ADVANCES IN CHEMICAL PHYSICS VOLUME 119 PART I
I. PRIGOGINE and STUART A. RICE, Series Editors

Edited by
MYRON EVANS

MODERN NONLINEAR OPTICS
Part I

MODERN NONLINEAR OPTICS
Part 1
Second Edition

ADVANCES IN CHEMICAL PHYSICS

VOLUME 119

EDITORIAL BOARD

BRUCE, J. BERNE, Department of Chemistry, Columbia University, New York, New York, U.S.A.

KURT BINDER, Institut für Physik, Johannes Gutenberg-Universität Mainz, Mainz, Germany

A. WELFORD CASTLEMAN, JR., Department of Chemistry, The Pennsylvania State University, University Park, Pennsylvania, U.S.A.

DAVID CHANDLER, Department of Chemistry, University of California, Berkeley, California, U.S.A.

M. S. CHILD, Department of Theoretical Chemistry, University of Oxford, Oxford, U.K.

WILLIAM T. COFFEY, Department of Microelectronics and Electrical Engineering, Trinity College, University of Dublin, Dublin, Ireland

F. FLEMING CRIM, Department of Chemistry, University of Wisconsin, Madison, Wisconsin, U.S.A.

ERNEST R. DAVIDSON, Department of Chemistry, Indiana University, Bloomington, Indiana, U.S.A.

GRAHAM R. FLEMING, Department of Chemistry, University of California, Berkeley, California, U.S.A.

KARL F. FREED, The James Franck Institute, The University of Chicago, Chicago, Illinois, U.S.A.

PIERRE GASPARD, Center for Nonlinear Phenomena and Complex Systems, Brussels, Belgium

ERIC J. HELLER, Institute for Theoretical Atomic and Molecular Physics, Harvard-Smithsonian Center for Astrophysics, Cambridge, Massachusetts, U.S.A.

ROBIN M. HOCHSTRASSER, Department of Chemistry, The University of Pennsylvania, Philadelphia, Pennsylvania, U.S.A.

R. KOSLOFF, The Fritz Haber Research Center for Molecular Dynamics and Department of Physical Chemistry, The Hebrew University of Jerusalem, Jerusalem, Israel

RUDOLPH A. MARCUS, Department of Chemistry, California Institute of Technology, Pasadena, California, U.S.A.

G. NICOLIS, Center for Nonlinear Phenomena and Complex Systems, Université Libre de Bruxelles, Brussels, Belgium

THOMAS P. RUSSELL, Department of Polymer Science, University of Massachusetts, Amherst, Massachusetts

DONALD G. TRUHLAR, Department of Chemistry, University of Minnesota, Minneapolis, Minnesota, U.S.A.

JOHN D. WEEKS, Institute for Physical Science and Technology and Department of Chemistry, University of Maryland, College Park, Maryland, U.S.A.

PETER G. WOLYNES, Department of Chemistry, University of California, San Diego, California, U.S.A.

MODERN NONLINEAR OPTICS

Part 1

Second Edition

ADVANCES IN CHEMICAL PHYSICS
VOLUME 119

Edited by

Myron W. Evans

Series Editors

I. PRIGOGINE

Center for Studies in Statistical Mechanics and Complex Systems
The University of Texas
Austin, Texas
and
International Solvay Institutes
Université Libre de Bruxelles
Brussels, Belgium

and

STUART A. RICE

Department of Chemistry
and
The James Franck Institute
The University of Chicago
Chicago, Illinois

AN INTERSCIENCE® PUBLICATION
JOHN WILEY & SONS, INC.

Designations used by companies to distinguish their products are often claimed as trademarks. In all instances where John Wiley & Sons, Inc., is aware of a claim, the product names appear in initial capital or ALL CAPITAL LETTERS. Readers, however, should contact the appropriate companies for more complete information regarding trademarks and registration.

Copyright © 2001 by John Wiley & Sons, Inc. All rights reserved.

No part of this publication may be reproduced, stored in a retrieval system or transmitted in any form or by any means, electronic or mechanical, including uploading, downloading, printing, decompiling, recording or otherwise, except as permitted under Sections 107 or 108 of the 1976 United States Copyright Act, without the prior written permission of the Publisher. Requests to the Publisher for permission should be addressed to the Permissions Department, John Wiley & Sons, Inc., 605 Third Avenue, New York, NY 10158-0012, (212) 850-6011, fax (212) 850-6008, E-Mail: PERMREQ @ WILEY.COM.

This publication is designed to provide accurate and authoritative information in regard to the subject matter covered. It is sold with the understanding that the publisher is not engaged in rendering professional services. If professional advice or other expert assistance is required, the services of a competent professional person should be sought.

ISBN 0-471-23147-9

This title is also available in print as ISBN 0-471-38930-7.

For more information about Wiley products, visit our web site at www.Wiley.com.

CONTRIBUTORS TO VOLUME 119
Part 1

PHILIP ALLCOCK, Research Officer, Department of Physics, University of Bath, Bath, United Kingdom

DAVID L. ANDREWS, School of Chemical Sciences, University of East Anglia, Norwich, United Kingdom

JIŘÍ BAJER, Department of Optics, Palacký University, Olomouc, Czech Republic

TADEUSZ BANCEWICZ, Nonlinear Optics Division, Adam Mickiewicz University, Poznań, Poland

V. V. DODONOV, Departamento de Física, Universidade Federal de São Carlos, São Carlos, SP, Brazil and Moscow Institute of Physics and Technology, Lebedev Physics Institute of the Russian Academy of Sciences, Moscow, Russia

MILOSLAV DUŠEK, Department of Optics, Palacký University, Olomouc, Czech Republic

ZBIGNIEW FICEK, Department of Physics and Centre for Laser Science, The University of Queensland, Brisbane, Australia

JAROMÍR FIURÁŠEK, Department of Optics, Palacký University, Olomouc, Czech Republic

JEAN-LUC GODET, Laboratoire de Propriétés Optiques des Matériaux et Applications, University d'Angers, Faculté des Sciences, Angers, France

ONDŘEJ HADERKA, Joint Laboratory of Optics of Palacký University and the Academy of Sciences of the Czech Republic, Olomouc, Czech Republic

MARTIN HENDRYCH, Joint Laboratory of Optics of Palacký University and the Academy of Sciences of the Czech Republic, Olomouc, Czech Republic

ZDENĚK HRADIL, Department of Optics, Palacký University, Olomouc, Czech Republic

NOBUYUKI IMOTO, CREST Research Team for Interacting Carrier Electronics, School of Advanced Sciences, The Graduate University of Advanced Studies (SOKEN), Hayama, Kanagawa, Japan

MASATO KOASHI, CREST Research Team for Interacting Carrier Electronics, School of Advanced Sciences, The Graduate University for Advanced Studies (SOKEN), Hayama, Kanagawa, Japan

YVES LE DUFF, Laboratoire de Propriétés Optiques des Matériaux et Applications, Université d'Angers, Faculté des Sciences, Angers, France

WIESŁAW LEOŃSKI, Nonlinear Optics Division, Adam Mickiewicz University, Poznań, Poland

ANTONÍN LUKŠ, Department of Optics, Palacký University, Olomouc, Czech Republic

ADAM MIRANOWICZ, CREST Research Team for Interacting Carrier Electronics, School of Advanced Sciences, The Graduate University for Advanced Studies (SOKEN), Hayama, Kanagawa, Japan and Nonlinear Optics Division, Institute of Physics, Adam Mickiewicz University, Poznan, Poland

JAN PEŘINA, Joint Laboratory of Optics of Palacký University and the Academy of Sciences of the Czech Republic, Olomouc, Czech Republic

JAN PEŘINA, JR., Joint Laboratory of Optics of Palacký University and the Academy of Sciences of the Czech Republic, Olomouc, Czech Republic

VLASTA PEŘINOVÁ, Department of Optics, Palacký University, Olomouc, Czech Republic

JAROSLAV ŘEHÁČEK, Department of Optics, Palacký University, Olomouc, Czech Republic

MENDEL SACHS, Department of Physics, State University of New York at Buffalo, Buffalo, NY

ALEXANDER S. SHUMOVSKY, Physics Department, Bilkent University, Bilkent, Ankara, Turkey

RYSZARD TANAŚ, Nonlinear Optics Division, Institute of Physics, Adam Mickiewicz University, Poznań, Poland

INTRODUCTION

Few of us can any longer keep up with the flood of scientific literature, even in specialized subfields. Any attempt to do more and be broadly educated with respect to a large domain of science has the appearance of tilting at windmills. Yet the synthesis of ideas drawn from different subjects into new, powerful, general concepts is as valuable as ever, and the desire to remain educated persists in all scientists. This series, *Advances in Chemical Physics*, is devoted to helping the reader obtain general information about a wide variety of topics in chemical physics, a field that we interpret very broadly. Our intent is to have experts present comprehensive analyses of subjects of interest and to encourage the expression of individual points of view. We hope that this approach to the presentation of an overview of a subject will both stimulate new research and serve as a personalized learning text for beginners in a field.

I. Prigogine
Stuart A. Rice

PREFACE

This volume, produced in three parts, is the Second Edition of Volume 85 of the series, *Modern Nonlinear Optics*, edited by M. W. Evans and S. Kielich. Volume 119 is largely a dialogue between two schools of thought, one school concerned with quantum optics and Abelian electrodynamics, the other with the emerging subject of non-Abelian electrodynamics and unified field theory. In one of the review articles in the third part of this volume, the Royal Swedish Academy endorses the complete works of Jean-Pierre Vigier, works that represent a view of quantum mechanics opposite that proposed by the Copenhagen School. The formal structure of quantum mechanics is derived as a linear approximation for a generally covariant field theory of inertia by Sachs, as reviewed in his article. This also opposes the Copenhagen interpretation. Another review provides reproducible and repeatable empirical evidence to show that the Heisenberg uncertainty principle can be violated. Several of the reviews in Part 1 contain developments in conventional, or Abelian, quantum optics, with applications.

In Part 2, the articles are concerned largely with electrodynamical theories distinct from the Maxwell–Heaviside theory, the predominant paradigm at this stage in the development of science. Other review articles develop electrodynamics from a topological basis, and other articles develop conventional or U(1) electrodynamics in the fields of antenna theory and holography. There are also articles on the possibility of extracting electromagnetic energy from Riemannian spacetime, on superluminal effects in electrodynamics, and on unified field theory based on an SU(2) sector for electrodynamics rather than a U(1) sector, which is based on the Maxwell–Heaviside theory. Several effects that cannot be explained by the Maxwell–Heaviside theory are developed using various proposals for a higher-symmetry electrodynamical theory. The volume is therefore typical of the second stage of a paradigm shift, where the prevailing paradigm has been challenged and various new theories are being proposed. In this case the prevailing paradigm is the great Maxwell–Heaviside theory and its quantization. Both schools of thought are represented approximately to the same extent in the three parts of Volume 119.

As usual in the *Advances in Chemical Physics* series, a wide spectrum of opinion is represented so that a consensus will eventually emerge. The prevailing paradigm (Maxwell–Heaviside theory) is ably developed by several groups in the field of quantum optics, antenna theory, holography, and so on, but the paradigm is also challenged in several ways: for example, using general relativity, using O(3) electrodynamics, using superluminal effects, using an

extended electrodynamics based on a vacuum current, using the fact that longitudinal waves may appear in vacuo on the U(1) level, using a reproducible and repeatable device, known as the *motionless electromagnetic generator*, which extracts electromagnetic energy from Riemannian spacetime, and in several other ways. There is also a review on new energy sources. Unlike Volume 85, Volume 119 is almost exclusively dedicated to electrodynamics, and many thousands of papers are reviewed by both schools of thought. Much of the evidence for challenging the prevailing paradigm is based on empirical data, data that are reproducible and repeatable and cannot be explained by the Maxwell–Heaviside theory. Perhaps the simplest, and therefore the most powerful, challenge to the prevailing paradigm is that it cannot explain interferometric and simple optical effects. A non-Abelian theory with a Yang–Mills structure is proposed in Part 2 to explain these effects. This theory is known as O(3) *electrodynamics* and stems from proposals made in the first edition, Volume 85.

As Editor I am particularly indebted to Alain Beaulieu for meticulous logistical support and to the Fellows and Emeriti of the Alpha Foundation's Institute for Advanced Studies for extensive discussion. Dr. David Hamilton at the U.S. Department of Energy is thanked for a Website reserved for some of this material in preprint form.

Finally, I would like to dedicate the volume to my wife, Dr. Laura J. Evans.

MYRON W. EVANS

Ithaca, New York

CONTENTS

QUANTUM NOISE IN NONLINEAR OPTICAL PHENOMENA

RYSZARD TANAŚ

Nonlinear Optics Division, Institute of Physics, Adam Mickiewicz University, Poznań, Poland

CONTENTS

I. INTRODUCTION

More than a century has passed since Planck discovered that it is possible to explain properties of the blackbody radiation by introducing discrete packets of energy, which we now call *photons*. The idea of discrete or quantized nature of energy had deep consequences and resulted in development of quantum mechanics. The quantum theory of optical fields is called *quantum optics*. The construction of lasers in the 1960s gave impulse to rapid development of nonlinear optics with a broad variety of nonlinear optical phenomena that have been

experimentally observed and described theoretically and now are the subject of textbooks [1,2]. In early theoretical descriptions of nonlinear optical phenomena, the quantum nature of optical fields has been ignored on the grounds that laser fields are so strong, that is, the number of photons associated with them are so huge, that the quantum properties assigned to individual photons have no chances to manifest themselves. However, it turned out pretty soon that quantum noise associated with the vacuum fluctuations can have important consequences for the course of nonlinear phenomena. Moreover, it appeared that the quantum noise itself can change essentially when the quantum field is subject to the nonlinear transformation that is the essence of any nonlinear process. The quantum states with reduced quantum noise for a particular physical quantity can be prepared in various nonlinear processes. Such states have no classical counterparts; that is, the results of some physical measurements cannot be explained without explicit recall to the quantum character of the field. The methods of theoretical description of quantum noise are the subject of Gardiner's book [3]. This chapter is not intended as a presentation of general methods that can be found in the book; rather, we want to compare the results obtained with a few chosen methods for the two, probably most important, nonlinear processes: second-harmonic generation and downconversion with quantum pump.

Why have we chosen the second-harmonic generation and the downconversion to illustrate consequences of field quantization, or a role of quantum noise, in nonlinear optical processes? The two processes are at the same time similar and different. Both of them are described by the same interaction Hamiltonian, so in a sense they are similar and one can say that they show different faces of the same process. However, they are also different, and the difference between them consists in the different initial conditions. This difference appears to be very important, at least at early stages of the evolution, and the properties of the fields produced in the two processes are quite different. With these two best-known and practically very important examples of nonlinear optical processes, we would like to discuss several nonclassical effects and present the most common theoretical approaches used to describe quantum effects. The chapter is not intended to be a complete review of the results concerning the two processes that have been collected for years. We rather want to introduce the reader who is not an expert in quantum optics into this fascinating field by presenting not only the results but also how they can be obtained with presently available computer software. The results are largely illustrated graphically for easier comparisons. In Section II we introduce basic definitions and the most important formulas required for later discussion. Section III is devoted to presentation of results for second-harmonic generation, and Section IV results for downconversion. In the Appendixes A and B we have added examples of computer programs that illustrate usage of really existing software and were

actually used in our calculations. We draw special attention to symbolic calculations and numerical methods, which can now be implemented even on small computers.

II. BASIC DEFINITIONS

In classical optics, a one mode electromagnetic field of frequency ω, with the propagation vector $\mathbf{k}$ and linear polarization, can be represented as a plane wave

$$E(\mathbf{r}, t) = 2E_0 \cos(\mathbf{k} \cdot \mathbf{r} - \omega t + \varphi) \tag{1}$$

where E_0 is the amplitude and φ is the phase of the field. Assuming the linear polarization of the field, we have omitted the unit polarization vector to simplify the notation. Classically, both the amplitude E_0 and the phase φ can be well-defined quantities, with zero noise. Of course, the two quantities can be considered as classical random variables with nonzero variances; thus, they can be noisy in a classical sense, but there is no relation between the two variances and, in principle, either of them can be rendered zero giving the noiseless classical field. Apart from a constant factor, the squared real amplitude, E_0^2, is the intensity of the field. In classical electrodynamics there is no real need to use complex numbers to describe the field. However, it is convenient to work with exponentials rather than cosine and sine functions and the field (1) is usually written in the form

$$E(\mathbf{r}, t) = E^{(+)} e^{i(\mathbf{k} \cdot \mathbf{r} - \omega t)} + E^{(-)} e^{-i(\mathbf{k} \cdot \mathbf{r} - \omega t)} \tag{2}$$

with the complex amplitudes $E^{\pm} = E_0 e^{\pm i\varphi}$. The modulus squared of such an amplitude is the intensity of the field, and the argument is the phase. Both intensity and the phase can be measured simultaneously with arbitrary accuracy.

In quantum optics the situation is dramatically different. The electromagnetic field E becomes a quantum quantity; that is, it becomes an operator acting in a Hilbert space of field states, the complex amplitudes $E^{\pm}$ become the annihilation and creation operators of the electromagnetic field mode, and we have

$$\hat{E} = \sqrt{\frac{\hbar\omega}{2\varepsilon_0 V}} [\hat{a} e^{i(\mathbf{k} \cdot \mathbf{r} - \omega t)} + \hat{a}^{+} e^{-i(\mathbf{k} \cdot \mathbf{r} - \omega t)}] \tag{3}$$

with the bosonic commutation rules

$$[\hat{a}, \hat{a}^{+}] = 1 \tag{4}$$

for the annihilation ($\hat{a}$) and creation ($\hat{a}^{+}$) operators of the field mode, where ε_0 is the electric permittivity of free space and V is the quantization volume. Because

of laws of quantum mechanics, optical fields exhibit an inherent quantum indeterminacy that cannot be removed for principal reasons no matter how smart we are. The quantity

$$\mathscr{E}_0 = \sqrt{\frac{\hbar\omega}{2\varepsilon_0 V}} \tag{5}$$

appearing in (3) is a measure of the quantum optical noise for a single mode of the field. This noise is present even if the field is in the vacuum state, and for this reason it is usually referred to as the *vacuum fluctuations of the field* [4]. Quantum noise associated with the vacuum fluctuations, which appears because of noncommuting character of the annihilation and creation operators expressed by (4), is ubiquitous and cannot be eliminated, but we can to some extent control this noise by 'squeezing' it in one quantum variable at the expense of "expanding" it in another variable. This noise, no matter how small it is in comparison to macroscopic fields, can have very important macroscopic consequences changing the character of the evolution of the macroscopic fields. We are going to address such questions in this chapter.

The electric field operator (3) can be rewritten in the form

$$\hat{E} = \mathscr{E}_0\left[\hat{Q}\cos(\mathbf{k}\cdot\mathbf{r} - \omega t) + \hat{P}\sin(\mathbf{k}\cdot\mathbf{r} - \omega t)\right] \tag{6}$$

where we have introduced two Hermitian quadrature operators, $\hat{Q}$ and $\hat{P}$, defined as

$$\hat{Q} = \hat{a} + \hat{a}^+ , \qquad \hat{P} = -i(\hat{a} - \hat{a}^+) \tag{7}$$

which satisfy the commutation relation

$$[\hat{Q}, \hat{P}] = 2i \tag{8}$$

The two quadrature operators thus obey the Heisenberg uncertainty relation

$$\langle(\Delta\hat{Q})^2\rangle\langle(\Delta\hat{P})^2\rangle \geq 1 \tag{9}$$

where we have introduced the quadrature noise operators

$$\Delta\hat{Q} = \hat{Q} - \langle\hat{Q}\rangle , \qquad \Delta\hat{P} = \hat{P} - \langle\hat{P}\rangle \tag{10}$$

For the vacuum state or a coherent state, which are the minimum uncertainty states, the inequality (9) becomes equality and, moreover, the two variances are equal

$$\langle(\Delta\hat{Q})^2\rangle = \langle(\Delta\hat{P})^2 = 1 \tag{11}$$

The Heisenberg uncertainty relation (9) imposes basic restrictions on the accuracy of the simultaneous measurement of the two quadrature components of the optical field. In the vacuum state the noise is isotropic and the two components have the same level of quantum noise. However, quantum states can be produced in which the isotropy of quantum fluctuations is broken—the uncertainty of one quadrature component, say, $\hat{Q}$, can be reduced at the expense of expanding the uncertainty of the conjugate component, $\hat{P}$. Such states are called *squeezed states* [5,6]. They may or may not be the minimum uncertainty states. Thus, for squeezed states

$$\langle(\Delta\hat{Q})^2\rangle < 1 \quad \text{or} \quad \langle(\Delta\hat{P})^2\rangle < 1 \tag{12}$$

Squeezing is a unique quantum property that cannot be explained when the field is treated as a classical quantity—field quantization is crucial for explaining this effect.

Another nonclassical effect is referred to as *sub-Poissonian photon statistics* (see, e.g., Refs. 7 and 8 and papers cited therein). It is well known that in a coherent state defined as an infinite superposition of the number states

$$|\alpha\rangle = \exp\left(-\frac{|\alpha|^2}{2}\right)\sum_{n=0}^{\infty}\frac{\alpha^n}{\sqrt{n!}}\,|n\rangle \tag{13}$$

the photon number distribution is Poissonian

$$p(n) = |\langle n|\alpha\rangle|^2 = \exp(-|\alpha|^2)\frac{|\alpha|^{2n}}{n!} = \exp(-\langle\hat{n}\rangle)\frac{\langle\hat{n}\rangle^n}{n!} \tag{14}$$

which means

$$\langle(\Delta\hat{n})^2\rangle = \langle\hat{n}^2\rangle - \langle\hat{n}\rangle^2 = \langle\hat{n}\rangle \tag{15}$$

If the variance of the number of photons is smaller than its mean value, the field is said to exhibit the sub-Poissonian photon statistics. This effect is related to the second-order intensity correlation function

$$G^{(2)}(\tau) = \langle:\hat{n}(t)\hat{n}(t+\tau):\rangle = \langle\hat{a}^+(t)\hat{a}^+(t+\tau)\hat{a}(t+\tau)\hat{a}(t)\rangle \tag{16}$$

where $::$ indicate the normal order of the operators. This function describes the probability of counting a photon at t and another one at $t+\tau$. For stationary fields, this function does not depend on t but solely on τ. The normalized

second-order correlation function, or second-order degree of coherence, is defined as

$$g^{(2)}(\tau) = \frac{G^{(2)}(\tau)}{\langle \hat{n} \rangle^2} \tag{17}$$

If $g^{(2)}(\tau) < g^{(2)}(0)$, the probability of detecting the second photon decreases with the time delay τ, indicating *bunching* of photons. On the other hand, if $g^{(2)}(\tau) > g^{(2)}(0)$, we have the effect of *antibunching* of photons. Photon antibunching is another signature of quantum character of the field. For $\tau = 0$, we have

$$g^{(2)}(0) = \frac{\langle \hat{a}^+ \hat{a}^+ \hat{a}\, \hat{a} \rangle}{\langle \hat{a}^+ \hat{a} \rangle^2} = \frac{\langle \hat{n}(\hat{n} - 1) \rangle}{\langle \hat{n} \rangle^2} = 1 + \frac{\langle (\Delta \hat{n})^2 \rangle - \langle \hat{n} \rangle}{\langle \hat{n} \rangle^2} \tag{18}$$

which gives the relation between the photon statistics and the second-order correlation function. Another convenient parameter describing the deviation of the photon statistics from the Poissonian photon number distribution is the Mandel q parameter defined as [9]

$$q = \frac{\langle (\Delta \hat{n})^2 \rangle}{\langle \hat{n} \rangle} - 1 = \langle \hat{n} \rangle (g^{(2)}(0) - 1) \tag{19}$$

Negative values of this parameter indicate sub-Poissonian photon statistics, namely, nonclassical character of the field. One obvious example of the nonclassical field is a field in a number state $|n\rangle$ for which the photon number variance is zero, and we have $g^{(2)}(0) = 1 - 1/n$ and $q = -1$. For coherent states, $g^{(2)}(0) = 1$ and $q = 0$. In this context, coherent states draw a somewhat arbitrary line between the quantum states that have "classical analogs" and the states that do not have them. The coherent states belong to the former category, while the states for which $g^{(2)}(0) < 1$ or $q < 0$ belong to the latter category. This distinction is better understood when the Glauber–Sudarshan quasidistribution function $P(\alpha)$ is used to describe the field.

The coherent states (13) can be used as a basis to describe states of the field. In such a basis for a state of the field described by the density matrix ρ, we can introduce the quasidistribution function $P(\alpha)$ in the following way:

$$\rho = \int d^2\alpha\, P(\alpha) |\alpha\rangle\langle\alpha| \tag{20}$$

where $d^2\alpha = d\,\mathrm{Re}(\alpha)\, d\,\mathrm{Im}(\alpha)$. In terms of $P(\alpha)$, the expectation value of the normally ordered products (creation operators to the left and annihilation

operators to the right) has the form

$$\langle(\hat{a}^+)^m\hat{a}^n\rangle = \mathrm{Tr}\,[\rho(\hat{a}^+)^m\hat{a}^n] = \int d^2\alpha\, P(\alpha)(\alpha^*)^m\alpha^n \tag{21}$$

For a coherent state $|\alpha_0\rangle$, $\rho = |\alpha_0\rangle\langle\alpha_0|$, and the quasiprobability distribution $P(\alpha) = \delta^{(2)}(\alpha - \alpha_0)$ giving $\langle(a^+)^m a^n\rangle = (\alpha^*)^m\alpha^n\rangle$. When $P(\alpha)$ is a well-behaved, positive definite function, it can be considered as a probability distribution function of a classical stochastic process, and the field with such a P function is said to have "classical analog." However, the P function can be highly singular or can take negative values, in which case it does not satisfy requirements for the probability distribution, and the field states with such a P function are referred to as *nonclassical states*.

From the definition (13) of coherent state it is easy to derive the completeness relation

$$\frac{1}{\pi}\int d^2\alpha\, |\alpha\rangle\langle\alpha| = 1 \tag{22}$$

and find that the coherent states do not form an orthonormal set

$$|\langle\alpha|\beta\rangle|^2 = \exp(-|\alpha - \beta|^2) \tag{23}$$

and only for $|\alpha - \beta|^2 \gg 1$ they are approximately orthogonal. In fact, coherent states form an overcomplete set of states.

To see the nonclassical character of squeezed states better, let us express the variance $\langle(\Delta\hat{Q})^2\rangle$ in terms of the P function

$$\begin{aligned}\langle(\Delta\hat{Q})^2\rangle &= \langle(\hat{a} + \hat{a}^+)^2\rangle - \langle(\hat{a} + \hat{a}^+)\rangle^2 \\ &= \langle\hat{a}^2 + \hat{a}^{+2} + 2\hat{a}^+\hat{a} + 1\rangle - \langle\hat{a} + \hat{a}^+\rangle^2 \\ &= 1 + \int d^2\alpha\, P(\alpha)[(\alpha + \alpha^*)^2 - \langle\alpha + \alpha^*\rangle^2]\end{aligned} \tag{24}$$

which shows that $\langle(\Delta\hat{Q})^2\rangle < 1$ is possible only if $P(\alpha)$ is not a positive definite function. The unity on the right-hand side of (24) comes from applying the commutation relation (4) to put the formula into its normal form, and it is thus a manifestation of the quantum character of the field ("shot noise").

Similarly, for the photon number variance, we get

$$\begin{aligned}\langle(\Delta\hat{n})^2\rangle &= \langle\hat{n}\rangle + \langle\hat{a}^{+2}\hat{a}^2\rangle - \langle\hat{a}^+\hat{a}\rangle^2 \\ &= \langle\hat{n}\rangle + \int d^2\alpha\, P(\alpha)[|\alpha|^2 - \langle|\alpha|^2\rangle]^2\end{aligned} \tag{25}$$

Again, $\langle(\Delta\hat{n})^2\rangle < \langle\hat{n}\rangle$ only if $P(\alpha)$ is not positive definite, and thus sub-Poissonian photon statistics is a nonclassical feature.

In view of (24), one can write

$$\langle(\Delta\hat{Q})^2\rangle = 1 + \langle:(\Delta\hat{Q})^2:\rangle\,, \qquad \langle(\Delta\hat{P})^2\rangle = 1 + \langle:(\Delta\hat{P})^2:\rangle \tag{26}$$

where : : indicate the normal form of the operator. Using the normal form of the quadrature component variances squeezing can be conveniently defined by the condition

$$\langle:(\Delta\hat{Q})^2:\rangle < 0 \quad \text{or} \quad \langle:(\Delta\hat{P})^2:\rangle < 0 \tag{27}$$

Therefore, whenever the normal form of the quadrature variance is negative, this component of the field is squeezed or, in other words, the quantum noise in this component is reduced below the vacuum level. For classical fields, there is no unity coming from the boson commutation relation, and the normal form of the quadrature component represents true variance of the classical stochastic variable, which must be positive.

The Glauber–Sudarshan P representation of the field state is associated with the normal order of the field operators and is not the only c-number representation of the quantum state. Another quasidistribution that is associated with antinormal order of the operators is the Q representation, or the Husimi function, defined as

$$Q(\alpha) = \frac{1}{\pi}\langle\alpha|\rho|\alpha\rangle \tag{28}$$

and in terms of this function the expectation value of the antinormally ordered product of the field operators is calculated according to the formula

$$\langle\hat{a}^m(\hat{a}^+)^n\rangle = \frac{1}{\pi}\int d^2\alpha\,\langle\alpha|\rho|\alpha\rangle\alpha^m(\alpha^*)^n \tag{29}$$

It is clear from (28) that $Q(\alpha)$ is always positive, since ρ is a positive definite operator. For a coherent state $|\alpha_0\rangle$, $Q(\alpha) = (1/\pi)\exp(-|\alpha-\alpha_0|^2)$ is a Gaussian in the phase space $\{\mathrm{Re}\,\alpha, \mathrm{Im}\,\alpha\}$ which is centered at α_0. The section of this function, which is a circle, represents isotropic noise in the coherent state (the same as for the vacuum). The anisotropy introduced by squeezed states means a deformation of the circle into an ellipse or another shape.

Generally, according to Cahill and Glauber [10], one can introduce the s-parametrized quasidistribution function $\mathscr{W}^{(s)}(\alpha)$ defined as

$$\mathscr{W}^{(s)}(\alpha) = \frac{1}{\pi}\mathrm{Tr}\{\rho\,\hat{T}^{(s)}(\alpha)\} \tag{30}$$

where the operator $\hat{T}^{(s)}(\alpha)$ is given by

$$\hat{T}^{(s)}(\alpha) = \frac{1}{\pi}\int d^2\xi \exp(\alpha\xi^* - \alpha^*\xi)\hat{D}^{(s)}(\xi) \tag{31}$$

and

$$\hat{D}^{(s)}(\xi) = \exp\left(\frac{s\xi^2}{2}\right)\hat{D}(\xi) \tag{32}$$

where $\hat{D}(\xi)$ is the displacement operator and ρ is the density matrix of the field. The operator $\hat{T}^{(s)}(\alpha)$ can be rewritten in the form

$$\hat{T}^{(s)}(\alpha) = \frac{2}{1-s}\sum_{n=0}^{\infty}\hat{D}(\alpha)|n\rangle\left(\frac{s+1}{s-1}\right)^n\langle n|\hat{D}^+(\alpha) \tag{33}$$

which gives explicitly its s dependence. So, the s-parametrized quasidistribution function $\mathscr{W}^{(s)}(\alpha)$ has the following form in the number-state basis

$$\mathscr{W}^{(s)}(\alpha) = \frac{1}{\pi}\sum_{m,n}\rho_{mn}\langle n|\hat{T}^{(s)}(\alpha)|m\rangle \tag{34}$$

where the matrix elements of the operator (31) are given by

$$\begin{aligned}\langle n|\hat{T}^{(s)}(\alpha)|m\rangle = \sqrt{\frac{n!}{m!}}\left(\frac{2}{1-s}\right)^{m-n+1}\left(\frac{s+1}{s-1}\right)^n e^{-i(m-n)\theta}|\alpha|^{m-n}\\ \times \exp\left(-\frac{2|\alpha|^2}{1-s}\right)L_n^{m-n}\left(\frac{4|\alpha|^2}{1-s^2}\right)\end{aligned} \tag{35}$$

in terms of the associate Laguerre polynomials $L_n^{m-n}(x)$. In this equation we have also separated explicitly the phase of the complex number α by writing

$$\alpha = |\alpha|e^{i\theta} \tag{36}$$

The phase θ is the quantity representing the field phase.

With the quasiprobability distributions $\mathscr{W}^{(s)}(\alpha)$, the expectation values of the s-ordered products of the creation and annihilation operators can be obtained by proper integrations in the complex α plane. In particular, for $s = 1, 0, -1$, the s-ordered products are normal, symmetric, and antinormal ordered products of the creation and annihilation operators, and the corresponding distributions are the Glauber–Sudarshan P function, Wigner function, and Husimi Q function. By

virtue of the relation inverse to (34), the field density matrix can be retrieved from the quasiprobability function

$$\rho = \int d^2\alpha\, \hat{T}^{(-s)}(\alpha)\mathscr{W}^{(s)}(\alpha) \tag{37}$$

Polar decomposition of the field amplitude, as in (36), which is trivial for classical fields becomes far from being trivial for quantum fields because of the problems with proper definition of the Hermitian phase operator. It was quite natural to associate the photon number operator with the intensity of the field and somehow construct the phase operator conjugate to the number operator. The latter task, however, turned out not to be easy. Pegg and Barnett [11–13] introduced the Hermitian phase formalism, which is based on the observation that in a finite-dimensional state space, the states with well-defined phase exist [14]. Thus, they restrict the state space to a finite $(\sigma + 1)$-dimensional Hilbert space $\mathrm{H}^{(\sigma)}$ spanned by the number states $|0\rangle, |1\rangle, \ldots, |\sigma\rangle$. In this space they define a complete orthonormal set of phase states by

$$|\theta_m\rangle = \frac{1}{\sqrt{\sigma+1}}\sum_{n}^{\sigma} \exp(in\theta_m)|n\rangle\,, \qquad m = 0, 1, \ldots, \sigma \tag{38}$$

where the values of θ_m are given by

$$\theta_m = \theta_0 + \frac{2\pi m}{\sigma+1} \tag{39}$$

The value of θ_0 is arbitrary and defines a particular basis set of $(\sigma + 1)$ mutually orthogonal phase states. The number state $|n\rangle$ can be expanded in terms of the $|\theta_m\rangle$ phase-state basis as

$$|n\rangle = \sum_{m=0}^{\sigma} |\theta_m\rangle\langle\theta_m|n\rangle = \frac{1}{\sqrt{\sigma+1}}\sum_{m=0}^{\sigma} \exp(-in\theta_m)|\theta_m\rangle \tag{40}$$

From Eqs. (38) and (40) we see that a system in a number state is equally likely to be found in any state $|\theta_m\rangle$, and a system in a phase state is equally likely to be found in any number state $|n\rangle$.

The Pegg–Barnett Hermitian phase operator is defined as

$$\hat{\Phi}_\theta = \sum_{m=0}^{\sigma} \theta_m|\theta_m\rangle\langle\theta_m| \tag{41}$$

Of course, the phase states (38) are eigenstates of the phase operator (40) with the eigenvalues θ_m restricted to lie within a phase window between θ_0 and $\theta_0 + 2\pi\sigma/(\sigma+1)$. The Pegg–Barnett prescription is to evaluate any observable of interest in the finite basis (38), and only after that to take the limit $\sigma \to \infty$.

Since the phase states (38) are orthonormal, $\langle\theta_m|\theta_{m'}\rangle = \delta_{mm'}$, the kth power of the Pegg–Barnett phase operator (41) can be written as

$$\hat{\Phi}_\theta^k = \sum_{m=0}^{\sigma} \theta_m^k |\theta_m\rangle\langle\theta_m| \tag{42}$$

Substituting Eqs. (38) and (39) into Eq. (41) and performing summation over m yields explicitly the phase operator in the Fock basis:

$$\hat{\Phi}_\theta = \theta_0 + \frac{\sigma\pi}{\sigma+1} + \frac{2\pi}{\sigma+1}\sum_{n\neq n'} \frac{\exp[i(n-n')\theta_0]|n\rangle\langle n'|}{\exp[i(n-n')2\pi/(\sigma+1)]-1} \tag{43}$$

It is readily apparent that the Hermitian phase operator $\hat{\Phi}_\theta$ has well-defined matrix elements in the number-state basis and does not suffer from the problems as those the original Dirac phase operator suffered. Indeed, using the Pegg–Barnett phase operator (43) one can readily calculate the phase-number commutator [13]

$$\left[\hat{\Phi}_\theta, \hat{n}\right] = -\frac{2\pi}{\sigma+1}\sum_{n\neq n'} \frac{(n-n')\exp[i(n-n')\theta_0]}{\exp[i(n-n')2\pi/(\sigma+1)]-1}|n\rangle\langle n'| \tag{44}$$

This equation looks very different from the famous Dirac postulate for the phase-number commutator.

The Pegg–Barnett Hermitian phase formalism allows for direct calculations of quantum phase properties of optical fields. As the Hermitian phase operator is defined, one can calculate the expectation value and variance of this operator for a given state $|f\rangle$. Moreover, the Pegg–Barnett phase formalism allows for the introduction of the continuous phase probability distribution, which is a representation of the quantum state of the field and describes the phase properties of the field in a very spectacular fashion. For so-called physical states, that is, states of finite energy, the Pegg–Barnett formalism simplifies considerably. In the limit as $\sigma \to \infty$ one can introduce the continuous phase distribution

$$P(\theta) = \lim_{\sigma\to\infty} \frac{\sigma+1}{2\pi}|\langle\theta_m|f\rangle|^2 \tag{45}$$

where $(\sigma+1)/2\pi$ is the density of states and the discrete variable θ_m is replaced by a continuous phase variable θ. In the number-state basis the

Pegg–Barnett phase distribution takes the form [15]

$$P(\theta) = \frac{1}{2\pi}\left\{1 + 2\mathrm{Re}\sum_{m>n}\rho_{mn}\exp\left[-i(m-n)\theta\right]\right\} \tag{46}$$

where $\rho_{mn} = \langle m|\rho|n\rangle$ are the density matrix elements in the number-state basis. The phase distribution (46) is 2π-periodic, and for all states with the density matrix diagonal in the number-state basis, the phase distribution is uniform over the 2π-wide phase window. Knowing the phase distribution makes the calculation of the phase operator expectation values quite simple; it is simply the calculation of all integrals over the continuous phase variable θ. For example,

$$\langle f|\hat{\Phi}_\theta^k|f\rangle = \int_{\theta_0}^{\theta_0+2\pi} d\theta\, \theta^k P(\theta) \tag{47}$$

When the phase window is chosen in such a way that the phase distribution is symmetrized with respect to the initial phase of the partial phase state, the phase variance is given by the formula

$$\langle(\Delta\hat{\Phi}_\theta)^2\rangle = \int_{-\pi}^{\pi} d\theta\, \theta^2 P(\theta) \tag{48}$$

For a partial phase state with the decomposition

$$|f\rangle = \sum_n b_n e^{in\varphi}|n\rangle \tag{49}$$

the phase variance has the form

$$\langle(\Delta\hat{\Phi}_\theta)^2\rangle = \frac{\pi^2}{3} + 4\sum_{n>k} b_n b_k \frac{(-1)^{n-k}}{(n-k)^2} \tag{50}$$

The value $\pi^2/3$ is the variance for the uniformly distributed phase, as in the case of a single-number state.

On integrating the quasiprobability distribution $\mathscr{W}^{(s)}(\alpha)$, given by (34), over the "radial" variable $|\alpha|$, we get a "phase distribution" associated with this quasiprobability distribution. The s-parametrized phase distribution is thus given by

$$P^{(s)}(\theta) = \int_0^\infty d|\alpha|\, \mathscr{W}^{(s)}(\alpha)|\alpha| \tag{51}$$

which, after performing of the integrations, gives the formula similar to the Pegg–Barnett phase distribution

$$P^{(s)}(\theta) = \frac{1}{2\pi}\left\{1 + 2\mathrm{Re}\sum_{m>n}\rho_{mn}\, e^{-i(m-n)\theta} G^{(s)}(m,n)\right\} \tag{52}$$

The difference between the Pegg–Barnett phase distribution (46) and the distribution (52) lies in the coefficients $G^{(s)}(m,n)$, which are given by [16]

$$G^{(s)}(m,n) = \left(\frac{2}{1-s}\right)^{(m+n)/2} \sum_{l=0}^{\min(m,n)} (-1)^l \left(\frac{1+s}{2}\right)^l \times \sqrt{\binom{n}{l}\binom{m}{l}}\, \frac{\Gamma\left(\dfrac{m+n}{2} - l + 1\right)}{\sqrt{(m-l)!(n-l)!}} \tag{53}$$

The phase distributions obtained by integration of the quasidistribution functions are different for different s, and all of them are different from the Pegg–Barnett phase distribution. The Pegg–Barnett phase distribution is always positive while the distribution associated with the Wigner distribution ($s = 0$) may take negative values. The distribution associated with the Husimi Q function is much broader than the Pegg–Barnett distribution, indicating that some phase information on the particular quantum state has been lost. Quantum phase fluctuations as fluctuations associated with the operator conjugate to the photon-number operator are important for complete picture of the quantum noise of the optical fields (for more details, see, e.g., Refs. 16 and 17).

III. SECOND-HARMONIC GENERATION

Second-harmonic generation, which was observed in the early days of lasers [18] is probably the best known nonlinear optical process. Because of its simplicity and variety of practical applications, it is a starting point for presentation of nonlinear optical processes in the textbooks on nonlinear optics [1,2]. Classically, the second-harmonic generation means the appearance of the field at frequency 2ω (second harmonic) when the optical field of frequency ω (fundamental mode) propagates through a nonlinear crystal. In the quantum picture of the process, we deal with a nonlinear process in which two photons of the fundamental mode are annihilated and one photon of the second harmonic is created. The classical treatment of the problem allows for closed-form solutions with the possibility of energy being transferred completely into the second-harmonic mode. For quantum fields, the closed-form analytical solution of the

problem has not been found unless some approximations are made. The early numerical solutions [19,20] showed that quantum fluctuations of the field prevent the complete transfer of energy into the second harmonic and the solutions become oscillatory. Later studies showed that the quantum states of the field generated in the process have a number of unique quantum features such as photon antibunching [21] and squeezing [9,22] for both fundamental and second harmonic modes (for a review and literature, see Ref. 23). Nikitin and Masalov [24] discussed the properties of the quantum state of the fundamental mode by calculating numerically the quasiprobability distribution function $Q(\alpha)$. They suggested that the quantum state of the fundamental mode evolves, in the course of the second-harmonic generation, into a superposition of two macroscopically distinguishable states, similar to the superpositions obtained for the anharmonic oscillator model [25–28] or a Kerr medium [29,30]. Bajer and Lisoněk [31] and Bajer and Peřina [32] have applied a symbolic computation approach to calculate Taylor series expansion terms to find evolution of nonlinear quantum systems. A quasiclassical analysis of the second harmonic generation has been done by Alvarez-Estrada et al. [33]. Phase properties of fields in harmonics generation have been studied by Gantsog et al. [34] and Drobný and Jex [35]. Bajer et al. [36] and Bajer et al. [37] have discussed the sub-Poissonian behavior in the second- and third-harmonic generation. More recently, Olsen et al. [38,38] have investigated quantum-noise-induced macroscopic revivals in second-harmonic generation and criteria for the quantum nondemolition measurement in this process.

Quantum description of the second harmonic generation, in the absence of dissipation, can start with the following model Hamiltonian

$$\hat{H} = \hat{H}_0 + \hat{H}_I \tag{54}$$

where

$$\hat{H}_0 = \hbar\omega\hat{a}^+\hat{a} + 2\hbar\omega\hat{b}^+\hat{b}\,, \qquad \hat{H}_I = \hbar\kappa(\hat{a}^2\hat{b}^+ + \hat{a}^{+2}\hat{b}) \tag{55}$$

and $\hat{a}$ ($\hat{a}^+$), $\hat{b}$ ($\hat{b}^+$) are the annihilation (creation) operators of the fundamental mode of frequency ω and the second harmonic mode at frequency 2ω, respectively. The coupling constant κ, which is real, describes the coupling between the two modes. Since $\hat{H}_0$ and $\hat{H}_I$ commute, there are two constants of motion: $\hat{H}_0$ and $\hat{H}_I$, $\hat{H}_0$ determines the total energy stored in both modes, which is conserved by the interaction $\hat{H}_I$. The free evolution associated with the Hamiltonian $\hat{H}_0$ leads to $\hat{a}(t) = \hat{a}(0)\exp(-i\omega t)$ and $\hat{b}(t) = \hat{b}(0)\exp(-i2\omega t)$. This trivial exponential evolution can always be factored out and the important part of the evolution described by the interaction Hamiltonian $\hat{H}_I$, for the slowly

varying operators in the Heisenberg picture, is given by a set of equations

$$\frac{d}{dt}\hat{a}(t) = \frac{1}{i\hbar}[\hat{a}, \hat{H}_I] = -2i\kappa\,\hat{a}^+(t)\hat{b}(t)$$
$$\frac{d}{dt}\hat{b}(t) = \frac{1}{i\hbar}[\hat{b}, \hat{H}_I] = -i\kappa\,\hat{a}^2(t) \tag{56}$$

where for notational convenience we use the same notation for the slowly varying operators as for the original operators — it is always clear from the context which operators are considered. In deriving the equations of motion (56), it is assumed that the operators associated with different modes commute, while for the same mode they obey the bosonic commutation rules (4).

Usually, the second-harmonic generation is considered as a propagation problem, not a cavity field problem, and the evolution variable is rather the path z the two beams traveled in the nonlinear medium. In the simplest, discrete two mode description of the process the transition from the cavity to the propagation problem is done by the replacement $t = -z/v$, where v denotes the velocity of the beams in the medium (we assume perfect matching conditions). We will use here time as the evolution variable, but it is understood that it can be equally well the propagation time in the propagation problem. So, we basically consider an idealized, one-pass problem. In fact, in the cavity situation the classical field pumping the cavity as well as the cavity damping must be added into the simple model to make it more realistic. Quantum theory of such a model has been developed by Drummond et al. [39,40]. Another interesting possibility is to study the second harmonic generation from the point of view of the chaotic behavior [41]. Such effects,however, will not be the subject of our concern here.

A. Classical Fields

Before we start with quantum description, let us recollect the classical solutions which will be used later in the method of classical trajectories to study some quantum properties of the fields. Equations (56) are valid also for classical fields after replacing the field operators $\hat{a}$ and $\hat{b}$ by the c-number field amplitudes α and β, which are generally complex numbers. They can be derived from the Maxwell equations in the slowly varying amplitude approximation [1] and have the form.

$$\frac{d}{dt}\alpha(t) = -2i\kappa\alpha^*(t)\beta(t)$$
$$\frac{d}{dt}\beta(t) = -i\kappa\alpha^2(t) \tag{57}$$

For classical fields the closed-form analytical solutions to equations (57) are known. Assuming that initially there is no second-harmonic field ($\beta(0) = 0$),

and the fundamental field amplitude is real and equal to $\alpha(0) = \alpha_0$ the solutions for the classical amplitudes of the second harmonic and fundamental modes are given by [1]

$$\begin{aligned}\alpha(t) &= \alpha_0 \operatorname{sech}(\sqrt{2}\,\alpha_0\kappa t)\\ \beta(t) &= \frac{\alpha_0}{\sqrt{2}}\tanh(\sqrt{2}\,\alpha_0\kappa t)\end{aligned} \tag{58}$$

The solutions (58) are monotonic and eventually all the energy present initially in the fundamental mode is transferred to the second-harmonic mode.

In a general case, when both modes initially have nonzero amplitudes, $\alpha_0 \neq 0$ and $\beta_0 \neq 0$, introducing $\alpha = |\alpha|e^{i\phi_a}$ and $\beta = |\beta|e^{i\phi_b}$, we obtain the following set of equations:

$$\begin{aligned}\frac{d}{dt}|\alpha| &= -2\kappa|\alpha||\beta|\sin\vartheta\\ \frac{d}{dt}|\beta| &= \kappa|\alpha|^2\sin\vartheta\\ \frac{d}{dt}\vartheta &= \kappa\left(\frac{|\alpha|^2}{|\beta|} - 4|\beta|\right)\cos\vartheta\\ \frac{d}{dt}\phi_a &= -2\kappa|\beta|\cos\vartheta\\ \frac{d}{dt}\phi_b &= -\kappa\frac{|\alpha|^2}{|\beta|}\cos\vartheta\end{aligned} \tag{59}$$

where $\vartheta = 2\phi_a - \phi_b$. The system (59) has two integrals of motion

$$C_0 = |\alpha|^2 + 2|\beta|^2, \qquad C_I = |\alpha|^2|\beta|\cos\vartheta \tag{60}$$

which are classical equivalents of the quantum constants of motion $\hat{H}_0$ and $\hat{H}_I$ ($C_0 = \langle\hat{H}_0\rangle$, $C_I = \langle\hat{H}_I\rangle$). Depending on the values of the constants of motion C_0 and C_I, the dynamics of the system (59) can be classified into several categories [42,43]:

1. *Phase-stable* motion, $C_I = 0$, in which the phases of each mode are preserved and the modes move radially in the phase space. The phase difference ϑ is also preserved, which appears for $\cos\vartheta = 0$ and $\vartheta = \pm\pi/2$. The solutions (58) belong to this category.
2. *Phase-changing* motion, $C_I \neq 0$, in which the dynamics of each mode involves both radial and phase motion. In this case both modes must be initially excited and their phase difference cannot be equal to $\pm\pi/2$.

3. *Phase-difference-stable* motion, which is a special case of the phase-changing motion that preserves the phase difference ϑ between the modes even though the phases of individual modes change. This corresponds to the *no-energy-exchange* regime when $\sin\vartheta = 0$ and the initial amplitudes of the modes are preserved.

Introducing new (scaled) variables

$$u_a = |\alpha|/\sqrt{C_0}\,, \qquad u_b = \sqrt{2}|\beta|/\sqrt{C_0}\,, \qquad u_a^2 + u_b^2 = 1 \tag{61}$$

$$\tau = \sqrt{2C_0}\,\kappa t \tag{62}$$

the set of equations (59) can be rewritten in the form

$$\begin{aligned}
\frac{d}{d\tau}u_a &= -u_a u_b \sin\vartheta \\
\frac{d}{d\tau}u_b &= u_a^2 \sin\vartheta \\
\frac{d}{d\tau}\vartheta &= \left(\frac{u_a^2}{u_b} - 2u_b\right)\cos\vartheta \\
\frac{d}{d\tau}\phi_a &= -u_b \cos\vartheta \\
\frac{d}{d\tau}\phi_b &= -\frac{u_a^2}{u_b}\cos\vartheta
\end{aligned} \tag{63}$$

Solutions to the set of equations (63) describe the evolution of the fields with the fundamental as well as second-harmonic frequencies.

From (60) we have

$$\cos\vartheta = \frac{\epsilon}{u_a^2 u_b} \tag{64}$$

where the constant of motion ϵ is defined by

$$\epsilon = \frac{\sqrt{2}C_I}{C_0^{3/2}} = u_a^2(0)u_b(0)\cos\vartheta(0) \tag{65}$$

From (63) and (64) one easily obtains the closed-form equations for the intensities $n_a = u_a^2$ and $n_b = u_b^2$ of the two modes

$$-\frac{dn_a}{d\tau} = \frac{dn_b}{d\tau} = 2\sqrt{n_b(1-n_b)^2 - \epsilon^2} \tag{66}$$

where $n_b = 1 - n_a$. Since the normalized variable n_a must be less, than or equal to unity, the maximum value that can be obtained by ϵ^2 is equal to $\frac{4}{27}$ (for $\cos\vartheta = 1$). From (66) we immediately obtain

$$2\,d\tau = \frac{dn_b}{\sqrt{n_b(1-n_b)^2 - \epsilon^2}} \tag{67}$$

which can be integrated, giving

$$2\tau = \int \frac{dn_b}{\sqrt{n_b(1-n_b)^2 - \epsilon^2}} \tag{68}$$

For $\epsilon = 0$, the integral on the right-hand side (r.h.s.) of (68) is elementary and has the form

$$\int \frac{dn_b}{\sqrt{n_b(1-n_b)^2}} = \ln\frac{1+\sqrt{n_b}}{1-\sqrt{n_b}} \tag{69}$$

In this case we get the well-known classical solution for the intensity of the second harmonic[1]

$$n_b(\tau) = \tanh^2\tau \tag{70}$$

which is a monotonic function of the scaled time $\tau = \sqrt{2C_0}\kappa t$. For $\epsilon \neq 0$ ($C_I \neq 0$), the r.h.s. of (68) is not elementary and the character of solution depends on the roots of the third order polynomial under the square root. Depending on the value of

$$\Delta = \epsilon^2\left(\epsilon^2 - \frac{4}{27}\right) \tag{71}$$

the polynomial has three different real roots ($\Delta < 0$) and two real roots, one of which is double ($\Delta = 0$). The third case with $\Delta > 0$, in which the polynomial has one real root and two complex conjugate roots, is excluded on physical grounds since $\epsilon^2 \leq \frac{4}{27}$.

In case of three different real roots $n_{b1} < n_{b2} < n_{b3}$ ($\Delta < 0$ or $\epsilon^2 < \frac{4}{27}$), we can effect a substitution

$$n_b = n_{b1} + (n_{b2} - n_{b1})\sin^2\phi \tag{72}$$

which leads to the elliptical integral

$$\int \frac{dn_b}{\sqrt{n_b(1-n_b)^2-\epsilon^2}} = \frac{2}{\sqrt{n_{b3}-n_{b1}}}\int \frac{d\phi}{\sqrt{1-k^2\sin^2\phi}} \tag{73}$$

where

$$k^2 = \frac{n_{b2}-n_{b1}}{n_{b3}-n_{b1}} \tag{74}$$

and we get from (68) and (73)

$$\sqrt{n_{b3}-n_{b1}}\,\tau = \int \frac{d\phi}{\sqrt{1-k^2\sin^2\phi}} \tag{75}$$

Using the definitions of the Jacobi elliptic functions we have

$$\sin\phi = \mathrm{sn}\left(\sqrt{n_{b3}-n_{b1}}\,\tau \,|\, k^2\right) \tag{76}$$

and inserting (76) into (72) we obtain the solution

$$n_b(\tau) = n_{b1} + (n_{b2}-n_{b1})\,\mathrm{sn}^2\left(\sqrt{n_{b3}-n_{b1}}\,\tau \,|\, k^2\right) \tag{77}$$

where sn is the Jacobi elliptic function sinusamplitude. The solution (77) is a periodic function of the scaled time τ with the period depending on the value of k^2. This means that even very small ϵ makes the solution periodic. The values of $n_b(\tau)$ are restricted to the region between the two smallest roots of the third order polynomial $n_{b1} \le n_b(\tau) \le n_{b2}$. To illustrate the behavior of the classical solutions, we plot in Fig. 1 the time evolution of the intensities of the two modes, $n_a(\tau)$ and $n_b(\tau)$, for the case when the second-harmonic mode is initially weak with respect to the fundamental mode ($n_b(0) = 0.001$) and the initial phases are both zeros ($\phi_a(0) = \phi_b(0) = 0$). In this case the constant of motion $\epsilon = 0.0316$. We see the regular periodic oscillations of the two intensities.

In the limiting case, for which $k = 1$, we have $n_{b1} = 0$, $n_{b2} = n_{b3} = 1$, and $\mathrm{sn}(x \,|\, 1) = \tanh(x)$ which is the phase-stable motion case and reproduces the classical result (70). The other limiting case appears when $k = 0$, which corresponds to the situation with $\epsilon^2 = \frac{4}{27}$ or $|\alpha|^2 = 4|\beta|^2$ $\left(n_{b1} = n_{b2} = \frac{1}{3}, n_{b3} = \frac{4}{3}\right)$. This is the phase-difference stable motion, or no-energy-exchange, case in which the solution is constant $n_b(\tau) = \frac{1}{3}$. This case has been discussed by Bajer et al. [36]. Thus the two extreme cases, $k = 1$ and $k = 0$, of the general solution (77) correspond to the phase-stable and phase-difference-stable

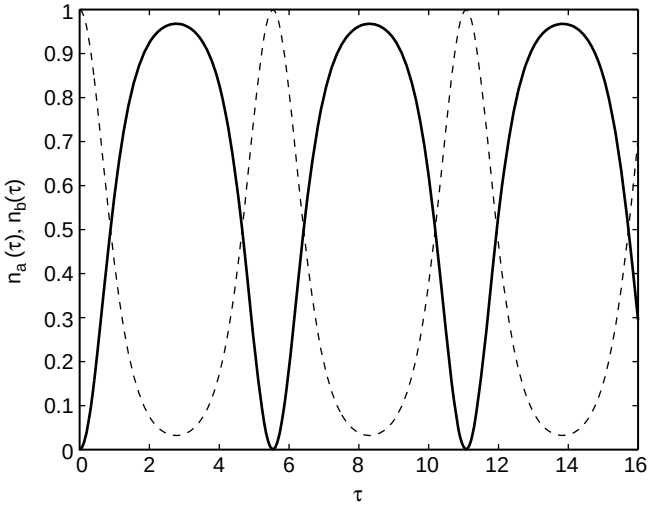

Figure 1. Intensities $n_a(\tau)$ (dashed line) and $n_b(\tau)$ (solid line) of the fundamental and second-harmonic modes for $n_b(0) = 0.001$, $\phi_a(0) = \phi_b(0) = 0$ ($\epsilon = 0.0316$).

motions in the phase space and they are special cases of the general case of the phase changing motion of the system.

The solution (77) for radial variables $u_a(\tau) = \sqrt{n_a(\tau)}$ and $u_b(\tau) = \sqrt{n_b(\tau)}$ must be supplemented with the corresponding solution for the phase variables $\phi_a(\tau)$ and $\phi_b(\tau)$ in order to find the trajectory in the phase space. The equations governing the evolution of the individual phases of the two modes can be rewritten in the form

$$\frac{d}{d\tau}\phi_a = -\frac{\epsilon}{n_a}\,, \qquad \frac{d}{d\tau}\phi_b = -\frac{\epsilon}{n_b} \tag{78}$$

where ϵ is given by (65). Of course, in the phase-stable regime ($\epsilon = 0$) both phases individually, and obviously the phase difference ϑ, are preserved. In Fig. 2 we have shown the evolution of the phases for the case of weak initial excitation of the second-harmonic mode. The initial values are same as in Fig. 1. Comparing Fig. 1 with Fig. 2, it is seen that there is a jump of the phase $\phi_a(\tau)$ by $\pi/2$ whenever the intensity $n_a(\tau)$ reaches its minimum and a jump by π of the phase $\phi_b(\tau)$ when $n_b(\tau)$ reaches its minimum. The phase difference $\vartheta(\tau) = 2\phi_a(\tau) - \phi_b(\tau)$ jumps between the values $\pm\pi/2$. To plot these figures, we have solved numerically the set of equations (63).

Solutions of equations (66) and (78), or equivalently the set (63), for given initial values describe the deterministic trajectories in the phase space for both

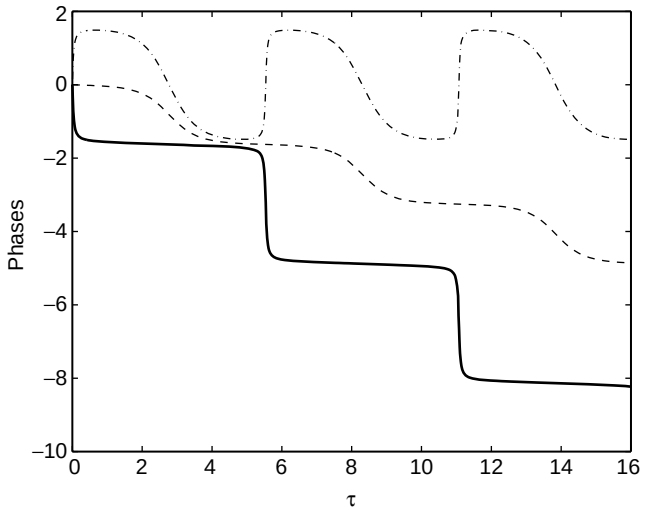

Figure 2. Evolution of the individual phases $\phi_a(\tau)$ (dashed line), $\phi_b(\tau)$ (solid line), and the phase difference $\vartheta(\tau)$ (dashed–dotted line). Initial values are same as in Fig. 1.

modes, the mode at frequency ω and the mode at frequency 2ω, in a general case of the system that describes coupling of the two modes via the $\chi^{(2)}$ nonlinearity. It is a matter of initial conditions whether we have a purely second-harmonic generation case $[n_b(0) = 0,\ n_a(0) = 1]$ or a purely downconversion case $[n_a(0) = 0,\ n_b(0) = 1]$. It is clear from (63) that for the purely downconversion regime $[u_a(0) = 0]$ the classical description does not allow for generating signal at the fundamental frequency from zero initial value. The quantum fluctuations are necessary to obtain such a signal. In a general case both processes take place simultaneously and compete with each other. If the initial amplitudes are well defined, that is, there is no classical noise, the amplitudes at time τ are also well defined. For quantum fields, however, the situation is different because of the inherent quantum noise associated with the vacuum fluctuations. Some quantum features, however, can be simulated with classical trajectories when the initial fields are chosen as random Gaussian variables with appropriately adjusted variances, and examples of such simulations will be shown later.

B. Linearized Quantum Equations

Assuming that the quantum noise is small in comparison to the mean values of the field amplitudes, one can introduce the operators

$$\Delta\hat{a} = \hat{a} - \langle\hat{a}\rangle\,, \qquad \Delta\hat{b} = \hat{b} - \langle\hat{b}\rangle \tag{79}$$

which describe the quantum fluctuations. On inserting the fluctuation operators (79) into the original evolution equations (56) and keeping only the linear terms in the quantum fluctuations, we get the equations

$$\begin{aligned}\frac{d}{dt}\Delta\hat{a} &= -2i\kappa(\Delta\hat{a}^{+}\langle\hat{b}\rangle + \langle\hat{a}^{+}\rangle\Delta\hat{b})\\ \frac{d}{dt}\Delta\hat{b} &= -2i\kappa\langle\hat{a}\rangle\Delta\hat{a}\end{aligned} \tag{80}$$

where $\langle\hat{a}\rangle$ and $\langle\hat{b}\rangle$ are the solutions for the mean fields and can be identified with the classical solutions. With the scaled variables (61) and (62) we can rewrite equations (80) in the form

$$\begin{aligned}\frac{d}{d\tau}\Delta\hat{a} &= -i(\Delta\hat{a}^{+}u_b\, e^{i\phi_b} + \sqrt{2}\, u_a\, e^{-i\phi_a}\Delta\hat{b})\\ \frac{d}{d\tau}\Delta\hat{b} &= -i\sqrt{2}\, u_a\, e^{i\phi_a}\Delta\hat{a}\end{aligned} \tag{81}$$

where $u_a = u_a(\tau)$, $u_b = u_b(\tau)$, $\phi_a = \phi_a(\tau)$, and $\phi_b = \phi_b(\tau)$ are the solutions of classical equations (66) and (78).

The analysis becomes easier if we introduce the following quadrature noise operators [44,45] (for further comparisons, we adjust the phase in quadrature definitions for the second harmonic mode in such a way as to take into account that $\vartheta = 2\phi_a - \phi_b = \pi/2$)

$$\begin{aligned}\Delta\hat{Q}_a(\tau) &= \Delta\hat{a}(\tau)e^{-i\phi_a(\tau)} + \Delta\hat{a}^{+}(\tau)e^{i\phi_a(\tau)}\\ \Delta\hat{P}_a(\tau) &= -i[\Delta\hat{a}(\tau)e^{-i\phi_a(\tau)} - \Delta\hat{a}^{+}(\tau)e^{i\phi_a(\tau)}]\\ \Delta\hat{P}_b(\tau) &= \Delta\hat{b}(\tau)e^{-i\phi_b(\tau)} + \Delta\hat{b}^{+}(\tau)e^{i\phi_b(\tau)}\\ \Delta\hat{Q}_b(\tau) &= i[\Delta\hat{b}(\tau)e^{-i\phi_b(\tau)} - \Delta\hat{b}^{+}(\tau)e^{i\phi_b(\tau)}]\end{aligned} \tag{82}$$

for which we get from (81) the following set of equations:

$$\begin{aligned}\frac{d}{d\tau}\Delta\hat{Q}_a &= -\Delta\hat{Q}_a u_b\sin\vartheta - 2\Delta\hat{P}_a u_b\cos\vartheta\\ &\quad - \Delta\hat{P}_b\sqrt{2}\, u_a\sin\vartheta - \Delta\hat{Q}_b\sqrt{2}u_a\cos\vartheta\\ \frac{d}{d\tau}\Delta\hat{P}_a &= \Delta\hat{P}_a u_b\sin\vartheta - \Delta\hat{P}_b\sqrt{2}\, u_a\cos\vartheta\\ &\quad + \Delta\hat{Q}_b\sqrt{2}\, u_a\sin\vartheta\end{aligned} \tag{83}$$

$$\frac{d}{d\tau}\Delta\hat{P}_b = \Delta\hat{Q}_a\sqrt{2}u_a\sin\vartheta + \Delta\hat{P}_a\sqrt{2}\,u_a\cos\vartheta + \Delta\hat{Q}_b\frac{u_a^2}{u_b}\cos\vartheta$$

$$\frac{d}{d\tau}\Delta\hat{Q}_b = \Delta\hat{Q}_a\sqrt{2}u_a\cos\vartheta - \Delta\hat{P}_a\sqrt{2}\,u_a\sin\vartheta - \Delta\hat{P}_b\frac{u_a^2}{u_b}\cos\vartheta$$

In the case of pure second-harmonic generation, that is, for $u_b(0) = 0$ and $u_a(0) = 1$, we have from (59) that $\cos\vartheta = 0$ or $\vartheta = \pm\pi/2$, which implies that, according to (77) for $k = 1$, the scaled intensities obey the equations

$$u_a(\tau) = \operatorname{sech}\tau\,, \qquad u_b(\tau) = \tanh\tau \tag{84}$$

Inserting $\vartheta = \pi/2$ and the solutions (84) into (83), we arrive at the following system of equations:

$$\begin{aligned}
\frac{d}{d\tau}\Delta\hat{Q}_a &= -\Delta\hat{Q}_a\tanh\tau - \Delta\hat{P}_b\sqrt{2}\,\operatorname{sech}\tau\\
\frac{d}{d\tau}\Delta\hat{P}_b &= \Delta\hat{Q}_a\sqrt{2}\,\operatorname{sech}\tau\\
\frac{d}{d\tau}\Delta\hat{P}_a &= \Delta\hat{P}_a\tanh\tau + \Delta\hat{Q}_b\sqrt{2}\,\operatorname{sech}\tau\\
\frac{d}{d\tau}\Delta\hat{Q}_b &= -\Delta\hat{P}_a\sqrt{2}\,\operatorname{sech}\tau
\end{aligned} \tag{85}$$

which shows that the quadratures $\Delta\hat{Q}_a$ and $\Delta\hat{P}_b$ of the two modes are coupled together independently from the quadratures $\Delta\hat{P}_a$ and $\Delta\hat{Q}_b$. This splits the system (85) into two independent subsystems. It was shown by Ou [44] that the two systems can be solved analytically, giving

$$\begin{aligned}
\Delta\hat{Q}_a(\tau) &= \Delta\hat{Q}_a(0)(1-\tau\tanh\tau)\operatorname{sech}\tau - \Delta\hat{P}_b(0)\sqrt{2}\,\tanh\tau\,\operatorname{sech}\tau\\
\Delta\hat{P}_b(\tau) &= \Delta\hat{Q}_a(0)\frac{1}{\sqrt{2}}(\tanh\tau + \tau\operatorname{sech}^2\tau) + \Delta\hat{P}_b(0)\,\operatorname{sech}^2\tau\\
\Delta\hat{P}_a(\tau) &= \Delta\hat{P}_a(0)\operatorname{sech}\tau + \Delta\hat{Q}_b(0)\frac{1}{\sqrt{2}}(\sinh\tau + \tau\,\operatorname{sech}\tau)\\
\Delta\hat{Q}_b(\tau) &= -\Delta\hat{P}_a(0)\sqrt{2}\,\tanh\tau + \Delta\hat{Q}_b(0)(1-\tau\tanh\tau)
\end{aligned} \tag{86}$$

Now, assuming that the two modes are not correlated at time $\tau = 0$, it is straightforward to calculate the variances of the quadrature field operators and check, according to the definition (12), whether the field is in a squeezed state. If the initial state of the field is a coherent state of the fundamental mode and a vacuum for the second-harmonic mode, $|\psi_0\rangle = |u_a(0)\rangle|0\rangle$, for which we have

$$\langle[\Delta\hat{Q}_a(0)]^2\rangle = \langle[\Delta\hat{Q}_b(0)]^2\rangle = \langle[\Delta\hat{P}_a(0)]^2\rangle = \langle[\Delta\hat{P}_b(0)]^2\rangle = 1 \tag{87}$$

the variances of the two quadrature noise operators are described by the following analytical formulas [44,45]:

$$\begin{aligned}
\langle[\Delta\hat{Q}_a(\tau)]^2\rangle &= (1-\tau\tanh\tau)^2\,\mathrm{sech}^2\,\tau + 2\,\tanh^2\tau\,\mathrm{sech}^2\,\tau \\
\langle[\Delta\hat{P}_a(\tau)]^2\rangle &= \mathrm{sech}^2\,\tau + \frac{1}{2}(\sinh\tau + \tau\,\mathrm{sech}\,\tau)^2 \\
\langle[\Delta\hat{Q}_b(\tau)]^2\rangle &= 2\,\tanh^2\tau + (1-\tau\,\tanh\tau)^2 \\
\langle[\Delta\hat{P}_b(\tau)]^2\rangle &= \frac{1}{2}\left(\tanh\tau + \tau\,\mathrm{sech}^2\,\tau\right)^2 + \mathrm{sech}^4\,\tau
\end{aligned} \tag{88}$$

The solutions (88) clearly indicate that the quantum noise present in the initial state of the field, which represents the vacuum fluctuations, undergoes essential changes due to the nonlinear transformation of the field as both modes propagate in the nonlinear medium. As $\tau \to \infty$, we have $\tanh\tau \to 1$, $\mathrm{sech}\,\tau \to 2e^{-\tau}$, and $\sinh\tau \to e^{\tau}/2$, which gives $\langle[\Delta\hat{Q}_a(\tau)]^2\rangle \to 4\tau^2 e^{-2\tau}$, $\langle[\Delta\hat{Q}_b(\tau)]^2\rangle \to \tau^2$, $\langle[\Delta\hat{P}_a(\tau)]^2\rangle \to e^{2\tau}/8$, and $\langle[\Delta\hat{P}_b(\tau)]^2\rangle \to \frac{1}{2}$. According to the definition of squeezing (12), we find that the quadratures $\hat{Q}_a$ and $\hat{P}_b$ become squeezed as τ increases while the other two quadratures, $\hat{P}_a$ and $\hat{Q}_b$, are stretched. For very long times (lengths of the nonlinear medium) the noise in the amplitude quadrature of the fundamental mode is reduced to zero (perfect squeezing), while for the second-harmonic mode it approaches the value $\frac{1}{2}$ (50% squeezing). Quantum fluctuations in the other quadratures of both modes explode to infinity as τ goes to infinity. Of course, we have to keep in mind that the results have been obtained from the linearized equations that require quantum fluctuations to be small. In Fig. 3a we have shown the evolution of the quadrature variances $\langle[\Delta\hat{Q}_a(\tau)]^2\rangle$ and $\langle[\Delta\hat{P}_b(\tau)]^2\rangle$ exhibiting squeezing of quantum fluctuations in both fundamental and second harmonic-modes. With dotted lines the classical amplitudes of the two modes are marked for reference. The value of unity for the quadrature variances sets the level of vacuum fluctuations (coherent states experience the same fluctuations), and we find that indeed the quantum noise can be suppressed below the vacuum level in the amplitude quadrature $\langle[\Delta\hat{Q}_a(\tau)]^2\rangle$ of the fundamental mode and the phase quadrature $\langle[\Delta\hat{P}(\tau)]^2\rangle$ of the harmonic mode. It becomes possible at the expense of increased fluctuations in the other quadratures as to preserve the

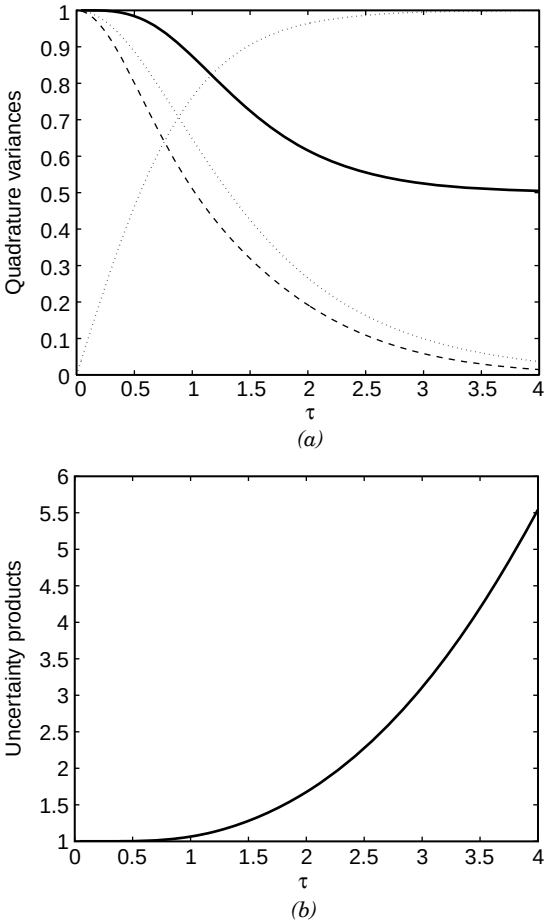

Figure 3. (a) Variances $\langle[\Delta\hat{Q}_a(\tau)]^2\rangle$ (dashed line) and $\langle[\Delta\hat{P}_a(\tau)]^2\rangle$ (solid line) [for reference, the amplitudes $u_a(\tau)$ and $u_b(\tau)$ are marked with dotted lines]; (b) uncertainty products.

validity of the Heisenberg uncertainty relation (9). We have

$$\begin{aligned}\langle[\Delta\hat{Q}_a(\tau)]^2\rangle\langle[\Delta\hat{P}_a(\tau)]^2\rangle &= \langle[\Delta\hat{Q}_b(\tau)]^2\rangle\langle[\Delta\hat{P}_b(\tau)]^2\rangle \\ &= \operatorname{sech}^2(\tau)[2\tanh^2\tau + (1-\tau\tanh\tau)^2] \\ &\quad\times\left[\operatorname{sech}^2\tau + \frac{1}{2}(\sinh\tau + \tau\operatorname{sech}\tau)^2\right] \qquad (89)\end{aligned}$$

and as $\tau \to \infty$ both uncertainty products are divergent as $\tau^2/2$. The evolution of the uncertainty products is illustrated in Fig. 3b. Since, except for the initial value, the value of the uncertainty product is larger than unity, the quantum states produced in the second-harmonic generation process are not the minimum uncertainty states.

The linear approximation to the quantum noise equations presented in this section shows that even in linear approximation the inherent property of quantum fields — the vacuum fluctuations which are ubiquitous and always present — undergo essential changes when transformed nonlinearly. The linearized solutions suggest that perfect squeezing (zero fluctuations) is possible in the fundamental mode for long evolution times (long interaction lengths). This means that one can produce highly nonclassical states of light in such a process. Later we will see to what extent we can trust in the linear approximation.

C. Symbolic Calculations

The linear approximation with respect to quantum noise operators, which assumes that the mean values of the fields evolve according to the classical equations and the quantum noise represents only small fluctuations around the classical solutions is a way to solve the operator equations (56). Another alternative is to use Taylor series expansion of the operator solution and make the short time (or short length of the medium) approximation to find the evolution of the quantum (operator) fields. This approach has been proposed by Tanaś [46] for approximate calculations of the higher-order field correlation functions in the process of nonlinear optical activity and later used by Kozierowski and Tanaś [21] for calculations of second order correlation function for the second-harmonic generation. Mandel [9] has used this approach to discuss squeezing and photon antibunching in harmonic generation. When doing calculations with operators it is crucial to keep track of the operator ordering and use the commutation relations to rearrange the ordering. This makes the calculations cumbersome and error-prone. The first calculations were performed by hand, but now we have computers that can do the job for us. The computer symbolic calculations of the subsequent terms in a series expansion have been performed by Bajer and Lisoněk [31] and Bajer and Peřina [32]. Bajer and Lisoněk [31] have written their own computer program for this purpose (about 3000 lines of code in Turbo Pascal). We want to show here how to do the same calculations with the freely available version of the computer program FORM [47] with only few lines of coding (see Appendix A).

The main idea of the approximate symbolic computations is based on the series expansion of any operator $\hat{O}(t)$ into a power series

$$\hat{O}(t) = \hat{O}(0) + \sum_{k=1}^{\infty} \frac{t^k}{k!} \frac{d^k}{dt^k} \hat{O}(t)\Big|_{t=0} \tag{90}$$

where the subsequent derivatives are obtained from the Heisenberg equations of motion

$$\frac{d}{dt}\hat{O} = \frac{1}{i\hbar}[\hat{O}, \hat{H}] \tag{91}$$

where $\hat{H}$ is the Hamiltonian. The higher derivatives are obtained recursively from (91), and the resulting expansion takes the form [31]

$$\hat{O}(t) = \hat{O}(0) + \sum_{k=1}^{\infty}\left(\frac{t}{i\hbar}\right)^k \frac{D_k}{k!} \tag{92}$$

where

$$D_k = [D_{k-1}, \hat{H}] = [\cdots[[\hat{O}(0), \hat{H}], \hat{H}], \ldots, \hat{H}] \tag{93}$$

is the kth-order commutator with $D_0 = \hat{O}(0)$.

Implementing the algorithm sketched above in the computer symbolic manipulation program FORM, as exemplified in Appendix A, and applying the method to the second-harmonic-generation (SHG) process, which is described by the interaction Hamiltonian $\hat{H}_I$ given by (55), one can easily calculate subsequent terms of the series (92). Restricting the calculations to the fourth-order terms, we get

$$\begin{aligned}\hat{a}(t) = \hat{a} &- 2\,i(\kappa t)\,\hat{a}^+\hat{b} - (\kappa t)^2\left(\hat{a}^+\hat{a}^2 - 2\hat{a}\hat{b}^+\hat{b}\right)\\ &- \frac{2}{3}\,i(\kappa t)^3\left(2\hat{a}^3\hat{b}^+ - 3\hat{a}^{+2}\hat{a}\hat{b} + 2\hat{a}^+\hat{b}^+\hat{b}^2 - \hat{a}^+\hat{b}\right)\\ &+ \frac{1}{6}(\kappa t)^4\left(5\hat{a}^{+2}\hat{a}^3 + 8\hat{a}^{+3}\hat{b}^2 - 28\hat{a}^+\hat{a}^2\hat{b}^+\hat{b} + 4\hat{a}\hat{b}^{+2}\hat{b}^2\right.\\ &\left.+ \hat{a}^+\hat{a}^2 - 20\hat{a}\hat{b}^+\hat{b}\right) + \cdots\end{aligned} \tag{94}$$

$$\begin{aligned}\hat{b}(t) = \hat{b} &- i(\kappa t)\hat{a}^2 - (\kappa t)^2\left(2\hat{a}^+\hat{a}\hat{b} + \hat{b}\right)\\ &+ \frac{1}{3}\,i(\kappa t)^3\left(2\hat{a}^+\hat{a}^3 - 4\hat{a}^2\hat{b}^+\hat{b} + 4\hat{a}^{+2}\hat{b}^2 + \hat{a}^2\right)\\ &+ \frac{1}{6}(\kappa t)^4\left(2\hat{a}^{+2}\hat{a}^2\hat{b} - 4\hat{a}^4\hat{b}^+ - 16\hat{a}^+\hat{a}\hat{b}^+\hat{b}^2\right.\\ &\left.+ 8\hat{a}^+\hat{a}\hat{b} - 8\hat{b}^+\hat{b}^2 + \hat{b}\right) + \cdots\end{aligned} \tag{95}$$

where the operators on the r.h.s. of equations (94) and (95) are at time $t = 0$. We can see that the terms that are of kth power in t contain the operator products that are of the $k+1$ order as well as the products that are of the order $k-1$,

$k-3, \ldots$. The latter products appeared as a result of application the bosonic commutation relations (4) for the operators of the two modes, and these terms represent purely quantum contributions that would not appear if the fields were classical. For classical fields, only the highest-order products survive. The quantum noise contributions appear in terms $\sim t^3$ and higher in the expansion (94) for the fundamental mode operators and in terms $\sim t^2$ and higher in the expansion (95) for the second harmonic mode operators. However, for the initial conditions representing the purely second-harmonic generation process, specifically, under the assumption that the harmonic mode is initially in the vacuum state such that $\hat{b}|0\rangle = 0$, we can drop all the terms containing operators $\hat{b}$ or $\hat{b}^+$ because they give zero due to the normal ordering of the operators. Assuming, moreover, that the pump beam is in a coherent state $|\alpha_0\rangle$ we find the following expansions for the mean values of the operators $\hat{a}(t)$ and $\hat{b}(t)$ [7]

$$\begin{aligned}\langle\hat{a}(t)\rangle &= \alpha_0\left[1-(\kappa t)^2|\alpha_0|^2+\frac{1}{6}(\kappa t)^4(5|\alpha_0|^4+|\alpha_0|^2)+\cdots\right]\\ \langle\hat{b}(t)\rangle &= -i\alpha_0^2\left[(\kappa t)-\frac{1}{3}(\kappa t)^3(2|\alpha_0|^2+1)+\cdots\right]\end{aligned} \tag{96}$$

or in the normalized variables (61) and scaled time (62), we have

$$\begin{aligned}u_a(\tau) &= u_a(0)e^{i\phi_a(0)}\left[1-\frac{\tau^2}{2}+\frac{5}{24}\tau^4\left(1+\frac{1}{5|\alpha_0|^2}\right)+\cdots\right]\\ u_b(\tau) &= u_a(0)^2e^{i(2\phi_a(0)-\pi/2)}\left[\tau-\frac{\tau^3}{3}\left(1+\frac{1}{2|\alpha_0|^2}\right)+\cdots\right]\end{aligned} \tag{97}$$

On neglecting the quantum noise terms, $\sim 1/|\alpha_0|^2$, one can easily recognize in (97) the first terms of the power series expansions of $\operatorname{sech}\tau$ and $\tanh\tau$, which are the classical solutions. When $|\alpha_0|^2 \gg 1$, the quantum noise introduces only small corrections to the classical evolution of the field amplitudes. It is also seen that the phase of the second harmonic field is phase-locked so as to satisfy $\vartheta = 2\phi_a - \phi_b = \pi/2$.

We can thus expect from the short-time approximation that quantum noise does not significantly affect the classical solutions when the initial pump field is strong. We will return to this point later on, but now let us try to find the short-time solutions for the evolution of the quantum noise itself—let us take a look at the quadrature noise variances and the photon statistics. Using the operator solutions (94) and (95), one can find the solutions for the quadrature operators $\hat{Q}$ and $\hat{P}$ as well as for $\hat{Q}^2$ and $\hat{P}^2$. It is, however, more convenient to use the computer program to calculate the evolution of these quantities directly. Let us consider the purely SHG process, we drop the terms containing $\hat{b}$ and $\hat{b}^+$ after performing the normal ordering and take the expectation value in the coherent

state $|\alpha_0\rangle$ of the fundamental frequency mode, and in effect we arrive at

$$\begin{aligned}
\langle \hat{Q}_a^2(t)\rangle &= 1 + 2|\alpha_0|^2 + \alpha_0^2 + \alpha_0^{*2} \\
&\quad - (\kappa t)^2\left[4|\alpha_0|^4 + (2|\alpha_0|^2+1)(\alpha_0^2+\alpha_0^{*2})\right] \\
&\quad + \frac{(\kappa t)^4}{6}\left[32|\alpha_0|^6 + 16|\alpha_0|^4 + \Big(16|\alpha_0|^4 \right. \\
&\quad \left. + 8|\alpha_0|^2 + 1\Big)\left(\alpha_0^{*2}+\alpha_0^2\right)\right] + \cdots \\
\langle \hat{P}_a^2(t)\rangle &= 1 + 2|\alpha_0|^2 - (\alpha_0^2 + \alpha_0^{*2}) \\
&\quad - (\kappa t)^2\left[4|\alpha_0|^4 - (2|\alpha_0|^2+1)(\alpha_0^2+\alpha_0^{*2})\right] \\
&\quad + \frac{(\kappa t)^4}{6}\left[32|\alpha_0|^6 + 16|\alpha_0|^4 - \Big(16|\alpha_0|^4 \right. \\
&\quad \left. + 8|\alpha_0|^2 + 1\Big)\left(\alpha_0^{*2}+\alpha_0^2\right)\right] + \cdots \\
\langle \hat{Q}_b^2(t)\rangle &= 1 + (\kappa t)^2\Big(2|\alpha_0|^4 - (\alpha_0^4+\alpha_0^{*4})\Big) - \frac{4}{3}(\kappa t)^4\Big[2|\alpha_0|^6 \\
&\quad + |\alpha_0|^4 - (|\alpha_0|^2+1)(\alpha_0^{*4}+\alpha_0^4)\Big] + \cdots \\
\langle \hat{P}_b^2(t)\rangle &= 1 + (\kappa t)^2\Big(2|\alpha_0|^4 + \alpha_0^4 + \alpha_0^{*4}\Big) - \frac{4}{3}(\kappa t)^4\Big[2|\alpha_0|^6 \\
&\quad + |\alpha_0|^4 + (|\alpha_0|^2+1)(\alpha_0^{*4}+\alpha_0^4)\Big] + \cdots
\end{aligned} \tag{98}$$

From equations (98) and (96) we obtain formulas for the field variances

$$\begin{aligned}
\langle[\Delta\hat{Q}_a(t)]^2\rangle &= 1 - (\kappa t)^2(\alpha_0^2+\alpha_0^{*2}) \\
&\quad + (\kappa t)^4\left[2|\alpha_0|^4 + \left(|\alpha_0|^2 + \frac{1}{6}\right)(\alpha_0^2+\alpha_0^{*2})\right] + \cdots \\
&= 1 - \tau^2\cos 2\phi_a + \frac{1}{2}\tau^4\left[1 + \left(1 + \frac{1}{6N_a}\right)\cos 2\phi_a\right] + \cdots \\
\langle[\Delta\hat{P}_a(t)]^2\rangle &= 1 + (\kappa t)^2(\alpha_0^2+\alpha_0^{*2}) \\
&\quad + (\kappa t)^4\left[2|\alpha_0|^4 - \left(|\alpha_0|^2 + \frac{1}{6}\right)(\alpha_0^2+\alpha_0^{*2})\right] \\
&= 1 + \tau^2\cos 2\phi_a + \frac{1}{2}\tau^4\left[1 - \left(1 + \frac{1}{6N_a}\right)\cos 2\phi_a\right] + \cdots \\
\langle[\Delta\hat{Q}_b(t)]^2\rangle &= 1 + \frac{2}{3}(\kappa t)^4(\alpha_0^4+\alpha_0^{*4}) + \cdots = 1 + \frac{\tau^4}{3}\cos 4\phi_a + \cdots \\
\langle[\Delta\hat{P}_b(t)]^2\rangle &= 1 - \frac{2}{3}(\kappa t)^4(\alpha_0^4+\alpha_0^{*4}) + \cdots = 1 - \frac{\tau^4}{3}\cos 4\phi_a + \cdots
\end{aligned} \tag{99}$$

It is easy to check, assuming $\phi_a = 0$, that the series expansion of the linearized solutions (88) agrees with (99) up to the leading terms, but in the higher-order terms there are already differences between the two solutions. Since the latter solutions are exact up to the fourth order, they show restricted applicability of the linearized solutions. We see that the quadratures $\langle[\Delta\hat{Q}_a(t)]^2\rangle$ and $\langle[\Delta\hat{P}_b(t)]^2\rangle$ become smaller than unity, showing squeezing, while the other two quadratures grow above unity.

The symbolic calculations using a computer allows for easy derivation of the approximate formulas for any operators for the two modes. Beside squeezing it is interesting to study the variance of the photon number operator for both modes in order to look for a possibility of obtaining the sub-Poissonian photon statistics in the process of second-harmonic generation. Let us calculate approximate formulas for the mean number of photons and the second order correlation function. Again, assuming initial conditions for pure second harmonic generation, $|\psi_0\rangle = |\alpha_0, 0\rangle$ with $|\alpha_0|^2 = N_a$, we have for the mean number of photons

$$\begin{aligned}\langle\hat{a}^+\hat{a}\rangle(t) &= |\alpha_0|^2\left[1 - 2(\kappa t)^2|\alpha_0|^2 + \frac{4}{3}(\kappa t)^4|\alpha_0|^2(2|\alpha_0|^2 + 1) + \cdots\right]\\ \langle\hat{b}^+\hat{b}\rangle(t) &= |\alpha_0|^4\left[(\kappa t)^2 - \frac{2}{3}(\kappa t)^4(2|\alpha_0|^2 + 1) + \cdots\right]\end{aligned} \tag{100}$$

or in the scaled variables (61) and (62) Eqs. (100) take a very simple form

$$\begin{aligned}n_a(\tau) &= u_a^2(\tau) = 1 - \tau^2 + \frac{2}{3}\tau^4\left(1 + \frac{1}{2N_a}\right) + \cdots\\ n_b(\tau) &= u_b^2(\tau) = \tau^2 - \frac{2}{3}\tau^4\left(1 + \frac{1}{2N_a}\right) + \cdots\end{aligned} \tag{101}$$

which explicitly shows the quantum noise contributions coming from the vacuum fluctuations.

The second order correlation functions can be obtained in the same manner giving

$$\begin{aligned}\langle\hat{a}^{+2}\hat{a}^2\rangle(t) &= |\alpha_0|^4\Big[1 - 2(\kappa t)^2(2|\alpha_0|^2 + 1)\\ &\qquad + \frac{4}{3}(\kappa t)^4(7|\alpha_0|^4 + 8|\alpha_0|^2 + 1)\cdots\Big]\\ \langle\hat{b}^{+2}\hat{b}^2\rangle(t) &= |\alpha_0|^8\left[(\kappa t)^4 - \frac{8}{3}(\kappa t)^6(|a_0|^2 + 1) + \cdots\right]\end{aligned} \tag{102}$$

and combining equations (100) and (102) we obtain

$$\langle \hat{a}^{+2}\hat{a}^2\rangle(t) - \langle \hat{a}^{+}\hat{a}\rangle^2(t) = -2(\kappa t)^2|\alpha_0|^4 + \frac{4}{3}(\kappa t)^4|\alpha_0|^4(6|\alpha_0|^2 + 1) + \cdots$$
$$\langle \hat{b}^{+2}\hat{b}^2\rangle(t) - \langle \hat{b}^{+}\hat{b}\rangle^2(t) = -\frac{4}{3}(\kappa t)^6|\alpha_0|^8 + \cdots \tag{103}$$

The results (103), obtained first by Kozierowski and Tanaś [21], explain a very important property of the second harmonic generation, that is, the appearance of the sub-Poissonian photon statistics, which is an effect of quantum properties of the fields. The leading terms in (103) are negative, indicating, according to (18) and (19), that the photon statistics in both modes becomes sub-Poissonian at the initial stages of the evolution. The computer software now makes the calculations of this kind almost trivial and less error-prone. However, the results that we obtain in this way are just few terms of the power series expansion that properly describe the evolution of the system only at the initial stages of the evolution. The results can be improved by taking into account more and more terms of the expansion [31,32], but the long-time behavior cannot be predicted with such methods.

Some conclusions about the role of quantum noise in the long-time behavior of the solutions for the SHG process can be drawn by closer inspection of the operator equations of motion for the number of photon operators and their approximate solutions for the expectation values [38,48]. From the equations of motion (56) it is easy to derive the equations for the number of photons operators $\hat{N}_a = \hat{a}^{+}\hat{a}$ and $\hat{N}_b = \hat{b}^{+}\hat{b}$ in the form

$$-2\frac{d}{dt}\hat{N}_b = \frac{d}{dt}\hat{N}_a = -2i\kappa(\hat{a}^{+2}\hat{b} - \hat{a}^2\hat{b}^{+}) \tag{104}$$

and taking the derivative of the operator on the r.h.s. of Eq. (104) (again the symbolic manipulation program makes it easy), we get the second-order differential equation

$$\frac{d^2}{dt^2}\hat{N}_a = -2\frac{d}{dt}\hat{N}_b = -4\kappa^2\left[\hat{N}_a(\hat{N}_a - 1) - 4\hat{N}_a\hat{N}_b - 2\hat{N}_b\right] \tag{105}$$

and taking into account that $\hat{N}_a + 2\hat{N}_b = \hat{C}_0$ is a constant of motion, we find

$$\frac{d^2}{dt^2}(2\hat{N}_b) = 4\kappa^2[3(2\hat{N}_b)^2 - \hat{C}_0(1 + 4(2\hat{N}_b) + \hat{C}_0^2] \tag{106}$$

This second-order equation cannot be solved exactly because it contains operators $\hat{N}_b^2$ and $\hat{N}_b\hat{C}_0$, which, in turn, obey their own equations of motion

and we come into an infinite hierarchy of equations. However, if we neglect the correlations and take

$$\langle \hat{N}_b^2 \rangle = \langle \hat{N}_b \rangle^2 , \qquad \langle \hat{N}_b \hat{C}_0 \rangle = \langle \hat{N}_b \rangle \langle \hat{C}_0 \rangle \tag{107}$$

and introduce the normalized intensity $n_b = 2\langle \hat{N}_b \rangle / C_0$ and the scaled time $\tau = \sqrt{2C_0}\,\kappa t$ with $C_0 = \langle \hat{C}_0 \rangle$, we obtain the equation for the mean value of the normalized intensity n_b in the form

$$\frac{d^2}{d\tau^2} n_b = 2\left[3n_b^2 - 4n_b + 1 - \frac{1}{C_0}\right] \tag{108}$$

This is the second-order differential equation, which reminds us of the equation for a particle moving under the action of a force, and the force can be derived from a potential. There is a quantity that is conserved during this motion, and we can write

$$\frac{d}{d\tau}\left[\frac{1}{2}\left(\frac{dn_b}{d\tau}\right)^2 - 2n_b[(1-n_b)^2 - \epsilon']\right] = 0 \tag{109}$$

where $\epsilon' = 1/C_0$ is the term representing the quantum noise contribution (it comes from application of the commutation rules to the field operators). The quantity in the square brackets can be considered as the total energy of a "particle" at position n_b, with the kinetic energy $\frac{1}{2}(dn_b/d\tau)^2$ and the potential energy $V = -2n_b[(1-n_b)^2 - \epsilon']$. The potential energy is shown in Fig. 4. The potential represents a well in which the particle will oscillate exhibiting fully periodic behavior. From Eq. (109) we get

$$\frac{dn_b}{d\tau} = 2\sqrt{n_b(1-n_b)^2 - n_b\epsilon'} \tag{110}$$

Comparing Eq. (110) with Eq. (66), we find that both equations have extra terms (the ϵ or ϵ' terms) which make the solutions oscillatory, but the physical reason for oscillations is different in both cases. In Eq. (66) different from zero ϵ comes from the nonzero initial value of the second-harmonic mode intensity, while in Eq. (110) the nonzero value of ϵ' comes from the quantum noise. We can interpret this fact in the following way. It is the spontaneous emission of photons, or vacuum fluctuations of the second harmonic mode, that contribute to the nonzero value of the initial intensity of the second harmonic mode and lead to the periodic evolution. This means that the very small quantum fluctuations can cause macroscopic effects, such as quantum-noise-induced macroscopic revivals [38], in the nonlinear process of second-harmonic generation.

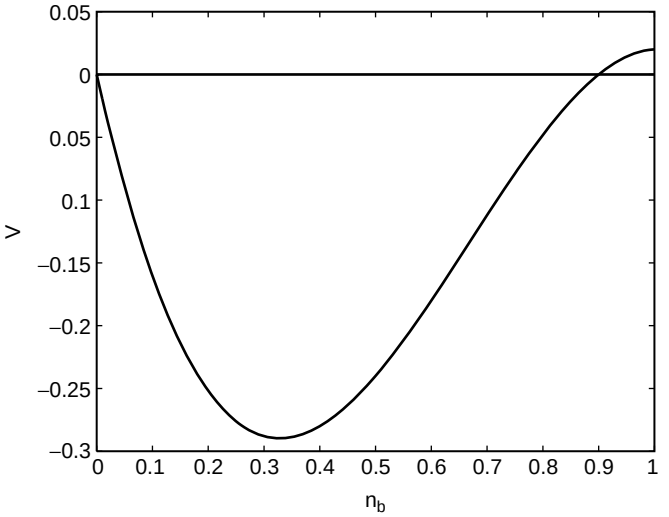

Figure 4. Plot of the pseudopotential curve for $\epsilon' = 0.01$.

A procedure similar to that used to solve equation (66) can be applied to solve equation (110). Again, the solution is given by the Jacobi elliptic functions. The third-order polynomial under the square root on the r.h.s. of (110) has the roots

$$n_{b1} = 0\,, \qquad n_{b2} = 1 - \sqrt{\epsilon'}\,, \qquad n_{b3} = 1 + \sqrt{\epsilon'} \tag{111}$$

and the solution has the form

$$n_b(\tau) = \sqrt{1 - \sqrt{\epsilon'}}\ \mathrm{sn}^2\left(\sqrt{1 + \sqrt{\epsilon'}}\,\tau \,|\, k^2\right) \tag{112}$$

where

$$k^2 = \frac{1 - \sqrt{\epsilon'}}{1 + \sqrt{\epsilon'}} \tag{113}$$

The results have been recently obtained by Olsen et al. [38], and they show that even for almost vanishingly small ϵ', which is inversely proportional to the initial mean value of the number of the pump mode photons, usually very large, the quantum fluctuations have huge macroscopic effect on the system dynamics. It is evident that the quantum noise, which is always present, is responsible for the oscillations between the two regimes of second-harmonic generation and downconversion. The period of oscillation is becoming infinite as ϵ' vanishes.

The solution (112) is fully periodic, but it does not allow for the complete transfer of energy from the fundamental to the second harmonic mode. The maximum that can be achieved by u_b is equal to $\sqrt{1-\sqrt{\epsilon'}}$. We have to remember, moreover, that the solution (112) has been obtained with the decorrelation (107), and it is only an approximate solution.

D. Numerical Methods

When analytical solutions are not known and the approximate analytical methods give results of limited applicability, the numerical methods may be a solution. Let us first discuss a method based on the diagonalization of the second-harmonic Hamiltonian [48,49]. As we have already said, the two parts of the Hamiltonian $\hat{H}_0$ and $\hat{H}_I$ given by (55), commute with each other, so they are both constants of motion. The $\hat{H}_0$ determines the total energy stored in both modes, which is conserved by the interaction $\hat{H}_I$. This means that we can factor the quantum evolution operator

$$\exp\left(\frac{-i\hat{H}t}{\hbar}\right) = \exp\left(\frac{-i\hat{H}_0 t}{\hbar}\right)\exp\left(\frac{-i\hat{H}_I t}{\hbar}\right) \tag{114}$$

If the Fock state basis is used to describe the field state, we find, for the initial state $|n,0\rangle = |n\rangle|0\rangle$ with n photons in the fundamental mode and zero photons in the second harmonic mode, that the Hamiltonian $\hat{H}_0$ splits the Hilbert space into orthogonal sectors. Since $\hat{H}_0$ is a constant of motion, we have for a given number of photons n the relation

$$\langle \hat{a}^+\hat{a}\rangle + 2\langle \hat{b}^+\hat{b}\rangle = n \tag{115}$$

which implies that the creation of k photons of the second-harmonic mode requires annihilation of $2k$ photons of the fundamental mode. Thus, for given n, we can introduce the states

$$|\psi_k^{(n)}\rangle = |n-2k,k\rangle\,, \qquad k = 0,1,\cdots,\left[\frac{n}{2}\right] \tag{116}$$

where $[n/2]$ means the integer part of $n/2$, which form a complete basis of states of the field in the sector with given n. We have

$$\langle \psi_{k'}^{(n')}|\psi_k^{(n)}\rangle = \delta_{nn'}\delta_{kk'} \tag{117}$$

which means that the subspace with given n has $[n/2]+1$ orthogonal states. In such a basis the interaction Hamiltonian $\hat{H}_I$ has the following nonzero matrix elements

$$\begin{aligned}\langle \psi_{k+1}^{(n)}|\hat{H}_I|\psi_k^{(n)}\rangle &= \langle \psi_k^{(n)}|\hat{H}_I|\psi_{k+1}^{(n)}\rangle = (\hat{H}_I)_{k+1,k}^{(n)} = (\hat{H}_I)_{k,k+1}^{(n)} \\ &= \hbar\kappa\sqrt{(k+1)(n-2k)(n-2k-1)}\end{aligned} \tag{118}$$

which form a symmetric matrix of dimension $([n/2]+1)\times([n/2]+1)$ with real nonzero elements (we assume that κ is real) that are located on the two diagonals immediately above and below the principal diagonal. Such a matrix can easily be diagonalized numerically [49]. To find the quantum state evolution, we need the matrix elements of the evolution operator. Since the evolution due to the Hamiltonian $\hat{H}_0$ at each sector of the Hilbert space with given n introduces only a constant phase factor $\exp(-in\omega t)$, we will drop this factor in our calculations and calculate the state at time t according to the formula

$$|\psi(t)\rangle = \exp\left(\frac{-i\hat{H}_I t}{\hbar}\right)|\psi(0)\rangle \tag{119}$$

where $|\psi(0)\rangle$ is the initial state of the field. In each subspace of the Hilbert space we can calculate the matrix elements of the evolution operator

$$c_{n,k}(t) = \langle\psi_k^{(n)}|\exp\left(\frac{-i\hat{H}_I t}{\hbar}\right)|\psi_0^{(n)}\rangle \tag{120}$$

by diagonalizing the Hamiltonian matrix (118). If the matrix U is the unitary matrix that diagonalizes the interaction Hamiltonian matrix (118)

$$U^{-1}\hat{H}_I^{(n)}U = \hbar\kappa\,\mathrm{diag}\left(\lambda_0,\lambda_1,\ldots,\lambda_{[n/2]}\right) \tag{121}$$

then the coefficients $c_{n,k}(t)$ can be written as

$$c_{n,k}(t) = \sum_{j=0}^{[n/2]} e^{-i\kappa t\lambda_j}U_{kj}U_{0j}^* \tag{122}$$

where λ_j are the eigenvalues of the interaction Hamiltonian in units of $\hbar\kappa$. Of course, the matrix U as well as the eigenvalues λ_j are defined for given n and should have an additional index n, which we have omitted to shorten the notation. Moreover, for real κ the interaction Hamiltonian matrix is real, and the transformation matrix U is a real orthogonal matrix, so the star can also be dropped.

The numerical diagonalization procedure gives the eigenvalues λ_j as well as the elements of the matrix U, and the coefficients $c_{n,k}(t)$ can thus be calculated according to (122). It is worthwhile to note, however, that because of the symmetry of the Hamiltonian, the eigenvalues λ_j are distributed symmetrically with respect to zero, with one eigenvalue equal to zero if there is an odd number of them. When the eigenvalues are numbered from the lowest to the highest

value, there is an additional relation

$$U_{kj}U_{0j} = (-1)^k U_{k,[n/2]-j}U_{0,[n/2]-j} \tag{123}$$

which makes the coefficients $c_{n,k}(t)$ either real (k even) or imaginary (k odd). This property of the coefficients $c_{n,k}(t)$ is very important and allows in some cases to get exact analytical results.

Knowing the coefficients $c_{n,k}(t)$ the resulting state of the field (119) in the particular sector can be written, for the initial state $|n,0\rangle$, as

$$|\psi^{(n)}(t)\rangle = \sum_{k=0}^{[n/2]} c_{n,k}(t)|\psi_k^{(n)}\rangle \tag{124}$$

The typical initial conditions for the second-harmonic generation are a coherent state of the fundamental mode and the vacuum of the second-harmonic mode. The initial state of the field can thus be written as

$$|\psi(0)\rangle = \sum_{n=0}^{\infty} \mathrm{e}^{in\phi_a} b_n |n,0\rangle \tag{125}$$

where

$$b_n = \exp\left(\frac{-N_a}{2}\right)\frac{N_a^{n/2}}{\sqrt{n!}} \tag{126}$$

is a Poissonian weighting factor of the coherent state $|\alpha_0\rangle$ represented as a superposition of the number states, $N_a = |\alpha_0|^2$ is the mean number of photons, and ϕ_a is the phase of the coherent state — $\alpha_0 = \sqrt{N_a}\exp(i\phi_a)$. With these initial conditions the resulting state of the field (119) takes the form

$$\begin{aligned} |\psi(t)\rangle &= \sum_{n=0}^{\infty} e^{in\phi_a} b_n |\psi^{(n)}(t)\rangle \\ &= \sum_{n=0}^{\infty} e^{in\phi_a} b_n \sum_{k=0}^{[n/2]} c_{n,k}(t)|n-2k,k\rangle \end{aligned} \tag{127}$$

Equation (127) describing the evolution of the system is our starting point for further discussion of the second-harmonic generation. If the initial state of the fundamental mode is not a coherent state but has a decomposition into a number states of the form (125) with different b_n, equation (127) is still valid when corresponding b_n are taken. It is true, for example, for the initially squeezed state of the fundamental mode.

It is interesting to consider one particular initial state of the field in which there are only two photons at the fundamental mode and no photons in the second-harmonic mode: $|2,0\rangle$. With this initial state the only state that can be created in the process is the state $|0,1\rangle$ with one photon in the second-harmonic mode and zero photons in the fundamental mode. Next, the second-harmonic photon can be downconverted into two photons of the fundamental mode, and we observe fully periodic evolution. The evolution is thus restricted to the two-dimensional subspace $\{|2,0\rangle, |0,1\rangle\}$. The Hamiltonian matrix in this subspace has the form

$$H_I = \hbar\kappa \begin{pmatrix} 0 & \sqrt{2} \\ \sqrt{2} & 0 \end{pmatrix} \tag{128}$$

the diagonalizing matrix U has the form

$$U = \frac{1}{\sqrt{2}} \begin{pmatrix} 1 & 1 \\ -1 & 1 \end{pmatrix}, \qquad U^{-1} = \frac{1}{\sqrt{2}} \begin{pmatrix} 1 & -1 \\ 1 & 1 \end{pmatrix} \tag{129}$$

and the two eigenvalues are $\lambda_0 = -\sqrt{2}$ and $\lambda_1 = \sqrt{2}$. We have two coefficients $c_{n,k}(t)$

$$c_{2,0}(t) = \cos(\sqrt{2}\,\kappa t), \qquad c_{2,1}(t) = -i\sin(\sqrt{2}\,\kappa t) \tag{130}$$

and the resulting state has the form

$$|\psi^{(2)}(t)\rangle = \cos(\sqrt{2}\,\kappa t)|2,0\rangle - i\sin(\sqrt{2}\,\kappa t)|0,1\rangle \tag{131}$$

The mean numbers of photons in the state (131) are given by

$$\langle \hat{a}^+\hat{a}\rangle(t) = 2\cos^2(\sqrt{2}\,\kappa t), \qquad \langle \hat{b}^+\hat{b}\rangle(t) = \sin^2(\sqrt{2}\,\kappa t) \tag{132}$$

which are exact analytical formulas for these particular initial conditions. We also have

$$\begin{aligned} \langle \hat{a}^{+2}\hat{a}^2\rangle - \langle \hat{a}^+\hat{a}\rangle^2 &= -2\cos^2\sqrt{2}\,\kappa t(2\cos^2\sqrt{2}\,\kappa t - 1) \\ \langle \hat{b}^{+2}\hat{b}^2\rangle - \langle \hat{b}^+\hat{b}\rangle^2 &= -\sin^4\sqrt{2}\,\kappa t \end{aligned} \tag{133}$$

From the definition (19) of the Mandel q parameter and Eq. (133) we immediately find that

$$q_a = 1 - 2\cos^2\sqrt{2}\,\kappa t, \qquad q_b = -\sin^2\sqrt{2}\,\kappa t \tag{134}$$

which shows that initially the fundamental mode has $q_a = -1$ denoting the sub-Poissonian statistics of the initial Fock state with two photons and the second harmonic mode initially has $q_b = 0$, as it should be for the vacuum state. At later times, however, the fundamental mode becomes super-Poissonian while the second-harmonic mode becomes sub-Poissonian. This simple example shows that even in the case of the evolution that is restricted to the two-dimensional subspace, there are essential changes in photon statistics.

Generally, the second-harmonic generation is described by the quantum state (127) and we use this state in our further calculations. Classical solutions discussed earlier, $u_a(\tau) = \operatorname{sech}\tau$ and $u_b(\tau) = \tanh\tau$, indicated that the amplitudes of the two modes are monotonic functions of time and that eventually all the energy from the fundamental mode will be transferred into the second-harmonic mode, assuming that there was no second-harmonic signal initially. It is well known [20,48], however, that the quantum solution has oscillatory character and does not allow for the complete power transfer. Using the state (127) we find that the mean photon numbers evolve in time according to the formulas

$$\begin{aligned}\langle\hat{N}_a(t)\rangle &= \langle\psi(t)|\hat{a}^+\hat{a}|\psi(t)\rangle = \sum_{n=0}^{\infty} b_n^2 \sum_{k=0}^{[n/2]}(n-2k)|c_{n,k}(t)|^2\\ \langle\hat{N}_b(t)\rangle &= \langle\psi(t)|\hat{b}^+\hat{b}|\psi(t)\rangle = \sum_{n=0}^{\infty} b_n^2 \sum_{k=0}^{[n/2]}k|c_{n,k}(t)|^2\end{aligned} \tag{135}$$

Because of the Poissonian factors, which are peaked at N_a, the summation over n can be performed numerically if N_a is not too great. On the other hand, some features of the classical solutions can be expected for $N_a \gg 1$. To evaluate numerically formulas (135) we use the computer program quoted in the Appendix B, which can be run using the freely available software OCTAVE [50] or the commercial software MATLAB [51]. The results are illustrated in Fig. 5. In Fig. 5a we have plotted the normalized second-harmonic intensity $n_b = 2\langle\hat{N}_b\rangle/N_a$, where N_a is the initial mean number of photons of the coherent state of the fundamental mode, against the scaled time τ for the initially coherent state with the mean number of photons equal to 2 (solid line) and compared it with the corresponding intensity obtained for the initial state of the fundamental mode being the Fock state with two photons [Eq. (132)]. In the latter case we see the perfectly periodic behavior with complete transfer of energy between the fundamental and second-harmonic modes. In the case of coherent state with the mean number of photons being the same as for the Fock state we already see the distorted oscillations, and the transfer of power is not complete. In Fig. 5b we have presented the results for initially coherent state of the fundamental mode with the mean number of photons satisfying the inequal-

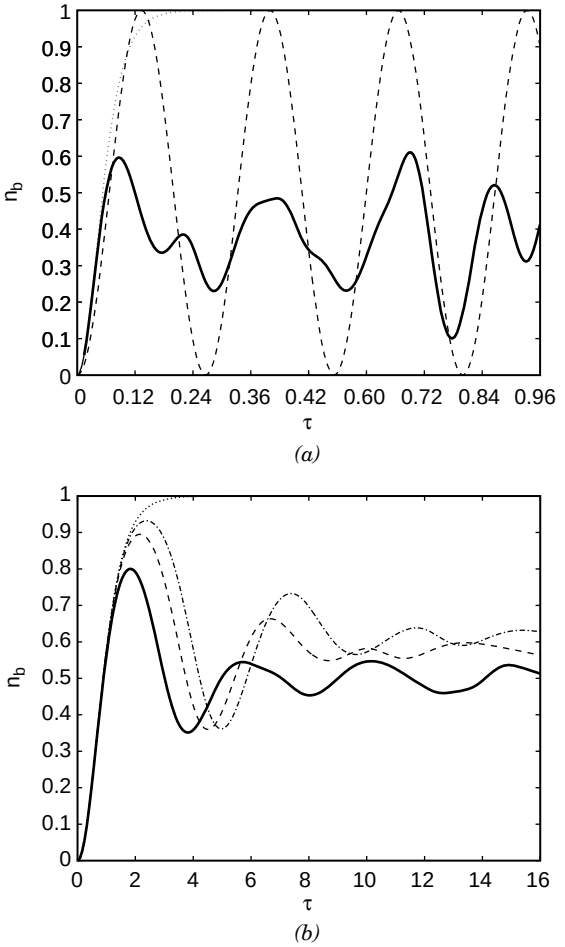

Figure 5. Intensity of the second-harmonic: (a) initial coherent state with $N_a = 2$ (solid line) and initial number state with two photons (dashed line); (b) initial coherent state with $N_a = 10$ (solid line), $N_a = 40$ (dashed line), and $N_a = 100$ (dashed–dotted line). Dotted line marks the classical solution.

ity $N_a \gg 1$. The curves are plotted for $N_a = 10$ (solid line), $N_a = 40$ (dashed line), and $N_a = 100$ (dashed-dotted line). For reference, with the dotted line the classical solution is marked on both figures. The solutions are oscillatory but the oscillations are damped rather quickly when the pump mode is strong. The higher is the intensity of the pump mode, the longer the solution sticks to the classical solution before the process is reversed from the second-harmonic

generation into the downconversion. The maximum reached by the second harmonic intensity increases, as the intensity of the pump mode increases, giving better efficiency of conversion of the fundamental mode field into the second harmonic. This tendency is clearly seen from Fig. 5b.

At this point it is interesting and worthwhile to compare the solution (112) that predicted fully periodic behavior resulting from the quantum noise with the fully quantum calculations performed in this section. In Fig. 6 we present both solutions for the initial mean number of photons $N_a = 100$, which gives $\epsilon' = 0.01$. Both solutions are almost identical up to the first maximum, but subsequent maxima are substantially damped with respect to the approximate solution. The approximate solution correctly predicts the transition from the second harmonic regime to the downconversion regime, which is the physical reason for starting oscillations. The quantum noise really induces macroscopic revivals, but subsequent maxima are smaller and smaller and the second harmonic intensity asymptotically approaches a certain value. Without quantum fluctuations the solution is a monotonic function as shown in the figure by the dotted curve. The quantum noise is necessary to trigger the macroscopic changes in the intensity of the second-harmonic mode.

Now, we can proceed further and ask the question about the evolution of the quantum fluctuations. We have already seen that there are essential changes in

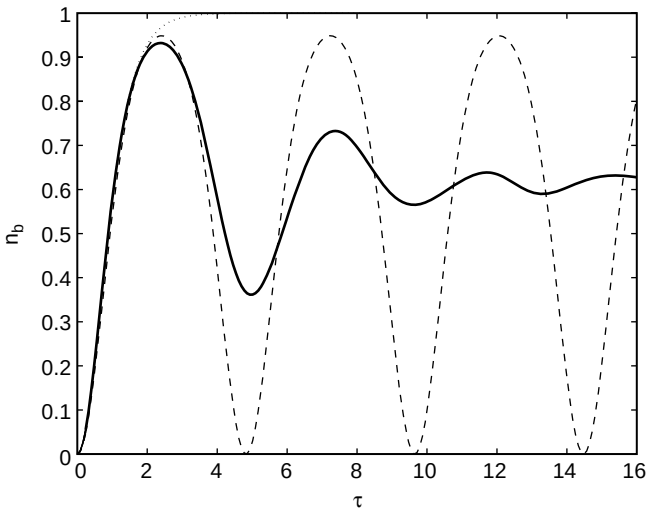

Figure 6. Comparison of the fully quantum numerical solution (solid line) and the approximate solution (112) (dashed line) for the initial mean number of photons $N_a = 100(\epsilon' = 0.01)$. Classical solution is marked by dotted curve.

the photon statistics when the evolution is restricted to the two-state subspace. Even in this simple case the fundamental mode evolved from the sub- to super-Poissonian photon statistics. The numerical method presented above is suitable for answering questions about photon statistics and squeezing equally well as the question about the mean intensity. To calculate the mean value of the square of the photon number operator for the fundamental mode, it is as simple as replacing $n - 2k$ by $(n - 2k)^2$ in (135), or replacing k by k^2 in order to calculate the mean value of the square of the photon number operator for the second-harmonic mode. All the rest is up to the computer. Let us calculate the Mandel q parameter as defined by (19). In Fig. 7 we have presented the results of the numerical calculations for the Mandel q parameters for both fundamental (Fig. 7a) and second harmonic (Fig. 7b) modes. Both modes exhibit sub-Poissonian photon statistics (negative values of the q parameter) at the initial stages of the evolution, but for long times the statistics becomes super-Poissonian. The sub-Poissonian statistics at initial stages of the evolution is in agreement with the short time approximation presented in Eq. (103).

In Fig. 8 we have plotted the quadrature variances for the two modes and compared them to their counterparts obtained from the linearized noise equations. In Fig. 8a we see the two squeezed quadratures, $\langle[\Delta Q_a]^2\rangle$ and $\langle[\Delta P_b]^2\rangle$, calculated numerically for the mean number of photons of the pump mode $N_a = 10$, and their counterparts obtained from the linearized theory, that is, plotted from the formulas (88). In Fig. 8b the nonsqueezed quadratures $\langle[\Delta P_a]^2\rangle$ and $\langle[\Delta Q_b]^2\rangle$ are compared. It is evident from the figures that, as one could expect, the linearized theory has only limited range of applicability. The linearized results are in good agreement with the exact numerical results roughly up to the scaled time $\tau \simeq 1$. The long-time evolution ($\tau > 1$) of the quadrature variances is principally different from their linearized approximation counterparts because the linearization fails to predict the quantum noise induced revival in the evolution. It is also clear from Fig. 8a that the degree of squeezing that can really be obtained is much smaller than that predicted from the linearized theory. The long time behavior of the quadrature variances is presented in Fig. 9 where the same quadratures are plotted as in Fig. 8 but for longer time τ showing irregular oscillations of the quantum noise with a general tendency for that noise to increase and we should not expect squeezing in the long time-limit. The reduction of the quantum noise below the vacuum level is thus a property that in second-harmonic generation appears at the beginning of the evolution and never reappears again.

Since $\hat{H}_0$ is a constant of motion, $\hat{H}_0^2$ is also a constant of motion, which gives, for the fluctuations of $\hat{H}_0$, the relation

$$\langle[\Delta\hat{H}_0]^2\rangle = \langle\hat{H}_0^2\rangle = \langle\hat{H}_0\rangle^2 = N_a(\hbar\omega)^2 \tag{136}$$

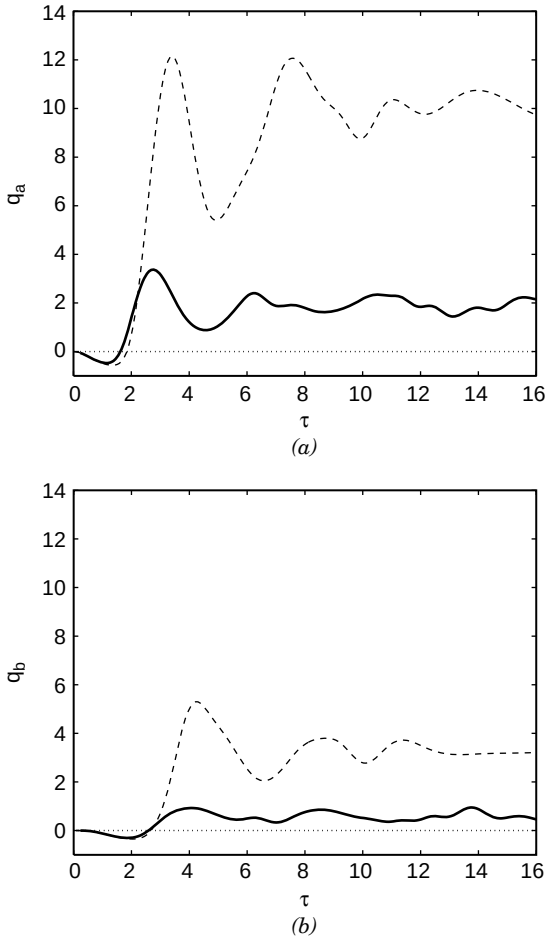

Figure 7. The Mandel q parameter for the (a) fundamental mode and; (b) second-harmonic mode. The mean number of photons is $N_a = 10$ (solid lines) and $N_a = 40$ (dashed lines).

which can be rewritten as

$$\langle[\Delta\hat{N}_a]^2\rangle + 4\langle[\Delta\hat{N}_b]^2\rangle + 4\langle\Delta\hat{N}_a\Delta\hat{N}_b\rangle = N_a \tag{137}$$

Formula (137) establishes the relation between the fluctuations of the individual-mode photon numbers and the intermode photon-number correlation. All the quantities on the left hand side (l.h.s.) of Eq. (137) can be calculated

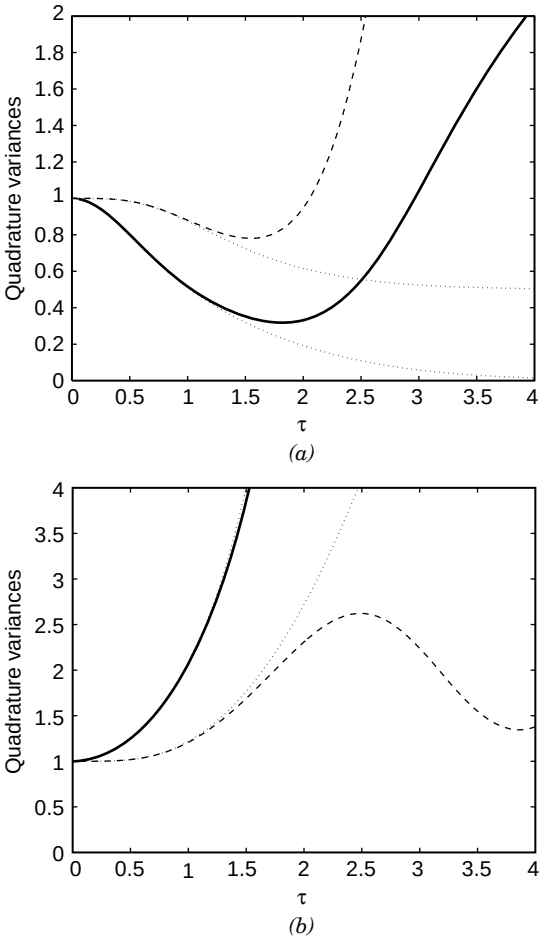

Figure 8. The quadrature variances: (a) squeezed variances $\langle[\Delta Q_a]^2\rangle$ (solid line) and $\langle[\Delta P_b]^2\rangle$ (dashed line) (b) nonsqueezed variances $\langle[\Delta P_a]^2\rangle$ (solid line) and $\langle[\Delta Q_b]^2\rangle$ (dashed line) for $N_a = 10$. The dotted lines are the linearized solutions.

numerically starting with the state (127), and formula (137) can serve as a test of numerical precision. The value of N_a sets the level of fluctuations for an initially coherent state with the mean number of photons N_a. In Fig. 10 we have visualized the evolution of the correlations between the photon-number fluctuations (normalized) $4\langle\Delta\hat{N}_a\Delta\hat{N}_b\rangle/N_a$ of the two modes. The two photon noises are negatively correlated. This negative correlation of photon fluctuations compensates for the large increase of the photon number variances in each

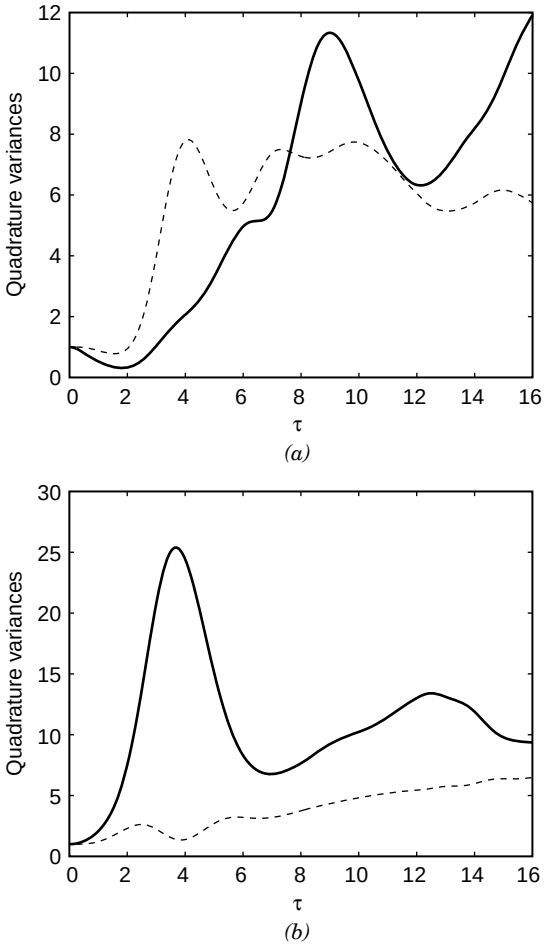

Figure 9. Same quadratures as in Fig. 8 but for longer time τ.

mode, which is clearly visible from Fig. 7. Thus the super-Poissonian photon statistics is related with the appearance of strong negative correlations between the photon-number fluctuations. The peak in the Mandel q parameter, indicating highly super-Poissonian photon statistics, is, on the other hand, related to the minimum of the quadrature variance, that is, it is related to the maximum of squeezing. This shows that quantum fluctuations of various physical quantities are related to each other, but this relation is not necessarily simple.

The statistical properties of the quantum fields are well characterized by the quasiprobability distribution functions defined in the Section II. Let us consider

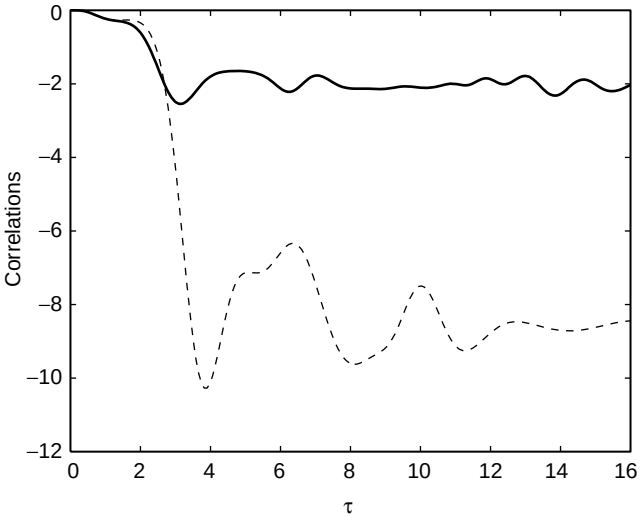

Figure 10. Correlations $4\langle\Delta\hat{N}_a\Delta\hat{N}_b\rangle/N_a$ between the photon-number fluctuations in the two modes for $N_a = 10$ (solid line) and $N_a = 40$ (dashed line). Compare to Fig. 7.

the Husimi Q function as defined by (28) for the fundamental mode. To find this function, we start with the more general function for the two-mode field

$$Q(\alpha,\beta) = \frac{1}{\pi^2}|\langle\alpha,\beta|\psi(t)\rangle|^2 \tag{138}$$

where $|\psi(t)\rangle$ is as given by (127). By integrating the function $Q(\alpha,\beta)$ over $d^2\beta$, we obtain the function $Q(\alpha)$ for the fundamental mode. We find

$$Q(\alpha,\beta) = \frac{1}{\pi^2}e^{-(|\alpha|^2+|\beta|^2)}\left|\sum_{n=0}^{\infty}e^{in\phi_a}b_n\sum_{k=0}^{[n/2]}\frac{(\alpha^*)^{n-2k}(\beta^*)^k}{\sqrt{(n-2k)!k!}}c_{n,k}(t)\right|^2 \tag{139}$$

and after integrating over $d^2\beta$ we get

$$\begin{aligned}Q(\alpha) = \frac{1}{\pi}e^{-|\alpha|^2}\Bigg\{&\sum_{n=0}^{\infty}|b_n|^2|\alpha|^{2n}\sum_{k=0}^{[n/2]}\frac{|\alpha|^{-4k}|c_{nk}(t)|^2}{(n-2k)!}\\&+2\mathrm{Re}\sum_{n=1}^{\infty}\sum_{n'=0}^{n-1}e^{i(n-n')\phi_a}b_nb_{n'}(\alpha^*)^n\alpha^{n'}\\&\times\sum_{k=0}^{[n'/2]}\frac{|\alpha|^{-4k}c_{n,k}(t)c^*_{n',k}(t)}{\sqrt{(n-2k)!(n'-2k)!}}\Bigg\}\end{aligned} \tag{140}$$

In a similar way, integrating (139) over $d^2\alpha$ we obtain the Q function for the second-harmonic mode, which has the form

$$Q(\beta) = \frac{1}{\pi} \mathrm{e}^{-|\beta|^2} \left\{ \sum_{n=0}^{\infty} \sum_{n'=0}^{\infty} e^{i(n-n')\phi_a} b_n b_{n'} \right.$$
$$\left. \times \sum_{k=0}^{[n/2]} \sum_{k'=0}^{[n'/2]} \frac{(\beta^*)^k \beta^{k'}}{\sqrt{k!k'!}} c_{n,k}(t) c^*_{n',k'}(t) \delta_{n-2k,n'-2k'} \right\} \tag{141}$$

The two functions can be evaluated numerically for a not-too-large mean number of photons N_a. In Fig. 11 we have shown the contour plots of the Q function for the fundamental mode (Fig. 11a) and the second-harmonic mode (Fig. 11b) for the initial mean number of photons of the fundamental mode $N_a = 10$. It is seen that the centroid of the distribution, in case of the fundamental mode, moves to the left along the Re α axis showing squeezing along this axis at initial stages of the evolution, and next it becomes a two-peak structure first noticed by Nikitin and Masalov [24]. Nikitin and Masalov [24] suggested that the two peaks appearing in the Q function indicated a macroscopic superposition of quantum states. In case of the second harmonic mode the Q function starts with the peak localized at the origin (initial vacuum state) and moves along the Im β axis undergoing deformation during the evolution. Motion of the centroid of the distribution along the Im β axis confirms again our earlier prediction that the phases of the two fields exhibit a shift by $\pi/2$. The Q function is one of the quasiprobalility distributions that describe quantum statistical properties of the field. It has advantage that it is always positive, so it can be treated in the way as the classical probability distributions are treated, but it also has disadvantages; for example, it does not lead to correct marginal distributions. In this context the Wigner function is more appropriate, but the Wigner function can take negative values, which precludes its treatment as classical probability distribution. In many cases, however, the Wigner function is very useful. All the quasidistribution functions take into account the fact that quantum fields are operator fields and are represented by noncommuting operators, which unavoidably introduce quantum noise. The different quasidistributions are related to different orderings of the field operators. The Q function is associated with the antinormal ordering of the operators.

As we have already seen, quantum noise changes the character of the evolution of the field in the second-harmonic generation by making it periodic. But periodic behavior is also seen for classical solution if we assume that there is a small classical signal of the second harmonic mode when the evolution starts. One can thus say that the quantum noise, or spontaneously emitted photons, play a role of the classical signal that makes the evolution periodic.

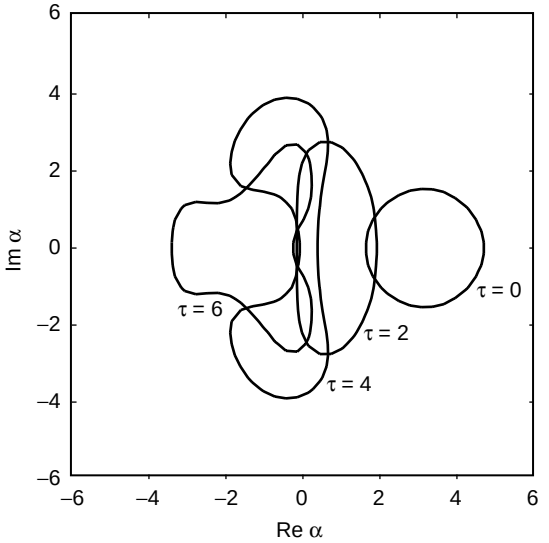

(a)

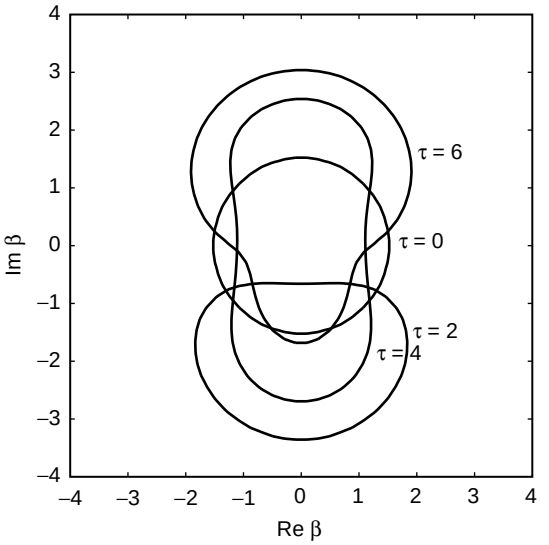

(b)

Figure 11. Contour plots for the Q function: (a) fundamental mode and (b) second-harmonic mode, for the mean number of photons $N_a = 10$. Contours are taken at 0.1 of the maximum.

This also prompts us a way to simulate the quantum noise by introducing randomly chosen initial values. We can use deterministic classical equation of motion to describe the evolution of the fields, but the initial conditions are chosen at random. Let us assume that $\alpha = \alpha_0 + \Delta\alpha$, $\beta = \beta_0 + \Delta\beta$, where α_0 and β_0 are the mean values of the initial amplitudes and $\Delta\alpha = \Delta x_a + i\Delta y_a$, $\Delta\beta = \Delta x_b + i\Delta y_b$ are the fluctuations of the two fields, where Δx_a, Δy_a, Δx_b, Δy_b being the independent real Gaussian processes with identical variances $\overline{\Delta x_a^2} = \overline{\Delta y_a^2} = \overline{\Delta x_b^2} = \overline{\Delta y_b^2} = \frac{1}{4}$, where we have denoted the classical averaging by the overline (vinculum). With these assumptions we find that the variances of the quadrature components $\hat{Q}$ and $\hat{P}$ of the fields, which for the vacuum state are equal to unity, can be expressed by the variances of these classical random variables $\langle[\Delta\hat{Q}_a]^2\rangle = 2(\overline{\Delta x_a^2} + \overline{\Delta y_a^2}) = 1$, and so on. Now, starting with the Gaussian distribution of the initial values of the field amplitudes, we can simulate some quantum properties of the fields using classical trajectories. It is interesting to compare the results obtained using the method of classical trajectories to the quantum results for the Q function. This kind of comparison has been done for second-harmonic process by Nikitin and Masalov [24]. Since it is really impressive to see how good the quantum Q function contours are reproduced by a cloud of points that undergone classical evolution starting from the initial conditions described by the Gaussian distribution, we show in Fig. 12 clouds of 1000 points for the same values of the evolution time as in Fig. 11 for $N_a = 10$. Why is the Q function reproduced so well with the classical trajectories? The Q function is a representative of a whole class of the quasidistribution functions. Generally, the s-parametrized quasiprobability distribution for a coherent state, defined by (30), is given by

$$\mathscr{W}^{(s)}(\alpha) = \frac{1}{\pi}\frac{2}{1-s}\exp\left(-\frac{2}{1-s}|\alpha-\alpha_0|^2\right) \tag{142}$$

which, for $s < 1$, is a Gaussian distribution. For $s = 1$, the distribution becomes the Dirac delta function, for $s = 0$ it is the Wigner function, and for $s = -1$, we have the Q function. The distribution (142) becomes narrower as s increases approaching unity. The Q function is the broadest distribution, but all of them for $s < 1$ are just Gaussians with various variances. In terms of classical description of the field noise, the most suitable function is the Wigner function [52], for which the variance of the Gaussian distribution is equal to $\frac{1}{4}$. The Q function is broader, with the variance equal to $\frac{1}{2}$, but because the state of the field has a large coherent component, the two functions are very similar in shape and the Q function is usually easier to calculate. For the nontrivial quantum states, the Wigner function can take negative values, and then it is difficult to simulate properties of such states by classical stochastic variables

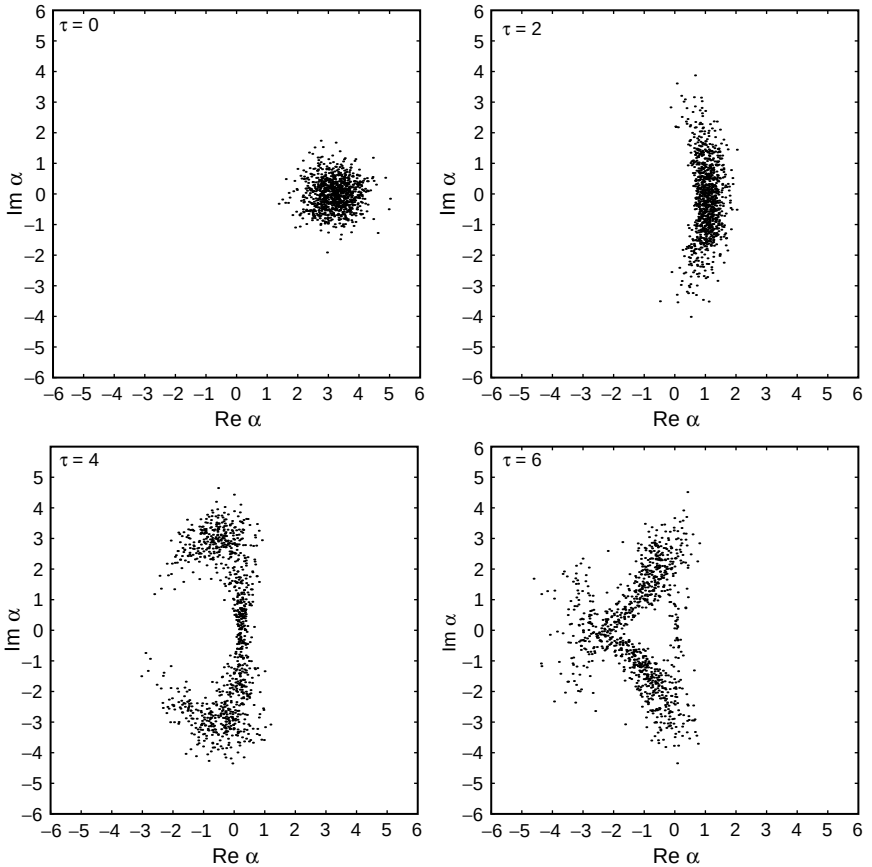

Figure 12. Classical trajectories for 1000 points for Gaussian distribution of initial values with unit variance and $N_a = 10$. Compare to Fig. 11a.

while the Q function does not suffer from such problems. When the initial state of the fundamental mode is a coherent state, the initial distribution is a Gaussian, and the result of simulation is pretty good. The method of classical trajectories has been used by Bajer et al. to explain the sub-Poissonian photon statistics in the second harmonic generation [36] as well as the third harmonic generation [37] in the no-energy-exchange regime. They have found that in this regime it is possible to obtain the steady-state solutions exhibiting sub-Poissonian photon statistics, and, surprisingly, they have shown that this quantum effect can be explained within the classical trajectories approach.

As we have already discussed in Section II, another characteristic of the quantum field is its phase distribution. The phase distribution of the quantum field can be calculated from the quasidistribution functions by integrating over the radial variable. In this way we get a kind of phase distribution that can be considered as an approximate description of the phase properties of the field. One can calculate the s-parametrized phase distributions, corresponding to the s-parametrized quasidistributions, for particular quantum states of the field [16]. However, a better way to study quantum phase properties is to use the Hermitian phase formalism introduced by Pegg and Barnett [11–13]. We have already introduced this formalism in Section II. Now, we apply this formalism to study the evolution of the phase properties of the two modes in the SHG process. In this case we have a two-mode field which requires a modification of the formulas presented in Section II into a two-mode case. The modification is rather trivial, and for the joint probability distribution for the continuous phase variables θ_a and θ_b describing phases of the two modes, we get the formula [53]

$$P(\theta_a, \theta_b) = \frac{1}{(2\pi)^2} \left| \sum_{n=0}^{\infty} b_n \sum_{k=0}^{[n/2]} c_{n,k}(t) \times \exp\{-i[(n-2k)\theta_a + k\theta_b - k(2\phi_a - \phi_b]\} \right|^2 \tag{143}$$

where ϕ_a and ϕ_b are the initial phases of the two modes, and the coefficients $c_{n,k}(t)$ are given by (122). The distribution (143) is normalized such that

$$\int_{-\pi}^{\pi} \int_{-\pi}^{\pi} P(\theta_a, \theta_b)\, d\theta_a\, d\theta_b = 1 \tag{144}$$

To choose the phase windows for θ_a and θ_b, we have to assign to ϕ_a and ϕ_b particular values. It is interesting to notice that formula (143) depends, in fact, on the difference $2\phi_a - \phi_b$, which reproduces the classical phase relation for the second harmonic generation, as seen in in classical equations (59). Classically, if there is no second-harmonic initially, this quantity must be $2\phi_a - \phi_b = \pm\pi/2$. This means that the phase of the second-harmonic mode is locked to the phase of the fundamental mode by this relation. It turns out that this is also a good choice to fix the phase windows in the quantum description. If the initial phase ϕ_a of the fundamental mode is zero, then $\phi_b = \pm\pi/2$ (depending on the sign of κ); that is, the second harmonic is shifted in phase by $\pi/2$ or $-\pi/2$ with respect to the fundamental mode.

The joint probability distribution given by Eq. (143) can be evaluated numerically and an example of such distribution is shown in Fig. 13, where the function $P(\theta_a, \theta_b)$ is plotted for several values of the scaled time τ and the initial mean number of photons of the fundamental mode $N_a = 10$. Initially the

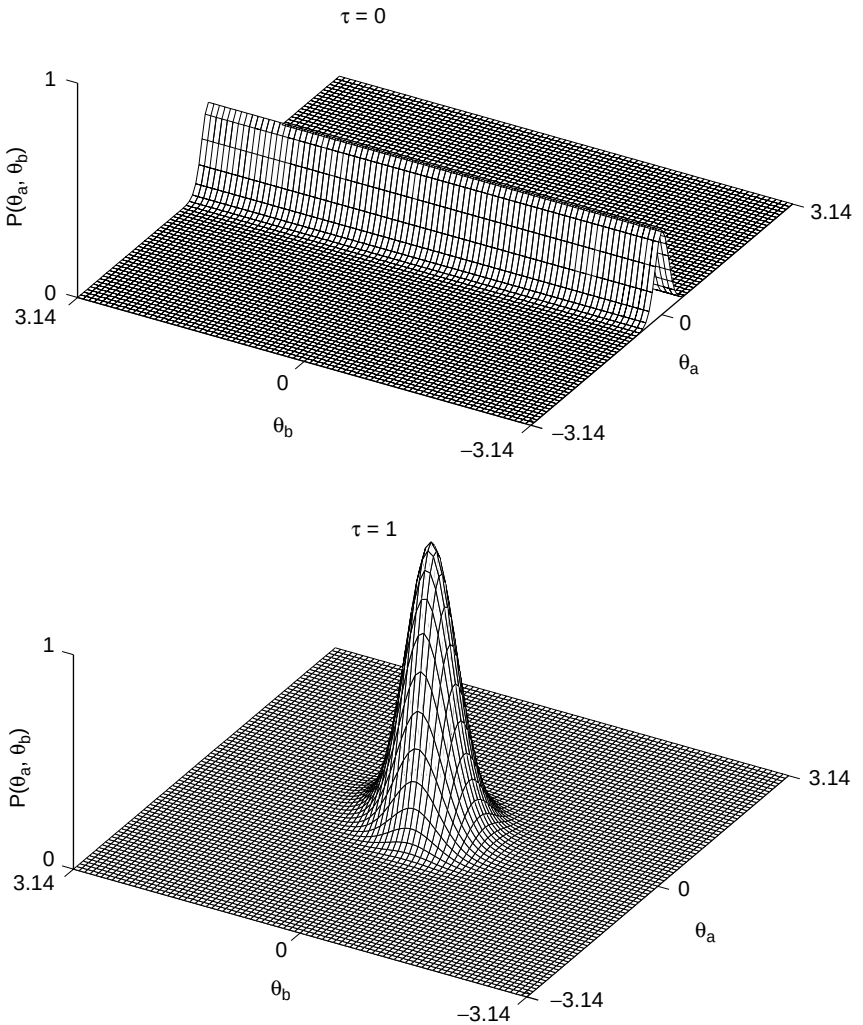

Figure 13. Joint phase probability distribution $P(\theta_a, \theta_b)$ of the fundamental and second-harmonic modes for various evolution time τ. In the last two figures the phase windows for θ_a and θ_b are shifted by π.

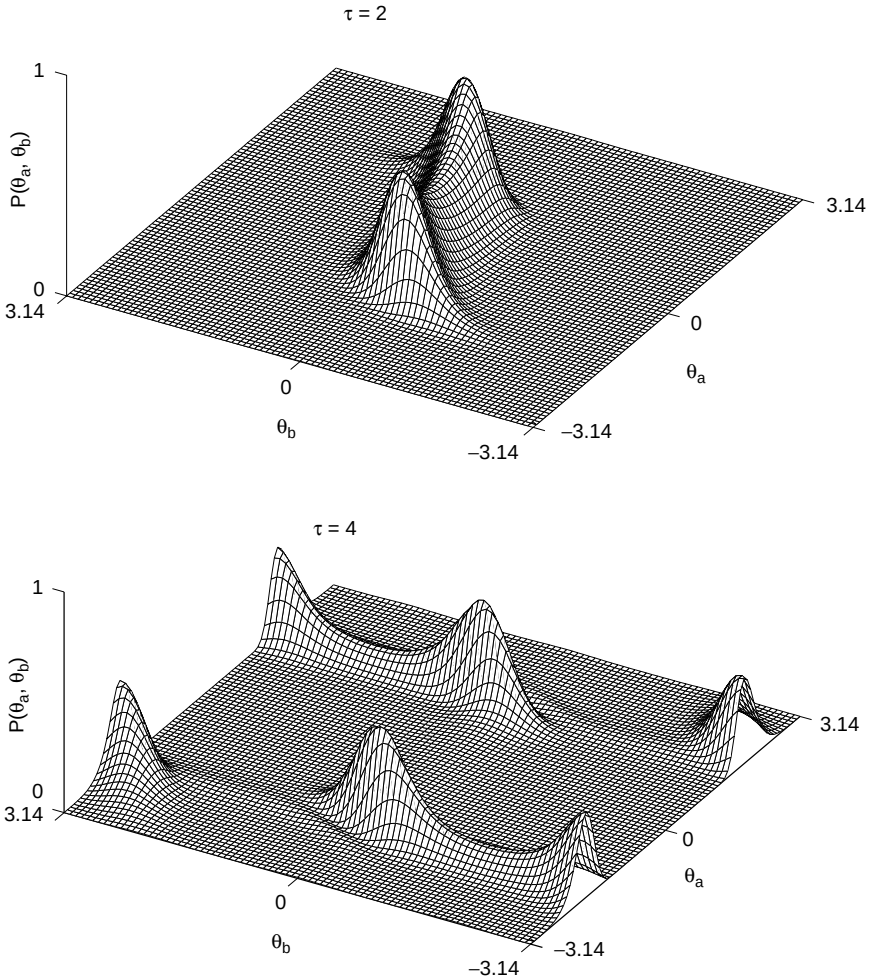

Figure 13. (*Continued*)

distribution is peaked at $\theta_a = 0$ in the θ_a direction reflecting the phase distribution of the coherent state of the fundamental mode, and it is completely flat in the θ_b direction reflecting the uniform phase distribution of the vacuum of the second-harmonic mode. At a later time, $\tau = 1$, a single, well-resolved peak of the distribution is visible, signifying a relatively well defined phase of the second-harmonic mode in conjunction with the phase of the fundamental mode. The fact that the peak appears for $\theta_a = \theta_b = 0$ corroborates the classical phase

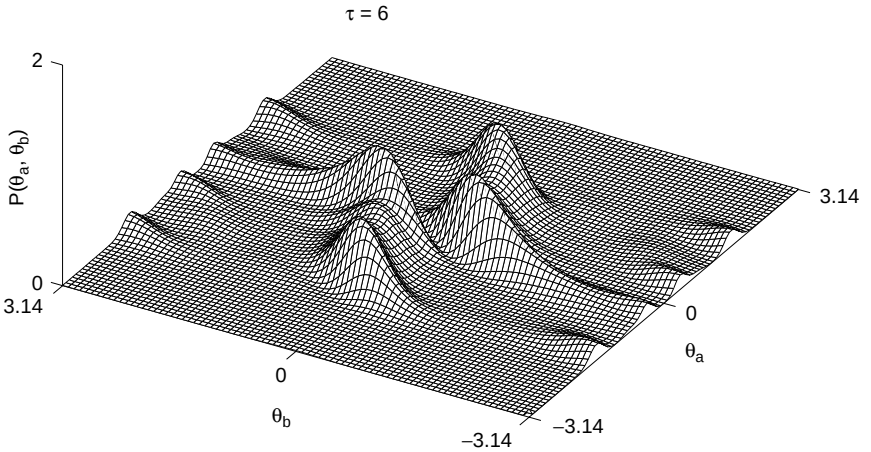

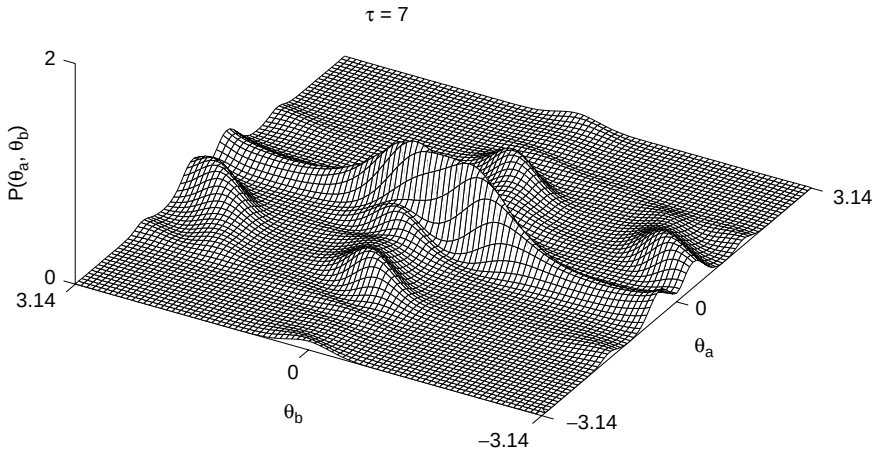

Figure 13. (*Continued*)

relation $2\phi_a - \phi_b = \pi/2$, which has been assumed here to choose the phase windows. As the evolution proceeds, for $\tau = 2$, the phase distribution $P(\theta_a, \theta_b)$ splits into two peaks. This is very interesting interval of time in which the second-harmonic mode achieves its maximum and the reverse process of downconversion start to predominate (can be seen from Fig. 5). The case of downconversion will be discussed later on, but now we can say that appearance of the two-peak phase distribution is a qualitative change in the phase properties

of the field, and it can be ascribed to the transition in the evolution from the harmonic generation regime into the downconversion regime. The two-peak structure of the ideal squeezed states has been indicated by Vaccaro and Pegg [54], and for the downconversion process with quantum pump by Gantsog et al. [55]. The splitting of the phase distribution into two peaks resembles the splitting of the Q function for the fundamental mode indicated by Nikitin and Masalov [24] which we have discussed earlier. The multipeak structure of the Q function or/and the phase distribution can be an indication that the field becomes a superposition of macroscopically distinguishable quantum states, the so-called Schrödinger cats [25,27,30,56]. For still longer times, $\tau = 4$, the intensity of the second-harmonic approaches its minimum and we observe a transition from the regime of downconversion back to the regime of second-harmonic generation, but this time with a quite different "initial" state. Such "bifurcations" of the phase distribution lead to a multipeak structure of the phase distribution, which means more and more uniform phase distribution. We would also draw attention to the jump in phase by π, which is clearly visible in the last two figures (compare to the classical phase evolution shown in Fig. 2). The fact that one peak splits into just two peaks is related to the fact that the process we discuss is the two-photon process. For example, for the three-photon downconversion the threefold symmetry of the distributions is observed [57]. Generally, the joint phase probability distribution carries quite a bit of useful information about the quantum state of the field. It is also important that for two-mode fields the joint phase probability distribution is a function of two variables θ_a and θ_b only, in contrast to the function $Q(\alpha, \beta)$, which is a function of four real variables Re α, Im α, Re β, Im β, so it is easy to visualize the two-mode field using the phase distribution while it is difficult to visualize the Q function in the phase space. Of course, the phase distribution obtained by integration of the quasidistributions is in this respect equally easy to handle as the Pegg–Barnett phase distribution even though the two functions are different. Generally, different distribution functions carry different information, but some properties of the field can be read out from all of them.

The phase distribution function (143) allows for calculations of the phase variances for the individual modes as well as the phase correlations between the two modes by performing simple integrations over the phase variables θ_a and θ_b. Detailed discussion of the phase properties of the fields can be found in Ref. 16, and we will not repeat it here. The material presented in this section has been chosen as to illustrate how quantum noise, which is an indispensable ingredient of quantum description of optical fields, can be incorporated into the theory of nonlinear optical phenomena, in particular the phenomenon of second-harmonic generation.

IV. DEGENERATE DOWNCONVERSION

A process on the one hand similar to the second-harmonic generation because it is described by the same Hamiltonian (54) but on the other hand opposite the second-harmonic generation because the initial conditions are interchanged, is the process of degenerate downconversion. For the second-harmonic generation initially there is no signal field at the second-harmonic frequency 2ω and there is a strong (coherent) field at the fundamental frequency ω. On the contrary, for the downconversion process initially there is no signal at frequency ω and there is a strong (coherent) field at the frequency 2ω, which is the pump mode in this process. As we have already discussed, we can talk about "pure" second-harmonic generation or downconversion only at the initial stage of the evolution with these particular initial conditions. At later times both processes compete with each other with domination of one of them between the subsequent maxima and minima of the signal intensity in a given mode. There is, however, one important difference between the two processes—the second-harmonic process can start even when the fields are classical, while the downconversion process must be triggered by quantum fluctuations.

The simplest and most often used approximation allowing for analytical solutions of the downconversion problem is the *parametric approximation*, in which it is assumed that the pump mode is a strong coherent field that remains undepleted during the evolution. The amplitude of this classical field is an external parameter on which the solutions for the signal field depend. Equations of motion for the downconversion process are the same as in (56)

$$\begin{aligned} \frac{d}{dt}\hat{a}(t) &= -2i\kappa\,\hat{a}^{+}(t)\hat{b}(t) \\ \frac{d}{dt}\hat{b}(t) &= -i\kappa\,\hat{a}^{2}(t) \end{aligned} \tag{145}$$

It is easy to note that for classical fields $\hat{a}(t) \to \alpha(t)$ and $\hat{b}(t) \to \beta(t)$, there is no nonzero solution for the signal field $\alpha(t)$ if $\alpha(0) = 0$. In the parametric approximation, the pump field at frequency 2ω is assumed to be constant classical field $\beta_0 = |\beta_0| \exp(i\phi_b)$. Within this approximation the first equation, Eq. 145, together with its Hermitian conjugate, can be solved analytically giving

$$\begin{aligned} \hat{a}(\tau) &= \hat{a}(0)\cosh\tau + \hat{a}^{+}(0)\sinh\tau\,\exp\left[i\left(\phi_b - \frac{\pi}{2}\right)\right] \\ \hat{a}^{+}(\tau) &= \hat{a}^{+}(0)\cosh\tau + \hat{a}(0)\sinh\tau\,\exp\left[-i\left(\phi_b - \frac{\pi}{2}\right)\right] \end{aligned} \tag{146}$$

where we have introduced the scaled time $\tau = 2|\beta_0|\kappa t$. The solutions (146) can be generated using the following squeezing operator

$$\hat{S}(\zeta) = \exp\left(\frac{1}{2}\zeta^* \hat{a}^2 - \frac{1}{2}\zeta \hat{a}^{+2}\right) \tag{147}$$

where the parameter $\zeta = i\tau$, in the following way [4]

$$\hat{a}(\tau) = \hat{S}^{-1}(\zeta)\hat{a}(0)\hat{S}(\zeta)\,, \qquad \hat{a}^+(\tau) = \hat{S}^{-1}(\zeta)\hat{a}^+(0)\hat{S}(\zeta) \tag{148}$$

Thus, the degenerate parametric oscillator, specifically, the downconversion process in the parametric approximation, performs the squeezing transformation, generating the *ideal squeezed states*, which have been widely discussed in the literature (see, e.g., Refs. 5 and 6 and papers cited therein). This material is well known, and we will not repeat it here. We rather concentrate on the cases when the parametric approximation is not applicable and the pump mode must be treated as a dynamical variable, the evolution of which must be taken into account. The quantum dynamics of the parametric oscillator has been studied by Kinsler and Drummond [58]. Reid and Krippner [59] have found that a macroscopic superposition states can be created in the nondegenerate parametric oscillator. Mode entanglement in such a system has been studied by Drobný et al. [60]. Here, we focus on comparison of the quantum properties of fields produced in the downconversion to those produced in the second-harmonic generation using the same theoretical methods.

A. Symbolic Calculations

Let us start with the short-time approximation in which we can use the symbolic manipulation computer program described in Appendix A to find the corrections coming from the quantum fluctuations of the fields. The operator formulas (94) and (95) are valid also for the degenerate downconversion because the two processes are governed by the same Hamiltonian, but now initially the second-harmonic mode is populated while the fundamental mode is initially in the vacuum state. Assuming that the pump mode at the frequency 2ω is in a coherent state $|\beta_0\rangle$ ($\beta_0 = \sqrt{N_b}\exp(i\phi_b)$), we have

$$\begin{aligned} \langle \hat{a}(t)\rangle &= 0 \\ \langle \hat{b}(t)\rangle &= \beta_0\left[1 - (\kappa t)^2 - \frac{1}{6}(\kappa t)^4(8|\beta_0|^2 - 1) + \cdots\right] \end{aligned} \tag{149}$$

It is interesting to note that the mean value of the signal mode at frequency ω is zero, and it is true for all powers in the expansion, reflecting the fact that photons are created in pairs. In case of pump mode, we see that the amplitude of the field will evolve in time and the lowest nonzero term is the quadratic term. The fact that the mean field of the signal mode is zero explains why the signal mode is said to be in the *squeezed vacuum*. Another interesting and characteristic feature of such field is the fact that the mean value of the square of the annihilation operator is nonzero

$$\begin{aligned}\langle \hat{a}^2(t)\rangle &= -2i\beta_0\left[(\kappa t) + \frac{1}{3}(\kappa t)^3(8|\beta_0|^2 - 1) + \cdots\right] \\ &= \exp\left[i(\phi_b - \pi/2)\right]\left[\tau + \frac{2}{3}\tau^3\left(1 - \frac{1}{8N_b}\right) + \cdots\right] \qquad (150)\end{aligned}$$

and this fact justifies the name the *two-photon coherent state* introduced by Yuen [61].

Let us take a look at the mean number of photons in the signal mode, which up to the fourth order is given by

$$\begin{aligned}\langle \hat{a}^+(t)\hat{a}(t)\rangle &= 4|\beta_0|^2\left[(\kappa t)^2 + \frac{2}{3}(\kappa t)^4(2|\beta_0|^2 - 1) + \cdots\right], \\ &= \tau^2 + \frac{\tau^4}{3}\left(1 - \frac{1}{2N_b}\right) + \cdots \qquad (151)\end{aligned}$$

where we have introduced the scaled time $\tau = 2\sqrt{N_b}\kappa t$, as suggested by the solutions (146) in the parametric approximation. The last term, $\sim N_b^{-1}$, comes from the field commutator and represents the quantum noise. The other terms are the terms of the expansion of $\sinh^2\tau$, which is the mean number of photons in the parametric approximation given by the solutions (146). For the pump mode we have

$$\begin{aligned}\langle \hat{b}^+(t)\hat{b}(t)\rangle &= |\beta_0|^2\left[1 - 2(\kappa t)^2 - \frac{4}{3}(\kappa t)^4(2|\beta_0|^2 - 1) + \cdots\right] \\ &= N_b - \frac{1}{2}\tau^2 - \frac{1}{6}\tau^4\left(1 - \frac{1}{2N_b}\right) + \cdots \qquad (152)\end{aligned}$$

Again, we can easily identify the noise term, and moreover, it is clear from Eqs. (151) and (152) that the quantity $\langle \hat{a}^+(t)\hat{a}(t)\rangle + 2\langle \hat{b}^+(t)\hat{b}(t)\rangle = 2|\beta_0|^2 = 2N_b$ is conserved including the quantum noise terms.

Similarly, we obtain corresponding expressions for the quadrature variances

$$\begin{aligned}\langle[\Delta\hat{Q}_a]^2\rangle &= 1 + 4(\kappa t)\,\mathrm{Im}\,\beta_0 + 8(\kappa t)^2|\beta_0|^2 + \frac{4}{3}(\kappa t)^3\,\mathrm{Im}\,\beta_0(8|\beta_0|^2 - 1) \\ &\quad + \frac{16}{3}(\kappa t)^4|\beta_0|^2(2|\beta_0|^2 - 1) + \cdots \\ &= 1 + 2\tau\sin\phi_b + 2\tau^2 + \frac{4}{3}\tau^3\sin\phi_b\left(1 - \frac{1}{8N_b}\right) \\ &\quad + \frac{2}{3}\tau^4\left(1 - \frac{1}{2N_b}\right) + \cdots \end{aligned} \tag{153}$$

$$\begin{aligned}\langle[\Delta\hat{P}_a]^2\rangle &= 1 - 4(\kappa t)\,\mathrm{Im}\,\beta_0 + 8(\kappa t)^2|\beta_0|^2 - \frac{4}{3}(\kappa t)^3\,\mathrm{Im}\,\beta_0(8|\beta_0|^2 - 1) \\ &\quad + \frac{16}{3}(\kappa t)^4|\beta_0|^2(2|\beta_0|^2 - 1) + \cdots \\ &= 1 - 2\tau\sin\phi_b + 2\tau^2 - \frac{4}{3}\tau^3\sin\phi_b\left(1 - \frac{1}{8N_b}\right) \\ &\quad + \frac{2}{3}\tau^4\left(1 - \frac{1}{2N_b}\right) + \cdots \end{aligned} \tag{154}$$

The sign of the linear terms in (153) and (154) depends on the sign of $\mathrm{Im}\beta_0$, and this sign decides whether the quadrature is squeezed. These examples illustrate the effectiveness of the symbolic manipulation programs in obtaining such expansions. Previously such calculations have been performed by hand. This approach belongs to the standard methods of quantum optics, and many results based on the power series expansion have been discussed in the book [62], so we restrict ourselves to these few examples only.

B. Numerical Methods

The exact operator expansions presented in the previous section indicated that the parametric approximation fails for sufficiently long evolution times, and, moreover, the quantum character of the pump mode introduces corrections to the field evolution coming from the quantum noise. Since the two parts of the Hamiltonian $\hat{H}_0$ and $\hat{H}_I$ given by Eq. (55) are constants of motion, again we can split the Hilbert space into orthogonal sectors, as before, and introduce for a given number n of the pump mode at frequency 2ω the states

$$|\psi_k^{(n)}\rangle = |2k, n-k\rangle\,, \qquad k = 0, 1, \ldots, n \tag{155}$$

which again form a complete orthogonal basis of states in a sector with given n. Now, however, n is the number of photons of the second-harmonic mode, which

would correspond energetically to the $2n$ photons of the fundamental mode, so the dimension of the sector with given n is $(n+1)\times(n+1)$. Assuming that the initial state of the pump mode is a coherent state $|\beta_0\rangle$ and the signal mode at frequency ω is in the vacuum, we can define the initial state of the field as

$$|\psi(0)\rangle = \sum_{n=0}^{\infty} b_n e^{in\phi_b}|0,n\rangle \tag{156}$$

where

$$b_n = \exp\left(\frac{-N_b}{2}\right)\frac{N_b^{n/2}}{\sqrt{n!}} \tag{157}$$

where $N_b = |\beta_0|^2$, and ϕ_b is the initial phase of the pump field $[\beta_0 = |\beta_0|\exp(i\phi_b)]$. With these initial conditions the resulting state of the field is given by

$$|\psi(t)\rangle = \sum_{n=0}^{\infty} b_n e^{in\phi_b}\sum_{k=0}^{n} c_{2n,k}(t)|2k, n-k\rangle \tag{158}$$

where the coefficients $c_{2n,k}(t)$ are the matrix elements of the evolution operator

$$\begin{aligned} c_{2n,k}(t) &= \left\langle 2k, n-k \middle| \exp\left(\frac{-i\hat{H}_I t}{\hbar}\right) \middle| 0, n \right\rangle \\ &= \sum_{j=0}^{n} e^{-i\lambda_j \kappa t} U_{n-k,j} U_{n,j}^* \end{aligned} \tag{159}$$

Comparing Eqs. (122) and (159), it is clear that the coefficients $c_{n,k}(t)$ and $c_{2n,k}(t)$ are derived from the same matrix U diagonalizing the Hamiltonian $\hat{H}_I$, but they include different elements of the matrix. As before, the coefficients (159) can be calculated numerically by diagonalizing the interaction Hamiltonian $\hat{H}_I$ [55]. The mean number of photons in both modes can be expressed, using the state (158), in the form

$$\begin{aligned} \langle \hat{N}_a(t)\rangle &= \langle\psi(t)|\hat{a}^+\hat{a}|\psi(t)\rangle = \sum_{n=0}^{\infty} b_n^2 \sum_{k=0}^{n} 2k|c_{2n,k}(t)|^2 \\ \langle \hat{N}_b(t)\rangle &= \langle\psi(t)|\hat{b}^+\hat{b}|\psi(t)\rangle = \sum_{n=0}^{\infty} b_n^2 \sum_{k=0}^{n} (n-k)|c_{2n,k}(t)|^2 \end{aligned} \tag{160}$$

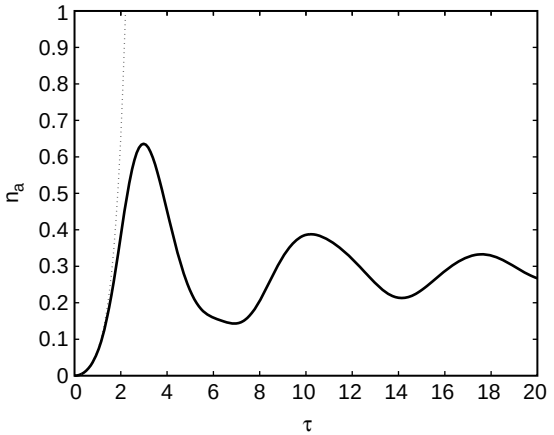

Figure 14. Signal intensity of the degenerate downconverter for the mean number of pump photons $N_b = 10$. Dotted line illustrates the parametric approximation.

where b_n is given by (157). In Fig. 14 we have plotted the signal intensity $n_a = \langle \hat{N}_a(\tau) \rangle / (2N_b)$ at frequency ω as a function of the scaled time $\tau = 2|\beta_0|\kappa t$. The intensity n_a is scaled in such a way that unity at the figure would mean the 100% conversion ratio. For reference we have plotted the normalized signal intensity in the parametric approximation, which is given by $\sinh^2 \tau/(2N_b)$. It is seen that the parametric approximation is valid for $\tau \leq 1$, and it fails for longer evolution times. As in the case of second-harmonic generation, the signal intensity exhibits damped oscillations; however, there is one important difference between the second-harmonic generation and the downconversion process, namely, the conversion ratio that can be achieved in both processes. As it is evident from Fig. 5b as the mean number of photons of the fundamental mode increases, the maximum conversion ratio also increases, becoming closer and closer to 100% efficiency. From Fig. 14 we see that the maximum conversion is below 70% for $N_b = 10$, and contrary to the second-harmonic generation, as the mean number of photons N_b of the pump mode increases the maximum conversion decreases. This effect is illustrated in Fig. 15, where we have plotted the maximum values of the scaled signal intensity n_a as a function of the mean number of photons of the pump mode N_b. This rather counterintuitive result has been discussed by Drobný and Bužek [63] who have found that there is a fundamental limit on the energy transfer in the k-photon downconversion. There is always a fraction of energy that is trapped in the pump mode and cannot be transferred to the downconversion signal and this fraction increases as the intensity of the pump mode becomes higher. If the dynamics of the pump mode

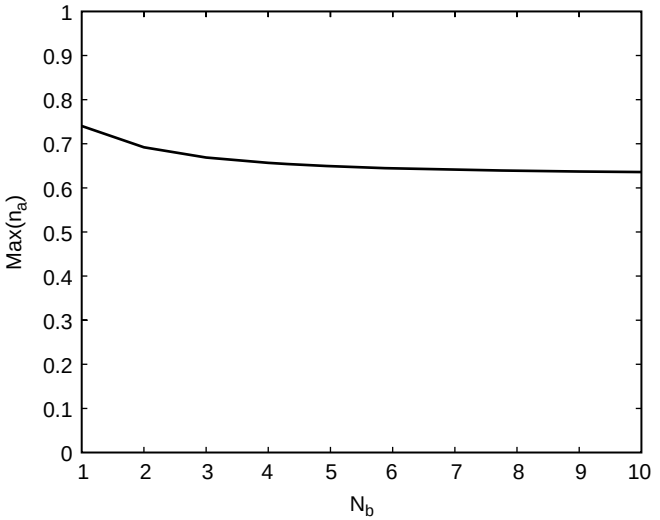

Figure 15. Maximum efficiency of energy transfer in the degenerate downconversion versus the initial mean photon number N_b of the pump mode.

is taken into account the downconversion signal behaves quite differently from the the idealized case when the parametric approximation is done.

The degenerate parametric downconversion is a source of squeezed light, which, as far as the parametric approximation is valid, produces the ideal squeezed states with the quadrature variances $\langle[\Delta\hat{Q}_a]^2\rangle = \exp(-2\tau)$ and $\langle[\Delta\hat{P}_a]^2\rangle = \exp(2\tau)$, which means that for $\tau \to \infty$, one of the variances goes to zero while the other goes to infinity. Thus, the idealized model allows for perfect squeezing. Of course, in a more realistic model in which the quantum noise of the pump mode is taken into account the amount of squeezing that can be obtained is limited. The two quadrature variances calculated numerically for $N_b = 10$ and $\phi_b = -\pi/2$ are illustrated in Fig. 16. For short evolution times τ the variance $\langle[\Delta\hat{Q}_a(\tau)]^2\rangle$ is squeezed, that is, it takes values below unity, that is below the vacuum fluctuations level. The $\hat{Q}$ quadrature is squeezed for the particular choice of the phase of the pump field, $\phi_b = -\pi/2$, in agreement with the analytical results presented in Eq. (99). For $\phi_b = 0$ both quadratures are unsqueezed. The dependence of squeezing on the field phase is a characteristic feature of this effect. The $\hat{Q}$ quadrature variance reaches a minimum below $\tau = 1$ and next shows maxima and minima that, however, do not fall below unity. It is a well-known fact that when the depletion of the pump mode and its quantum character is taken into account, the quadrature noise has finite minimum, and it has been shown [64–66] that the value of squeezing is

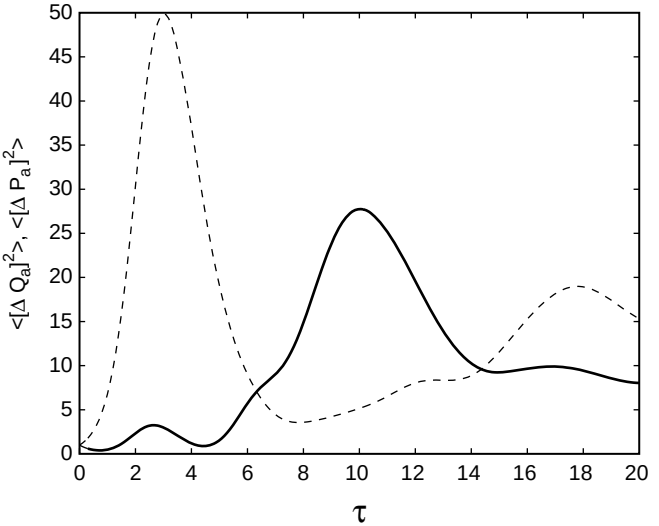

Figure 16. Quadrature variances of the signal mode for $N_b = 10$ and $\phi_b = -\pi/2$: $\langle[\Delta\hat{Q}_a(\tau)]^2\rangle$ (solid line) and $\langle[\Delta\hat{P}_a(\tau)]^2\rangle$ (dashed line).

bounded by $(2\sqrt{N_b})^{-1}$. Kinsler et al. [66] compared various numerical methods, including the number-state calculations and stochastic simulations based on the stochastic differential equations derived from the positive P representation. Here, we use the method of diagonalization of the Hamiltonian in the number-state basis, which is simple but it is applicable only for the pump fields with a not-too-large mean number of photons. Nevertheless, the results obtained in this simple way illustrate pretty well the features of the field produced in the degenerate down converter with quantum pump. In Fig. 17 we have plotted the quadrature variances for several values of the mean number of photons of the pump mode. It is seen that, as the number of photons increases, the solutions remain close to the parametric approximation for longer times, or in other words, the parametric approximation is valid longer as the pump fields are becoming stronger.

Similarly to the second-harmonic generation, we can calculate the Q function for the fields. With the state (158) we find for the two-mode field the formula

$$Q(\alpha,\beta) = \frac{1}{\pi^2}\mathrm{e}^{-(|\alpha|^2+|\beta|^2)}\left|\sum_{n=0}^{\infty} e^{in\phi_b} b_n \sum_{k=0}^{n} \frac{(\alpha^*)^{2k}(\beta^*)^{n-k}}{\sqrt{(2k)!(n-k)!}} c_{2n,k}(t)\right|^2 \tag{161}$$

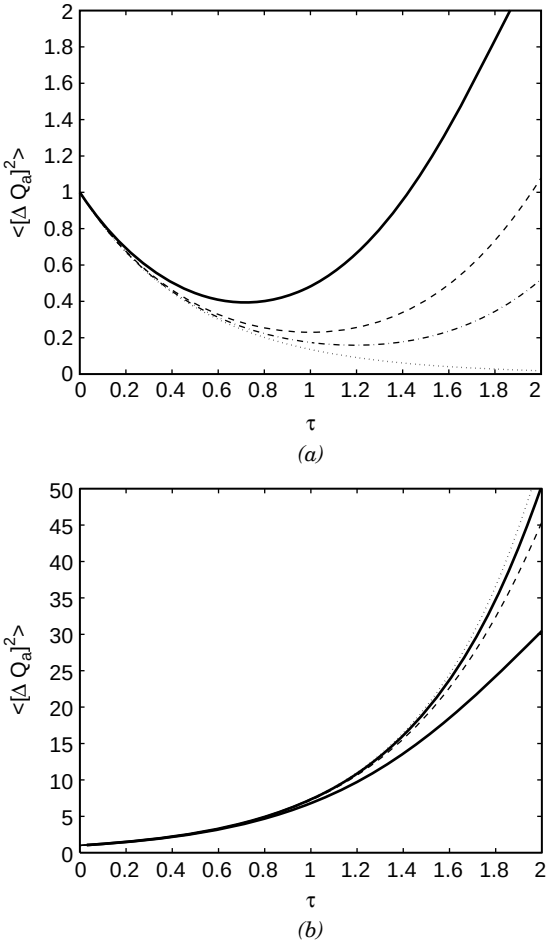

Figure 17. Quadrature variances (a) $\langle[\Delta\hat{Q}_a(\tau)]^2\rangle$ and (b) $\langle[\Delta\hat{P}_a(\tau)]^2\rangle$ for the signal mode with $\phi_b = -\pi/2$ and $N_b = 10$ (solid line), $N_b = 40$ (dashed line), and $N_b = 100$ (dashed–dotted line). Dotted lines represent parametric approximation.

which after corresponding integrations gives the Q functions for individual modes. For the signal mode, we have

$$Q(\alpha) = \frac{1}{\pi} e^{-|\alpha|^2} \sum_{n=0}^{\infty} \sum_{n'=0}^{\infty} e^{i(n-n')\phi_b} b_n b_{n'} \times \sum_{k=0}^{n} \sum_{k'=0}^{n'} \frac{(\alpha^*)^{2k} \alpha^{2k'}}{\sqrt{(2k)!(2k')!}} c_{2n,k}(t) c^*_{2n',k'}(t) \delta_{n-k,n'-k'} \tag{162}$$

and for the pump mode

$$Q(\beta) = \frac{1}{\pi} e^{-|\beta|^2} \sum_{n=0}^{\infty} \sum_{n'=0}^{\infty} e^{i(n-n')\phi_b} b_n b_{n'}$$
$$\times \sum_{k=0}^{\min(n,n')} \frac{(\beta^*)^{n-k} \beta^{n'-k}}{\sqrt{(n-k)!(n'-k)!}} c_{2n,k}(t) c^*_{2n',k}(t) \tag{163}$$

where the coefficients $c_{2n,k}(t)$ are given by (159) and the Poissonian factors b_n, by (157). The contours of the Q functions for the signal (Fig. 18a) and pump (Fig. 18b) modes, for a particular choice of the evolution times, are illustrated in Fig. 18. The squeezing property of the signal is clearly seen for $\tau = 1$, and for a longer time $\tau = 3$ the Q function of the signal mode develops a two-peak structure. All the time the mean amplitude of the signal mode is zero — the quasidistribution exhibits a twofold symmetry around the origin. The pump mode starts from a coherent state with the amplitude $-i\sqrt{10}$, and next the distribution is smeared along the imaginary axis ($\tau = 3$) and concentrates again to an approximately coherent state with the amplitude $i\sqrt{10}$ ($\tau = 6$). It is interesting to compare the shape of the Q functions with the maxima and minima of the intensity of the signal mode shown in Fig. 14.

The classical trajectories approach, described in Section III.D, applied to the downconversion regime confirms pretty well the fully quantum calculations for the quasidistribution functions presented in Fig. 18. Examples of the classical trajectories approach are shown in Fig. 19. Similarly to the second-harmonic generation (see Section III.D), the initial values are taken from the Gaussian distribution with the appropriately adjusted variance and the set of classical equations (59) is solved numerically for 1000 trajectories. As it is evident from Fig. 19, the cloud of points reproduces very well the quasidistribution functions for both modes. The classical trajectories approach has an advantage over the direct quantum calculations with the diagonalization of the Hamiltonian in this that it can be applied to the fields with large number of photons where the diagonalization method cannot be used because of the computer limitations. It has been shown [52] that the Wigner function is the most adequate quasidistribution function to use with classical trajectories approach, and the symmetric ordering associated with the Wigner function should be used to calculate mean values of the physical quantities by averaging over ensembles of classical trajectories. Here we have illustrated both approaches, choosing the mean number of photons $N_b = 10$ for which the calculations can be performed even on small computers.

The Hermitian operator phase formalism of Pegg and Barnett [11–13] allows for quantum calculations of phase distribution for the fields produced in the

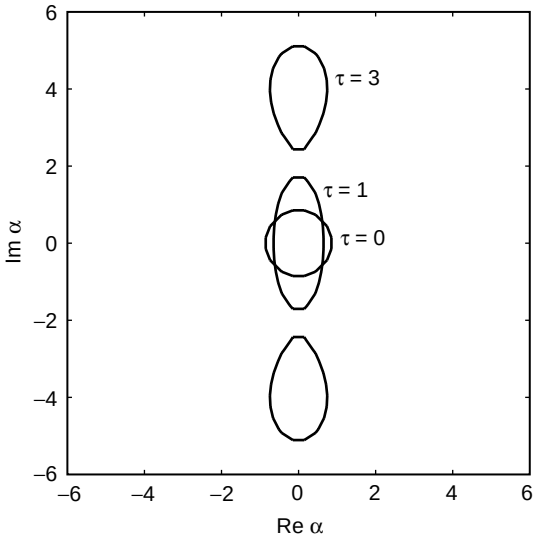

(a)

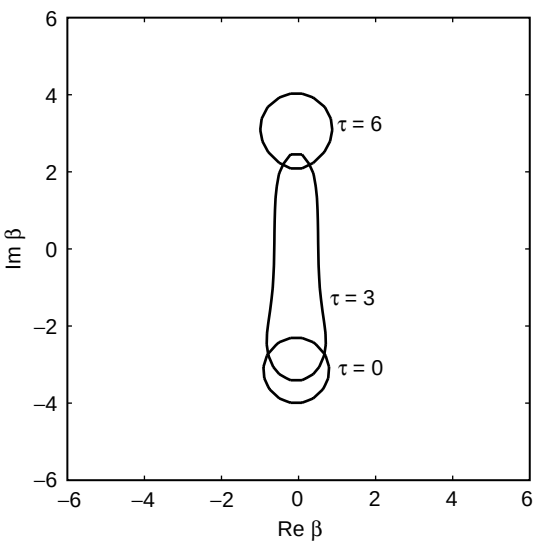

(b)

Figure 18. Contour plots of the Q function for (a) the signal mode and (b) pump mode for $N_b = 10, \phi_b = -\pi/2$, and several values of the evolution time τ. Contours are taken at half the maximum.

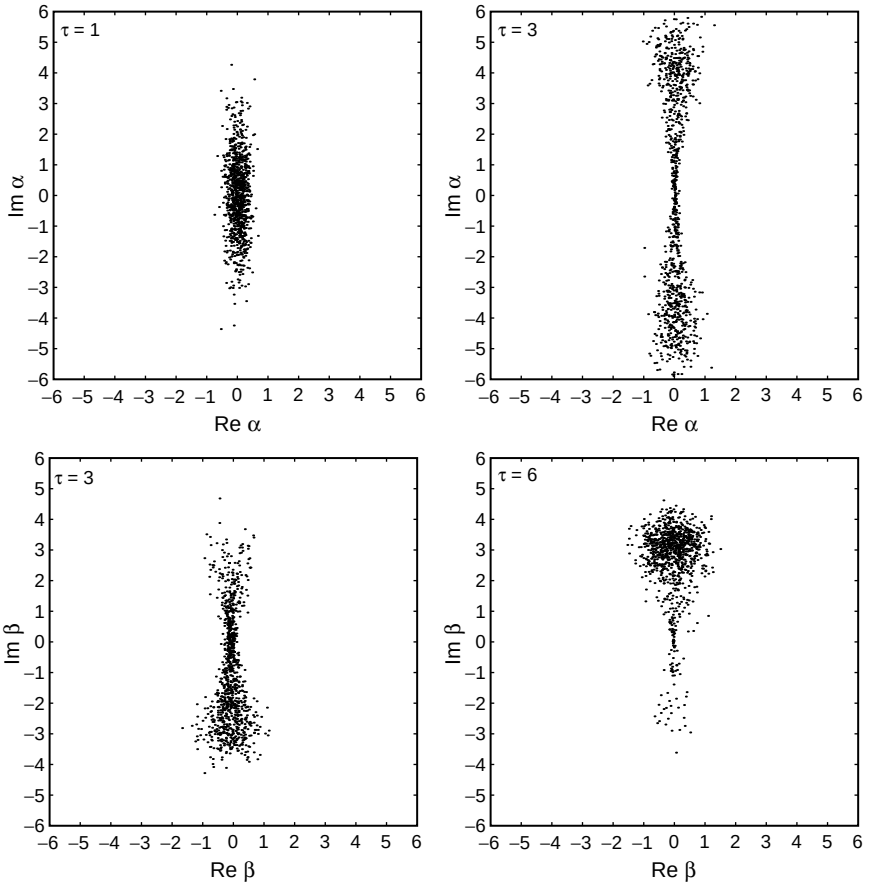

Figure 19. Classical trajectories for 1000 points for Gaussian distribution of initial values and $N_b = 10, \phi_b = -\pi/2$ for the signal mode (upper figures) and the pump mode (lower figures). The evolution times are chosen as to compare with Fig. 18.

downconversion process [55]. The joint phase probability distribution has the following form in this case [16,55]:

$$P(\theta_a, \theta_b) = \frac{1}{(2\pi)^2} \left| \sum_{n=0}^{\infty} b_n \sum_{k=0}^{n} c_{2n,k}(t) \right.$$
$$\left. \times \exp\{-i[2k\theta_a + (n-k)\theta_b + k(2\phi_a - \phi_b)]\} \right. \qquad (164)$$

It is very instructive to compare the joint phase probability distributions for the signal and pump modes produced in the downconversion process shown in

Fig. 20 to the same distribution for the fields produced in the second-harmonic generation process shown in Fig. 13. The differences are clearly visible. The distribution for the downconverted field from the beginning develops a two-peak phase structure, which is a consequence of the two-fold rotational symmetry of the Q function for the signal mode. It is known [57,67] that for k-photon downconversion the Q function has k-fold rotational symmetry and the phase distribution has k peaks, at least at the initial stages of the evolution. From Fig. 20 it is also clear that when the intensity of the signal mode reaches its

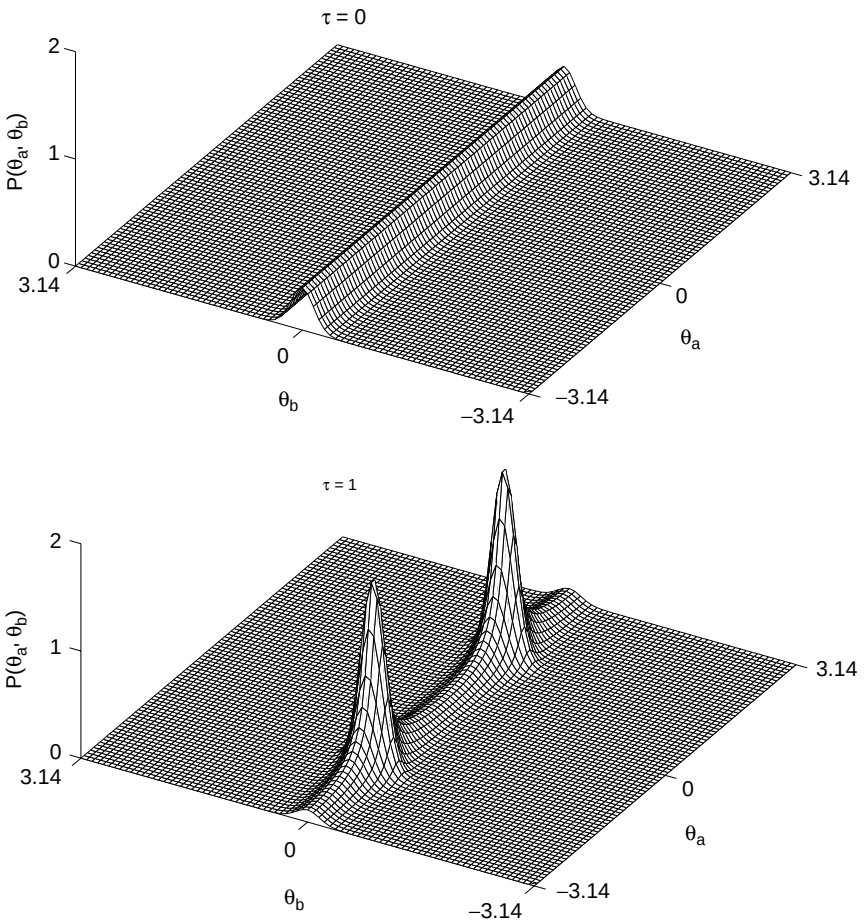

Figure 20. Joint phase probability distribution $P(\theta_a, \theta_b)$ for the signal and pump modes at several evolution times τ and $N_b = 10$. In the last two figures the window for θ_b is shifted $\theta_b \to \theta_b + \pi/2$ and $\theta_b \to \theta_b + \pi$, correspondingly.

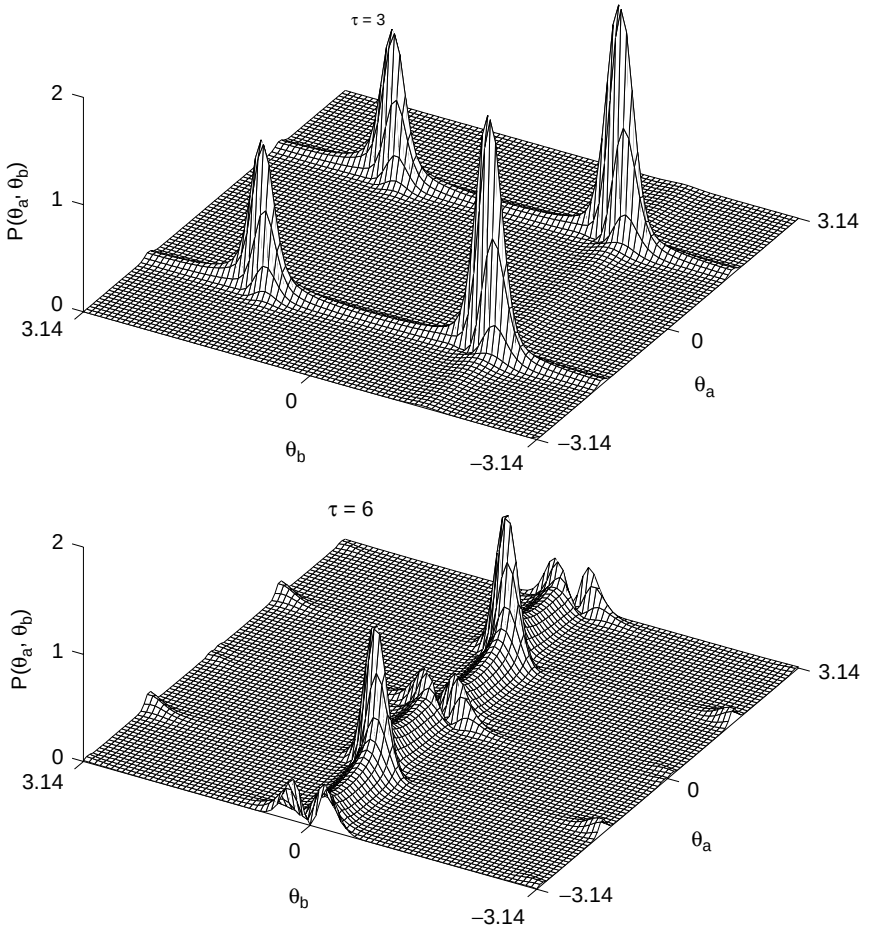

Figure 20. (*Continued*)

maximum ($\tau = 3$), the process is reversed from the downconversion regime to the harmonics generation regime and the phase distribution for θ_b splits into two peaks and a jump in phase by $\pi/2$ appears. For $\tau = 6$, the phase distribution confirms the fact seen from the contours of the Q function, that the pump mode reaches the state close to the initial coherent state but shifted in phase by π. To avoid splitting of the peaks in the phase distribution, we have made corresponding shifts of the phase window for θ_b variable for the last two pictures of Fig. 20, so $\theta_b \to \theta_b + \pi/2$ and $\theta_b \to \theta_b + \pi$, correspondingly. The two-peak structure of the phase distribution is a characteristic feature of the ideal squeezed states. To

compare the ideal squeezed state phase distribution with the distribution for downconversion with quantum pump, we can calculate the marginal phase distribution functions, which are obtained by integrating (164) over one of the phase variables. The result is

$$P(\theta_a) = \frac{1}{2\pi}\left\{1 + 2\,\mathrm{Re}\sum_{n>n'} b_n b_{n'} \sum_{k=0}^{n}\sum_{k'=0}^{n'} c_{2n,k}(t)c^*_{2n',k'}(t) \times \exp[-i(k-k')(2\theta_a + 2\phi_a - \phi_b)]\delta_{n-n',k-k'}\right\}$$

$$P(\theta_b) = \frac{1}{2\pi}\left\{1 + 2\,\mathrm{Re}\sum_{n>n'} b_n b_{n'} \sum_{k=0}^{n'} c_{2n,k}(t)c^*_{2n',k}(t) \times \exp[-i(n-n')\theta_b]\right\} \tag{165}$$

The marginal phase distributions are illustrated in Fig. 21a, where we have plotted the phase distribution $P(\theta_a)$ for the signal mode at the evolution time $\tau = 1$ and the phase distribution for the ideal squeezed state for the same squeezing parameter. The mean number of photons for the pump mode is equal to 10. It is clear that quantum fluctuations of the pump mode cause broadening of the phase distribution, but the two-peak structure of the distribution with the peaks at $\pm\pi/2$ is obvious. For large squeezing, the phase distribution of the ideal squeezed state becomes the sum of two symmetrically placed delta functions

$$P(\theta_a) = \frac{1}{2}\left[\delta\left(\theta_a - \frac{\pi}{2}\right) + \delta\left(\theta_a + \frac{\pi}{2}\right)\right] \tag{166}$$

but the quantum noise present in the pump mode broadens the phase distribution which can never become the delta function distribution. In Fig. 21b we have shown the distribution for the pump mode at the evolution time $\tau = 6$, which is compared to the initial coherent state phase distribution (dotted line). The window for θ_b is shifted by π to be consistent with Fig. 20. The phase distribution of the pump mode for this particular evolution time corroborates what has already been found from previous figures, that at time $\tau = 6$ the state of the pump mode becomes close to the coherent state but shifted in phase by π with respect to the initial state. This illustrates that the phase distribution is a very convenient function to study in order to get information about the quantum state of the field.

Because of the oscillatory behavior of the intensity of the signal mode, which switches the process from the downconversion regime to the second-harmonic

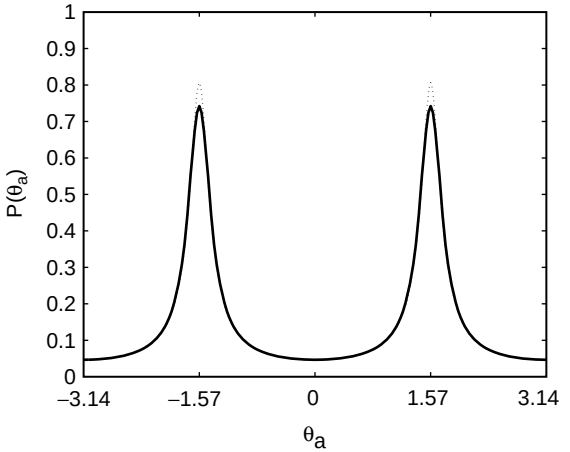

(a)

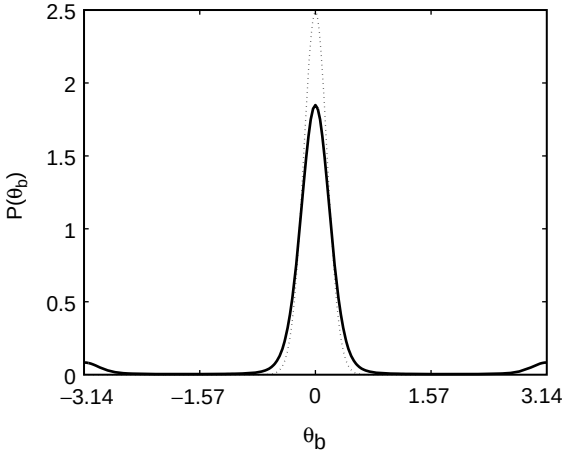

(b)

Figure 21. Marginal phase distributions: (a) $P(\theta_a)$ for $\tau = 1$ (solid line) and ideal squeezed vacuum (dotted line); (b) $P(\theta_b)$ for $\tau = 6$ (solid line) and coherent state with $N_b + 10$ (dotted line). The window for θ_b is shifted by π.

generation regime and back, the structure of the joint phase distribution $P(\theta_a, \theta_b)$ for longer evolution times becomes more complicated. This is true for both the phase distribution that started in the pure SHG regime and the distribution that started in the pure downconversion regime. As the evolution proceeds the subsequent bifurcations of the distribution take place and the effect

of quantum noise accumulates, making the phase distributions more and more flat indicating randomization of the phase. More details on the quantum phase properties of the fields produced in nonlinear optical phenomena can be found in Ref. 16.

V. SUMMARY

In this chapter we have discussed two best-known nonlinear optical phenomena — second-harmonic generation and parametric downconversion — drawing particular attention to the signatures of quantum fluctuations of the optical fields that can be found in the phenomena. The ubiquitous vacuum fluctuations can manifest themselves in various ways when an optical field undergoes nonlinear transformation. The two processes considered here are only examples of a rich variety of nonlinear phenomena, but they are of great practical importance and thus they have been studied for years and a lot of knowledge has been accumulated. It was not our intention to collect all the facts known about the two processes, but rather to select some specific effects illustrating the role of quantum character of the field in the process. We have also presented several theoretical methods that are used to describe quantum properties of the field and are now available to everybody owing to common access to computers and software. Quantum fields are operator quantities that cannot be treated on computers in the same way as ordinary numbers describing classical quantities. However, presently existing computer software allows for symbolic manipulation, which makes it trivial to obtain formulas that would be very difficult or even impossible to obtain by hand. The early results indicating possibility of nonclassical effects such as sub-Poissonian photon statistics or squeezing were based on the power expansions of operator products. We have shown here how it can be done with freely available software using a computer. Also traditional numerical calculations became easy with the use of now existing numerical packages. We have presented examples of such calculations. We have compared quantum statistical properties of the fields produced in the idealized models of second-harmonic generation and downconversion with quantum pump using the same methods of symbolic calculations, approximate analytical methods, the method of classical trajectories with stochastic initial conditions and direct, fully quantum-mechanical calculations using the method of diagonalization of the interaction Hamiltonian. Since both processes discussed in this chapter are described by the same Hamiltonian, the differences between the quantum properties of the field generated in them have their origin in the initial conditions, in particular, in the presence of quantum fluctuations. As we have shown, the differences are quite important and their comparison is very instructive.

APPENDIX A

An example of the FORM [47] program calculating symbolically evolution of the operator $\hat{a}^+(t)\hat{a}(t)$ in the SHG process and the results produced by the program. The program calculates the Taylor series expansion terms up to given order (16 in the example). `T'n'` is the `n`th order term which must be multiplied by $(\kappa t)^n$, and the notation `ad(n)` means $(\hat{a}^+)^n$, and correspondingly `a(n)` means $\hat{a}^n$, where $\hat{a}$ and $\hat{a}^+$ are the annihilation and creation operators for the fundamental beam. In the calculations we assume that initially there are no photons of the second-harmonic beam, that is, after operator calculations we take the expectation value over the vacuum state for the second-harmonic beam. In the program this is performed by identifying $\hat{b}$ and $\hat{b}^+$ as zero after the normal ordering of the operators. The program is very simple (just few lines of code) and very effective (just few seconds on a Dual PIII 450 MHz machine under Linux).

```
FORM by J.Vermaseren. Version 1.1 Dec 14 1998

* calculates Taylor series terms for harmonics generation

  nwrite statistics;
  Symbols n,k;
  Function T,a,ad,b,bd,x,y;
  Set aa:a,ad;
  Set bb:b,bd;

* definitions

  #define MAX "16"
  * Hamiltonian
  Local H=ad*ad*b+a*a*bd;
  * operator the evolution we are looking for
  Local T0=ad*a;
  .sort

* main loop

  #do i=1,'MAX'
  Local T{'i'} = (T{'i'-1}*H-H*T{'i'-1})/i_/'i';
  repeat;
  id x?bb*y?aa=y*x;
  endrepeat;
  .sort
```

```
 repeat;
 id a*ad=ad*a+1;
 id b*bd=bd*b+1;
 endrepeat;
 .sort
 #enddo;
 id b=0;
 id bd=0;
 id x?=x(1);
 repeat;
 id x?(n?)*x?(k?)=x(n+k);
 endrepeat;
 print;
 .end

* results

 T0 = ad(1)*a(1);

 T1 = 0;

 T2 = - 2*ad(2)*a(2);

 T3 = 0;

 T4 = 8/3*ad(3)*a(3) + 4/3*ad(2)*a(2);

 T5 = 0;

 T6 = - 136/45*ad(4)*a(4) - 128/45*ad(3)*a(3) - 16/45*ad(2)*a(2);

 T7 = 0;

 T8 = 992/315*ad(5)*a(5) + 184/35*ad(4)*a(4) + 416/315*ad(3)*a(3)
     + 16/315*ad(2)*a(2);

 T9 = 0;

 T10 = - 44224/14175*ad(6)*a(6) - 4544/567*ad(5)*a(5) - 12128/
   2835*ad(4)*a(4)
     - 1024/2835*ad(3)*a(3) - 64/14175*ad(2)*a(2);

 T11 = 0;
```

```
T12 = 1398016/467775*ad(7)*a(7) + 730976/66825*ad(6)*a(6)
    + 914944/93555*ad(5)*a(5) + 67904/31185*ad(4)*a(4)
    + 2816/42525*ad(3)*a(3) + 128/467775*ad(2)*a(2);

T13 = 0;

T14 = - 118984832/42567525*ad(8)*a(8) - 65317888/4729725*
  ad(7)*a(7)
    - 12242816/654885*ad(6)*a(6) - 1856000/243243*ad(5)*a(5)
    - 4741376/6081075*ad(4)*a(4) - 4096/467775*ad(3)*a(3)
    - 512/42567525*ad(2)*a(2);

T15 = 0;

T16 = 1639572992/638512875*ad(9)*a(9) + 2102147456/
127702575*ad(8)*a(8)
    + 20049444736/638512875*ad(7)*a(7) + 378236224/
   18243225*ad(6)*a(6)
    + 43331584/10135125*ad(5)*a(5) + 6365056/30405375*ad(4)*a(4)
    + 559616/638512875*ad(3)*a(3) + 256/638512875*ad(2)*a(2);
```

APPENDIX B

An example of the program that can be run using the free available software OCTAVE [50] (under Linux) or the commercial software MATLAB [51] (under Linux or MS Windows). The program calculates numerically the intensity of the second-harmonic using the procedure of diagonalizing the interaction Hamiltonian described in the text (Section III.D).

```
% program intensity.m
% calculates the intensity of the second-harmonic
% using diagonalization of the interaction Hamiltonian
% int2 - second-harmonic intensity
% int1 - fundamental mode intensity

clear
nav=input(' mean number of photons: ');
nmax=input(' nmax:  ');
tmax=input(' taumax: ');
t=0:tmax/511:tmax;

tic;
int2=zeros(1,512);
```

```
% Poisson distribution
b(1)=exp(-nav);
b(2)=b(1)*nav;
for n=2:nmax
b(n+1)=b(n)*nav/n;

% calculates the Hamiltonian H
nd=floor(n/2)+1;
nd1=floor((nd-1)/2);
hk=zeros(nd-1,1);
 for k=0:nd-2
 hk(k+1,1)=sqrt((k+1)*(n-2*k)*(n-2*k-1));
 end
 H=diag(hk,1)+diag(hk,-1);

% diagonalization with scaling
 [u e]=eig(H./sqrt(2*nav));
% [u e]=eig(H);
 [e l]=sort(diag(e));
 u=u(:,l);

% calculation of the intensity
 cz=0;
  for k=0:nd-1;
  c=0;
   if rem(k,2)==0;
    for l=0:nd1;
    c=c+u(k+1,l+1)*u(1,l+1)*cos(e(l+1,1)*t);
    end
   else
    for l=0:nd1;
    c=c+u(k+1,l+1)*u(1,l+1)*sin(e(l+1,1)*t);
    end
   end
  c=2*c;
    if rem(nd+1,2)==0;
    c=c-u(k+1,nd1+1)*u(1,nd1+1);
    end
  cz=cz+k*c.^2;
  end
 int2=int2+b(n+1)*cz;     % second-harmonic intensity
end
```

```
int1=nav-2*int2;        % fundamental intensity
r=int1/nav;
toc
plot(t,r);
xlabel('time'),ylabel('intensity ');
```

References

1. Y. R. Shen, *The Principles of Nonlinear Optics*, Wiley, New York, 1985.
2. S. Kielich, *Nonlinear Molecular Optics*, Nauka, Moscow, 1981 (in Russian).
3. C. W. Gardiner, *Quantum Noise*, Springer, Berlin, 1991.
4. P. L. Knight and R. Loudon, *J. Mod. Opt.* **34**, 709 (1987).
5. R. Loudon and P. L. Knight, *J. Mod. Opt.* **34**, 709 (1987).
6. M. C. Teich and B. E. A. Saleh, *Quantum Opt.* **1**, 153 (1989).
7. J. Peřina, *Quantum Statistics of Linear and Nonlinear Optical Phenomena*, 2 ed., Kluwer, Dordrecht, 1991.
8. L. Davidovich, *Rev. Mod. Phy.* **68**, 127 (1996).
9. L. Mandel, *Opt. Commun.* **42**, 437 (1982).
10. K. E. Cahill and R. J. Glauber, *Phys. Rev.* **177**, 1857 (1969).
11. D. T. Pegg and S. M. Barnett, *Europhys. Lett.* **6**, 483 (1988).
12. S. M. Barnett and D. T. Pegg, *J. Mod. Opt.* **36**, 7 (1989).
13. D. T. Pegg and S. M. Barnett, *Phys. Rev. A* **39**, 1665 (1989).
14. W. H. Louisell, *Quantum Statistical Properties of Radiation*, J Wiley, New York, 1973.
15. D. T. Pegg and S. M. Barnett, *Phys. Rev. A* **43**, 2579 (1991).
16. R. Tanaś, A. Miranowicz, and T. Gantsog, in E. Wolf (Ed.), *Progress in Optics*, Elsevier Scientific, Amsterdam, 1996, Vol. XXXV, pp. 355–446.
17. V. Peřinová, A. Lukš, and J. Peřina, *Phase in Optics*, World Scientific, Singapore, 1998.
18. P. A. Franken, A. E. Hill, C. W. Peters, and G. Weinreich, *Phys. Rev. Lett.* **7**, 118 (1961).
19. D. F. Walls and C. T. Tindle, *Nuovo Cimento Lett.* **2**, 915 (1971).
20. D. F. Walls and C. T. Tindle, *J. Phys. A* **5**, 534 (1972).
21. M. Kozierowski and R. Tanaś, *Opt. Commun.* **21**, 229 (1977).
22. L. A. Wu, H. J. Kimble, J. L. Hall, and H. Wu, *Phys. Rev. Lett.* **57**, 2520 (1986).
23. S. Kielich, M. Kozierowski, and R. Tanaś, *Optica Acta* **32**, 1023 (1985).
24. S. P. Nikitin and A. V. Masalov, *Quantum Opt.* **3**, 105 (1991).
25. B. Yurke and D. Stoler, *Phys. Rev. Lett.* **57**, 13 (1986).
26. P. Tombesi and A. Mecozzi, *J. Opt. Soc. Am. B* **4**, 1700 (1987).
27. A. Miranowicz, R. Tanaś, and S. Kielich, *Quantum Opt.* **2**, 253 (1990).
28. T. Gantsog and R. Tanaś, *J. Mod. Opt.* **38**, 1021 (1991).
29. G. S. Agarwal and R. R. Puri, *Phys. Rev. A* **40**, 5179 (1989).
30. T. Gantsog and R. Tanaś, *Quantum Opt.* **3**, 33 (1991).
31. J. Bajer and P. Lisoněk, *J. Mod. Opt.* **38**, 719 (1991).
32. J. Bajer and J. Peřina, *Opt. Commun.* **92**, 99 (1992).

33. R. F. Alvarez-Estrada, A. Gómez-Nicola, L. L. Sánchez-Soto, and A. Luis, *J. Phys. A* **28**, 3439 (1995).
34. T. Gantsog, R. Tanaś, and R. Zawodny, *Phys. Lett. A* **155**, 1 (1991).
35. G. Drobný and I. Jex, *Phys. Lett. A* **169**, 273 (1992).
36. J. Bajer, O. Haderka, and J. Peřina, *J. Opt. B: Quantum Semiclass. Opt.* **1**, 529 (1999).
37. J. Bajer, J. Peřina, O. Haderka, and A. Miranowicz, *Czech. J. Phys.* **50**, 717 (2000).
38. M. K. Olsen, R. J. Horowicz, L. I. Plimak, N. Treps, and C. Fabre, *Phys. Rev. A* **61**, 021803 (2000).
39. P. D. Drummond, K. J. McNeil, and D. F. Walls, *Optica Acta* **27**, 321 (1980).
40. P. D. Drummond, K. J. McNeil, and D. F. Walls, *Optica Acta* **28**, 211 (1981).
41. P. Szlachetka and K. Grygiel, "Chaos in optical systems", this volume.
42. A. Bandilla, G. Drobný, and I. Jex, *Opt. Commun.* **128**, 353 (1996).
43. G. Drobný, A. Bandilla, and I. Jex, *Phys. Rev. A* **55**, 78 (1997).
44. Z. Y. Ou, *Phys. Rev. A* **49**, 2106 (1994).
45. R. D. Li and P. Kumar, *Phys. Rev. A* **49**, 2157 (1994).
46. R. Tanaś, *Optik* **40**, 109 (1974).
47. J. A. M. Vermaseren, *FORM*, 1989, version 1 of the program is available from ftp.nikhef.nl.
48. J. Mostowski and K. Rzązewski, *Phys. Lett. A* **66**, 275 (1978).
49. D. F. Walls and R. Barakat, *Phys. Rev. A* **1**, 446 (1970).
50. J. W. Eaton, *GNU Octave. A High-Level Interactive Language for Numerical Computations*, (1997), OCTAVE is available from http://www.octave.org/,.
51. Matlab, is a product of The MathWorks, Inc., see http://www.mathworks.com.
52. D. Kupiszewska and K. Rzązewski, *Phys. Rev. A* **42**, 6869 (1990).
53. R. Tanaś, T. Gantsog, and R. Zawodny, *Quantum Opt.* **3**, 221 (1991).
54. J. A. Vaccaro and D. T. Pegg, *Opt. Commun.* **70**, 529 (1989).
55. T. Gantsog, R. Tanaś, and R. Zawodny, *Opt. Commun.* **82**, 345 (1991).
56. T. Gantsog and R. Tanaś, *J. Mod. Opt.* **38**, 1537 (1991).
57. R. Tanaś and T. Gantsog, *Phys. Rev. A* **45**, 5031 (1992).
58. P. Kinsler and P. D. Drummond, *Phys. Rev. A* **43**, 6194 (1991).
59. M. D. Reid and L. Křippner, *Phys. Rev. A* **47**, 552 (1993).
60. G. Drobný, I. Jex, and V. Buzek, *Phys. Rev. A* **48**, 569 (1993).
61. H. P. Yuen, *Phys. Rev. A* **13**, 2226 (1976).
62. J. Peřina, *Quantum Statistics of Linear and Nonlinear Optical Phenomena*, 2nd ed., Kluwer, Dordrecht, 1991.
63. G. Drobný and V. Bužek, *Phys. Rev. A* **50**, 3492 (1994).
64. M. Hillery and M. S. Zubairy, *Phys. Rev. A* **29**, 1275 (1984).
65. D. D. Crouch and S. L. Braunstein, *Phys. Rev. A* **38**, 4696 (1988).
66. P. Kinsler, M. Fernée, and P. D. Drummond, *Phys. Rev. A* **48**, 3310 (1993).
67. S. L. Braunstein and C. M. Caves, *Phys. Rev. A* **42**, 4115 (1990).

QUANTUM INTERFERENCE IN ATOMIC AND MOLECULAR SYSTEMS

ZBIGNIEW FICEK

Department of Physics and Centre for Laser Science,
The University of Queensland, Brisbane, Australia

CONTENTS

I. INTRODUCTION

The concept of optical interference began with the Michelson and Young's experiments [1], in which a beam of light is divided into two beams and, after traveling a distance long compared to the optical wavelength, these two beams are recombined at an observation point. If there is a small path difference between the beams, interference fringes are found in the observation (recombination) point. The observation of the fringes is a manifestation of temporal coherence (Michelson interferometer) or spatial coherence (Young interferometer) between the two light beams. The interference experiments played a central role in early discussions of the dual nature of light, and the appearance of an interference pattern was recognized as a demonstration that light is a wave. The interpretation of the interference experiments changed with the birth of quantum mechanics, when corpuscular properties of light showed up in many experiments. According to the quantum-mechanical interpretation, given by Dirac [2], the interference pattern observed in the Young double-slit experiment results from a superposition of the probability amplitudes of a single photon to take either of two possible pathways.

The phenomenon of optical interference can be observed not only between two light beams but also between radiation fields emitted from a small number of atoms or molecules, or even in the radiation field emitted from a single multilevel system [3]. The atoms or atomic transitions can be regarded as point sources of radiation, similar to the slits in Young's original experiment. In this case interference results from a superposition of the transition amplitudes between quantum states of the atom, and this phenomenon has been designated as quantum interference. The essential feature of quantum interference is the existence of linear superpositions of the atomic states that can be induced by external or internal fields, or even by the coupling of the atomic states through the environment (vacuum field). The existence of interference among multichannel transitions in atoms or molecules is one of the fundamental aspects of

quantum mechanics that demonstrates the difference between a superposition of states and a mixture of states.

The interest in quantum interference stems from the early 1970s when Agarwal [4] showed that the ordinary spontaneous decay of an excited degenerate V-type three-level atom can be modified due to interference between the two atomic transitions. The analysis of quantum interference has since been extended to other configurations of three- and multilevel atoms and many interesting effects have been predicted, which can be used to control optical properties of quantum systems, such as high-contrast resonances [5,6], electromagnetically induced transparency [7], amplification without population inversion [8], and enhancement of the index of refraction without absorption [9].

Spontaneous emission arises from the coupling of a system to the environment and is a source of undesirable noise (decoherence), which imposes limits on spectroscopic measurements, population inversion, and quantum information processing. The control and suppression of spontaneous emission is very significant in the context of quantum computation, teleportation, and quantum information theory. Thus, ways of reducing decoherence are of particular importance. Among the different methods proposed to suppress spontaneous emission, quantum interference has been recognized as the most significant mechanism for modifying and suppression of spontaneous emission.

The effect of quantum interference on spontaneous emission in atomic and molecular systems is the generation of superposition states that can be manipulated, to reduce the interaction with the environment, by adjusting the polarizations of the transition dipole moments, or the amplitudes and phases of the external driving fields. With a suitable choice of parameters, the superposition states can decay with controlled and significantly reduced rates. This modification can lead to subnatural linewidths in the fluorescence and absorption spectra [5,10]. Furthermore, as will be shown in this review, the superposition states can even be decoupled from the environment and the population can be trapped in these states without decaying to the lower levels. These states, known as dark or trapped states, were predicted in many configurations of multilevel systems [11], as well as in multiatom systems [12].

Although the trapping states have the common property that the population will stay in such a state for an extremely long time, they can be implemented in different ways. In a multilevel system the population can be trapped in a linear superposition of the bare atomic states, or in a dressed state corresponding to an eigenstate of the atoms plus external fields, or in some cases, in one of the excited states of the system.

In this review we discuss the major effects resulting from the modification of spontaneous emission by quantum interference. We begin in Section II by presenting elementary concepts and definitions of the first- and second-order correlation functions, which are frequently used in the analysis of the inter-

ference phenomena. Section III describes the master equation approach used for analyzing quantum interference effects in atomic and molecular systems. In Sections IV and V we review the fundamental quantum interference effects in spontaneous emission and in coherently driven systems. We discuss different schemes for suppression of spontaneous emission and population trapping and give an alternative explanation of these effects in the dressed-atom picture. Sections VI deals with the problem of amplification on dark transitions, which are important for information processing without spontaneous emission. The effect of quantum interference on photon correlations is discussed in Section VII. Multilevel systems composed of two transitions with parallel dipole moments and methods for generating two transitions with nonorthogonal dipole moments are briefly discussed in Section VIII. The final section (Section IX) deals with the experimental demonstration of constructive and destructive interference effects in a driven molecular system.

II. INTERFERENCE AND OPTICAL COHERENCE

The phenomenon of optical interference is commonly describable in completely classical terms, in which optical fields are represented by classical waves. Classical and quantum theories of optical interference readily explain the presence of an interference pattern, but there are interference effects that distinguish the quantum (photon) nature of light from the wave nature. In this section, we present elementary concepts and definitions of both the classical and quantum theories of optical interference and illustrate the role of optical coherence.

A. Classical Interference

1. *First-Order Coherence*

The Young's double-slit experiment is the prototype for a demonstration of an optical interference and for all quantitative measurements of so-called first-order coherence. The presence of the interference fringes in the experiment may be regarded as a manifestation of the first-order coherence.

A schematic diagram of an interference experiment of the Young type is shown in Fig. 1. Two light beams of amplitudes $\mathbf{E}_1(\mathbf{r}_1, t_1)$ and $\mathbf{E}_2(\mathbf{r}_2, t_2)$ produced at two slits S_1 and S_2 located at $\mathbf{r}_1$ and $\mathbf{r}_2$, respectively, incident on the screen at a point P. The resulting field detected at the point P is a linear superposition of the two fields

$$\mathbf{E}(\mathbf{R}, t) = \mathbf{E}_1(\mathbf{R}, t) + \mathbf{E}_2(\mathbf{R}, t) \tag{1}$$

where $\mathbf{E}_i(\mathbf{R}, t)$ is the electric field produced by the ith slit and evaluated at the position $\mathbf{R}$ of the observation point P. We can relate the field $\mathbf{E}_i(\mathbf{R}, t)$ to the field

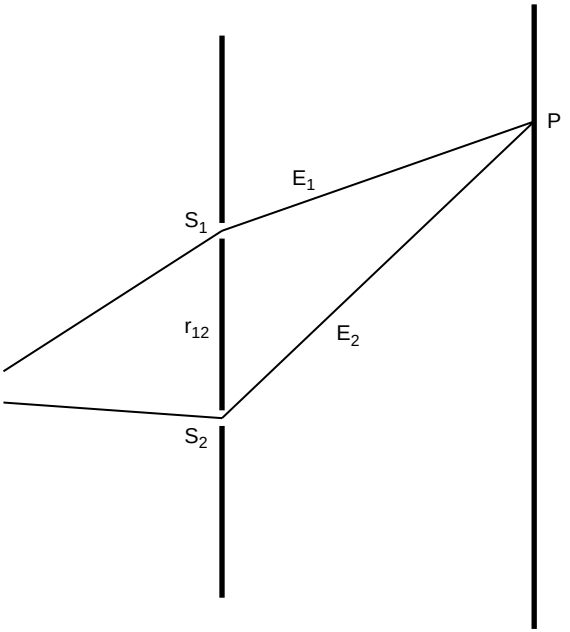

Figure 1. Schematic diagram of the Young's double-slit experiment.

$\mathbf{E}_i(\mathbf{r}_i, t - t_i)$ at the position of the ith slit. This is given by the relation [1]

$$\mathbf{E}_i(\mathbf{R}, t) = \frac{a_i}{R_i}\mathbf{E}_i(\mathbf{R}_i, t - t_i) \tag{2}$$

where $R_i = |\mathbf{R} - \mathbf{r}_i|$ denotes the distance between the point $\mathbf{R}$ on the screen and the position of the ith slit, $t_i = R_i/c$, and a_i is a constant that depends on the geometry and the size of the ith slit.

The instantaneous intensity $I(\mathbf{R}, t)$ of the combined field detected at the point P at time t is defined by a scalar product of the field amplitude and its complex conjugate as

$$I(\mathbf{R}, t) = \mathbf{E}^*(\mathbf{R}, t) \cdot \mathbf{E}(\mathbf{R}, t) \tag{3}$$

and substituting Eqs. (1) and (2), we obtain

$$\begin{aligned} I(\mathbf{R}, t) = {} & |u_1|^2 I_1(\mathbf{R}_1, t - t_1) + |u_2|^2 I_2(\mathbf{R}_2, t - t_2) \\ & + 2\mathrm{Re}(u_1^* u_2 \mathbf{E}_1^*(\mathbf{R}_1, t - t_1) \cdot \mathbf{E}_2(\mathbf{R}_2, t - t_2)) \end{aligned} \tag{4}$$

where $I_i(\mathbf{R}_i, t - t_i)$ is the intensity from the ith slit in the absence of the other, and $u_i = a_i/R_i$.

Hence, the average value of $I(\mathbf{R}, t)$ over an ensemble of different realizations of the field may be written as

$$\begin{aligned}\langle I(\mathbf{R}, t)\rangle = |u_1|^2\langle I_1(\mathbf{R}_1, t - t_1)\rangle + |u_2|^2\langle I_2(\mathbf{R}_2, t - t_2)\rangle \\ + 2\mathrm{Re}\{u_1^* u_2 G^{(1)}(\mathbf{R}_1, t - t_1; \mathbf{R}_2, t - t_2)\}\end{aligned} \tag{5}$$

where

$$G^{(1)}(\mathbf{R}_1, t - t_1; \mathbf{R}_2, t - t_2) = \langle \mathbf{E}_1^*(\mathbf{R}_1, t - t_1) \cdot \mathbf{E}_2(\mathbf{R}_2, t - t_2)\rangle \tag{6}$$

is the first-order correlation function between the field at $\mathbf{R}_2$ and the complex conjugate field at $\mathbf{R}_1$, at times t_2 and t_1, respectively.

It is convenient to introduce the normalized first-order correlation function as

$$\begin{aligned}g^{(1)}(\mathbf{R}_1, t_1; \mathbf{R}_2, t_2) &= \frac{G^{(1)}(\mathbf{R}_1, t_1; \mathbf{R}_2, t_2)}{\sqrt{G^{(1)}(\mathbf{R}_1, t_1; \mathbf{R}_1, t_1) G^{(1)}(\mathbf{R}_2, t_2; \mathbf{R}_2, t_2)}} \\ &= \frac{G^{(1)}(\mathbf{R}_1, t_1; \mathbf{R}_2, t_2)}{\sqrt{I_1(\mathbf{R}_1, t_1) I_2(\mathbf{R}_2, t_2)}},\end{aligned} \tag{7}$$

satisfying the condition $1 \leq |g^{(1)}| \leq 1$. The normalized correlation function (7) is often called the *degree of coherence* and $g^{(1)} = 0$ for two independent fields, whereas $g^{(1)} = 1$ for the perfectly correlated fields. The intermediate values of $g^{(1)}$ $(0 < |g^{(1)}| < 1)$ characterize a partial correlation (coherence) between the fields.

The average intensity $\langle I(\mathbf{R}, t)\rangle$ at the point P depends on $g^{(1)}$ and in the case of identical slits $(u_1 = u_2)$ and the perfectly correlated fields $(|g^{(1)}| = 1)$, the intensity can vary from $(\sqrt{I_1} - \sqrt{I_2})^2$ to $(\sqrt{I_1} + \sqrt{I_2})^2$, giving so-called interference pattern. Thus, for equal intensities of the two fields $(I_1 = I_2 = I_0)$, the total average intensity can vary at the point P from $\langle I\rangle_{\min} = 0$ to $\langle I\rangle_{\max} = 4\langle I_0\rangle$, giving maximal interference pattern. For two independent fields, $g^{(1)} = 0$, and than the resulting intensity at P is just a sum of the intensities of the two fields that does not vary with the position of P.

The usual measure of the depth of modulation (sharpness) of interference fringes is a visibility in an interference pattern defined as

$$\mathscr{V}(\mathbf{R}) = \frac{\langle I(\mathbf{R}, t)\rangle_{\max} - \langle I(\mathbf{R}, t)\rangle_{\min}}{\langle I(\mathbf{R}, t)\rangle_{\max} + \langle I(\mathbf{R}, t)\rangle_{\min}}, \tag{8}$$

where $\langle I(\mathbf{R}, t)\rangle_{\max}$ and $\langle I(\mathbf{R}, t)\rangle_{\min}$ represent the intensity maxima and minima at the point P.

Since

$$\langle I \rangle_{\max} = \langle I_1 \rangle + \langle I_2 \rangle + 2\sqrt{I_1 I_2}|g^{(1)}| \tag{9}$$

and

$$\langle I \rangle_{\min} = \langle I_1 \rangle + \langle I_2 \rangle - 2\sqrt{I_1 I_2}|g^{(1)}| \tag{10}$$

we obtain

$$\mathscr{V}(\mathbf{R}) = \frac{2\sqrt{I_1 I_2}}{(I_1 + I_2)}|g^{(1)}| \tag{11}$$

Thus, $|g^{(1)}|$ determines the visibility of the interference fringes. In the special case of equal intensities of the two fields $(I_1 = I_2)$, Eq. (11) reduces to $\mathscr{V}(\mathbf{R}) = |g^{(1)}|$; $|g^{(1)}|$ is then simply equal to the visibility. For perfectly correlated fields $|g^{(1)}| = 1$, and then $\mathscr{V}(\mathbf{R}) = 1$, while $\mathscr{V}(\mathbf{R}) = 0$ for uncorrelated fields. When $I_1 \neq I_2$, the visibility is always smaller than one even for perfectly correlated fields. This fact is related to the problem of extracting which-way information has been transferred through the slits into the point P. The observation of an interference pattern and the acquisition of which-way information has been transmitted are mutually exclusive. We can introduce an inequality according to which the fringe visibility $\mathscr{V}$ displayed at the point P and an absolute upper bound on the amount of which-way information $\mathscr{D}$ that can be detected at the point P are related by [13]

$$\mathscr{D}^2 + \mathscr{V}^2 \leq 1 \tag{12}$$

Hence, the extreme situations characterized by perfect fringe visibility $(\mathscr{V} = 1)$ or full knowledge of which way information has been transmitted $(\mathscr{D} = 1)$ are mutually exclusive. In order to distinguish which-way information has been transmitted, one can locate an intensity detector at the point P and adjust it to measure a field of a particular intensity I_d. When the fields coming from the slits have the same intensities, the detector cannot distinguish which-way the detected field came to the point P, so there is no which-way information available $(\mathscr{D} = 0)$ resulting in perfect fringe visibility $(\mathscr{V} = 1)$. On the other hand, when the intensities of the fields are different $(I_1 \neq I_2)$, the detector adjusted to measure a particular intensity can distinguish which way the field came to the point P resulting in the disappearance of the interference fringes. This is clearly seen from Eq. (11); if $I_1 \gg I_2$ or $I_1 \ll I_2$, the visibility $\mathscr{V} \approx 0$ even for $|g^{(1)}| = 1$. The same arguments apply to frequencies and phases of the detected fields.

The information about the frequencies and phases of the detected fields is provided by the argument (phase) of $g^{(1)}$. Moreover, the phase of $g^{(1)}$ determines positions of the fringes in the interference pattern. If the observation point P lies in the far-field zone of the radiation emitted by the slits, the fields at the observation point can be approximated by plane waves for which we can write

$$\begin{aligned}\mathbf{E}(\mathbf{R}_i, t - t_i) &\approx \mathbf{E}(\mathbf{R}_i, t)e^{-i(\omega_i t_i + \phi_i)} \\ &= \mathbf{E}(\mathbf{R}_i, t)e^{-i(\omega_i R_i/c + \phi_i)}, \quad i = 1, 2\end{aligned} \tag{13}$$

where ω_i is the angular frequency of the ith field and ϕ_i is its initial phase, which, in general, can depend on time. We can center the frequencies around the average frequency of the two fields as

$$\begin{aligned}\omega_1 &= \omega_0 + \frac{1}{2}\Delta \\ \omega_2 &= \omega_0 - \frac{1}{2}\Delta\end{aligned} \tag{14}$$

where $\omega_0 = (\omega_1 + \omega_2)/2$ is the average frequency of the fields, and $\Delta = \omega_1 - \omega_2$.

Since the observation point lies in far-field zone of the radiation emitted by the slits, that is, the separation between the slits is very small compared to the distance to the point P, we can write approximately

$$R_i = |\mathbf{R} - \mathbf{r}_i| \approx R - \bar{\mathbf{R}} \cdot \mathbf{r}_i \tag{15}$$

where $\bar{\mathbf{R}} = \mathbf{R}/R$ is the unit vector in the direction $\mathbf{R}$. Hence, substituting Eq. (13) with (14) and (15) into Eq. (7), we obtain

$$g^{(1)}(\mathbf{R}_1, t_1; \mathbf{R}_2, t_2) = |g^{(1)}(\mathbf{R}_1, t; \mathbf{R}_2, t)|e^{ik_0\bar{\mathbf{R}}\cdot\mathbf{r}_{12}}e^{i(k_0\tilde{R}\frac{\Delta}{\omega_0} + \delta\phi)} \tag{16}$$

where $\mathbf{r}_{12} = \mathbf{r}_2 - \mathbf{r}_1$ is the distance between the slits, $\tilde{R} = R + \frac{1}{2}\bar{\mathbf{R}} \cdot (\mathbf{r}_1 + \mathbf{r}_2)$, $\delta\phi = \phi_1 - \phi_2$, $k_0 = \omega_0/c = 2\pi/\lambda_0$, and λ_0 represents the mean wavelength of the fields. Let us analyze the physical meaning of the exponences appearing on the right-hand side (r.h.s) of Eq. (16). The first exponence depends on the separation between the slits and the position $\mathbf{R}$ of the point P. For small separations the exponence slowly changes with the position $\mathbf{R}$ and leads to minima and maxima in the interference pattern. The minima appear whenever

$$k_0\bar{\mathbf{R}} \cdot \mathbf{r}_{12} = (2n + 1)\pi, \quad n = 0, \pm 1, \pm 2, \ldots \tag{17}$$

The second exponence, appearing in Eq. (16), depends on the sum of the position of the slits, the ratio Δ/ω_0, and the difference $\delta\phi$ between the initial phases of the fields. This term introduces limits on the visibility of the interference pattern and can affect the pattern only if the frequencies and the initial phases of the fields are different. Even for equal and well-stabilized phases, but significantly different frequencies of the fields such that $\Delta/\omega_0 \approx 1$, the exponence oscillates rapidly, with $\mathbf{R}$ leading to the disappearance of the interference pattern. Thus, in order to observe an interference pattern, it is important to have two fields of well stabilized phases and equal or nearly equal frequencies. Otherwise, no interference pattern can be observed even if the fields are perfectly correlated.

The dependence of the interference pattern on the frequencies and phases of the fields is related to the problem of extracting which way information has been transferred to the observation point P. For perfectly correlated fields with equal frequencies ($\Delta = 0$) and equal initial phases ($\phi_1 = \phi_2$), the total intensity at the point P is

$$\langle I(\mathbf{R})\rangle = 2\langle I_0\rangle(1 + \cos k_0\bar{\mathbf{R}} \cdot \mathbf{r}_{12}) \tag{18}$$

giving maximum possible interference pattern with the maximum visibility of 100%. When $\Delta \neq 0$ and/or ($\phi_1 \neq \phi_2$), the total intensity at the point P is given by

$$\langle I(\mathbf{R})\rangle = 2\langle I_0\rangle\left\{1 + (\cos k_0\bar{\mathbf{R}} \cdot \mathbf{r}_{12})\cos\left(k_0\tilde{R}\frac{\Delta}{\omega_0} + \delta\phi\right) - (\sin k_0\bar{\mathbf{R}} \cdot \mathbf{r}_{12})\sin\left(k_0\tilde{R}\frac{\Delta}{\omega_0} + \delta\phi\right)\right\} \tag{19}$$

In this case the intensity exhibits additional cosine and sine modulations, and at the minima the intensity is different from zero, indicating that the maximum depth of modulation of 100% is not possible for two fields of different frequencies and/or initial phases. Moreover, for large differences between the frequencies of the fields ($\Delta/\omega_0 \gg 1$) the $\cos(k_0\tilde{R}\frac{\Delta}{\omega_0} + \delta\phi)$ and $\sin(k_0\tilde{R}\frac{\Delta}{\omega_0} + \delta\phi)$ terms rapidly oscillate with $\mathbf{R}$ and average to zero that washes out the interference pattern. In terms of which-way information has been transferred, a detector located in the point P and adjusted to measure a particular frequency or phase could distinguish the frequency or the phase of the two fields. Clearly, one could tell which way the detected field came to the point P. Thus, whether which-way information is available depends on the intensities as well as frequencies and phases of the interfering fields. Maximum possible which-way information results in the lack of the interference pattern, and vice versa, the lack of which-way information results in maximum interference pattern.

2. *Second-Order Coherence*

The analysis of the interference phenomenon can be extended into higher-order correlation functions. The first experimental demonstration that such correlations exist in optical fields was given by Hanbury-Brown and Twiss [14], who measured the second-order correlation function of a thermal field.

The second-order (intensity) correlation function of a field of a complex amplitude $E(\mathbf{R}, t)$ is defined as

$$\begin{aligned} G^{(2)}(\mathbf{R}_1, t_1; \mathbf{R}_2, t_2) &= \langle \mathbf{E}^*(\mathbf{R}_1, t_1)\mathbf{E}^*(\mathbf{R}_2, t_2)\mathbf{E}(\mathbf{R}_2, t_2)\mathbf{E}(\mathbf{R}_1, t_1)\rangle \\ &= \langle I(\mathbf{R}_1, t_1)I(\mathbf{R}_2, t_2)\rangle \end{aligned} \tag{20}$$

where $I(\mathbf{R}_1, t_1)$ and $I(\mathbf{R}_2, t_2)$ are the instantaneous intensities of the field detected at a point $\mathbf{R}_1$ at time t_1 and at a point $\mathbf{R}_2$ at time t_2, respectively.

We can define the normalized second-order correlation function as

$$g^{(2)}(\mathbf{R}_1, t_1; \mathbf{R}_2, t_2) = \frac{G^{(2)}(\mathbf{R}_1, t_1; \mathbf{R}_2, t_2)}{G^{(1)}(\mathbf{R}_1, t_1)G^{(1)}(\mathbf{R}_2, t_2)} \tag{21}$$

where $G^{(1)}(\mathbf{R}_i, t_i) \equiv G^{(1)}(\mathbf{R}_i, t_i; \mathbf{R}_i, t_i)$.

In the plane-wave approximation, the second-order correlation function (20) can be written as

$$\begin{aligned} G^{(2)}(\mathbf{R}_1, t_1; \mathbf{R}_2, t_2) = &\sum_{i,j,k,l=1}^{2} \langle \mathbf{E}_i^*(t_1)\mathbf{E}_k^*(t_2)\mathbf{E}_l(t_2)\mathbf{E}_j(t_1)\rangle \\ &\times e^{ik(\bar{\mathbf{R}}_1\cdot\mathbf{r}_{ij}+\bar{\mathbf{R}}_2\cdot\mathbf{r}_{kl})} e^{i(\phi_i+\phi_k-\phi_l-\phi_j)} \end{aligned} \tag{22}$$

where $k = 2\pi/\lambda$ and λ is the wavelength of the field. There are 16 correlation functions contributing to the r.h.s. of Eq. (22), each accompanied by a phase factor that depends on the relative phase of the fields.

The second-order correlation function has coherence properties completely different from those of the first-order correlation function. An interference pattern can be observed in the second-order correlation function, but in contrast to the first-order correlation function, the interference appears between two points located at $\mathbf{R}_1$ and $\mathbf{R}_2$. Moreover, an interference pattern can be observed even if the fields are produced by two independent sources for which the phase difference $\phi_1 - \phi_2$ is completely random [15]. In this case the second-order correlation function (22) is given by

$$\begin{aligned} G^{(2)}(\mathbf{R}_1, t_1; \mathbf{R}_2, t_2) = &\langle I_1^2(t_1)\rangle + \langle I_2^2(t_2)\rangle + 2\langle I_1(t_1)I_2(t_2)\rangle \\ &+ 2\langle I_1(t_1)I_2(t_2)\rangle \cos k\mathbf{r}_{12}\cdot(\bar{\mathbf{R}}_1 - \bar{\mathbf{R}}_2). \end{aligned} \tag{23}$$

Clearly, the second-order correlation function exhibits a cosine modulation with the separation $\mathbf{R}_1 - \mathbf{R}_2$ of the two detectors. This is an interference, although it involves a correlation function that is of the second order in the intensity. Hence an interference pattern can be observed even for two completely independent fields. Similar to the first-order correlation function, the sharpness of the fringes depends on the relative intensities of the fields. For equal intensities, $I_1 = I_2 = I_0$, the correlation function (23) reduces to

$$G^{(2)}(\mathbf{R}_1, t; \mathbf{R}_2, t) = 4\langle I_0^2 \rangle \left[1 + \frac{1}{2} \cos k\mathbf{r}_{12} \cdot (\bar{\mathbf{R}}_1 - \bar{\mathbf{R}}_2) \right] \tag{24}$$

where $\langle \Delta I_0^2 \rangle = \langle I_0^2 \rangle - \langle I_0 \rangle^2$ is the variance of the field intensity.

In analogy to the visibility in the first-order correlation function, we can define the visibility of the interference pattern of the intensity correlations as

$$\mathscr{V} = \frac{G^{(2)}_{\max} - G^{(2)}_{\min}}{G^{(2)}_{\max} + G^{(2)}_{\min}} \tag{25}$$

and find from Eq. (24) that in the case of a classical field, an interference pattern can be observed with the maximum possible visibility of $\mathscr{V} = \frac{1}{2}$. Thus, two independent fields of random and uncorrelated phases can exhibit an interference pattern in the intensity correlation with a maximum visibility of 50%.

B. Quantum Interference

In the classical theory of light and optical coherence the field is represented by complex vectorial amplitudes $\mathbf{E}(\mathbf{r}, t)$ and $\mathbf{E}^*(\mathbf{r}, t)$, which absolute values are complex numbers (c- numbers). In quantum theory of light the most important physical quantity is the electric field, which is represented by the field operator $\hat{\mathbf{E}}(\mathbf{r}, t)$. This Hermitian operator is usually expressed by the sum of two non-Hermitian operators as

$$\hat{\mathbf{E}}(\mathbf{r}, t) = \hat{\mathbf{E}}^{(+)}(\mathbf{r}, t) + \hat{\mathbf{E}}^{(-)}(\mathbf{r}, t) \tag{26}$$

where $\hat{\mathbf{E}}^{(+)}$ ($\hat{\mathbf{E}}^{(-)}$) is the positive (resp. negative) frequency component of the field.

In free space the frequency components can be expressed in terms of plane waves as

$$\hat{\mathbf{E}}^{(+)}(\mathbf{r}, t) = (\hat{\mathbf{E}}^{(-)}(\mathbf{r}, t))^{\dagger} = i \sum_{\mathbf{k}s} \left(\frac{\hbar \omega_k}{2\epsilon_0 V} \right)^{1/2} \mathbf{e}_{\mathbf{k}s} \hat{a}_{\mathbf{k}s} e^{i(\mathbf{k} \cdot \mathbf{r} - \omega_k t)} \tag{27}$$

where V is the volume occupied by the field, $\hat{a}_{\mathbf{k}s}$ is the annihilation operator for the $\mathbf{k}$th mode of the field of the polarization s, and $\mathbf{e}_{\mathbf{k}s}$ and ω_k are, respectively, the unit polarization vector and the angular frequency of the mode.

In the case of the quantum description of the field, the first- and second-order correlation functions are defined in terms of the normally ordered field operators $\hat{\mathbf{E}}^{(+)}$ and $\hat{\mathbf{E}}^{(-)}$ as

$$\begin{aligned} G^{(1)}(\mathbf{R}_1, t_1; \mathbf{R}_2, t_2) &= \langle \hat{\mathbf{E}}^{(-)}(\mathbf{R}_1, t_1) \cdot \hat{\mathbf{E}}^{(+)}(\mathbf{R}_2, t_2) \rangle \\ G^{(2)}(\mathbf{R}_1, t_1; \mathbf{R}_2, t_2) &= \langle \hat{\mathbf{E}}^{(-)}(\mathbf{R}_1, t_1) \hat{\mathbf{E}}^{(-)}(\mathbf{R}_2, t_2) \\ &\quad \times \hat{\mathbf{E}}^{(+)}(\mathbf{R}_2, t_2) \hat{\mathbf{E}}^{(+)}(\mathbf{R}_1, t_1) \rangle \end{aligned} \tag{28}$$

where the average is taken over a state $|i\rangle$ of the field. Usually the state $|i\rangle$ is an initial state of the field.

If we introduce the density operator ρ for the field, we can rewrite the correlation functions as

$$\begin{aligned} G^{(1)}(\mathbf{R}_1, t_1; \mathbf{R}_2, t_2) &= \mathrm{Tr}[\rho \hat{\mathbf{E}}^{(-)}(\mathbf{R}_1, t_1) \cdot \hat{\mathbf{E}}^{(+)}(\mathbf{R}_2, t_2)] \\ G^{(2)}(\mathbf{R}_1, t_1; \mathbf{R}_2, t_2) &= \mathrm{Tr}\{\rho \hat{\mathbf{E}}^{(-)}(\mathbf{R}_1, t_1) \hat{\mathbf{E}}^{(-)}(\mathbf{R}_2, t_2) \\ &\quad \times \hat{\mathbf{E}}^{(+)}(\mathbf{R}_2, t_2) \hat{\mathbf{E}}^{(+)}(\mathbf{R}_1, t_1)\} \end{aligned} \tag{29}$$

where the trace is taken over the initial state $|i\rangle$.

The correlation functions (28) described by the field operators are similar to the correlation functions (6) and (20) of the classical field. A closer look into Eqs. (6), (20), and (28) could suggest that the only difference between the classical and quantum correlation functions is that the classical amplitudes $\mathbf{E}^*(\mathbf{R}, t)$ and $\mathbf{E}(\mathbf{R}, t)$ are replaced by the field operators $\hat{\mathbf{E}}^{(-)}(\mathbf{R}, t)$ and $\hat{\mathbf{E}}^{(+)}(\mathbf{R}, t)$. This is true as long as the first-order correlation functions are considered, where the interference effects do not distinguish between the quantum and classical theories of the electromagnetic field. However, there are significant differences between the classical and quantum descriptions of the field in the properties of the second-order correlation function [16].

As an example, consider the simple case of two single-mode fields of equal frequencies and polarizations. Assume that there are initially n photons in field 1 and m photons in the field 2, and that the state vectors of the fields are the Fock states $|\psi_1\rangle = |n\rangle$ and $|\psi_2\rangle = |m\rangle$. The initial state of the two fields is the direct product of the single-field states, $|\psi\rangle = |n\rangle|m\rangle$. Inserting Eq. (27) into Eq. (28) and taking the expectation value with respect to the initial state of the fields, we find

$$\begin{aligned} G^{(2)}(\mathbf{R}_1, t_1; \mathbf{R}_2, t_2) &= \left(\frac{\hbar\omega}{2\epsilon_0 V}\right)^2 \{n(n-1) + m(m-1) \\ &\quad + 2nm[1 + \cos k\mathbf{r}_{12} \cdot (\bar{\mathbf{R}}_1 - \bar{\mathbf{R}}_2)]\} \end{aligned} \tag{30}$$

We note that the first two terms on the r.h.s. of Eq. (30) vanish when the number of photons in each field is smaller than 2, that is, $n < 2$ and $m < 2$. In this limit the correlation function (30) reduces to

$$G^{(2)}(\mathbf{R}_1, t_1; \mathbf{R}_2, t_2) = 2\left(\frac{\hbar\omega}{2\epsilon_0 V}\right)^2 [1 + \cos k\mathbf{r}_{12} \cdot (\bar{\mathbf{R}}_1 - \bar{\mathbf{R}}_2)] \tag{31}$$

Thus, perfect interference pattern with visibility $\mathscr{V} = 1$ can be observed in the second-order correlation function of two quantum fields each containing only one photon. As we have noted in Section II.A, the classical theory predicts only a visibility of $\mathscr{V} = 0.5$. For $n, m \gg 1$, the first two terms on the r.h.s. of Eq. (30) are different from zero $(m(m-1) \approx n(n-1) \approx n^2)$, and then the quantum correlation function (30) reduces to that of the classical field.

It follows from Eq. (31) that the second-order correlation function vanishes when

$$k\mathbf{r}_{12} \cdot (\bar{\mathbf{R}}_1 - \bar{\mathbf{R}}_2) = (2n+1)\pi, \quad n = 0, \pm 1, \pm 2, \ldots \tag{32}$$

In other words, two photons can never be detected at two points separated by an odd number of $\lambda/2r_{12}$, despite the fact that one photon can be detected anywhere. The vanishing of $G^{(2)}(\mathbf{R}_1, t_1; \mathbf{R}_2, t_2)$ for two photons at widely separated points $\mathbf{R}_1$ and $\mathbf{R}_2$ is an example of quantum-mechanical nonlocality, that the outcome of a detection measurement at $\mathbf{R}_1$ appears to be influenced by where we have chosen to locate the $\mathbf{R}_2$ detector. At certain positions $\mathbf{R}_2$ we can never detect a photon at $\mathbf{R}_1$ when there is a photon detected at $\mathbf{R}_2$, whereas at other position $\mathbf{R}_2$ it is possible. The photon correlation argument shows clearly that quantum theory does not in general describe an objective physical reality independent of observation [17].

The visibility of the interference pattern of the intensity correlations provides a means of testing for quantum correlations between two light fields. Mandel et al. [18] have measured the visibility in the interference of signal and idler modes simultaneously generated in the process of degenerate parametric downconversion, and observed a visibility of about 75%, that is a clear violation of the upper bound of 50% allowed by classical correlations. Richter [19] has extended the analysis of the visibility into the third-order correlation function and also found significant differences in the visibility of the interference pattern of the classical and quantum fields.

III. MASTER EQUATION OF TWO COUPLED DIPOLE MOMENTS

In this section, we present a derivation of the master equation for the density operator of two arbitrary dipole moments driven by an external field and

coupled to the quantized three-dimensional vacuum field. The dipole moments, which we will call "bare" systems, are represented by dipole operators

$$\begin{aligned}\hat{\boldsymbol{\mu}}_1 &= \boldsymbol{\mu}_1 S_1^+ + \boldsymbol{\mu}_1^* S_1^- \\ \hat{\boldsymbol{\mu}}_2 &= \boldsymbol{\mu}_2 S_2^+ + \boldsymbol{\mu}_2^* S_2^-\end{aligned} \tag{33}$$

where S_i^+ (S_i^-) is the dipole raising (resp. lowering) operator and μ_i is the dipole matrix element of the ith system. The dipole moments are assumed to oscillate with different frequencies ω_1 and ω_2, and are coupled to the quantized three-dimensional multimode electromagnetic field whose modes are in a vacuum state. The knowledge of the density operator of the two systems, coupled through the vacuum field, will allow us to calculate correlation functions of the dipole operators that contain the information about correlations and coherences between the two systems.

A. Correlation Functions for Atomic Operators

In the preceding section we have shown that the correlation functions of the quantized field can be calculated if we know an initial state or the density operator of the field. As we see in this section, the phenomenon of interference can be described not only for light beams but also for electromagnetic (EM) fields spontaneously emitted from atoms, molecules, or even for the EM field emitted from single multilevel systems. In this case the correlation functions of the EM field can be related to the correlation functions of the variables of the systems, such as the dipole operators $S_i^{\pm}$.

The relation between the positive frequency part of the electric field operator at a point $\mathbf{R} = R\bar{\mathbf{R}}$ in the far-field zone of the radiating systems and the dipole moments is given by the well-known expression [4,20]

$$\hat{\mathbf{E}}^{(+)}(\mathbf{R}, t) = \hat{\mathbf{E}}_0^{(+)}(\mathbf{R}, t) - \frac{1}{c^2}\sum_{i=1}^{2} \frac{\bar{\mathbf{R}} \times (\bar{\mathbf{R}} \times \boldsymbol{\mu}_i)}{R} \omega_i S_i^- \left(t - \frac{R}{c}\right) \tag{34}$$

where S_i^- is the dipole lowering operator of the ith system $\boldsymbol{\mu}_i$ and ω_i are the transition dipole matrix element and the angular frequency, respectively, and $\hat{\mathbf{E}}_0^{(+)}(\mathbf{R}, t)$ denotes the positive frequency part of the field in the absence of the radiating systems.

If we assume that initially the field is in the vacuum state, then the free-field part $\hat{\mathbf{E}}_0^{(+)}(\mathbf{R}, t)$ does not contribute to the expectation values of the normally ordered field operators, and we obtain the following expressions for the first- and second-order correlation functions

$$G^{(1)}(\mathbf{R}, t) = \sum_{i,j=1}^{2} \Gamma_{ij} \langle S_i^+(t) S_j^-(t) \rangle \tag{35}$$

and

$$G^{(2)}(\mathbf{R}, t_1; \mathbf{R}, t_2) = \sum_{i,j,k,l=1}^{2} \Gamma_{il}\Gamma_{jk}\langle S_i^+(t_1)S_j^+(t_2)S_k^-(t_2)S_l^-(t)\rangle \tag{36}$$

where $\Gamma_{ii} = \Gamma_i$ is the spontaneous decay rate of the ith system, while

$$\Gamma_{ij} = \frac{2\sqrt{\omega_i^3\omega_j^3}}{3\hbar c^3}\boldsymbol{\mu}_i \cdot \boldsymbol{\mu}_j = \sqrt{\Gamma_i\Gamma_j}\cos\theta \qquad (i \neq j) \tag{37}$$

is the so-called cross-damping rate arising from the vacumm induced coupling between the dipole moments. The cross-damping rate is sensitive to the mutual polarization of the dipole moments of the two systems, which we represent by the angle θ. If the dipole moments are parallel, $\theta = 0^o$, and the cross-damping rate is maximal with $\Gamma_{12} = \sqrt{\Gamma_1\Gamma_2}$, while $\Gamma_{12} = 0$ if the dipole moments are perpendicular ($\theta = 90^o$).

It is seen from Eq. (36) that the second-order correlation function of the EM field emitted from the two systems depends on various two-time dipole correlation functions of the form $\langle S_i^+(t_1)S_j^+(t_2)S_j^-(t_2)S_i^-(t_1)\rangle$. The functions are proportional to the probabilities of detecting two photons emitted from the same $(i = j)$ or different $(i \neq j)$ bare systems. For example, the correlation function $\langle S_1^+(t_1)S_2^+(t_2)S_2^-(t_2)S_1^-(t_1)\rangle$ is proportional to the probability of detecting a photon at time t_2 emitted from system 2 if a photon emitted from the system 1 was detected at time t_1.

The second-order correlation function (36) also depends on the dipole correlation functions of the form $\langle S_1^+(t_1)S_2^+(t_2)S_1^-(t_2)S_2^-(t_1)\rangle$, which result from correlations of photons emitted from a superposition of the bare systems.

B. Hamiltonian of the System

The total Hamiltonian describing the energies of the systems, electromagnetic field and interactions, in the electric dipole and RWA (rotating-wave approximation) approximations [21], is composed of four terms

$$H = H_s + H_v + H_{sL} + H_{sv}, \tag{38}$$

where

$$H_s = \hbar\omega_1 S_1^+ S_1^- + \hbar\omega_2 S_2^+ S_2^- \tag{39}$$

is the Hamiltonian of the two bare systems

$$H_v = \sum_{\mathbf{k}s} \hbar\omega_{\mathbf{k}s}\left(\hat{a}_{\mathbf{k}s}^\dagger \hat{a}_{\mathbf{k}s} + \frac{1}{2}\right) \tag{40}$$

is the Hamiltonian of the three-dimensional multimode electromagnetic field

$$H_{sL} = -\frac{1}{2}\hbar[(\Omega_1 S_1^+ + \Omega_2 S_2^+)e^{-i(\omega_L t+\phi_L)} + \text{H.c.}] \tag{41}$$

is the interaction of the systems with the coherent laser field, and

$$H_{sv} = \sum_{\mathbf{k}s}\{[\boldsymbol{\mu}_1 \cdot \mathbf{g}_{\mathbf{k}s}(\mathbf{r})S_1^+ + \boldsymbol{\mu}_2 \cdot \mathbf{g}_{\mathbf{k}s}(\mathbf{r})S_2^+]\hat{a}_{\mathbf{k}s} + \text{H.c.}\} \tag{42}$$

is the interaction of the bare systems with the multimode vacuum field (H.c. denotes Hermitian conjugation). Here, ω_L and ϕ_L are the frequency and the phase of the driving laser field, respectively, $\hat{a}^\dagger_{\mathbf{k}s}$ and $\hat{a}_{\mathbf{k}s}$ are the creation and annihilation operators of a photon in the mode $(\mathbf{k}, s)$ with wavevector $\mathbf{k}$ and polarization s

$$\mathbf{g}_{\mathbf{k}s}(\mathbf{r}) = \left(\frac{ck}{2\pi\epsilon_0\hbar(2\pi)^3}\right)^{1/2} \mathbf{e}_{\mathbf{k}s}e^{i\mathbf{k}\cdot\mathbf{r}} \tag{43}$$

is the mode function of the three-dimensional multimode vacuum field, evaluated at the position $\mathbf{r}$ of the radiating dipole moment, and

$$\Omega_i = \frac{\boldsymbol{\mu}_i \cdot \mathbf{E}_L e^{i\mathbf{k}_L\cdot\mathbf{r}}}{\hbar} \tag{44}$$

is the Rabi frequency of the ith system with $\mathbf{E}_L$ and $\mathbf{k}_L$ denoting the amplitude and the wave vector of the driving field, respectively. For a single laser coupled to both systems the Rabi frequencies Ω_1 and Ω_2 are related by

$$\Omega_2 = \Omega_1 \frac{\mu_2 \cos\theta_1}{\mu_1 \cos\theta_2} \tag{45}$$

where θ_i is the angle between $\boldsymbol{\mu}_i$ and the polarization vector of the laser field and $\mu_i = |\boldsymbol{\mu}_i|$ is the magnitude of the ith dipole moment.

C. Master Equation

Having available the total Hamiltonian of the system, Eq. (38), we can write the Schrödinger equation for the density operator ρ_T of the total system, the bare dipole systems plus the EM field, as

$$i\hbar\frac{\partial}{\partial t}\rho_T = [H, \rho_T] \tag{46}$$

Since we are interested in the interaction of the bare dipole systems with the vacuum field, which is the source of spontaneous emission, we make the unitary transformation

$$\tilde{\rho}_T(t) = e^{iUt/\hbar}\rho_T e^{-iUt/\hbar} \tag{47}$$

and find that the transformed density operator satisfies the equation

$$i\hbar\frac{\partial}{\partial t}\tilde{\rho}_T(t) = [\tilde{H}_{sv}(t), \tilde{\rho}_T(t)] \tag{48}$$

where

$$\tilde{H}_{sv}(t) = e^{iUt/\hbar}H_{sv}e^{-iUt/\hbar} \tag{49}$$

and

$$U = H_s + H_v + H_{sL} \tag{50}$$

Formally integrating the equation of motion (48) gives

$$\tilde{\rho}_T(t) = \tilde{\rho}_T(0) + \frac{1}{i\hbar}\int_0^t dt'[\tilde{H}_{sv}(t'), \tilde{\rho}_T(t')] \tag{51}$$

Substituting Eq. (51) into the r.h.s. of Eq. (48), and after tracing over the field variables, we find that the reduced density operator $\tilde{\rho}(t) = \mathrm{Tr}_F\tilde{\rho}_T(t)$ of the bare systems satisfies the integrodifferential equation

$$\begin{aligned}\frac{\partial}{\partial t}\tilde{\rho}(t) = &\frac{1}{i\hbar}\mathrm{Tr}_F[\tilde{H}_{sv}(t), \tilde{\rho}_T(0)] \\ &-\frac{1}{\hbar^2}\int_0^t d\tau \mathrm{Tr}_F\{[\tilde{H}_{sv}(t), [\tilde{H}_{sv}(t-\tau), \tilde{\rho}_T(t-\tau)]]\}\end{aligned} \tag{52}$$

We now make two approximations [22] regarding to the density operator of the total system appearing on the r.h.s. of Eq. (52):

1. The *Born approximation*, in which the interaction between the systems and the field is supposed to be weak, so there is no the backreaction effect of the systems on the field

$$\tilde{\rho}_T(t-\tau) = \tilde{\rho}(t-\tau)\tilde{\rho}_F(0), \tag{53}$$

where $\tilde{\rho}_F(0)$ is the density operator of the field.

2. The *Markov approximation*, in which we assume that the correlation time of the EM field is much shorter than the timescale of radiation processes of the bare systems. This approximation is equivalent to the white-noise (broadband) description of the EM field modes, and allows us to replace $\tilde{\rho}(t-\tau)$ by $\tilde{\rho}(t)$.

Applying the Born and Markov approximations to Eq. (52) and assuming that all modes of the EM field are in a vacuum state, defined by

$$\begin{aligned}
\mathrm{Tr}_F[\rho_F(0)\hat{a}_{\mathbf{k}s}] &= \mathrm{Tr}_F[\rho_F(0)\hat{a}^\dagger_{\mathbf{k}s}] = 0 \\
\mathrm{Tr}_F[\rho_F(0)\hat{a}_{\mathbf{k}s}\hat{a}^\dagger_{\mathbf{k}'s'}] &= \delta^3(\mathbf{k}-\mathbf{k}')\delta_{ss'}, \quad \mathrm{Tr}_F[\rho_F(0)\hat{a}^\dagger_{\mathbf{k}s}\hat{a}_{\mathbf{k}'s'}] = 0 \\
\mathrm{Tr}_F[\rho_F(0)\hat{a}^\dagger_{\mathbf{k}s}\hat{a}^\dagger_{\mathbf{k}'s'}] &= \mathrm{Tr}_F[\rho_F(0)\hat{a}_{\mathbf{k}s}\hat{a}_{\mathbf{k}'s'}] = 0
\end{aligned} \tag{54}$$

we obtain

$$\begin{aligned}
\frac{\partial}{\partial t}\tilde{\rho}(t) = &-\frac{i}{\hbar}[H_c, \tilde{\rho}(t)] \\
&-\frac{1}{2}\sum_{i,j=1}^{2}\Gamma_{ij}(S_i^+S_j^-\tilde{\rho}(t) + \tilde{\rho}(t)S_i^+S_j^- - 2S_j^-\tilde{\rho}(t)S_i^+)
\end{aligned} \tag{55}$$

where

$$\begin{aligned}
H_c = &\hbar\delta_1^{(-)}S_1^+S_1^- + \hbar\delta_2^{(-)}S_2^+S_2^- + \hbar\delta_1^{(+)}S_1^-S_1^+ + \hbar\delta_2^{(+)}S_2^-S_2^+ \\
&+ \hbar\delta_{12}^{(-)}(S_1^+S_2^- + S_2^+S_1^-) + \hbar\delta_{12}^{(+)}(S_1^-S_2^+ + S_2^-S_1^+)
\end{aligned} \tag{56}$$

is the vacuum induced coherent term. The parameter

$$\Gamma_i \equiv \Gamma_{ii} = \pi\sum_{\mathbf{k}s}|\boldsymbol{\mu}_i\cdot\mathbf{g}_{\mathbf{k}s}(\mathbf{r})|^2\delta^3(\mathbf{k}-\mathbf{k}_0) \qquad (i=1,2) \tag{57}$$

is the spontaneous damping rate of the ith system resulting from the coupling of the system to the vacuum field, and

$$\Gamma_{ij} = \Gamma_{ji} = \pi\sum_{\mathbf{k}s}[\boldsymbol{\mu}_1\cdot\mathbf{g}_{\mathbf{k}s}(\mathbf{r})][\boldsymbol{\mu}_2^*\cdot\mathbf{g}_{\mathbf{k}s}^*(\mathbf{r})]\delta^3(\mathbf{k}-\mathbf{k}_0) \quad (i\neq j) \tag{58}$$

are cross-damping rates arising from the coupling of the bare systems through the vacuum field, and $k_0 = (k_1+k_2)/2$.

The remaining parameters appearing in Eq. (55) are

$$\delta_i^{(\pm)} = \frac{P}{c}\sum_{\mathbf{k}s}|\boldsymbol{\mu}_i\cdot\mathbf{g}_{\mathbf{k}s}(\mathbf{r}_i)|^2\frac{1}{k\pm k_0} \tag{59}$$

and

$$\delta_{12}^{(\pm)} = \frac{P}{c}\sum_{\mathbf{k}s}[\boldsymbol{\mu}_1 \cdot \mathbf{g}_{\mathbf{k}s}(\mathbf{r})][\boldsymbol{\mu}_2^* \cdot \mathbf{g}_{\mathbf{k}s}^*(\mathbf{r})]\frac{1}{k \pm k_0} \tag{60}$$

which represent a part of the Lamb shift of the frequencies of the bare systems and the vacuum induced coherent coupling between the systems, respectively, and P refers to the Cauchy principal value.

The Γ_1 and Γ_2 terms appearing in Eq. (55) are the standard damping terms of the bare systems. The Γ_{12} and Γ_{21} terms in this equation arise from the coupling of the bare systems through the vacuum field. These two terms distinguish the dissipative part from master equations of independent systems. The parameters $\delta_i^{(\pm)}$ can be considered as a part of the frequencies ω_1 and ω_2, and thus they can be included into the dynamics by redefining the frequencies to $\tilde{\omega}_i = \omega_i + \delta_i^{(-)}$. However, the parameter $\delta_{12}^{(\pm)}$ does not appear as a shift of the energies, but contributes to the coherent coupling between the bare systems [23,24]. Thus, the interaction of the systems with the vacuum field not only produces spontaneous emission but also leads to a coherent coupling between the systems.

To carry out the sums appearing in Eqs. (57–60), we use the plane-wave representation (43) of the vacuum modes and work in the spherical representation of the unit orthogonal polarization vectors $\mathbf{e}_{\mathbf{k}1}$ and $\mathbf{e}_{\mathbf{k}2}$. Substituting Eq. (43) into Eqs. (57–60), and evaluating the sums over $\mathbf{k}$ and s, we obtain

$$\Gamma_i = \frac{k_i^3 \mu_i^2}{6\pi\epsilon_0\hbar} \qquad (i = 1, 2) \tag{61}$$

$$\Gamma_{12} = \sqrt{\Gamma_1\Gamma_2}(\bar{\boldsymbol{\mu}}_1 \cdot \bar{\boldsymbol{\mu}}_2) = \sqrt{\Gamma_1\Gamma_2}\cos\theta = p\sqrt{\Gamma_1\Gamma_2} \tag{62}$$

and

$$\delta_{12}^{(\pm)} = \frac{\Gamma_{12}}{\pi}P\int_{-\infty}^{\infty} dk \frac{1}{k \pm k_0} \tag{63}$$

where $\bar{\boldsymbol{\mu}}_i$ is the unit vector along the ith dipole moment, $k = |\mathbf{k}|$ and $k_i = \omega_i/c$. The magnitude of the parameters (62) and (63) depends on the mutual orientation of the dipole moments, which can be represented by the angle θ or equivalently by the parameter $p = \cos\theta$. The vacuum induced terms vanish when the dipole moments of the two systems are perpendicular ($p = 0$). For parallel dipole moments ($p = 1$) the parameters attain their maximal values.

On transforming Eq. (55) into the Schrödinger picture, the master equation of the system takes the form

$$\frac{\partial}{\partial t}\rho = -\frac{i}{\hbar}[H', \rho] - \frac{1}{2}\sum_{i,j=1}^{2}\Gamma_{ij}(S_i^+ S_j^- \rho + \rho S_i^+ S_j^- - 2S_j^- \rho S_i^+) \tag{64}$$

where

$$H' = H_s + H_{sL} + \hbar\delta_{12}^{(-)}(S_1^+ S_2^- + S_2^+ S_1^-) + \hbar\delta_{12}^{(+)}(S_1^- S_2^+ + S_2^- S_1^+) \tag{65}$$

Equation (64) is the final form of the master equation that gives us an elegant description of the physics involved in the dynamics of two interacting systems. An important point is that the master equation is quite general and can be applied to an arbitrary system composed of two dipole moments.

The presence of the additional damping terms Γ_{12} may suggest that quantum interference enhances spontaneous emission from two coupled systems. However, as we shall illustrate in the following sections, the presence of these terms in the master equation can, in fact, lead to a reduction or even suppression of spontaneous emission. According to Eq. (62), the reduction and suppression of spontaneous emission can be controlled by changing the mutual orientation of the dipole moments of the bare systems.

IV. QUANTUM INTERFERENCE AS A CONTROL OF SPONTANEOUS EMISSION

The control and suppression of spontaneous emission is a topic of much current interest because of the many possible applications in quantum computation, teleportation, and quantum information theory. As spontaneous emission arises from the interaction of an atomic system with the environmental modes, the most obvious mechanism for modifying spontaneous emission is to place the system in a frequency-dependent reservoir such as an electromagnetic cavity, an optical waveguide, or a photonic bandgap material, which changes the density of modes of the vacuum field into which the system can emit. For atoms in free space, quantum interference has been recognized as the basic phenomenon for controlling spontaneous emission. It was first shown by Agarwal [4] that the decay of an excited degenerate V-type three-level atom can be modified by interference between the two coupled atomic transitions, and a population trapping can occur.

A. Modification of Spontaneous Emission Rates

The traditional method to analyze conditions for modification of spontaneous emission is to derive equations of motion for the probability amplitudes or density matrix elements and solve them by direct integration, or by a transformation to easily solvable algebraic equations. Here, we discuss an alternative approach proposed by Akram et al. [24] that allows us to identify conditions for a modification of spontaneous emission directly in the master equation of two arbitrary systems. In this approach, we introduce linear superpositions of the dipole operators

$$\begin{aligned} S_s^+ &= uS_1^+ + vS_2^+ \\ S_a^+ &= vS_1^+ - uS_2^+ \end{aligned} \tag{66}$$

where

$$u = \frac{\sqrt{\Gamma_1}}{\sqrt{\Gamma_1 + \Gamma_2}}, \qquad v = \frac{\sqrt{\Gamma_2}}{\sqrt{\Gamma_1 + \Gamma_2}} \tag{67}$$

and

$$|u|^2 + |v|^2 = 1 \tag{68}$$

which ensure that the transition to the superposition operators is an unitary transformation. The operators S_s^+ and S_a^+ represent, respectively, symmetric and antisymmetric superpositions of the dipole moments of the two bare systems. In terms of the operators (66), we can rewrite the dissipative part of the master equation (64) in a form

$$\begin{aligned} \mathscr{L}_d\rho = &-\Gamma_{ss}(S_s^+S_s^-\rho + \rho S_s^+S_s^- - 2S_s^-\rho S_s^+) \\ &- \Gamma_{aa}(S_a^+S_a^-\rho + \rho S_a^+S_a^- - 2S_a^-\rho S_a^+) \\ &- \Gamma_{sa}(S_s^+S_a^-\rho + \rho S_s^+S_a^- - 2S_a^-\rho S_s^+) \\ &- \Gamma_{as}(S_a^+S_s^-\rho + \rho S_a^+S_s^- - 2S_s^-\rho S_a^+) \end{aligned} \tag{69}$$

where

$$\begin{aligned} \Gamma_{ss} &= \frac{1}{2}\frac{(\Gamma_1^2 + \Gamma_2^2 + 2\Gamma_{12}\sqrt{\Gamma_1\Gamma_2})}{\Gamma_1 + \Gamma_2} \\ \Gamma_{aa} &= \frac{(\sqrt{\Gamma_1\Gamma_2} - \Gamma_{12})\sqrt{\Gamma_1\Gamma_2}}{\Gamma_1 + \Gamma_2} \\ \Gamma_{sa} = \Gamma_{as} &= \frac{1}{2}\frac{(\Gamma_1 - \Gamma_2)(\sqrt{\Gamma_1\Gamma_2} - \Gamma_{12})}{\Gamma_1 + \Gamma_2} \end{aligned} \tag{70}$$

Although in general the two forms (64) and (69) look similar, the advantage of the transformed form (69) over (64) is obtained when the damping rates of the original systems are equal ($\Gamma_1 = \Gamma_2$). In this case $\Gamma_{sa} = \Gamma_{as} = 0$, and then the symmetric and antisymmetric superpositions decay independently with the decay rates $\frac{1}{2}(\Gamma + \Gamma_{12})$ and $\frac{1}{2}(\Gamma - \Gamma_{12})$, respectively. In other words, for $\Gamma_1 = \Gamma_2$ the transformation (66) diagonalizes the dispersive part of the master equation. Furthermore, if $\Gamma_{12} = \sqrt{\Gamma_1\Gamma_2}$, then $\Gamma_{aa} = \Gamma_{sa} = \Gamma_{as} = 0$ regardless of the ratio between Γ_1 and Γ_2. In this case the antisymmetric superposition does not decay. This implies that spontaneous emission can be controlled and even suppressed by appropriately engineering the cross-damping rate Γ_{12} arising from the dissipative interaction between the systems.

B. Phase Control of Spontaneous Emission

Spontaneous emission in a multilevel atom can be controlled by changing not only the mutual orientation of the dipole moments of two interfering transitions but also the phase difference of driving lasers used for the excitation of the atom.

Phase dependent effects in spontaneous emission have been predicted in atomic systems with nonorthogonal as well as with orthogonal dipole moments. In the first case the phase-dependent effects, which arise from quantum interference between two nonorthogonal dipole moments, can be observed with two driving fields [25–28]. In the latter case the observation of phase-dependent effects requires at least three driving fields [29,30]. It is of particular interest to observe the phase-dependent effects, as they represent interference effects that can be induced by driving fields even in the absence of the vacumm-induced quantum interference.

Our review of the phase control of spontaneous emission will concentrate on the example of a V-type atom with nondegenerate transitions and nonorthogonal dipole moments driven by two laser fields. The lasers can have equal or different frequencies and each laser can couple to only one or both atomic transitions.

The interaction Hamiltonian of the atom with two laser fields can be written as

$$\begin{aligned} H_{\text{int}} = -\frac{1}{2}\hbar\{&\Omega_1(S_1^+ + \eta S_2^+)e^{-i(\omega_{L_1}t+\phi_1)} \\ &+ \Omega_2(\eta S_1^+ + S_2^+)e^{-i(\omega_{L_2}t+\phi_2)} + \text{H.c.}\} \end{aligned} \tag{71}$$

where Ω_1, Ω_2 are the Rabi frequencies and $\omega_{L_1}, \omega_{L_2}$ are the angular frequencies of the laser fields. The paramenters η stands for two possible configurations of the coupling of the lasers to the atomic transitions. The case of $\eta = 0$ corresponds to each laser only coupled to one of the atomic transitions, whereas $\eta = 1$ corresponds to the case of each laser coupled to both transitions.

The dynamics of the system are determined by the master equation with the interaction Hamiltonian (71). We make the following unitary transformation of the density operator of the system

$$\tilde{\rho} = e^{iH_{0L}t}\rho e^{-iH_{0L}t} \tag{72}$$

with $H_{0L} = \omega_{L_1}|1\rangle\langle 1| + \omega_{L_2}|3\rangle\langle 3|$, and find that the master equation of the system takes the form

$$\begin{aligned}\frac{d\tilde{\rho}}{dt} = &-\frac{i}{\hbar}[\tilde{H}_0 + \tilde{H}_{\text{int}}, \tilde{\rho}] \\ &-\frac{1}{2}\Gamma_1(S_1^+S_1^-\tilde{\rho} + \tilde{\rho}S_1^+S_1^- - 2S_1^-\tilde{\rho}S_1^+) \\ &-\frac{1}{2}\Gamma_2(S_2^+S_2^-\tilde{\rho} + \tilde{\rho}S_2^+S_2^- - 2S_2^-\tilde{\rho}S_2^+) \\ &-\frac{1}{2}\Gamma_{12}(S_2^+S_1^-\tilde{\rho} + \tilde{\rho}S_2^+S_1^- - 2S_1^-\tilde{\rho}S_2^+)e^{-i[(\omega_{L_1}-\omega_{L_2})t+\delta\phi]} \\ &-\frac{1}{2}\Gamma_{12}(S_1^+S_2^-\tilde{\rho} + \tilde{\rho}S_1^+S_2^- - 2S_2^-\tilde{\rho}S_1^+)e^{i[(\omega_{L_1}-\omega_{L_2})t+\delta\phi]}\end{aligned} \tag{73}$$

where

$$\tilde{H}_0 = \Delta_1|1\rangle\langle 1| + \Delta_2|3\rangle\langle 3| \tag{74}$$

$$\begin{aligned}\tilde{H}_{\text{int}} = &-\frac{1}{2}\hbar\{\Omega_1(S_1^+ + \eta S_2^+ e^{-i[(\omega_{L_1}-\omega_{L_2})t+\delta\phi]}) \\ &+ \Omega_2(\eta S_1^+ e^{i[(\omega_{L_1}-\omega_{L_2})t+\delta\phi]} + S_2^+) + \text{H.c.}\}\end{aligned} \tag{75}$$

and $\Delta_1 = \omega_1 - \omega_{L_1}$, $\Delta_2 = \omega_2 - \omega_{L_2}$ are the detunings of the laser fields from the atomic transitions.

In the transformed form the η- and Γ_{12}-dependent terms are accompanied by a phase-dependent term, $\exp(\pm\delta\phi)$. These terms are also accompanied by the time-dependent terms $\exp[i(\omega_{L_1} - \omega_{L_2})t]$, which oscillate with the difference of the laser frequencies. This shows that in any attempt to calculate phase-dependent effects, it is important to assume that the lasers have equal frequencies. Otherwise, for unequal frequencies the time-dependent terms rapidly oscillate in time and average out over a long period of the detection time. Furthermore, we note from Eq. (75) that in the case of $\eta = 1$ a phase dependence can be observed even in the absence of the vacuum induced quantum interference terms ($\Gamma_{12} = 0$). Only for $\eta = 0$, that is, when each laser couples to only one of the transitions, the phase terms solely depend on the vacuum induced quantum interference. However, this condition can be achieved only for an imperfect interference ($p \neq 1$) between the atomic transitions that the dipole

moments of the transitions are not parallel. From an experimental point of view the condition that each laser should only couple to one of two almost parallel dipole moments may be difficult to achieve. Menon and Agarwal [26] have proposed a scheme to overcome this difficulty using linearly polarized laser fields. In this scheme one can select the polarizations of the laser fields $\mathbf{E}_1$ and $\mathbf{E}_2$ such that $\boldsymbol{\mu}_1 \cdot \mathbf{E}_2 = \boldsymbol{\mu}_2 \cdot \mathbf{E}_1 = 0$. Since $\boldsymbol{\mu}_1$ is not parallel to $\boldsymbol{\mu}_2$, we obtain that $\boldsymbol{\mu}_1 \cdot \mathbf{E}_1 \neq 0$ and $\boldsymbol{\mu}_2 \cdot \mathbf{E}_2 \neq 0$.

In Fig. 2, we present the steady-state population inversion between the upper state $|1\rangle$ and the ground state $|2\rangle$, computed from the master equation (73), for $\eta = 0$ and different values of the phase difference $\delta\phi$ and the interference parameter p. It is seen that in the presence of quantum interference the population can be inverted on the $|1\rangle \rightarrow |2\rangle$ transition and the inversion can be controlled by the phase difference between the driving laser fields [27].

Paspalakis and Knight [28] have considered a V-type three-level system driven from an auxiliary level by two laser fields of the same frequencies. They have predicted linewidth narrowing and cancellation of the fluorescenc, which can be controlled via the phase difference between the two laser fields used for the excitation. Ghafoor et al. [29] have considered a four-level system in which quantum interference can be generated by three driving fields and have shown that the linewidths and intensities of the spectral lines can be controlled by the phases and amplitudes of the driving fields.

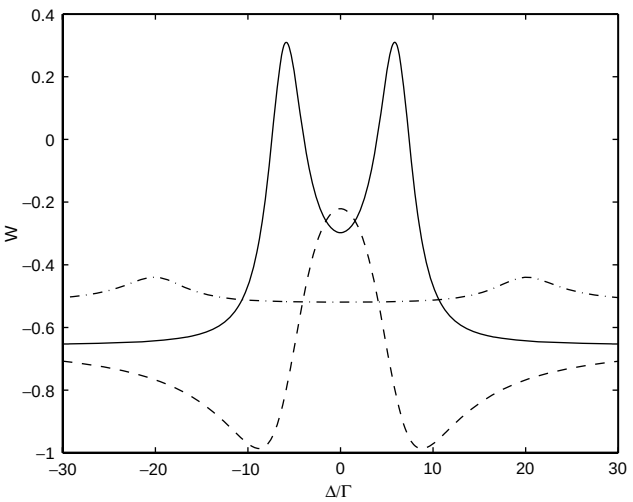

Figure 2. The steady-state population inversion $W = \rho_{11} - \rho_{22}$ as a function of $\Delta = \Delta_1 + \Delta_2$ for two fields of the same angular frequencies, $\Gamma_1 = 6\Gamma, \Gamma_2 = \Gamma, \Omega_1 = 20\Gamma, \Omega_2 = \Gamma$ and different p and $\delta\phi$: $p = 0.95, \delta\phi = 0$ (solid line), $p = 0.95, \delta\phi = \pi$ (dashed–line), $p = 0, \delta\phi = 0$ (dashed-dotted line).

C. Population Trapping and Dark States

In the literature, the population trapping is often referred to as a consequence of a cancellation of spontaneous emission. However, the cancellation of spontaneous emission from an atomic state not always leads to the trapping of the population in this nondecaying state. We shall illustrate this by considering the process of spontaneous emission from a V-type atom composed of two excited states $|1\rangle$, $|3\rangle$ and the ground state $|2\rangle$. For simplicity, we assume that spontaneous emission occurs from the excited states to the ground state with the same decay rates $\Gamma_1 = \Gamma_2 = \Gamma$, and the transition between the excited states is forbidden in the electric dipole approximation. The allowed transitions are represented by the dipole operators $S_1^+ = (S_1^-)^\dagger = |1\rangle\langle 2|$ and $S_2^+ = (S_2^-)^\dagger = |3\rangle\langle 2|$. In the absence of the driving field ($\Omega_1 = \Omega_2 = 0$), the master equation (64) leads to the following equations of motion for the density matrix elements

$$\begin{aligned}
\dot{\rho}_{11} &= -\Gamma\rho_{11} - \frac{1}{2}\Gamma_{12}(\rho_{13} + \rho_{31}) \\
\dot{\rho}_{33} &= -\Gamma\rho_{33} - \frac{1}{2}\Gamma_{12}(\rho_{13} + \rho_{31}) \\
\dot{\rho}_{22} &= \Gamma(\rho_{11} + \rho_{33}) + \Gamma_{12}(\rho_{13} + \rho_{31}) \\
\dot{\rho}_{13} &= -(\Gamma + i\Delta)\rho_{13} - \frac{1}{2}\Gamma_{12}(\rho_{11} + \rho_{33}) \\
\dot{\rho}_{31} &= -(\Gamma - i\Delta)\rho_{31} - \frac{1}{2}\Gamma_{12}(\rho_{11} + \rho_{33})
\end{aligned} \tag{76}$$

where $\Delta = \omega_1 - \omega_2$ is the frequency difference between the excited states and, for simplicity, we have ignored the small coherent coupling terms $\delta_{12}^{(\pm)}$.

There are two different steady-state solutions of Eq. (76) depending on whether the transitions are degenerate ($\Delta = 0$) or nondegenerate ($\Delta \neq 0$). This fact is connected with the existence of a linear combination of the density matrix elements

$$\alpha(t) = \rho_{11}(t) + \rho_{33}(t) - \rho_{13}(t) - \rho_{31}(t) \tag{77}$$

which, for $\Delta = 0$ and $\Gamma_{12} = \Gamma$ is a constant of motion [4,31].

In this case the steady-state solutions for the density matrix elements are

$$\begin{aligned}
\rho_{11}(\infty) &= \rho_{33}(\infty) = \frac{1}{4}\alpha(0) \\
\rho_{13}(\infty) &= \rho_{31}(\infty) = -\frac{1}{4}\alpha(0) \\
\rho_{22}(\infty) &= \frac{1}{2}\alpha(0)
\end{aligned} \tag{78}$$

Therefore, if $\alpha(0) \neq 0$, then a part of the population remains in the excited states for all times $t > 0$.

On the other hand, for $\Delta \neq 0$ and/or $\Gamma_{12} \neq \Gamma$ the linear combination (77) is no longer a constant of motion, and then the steady-state solutions for the density matrix elements are

$$\begin{aligned} &\rho_{11}(\infty) = \rho_{33}(\infty) = \rho_{13}(\infty) = \rho_{31}(\infty) = 0 \\ &\rho_{22}(\infty) = 1 \end{aligned} \tag{79}$$

In this case the steady-state solutions for the density matrix elements do not depend on the initial state of the atom.

The steady-state behavior of the system can be explained in terms of superposition states induced by the cross-damping Γ_{12}. Introducing superposition states

$$\begin{aligned} |s\rangle &= \frac{1}{\sqrt{2}}(|1\rangle + |3\rangle) \\ |a\rangle &= \frac{1}{\sqrt{2}}(|1\rangle - |3\rangle) \end{aligned} \tag{80}$$

we find from Eq. (76) the following equations of motion for the populations of the superposition states:

$$\begin{aligned} \dot{\rho}_{ss} &= -\frac{1}{2}(\Gamma + \Gamma_{12})\rho_{ss} - \frac{1}{2}i\Delta(\rho_{sa} - \rho_{as}) \\ \dot{\rho}_{aa} &= -\frac{1}{2}(\Gamma - \Gamma_{12})\rho_{aa} + \frac{1}{2}i\Delta(\rho_{sa} - \rho_{as}) \end{aligned} \tag{81}$$

A number of interesting conclusions follow from Eq. (81). In the first place, we note that the superposition states decay at different rates, the symmetric state decays with an enhanced rate $(\Gamma + \Gamma_{12})$, while the antisymmetric state decays at a reduced rate $(\Gamma - \Gamma_{12})$. For $\Gamma_{12} = \Gamma$, the antisymmetric state does not decay at all. In this case the antisymmetric state can be regarded as a *dark state* in the sense that the state is decoupled from the environment. Second, we note from Eq. (81) that the state $|a\rangle$ is coupled to the state $|s\rangle$ through the splitting Δ, which plays a role here similar to the Rabi frequency of the coherent interaction between the symmetric and antisymmetric states. Consequently, an initial population in the state $|a\rangle$ can be coherently transferred to the state $|s\rangle$, which rapidly decays to the ground state. When $\Delta = 0$, that is, the excited states are degenerate, the coherent interaction does not take place and then any initial population in $|a\rangle$ will stay in this state for all times. In this case we can say that the population is *trapped* in the state $|a\rangle$.

We can conclude that the cancellation of spontaneous emission not necessary leads to the population trapping. The population can be trapped in a nondecaying state only if the state is completely decoupled from any interactions.

V. QUANTUM INTERFERENCE EFFECTS IN COHERENTLY DRIVEN SYSTEMS

The discussion, presented in Section IV, has been concentrated on analysis of the effect of quantum interference on spontaneous emission in a V-type three-level atom. With the specific examples we have demonstrated that spontaneous emission can be controlled and even suppressed by quantum interference. In this section, we extend the analysis to the case of coherently driven systems. We will present simple models for quantum interference in which atomic systems are composed of two coupled dipole subsystems. In particular, we consider interference effects in coherently driven V and Λ-type three-level atoms. Each of the three systems is represented by two dipole moments, $\boldsymbol{\mu}_1$ and $\boldsymbol{\mu}_2$, interacting through the vacuum field.

A. Three-Level V System

Our first example for quantum interference in driven atomic systems is a three-level atom in the V configuration composed of two nondegenerate excited levels $|1\rangle$ and $|3\rangle$ and a single ground level $|2\rangle$. The upper levels $|1\rangle$ and $|3\rangle$ can decay to the ground level by spontaneous emission with decay rates Γ_1 and Γ_2, respectively, whereas transitions between the excited levels are forbidden in the electric dipole approximation. The two decaying transitions have dipole moments $\boldsymbol{\mu}_{12}$ and $\boldsymbol{\mu}_{32}$ sharing the same ground level $|2\rangle$ and are represented by the operators $S_1^+ = (S_1^-)^\dagger = |1\rangle\langle 2|$ and $S_2^+ = (S_2^-)^\dagger = |3\rangle\langle 2|$. The system can be driven by a coherent laser field from an auxiliary level or the laser field can directly couple to the decaying transitions.

1. *Driving from an Auxiliary Level*

Zhu and Scully [32] have shown that quantum interference in a V-type system, driven by a laser field from an auxiliary level, can lead to the elimination of the spectral line at the driving laser frequency.

The four-level system considered by Zhu and Scully is shown in Fig. 3. The laser field is coupled to nondecaying $|1\rangle - |b\rangle$ and $|3\rangle - |b\rangle$ transitions, whereas spontaneous emission occurs from the levels $|1\rangle, |3\rangle$ to the ground level $|2\rangle$.

The most direct approach to the analysis of the dynamics of the system is the master equation (64) with the Hamiltonian H' given by

$$H' = \hbar\omega_1 S_1^+ S_1^- + \hbar\omega_2 S_2^+ S_2^- + \hbar\omega_b |b\rangle\langle b| - \frac{1}{2}\hbar[(\Omega_1 S_{1b}^+ + \Omega_2 S_{3b}^+)e^{-i\omega_L t} + \text{H.c.}] \tag{82}$$

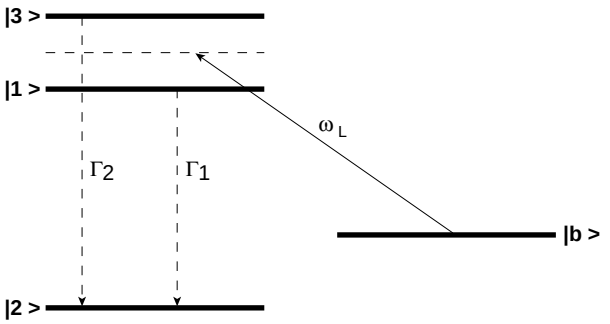

Figure 3. Three-level V-type system driven from an auxiliary level.

where $S_{1b}^{+} = |1\rangle\langle b|$ and $S_{3b}^{+} = |3\rangle\langle b|$ are the dipole raising operators for the transitions between the upper levels $|1\rangle, |3\rangle$ and the auxiliary level $|b\rangle$.

The spectrum of the fluorescence field emitted on the $|1\rangle \to |2\rangle$ and $|3\rangle \to |2\rangle$ transitions is given by the Fourier transform of the average two-time correlation function of the dipole moments of the transitions that, according to the quantum regression theorem [33], satisfy the same equations of motion as the density matrix elements $\rho_{12}(t)$ and $\rho_{32}(t)$. Using the master equation (64) with the Hamiltonian (82), we obtain the following set of coupled equations of motion for the density matrix elements

$$\frac{\partial}{\partial t}\mathbf{X}(t) = M\mathbf{X}(t) \tag{83}$$

where $\mathbf{X}(t) = [\rho_{12}(t), \rho_{32}(t), \rho_{b2}(t)]$ is a column vector composed of the density matrix elements, and M is the 3×3 matrix

$$M = \begin{pmatrix} -(\frac{1}{2}\Gamma_1 + i\Delta_1) & -\frac{1}{2}\Gamma_{12} & \frac{1}{2}i\Omega_1 \\ -\frac{1}{2}\Gamma_{12} & -(\frac{1}{2}\Gamma_2 + i\Delta_2) & \frac{1}{2}i\Omega_2 \\ \frac{1}{2}i\Omega_1 & \frac{1}{2}i\Omega_2 & 0 \end{pmatrix} \tag{84}$$

where $\Delta_1 = \omega_{1b} - \omega_L$ and $\Delta_2 = \omega_{3b} - \omega_L$ are the detunings of the laser field from the $|1\rangle - |b\rangle$ and $|3\rangle - |b\rangle$ transitions, respectively.

Since we are interested in the time evolution of the density matrix elements, we will need explicit expressions for the components X_i of the vector $\mathbf{X}(t)$ in terms of their initial values. This can be done by a direct integration of (83). Thus, if t_0 denotes an arbitrary initial time, the integration of (83) leads to the following formal solution for $\mathbf{X}(t)$

$$\mathbf{X}(t) = \mathbf{X}(t_0)e^{Mt} \tag{85}$$

Because the determinant of the matrix M is different from zero, there exists a complex invertible matrix T that diagonalize M, and $\lambda = T^{-1}MT$ is the diagonal matrix of complex eigenvalues, which can be found from the eigenvalue equation

$$\lambda\left(\lambda + \frac{1}{2}\Gamma_1 + i\Delta_1\right)\left(\lambda + \frac{1}{2}\Gamma_2 + i\Delta_2\right) - \frac{1}{4}\Gamma_{12}(\Gamma_{12}\lambda + \Omega_1\Omega_2) + \frac{1}{4}\Omega_1\left(\lambda + \frac{1}{2}\Gamma_2 + i\Delta_2\right) + \frac{1}{4}\Omega_2\left(\lambda + \frac{1}{2}\Gamma_1 + i\Delta_1\right) = 0 \tag{86}$$

Following Zhu and Scully, we assume that $\Gamma_1 = \Gamma_2 = \Gamma$, $\Omega_1 = \Omega_2 = \Omega$ and that the laser field is tuned to the middle of the upper-level splitting; $\Delta_2 = -\Delta_1 = \frac{1}{2}\Delta$. In this case, the cubic equation, Eq. (86), simplifies to

$$\lambda\left[\lambda^2 + \Gamma\lambda + \frac{1}{4}\Delta^2 + \frac{1}{4}\left(\Gamma^2 - \Gamma_{12}^2\right)\right] + \frac{1}{2}\Omega^2\left[\lambda + \frac{1}{2}(\Gamma - \Gamma_{12})\right] = 0 \tag{87}$$

There are two different solutions of Eq. (87) depending on whether $\Gamma_{12} = \Gamma$ or $\Gamma_{12} \neq \Gamma$. For $\Gamma_{12} = \Gamma$, which corresponds to parallel dipole moments of the transitions, and $\Omega \gg \Gamma$ the roots of the cubic equation (87) are

$$\begin{aligned}
\lambda_1 &= 0 \\
\lambda_2 &= -\frac{1}{2}\Gamma + \frac{1}{2}i\sqrt{\Delta^2 + 2\Omega^2} \\
\lambda_3 &= -\frac{1}{2}\Gamma - \frac{1}{2}i\sqrt{\Delta^2 + 2\Omega^2}
\end{aligned} \tag{88}$$

while for $\Gamma_{12} = 0$, which corresponds to perpendicular dipole moments, and $\Omega \gg \Gamma$ the roots are

$$\begin{aligned}
\lambda_1 &= -\frac{1}{2}\Gamma \\
\lambda_2 &= -\frac{1}{4}\Gamma + \frac{1}{2}i\sqrt{\Delta^2 + 2\Omega^2} \\
\lambda_3 &= -\frac{1}{4}\Gamma - \frac{1}{2}i\sqrt{\Delta^2 + 2\Omega^2}
\end{aligned} \tag{89}$$

Thus, in the case of parallel dipole moments the spectrum is composed of two lines of equal bandwidths ($\frac{1}{2}\Gamma$) located at frequencies $\pm\frac{1}{2}\sqrt{\Delta^2 + 2\Omega^2}$ and there is no the central component in the fluorescence spectrum at the laser frequency ω_L. The eigenvalue $\lambda = 0$ contributes to the coherent scattering of the laser field. When $\Gamma_{12} = 0$, the spectrum is composed of three lines: the central line of the bandwidth $\frac{1}{2}\Gamma$ located at the laser frequency and two sidebands of bandwidths $\frac{1}{4}\Gamma$

located at $\pm\frac{1}{2}\sqrt{\Delta^2+2\Omega^2}$. The absence of the central line for $\Gamma_{12}=\Gamma$ is clear evidence of the quantum interference cancellation of spontaneous emission into the vacuum modes around the laser frequency.

Lee et al. [34] have shown that the physical origin of the cancellation of the central line in the spectrum can be explained clearly by the dressed-atom model of the system [35]. In this model we use a fully quantum-mechanical description of the Hamiltonian (65), which in a frame rotating with the laser frequency ω_L can be written as

$$H' = H_{0b} + V_b \tag{90}$$

where

$$H_{0b} = \hbar\Delta_1 S_1^+ S_1^- + \hbar\Delta_2 S_2^+ S_2^- + \hbar\omega_L a_L^\dagger a_L \tag{91}$$

is the Hamiltonian of the uncoupled system and the laser field, and

$$V_b = -\frac{\hbar}{2} g[(S_{1b}^+ + S_{2b}^+)a_L + a_L^\dagger(S_{1b}^- + S_{2b}^-)] \tag{92}$$

is the interaction of the laser with the atom. In Eq. (92), g is the system field coupling constant and a_L ($a_L^\dagger$) is the annihilation (creation) operator for the driving field mode.

For $\Delta_2 = -\Delta_1 = \frac{1}{2}\Delta$, the Hamiltonian H_{0b} has four nondegenerate eigenstates $|2,N\rangle$, $|b,N\rangle$, $|1,N-1\rangle$, and $|3,N-1\rangle$, where $|i,N\rangle$ is the state with the atom in state $|i\rangle$ and N photons present in the driving laser mode. When we include the interaction V_b, the diagonalization of the Hamiltonian $H_{0b}+V_b$ leads to the following dressed states of the system

$$\begin{aligned}
|+,N\rangle &= \frac{1}{2}[(1-\alpha)|1,N-1\rangle + (1+\alpha)|3,N-1\rangle - 2\beta|b,N\rangle] \\
|0,N\rangle &= -\beta(|1,N-1\rangle - |3,N-1\rangle) + \alpha|b,N\rangle \\
|-,N\rangle &= \frac{-1}{2}[(1+\alpha)|1,N-1\rangle + (1-\alpha)|3,N-1\rangle + 2\beta|b,N\rangle] \\
|2,N\rangle &= |2,N\rangle
\end{aligned} \tag{93}$$

with energies

$$\begin{aligned}
E_{N,+} &= \hbar(N\omega_L + \Omega') \\
E_{N,0} &= \hbar N\omega_L \\
E_{N,-} &= \hbar(N\omega_L - \Omega') \\
E_{N,2} &= \hbar N\omega_L
\end{aligned} \tag{94}$$

where $\Omega' = \frac{1}{2}\sqrt{\Delta^2+2\Omega^2}$, $\alpha = \Delta/2\Omega'$, and $\beta = \Omega/2\Omega'$.

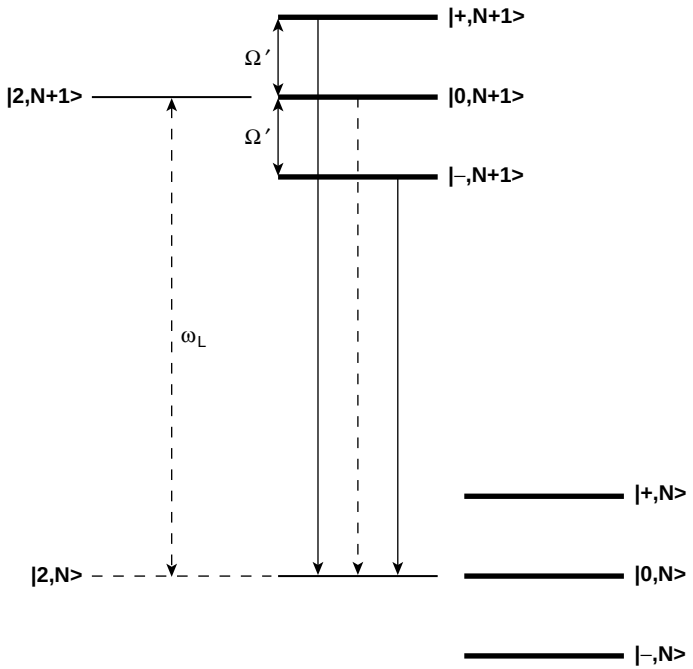

Figure 4. Dressed states of two neighboring manifolds, $N+1$ and N. Solid arrows indicate transitions at $\omega_L \pm \Omega'$ that are only slightly affected by quantum interference, while the dashed arrow indicates the transition at the laser frequency ω_L, which is strongly affected by quantum interference and vanishes for parallel dipole moments and $|\boldsymbol{\mu}_{12}| = |\boldsymbol{\mu}_{32}|$.

Dressed states of two neighboring manifolds are shown in Fig. 4. The manifolds are separated by ω_L, while the states inside each manifold are separated by Ω'. The dressed states are connected by transition dipole moments. It is easily verified that nonzero dipole moments occur only between states within neighboring manifolds. Using Eq. (93), we find that the transition dipole moments between $|i, N+1\rangle$ $(i = 0, -, +)$ and $|2, N\rangle$ are

$$\begin{aligned}
\langle N+1, +|\boldsymbol{\mu}|2, N\rangle &= (1-\alpha)\boldsymbol{\mu}_{12} + (1+\alpha)\boldsymbol{\mu}_{32} \\
\langle N+1, 0|\boldsymbol{\mu}|2, N\rangle &= -\beta(\boldsymbol{\mu}_{12} - \boldsymbol{\mu}_{32}) \\
\langle N+1, -|\boldsymbol{\mu}|2, N\rangle &= -[(1+\alpha)\boldsymbol{\mu}_{12} + (1-\alpha)\boldsymbol{\mu}_{32}]
\end{aligned} \tag{95}$$

whereas the transition dipole moments $\langle N, 2|\boldsymbol{\mu}|i, N-1\rangle$ between $|2, N\rangle$ and the dressed states $|i, N-1\rangle$ of the manifold below are equal to zero. It is evident from Eq. (95) that transitions to the state $|2, N\rangle$ depend on the mutual

polarization of the dipole moments $\boldsymbol{\mu}_{12}$ and $\boldsymbol{\mu}_{32}$. For $\boldsymbol{\mu}_{12} \parallel \boldsymbol{\mu}_{32}$ and $|\boldsymbol{\mu}_{12}| = |\boldsymbol{\mu}_{32}|$, the transition dipole moment $\langle N+1, 0|\boldsymbol{\mu}|2, N\rangle$ vanishes, resulting in the disappearance of the central component of the fluorescence spectrum. When $\boldsymbol{\mu}_{12}$ and $\boldsymbol{\mu}_{32}$ are not parallel, all the transitions are allowed and three lines can be seen in the spectrum.

The dressed-atom predictions clearly explain the origin of the cancellation of the spectral line arising from the cancellation of the transition dipole moment due to quantum interference between the two atomic transitions.

2. *Direct Driving of the Atomic Transitions*

Another area of interest in quantum interference effects, which has been studied extensively, is the response of a V-type three-level atom to a coherent laser field directly coupled to the decaying transitions. This was studied by Cardimona et al. [36], who found that the system can be driven into a trapping state in which quantum interference prevents any fluorescence from the excited levels, regardless of the intensity of the driving laser. Similar predictions have been reported by Zhou and Swain [5], who have shown that ultrasharp spectral lines can be predicted in the fluorescence spectrum when the dipole moments of the atomic transitions are nearly parallel and the fluorescence can be completely quenched when the dipole moments are exactly parallel.

When the atomic transitions $|1\rangle \to |2\rangle$ and $|3\rangle \to |2\rangle$ are directly driven by a laser field, the master equation (64) leads to the following set of equations of motions for the density matrix elements

$$
\begin{aligned}
\dot{\tilde{\rho}}_{12} = (\dot{\tilde{\rho}}_{21})^* &= \frac{1}{2} i\Omega_1 - \left[\frac{1}{2}\Gamma_1 - i\left(\Delta_L - \frac{1}{2}\Delta\right)\right]\tilde{\rho}_{12} - \frac{1}{2}\Gamma_{12}\tilde{\rho}_{32} \\
&\quad - \frac{1}{2} i\Omega_2 \rho_{13} - \frac{1}{2} i\Omega_1 (2\rho_{11} + \rho_{33}) \\
\dot{\tilde{\rho}}_{32} = (\dot{\tilde{\rho}}_{23})^* &= \frac{1}{2} i\Omega_2 - \left[\frac{1}{2}\Gamma_2 - i\left(\Delta_L + \frac{1}{2}\Delta\right)\right]\tilde{\rho}_{32} - \frac{1}{2}\Gamma_{12}\tilde{\rho}_{12} \\
&\quad - \frac{1}{2} i\Omega_1 \rho_{31} - \frac{1}{2} i\Omega_2 (2\rho_{33} + \rho_{11}) \\
\dot{\rho}_{31} = (\dot{\rho}_{13})^* &= -\left[\frac{1}{2}(\Gamma_1 + \Gamma_2) - i\Delta\right]\rho_{31} - \frac{1}{2}\Gamma_{12}(\rho_{33} + \rho_{11}) \\
&\quad - \frac{1}{2} i\Omega_1 \tilde{\rho}_{32} + \frac{1}{2} i\Omega_2 \tilde{\rho}_{21}, \\
\dot{\rho}_{11} &= -\Gamma_1 \rho_{11} - \frac{1}{2}\Gamma_{12}(\rho_{13} + \rho_{31}) + \frac{1}{2} i\Omega_1 (\tilde{\rho}_{21} - \tilde{\rho}_{12}) \\
\dot{\rho}_{33} &= -\Gamma_2 \rho_{33} - \frac{1}{2}\Gamma_{12}(\rho_{13} + \rho_{31}) + \frac{1}{2} i\Omega_2 (\tilde{\rho}_{23} - \tilde{\rho}_{32})
\end{aligned}
\tag{96}
$$

where

$$\tilde{\rho}_{j2} = \rho_{j2} e^{i(\omega_L t + \phi_L)}, \quad (j = 1, 3) \tag{97}$$

and $\Delta_L = \omega_L - \frac{1}{2}(\omega_1 + \omega_2)$ is the detuning of the laser frequency from the middle of the upper-level splitting.

The equations of motion (96) can be used to calculate the steady-state fluorescence spectrum of the driven atom. The spectrum is defined as the Fourier transform of the stationary value of the two-time correlation function of the electric field operators

$$\Lambda(\omega) = \mathrm{Re} \int_0^\infty d\tau \lim_{t\to\infty} \langle \hat{\mathbf{E}}^{(-)}(\mathbf{R}, t) \cdot \hat{\mathbf{E}}^{(+)}(\mathbf{R}, t + \tau) \rangle e^{i\omega\tau} \tag{98}$$

According to Eq. (34), the spectrum can be expressed in terms of the atomic correlation functions as

$$\begin{aligned} \Lambda(\omega) = \mathrm{Re} \int_0^\infty d\tau \lim_{t\to\infty} \{ & \Gamma_1 \langle S_1^+(t) S_1^-(t+\tau) \rangle + \Gamma_2 \langle S_2^+(t) S_2^-(t+\tau) \rangle \\ & + \Gamma_{12} (\langle S_1^+(t) S_2^-(t+\tau) \rangle + \langle S_2^+(t) S_1^-(t+\tau) \rangle) \} e^{i\omega\tau} \end{aligned} \tag{199}$$

From the quantum regression theorem [33], it is well known that the two-time averages $\langle S_m^+(t) S_n^-(t+\tau) \rangle$ satisfy the same equations of motion as do the one-time averages $\langle S_n^-(t) \rangle$ which, on the other hand, satisfy the same equations of motion as do the density matrix elements $\rho_{ij}(t)$.

In Fig. 5 we plot the fluorescence spectrum for a strong driving field tuned to the middle of the upper-level splitting Δ. For small Δ the spectrum exhibits a three-peak structure, similar to the Mollow spectrum of a two-level atom [37], while for large Δ the spectrum consists of five peaks whose the intensities and widths vary with the cross-damping term Γ_{12}. When the dipole moments are nearly parallel, $\Gamma_{12} = 0.999\Gamma$, a significant sharp peak appears at the central frequency superimposed on a broad peak. However, in the case of exactly parallel dipole moments, $\Gamma_{12} = \Gamma$, and the fluorescence emission quenches completely at all frequencies.

The dependence of the number of peaks on the splitting Δ, and the variation of their intensities and widths with Γ_{12} can be readily explained in terms of transition rates between dressed states of the system. For the three-level system discussed here, the Hamiltonian (65) takes the form

$$H' = H_0 + V_L \tag{100}$$

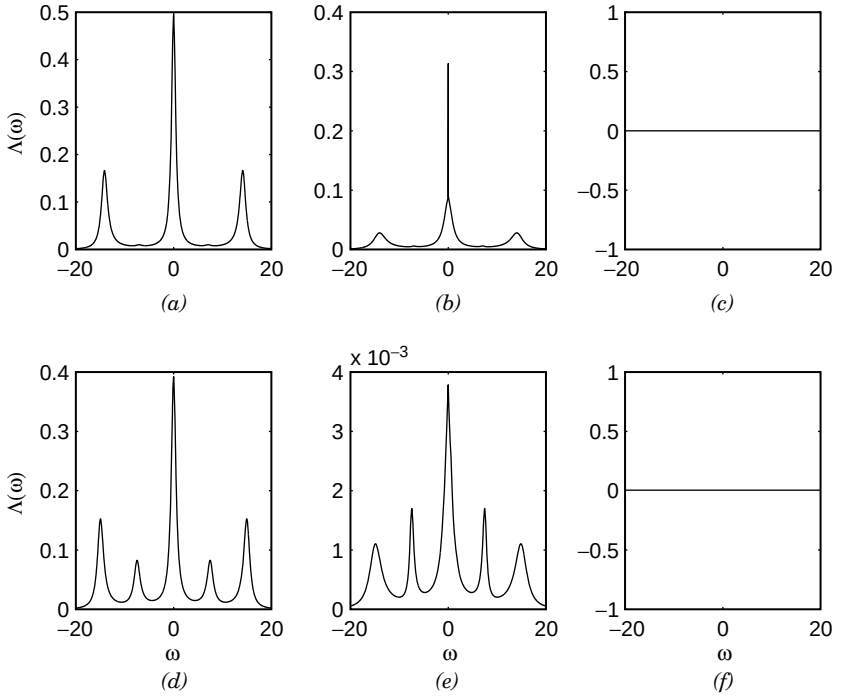

Figure 5. The fluorescence spectrum for the V-type three-level atom with nondegenerate transitions driven by a strong laser field of the Rabi frequency $\Omega = 5\Gamma_1$, $\Delta_L = 0, \Gamma_1 = \Gamma_2 = \Gamma$, and different Δ and Γ_{12}: (a) $\Delta = \Gamma, \Gamma_{12} = 0$; (b) $\Delta = \Gamma, \Gamma_{12} = 0.999\Gamma$; (c) $\Delta = \Gamma, \Gamma_{12} = \Gamma$; (d) $\Delta = 5\Gamma, \Gamma_{12} = 0$; (e) $\Delta = 5\Gamma, \Gamma_{12} = 0.999\Gamma$; (f) $\Delta = 5\Gamma, \Gamma_{12} = \Gamma$.

where

$$H_0 = -\hbar\left(\Delta_L - \frac{1}{2}\Delta\right)S_1^+S_1^- - \hbar\left(\Delta_L + \frac{1}{2}\Delta\right)S_2^+S_2^- + \hbar\omega_L a_L^\dagger a_L \tag{101}$$

is the Hamiltonian of the uncoupled system and the laser field, and

$$V_L = -\frac{\hbar}{2}g[a_L^\dagger(S_1^- + S_2^-) + (S_1^+ + S_2^+)a_L] \tag{102}$$

is the interaction between the laser field and the atomic transitions.

For $\Delta_L = 0$, the Hamiltonian H_0 has three nondegenerate eigenstates $|2, N\rangle$, $|1, N-1\rangle$, and $|3, N-1\rangle$, where $|i, N\rangle$ is the state with the atom in state $|i\rangle$ and

N photons present in the driving laser mode. When we include the interaction V_L the triplets recombine into new triplets with eigenvectors (dressed states)

$$\begin{aligned}
|+,N\rangle &= \frac{1}{2}[(1-\alpha)|1,N-1\rangle + (1+\alpha)|3,N-1\rangle - 2\beta|2,N\rangle] \\
|0,N\rangle &= -\beta(|1,N-1\rangle - |3,N-1\rangle) + \alpha|2,N\rangle \\
|-,N\rangle &= \frac{-1}{2}[(1+\alpha)|1,N-1\rangle + (1-\alpha)|3,N-1\rangle + 2\beta|2,N\rangle]
\end{aligned} \tag{103}$$

corresponding to energies

$$\begin{aligned}
E_{N,+} &= \hbar(N\omega_L + \tilde{\Omega}) \\
E_{N,0} &= \hbar N\omega_L \\
E_{N,-} &= \hbar(N\omega_L - \tilde{\Omega})
\end{aligned} \tag{104}$$

where $\tilde{\Omega} = \sqrt{\Delta^2 + \frac{1}{2}\Omega^2}$, $\alpha = \Delta/2\tilde{\Omega}$, and $\beta = \Omega/2\tilde{\Omega}$.

The dressed states (103) group into manifolds, each containing three states. Neighboring manifolds are separated by ω_L, while the states inside each manifold are separated by $\tilde{\Omega}$. Interaction between the atom and the vacuum field leads to a spontaneous emission cascade down its energy manifold ladder. The probability of a transition between any two dressed states is proportional to the absolute square of the the dipole transition moment between these states. It is easily verified that nonzero dipole moments occur only between states within neighboring manifolds. Using (103) and assuming that $\boldsymbol{\mu}_{13} = \boldsymbol{\mu}_{23} = \boldsymbol{\mu}$, we find that the transition dipole moments between $|0,N\rangle$ and the dressed states of the manifold above are

$$\begin{aligned}
\langle N+1,+|\boldsymbol{\mu}|0,N\rangle &= \frac{1}{2}\alpha\boldsymbol{\mu}[(1-\alpha) + (1+\alpha)\cos\theta] \\
\langle N+1,0|\boldsymbol{\mu}|0,N\rangle &= -\alpha\beta\boldsymbol{\mu}(1-\cos\theta) \\
\langle N+1,-|\boldsymbol{\mu}|0,N\rangle &= -\frac{1}{2}\alpha\boldsymbol{\mu}[(1+\alpha) + (1-\alpha)\cos\theta]
\end{aligned} \tag{105}$$

whereas the transition dipole moments between $|0,N\rangle$ and the dressed states of the manifold below are

$$\begin{aligned}
\langle N,0|\boldsymbol{\mu}|+,N-1\rangle &= \beta^2\boldsymbol{\mu}(1-\cos\theta) \\
\langle N,0|\boldsymbol{\mu}|0,N-1\rangle &= -\alpha\beta\boldsymbol{\mu}(1-\cos\theta) \\
\langle N,0|\boldsymbol{\mu}|-,N-1\rangle &= \beta^2\boldsymbol{\mu}(1-\cos\theta)
\end{aligned} \tag{106}$$

where θ is the angle between the dipole moments.

It is apparent from Eq. (106) that transitions from the state $|0,N\rangle$ to the dressed states of the manifold below are allowed only if the dipole moments are not parallel. The transitions occur with significantly reduced rates, proportional to $(1-\cos\theta)$, giving very narrow lines when $\theta \approx 0^o$. For parallel dipole moments the transitions to the state $|0,N\rangle$ are allowed from the dressed states of the manifold above, but are forbidden to the states of the manifold below. Therefore, the state $|0,N\rangle$ is a trapping state such that the population can flow into this state, but cannot leave it resulting in the disappearance of the fluorescence from the driven atom. The nonzero transition rates to the state $|0,N\rangle$ are proportional to α and are allowed only when $\Delta \neq 0$. Otherwise, for $\Delta = 0$, the state $|0,N\rangle$ is completely decoupled from the remaining dressed states. In this case the three-level system reduces to that equivalent to a two-level atom.

The preceding dressed-atom analysis shows that quantum interference and the driving laser field create a "dressed" trapping state that is a linear superposition of the $|a\rangle$ and $|2\rangle$ states. This trapping state is different from the trapping state created by quantum interference in the absence of the driving field [see Eq. (80)], which is the antisymmetric state $|a\rangle$ alone. As is seen from Eq. (103), the dressed trapping state reduces to the state $|a\rangle$ for a very strong driving field ($\Omega \gg \Delta$).

An alternative way of viewing the process of the reduction of the dressed trapping state to the state $|a\rangle$ in a very strong field is to analyze the equations of motion for the density matrix elements in terms of the symmetric and antisymmetric superpositions of the atomic excited states

$$|s\rangle = \frac{1}{\sqrt{1+r}}(|1\rangle + \sqrt{r}|3\rangle) \tag{107}$$

$$|a\rangle = \frac{1}{\sqrt{1+r}}(\sqrt{r}|1\rangle - |3\rangle) \tag{108}$$

where $r = \Gamma_2/\Gamma_1$.

For $\Gamma_1 = \Gamma_2 = \Gamma$ and $\Omega_1 = \Omega_2 = \Omega$ the equations of motion for the populations ρ_{ss} and ρ_{aa} of the symmetric and antisymmetric states are

$$\begin{aligned}\dot{\rho}_{ss} &= -\frac{1}{2}(1+p)\Gamma\rho_{ss} - \frac{1}{2}i\Delta(\rho_{sa} - \rho_{as}) - i\sqrt{2}\Omega(\rho_{2s} - \rho_{s2})\\ \dot{\rho}_{aa} &= -\frac{1}{2}(1-p)\Gamma\rho_{aa} + \frac{1}{2}i\Delta(\rho_{sa} - \rho_{as})\end{aligned} \tag{109}$$

The first terms on the right-hand side of Eq. (109) determine the spontaneous emission rates from the symmetric and antisymmetric states, while the second terms determine the coherent interaction between these two states. Note that the

antisymmetric state is not driven by the laser field and the equation of motion for ρ_{aa} has the same form as that in the absence of the driving field [see Eq. (81)].

We have shown in Section III, that in the absence of a driving field the coherent interaction Δ between the symmetric and antisymmetric states can destroy the population trapping. However, as it has been shown by Akram et al. [24], the role of the coherent interaction can reverse in the presence of the driving field. In this case the coherent interaction Δ can transfer the population from the driven $|s\rangle$ state to the undriven and nondecaying $|a\rangle$ state. This is shown in Fig. 6, where we plot the steady-state population ρ_{aa} as a function of Δ_L for different Ω. It is seen that the antisymmetric state is populated by the presence of the coherent interaction Δ. The amount of population in $|a\rangle$ increases with increasing Ω and attains the maximum value $\rho_{aa} \approx 1$ at $\Delta_L = 0$ and a very strong driving field. This effect can be interpreted as a population trapping induced by the laser field and the coherent interaction between the symmetric and antisymmetric states.

3. *Quantum Interference in Probe Absorption*

The narrow resonances produced by quantum interference may also be observed in the absorption spectrum of a three-level atom probed by a weak field of the frequency ω_p. Zhou and Swain [10] have calculated the absorption spectrum of a probe field monitoring V-type three-level atoms with degenerate $(\Delta = 0)$ as well as nondegenerate $(\Delta \neq 0)$ transitions and have demonstrated that quantum

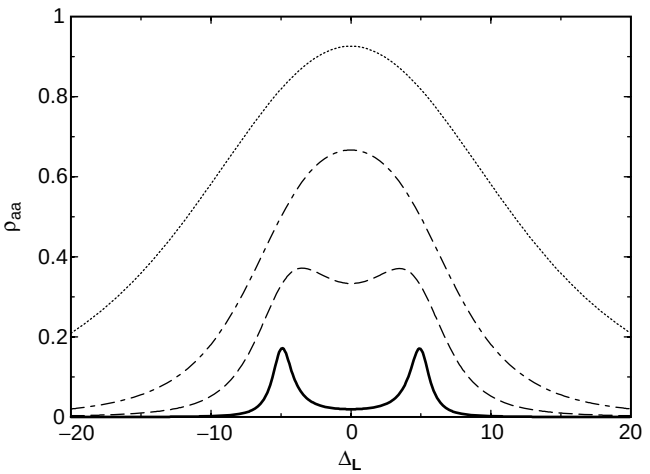

Figure 6. The steady-state population of the antisymmetric state $|a\rangle$ as a function of Δ_L for $\Gamma_1 = \Gamma_2 = \Gamma, \Delta = 5\Gamma, p = 1$, and different Ω: $\Omega = \Gamma$ (solid line), $\Omega = 5\Gamma$ (dashed–line), $\Omega = 10\Gamma$ (dashed-dotted line), $\Omega = 25\Gamma$ (dotted line).

interference between the two atomic transitions can result in very narrow spectral lines, transparency, and even gain without population inversion.

The absorption spectrum can be given in terms of the Fourier transform of the average value of the two-time commutator of the atomic dipole operators as [38]

$$\begin{aligned} A(\omega) = \mathrm{Re}\int_0^\infty d\tau e^{i\omega_p\tau} \\ \times \lim_{t\to\infty}\{\Gamma_1\langle[S_1^-(t+\tau), S_1^+(t)]\rangle + \Gamma_2\langle[S_2^-(t+\tau), S_2^+(t)]\rangle. \\ + .\Gamma_{12}(\langle[S_1^-(t+\tau), S_2^+(t)]\rangle + \langle[S_2^-(t+\tau), S_1^+(t)]\rangle)\} \end{aligned} \tag{110}$$

where the terms $\langle S_i^-(t+\tau)S_j^+(t)\rangle$ are associated with absorption and the terms $\langle S_i^+(t+\tau)S_j^-(t)\rangle$ with stimulated emission of the probe field. The absorption spectrum can be calculated from the equations of motion (96) in conjugation with the quantum regression theorem. In the absence of the driving laser field ($\Omega = 0$) and $\Gamma_{12} \approx \Gamma$, the absorption spectrum of a three-level atom with degenerate transitions ($\Delta = 0$) consists of a subnatural linewidth peak superimposed on a broad peak, both centered on the resonant frequency $\omega_p = \omega_0$, where $\omega_0 = \frac{1}{2}(\omega_1 + \omega_2)$.

This is shown in Fig. 7 and can be easily interpreted in terms of the symmetric and antisymmetric superpositions of the excited atomic states. For $\Delta = 0$ and $\Gamma_{12} \neq \Gamma$, the superposition states decay independently with the rates $(\Gamma + \Gamma_{12})$ and $(\Gamma - \Gamma_{12})$, respectively. The broad peak, seen in Fig. 7, corresponds to the absorption on the $|2\rangle - |s\rangle$ transition of the linewidth $(\Gamma + \Gamma_{12})$, whereas the narrow peak of the linewidth $(\Gamma - \Gamma_{12})$ arises from the absorption of the probe field on the $|2\rangle - |a\rangle$ transition. When the dipole moments of the atomic transitions are parallel, $\Gamma_{12} = \Gamma$, and then the dipole moment of the $|2\rangle - |a\rangle$ transition vanishes. In this case the probe only couples to the $|2\rangle - |s\rangle$ transition resulting in a single broad peak in the absorption spectrum, as seen in Fig. 7d.

Figure 8 shows the absorption spectrum of a three-level atom with nondegenerate transitions ($\Delta \neq 0$). One notable feature of the absorption spectrum is a single broad peak with a narrow hole burned at the average atomic transition frequency ω_0. The hole changes into a dispersive structure for unequal damping rates of the atomic transitions. The origin of the hole burning is in the coherent oscillations of the population between the symmetric and antisymmetric states. The oscillations are induced by the coherent interaction Δ, and can be readily understand from Eq. (109), which shows that the population coherently oscillates between the $|s\rangle$ and $|a\rangle$ states with frequency $\Delta/2$.

The shape of the dip in the absorption spectrum can be obtained by finding the analytical form of the absorption spectrum. Using Eqs. (96) and (110), we

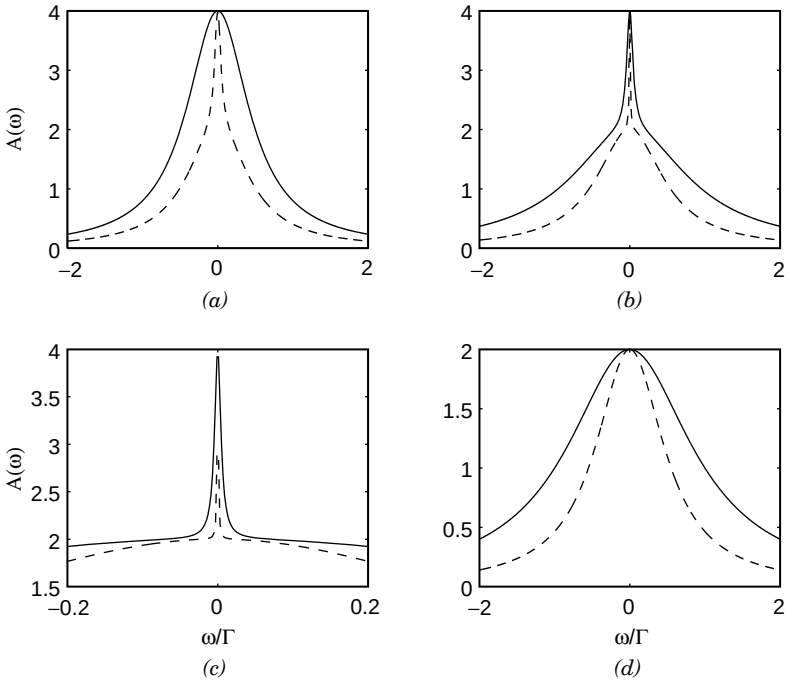

Figure 7. The absorption spectrum as a function of $\omega = \omega_p - \omega_0$ for degenerate transitions with $\Delta = 0$ and various Γ_{12}: (a) $\Gamma_{12} = 0$; (b) $\Gamma_{12} = 0.9\sqrt{\Gamma_1\Gamma_2}$; (c) $\Gamma_{12} = 0.99\sqrt{\Gamma_1\Gamma_2}$; (d) $\Gamma_{12} = \sqrt{\Gamma_1\Gamma_2}$. The solid line represents $\Gamma_1 = \Gamma_2$, while the dashed line corresponds to $\Gamma_2 = 0.1\Gamma_1$.

find that in the limit of a small splitting of the upper states ($\Delta \ll \Gamma_1, \Gamma_2$), the spectrum is given by

$$A(\omega) \simeq 2\left[\frac{\Gamma^2}{\Gamma^2 + \omega^2} - \frac{(\Delta/4\Gamma)^2}{(\Delta/4\Gamma)^2 + \omega^2}\right] \tag{111}$$

where, for simplicity, we have assumed $\Gamma_1 = \Gamma_2 = \Gamma$. We see from Eq. (111) that the width of the hole depends on Δ and can be very narrow for $\Delta \ll \Gamma$. Moreover, for $\Delta \simeq 2\Gamma$, the absorption at the centre of the hole approaches zero, resulting in transparency of the probe field at this frequency. The simple formula in Eq. (111) predicts accurately the depth and width of the dip seen in Fig. 8.

Zhou and Swain [10] have shown that in the presence of initial correlations between the upper states, the hole in the center of the spectrum can reach negative values, indicating that the probe can be amplified as a result of quantum interference. Paspalakis and Knight [39] have calculated the absorption

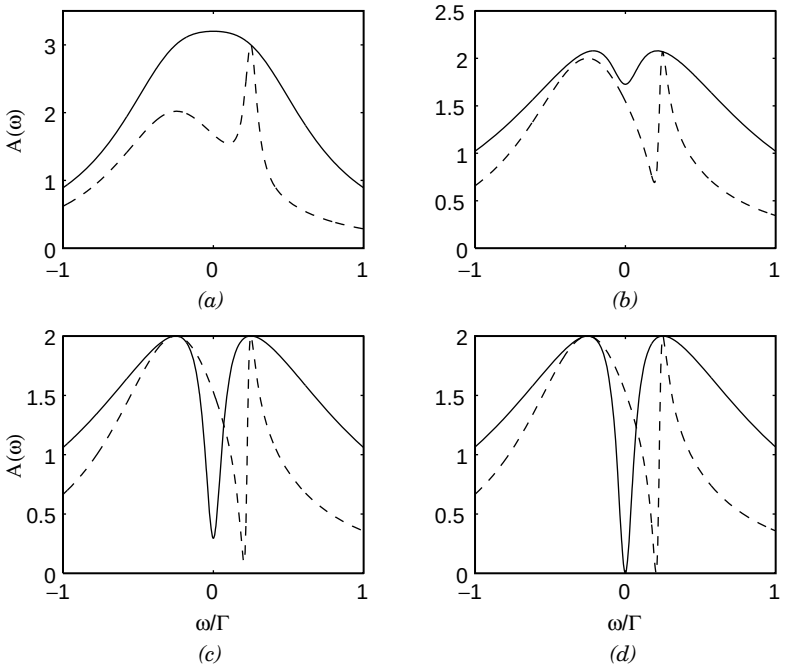

Figure 8. The absorption spectrum as a function of $\omega = \omega_p - \omega_0$ for nondegenerate transitions with $\Delta = \frac{1}{2}\Gamma_1$ and various Γ_{12}: (a) $\Gamma_{12} = 0$; (b) $\Gamma_{12} = 0.9\sqrt{\Gamma_1\Gamma_2}$; (c) $\Gamma_{12} = 0.99\sqrt{\Gamma_1\Gamma_2}$; (d) $\Gamma_{12} = \sqrt{\Gamma_1\Gamma_2}$. The solid line represents $\Gamma_1 = \Gamma_2$, while the dashed line corresponds to $\Gamma_2 = 0.1\Gamma_1$.

spectrum and refractive index of a V-type three-level atom driven by coherent and incoherent fields and have found that quantum interference enhances the index of refraction and can produce a very strong gain without population inversion.

B. Three-Level Λ System

It has been known for a long time that in a Λ-type three-level atom with two transitions of perpendicular dipole moments $(\Gamma_{12} = 0)$ driven by two laser fields, the population can be trapped in the ground states of the atom. This phenomenon, known as coherent population trapping (CPT) has been theoretically investigated by Arimondo and Orriols [40], Gray et al. [41], Orriols [42], and experimentally observed by Alzeta et al. [43]. Coherent population trapping has been examined in review articles by Dalton and Knight [44] and Arimondo [45]. Javanainen [46], Ferguson et al. [47], and Menon and Agarwal [26] have examined the effect of quantum interference between the

atomic transitions on the CPT and have demonstrated that the CPT effect strongly depends on the cross-damping term Γ_{12} and disappears when $\Gamma_{12} = \Gamma$.

The CPT effect and its dependence on quantum interference can be easily explained by examining the population dynamics in terms of the superposition states $|s\rangle$ and $|a\rangle$. Assume that a three-level Λ-type atom is composed of a single upper state $|3\rangle$ and two ground states $|1\rangle$ and $|2\rangle$. The upper state is connected to the lower states by transition dipole moments $\boldsymbol{\mu}_{31}$ and $\boldsymbol{\mu}_{32}$. After introducing superposition operators $S_s^+ = (S_s^-)^\dagger = |3\rangle\langle s|$ and $S_a^+ = (S_a^-)^\dagger = |3\rangle\langle a|$, where $|s\rangle$ and $|a\rangle$ are the superposition states of the same form as Eqs. (107) and (108), the Hamiltonian (65) can be written as

$$H' = -\hbar\left\{\left(\Delta_L - \frac{1}{2}\Delta'\right)S_s^- S_s^+ + \left(\Delta_L + \frac{1}{2}\Delta'\right)S_a^- S_a^+ + \Delta_c(S_s^- S_a^+ + S_a^- S_s^+) + \frac{1}{2}\frac{\sqrt{\Gamma_1}\Omega}{\sqrt{\Gamma_1+\Gamma_2}}(S_s^+ + S_s^-)\right\} \tag{112}$$

where

$$\Delta' = \frac{1}{\Gamma_1+\Gamma_2}[(\Gamma_1 - \Gamma_2)\Delta + 4\delta_{12}\sqrt{\Gamma_1\Gamma_2}] \tag{113}$$

and

$$\Delta_c = \frac{1}{\Gamma_1+\Gamma_2}[\delta_{12}(\Gamma_1 - \Gamma_2) - \Delta\sqrt{\Gamma_1\Gamma_2}] \tag{114}$$

As before, $\Delta = \omega_1 - \omega_2$, $\Delta_L = \omega_L - \frac{1}{2}(\omega_1 + \omega_2)$, and we have assumed that $\Omega_1 = \Omega_2 = \Omega$.

From the master equation (64) with the Hamiltonian (112), we derive the following equation of motion for the population ρ_{aa} of the antisymmetric state:

$$\dot{\rho}_{aa} = \frac{2\Gamma_1\Gamma_2}{\Gamma_1+\Gamma_2}(1-p)\rho_{33} - i\Delta_c(\rho_{as} - \rho_{sa}) \tag{115}$$

The equation of motion (115) allows us to analyze conditions for population trapping in the driven Λ system. In the steady state ($\dot{\rho}_{aa} = 0$) with $p \neq 1$ and $\Delta_c = 0$ the population in the upper state $\rho_{33} = 0$. Thus the state $|3\rangle$ is not populated even though it is continuously driven by the laser. In this case the population is entirely trapped in the antisymmetric superposition of the ground states. This is the CPT effect. However, for $p = 1$ and $\Delta_c = 0$, the antisymmetric state decouples from the interactions, and then the steady-state population ρ_{33} is different from zero [46]. This shows that coherent population trapping is possible

only in the presence of spontaneous emission from the upper state to the antisymmetric superposition state. Thus, we can conclude that quantum interference has a destructive effect on the CPT. Menon and Agarwal [26] have shown that the CPT effect can be preserved in the presence of quantum interference provided that the atom is driven by two coherent field each coupled to only one of the atomic transitions.

According to Eq. (115), the CPT can also be destroyed by the presence of the coherent interaction Δ_c between the symmetric and antisymmetric states. This is shown in Fig. 9, where we plot the steady-state population ρ_{33} as a function of Δ for different values of Γ_2/Γ_1. It is evident that the cancellation of the population ρ_{33} appears only at $\Delta_c = 0$, that is, in the absence of the coherent interaction between the antisymmetric and symmetric states. For $\Gamma_1 = \Gamma_2$ the cancellation appears at $\Delta = 0$, while for $\Gamma_1 \neq \Gamma_2$ the effect shifts toward nonzero Δ given by

$$\Delta = \frac{\Gamma_1 - \Gamma_2}{\sqrt{\Gamma_1 \Gamma_2}} \delta_{12} \tag{116}$$

The shift depends on the ratio r, and for either $r \ll 1$ or $r \gg 1$ can be large even though δ_{12} is very small. Therefore, the vacuum-induced coherent coupling can be experimentally observed in the Λ system as a shift of the zero of the population ρ_{33} of the upper state [24].

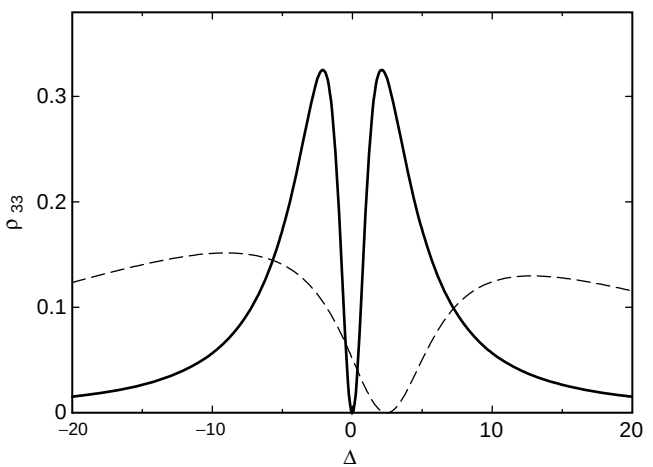

Figure 9. The stationary population of the upper state $|3\rangle$ of a Λ-type atom as a function of the splitting Δ for $\Delta_L = 0, \Omega = 5\Gamma_1, \delta_{12} = 0.1\Gamma_1, p = 0.5$, and different Γ_2: $\Gamma_2 = \Gamma_1$ (solid line), $\Gamma_1 = 50\Gamma_2$ (dashed line).

We have shown in Section V.A.2 that a laser field can drive the V-type system into the antisymmetric (trapping) state through the coherent interaction between the symmetric and antisymmetric states. Akram et al. [24] have shown that in the Λ system there are no trapping states to which the population can be transferred by the laser field. This can be illustrated by calculating the transition dipole moments between the dressed states of the driven Λ system. The procedure of calculating the dressed states of the Λ system is the same as for the V system. The only difference is that now the eigenstates of the unperturbed Hamiltonian H_0 are $|3, N-1\rangle, |1, N\rangle, |2, N\rangle$, and the dressed states are given by

$$\begin{aligned}
|+, N\rangle &= \frac{1}{\sqrt{2}}[-\alpha|a, N\rangle + |s, N\rangle - \sqrt{2}\beta|3, N-1\rangle] \\
|0, N\rangle &= -\sqrt{2}\beta|a, N\rangle + \alpha|3, N-1\rangle \\
|-, N\rangle &= \frac{1}{\sqrt{2}}[-\alpha|a, N\rangle - |s, N\rangle - \sqrt{2}\beta|3, N-1\rangle]
\end{aligned} \tag{117}$$

Although the dressed states (117) are similar to that of the V system [see Eq. (103)], there is a crucial difference between the transition dipole moments. For the Λ system the transition dipole moments between the dressed states $|i, N+1\rangle$ and the state $|0, N\rangle$ of the manifold below are all zero, but there are nonzero transition dipole moments between $|0, N\rangle$ and the dressed states $|i, N-1\rangle$ of the manifold below

$$\begin{aligned}
\langle N, 0|\boldsymbol{\mu}|\pm, N-1\rangle &= \pm\alpha\boldsymbol{\mu} \\
\langle N, 0|\boldsymbol{\mu}|0, N-1\rangle &= 0
\end{aligned} \tag{118}$$

Therefore, the population is unable to flow into the state $|0, N\rangle$, but can flow away from it. If $\Delta = 0$, then $\alpha = 0$, and the state $|0, N\rangle$ completely decouples from the remaining states. For $\Delta \neq 0$ the state $|0, N\rangle$ is coupled to the remaining states, but does not participate in the dynamics of the system because it cannot be populated by transitions from the other states. Thus, there is no trapping state among the dressed states of the driven Λ system.

VI. AMPLIFICATION ON DARK TRANSITIONS

Menon and Agarwal [48] have predicted that in the presence of quantum interference the Autler–Townes spectrum of a weak probe beam monitoring a driven three-level V-type atom can exhibit gain features instead of the usual absorption doublet. This unexpected feature requires the condition that the Rabi frequency Ω of the driving field be such that $\Omega = 2\Delta$, where Δ is the splitting between the excited states. The gain features have been explained as arising

from a large difference in population between the dressed states produced by the driving field and the undriven atomic level.

A. Amplification on Inverted Transitions

In the process of amplification with population inversion, spontaneous emission imposes a serious restriction in creating an inversion between atomic levels. For example, in a two-level system with ground state $|g\rangle$ and excited state $|e\rangle$, the stationary absorptive and emissive processes are governed by the balance condition

$$P_g\Gamma_{ge} = P_e\Gamma_{eg}, \tag{119}$$

where $P_g(P_e)$ is the steady-state population of the ground (excited) level, Γ_{ge} is the absorptive, and Γ_{eg} is the emissive rate between the atomic levels. It follows from Eq. (119) that inversion $(P_e > P_g)$ can be produced only if $\Gamma_{ge} > \Gamma_{eg}$. This condition may not be achieved in two-level systems since the stimulated absorptive and emissive rates are the same and spontaneous emission contributes only to the emissive rate, giving $\Gamma_{eg} > \Gamma_{ge}$ [49]. Population inversions involving the ground level can, however, be produced in multilevel systems where population can be transferred into level $|e\rangle$ through other channels (levels) [50]. If we introduce a third level $|3\rangle$, which has its absorptive rate Γ_{g3} from the ground level and the spontaneous rate Γ_{3e} to the excited level much larger than the emissive rate Γ_{eg}, a pumping field applied to the $|g\rangle \to |3\rangle$ transition will create a steady-state inversion on the $|e\rangle \to |g\rangle$ transition. Using rate equations for the atomic populations, the ratio P_e/P_g of the steady-state populations of the excited and ground states can be expressed as

$$\frac{P_e}{P_g} = \frac{\Gamma_{3e}\Gamma_{g3}}{\Gamma_{eg}(\Gamma_{3e} + \Gamma_{3g})} \tag{120}$$

It is seen that the ratio (120) depends crucially on the spontaneous emission rate Γ_{eg}, which depopulates the state $|e\rangle$. Maximum inversion, with $P_e = 1$ and $P_g = 0$, is obtained for $\Gamma_{eg} = 0$, when the population is said to be "shelved" (trapped) in the state $|e\rangle$ from which it cannot decay to the ground state. Thus, in the case of maximum inversion one could expect maximum amplification of a probe beam on the $|e\rangle \to |g\rangle$ transition. However, the absorption rate $W(\omega_p)$ of a probe beam of amplitude $\mathbf{E}_p$ and frequency ω_p monitoring the $|e\rangle \to |g\rangle$ transition, as defined by Mollow [38], is

$$W(\omega_p) = \frac{1}{i\hbar}\int_{-\infty}^{t} dt' \left\langle \left[\frac{dH_p(t)}{dt}, H_p(t')\right]\right\rangle \tag{121}$$

where

$$H_p(t) = \frac{1}{2}\boldsymbol{\mu}_{eg} \cdot \mathbf{E}_p(S^+ e^{-i\omega_p t} + S^- e^{i\omega_p t}) \tag{122}$$

is the interaction Hamiltonian of the probe field with dipole moment $\boldsymbol{\mu}_{eg}$, and $S^+ = |e\rangle\langle g|$ ($S^- = |g\rangle\langle e|$) is the dipole raising (lowering) operator. For a long interaction time ($t \to \infty$) the absorption rate satisfies the integral relation [38]

$$\bar{W} = \int_{-\infty}^{\infty} d\omega_p W(\omega_p) = \frac{2\pi}{\hbar}|\boldsymbol{\mu}_{eg} \cdot \mathbf{E}_p|^2 (P_g - P_e) \tag{123}$$

Thus, two factors determine the magnitude of amplification ($\bar{W} < 0$) of the probe field: (1) the population must be inverted ($P_e > P_g$) and (2) the dipole moment of the transition, which determines the coupling strength of the probe field to the atom, must be nonzero. According to the balance condition (119), an increase of the population inversion can be achieved by decreasing the emissive rate and the population can be completely inverted only if $\Gamma_{eg} = 0$, that is, only if the state $|e\rangle$ is a trapping state. Since $\Gamma_{eg} \sim |\boldsymbol{\mu}_{eg}|^2$, the trapping results in cancellation of the dipole moment to the ground state, and then the inverted transition becomes transparent for the probe beam. Therefore, in order to obtain a significant amplification, one should produce a large population inversion and simultaneously maintain a strong coupling of the probe field to the inverted transition. The preceding analysis suggests that this is impossible to achieve in atomic systems.

B. Autler–Townes Absorption Spectra

Consider the Menon–Agarwal approach to the Autler–Townes spectrum of a V-type three-level atom. The atom is composed of two excited states, $|1\rangle$ and $|3\rangle$, and the ground state $|2\rangle$ coupled by transition dipole moments with matrix elements $\boldsymbol{\mu}_{12}$ and $\boldsymbol{\mu}_{32}$, but with no dipole coupling between the excited states. The excited states are separated in frequency by Δ. The spontaneous emission rates from $|1\rangle$ and $|3\rangle$ to the ground state $|2\rangle$ are Γ_1 and Γ_2, respectively. The atom is driven by a strong laser field of the Rabi frequency Ω, coupled *solely* to the $|1\rangle \to |2\rangle$ transition. This is a crucial assumption, which would be difficult to realize in practice since quantum interference requires almost parallel dipole moments. However, the difficulty can be overcome in atomic systems with specific selection rules for the transition dipole moments, or by applying fields with specific polarization properties [26].

We consider two different coupling configurations of the probe beam to the driven atom. In the first case, we assume that the probe beam is coupled to the driven $|1\rangle \to |2\rangle$ transition [51]. In the second case, that has been considered by

Menon and Agarwal [48], we will assume that the probe beam is coupled to the undriven $|3\rangle \rightarrow |2\rangle$ transition.

The absorption rate of a probe beam of a tunable frequency ω_p monitoring the $|1\rangle \rightarrow |2\rangle$ transition is defined as [38,48]

$$W_{12}(\omega_p) = \mathrm{Re}[\Omega_p \rho_{12}^{(+1)}] \tag{124}$$

where Ω_p is the Rabi frequency of the probe beam and $\rho_{12}^{(+1)}$ is the stationary component (harmonic) of the coherence ρ_{12} oscillating with the probe detuning $\delta = \omega_p - \omega_2$.

In Fig. 10, we plot the absorption rate W_{12} as a function of δ for $p = 0.95$ and different Ω. When $\Omega \neq 2\Delta$ the absorption rate exhibits the familar Mollow absorption spectrum [38] with small dispersive structures at $\delta = \pm\Omega$. The absorption rate changes dramatically when $\Omega = 2\Delta$. Here, the dominant features of the rate are emissive and absorptive components at $\delta = \pm\Omega$, indicating that at $\delta = -\Omega$ the weaker field is absorbed, whereas at $\delta = \Omega$ is amplified at the expense of the strong field. The weaker field is always absorbed (amplified) at $\delta = -\Omega$ ($\delta = \Omega$) independent of the ratio $r = \Gamma_1/\Gamma_2$ between the spontaneous emission rates Γ_1 and Γ_2. We illustrate this in Fig. 11, where we plot the absorptive rate for different values of r. The absorptive (emissive) peak remains absorptive (emissive) independent of the ratio r.

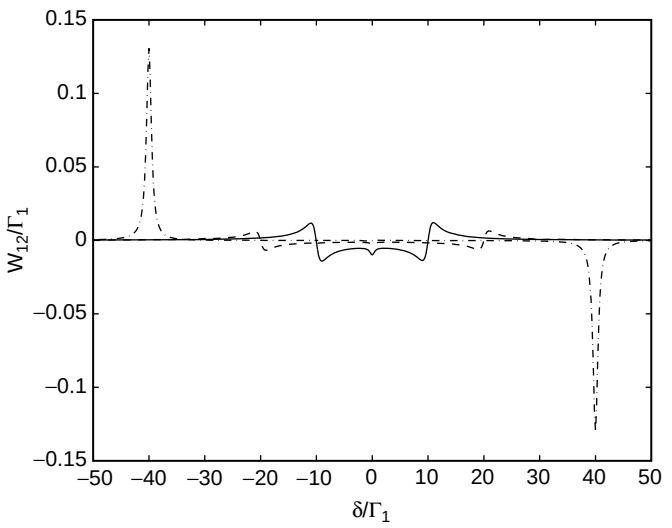

Figure 10. The absorption rate W_{12} as a function of δ/Γ_1 for $p = 0.95, \Gamma_1 = \Gamma_2, \Omega_p = \Gamma_1, \Delta = 20\Gamma_1$, and different Ω: $\Omega = 10\Gamma_1$ (solid line), $\Omega = 20\Gamma_1$ (dashed line) and $\Omega = 40\Gamma_1$ (dashed–dotted line).

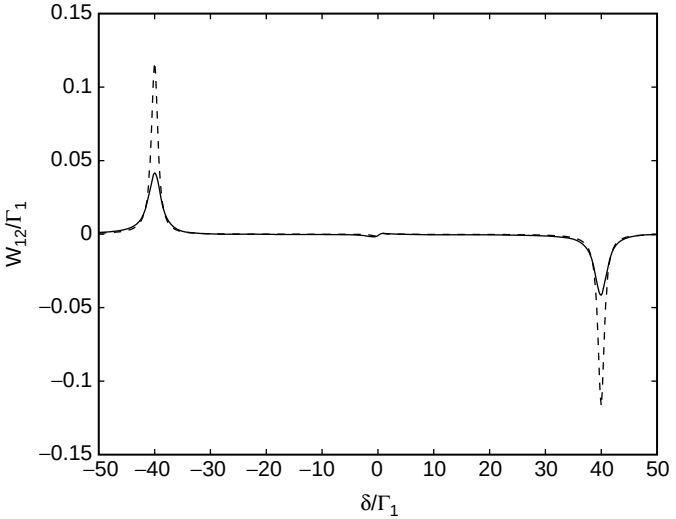

Figure 11. The absorptive rate W_{12} as a function of δ/Γ_1 for $p = 0.95, \Omega = 40\Gamma_1, \Omega_p = \Gamma_1, \Delta = 20\Gamma_1$, and different values of $r = \Gamma_1/\Gamma_2$: $r = 2$ (dashed line) and $r = 5$ (solid line).

Note that the absorption rate shown in Figs. 10 and 11 is similar to the Mollow absorption spectrum for an off-resonance driving field [38]. However, there is a significant difference in that the ratio between the magnitudes of the emissive and absorptive peaks in the Mollow spectrum is always less than one and the ratio varies with the detuning and Rabi frequency of the driving field. The ratio of the absorption rates, shown in Figs. 10 and 11, is equal to one and constant independent of the values of the parameters involved.

In Fig. 12, we present the absorption rate for the case considered by Menon and Agarwal [48], in which the probe beam is coupled to the undriven $|3\rangle - |2\rangle$ transition

$$W_{23}(\omega_p) = 2\mathrm{Re}[\Omega_p \rho_{23}^{(+1)}] \tag{125}$$

The absorption rate is plotted as a function of δ for $\Omega = 2\Delta$. We see that the absorption rate exhibits an emissive feature at $\delta = \Omega$. Moreover, there is a central component at $\delta = 0$, whose absorptive/emissive properties depend on the ratio r. For $r < 2$ the rate is positive indicating that the weaker field is absorbed by the system. As r increases the absorptive feature decreases and vanishes for $r \approx 2$. When we further increase r $(r > 2)$ the absorptive features at $\delta = 0$ switch into emissive features and the magnitude of the emissive peak increases with increasing r. The threshold value for r, at which absorption switches to emission,

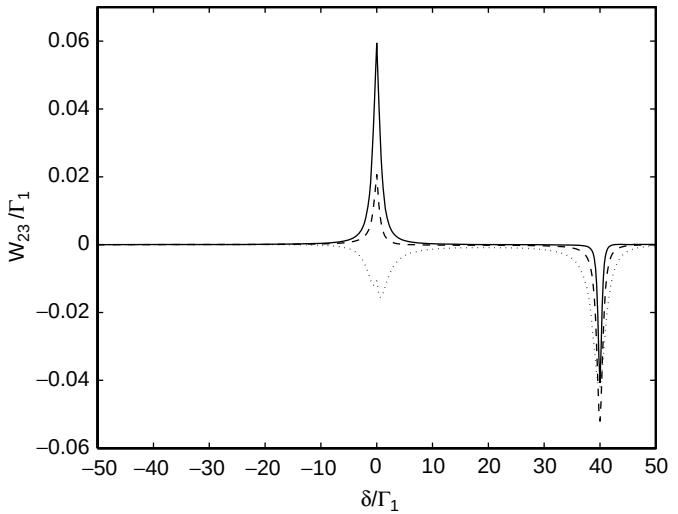

Figure 12. The absorption rate W_{23} as a function of δ for $\Omega = 40\Gamma_1$, $\Omega_p = \Gamma_1$, $\Delta = 20\Gamma_1$, $p = 0.95$, and different values of r: $r = 1$ (solid line), $r = 2$ (dashed line) and $r = 5$ (dotted line).

depends on p. For $p = 1$ the threshold is exactly at $r = 2$, and shifts toward larger r as p decreases.

C. Dressed-Atom Model of the Amplification on Dark Transitions

The physics associated with the unusual properties of the absorption rate of the probe beam, shown in Figs. 10–12, can be easily explored by working in the basis of quantum dressed states of the system [35]. In this approach, we work with the quantum version of the Hamiltonian (65) which, in the case of the driving laser coupled exclusively to the $|1\rangle \rightarrow |2\rangle$ transition, can be written as

$$H_S = H_0 + H_{\text{int}} \tag{126}$$

where

$$H_0 = \hbar\omega_1 S_1^+ S_1^- + \hbar\omega_2 S_2^+ S_2^- + \hbar\omega_1 a_{L_1}^\dagger a_{L_1} \tag{127}$$

is the Hamiltonian of the system atom plus driving field

$$H_{\text{int}} = -\frac{1}{2}\hbar g(a_{L_1}^\dagger S_1^- + a_{L_1} S_1^+) \tag{128}$$

is the interaction between the atom and the laser field.

The Hamiltonian H_0 has the "undressed" eigenstates $|1, N-1\rangle$, $|3, N-1\rangle$, and $|2, N\rangle$. The states $|1, N-1\rangle$ and $|2, N\rangle$ are degenerate with energies $E_{1,N} = E_{2,N} = \hbar N\omega_1$, while the state $|3, N-1\rangle$ has energy $E_{3,N} = \hbar(N\omega_1 + \Delta)$, where N is the number of photons in the laser mode. When we include the interaction (128) between the atom and the laser field, the degeneracy is lifted, resulting in triplets of dressed states

$$\begin{aligned} |+, N\rangle &= \frac{1}{\sqrt{2}}(|2, N\rangle + |1, N-1\rangle) \\ |-, N\rangle &= \frac{1}{\sqrt{2}}(|2, N\rangle - |1, N-1\rangle) \\ |\tilde{3}, N\rangle &= |3, N-1\rangle, \end{aligned} \tag{129}$$

with energies

$$\begin{aligned} E_{+,N} &= \hbar\left(N\omega_1 + \frac{1}{2}\Omega\right) \\ E_{-,N} &= \hbar\left(N\omega_1 - \frac{1}{2}\Omega\right) \\ E_{\tilde{3},N} &= \hbar(N\omega_1 + \Delta) \end{aligned} \tag{130}$$

The dressed states (129) group into manifolds of nondegenerate triplets unless $\Delta = \frac{1}{2}\Omega$ and then the states $|+, N\rangle$, $|\tilde{3}, N\rangle$ in each manifold are degenerate.

Since the driven and undriven transitions are coupled through the Γ_{12} terms, it is convenient to introduce symmetric and antisymmetric superposition states of the dressed states $|+, N\rangle$ and $|\tilde{3}, N\rangle$. According to Eq. (68), the superposition states diagonalise the dissipative (damping) part of the master equation of the system. The superposition states can be written as [51]

$$|s, N\rangle = \alpha|+, N\rangle + \beta|\tilde{3}, N\rangle \tag{131}$$

$$|a, N\rangle = \beta|+, N\rangle - \alpha|\tilde{3}, N\rangle \tag{132}$$

where

$$\alpha = \frac{\sqrt{\frac{1}{2}\Gamma_1}}{\sqrt{\frac{1}{2}\Gamma_1 + \Gamma_2}} \tag{133}$$

$$\beta = \frac{\sqrt{\Gamma_2}}{\sqrt{\frac{1}{2}\Gamma_1 + \Gamma_2}} \tag{134}$$

such that

$$\alpha^2 + \beta^2 = 1 \tag{135}$$

With the dressed states of the driven system available, we can easily predict transition frequencies and calculate transition dipole moments and spontaneous emission rates between the dressed states of the system. It is easily verified that nonzero dipole moments occur only between dressed states within neighboring manifolds. Using Eqs. (131) and (132), we find that the transition dipole moments between $|N, i\rangle$ and $|N-1, j\rangle$ are

$$\begin{aligned}
\boldsymbol{\mu}_{s,N;s,N-1} &= \frac{1}{2}\alpha^2\boldsymbol{\mu}_{12} + \frac{\alpha\beta}{\sqrt{2}}\boldsymbol{\mu}_{32}, \quad \boldsymbol{\mu}_{s,N;-,N-1} = \frac{1}{2}\alpha\boldsymbol{\mu}_{12} + \frac{1}{\sqrt{2}}\beta\boldsymbol{\mu}_{32} \\
\boldsymbol{\mu}_{-,N;s,N-1} &= -\frac{1}{2}\alpha\boldsymbol{\mu}_{12}, \quad \boldsymbol{\mu}_{-,N;-,N-1} = -\frac{1}{2}\boldsymbol{\mu}_{12} \\
\boldsymbol{\mu}_{-,N;a,N-1} &= -\frac{1}{2}\beta\boldsymbol{\mu}_{12}, \quad \boldsymbol{\mu}_{s,N;a,N-1} = \frac{1}{2}\alpha\beta\boldsymbol{\mu}_{12} + \frac{1}{\sqrt{2}}\beta^2\boldsymbol{\mu}_{32} \\
\boldsymbol{\mu}_{a,N;s,N-1} &= \frac{1}{2}\alpha\beta\boldsymbol{\mu}_{12} - \frac{1}{\sqrt{2}}\alpha^2\boldsymbol{\mu}_{32}, \quad \boldsymbol{\mu}_{a,N;-,N-1} = \frac{1}{2}\beta\boldsymbol{\mu}_{12} - \frac{1}{\sqrt{2}}\alpha\boldsymbol{\mu}_{32} \\
\boldsymbol{\mu}_{a,N;a,N-1} &= \frac{1}{2}\beta^2\boldsymbol{\mu}_{12} - \frac{1}{\sqrt{2}}\alpha\beta\boldsymbol{\mu}_{32}
\end{aligned} \tag{136}$$

where $\boldsymbol{\mu}_{i,N;j,N-1} = \langle i, N|\tilde{\boldsymbol{\mu}}|j, N-1\rangle$, and $\tilde{\boldsymbol{\mu}} = \tilde{\boldsymbol{\mu}}_1 + \tilde{\boldsymbol{\mu}}_2$ is the total dipole moment of the atom.

The spontaneous transitions occur with probabilities

$$\Gamma_{i,N;j,N-1} = \frac{\Gamma_n}{|\boldsymbol{\mu}_{2n-1,2}|^2}|\langle i, N|\tilde{\boldsymbol{\mu}}|j, N-1\rangle|^2, \quad n = 1, 2 \tag{137}$$

given by the expressions

$$\begin{aligned}
\Gamma_{s,N;s,N-1} &= \frac{1}{4}\Gamma_1[1 - \frac{\Gamma_1\Gamma_2}{(\Gamma_2 + \frac{1}{2}\Gamma_1)^2}(1 - \cos\theta)] \\
\Gamma_{s,N;-,N-1} &= \frac{1}{2}\left(\Gamma_2 + \frac{1}{2}\Gamma_1\right)\left[1 - \frac{\Gamma_1\Gamma_2}{(\Gamma_2 + \frac{1}{2}\Gamma_1)^2}(1 - \cos\theta)\right] \\
\Gamma_{s,N;a,N-1} &= \frac{1}{2}\Gamma_2\left[1 - \frac{\Gamma_1\Gamma_2}{(\Gamma_2 + \frac{1}{2}\Gamma_1)^2}(1 - \cos\theta)\right] \\
\Gamma_{-,N;-,N-1} &= \frac{1}{4}\Gamma_1
\end{aligned}$$

$$
\begin{aligned}
\Gamma_{-,N;s,N-1} &= \frac{1}{8}\frac{\Gamma_1^2}{(\Gamma_2+\frac{1}{2}\Gamma_1)} \\
\Gamma_{-,N;a,N-1} &= \frac{1}{4}\frac{\Gamma_1\Gamma_2}{(\Gamma_2+\frac{1}{2}\Gamma_1)} \\
\Gamma_{a,N;s,N-1} &= \frac{1}{4}\frac{\Gamma_1^2\Gamma_2}{(\Gamma_2+\frac{1}{2}\Gamma_1)^2}(1-\cos\theta) \\
\Gamma_{a,N;-,N-1} &= \frac{1}{2}\frac{\Gamma_1\Gamma_2}{(\Gamma_2+\frac{1}{2}\Gamma_1)}(1-\cos\theta) \\
\Gamma_{a,N;a,N-1} &= \frac{1}{2}\frac{\Gamma_1\Gamma_2^2}{(\Gamma_2+\frac{1}{2}\Gamma_1)^2}(1-\cos\theta)
\end{aligned}
\tag{138}
$$

where θ is the angle between $\boldsymbol{\mu}_1$ and $\boldsymbol{\mu}_2$.

In Fig. 13, we present the dressed states of two neighboring manifolds, N and $N-1$, and the possible transitions among them. Solid lines indicate transitions

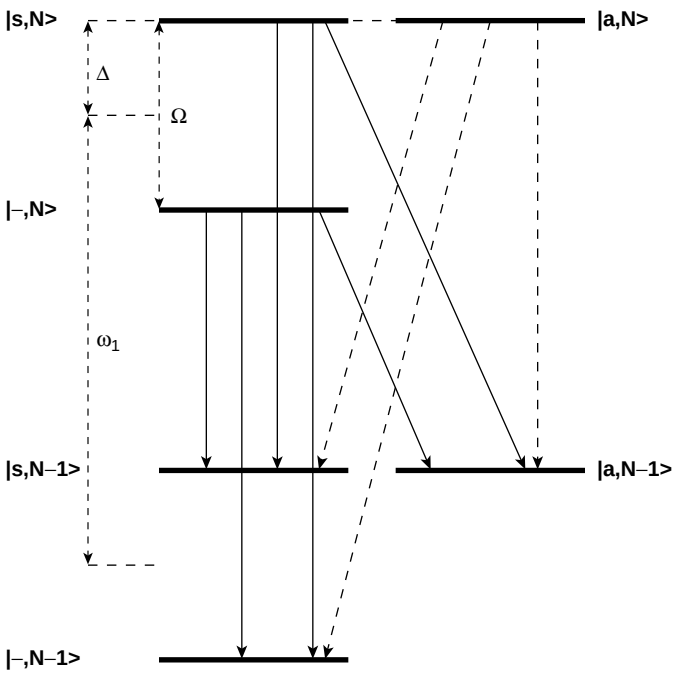

Figure 13. Energy-level diagram of the superposition dressed states for $\Delta = \frac{1}{2}\Omega$. The solid lines indicate spontaneous transitions that occur independently of quantum interference, whereas the dashed lines indicate transitions that are significantly reduced by quantum interference.

that are not significantly affected by quantum interference, whereas dashed lines indicate transitions that are strongly modified by quantum interference, in that their transition dipole moments decrease with increasing p and vanish for $p = 1$. We see from Fig. 13 that quantum interference strongly affects transition rates from the antisymmetric state to the states of the manifold below. Thus, the antisymmetric state becomes a dark state in the limit of a strong interference, $p \approx 1$. Moreover, it can be found from the master equation (64) and the dressed state (132) that the steady-state population $P_a = \sum_N \langle a, N|\rho|a, N\rangle$ of the antisymmetric state is given by

$$P_a = \frac{1}{1 + \frac{u}{w}(1 - \cos\theta)} \tag{139}$$

where

$$u = 2\Gamma_2\left[\Gamma_{sa} + \Gamma_{s-} + \Gamma_{-s} + \frac{\Gamma_1(\Gamma_{s-} + \frac{1}{4}\Gamma_1)}{2(\Gamma_2 + \frac{1}{2}\Gamma_1)}\right]$$

$$w = \Gamma_2(\Gamma_{sa} + \Gamma_{s-}) + \frac{1}{2}\Gamma_1\Gamma_{sa} \tag{140}$$

and $\Gamma_{ij} = \Gamma_{i,N;j,N-1}$. Hence, for small θ the antisymmetric state is strongly populated, and the population can be trapped in the antisymmetric state ($P_a = 1$) when $\theta = 0$.

Figure 13, together with the transition dipole moments and transition rates, provides a simple interpretation of the absorption rate shown in Fig. 11. According to Eq. (139), the emissive peak in the absorption rate appears on an almost completely inverted transition ($|a, N\rangle - |-, N-1\rangle$), whose dipole moment is significantly reduced by quantum interference. One could expect that the weaker field should not couple to an almost canceled dipole moment. However, we have assumed that the probe field couples *only* to the dipole moment $\boldsymbol{\mu}_{12}$. From Eq. (136), we find that the coupling strength of the probe field to the transition $|a, N\rangle - |-, N-1\rangle$ is proportional to $\frac{1}{2}\beta\boldsymbol{\mu}_{12}$ despite the fact that the total dipole moment of the transition is much smaller, $\boldsymbol{\mu}_{a,N;-,N-1} = \frac{1}{2}\beta\boldsymbol{\mu}_{12} - \frac{1}{\sqrt{2}}\alpha\boldsymbol{\mu}_{32}$. The absorptive peak, seen in Fig. 11 at the frequency $\omega_1 - \Omega$, appears on the noninverted transition $|-, N\rangle - |a, N-1\rangle$ with the transition dipole moment $\frac{1}{2}\beta\boldsymbol{\mu}_{12}$. Since the absolute values of the population difference on the $|a, N\rangle - |-, N-1\rangle$ and $|-, N\rangle - |a, N-1\rangle$ transitions are the same and the coupling strengths of the weaker field to the transitions are equal, $\boldsymbol{\mu}_{a,N;-,N-1} = \boldsymbol{\mu}_{-,N;a,N-1} = \frac{1}{2}\beta\boldsymbol{\mu}_{12}$, the absolute values of the absorptive and emissive peaks in the absorption rate are the same indepen-

dent of the ratio $r = \Gamma_1/\Gamma_2$. One can see from Fig. 13 that there are two transitions, one emissive $(|a,N\rangle - |s,N-1\rangle)$ and one absorptive $(|s,N\rangle - |a,N-1\rangle)$, which contribute to the central structure at $\delta = 0$. Since the absolute values of the population difference on these transitions are the same and the coupling strengths of the weaker field to these transitions are equal, $\boldsymbol{\mu}_{s,N;a,N-1} = \boldsymbol{\mu}_{a,N;s,N-1} = \frac{1}{2}\alpha\beta\boldsymbol{\mu}_{12}$, these two contributions cancel each other leading to a transparency of the weaker field at $\delta = 0$.

The physical origin of the gain features predicted by Menon and Agarwal [48], shown in Fig. 12, can also be explained with the help of the energy-level diagram of Fig. 13 and the transition dipole moments (136). As we have already shown in Eq. (139), for $p \approx 1$ almost all the population is trapped in the state $|a,N\rangle$. Therefore, the weaker field can be amplified on the $|a,N\rangle - |s,N-1\rangle$ and $|a,N\rangle - |-,N-1\rangle$ transitions, and can be absorbed on the $|a,N-1\rangle - |s,N\rangle$ and $|a,N-1\rangle - |-,N\rangle$ transitions. Since the weaker field couples exclusively to $\boldsymbol{\mu}_{32}$, the transition $|a,N-1\rangle - |-,N\rangle$, whose dipole moment is proportional to $\boldsymbol{\mu}_{12}$, is transparent for the weaker field. The coupling strength of the weaker field to the $|a,N\rangle - |-,N-1\rangle$ transition is proportional to $\frac{\alpha}{\sqrt{2}}\boldsymbol{\mu}_{32}$, indicating that the field can be amplified on this transition and the amplification is not much affected by the ratio r. It is seen from Fig. 13 that at $\delta = 0$ the probe couples to three transitions. The transition $|a,N\rangle \to |a,N-1\rangle$ is transparent for the probe because it occurs between two states of the same population. Therefore, the absorptive/emissive properties result from the coupling of the probe to the $|s,N\rangle - |a,N-1\rangle$ and $|a,N\rangle - |s,N-1\rangle$ transitions. For $\theta \approx 0$ almost all the population is trapped in the antisymmetric state, and then the probe is strongly absorbed on the $|s,N\rangle \to |a,N-1\rangle$ transition, but is amplified on the $|a,N\rangle \to |s,N-1\rangle$ transition. According to Eq. (138), the later is a dark transition. Since the absolute values of the population difference between the states are the same for both transitions, the absorptive/emissive properties at $\delta = 0$ depend solely on the relation between the transition rates. From Eq. (136), we find that the coupling strength of the probe beam to the transition $|a,N\rangle - |s,N-1\rangle$ is proportional to $\frac{1}{\sqrt{2}}\alpha^2\boldsymbol{\mu}_{32}$, whereas the coupling strength to the transition $|s,N\rangle - |a,N-1\rangle$ is proportional to $\frac{1}{\sqrt{2}}\beta^2\boldsymbol{\mu}_{32}$. Thus, the absorptive/emissive properties at $\delta = 0$ depend on the difference $(\beta^2 - \alpha^2) = \frac{1}{2}\beta^2(2-r)$. For $r < 2$ the difference is positive, indicating that the weaker field is absorbed at $\delta = 0$, and is amplified for $r > 2$. These simple dressed-atom predictions are in excellent agreement with the numerical calculations shown in Fig. 12.

Thus, in terms of the quantum dressed states, the gain features predicted by Menon and Agarwal [48] actually appear on completely inverted transitions whose dipole moments are canceled by quantum interference. Therefore, the gain features can be regarded as the amplification on dark transitions [51].

VII. EFFECT OF QUANTUM INTERFERENCE ON PHOTON CORRELATIONS

In view of the interesting quantum interference effects in the fluorescence and absorption spectra, it is natural to study the influence of quantum interference on the second-order correlation function of the fluorescence field emitted from a three-level atom. We will illustrate this for a V-type three-level atom consisting of two excited states coupled to a ground state by electric dipole interactions and driven by a coherent laser field. These correlations have been investigated by Hegerfeldt and Plenio [52] for an incoherently driven atom. The results show that the intensity correlation may exhibit quantum beats despite the incoherent pumping. The case of excitation by two coherent fields has been considered by Manka et al. [53], who showed how the resonance fluorescence and intensity–intensity correlation spectra on one transition can be influenced by the intensity of the driving field on the other transition [54,55]. In particular, they demonstrated that the decay rate of the intensity–intensity correlation spectrum could be reduced in this way. Jagatap et al. [56] and Huang et al. [57] have also calculated the intensity correlations in a three-level ladder system driven by two coherent fields and have shown that the correlations can have secondary oscillations, in addition to the Rabi oscillations.

We concentrate on the role of quantum interference in the correlation of photons emitted from a coherently driven V-type atom, recently analyzed by Swain et al. [58]. We calculate the normalized second-order two-time correlation function $g^{(2)}(\mathbf{R}, t; \mathbf{R}, t+\tau)$ for the fluorescent field emitted from a three-level V-type atom driven by a coherent laser field coupled to both atomic transitions. The fluorescence field is observed by a single detector located at a point $\mathbf{R} = R\bar{\mathbf{R}}$, where $\bar{\mathbf{R}}$ is the unit vector in the direction of the observation.

As we have shown in Sec. III.A, the second-order correlation function of the fluorescence field depends on correlation functions of the atomic dipole moments $\langle S_i^+(t) S_j^+(t+\tau) S_l^-(t) S_j^-(t)\rangle$, which correspond to different processes including photon emissions from a superposition of the excited levels. Therefore, we write the correlation functions $G^{(1)}(\mathbf{R}, t)$ and $G^{(2)}(\mathbf{R}, t; \mathbf{R}, t+\tau)$ in terms of the symmetric and antisymmetric superposition states as

$$
\begin{aligned}
G^{(1)}(\mathbf{R}, t) = \frac{1}{(\Gamma_1 + \Gamma_2)} \{ & (\Gamma_1^2 + \Gamma_2^2 + 2p\Gamma_1\Gamma_2)\langle S_s^+(t) S_s^-(t)\rangle \\
& + 2(1-p)\Gamma_1\Gamma_2 \langle S_a^+(t) S_a^-(t)\rangle \\
& + (1-p)\sqrt{\Gamma_1\Gamma_2}(\Gamma_1 - \Gamma_2) \\
& \times \langle S_s^+(t) S_a^-(t) + S_a^+(t) S_s^-(t)\rangle \}
\end{aligned} \tag{141}
$$

and

$$
\begin{aligned}
G^{(2)}(\mathbf{R},t;\mathbf{R},t+\tau) = \frac{1}{(\Gamma_1+\Gamma_2)^2}\{&(\Gamma_1^2+\Gamma_2^2+2p\Gamma_1\Gamma_2)\\
&\times\langle S_s^+(t)U(t+\tau)S_s^-(t)\rangle\\
&+(1-p)\sqrt{\Gamma_1\Gamma_2}[2\sqrt{\Gamma_1\Gamma_2}\langle S_a^+(t)U(t+\tau)S_a^-(t)\rangle\\
&+(\Gamma_1-\Gamma_2)\langle S_s^+(t)U(t+\tau)S_a^-(t)\rangle\\
&+..\langle S_a^+(t)U(t+\tau)S_s^-(t)\rangle]\}
\end{aligned}
\tag{142}
$$

where

$$
\begin{aligned}
U(t+\tau) = (\Gamma_1^2+\Gamma_2^2+2p\Gamma_1\Gamma_2)&S_s^+(t+\tau)S_s^-(t+\tau)\\
&+(1-p)\sqrt{\Gamma_1\Gamma_2}\{2\sqrt{\Gamma_1\Gamma_2}S_a^+(t+\tau)S_a^-(t+\tau)\\
&+(\Gamma_1-\Gamma_2)\{S_s^+(t+\tau)S_a^-(t+\tau)\\
&+S_a^+(t+\tau)S_s^-(t+\tau)\}\}
\end{aligned}
\tag{143}
$$

It is seen that in the bases of the symmetric and antisymmetric states, there are three terms contributing to the first- and the second-order correlation functions. The first term is from the transition $|s\rangle \to |2\rangle$, the second is from the transition $|a\rangle \to |2\rangle$, and the third term arises from the coupling between them. When the decay rates are equal, $\Gamma_1 = \Gamma_2$, then the transitions are independent regardless of the mutual orientation of the atomic transition dipole moments. Moreover, for parallel dipole moments ($p = 1$), only the transition $|s\rangle \to |2\rangle$ contributes to the first- and second-order correlation functions, indicating that in this case the system reduces to a two-level system. However, correlations between the emitted photons can be significantly different from those one would expect for a two-level system. We will illustrate this in two examples of distinguishable and indistinguishable photons.

A. Distinguishable Photons

If the photons emitted from the excited states to the ground state are distinguishable, such as by having significantly different polarizations or frequencies, then the following normalized second-order correlation functions of the steady-state fluorescence intensity can be written as [57]

$$
g_{ij}^{(2)}(\tau) = \lim_{t\to\infty} g^{(2)}(\mathbf{R},t;\mathbf{R},t+\tau) = \frac{P_{2\to j}(\tau)}{P_j}, \quad i,j = 1,3 \tag{144}
$$

where

$$P_{2\to j}(\tau) = \frac{\langle S_i^+ S_j^+(\tau) S_j^-(\tau) S_i^- \rangle}{\langle S_i^+ S_i^- \rangle} \tag{145}$$

is the probability that at time $t+\tau$ the atom is in the upper state $|j\rangle$ of the transition $|j\rangle \to |2\rangle$ if it was in the lower state $|2\rangle$ of the $|i\rangle \to |2\rangle$ transition at time t, and $P_i = \langle S_i^+ S_i^- \rangle$ is the steady-state population of the state $|i\rangle$. In particular, we consider the following correlation functions

$$g_{11}^{(2)}(\tau) = g_{31}^{(2)}(\tau) = \frac{P_{2\to 1}(\tau)}{P_1} \tag{146}$$

$$g_{33}^{(2)}(\tau) = g_{13}^{(2)}(\tau) = \frac{P_{2\to 3}(\tau)}{P_3} \tag{147}$$

In Fig. 14, we plot the correlation functions (146) and (147) computed from the equations of motion (96) for the case of degenerate transitions ($\Delta = 0$) and two different values of p: $p = 0$ corresponding to the case of perpendicular dipole moments, and $p = 0.99$ corresponds to almost parallel dipole moments. We have chosen $p < 1$ to avoid population trapping, which can appear for $p = 1$. The correlations show the characteristic photon antibunching effect [59] that $g^{(2)}(\tau)$

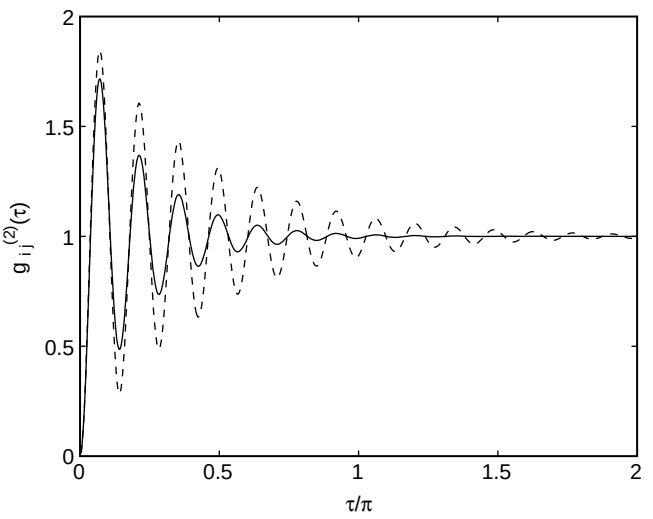

Figure 14. Second-order correlation functions $g_{11}^{(2)}(\tau)$ and $g_{33}^{(2)}(\tau)$ for $\Gamma_1 = \Gamma_2 = \Gamma, \Delta_L = \Delta = 0, \Omega_1 = \Omega_2 = 5\Gamma$, and different values of p: $p = 0.99$ (solid line), $p = 0$ (dashed line).

vanishes identically for $\tau = 0$ and increases with increasing τ. This reflects the fact that the detection of a photon at time $t + \tau$, after the detection of a photon at time t, is impossible if $\tau = 0$, and is unlikely until τ increases to a value of the order of $(2\Omega)^{-1}\pi$. For both values of p the correlation function oscillates with the Rabi frequency of the driving field and there is little difference between the plots for $p = 0$ and $p = 0.99$. The shape of the oscillations resembles that known for a two-level atom [59], which indicates that the atomic dipole moments oscillate independently, regardless of the value of p.

In Fig. 15, we plot the correlation functions for the same parameters as in Fig. 14, but now $\Delta \neq 0$. We first observe that the behavior of the correlation functions is qualitatively different to the case where $\Delta = 0$. For correlated dipole moments with $p = 0.99$, the values of $g_{11}^{(2)}(\tau)$ and $g_{33}^{(2)}(\tau)$ remain below unity for all times. This shows that for any τ the probability of emission of two photons from levels $|1\rangle$ or $|3\rangle$ is very small. We can interpret this as extended *simultaneous* periods of darkness in the fluorescence from the two atomic transitions; after detection of a photon at time $\tau = 0$, detection of another photon at time $\tau > 0$, emitted from levels $|1\rangle$ or $|3\rangle$, is very unlikely. We point out that the simultaneous periods of darkness appear only for correlated transitions with $p \neq 0$. Dark periods of fluorescence have been predicted by Cook and Kimble [60] and Pegg et al. [61] for a V-type atom with orthogonal dipole moments of the transitions and significantly different decay rates Γ_1 and

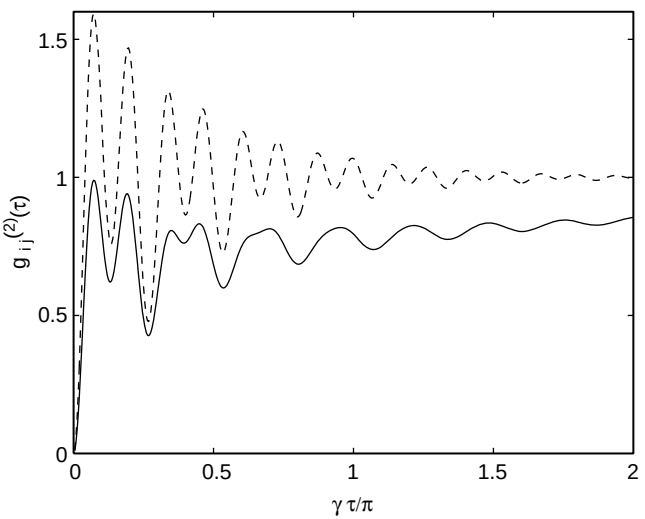

Figure 15. Second-order correlation functions $g_{11}^{(2)}(\tau)$ and $g_{33}^{(2)}(\tau)$ as a function of $\gamma\tau/\pi$ $(\gamma = (\Gamma_1 + \Gamma_2)/2)$ for $\Gamma_1 = \Gamma_2 = \Gamma, \Delta_L = 0, \Delta = 5\Gamma, \Omega_1 = \Omega_2 = 5\Gamma$, and different values of p: $p = 0.99$ (solid line), $p = 0$ (dashed line).

Γ_2. In their case the atom "prefers" to stay in the transition with the larger decay rate (strong transition) and there is a small probability of finding the system in the other (weak) transition. The extended dark periods, predicted for the V-type atom with almost parallel dipole moments, appear simultaneously on both transitions independent of the decay rates. This indicates that in the presence of quantum interference the atomic states $|1\rangle$ and $|3\rangle$ are not the preferred radiative states of the atom.

B. Indistinguishable Photons

We now turn to the situation in which the photons emitted from the two atomic transitions are not distinguishable. This can happen when the atomic transition dipole moments are exactly parallel. Then the detector responds to the total field (30) for which the correlation functions are given by Eqs. (141) and (142). However, even for $p \approx 1$, we can still distinguish between photons emitted from the $|s\rangle \to |2\rangle$ and $|a\rangle \to |2\rangle$ transitions as they can have different polarizations. This is easy to see from Eqs. (107) and (108), where the dipole moments $\boldsymbol{\mu}_s$ and $\boldsymbol{\mu}_a$ of the $|s\rangle \to |2\rangle$ and $|a\rangle \to |2\rangle$ transitions, respectively, are oriented in different directions, unless $\boldsymbol{\mu}_1 = \boldsymbol{\mu}_2$ and then $\boldsymbol{\mu}_a = 0$.

Therefore, we consider separately the following correlation functions

$$g_{ss}^{(2)}(\tau) = \frac{P_{2\to s}(\tau)}{P_s} \tag{148}$$

$$g_{aa}^{(2)}(\tau) = \frac{P_{2\to a}(\tau)}{P_a} \tag{149}$$

In Fig. 16, we plot the correlation functions (148) and (149) for non-degenerate transitions with $\Delta = 5\Gamma$. Again, the solid line represents $p = 0.99$ and the dashed line, $p = 0$. It is apparent from the graphs that with quantum interference ($p = 0.99$), there are very strong correlations of photons on the $|s\rangle \to |2\rangle$ transition, whereas the photons are strongly anticorrelated on the $|a\rangle \to |2\rangle$ transition. The correlation function $g_{ss}^{(2)}(\tau)$ oscillates with $2\sqrt{2}\Omega$ and attains the maximum value at time $\tau = (2\sqrt{2}\Omega)^{-1}\pi$. Moreover, the correlations decay at a very low rate and it takes a time in excess of 300π before it gets close to unity. The correlation function $g_{aa}^{(2)}(\tau)$ oscillates with $\sqrt{2}\Omega$ and in the presence of quantum interference is smaller than unity for all times, whereas the values can be larger than unity, with the maximum value of around 2.8, for $p = 0$.

We wish to emphasize that under appropriate conditions of $p \approx 1$ the maximum value of $g_{ss}^{(2)}(\tau)$ can be made huge, with values of the order of hundreds, whereas the maximum value of $g_{ss}^{(2)}(\tau)$ remains of the order of unity for $p = 0$. Indeed, it is seen from Fig. 16 that the maximum value of $g_{ss}^{(2)}(\tau)$ is about 22.5 for $p \simeq 1$. Swain et al. [58] have shown that even larger values are

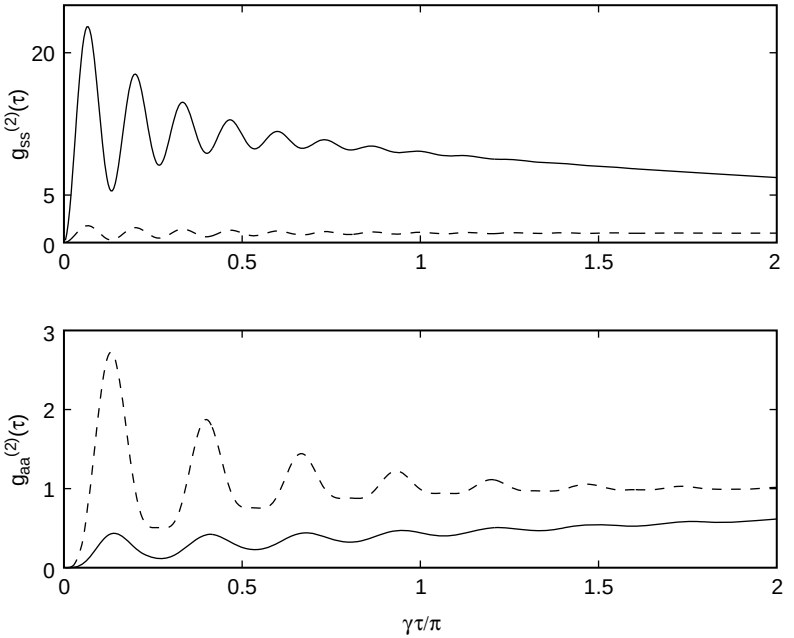

Figure 16. Second-order correlation functions $g_{ss}^{(2)}(\tau)$ and $g_{aa}^{(2)}(\tau)$ for $\Gamma_1 = \Gamma_2 = \Gamma$, $\Delta = 5\Gamma, \Omega_1 = \Omega_2 = 5\Gamma$, and different values of p: $p = 0.99$ (solid line), $p = 0$ (dashed line).

possible. For example, if we reduce the value Ω to 0.5Γ, leaving other parameters unchanged, then the maximum value can increase to almost 1500.

As we have seen from Figs. 14–16, the effect of quantum interference on the second-order correlation function, is very sensitive to the splitting Δ of the excited levels. For degenerate excited levels ($\Delta = 0$), the photon emissions are similar to those of a two-level atom, independent of quantum interference. For large splittings, the correlation functions $g_{aa}^{(2)}(\tau)$ and $g_{ij}^{(2)}(\tau)$, $i,j = 1,3$ are smaller than unity for all times τ, while $g_{ss}^{(2)}(\tau)$ exhibits strong correlations ($g_{ss}^{(2)}(\tau) \gg 2$) for $\tau \approx (2\sqrt{2}\Omega)^{-1}\pi$, which decay at a very low rate.

We can explain these features by considering the equations of motion (96) for the density matrix elements. When $\Delta = 0$, and the laser is tuned to the middle of the upper levels splitting the states $|1\rangle$ and $|3\rangle$ are equally driven by the laser and the coherences ρ_{12} and ρ_{32} oscillate in phase with frequency Δ_L. The coherences are directly coupled by the cross-damping term Γ_{12}. However, for a strong driving field ($\Omega \gg \Gamma$) the Rabi oscillations dominate over the spontaneous exchange of photons, resulting in independent oscillations of the atomic dipole moments.

The situation is different when $\Delta \neq 0$. In this case the coherences oscillate with opposite phases indicating that there is an exchange of photons between the states $|1\rangle$ and $|3\rangle$, which prevents photons being emitted from the atomic levels. The coherences oscillate with $\pm\Delta/2$, which introduces the modulation of the Rabi oscillations, seen in Fig. 15. The exchange of photons between the atomic levels is better seen in the basis of the symmetric and antisymmetric states (107) and (108). In terms of these states, setting $\Gamma_1 = \Gamma_2 = \Gamma$ for simplicity, the equations of motion for the populations

$$\dot{\rho}_{ss} = -\frac{1}{2}\Gamma(1+p)\rho_{ss} - \frac{1}{2}i\Delta(\rho_{sa} - \rho_{as}) - i\sqrt{2}\Omega(\rho_{s2} - \rho_{2s}) \tag{150}$$

$$\dot{\rho}_{aa} = -\frac{1}{2}\Gamma(1-p)\rho_{aa} + \frac{1}{2}i\Delta(\rho_{sa} - \rho_{as}) \tag{151}$$

It is evident that the antisymmetric state is populated by the coherent coupling to the symmetric state. Since the decay rate of the antisymmetric state, $\Gamma(1-p)$, is very small for $p \approx 1$, the population stays in this state for a long time. If $\Delta = 0$ the state is decoupled from the symmetric state and $\rho_{aa}(t)$ is zero if its initial value is zero. In the latter case the system reduces to a two-level atom. In the former case the transfer of the population to a slowly decaying state leaves the symmetric state almost unpopulated even if the driving field is strong. This is shown in Fig. 17, where we plot the steady-state populations ρ_{ss} as a

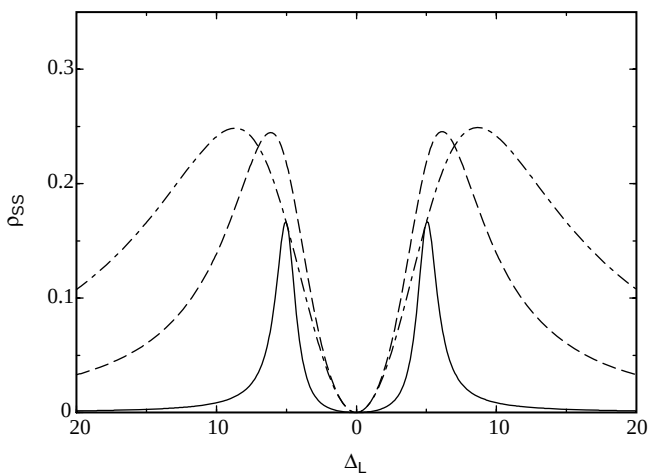

Figure 17. The stationary population of the symmetric state $|s\rangle$ as a function of Δ_L for $\Gamma_2 = \Gamma_1 = \Gamma, \delta_{12} = 0.1\Gamma, \Delta = 5\Gamma, p = 1$, and different Ω: $\Omega = \Gamma$ (solid line), $\Omega = 5\Gamma$ (dashed line), $\Omega = 10\Gamma$ (dashed–dotted line).

function of Δ_L. It is seen that the symmetric state is unpopulated for $\Delta_L = 0$. This indicates that in the presence of quantum interference, the driving field does not saturate the transition $|2\rangle \rightarrow |s\rangle$, even for very large Rabi frequencies. The lack of population in the state $|s\rangle$ increases the probability of returning the atom to this state from the ground state by the driving field. Consequently, $g_{ss}^{(2)}(\tau)$ attains a very large value at time $\tau = (2\sqrt{2}\Omega)^{-1}\pi$, corresponding to half of the Rabi cycle between $|2\rangle$ and $|s\rangle$.

VIII. PREPARATION OF TWO NON-ORTHOGONAL DIPOLE MOMENTS

The unusual effects induced by the quantum interference between two transitions in the multilevel systems, discussed in the previous sections, may occur only if the dipole matrix elements of the transitions involved are nonorthogonal:

$$\boldsymbol{\mu}_1 \cdot \boldsymbol{\mu}_2 \neq 0 \tag{152}$$

This represents a formidable practical problem, as one is very unlikely to find isolated atoms with two nonorthogonal dipole moments and quantum states close in energy. Consider, for example, a V-type atom with the upper states $|1\rangle$, $|3\rangle$ and the ground state $|2\rangle$. The evaluation of the dipole matrix elements produces the following selection rules in terms of the angular momentum quantum numbers: $J_1 - J_2 = \pm 1, 0$, $J_3 - J_2 = \pm 1, 0$, and $M_1 - M_2 = M_3 - M_2 = \pm 1, 0$. Since $M_1 \neq M_3$, in many atomic systems, $\boldsymbol{\mu}_{12}$ is perpendicular to $\boldsymbol{\mu}_{32}$ and the atomic transitions are independent. Xia et al. [62] have found transitions with parallel and antiparallel dipole moments in sodium molecules (dimers) and have demonstrated experimentally the effect of quantum interference on the fluorescence intensity. We discuss the experiment in more details in the next section. Here, we point out that the transitions with parallel and antiparallel dipole moments in the sodium dimers result from a mixing of the molecular states due to the spin–orbit coupling.

A. External Driving Field Method

A mixing of atomic or molecular states can be implemented by applying external fields. To illustrate this method, we consider a V-type atom with the upper states connected to the ground state by perpendicular dipole moments ($\boldsymbol{\mu}_{12} \perp \boldsymbol{\mu}_{32}$). When the two upper states are coupled by a resonant microwave field, the states become a linear superposition of the bare states

$$\begin{aligned} |a\rangle &= \frac{1}{\sqrt{2}}(|1\rangle + |3\rangle) \\ |b\rangle &= \frac{1}{\sqrt{2}}(|1\rangle - |3\rangle) \end{aligned} \tag{153}$$

It is easily to find from Eq (153) that the dipole matrix elements between the superposition states and the ground state $|2\rangle$ are

$$\begin{aligned}\boldsymbol{\mu}_{a2} &= \frac{1}{\sqrt{2}}(\boldsymbol{\mu}_{12} + \boldsymbol{\mu}_{32}) \\ \boldsymbol{\mu}_{b2} &= \frac{1}{\sqrt{2}}(\boldsymbol{\mu}_{12} - \boldsymbol{\mu}_{32})\end{aligned} \tag{154}$$

When $|\boldsymbol{\mu}_{12}| \neq |\boldsymbol{\mu}_{32}|$, the dipole moments $\boldsymbol{\mu}_{a2}$ and $\boldsymbol{\mu}_{b2}$ are not perpendicular. However, the dipole moments cannot be made parallel or antiparallel.

An alternative method in which one could create a V-type system with parallel or antiparallel dipole moments is to apply a strong laser field to one of the two transitions in a Λ-type atom. The scheme is shown in Fig. 18. When the dipole moments of the $|1\rangle \to |3\rangle$ and $|2\rangle \to |3\rangle$ transitions are perpendicular, the laser exclusively couples to the $|2\rangle \to |3\rangle$ transition and produces dressed states

$$\begin{aligned}|a\rangle &= \sin\phi|2\rangle + \cos\phi|3\rangle \\ |b\rangle &= \cos\phi|2\rangle - \sin\phi|3\rangle\end{aligned} \tag{155}$$

where

$$\cos^2\phi = \frac{1}{2} + \frac{\Delta_L}{2\sqrt{\Omega_0^2 + \Delta_L^2}} \tag{156}$$

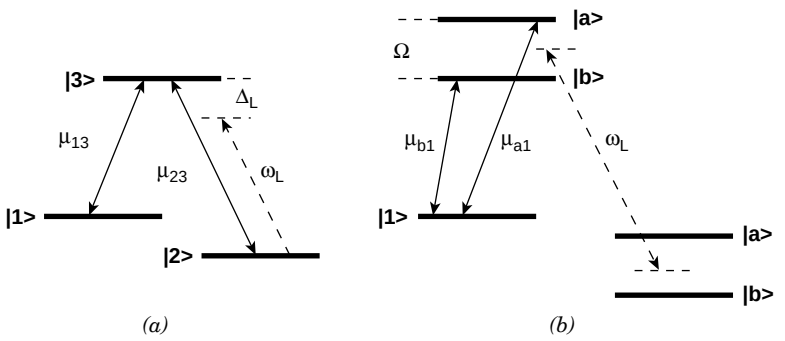

Figure 18. Laser induced V-type system with nondegenerate transitions. A laser field applied to the $|2\rangle \to |3\rangle$ transition of a Λ system creates nondegenerate dressed states separated by $\Omega = \sqrt{\Omega_0^2 + \Delta_L^2}$. The subsystem with the upper dressed atates $|a\rangle$, $|b\rangle$ and the ground state $|1\rangle$ behaviors as a V-type system with parallel dipole moments.

where Δ_L is the detuning of the laser frequency from the atomic transition and Ω_0 is the on-resonance Rabi frequency of the laser field.

From Eq (155), we find that the dipole matrix elements between the dressed states and the ground state $|1\rangle$ are

$$\begin{aligned} \boldsymbol{\mu}_{a1} &= \boldsymbol{\mu}_{13} \sin\phi \\ \boldsymbol{\mu}_{b1} &= \boldsymbol{\mu}_{13} \cos\phi \end{aligned} \tag{157}$$

Thus, the subsystem with the upper dressed states $|a\rangle$, $|b\rangle$ and the ground state $|1\rangle$ behaviors as a V-type system with parallel dipole moments. This system has an advantage that the magnitudes of the transition dipole moments, and the upper-level splitting can be controlled by the Rabi frequency and detuning of the driving laser field.

B. Dressed-Atom Approach

Transitions with parallel or antiparallel dipole moments can be created not only in multilevel systems but also in a two-level system driven by a polychromatic field [63]. In order to show this, we consider a two-level atom driven by a bichromatic field composed of a strong resonant laser field and a weaker laser field detuned from the atomic resonance by the Rabi frequency of the strong field. The effect of the strong field alone is to produce dressed states [35]

$$\begin{aligned} |1, N\rangle &= \frac{1}{\sqrt{2}}(|g, N\rangle - |e, N-1\rangle) \\ |2, N\rangle &= \frac{1}{\sqrt{2}}(|g, N\rangle + |e, N-1\rangle) \end{aligned} \tag{158}$$

with energies $E_{1,2} = \hbar(N\omega_0 \pm \frac{1}{2}\Omega)$, where N is the number of photons in the field mode, Ω is the Rabi frequency, and ω_0 is the atomic transition frequency.

The dressed states are shown in Fig. 19a. We see that in the dressed atom basis the system is no longer a two-level system. It is a multilevel system with three different transition frequencies, ω_0 and $\omega_0 \pm \Omega$, and four nonvanishing dipole matrix elements $\boldsymbol{\mu}_{ij,N} = \langle N, i|\boldsymbol{\mu}|j, N-1\rangle$:

$$\boldsymbol{\mu}_{11,N} = \boldsymbol{\mu}_{12,N} = -\boldsymbol{\mu}_{21,N} = -\boldsymbol{\mu}_{22,N} = \frac{1}{2}\boldsymbol{\mu} \tag{159}$$

connecting dressed states between neighboring manifolds. There are transitions with parallel and antiparallel dipole moments that oscillate with frequencies ω_0 and $\omega_0 \pm \Omega$. This makes the system an ideal candidate for quantum interference. Moreover, there are two transitions with antiparallel dipole moments, $\boldsymbol{\mu}_{11,N}$ and $\boldsymbol{\mu}_{22,N}$, which oscillate with the same frequency ω_0. However, they are not coupled

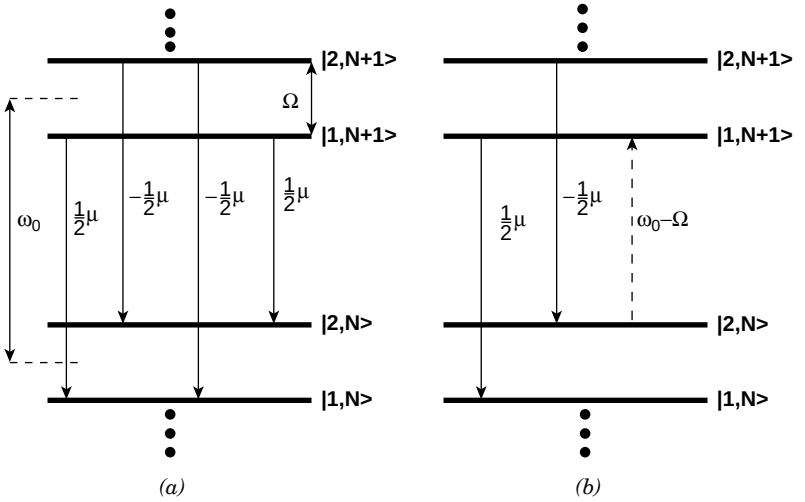

Figure 19. (a) Dressed states of a strongly driven two-level atom. The arrows indicate the allowed spontaneous transitions with dipole moments $\pm\frac{1}{2}\mu$. (b) A second coherent field (dashed arrow) of frequency $\omega_0 - \Omega$ couples the dipole moments of the two degenerate transitions at ω_0.

(correlated), preventing these dipole moments from being a source of quantum interference. This can be shown by calculating the correlation functions of the dipole moment operators of the dressed-atom transitions $\sigma^{+}_{ijN} = |i,N\rangle\langle N-1,j|$, $(i,j = 1,2)$. The correlation functions $\langle\sigma^{+}_{iiN}\sigma^{-}_{jjN}\rangle$, $(i \neq j)$, are equal to zero, showing that the dipole moments oscillate independently.

In order to correlate them, we can introduce a second (weaker) laser field of frequency $\omega_0 - \Omega$ and the Rabi frequency $\Omega_2 < \Omega$, which couples the degenerate transitions with dipole moments $\boldsymbol{\mu}_{11,N}$ and $\boldsymbol{\mu}_{22,N-1}$, as indicated in Fig. 19b. Treating the second field perturbatively, at zeroth order the coupling results in new "doubly dressed" states [63]

$$|\bar{N}, n\pm\rangle = \frac{1}{\sqrt{2}}(|2, N-n-1, M+n+1\rangle \pm |1, N-n, M+n\rangle) \qquad (160)$$

where M is the number of photons in the weaker-field mode, and $\bar{N} = N + M$ is the total number of photons. The doubly dressed states are entangled states of the "singly" dressed states (158), and the states of the second driving field.

We now can calculate the transition dipole moments $\boldsymbol{\mu}_{n\pm,n\pm}$ between the doubly dressed states, corresponding to the transitions at ω_0, and find that the dipole moments are equal to zero. Thus, in the doubly driven atom the effective dipole moments at ω_0 are zero due to quantum interference between the two

degenerate dipole moments of opposite phases. A dramatic consequence of this cancellation of the dipole moments is the disappearance of the central component in the fluorescence spectrum of the doubly driven two-level atom [63].

C. Preselected Polarization Method

Patnaik and Agarwal [64] and Zhou and Swain [65] have proposed a method involving a three-level atom with perpendicular dipole moments interacting with a single-mode cavity of a preselected polarization. In this system the polarization index s of the cavity mode is fixed to only one of the two possible directions. This arrangement of the polarization can lead to a nonzero coherence term Γ_{12} in the master equation of the system, even if the dipole moments of the atomic transitions are perpendicular. If the polarization of the cavity field is fixed, say, $\mathbf{e}_{ks} = \mathbf{e}_{kx}$, the polarization direction along the x-quantization axis, then the cross-damping rate (58) is given by

$$\Gamma_{12} = \sqrt{\Gamma_1 \Gamma_2} \cos\alpha \cos\beta \tag{161}$$

where $\alpha(\beta)$ is the angle between $\boldsymbol{\mu}_1(\boldsymbol{\mu}_2)$ and the preselected polarization vector, and $\alpha + \beta = 90^o$.

Zhou and Swain [65] have also shown that the idea of the preselected polarization can be applied to engineer a system with antiparallel dipole moments. Zhou [66] has extended the method to a cascade three-level atom coupled to a frequency-tunable cavity mode in a thermal state.

D. Anisotropic Vacuum Approach

Agarwal [67] has proposed a totally different mechanism to produce atomic transitions with parallel dipole moments. In this method the interference between two perpendicular dipole moments can be induced by an anisotropic vacuum field. Using the second-order perturbation theory, it can be shown that transition probability from the ground state $|g\rangle$ of a four-level system to the final state $|f\rangle$ through two intermediate states $|i\rangle$ and $|j\rangle$ is given by

$$T_{gf} = \frac{1}{\hbar^2} \sum_{i,j} \Omega_i \Omega_j \frac{\boldsymbol{\mu}_{fj}^* \mathbf{C}(\omega_L - \omega_{fg}) \boldsymbol{\mu}_{fi}}{(\omega_{ig} - \omega_L)(\omega_{jg} - \omega_L)} \tag{162}$$

where $\Omega_i(\Omega_j)$ is the Rabi frequency of the $|g\rangle \to |i\rangle(|g\rangle \to |j\rangle)$ transition, ω_L is the frequency of the driving laser, and $\mathbf{C}(\omega_L - \omega_{fg})$ is the Fourier transform of the tensor the antinormally ordered correlation function of the vacuum field operators. The anisotropy of the vacuum enters through the tensor $\mathbf{C}$. With the perpendicular dipole moments $\boldsymbol{\mu}_{fj}$ and $\boldsymbol{\mu}_{fi}$, the transition probability responsible for the quantum interference between the $|i\rangle \to |f\rangle$ and $|j\rangle \to |f\rangle$ transitions can be different from zero only if the tensor $\mathbf{C}$ is anisotropic. For isotropic vacuum

the tensor **C** is proportional to the unit tensor and then the transition probability vanishes for $\boldsymbol{\mu}_{fi} \perp \boldsymbol{\mu}_{fj}$.

IX. EXPERIMENTAL EVIDENCE OF QUANTUM INTERFERENCE

In 1996, Xia et al. [62] published the first experimental demonstration of constructive and destructive interference effects in spontaneous emission. In the experiment they used sodium dimers, which can be modeled as five-level molecular systems with a single ground level, two intermediate and two upper levels, driven by a two-photon process from the ground level to the upper doublet. By monitoring the fluorescence from the upper levels, they observed that the total fluorescence intensity, as a function of two-photon detuning, is composed of two peaks on transitions with parallel and three peaks on transitions with antiparallel dipole moments. The observed variation of the number of peaks with the mutual polarization of the dipole moments gives compelling evidence for quantum interference in spontaneous emission. Agarwal [68] has provided an intuitive picture for the observed spontaneous emission cancellation in terms of interference pathways involving a two-photon absorption process. Berman [69] has shown that the experimentally observed cancellation of spontaneous emission involving a two-photon absorption process can be interpreted in terms of population trapping. Although a cancellation of spontaneous emission is present with a two-photon excitation process, no variation of the number of peaks with the polarization of the dipole moments exist in the fluorescent intensity. Wang et al. [70] have presented a theoretical model of the observed fluorescence intensity that explains the variation of the number of the observed peaks with the mutual polarization of the molecular dipole moments.

The purpose of this section is to discuss the experimental scheme demonstrating the quantum interference effects in the fluorescence intensity and to explore the theoretical approach of Wang et al. [70] that explains the observed intensity profile.

A. Energy Levels of the Molecular System

The energy-level scheme of the molecular system considered in the experiment is shown in Fig. 20. The five-level molecule consists of two upper levels $|a_1\rangle$ and $|a_2\rangle$, two intermediate levels $|b\rangle$ and $|d\rangle$, and a single ground level $|c\rangle$. The upper levels are separated by the frequency ω_{12}, which is much smaller than the frequencies ω_{1b} and ω_{2b} of the $|a_1\rangle \to |b\rangle$ and $|a_2\rangle \to |b\rangle$ transitions and the frequencies ω_{1d} and ω_{2d} of the $|a_1\rangle \to |d\rangle$ and $|a_2\rangle \to |d\rangle$ transitions. As in the sodium dimers used in the experiment, we assume that the frequencies ω_{1b} and ω_{2b} correspond to the visible region, while the frequencies ω_{1d} and ω_{2d}

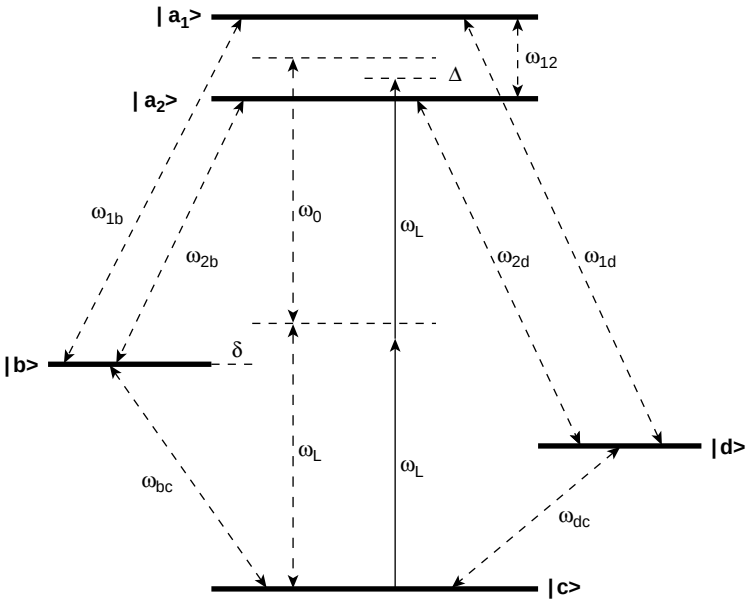

Figure 20. Energy-level structure of the molecular system considered by Xia et al. [62].

correspond to ultravioled region and are significantly different from the remaining frequencies.

In the molecule, the one-photon transitions $|a_1\rangle, |a_2\rangle \to |b\rangle, |d\rangle \to |c\rangle$ are connected by electric dipole moments, whereas the transition $|a_1\rangle \to |a_2\rangle$ and the two-photon transitions $|a_1\rangle, |a_2\rangle \to |c\rangle$ are forbidden in the electric dipole approximation. The transition dipole moments $\boldsymbol{\mu}_{ba_1}$ and $\boldsymbol{\mu}_{ba_2}$ are parallel, whereas the transition dipole moments $\boldsymbol{\mu}_{da_1}$ and $\boldsymbol{\mu}_{da_2}$ are antiparallel.

The system is driven by a single-mode tunable laser of an amplitude $\mathbf{E}_L$ and frequency ω_L coupled to the two-photon transitions $|c\rangle \to |a_1\rangle, |a_2\rangle$. The coupling strength of the laser field to the transitions is determined by the two-photon Rabi frequency

$$Q = \frac{1}{2}\sum_m \frac{\mu_{mc}\mu_{ma_1}E_L^2}{\omega_L - \omega_{mc}} = \frac{1}{2}\sum_m \frac{\mu_{mc}\mu_{ma_2}E_L^2}{\omega_L - \omega_{mc}} \tag{163}$$

where $E_L = |\mathbf{E}_L|$, and the sums are taken over intermediate virtual levels m.

B. Master Equation of the System

In the experiment Xia et al. [62] observed the steady-state intensity of the fluorescence field emitted on the visible and ultraviolet molecular transitions.

The intensity is proportional to the first-order correlation function $G^{(1)}(\mathbf{R}, t)$ which, according to Eq. (35), can be expressed in terms of the molecular dipole operators, or equivalently, in terms of matrix elements of the density operator of the molecular system. Using Eq. (35), we can write the intensities of the observed fluorescence fields on the visible (I_v) and ultraviolet (I_u) transitions as

$$\begin{aligned} I_v &= \Gamma_{a_1 b}\rho_{11} + \Gamma_{a_2 b}\rho_{22} + 2p_v\sqrt{\Gamma_{a_1 b}\Gamma_{a_2 b}}\mathrm{Re}(\rho_{12}) \\ I_u &= \Gamma_{a_1 d}\rho_{11} + \Gamma_{a_2 d}\rho_{22} + 2p_u\sqrt{\Gamma_{a_1 d}\Gamma_{a_2 d}}\mathrm{Re}(\rho_{12}) \end{aligned} \tag{164}$$

where Γ_{ij} is the spontaneous decay rate of the $|i\rangle \to |j\rangle$ transition, ρ_{11} and ρ_{22} are the steady-state populations of the levels $|a_1\rangle$ and $|a_2\rangle$, ρ_{12} is the steady-state coherence between them, and u and v stand for the ultraviolet and visible transitions, respectively.

We find the density matrix elements from the master equation of the system. In the frame rotating with the laser frequency ω_L and within a secular approximation, in which we ignore all terms oscillating with $(\omega_{1d} - \omega_L)$ and $(\omega_{2d} - \omega_L)$, the master equation for the density operator of the system is given by

$$\frac{\partial}{\partial t}\rho(t) = -\frac{i}{\hbar}[H(t), \rho(t)] + \mathscr{L}_d\rho(t) \tag{165}$$

where

$$\begin{aligned} H(t) = &-\hbar(\Delta - \frac{1}{2}\omega_{12})S_{a_1a_1} - \hbar(\Delta + \frac{1}{2}\omega_{12})S_{a_2a_2} \\ &- \frac{\hbar}{2}(\Delta + 2\delta)S_{bb} + \hbar[Q(S_{a_1c} + S_{a_2c}) + \mathrm{H.c.}] \end{aligned} \tag{166}$$

$$\begin{aligned} \mathscr{L}_d = &\frac{1}{2}\Gamma_v(1+p_v)\mathscr{D}[S_{ba_1} + S_{ba_2}] + \frac{1}{2}\Gamma_v(1-p_v)\mathscr{D}[S_{ba_1} - S_{ba_2}] \\ &+ \frac{1}{2}\Gamma_u(1+p_u)\mathscr{D}[S_{da_1} + S_{da_2}] + \frac{1}{2}\Gamma_u(1-p_u)\mathscr{D}[S_{da_1} - S_{da_2}] \\ &+ \Gamma_b\mathscr{D}[S_{cb}] + \Gamma_d\mathscr{D}[S_{cd}], \end{aligned} \tag{167}$$

and $S_{ij} \equiv |i\rangle\langle j|$ are projection operators that represent the energies of the molecular levels $(i = j)$ and transition dipole moments $(i \neq j)$. In Eqs. (166) and (167), $\Delta = 2(\omega_L - \omega_0)$ is the two-photon detuning between the laser frequency ω_L and the mean frequency ω_0 of the upper levels relative to the ground level, $\delta = \omega_0 - \omega_b$ is the frequency difference between ω_0 and the frequency ω_b of the $|b\rangle \to |c\rangle$ transition. The parameters $\Gamma_v = \Gamma_{a_1 b} = \Gamma_{a_2 b}$ and $\Gamma_u = \Gamma_{a_1 d} = \Gamma_{a_2 d}$ denote the spontaneous decay rates of the visible and

ultraviolet transitions, respectively; Γ_b (Γ_d) stands for the spontaneous decay rate from the intermediate level $|b\rangle$ ($|d\rangle$) to the ground level $|c\rangle$; and $\mathscr{D}$ is a superoperator defined for arbitrary operators A and B as

$$\mathscr{D}[A]B \equiv ABA^{\dagger} - \frac{1}{2}\{A^{\dagger}A, B\} \tag{168}$$

The master equation (165) provides the basis for our analytical and numerical discussions of quantum interference effects in the molecular system.

C. Two-Photon Excitation

The master equation (165) leads to a closed system of 25 equations of motion for the density matrix elements. Since the laser field does not couple to the level $|d\rangle$, the system of equations splits into two subsystems: a set of 17 equations of motion directly coupled to the driving field and the other of 8 equations of motion not coupled to the driving field. It is not difficult to show that the steady-state solutions for the 8 density matrix elements are zero. Using the trace property, one of the remaining equations can be eliminated, and the system of equations reduces to the 16 coupled linear inhomogeneous equations.

Consider the weak-field limit where Q is much smaller than the spontaneous decay rates and assume, for simplicity, that the decay rates of the upper levels on the visible and ultraviolet transitions are equal, $\Gamma_v = \Gamma_u = \Gamma$. In this case, we can solve the system analytically, and find that the steady-state populations and coherences appearing in Eq. (164) are

$$\rho_{11} = \frac{Q^2}{(\Delta + \frac{1}{2}\omega_{12})^2 + \Gamma^2} \tag{169}$$

$$\rho_{22} = \frac{Q^2}{(\Delta - \frac{1}{2}\omega_{12})^2 + \Gamma^2} \tag{170}$$

$$\mathrm{Re}(\rho_{12}) = \frac{Q^2(\Delta^2 - \frac{1}{4}\omega_{12}^2 + \Gamma^2)}{[(\Delta + \frac{1}{2}\omega_{12})^2 + \Gamma^2][(\Delta - \frac{1}{2}\omega_{12})^2 + \Gamma^2]} \tag{171}$$

It is seen that the populations and coherence exhibit resonances at $\Delta = \pm\frac{1}{2}\omega_{12}$, corresponding to the two-photon resonances of the laser field with the $|c\rangle \to |a_1\rangle$ and $|c\rangle \to |a_2\rangle$ transitions. Hence, the fluorescence intensity will exhibit two peaks located at $\Delta = \pm\frac{1}{2}\omega_{12}$.

In Fig. 21, we plot the fluorescence intensity as a function of Δ for the visible and unvisible transitions. It is evident that the intensity profile is composed of two peaks located at $\Delta = \pm\frac{1}{2}\omega_{12}$, and the amplitudes of the peaks are not sensitive to p. The intensity is sensitive to p only about $\Delta = 0$ and can be

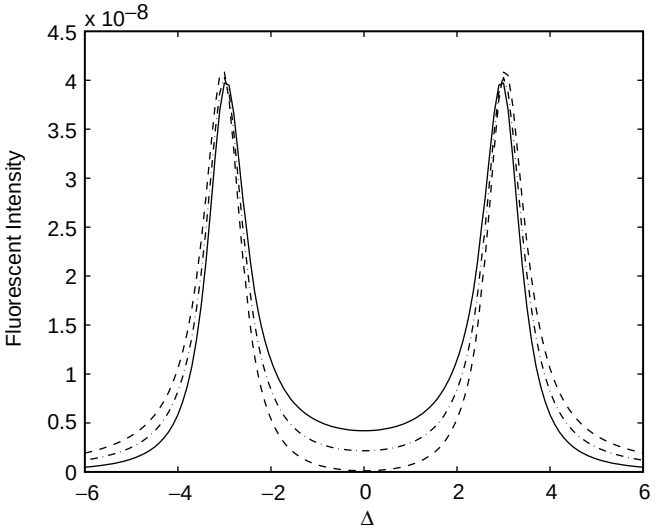

Figure 21. The fluorescence intensity as a function of Δ for $Q = 10^{-4}\Gamma$, $\delta = 0$, $\omega_{12} = 6\Gamma$ and $\Gamma_b = \Gamma_d = \Gamma$. The solid line shows the intensity on the ultraviolet transition ($p_u = -1$), the dashed line shows the intensity on the visible transition ($p_v = 1$), and the dashed–dotted line indicates the intensity for a transition with perpendicular dipole moments ($p = 0$).

completely suppressed for $p_v = 1$ transitions. This is in agreement with the prediction by Agarwal [68] that the two-photon excitation process involving the $|a_1\rangle$ and $|a_2\rangle$ levels can lead to cancellation of spontaneous emission at the two-photon resonance $\Delta = 0$.

In the experiment [62], however, a pronounced central peak at $\Delta = 0$ was observed, in addition to the sideband peaks located at $\Delta = \pm\frac{1}{2}\omega_{12}$, on the ultraviolet transitions with antiparallel dipole moments. According to Eq. (164), the theory does not predict the central peak for the $p_u = -1$ transitions. Thus, with the two-photon excitation the fluorescence intensity exhibits two peaks regardless of the mutual orientation of the transition dipole moments. Wang et al. [70] have concluded that apart from the two-photon excitation process there must be some other processes involved in the dynamics of the system, and have suggested a two-step one-photon excitation in addition to the two-photon process.

D. One- and Two-Photon Excitations

Following the approach of Wang et al. [70], we suppose that the molecule is excited not only by the two-photon process but also by a two-step one-photon process involving the intermediate level $|b\rangle$. This channel of the excitation was

possible in the experiment as the one-photon transitions in the molecule are in the visible region and their dipole moments are parallel [62]. Moreover, it is stated in the experimental paper [62] that the two-photon transition in sodium dimers was enhanced by a near-resonant intermediate level, indicating that the laser could also couple the ground state $|c\rangle$ to the upper states $|a_1\rangle, |a_2\rangle$ via cascaded one-photon transitions. Thus, the laser could also couple to the one-photon transitions $|c\rangle \to |b\rangle$ and $|b\rangle \to |a_1\rangle, |a_2\rangle$.

To illustrate the effect of the two-step one-photon coupling on the fluorescence intensity, we include into the Hamiltonian (166) the interaction of the laser field with the one-photon transitions, and obtain

$$\begin{aligned} H(t) = &-\hbar\left(\Delta - \frac{1}{2}\omega_{12}\right)S_{a_1a_1} - \hbar\left(\Delta + \frac{1}{2}\omega_{12}\right)S_{a_2a_2} \\ &- \frac{\hbar}{2}(\Delta + 2\delta)S_{bb} + \hbar[Q(S_{a_1c} + S_{a_2c}) + \text{H.c.}] \\ &+ \frac{\hbar}{2}[\Omega_a(S_{a_1b} + S_{a_2b}) + \Omega_b S_{bc} + \text{H.c.}] \end{aligned} \tag{172}$$

where $\Omega_a = \boldsymbol{\mu}_{ba_1} \cdot \mathbf{E}_L/\hbar = \boldsymbol{\mu}_{ba_2} \cdot \mathbf{E}_L/\hbar$, and $\Omega_b = \boldsymbol{\mu}_{bc} \cdot \mathbf{E}_L/\hbar$ are the one-photon Rabi frequencies of the $|b\rangle \to |a_1\rangle, |a_2\rangle$ and $|c\rangle \to |b\rangle$ transitions, respectively.

Following the same procedure as in Section III.C, we find that in the presence of the two-step one-photon excitation and in the weak-field limit $(\Omega_a, \Omega_b, Q \ll \Gamma, \Gamma_b, \Gamma_d)$ the steady-state solutions for the relevant populations and the coherence are

$$\begin{aligned} \rho_{11} &= \frac{4\Omega_a^2\Omega_b^2}{[(\Delta + 2\delta)^2 + \Gamma_b^2][(\Delta - \frac{1}{2}\omega_{12})^2 + \Gamma^2]} \\ \rho_{22} &= \frac{4\Omega_a^2\Omega_b^2}{[(\Delta + 2\delta)^2 + \Gamma_b^2][(\Delta + \frac{1}{2}\omega_{12})^2 + \Gamma^2]} \\ \text{Re}(\rho_{12}) &\simeq \frac{-16\Omega_a^2\Omega_b^2}{(\omega_{12})^2[(\Delta + 2\delta)^2 + \Gamma_b^2]} \end{aligned} \tag{173}$$

The steady-state solution (173) shows that the populations of the upper levels as well as the coherences exhibit resonant behaviors not only on the two-photon resonances $\Delta = \pm\frac{1}{2}\omega_{12}$ but also on the one-photon resonance $\Delta = -2\delta$. The existence of the resonance at $\Delta = 2\delta$ illustrates the occurrence of the two-step one-photon excitation process. Hence, the fluorescence intensity will exhibit a peak at $\Delta = -2\delta$ of the linewidth Γ_b, and two sideband peaks located at$\Delta = \pm\frac{1}{2}\omega_{12}$ of the linewidth Γ.

Substituting Eq. (173) into Eqs. (164), we find that the fluorescence intensity for the ultraviolet and visible transitions can be written as

$$I_{u/v} = \frac{16\Gamma\Omega_a^2\Omega_b^2}{\omega_{12}^2}\left\{\frac{2(1-p_{u/v})}{(\Delta+2\delta)^2+\Gamma_b^2}\right.$$
$$\left.+\frac{1}{(\Delta-\frac{1}{2}\omega_{12})^2+\Gamma^2}+\frac{1}{(\Delta+\frac{1}{2}\omega_{12})^2+\Gamma^2}\right\} \tag{174}$$

Thus, the fluorescence intensity is composed of three Lorentzians: the central peak located at $\Delta = -2\delta$ and two sidebands located at $\Delta = \pm\frac{1}{2}\omega_{12}$. In Fig. 22, we plot the fluorescence intensity for a strong driving field obtained by numerical integration of the master equation (165) for three different values of the parameter p.

It is seen that the amplitude of the central peak depends strongly on the mutual polarization of the dipole moments. The peak is absent in the intensity I_v observed in the visible region with $p_v = 1$. For the fluorescence intensity I_u observed in the ultravioled region with $p_u = -1$, the amplitude of the peak is enhanced. The strong dependence of the amplitude of the central peak on the mutual orientation of the molecular dipole moments is precisely the effect observed in the experiment. We emphasize again that the presence of the central peak in the fluorescent intensity results from the coupling of the driving laser to the one-photon transitions. This peak would be present even if there were no interference between the transitions (i.e., even if the dipole moments were orthogonal with $p = 0$). The interference leads to an enhancement ($p_u = -1$) or cancellation ($p_v = 1$) of this central peak arising from cascaded one-photon excitations.

The intensity profile shown in Fig. 22 is symmetric about $\Delta = 0$. However, the experimentally observed fluorescent intensity was asymmetric about $\Delta = 0$. Few factors could contribute toward the observed asymmetry. For example, the decay rates from the two upper levels to the intermediate levels could be unequal. Another reason could be that the central peak is not exactly at $\Delta = 0$. The analytical solution (174) predicts the central peak to be at $\Delta = -2\delta$, and the condition of $\delta = 0$ implies that the energy of the level $|b\rangle$ is exactly half of the mean energy of the upper levels. There is no reason to expect this condition to be satisfied in the real molecule, and in fact it appears from the experimental results that δ is positive. In Fig. 23 we plot the fluorescence intensity for a nonzero δ. In this case the intensity profile is asymmetric and the asymmetry increases with increasing δ.

The experiment of Xia et al. [62] provides a nice demonstration of the quantum interference effects in a multilevel system. Li et al. [71] have repeated the two-photon experiment and claim that they have no observed the fluore-

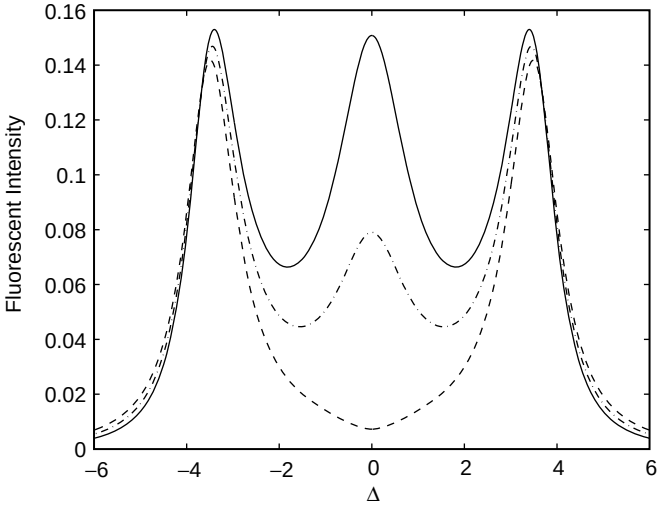

Figure 22. The fluorescence intensity as a function of Δ for $\Omega_a = \Omega_b = \Gamma, Q = 10^{-4}\Gamma$, $\delta = 0, \omega_{12} = 6\Gamma$ and $\Gamma_b = \Gamma_d = 0.15\Gamma$. The solid line shows the intensity on the ultraviolet transition ($p_u = -1$), the dashed line shows the intensity on the visible transition ($p_v = 1$), and the dashed–dotted line represents the intensity for a transition with perpendicular dipole moments ($p = 0$).

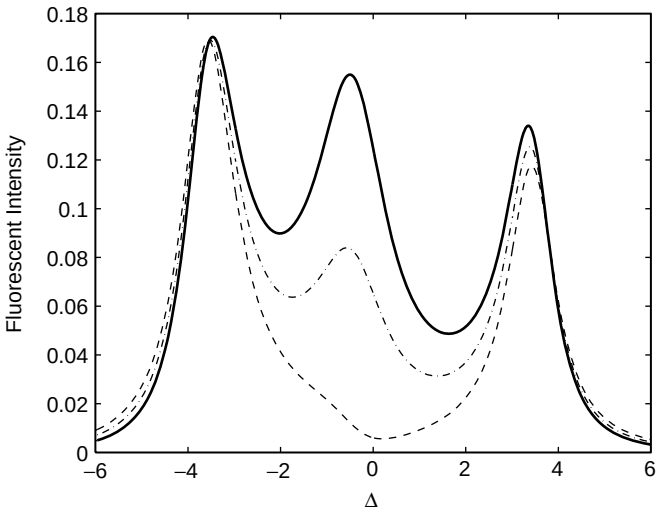

Figure 23. Same as in Fig. 22, but $\delta = 0.3\Gamma$.

scence signal reported by Xia et al. [62]. The major disagreement between these two experiments is found in the linewidths of the observed signals. However, a detailed comparison of these two experiments and theoretical calculations of the linewidths are rather difficult. In particular, the experimental conditions were not sufficiently well defined, which considerably complicates the interpretation of the observed signals and makes it difficult to resolve the disagreement between the experiments. Despite these disagreements, the theoretical model proposed by Wang et al. [70] correctly predicts the shape of the observed intensity profile and the variation of the number of peaks with the polarization of the dipole moments.

Acknowledgments

This work was supported by the Australian Research Council. I wish to thank especially Stuard Swain, Helen Freedhoff, Paul Berman, Peng Zhou, Terry Rudolph, Howard Wiseman, Uzma Akram, and Jin Wang for helpful discussions relating directly to the research reviewed in this chapter.

References

1. L. Mandel and E. Wolf, *Optical Coherence and Quantum Optics*, Cambridge Univ. Press, New York, 1995.
2. P. A. M. Dirac, *The Principles of Quantum Mechanics*, Oxford Univ. Press, Oxford, 1981.
3. M. O. Scully and M. S. Zubairy, *Quantum Optics*, Cambridge Univ. Press, New York, 1997.
4. G. S. Agarwal, in G. Höhler (Ed.), *Quantum Statistical Theories of Spontaneous Emission and Their Relation to Other Approaches*, Springer Tracts in Modern Physics, Vol. 70, Springer-Verlag, Berlin, 1974.
5. P. Zhou and S. Swain, *Phys. Rev. Lett.* **77**, 3995 (1996); Phys. Rev. A **56**, 3011 (1997).
6. C. H. Keitel, *Phys. Rev. Lett.* **83**, 1307 (1999).
7. K. J. Boller, A. Imamoglu, and S. E. Harris, *Phys. Rev. Lett.* **66**, 2593 (1991); K. Hakuta, L. Marmet, and B. Stoicheff, *Phys. Rev. Lett.* **66**, 596 (1991); J. C. Petch, C. H. Keitel, P. L. Knight, and J. P. Marangos, *Phys. Rev.* A **53**, 543 (1996); Y.-Q. Li and M. Xiao, Phys. Rev. A **51**, R2703, 4959 (1995).
8. S. E. Harris, *Phys. Rev. Lett.* **62**, 1033 (1989); M. O. Scully, S.-Y. Zhu, and A. Gavrielides, Phys. Rev. Lett. **62**, 2813 (1989); G. S. Agarwal, *Phys. Rev. A* **44**, R28 (1991); Z.-F. Luo and Z.-Z. Xu, *Phys. Rev. A* **45**, 8292 (1992); W. Tan, W. Lu, and R. G. Harrison, *Phys. Rev. A* **46**, R3613 (1992); C. H. Keitel, O. Kocharovskaya, L. M. Narducci, M. O. Scully, S.-Y. Zhu, and H. M. Doss, *Phys. Rev. A* **48**, 3196 (1993); W. Gawlik, *Comments Atom. Mol. Phys.* **29**, 189 (1993); G. Grynberg, M. Pinard, and P. Mandel, *Phys. Rev. A* **54**, 776 (1996); J. Kitching and L. Hollberg, *Phys. Rev. A* **59**, 4685 (1999).
9. M. O. Scully, *Phys. Rev. Lett.* **67**, 1855 (1991); M. O. Scully and M. Fleischhauer, *Phys. Rev. Lett.* **69**, 1360 (1992); A. D. Wilson-Gordon and H. Friedmann, *Opt. Commun.* **94**, 238 (1992); T. Quang and H. Freedhoff, *Phys. Rev. A* **48**, 3216 (1993); U. Akram, M. R. B. Wahiddin, and Z. Ficek, Phys. Lett. **A238**, 117 (1998).
10. P. Zhou and S. Swain, *Phys. Rev. Lett.* **78**, 832 (1997).
11. G. C. Hegerfeldt and M. B. Plenio, *Phys. Rev. A* **46**, 373 (1992); S.-Y. Zhu, R. C. F. Chan, and C. P. Lee, *Phys. Rev. A* **52**, 710 (1995); A. H. Toor, S.-Y. Zhu, and M. S. Zubairy, *Phys. Rev. A* **52**, 4803 (1995); M. B. Plenio and P. L. Knight, *Rev. Mod. Phys.* **70**, 101 (1998); F.-L. Li and S.-Y. Zhu,

Phys. Rev. A **59**, 2330 (1999); M. D. Lukin, S. F. Yelin, M. Fleischhauer, and M. O. Scully, Phys. Rev. A **60**, 3225 (1999); F. Plastina and F. Piperno, *Phys. Rev. A* **62**, 053801 (2000).

12. R. H. Dicke, *Phys. Rev.* **93**, 99 (1954); P. W. Milonni and P. L. Knight, *Phys. Rev. A* **10**, 1090 (1974); H. S. Freedhoff, *J. Phys. B* **19**, 3035 (1986); Z. Ficek, R. Tanaś, and S. Kielich, *Physica* **146A**, 452 (1987); G. J. Yang, O. Zobay, and P. Meystre, *Phys. Rev. A* **59**, 4012 (1999); A. Beige and G. C. Hegerfeldt, *Phys. Rev. A* **59**, 2385 (1999).
13. L. C. Ryff, *Phys. Rev. A* **52**, 2591 (1995); B.-G. Englert, *Phys. Rev. Lett.* **77**, 2154 (1996).
14. R. Hanbury-Brown and R. Q. Twiss, *Nature* **177**, 27 (1956).
15. A. Javan, E. A. Ballik, and W. L. Bond, *J. Opt. Soc. Am.* **52**, 96 (1962); M. S. Lipsett and L. Mandel, *Nature* **199**, 553 (1963).
16. Th. Richter, *Ann. Phys.* (*Leipzig*) **36**, 266 (1979); L. Mandel, *Phys. Rev. A* **28**, 1929 (1983); R. Gosh, C. K. Hong, Z. Y. Ou, and L. Mandel, *Phys. Rev. A* **34**, 3962 (1986); Z. Ficek, R. Tanás, and S. Kielich, *J. Mod. Opt.* **35**, 81 (1988).
17. D. F. Walls and G. J. Milburn, *Quantum Optics*, Springer, Berlin, 1994.
18. R. Gosh and L. Mandel, *Phys. Rev. Lett.* **59**, 1903 (1987); C. K. Hong, Z. Y. Ou, and L. Mandel, *Phys. Rev. Lett.* **59**, 2044 (1987); Z. Y. Ou and L. Mandel, *Phys. Rev. Lett.* **62**, 2941 (1989).
19. T. Richter, *Phys. Rev. A* **42**, 1817 (1990).
20. R. H. Lehmberg, *Phys. Rev. A* **2**, 883 (1970).
21. L. Allen and J. H. Eberly, *Resonance Fluorescence and Two-Level Atoms*, Wiley, New York, 1975.
22. W. H. Louisell, *Statistical Properties of Radiation*, Wiley, New York, 1973.
23. D. A. Cardimona and C. R. Stroud, Jr., *Phys. Rev. A* **27**, 2456 (1983).
24. U. Akram, Z. Ficek, and S. Swain, *Phys. Rev. A* **62**, 013413 (2000).
25. M. A. G. Martinez, P. R. Herczfeld, C. Samuel, L. M. Narducci, and C. H. Keitel, *Phys. Rev. A* **55**, 4483 (1997).
26. S. Menon and G. S. Agarwal, *Phys. Rev. A* **57**, 4014 (1998).
27. S.-Q. Gong, E. Paspalakis, and P. L. Knight, *J. Mod. Opt.* **45**, 2433 (1998).
28. E. Paspalakis, S.-Q. Gong, and P. L. Knight, *Opt. Commun.* **152**, 293 (1998).
29. F. Ghafoor, S.-Y. Zhu, and M. S. Zubairy, *Phys. Rev.* **62**, 013811 (2000).
30. Z. Ficek, J. Seke, A. Soldatov, and G. Adam, *Opt. Commun.* **182**, 143 (2000).
31. V. Bužek, P. L. Knight, and I. K. Kudryavtsev, *Phys. Rev. A* **44**, 1931 (1991).
32. S.-Y. Zhu and M. O. Scully, *Phys. Rev. Lett.* **76**, 388 (1996).
33. M. Lax, *Phys. Rev.* **172**, 350 (1968).
34. H. Lee, P. Polynkin, M. O. Scully, and S.-Y. Zhu, *Phys. Rev. A* **55**, 4454 (1997).
35. C. Cohen-Tannoudji and S. Reynaud, *J. Phys. B* **10**, 345 (1977); C. Cohen-Tannoudji, J. Dupont-Roc, and G. Grynberg, *Atom-Photon Interactions*, Wiley, New York, 1992.
36. D. A. Cardimona, M. G. Raymer, and C. R. Stroud, Jr., *J. Phys. B* **15**, 55 (1982).
37. B. R. Mollow, *Phys. Rev.* **188**, 1969 (1969).
38. B. R. Mollow, *Phys. Rev. A* **5**, 1522, 2217 (1972).
39. E. Paspalakis, and P. L. Knight, *Phys. Rev. Lett.* **81**, 293 (1998).
40. E. Arimondo and G. Orriols, *Lett. Nuovo Cimento* **17**, 333 (1976).
41. H. R. Gray, R. M. Whitley, and C. R. Stroud, Jr., *Opt. Lett.* **3**, 218 (1978).
42. G. Orriols, *Nuovo Cimento B* **53**, 1 (1979).
43. G. Alzetta, A. Gozzini, L. Moi, and G. Orriols, *Nuovo Cimento B* **36**, 5 (1976).

44. B. J. Dalton and P. L. Knight, in: J. D. Harvey and D. F. Walls (Eds.), *Laser Physics, Lecture Notes in Physics*, Vol. 182, Springer, Berlin, 1983, p. 213.
45. E. Arimondo, in E. Wolf (Ed.) *Progress in Optics*, Vol. Elsevier, Amsterdam, 1996, p. 257.
46. J. Javanainen, *Europhys. Lett.* **17**, 407 (1992).
47. M. R. Ferguson, Z. Ficek, and B. J. Dalton, *J. Mod. Opt.* **42**, 679 (1995).
48. S. Menon and G. S. Agarwal, *Phys. Rev. A* **61**, 013807 (2000).
49. R. Loudon, *The Quantum Theory of Light*, Oxford Univ. Press, Oxford, 1985, p. 23.
50. M. Sargent, M. O. Scully, and W. E. Lamb, *Laser Physics*, Addison-Wesley, Reading, MA, 1974.
51. Z. Ficek, S. Swain, and U. Akram, *J. Phys. B* **34**, 671 (2001); U. Akram, Z. Ficek, and S. Swain, *J. Mod. Opt.* **48**, 1059 (2001).
52. G. C. Hegerfeldt and M. B. Plenio, *Phys. Rev. A* **47**, 2186 (1993).
53. A. S. Manka, E. J. D'Angelo, L. M. Narducci, and M. O. Scully, *Phys. Rev. A* **47**, 4236 (1993).
54. L. M. Narducci, M. O. Scully, G.-L. Oppo, P. Ru, and J. R. Tredicci, *Phys. Rev. A* **42**, 1630 (1990).
55. D. J. Gauthier, Y. Zhu, and T. W. Mossberg, *Phys. Rev. Lett.* **66**, 2460 (1991).
56. B. N. Jagatap, Q. V. Lawande, and S. V. Lawande, *Phys. Rev. A* **43**, 535 (1991).
57. H. Huang, S.-Y. Zhu, M. S. Zubairy, and M. O. Scully, *Phys. Rev. A* **53**, 1834 (1996).
58. S. Swain, P. Zhou, and Z. Ficek, *Phys. Rev. A* **61**, 043410 (2000).
59. H. J. Carmichael and D. F. Walls, *J. Phys. B* **9**, L43 (1976); H. J. Kimble and L. Mandel, *Phys. Rev. A* **13**, 2123 (1976); H. J. Kimble, M. Dagenais, and L. Mandel, *Phys. Rev. Lett.* **39**, 691 (1977); M. Dagenais and L. Mandel, *Phys. Rev. A* **18**, 2217 (1978).
60. R. J. Cook and H. J. Kimble, *Phys. Rev. Lett.* **54**, 1023 (1985).
61. D. T. Pegg, R. Loudon, and P. L. Knight, *Phys. Rev. A* **33**, 4085 (1986).
62. H. R. Xia, C. Y. Ye, and S.-Y. Zhu, *Phys. Rev. Lett.* **77**, 1032 (1996).
63. Z. Ficek and H. S. Freedhoff, *Phys. Rev. A* **53**, 4275 (1996); T. Rudolph, H. S. Freedhoff, and Z. Ficek, *J. Opt. Soc. Am. B* **15**, 2345 (1998); C. C. Yu, J. R. Bochinski, T. M. V. Kordich, T. W. Mossberg, and Z. Ficek, *Phys. Rev. A* **56**, R4381 (1997); Z. Ficek and T. Rudolph, *Phys. Rev. A* **60**, R4245 (1999).
64. A. K. Patnaik and G. S. Agarwal, *Phys. Rev. A* **59**, 3015 (1999).
65. P. Zhou and S. Swain, *Opt. Commun.* **179**, 267 (2000).
66. P. Zhou, *Opt. Commun.* **178**, 141 (2000).
67. G. S. Agarwal, *Phys. Rev. Lett.* **84**, 5500 (2000); G. S. Agarwal and A. K. Patnaik, *Phys. Rev. A* **63**, 043805 (2001).
68. G. S. Agarwal, *Phys. Rev. A* **55**, 2457 (1997).
69. P. R. Berman, *Phys. Rev. A* **58**, 4886 (1998).
70. J. Wang, H. M. Wiseman, and Z. Ficek, *Phys. Rev. A* **61**, 063811 (2000).
71. L. Li, X. Wang, J. Jang, G. Lazarov, J. Qi, and A. M. Lyyra, *Phys. Rev. Lett.* **84**, 4016 (2000).

QUANTUM-OPTICAL STATES IN FINITE-DIMENSIONAL HILBERT SPACE. I. GENERAL FORMALISM

ADAM MIRANOWICZ

CREST Research Team for Interacting Carrier Electronics, School of Advanced Sciences, The Graduate University for Advanced Studies (SOKEN), Hayama, Kanagawa, Japan and Nonlinear Optics Division, Institute of Physics, Adam Mickiewicz University, Poznań, Poland

WIESŁAW LEOŃSKI

Nonlinear Optics Division, Institute of Physics, Adam Mickiewicz University, Poznań, Poland

NOBUYUKI IMOTO

CREST Research Team for Interacting Carrier Electronics, School of Advanced Sciences, The Graduate University for Advanced Studies (SOKEN), Hayama, Kanagawa, Japan

CONTENTS

I. INTRODUCTION

In the late twentieth century much attention has been paid to the investigation of various quantum-optical states defined in a *finite-dimensional Hilbert space* of operators, which are bounded and have a discrete spectrum. Yet, the idea of creating finite-dimensional quantum-optical states was conceived much earlier. In fact, back in 1931, Weyl's formulation of quantum mechanics [1] opened the possibility of studying the dynamics of quantum systems both in infinite-dimensional (ID) and finite-dimensional (FD) Hilbert spaces. Weyl's approach, generalized by Schwinger [2], is based on the fact that the kinematical structure of a physical system can be expressed by an irreducible Abelian group of unitary representations of system space. For a given finite Abelian group there is a unique class of unitarily equivalent, irreducible representations in FD space. Hence, this formulation has provided the basis for studies of the behavior of the harmonic oscillator in FD Hilbert spaces. In the 1970s, Santhanam and co-workers contributed to the above-mentioned formulation in a series of papers [3]. To describe the interaction of an assembly of two-level atoms with a transverse electromagnetic field, Radcliffe [4] and Arecchi et al. [5] introduced the atomic (or spin) coherent states (also referred to as the directed angular-momentum states [6]) as FD analogs of the conventional optical coherent states (CS) [7–9]. General formulation of coherent states in FD and ID Hilbert spaces was then developed by Perelomov [10] and Gilmore et al. [11,12] (see also Refs. 13–15). In the 1990s, various quantum-optical states were constructed in FD Hilbert spaces in analogy to those in the ID spaces. In particular, (1) various kinds of FD coherent states [16–24], (2) FD displaced number states [21], (3) FD even and odd coherent states [21,24,25], (4) FD phase states [26], (5) FD phase coherent states (also referred to as coherent phase states) [27–30], (6) FD squeezed states

[31–34], (7) FD displaced phase states [28], or (8) FD even and odd phase coherent states [35].

The interest in the FD quantum-optical states has been stimulated by the progress in quantum-optical state preparation and measurement techniques [36], in particular, by the development of the discrete quantum-state tomography [37–42]. There are several other reasons for studying states in FD spaces:

1. We can treat FD quantum-optical states as those of a real single-mode electromagnetic field, which fulfill the condition of truncated Fock expansion. These states can *directly* be generated by the truncation schemes (the *quantum scissors*) proposed by Pegg et al. [44] and then generalized by other authors [45–47]. Alternatively, one can analyze states obtained by a direct truncation of operators rather then of their Fock expansion. Such an operator truncation scheme, proposed by Leoński et al. [48–50], will be discussed in detail in the next chapter [51].
2. The formalism of FD quantum-optical states is applicable to other systems described by the FD models as well, such as spin systems or ensembles of two-level atoms or quantum dots. In such cases we should talk about, for instance the z component of the spin and its azimuthal orientation rather than about the photon number and phase. However, the states studied here were first discussed in the quantum-optical papers and we also will keep the terminology of quantum optics.
3. This analysis gives us a deeper insight into the Pegg–Barnett phase formalism [26] (for a review, see Ref. 43) of the Hermitian optical phase operator constructed in $(s+1)$-dimensional state Hilbert space. The key idea of the Pegg–Barnett procedure is to calculate all the physical quantities such as expectation values or variances in the FD space and only then to take the limit of $s \to \infty$. Bužek et al. [16] pointed out that all quantities (in particular states) analyzed within the Pegg–Barnett formalism should properly be defined in the same $(s+1)$-dimensional state space before finally going over into the infinite limit. So, for better understanding of the Pegg–Barnett formalism, it is useful to construct finite-dimensional states and to know what exactly happens before taking the limit.

In this chapter, we apply a discrete Wigner function to describe FD quantum-optical states. Wigner function is widely used in nonrelativistic quantum mechanics as an alternative to the density matrix of quantum systems [52]. Although the original Wigner function applies only to systems with continuous degrees of freedom, it can be generalized for finite-state systems as well [53]. Discrete Wigner function for spin-$\frac{1}{2}$ systems was introduced by O'Connell and Wigner [54] and generalized for arbitrary spins by Wootters [55]. His definition takes the simplest form for prime-number-dimensional systems. A similar

construction of a discrete Wigner function for odd-dimensional systems was suggested by a Cohendet et al. [56]. A number-phase discrete Wigner function, a special case of the Wootters definition, was analyzed in detail by Vaccaro and Pegg [57]. Another definition of Wigner function (for odd dimensions equivalent to that of Wootters) was proposed by Leonhardt [37]. This approach can readily be generalized to define a discrete Husimi Q function or, moreover, discrete parameterized phase-space functions as was studied by Opatrný et al. [58,59]. Another generalization of discrete Wigner function for Schwinger's FD periodic Hilbert space was analyzed by, for instance, Hakioğlu [60]. The Wigner function approach to FD systems can be developed from basic principles as was shown, for example, by Wootters [55], Leonhardt [37], Lukš and Peřinová [61], or Luis and Peřina [62]. Discrete Wigner function has successfully been applied to quantum-state tomography of FD systems [37] (for a review, see Ref. 42).

This work is intended as an attempt to present two essentially different constructions of harmonic oscillator states in a FD Hilbert space. We propose some new definitions of the states and find their explicit forms in the Fock representation. For the convenience of the reader, we also bring together several known FD quantum-optical states, thus making our exposition more self-contained. We shall discuss FD coherent states, FD phase coherent states, FD displaced number states, FD Schrödinger cats, and FD squeezed vacuum. We shall show some intriguing properties of the states with the help of the discrete Wigner function.

II. FD HILBERT SPACE

We shall discuss various states constructed in FD Hilbert space of harmonic oscillator. Let us denote by $\mathscr{H}^{(s)}$ the $(s+1)$-dimensional Hilbert space spanned by number states $\{|0\rangle, |1\rangle, \ldots, |s\rangle\}$ fulfilling the completeness and orthogonality relations

$$\hat{1}_s = \sum_{n=0}^{s} |n\rangle\langle n|\,, \qquad \langle n|m\rangle = \delta_{n,m} \tag{1}$$

where $n, m = 0, \ldots, s$ and $\hat{1}_s$ is the unit operator in $\mathscr{H}^{(s)}$. Thus, arbitrary quantum-optical pure state in the FD Hilbert space can be defined by its Fock expansion

$$|\psi\rangle_{(s)} = \sum_{n=0}^{s} C_n^{(s)}|n\rangle \equiv \sum_{n=0}^{s} b_n^{(s)} e^{i\varphi_n}|n\rangle \tag{2}$$

where $C_n^{(s)} = b_n^{(s)} e^{i\varphi_n}$ and $b_n^{(s)}$ are real superposition coefficients fulfilling the normalization condition

$$ {}_{(s)}\langle\psi|\psi\rangle_{(s)} = \sum_{n=0}^{s} [b_n^{(s)}]^2 = 1 \tag{3} $$

for arbitrary dimension $(s+1)$ of Hilbert space. It is sometimes useful to represent the optical state, given by (2), via the phase states defined to be [26]

$$ |\theta_m\rangle \equiv |\theta_m\rangle_{(s)} = \frac{1}{\sqrt{s+1}} \sum_{n=0}^{s} \exp(in\theta_m)|n\rangle \tag{4} $$

with the phases θ_m given by

$$ \theta_m = \theta_0 + \frac{2\pi}{s+1} m \tag{5} $$

where θ_0 is the initial reference phase and $m = 0, \ldots, s$. States (4) also form a complete and orthonormal basis:

$$ \hat{1}_s = \sum_{m=0}^{s} |\theta_m\rangle\langle\theta_m| , \qquad \langle\theta_m|\theta_n\rangle = \delta_{m,n} \tag{6} $$

The phase states were applied by Pegg and Barnett in their definition of the Hermitian quantum-optical phase operator [26]:

$$ \hat{\Phi}_s \equiv \hat{\Phi}_s(\theta_0) = \sum_{m=1}^{s} \theta_m |\theta_m\rangle\langle\theta_m| \tag{7} $$

The phase states can also be used in construction of a discrete Wigner function as will be described in Section III. The FD annihilation and creation operators in $\mathscr{H}^{(s)}$ are defined by

$$ \begin{aligned} \hat{a}_s &= \sum_{n=1}^{s} \sqrt{n}|n-1\rangle\langle n| \\ \hat{a}_s^\dagger &= \sum_{n=1}^{s} \sqrt{n}|n\rangle\langle n-1| \end{aligned} \tag{8} $$

The FD and ID annihilation operators act on a number state in the same manner. However, the actions of the creation operators on $|n\rangle$ are different in $\mathscr{H}^{(s)}$ and

$\mathscr{H}^{(\infty)}$. Equation (8) implies that

$$(\hat{a}_s^\dagger)^k|n\rangle = 0 \tag{9}$$

if $n + k > s$. By contrast, the action of the ID creation operator (in any power) on $|n\rangle$ gives always nonzero result. The commutation relation for the annihilation and creation operators in $\mathscr{H}^{(s)}$ reads as

$$[\hat{a}_s, \hat{a}_s^\dagger] = 1 - (s+1)|s\rangle\langle s| \tag{10}$$

which differs from the conventional boson canonical relation in $\mathscr{H}^{(\infty)}$. Thus, $\hat{a}_s$ and $\hat{a}_s^\dagger$ are not related to the Weyl–Heisenberg algebra. Even the double commutators $[\hat{a}_s, [\hat{a}_s, \hat{a}_s^\dagger]]$ and $[\hat{a}_s^\dagger, [\hat{a}_s, \hat{a}_s^\dagger]]$ do not vanish, precluding the application of the Baker–Hausdorff theorem. These properties of the FD annihilation and creation operators considerably complicate analytical approaches to the quantum mechanics in $\mathscr{H}^{(s)}$, including the explicit construction of the FD harmonic oscillator states.

Creation and annihilation of phase quanta in FD Hilbert space can be defined in a close analogy to the creation and annihilation of photons, as given by Eq. (8). Phase annihilation, $\hat{\phi}_s$, and phase creation, $\hat{\phi}_s^\dagger$, operators can be introduced with the help of the relation $\hat{\Phi}_s = \hat{\phi}_s^\dagger \hat{\phi}_s$ for the Pegg–Barnett phase operator, given by (7). The FD phase annihilation and creation operators in the phase-state basis, have the following form [16]

$$\begin{aligned} \hat{\phi}_s &\equiv \hat{\phi}_s(\theta_0) = \sum_{m=1}^{s} \sqrt{\theta_m}|\theta_{m-1}\rangle\langle\theta_m| + \sqrt{\theta_0}|\theta_s\rangle\langle\theta_0| \\ \hat{\phi}_s^\dagger &\equiv \hat{\phi}_s^\dagger(\theta_0) = \sum_{m=1}^{s} \sqrt{\theta_m}|\theta_m\rangle\langle\theta_{m-1}| + \sqrt{\theta_0}|\theta_0\rangle\langle\theta_s| \end{aligned} \tag{11}$$

respectively. Their commutator is

$$[\hat{\phi}_s, \hat{\phi}_s^\dagger] = \frac{2\pi}{s+1} - 2\pi|\theta_s\rangle\langle\theta_s| \tag{12}$$

The phase annihilation and creation operators act on the phase states in a similar way (particularly for $\theta_0 = 0$) as the conventional (photon number) annihilation and creation operators act on number states.

III. DISCRETE WIGNER FUNCTION FOR FD STATES

The expression of quantum-optical states by quasidistributions enables a very intuitive description of their properties. Here, we give a general definition of the

discrete Wigner function. We also present its graphical representations for several FD quantum-optical states, often discussed in more recent works. The Wigner function will be studied in greater detail in the following sections.

The number–phase characteristic function in $\mathscr{H}^{(s)}$ can be defined as [37]

$$C_s(\nu, \theta_\mu) = \sum_{m=0}^{s} \exp\left(-\frac{4\pi i}{s+1}\nu(m+\mu)\right)\langle\theta_m|\hat{\rho}|\theta_{m+2\mu}\rangle \tag{13}$$

in terms of the phase states (4). A discrete Fourier transform applied to $C_s(\nu, \theta_\mu)$ leads to the following discrete Wigner function (for brevity referred to as the W function) for phase and number

$$W_s(n, \theta_m) = \frac{1}{(s+1)^2}\sum_{\nu=0}^{s}\sum_{\mu=0}^{s} \exp\left(\frac{4\pi i}{s+1}(n\mu + \nu m)\right) C_s(\nu, \theta_\mu) \tag{14}$$

or, explicitly, as [37,55]

$$W_s(n, \theta_m) = \frac{1}{s+1}\sum_{\mu=0}^{s} \exp\left(\frac{4\pi i}{s+1} n\mu\right)\langle\theta_{m-\mu}|\hat{\rho}|\theta_{m+\mu}\rangle \tag{15}$$

The Wigner function $W_s(n, \theta_m)$ is periodic both in n and θ_m:

$$\begin{aligned} W_s(n, \theta_m) &= W_s(n \pm \{s+1\}, \theta_m) \\ &= W_s(n, \theta_{m\pm(s+1)}) \\ &= W_s(n, \theta_m \pm 2\pi) \end{aligned} \tag{16}$$

Thus, it is represented graphically on torus [20]. The Wigner function for any FD pure state of the form (2) can be expressed as follows [57]

$$\begin{aligned} W_s(n, \theta_m) = \frac{1}{s+1}\Bigg\{ &\sum_{k=0}^{M} b_k^{(s)} b_{M-k}^{(s)} \exp[i(2k-M)\theta_m + \varphi_{M-k} - \varphi_k] \\ &+ \sum_{k=M+1}^{s} b_k^{(s)} b_{M-k+s+1}^{(s)} \exp[i(2k-M-s-1)\theta_m + \varphi_{M-k+s+1} - \varphi_k] \Bigg\} \end{aligned} \tag{17}$$

in terms of the decomposition coefficients $b_k^{(s)}$ and $M \equiv 2n \bmod (s+1)$. Several graphs of these functions of various states are presented here (Fig. 1) and in the next sections. The physical interpretation of the Wigner functions is based on the

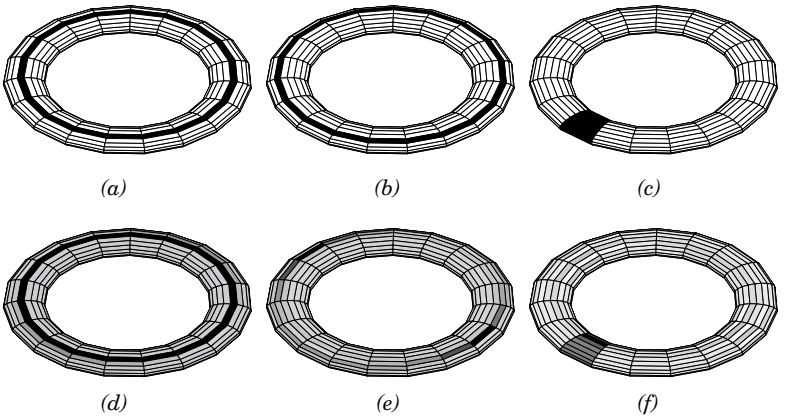

Figure 1. Examples of discrete Wigner function on a torus in 19-dimensional Hilbert space ($s = 18$): (a) vacuum $|0\rangle$; (b) single-photon number state $|1\rangle$; (c) FD preferred phase state ("phase vacuum") $|\theta_0\rangle_{(s)}$; (d) FD coherent state, $|\alpha\rangle_{(s)} \approx |\bar{\alpha}\rangle_{(s)}$; (e) FD displaced number state, $|\alpha, 1\rangle_{(s)} \approx |\bar{\alpha}, 1\rangle_{(s)}$; (f) FD phase coherent state, $|\beta, \theta_0\rangle_{(s)} \approx |\bar{\beta}, \theta_0\rangle_{(s)}$, with equal displacement parameters, $\alpha = \bar{\alpha} = \beta = \bar{\beta} = 0.5$ and $\theta_0 = 0$. The darker is a region, the higher is the value of the Wigner function.

fact that the marginal sum of their values over a generalized line gives the probability that the system will be in some state [37,55]. In the ID Hilbert space, where the W-function arguments are continuous (quadratures X and Y), a marginal integral along any straight line $aX + bY + c = 0$ is nonnegative and can be considered to be the probability. A similar situation arises in the FD case; we can define lines as sets of discrete points (n, θ_m), or equivalently (n, m), for which the relation $(an + bm + c) \bmod N = 0$ holds (here, a, b, c are integers). Again, sums of the discrete W-function values on such sets are non-negative. The mod $(s + 1)$ relations are essential and are connected to some periodic properties of the discrete W function—the maximum value of each argument (m or n) is topologically followed by its minimum (zero in our case). This means that the discrete W function is defined on a torus (or more precisely on a discrete set of points of a torus). The "lines" are then points of closed toroidal spirals or, in a special case, points of a circle. The periodic property is quite natural for the phase index m, but may seem strange for the photon number n. In the next sections, we shall draw attention to some consequences of the periodicity in n for generalized coherent states, for instance.

One aim of this chapter is to show graphs of the discrete W functions for FD quantum-optical states. Because of the discreteness of the arguments, the W-function graph should be a histogram. However, two-dimensional projections of such three-dimensional histograms could be very confusing. Therefore, for

better legibility of the graphs, we have decided to depict them topographically. The darker is a region, the higher is the value of the W function it represents. Moreover, negative values of the W function are marked by crosses. As mentioned above, the most natural way of presenting the discrete W-function graphs is to construct them on toruses. A few simple examples of the toroidal discrete Wigner functions are given in Fig. 1. Unfortunately, this graphical representation is seldom transparent enough for its interpretation. In what follows we shall work with two-dimensional graphs. Here, one should keep in mind that some consequences of the periodicity in n and m can appear; for instance, some peaks can be located partially at the outer boundary at $n \approx s$ (or $m \approx s$) and can "continue" near the center $n \approx 0$ (or $m \approx 0$). In the next section, the W functions of various FD states will be presented.

For a better understanding of the discrete Wigner function, let us recall its close correspondence to the discrete Pegg–Barnett phase distribution [26]

$$P_s(\theta_m) = \sum_{n=0}^{s} W_s(n, \theta_m) = \left|{}_{(s)}\langle\theta_m|\psi\rangle_{(s)}\right|^2 \tag{18}$$

and to the photon-number distribution

$$P_s(n) = \sum_{m=0}^{s} W_s(n, \theta_m) = \left|\langle n|\psi\rangle_{(s)}\right|^2 = |b_n^{(s)}|^2 \tag{19}$$

Thus, the sum of the W function values, at constant θ_m, over all n values gives the probability of the phase θ_m and, analogously, the sum with constant n over all arguments θ_m gives the probability of n photons—at least in systems, which are fully described by finite-number state models. If we want to interpret our results as describing states of a usual one-mode field under the condition that all Fock components of $|n\rangle$ with $n > s$ are absent, then the real phase probability distribution is obviously continuous. Let us briefly discuss its connection to the obtained discrete distribution. If s is greater than or equal to the largest Fock state component of a given state, which by definition is our case, then the discrete probabilities (from the discrete Wigner phase marginal) are proportional to the values of the continuous phase probability distribution in the discrete set of points (5). One can easily obtain other values also, although not directly. We could use a FD version of the sampling theorem—if the n distribution is limited, then for description a state in the phase representation only a discrete set of phase amplitudes is necessary. It is clear that the $(s+1)^2$ real values of the discrete W function yield the same information as the $(s+1)^2$ real nonzero parameters of the related density matrix.

IV. FD COHERENT STATES

The most common states in quantum optics are the *coherent states* (CS) introduced by Schrödinger [7] in connection with classical states of the quantum harmonic oscillator. First modern description and specific application of CS is due to Glauber [8] and Sudarshan [9]. The literature on CS and their generalizations is truly prodigious and has been summarized in a number of excellent monographs [10,13,14,63] and reviews [12]. There are several ways of generalizing the conventional ID coherent states to comprise the FD case. It is possible to define CS using the concept of Lie group representations [63], or to postulate the validity of some properties of the ID CS for their FD analogs. In this chapter, we are interested in two definitions of the latter kind. First, CS in a FD space are usually treated as the displaced vacuum, where the displacement operator is defined analogously to the conventional displacement operator in the ID space (the Glauber treatment of CS [8]). This idea was applied in the work of Bužek and co-workers [16] and further studied by Miranowicz et al. [18] and Opatrný et al. [20]. Here, we refer to such states as the *generalized CS*. Another definition is based on the postulate that the Fock expansion of the FD CS is equal to the truncated expansion of the conventional ID CS. This approach was extensively developed by Kuang et al. [17] and Opatrný et al. [20]. Here, we shall refer to CS of this kind as the *truncated CS*. An experimental scheme, known as the *quantum scissors*, for generation of the truncated CS was proposed by Pegg et al. [44]. Quantum scissors were generalized by Koniorczyk et al. [45], Paris [46], and Miranowicz et al. [47]. A physical system for preparation of the generalized CS was proposed by Leoński [49] (see also Ref. 50) as a modification of the Fock state engineering technique of Leoński and Tanaś [48]. These schemes are presented in the next chapter [51].

A. Generalized Coherent States

Glauber [8] constructed coherent states in the ID Hilbert space by applying the displacement operator $\hat{D}(\alpha,\alpha^*) \equiv \exp(\alpha\hat{a}^\dagger - \alpha^*\hat{a})$ on vacuum state $|0\rangle$. Analogously, one can define the *generalized coherent state* [16]

$$|\alpha\rangle_{(s)} = \hat{D}_s(\alpha,\alpha^*)|0\rangle \tag{20}$$

constructed in the FD Hilbert space by the action of the generalized FD given by displacement operator

$$\hat{D}_s(\alpha,\alpha^*) = \exp\left[\alpha\hat{a}_s^\dagger - \alpha^*\hat{a}_s\right] \tag{21}$$

where the FD annihilation and creation operators are given by (8). Definitions of CS based on displacement operators are usually applied in various general-

izations of CS [4,5,10,12,16,18]. The generalized coherent state, $|\alpha\rangle_{(s)}$ with $\alpha = |\alpha|\exp(i\varphi)$, has the following Fock expansion [18]

$$|\alpha\rangle_{(s)} = \sum_{n=0}^{s} e^{in\varphi}\, b_n^{(s)}\, |n\rangle \tag{22}$$

where

$$b_n^{(s)} = \frac{s!}{s+1}\frac{(-\mathrm{i})^n}{\sqrt{n!}}\sum_{k=0}^{s} e^{ix_k|\alpha|}\,\frac{\mathrm{He}_n(x_k)}{\mathrm{He}_s^2(x_k)} \tag{23}$$

Here, $x_k \equiv x_k^{(s+1)}$ are the roots, $\mathrm{He}_{s+1}(x_k) = 0$, of the Hermite polynomial $\mathrm{He}_n(x) \equiv 2^{-n/2}\mathrm{H}_n(x/\sqrt{2})$. A method for deriving the coefficients (23) is presented in the Appendix. In the special cases for $s = 1, 2, 3$, the generalized CS are as follows

$$|\alpha\rangle_{(1)} = \cos|\alpha||0\rangle + e^{i\varphi}\sin|\alpha||1\rangle \tag{24}$$

$$\begin{aligned}|\alpha\rangle_{(2)} = {} & \frac{1}{3}[\cos(\sqrt{3}|\alpha|) + 2]|0\rangle + \frac{1}{\sqrt{3}}\, e^{i\varphi}\sin(\sqrt{3}|\alpha|)|1\rangle \\ & + \frac{\sqrt{2}}{3}\, e^{2i\varphi}[1 - \cos(\sqrt{3}|\alpha|)]|2\rangle\end{aligned} \tag{25}$$

$$\begin{aligned}|\alpha\rangle_{(3)} = {} & \frac{x_2^2 c_1 + x_1^2 c_2}{2x_1^2 x_2^2}|0\rangle + \frac{x_2 s_1 + x_1 s_2}{2x_1 x_2}\, e^{i\varphi}|1\rangle \\ & - \frac{c_1 - c_2}{2\sqrt{3}}\, e^{2i\varphi}|2\rangle - \frac{x_2 s_1 - x_1 s_2}{2x_1 x_2}\, e^{3i\varphi}|3\rangle\end{aligned} \tag{26}$$

where $s_k = \sin(x_k^{(4)}|\alpha|)$ and $c_k = \cos(x_k^{(4)}|\alpha|)$ are functions of the roots $x_{1,2}^{(4)} = \sqrt{3 \pm \sqrt{6}}$. The state (24) in the two-dimensional Hilbert space is studied in greater detail in Section IV.C. The simplicity of (24) comes from the fact that the only nonvanishing coefficients $d_{nk}^{(1)}$, given by Eq. (A.7), are equal to unity. In Fig. 2, the coefficients $b_n^{(s)}$ are presented in their dependence on the parameter $|\alpha|$ for $s = 1, 2, 3$ and $s = \infty$. It is seen that the coefficients (23) are periodic (for s=1, 2) or quasiperiodic (for higher s) in $|\bar{\alpha}|$. The generalized CS go over into the conventional CS in the limit of $s \to \infty$. This conclusion can be drawn by analyzing Fig. 3, where the photon-number distribution $P_s(n) = |b_n^{(s)}|^2$ for the generalized CS is presented for different values of s and fixed $\alpha = 4$. The differences between $|\alpha\rangle_{(s)}$ and $|\alpha\rangle_{(\infty)}$ vanish even for $s = 50$ on the scale of Fig. 3. In order to prove this property analytically, let us expand the scalar product

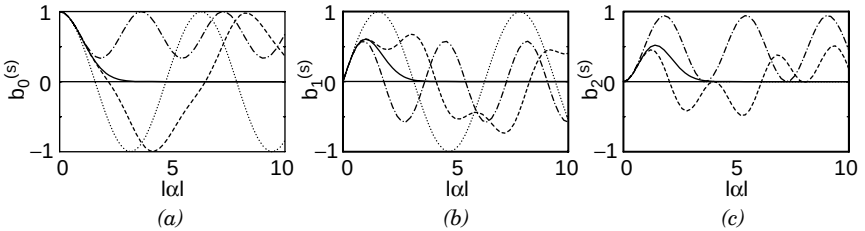

Figure 2. Generalized coherent states. The superposition coefficients $b_n^{(s)}$ for $|\alpha\rangle_{(s)}$ versus displacement parameter amplitude $|\alpha|$ for: (a) $n = 0$, (b) $n = 1$, and (c) $n = 2$ in the Hilbert spaces of different dimensionality: $s = 1$ (dotted), $s = 2$ (dot–dashed), $s = 3$ (dashed), and $s = \infty$ (solid curves).

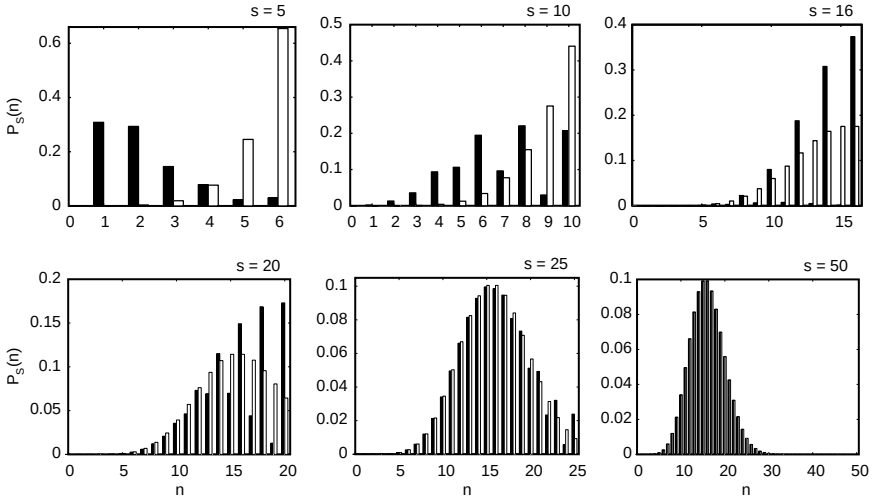

Figure 3. Generalized coherent states (black bars) versus truncated coherent states (white bars): photon-number distribution $P_s(n)$ as a function of n in FD Hilbert spaces with $s = 5, \ldots, 50$ for the same displacement parameters $\alpha = \bar{\alpha} = 4$.

between $|\alpha\rangle_{(s)}$ and $|\alpha\rangle_{(\infty)}$ in series of parameter $|\alpha|$. One finds the following power series expansions [20]

$$
\begin{aligned}
{}_{(\infty)}\langle\alpha|\alpha\rangle_{(1)} &= 1 - \frac{1}{4}|\alpha|^4 + \frac{1}{9}|\alpha|^6 - \mathcal{O}(|\alpha|^8) \\
{}_{(\infty)}\langle\alpha|\alpha\rangle_{(2)} &= 1 - \frac{1}{12}|\alpha|^6 + \frac{3}{64}|\alpha|^8 - \mathcal{O}(|\alpha|^{10}) \\
{}_{(\infty)}\langle\alpha|\alpha\rangle_{(3)} &= 1 - \frac{1}{48}|\alpha|^8 + \frac{1}{75}|\alpha|^{10} - \mathcal{O}(|\alpha|^{12})
\end{aligned}
\tag{27}
$$

for particular values of s. We see that, with increasing dimension, the generalized CS approach the conventional CS as

$$_{(\infty)}\langle\alpha|\alpha\rangle_{(s)} = 1 - \frac{|\alpha|^{2(s+1)}}{2(s+1)!} + \mathcal{O}(|\alpha|^{2(s+2)}) \tag{28}$$

for $|\alpha|^2 \ll s$.

On insertion of the coefficients (23) into the general formula (17), we get the Wigner function for $|\alpha\rangle_{(s)}$ in the form

$$\begin{aligned} W_s(n,\theta_m) = &\sum_{k=M+1}^{s} \frac{\exp[i(2k-M-s-1)(\theta_m-\varphi+\pi/2)]}{[k!(M-k+s+1)!]^{1/2}} G_{1k} \\ &+ \sum_{k=0}^{M} \frac{\exp[i(2k-M)(\theta_m-\varphi+\pi/2)]}{[k!(M-k)!]^{1/2}} G_{0k} \end{aligned} \tag{29}$$

where

$$G_{\eta k} = \frac{(s!)^2}{(s+1)^3} \sum_{p=0}^{s}\sum_{q=0}^{s} \exp[\mathrm{i}(x_q-x_p)|\alpha|] \frac{\mathrm{He}_k(x_p)\mathrm{He}_{M-k+\eta(s+1)}(x_q)}{[\mathrm{He}_s(x_p)\mathrm{He}_s(x_q)]^2} \tag{30}$$

with $\eta = 0, 1$. By writing Eq. (29) in a form more similar to the Vaccaro–Pegg expression, we arrive at

$$\begin{aligned} W_s(n,\theta_m) = &\sum_{k=2n+1}^{s} (-1)^{k-n-s/2} \frac{\sin[(2k-2n-s-1)(\theta_m-\varphi)]}{[k!(2n-k+s+1)!]^{1/2}} G_{1k} \\ &+ \sum_{k=0}^{2n} (-1)^{k-n} \frac{\cos[(2k-2n)(\theta_m-\varphi)]}{[k!(2n-k)!]^{1/2}} G_{0k} \end{aligned} \tag{31}$$

for $n \le s/2$, and

$$\begin{aligned} W_s(n,\theta_m) = &\sum_{k=0}^{2n-s-1} (-1)^{k-n-s/2} \frac{\sin[(2k-2n+s+1)(\theta_m-\varphi)]}{[k!(2n-k-s-1)!]^{1/2}} G_{0k} \\ &+ \sum_{k=2n-s}^{s} (-1)^{k-n} \frac{\cos[(2k-2n)(\theta_m-\varphi)]}{[k!(2n-k)!]^{1/2}} G_{1k} \end{aligned} \tag{32}$$

for $n > s/2$. As readily seen, we cannot generally factorize this function into a product of amplitude $|\alpha|$- and phase φ-dependent parts. The Wigner functions for the generalized CS are presented for $s = 18$ in Fig. 4. We observe the following

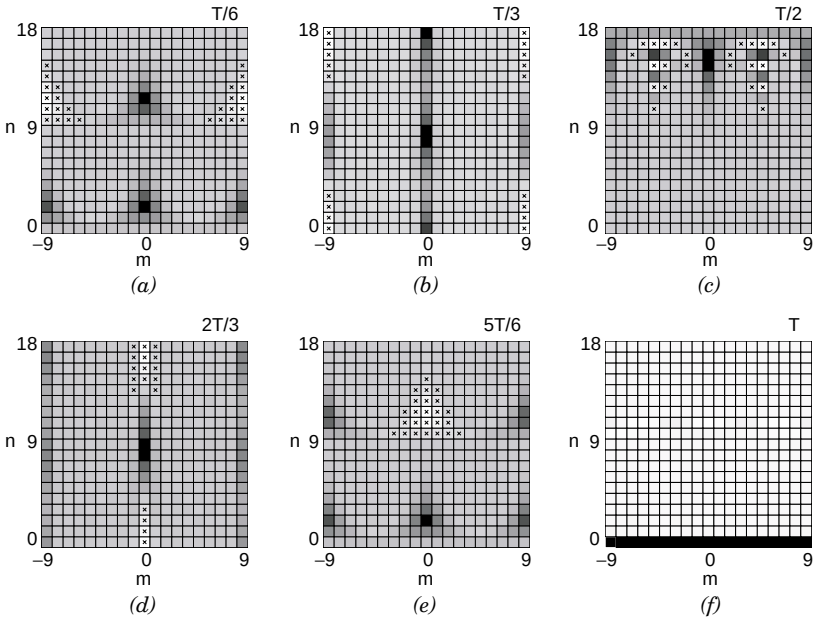

Figure 4. Generalized coherent states: Wigner function $W_s(n, \theta_m)$ in FD Hilbert space with $s = 18$ for $|\alpha\rangle_{(18)}$ with different values of displacement parameter α, chosen as fractions of the quasiperiod $T \equiv T_{18} \approx 8.8$. As in Fig. 1, higher values of Wigner function are depicted darker. Negative regions are marked additionally by crosses.

behavior of the Wigner function. The shape of the respective graph is approximately periodic (referred to as the *quasiperiodic*) in the parameter $|\alpha|$ with quasi-period $T_s \approx 8.8$. We find that for small $|\bar{\alpha}|$ the shape is essentially the same as that described in Ref. [57]—for $n \leq s/2$, there are two peaks for opposite phases, whereas for $n > s/2$ we observe a peak and an antipeak. Note, the peaks at the borders are artificially split up in our Cartesian representation of the Wigner function. The peaks or antipeaks are located at such positions that on summing the W function with constant n (or θ_m) over θ_m (or n), we get the probability distribution of n (or θ_m, respectively). Then, with increasing $|\alpha|$, interesting oscillations in photon number appear. Their culmination is at $|\alpha| = T_s/2$ (Fig. 4c), where only even photon numbers are present. For this value of α, the generalized coherent state approaches an even CS, namely, the case of a Schrödinger cat state, described in detail in Section V.C. By further enlarging $|\alpha|$, the W function returns to its previous shapes through the transition regime (for $|\alpha| \approx 2T_s/3$ in Fig. 4d) to the case of the inner two-peak and outer peak–antipeak structure, similar to the Vaccaro–Pegg results. For $|\alpha| \approx 5T_s/6$ as

given in Fig. 4e, the W function is very similar to that presented in Fig. 4a for $|\alpha| \approx T_s/6$, but with opposite phase. Finally, for $|\alpha| = T_s$ as presented in Fig. 4f, we arrive at an almost vacuum state. By further increasing $|\alpha|$, these shapes of the W-function graph reappeared for several quasiperiods T_s. Similar behavior can be observed also for other values of s.

This quasiperiodicity can be explained as follows. By applying the fitting procedure, based on the WKB (Wentzel–Kramers–Brillouin) method, one can find that the smallest positive root $x_1 \equiv x_1^{(s+1)}$ of the Hermite polynomial $\mathrm{He}_{s+1}(x)$ is approximately equal to

$$x_1^{(s+1)} \approx \frac{2\pi}{\sqrt{4s+6}} \tag{33}$$

(for even s). Besides, it is well known that the nearest-to-zero roots of the Hermite polynomials are approximately equidistant. Thus, their difference $\Delta x \equiv x_{k+1} - x_k$ is approximately given by (33), which is 0.71 for $s = 18$. The predominant terms of the sum in (23) depend on $|\alpha|$ approximately as $\exp(ig\Delta x|\alpha|)$, where $g = 0, \pm 1, \pm 2, \ldots$. These exponential functions are quasiperiodic with approximate mean period (referred to as the *quasiperiod*) given by [20,64]

$$T_s \approx \sqrt{4s+6} \tag{34}$$

for even s. From Eq. (34), the quasiperiod for $s = 18$ is approximately equal to 8.8. For odd n, the property $\mathrm{He}_n(-x_k) = (-1)^n \mathrm{He}_n(x_k)$ holds. On the other hand, the odd coefficients n in the sum (23) contain sine functions, which are zero in the middle of their period. Therefore, for $|\alpha| = T_s/2$, the odd n terms almost disappear, and we get an approximately even coherent state. We analyze in detail the W functions for even s only. Nonetheless, for completeness of our discussion, we give the explicit approximate expression for the quasiperiod

$$T_s \approx 2\sqrt{4s+6} \tag{35}$$

for odd s, which is twice larger than the quasi-period given by (34) for a chosen value of s.

B. Truncated Coherent States

Kuang et al. [17] defined the normalized FD coherent states by truncating the Fock expansion of the conventional ID coherent states or equivalently by the action of the operator $\exp(\bar{\alpha}\,\hat{a}^\dagger)$ (with proper normalization) on vacuum state. The Kuang et al. approach is similar to the Vaccaro–Pegg treatment [57] of the

Wigner function for CS. The state $|\bar{\alpha}\rangle_{(s)}$, where $\bar{\alpha} = |\bar{\alpha}|\exp(i\varphi)$, can be defined by its Fock expansion [17]

$$|\bar{\alpha}\rangle_{(s)} = \mathcal{N}_s \exp(\bar{\alpha}\hat{a}_s^\dagger)|0\rangle = \sum_{n=0}^{s} b_n^{(s)}|n\rangle \tag{36}$$

with the Poissonian superposition coefficients

$$b_n^{(s)} = \mathcal{N}_s \sum_{n=0}^{s} \frac{\bar{\alpha}^n}{\sqrt{n!}} \tag{37}$$

normalized by

$$\mathcal{N}_s = \left(\sum_{n=0}^{s} \frac{|\bar{\alpha}|^{2n}}{n!}\right)^{-1/2} = \{(-1)^s L_s^{-s-1}(|\bar{\alpha}|^2)\}^{-1/2} \tag{38}$$

where $L_s^n(x)$ is the generalized Laguerre polynomial. Equation (36) is just the Fock expansion of the conventional ID CS, which are truncated at an sth term and properly normalized. For this reason we shall refer to the state (36) as the *truncated CS*. In Fig. 5, the superposition coefficients $b_n^{(s)}$, given by Eq. (37) for the truncated CS $|\bar{\alpha}\rangle_{(s)}$ are presented as a function of the parameter $|\bar{\alpha}| \equiv |\alpha|$ in $\mathscr{H}^{(s)}$ with $s = 1, 2, 3$ and $s = \infty$. As seen in Fig. 5, the coefficients $b_n^{(s)}$ are aperiodic functions of $|\bar{\alpha}|$. We emphasize the essential difference between the generalized and truncated CS. The former are periodic or quasiperiodic, while the latter are aperiodic in $|\bar{\alpha}| = |\alpha|$. Nevertheless, both $|\alpha\rangle_{(s)}$ and $|\bar{\alpha}\rangle_{(s)}$, go over into the conventional Glauber CS in the limit of $s \to \infty$ as is convincingly depicted in Fig. 3. By definition, the truncated CS go over into the Glauber CS in the limit of $s \to \infty$. Nevertheless, for better comparison with the generalized CS, given by (20), we show this property explicitly by expanding the scalar products

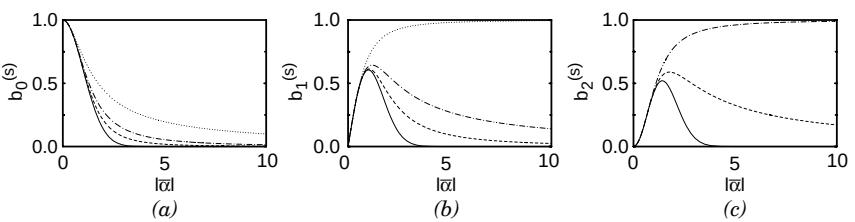

Figure 5. Truncated coherent states. Superposition coefficients $b_n^{(s)}$ of $|\bar{\alpha}\rangle_{(s)}$ versus displacement parameter amplitude $|\bar{\alpha}|$ for the same cases as in Fig. 2.

between $|\bar{\alpha}\rangle_{(s)}$ and $|\alpha\rangle_{(\infty)}$ in power series of $|\alpha|$. We have [20]

$$
\begin{aligned}
{}_{(\infty)}\langle\alpha|\bar{\alpha}\rangle_{(1)} &= 1 - \frac{1}{4}|\alpha|^4 + \frac{1}{6}|\alpha|^6 - \mathcal{O}(|\alpha|^8) \\
{}_{(\infty)}\langle\alpha|\bar{\alpha}\rangle_{(2)} &= 1 - \frac{1}{12}|\alpha|^6 + \frac{1}{16}|\alpha|^8 - \mathcal{O}(|\alpha|^{10}) \\
{}_{(\infty)}\langle\alpha|\bar{\alpha}\rangle_{(3)} &= 1 - \frac{1}{48}|\alpha|^8 + \frac{1}{60}|\alpha|^{10} - \mathcal{O}(|\alpha|^{12})
\end{aligned} \tag{39}
$$

where we put $\alpha = \bar{\alpha}$. We find by induction that, with increasing dimension $(s+1)$, the truncated CS approach the conventional CS

$$
{}_{(\infty)}\langle\alpha|\bar{\alpha}\rangle_{(s)} = 1 - \frac{|\alpha|^{2(s+1)}}{2\,(s+1)!} + \mathcal{O}(|\alpha|^{2(s+2)}) \tag{40}
$$

for $|\alpha| \equiv |\bar{\alpha}|^2 \ll s$. Although Eqs. (28) and (40) have the same form, a closer comparison of Eqs. (27) and (39) shows that the states $|\alpha\rangle_{(s)}$ approach $|\alpha\rangle_{(\infty)}$ slower than $|\bar{\alpha}\rangle_{(s)}$ do and, in fact, the corrections $\mathcal{O}(|\alpha|^{2(s+2)})$ in Eq. (39) are smaller than those in Eq. (27). Finally, let us expand the scalar product between $|\alpha\rangle_{(s)}$ and $|\bar{\alpha}\rangle_{(s)}$ for $s=1, 2, 3$ in power series of $\alpha \equiv \bar{\alpha}$. We find that

$$
\begin{aligned}
{}_{(1)}\langle\alpha|\bar{\alpha}\rangle_{(1)} &= 1 - \frac{1}{18}|\alpha|^6 + \frac{1}{15}|\alpha|^8 - \mathcal{O}(|\alpha|^{10}) \\
{}_{(2)}\langle\alpha|\bar{\alpha}\rangle_{(2)} &= 1 - \frac{1}{64}|\alpha|^8 + \frac{9}{800}|\alpha|^{10} - \mathcal{O}(|\alpha|^{12}) \\
{}_{(3)}\langle\alpha|\bar{\alpha}\rangle_{(3)} &= 1 - \frac{1}{300}|\alpha|^{10} + \frac{13}{5040}|\alpha|^{12} - \mathcal{O}(|\alpha|^{14})
\end{aligned} \tag{41}
$$

The expansions up to $|\alpha|^{2(s+2)}$ can be written in general form as

$$
{}_{(s)}\langle\alpha|\bar{\alpha}\rangle_{(s)} = 1 - \frac{|\alpha|^{2(s+2)}}{2s!(s+2)^2} + \mathcal{O}(|\alpha|^{2(s+3)}) \tag{42}
$$

All these three types of CS are approximately equal for $|\bar{\alpha}|^2 = |\alpha|^2 \ll s$, since the scalar products between them tend to unity. The higher s, the greater is the range of $|\alpha|$, where the scalar product tends to unity. However, the states are significantly different for values $|\alpha|^2 \approx s$. By comparing Eqs. (28), (40), and (42) for the same s, we observe that $|\alpha\rangle_{(s)}$ and $|\bar{\alpha}\rangle_{(s)}$ approach each other faster than $|\alpha\rangle_{(\infty)}$.

In order to calculate the Wigner function, we substitute Eq. (37) into Eq. (17), arriving at

$$W_s(n,\theta_m) = \frac{\mathcal{N}_s^2}{s+1}\left(\sum_{k=0}^{M}\frac{|\bar{\alpha}|^M}{\sqrt{k!(M-k)!}}\exp[i(2k-M)(\theta_m-\varphi)] + \sum_{k=M+1}^{s}\frac{|\bar{\alpha}|^{M+s+1}}{\sqrt{k!(M-k+s+1)!}}\right) \tag{43}$$

where $M = 2n \bmod (s+1)$. Equation (43) can be written in a form useful for a comparison with the Vaccaro–Pegg result

$$W_s(n,\theta_m) = \frac{1}{s+1}[\Lambda_1(n,|\bar{\alpha}|)\Phi_1(n,\theta_m,\varphi) + \Lambda_2(n,|\bar{\alpha}|)\Phi_2(n,\theta_m,\varphi)] \tag{44}$$

where

$$\Lambda_1(n,|\bar{\alpha}|) = \frac{\mathcal{N}_s^2|\bar{\alpha}|^M}{\mu_1!}$$
$$\Phi_1(n,\theta_m,\varphi) = \mu_1!\sum_{k=0}^{M}\frac{\cos[(2k-M)(\theta_m-\varphi)]}{[k!(M-k)!]^{1/2}} \tag{45}$$

and

$$\Lambda_2(n,|\bar{\alpha}|) = \frac{\mathcal{N}_s^2|\bar{\alpha}|^{M+s+1}}{\mu_2!}$$
$$\Phi_2(n,\theta_m,\varphi) = \mu_2!\sum_{k=M+1}^{s}\frac{\cos[(2k-M-s-1)(\theta_m-\varphi)]}{[k!(M-k+s+1)!]^{1/2}} \tag{46}$$

Here, $\mu_1 = [\![M/2]\!]$ is the integer part of $M/2$, and similarly $\mu_2 = [\![(M+1+s)/2]\!]$. We note that the functions Λ_i do not depend on the phase φ of $\bar{\alpha}$ and similarly the functions Φ_i do not depend on its amplitude $|\bar{\alpha}|$. In the Vaccaro–Pegg treatment, $|\bar{\alpha}|^2$ was always much less than s, so that the second term of Eq. (44) could be neglected. Then the Wigner function was factorizable into the amplitude-dependent function Λ_1 and the phase-dependent function Φ_1, and the normalizing constant $\mathcal{N}_s$ was approximated by $\exp(-|\bar{\alpha}|^2/2)$. It can be seen that for general values of $\bar{\alpha}$ of the truncated CS this factorization is no longer feasible. Moreover, for large $|\bar{\alpha}|$, the second term of Eq. (44) becomes predominant. We compare different shapes of the W functions for various $\bar{\alpha}$ in Fig. 6. The functions are computed for $s = 18$. With $|\alpha|$ increasing from zero, the shape of the generalized CS is initially very similar to that of the truncated CS (see Fig. 4).

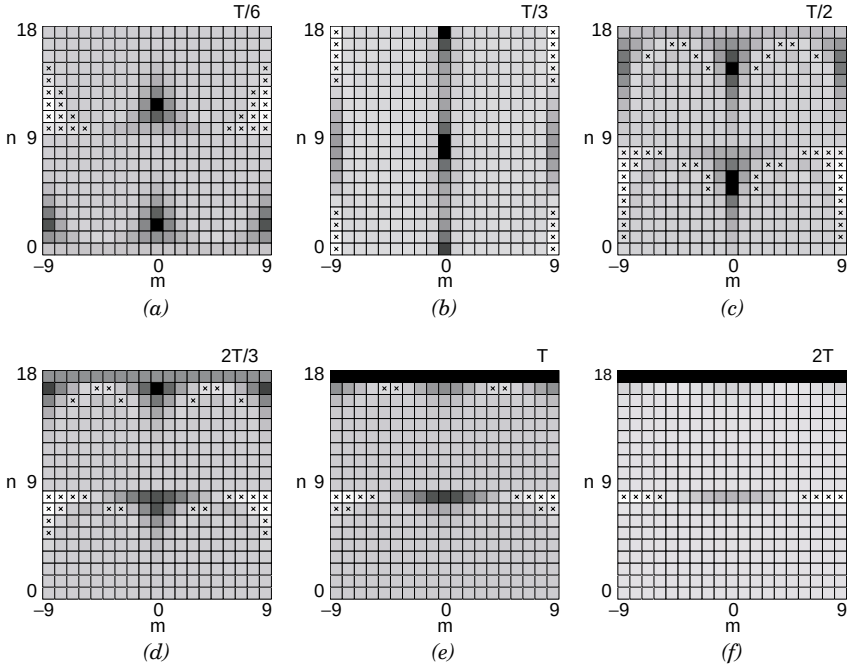

Figure 6. Truncated coherent states. Wigner function for $|\bar{\alpha}\rangle_{(18)}$ with different displacement parameters $\bar{\alpha}$ given by fractions of $T = 8.8$.

It occurs up to the peak–antipeak transition from $n = s$ to $n = 0$ around the value $|\bar{\alpha}|^2 \approx s/2$ (corresponding to $|\alpha| \approx T_s/3$ in Fig. 6b). However, if $|\bar{\alpha}|^2 \gg s/2$, the situation is inverse: the second term of Eq. (44) is now predominant and we observe two peaks for $n > s/2$ and a peak–antipeak structure for $n \leq s/2$ (e.g., Fig. 6d). In the case when $|\bar{\alpha}|^2 \approx s$ (Fig. 6c), the W function has a more general shape. With increasing $|\bar{\alpha}|$ the two-peak structure shifts to larger values of n, while the peak–antipeak structure gradually vanishes at $n \leq s/2$ (Fig. 6d,e). The shape is still comparatively simple because the function Eq. (44) is a sum of only two factorizable terms. By further increasing $|\bar{\alpha}| \gg T_s$, the Wigner function has a very simply structure representing the number state $|s\rangle$. Even for $|\bar{\alpha}| = 2T_s$, as presented in Fig. 6f, the peak–antipeak structure at $n \leq s/2$ vanishes almost completely. In the limit of $|\bar{\alpha}|^2/s \to \infty$, the truncated CS approaches the number state $|s\rangle$. This conclusion can also be deduced from the behavior of the superposition coefficients $b_n^{(s)}$ in their dependence on $|\bar{\alpha}|$ as depicted Fig. 5. In contrast to the generalized CS, the behavior of the truncated CS is aperiodic in $|\bar{\alpha}|$.

C. Example: Two-Dimensional Coherent States

The simplest nontrivial FD states are those spanned in a two-dimensional system, namely, for $s = 1$. States in such a system have intensively been studied by authors dealing with the general problem of finite-dimensional quantum optical states [16,17,28]. Here, we would like to discuss this problem from other points of view. Two-dimensional systems are well known in various fields of physics, and we thus can apply the results and concepts to describe our situation. Examples of realizations of such a system can be given by the spin projection of spin-$\frac{1}{2}$ particle, two-level atom, or quantum dot. Hence, the CS in $\mathscr{H}^{(1)}$ [see Eqs. (48) and (50)] can, in fact, be identified with the coherent spin-$\frac{1}{2}$ state [4] or equivalently with the two-level atomic coherent state [5]. In the case of $s = 1$, the terms *photon number*, *phase*, and *FD harmonic oscillator* are a bit confusing and should be understood, for example, as [55] *z component of spin divided by ħ*, *angle of orientation about the z axis*, and *spin*, respectively, or equivalently as atomic quantities [5,16]. We use the notion *two-dimensional* space or states to be consistent with our general terminology applied in earlier sections. Although, we are aware that this terminology might be misleading. In this section we use a Poincaré sphere representation for the description of the states discussed and their properties, like various operator averages and squeezing degrees. Finally, we present the W function for two-dimensional CS.

It is well known that states in a two-dimensional system can be described by means of the Stokes parameters and visualized by means of the Poincaré sphere. The density matrix of any two-state system can be written in the form

$$\hat{\rho} = \frac{1}{2}\begin{pmatrix} 1 + \mathscr{S}_z & S_x + \mathrm{i}\mathscr{S}_y \\ \mathscr{S}_x - \mathrm{i}\mathscr{S}_y & 1 - \mathscr{S}_z \end{pmatrix} \tag{47}$$

where $\mathscr{S}_x$, $\mathscr{S}_y$, and $\mathscr{S}_z$ are the Stokes parameters. Using these parameters as coordinates of a point in three-dimensional space, any state corresponds to a point on a unit radius sphere, the so-called Poincaré sphere. Pure states are represented by points on the surface, while mixed-state points lie inside the sphere. Now, using this tool, we can display both the two-dimensional generalized and truncated CS and compare their expressions.

For the two-dimensional generalized CS, given by

$$|\alpha\rangle_{(1)} = \cos|\alpha||0\rangle + \exp(\mathrm{i}\varphi)\sin|\alpha|\,|1\rangle \tag{48}$$

the Stokes parameters are found to be

$$\begin{aligned} \mathscr{S}_x &= \sin 2|\alpha| \cos\varphi \\ \mathscr{S}_y &= -\sin 2|\,\alpha|\sin\varphi \\ \mathscr{S}_z &= \cos 2|\alpha| \end{aligned} \tag{49}$$

We note that any pure state in $\mathscr{H}^{(1)}$ is coherent. The interpretation of the parameter α is very simple; its module is proportional to the polar coordinate, while its argument φ is the azimuthal coordinate of the representative Poincaré sphere point.

Similarly, we find the Stokes parameters for the truncated CS, given by (36). The two-dimensional state $|\bar{\alpha}\rangle_{(1)}$, with the parameter $\bar{\alpha} = |\bar{\alpha}|\exp(i\varphi)$, is expressed by

$$\begin{aligned} |\bar{\alpha}\rangle_{(1)} &= \frac{1}{\sqrt{1+|\bar{\alpha}|^2}}\,|0\rangle + \exp(i\varphi)\frac{|\bar{\alpha}|}{\sqrt{1+|\bar{\alpha}|^2}}\,|1\rangle \\ &= \cos(\arctan|\bar{\alpha}|)|0\rangle + \exp(i\varphi)\sin(\arctan|\bar{\alpha}|)\,|1\rangle \end{aligned} \tag{50}$$

The Stokes parameters are now

$$\begin{aligned} \mathscr{S}_x &= 2\frac{|\bar{\alpha}|}{1+|\bar{\alpha}|^2}\cos\varphi \\ \mathscr{S}_y &= -2\frac{|\bar{\alpha}|}{1+|\bar{\alpha}|^2}\sin\varphi \\ \mathscr{S}_z &= \frac{1-|\bar{\alpha}|^2}{1+|\bar{\alpha}|^2} \end{aligned} \tag{51}$$

The function of the argument φ is the same as for the generalized CS, while the meaning of module $|\bar{\alpha}|$ is different from that of $|\alpha|$. We observe, for instance, neither periodicity nor quasiperiodicity in $|\bar{\alpha}|$. To interpret $|\bar{\alpha}|$, we write the last equation in (51) in the form $|\bar{\alpha}|/(1-\mathscr{S}_z^2)^{1/2} = 1/(1+\mathscr{S}_z)$. Thus, for a given $\bar{\alpha}$, one can construct the corresponding Poincaré sphere point as follows [20]: (1) by locating the complex number $\bar{\alpha}$ in the $\mathscr{S}_x\mathscr{S}_y$ plane, so that the $\mathscr{S}_x$ $(-\mathscr{S}_y)$ coordinate is the real (imaginary) part of $\bar{\alpha}$, respectively; and (2) by connecting this point with the lower pole of the Poincaré sphere by a straight line. The other intersection of the line and the sphere is then the point representing the coherent state.

For the case of two-dimensional CS, there have been computed quantities such as the mean values and variances of the various operators, including $\hat{N}$ and $\hat{\Phi}$ quadratures and their commutators [16,17]. Most of these quantities can easily be displayed on the Poincaré sphere and expressed by means of the Stokes parameters. We find that the following mean values and variances are given respectively by

$$\begin{aligned} \langle\hat{N}\rangle &= \frac{1-\mathscr{S}_z}{2} \\ \langle(\Delta\hat{N})^2\rangle &= \frac{\mathscr{S}_x^2+\mathscr{S}_y^2}{4} \\ \langle\hat{\Phi}\rangle &= \frac{(1-\mathscr{S}_x)\pi}{2} \\ \langle(\Delta\hat{\Phi})^2\rangle &= \frac{(\mathscr{S}_y^2+\mathscr{S}_z^2)\pi^2}{4} \end{aligned} \tag{52}$$

and the mean value of the $\hat{N} - \hat{\Phi}$ commutator is

$$\langle[\hat{N}, \hat{\Phi}]\rangle = \frac{i\pi\mathscr{S}_y}{2} \tag{53}$$

The degrees of squeezing S_N and S_Φ are defined by

$$\begin{aligned} S_N &= 2\langle(\Delta\hat{N})^2\rangle\, |\langle[\hat{N}, \hat{\Phi}]\rangle|^{-1} - 1 \\ S_\Phi &= 2\langle(\Delta\hat{\Phi})^2\rangle\, |\langle[\hat{N}, \hat{\Phi}]\rangle|^{-1} - 1 \end{aligned} \tag{54}$$

They can be written in terms of the Stokes parameters as

$$\begin{aligned} S_N &= \frac{1}{\pi}\frac{\mathscr{S}_x^2 + \mathscr{S}_y^2}{|\mathscr{S}_y|} - 1 \\ S_\Phi &= \pi\frac{\mathscr{S}_y^2 + \mathscr{S}_z^2}{|\mathscr{S}_y|} - 1 \end{aligned} \tag{55}$$

We found for the case of $s = 1$ that the averages of the quantum optical quantities are simply related to the Stokes parameters. The correspondence can also be expressed in terms of the operators $\hat{N}$ and $\hat{\Phi}$ in relation to the Pauli matrices $\hat{\sigma}_z$ and $\hat{\sigma}_x$, or the quadratures $\hat{X}_a$ and $\hat{Y}_a$ related to $\hat{\sigma}_x$ and $\hat{\sigma}_y$.

Finally, we find the explicit expression for the Wigner function in n and θ for two-dimensional generalized CS. We get

$$\begin{aligned} W_s(n, \theta_m) = \frac{1}{4}\Big[&1 + (-1)^n\cos(2|\alpha|) \\ &+ (-1)^m\sqrt{2}\sin(2|\alpha|)\cos\left(\varphi - (-1)^n\frac{\pi}{4}\right)\Big] \end{aligned} \tag{56}$$

On simple replacement of $|\alpha|$ by $\arctan|\bar{\alpha}|$ in Eq. (56), one obtains the W-function for the two-dimensional truncated CS.

V. OTHER FD QUANTUM-OPTICAL STATES

Analogously to the *generalized CS* in a FD Hilbert space, analyzed in Section IV.A, other states of the electromagnetic field can be defined by the action of the FD displacement or squeeze operators. In particular, FD displaced phase states and coherent phase states were discussed by Gangopadhyay [28]. Generalized displaced number states and Schrödinger cats were analyzed in Ref. 21 and generalized squeezed vacuum was studied in Ref. 34. A different approach to construction of FD states can be based on truncation of the Fock expansion of the well-known ID harmonic oscillator states. The same construction, as for the

truncated CS, was applied to analyze, for instance, truncated Schrödinger cats by Zhu and Kuang [25,35], Miranowicz et al. [21], and Roy and Roy [24]; truncated phase CS by Kuang and Chen [27]; truncated displaced number states by Miranowicz et al. [21], or truncated squeezed vacuum by Miranowicz et al. [34].

A. FD Phase Coherent States

Here, we study two kinds of FD phase coherent states associated with the Pegg–Barnett Hermitian optical phase formalism [26]. First states, referred to as the *generalized phase CS* or coherent phase states, are generated by the action of the phase displacement operator. This definition of the phase CS was applied by Gangopadhyay [28] in close analogy to Glauber's idea of the conventional CS. The second definition of phase CS is based on another phase "displacement" operator formally designed by Kuang and Chen [27]. We shall refer to these states as the *truncated phase CS* to stress its similarity to the *truncated CS* described in Section IV.B. We construct the phase CS explicitly and derive their discrete Wigner representation. The FD phase CS are not only mathematical structures. A framework for their physical interpretation is provided by cavity quantum electrodynamics and atomic physics.

1. *Generalized Phase CS*

Gangopadhyay [28] has proposed a definition of the generalized phase CS in formal analogy to the generalized CS, defined by Eq. (20). The main idea is to choose a preferred phase state $|\theta_0\rangle$, and then to construct the phase creation ($\hat{\phi}_s^\dagger$) and phase annihilation ($\hat{\phi}_s$) operators analogously to the conventional (photon-number) creation and annihilation operators. The phase CS are then constructed by replacing vacuum $|0\rangle$ by $|\theta_0\rangle$, and the operators $\hat{a}_s$ and $\hat{a}_s^\dagger$ by $\hat{\phi}_s$ and $\hat{\phi}_s^\dagger$, respectively, as given by Eq. (11). Thus, the generalized phase CS is defined to be [28]

$$|\beta, \theta_0\rangle_{(s)} = \hat{D}_s(\beta, \theta_0)\,|\theta_0\rangle \tag{57}$$

by the action of the phase displacement operator

$$\hat{D}^{(s)}(\beta, \theta_0) = \exp[\beta\hat{\phi}_s^\dagger - \beta^*\hat{\phi}_s] \tag{58}$$

on the preferred phase state $|\theta_0\rangle$. By generalizing the method described in Appendix, one can find the following phase-state representation of the generalized phase CS [29]

$$|\beta, \theta_0\rangle_{(s)} = \sum_{m=0}^{s} e^{i(\mu - m_0)\varphi}\, b_m^{(s)}\,|\theta_m\rangle \tag{59}$$

where $\varphi = \mathrm{Arg}\,\beta$ and the decomposition coefficients are

$$b_m^{(s)} \equiv b_m^{(s)}(\theta_0) = \frac{s!}{s+1}(-1)^{m+m_0}\frac{i^{m_0+\mu}}{\sqrt{\mu! m_0!}} \times \sum_{k=0}^{s} \exp(ix_k\gamma_s|\beta|)\frac{\mathrm{He}_\mu(x_k)\mathrm{He}_{m_0}(x_k)}{\mathrm{He}_s^2(x_k)} \tag{60}$$

Here, $x_l \equiv x_l^{(s+1)}$ are the roots of the Hermite polynomial, $\mathrm{He}_{s+1}(x_l) = 0$. For brevity, we have denoted $\mu = m + m_0 \mod(s+1)$ and $\gamma_s = \sqrt{\frac{2\pi}{s+1}}$. The values θ_m are chosen $\mod(2\pi)$. We also assume that the permitted values of θ_0 are not completely arbitrary but restricted to $\frac{2\pi}{s+1}m_0 \mod(2\pi)$ (where $m_0 = 0, 1, \ldots$). In a special case, for $\theta_0 = 0$ and $s = 1$, the phase CS reduce to the state $|\beta, \theta_0 = 0\rangle_{(1)}$ studied by Gangopadhyay [28]. Here, for simplicity, we also consider the case of $\theta_0 = 0$.

2. *Truncated Phase CS*

Kuang and Chen [27] defined the FD phase CS, denoted as $|\bar{\beta}, \theta_0\rangle_{(s)}$, by the action of the FD operator $\exp(\bar{\beta}\hat{\phi}_s^\dagger)$ on the phase state $|\theta_0\rangle$. The reference phase θ_0 is chosen as zero [27]. Therefore, on comparing the explicit expressions for $\hat{a}_s$ and $\hat{\phi}_s$, it is clear that the states $|\bar{\beta}, \theta_0\rangle_{(s)}$ are in close analogy to the truncated CS [20]. For this reason we shall refer to the states $|\bar{\beta}, \theta_0\rangle_{(s)}$ as the *truncated phase CS* in $\mathscr{H}^{(s)}$. For completeness, we present the phase-space expansion with $\bar{\beta} = |\bar{\beta}|\exp(i\varphi)$ given by [27]

$$|\bar{\beta}, \theta_0\rangle_{(s)} = \mathscr{N}_s \exp(\bar{\beta}\hat{\phi}_s^\dagger)|\theta_0\rangle = \sum_{m=0}^{s} e^{im\varphi}\, b_m^{(s)}|\theta_m\rangle \tag{61}$$

where

$$b_m^{(s)} = \mathscr{N}_s \frac{(\gamma_s|\bar{\beta}|)^m}{\sqrt{m!}}, \qquad \mathscr{N}_s = \left(\sum_{n=0}^{s}\frac{(\gamma_s|\bar{\beta}|)^{2n}}{n!}\right)^{-1/2} \tag{62}$$

and $\gamma_s = \sqrt{\frac{2\pi}{s+1}}$ as in Eq. (60). In particular, squeezing properties of the truncated phase CS were analyzed by Kuang and Chen [27]. They have paid special attention to the two-dimensional case.

Although many properties of the phase CS are known by now, for their better understanding it is very useful to analyze graphs of their quasidistributions. The discrete Wigner function, as defined by Wootters [55] (see also Ref. 57), takes the following form for $s > 1$

$$W_s(n, \theta_m) = \frac{1}{s+1}\sum_{p=0}^{s} b_{m+p}^{(s)}\, b_{m-p}^{(s)} \exp\left[-2ip\left(\frac{2\pi}{s+1}n + \varphi\right)\right] \tag{63}$$

for the generalized phase CS with $b_n^{(s)}$ given by (60) and for the truncated phase CS with superposition coefficients (62). In Eq. (63), the subscripts $m \pm p$ are assumed to be $\mathrm{mod}(s+1)$. One can obtain the particularly simple Wigner function for $s = 1$ [55].

The generalized phase CS, $|\beta, \theta_0\rangle_{(s)}$, and truncated phase CS, $|\bar{\beta}, \theta_0\rangle_{(s)}$, are associated with the Pegg–Barnett formalism of the Hermitian phase operator $\hat{\Phi}_s$. The operators $\hat{\Phi}_s$, $\hat{\phi}_s$, and $\hat{\phi}_s^\dagger$ do not exist in the conventional ID Hilbert space $\mathscr{H}^{(\infty)}$. Thus the generalized and truncated phase CS are properly defined *only* in $\mathscr{H}^{(s)}$ of finite dimension. States $|\beta, \theta_0\rangle_{(s)}$ and $|\bar{\beta}, \theta_0\rangle_{(s)}$, similar to $|\alpha\rangle_{(s)}$ and $|\bar{\alpha}\rangle_{(s)}$, approach each other for $|\beta|^2 = |\bar{\beta}|^2 \ll s/\pi$ [20]. This can be shown explicitly by calculating the scalar product between generalized and truncated phase CS. We find ($\beta = \bar{\beta}$)

$$_{(s)}\langle\beta, \theta_0|\bar{\beta}, \theta_0\rangle_{(s)} = 1 - \frac{(\sqrt{\pi}|\beta|)^{2(s+2)}}{2s!(s+2)^2} + \mathcal{O}(|\beta|^{2(s+3)}) \tag{64}$$

For values $|\beta|^2 = |\bar{\beta}|^2 \approx s/\pi$ or greater than s/π, the differences between $|\beta, \theta_0\rangle_{(s)}$ and $|\bar{\beta}, \theta_0\rangle_{(s)}$ become significant.

In Fig. 7, a few examples of the Wigner function for $|\beta, 0\rangle_{(18)}$ are presented for different values of the phase displacement parameter β. Because of space limits in this chapter, the corresponding figures for the truncated phase CS are not presented. In Fig. 7c, we observe that $|\beta, 0\rangle_{(s)}$ is quasiperiodic in β. Closer analysis of Eq. (60), in comparison to (23), shows that the quasiperiod T_s for $|\beta, 0\rangle_{(s)}$ is the same as that for the generalized coherent states. Thus, it is given by Eq. (34) for even s and Eq. (35) for odd s. Yet, the evolution of the generalized phase CS is more complicated than that for the generalized CS, as seen on comparing Figs. 7a,b with the corresponding Figs. 4b,d. As was

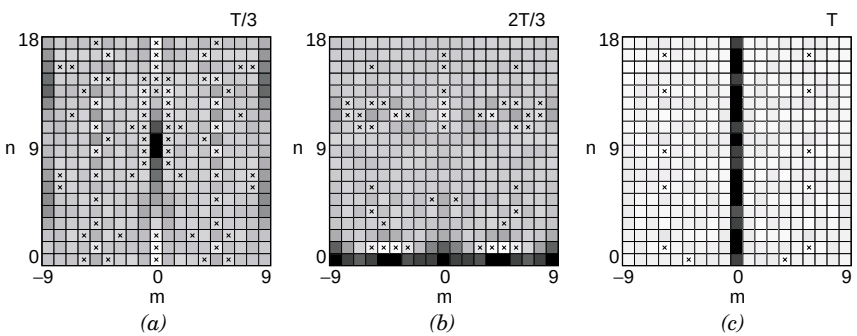

Figure 7. Generalized phase coherent states. Wigner function for $|\beta, 0\rangle_{(18)}$ with different phase displacement parameters β chosen to be fractions of the quasiperiod $T = T_{18} = 8.8$.

discussed in Ref. 29, the truncated phase CS are aperiodic in $\bar{\beta}$ for any dimension.

B. FD Displaced Number States

In this section, we propose two nonequivalent definitions of the *displaced number states* (DNS) in the FD Hilbert space and show that the FD states go over into the conventional DNS discussed, for instance, by de Oliveira et al. [65].

1. *Generalized DNS*

Analogously to the generalized CS, given by Eq. (20), we define the generalized DNS as follows

$$|\alpha, n_d\rangle_{(s)} = \hat{D}^{(s)}(\alpha)|n_d\rangle \tag{65}$$

as the result of action of the displacement operator $\hat{D}^{(s)}(\alpha)$, given by Eq. (21), on the number state $|n_d\rangle$. By using the same method as described in Appendix for $|\alpha\rangle_{(s)}$, we find the following explicit Fock representation of the generalized DNS

$$|\alpha, n_d\rangle_{(s)} = \hat{D}_s(\alpha)|n_d\rangle = \sum_{n=0}^{s} e^{\mathrm{i}(n-n_d)\varphi}\, b_n^{(s)}|n\rangle \tag{66}$$

where

$$b_n^{(s)} \equiv b_n^{(s)}(n_d) = \frac{s!}{s+1}\,\frac{i^{n_d}(-\mathrm{i})^n}{\sqrt{n!n_d!}}\sum_{k=0}^{s} e^{i}x_k|\alpha|\,\frac{\mathrm{He}_n(x_k)\mathrm{He}_{n_d}(x_k)}{\mathrm{He}_s^2(x_k)} \tag{67}$$

and $\alpha = |\alpha|\exp(i\varphi)$. In the dimension limit, $s \to \infty$, the generalized DNS go over into the conventional DNS defined, for example, in Refs. 65 and 43. This property can readily be deduced from $\lim_{s\to\infty}\hat{D}_s = \hat{D}_\infty \equiv \hat{D}$. Obviously, in the special case of $n_d = 0$ the generalized DNS reduce to the generalized CS defined by Eq. (20).

2. *Truncated DNS*

Let us define the finite-dimensional DNS, which in a special case go over into the truncated CS of Kuang et al. [17] and into the conventional DNS [65] in the limit of $s \to \infty$. We define the truncated displaced number states, $|\bar{\alpha}, n_d\rangle_{(s)}$, by the following Fock representation

$$|\bar{\alpha}, n_d\rangle_{(s)} = \sum_{n=0}^{s} b_n^{(s)} e^{i(n-n_d)\varphi}|n\rangle \tag{68}$$

where

$$b_n^{(s)} \equiv b_n^{(s)}(n_d) = \mathcal{N}_s \left(\frac{n_1!}{n_2!}\right)^{1/2} (-1)^{n_2-n} |\bar{\alpha}|^{n_2-n_1} L_{n_1}^{n_2-n_1}(|\bar{\alpha}|^2) \tag{69}$$

$$\mathcal{N}_s \equiv \mathcal{N}_s(|\bar{\alpha}|, n_d) = \left(\sum_{n=0}^{s} \frac{n_1!}{n_2!} |\bar{\alpha}|^{2(n_2-n_1)} [L_{n_1}^{n_2-n_1}(|\bar{\alpha}|^2)]^2\right)^{-1/2} \tag{70}$$

For brevity, we have introduced the indices $n_1 \equiv \min(n, n_d)$ and $n_2 \equiv \max(n, n_d)$. The state (68) is, in fact, given by the Fock expansion of the conventional ID DNS [43,65], which are truncated at the $(s+1)$th term and properly normalized. This construction justifies our name for Eq. (68). Alternatively, the states (68) can be defined by the action of the FD factorized displacement operator, $\exp(\bar{\alpha}\ \hat{a}_s{}^\dagger)\exp(-\bar{\alpha}^*\hat{a}_s)$, on a number state $|n_d\rangle$:

$$|\bar{\alpha}, n_d\rangle_{(s)} = \mathcal{N}_s \exp(\bar{\alpha}\hat{a}_s{}^\dagger)\exp(-\bar{\alpha}^*\hat{a}_s)|n_d\rangle \tag{71}$$

The equation explicitly shows how the concept of the truncated CS, given by (36), is generalized. The truncated DNS are different from the generalized DNS, given by (65). The differences are particularly distinct for values $|\bar{\alpha}|^2 \equiv |\alpha|^2$ of the order s or greater. However, for $|\bar{\alpha}|^2 \equiv |\alpha|^2 \ll s$, the FD displaced number states $|\alpha, n_d\rangle_{(s)}$ and $|\bar{\alpha}, n_d\rangle_{(s)}$ approach each other.

In Fig. 8, we present a few examples of the Wigner function for the generalized DNS with $n_d = 1$, and 2. We observe that $|\alpha, n_d\rangle_{(s)}$ are quasiperiodic in $|\alpha|$ with the same quasiperiods as those for the generalized CS given by Eqs. (34) and (35) for even and odd s, respectively. At multiples of T_s, the initial number state $|n_d\rangle$ is partially recovered, as observed in Figs. 4f and 8c,f. However, the periodicity is deteriorated with increasing photon number n_d. The most precise periodicity is observed for $|\alpha, 0\rangle_{(s)}$, as depicted in Fig. 4f. It is worse for $|\alpha, 1\rangle_{(s)}$ (Fig. 8c), and even worse for $|\alpha, 2\rangle_{(s)}$ as seen in Fig. 8f. In fact, the entire evolution of $|\alpha, n_d\rangle_{(s)}$ becomes more complicated with increasing number n_d as can be observed by comparing Figs. 4b,c,f, 8a–c and 8d–f, respectively. For brevity, we omit the corresponding figures for the truncated DNS. The Wigner functions for $|\alpha, n_d\rangle_{(s)}$ and $|\bar{\alpha}, n_d\rangle_{(s)}$ are almost indistinguishable for the displacement parameter $|\alpha| = |\bar{\alpha}|$ and n_d much less than s. However, for higher values of these parameters, the generalized and truncated DNS behave qualitatively different. As discussed, the former states are periodic or quasiperiodic, but the latter are aperiodic with the increasing displacement parameter.

C. FD Schrödinger Cats

Superpositions of two CS have attracted much attention [13,66] as simple examples of Schrödinger cats. In this Section, we will discuss two kinds of FD

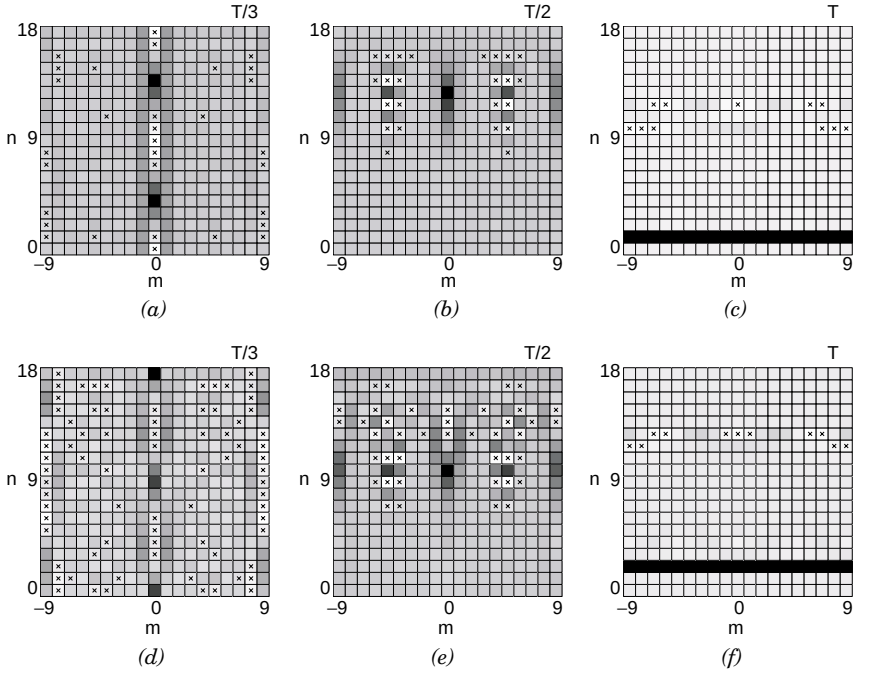

Figure 8. Generalized displaced number states. Wigner function for $|\alpha, n_d\rangle_{(s)} = |\alpha, 1\rangle_{(18)}$ (a–c) and $|\alpha, 2\rangle_{(18)}$ (d–f) with different displacement parameters α given by fractions of the quasiperiod $T = T_{18} = 8.8$.

analogs of the conventional ID even and odd CS of Malkin and Man'ko [13]. The Schrödinger cats in FD Hilbert spaces were discussed, for example, by Zhu and Kuang [25], Miranowicz, Opatrný and Bajer [21], and Roy and Roy [24].

1. *Generalized Schrödinger Cats*

Let us define the generalized even CS by [21]

$$|\alpha_0\rangle_{(s)} = \mathscr{M}_{0s}\left(|\alpha\rangle_{(s)} + |-\alpha\rangle_{(s)}\right) \tag{72}$$

and odd CS by

$$|\alpha_1\rangle_{(s)} = \mathscr{M}_{1s}\left(|\alpha\rangle_{(s)} - |-\alpha\rangle_{(s)}\right) \tag{73}$$

where the normalization is guaranteed by $\mathscr{M}_{\delta s}$ ($\delta = 0, 1$). On inserting Eq. (22) into (72) and (73), we find the Fock expansions of the Schrödinger cats in

the forms

$$|\alpha_0\rangle_{(s)} = \mathcal{N}_{0s} \sum_{n=0}^{[\![s/2]\!]} e^{i2n\varphi}\, b_{2n}^{(s)} |2n\rangle$$
$$|\alpha_1\rangle_{(s)} = \mathcal{N}_{1s} \sum_{n=0}^{[\![s/2]\!]} e^{i(2n+1)\varphi}\, b_{2n+1}^{(s)} |2n+1\rangle \tag{74}$$

where the coefficients $b_n^{(s)}$ are given by Eq. (23); $[\![s/2]\!]$ is the integer part of $s/2$, and the normalizations are ($\delta = 0, 1$):

$$\mathcal{N}_{\delta s} = \left(\sum_{n=0}^{[\![s/2]\!]} \left(b_{2n+\delta}^{(s)}\right)^2 \right)^{-1/2} \tag{75}$$

Analogously one can construct FD superpositions of several CS, that is, FD Schrödinger cat-like or kitten states, which in the limit go over into the conventional ID ones [66,67].

2. *Truncated Schrödinger Cats*

FD even and odd CS can be constructed in a way slightly different from that presented in the preceding paragraph. Instead of the generalized CS, the truncated CS can be used in the definitions (72) and (73). This approach was explored by Zhu and Kuang [25], and Roy and Roy [24]. We rewrite briefly their explicit expressions for $|\bar{\alpha}_0\rangle_{(s)}$ and $|\bar{\alpha}_1\rangle_{(s)}$ in Fock representation

$$|\bar{\alpha}_\delta\rangle_{(s)} = \mathcal{N}_{\delta s} \sum_{n=0}^{[\![s/2]\!]} \frac{\bar{\alpha}^{\,2n+\delta}}{\sqrt{(2n+\delta)!}} |2n+\delta\rangle \tag{76}$$

where $\delta = 0$ for even cats and $\delta = 1$ for odd cats. The normalization is

$$\mathcal{N}_{\delta s} = \left(\sum_{n=0}^{[\![s/2]\!]} \frac{|\bar{\alpha}|^{2(2n+\delta)}}{(2n+\delta)!} \right)^{-1/2} \tag{77}$$

Equation (76) can directly be calculated from Eqs. (72) and (73) after replacing $|\pm\alpha\rangle_{(s)}$ by $|\pm\bar{\alpha}\rangle_{(s)}$, given by their Fock expansion (36). Therefore, we refer to the states (76) as the *truncated* states.

Several examples of the Wigner function for the generalized even and odd CS are presented in Fig. 9. Their interpretation is quite clear. These are two-peak structures with many interference fringes. The fringes in the Wigner

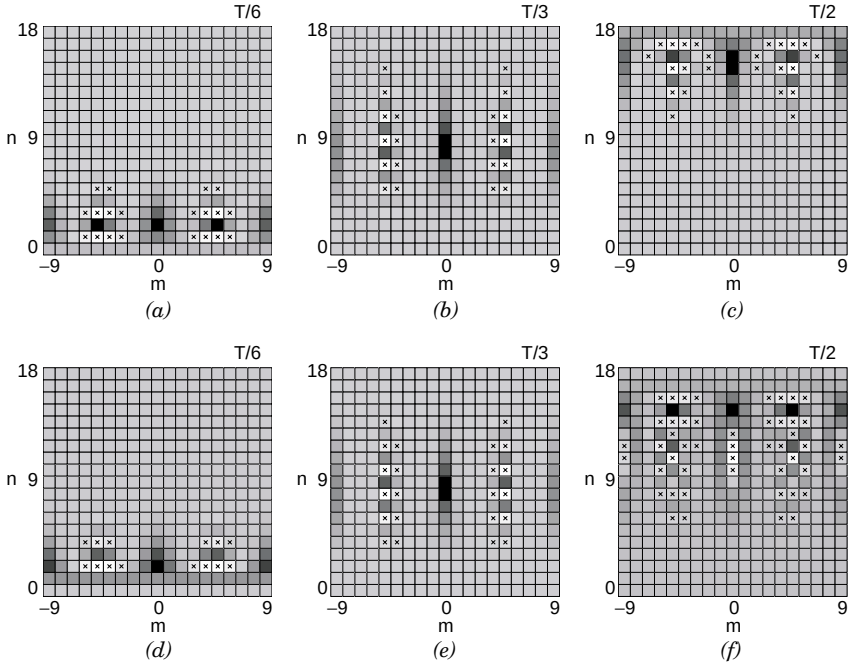

Figure 9. Generalized Schrödinger cats. Wigner function for $|\alpha_0\rangle_{(18)}$ (a–c) and $|\alpha_1\rangle_{(18)}$ (d–f) with α given by fractions of the quasiperiod $T = T_{18} = 8.8$.

function are typical of superposition states, and are not observed for a mixture of states. The main difference between the Wigner functions presented in Fig. 9a–c and d–f consists in a shift of the interference fringes. Let us note that the generalized CS for $|\alpha| = T_s/2$, presented in Fig. 4c, is approximately equal to the even CS for the same value of $|\alpha|$. Unfortunately, because of space limitations here, the corresponding Wigner functions for the truncated cats are skipped. Let us mention that only for small displacement parameter $|\bar{\alpha}|^2 = |\alpha|^2 \ll s$, the truncated and generalized cats have similar properties since approximately holds $|\alpha_0\rangle_{(s)} \approx |\bar{\alpha}_0\rangle_{(s)}$ and $|\alpha_1\rangle_{(s)} \approx |\bar{\alpha}_1\rangle_{(s)}$. However, for higher values of $|\alpha|^2$ (roughly estimated to be greater than $T_s/3$), discrepancies between the generalized and truncated Schrödinger cats become essential since they are defined in terms of the CS $|\pm\alpha\rangle_{(s)}$ and $|\pm\bar{\alpha}\rangle_{(s)}$ exhibiting different properties for large $|\alpha|^2$ as seen by comparing Figs. 4c–f and 6c–f. These discrepancies result from periodic or quasiperiodic behavior of the generalized states and aperiodic behavior of the truncated states.

D. FD Squeezed Vacuum

Here, we discuss two kinds of FD squeezed vacuum. We will present explicit forms of these states, which reveal the differences and similarities between them and the conventional IF squeezed vacuum [68] or FD coherent state. We will show that our states are properly normalized in $\mathscr{H}^{(s)}$ of arbitrary dimension and go over into the conventional squeezed vacuum if the dimension is much greater than the square of the squeeze parameter. Squeezing and squeezed states in FD Hilbert spaces were analyzed, in particular, by Wódkiewicz et al. [31], Figurny et al. [32], Wineland et al. [33], Bužek et al. [16], and Opatrný et al. [20]. An FD analog of the conventional squeezed vacuum was proposed by Miranowicz et al. [34].

1. *Generalized Squeezed Vacuum*

By analogy with the conventional squeezed vacuum [68], we define the generalized squeezed vacuum in the $(s+1)$-dimensional Hilbert space by [34]

$$|\zeta\rangle_{(s)} = \hat{S}_s(\zeta)\,|0\rangle \tag{78}$$

as the result of action of the generalized FD squeeze operator

$$\hat{S}_s(\zeta) = \exp\left\{\tfrac{1}{2}\left(\zeta\hat{a}_s^{\dagger 2} - \zeta^*\hat{a}_s^2\right)\right\} \tag{79}$$

on vacuum. Here, $\zeta = |\zeta|\exp(\mathrm{i}\varphi)$ is the complex squeeze parameter; $\hat{a}_s$ and $\hat{a}_s^\dagger$ are, respectively, the FD annihilation and creation operators defined by Eq. (8). The method for finding explicit number-state representation of the generalized CS, presented in Appendix, can also be applied here. We find the following explicit Fock expansion of the generalized squeezed vacuum

$$|\zeta\rangle_{(s)} = \sum_{n=0}^{\sigma} b_{2n}^{(s)} e^{in\varphi}|2n\rangle \tag{80}$$

with the superposition coefficients given by

$$b_{2n}^{(s)} = (-i)^n \frac{(2\sigma)!}{\sqrt{(2n)!}} \sum_{k=0}^{\sigma} \exp\left(\tfrac{i}{2}|\zeta|x_k\right) \frac{G_n(x_k)}{G_\sigma(x_k)G'_{\sigma+1}(x_k)} \tag{81}$$

where $\sigma = [\![s/2]\!]$ and $G_n(x)$ are the Meixner–Sheffer orthogonal polynomials defined by the recurrence relation [69]

$$G_{n+1} = xG_n - 2n(2n-1)G_{n-1} \tag{82}$$

for $n = 2, 3, \ldots$, together with $G_0(x) = 1$ and $G_1(x) = x$. In Eq. (81), $x_k \equiv x_k^{(\sigma+1)}$ is the kth root ($k = 0, \ldots, \sigma$) of the polynomial $G_{\sigma+1}(x)$ and $G'_{\sigma+1}(x_k)$ denotes the x derivative at $x = x_k$. Since Eq. (81) is of a rather complicated form, we present a few examples of the FD squeezed vacuum for small dimensions. For $s = 2$ and 3, we find

$$|\zeta\rangle_{(2)} = |\zeta\rangle_{(3)} = \cos\beta|0\rangle + e^{i\varphi}\sin\beta|2\rangle \tag{83}$$

where $\beta = \frac{1}{2}|\zeta x_0^{(2)}| = \frac{1}{\sqrt{2}}|\zeta|$. For $s = 4, 5$, we have

$$|\zeta\rangle_{(4)} = |\zeta\rangle_{(5)} = \frac{1}{7}(6 + \cos\beta)|0\rangle + e^{i\varphi}\frac{1}{\sqrt{7}}\sin\beta|2\rangle + e^{2i\varphi}\frac{2}{7}\sqrt{6}\sin^2\left(\frac{1}{2}\beta\right)|4\rangle \tag{84}$$

where $\beta = \frac{1}{2}|\zeta x_0^{(3)}| = \sqrt{\frac{7}{2}}|\zeta|$. The generalized squeezed vacuum, given by (80), has more complicated form in Fock basis than that for the generalized CS, described by (22). In particular, the solution (81) contains rather complicated Meixner–Sheffer polynomials instead of the well-known Hermite polynomials, which occur in the expansions for the generalized CS.

Here, we discuss only a few basic properties of generalized squeezed vacuum, given by (78). By definition, it is properly normalized for arbitrary dimension of the Hilbert space. There are several ways to prove that the generalized squeezed vacuum goes over into the conventional squeezed vacuum ($|\zeta\rangle$) in the limit of $s \to \infty$. By definition (78), one can conclude that the property $\lim_{s\to\infty}|\zeta\rangle_{(s)} = |\zeta\rangle_{(\infty)} = |\zeta\rangle$ holds, since the FD annihilation and creation operators go over into the conventional ones: $\lim_{s\to\infty}\hat{a}_s = \hat{a}$ and $\lim_{s\to\infty}\hat{a}_s^\dagger = \hat{a}^\dagger$. One can also show, at least numerically, that the superposition coefficients (81) approach the coefficients b_n for the conventional squeezed vacuum: $\lim_{s\to\infty} b_n^{(s)} = b_n$ for $n = 0, \ldots, s$. We apply another method based on the calculation of the scalar product $\langle\zeta|\zeta\rangle_{(s)}$. We show the analytical results for $|\zeta| \leq 1$ only. We have found the scalar product between conventional and generalized squeezed vacuums in the form (for even s)

$$\langle\zeta|\zeta\rangle_{(s)} = \langle\zeta|\zeta\rangle_{(s+1)} = 1 + \sum_{k=1}^{\infty}(-1)^k c_k^{(s)}|\zeta|^{s+2k} \leq 1 \tag{86}$$

where the coefficients $c_k^{(s)}$ are positive and less than one for any k and s. We find that the explicit expansion up to $|\zeta|^{s+2}$ can be given in terms of the binomial coefficient as follows:

$$\langle\zeta|\zeta\rangle_{(s)} = \langle\zeta|\zeta\rangle_{(s+1)} = 1 - \binom{s+1}{\frac{1}{2}s+1}\left(\frac{|\zeta|}{2}\right)^{s+2} + \mathcal{O}(|\zeta|^{s+4}) \tag{87}$$

In particular, for $s = 2, \ldots, 7$, we have

$$\langle\zeta|\zeta\rangle_{(2)} = \langle\zeta|\zeta\rangle_{(3)} = 1 - \frac{3}{16}|\zeta|^4 + \frac{1}{8}|\zeta|^6 - \mathcal{O}(|\zeta|^8)$$

$$\langle\zeta|\zeta\rangle_{(4)} = \langle\zeta|\zeta\rangle_{(5)} = 1 - \frac{5}{32}|\zeta|^6 + \frac{185}{1024}|\zeta|^8 - \mathcal{O}(|\zeta|^{10})$$

$$\langle\zeta|\zeta\rangle_{(6)} = \langle\zeta|\zeta\rangle_{(7)} = 1 - \frac{35}{256}|\zeta|^8 + \frac{7}{30}|\zeta|^{10} - \mathcal{O}(|\zeta|^{12}) \tag{88}$$

It is clearly seen that, for a given ζ, the scalar products become closer to unity with increasing space dimension. We conclude that the generalized state (78) approaches the conventional squeezed vacuum in the dimension limit.

2. *Truncated Squeezed Vacuum*

One can propose another definition of a FD squeezed vacuum, such as by truncation of the Fock expansion of the conventional squeezed vacuum at the state $|s\rangle$. Thus, we define the truncated squeezed vacuum as follows [34]

$$|\bar{\zeta}\rangle_{(s)} = \sum_{n=0}^{\sigma+1} b_{2n}^{(s)} e^{in\varphi}|2n\rangle \tag{89}$$

with the superposition coefficients

$$b_{2n}^{(s)} = \mathcal{N}_s \frac{\sqrt{(2n)!}}{n!} t^n \tag{90}$$

normalized by

$$\mathcal{N}_s^{-2} = \cosh|\bar{\zeta}| - 2t^{2\sigma+2}\binom{2\sigma+1}{\sigma}\,{}_2\mathrm{F}_1\left(1, \left\{\frac{3}{2}+\sigma, 2+\sigma\right\}, 4t^2\right) \tag{91}$$

where $\sigma = [\![s/2]\!]$; $t = \frac{1}{2}\tanh|\bar{\zeta}|$, and ${}_2\mathrm{F}_1$ is the generalized hypergeometric function. We marked with a bar the complex squeeze parameter $\bar{\zeta}$ for the truncated states in order to distinguish it from the generalized squeezed vacuum defined by applying the FD squeeze operator. We give an example of the truncated squeezed vacuum. For $s = 2,3$, Eq. (89) reduces to

$$|\bar{\zeta}\rangle_{(2)} = |\bar{\zeta}\rangle_{(3)} = \frac{|0\rangle + \sqrt{2}t|2\rangle}{\sqrt{1+2t^2}} \tag{92}$$

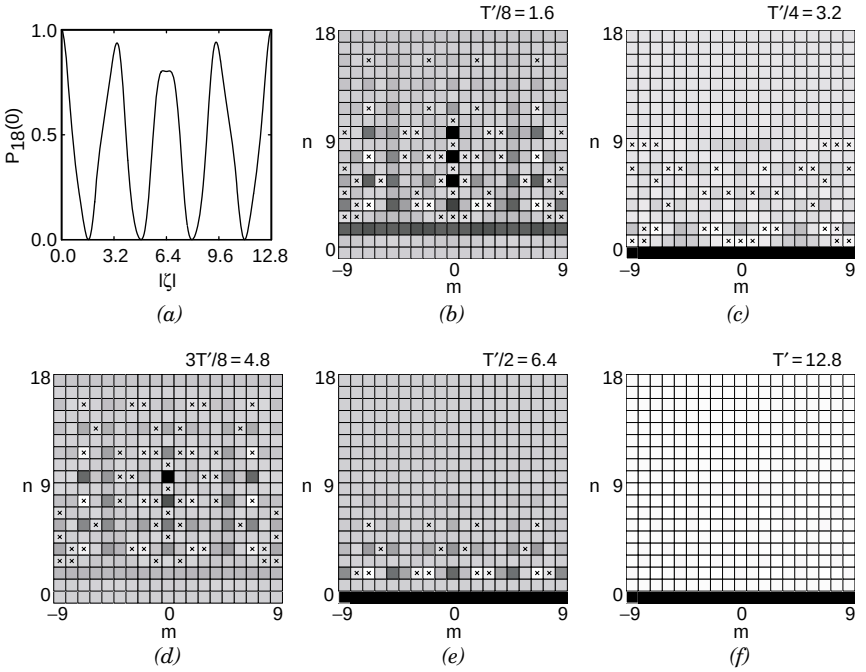

Figure 10. Generalized squeezed vacuum. (a) Vacuum-state probability, $P_{18}(0) = |b_0^{(18)}|^2$, for $|\zeta\rangle_{(18)}$ as a function of the squeeze parameter amplitude $|\zeta|$; (b–f) Wigner function for $|\zeta\rangle_{(18)}$ with ζ given by fractions of the quasiperiod $T' = T'_{18} = 12.8$.

The state (89), by definition, goes over into the conventional squeezed vacuum in the limit of large dimension: $\lim_{s\to\infty} |\bar{\zeta}\rangle_{(s)} = |\bar{\zeta}\rangle \equiv |\zeta\rangle$. We can explicitly show this by expanding the scalar products between them in power series with respect to $|\zeta|^2 = |\bar{\zeta}|^2 \ll s$. We find (for even s)

$$ {}_{(\infty)}\langle\zeta|\bar{\zeta}\rangle_{(s)} = {}_{(\infty)}\langle\zeta|\bar{\zeta}\rangle_{(s+1)} \tag{93} $$

under assumption $\varphi = \bar{\varphi}$. In particular, we have

$$ \begin{aligned} {}_{(\infty)}\langle\zeta|\bar{\zeta}\rangle_{(2)} = {}_{(\infty)}\langle\zeta|\bar{\zeta}\rangle_{(3)} &= 1 - \frac{3}{16}|\zeta|^4 + \frac{3}{16}|\zeta|^6 - \mathcal{O}(|\zeta|^8) \\ \langle\zeta|\bar{\zeta}\rangle_{(4)} = \langle\zeta|\bar{\zeta}\rangle_{(5)} &= 1 - \frac{5}{32}|\zeta|^6 + \frac{65}{256}|\zeta|^8 - \mathcal{O}(|\zeta|^{10}) \\ \langle\zeta|\bar{\zeta}\rangle_{(6)} = \langle\zeta|\bar{\zeta}\rangle_{(7)} &= 1 - \frac{35}{256}|\zeta|^8 + \frac{119}{384}|\zeta|^{10} - \mathcal{O}(|\zeta|^{10}) \end{aligned} \tag{94} $$

We can also explicitly compare $|\bar{\zeta}, 2n_0\rangle_{(s)}$ with $|\zeta, 2n_0\rangle_{(s)}$ with the help of their scalar products. In particular, by putting $\varphi = \overline{\varphi}$, we have

$$
\begin{aligned}
{}_{(2)}\langle\zeta|\bar{\zeta}\rangle_{(2)} &= {}_{(2)}\langle\zeta|\bar{\zeta}\rangle_{(3)} = 1 - \frac{1}{16}|\zeta|^6 + \frac{7}{80}|\zeta|^8 - \mathcal{O}(|\zeta|^{10}) \\
{}_{(4)}\langle\zeta|\bar{\zeta}\rangle_{(4)} &= {}_{(5)}\langle\zeta|\bar{\zeta}\rangle_{(5)} = 1 - \frac{75}{2^{10}}|\zeta|^8 + \frac{131}{2^{10}}|\zeta|^{10} - \mathcal{O}(|\zeta|^{12}) \\
{}_{(6)}\langle\zeta|\bar{\zeta}\rangle_{(6)} &= {}_{(7)}\langle\zeta|\bar{\zeta}\rangle_{(7)} = 1 - \frac{49}{640}|\zeta|^{10} + \frac{189}{2^{10}}|\zeta|^{12} - \mathcal{O}(|\zeta|^{14})
\end{aligned}
\tag{95}
$$

By comparing Eq. (95) with Eqs. (88) and (94), we can conclude that the differences between the generalized and truncated squeezed vacuums are smaller than those between them and the conventional squeezed vacuum. All these states coincide in the high-dimension limit. In Fig. 10b–f, we have presented the Wigner representation of the generalized squeezed vacuum for those values of the squeeze parameter $|\zeta|$, which correspond to maximum and minimum values of the vacuum-state probability given by $P_s(0) = |b_0^{(s)}|^2$ (see Fig. 10a). We find that the generalized squeezed vacuum is quasiperiodic in $|\zeta|$. Although, its quasi-period T_s' differs from T_s for the generalized CS, phase CS, displaced number states or Schrödinger cats, as given by Eqs. (34) and (35). The truncated squeezed vacuum is aperiodic in $|\bar{\zeta}|$, similarly to other truncated quantum-optical states discussed in Sections IV and V.

VI. CONCLUSION

We have compared two approaches to define finite-dimensional (FD) analogs of the conventional quantum-optical states of infinite-dimensional Hilbert space. We have contrasted (1) the generalized coherent states (CS), defined by the action of the generalized FD displacement operator on vacuum, with (2) the truncated CS, defined by the normalized truncated Fock expansion of the conventional Glauber CS. We have shown both analytically and graphically that these CS constructed in FD Hilbert spaces exhibit essentially different behaviors; the generalized CS are periodic (for $s = 1,2$) or quasi-periodic (for higher $s < \infty$) functions of the displacement parameter, whereas the truncated CS are aperiodic for any s (even for $s = 1$). Both the generalized and truncated CS go over into the conventional CS in the dimension limit. Nevertheless, the truncated CS approach the conventional Glauber CS faster than the generalized CS do. Besides, as the special case, we have compared in detail the two-dimensional CS. We have analyzed other finite-dimensional quantum-optical states. In particular, we have discussed: (1) FD phase coherent states, (2) FD displaced number states; (3) FD Schrödinger cats, including even and odd CS; and (4) FD squeezed vacuums. We have confronted two essentially different

ways of defining states in FD Hilbert spaces. We have constructed explicitly all of these states generated by various finite-dimensional displacement or squeeze operators using the method developed in Ref. 18 for the generalized CS. We have also presented graphical representations of the discrete number-phase Wigner function, which enabled us a very intuitive understanding of the properties of the generalized and truncated quantum-optical states.

APPENDIX

Here, after Ref. 18, we present a method for finding the coefficients $b_n^{(s)}$ of Fock representation of the generalized CS, given by Eq. (22).

The Baker–Hausdorf formula cannot be used to solve this problem because the commutator of the annihilation $\hat{a}_s$ and creation $\hat{a}_s^\dagger$ operators is not a c number. A numerical procedure, leading to the coefficients $b_n^{(s)}$, was proposed by Bužek et al. [16]. In order to solve this problem analytically [18], it is of advantage to express the conventional coherent state, $|\alpha\rangle$, in the Fock representation in a different manner

$$\begin{aligned}|\alpha\rangle &= \sum_{n=0}^{\infty} \frac{(\alpha a^\dagger - \alpha^* a)^n}{n!}|0\rangle \\ &= \sum_{n=0}^{\infty} \sum_{k=0}^{[\![n/2]\!]} \frac{\sqrt{(n-2k)!}}{n!}\, d_{n,n-2k}(-\alpha^*)^k \alpha^{n-k}|n-2k\rangle \end{aligned} \tag{A.1}$$

where

$$d_{n,k} = \binom{n}{k}(n-k-1)!! \tag{A.2}$$

and $[\![x]\!]$ is the integer part of x. Thus, Eq. (A.1) for the generalized CS can be rewritten as

$$|\alpha\rangle_{(s)} = \sum_{k=0}^{s}\left[\sum_{n=k}^{\infty} \frac{\sqrt{k!}}{n!}\, d_{nk}^{(s)}(-\alpha^*)^{(n-k)/2}\alpha^{(n+k)/2}\right]|k\rangle \equiv \sum_{k=0}^{s} c_k^{(s)}|k\rangle \tag{A.3}$$

The problem reduces to derivation of the coefficients $d_{n,k}^{(s)}$ satisfying the condition in the dimension limit

$$\lim_{s\to\infty} d_{nk}^{(s)} = d_{n,k}^{(\infty)} \equiv d_{nk} = \binom{n}{k}(n-k-1)!! \tag{A.4}$$

We obtain the following simple recurrence formula

$$d_{nk}^{(s)} = \theta_k d_{n-1,k-1}^{(s)} + (k+1)\theta_{k+1} d_{n-1,k+1}^{(s)} \tag{A.5}$$

with the conditions $d_{00}^{(s)} = 1$ and $d_{n,n+k}^{(s)} = 0$ for $s, k > 0$. In Eq. (A.5), θ_n is the Heaviside function defined to be

$$\theta_n \equiv \theta(s-n) = \begin{cases} 1 & \text{for} \quad s \geq n \\ 0 & \text{for} \quad s < n \end{cases} \tag{A.6}$$

The solution of the recurrence formula (A.5) is

$$d_{nk}^{(s)} = \frac{s!}{k!(s+1)} \sum_{l=0}^{s} \frac{\mathrm{He}_k(x_l)}{[\mathrm{He}_s(x_l)]^2} x_l^n \tag{A.7}$$

where $x_l \equiv x_l^{(s+1)}$ are the roots of the Hermite polynomial $\mathrm{He}_{s+1}(x)$. A solution similar to ours (A.7) was found by Figurny et al. [32] in their analysis of the eigenvalues of the truncated quadrature operators. On performing summation in Eq. (A.3) with the coefficients $d_{nk}^{(s)}$, given by (A.7), one readily arrives at

$$C_n^{(s)} = \frac{s!}{s+1} \frac{1}{\sqrt{n!}} \sum_{k=0}^{s} \exp\left\{ i \left[n \left(\frac{\varphi - \pi}{2} \right) + x_k \, |\alpha| \right] \right\} \frac{\mathrm{He}_n(x_k)}{[\mathrm{He}_s(x_k)]^2} \equiv \mathrm{e}^{\mathrm{i}n\varphi} b_n^{(s)} \tag{A.8}$$

or, equivalently, Eq. (23). Our procedure provides the coefficients $b_n^{(s)}$ in a closed analytical form. This is the solution of the problem formulated by Bužek et al. [16].

Acknowledgments

A. M. and W. L. thank J. Bajer, S. Dyrting, M. Koashi, T. Opatrný, S. K. Özdemir, J. Peřina, K. Piątek, and R. Tanaś for their stimulating discussions. A. M. is indebted to Prof. Nobuyuki Imoto for his hospitality at SOKEN.

References

1. H. Weyl, *Theory of Groups and Quantum Mechanics*, Dover, New York, 1931.
2. J. Schwinger, *Proc. Natl. Acad. Sci. (USA)* **46**, 570 (1960); reprinted in *Quantum Kinematics and Dynamics*, Benjamin, New York, 1970, p. 63.
3. T. S. Santhanam and A. R. Tekumalla, *Found. Phys.* **6**, 583 (1976); T. S. Santhanam, *Phys. Lett. A* **56**, 345 (1976); T. S. Santhanam and K. B. Sinha, *Aust. J. Phys.* **31**, 233 (1978); T. S. Santhanam, in B. Gruber and S. Millmann (Eds.), *Symmetries in Science*, Plenum, New York, 1980, p. 337.
4. J. M. Radcliffe, *J. Phys. A* **4**, 313 (1971).
5. C. Arecchi, E. Courtens, R. Gilmore and H. Thomas, *Phys. Rev. A* **6**, 2211 (1972).
6. R. J. Glauber and F. Haake, *Phys. Rev. A* **13**, 357 (1976).
7. E. Schrödinger, *Naturwissenschaften* **14**, 664 (1926).
8. R. J. Glauber, *Phys. Rev. A* **130**, 2529 (1963); *ibid.* **131**, 2766 (1963).
9. E. C. G. Sudarshan, *Phys. Rev. Lett.* **10**, 277 (1963).
10. A. M. Perelomov, *Commun. Math. Phys.* **26**, 222 (1972); *Usp. Fiz. Nauk* **123**, 23 (1977) [*Sov. Phys. Usp.* **20**, 703 (1977)]; *Generalized Coherent States and their Applications*, Springer, Berlin, 1986.

11. R. Gilmore, *Ann. Phys.* (*NY*) **74**, 391 (1972); *Rev. Mex. Fis.* **23**, 142 (1974); *J. Math. Phys.* **15**, 2090 (1974).
12. W. M. Zhang, D. H. Feng, and R. Gilmore, *Rev. Mod. Phys.* **62**, 867 (1990).
13. I. A. Malkin and V. I. Man'ko, *Dynamical Symmetries and Coherent States of Quantum Systems*, Nauka, Moscow, 1979.
14. J. R. Klauder and B. S. Skagerstam (Eds.), *Coherent States: Applications in Physics and Mathematical Physics*, World Scientific, Singapore, 1985.
15. D. H. Feng and J. Klauder (Eds.), *Coherent States: Past, Present and Future*, World Scientific, Singapore, 1994.
16. V. Bužek, A. D. Wilson-Gordon, P. L. Knight, and W. K. Lai, *Phys. Rev. A* **45**, 8079 (1992).
17. L. M. Kuang, F. B. Wang, and Y. G. Zhou, *Phys. Lett. A* **183**, 1 (1993); *J. Mod. Opt.* **41**, 1307 (1994).
18. A. Miranowicz, K. Piątek, and R. Tanaś, *Phys. Rev. A* **50**, 3423 (1994).
19. A. K. Pati and S. V. Lawande, *Phys. Rev. A* **51**, 5012 (1995).
20. T. Opatrný, A. Miranowicz, and J. Bajer, *J. Mod. Opt.* **43**, 417 (1996).
21. A. Miranowicz, T. Opatrný, and J. Bajer, in T. Hakioğlu and A. S. Shumovsky (Eds.), *Quantum Optics and the Spectroscopy of Solids: Concepts and Advances*, Vol. 83, *Fundamental Theories of Physics*, Kluwer, Dordrecht, 1997, p. 225.
22. B. Roy and R. Roychoudhury, *Int. J. Theor. Phys.* **36**, 1525 (1997).
23. B. Roy, *Modern Phys. Lett. B* **11**, 963 (1997).
24. B. Roy and P. Roy, *J. Phys. A* **31**, 1307 (1998).
25. J. Y. Zhu and L. M. Kuang, *Phys. Lett. A* **193**, 227 (1994); *Chinese Phys. Lett. A* **11**, 424 (1994).
26. D. T. Pegg, and S. M. Barnett, *Europhys. Lett.* **6**, 483 (1988); *Phys. Rev. A* **41**, 3427 (1989); S. M. Barnett and D. T. Pegg, *J. Mod. Opt.* **36**, 7 (1989).
27. L. M. Kuang and X. Chen, *Phys. Rev. A* **50**, 4228 (1994); *Phys. Lett. A* **186**, 8 (1994).
28. G. Gangopadhyay, *J. Mod. Opt.* **41**, 525 (1994).
29. A. Miranowicz, K. Piątek, T. Opatrný, and R. Tanaś, *Acta Phys. Slov.* **45**, 391 (1995).
30. P. Roy and B. Roy, *Quantum and Semiclas. Optics* **9**, L37 (1997).
31. K. Wódkiewicz, P. L. Knight, S. J. Buckle, and S. M. Barnett, *Phys. Rev. A* **35**, 2567 (1987).
32. P. Figurny, A. Orłowski, and K. Wódkiewicz, *Phys. Rev A* **47**, 5151 (1993).
33. D. J. Wineland, J. J. Bollinger, W. M. Itano, and D. J. Heinzen, *Phys. Rev. A* **50**, 67 (1994).
34. A. Miranowicz, W. Leoński, and R. Tanaś, in D. Han et al. (Eds.), NASA Conference Publication 206855, Greenbelt, MD, 1998, p. 91.
35. L. M. Kuang and J. Y. Zhu, *J. Phys. A* **29**, 895 (1996).
36. Special issue on quantum state preparation and measurement, *J. Mod. Opt.* **44** (11/12) (1997).
37. U. Leonhardt, *Phys. Rev. Lett.* **74**, 4101 (1995); ibid. **76**, 4293 (1996); *Phys. Rev. A* **53**, 2998 (1996).
38. V. I. Man'ko, O. V. Man'ko, *JETP* **85**, 430 (1997); V. A. Andreev, V. I. Man'ko, *JETP* **87**, 239 (1998); V. I. Man'ko, S. S. Safonov, *Phys. Atom. Nuclei* **61**, 585 (1998).
39. V. Bužek, G. Drobný, G. Adam, R. Derka, P. L. Knight, *J. Mod. Opt.* **44**, 2607 (1997); V. Bužek, R. Derka, G. Adam, P. L. Knight, *Ann. Phys.* (*San Diego*) **266**, 454 (1998).
40. R. Walser, J. I. Cirac, P. Zoller, *Phys. Rev. Lett.* **77**, 2658 (1996).
41. J.-P. Amiet and S. Weigert, *J. Phys. A* **31**, L543 (1998); ibid. **32**, L269 (1999); *J. Opt. B* **1**, L5 (1999).

42. D.-G. Welsch, W. Vogel, and T. Opatrný, in E. Wolf (Ed.), *Progress in Optics*, Vol. 39, North-Holland, Amsterdam, 1999, p. 63.
43. R. Tanaś, A. Miranowicz, and T. Gantsog, in E. Wolf (Ed.), *Progress in Optics*, Vol. 35, North-Holland, Amsterdam, 1996, p. 355.
44. D. T. Pegg, L. S. Phillips, and S. M. Barnett, *Phys. Rev. Lett.* **81**, 1604 (1998); S. M. Barnett and D. Pegg, *Phys. Rev. A* **60**, 4965 (1999).
45. M. Koniorczyk, Z. Kurucz, A. Gábris, and J. Janszky, *Phys. Rev. A* **62**, 013802 (2000).
46. M. G. A. Paris, *Phys. Rev. A* **62**, 033813 (2000).
47. A. Miranowicz, S. K. Özdemir, N. Imoto, and M. Koashi, *Mtg. Abstr. Phys. Soc. Jpn.* **62**, 108 (2000).
48. W. Leoński and R. Tanaś, *Phys. Rev. A* **49**, R20 (1994); W. Leoński, *Phys. Rev. A* **54**, 3369 (1996); W. Leoński, S. Dyrting, and R. Tanaś, *J. Mod. Opt.* **44**, 2105 (1997).
49. W. Leoński, *Phys. Rev. A* **55**, 3874 (1997).
50. A. Miranowicz, W. Leoński, S. Dyrting, and R. Tanaś, *Acta Phys. Slov.* **46**, 451 (1996).
51. W. Leoński and A. Miranowicz, "Quantum-optical states in finite-dimensional Hilbert space. II. State generation," Chapter 4, this volume.
52. E. P. Wigner, *Phys. Rev.* **40**, 749 (1932); for a review, see M. Hillery, R. F. O'Connell, M. O. Scully, and E. P. Wigner, *Phys. Rep.* **106**, 121 (1984); V. I. Tatarskii, *Sov. Phys. Usp.* **26**, 311 (1983).
53. R. L. Stratonovich, *Sov. Phys. JETP* **4**, 891 (1957); L. Cohen and M. O. Scully, *Found. Phys.* **16**, 295 (1986).
54. R. F. O'Connell, and E. P. Wigner, *Phys. Rev. A* **30**, 2613 (1984).
55. W. K. Wootters, *Ann. Phys.* **176**, 1 (1987).
56. O. Cohendet, P. Combe, M. Sirugue, and M. Sirugue-Collin, *J. Phys. A* **21**, 2875 (1988).
57. J. A. Vaccaro and D. T. Pegg, *Phys. Rev. A* **41**, 5156 (1990).
58. T. Opatrný, V. Bužek, J. Bajer, and G. Drobný, *Phys. Rev. A* **52**, 2419 (1995).
59. T. Opatrný, D.-G. Welsch, and V. Bužek, *Phys. Rev. A* **53**, 3822 (1996).
60. T. Hakioğlu, *J. Phys. A* **31**, 6975 (1998).
61. A. Lukš and V. Peřinová, *Phys. Scr. T* **48**, 94 (1993).
62. A. Luis and J. Peřina, *J. Phys. A* **31**, 1423 (1998).
63. J. Peřina, Z. Hradil, and B. Jurčo, *Quantum Optics and Fundamentals of Physics*, Vol. 63, *Fundamental Theories in Physics*, Kluwer Academic, Dordrecht, 1994.
64. W. Leoński and A. Miranowicz, *Acta Phys. Slov.* **46**, 433 (1996); W. Leoński, A. Miranowicz, and R. Tanaś, *Laser Physics* **7**, 126 (1997).
65. F. A. M. de Oliveira, M. S. Kim, P. L. Knight, and V. Bužek, *Phys. Rev. A* **41**, 2645 (1990).
66. V. Bužek, and P. L. Knight, in E. Wolf (Ed.), *Progress in Optics*, Vol. 34, North-Holland, Amsterdam, 1995, p. 1.
67. A. Miranowicz, R. Tanaś, and S. Kielich, *Quantum Opt.* **2**, 253 (1990).
68. R. Loudon and P. L. Knight, *J. Mod. Opt.* **34**, 709 (1987); K. Zaheer and M. S. Zubairy, in D. Bates and B. Bederson (Eds.), *Advances in Atomic, Molecular and Optical Physics*, Vol. 28, Academic Press, New York, 1990, p. 143.
69. J. Meixner, *J. London Math. Soc.* **9**, 6 (1934); I. M. Sheffer, *Duke Math. J.* **5**, 590 (1939).

QUANTUM-OPTICAL STATES IN FINITE-DIMENSIONAL HILBERT SPACE. II. STATE GENERATION

WIESŁAW LEOŃSKI

Nonlinear Optics Division, Institute of Physics, Adam Mickiewicz University, Poznań, Poland

ADAM MIRANOWICZ

CREST Research Team for Interacting Carrier Electronics, School of Advanced Sciences, The Graduate University for Advanced Studies (SOKEN), Hayama, Kanagawa, Japan and Nonlinear Optics Division, Institute of Physics, Adam Mickiewicz University, Poznań, Poland

CONTENTS

I. INTRODUCTION

As it was mentioned in the first part of this study [1], the *finite-dimensional* (FD) quantum-optical states have been a subject of numerous papers. For instance,

various kinds of FD coherent states [2–6], FD Schrödinger cats [5–7], FD displaced number states [5], FD phase states [8], and FD squeezed states [9,10] were studied by many authors. In this chapter we concentrate on some schemes of generation of the FD quantum-optical states. These states can be produced as a finite superposition of n-photon Fock states. As a consequence, the problem of generation of FD states can be reduced to the choice of the mechanism of n-photon Fock state generation. For instance, Fock states can be achieved in the systems with externally driven cavity filled with the Kerr media [11–13]. Moreover, they can be produced in the cavities using micromaser trapped states [14]. Another way to obtain Fock states is that proposed by D'Ariano et al. [15] based on the *optical Fock-state synthesizer*, in which the conditional measurements have been performed for the interferometer containing Kerr medium. The cavities with moving mirror [16] can also be utilized for the FD state generation. Recently, several schemes for the optical-state truncaction (*quantum scissors*), by which FD quantum-optical states can be produced via teleportation, have been analyzed [17,18]. Various other methods for preparation of Fock states [19] and their arbitrary superpositions [20] have been developed (see also Ref. 21).

However, we concentrate here on the generation methods in which we are able to get directly the FD quantum state desired. Namely, we shall describe the models involving quantum nonlinear oscillator driven by an external field [11–13,22]. For this class of systems we are able to get the quantum states that are very close for instance, to the FD coherent states [2,3] or to the FD squeezed vacuum [10].

II. FD COHERENT STATES GENERATED BY NONLINEAR OSCILLATOR SYSTEMS

This section is devoted to the method of generation of the FD coherent states making a class of states defined in FD Hilbert space. We shall concentrate on the states proposed by Bužek et al. [2] and further discussed by Miranowicz et al. [3,23], where both the Glauber displacement operator and the states are defined in the FD Hilbert space [1]. The method of generation discussed here is based on the quantum systems containing a *Kerr medium* represented by nonlinear oscillator. It was introduced in Ref. 12 as a way of generating one-photon Fock states and was further adapted for the FD coherent-state generation [24]. The model discussed here represents a quantum nonlinear oscillator that interacts with an external field. Systems of this kind can be a source of various quantum states. For example, quantum nonlinear evolution can lead to generation of squeezed states [25], minimum uncertainty states [26], n-photon Fock states [11–13,22], displaced Kerr states [27], macroscopically distinguishable superpositions of two states (Schrödinger cats) [28,29], or higher number of states

(Schrödinger kittens) [30]. Of course, the problem of practical realization of the system arises. At this point one should emphasize that the most commonly proposed practical realization is that in which a nonlinear medium is located inside one arm of the Mach–Zehnder interferometer [26]. However, models of a quantum nonlinear oscillator can be achieved in various ways. For instance, systems comprising trapped ions [31], trapped atoms [32], or cavities with moving mirrors [16] can be utilized to generate states of our interest.

A. Two-Dimensional Coherent States

Let us start the discussion of practical possibilities of the FD coherent-state generation from the simplest case, where only superpositions of vacuum and single-photon state are involved (the Hilbert space discussed is reduced to two dimensions). We consider the system governed by the following Hamiltonian defined in the interaction picture (in units of $\hbar = 1$) to be

$$\hat{H}(t) = \frac{\chi}{2}(\hat{a}^\dagger)^2\hat{a}^2 + \epsilon(\hat{a}^\dagger + \hat{a})f(t) \tag{1}$$

where χ denotes the nonlinearity constant, which can be related to the third-order susceptibility of the Kerr medium; ϵ is the strength of the interaction with the external field, and $\hat{a}^\dagger$ and $\hat{a}$ are bosonic creation and annihilation operators, respectively. Moreover, using function $f(t)$ we are able to define the shape of the envelope of external field. For simplicity, we shall assume that the excitation is of the constant amplitude and hence, we put $f(t) = 1$. Obviously, one should keep in mind that models discussed here concern a real physical situation (although they naturally involve certain limitation) and all operators, appearing in Eq. (1), are defined in the infinite-dimensional Hilbert space.

Let us express the wave function for our system in the Fock basis as

$$|\psi(t)\rangle = \sum_{n=0}^{\infty} C_n(t)|n\rangle \tag{2}$$

where the complex probability amplitude $C_n(t)$ corresponds to the nth Fock state $|j\rangle$ and determines its time evolution. This wave function obeys the following Schrödinger equation

$$i\frac{d}{dt}|\psi(t)\rangle = \left(\frac{\chi}{2}(\hat{a}^\dagger)^2\hat{a}^2 + \epsilon(\hat{a}^\dagger + \hat{a})\right)|\psi(t)\rangle \tag{3}$$

for the Hamiltonian (1). Applying the standard procedure to our wavefunction (2) and Hamiltonian (1), we obtain a set of equations for the probability amplitudes $C_n(t)$. They are of the form

$$i\frac{d}{dt}C_n(t) = \frac{\chi}{2}n(n-1)C_n(t) + \epsilon[\sqrt{n}C_{n-1}(t) + \sqrt{n+1}C_{n+1}(t)] \tag{4}$$

where n corresponds to the n-photon Fock state. Obviously, one should keep in mind that we deal with the infinite-dimensional Hilbert space and so the set of equations for $C_n(t)$, given by (4), is infinite, too. However, our aim here is to show that under special conditions our system behaves as one defined in the FD Hilbert space. The first step is to assume that the external excitation is weak ($\epsilon \ll \chi$). As a consequence, we assume a perturbative approach. Moreover, and this is the main point of our considerations, the part of Hamiltonian (1) corresponding to the nonlinear evolution of the system

$$\hat{H}_{\mathrm{NL}} = \frac{\chi}{2}(\hat{a}^\dagger)^2\hat{a}^2 \tag{5}$$

produces degenerate states corresponding to $n = 0$ and $n = 1$. As we take into account not only the first part of Hamiltonian (1) but also the second part, we see that a resonance arises between the interaction described by the latter and the degenerate states generated by $\hat{H}_{\mathrm{NL}}$. This resonance and the weak interaction lead to a situation when the system dynamics becomes of the closed form and cuts some subspace of states out of all the n-photon Fock states. As a consequence, assuming that the dynamics of the physical process starts from vacuum $|0\rangle$, the evolution of the system is restricted to the states $|0\rangle$ and $|1\rangle$ solely. This situation resembles in some sense the problem of two degenerate atomic levels coupled by a zero-frequency field, where this resonant coupling selects, from the whole set of atomic levels, only those of them that lead to a closed system dynamics. For the case discussed here our system evolution corresponds to the two-level atom problem, where the interaction with remaining atomic states can be treated as a negligible perturbation [34]. Obviously, one should note that the character of the resonances commonly discussed in various papers, where the cavity field and the difference between the energies of the atomic levels (or cavity frequencies) have identical values, is different than that of those discussed here.

Thus, we write following equations of motion

$$\begin{aligned} i\frac{d}{dt}C_0(t) &= \epsilon C_1(t) \\ i\frac{d}{dt}C_1(t) &= \epsilon[C_0(t) + \sqrt{2}C_2(t)] \\ i\frac{d}{dt}C_2(t) &= \chi C_2(t) + \epsilon[\sqrt{2}C_1(t) + \sqrt{3}C_3(t)] \\ &\vdots \end{aligned} \tag{6}$$

for the probability amplitudes corresponding to the system discussed here. Since we have assumed $\epsilon \ll \chi$, Eqs. (6) indicate that the amplitude $C_n(t)$ rapidly

oscillates in comparison with the amplitudes $C_N(t)$ if $n > N$. Hence, analogously to the description of driven atomic systems within the rotating-wave approximation (RWA) [34], we neglect the influence of the probability amplitudes $C_n(t)$ for $n \geq 2$. Therefore, the dynamics of our system can be described by the following set of two equations

$$\begin{aligned} i\frac{d}{dt}C_0(t) &= \epsilon C_1(t) \\ i\frac{d}{dt}C_1(t) &= \epsilon C_0(t) \end{aligned} \tag{7}$$

and their solution

$$\begin{aligned} C_0(t) &= i\cos(\epsilon t) \\ C_1(t) &= \sin(\epsilon t) \end{aligned} \tag{8}$$

where we have assumed that the system starts its evolution from vacuum $|0\rangle$. Clearly, this result resembles that for a two-level atom in an external field [34] and the dynamics of the system exhibits well-known oscillatory behavior. This result is identical to that derived for the simplest case (i.e., for $N = s + 1 = 2$) of the FD generalized coherent states discussed by us in the first part of this work [1]. Of course, one should keep in mind that the set of Eqs. (7) gives zero-order solutions in perturbative treatment. As a consequence, the FD coherent states can be produced by the system discussed within the error following from this approximation.

The preceding result concerns the situation where the external excitation is characterized by a constant envelope: $f(t) = 1$. For the general case, the solution can be obtained easily, applying the same procedure as for a resonantly driven two-level atom [34]. Then, the general solution can be expressed as

$$\begin{aligned} C_0(t) &= i\cos\Theta(t) \\ C_1(t) &= \sin\Theta(t) \end{aligned} \tag{9}$$

where the symbol $\Theta(t)$ denotes the pulse area and is defined to be

$$\Theta(t) = \epsilon \int_0^t f(t')\,dt' \tag{10}$$

B. *N*-Dimensional Coherent States

It is possible to extend our considerations to the case of the FD Hilbert space with arbitrary dimension. Similarly as in [24] we introduce a system comprising

a nonlinear oscillator with the Nth-order nonlinearity and governed by the following Hamiltonian:

$$\hat{H}(t) = \frac{\chi}{N}(\hat{a}^\dagger)^N \hat{a}^N + \epsilon(\hat{a}^\dagger + \hat{a})f(t) \tag{11}$$

The first term in (11) is the N-photon Kerr Hamiltonian [35], giving rise to optical bistability, and χ is related to the $(2N-1)$-order susceptibility of the medium. The second term in (11) represents coherent pumping modulated by classical function $f(t)$. Similarly, as in the previous section, we assume that the excitation has a constant envelope: i.e. $f(t) = 1$. Applying the procedure analogous to that described in the previous section we get the following equations

$$\begin{aligned}
i\frac{d}{dt}C_0(t) &= \epsilon C_1(t) \\
i\frac{d}{dt}C_1(t) &= \epsilon[C_0(t) + \sqrt{2}C_2(t)] \\
&\vdots \\
i\frac{d}{dt}C_{N-1}(t) &= \epsilon[\sqrt{N-1}C_{N-2}(t) + \sqrt{N}C_N(t)] \\
i\frac{d}{dt}C_N(t) &= \chi(N-1)!C_N(t) + \epsilon[\sqrt{N}C_{N-1}(t) + \sqrt{N+1}C_{N+1}(t)] \\
&\vdots
\end{aligned} \tag{12}$$

for the probability amplitudes $C_n(t)$. As is assumed that $\epsilon \ll \chi$, we can exclude all probability amplitudes $C_n(t)$ for $n > N-1$. Hence, we get the set of equations in the closed form and the dynamics of the system is practically restricted within a space spanned over N Fock states. For instance, for $N = 3$ Eqs. (12) reduce to

$$\begin{aligned}
i\frac{d}{dt}C_0(t) &= \epsilon C_1(t) \\
i\frac{d}{dt}C_1(t) &= \epsilon[C_0(t) + \sqrt{2}C_2(t)] \\
i\frac{d}{dt}C_2(t) &= \epsilon\sqrt{2}C_1(t)
\end{aligned} \tag{13}$$

and have the solutions

$$C_0(t) = \frac{1}{3}[2 + \cos(\sqrt{3}\epsilon t)]$$
$$C_1(t) = \frac{-i}{\sqrt{3}}\sin(\sqrt{3}\epsilon t)$$
$$C_2(t) = \frac{\sqrt{2}}{3}[\cos(\sqrt{3}\epsilon t) - 1] \tag{14}$$

Again, these solutions are identical to those derived by Miranowicz et al. [3] [compare Eq. (25) in Ref. 1]. Of course, we can write the equations for arbitrary value of the parameter N and hence, get the formulas for the probability amplitudes for the n-photon state expansion of the FD coherent state defined in the N-dimensional Hilbert space. In general, for any dimension N and arbitrary real periodic function $f(t)$ with the period T, we find that the system evolves at $t = kT$ into the state [33]

$$|\phi(kT)\rangle = \sum_{n=0}^{N-1} C_n|n\rangle + \epsilon C_N|N\rangle + \mathcal{O}(\epsilon^2) \tag{15}$$

where the superposition coefficients $C_n = \langle n|\phi(kT)\rangle$ for $n = 0, \ldots, N-1$ are given by

$$C_n = \frac{(N-1)!}{N}\frac{(-1)^n}{\sqrt{n!}}\sum_{m=0}^{N-1}\exp(ikx_m\epsilon c_0)\frac{\mathrm{He}_n(x_m)}{[\mathrm{He}_{N-1}(x_m)]^2} \tag{16}$$

and for $n = N$ are

$$C_N = \sqrt{N}BC_{N-1} = (-1)^{N-1}B\sqrt{\frac{(N-1)!}{N}}\sum_{m=0}^{N-1}\frac{\exp(ikx_m c_0\epsilon)}{\mathrm{He}_{N-1}(x_m)} \tag{17}$$

Here, $x_m \equiv x_m^{(N)}$ are the roots of the Hermite polynomial of order N, $\mathrm{He}_N(x_m) = 0$. The coefficient B is defined to be

$$B = \frac{1}{2\pi}\sum_{n=-\infty}^{\infty}\frac{c_n}{n+a} \tag{18}$$

where

$$c_n = \int_0^T f(t)\exp\left(-i2\pi n\frac{t}{T}\right)dt \tag{19}$$

is the Fourier transform and $a = T\chi(N-1)!/(2\pi)$. In the first part of this work [see Eq. (20) in Ref. 1], we have defined the N-dimensional generalized coherent states to be ($N \equiv s+1$)

$$|\alpha\rangle_{(s)} = \exp\left[\alpha\hat{a}_s^\dagger - \alpha^*\hat{a}_s\right]|0\rangle \tag{20}$$

in terms of the FD annihilation and creation operators

$$\hat{a}_s = \sum_{n=1}^{s}\sqrt{n}|n-1\rangle\langle n|, \qquad \hat{a}_s^\dagger = \sum_{n=1}^{s}\sqrt{n}|n\rangle\langle n-1| \tag{21}$$

respectively. On omitting terms proportional to ϵ, we explicitly show that

$$|\alpha = -ikc_0\epsilon\rangle_{(s)} = |\phi(kT)\rangle + \mathcal{O}(\epsilon) \tag{22}$$

Thus, the state created in the process governed by the Hamiltonian (11) is the finite-dimensional coherent state.

III. NUMERICAL CALCULATIONS

It is possible to verify our considerations performing appropriate numerical calculations. As, we have excluded here all damping processes, the dynamics of our system can be described by the unitary evolution. Therefore, we define the unitary evolution operator

$$\hat{U} = \exp\left\{-i\left[\frac{\chi}{N}(\hat{a}^\dagger)^N\hat{a}^N + \epsilon(\hat{a}^\dagger + \hat{a})\right]t\right\} \tag{23}$$

on the basis of Hamiltonian (1). In (23) all operators are defined in the N-dimensional Hilbert space. For example, for $N = 4$ the wavefunction $|\psi(t)\rangle$ can be expressed as

$$|\psi(t)\rangle = \begin{pmatrix} C_0(t) \\ C_1(t) \\ C_2(t) \\ C_3(t) \end{pmatrix} \tag{24}$$

whereas the annihilation and creation operators ($\hat{a}$ and $\hat{a}^\dagger$, respectively) can be represented by the following matrices

$$\hat{a} = \begin{bmatrix} 0 & 1 & 0 & 0 \\ 0 & 0 & \sqrt{2} & 0 \\ 0 & 0 & 0 & \sqrt{3} \\ 0 & 0 & 0 & 0 \end{bmatrix}, \qquad \hat{a}^\dagger = \begin{bmatrix} 0 & 0 & 0 & 0 \\ 1 & 0 & 0 & 0 \\ 0 & \sqrt{2} & 0 & 0 \\ 0 & 0 & \sqrt{3} & 0 \end{bmatrix} \tag{25}$$

which are special cases of (21) for $s = 3$. As a consequence, the Hamiltonian (11) can be constructed using the Eq. (25) matrix representations. Next we should construct the evolution operator $\hat{U}$. Since this operator is in the form of the matrix exponential, it could be necessary to solve eigensystem with the Hamiltonian $\hat{H}$. This step can be easily done by applying standard numerical procedures [36]. Obviously, other methods of calculating matrix exponentials can be utilized as well. For instance, the Taylor series expansion of the operator $\hat{U}$ can be helpful in this case. Using the evolution operator derived, we are in a position to generate the wave function for arbitrary time t.

Thus, assuming that the system starts its evolution from vacuum $|0\rangle$, we act (numerically) $\hat{U}$ on the wavefunction of the system represented by the N-element vector

$$|\psi(0)\rangle = \begin{pmatrix} 1 \\ 0 \\ 0 \\ \vdots \\ 0 \end{pmatrix} \tag{26}$$

and obtain the vector representation of the desired wavefunction $|\psi(t)\rangle$ corresponding to the state of our system for the time t:

$$|\psi(t)\rangle = \hat{U}|\psi(0)\rangle \tag{27}$$

It would be interesting to compare Eqs. (26) and (27) with the Glauber definition of the coherent state [37]

$$|\alpha >_{(\infty)} = \hat{D}(\alpha, \alpha^*)|0 > \tag{28}$$

where the Glauber displacement operator $\hat{D}(\alpha, \alpha^*)$ is defined as

$$\hat{D}(\alpha, \alpha^*) = \exp(\alpha\hat{a}^\dagger - \alpha^*\hat{a}) \tag{29}$$

It is seen that the operator $\hat{U}$ defined in Eq. (23) plays the same role as the Glauber displacement operator $\hat{D}(\alpha, \alpha^*)$. Obviously, it should be kept in mind that $\hat{U}$ is defined in the FD Hilbert space, contrary to the definition of $\hat{D}$ in which the space has been assumed to be infinite-dimensional. Therefore, we conclude that within the assumptions introduced here we deal with the following correspondence:

$$\hat{U}\big|_{\infty} \leftrightarrow \hat{D} \tag{30}$$

To check our analytical formulas derived in the previous sections, we shall concentrate on the two cases where the parameter $N = 2, 3$. First, for $N = 2$ we apply the evolution operator

$$\hat{U} = \exp\left\{-i\left[\frac{\chi}{2}\left(\hat{a}^\dagger\right)^2\hat{a}^2 + \epsilon\left(\hat{a}^\dagger + \hat{a}\right)\right]t\right\} \tag{31}$$

and the results are shown in Fig. 1, which also shows the analytical results for the probabilities of finding the system in vacuum $|0\rangle$ and one-photon $|1\rangle$ states together with those of the numerical method. The analytical and numerical results agree almost perfectly and for these two cases we obtain the well-known oscillatory behavior. Obviously, one should keep in mind that the interaction with the external field is weak ($\epsilon \ll \chi$) and we assume that $\epsilon = \pi/50$ contrary to $\chi = 1$.

Analogously, for $N = 3$ three states are involved in the system evolution. For this case the evolution operator should be of the form

$$\hat{U} = \exp\left(-i\left[\frac{\chi}{3}\left(\hat{a}^\dagger\right)^3\hat{a}^3 + \epsilon\left(\hat{a}^\dagger + \hat{a}\right)\right]t\right) \tag{32}$$

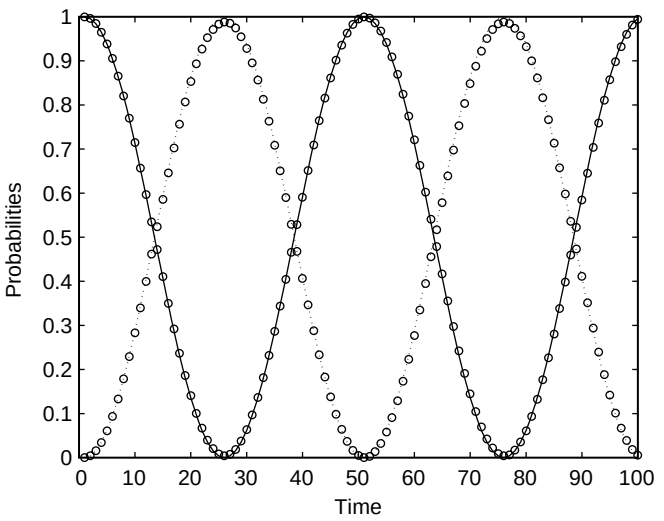

Figure 1. Time-evolution of the probabilities (analytical results) for vacuum $|0\rangle$ (solid curve) and one-photon state $|1\rangle$ (dotted curve) for the system with Kerr medium described by the Hamiltonian $\frac{1}{2}\chi(\hat{a}^\dagger)^2\hat{a}^2$. The circle marks denote numerical results. The pulse strength is $\epsilon = \pi/50$.

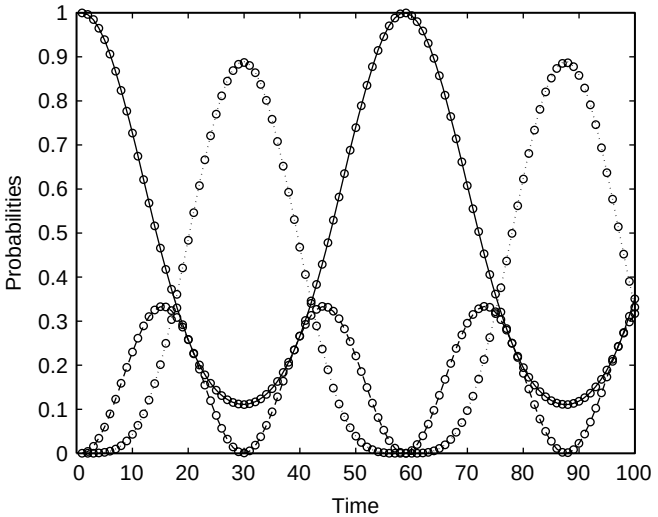

Figure 2. The same as in Fig. 1 but for the system with the Kerr medium described by $\frac{1}{3}\chi(\hat{a}^\dagger)^3\hat{a}^3$. Analytical results for: vacuum $|0\rangle$ (solid curve), one-photon state $|1\rangle$ (dashed curve), and two-photon state $|2\rangle$ (dotted curve). The numerical results are marked by circles.

whereas the parameters ϵ and χ are the same as for the case of $N = 2$. Similarly as for $N = 2$, the agreement of the analytical results with their numerical counterparts is very good. Thus, Fig. 2 depicts oscillations of the probabilities for the states $|0\rangle$, $|1\rangle$ and $|2\rangle$. The amplitude of the oscillations for one-photon state $|1\rangle$ is considerably smaller than that for other two states involved in the evolution. This fact agrees with the properties of the Fock expansion of the FD coherent state [3].

Applying the numerical method described here we, can also estimate the error of the perturbative treatment introduced in the previous sections. In Fig. 3 we show the probability corresponding to the three-photon state $|3\rangle$ as a function of time. It is seen that the probability oscillates in a similar way as those corresponding to the states $|0\rangle$, $|1\rangle$, and $|2\rangle$. However, the amplitudes of the oscillations differ significantly. Thus, the probability for the state $|3\rangle$ oscillates between 0 and $\sim 1.2 \times 10^{-3}$ whereas that corresponding to the state $|1\rangle$ changes its value from 0 to ~ 0.3 (Fig. 2). We see that the dynamics of the system described by the Hamiltonian (1) is restricted in practice to the closed set of the Fock states. This fact and the behavior of the probabilities shown in Figs. 1 and 2 proves that the quantum states generated by the system described by Hamiltonian (1) are very close to the FD coherent states described in Ref. 3.

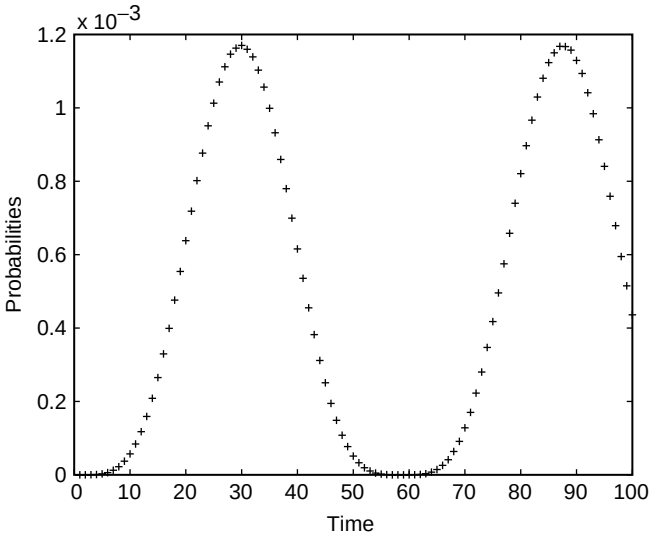

Figure 3. The probability for the three-photon state $|3\rangle$ obtained from the numerical calculations. All parameters are the same as for Fig. 2.

IV. STATE GENERATION IN DISSIPATIVE SYSTEMS

It is obvious that in the real physical situations we are not able to avoid dissipation processes. For dissipative systems, we cannot take an external excitation too weak (the parameter ϵ cannot be too small) since the field interacting with the nonlinear oscillator could be completely damped and hence, our model could become completely unrealistic. Moreover, the dissipation in the system leads to a mixture of the quantum states instead of their coherent superpositions. Therefore, we should determine the influence of the damping processes on the systems discussed here. To investigate such processes we can utilize various methods. For instance, the quantum jumps simulations [38] and quantum state diffusion method [39] can be used. Description of these two methods can be found in Ref. 40, where they were discussed and compared. Another way to investigate the damping processes is to apply the approach based on the density matrix formalism. Here, we shall concentrate on this method [12,41,42].

As we have discussed earlier, the time dependence of the envelope of external excitation does not influence the final analytical result discussed here. The parameter $f(t)$ appears only inside the integral determining the external pulse area $\theta(t)$ [Eq. (10)]. Therefore, we can assume without losing generality of our considerations that the excitation is in the form of a series of ultrashort

pulses. Then the function $f(t)$ can be modeled by the Dirac delta functions as

$$f(t) = \sum_{k=0}^{\infty} \delta(t - kT) \tag{33}$$

where T is a time between two subsequent pulses. For such situation the time evolution of the system can be divided into two different stages. When the damping processes are absent, the first stage is a "free" evolution of the nonlinear oscillator determined by the unitary evolution operator

$$\hat{U}_{\mathrm{NL}} = \exp\left[-i\frac{\chi T}{2}\left(\hat{a}^{\dagger}\right)^2\hat{a}^2\right] \tag{34}$$

We assume the simplest case, where the time evolution is restricted to two quantum states, $|0\rangle$ and $|1\rangle$. The second stage of the time-evolution of the system is caused by its interaction with an infinitely short external pulse. This part of the evolution is described by the second term of the Hamiltonian (1) and can be described by the following evolution operator

$$\hat{U}_K = \exp[-i\epsilon(\hat{a}^{\dagger} + \hat{a})] \tag{35}$$

The overall evolution of the system can be described as a subsequent action of the operators $\hat{U}_{\mathrm{NL}}$ and $\hat{U}_K$ on the initial state. When we take into account losses during the time evolution between two pulses we should solve the appropriate master equation. It can be written as

$$\frac{d\rho}{dt} = -i\frac{\chi}{2}\left(\hat{a}^{\dagger}\right)^2\hat{a}^2 + \frac{\gamma}{2}\left(2\hat{a}\rho\hat{a}^{\dagger} - \hat{a}^{\dagger}\hat{a}\rho - \rho\hat{a}^{\dagger}\hat{a}\right) \tag{36}$$

The solution of this master equation in the Fock number states basis is given by [41,42]

$$\begin{aligned}\langle p|\rho(t+T)|q\rangle = {} & \exp\left[i\frac{\vartheta}{2}(p-q)\right]\frac{[g(T)]^{(p+q)/2}}{\sqrt{p!q!}}\sum_{n=p}^{\infty}\langle n|\rho(t)|n-(p-q)\rangle \\ & \times\frac{\sqrt{n![n-(p-q)]!}}{(n-p)!}(1+i\delta)^{-(n-p)}[1-g(T)]^{(n-p)}\end{aligned} \tag{37}$$

where

$$\begin{aligned}\delta &= \frac{p-q}{\kappa} \\ g(T) &= \exp[-\kappa\vartheta - i\vartheta(p-q)] \\ \kappa &= \frac{\gamma}{\chi} \\ \vartheta &= \chi T\end{aligned} \tag{38}$$

The symbol γ appearing above is a damping constant responsible for the cavity loss. Thus, solving the master equation (36), we can determine the probabilities of finding the system in an arbitrary n-photon state. Of course, the evolution during single ultrashort, external pulse is determined by the operator $\hat{U}_K$ as before.

Thus Fig. 4 shows probabilities for vacuum $|0\rangle$ and one-photon $|1\rangle$ state for weak external excitation once more. We have chosen two values of the damping

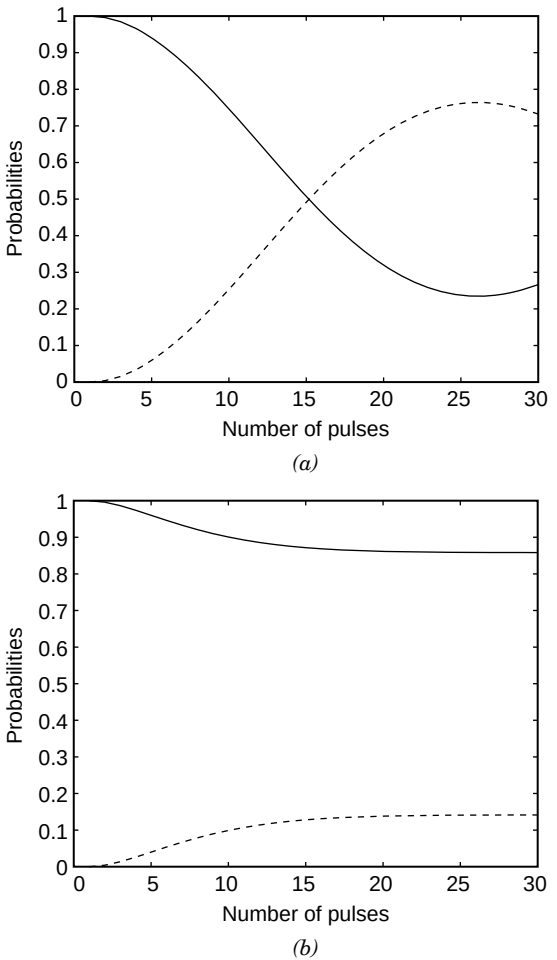

Figure 4. The probabilities for vacuum $|0\rangle$ (solid curve) and one-photon state $|1\rangle$ (dashed curve) for the Kerr medium described by $\frac{1}{2}\chi(\hat{a}^\dagger)^2\hat{a}^2$. The damping constants are (a) $\gamma = 0.01$ and (b) $\gamma = 0.1$. The pulse strength in $\epsilon = \pi/50$ and the time $T = \pi$.

parameter: $\gamma = 0.1$ (Fig. 4a) and $\gamma = 0.01$ (Fig. 4b). It is seen that for weak damping we observe slow oscillations of the probabilities, similarly as for the case of the quantum nonlinear oscillator without dissipation. Moreover, for ($\gamma = 0.01$) the amplitude of the oscillations reaches over 75% of its value for the case of $\gamma = 0$. As a consequence, we are able to get the field very close to the desired quantum state. However, as the damping increases the situation changes considerably. For $\gamma = 0.1$ the oscillations of the probabilities vanish, and the resulting state is far from the FD coherent state defined in the two-dimensional Hilbert space. We see that the dissipation in the system can drastically lower the effectiveness of producing the FD coherent states. Nevertheless, one should keep in mind one of the crucial points of our considerations: the assumption of weak external excitation. Hence, we hope that for sufficiently weak damping, our system can evolve to a state that is very close to the quantum state of our interest.

V. GENERALIZED METHOD FOR FD SQUEEZED VACUUM GENERATION

The method described in the previous sections can be easily generalized to be useful for generation of various FD quantum-optical states different from the FD coherent state. Thus, we shall show an example of how to adapt our method to generate the FD squeezed vacuum [10]. In the first part of this work [see Eq. (78) in Ref. 1], we have defined the $(s+1)$-dimensional generalized squeezed vacuum to be

$$|\xi\rangle_{(s)} = \exp\left[\frac{\xi}{2}(\hat{a}_s^\dagger)^2 - \frac{\xi^*}{2}\hat{a}_s^2\right]|0\rangle \tag{39}$$

where $\xi = |\xi|\exp(i\phi)$ is the complex squeeze parameter, whereas $\hat{a}_s$ and $\hat{a}_s^\dagger$ are, respectively, the FD annihilation and creation operators defined by (21). Since the properties of the FD squeezed vacuum have already been discussed [1], here we shall concentrate on the method of its generation.

We assume that our system consists of a Kerr medium of the $(s+1)$th-order nonlinearity and a parametric amplifier driven by a series of ultrashort external classical light pulses. Thus, the Hamiltonian describing our system can be written in the interaction picture as

$$\hat{H} = \frac{\chi}{(s+1)}(\hat{a}^\dagger)^{s+1}\hat{a}^{s+1} + \epsilon(\hat{a}^{\dagger 2} + \hat{a}^2)f(t) \tag{40}$$

where the first term describes the $(s+1)$-photon nonlinear oscillator (Kerr medium) as in (11), and the second term represents a pulsed parametric

oscillator modulated by $f(t)$, given by (33). This situation differs from those discussed in the previous sections in one important point, namely, in the character of external excitation. For this case we assume that the oscillator is driven by a second-order parametric process instead of linear excitation involved in the FD coherent-state generation. The model, described by (40) with the two-photon Kerr Hamiltonian, was studied by Milburn and Holmes [42] in their analysis of quantum coherence and classical chaos. The system for $s = 1$ and $f(t) = 1$ is referred to as the *Cassinian oscillator* and has been analyzed in the context of squeezing by, for instance, Gerry et al. [43] and DiFilippo et al. [44]. The time evolution of the system leads to the generation of the quantum states that differ significantly from the FD coherent states. In a similar way as for the generation of the latter, we assume that the excitation is weak ($\epsilon \ll \chi$), and we can apply the perturbative treatment again. As a consequence, we get the formula for the n-photon state expansion

$$|\phi(t)\rangle = \sum_{n=0}^{\sigma} C_{2n}(t)|2n\rangle + \epsilon C_{2\sigma+2}(t)|2\sigma+2\rangle + O(\epsilon^2) \tag{41}$$

where the expansion coefficients $C_{2n} = \langle 2n|\phi(t)\rangle$ for $n = 0, \ldots, \sigma$ are

$$C_{2n}(t) = (-1)^n \frac{(2\sigma)!}{\sqrt{(2n)!}} \sum_{k=0}^{\sigma} \exp\,(ix_k\epsilon t) \frac{G_n(x_k)}{G_\sigma(x_k)G'_{\sigma+1}(x_k)} \tag{42}$$

and

$$C_{2\sigma+2}(t) = 2^{-\sigma-1}\sqrt{(2\sigma+1)(2\sigma+2)}\, C_{2\sigma}(t) \tag{43}$$

The functions $G_n(x)$ appearing above are the Meixner–Sheffer orthogonal polynomials; the prime sign in (42) denotes their x derivative, and $\sigma = \mathrm{Int}\,(s/2)$ is the integer part of $s/2$. If we omit the terms proportional to ϵ and higher, we get the expansion for the FD squeezed vacuum as

$$|\xi = -2\epsilon t\rangle_{(s)} = |\phi(t)\rangle + O(\epsilon) \tag{44}$$

So, our system evolves to a state close to the FD squeezed vacuum discussed in Ref. 10.

VI. SUMMARY

We have discussed one of the possible methods of generation of the FD quantum-optical states. Although, it is possible to generate n-photon Fock states

and then to construct a desired state from these states, we have concentrated on the generation schemes that can lead directly to the FD coherent states and FD squeezed vacuum. The method described here is based on the quantum nonlinear oscillator evolution. We have assumed that this oscillator is driven by an external excitation. We have shown that within the weak excitation regime we are able to generate with high accuracy the appropriate FD quantum state. Thus, depending on the character of the excitation, we can produce various FD states. For instance, for the linear excitation case we generate the FD coherent state, whereas for the parametric excitation, the FD squeezed vacuum can be achieved. Moreover, we have shown that the mechanism of the generation does not depend on the shape of the excitation envelope. Hence, various forms of the latter can be assumed depending of the feasibility of our model from the experimental or mathematical point of view.

For the situations discussed here appropriate analytical formulas for the generated states have been derived. These results have been obtained within the perturbation theory, and they agree with those of the n-photon expansion of the appropriate FD states. Moreover, we have proposed methods for checking our results numerically, and we have shown that numerical results agree very well with the analytical ones. Since we are not able to avoid dissipation processes from real physical situations, we have discussed damping processes two. It has been shown that although dissipation can play crucial role in the whole system dynamics and is able to destroy the effect of the FD state generation completely, under special assumptions these states can be achieved.

Acknowledgments

The authors thank J. Bajer, S. Dyrting, N. Imoto, M. Koashi, T. Opatrný, S. K. Özdemir, J. Peřina, K. Piątek, and R. Tanaś for their helpful discussions. A. M. is indebted to Prof. Nobuyuki Imoto for his hospitality and stimulating research at SOKEN.

References

1. A. Miranowicz, W. Leoński, and N. Imoto, "Quantum-optical states in finite-dimensional Hilbert space. I. General formalism," chapter 3, this volume.
2. V. Bužek, A. D. Wilson-Gordon, P. L. Knight, and W. K. Lai, *Phys. Rev. A* **45**, 8079 (1992).
3. A. Miranowicz, K. Piątek, and R. Tanaś, *Phys. Rev. A* **50**, 3423 (1994); T. Opatrný, A. Miranowicz, and J. Bajer, *J. Mod. Opt.* **43**, 417 (1996).
4. L. M. Kuang, F. B. Wang, and Y. G. Zhou, *Phys. Lett.* **183**, 1 (1993) and *J. Mod. Opt.* **42**, 1307 (1994); A. K. Pati and S. V. Lawande, *Phys. Rev. A* **51**, 5012 (1995); B. Roy and R. Roychoudhury, *Int. J. Theor. Phys.* **36**, 1525 (1997); B. Roy, *Modern Phys. Lett.* **11**, 963 (1997).
5. A. Miranowicz, T. Opatrný, and J. Bajer, in T. Hakioğlu and A. S. Shumovsky (Eds.), *Quantum Optics and the Spectroscopy of Solids: Concepts and Advances,* Ser. on *Fundamental Theories in Physics*, Kluwer, Dordrecht, 1997, p. 225.
6. B. Roy and P. Roy, *J. Phys. A* **31**, 1307 (1998).
7. J. Y. Zhu and L. M. Kuang, *Phys. Lett. A* **193**, 227 (1994).

8. D. Pegg and S. M. Barnett, *Phys. Rev. A* **41**, 3427 (1989); S. M. Barnett and D. T. Pegg, *J. Mod. Opt.* **36**, 7 (1989).
9. K. Wódkiewicz, P. L. Knight, S. J. Buckle, and S. M. Barnett, *Phys. Rev. A* **35**, 2567 (1987); P. Figurny, A. Orłowski, and K. Wódkiewicz, *Phys. Rev. A* **47**, 5151 (1993); D. J. Wineland, J. J. Bollinger, W. M. Itano, and D. J. Heinzen, *Phys. Rev. A* **50**, 67 (1994).
10. A. Miranowicz, W. Leoński, and R. Tanaś, in D. Han et al. (Eds.), NASA Conference Publication 206855, Greenbelt, MD, 1998, p. 91.
11. J. R Kukliński, *Phys. Rev. Lett.* **64**, 2507 (1990).
12. W. Leoński and R. Tanaś, *Phys. Rev. A* **49**, R20 (1994).
13. W. Leoński, S. Dyrting, and R. Tanaś, *J. Mod. Opt.* **44**, 2105 (1997).
14. J. Krause, M. O. Scully, T. Walther, and H. Walther, *Phys. Rev. A* **39**, 1915 (1989); M. Kozierowski and S. M. Chumakov, *Phys. Rev. A* **52**, 4194 (1995); P. Domokos, M. Brune, J. M. Raimond, and S. Haroche, *Eur. Phys. J.* **1**, 1 (1998).
15. G. M. D'Ariano, L. Maccone, M. G. A. Paris, and M. F. Sacchi, *Phys. Rev. A* **61**, 053817 (2000).
16. S. Bose, K. Jacobs, and P. L. Knight, *Phys. Rev. A* **56**, 4175 (1997).
17. D. T. Pegg, L. S. Philips, and S. M. Barnett, *Phys. Rev. Lett.* **81**, 1604 (1998).
18. M. Koniorczyk, Z. Kurucz, A. Gábris, and J. Janszky, *Phys. Rev. A* **62**, 013802 (2000); M. G. A. Paris, ibid. 033813; A. Miranowicz, S. K. Özdemir, N. Imoto, and M. Koashi, *Mtg. Abstr. Phys. Soc. Jpn.* **62**, 108 (2000).
19. M. Brune, S. Haroshe, V. Lefevre, J. M. Raimond, and N. Zagury, *Phys. Rev. Lett.* **65**, 976 (1990); M. J. Holland, D. F. Walls, and P. Zoller, *Phys. Rev. Lett.* **67**, 1716 (1991).
20. K. Vogel, V. M. Akulin, and W. P. Schleich, *Phys. Rev. Lett.* **71**, 1816 (1993); B. M. Garraway, B. Sherman, H. Moya-Cessa, P. L. Knight, and G. Kurizki, *Phys. Rev. A* **49**, 535 (1994); J. Janszky, P. Domokos, S. Szabó, and P. Adam, *Phys. Rev. A* **51**, 4191 (1995); M. Dakna, J. Clausen, L. Knöll, D.-G. Welsch, *Phys. Rev. A* **59**, 1658 (1999).
21. Special issue on quantum state preparation and measurement, *J. Mod. Opt.* **44** (11/12) (1997).
22. W. Leoński, *Phys. Rev. A* **54**, 3369 (1996).
23. A. Miranowicz, K. Piątek, and T. Opatrný, and R. Tanaś, *Acta. Phys. Slov.* **45**, 391 (1995).
24. W. Leoński, *Phys. Rev. A* **55**, 3874 (1997).
25. Y. Yamamoto, N. Imoto, and S. Machida, *Phys. Rev. A* **33**, 3243 (1986).
26. M. Kitagawa and Y. Yamamoto, *Phys. Rev. A* **34**, 3974 (1986).
27. A. D. Wilson-Gordon, V. Bužek, and P. L. Knight, *Phys. Rev. A* **44**, 7647 (1991).
28. B. Yurke and D. Stoller, *Phys. Rev. Lett.* **57**, 13 (1986).
29. P. Tombessi and A. Mecozzi, *J. Opt. Soc. Am. B* **4**, 1700 (1987).
30. A. Miranowicz, R. Tanaś, and S. Kielich, *Quantum Opt.* **2**, 253 (1990).
31. V. Bužek, G. Drobný, M. S. Kim, G. Adam, and P. L. Knight, *Phys. Rev. A* **56**, 2352 (1997).
32. S. Walentowitz and W. Vogel, *Phys. Rev. A* **55**, 4438 (1997); ibid. **58**, 679 (1998); S. Walentowitz, W. Vogel, and P. L. Knight, *Phys. Rev. A* **59**, 531 (1999).
33. A. Miranowicz, W. Leoński, S. Dyrting, and R. Tanaś, *Acta Phys. Slov.* **46**, 451 (1996).
34. L. Allen and J. H. Eberly, *Optical Resonance and Two-Level Atoms*, Wiley, New York, 1975.
35. C. C. Gerry, *Phys. Lett. A* **124**, 237 (1987); V. Bužek and I. Jex, *Acta Phys. Slov.* **39**, 351 (1989); M. Paprzycka and R. Tanaś, *Quantum Opt.* **4**, 331 (1992).
36. W. H. Press, B. P. Flannery, S. A. Teukolsky, and W. T. Vetterling, *Numerical Recipes. The Art of Scientific Computing*, Cambridge Univ. Press, 1986.

37. R. J. Glauber, *Phys. Rev. A* **131**, 2766 (1963).

38. J. Dalibard, Y. Castin, and K. Mölmer, *Phys. Rev. Lett.* **68**, 580 (1992); K. Mölmer, Y. Castin, and J. Dalibard, *J. Opt. Soc. Am.* **10**, 524 (1993); H. J. Carmichael, *An Open Systems Approach to Quantum Optics*, *Lecture Notes in Physics*, Series, Springer, Berlin, 1993.

39. N. Gisin and I. C. Percival, *J. Phys. A* **25**, 5677 (1992); ibid. **26**, 2233 and 2245 (1993).

40. B. M. Garraway and P. L. Knight, *Phys. Rev. A* **49**, 1266 (1994).

41. G. J. Milburn and C. A. Holmes, *Phys. Rev. Lett.* **56**, 2237 (1986).

42. G. J. Milburn and C. A. Holmes, *Phys. Rev. A* **44**, 4704 (1991).

43. C. C. Gerry and S. Rodrigues, *Phys. Rev. A* **36**, 5444 (1987); C. C. Gerry, R. Grobe, and E. R. Vrscay, *Phys. Rev. A* **43**, 361 (1991).

44. F. DiFilippo, V. Natarajan, K. R. Boyce, and D. E. Pritchard, *Phys. Rev. Lett.* **68**, 2859 (1992).

CORRELATED SUPERPOSITION STATES IN TWO-ATOM SYSTEMS

ZBIGNIEW FICEK

Department of Physics and Centre for Laser Science, The University of Queensland, Brisbane, Australia

RYSZARD TANAŚ

Nonlinear Optics Division, Institute of Physics, Adam Mickiewicz University, Poznań, Poland

CONTENTS

I. INTRODUCTION

The subject of correlated or collective spontaneous emission by a system of a large number of atoms was first proposed by Dicke [1], who introduced the concept of superradiance that the influence on each atomic dipole of the electromagnetic field produced by the other atomic dipoles could, in certain circumstances, cause each atom to decay with an enhanced spontaneous emission rate. The shortening of the atomic lifetime resulting from the interaction between N atoms could involve an enhancement of the intensity of radiation up to N^2.

The earliest investigations into correlated spontaneous emission from multiatom systems were motivated by attempts to detect coherent effects in the interaction of light with resonant atomic systems [2–4]. Another intrinsic feature of correlated spontaneous emission is that the emitted field exhibits strong nonlinear and directional behavior [5]. Moreover, the interest in correlated spontaneous emission lies in its close connection with the quantum and classical as well as with the spontaneous and stimulated aspects of atomic emission [6].

The phenomenon of collective emission is, in general, characteristic of macroscopic systems with a large number of emitting atoms confined a region much smaller than the optical wavelength. However, to understand collective effects from a macroscopic system of atoms, it is necessary to have a microscopic formulation of the interaction between the atoms and the electromagnetic field. Therefore, some previous work has been devoted to study collective effects in the case of few atoms [7–10]. Although a system of two or three atoms is admittedly an elementary model, it offers some advantages over the multiatom problem. Because of its simplicity, one obtains detailed and almost exact dynamical solutions with a variety of initial conditions. Many of the results predicted for the system of two or three atoms are analogous to phenomena that one could expect in multiatom systems. Early treatments of two or three-atom systems assumed a constant interatomic separation during the radiation process. When averaged over all such possible interatomic separations the collective effects average out, which made them difficult to observe experimentally.

In the 1990s, advances in trapping and cooling of small number of ions and neutral atoms greatly renewed the interest in collective effects in the interaction

of atoms with the electromagnetic field [11–13]. The trapped atoms are essentially motionless and lie at a known and controllable distance from one another, permitting qualitatively new studies of interatomic interactions not accessible in a gas cell or an atomic beam. The advantage of the trapped atoms is that it allows separation of collective effects, arising from the correlations between the atoms, from the single-atom effects. The question of to what extent the interatomic interactions can alter the dynamics of a multiatom system has become of interest as it contains information about the internal structure of the collective system.

A central topic in the current studies of collective effects is the theoretical and experimental investigation of the concept of correlated superposition states (entangled states) of a multiatom system [14]. The entangled states are linear superpositions of the internal states of the system that cannot be separated into product states of the individual atoms. This property is recognized as an entirely quantum-mechanical effect and has played a crucial role in many discussions of the nature of quantum measurements and, in particular, in the development of quantum communications. It has been realized that entangled states can have many practical applications, ranging from quantum computation [15,16], information processing [17,18], and cryptography [19] to atomic spectroscopy [20].

An example of entangled states in a two-atom system are the symmetric and antisymmetric states, which correspond to the symmetric and antisymmetric combinations of the atomic dipole moments, respectively [1,7,21]. These states are created by the dipole–dipole interaction between the atoms and are characterized by different spontaneous decay rates that the symmetric state decays with an enhanced, whereas the antisymmetric state decays with a reduced spontaneous emission rate [7]. For the case of two atoms confined into the region much smaller than the optical wavelength, the antisymmetric state does not decay at all, and therefore can be regarded as a decoherence-free state.

Another particularly interesting entangled states of the two-atom system are two-photon entangled states that are superpositions of only those states of the two-atom system in which both or neither of the atoms are excited. These states have been known for a long time as pairwise atomic states [22] or multiatom squeezed states [23]. The two-photon entangled states cannot be generated by a coherent laser field coupled to the atomic dipole moments. The states can be created by a two-photon excitation process with nonclassical correlations that can transfer the population from the two-atom ground state to the upper state without populating the intermediate one-photon states. An obvious candidate for the creation of the two-photon entangled states is a broadband squeezed vacuum field that is characterized by strong nonclassical two-photon correlations [24,25].

A number of theoretical methods have been proposed to prepare a two-atom system in an entangled state [26–29,31–34], and two-atom entangled states have

already been demonstrated experimentally using ultracold trap ions [35] and cavity quantum electrodynamic (QED) schemes [36]. The preparation of correlated superposition states in multiatom system has been performed using a quantum nondemolition (QND) measurement technique [37]. A mapping of entangled states of light on atoms has also been proposed [38,39] and experimentally demonstrated [40].

In this chapter, we review schemes proposed for the preparation of two 2-level atoms in an entangled state. Since we focus here on basis aspects of the atom–atom entanglement, we begin in Section II with a derivation of the master equation for two nonidentical two-level atoms interacting with the quantized three-dimensional vacuum field and driven by a single-mode coherent laser field. Sections III and IV are concerned mainly with techniques proposed for the preparation of a two-atom system in entangled states. The cases of maximally and nonmaximally entangled states are discussed. In Section V, we discuss methods of detecting of a particular entangled state. In Section VI, we describe the method of preparation of a two-atom system in two-photon entangled states. We also present a method of mapping of the entanglement of light on atoms.

II. MASTER EQUATION OF TWO COUPLED ATOMS

There are several theoretical approaches that can be used to calculate the dynamics and correlation properties of two atoms interacting with the quantized electromagnetic field. One of the methods is the wavefunction approach in which the dynamics are given in terms of the probability amplitudes [9]. Another approach is the Heisenberg equation method, in which equations of motion for the atomic and field operators are found from the Hamiltonian of a given system [10]. The most popular approach is the master equation method, in which the equation of motion is found for the density operator of an atomic system weakly coupled to a system regarded as a reservoir [7,8,41]. There are many possible realizations of reservoirs. The typical reservoir to which atomic systems are coupled is the quantized three-dimensional multimode vacuum field. The major advantage of the master equation is that it allows us to consider the evolution of the atoms plus field system entirely in terms of atomic operators.

A. Atomic System and Hamiltonian

We consider a system of two nonidentical and nonoverlapping atoms at positions $\mathbf{r}_1$ and $\mathbf{r}_2$, coupled to the quantized three-dimensional electromagnetic field. The initial state of the field is the product of a single-mode coherent state of a driving laser field, and the vacuum state of the rest of the modes. Each atom is assumed to have only two levels: the ground level $|g_i\rangle$ and the excited level $|e_i\rangle (i = 1, 2)$, separated by an energy $\hbar\omega_i = E_{e_i} - E_{g_i}$, and connected by an

electric dipole transition with the dipole matrix elements $\boldsymbol{\mu}_1$ and $\boldsymbol{\mu}_2$. The dipole transitions are represented by the dipole raising S_i^+ and lowering S_i^- operators defined as

$$S_i^+ = |e_i\rangle\langle g_i|, \quad S_i^- = |g_i\rangle\langle e_i| \tag{1}$$

and satisfying the relations

$$[S_i^+, S_j^-] = 2S_i^z\delta_{ij}, \quad S_i^+S_i^- + S_i^-S_i^+ = 1 \tag{2}$$

where $S_i^z = \frac{1}{2}(|e_i\rangle\langle e_i| - |g_i\rangle\langle g_i|)$ is the energy operator of the ith atom. If the ith atom is in its ground state $|g_i\rangle$, then $\langle S_i^z\rangle = -\frac{1}{2}$, whereas $\langle S_i^z\rangle = \frac{1}{2}$ if the atom is in its excited state.

The atoms interact with the quantized three-dimensional vacuum field and are also driven by a single-mode coherent laser field. We express the quantized multimode field in terms of the annihilation and creation operators $\hat{a}_{\mathbf{k}s}$ and $\hat{a}_{\mathbf{k}s}^\dagger$ of field mode $\mathbf{k}s$, which has wavevector $\mathbf{k}$, frequency ω_k, and polarization $\bar{\mathbf{e}}_{\mathbf{k}s}$. Thus, we write the electric field operator at position $\mathbf{r}$ in the form

$$\hat{\mathbf{E}}(\mathbf{r}, t) = i\hbar \sum_{\mathbf{k}s} \left(\frac{\omega_k}{2\epsilon_0\hbar V}\right)^{1/2} \bar{\mathbf{e}}_{\mathbf{k}s}(\hat{a}_{\mathbf{k}s}e^{i\mathbf{k}\cdot\mathbf{r}} - \hat{a}_{\mathbf{k}s}^\dagger e^{-i\mathbf{k}\cdot\mathbf{r}}) \tag{3}$$

where V is the normalization volume.

The total Hamiltonian of the interacting systems in the electric dipole and RWA approximations [42] is given by

$$H = H_A + H_F + H_I \tag{4}$$

where

$$H_A = \hbar\omega_1 S_1^z + \hbar\omega_2 S_2^z \tag{5}$$

is the Hamiltonian of the atoms

$$H_F = \sum_{\mathbf{k}s} \hbar\omega_k \left(\hat{a}_{\mathbf{k}s}^\dagger \hat{a}_{\mathbf{k}s} + \frac{1}{2}\right) \tag{6}$$

is the Hamiltonian of the field, and $H_I = H_v + H_L$ is the interaction Hamiltonian composed of two terms:

$$\begin{aligned} H_v &= -i\hbar \sum_{\mathbf{k}s} \{[\boldsymbol{\mu}_1 \cdot \mathbf{g}_{\mathbf{k}s}(\mathbf{r}_1)S_1^+ + \boldsymbol{\mu}_2 \cdot \mathbf{g}_{\mathbf{k}s}(\mathbf{r}_2)S_2^+]\hat{a}_{\mathbf{k}s}e^{i\omega_k t} - \text{H.c.}\} \\ H_L &= -\frac{1}{2}i\hbar[(\Omega_1 S_1^+ + \Omega_2 S_2^+)e^{i(\omega_L t + \phi_L)} - \text{H.c.}] \end{aligned} \tag{7}$$

The first term in Eq. (7) represents the interaction of the atoms with the quantized multimode vacuum field, while the second term is the interaction of the atoms with a classical driving laser field (H.c. denotes Hermitian conjugation). Here, ω_L and ϕ_L are the frequency and the phase of the driving field, respectively

$$\mathbf{g}_{\mathbf{k}s}(\mathbf{r}_i) = \left(\frac{\omega_k}{2\epsilon_0 \hbar V}\right)^{1/2} \bar{\mathbf{e}}_{\mathbf{k}s}\, e^{i\mathbf{k}\cdot\mathbf{r}_i} \tag{8}$$

is the mode function of the three-dimensional vacuum field, evaluated at the position $\mathbf{r}_i$ of the ith atom, and

$$\Omega_i = \frac{\boldsymbol{\mu}_i \cdot \mathbf{E}_L e^{i\mathbf{k}_L\cdot\mathbf{r}_i}}{\hbar} \tag{9}$$

is the Rabi frequency of the ith atom with $\mathbf{E}_L$ and $\mathbf{k}_L$ denoting the amplitude and the wave vector of the driving field, respectively.

If the dipole moments of the atoms are parallel, the Rabi frequencies Ω_1 and Ω_2 are related by

$$\Omega_2 = \Omega_1 \frac{|\boldsymbol{\mu}_2|}{|\boldsymbol{\mu}_1|} e^{i\mathbf{k}_L\cdot\mathbf{r}_{12}} \tag{10}$$

where $\mathbf{r}_{12} = \mathbf{r}_2 - \mathbf{r}_1$ is the vector in the direction of the interatomic axis and $|\mathbf{r}_{12}| = r_{12}$ is the distance between the atoms. Thus, for two atoms with equal magnitudes of the dipole moments ($|\boldsymbol{\mu}_1| = |\boldsymbol{\mu}_2|$), the Rabi frequencies differ only by the phase factor $\exp(i\mathbf{k}_L \cdot \mathbf{r}_{12})$ arising from different positions of the atoms. However, the phase factor $\exp(i\mathbf{k}_L \cdot \mathbf{r}_{12})$ also depends on the orientation of the interatomic axis in respect to the direction of propagation of the driving field, and $\exp(i\mathbf{k}_L \cdot \mathbf{r}_{12})$ can be equal to one even for large interatomic separations r_{12}. This happens when the direction of propagation of the driving field is perpendicular to the interatomic axis, $\mathbf{k}_L \cdot \mathbf{r}_{12} = 0$. When $\mathbf{k}_L \cdot \mathbf{r}_{12} \neq 0$, the atoms are subject to different Rabi frequencies ($\Omega_1 \neq \Omega_2$).

B. Master Equation

Starting from the Hamiltonian (4), we can write the Schrödinger equation for the density operator ρ_T of the total system, two atoms plus the electromagnetic fields, as

$$\frac{\partial}{\partial t}\rho_T = \frac{1}{i\hbar}[H, \rho_T] \tag{11}$$

We are interested in the interaction of two atoms with the vacuum field, and therefore we transform Eq. (11) into the interaction picture with

$$\tilde{\rho}_T(t) = e^{i(H_A+H_F+H_L)t/\hbar}\rho_T\, e^{-i(H_A+H_F+H_L)t/\hbar} \tag{12}$$

and find that the transformed density operator satisfies the equation

$$\frac{\partial}{\partial t}\tilde{\rho}_T(t) = \frac{1}{i\hbar}[\tilde{H}_v(t), \tilde{\rho}_T(t)] \tag{13}$$

where

$$\tilde{H}_v(t) = e^{i(H_A+H_F+H_L)t/\hbar} H_v e^{-i(H_A+H_F+H_L)t/\hbar} \tag{14}$$

The master equation involves the so-called reduced density operator ρ describing the system of two atoms, which is obtained from the total density operator ρ_T by tracing over vacuum field (reservoir) states

$$\tilde{\rho}(t) = \mathrm{Tr}_F \tilde{\rho}_T(t) \tag{15}$$

We will assume that the interaction is turned on at $t = 0$, and no correlations exist between the atoms and the vacuum field at this initial time. Hence, we can write the density operator $\tilde{\rho}_T(0)$ as a product of the density operator of the atoms $\tilde{\rho}(0)$ and the density operator of the reservoir $\tilde{\rho}_F(0)$:

$$\tilde{\rho}_T(0) = \tilde{\rho}(0)\tilde{\rho}_F(0) \tag{16}$$

The properties of the vacuum field are specified by the density operator $\tilde{\rho}_F(0)$, from which correlation functions of the field operators can be determined as

$$\begin{aligned}
\langle \hat{a}_{\mathbf{k}s}\rangle &= \mathrm{Tr}_F[\rho_F(0)\hat{a}_{\mathbf{k}s}] = 0, \quad \langle \hat{a}^\dagger_{\mathbf{k}s}\rangle = \mathrm{Tr}_F[\rho_F(0)\hat{a}^\dagger_{\mathbf{k}s}] = 0 \\
\langle \hat{a}_{\mathbf{k}s}\hat{a}^\dagger_{\mathbf{k}'s'}\rangle &= \mathrm{Tr}_F[\rho_F(0)\hat{a}_{\mathbf{k}s}\hat{a}^\dagger_{\mathbf{k}'s'}] = \delta^3(\mathbf{k}-\mathbf{k}')\delta_{ss'} \\
\langle \hat{a}^\dagger_{\mathbf{k}s}\hat{a}_{\mathbf{k}'s'}\rangle &= \mathrm{Tr}_F[\rho_F(0)\hat{a}^\dagger_{\mathbf{k}s}\hat{a}_{\mathbf{k}'s'}] = 0 \\
\langle \hat{a}^\dagger_{\mathbf{k}s}\hat{a}^\dagger_{\mathbf{k}'s'}\rangle &= \mathrm{Tr}_F[\rho_F(0)\hat{a}^\dagger_{\mathbf{k}s}\hat{a}^\dagger_{\mathbf{k}'s'}] = 0 \\
\langle \hat{a}_{\mathbf{k}s}\hat{a}_{\mathbf{k}'s'}\rangle &= \mathrm{Tr}_F[\rho_F(0)\hat{a}_{\mathbf{k}s}\hat{a}_{\mathbf{k}'s'}] = 0
\end{aligned} \tag{17}$$

We now integrate Eq. (13), substitute the solution for $\tilde{\rho}_T(t)$ inside the commutator on the right-hand side (r.h.s.) of Eq. (13), and after taking the trace over the reservoir states, we find that the reduced density operator $\tilde{\rho}(t)$ satisfies the integrodifferential equation

$$\begin{aligned}
\frac{\partial}{\partial t}\tilde{\rho}(t) = &\frac{1}{i\hbar}\mathrm{Tr}_F[\tilde{H}_v(t), \tilde{\rho}(0)\tilde{\rho}_F(0)] \\
&-\frac{1}{\hbar^2}\int_0^t d\tau \mathrm{Tr}_F\{[\tilde{H}_v(t), [\tilde{H}_v(t-\tau), \tilde{\rho}_T(t-\tau)]]\}
\end{aligned} \tag{18}$$

In the derivation of Eq. (18), we have assumed that the total density operator $\tilde{\rho}_T(t)$ factorizes at $t = 0$. At later times correlations between the atoms and the field may arise as a result of the coupling through the Hamiltonian H_v. Here, we assume that the interaction between the atoms and the field is weak, which allows us to make the so-called Born approximation that ignores the back-reaction effects of the atoms on the field. Thus, $\tilde{\rho}_T(t-\tau) = \tilde{\rho}(t-\tau)\,\tilde{\rho}_F(t-\tau) = \tilde{\rho}(t-\tau)\tilde{\rho}_F(0)$ for all times $t - \tau > 0$. Moreover, we make the Markov approximation in which we assume that the correlation time of the field is much shorter than the timescale of radiation processes in the atoms. This allows us to replace $\tilde{\rho}(t-\tau)$ by $\tilde{\rho}(t)$.

Substituting Eq. (17) into Eq. (18) and after the Born–Markov approximation, the master equation takes the form

$$\frac{\partial}{\partial t}\tilde{\rho}(t) = -\frac{i}{\hbar}[H_c, \tilde{\rho}(t)] - \frac{1}{2}\sum_{i,j=1}^{2}\Gamma_{ij}(S_i^+ S_j^-\,\tilde{\rho}(t) + \tilde{\rho}(t)S_i^+ S_j^- - 2S_j^-\,\tilde{\rho}(t)S_i^+) \tag{19}$$

where

$$H_c = \hbar\delta_1 S_1^+ S_1^- + \hbar\delta_2 S_2^+ S_2^- + \hbar\Omega_{12}(S_1^+ S_2^- + S_2^+ S_1^-) \tag{20}$$

represents the vacuum-induced shifts of the atomic transition frequencies and the coherent interaction between the atoms. The parameter

$$\Gamma_i \equiv \Gamma_{ii} = \pi\sum_{\mathbf{k}s}|\boldsymbol{\mu}_i \cdot \mathbf{g}_{\mathbf{k}s}(\mathbf{r}_i)|^2\delta^3(\mathbf{k}-\mathbf{k}_0) \qquad (i = 1, 2) \tag{21}$$

describes the spontaneous emission rate of the ith atom resulting from the interaction of the individual atoms with the vacuum field, and

$$\Gamma_{ij} = \Gamma_{ji} = \pi\sum_{\mathbf{k}s}[\boldsymbol{\mu}_1 \cdot \mathbf{g}_{\mathbf{k}s}(\mathbf{r}_1)][\boldsymbol{\mu}_2^* \cdot \mathbf{g}_{\mathbf{k}s}^*(\mathbf{r}_2)]\delta^3(\mathbf{k}-\mathbf{k}_0), \quad (i \neq j) \tag{22}$$

are collective spontaneous emission rates arising from the coupling between the atoms through the vacuum field, and $k_0 = (k_1 + k_2)/2$.

The parameters

$$\delta_i = P\sum_{\mathbf{k}s}|\boldsymbol{\mu}_i \cdot \mathbf{g}_{\mathbf{k}s}(\mathbf{r}_i)|^2\left(\frac{1}{\omega_k + \omega_i} - \frac{1}{\omega_k - \omega_i}\right) \tag{23}$$

represent a part of the Lamb shift, induced by the first-order coupling in the Hamiltonian H_v, of the ground and excited states of the atoms, while

$$\Omega_{12} = P\sum_{\mathbf{k}s}[\boldsymbol{\mu}_1 \cdot \mathbf{g}_{\mathbf{k}s}(\mathbf{r}_1)][\boldsymbol{\mu}_2^* \cdot \mathbf{g}_{\mathbf{k}s}^*(\mathbf{r}_2)]\left(\frac{1}{\omega_k + \omega_0} + \frac{1}{\omega_k - \omega_0}\right) \tag{24}$$

represents the vacuum-induced coherent interaction between the atoms, P refers to the Cauchy principal value, and $\omega_0 = (\omega_1 + \omega_2)/2$ is the average frequency of the atomic transitions.

The parameters δ_i are usually considered to be absorbed into the atomic frequencies ω_1 and ω_2, by redefining the frequencies $\tilde{\omega}_i = \omega_i + \delta_i$ and are not explicitly included in the master equations. However, we are interested in the qualitative effects of the interactions between the atoms, and the role played by Ω_{12} in their dynamics. It is evident from Eq. (20) that the parameter Ω_{12} does not appear as a shift of the energies, but rather as a coherent coupling between the atoms. Thus, the interaction with the vacuum field not only gives rise to the dissipative spontaneous emission but also leads to a coherent coupling between the atoms.

We may find the explicit form of the collective parameters Γ_{12} and Ω_{12} by using the spherical representation of the unit orthogonal polarization vectors [41]

$$\begin{aligned}\bar{\mathbf{e}}_{\mathbf{k}1} &= (-\cos\theta\cos\phi, -\cos\theta\sin\phi, \sin\theta),\\ \bar{\mathbf{e}}_{\mathbf{k}2} &= (\sin\phi, -\cos\phi, 0)\end{aligned} \tag{25}$$

and changing the sum over $\mathbf{k}$ into an integral

$$\frac{1}{V}\sum_{\mathbf{k}s} \longrightarrow \frac{1}{(2\pi c)^3}\sum_{s=1}^{2}\int_0^\infty \omega_k^2\, d\omega_k \int_0^\pi \sin\theta\, d\theta \int_0^{2\pi} d\phi \tag{26}$$

where (k, θ, ϕ) denote spherical coordinates.

Substituting Eq. (26) into Eqs. (22) and (24), we obtain the following explicit expressions for the collective spontaneous emission rate

$$\begin{aligned}\Gamma_{12} = \frac{3}{4}\sqrt{\Gamma_1\Gamma_2}\Bigg\{&[1 - (\bar{\boldsymbol{\mu}} \cdot \bar{\mathbf{r}}_{12})^2]\frac{\sin(k_0 r_{12})}{k_0 r_{12}}\\ &+[1 - 3(\bar{\boldsymbol{\mu}} \cdot \bar{\mathbf{r}}_{12})^2]\left[\frac{\cos(k_0 r_{12})}{(k_0 r_{12})^2} - \frac{\sin(k_0 r_{12})}{(k_0 r_{12})^3}\right]\Bigg\}\end{aligned} \tag{27}$$

and the collective coupling between the atoms

$$\Omega_{12} = \frac{3}{4}\sqrt{\Gamma_1\Gamma_2}\left\{-[1-(\bar{\boldsymbol{\mu}}\cdot\bar{\mathbf{r}}_{12})^2]\frac{\cos(k_0 r_{12})}{k_0 r_{12}} + [1-3(\bar{\boldsymbol{\mu}}\cdot\bar{\mathbf{r}}_{12})^2]\left[\frac{\sin(k_0 r_{12})}{(k_0 r_{12})^2}+\frac{\cos(k_0 r_{12})}{(k_0 r_{12})^3}\right]\right\} \tag{28}$$

where $\bar{\boldsymbol{\mu}}$ is the unit vector along the dipole moments of the atoms, which we have assumed to be parallel ($\bar{\boldsymbol{\mu}} = \bar{\boldsymbol{\mu}}_1 = \bar{\boldsymbol{\mu}}_2$), and $\bar{\mathbf{r}}_{12}$ is the unit vector along the interatomic axis.

The collective parameters (27) and (28), which both depend on the interatomic separation, determine the collective properties of the two-atom system. The parameter (28) is the familiar retarded dipole–dipole interaction between the atoms [7,9,10,21], while Γ_{12} gives rise to the collective spontaneous emission. In Fig. 1, we plot $\Gamma_{12}/\sqrt{\Gamma_1\Gamma_2}$ and $\Omega_{12}/\sqrt{\Gamma_1\Gamma_2}$ as a function of r_{12}/λ_0, where λ_0 is the resonant wavelength. For large separations ($r_{12} \gg \lambda_0$) the parameters are very small ($\Gamma_{12} = \Omega_{12} \approx 0$). By contrast, for atomic separations much smaller than the resonant wavelength (the small sample model), the parameters reduce to

$$\Gamma_{12} = \sqrt{\Gamma_1\Gamma_2} \tag{29}$$

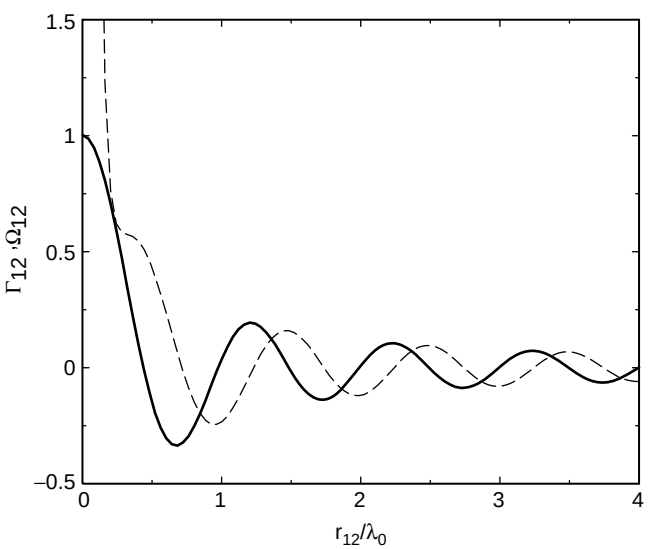

Figure 1. Collective parameters $\Gamma_{12}/\sqrt{\Gamma_1\Gamma_2}$ (solid line) and $\Omega_{12}/\sqrt{\Gamma_1\Gamma_2}$ (dashed line) as a function of r_{12}/λ_0 for $\bar{\boldsymbol{\mu}} \perp \bar{r}_{12}$.

and

$$\Omega_{12} \approx \frac{3\sqrt{\Gamma_1\Gamma_2}}{4(k_0 r_{12})^3}[1 - 3(\bar{\boldsymbol{\mu}} \cdot \bar{\mathbf{r}}_{12})^2] \tag{30}$$

For this case Ω_{12} corresponds to the quasistatic dipole–dipole interaction potential.

On transforming Eq. (19) into the Schrödinger picture, the master equation of the two-atom system takes the form

$$\begin{aligned}\frac{\partial}{\partial t}\rho = &-\frac{i}{\hbar}[H', \rho] \\ &-\frac{1}{2}\sum_{i,j=1}^{2}\Gamma_{ij}(S_i^+ S_j^- \rho + \rho S_i^+ S_j^- - 2S_j^- \rho S_i^+)\end{aligned} \tag{31}$$

where

$$H' = H_s + H_L + \hbar\Omega_{12}(S_1^+ S_2^- + S_2^+ S_1^-) \tag{32}$$

Equation (31) is the final form of the master equation that gives us an elegant description of the physics involved in the dynamics of two interacting atoms. The collective parameters Γ_{12} and Ω_{12}, which arise from the mutual interaction between the atoms, significantly modify the master equation of a two-atom system. The parameter Γ_{12} introduces a coupling between the atoms through the vacuum field that the spontaneous emission from one of the atoms influences the spontaneous emission from the other. The dipole–dipole interaction Ω_{12} introduces a coherent coupling between the atoms. Owing to the dipole–dipole interaction, the population is coherently transferred back and forth from one atom to the other. Here, the dipole–dipole interaction parameter Ω_{12} plays a role similar to that of the Rabi frequency in the atom–field interaction.

III. COLLECTIVE ATOMIC STATES

The presence of the collective parameters Γ_{12} and Ω_{12} introduces off-diagonal terms in the Hamiltonian H' and in the dissipative part of the master equation. This suggests that in the presence of the interaction between the atoms the bare atomic states are no longer the eigenstates of the two-atom system. We can diagonalize the Hamiltonian (32) with respect to the dipole–dipole interaction and find collective states of the two-atom system.

In the absence of the driving laser field and the dipole–dipole interaction, the basis states of the two-atom system are the four direct products states

$$|g_1\rangle|g_2\rangle, \quad |e_1\rangle|g_2\rangle, \quad |g_1\rangle|e_2\rangle, \quad |e_1\rangle|e_2\rangle \tag{33}$$

In the basis of these states the matrix representation of the Hamiltonian H', with $\Omega_1 = \Omega_2 = 0$, is given by

$$\frac{H'}{\hbar} = \begin{pmatrix} 0 & 0 & 0 & 0 \\ 0 & \omega_0 - \frac{1}{2}\Delta & \Omega_{12} & 0 \\ 0 & \Omega_{12} & \omega_0 + \frac{1}{2}\Delta & 0 \\ 0 & 0 & 0 & 2\omega_0 \end{pmatrix} \tag{34}$$

where $\omega_0 = \frac{1}{2}(\omega_1 + \omega_2)$ and $\Delta = \omega_2 - \omega_1$.

Evidently, in the presence of the dipole–dipole interaction the matrix (34) is not diagonal, which indicates that the product states (33) are not the eigenstates of the two-atom system. We will diagonalize the matrix (34) for the case of identical ($\Delta = 0$) as well as nonidentical ($\Delta \neq 0$) atoms to find eigenstates of the system and their energies.

A. Collective States of Two Identical Atoms

We begin by studying the collective properties of the system of two identical atoms ($\Delta = 0$). In order to find eigenstates and corresponding energies of the system, we diagonalize the matrix (34), and find that in the case of two identical atoms the eigenstates are given by [1,7]

$$\begin{aligned} |g\rangle &= |g_1\rangle|g_2\rangle \\ |s\rangle &= \frac{1}{\sqrt{2}}(|e_1\rangle|g_2\rangle + |g_1\rangle|e_2\rangle) \\ |a\rangle &= \frac{1}{\sqrt{2}}(|e_1\rangle|g_2\rangle - |g_1\rangle|e_2\rangle) \\ |e\rangle &= |e_1\rangle|e_2\rangle \end{aligned} \tag{35}$$

with corresponding energies

$$\begin{aligned} E_g &= 0 \\ E_s &= \hbar(\omega_0 + \Omega_{12}) \\ E_a &= \hbar(\omega_0 - \Omega_{12}) \\ E_e &= 2\hbar\omega_0 \end{aligned} \tag{36}$$

The eigenstates (35) are the collective states of two interacting atoms and are known in quantum optics as the Dicke states of the two-atom system [1]. We note here that the collective states $|s\rangle$ and $|a\rangle$ are an example of maximally entangled states of the two-atom system that the eigenstates of the system are linear superpositions which cannot be separated into product states of the individual atoms.

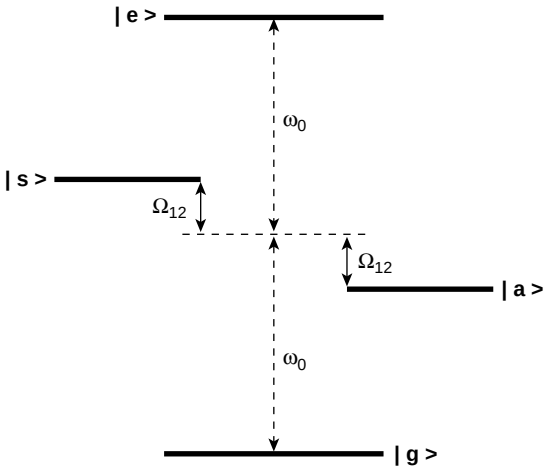

Figure 2. Collective states of two identical atoms. The dipole–dipole interaction Ω_{12} shifts the energies of the symmetric and antisymmetric states in the opposite directions.

The collective states are shown in Fig. 2. It is seen that in the collective states representation, the two-atom system behaves as a single four-level system with the ground state $|g\rangle$, the upper state $|e\rangle$, and two intermediate states: the symmetric state $|s\rangle$ and the antisymmetric state $|a\rangle$. The energies of the intermediate states depend on the dipole–dipole interaction and these states suffer a large shift when the interatomic separation is small.

From Eqs. (1) and (35), we find the following relations between the atomic and collective operators

$$S_1^+ = \frac{1}{\sqrt{2}}(A_{es} - A_{ea} + A_{sg} + A_{ag})$$
$$S_2^+ = \frac{1}{\sqrt{2}}(A_{es} + A_{ea} + A_{sg} - A_{ag}) \tag{37}$$

where $A_{ij} = |i\rangle\langle j|, \quad (i,j = e,a,s,g)$ are the collective operators that represent the energies $(i = j)$ of the collective states and transition dipole moments $(i \neq j)$.

Substituting the relations (37) into Eq. (31), we find that in terms of the collective operators, the master equation is given by

$$\begin{aligned}\frac{\partial}{\partial t}\rho = &-\frac{i}{\hbar}[H_{cs}, \rho] - \frac{1}{2}(\Gamma + \Gamma_{12})\{(A_{ee} + A_{ss})\rho + \rho(A_{ee} + A_{ss}) \\ &- 2(A_{se} + A_{gs})\rho(A_{es} + A_{sg})\} - \frac{1}{2}(\Gamma - \Gamma_{12})\{(A_{ee} + A_{aa})\rho \\ &+ \rho(A_{ee} + A_{aa}) - 2(A_{ae} + A_{ga})\rho(A_{ea} + A_{ag})\}\end{aligned} \tag{38}$$

where the Hamiltonian H_{cs} reads

$$\begin{aligned} H_{cs} = \hbar[2\omega_0 A_{ee} + (\omega_0 + \Omega_{12})A_{ss} + (\omega_0 - \Omega_{12})A_{aa}] \\ - \frac{\hbar}{2\sqrt{2}}\{(\Omega_1 + \Omega_2)[(A_{es} + A_{sg})e^{i(\omega_L t + \phi_L)} + \text{H.c.}] \\ + (\Omega_1 - \Omega_2)[(A_{ea} + A_{ag})e^{i(\omega_L t + \phi_L)} + \text{H.c.}]\} \end{aligned} \tag{39}$$

The master equation (38) provides the simplest example of the effects introduced by the coherent interaction of atoms with the radiation field. These effects include the shifts of the energy levels of the system, produced by the dipole–dipole interaction, and the phenomena of enhanced (superradiant) and reduced (subradiant) spontaneous emission, which appear in the changed damping rates to $\frac{1}{2}(\Gamma + \Gamma_{12})$ and $\frac{1}{2}(\Gamma - \Gamma_{12})$, respectively.

B. Collective States of Two Nonidentical Atoms

The collective states (35) are eigenstates of the system of two identical atoms. If the atoms are not identical, the situation becomes more complicated and we will discuss here some consequences of the fact that the atoms could have different transition frequencies and/or different spontaneous emission rates. When the atoms are nonidentical with different transition frequencies, the states (35) are no longer the eigenstates of the Hamiltonian (32). The diagonalization of the matrix (34) with $\Delta \neq 0$ leads to the following eigenstates [43]

$$\begin{aligned} |g\rangle &= |g_1\rangle|g_2\rangle \\ |s'\rangle &= \beta|e_1\rangle|g_2\rangle + \alpha|g_1\rangle|e_2\rangle \\ |a'\rangle &= \alpha|e_1\rangle|g_2\rangle - \beta|g_1\rangle|e_2\rangle \\ |e\rangle &= |e_1\rangle|e_2\rangle \end{aligned} \tag{40}$$

with energies

$$\begin{aligned} E_g &= 0 \\ E_{s'} &= \hbar\left(\omega_0 + \sqrt{\Omega_{12}^2 + \frac{1}{4}\Delta^2}\right) \\ E_{a'} &= \hbar\left(\omega_0 - \sqrt{\Omega_{12}^2 + \frac{1}{4}\Delta^2}\right) \\ E_e &= 2\hbar\omega_0, \end{aligned} \tag{41}$$

where

$$\alpha = \frac{w}{\sqrt{w^2 + \Omega_{12}^2}}, \quad \beta = \frac{\Omega_{12}}{\sqrt{w^2 + \Omega_{12}^2}} \tag{42}$$

and $w = \frac{1}{2}\Delta + \sqrt{\Omega_{12}^2 + \frac{1}{4}\Delta^2}$.

The energy system of two nonidentical atoms is similar to that of the identical atoms, with the ground state $|g\rangle$, the upper state $|e\rangle$, and two intermediate states $|s'\rangle$ and $|a'\rangle$. It is apparent that the effect of the frequency difference Δ on the collective atomic states is to increase the splitting between the intermediate levels, which now is equal to $\sqrt{\Omega_{12}^2 + \frac{1}{4}\Delta^2}$. However, the most dramatic effect of the detuning Δ is on the degree of entanglement of the states $|s'\rangle$ and $|a'\rangle$ that in the case of nonidentical atoms the states $|s'\rangle$ and $|a'\rangle$ are not maximally entangled states. For $\Delta = 0$ the states $|s'\rangle$ and $|a'\rangle$ reduce to the maximally entangled states $|s\rangle$ and $|a\rangle$, whereas for $\Delta \gg \Omega_{12}$ the entangled states $|s'\rangle$ and $|a'\rangle$ reduce to the product states $|e_1\rangle|g_2\rangle$ and $-|g_1\rangle|e_2\rangle$, respectively.

We follow exactly the same route as in the preceding section, and rewrite the master equation (31) in terms of the collective operators $A_{ij} = |i\rangle\langle j|$, where now the collective states are given in Eq. (40). First, we find that in the case of nonidentical atoms the atomic and collective operators are related by

$$\begin{aligned} S_1^+ &= \beta A_{es'} - \alpha A_{ea'} + \alpha A_{s'g} + \beta A_{a'g} \\ S_2^+ &= \alpha A_{es'} + \beta A_{ea'} + \beta A_{s'g} - \alpha A_{a'g} \end{aligned} \tag{43}$$

In terms of the collective operators A_{ij} the master equation can be written as

$$\frac{\partial}{\partial t}\rho = -\frac{i}{\hbar}[H_{na}, \rho] - \mathscr{L}_d\rho - \mathscr{L}_{nd}\rho \tag{44}$$

where

$$\begin{aligned} H_{na} = \hbar\Bigg\{ & 2\omega_0 A_{ee} + \left(\omega_0 + \sqrt{\Omega_{12}^2 + \frac{1}{4}\Delta^2}\right)A_{s's'} \\ & + \left(\omega_0 - \sqrt{\Omega_{12}^2 + \frac{1}{4}\Delta^2}\right)A_{a'a'}\Bigg\} \\ & - \frac{\hbar}{2}\{(\alpha\Omega_1 + \beta\Omega_2)[(A_{es'} + A_{s'g})e^{i(\omega_L t + \phi_L)} + \text{H.c.}]. \\ & + (\alpha\Omega_1 - \beta\Omega_2)[(A_{ea'} + A_{a'g})e^{i(\omega_L t + \phi_L)} + \text{H.c.}]\} \end{aligned} \tag{45}$$

is the Hamiltonian of the system in the collective states basis. The diagonal dissipative part of the master equation reads

$$\begin{aligned} \mathscr{L}_d\rho = & -\Gamma_{es'}(A_{ee}\rho + \rho A_{ee} - 2A_{s'e}\rho A_{es'}) \\ & - \Gamma_{s'g}(A_{s's'}\rho + \rho A_{s's'} - 2A_{gs'}\rho A_{s'g}) \\ & - \Gamma_{a'g}(A_{a'a'}\rho + \rho A_{a'a'} - 2A_{ga'}\rho A_{a'g}) \\ & - \Gamma_{ea'}(A_{ee}\rho + \rho A_{ee} - 2A_{a'e}\rho A_{ea'}) \end{aligned} \tag{46}$$

while the off-diagonal is given by

$$\begin{aligned}\mathscr{L}_{nd}\rho = &-\Gamma_{a's'}\{(A_{a's'}+A_{s'a'})\rho+\rho(A_{a's'}+A_{s'a'})\\ &-2A_{ga'}\rho A_{s'g}-2A_{gs'}\rho A_{a'g}\}\\ &-[\alpha\beta(\Gamma_1+\Gamma_2)+\Gamma_{12}](A_{s'e}\rho A_{s'g}+A_{gs'}\rho A_{es'})\\ &+[\alpha\beta(\Gamma_1+\Gamma_2)-\Gamma_{12}](A_{a'e}\rho A_{a'g}+A_{ga'}\rho A_{ea'})\\ &+[\Gamma_{a's'}-2(\beta^2-\alpha^2)\Gamma_{12}](A_{s'e}\rho A_{ea'}+A_{a'e}\rho A_{es'})\\ &+(\alpha^2\Gamma_1-\beta^2\Gamma_2)(A_{a'e}\rho A_{s'g}+A_{gs'}\rho A_{ea'})\\ &-(\beta^2\Gamma_1-\alpha^2\Gamma_2)(A_{s'e}\rho A_{a'g}+A_{ga'}\rho A_{es'})\end{aligned} \tag{47}$$

with the coefficients

$$\begin{aligned}\Gamma_{es'} &= \frac{1}{2}(\beta^2\Gamma_1+\alpha^2\Gamma_2+2\alpha\beta\Gamma_{12})\\ \Gamma_{s'g} &= \frac{1}{2}(\alpha^2\Gamma_1+\beta^2\Gamma_2+2\alpha\beta\Gamma_{12})\\ \Gamma_{ea'} &= \frac{1}{2}(\alpha^2\Gamma_1+\beta^2\Gamma_2-2\alpha\beta\Gamma_{12})\\ \Gamma_{a'g} &= \frac{1}{2}(\beta^2\Gamma_1+\alpha^2\Gamma_2-2\alpha\beta\Gamma_{12})\\ \Gamma_{a's'} &= \frac{1}{2}[\alpha\beta(\Gamma_1-\Gamma_2)+(\beta^2-\alpha^2)\Gamma_{12}]\end{aligned} \tag{48}$$

In the absence of the driving field, the Hamiltonian (45) has a simple diagonal form, where the different terms represent energies of the collective states. In contrast, the dissipative part of the master equation is very extensive and complicated and unlike the case of identical atoms, is not diagonal. The diagonal dissipative part of the master equation, Eq. (46), contains the familiar relaxation terms corresponding to spontaneous transitions between the collective states, and the coefficients $\Gamma_{es'}$, $\Gamma_{s'g}$, $\Gamma_{ea'}$, and $\Gamma_{a'g}$ are the spontaneous emission rates of the transitions. The off-diagonal part, Eq. (47), contains spontaneously induced coherences between the transitions. They are of importance only in systems of atoms with different transition frequencies ($\Delta \neq 0$).

Similar to the case of identical atoms, there are two channels of transitions $|e\rangle \to |s'\rangle \to |g\rangle$ and $|e\rangle \to |a'\rangle \to |g\rangle$ which decay with the rates $\Gamma_{es'}$, $\Gamma_{s'g}$ and $\Gamma_{ea'}$, $\Gamma_{a'g}$, respectively. However, in contrast to the case of identical atoms, these two channels of transitions are not independent and their decays are correlated through various off-diagonal terms. The decay rates $\Gamma_{ea'}$ and $\Gamma_{a'g}$ are much smaller than the decay rates $\Gamma_{es'}$, $\Gamma_{s'g}$ involving the symmetric state and can be reduced to zero. This happens only for atomic separations much smaller than the optical wavelenght (the small sample model). In particular, the decay rate $\Gamma_{a'g}$

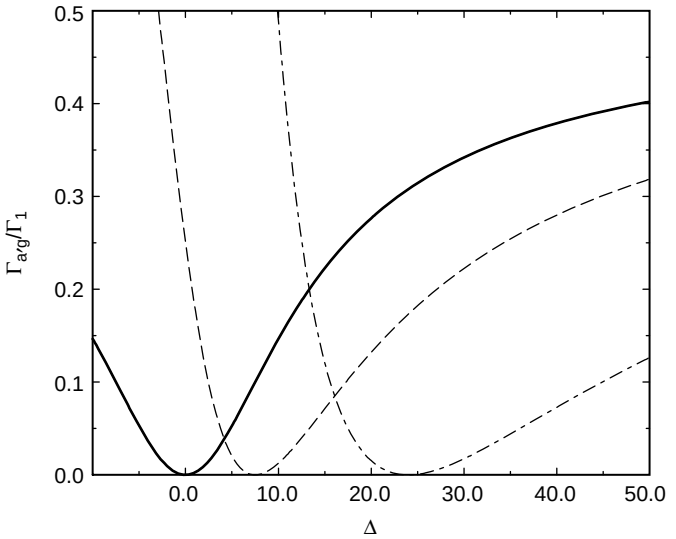

Figure 3. The spontaneous emission damping rate $\Gamma_{a'g}$ as a function of Δ for $\Omega_{12} = 5\Gamma_1$, and different Γ_2: $\Gamma_2 = \Gamma_1$ (solid line), $\Gamma_2 = 2\Gamma_1$ (dashed line), $\Gamma_2 = 5\Gamma_1$ (dashed–dotted line).

of the antisymmetric state to the ground state, shown in Fig. 3, vanishes when [43]

$$\Gamma_{12} = \sqrt{\Gamma_1\Gamma_2} \quad \text{and} \quad \frac{\beta}{\alpha} = \sqrt{\frac{\Gamma_2}{\Gamma_1}} \tag{49}$$

The first condition, $\Gamma_{12} = \sqrt{\Gamma_1\Gamma_2}$, is satisfied when the atoms are separated by distances much smaller than the optical wavelength. The second condition is satisfied when

$$\Delta = -\frac{\Omega_{12}(\Gamma_1 - \Gamma_2)}{2\sqrt{\Gamma_1\Gamma_2}} \tag{50}$$

Thus, with the condition (49) the antisymmetric state does not decay to the ground state. Moreover, at the condition (49) the interference term vanishes, $\Gamma_{a's'} = 0$. Since in the trapping condition (49) the state $|a'\rangle$ is also decoupled from the interaction with the laser field, the only way to populate this state is by spontaneous emission from the upper state $|e\rangle$.

The decoupling of the antisymmetric state $|a'\rangle$ from the coherent field prevents the state from the external coherent interactions. This is not, however, a useful property in terms of quantum computation, where it is required to

prepare entangled states which are decoupled from the external environment and simultaneously should be accessible by coherent processes.

C. Maximally Entangled States of Two Nonidentical Atoms

The choice of the collective states (40) as a basis leads to a complicated master equation whose physical properties are tractable only for very specific values of the parameters involved. A different choice of basis collective states is proposed here, which allows us to obtain a simple master equation of the system of two nonidentical atoms. Moreover, we will show that it is possible to create a maximally entangled state in the system of two nonidentical atoms that can be decoupled from the external environment and, at the same time, the state exhibits a strong coherent coupling with the remaining states.

In order to show this, we introduce superposition operators $S_s^{\pm}$ and $S_a^{\pm}$, which are linear combinations of the atomic operators $S_1^{\pm}$ and $S_2^{\pm}$, as

$$\begin{aligned} S_s^+ &= uS_1^+ + vS_2^+, \quad S_s^- = u^*S_1^- + v^*S_2^- \\ S_a^+ &= vS_1^+ - uS_2^+, \quad S_a^- = v^*S_1^- - u^*S_2^- \end{aligned} \tag{51}$$

where the parameters u and v are in general complex numbers such that

$$|u|^2 + |v|^2 = 1 \tag{52}$$

The operators $S_s^{\pm}$ and $S_a^{\pm}$ represent, respectively, symmetric and antisymmetric superpositions of the atomic dipole operators. In terms of the operators (51), we can rewrite the dissipative part $\mathscr{L}\rho$ of the master equation as

$$\begin{aligned} \mathscr{L}\rho = &-\Gamma_{ss}(S_s^+S_s^-\rho + \rho S_s^+S_s^- - 2S_s^-\rho S_s^+) \\ &- \Gamma_{aa}(S_a^+S_a^-\rho + \rho S_a^+S_a^- - 2S_a^-\rho S_a^+) \\ &- \Gamma_{sa}(S_s^+S_a^-\rho + \rho S_s^+S_a^- - 2S_a^-\rho S_s^+) \\ &- \Gamma_{as}(S_a^+S_s^-\rho + \rho S_a^+S_s^- - 2S_s^-\rho S_a^+) \end{aligned} \tag{53}$$

where the coefficients Γ_{mn} are

$$\begin{aligned} \Gamma_{ss} &= |u|^2\Gamma_1 + |v|^2\Gamma_2 + (uv^* + u^*v)\Gamma_{12} \\ \Gamma_{aa} &= |v|^2\Gamma_1 + |u|^2\Gamma_2 - (uv^* + u^*v)\Gamma_{12} \\ \Gamma_{as} &= uv^*\Gamma_1 - u^*v\Gamma_2 - (|u|^2 - |v|^2)\Gamma_{12} \\ \Gamma_{sa} &= u^*v\Gamma_1 - uv^*\Gamma_2 - (|u|^2 - |v|^2)\Gamma_{12} \end{aligned} \tag{54}$$

The first two terms in Eq. (53) are familiar spontaneous transitions terms and the parameters Γ_{ss} and Γ_{aa} are spontaneous emission rates of the symmetric and antisymmetric superpositions, respectively. The last two terms are due to

coherence between the superposition states and the parameters Γ_{as} and Γ_{sa} appear as cross-damping rates between the superpositions.

If we make the identification

$$u = \sqrt{\frac{\Gamma_1}{\Gamma_1 + \Gamma_2}}, \quad v = \sqrt{\frac{\Gamma_2}{\Gamma_1 + \Gamma_2}}, \tag{55}$$

then the parameters (54) simplify to

$$\begin{aligned}
\Gamma_{ss} &= \frac{1}{2}(\Gamma_1 + \Gamma_2) + \frac{\sqrt{\Gamma_1\Gamma_2}(\Gamma_{12} - \sqrt{\Gamma_1\Gamma_2})}{\Gamma_1 + \Gamma_2} \\
\Gamma_{aa} &= \frac{(\sqrt{\Gamma_1\Gamma_2} - \Gamma_{12})\sqrt{\Gamma_1\Gamma_2}}{\Gamma_1 + \Gamma_2} \\
\Gamma_{sa} = \Gamma_{as} &= \frac{1}{2}\frac{(\Gamma_1 - \Gamma_2)\left(\sqrt{\Gamma_1\Gamma_2} - \Gamma_{12}\right)}{\Gamma_1 + \Gamma_2}
\end{aligned} \tag{56}$$

Clearly, the cross-damping terms Γ_{as} and Γ_{sa} vanish when the damping rates of the atoms are equal $(\Gamma_1 = \Gamma_2)$. Furthermore, if $\Gamma_{12} = \sqrt{\Gamma_1\Gamma_2}$, then the spontaneous emission rates Γ_{aa}, Γ_{as}, and Γ_{sa} vanish regardless of the ratio between the Γ_1 and Γ_2. In this limit, which corresponds to the case of the atoms confined to the region much smaller than the optical wavelength, the antisymmetric superposition does not decay and also decouples from the symmetric superposition.

An interesting question arises as to whether the nondecaying antisymmetric superposition can still be coupled to the symmetric superposition through the coherent terms contained in the Hamiltonian H'. To check it, we first transform the Hamiltonian (32) into the interaction picture and next rewrite the transformed Hamiltonian in terms of the $S_s^{\pm}$ and $S_a^{\pm}$ operators as

$$\begin{aligned}
H' = -\hbar\Bigg\{ &\left[\Delta_L - \frac{1}{2}\left(u^2 - v^2\right)\Delta\right] S_s^+ S_s^- + \left[\Delta_L + \frac{1}{2}\left(u^2 - v^2\right)\Delta\right] S_a^+ S_a^- . \\
&-\Delta uv\left(S_s^+ S_a^- + S_a^+ S_s^-\right)\Big\} + \hbar\Omega_{12}\left[2uv\left(S_s^+ S_s^- - S_a^+ S_a^-\right)\right. \\
&\left. + \left(u^2 - v^2\right)\left(S_s^+ S_a^- + S_a^+ S_s^-\right)\right] - \frac{\hbar}{2}\left\{(u\Omega_1 + v\Omega_2)S_s^+\right. \\
&\left. + (v\Omega_1 - u\Omega_2)S_a^+ + \text{H.c.}\right\}
\end{aligned} \tag{57}$$

where $\Delta_L = \omega_0 - \omega_L$.

In Eq. (57), the first term arises from the Hamiltonian H_A and shows that the energies of the symmetric and antisymmetric superpositions depend on the energy difference Δ between the atomic transition frequencies and the spontaneous emission rates Γ_i. It is interesting to note that the energy difference Δ

introduces a coherent coupling between the superpositions. If the atoms are identical, $\Delta = 0$ $\Gamma_1 = \Gamma_2$, and then the superpositions have the same energies and there is no contribution to the coherent interaction from the Hamiltonian H_A.

The second term in Eq. (57), proportional to the dipole–dipole interaction between the atoms, has two effects on the dynamics of the symmetric and antisymmetric superpositions. The first is a shift of the energies, and the second is the coherent interaction between the superpositions. It is seen from Eq. (57) that the contribution of Ω_{12} to the coherent interaction between the superpositions vanishes for $\Gamma_1 = \Gamma_2$, and then the effect of Ω_{12} is only the shift of the energies from their unperturbed values. Note that the dipole–dipole interaction Ω_{12} shifts the energies in the opposite directions.

The third term in Eq. (57) represents the interaction of the superpositions with the driving laser field. We see that the symmetric superposition couples to the laser field with an enhanced Rabi frequency proportional to $u\Omega_1 + v\Omega_2$, whereas the Rabi frequency of the antisymmetric superposition is proportional to $v\Omega_1 - u\Omega_2$ and vanishes for $v\Omega_1 = u\Omega_2$.

We may rewrite the Hamiltonian (57) in a physically transparent form that shows explicitly the presence of the coherent coupling between the superpositions

$$\begin{aligned} H' = -\hbar\Big\{ &\left(\Delta_L - \frac{1}{2}\Delta'\right) S_s^+ S_s^- + \left(\Delta_L + \frac{1}{2}\Delta'\right) S_a^+ S_a^- \\ &+ \Delta_c \left(S_s^+ S_a^- + S_a^+ S_s^-\right)\Big\} - \frac{\hbar}{2}\{(u\Omega_1 + v\Omega_2) S_s^+ \\ &+ (v\Omega_1 - u\Omega_2) S_a^+ + \text{H.c.}\} \end{aligned} \tag{58}$$

where Δ' and Δ_c are given by

$$\begin{aligned} \Delta' &= [(u^2 - v^2)\Delta + 4\Omega_{12} uv] \\ \Delta_c &= [(u^2 - v^2)\Omega_{12} - \Delta uv] \end{aligned} \tag{59}$$

The parameters Δ' and Δ_c allow us to gain physical insight into how the dipole–dipole interaction Ω_{12} and the frequency difference Δ can modify the dynamics of the two-atom system. The parameter Δ' appears as a shift of the energies of the superposition systems, while Δ_c determines the magnitude of the coherent interaction between the superpositions. For $\Omega_{12} \neq 0$ and identical atoms the shift $\Delta' \neq 0$, but can vanish for nonidentical atoms. This occurs for

$$\Omega_{12} = -\frac{1}{4}\frac{(\Gamma_1 - \Gamma_2)\Delta}{\sqrt{\Gamma_1 \Gamma_2}} \tag{60}$$

In contrast to the shift Δ', which is different from zero for identical atoms, the coherent coupling Δ_c can be different from zero only for nonidentical atoms. However, even in this case the coupling can vanish, which happens for

$$\Delta = \frac{\Omega_{12}(\Gamma_1 - \Gamma_2)}{\sqrt{\Gamma_1\Gamma_2}} \tag{61}$$

Obviously, with the condition (61) and $\Gamma_{12} = \sqrt{\Gamma_1\Gamma_2}$ the antisymmetric superposition of two nonidentical atoms completely decouples from the interactions.

Thus, the condition $\Gamma_{12} = \sqrt{\Gamma_1\Gamma_2}$ for suppression of spontaneous emission from the antisymmetric state is valid for identical as well as nonidentical atoms, whereas the coherent interaction between the superpositions appears only for nonidentical atoms with different transition frequencies and/or spontaneous damping rates.

The symmetric and antisymmetric superpositions (51) can be represented by collective states of the system

$$\begin{aligned} |e\rangle &= |e_1\rangle|e_2\rangle \\ |+\rangle &= u|e_1\rangle|g_2\rangle + v|g_1\rangle|e_2\rangle \\ |-\rangle &= v|e_1\rangle|g_2\rangle - u|g_1\rangle|e_2\rangle \\ |g\rangle &= |g_1\rangle|g_2\rangle \end{aligned} \tag{62}$$

In the general case of $\Gamma_1 \neq \Gamma_2$, the superposition states $|+\rangle$ and $|-\rangle$ are nonmaximally entangled states. However, the states $|+\rangle$ and $|-\rangle$ can be represented by linear superpositions of the maximally entangled states of two identical atoms as

$$\begin{aligned} |+\rangle &= (u+v)|s\rangle + (u-v)|a\rangle \\ |-\rangle &= (u+v)|a\rangle - (u-v)|s\rangle \end{aligned} \tag{63}$$

The entangled states $|+\rangle$ and $|-\rangle$ are independent of Δ, but depend on the damping rates Γ_1 and Γ_2. For $\Gamma_1 = \Gamma_2$ $(u = v)$ the states are maximally entangled, whereas for either $\Gamma_1 \ll \Gamma_2$ or $\Gamma_1 \gg \Gamma_2$ the entangled states reduce to the product states.

IV. SELECTIVE EXCITATION OF THE COLLECTIVE ATOMIC STATES

We now consider excitation and population transfer processes that can lead to a preparation of the two-atom system in one of the collective states. In particular, we will focus on processes that can prepare the two-atom system in the

entangled symmetric state $|s\rangle$. Our main interest, however, is in the preparation of the system in the maximally entangled antisymmetric state $|a\rangle$, which, under the condition $\Gamma_{12} = \sqrt{\Gamma_1\Gamma_2}$, is a decoherence-free state.

A. Preparation of the Symmetric State by a Pulse Laser

It has been shown [31] that a system of two identical two-level atoms may be prepared in the symmetric state $|s\rangle$ by a short laser pulse. The conditions for a selective excitation of the collective atomic states can be analyzed from the interaction Hamiltonian of the laser field with the two-atom system. We make the unitary transformation

$$\tilde{H}_L = e^{iH_0t/\hbar}H'e^{-iH_0t/\hbar} \tag{64}$$

where

$$H_0 = \hbar\{2\Delta_L|e\rangle\langle e| + (\Delta_L + \Omega_{12})|s\rangle\langle s| + (\Delta_L - \Omega_{12})|a\rangle\langle a|\} \tag{65}$$

and find that in the case of identical atoms, $\Gamma_1 = \Gamma_2$ and $\Delta = 0$, the transformed interaction Hamiltonian $\tilde{H}_L$ is given by

$$\begin{aligned}\tilde{H}_L = -\frac{\hbar}{2\sqrt{2}}\{&(\Omega_1 + \Omega_2)(S^+_{es}e^{i(\Delta_L-\Omega_{12})t} + S^+_{sg}e^{i(\Delta_L+\Omega_{12})t}) \\ &+ (\Omega_1 - \Omega_2)(S^+_{ag}e^{i(\Delta_L-\Omega_{12})t} + S^+_{ea}e^{i(\Delta_L+\Omega_{12})t}) + \text{H.c.}\}\end{aligned} \tag{66}$$

where Hamiltonian represents the interaction of the laser field with the collective two-atom system, and in the transformed form contains terms oscillating at frequencies $(\Delta_L \pm \Omega_{12})$, which correspond to the two separate groups of transitions between the collective atomic states at frequencies $\omega_L = \omega_0 + \Omega_{12}$ and $\omega_L = \omega_0 - \Omega_{12}$. The $\Delta_L + \Omega_{12}$ frequencies are separated from $\Delta_L - \Omega_{12}$ frequencies by $2\Omega_{12}$, and hence the two groups of the transitions evolve separately when $\Omega_{12} \gg \Gamma$. Depending on the frequency, the laser can be selectively tuned to one of the two groups of the transitions. When $\omega_L = \omega_0 + \Omega_{12}$ $(\Delta_L + \Omega_{12} = 0)$, the laser is tuned to exact resonance with the $|e\rangle - |a\rangle$ and $|g\rangle - |s\rangle$ transitions, and then the terms appearing in the Hamiltonian (66) and corresponding to these transitions have no explicit time dependence. In contrast, the $|g\rangle - |a\rangle$ and $|e\rangle - |s\rangle$ transitions are off-resonance and the terms corresponding to these transitions have an explicit time dependence $\exp(\pm 2i\Omega_{12}t)$. If $\Omega_{12} \gg \Gamma$, the off-resonance terms rapidly oscillate with the frequency $2\Omega_{12}$, and then we can make a secular approximation in which we neglect all those rapidly oscillating terms. The interaction Hamiltonian can then be written in the simplified form:

$$\tilde{H}_L = -\frac{\hbar}{2\sqrt{2}}[(\Omega_1 + \Omega_2)S^+_{sg} + (\Omega_1 - \Omega_2)S^+_{ea} + \text{H.c.}] \tag{67}$$

It is seen that the laser field couples to the transitions with significantly different Rabi frequencies. The coupling strength of the laser to the $|g\rangle - |s\rangle$ transition is proportional to the sum of the Rabi frequencies $\Omega_1 + \Omega_2$, whereas the coupling strength of the laser to the $|a\rangle - |e\rangle$ transition is proportional to the difference of the Rabi frequencies $\Omega_1 - \Omega_2$. According to Eq. (10), the Rabi frequencies Ω_1 and Ω_2 of two identical atoms differ only by the phase factor $\exp(i\mathbf{k}_L \cdot \mathbf{r}_{12})$. Thus, in order to selectively excite the $|g\rangle - |s\rangle$ transition, the driving laser field should be in phase with both atoms: $\Omega_1 = \Omega_2$. This can be achieved by choosing the propagation vector $\mathbf{k}_L$ of the laser orthogonal to the line joining the atoms. Under this condition we can make a further simplification and truncate the state vector of the system into two states $|g\rangle$ and $|s\rangle$. In this two-state approximation we find from the Schrödinger equation the time evolution of the population $P_s(t)$ of the state $|s\rangle$ as

$$P_s(t) = \sin^2\left(\frac{1}{\sqrt{2}}\Omega t\right) \tag{68}$$

where $\Omega = \Omega_1 = \Omega_2$.

The population oscillates with the Rabi frequency of the $|g\rangle - |s\rangle$ transition and at certain times $P_s(t) = 1$, indicating that all the population is in the symmetric state. This happens at times

$$T_n = (2n+1)\frac{\pi}{\sqrt{2}\Omega}, \quad n = 0, 1, \ldots \tag{69}$$

Hence, the system can be prepared in the state $|s\rangle$ by simply applying a laser pulse, for example, with the duration T_0, that is a standard π pulse.

The two-state approximation is of course an idealization, and a possibility that all the transitions can be driven by the laser imposes significant limits on the Rabi frequency and the duration of the pulse. Namely, the Rabi frequency cannot be too strong in order to avoid the coupling of the laser to the $|s\rangle - |e\rangle$ transition, which could lead to a slight pumping of the population to the state $|e\rangle$. On the other hand, the Rabi frequency cannot be too small as for a small Ω the duration of the pulse, required for the complete transfer of the population into the state $|s\rangle$, becomes longer and then spontaneous emission can occur during the excitation process. Therefore, the transfer of the population to the state $|s\rangle$ cannot be made arbitrarily fast and, in addition, requires a careful estimation of the optimal Rabi frequency, which could be difficult to achieve in a real experimental situation.

B. Preparation of the Antisymmetric State

1. *Pulse Laser*

If we choose the laser frequency such that $\Delta_L - \Omega_{12} = 0$, the laser field is then resonant to the $|a\rangle - |g\rangle$ and $|e\rangle - |s\rangle$ transitions and, after the secular

approximation, the Hamiltonian (66) reduces to

$$\tilde{H}_L = -\frac{\hbar}{2\sqrt{2}}[(\Omega_1 - \Omega_2)S_{ag}^+ + (\Omega_1 + \Omega_2)S_{es}^+ + \text{H.c.}] \tag{70}$$

Clearly, for $\Omega_1 = -\Omega_2$ the laser couples only to the $|a\rangle - |g\rangle$ transition. Thus, in order to selectively excite the $|g\rangle - |a\rangle$ transition, the atoms should experience opposite phases of the laser field. This can be achieved by choosing the propagation vector $\mathbf{k}_L$ of the laser along the interatomic axis, and the atomic separations such that

$$\mathbf{k}_L \cdot \mathbf{r}_{12} = (2n+1)\pi, \quad n = 0, 1, 2, \ldots \tag{71}$$

which corresponds to a situation that the atoms are separated by a distance $r_{12} = (2n+1)\lambda_0/2$.

The smallest distance at which the atoms could experience opposite phases corresponds to $r_{12} = \lambda_0/2$. However, at this particular separation the dipole–dipole interaction parameter Ω_{12} is small (see Fig. 1), and then all of the transitions between the collective states occur at approximately the same frequency. In this case the secular approximation is not valid, and we cannot separate the transitions at $\Delta_L + \Omega_{12}$ from the transitions at $\Delta_L - \Omega_{12}$.

One possible solution to the problem of the selective excitation with opposite phases is to use a standing laser field instead of the running wave field. If the laser amplitudes differ by the sign, namely, $\mathbf{E}_{L_1} = -\mathbf{E}_{L_2} = \mathbf{E}_0$, and $\mathbf{k}_{L_1} \cdot \mathbf{r}_1 = -\mathbf{k}_{L_2} \cdot \mathbf{r}_2$, the Rabi frequencies experienced by the atoms are

$$\begin{aligned} \Omega_1 &= \frac{2i}{\hbar}\boldsymbol{\mu}_1 \cdot \mathbf{E}_0 \sin\left(\frac{1}{2}\mathbf{k}_L \cdot \mathbf{r}_{12}\right) \\ \Omega_2 &= -\frac{2i}{\hbar}\boldsymbol{\mu}_2 \cdot \mathbf{E}_0 \sin\left(\frac{1}{2}\mathbf{k}_L \cdot \mathbf{r}_{12}\right) \end{aligned} \tag{72}$$

where $\mathbf{k}_L = \mathbf{k}_{L_1} = \mathbf{k}_{L_2}$ and we have chosen the reference frame such that $\mathbf{r}_1 = \frac{1}{2}\mathbf{r}_{12}$ and $\mathbf{r}_2 = -\frac{1}{2}\mathbf{r}_{12}$. It follows from Eq. (72) that the Rabi frequencies oscillate with opposite phases independent of the separation between the atoms. However, the magnitude of the Rabi frequencies decreases with decreasing r_{12}.

2. *Indirect Driving through the Symmetric State*

We now turn to the situation of nonidentical atoms and consider different possible processes of the population transfer to the antisymmetric state that could be present even if the antisymmetric state does not decay to the ground level. This can happen when $\Gamma_{12} = \sqrt{\Gamma_1\Gamma_2}$, that is, when the separation between the atoms is negligible small. Under this condition the antisymmetric state is also decoupled from the driving field. According to Eq. (58), the antisymmetric

state can still be coupled, through the coherent interaction Δ_c, to the symmetric state $|+\rangle$. However, this coupling appears only for nonidentical atoms.

From the master equation (31), we find that under the condition $\Gamma_{12} = \sqrt{\Gamma_1\Gamma_2}$ the equation of motion for the population of the state $|-\rangle$ is given by [33]

$$\begin{aligned}\dot{\rho}_{--} = {} & \frac{(\Gamma_1 - \Gamma_2)^2}{\Gamma_1 + \Gamma_2}\rho_{ee} + i\Delta_c(\rho_{+-} - \rho_{-+}) \\ & - \frac{1}{2}i\Omega\frac{(\Gamma_1 - \Gamma_2)}{\sqrt{\Gamma_1^2 + \Gamma_2^2}}(\rho_{e-} - \rho_{-e})\end{aligned} \tag{73}$$

This equation shows that the nondecaying antisymmetric state $|-\rangle$ can be populated by spontaneous emission from the upper state $|e\rangle$ and also by the coherent interaction with the state $|+\rangle$. The first condition is satisfied only when $\Gamma_1 \neq \Gamma_2$, while the other condition is satisfied only when $\Delta_c \neq 0$. Thus, the transfer of population to the state $|-\rangle$ from the upper state $|e\rangle$ and the symmetric state $|s\rangle$ does not appear when the atoms are identical, but is possible for nonidentical atoms.

We illustrate this effect in Fig. 4, where we plot the steady-state population of the state $|-\rangle$ as a function of Δ_L for two different types of nonidentical atoms. In the first case the atoms have the same damping rates ($\Gamma_1 = \Gamma_2$) but different transition frequencies ($\Delta \neq 0$), while in the second case the atoms have the same frequencies ($\Delta = 0$) but different damping rates ($\Gamma_1 \neq \Gamma_2$). It is

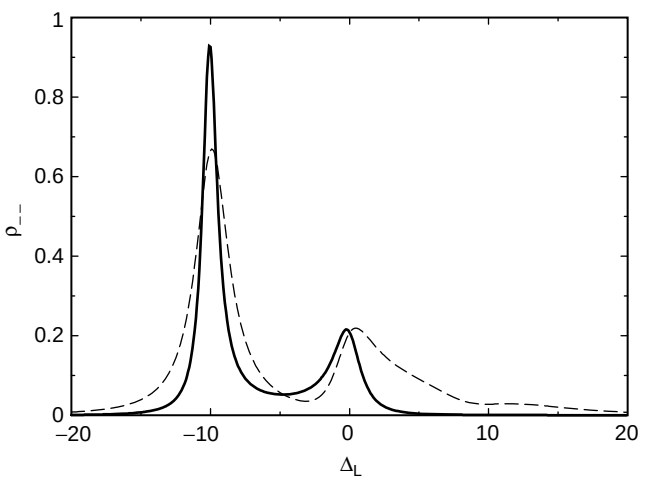

Figure 4. The steady-state population of the antisymmetric state $|-\rangle$ for $\Omega = 5\Gamma_1, \Omega_{12} = 10\Gamma_1$ and $\Gamma_2 = \Gamma_1, \Delta = \Gamma_1$ (solid line), $\Gamma_2 = 2\Gamma_1, \Delta = 0$ (dashed line).

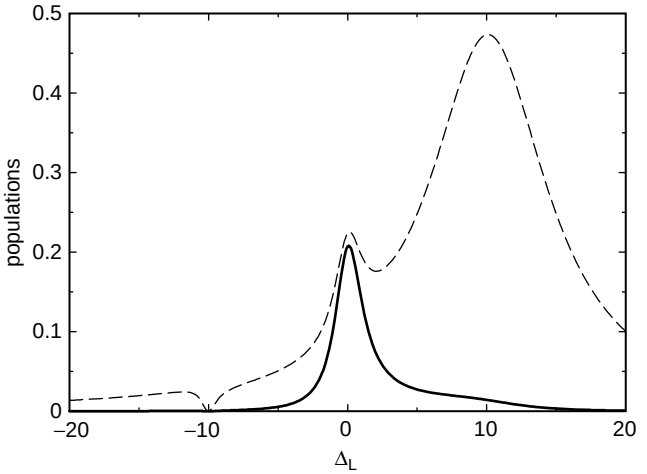

Figure 5. The steady-state populations of the upper state $|e\rangle$ (solid line) and the symmetric state $|+\rangle$ (dashed line) for $\Gamma_2 = \Gamma_1, \Omega = 5\Gamma_1, \Omega_{12} = 10\Gamma_1$ and $\Delta = \Gamma_1$.

seen from Fig. 4 that in both cases the antisymmetric state can be populated even if is not directly driven from the ground state. The population is transferred to $|-\rangle$ through the coherent interaction Δ_c, which leaves the other excited states completely unpopulated. This is shown in Fig. 5, where we plot the steady-state populations ρ_{++} and ρ_{ee} of the states $|+\rangle$ and $|e\rangle$. It is apparent from Fig. 5 that at $\Delta_L = -\Omega_{12}$ the states $|+\rangle$ and $|e\rangle$ are not populated. However, the population is not entirely trapped in the antisymmetric state $|-\rangle$, but rather in a linear superposition of the antisymmetric and ground states. This is shown in Fig. 6, where we plot the steady-state population ρ_{--} for the same parameters as in Fig. 5, but different Ω. Clearly, for a small Ω the steady-state population $\rho_{--} \approx \frac{1}{2}$, and the amount of the population increases with increasing Ω. The population ρ_{--} attains the maximum value $\rho_{--} \approx 1$ for a very strong driving field.

This result shows that we can relatively easily prepare two nonidentical atoms in the maximally entangled antisymmetric state. The closeness of the prepared state to the ideal one is measured by the fidelity F. Here F is equal to the obtained maximum population in the state $|-\rangle$. For $\Omega \gg \Gamma$ the fidelity of the prepared state is maximal, equal to 1. As we have already mentioned, the system has the advantage that the maximally entangled state $|-\rangle$ does not decay, that is, is a decoherence-free state.

3. *Atom–Cavity–Field Interaction*

There have been several proposals to generate the antisymmetric state $|a\rangle$ in a system of two identical atoms interacting with a single-mode cavity field. For

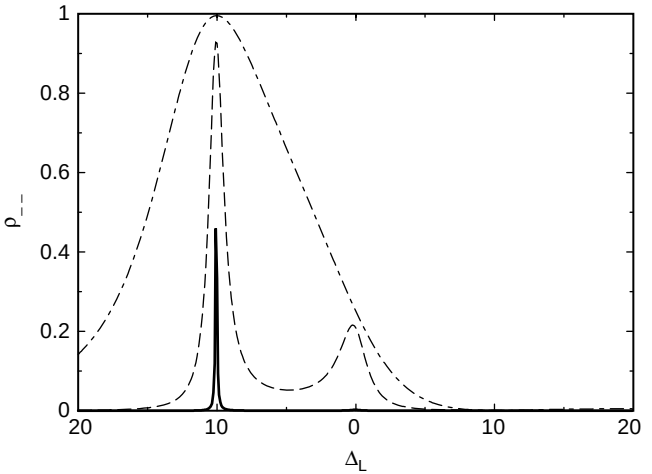

Figure 6. The Steady-state population of the antisymmetric state $|-\rangle$ for $\Gamma_2 = \Gamma_1, \Omega_{12} = 10\Gamma_1, \Delta = \Gamma_1$ and different Ω: $\Omega = \Gamma_1$ (solid line), $\Omega = 5\Gamma_1$ (dashed line), $\Omega = 20\Gamma_1$ (dashed–dotted line).

example, Plenio et al. [30] have considered a system of two atoms trapped inside an optical cavity and separated by a distance much larger than the optical wavelength. This allows for the selective excitation of only one of the atoms. In this scheme the generation of the antisymmetric state relies on the concept of conditional dynamics due to continuous observation of the cavity field. If only one atom is excited and no photon is detected outside the cavity, the atoms are prepared in a dark state [44], which is equivalent to the antisymmetric state $|a\rangle$.

Several investigators [26–28] have analyzed two-atom Jaynes-Cummings models for a violation of Bell's inequality, and have shown that the atoms moving across a single-mode cavity can be prepared in the antisymmetric state via the interaction with the cavity field. In this scheme, the preparation of the antisymmetric state takes place in two steps. In the first step, one atom initially prepared in its excited state $|e_1\rangle$ is sent through a single-mode cavity being in the vacuum state $|0\rangle_c$. During the interaction with the cavity mode, the atomic population undergoes the vacuum Rabi oscillations, and the interaction time was varied by selecting different atomic velocities. If the velocity of the atom is such that the interaction time of the atom with the cavity mode is equal to a quarter of the vacuum Rabi oscillations, then the state of the combined system, the atom plus the cavity mode, is a superposition state:

$$|a_1 c\rangle = \frac{1}{\sqrt{2}}(|e_1\rangle|0\rangle_c - |g_1\rangle|1\rangle_c) \tag{74}$$

Hence, the state of the total system, two atoms plus the cavity mode, after the first atom has crossed the cavity is

$$|\Psi_1\rangle = \frac{1}{\sqrt{2}}(|e_1\rangle|0\rangle_c - |g_1\rangle|1\rangle_c)|g_2\rangle \tag{75}$$

If we now send the second atom, which is in its ground state, with the selected velocity such that during the interaction with the cavity mode the atom undergoes half of the vacuum Rabi oscillation, the final state of the system becomes

$$\begin{aligned}|\Psi_{12}c\rangle &= \frac{1}{\sqrt{2}}(|e_1\rangle|0\rangle_c|g_2\rangle - |g_1\rangle|0\rangle_c|e_2\rangle) \\ &= \frac{1}{\sqrt{2}}(|e_1\rangle|g_2\rangle - |g_1\rangle|e_2\rangle)|0\rangle_c = |a\rangle|0\rangle_c\end{aligned} \tag{76}$$

Thus, the final state of the system is a product state of the atomic antisymmetric state $|a\rangle$ and the vacuum state of the cavity mode. In this scheme the cavity mode is left in the vacuum state, which protects the antisymmetric state against any noise of the cavity. The scheme to entangle two atoms in a cavity, proposed by Cirac and Zoller [28], has been realized experimentally by Hagly et al. [36].

Gerry [29] has proposed a similar method based on a dispersive interaction of the atoms with a cavity mode prepared in a coherent state $|\alpha\rangle$. The atoms enter the cavity in superposition states

$$\begin{aligned}|a_1\rangle &= \frac{1}{\sqrt{2}}(|e_1\rangle + i|g_1\rangle) \\ |a_2\rangle &= \frac{1}{\sqrt{2}}(|e_2\rangle - i|g_2\rangle)\end{aligned} \tag{77}$$

After passage of the second atom, the final state of the system is

$$\begin{aligned}|\Psi_{12}c\rangle = \frac{1}{2}\{&(|g_1\rangle|g_2\rangle + |e_1\rangle|e_2\rangle)|-\alpha\rangle \\ &+ i(|e_1\rangle|g_2\rangle - |g_1\rangle|e_2\rangle)|\alpha\rangle\}\end{aligned} \tag{78}$$

Thus, if the cavity field is measured and found in the state $|\alpha\rangle$, the atoms are in the antisymmetric state. If the cavity field is found in the state $|-\alpha\rangle$, the atoms are in the entangled state:

$$|\Psi_{12}(-\alpha)\rangle = \frac{1}{2}(|g_1\rangle|g_2\rangle + |e_1\rangle|e_2\rangle) \tag{79}$$

The state (79) is called a *two-photon entangled state*. In Section VI, we will discuss another method of preparing the system in the two-photon entangled state based on the interaction of two atoms with a squeezed vacuum field.

C. Preparation of a Superposition of Antisymmetric and Ground States

In the section IV.B.2, we have shown that two nonidentical two-level atoms can be prepared in an arbitrary superposition of the maximally entangled antisymmetric state $|a\rangle$ and the ground state $|g\rangle$

$$|\Phi\rangle = \eta|a\rangle + \sqrt{1-|\eta|^2}|g\rangle \tag{80}$$

However, the preparation of the superposition state requires that the atoms have different transition frequencies. Beige et al. [32] have proposed a scheme in which the superposition state $|\Phi\rangle$ can be prepared in a system of two identical atoms placed at fixed positions inside an optical cavity.

Here, we discuss an alternative scheme where the superposition state $|\Phi\rangle$ can be generated in two identical atoms driven in free space by a coherent laser field. This can happen when the atoms are in nonequivalent positions in the driving field, where the atoms experience different intensities and phases of the driving field. The populations of the collective states of the system can be found from the master equation (31). We use the set of the collective states (35) as an appropriate representation for the density operator

$$\rho = \sum_{ij} \rho_{ij}|i\rangle\langle j|, \quad i,j = g,s,a,e \tag{81}$$

where ρ_{ij} are the density matrix elements in the basis of the collective states.

After transforming to the collective state basis, the master equation (31) leads to a closed system of 15 equations of motion for the density matrix elements [46]. However, for a specifically chosen geometry for the driving field, namely, that the field is propagated perpendicularly to the atomic axis ($\mathbf{k}_L \cdot \mathbf{r}_{12} = 0$), the system of equations decouples into 9 equations for symmetric and 6 equations for antisymmetric combinations of the density matrix elements [45–50]. In this case, we can solve the system analytically, and find that the steady-state values of the populations are [45,46]

$$\begin{aligned}
\rho_{ee} &= \frac{1}{4}\frac{\Omega^4}{D} \\
\rho_{ss} &= \frac{1}{4}\frac{2\Omega^2(\Gamma^2+\Delta_L^2)+\Omega^4}{D} \\
\rho_{aa} &= \frac{1}{4}\frac{\Omega^4}{D}
\end{aligned} \tag{82}$$

where

$$D = \Omega^4 + (\Gamma^2 + \Delta_L^2)\left\{\Omega^2 + \frac{1}{4}[(\Gamma + \Gamma_{12})^2 + (\Delta_L - \Omega_{12})^2]\right\} \tag{83}$$

and $\Delta_L = \omega_0 - \omega_L$.

In this case all of the collective states are populated with the population distribution $\rho_{ee} = \rho_{aa} < \rho_{ss}$. Moreover, for a very strong driving field ($\Omega \gg \Gamma, \Delta_L$), the excited states are equally populated with $\rho_{ee} = \rho_{ss} = \rho_{aa} = \frac{1}{4}$. The population distribution changes dramatically when the driving field propagates in directions different from perpendicular to the interatomic axis [49–50]. In this situation the populations strongly depend on the interatomic separation and the detuning Δ_L. This can produce the interesting modification that the collective states can be selectively populated. We show this by solving numerically the system of 15 equations for the density matrix elements. The populations are plotted against the detuning Δ_L in Fig. 7 for the laser field propagating in the direction of the interatomic axis. We see from Fig. 7 that the collective excited states are populated for most values of Δ_L, except $\Delta_L = -\Omega_{12}$. At this detuning the antisymmetric state is significantly populated, whereas the population of the symmetric and upper states is close to zero. Since $\rho_{aa} < 1$, the population is distributed between the antisymmetric and the ground

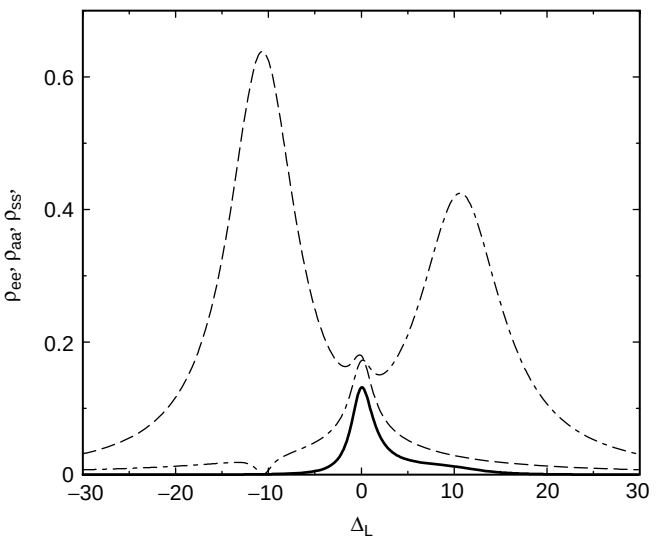

Figure 7. The steady-state populations of the collective atomic states of two identical atoms as a function of Δ_L for the driving field propagating in the direction of the interatomic axis, $\Omega = 2.5\Gamma$, $r_{12}/\lambda_0 = 0.08$ and $\bar{\boldsymbol{\mu}} \perp \bar{r}_{12}$: ρ_{ee} (solid line), ρ_{aa} (dashed line), ρ_{ss} (dashed–dotted line).

states, and therefore at $\Delta_L = -\Omega_{12}$ the system is in a superposition of the maximally entangle state $|a\rangle$ and the ground state $|g\rangle$.

Turchette et al. [35] have realized experimentally a superposition state of the ground state and a nonmaximally entangled antisymmetric state in two trapped ions. In the experiment two trapped barium ions were sideband-cooled to their motional ground states. Transitions between the states of the ions were induced by Raman pulses using copropagating lasers. The ions were at positions that experience different Rabi frequencies Ω_1 and Ω_2 of the laser fields. By preparing the initial motional ground state with one ion excited $|e_1\rangle|g_2\rangle|0\rangle$, and applying the laser fields for a time t, the following entangled state $|\Psi(t)\rangle$ was created

$$|\Psi(t)\rangle = -\frac{i\Omega_2}{\Omega}\sin(\Omega t)|g\rangle|1\rangle + \left\{\left[\frac{\Omega_2^2}{\Omega^2}(\cos\Omega t - 1) + 1\right]|e_1\rangle|g_2\rangle + \left[\frac{\Omega_1\Omega_2}{\Omega^2}(\cos\Omega t - 1)\right]|g_1\rangle|e_2\rangle\right\}|0\rangle \tag{84}$$

where $\Omega^2 = \Omega_1^2 + \Omega_2^2$.

For $\Omega t = \pi$ the entangled state (84) reduces to a nonmaximally entangled antisymmetric state

$$|\Psi_a\rangle = \left[\frac{\Omega_1^2 - \Omega_2^2}{\Omega^2}|e_1\rangle|g_2\rangle - \frac{2\Omega_1\Omega_2}{\Omega^2}|g_1\rangle|e_2\rangle\right]|0\rangle \tag{85}$$

Franke et al. [51] proposed using the nonmaximally entangled state (85) to demonstrate the intrinsic difference between quantum and classical information transfers. The difference arises from the different ways in which the probabilities occur and is particularly clear in terms of entangled states.

V. DETECTION OF THE ENTANGLED STATES

In this section we discuss problems that could be involved in any attempt to detect an internal entangled state of two coupled atoms in free space. Beige et al. [34] have proposed a scheme, based on the quantum Zeno effect, to observe a decoherence-free state in a system of two 3-level atoms located inside an optical cavity. Here, we discuss possible schemes to detect entangled states of two 2-level atoms in free space.

A. Fluorescence Intensity

One of the possible ways to detect an internal state of two coupled atoms is to observe the fluorescence field emitted from the system. It is well known that the fluorescence from the two-atom system exhibits strong directional properties [7,10,48,52].

To show this, we consider the fluorescence intensity detected at a point $\mathbf{R}$ in the far-field zone of the radiation emitted by the atomic system. The intensity is proportional to the first-order correlation functions of the atomic dipole operators as [7,8]

$$I(\mathbf{R},t) = U(\mathbf{R}) \sum_{i,j=1}^{2} \left\langle S_i^+\left(t - \frac{R}{c}\right) S_j^-\left(t - \frac{R}{c}\right) \right\rangle e^{ik\bar{\mathbf{R}}\cdot\mathbf{r}_{ij}}, \tag{86}$$

where

$$U(\mathbf{R}) = \left(\frac{\omega_0^4 \mu^2}{2R^2 \pi \varepsilon_0}\right) \sin^2\varphi \tag{87}$$

is the geometric factor with φ the angle between the observation direction $\mathbf{R} = R\bar{\mathbf{R}}$ and the atomic dipole moment $\boldsymbol{\mu}$.

From Eqs. (86) and (81) the fluorescence intensity can be written in terms of the density matrix elements in the collective states representation as

$$\begin{aligned} I(\mathbf{R},t) = U(\mathbf{R})\{&(\rho_{ee} + \rho_{ss})[1 + \cos(kr_{12}\cos\theta)] \\ &+ (\rho_{ee} + \rho_{aa})[1 - \cos(kr_{12}\cos\theta)] \\ &+ i(\rho_{sa} - \rho_{as})\sin(kr_{12}\cos\theta)\} \end{aligned} \tag{88}$$

where θ is the angle between the observation direction $\bar{\mathbf{R}}$ and the vector $\mathbf{r}_{12}$.

The first term in Eq. (88) arises from the fluorescence emitted on the $|e\rangle \to |s\rangle \to |g\rangle$ transitions, which involve the symmetric state. The second term arises from the $|e\rangle \to |a\rangle \to |g\rangle$ transitions through the antisymmetric state. These two terms describe two different channels of transitions for which the angular distribution is proportional to $[1 \pm \cos(kr_{12}\cos\theta)]$. The last term in Eq. (88) originates from interference between these two radiation channels. It is seen from Eq. (1.88) that the angular distribution of the fluorescence field depends on the population of the entangled states $|s\rangle$ and $|a\rangle$. Moreover, independent of the interatomic separation r_{12}, the antisymmetric state does not radiate in the direction perpendicular to the atomic axis, as for $\theta = \pi/2$ the factor $[1 - \cos(kr_{12}\cos\theta)]$ vanishes. In contrast, the symmetric state radiates in all directions.

It is evident from Eq. (88) that the radiation pattern is nonspherical unless $\rho_{ss} = \rho_{aa}$ and then the pattern is spherically symmetric independent of the interatomic separation. Therefore, an asymmetry in the radiation pattern would be compelling evidence that the entangled states $|s\rangle$ and $|a\rangle$ are not equally populated. If the fluorescence were detected in the direction perpendicular to the atomic axis, the observed intensity (if any) would correspond to the fluorescence field emitted from the symmetric state $|s\rangle$ and/or the upper state $|e\rangle$. On the other hand, if there is no fluorescence detected in the direction perpendicular

to the atomic axis, the population is entirely in a superposition of the antisymmetric state $|a\rangle$ and the ground state $|g\rangle$.

Guo and Yang [53] have analyzed spontaneous decay from two atoms initially prepared in an entangled state. They have shown that the time evolution of the population inversion, which is proportional to the intensity (87), depends on the degree of entanglement of the initial state of the system. Ficek et al. [10] have shown that in the case of two nonidentical atoms, the time evolution of the intensity $I(\mathbf{R}, t)$ can exhibit quantum beats that result from the presence of correlations between the symmetric and antisymmetric states. In fact, quantum beats are present only if initially the system is in a nonmaximally entangled state, and no quantum beats are predicted for maximally entangled as well as unentangled states.

B. Interference Pattern

An alternative way to detect an internal state of the two atom system is to observe an interference pattern of the fluorescence field emitted in the direction $\mathbf{R}$, not necessary perpendicular to the interatomic axis. The usual measure of the depth of modulation of the interference fringes is a visibility defined as

$$\mathscr{V} = \frac{I_{\max} - I_{\min}}{I_{\max} + I_{\min}} \tag{89}$$

where $I_{\max}$ corresponds to $\cos(k\bar{\mathbf{R}} \cdot \mathbf{r}_{12}) = 1$, whereas I_{min} corresponds to $\cos(k\bar{\mathbf{R}} \cdot \mathbf{r}_{12}) = -1$. This scheme is particularly useful when the antisymmetric state is a decoherence-free (dark) state.

Using Eq. (88), we can write the visibility in the basis of the collective states as

$$\mathscr{V} = \frac{\rho_{ss} - \rho_{aa}}{\rho_{ss} + \rho_{aa} + 2\rho_{ee}} \tag{90}$$

This equation shows that the sign of $\mathscr{V}$ depends on the population difference between the symmetric and antisymmetric states. For $\rho_{ss} > \rho_{aa}$ the visibility $\mathscr{V}$ is positive, and then the interference pattern exhibits a maximum (bright center), whereas for $\rho_{ss} < \rho_{aa}$ the visibility $\mathscr{V}$ is negative and then there is a minimum (dark center). The optimum positive (negative) value is $\mathscr{V} = 1$ ($\mathscr{V} = -1$), and there is no interference pattern when $\mathscr{V} = 0$. The later happens when $\rho_{ss} = \rho_{aa}$.

Similar to the fluorescence intensity distribution, the visibility can provide us an information about the internal state of the system. When the system is prepared in the antisymmetric state or in a superposition of the antisymmetric and the ground states, $\rho_{ss} = \rho_{ee} = 0$, and then the visibility has the optimum negative value $\mathscr{V} = -1$. On the other hand, when the system is prepared in the symmetric state or in a linear superposition of the symmetric and ground states, the visibility has the maximum positive value $\mathscr{V} = 1$.

There have been several theoretical studies of the fringe visibility in the fluorescence field emitted by two coupled atoms, and the Young's interference-type pattern has been observed experimentally in the resonance fluorescence of two trapped ions [11]. The experimental results have been explained theoretically by Wong et al. [54], and can be understood by treating the ions as independent radiators that are synchronized by the constant phase of the driving field. It has been shown that for a weak driving field, the fluorescence field is predominantly composed of an elastic component and therefore the ions behave as point sources of coherent light producing an interference pattern. Under strong excitation the fluorescence field is mostly composed of the incoherent part and consequently there is no interference pattern. Dung and Ujihara [52] have shown that an interference pattern can be observed in spontaneous emission from two interacting atoms even if it is known for certain which atom is excited initially. Michelson type (temporary) interference pattern has been predicted in spontaneous emission from two non-identical atoms [43]. Kochan et al. [55] have shown that the interference pattern of the strongly driven atoms can be partially recovered by placing the atoms inside an optical cavity. The coupling of the atoms to the cavity mode induces atomic correlations, which improves the fringe visibility. Meyer and Yeoman [56] have reported an even stronger cavity induced modification of the interference pattern that occurs when the coherent driving field is replaced by an incoherent field. They have shown that in contrast to the coherent excitation, the incoherent field produces an interference pattern with a dark center. Interference pattern with a dark center has also been predicted when the atoms experience different intensities of the driving field [57] or in the case where the driving field is replaced by a squeezed vacuum field [58].

VI. TWO-PHOTON ENTANGLED STATES

We have already discussed different methods of generating two-atom entangled states of the form

$$|\Psi\rangle = c_1|e_1\rangle|g_2\rangle \pm c_2|g_1\rangle|e_2\rangle \tag{91}$$

These states are generated by the dipole–dipole interaction between the atoms and the preparation of these states is sensitive to the difference Δ between the atomic transition frequencies and to the atomic decay rates.

There are two other collective states of the two-atom system: the double atomic ground state $|g\rangle = |g_1\rangle|g_2\rangle$ and the double atomic excited state $|e\rangle = |e_1\rangle|e_2\rangle$, which are also product states of the individual atomic states. These states are not affected by the dipole–dipole interaction Ω_{12}, the detuning Δ and the spontaneous emission rates.

Here, we discuss a method of preparing a two atom system in entangled states involving only the double atomic ground $|g\rangle$ and excited $|e\rangle$ states

$$|\Upsilon\rangle = c_g|g\rangle \pm c_e|e\rangle \tag{92}$$

where c_g and c_e are constant parameters such that $|c_g|^2 + |c_e|^2 = 1$. The entangled states of the form (92) are known in the literature as *pairwise atomic states* [22] or *multiatom squeezed states* [23]. According to Eq. (36), the collective ground and excited states are separated in energy by $2\hbar\omega_0$, and therefore we can call the states $|\Upsilon\rangle$ as two-photon entangled (TPE) states.

The two-photon entangled states cannot be generated by a simple coherent excitation. A coherent field applied to the two-atom system couples to one-photon transitions. The problem is that coherent excitation populates the upper state $|e\rangle$ but also populated the intermediate states $|s\rangle$ and $|a\rangle$. The two-photon entangled states (92) are superpositions of the collective ground and excited states with no contribution from the intermediate collective states $|s\rangle$ and $|a\rangle$.

The two-photon behavior of the entangled states (92) suggests that the simplest technique for generating the TPE states would be by applying a two-photon excitation process. An obvious candidate is a squeezed vacuum field, which is characterized by strong two-photon correlations that would enable the transition $|g\rangle \rightarrow |e\rangle$ to occur effectively in a single step without populating the intermediate states. We will illustrate this effect by analyzing the populations of the collective atomic states.

A. Two Atoms in a Squeezed Vacuum

The dynamics of the collective two-atom system in a squeezed vacuum can be determined from the master equation of the density operator of the system or from the equations of motion for the transition probability amplitudes [22]. In Section II.B, we derived the master equation for the density operator of a two atom system interacting with the ordinary vacuum field. It is our purpose to extend the master equation to the case of a squeezed vacuum field. The method of derivation of the master equation is a straightforward extension of that presented in Section II.B.

The correlation functions for the field operators $\hat{\mathbf{a}}_{\mathbf{k}s}$ and $\hat{\mathbf{a}}^\dagger_{\mathbf{k}s}$, which describe a three-dimensional field in a squeezed vacuum state, are given by [24,25]

$$\begin{aligned}
\langle \hat{a}_{\mathbf{k}s}\rangle &= \langle \hat{a}^\dagger_{\mathbf{k}s}\rangle = 0\\
\langle \hat{a}_{\mathbf{k}s}\hat{a}^\dagger_{\mathbf{k}'s'}\rangle &= (N(\omega_k)+1)\delta^3(\mathbf{k}-\mathbf{k}')\delta_{ss'}\\
\langle \hat{a}^\dagger_{\mathbf{k}s}\hat{a}_{\mathbf{k}'s'}\rangle &= N(\omega_k)\delta^3(\mathbf{k}-\mathbf{k}')\delta_{ss'}\\
\langle \hat{a}^\dagger_{\mathbf{k}s}\hat{a}^\dagger_{\mathbf{k}'s'}\rangle &= M(\omega_k)\delta^3(2\mathbf{k}_s-\mathbf{k}-\mathbf{k}')\delta_{ss'}\\
\langle \hat{a}_{\mathbf{k}s}\hat{a}_{\mathbf{k}'s'}\rangle &= M^*(\omega_k)\delta^3(2\mathbf{k}_s-\mathbf{k}-\mathbf{k}')\delta_{ss'}
\end{aligned} \tag{93}$$

where $N(\omega_k)$ is the number of photons in the mode ω_k and $M(\omega_k) = M(2\omega_s - \omega_k)$ is the two-photon correlation function, which is symmetric about the squeezing carrier frequency $2\omega_s$. The parameters $N(\omega_k)$ and $M(\omega_k) = |M(\omega_k)|\exp(i\phi)$ are not independent of each other but are related by the inequality

$$|M(\omega_k)|^2 \leq N(\omega_k)(N(2\omega_s - \omega_k) + 1) \tag{94}$$

where the term $+1$ on the r.h.s arises from the quantum nature of the squeezed field [25], and ϕ is the phase of the squeezed vacuum field.

Substituting the interaction Hamiltonian (7), we find that the evolution of the density operator depends on the second order correlation functions of the reservoir operators. We assume that a part of the reservoir modes is in a squeezed vacuum state for which the correlation functions are given by Eq. (93).

In order to optimize the squeezing effects on the atom, the mode function $U_s(\omega_k)$ of the squeezed vacuum field should be perfectly matched to the mode function $\mathbf{g}_{\mathbf{k}s}(\mathbf{r}_i)$ of the three-dimensional vacuum field coupled to the atoms. Such a requirement of the perfect matching is practically impossible to achieve in present experiments [59]. Therefore, we consider mode functions that correspond to an imperfect matching of the squeezing modes to the vacuum modes surrounding the atoms. In this case, we can write the mode function $U_s(\omega_k)$ as

$$U_s(\omega_k) = \begin{cases} [\mathcal{N}(\omega_k)]^{-1/2}\boldsymbol{\mu}_i^* \cdot \mathbf{g}_{\mathbf{k}s}^*(\mathbf{r}_i)D(\omega_k) & \text{for} \quad \theta_k \leq \theta_m \\ 0 & \text{for} \quad \theta_k > \theta_m \end{cases} \tag{95}$$

where $\mathcal{N}(\omega_k)$ is the normalization constant such that $|U_s(\omega_k)|^2 = 1$, the parameter $D(\omega_k)$ determines the coupling efficiency of the squeezed field mode function $U_s(\omega_k)$ to the vacuum field mode function $g_{\mathbf{k}s}(\mathbf{r}_i)$, and θ_m is the maximum angle over which the squeezed modes are propagated. For perfect coupling efficiency $|D(\omega_k)| = 1$, whereas $|D(\omega_k)| < 1$ for an imperfect coupling. The parameter $D(\omega_k)$ contains both the amplitude and phase coupling, and its explicit form depends on the method of propagation and focusing the squeezed field. For example, in the case of a Gaussian profile of a focused squeezed field, the parameter $D(\omega_k)$ is given by [60,61]

$$D(\omega_k) = \exp[-W_0 \sin^2\theta_k - ikz_f \cos\theta_k] \tag{96}$$

where W_0 is the beam spot size at the focal point z_f. In a cavity situation, for example, the parameter $D(\omega_k)$ is identified as the cavity transfer function, the absolute value square of which is the Airy function of the cavity [61,62].

Before returning to the derivation of the master equation, we should remark that in the squeezing propagation case in which the squeezed modes lie inside the cone of angle $\theta_m < \pi$, we assume that the modes outside the cone are in their ordinary vacuum state. In practice, the modes will be in a finite-temperature

blackbody state, which means that inside the cone the modes are in mixed squeezed vacuum and blackbody states. However, this is not a serious practical problem as experiments are usually performed at low temperatures where the blackbody radiation is negligible. In principle, we can include the blackbody radiation effect (thermal noise) to the problem replacing $N(\omega_k)$ in (93) by $N(\omega_k) + \bar{N}$, where $\bar{N}$ is proportional to the photon number in the blackbody radiation.

We now return to the derivation of the master equation of the atom in a squeezed vacuum field. Substituting the interaction Hamiltonian (7) into Eq. (18) and using the correlation functions (93), we obtain

$$\begin{aligned}\frac{\partial}{\partial t}\tilde{\rho}(t) = \sum_{i,j=1}^{2}\{&[S_i^- Y_{ij}(t,\tau), S_j^+] + [S_i^-, Y_{ij}(t,\tau)S_j^+] \\ &+ [S_i^+ N_{ij}(t,\tau), S_j^-] + [S_i^+, N_{ij}(t,\tau)S_j^-] \\ &+ [S_i^+ M_{ij}(t,\tau), S_j^+] + [S_i^+, M_{ij}(t,\tau)S_j^+] \\ &+ [S_i^- M_{ij}^*(t,\tau), S_j^-] + [S_i^-, M_{ij}^*(t,\tau)S_j^-]\} \\ &- i\sum_{i\neq j}\Omega_{ij}[S_i^+ S_j^-, \tilde{\rho}(t)]\end{aligned} \tag{97}$$

where Ω_{ij} is given in Eq. (28),

$$\begin{aligned}Y_{ij}(t,\tau) &= \frac{1}{c^3}\int d\omega_k \omega_k^2[\chi_{ij}^{(N)}(t) + \chi_{ij}(t)]\int_0^t d\tau\tilde{\rho}(t-\tau)e^{i(\omega_i-\omega_k)\tau} \\ N_{ij}(t,\tau) &= \frac{1}{c^3}\int d\omega_k \omega_k^2\chi_{ij}^{(N)}(t)\int_0^t d\tau\tilde{\rho}(t-\tau)e^{-i(\omega_i-\omega_k)\tau} \\ M_{ij}(t,\tau) &= \frac{1}{c^3}\int d\omega_k \omega_k(2\omega_s-\omega_k)\chi_{ij}^{(M)}(t)\int_0^t d\tau\tilde{\rho}(t-\tau)e^{i(\omega_i-\omega_k)\tau}\end{aligned} \tag{98}$$

with

$$\begin{aligned}\chi_{ij}(t) &= \int d\Omega_k \sum_s [\boldsymbol{\mu}_i\cdot\mathbf{g}_{\mathbf{k}s}(\mathbf{r}_i)][\boldsymbol{\mu}_j^*\cdot\mathbf{g}_{\mathbf{k}s}^*(\mathbf{r}_j)]e^{i(\omega_i-\omega_j)t} \\ \chi_{ij}^{(N)}(t) &= N(\omega_k)|D(\omega_k)|^2 e^{-i(\omega_i-\omega_j)t} \\ &\quad\times\sum_s\int_{\Omega_s} d\Omega_k[\boldsymbol{\mu}_i^*\cdot\mathbf{g}_{\mathbf{k}s}^*(\mathbf{r}_i)][\boldsymbol{\mu}_j\cdot\mathbf{g}_{\mathbf{k}s}(\mathbf{r}_j)] \\ \chi_{ij}^{(M)}(t) &= M(\omega_k)|D(\omega_k)|^2 e^{i(2\omega_o-\omega_i-\omega_j)t} \\ &\quad\times\sum_s\int_{\Omega_s} d\Omega_k[\boldsymbol{\mu}_i\cdot\mathbf{g}_{\mathbf{k}s}(\mathbf{r}_i)][\boldsymbol{\mu}_j\cdot\mathbf{g}_{\mathbf{k}s}(\mathbf{r}_j)]\end{aligned} \tag{99}$$

and Ω_s is the solid angle over which the squeezed modes are propagated.

The master equation (97) with parameters (98) is quite general in terms of the matching of the squeezed modes to the vacuum modes and the bandwidth of the squeezed field relative to the atomic linewidths. The master equation is in the

form of a differential integral equation, and we can simplify the form employing the Markov approximation. In this approximation the integral over the time delay τ contains functions that decay to zero over a short correlation time τ_c. This correlation time is of the order of the inverse bandwidth of the squeezed field, and the short correlation time approximation is formally equivalent to assume that squeezing bandwidths are much larger than the atomic linewidths. Over this short timescale, the density operator would hardly have changed from $\rho(t)$, thus we can replace $\tilde{\rho}(t-\tau)$ by $\tilde{\rho}(t)$ in (98) and extend the integral to infinity. Next, we can perform the integration and find

$$\lim_{t\to\infty}\int_0^t d\tau\tilde{\rho}(t-\tau)e^{ix\tau} \approx \tilde{\rho}(t)\left[\pi\delta(x)+i\frac{P}{x}\right] \tag{100}$$

where P indicates the principal value of the integral. Finally, to carry out the polarization sums and integrals over $d\Omega_k$ in (99), we use the plane-wave description of the vacuum mode function $\mathbf{g}_{\mathbf{k}s}(\mathbf{r})$, and assuming that the dipole moments are parallel ($\boldsymbol{\mu}_1 \| \boldsymbol{\mu}_2$), the sums over s and the integrals over $d\Omega_k$ in (99) lead to

$$\begin{aligned}
Y_{ij}(t,\tau) &= \Gamma_{ij}[1+N(\omega_i)|D(\omega_i)|^2 v(\theta_m)]\tilde{\rho}(t)e^{i(\omega_i-\omega_j)t}\\
N_{ij}(t,\tau) &= \Gamma_{ij}N(\omega_i)|D(\omega_i)|^2 v(\theta_m)\tilde{\rho}(t)e^{-i(\omega_i-\omega_j)t}\\
M_{ij}(t,\tau) &= \Gamma_{ij}M(\omega_i)|D(\omega_i)|^2 v(\theta_m)\tilde{\rho}(t)e^{i\left(2\omega_s-\omega_i-\omega_j\right)t}
\end{aligned} \tag{101}$$

where

$$v(\theta_m) = \frac{1}{2}\left[1-\frac{1}{4}\left(3+\cos^2\theta_m\right)\cos\theta_m\right] \tag{102}$$

In the derivation of (101), we have ignored the principal value parts that contribute to the energy shifts of the atomic levels. In fact, the shifts are very small for a broadband squeezed field, and their contribution to the atomic dynamics are negligible [63].

With the parameters (101), the master equation of two atoms in a broadband squeezed vacuum, written in the Schrödinger picture, reads as

$$\begin{aligned}
\frac{\partial\rho}{\partial t} = &-\frac{1}{2}\sum_{i,j=1}^{2}\Gamma_{ij}[1+\tilde{N}(\omega_i)](\rho S_i^+S_j^- + S_i^+S_j^-\rho - 2S_j^-\rho S_i^+)\\
&-\frac{1}{2}\sum_{ij}\Gamma_{ij}\tilde{N}(\omega_i)(\rho S_i^-S_j^+ + S_i^-S_j^+\rho - 2S_j^+\rho S_i^-)\\
&-\frac{1}{2}\sum_{ij}\Gamma_{ij}\tilde{M}(k_i)([S_i^+\rho, S_j^+] + [S_j^+, \rho S_i^+])\\
&-\frac{1}{2}\sum_{ij}\Gamma_{ij}\tilde{M}^*(\omega_i)([S_i^-\rho, S_j^-] + [S_j^-, \rho S_i^-]) - \frac{i}{\hbar}[H', \rho]
\end{aligned} \tag{103}$$

where

$$\tilde{N}(\omega_i) = \eta N(\omega_i)$$
$$\tilde{M}(\omega_i) = \eta M(\omega_i) \tag{104}$$

with $\eta = |D(\omega_i)|^2 v(\theta_m)$, and the Hamiltonian H' as given in Eq. (32).

The parameter η determines the matching of the squeezed modes to the modes surrounding the atom. This includes the coupling efficiency of the mode functions, given by the parameter $D(\omega_k)$, and the angular dimensions, given by the angle θ_m, of the squeezed modes. For an imperfect matching the master equation (103) is formally identical to that for perfect matching: the only difference is the replacement of the squeezing parameters N and M by the matching modified parameters $\tilde{N}$ and $\tilde{M}$. The master equation (103) is a starting equation to calculate the stationary state of a two-atom system interacting with a squeezed vacuum field.

B. Steady-State Populations

In order to calculate the stationary state of the two-atom system, we have to know the steady-state populations ρ_{ii} of the collective atomic states and the coherencies $\rho_{ij}(i \neq j)$. First, we consider a system of two identical atoms $(\Delta = 0, \Gamma_1 = \Gamma_2)$ separated by an arbitrary distance r_{12} and interacting with a squeezed vacuum field. Moreover, we assume that the carrier frequency ω_s of the squeezed vacuum field is resonant to the atomic transition frequencies $(\omega_s = \omega_0)$.

From the master equation (103), we find equations of motion for the populations of the collective atomic states, which in the absence of the coherent driving field $(\Omega_1 = \Omega_2 = 0)$ can be written as

$$\begin{aligned}
\frac{\partial}{\partial t}\rho_{ee} &= -\Gamma(n+1)\rho_{ee} + \frac{1}{2}(n-1)[(\Gamma+\Gamma_{12})\rho_{ss} + (\Gamma-\Gamma_{12})\rho_{aa}] \\
&\quad + \Gamma_{12}(\tilde{M}^*\rho_{eg} + \tilde{M}\rho_{ge}) \\
\frac{\partial}{\partial t}\rho_{ss} &= \frac{1}{2}(\Gamma+\Gamma_{12})\{(n-1) - (3n-1)\rho_{ss} - (n-1)\rho_{aa} + 2\rho_{ee} \\
&\quad - 2(\tilde{M}^*\rho_{eg} + \tilde{M}\rho_{ge})\} \\
\frac{\partial}{\partial t}\rho_{aa} &= \frac{1}{2}(\Gamma-\Gamma_{12})\{(n-1) - (3n-1)\rho_{aa} - (n-1)\rho_{ss} + 2\rho_{ee} \\
&\quad + 2(\tilde{M}^*\rho_{eg} + \tilde{M}\rho_{ge})\} \\
\frac{\partial}{\partial t}\rho_{eg} &= \left(\frac{\partial}{\partial t}\rho_{ge}\right)^* = \Gamma_{12}\tilde{M} - n\Gamma\rho_{eg} \\
&\quad - \tilde{M}[(\Gamma+2\Gamma_{12})\rho_{ss} - (\Gamma-2\Gamma_{12})\rho_{aa}]
\end{aligned} \tag{105}$$

where $n = 2\tilde{N}(\omega_0) + 1$ and $\tilde{M} = \tilde{M}(\omega_0)$.

It is seen from Eq. (105) that the evolution of the populations depends on the two-photon coherencies ρ_{eg} and ρ_{ge}, which can transfer the population from the ground state $|g\rangle$ directly to the upper state $|e\rangle$ leaving the states $|s\rangle$ and $|a\rangle$ unpopulated. The evolution of the populations depends on Γ_{12}, but is completely independent of the dipole–dipole interaction Ω_{12}.

There are two different steady-state solutions of Eqs. (105) depending on whether $\Gamma_{12} = \Gamma$ or $\Gamma_{12} \neq \Gamma$. This fact is connected with the existence of a combination of the density matrix elements involving the antisymmetric state

$$S^2(t) = 2 - 2\rho_{aa}(t) \tag{106}$$

which, for $\Gamma_{12} = \Gamma$ is a constant of motion. In this case the population in the antisymmetric state does not change in time. Thus an initially unpopulated antisymmetric state remains unpopulated for all times, and then the population is distributed only between three collective states $|e\rangle$, $|s\rangle$, and $|g\rangle$.

Assuming that $\Gamma_{12} = \Gamma$ and setting the left-hand side of Eqs. (105) equal to zero, we obtain the steady-state solutions for the populations of the states $|e\rangle$ and $|s\rangle$, and the two-photon coherence $|\rho_{eg}|$. A straightforward algebraic manipulation of Eqs. (105) leads to the following steady-state solutions

$$\begin{aligned}
\rho_{ee} &= \frac{n(n-1)^2 - 4(n-2)|\tilde{M}|^2}{n(3n^2 + 1 - 12|\tilde{M}|^2)} \\
\rho_{ss} &= \frac{(n^2-1) - 4|\tilde{M}|^2}{3n^2 + 1 - 12|\tilde{M}|^2} \\
\rho_u &= \frac{8|\tilde{M}|}{n(3n^2 + 1 - 12|\tilde{M}|^2)}
\end{aligned} \tag{107}$$

where $\rho_u = \rho_{eg}e^{-i\phi} + \rho_{ge}e^{i\phi}$.

The steady-state populations depend on the squeezing correlations M and the coupling efficiency η. For a classical squeezed field with the maximal correlations $M = N$, the steady-state populations reduces to

$$\begin{aligned}
\rho_{ss} &= \frac{\eta N}{3\eta N + 1} \\
\rho_{ee} &= \frac{\eta^2 N^2}{(\eta N + 1)(3\eta N + 1)}
\end{aligned} \tag{108}$$

In this case both the excited states are populated and the populations obey a Boltzmann distribution with $\rho_{gg} > \rho_{ss} > \rho_{ee}$.

The population distribution is qualitatively different for a quantum squeezed field with $|M|^2 = N(N+1)$. In this case the populations are given by

$$\rho_{ss} = \frac{\eta N(1-\eta)}{3\eta N(1-\eta)+1}$$
$$\rho_{ee} = \frac{\eta N[1+2(1-\eta)N]}{(2\eta N+1)[3\eta(1-\eta)N+1]} \tag{109}$$

Clearly, the population in the symmetric state can be reduced to zero. This happens for $\eta = 1$, that is, when the squeezed field is perfectly matched to the atoms. In this case the population is distributed only between the ground state $|g\rangle$ and the upper state $|e\rangle$.

The issue we are interested in concerns the final state of the system and its purity. To answer this question, we apply the steady-state solutions (107) and find the stationary density matrix of the system

$$\rho = \begin{pmatrix} \rho_{gg} & 0 & \rho_{ge} \\ 0 & \rho_{ss} & 0 \\ \rho_{eg} & 0 & \rho_{ee} \end{pmatrix} \tag{110}$$

where ρ_{ij} are the nonzero steady-state density matrix elements.

It is evident from Eq. (110) that in the squeezed vacuum the density matrix of the system is not diagonal, due to the presence of the two-photon coherencies ρ_{ge} and ρ_{eg}. In this case the collective states $|g\rangle$, $|s\rangle$ and $|e\rangle$ are no longer eigenstates of the system. The density matrix can be rediagonalized by including ρ_{eg} and ρ_{ge} to give the new (entangled) states

$$|\Upsilon_1\rangle = \left[(P_1-\rho_{ee})|g\rangle + \rho_{eg}|e\rangle\right]/[(P_1-\rho_{ee})^2 + |\rho_{eg}|^2]^{1/2}$$
$$|\Upsilon_2\rangle = [\rho_{ge}|g\rangle + (P_2-\rho_{gg})|e\rangle]/[(P_2-\rho_{gg})^2 + |\rho_{eg}|^2]^{1/2}$$
$$|\Upsilon_3\rangle = |s\rangle \tag{111}$$

where the diagonal probabilities are

$$P_1 = \frac{1}{2}(\rho_{gg}+\rho_{ee}) + \frac{1}{2}[(\rho_{gg}-\rho_{ee})^2 + 4|\rho_{eg}|^2]^{1/2}$$
$$P_2 = \frac{1}{2}(\rho_{gg}+\rho_{ee}) - \frac{1}{2}[(\rho_{gg}-\rho_{ee})^2 + 4|\rho_{eg}|^2]^{1/2}$$
$$P_3 = \rho_{ss} \tag{112}$$

In view of Eq. (111), it is easy to see that the squeezed vacuum causes the system to decay into entangled states $|\Upsilon_i\rangle$, which are linear superpositions of the collective ground state $|g\rangle$ and the upper state $|e\rangle$. The intermediate symmetric state remains unchanged under the squeezed vacuum excitation. In general, the states (111) are mixed states. However, for perfect coupling of the squeezed vacuum to the atoms ($\eta = 1$) and $|M|^2 = N(N+1)$ the populations P_2 and P_3 are zero, leaving the population only in the state $|\Upsilon_1\rangle$. Hence, in the limit of perfect coupling $\eta = 1$ the state $|\Upsilon_1\rangle$ is a pure state of the system of two atoms driven by a squeezed vacuum field. From Eqs. (111), we find that the pure entangled state $|\Upsilon_1\rangle$ is given by

$$|\Upsilon_1\rangle = \frac{1}{\sqrt{2n}}[\sqrt{n+1}|g\rangle + \sqrt{n-1}|e\rangle] \tag{113}$$

The pure state (113) is nonmaximally entangled state; it reduces to a maximally entangled state for $N \gg 1$. The entangled state is analogous to the pairwise atomic state [22] or the multiatom squeezed state [23], (see also Ref. 24), predicted in the small sample model of two coupled atoms.

C. Effect of the Antisymmetric State on the Purity of the System

The preparation of a two-atom system in the pure entangled state $|\Upsilon_1\rangle$ requires perfect matching of the squeezed modes to the atoms and interatomic separations much smaller than the optical wavelength. To achieve perfect matching ($\eta = 1$), it is necessary to squeeze of all the modes to which the atoms are coupled: that is, the squeezed modes must occupy the whole 4π solid angle of the space surrounding the atoms. This is not possible to achieve with the present experiments in free space, and in order to avoid the difficulty cavity environments have been suggested [59]. Inside a cavity the atoms interact strongly only with the privileged cavity modes. By the squeezing of these cavity modes, which occupy only a small solid angle about the cavity axis, it would be possible to achieve perfect matching of the squeezed field to the atoms.

However, it is difficult experimentally to fulfil the second requirement that interatomic separations should be much smaller than the resonant wavelength. In fact, present atom trapping and cooling techniques can trap two atoms only within distances of the order of a resonant wavelength [11–13]. It is therefore of interest to examine the effect of increasing the interatomic separation so that the simple three-state representation of two atoms, presented in the preceding section, eventually ceases to be valid. With a finite interatomic separation, the two-atom system is represented by the full four-level system of (35).

With the interatomic separation included, the antisymmetric state $|a\rangle$ fully participates in the dynamics of the two-atom system. In this case $\Gamma_{12} \neq \Gamma$ and

the steady-state solutions of Eqs. (105) are

$$\begin{aligned}
\rho_{ee} &= \frac{(n-1)^2}{4n^2} + \frac{a^2|\tilde{M}|^2(2n-1)}{Q} \\
\rho_{ss} &= \frac{(n^2-1)}{4n^2} - \frac{a|\tilde{M}|^2(2n^2-a)}{Q} \\
\rho_{aa} &= \frac{(n^2-1)}{4n^2} + \frac{a|\tilde{M}|^2(2n^2+a)}{Q} \\
\rho_{u} &= \frac{2an^3|\tilde{M}|}{Q}
\end{aligned} \tag{114}$$

where

$$Q = n^2[n^4 + 4|\tilde{M}|^2(a^2 - n^2)] \tag{115}$$

This result shows that the antisymmetric state is populated in the steady-state even for small interatomic separations ($a \approx 1$). For large interatomic separations $a \approx 0$, and then the symmetric and antisymmetric states are equally populated. When the interatomic separation decreases, the population of the state $|a\rangle$ increases, whereas the population of the state $|s\rangle$ decreases and $\rho_{ss} = 0$ for very small interatomic separations. In Fig. 8, we plot the steady-state populations as a function of the interatomic separation. We see that the collective states are unequally populated and for small r_{12} the state $|a\rangle$ is the most populated state of the system, whereas the state $|s\rangle$ is not populated.

However, the vanishing of the population in the state $|s\rangle$ does not mean that the system is in a pure TPE state. This is due to the presence of the antisymmetric state $|a\rangle$ which is significantly populated for small interatomic separations. To show this, we calculate the quantity

$$\mathrm{Tr}(\rho^2) = \rho_{gg}^2 + \rho_{ss}^2 + \rho_{aa}^2 + \rho_{ee}^2 + |\rho_u|^2 \tag{116}$$

which determines the purity of the system. $\mathrm{Tr}(\rho^2) = 1$ corresponds to a pure state of the system, while $\mathrm{Tr}(\rho^2) < 1$ corresponds to a mixed state. $\mathrm{Tr}(\rho^2) = \frac{1}{4}$ describes a completely mixed state of the system. In Fig. 9, we display $\mathrm{Tr}(\rho^2)$ as a function of the interatomic separation r_{12} for perfect matching $\eta = 1$, $|M|^2 = N(N+1)$, and various N. Clearly, the system is in a mixed state independent of the interatomic separation. Moreover, the purity decreases as N increases.

For small interatomic separation, the mixed state of the system is composed of two states: the TPE state $|\Upsilon_1\rangle$ and the antisymmetric state $|a\rangle$. We can

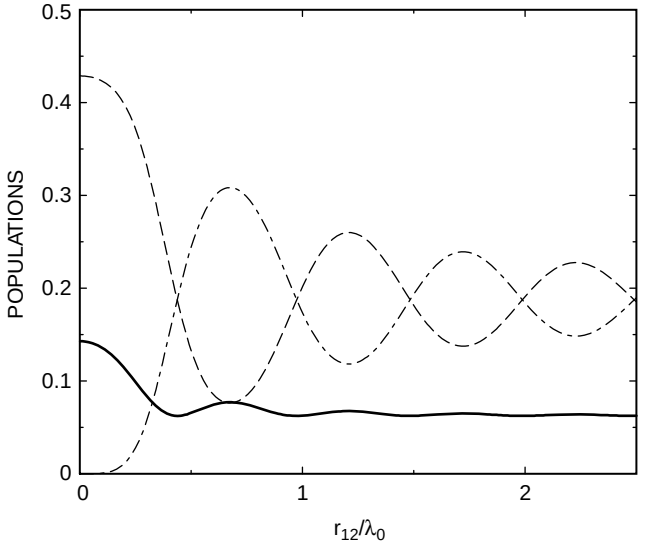

Figure 8. The steady-state populations of the collective atomic states as a function of the interatomic separation for $\eta = 1, |M|^2 = N(N+1), N = 0.5$, $\bar{\boldsymbol{\mu}} \perp \bar{r}_{12}$ and ρ_{ee} (solid line), ρ_{aa} (dashed line), ρ_{ss} (dashed–dotted line).

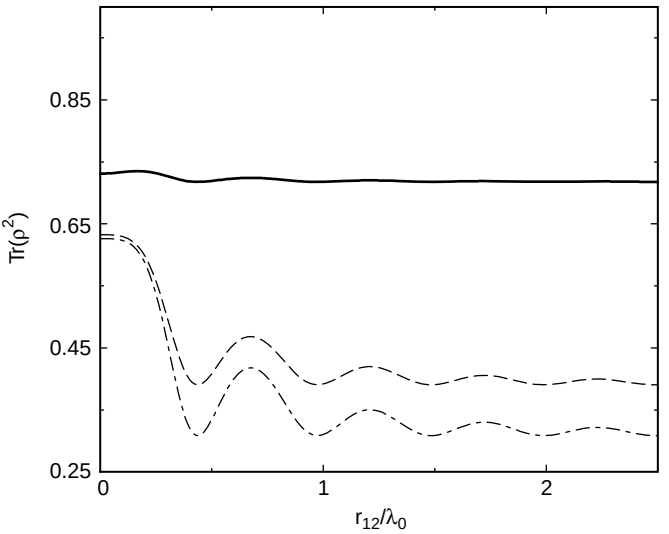

Figure 9. $\mathrm{Tr}(\rho^2)$ as a function of the interatomic separation for $\eta = 1, |M|^2 = N(N+1)$, $\bar{\boldsymbol{\mu}} \perp \bar{r}_{12}$ and different N: $N = 0.1$ (solid line), $N = 0.5$ (dashed line), $N = 1$ (dashed–dotted line).

illustrate this by diagonalizing the steady-state density matrix of the system

$$\rho = \begin{pmatrix} \rho_{gg} & 0 & 0 & \rho_{ge} \\ 0 & \rho_{aa} & 0 & 0 \\ 0 & 0 & \rho_{ss} & 0 \\ \rho_{eg} & 0 & 0 & \rho_{ee} \end{pmatrix} \tag{117}$$

When we diagonalize the matrix (117), we find the new (entangled) states

$$\begin{aligned} |\Upsilon_1\rangle &= \frac{(P_1 - \rho_{ee})|g\rangle + \rho_{eg}|e\rangle}{[(P_1 - \rho_{ee})^2 + |\rho_{eg}|^2]^{1/2}} \\ |\Upsilon_2\rangle &= \frac{\rho_{ge}|g\rangle + (P_2 - \rho_{gg})|e\rangle}{[(P_2 - \rho_{gg})^2 + |\rho_{eg}|^2]^{1/2}} \\ |\Upsilon_3\rangle &= |s\rangle \\ |\Upsilon_4\rangle &= |a\rangle \end{aligned} \tag{118}$$

where the diagonal probabilities (populations of the entangled states) are

$$\begin{aligned} P_1 &= \frac{1}{2}(\rho_{gg} + \rho_{ee}) + \frac{1}{2}[(\rho_{gg} - \rho_{ee})^2 + 4|\rho_{eg}|^2]^{1/2} \\ P_2 &= \frac{1}{2}(\rho_{gg} + \rho_{ee}) - \frac{1}{2}[(\rho_{gg} - \rho_{ee})^2 + 4|\rho_{eg}|^2]^{1/2} \\ P_3 &= \rho_{ss} \\ P_4 &= \rho_{aa} \end{aligned} \tag{119}$$

Note that the states $|\Upsilon_1\rangle, |\Upsilon_2\rangle$ and $|\Upsilon_3\rangle$ are the same as for the small sample model, discussed in the preceding section. This means that the presence of the antisymmetric state does not affect the two-photon entangled states, but it can affect the population distribution between the states and the purity of the system. In Fig. 10, we plot the populations P_i of the states $|\Upsilon_i\rangle$ as a function of the interatomic separation. The figure demonstrates that the atoms are driven into a mixed state composed of two states $|\Upsilon_1\rangle$ and $|a\rangle$, and there is a vanishing probability that the system is in the states $|\Upsilon_2\rangle$ and $|s\rangle$.

However, the system can decay to the pure TPE state $|\Upsilon_1\rangle$ with the interatomic separation included, provided the observation time is shorter than Γ^{-1}. The antisymmetric state $|a\rangle$ decays on a time scale $\sim(\Gamma - \Gamma_{12})^{-1}$, and for $\Gamma_{12} \approx \Gamma$ the decay rate of the antisymmetric state is much longer than Γ^{-1}. By contrast, the state $|s\rangle$ decays on a time scale $\sim(\Gamma + \Gamma_{12})^{-1}$, which for $\Gamma_{12} \approx \Gamma$ is shorter than Γ^{-1}. Clearly, for observation times shorter than Γ^{-1}, the antisymmetric state does not participate in the interaction and the system reaches the steady-state only between the triplet states. Thus, for perfect

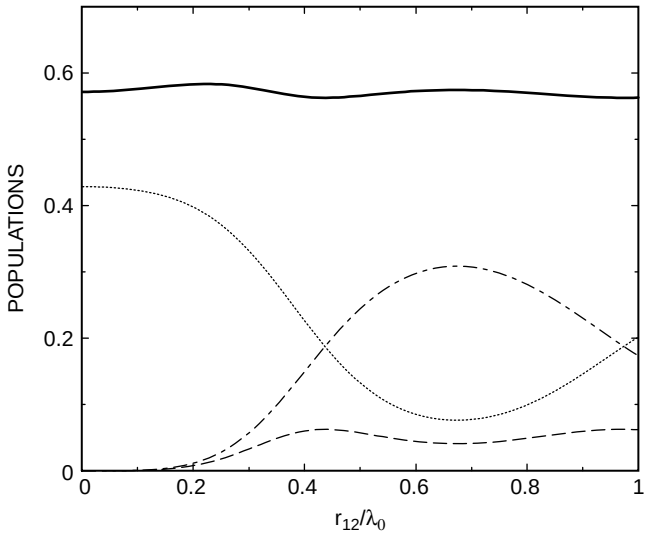

Figure 10. The populations P_i of the entangled states (115) as a function of the interatomic separation for $\eta = 1, |M|^2 = N(N+1)$, $\bar{\boldsymbol{\mu}} \perp \bar{r}_{12}$ and $N = 0.5$; P_1 (solid line), P_2 (dashed line), P_3 (dashed–dotted line), P_4 (dotted line).

matching of the squeezed modes to the atoms the symmetric state is not populated and then the system is in the pure TPE state $|\Upsilon_1\rangle$.

D. Two-Photon Entangled States for Two Nonidentical Atoms

By employing two nonidentical atoms of significantly different transition frequencies ($\Delta \gg \Gamma$), it is possible to achieve the pure TPE state with the interatomic separation comparable to the resonant wavelength, and the anti-symmetric state fully participating in the interaction.

Assuming that $\Delta \neq 0$, the master equation (103) leads to the following equations of motion for the density matrix elements

$$\begin{aligned}
\frac{\partial}{\partial t}\rho_{ee} &= -\Gamma(n+1)\rho_{ee} + \frac{1}{2}(n-1)\left[\Gamma(\rho_{ss}+\rho_{aa}) + \Gamma_{12}(\rho_{ss}-\rho_{aa})e^{i\Delta t}\right] \\
&\quad + \Gamma_{12}|\tilde{M}|\left(\rho_{eg}e^{-i[2(\omega_s-\omega_0)t+\phi]} + \rho_{ge}e^{i[2(\omega_s-\omega_0)t+\phi]}\right) \\
\frac{\partial}{\partial t}\rho_{ss} &= \frac{1}{2}(\Gamma + \Gamma_{12}e^{i\Delta t})\left[(n-1) - (3n-1)\rho_{ss} - (n-1)\rho_{aa} + 2\rho_{ee}\right] \\
&\quad - \Gamma|\tilde{M}|\left(\rho_{eg}e^{-i[2(\omega_s-\omega_1)t+\phi]} + \rho_{ge}e^{i[2(\omega_s-\omega_1)t+\phi]}\right) \\
&\quad - \Gamma_{12}|\tilde{M}|\left(\rho_{eg}e^{-i[2(\omega_s-\omega_0)t+\phi]} + \rho_{ge}e^{i[2(\omega_s-\omega_0)t+\phi]}\right)
\end{aligned}$$

$$\begin{aligned}\frac{\partial}{\partial t}\rho_{aa} &= \frac{1}{2}\left(\Gamma - \Gamma_{12}e^{i\Delta t}\right)[(n-1) - (3n-1)\rho_{aa} - (n-1)\rho_{ss} + 2\rho_{ee}] \\ &\quad + \Gamma|\tilde{M}|(\rho_{eg}e^{-i[2(\omega_s-\omega_1)t+\phi]} + \rho_{ge}e^{i[2(\omega_s-\omega_1)t+\phi]}) \\ &\quad - \Gamma_{12}|\tilde{M}|(\rho_{eg}e^{-i[2(\omega_s-\omega_0)t+\phi]} + \rho_{ge}e^{i[2(\omega_s-\omega_0)t+\phi]}) \\ \frac{\partial}{\partial t}\rho_{eg} &= \left(\frac{\partial}{\partial t}\rho_{ge}\right)^* = \Gamma_{12}\tilde{M}e^{i[2(\omega_s-\omega_1)t+\phi]} - n\Gamma\rho_{eg} \\ &\quad - \Gamma\tilde{M}e^{i[2(\omega_s-\omega_1)t+\phi]}(\rho_{ss} - \rho_{aa}) \\ &\quad + 2\Gamma_{12}\tilde{M}e^{i[2(\omega_s-\omega_0)t+\phi]}(\rho_{ss} + \rho_{aa}) \end{aligned} \tag{120}$$

where $\omega_0 = \frac{1}{2}(\omega_1 + \omega_2)$.

Equations (120) contain time-dependent terms that oscillate at frequencies $\exp(\pm i\Delta t)$ and $\exp[\pm 2i(\omega_s - \omega_0)t + \phi]$. If we tune the squeezed vacuum field to the middle of the frequency difference between the atomic frequencies, namely, $\omega_s = (\omega_1 + \omega_2)/2$, the terms proportional to $\exp[\pm 2i(\omega_s - \omega_0)t + \phi]$ become stationary in time. None of the other time-dependent components is resonant with the frequency of the squeezed vacuum field. Consequently, for $\Delta \gg \Gamma$, the time-dependent components oscillate rapidly in time and average to zero over long times. Therefore, we can formulate a secular approximation in which we ignore the rapidly oscillating terms, and find that Eqs. (120) give us the following steady-state solutions [64]:

$$\begin{aligned}\rho_{ee} &= \frac{1}{4}\left[\frac{(n-2)}{n} + \frac{1}{(n^2 - 4a^2|\tilde{M}|^2)}\right] \\ \rho_{ss} = \rho_{aa} &= \frac{1}{4}\left[1 - \frac{1}{(n^2 - 4a^2|\tilde{M}|^2)}\right] \\ \rho_u &= \frac{2a|\tilde{M}|}{n(n^2 - 4a^2|\tilde{M}|^2)}\end{aligned} \tag{121}$$

These equations are quite different from Eqs. (114) that in the case of non-identical atoms the symmetric and antisymmetric states are equally populated independent of the interatomic separation. These are, however, similar to the steady-state solutions for the small sample model that for small interatomic separations $\rho_{ss} = \rho_{aa} \approx 0$ and then only the collective ground and the upper states are populated.

E. Mapping of the Entanglement of Light on Atoms

The generation of the pure TPE state is an example of mapping of a state of quantum correlated light onto an atomic system. The two-photon correlations

contained in the squeezed vacuum field can be completely transferred to the atomic system. It is seen from Eq. (121) that the collective damping parameter $a(a = \Gamma_{12}/\sqrt{\Gamma_1\Gamma_2})$ plays the role of a degree of the correlation transfer from the squeezed vacuum to the atomic system. For large interatomic separations, $\Gamma_{12} \approx 0$, and there is no transfer of the correlations to the system. In contrast, for very small separations, $\Gamma_{12} \approx \Gamma$, and then the correlations are completely transferred to the atomic system.

However, the complete transfer of the correlations does not necessary mean that the two-photon correlations are stored in the pure TPE state. This happens only for the small sample model and two atoms with significantly different transition frequencies, where the steady state is the pure TPE state. For identical atoms separated by a finite distance r_{12}, a part of the correlations is stored in the antisymmetric state. This fact can lead to an interesting modification of the interference pattern of the fluorescence field. Using the steady-state solutions (114), we find that the visibility in the interference pattern is given by [58]

$$\mathscr{V} = -\frac{4a\eta^2|M|^2}{n^3(n-1) + 4\eta^2|M|^2(a+n-n^2)} \tag{122}$$

This visibility is negative, indicating that the squeezing correlations stored in the antisymmetric state generate an interference pattern with a dark center. In Fig. 11, we plot the visibility $\mathscr{V}$ as a function of the interatomic separation for

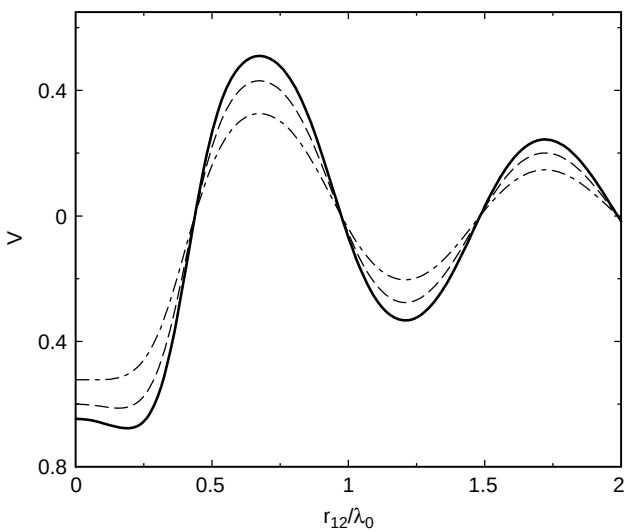

Figure 11. The visibility $\mathscr{V}$ as a function of the interatomic separation for $\eta = 1, |M|^2 = N(N+1)$, $\bar{\boldsymbol{\mu}} \perp \bar{r}_{12}$ and different N: $N = 0.1$ (solid line), $N = 0.5$ (dashed line), $N = 5$ (dashed–dotted line).

$\eta = 1$ and $|M| = \sqrt{N(N+1)}$. An interference pattern with a dark center is observed for small interatomic separations ($r_{12} < \lambda_0$) with the maximal negative value $\mathscr{V} \approx -\frac{1}{2}$. The value $\mathscr{V} \approx -\frac{1}{2}$ compared to the possible negative value $\mathscr{V} = -1$ indicates that 50% of the squeezing correlations are stored in the antisymmetric state. Thus, the visibility can be used to measure the degree of correlations stored in the entangled state $|a\rangle$.

The two-photon correlations stored in the pure TPE state can be measured by detecting fluctuations of the fluorescence field emitted by the atomic system. Squeezing in the fluorescence field is proportional to the squeezing in the atomic dipole operators (squeezing in the atomic spins) which, on the other hand, can be found from the steady-state solutions for the density matrix elements.

The fluctuations of the electric field are determined by the normally ordered variance of the field operators as

$$\langle :(\Delta E_\theta)^2: \rangle = \sum_{\mathbf{k}s} E_k (2\langle a^\dagger_{\mathbf{k}s} a_{\mathbf{k}s}\rangle + \langle a_{\mathbf{k}s} a_{\mathbf{k}s}\rangle e^{2i\theta} + \langle a^\dagger_{\mathbf{k}s} a^\dagger_{\mathbf{k}s}\rangle e^{-2i\theta}) \tag{123}$$

Using the correlation functions (93) and choosing $\theta = \pi/2$, the variance of the incident squeezed vacuum field can be written as

$$\langle :(\Delta E^v_{\pi/2})^2: \rangle = 2E_0(N - |M|) \tag{124}$$

where E_0 is a constant.

Since $|M| = \sqrt{N(N+1)}$, the variance (124) is negative, indicating that we have a squeezed field.

On the other hand, the normally ordered variance of the emitted fluorescence field can be expressed in terms of the density matrix elements of the two-atom system as

$$\langle :\left(\Delta E^F_\theta\right)^2: \rangle = E_0(2\rho_{ss} + 2\rho_{ee} + |\rho_u| \cos 2\theta) \tag{125}$$

Using the steady-state solutions (107) and choosing $\theta = \pi/2$, we find

$$\langle :(\Delta E^F_{\pi/2})^2: \rangle = 2E_0 \frac{(N - |M|)}{2N+1} \tag{126}$$

Thus, at low intensities of the squeezed vacuum field ($N \ll 1$) the fluctuations in the incident squeezed vacuum field are perfectly mapped onto the atomic system. For large intensities ($N > 1$), the thermal fluctuations of the atomic dipoles dominate over the squeezed fluctuations, resulting in a reduction of squeezing in the fluorescence field.

Kozhekin et al. [38] proposed a method of mapping of quantum states onto an atomic system based on the stimulated Raman absorption of propagating quantum light by a cloud of three-level atoms. Hald et al. [40] have experimentally observed the squeezed spin states of a system of three-level atoms driven by a squeezed field. The observed squeezed spin states have been generated via entanglement exchange with the squeezed field completely absorbed in the process. Fleishhauer et al. [39] have considered a similar system of three-level atoms and have found that quantum states of single-photon fields can be mapped onto collective states of the atomic system. In this case the quantum state of the field is stored in a dark state of the collective states of the system.

Acknowledgments

This work was supported by the Australian Research Council. We gratefully acknowledge helpful conversations with Stuart Swain and Almut Beige.

References

1. R. H. Dicke, *Phys. Rev.* **93**, 99 (1954).
2. G. S. Agarwal, *Phys. Rev. A* **2**, 2038 (1970).
3. R. Bonifacio and L. A. Lugiato, *Phys. Rev. A* **11**, 1507 (1975).
4. M. Gross and S. Haroche, *Phys. Rep.* **93**, 301 (1982).
5. J. H. Eberly and N. E. Rehler, *Phys. Rev. A* **2**, 1607 (1970).
6. C. Greiner, B. Boggs, and T. W. Mossberg, *Phys. Rev. Lett.* **85**, 3793 (2000).
7. R. H. Lehmberg, *Phys. Rev. A* **2**, 883, 889 (1970).
8. G. S. Agarwal, in G. Höhler (Ed.),*Quantum Statistical Theories of Spontaneous Emission and Their Relation to Other Approaches*, *Springer Tracts in Modern Physics*, Vol. 70, Springer-Verlag , Berlin, 1974.
9. P. W. Milonni and P. L. Knight, *Phys. Rev. A* **10**, 1096 (1974).
10. Z. Ficek, R. Tanaś, and S. Kielich, *Physica* **146A**, 452 (1987).
11. U. Eichmann, J. C. Bergquist, J. J. Bollinger, J. M. Gilligan, W. M. Itano, D. J. Wineland, and M. G. Raizen, *Phys. Rev. Lett.* **70**, 2359 (1993).
12. R. G. DeVoe and R. G. Brewer, *Phys. Rev. Lett.* **76**, 2049 (1996).
13. D. J. Berkeland, in R. Blatt, J. Eschner, D. Leibfried, and F. Schmidt-Kaler (Eds.), *Laser Spectroscopy* World Scientific, Singapore, 1999, p. 352.
14. M. B. Plenio and V. Vedral, *Contemp. Phys.* **39**, 431 (1998).
15. A. Barenco, *Contemp. Phys.* **37**, 375 (1996).
16. L. K. Grover, *Phys. Rev. Lett.* **79**, 325 (1997).
17. A. Barenco and A. Ekert, *J. Mod. Opt.* **42**, 1253 (1995).
18. S. F. Pereira, Z. Y. Ou, and H. J. Kimble, *Phys. Rev. A* **62**, 042311 (2000).
19. A. Ekert, *Phys. Rev. Lett.* **67**, 661 (1991).
20. J. J. Bollinger, W. M. Itano, D. J. Wineland, and D. J. Heinzen, *Phys. Rev. A* **54**, R4649 (1996); S. F. Huelga, C. Macchiavello, T. Pellizzari, A. K. Ekert, M.B. Plenio, and J. I. Cirac, *Phys. Rev. Lett.* **79**, 3865 (1997).

21. M. J. Stephen, J. Chem. Phys. **40**, 669 (1964).
22. G. M. Palma and P. L. Knight, *Phys. Rev. A* **39**, 1962 (1989); A. K. Ekert, G. M. Palma, S. M. Barnett, and P. L. Knight, *Phys. Rev. A* **39**, 6026 (1989); G.S. Agarwal and R. R. Puri, *Phys. Rev. A* **41**, 3782 (1990); Z. Ficek, *Phys. Rev. A* **44**, 7759 (1991).
23. S. M. Barnett and M. A. Dupertuis, *J. Opt. Soc. Am. B* **4**, 505 (1987).
24. A. S. Parkins, in M. Evans and S. Kielich (Eds.), *Modern Nonlinear Optics*, Part II, Wiley, New York, 1993, p. 607.
25. Z. Ficek and P. D. Drummond, *Physics Today* 34 (Sept. 1997); B. J. Dalton, Z. Ficek, and S. Swain, *J. Mod. Opt.* **46**, 379 (1999).
26. S. J. D. Phoenix and S. M. Barnett, *J. Mod. Opt.* **40**, 979 (1993).
27. I. K. Kudrayvtsev and P. L. Knight, *J. Mod. Opt.* **40**, 1673 (1993).
28. J. I. Cirac and P. Zoller, *Phys. Rev. A* **50**, R2799 (1994).
29. C. C. Gerry, *Phys. Rev. A* **53**, 2857 (1996).
30. M. B. Plenio, S. F. Huelga, A. Beige, and P. L. Knight, *Phys. Rev. A* **59**, 2468 (1999).
31. A. Beige, S. F. Huelga, P. L. Knight, M. B. Plenio, and R. C. Thompson, *J. Mod. Opt.* **47**, 401 (2000).
32. A. Beige, W. J. Munro, and P. L. Knight, *Phys. Rev. A* **62**, 052102 (2000).
33. U. Akram, Z. Ficek, and S. Swain, *Phys. Rev. A* **62**, 013413 (2000).
34. A. Beige, D. Braun, B. Tregenna, and P. L. Knight, *Phys. Rev. Lett.* **85**, 1762 (2000).
35. Q. A. Turchette, C. S. Wood, B. E. King, C. J. Myatt, D. Leibfried, W. M. Itano, C. Monroe, and D. J. Wineland, *Phys. Rev. Lett.* **81**, 3631 (1998).
36. E. Hagley, X. Maitre, G. Nogues, C. Wunderlich, M. Brune, J. M. Raimond, and S. Haroche, *Phys. Rev. Lett.* **79**, 1 (1997).
37. A. Kuzmich, L. Mandel, and N. P. Bigelow, *Phys. Rev. Lett.* **85**, 1594 (2000).
38. A. E. Kozhekin, K. Molmer, and E. Polzik, *Phys. Rev. A* **62**, 033809 (2000).
39. M. Fleischhauer, S. F. Yelin, and M. D. Lukin, *Opt. Commun.* **179**, 395 (2000).
40. J. Hald, J. L. Sorensen, L. Leich, and E. S. Polzik, *Opt. Express* **2**, 93 (1998); J. Hald, J. L. Sorensen, C. Schori, and E. S. Polzik, *Phys. Rev. Lett.* **83**, 1319 (1999).
41. W. H. Louisell, *Statistical Properties of Radiation*, Wiley, New York, 1973.
42. L. Allen and J. H. Eberly, *Resonance Fluorescence and Two-Level Atoms*, Wiley, New York, 1975.
43. Z. Ficek, R. Tanaś, and S. Kielich, *Optica Acta* **33**, 1149 (1986).
44. G. J. Yang, O. Zobay, and P. Meystre, *Phys. Rev. A* **59**, 4012 (1999).
45. T. Richter, *Optica Acta* **29**, 265 (1982).
46. Z. Ficek, R. Tanaś, and S. Kielich, *Optica Acta* **30**, 713 (1983).
47. T. Richter, *Optica Acta* **30**, 1769 (1983).
48. T. G. Rudolph, Z. Ficek, and B. J. Dalton, *Phys. Rev. A* **52**, 636 (1995).
49. H. S. Freedhoff, *Phys. Rev. A* **26**, 684 (1982).
50. Z. Ficek and B. C. Sanders, *Phys. Rev. A* **41**, 359 (1990).
51. S. Franke, G. Huyet, and S. M. Barnett, *J. Mod. Opt.* **47**, 145 (2000).
52. H. T. Dung and K. Ujihara, *Phys. Rev. Lett.* **84**, 254 (2000).
53. G. C. Guo and C. P. Yang, *Physica* **A260**, 173 (1998); C. P. Yang and G. C. Guo, *Physica* **A273**, 352 (1999).

54. T. Wong, S. M. Tan, M. J. Collett, and D. F. Walls, *Phys. Rev. A* **55**, 1288 (1997).
55. P. Kochan, H. J. Carmichael, P. R. Morrow, and M. G. Raizen, *Phys. Rev. Lett.* **75**, 45 (1995).
56. G. M. Meyer and G. Yeoman, *Phys. Rev. Lett.* **79**, 2650 (1997).
57. T. Rudolph and Z. Ficek, *Phys. Rev. A* **58**, 748 (1998).
58. Z. Ficek and R. Tanaś, *Opt. Commun.* **153**, 245 (1998).
59. Q. A. Turchette, N.P. Georgiades, C. J. Hood, H. J. Kimble, and A. S. Parkins, *Phys. Rev. A* **58**, 4056 (1998); N.P. Georgiades, E. S. Polzik, and H. J. Kimble, *Phys. Rev. A* **59**, 123 (1999).
60. Z. Ficek and P. D. Drummond, *Europhys. Lett.* **24**, 455 (1993).
61. A. Yariv, *Quantum Electronics*, Wiley, New York, 1989.
62. M. Born and E. Wolf, *Principles of Optics*, Macmillan, New York, 1964, Chapter 7.
63. Z. Ficek and P. D. Drummond, *Phys. Rev. A* **43**, 6247 (1991); **43**, 6258 (1991).
64. Z. Ficek and M. R. B. Wahiddin, *Opt. Commun.* **134**, 387 (1997).

MULTIPOLAR POLARIZABILITIES FROM INTERACTION-INDUCED RAMAN SCATTERING

TADEUSZ BANCEWICZ

Nonlinear Optics Division, Faculty of Physics, Adam Mickiewicz University, Poznań, Poland

YVES LE DUFF AND JEAN-LUC GODET

Laboratoire des Propriétés Optiques des Matériaux et Applications, Université d'Angers, Faculté des Sciences, Angers, France

CONTENTS

I. INTRODUCTION

Multipolar polarizabilities contribute to molecular interactions in dense media and may influence macroscopic properties of matter (e.g., dielectric virial coefficient, susceptibilities, light scattering intensities) [1]. However, until the late 1970s or so, these molecular constants have not been studied very extensively. In 1978, it was shown for the first time that the induced rotational transitions associated to dipole-multipole polarizabilities of molecules induce depolarized scattering in compressed gases [2]. Then scattering experiments have been used to study multipolar polarizability for several types of molecules. For isotropic molecules, for which the polarizability tensor is a scalar, there are no allowed rotational bands around the Rayleigh line and multipolar contributions have been observed in the depolarized Rayleigh wings where they appear mixed with a strong contribution from the dipole-induced dipole (DID) effect [2–8]. In this way, the dipole quadrupole polarizability A and/or the dipole octopole polarizability E have been measured for CH_4, CD_4, neopentane, CF_4, and SF_6 [2–12]. Recently it has been shown that these multipolar contributions may also be measured in the isotropic Rayleigh wings without any perturbation from DID interactions [13,14]. In the case of linear molecules the allowed rotational lines of each individual molecule yield a large scattering around the Rayleigh line and hide multipolar polarizabilities contributions at low frequency shifts. However in the case of N_2 and CO_2 [15,16] from studies of scattering intensities in the very far wings of the Rayleigh band, the dipole–octopole polarizability E may be deduced. Consideration of isotropic scattering intensities in these molecules allows us to avoid any perturbation from the rotational bands of free molecules contrary to the depolarized scattering spectrum [15]. Multipolar polarizabilities effects may also be observed outside the Rayleigh

frequency domain and in particular in the vibrational Raman bands. For CF_4 and SF_6 the measurement of scattering intensities in the totally symmetric ν_1 Raman band have provided experimental value for their normal coordinate derivative multipolar polarizabilities dA/dR and/or dE/dR [14,17,18].

In this chapter we first give a general presentation of collision-induced scattering (CIS) also named interaction induced scattering. The different types of molecular interaction are mentioned with a special emphasis on the multipolar polarizabilities contributions studied in our laboratories [19] since the beginning of 1990s. Then we describe the setup and the experimental procedure used for the measurement of the scattering on an absolute scale. In the following paragraphs we discuss the multipolar contributions to depolarized and isotropic CIS for specific molecular symmetries. We present studies in the Rayleigh wings of isotropic molecules such as CF_4 and SF_6 and of linear molecules such as N_2 and CO_2. Finally we report on observations made in the wings of vibrational Raman bands of CF_4 and SF_6.

II. THEORY OF LIGHT SCATTERING

A. Historical Background

The approach of the molecules or atoms and their dispersal accompanying the collisions between them involve temporary changes in the resultant polarizability of an interacting pair or in general a cluster of molecules. The polarizability $A_{\alpha\beta}$ of the pair of molecules A and B:

$$A_{\alpha\beta} = A_{\alpha\beta}(A) + A_{\alpha\beta}(B) + \Delta A_{\alpha\beta}(AB) \tag{1}$$

is no longer a simple sum of the internal polarizabilities $A_{\alpha\beta}(A)$ and $A_{\alpha\beta}(B)$ and some additional polarizability $\Delta A_{\alpha\beta}(AB)$ appears known as the collision-induced or interaction-induced polarizability, originating from all possible interactions between the molecules. At least two reasons for its appearance can be identified: (1) the fluctuating electric field produced by the neighboring molecule different from the electric field of the external source of radiation and (2) short-range interactions, such as of the overlap type and the dispersion interactions deforming the electron clouds of the interacting molecules and thus changing their internal polarizabilities. This incremental polarizability is manifested in the dielectric and optical properties of the concentrated gases and liquids. Changes in the mean polarizability (α) of a pair of interacting molecules determine the second dielectric virial coefficient [20], the second virial coefficient of the light refraction index and rototranslational wings of the isotropic Rayleigh and Raman light scattering [1,21]. The collision-induced anisotropy contributes to the second virial coefficient for the Kerr effect, to the electric-field-induced birefringence, and is a source of rototranslational wings in

the vicinity of the Rayleigh and Raman lines [22]. Besides, in the system of two molecules or atoms, the above-described mechanisms cause the appearance of collision-induced additional dipole moment (static or modulated by vibrations) which is a source of the collision-induced absorption [23]. In this chapter we concentrate on the processes prompted by the collision-induced polarizability, or to be more exact, its spectral manifestations. Thus, we consider the effect of the excess polarizability on the Rayleigh and Raman light scattering for the systems whose density implies a significant role of binary interactions. As follows from our measurements, at room temperature the binary interaction approximation can be used for gas N_2 up to 150 amagat [15] and for CO_2 [16] and CF_4 [8,13] up to 100 amagat. For greater densities higher order correlations begin to play an important role and interpretation of the collision-induced mechanisms becomes more complex or even problematic.

Naturally, collision-induced contributions are present in all kinds of spectra. They are much less sensitive to the limitations imposed by the selection rules and always accompany the allowed transitions. In interpretation of such single-molecule spectra, the collision-induced part should be recognized so that it could be correctly separated from the single-molecule mechanism. In some circumstances, such a collision-induced part of the spectrum may be identified more easily; it is the case of: (1) the spectrum of H_2 (because of large distances between the rotation lines of permanent anisotropy) [24], and (2) the spectrum of H_2S (because of a very low value of the anisotropy constant) [25] . In most cases, however, the collision-induced spectra accompanying the allowed transitions are difficult for interpretation (e.g., the problem of cross effects) and the information they provide are less reliable—this concerns in particular the depolarized component of the scattered light. The situation is generally different for the polarized component which includes an anisotropic part and an isotropic part where the latter is caused by the mean polarizability α of the molecular pair. The intrinsic mean polarizability of an isolated molecule is the source of a strong and very narrow central line of the spectrum (the Q branch). Thus, the wings of the isotropic part of the scattered radiation are of a collision-induced nature [15] and can provide much information on the rotational collision effects (they have a relatively weak translation spectrum of only second-order DID type) [13]. However, the spectral studies of the wings (in particular its high-frequency domain) in the isotropic part of the scattered radiation are very difficult to measure and for molecules only a few works have been devoted to this subject [13,15,18,25,26].

The collision-induced polarizability is best manifested if it is the only reason for the phenomenon observed. In such a case the intermolecular interactions break the selection rules of isolated molecules and a process forbidden in the single-molecule approximation becomes allowed in concentrated gas or liquid. For example, it occurs when we observe the depolarized component of light

scattered by noble gases or gases composed of isotropically polarized molecules such as CH_4, CF_4, or SF_6 [8,13,17,18] or when we observe vibrations ν_2 and ν_3 (forbidden in single-molecule Raman spectroscopy) of such molecules as CO_2 and CS_2. Then, investigation of the scattered radiation spectrum allows direct insight into the mechanisms responsible for the excess polarizability $\Delta A_{\alpha\beta}(AB)$ and dynamics of intermolecular interactions.

We begin our review by describing collision-induced light scattering mechanisms in the language of Cartesian tensors. We continue our description by the way of irreducible spherical tensors showing that the irreducible spherical tensors approach is indispensable for the spectral lineshape computation.

B. Pair Polarizability Tensor

In a dense medium, collisional effects as well as time and space fluctuations of multipolar molecular fields will in general lead to changes in the molecular polarizability tensor. Then, according to Eq. (1), the pair polarizability tensor of two molecules A and B, $A_{\alpha\beta}$, acquires an incremental collision-induced polarizability of linear origin $\Delta A^{(L)}_{\alpha\beta}(AB)$ and of nonlinear origin $\Delta A^{(NL)}_{\alpha\beta}(AB)$:

$$A_{\alpha\beta} = A_{\alpha\beta}(A) + A_{\alpha\beta}(B) + \Delta A^{(L)}_{\alpha\beta}(AB) + \Delta A^{(NL)}_{\alpha\beta}(AB) \tag{2}$$

The excess collision-induced pair polarizability of molecules A and B results as a self-consistent solution of a set of equations for local fields polarizing molecules A and B and the multipolar moments induced in molecules A and B. In a first approximation, the long range field-induced change in the pair polarizability, related to the linear multipolar polarizabilities of molecules, is [27]:

$$\Delta \mathbf{A}^{(L)}_{\alpha\beta} = (1 + \mathscr{P}_{\mathscr{A}\mathscr{B}}) \left\{ \sum_{m=1}^{\infty} \sum_{n=1}^{\infty} (-1)^n \frac{2^{m+n} m! n!}{(2m)!(2n)!} \right.$$
$$\left. {}^{(1)}\mathbf{A}^{(m)}(\omega_A)[m]^{(m)}\mathbf{T}^{(n)}(\mathbf{R}_{AB})[n]^{(n)}\mathbf{A}^{(1)}(\omega_B) \right\}_{\alpha\beta} \tag{3}$$

where the tensor ${}^{(1)}\mathbf{A}^{(m)}(\omega_i)$ of rank $1 + m$ determines the linear dipole mth-rank multipole polarizability due to dipole–$2^{**}m$-pole electric transitions in a molecule i, the symbol $[m]$ denotes m-fold contraction whereas $\mathscr{P}_{\mathscr{A}\mathscr{B}}$ permutes the indices A and B. Moreover, the tensor

$${}^{(m)}\mathbf{T}^{(n)}(\mathbf{R}_{AB}) = \nabla_A^m \nabla_B^n \left(\frac{1}{R_{AB}} \right) \tag{4}$$

of $m + n$ rank defines $2^{**}m$-pole–$2^{**}n$-pole interaction between molecules A and B separated by a distance $\mathbf{R}_{AB}$.

The additional variation in the pair polarizability due to nonlinear molecular polarizabilities combined with permanent multipoles in a first approximation has the form [27]

$$\Delta \mathbf{A}_{\alpha\beta}^{(NL)} = (1+\mathscr{P}_{\mathscr{A}\mathscr{B}})\left\{\sum_{m=1}^{\infty}\sum_{n=1}^{\infty}(-1)^n \frac{2^{m+n}m!n!}{(2m)!(2n)!}\cdot \right.$$
$$\left. {}^{(1)}\mathbf{B}^{(1+m)}(\omega_A)[m]^{(m)}\mathbf{T}^{(n)}(\mathbf{R}_{AB})[n]\mathbf{Q}^{(n)}(\omega_B)\right\}_{\alpha\beta} \tag{5}$$

where the tensor ${}^{(1)}\mathbf{B}^{(1+m)}(\omega_i)$ of rank $2+m$ determines the nonlinear (second order) dipole-mth rank multipole hyperpolarizability due to dipole–dipole-$2^{**}m$-pole electric transitions in a molecule i. Moreover $\mathbf{Q}^{(n)}(\omega_i)$ defines the $2^{**}n$ order intrinsic molecular multipole moment of molecule i.

Some time ago we contributed to the development of the irreducible spherical tensor multipolar theory of light scattering [13,28]. According to Ref. 13, the M component of the Kth-rank dipole–arbitrary order multipole linear polarizability of a pair of interacting molecules A and B reads as

$$\Delta A_{KM}^{(L)} = 2\sum_{\substack{j_A j_B \times \\ l_A l_B}}(-1)^{j_A+N}\left(\frac{2^N}{(2l_A)!(2l_B)!}\right)^{1/2} X_{j_A j_B N x}\begin{Bmatrix} j_A & j_B & x \\ 1 & 1 & K \\ l_A & l_B & N \end{Bmatrix}$$
$$\left[\mathbf{T}_N(\mathbf{R}_{AB})\otimes\left(\boldsymbol{\alpha}_{j_A}^{(1l_A)}\otimes\boldsymbol{\alpha}_{j_B}^{(1l_B)}\right)_{(x)}\right]_{KM} \tag{6}$$

whereas the nonlinear part of the pair polarizability has the form

$$\Delta A_{KM}^{(NL)} = -(1+\mathscr{P}_{\mathscr{A}\mathscr{B}})\sum_{J_A l_A l_B}\left(\frac{2^N}{(2l_A)!(2l_B)!}\right)^{1/2}(-1)^{l_B}\frac{X_{NJ_A x}}{X_K}$$
$$\begin{Bmatrix} N & l_B & l_A \\ J_A & K & x \end{Bmatrix}\left\{\mathbf{T}_N^{(AB)}(\mathbf{R}_{12})\otimes\left[\boldsymbol{\beta}_{J_A}[(11)Kl_A]\otimes\mathbf{Q}_{l_B}\right]_{(x)}\right\}_{KM} \tag{7}$$

where

$$\begin{Bmatrix} a & b & c \\ d & e & f \\ g & h & j \end{Bmatrix} \tag{8}$$

is the $9-j$ Wigner symbol, whereas

$$\begin{Bmatrix} a & b & c \\ d & e & f \end{Bmatrix} \tag{9}$$

stands for the $6-j$ Wigner symbol. Moreover, $\mathbf{A}_{j_i}^{(1,l_i)}$ is the irreducible j_ith-rank spherical tensor of dipole-l_ith-rank multipole polarizability tensor of molecule i and $\mathbf{T}_N$ denotes the spherical multipole interaction tensor, $X_{ab\ldots f} = [(2a+1)(2b+1)\cdots(2f+1)]^{1/2}, N = l_A + l_B$ and $\otimes$ stands for the irreducible tensor product. Besides, in Eq. (7) $Q_{l_i m_i}$ denotes the m_i component of the l_ith-order spherical electric multipole moment of the molecule i and $\beta_{J_i M_i}[(11)al_i]$ stands for the irreducible J_i rank spherical tensor of dipole–dipole–$2^{**}a$-pole hyperpolarizability of molecule i in a coupling scheme where two dipoles are first connected and, subsequently the $2^{**}a$-pole multipolar moment.

C. Pair Correlation Function

When induction operators of high-order multipoles are taken into account intensity calculations tend to become very cumbersome [30,31]. We propose a relatively easy way of performing these calculations using the irreducible spherical tensor theory of multipole light scattering [e.g., Eqs. (6) and (7)] together with symbolic calculations of the Wigner coefficients by computer.

We consider a macroscopically isotropic system composed of N-like molecules in an active scattering volume V illuminated by laser radiation of frequency ω_i, linearly polarized in the direction $\mathbf{e}$. We analyze the secondary electromagnetic radiation emitted by the system in response to that perturbation. At a point $\mathbf{R}$ distant from the center of the sample, the radiation scattered at ω is measured on traversal of an analyzer with polarization $\mathbf{n}$. The pair double-differential cross sections for scattered interaction-induced radiation becomes

$$\frac{\partial^2\sigma}{\partial\Omega\partial\omega} = k_i k_s^3 \frac{1}{2\pi}\int \exp(-i\omega t)F(t)dt \tag{10}$$

where

$$F(t) = \sum_{k=0,2} \Phi_{kk} F_{kk}(t) \tag{11}$$

with geometric factors equal to $\Phi_{00} = \frac{1}{3}(\mathbf{e}\cdot\mathbf{n})^2$ for the isotropic spectrum and $\Phi_{22} = \frac{1}{30}[3 + (\mathbf{e}\cdot\mathbf{n})^2]$ for the anisotropic spectrum. First we analyze the multipolar collision-induced light scattering. Then $F_{kk}(t)$ becomes the autocorrelation function of (6)

$$F_{kk}(t) = \langle \Delta\mathbf{A}_{(k)}(0) \odot \Delta\mathbf{A}_{(k)}(t)\rangle \tag{12}$$

where $\odot$ denotes a scalar tensor product and $\langle\ \rangle$ is a canonical average.

Using Eq. (6) and decoupling procedures for irreducible spherical tensors [32], we easily derive the following general form of the autocorrelation function

(13) for the dipole–arbitrary-order multipole light scattering induction operator [33]:

$$F_{kk}(t) = 4(2k+1)\sum_{\substack{j_1,j_2\\ l_1,l_2}}\sum_{\substack{k_1,k_2\\ m_1,m_2}}(-1)^{g+h+l_1+m_1}\left[\frac{2^{N_1+N_2}}{(2l_1)!(2l_2)!(2m_1)!(2m_2)!}\right]^{1/2}$$
$$X_{j_1j_2k_1k_2N_1N_2gh}\begin{Bmatrix} h & & k_2 & & 1 & k & 1 & & k_1 & & g \\ & j_2 & & m_2 & & & & l_1 & & k_1 & \\ 1 & & l_2 & & N_1 & a & N_2 & & m_1 & & 1 \end{Bmatrix}$$
$$\langle[\mathbf{T}_{N_1}(\mathbf{R}_{12}(0))\otimes\mathbf{T}_{N_2}(\mathbf{R}_{12}(t))]^{(a)}\odot[(\mathbf{A}_{j_1}^{(1,l_1)}(1,0)\otimes$$
$$\mathbf{A}_{k_1}^{(1,m_1)}(1,t))^{(g)}\otimes(\mathbf{A}_{j_2}^{(1,l_2)}(2,0)\otimes\mathbf{A}_{k_2}^{(1,m_2)}(2,t))^{(h)}]^{(a)}\rangle \tag{13}$$

where we used the 18-j coefficient of ${}^{28}\mathbf{M}_1$ type defined as [34]

$$\begin{Bmatrix} a & & b & & g & k & h & & r & & s \\ & c & & f & & & & p & & t & \\ d & & e & & j & l & m & & u & & w \end{Bmatrix} = \sum_{x_1x_2}(-1)^{\psi}(2x_1+1)$$
$$(2x_2+1)\begin{Bmatrix} l & x_1 & x_2 \\ k & j & m \end{Bmatrix}\begin{Bmatrix} l & x_1 & x_2 \\ a & b & c \\ s & t & r \end{Bmatrix}\begin{Bmatrix} m & k & x_1 \\ f & g & b \\ u & w & t \end{Bmatrix}$$
$$\begin{Bmatrix} j & k & x_2 \\ p & h & r \\ e & d & c \end{Bmatrix} \tag{14}$$

and $\psi = a+s+j+m+c+t+w+d-u-e$.

With symbolic computation programs [35], we calculate rather easily the values of the $18-j$ symbols of (6) for selected multipole light scattering mechanisms. For instance, taking $N_1 = N_2 = 3; j_1 = k_1 = 3,\ l_1 = m_1 = 2;$ $j_2 = k_2 = 0, l_2 = m_2 = 1$, we obtain excellent agreement with the dipole-induced quadrupole autocorrelation function derived by Posch [7]. The correlation function (13) deals with a general situation when rotational and translational degrees of freedom are coupled. However, when considering radiation scattered by low-density gaseous systems, we usually are justified in assuming that the molecules of the scattering volume are correlated radially but uncorrelated orientationally [2,7,36]. That assumption was used when the theory of collision-induced rotational Raman (CIRR) effect was developed by Buckingham and Tabisz [2,37]. Our general autocorrelation function (13) reduces to the autocorrelation function of CIRR if $g = h = a = 0$. Then, taking into account the

explicit form of the spherical interaction tensor [33,38]:

$$\mathbf{T}_N(\mathbf{R}_{12}) = (-1)^N \left(\frac{(2N)!}{2^N}\right)^{1/2} \sqrt{\frac{4\pi}{2N+1}} R_{12}^{-(N+1)} \mathbf{Y}_N(\widehat{\mathbf{R}}_{12}) \tag{15}$$

where $\mathbf{Y}_N(\widehat{\mathbf{R}}_{12})$ stands for spherical harmonic function, our Eq. (13) becomes:

$$\begin{aligned} F_{kk}(t) = {} & \frac{16\,\pi\,(2k+1)}{2\,N_1+1} \sum_{\substack{j_1,j_2\\ l_1,l_2}} \sum_{\substack{k_1,k_2\\ m_1,m_2}} \frac{(-1)^{l_1+m_1}\,2^{N_1}}{[(2\,l_1)!\,(2\,l_2)!\,(2\,m_1)!\,(2\,m_2)!]^{1/2}} \\ & \begin{bmatrix} 1 & 1 & l_2 & m_2 \\ 1 & l_1 & 1 & m_1 \\ k & j_2 & j_1 & N_1 \end{bmatrix} \left\langle \left(\mathbf{A}_{j_1}^{(1,l_1)}(1,0) \odot \mathbf{A}_{j_1}^{(1,m_1)}(1,t) \right) \right\rangle_{\Omega_1(0)} \\ & \left\langle \left(\mathbf{A}_{j_2}^{(1,l_2)}(2,0) \odot \mathbf{A}_{j_2}^{(1,m_2)}(2,t) \right) \right\rangle_{\Omega_2(0)} \left\langle \left(R_{12}^{-(N_1+1)}(0) \mathbf{Y}_{N_1}(\widehat{\mathbf{R}}_{12}(0) \odot \right.\right. \\ & \left.\left. R_{12}^{-(N_1+1)}(t) \mathbf{Y}_{N_1}(\widehat{\mathbf{R}}_{12}(t) \right) \right\rangle_{\Omega_{12}(0)} \end{aligned} \tag{16}$$

where

$$\begin{aligned} \begin{bmatrix} a & b & e & f \\ d & h & c & g \\ p & q & s & r \end{bmatrix} = {} & (-1)^{-p+q-r+s} \sum_{x_1} X_{x_1}^2 \\ & \begin{Bmatrix} a & b & x_1 \\ c & d & p \end{Bmatrix} \begin{Bmatrix} c & d & x_1 \\ e & f & q \end{Bmatrix} \begin{Bmatrix} e & f & x_1 \\ g & h & r \end{Bmatrix} \begin{Bmatrix} g & h & x_1 \\ a & b & s \end{Bmatrix} \end{aligned} \tag{17}$$

stands for the 12–j Wigner symbol of the second kind [32]. Introducing the notation

$$S_N(t) = \langle D_{00}^N(\delta\Omega_{12}(t))\, R_{12}(0)^{-(N+1)}\, R_{12}(t)^{-(N+1)} \rangle \tag{18}$$

$$R_j(t) = \left\langle D_{nn}^j(\delta\Omega(t)) \right\rangle$$

and averaging isotropically over the initial orientation Ω_i of molecule i, we obtain

$$\left\langle \left(\mathbf{A}_{j_i}^{(1,l_i)}(i,0) \odot \mathbf{A}_{j_i}^{(1,m_i)}(i,t) \right) \right\rangle_{\Omega_i(0)} = \left(\tilde{\mathbf{A}}_{j_i}^{(1,l_i)} \odot \tilde{\mathbf{A}}_{j_i}^{(1,l_i)} \right) R_{j_i}(t) \tag{20}$$

where $\tilde{\mathbf{A}}_{j_i}^{(1,l_i)}$ stands for the irreducible multipolar polarizability tensor of the ith molecule in its molecular frame reference system. Averaging over the initial orientation of the intermolecular vector gives us

$$\left\langle \left(R_{12}^{-(N_1+1)}(0)\mathbf{Y}_{N_1}(\widehat{\mathbf{R}}_{12}(0) \odot R_{12}^{-(N_1+1)}(t)\mathbf{Y}_{N_1}(\widehat{\mathbf{R}}_{12}(t)\right) \right\rangle_{\Omega_{12}(0)} = \frac{2N_1+1}{4\pi} S_{N_1}(t) \tag{21}$$

In this way we transform our key equation, (16), to the form suitable for computer programming:

$$F_{kk}(t) = \frac{4(2k+1)}{2N_1+1} \sum_{\substack{j_1,j_2 \\ l_1,l_2}} \sum_{m_1,m_2} (-1)^{l_1+m_1} \frac{2^{N_1}}{[(2l_1)!\,(2l_2)!\,(2m_1)!\,(2m_2)!]^{1/2}}$$
$$\begin{bmatrix} 1 & 1 & l_2 & m_2 \\ 1 & l_1 & 1 & m_1 \\ k & j_2 & j_1 & N_1 \end{bmatrix} \left(\tilde{\mathbf{A}}_{j_1}^{(1,l_1)}(1) \odot \tilde{\mathbf{A}}_{j_1}^{(1,m_1)}(1)\right) \left(\tilde{\mathbf{A}}_{j_2}^{(1,l_2)}(2) \odot \tilde{\mathbf{A}}_{j_2}^{(1,m_2)}(2)\right)$$
$$\times R_{j_1}(t)\, R_{j_2}(t)\, S_{N_1}(t) \tag{22}$$

It would be relatively easy to extend here our computer symbolic calculations to "the hyperpolarizability part" of the pair polarizability [see Eqs. (5) and (7)]. However, from all our numerical computations done for N_2, CO_2, and CF_4, it results that nonlinear part of the pair polarizability has a weak influence on the resulting spectrum (for details, see Refs. 8, 13, and 15–18). Bearing in mind these results in this review, we restrict our discussion to multipolar light scattering mechanisms. Formula (22) allows us to write the following simple symbolic program in Mathematica calculating the analytical form of the autocorrelation function (16) for a selected dipole-arbitrary order multipole induction operator:

```
Fkk=(2 k+1) 4 (-1)^(l1+m1) (2 N1)!/Sqrt[(2 l1)! (2 (N1-l1))! (
2 m1)! (2 (N1-m1))!] Sum[(2 x+1) SixJSymbol[{1,1,x},{1,1,k}
] SixJSymbol[{1,1,x},{N1-l1,N1-m1,j2}
] SixJSymbol[{N1-l1,N1-m1,x},{m1,l1,N1}] SixJSymbol[{m1,l1,x},
{1,1,j1}],{x,0,2}] (Sum[(-1)^m A[1,j1,l1,m] A[1,j1,m1,-m],{m,
-j1,j1}] Sum[(-1)^m A[2,j2,(N1-l1),m] A[2,j2,(N1-m1),-m],{m,
-j2,j2}]) R[j1,t] R[j2,t] S[N1,t]
```

In our program we distinguish multipolarizabilities of molecules 1: `A[1,j1,l1,m]` and molecule 2: `A[2,j2,l2,m]` so in practice our program can be used to light scattering computations for mixtures. Having an analytical form

of the autocorrelation function, one easily calculates [see (10)] the double differential cross section of scattered radiation. Before running the above program, we must specify the value of k ($k = 0$, *isotropic scattering*; or $k = 2$, *anisotropic scattering*) the rank of the interaction tensor N_1 and the set of indices j_1, j_2, l_1, and m_1. Our program easily gives the double differential cross section for molecules of an arbitrary symmetry and selected multipole light scattering mechanisms, provided, however, that the explicit form of the respective irreducible multipole polarizability molecular frame tensors $\tilde{\mathbf{A}}_{j_n}^{(1,l_n)}$ is available [29]. In other words, once we know the irreducible form of the multipole polarizability tensors involved in the light scattering mechanism considered, our program gives the double differential cross section due to this mechanism without often cumbersome (especially for high-order tensors) unweighted rotational averaging of many directional cosines [30,31]. For tetrahedral molecules, these sets are assembled in Table I for the successive multipolar induction operators up to dipole-induced octopole light scattering mechanism. For octahedral molecules, symmetry constraints reduce the number of possible light scattering mechanisms allowed; for instance, $\mathbf{A} \equiv 0$. However, Table I can be used as well for all light scattering mechanisms active in collision-induced spectra of octahedral molecules. Moreover, in general, before running our program we must define the form of the molecular frame spherical irreducible multipole polarizability tensor for the considered light scattering mechanism. In Table II we specify this form for tetrahedral molecules and light scattering mechanisms ranging from the dipole–dipole induction operator up to the dipole–octopole one. The way of utilizing of our program for linear molecules is discussed in section II.C.2.

1. *Globular Molecules*

We start illustrate our program considering tetrahedral and octahedral molecules. Let us begin the calculation of the double differential cross section of the isotropic component of the light scattered due to *octopole–octopole* (OO) **ETE** mechanism. In this case `k=0, j1=4, j2=4, l1=3, m1=3, N1=6`. It is

TABLE I
The Set of Indices j_1, j_2, l_1 and m_1 for Induction Operators Ranging from Dipole–Dipole to Dipole–Octopole

Operator	j_1	j_2	l_1	m_1	Operator	j_1	j_2	l_1	m_1
$\alpha\mathbf{T}^{(2)}\alpha$	0	0	1	1	$\mathbf{A}\,\mathbf{T}^{(4)}\,\mathbf{A}$	3	3	2	2
$\alpha\,\mathbf{T}^{(3)}\,\mathbf{A}$	0	3	1	1	$\mathbf{A}\,\mathbf{T}^{(5)}\,\mathbf{E}$	3	4	2	2
	3	0	2	2		4	3	3	3
$\alpha\,\mathbf{T}^{(4)}\,\mathbf{E}$	0	4	1	1	$\mathbf{E}\,\mathbf{T}^{(6)}\,\mathbf{E}$	4	4	3	3
	4	0	3	3					

TABLE II
The Form of the Molecular Frame Multipole Polarizability Tensor Ranging from Dipole–Dipole to Dipole–Octopole Light Scattering Mechanisms

Light Scattering Mechanisms	The Molecular Frame Multipole Polarizability Tensor
Dipole-Dipole	$A[1,0,1,0]=-\sqrt{3}a1$
	$A[2,0,1,0]=-\sqrt{3}a2$
	$A[1,2,1,0]=0$
	$A[2,2,1,0]=0$
	$A[1,2,1,1]=0$
	$A[2,2,1,-1]=0$
	$A[1,2,1,2]=0$
	$A[2,2,1,-2]=0$
Dipole–quadrupole	$A[1,3,2,0]=0$
	$A[2,3,2,0]=0$
	$A[1,3,2,1]=0$
	$A[1,3,2,-1]=0$
	$A[2,3,2,1]=0$
	$A[2,3,2,-1]=0$
	$A[1,3,2,2]=I\sqrt{2}A1$
	$A[1,3,2,-2]=-I\sqrt{2}A1$
	$A[2,3,2,2]=I\sqrt{2}A2$
	$A[2,3,2,-2]=-I\sqrt{2}A2$
	$A[1,3,2,3]=0$
	$A[1,3,2,-3]=0$
	$A[2,3,2,3]=0$
	$A[2,3,2,-3]=0$
Dipole–octopole	$A[1,4,3,0]=\sqrt{7}/2E1$
	$A[2,4,3,0]=\sqrt{7}/2E2$
	$A[1,4,3,1]=0$
	$A[1,4,3,-1]=0$
	$A[2,4,3,1]=0$
	$A[2,4,3,-1]=0$
	$A[1,4,3,2]=0$
	$A[1,4,3,-2]=0$
	$A[2,4,3,2]=0$
	$A[2,4,3,-2]=0$
	$A[1,4,3,3]=0$
	$A[1,4,3,-3]=0$
	$A[2,4,3,3]=0$
	$A[2,4,3,-3]=0$
	$A[1,4,3,4]=\sqrt{10}/4E1$
	$A[1,4,3,-4]=\sqrt{10}/4E1$
	$A[2,4,3,4]=\sqrt{10}/4E2$
	$A[2,4,3,-4]=\sqrt{10}/4E2$

straightforward to find that in utilizing our program after one push of a computer key, we obtain

$$F00(t) = \frac{55}{3}\, E^4\, R[4,t]^2\, S[6,t] \tag{23}$$

Looking for depolarized component of this scattering, we use `k=2, j1=4, j2=4, l1=3, m1=3, N1=6`. Then the result of our program reads as

$$F22(t) = \frac{11330}{21}\, E^4\, R[4,t]^2\, S[6,t] \tag{24}$$

In this way using Tables I and II we calculate double differential cross sections for all light scattering mechanisms of globular molecules consider in our work.

2. *Linear Molecules*

The symmetry of linear molecules imposes less constraints on the multipole polarizability tensors than does tetrahedral symmetry, so the forms of the respective tensors for linear molecules are usually more highly complicated than for tetrahedral ones. This certainly complicates interpretation of light scattering results but has much less influence on complications in running our program. By means of the same methods as in the case of tetrahedral molecules we calculate the spherical irreducible components of the dipole–dipole, dipole–quadrupole, and dipole–octopole polarizability tensors as dipole–dipole

$$A_{00}^{(11)} = -\sqrt{3}\,\alpha \tag{25}$$

$$A_{20}^{(11)} = \sqrt{\frac{2}{3}}\,\gamma \tag{26}$$

dipole–quadrupole

$$A_{10}^{(12)} = -\frac{\sqrt{10}}{5}\,(A_{\parallel} + 2A_{\perp}) \tag{27}$$

$$A_{30}^{(12)} = \frac{\sqrt{15}}{15}\,(3A_{\parallel} - 4A_{\perp}) \tag{28}$$

or dipole–octopole:

$$A_{20}^{(13)} = \frac{\sqrt{21}}{21}\,E2 \tag{29}$$

$$A_{40}^{(13)} = \frac{2\sqrt{7}}{7}\,E4 \tag{30}$$

Putting in our program N1=4 and the following sets of j_1, j_2, l_1, m_1 indices — (0,2,1,1); (2,0,3,3); (0,4,1,1); (4,0,3,3); (2,2,1,1); (2,2,3,3); (2,2,1,3); (2,2,3,1) — we easily obtain the anisotropic $F22(t)$ and isotropic $F00(t)$ correlation functions for the dipole–octopole $\alpha\mathbf{TE}$) induction operator [15,36]:

$$F22(t) = \left[\frac{32}{21}\,(\alpha\,E2)^2\,R[0,t]\,R[2,t] + \frac{880}{189}\,(\alpha\,E4)^2\,R[0,t]\,R[4,t] + \frac{16}{105}\,(\gamma\,E2)^2\,R[2,t]^2 + \frac{704}{243}\,(\gamma\,E4)^2\,R[2,t]\,R[4,t]\right] S[4,t] \tag{31}$$

$$F00(t) = \left[\frac{128}{27}\,(\alpha\,E4)^2\,R[0,t]\,R[4,t] + \frac{128}{945}\,(\gamma\,E2)^2\,R[2,t]^2 + \frac{352}{1701}\,(\gamma\,E4)^2\,R[2,t]\,R[4,t]\right] S[4,t] \tag{32}$$

with $\alpha, \gamma, E2, E4$ polarizability invariants of molecule i defined as in Ref. 15.

III. EXPERIMENTAL CONSIDERATIONS

A. Setup

Interaction-induced light scattering intensities may be measured by a conventional scattering experimental setup. However these intensities are generally weak and the collection of accurate data needs some specific arrangements, especially when polarization studies are concerned. For the data reported here we used the experimental apparatus shown in Fig. 1. The light source is a 15-W argon ion laser operating on the green line at $\lambda_L = 514.5$ nm. The laser light is linearly polarized perpendicularly to the scattering plane, which is defined by the laser beam and the axis of the scattered light. The direction of the laser polarization may be rotated and set parallel to the scattering plane using a half-wave plate associated with a glan polarizer. The laser beam is focused on a sample cell with a convergent lens (L1) and the light scattered at 90° is collected with an another lens (L2). The collection angle is kept as small as possible (7° maximum). The scattered light is analyzed by a double monochromator with two holographic gratings. Then it is detected by either a photomultiplier (PM) or a charge-coupled-device (CCD). The PM is a low-noise tube with a bialkali photocathode cooled at −5°C associated with a photon counter. It gives the signal intensity at one frequency. The CCD is a silicon chip detector that consists of 1024 × 256 pixels. It is associated to a holographic filter to stop the light at the laser frequency and gives the intensities for any frequency of a spectral domain above 160 cm^{-1}. By cooling the CCD at 140 K and using specific software, we have been able to measure very weak signals with this detector corresponding to *one photon per week and per pixel*. For gaseous

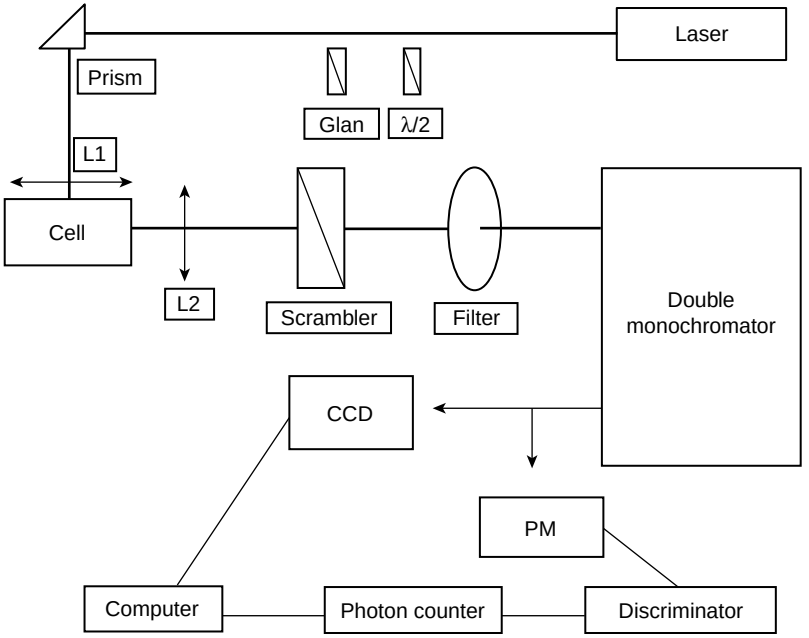

Figure 1. Experimental arrangement for the study of collision-induced light scattering. L1 and L2 are convergent lens.

sample we used high-pressure cells with four fused silica windows of high optic quality and with diaphragms inside to stop the parasitic light. When low temperature studies were performed, the cell was set in a specially designed continuous-flow cryostat from the Air Liquide Company. The temperature was monitored with an accuracy of about 1 K using a platinum calibrate resistance inside the cell. With this apparatus our cell can work with several hundred bars of gas from liquid helium to room temperature.

B. Experimental Procedure

The scattering spectra induced by binary interactions at the low-density limit for the gaseous samples studied have been deduced from the analysis of the density behavior of the spectral Stokes intensities. For each Raman frequency ν studied, we have measured the scattering intensities $I(\nu)$ at several densities ρ and fitted the resulting data to a power series expansion in density of the form

$$I(\nu) = I_0(\nu) + I_1(\nu)\,\rho + I_2(\nu)\,\rho^2 + I_3(\nu)\,\rho^3 + \cdots \tag{33}$$

where $I_0(\nu)$ represents an intensity contribution independent of the gas density and due mostly to laser light reflections, $I_1(\nu)$ is the scattering from monomers

and is proportional to the gas density, $I_2(\nu)$ is the binary intensity induced by the two-body interactions that we are looking for, and $I_3(\nu)$ describes three-body contributions to the scattering. The density expansion given by Eq. (33) is an approximation and must be used with caution. It may be consider valid for relatively low densities. The spectral response of the apparatus has been taken into account in order to compare experimental intensities obtained at different frequencies. This has been done by means of a spectral correction factor determined from measurement of the sensitivity of our device using a precalibrated spectral lamp. Since intensities obtained in a first step from the experiment are on a relative scale, a calibration is needed to put them on an absolute scale. In our case, we used an external calibration, in which two types of experiments are conducted under the same experimental conditions. The first one was to measure the induced interaction signal S_p [in counts per second (cps)] scattered by the sample at a specific frequency shift ν_0. The second one was to measure the frequency integrated intensity S_r^i (in $\mathrm{cm}^{-1}\cdot\mathrm{cps}$) for a reference rotational line of a molecule B serving as a standard. If the integrated cross section of the reference line ($d\sigma/d\Omega$) is known, the interaction-induced intensity at ν_0 per unit of frequency shift, $I(\nu_0)$, can be calculated from [39]

$$I(\nu_0) = \frac{d\sigma}{d\Omega}\frac{S_p}{S_r^i}\frac{2\,n_r}{n_p^2} \tag{34}$$

where n_p and n_r are the number density of the sample studied and of the molecule B, respectively. For several of our studies, the rotational line $S_0(1)$ of hydrogen was used as reference line. In order to study polarization properties of CIS, two scattering components are measured with different optical arrangement. The perpendicular scattering component $I_\perp$ is obtained when the polarization of the laser beam in the cell is perpendicular to the scattering plane. The parallel scattering component $I_\parallel$ is measured when this laser polarization inside the cell is parallel to the scattering plane. However, some mixing between perpendicular and parallel components may occur because of the nonzero value of the collection angle of the light scattered by the sample. To obtain the values of the perpendicular and the parallel intensities scattered at 90°, $I'_\perp$ and $I'_\parallel$, respectively, and corresponding to a collection angle close to zero, a correction may be applied [16,40]. In our experiment the scattered beam was collected in a cone with a half-angle about 6.2°, and we now have

$$I'_\parallel = 1.006 I_\parallel - 0.006 I_\perp \tag{35}$$

$$I'_\perp = 1.003 I_\perp - 0.003 I_\parallel \tag{36}$$

Then the depolarized and the isotropic spectra, $I_{\text{dep}}(\nu)$ and $I_{\text{iso}}(\nu)$ respectively, can be obtained on an absolute scale from the calibrated values of intensities $I'_{\parallel}$ and $I'_{\perp}$ for each studied frequency ν. We thus have [41]

$$I_{\text{dep}}(\nu) = I'_{\parallel}(\nu) \tag{37}$$

$$I_{\text{iso}}(\nu) = I'_{\perp}(\nu) - \frac{7}{6} I'_{\parallel}(\nu) \tag{38}$$

IV. SCATTERING IN THE RAYLEIGH FREQUENCY REGION

A. Optically Isotropic Molecules

1. Theory

One particular feature of the light scattering by noble gases and optically isotropic molecules is the collision-induced (CI) origin of spectral wings around the Rayleigh line. There are two kinds of CI spectra: the depolarized and the isotropic ones. Whereas first-order DID contribution to the depolarized spectrum is predominant at low-frequency shifts, DID mechanism is of second-order in the isotropic case so that other contributions may be more distinctively displayed. These other contributions are due to short-range effects such as overlap, exchange, orientational, and, in the case of globular molecules, collision-induced multipolar effects. Models of various contributions and their numerical evaluations allow us to determine the relative importance of multipolar mechanisms in depolarized or isotropic CIS spectra for optically isotropic molecules.

a. DID: A Pure Translational Mechanism. Based on a point-like molecule approximation, the DID model involves only the relative translational motion of a pair of molecules. All computations may be done by considering the scalar distance R_{12} between two interacting molecules, an isotropic intermolecular potential $V(R_{12})$, and the DID pair polarizability tensor. The trace of this tensor, $\alpha_{\text{DID}}(R_{12}) = 6\,\alpha^3\,R_{12}^{-6}$, is a second-order term that weakly affects the isotropic CI spectrum. On the contrary its first-order anisotropy, $\beta_{\text{DID}}(R_{12}) = 6\,\alpha^2\,R_{12}^{-3}$, is responsible for most of the integrated intensity for the depolarized CI spectrum $I_{\text{dep}}(\nu)$ (where ν stands for the frequency shift relatively to the Rayleigh line). This means that the zero-order spectral moment of the depolarized spectrum $M_{0,d} = \frac{15}{2}\left(\frac{\lambda_L}{2\pi}\right)^4 \int_{-\infty}^{\infty} I_d(\nu)\,d\nu$ [74] may be in first approximation identified to the canonical average of the DID anisotropy:

$$\begin{aligned} M_{0,d}^{\text{DID}} &= \left\langle \beta_{\text{DID}}^2(R_{12}) \right\rangle \\ &= \int \beta_{\text{DID}}^2(R_{12})\, g(R_{12})\, 4\pi R_{12}^2\, dR_{12} \end{aligned} \tag{39}$$

where [43]

$$g(R_{12}) = \left(1 + \frac{\hbar^2}{12mk_BT}\left[\frac{1}{2}\left(\frac{d}{dR_{12}}\frac{V(R_{12})}{k_BT}\right)^2 - \frac{2}{r}\frac{d}{dR_{12}}\frac{V(R_{12})}{k_BT} - \frac{d^2}{dR_{12}^2}\frac{V(R_{12})}{k_BT}\right]\right)\exp\left(\frac{-V(R_{12})}{k_BT}\right) \tag{40}$$

is close to $\exp(-V(R_{12})/k_BT)$ for heavy molecules such as globular ones. On the other hand, the DID depolarized intensities $I_d^{\mathrm{DID}}(\nu)$ may be calculated either quantally (by solving Schrödinger's equation) or classically (via Newton's equations of motion) [44]. Quantum-mechanical methods consist in computing the various matrix elements corresponding to level transitions of an interacting pair of molecules. Till now, they have been used mainly for noble gases [44–46]). Classical method consists in computing molecular trajectories of free dimers (a pair of colliding molecules coming from infinite). This method has been exhaustively described in many publications [47]. For a relatively heavy noble gas such as argon, it has been shown that quantal and classical methods provide very similar intensities, at least for $15 < \nu < 200\,\mathrm{cm}^{-1}$ [39,48]; a similar result is a fortiori expected in spectral regions of experimental data for heavier systems such as globular molecules. However, the contribution of bound dimers (pair of interacting molecules trapped in the well of the effective intermolecular potential) must also be considered. This accounts for $100x\%$ of the zero-order moment, where $x \approx 0.1$–0.5 can be evaluated by using a statistical method described by Levine [49] and depends strongly on the choice of the potential. For each frequency shift ν, bound dimer contribution can be calculated by way of quantum mechanics [48,50] as well as by using a semiclassical method that provides intensities due to bound and free dimers [51,52]. The contribution of bound dimers to the DID spectral lineshape is limited to the lower-frequency range ($0 < \nu < 15\,\mathrm{cm}^{-1}$) and does not influence directly spectral studies focused on the determination of multipolar effects (which take place in a higher-frequency range).

b. Other Mechanisms Involved in the Pure Translational Spectrum. Other processes must be considered in the computation of the theoretical pure translational depolarized spectrum: terms in R_{12}^{-6}, overlap and exchange effects, and consequences of the non-point-like size and of the nonspherical shape of globular molecules. The R_{12}^{-6} terms (involving the second-order DID term, the second hyperpolarizability γ, and the coefficient C_6 of the dispersion interaction) may be easily inserted in the anisotropy equation, but do not contribute significantly to the spectrum in the low-frequency region, where pure translational mechanisms predominate. Overlap and exchange effects probably

play a more important role. Unfortunately, a quantum-mechanical analysis of effects concerning a pair of globular molecules is very complicated and has not yet been done. Several authors propose to modelize overlap and exchange effects by adding an exponential term to the anisotropy [10,53]:

$$\beta(R_{12}) = \beta_{\mathrm{DID}}(R_{12}) + \left(6\alpha^3 + \frac{\gamma C_6}{3\alpha}\right) R_{12}^{-6} - B\exp\left(\frac{-R_{12}}{R_0}\right) \tag{41}$$

Here, the exponential term accounts for the electron overlap and exchange effects. The adjustable parameters B and R_0 are deduced from measurements relative to noble gases and CH_4 and by using a law of corresponding states [53]: $R_0 = 0.09531\, R_{\min}$ and $B = 2580\,(6\alpha_0^2)/(4\pi\epsilon_0 R_{\min}^3)$, where $R_{\min}$ is the intermolecular separation at the minimum of the potential. A similar method can be used in order to compute the trace of the polarizability [54]. However, the correspondence between results concerning noble gases and results concerning other atomic or molecular systems is not well established. It has been shown that the anisotropy model given in Eq. (41) is not satisfactory in the case of hot mercury vapor [55], and that the DID contribution must be suppressed at short interatomic distances [55,56]. Damping functions are then introduced in order to avoid nonphysical singularities of R_{12}^{-n} terms when the interatomic distance R_{12} tends to zero [55–57]. As they take account of some of the negative contribution due to overlap effects, the B value of the exponential term of Eq. (41) is necessarily affected by the choice of these functions [56]. Therefore, in the case of globular molecules, the use of semiempirical terms such as the exponential one must be done very carefully. The consequences of the molecular frame distortion and of the spatial charge distribution of the non-point-like globular molecules might also be taken into account in the anisotropy model. Moreover, any calculation might consider that intermolecular potentials of globular molecules are partly anisotropic. All these uncertainties shed a shadow on a procedure that would be founded on the study of the depolarized CI spectrum alone and would attempt to discriminate pure translational and rototranslational mechanisms in the frequency range where these two contributions may have the same order of magnitude (e.g. for CF_4: about $\nu \approx 60\,\mathrm{cm}^{-1}$). In fact, the depolarized CI spectrum must be analyzed together with the isotropic one (where rototranslational contributions due to multipolar mechanisms play the leading role).

c. Rototranslational Spectrum. Considering the spectral frequency range of experimental data, only the first-order Rayleigh rototranslational mechanisms must be taken into account: $\alpha\,\mathbf{T}\,\mathbf{A}$ (DQ), $\alpha\,\mathbf{T}\,\mathbf{E}$ (DO), $\mathbf{A}\,\mathbf{T}\,\mathbf{A}$ (QQ), $\mathbf{A}\,\mathbf{T}\,\mathbf{E}$ (QO) and $\mathbf{E}\,\mathbf{T}\,\mathbf{E}$ (OO). Here, the tensors α, $\mathbf{A}$, and $\mathbf{E}$ stand for dipole–dipole, dipole–

TABLE III
Coefficients φ_{LL}^{N,j_1,j_2} Involved in the Rayleigh Isotropic and Depolarized light Scattering Correlation Functions $F_{LL}(t) = \sum_{N,j_1,j_2} \varphi_{LL}^{N,j_1,j_2} S_N(t) R_{j_1}(t) R_{j_2}(t)$ for the Successive Multipolar Induction Operators

CIS Mechanism	Rayleigh Case	N	j_1	j_2	Isotropic φ_{00}^{N,j_1,j_2}	Depolarized φ_{22}^{N,j_1,j_2}
DID	$\alpha\mathbf{T}\alpha$	2	0	0	0	$24\,\alpha^4$
DQ	$\alpha\mathbf{T}\mathbf{A}$	3	0	3	$\frac{160}{7}\,\alpha^2 A^2$	$\frac{192}{7}\,\alpha^2 A^2$
DO	$\alpha\mathbf{T}\mathbf{E}$	4	0	4	$\frac{224}{9}\,\alpha^2 E^2$	$\frac{220}{9}\,\alpha^2 E^2$
QQ	$\mathbf{A}\,\mathbf{T}\,\mathbf{A}$	4	3	3	$\frac{1408}{189} A^4$	$\frac{125{,}824}{945} A^4$
QO	$\mathbf{A}\,\mathbf{T}\,\mathbf{E}$	5	3	4	$\frac{416}{21} A^2 E^2$	$\frac{9280}{21} A^2 E^2$
OO	$\mathbf{E}\,\mathbf{T}\,\mathbf{E}$	6	4	4	$\frac{55}{3} E^4$	$\frac{11{,}330}{21} E^4$

quadrupole, and dipole–octopole polarizability ones respectively, whereas **T** is the spherical interaction tensor of Eq. (4). The correlation functions defined in Eq. (22) of these successive multipolar induction operators for depolarized and isotropic CI spectra may be directly deduced from Table III in the case of tetrahedral molecules [8,13]. It is noteworthy that, in the case of centrosymmetric molecules like octahedral ones, the terms including the independent component $A = A_{x,yz}$ of the dipole–quadrupole polarizability tensor vanish (the dipole–octopole independent component $E = E_{z,zzz}$ remains alone). For each correlation function, rotational and translational motions are represented separately by functions $R_j(t)$ and $S_N(t)$ defined in Eqs. (18) and (19), respectively. Therefore, a Fourier transform of a correlation function is a convolution product of a rotational spectrum $\mathscr{R}(\nu)$ and of a translational contribution $\mathscr{S}(\nu)$. The Fourier transform of any rotational function $R_j(t)$ may be done by using spherical top wave functions for the evaluation of transition matrix elements. The Fourier transform of $R_{j_1}(t)\,R_{j_2}(t)$ then has the form [7]

$$\mathscr{R}_{j_1,j_2}(\nu) = g_{I_1}\ g_{I_2}\ \frac{(2J_1+1)\,(2J_2+1)\,(2J_1'+1)\,(2J_2'+1)}{Z_1 Z_2}$$
$$\exp\left[-\frac{(E_{J_1}+E_{J_2})}{k_B T}\right]\delta(\nu\ -\ \nu_{J_1 J_2 J_1' J_2'}) \tag{42}$$

where g_{I_i} stands for the nuclear spin statistical factor of molecule i and $E_J = J(J+1)B$ whereas

$$\nu_{J_1 J_2 J_1' J_2'} = -\left[J_1'(J_1'+1) + J_2'(J_2'+1) - J_1(J_1+1) - J_2(J_2+1)\right]B \tag{43}$$

Here, B is the rotational constant and Z_i denotes the rotational partition function. The selection rules have the following form:

$$\Delta J_1 = 0, \pm 1, \pm 2 \ldots \pm j_1 \qquad J_1 + J_1' \geq j_1 \tag{44}$$

$$\Delta J_2 = 0, \pm 1, \pm 2 \ldots \pm j_2 \qquad J_2 + J_2' \geq j_2 \tag{45}$$

Using Eqs. (42)–(45), a rotational stick spectrum $\mathscr{R}(\nu)$ can be calculated for each multipolar mechanism (where each stick is separated from the neighboring one by a frequency shift equal to a few B). Concerning Fourier transforms of the translational functions $S_N(t)$, no exact solution can be found easily. Nevertheless, an accurate knowledge of their spectral profile is not essential because they are convoluted with the rotational contributions. They serve to fill in the intensity between the sticks of each rotational spectrum with the result that the convolution product is not very sensitive to their particular lineshapes [12]. Therefore, it is possible to make use models of the translational parts involved. This model, by Birnbaum and Cohen (BC) [58], needs only the calculation of translational spectral moments. For relatively large molecules such as CF_4 and SF_6, these moments may be either classical or semiclassical (including quantum mechanical corrections) [13]. More generally, however, it is better to base computations on semiclassical moments of zeroth, first and second order. For a light scattering mechanism of order N, these moments may be written [59]

$$M_0^{(N)} = \langle R_{12}^{-2(N+1)} \rangle \tag{46}$$

$$M_1^{(N)} = \frac{\hbar}{2m} (N+1)(2N+1) \langle R_{12}^{-2(N+2)} \rangle \tag{47}$$

$$M_2^{(N)} = \frac{2k_BT}{\hbar} M_1 + \frac{1}{3} \left(\frac{\hbar}{2k_BT} \right)^2 {}^{\mathrm{cl}}M_4^{(N)} + O(\hbar^4) \tag{48}$$

where the fourth-order classical moment ${}^{\mathrm{cl}}M_4^{(N)}$ is [60]

$$\begin{aligned} {}^{\mathrm{cl}}M_4^{(N)} &= 2(N+1)(N+2)(2N+1)(2N+3) \left(\frac{k_BT}{m} \right)^2 \langle R_{12}^{-2(N+3)} \rangle \\ &\quad + \frac{(N+1)^2}{m^2} \left\langle R_{12}^{-2(N+2)} \left(\frac{dV(R_{12})}{dR_{12}} \right)^2 \right\rangle \end{aligned} \tag{49}$$

From these moments, characteristic times τ_i may be deduced

$$\tau_1 = \frac{M_0}{M_1} \sqrt{\frac{M_2}{M_1}\tau_1 - \frac{M_1}{M_0}\tau_0 - 1} \tag{50}$$

$$\tau_2 = \tau_0 \left(\frac{M_2}{M_1}\tau_1 - \frac{M_1}{M_0}\tau_0 - 1 \right)^{-1/2} \tag{51}$$

where $\tau_0 = \hbar/(2k_B T)$. Finally, the BC model for translational contribution of consecutive light scattering mechanisms may be written as [58]

$$S_{BC}(\nu) = M_0 \frac{\sqrt{\tau_0^2 + \tau_2^2}}{\pi} \exp\left(\frac{\tau_1}{\tau_2}\right) \frac{\exp(\nu\tau_0)}{\sqrt{1 + (\nu\tau_1)^2}} K_1\left(\frac{\sqrt{\tau_0^2 + \tau_2^2}}{\tau_1}\sqrt{1 + (\nu\tau_1)^2}\right) \tag{52}$$

where $K_1(z)$ is a modified Bessel function of the second kind. It is noteworthy that this translational contribution depends on moments and thus on the potential $V(R_{12})$. The intensity of the rototranslational spectrum can therefore be affected by the choice of the intermolecular potential.

d. Nonlinear Contributions to Rototranslational Spectrum. According to Eqs. (5) and (7), the pair polarizability results as well from nonlinear light scattering mechanisms. These mechanisms are induced by hyperpolarizability tensors and permanent multipole moments. For tetrahedral molecules, they contribute only to the correlation functions related to the depolarized spectrum and governed by double rotational transitions. Consequently, some corrections $\Delta\varphi_{22}^{N,j_1,j_2}$ must be added to the linear-origin terms φ_{22}^{N,j_1,j_2} of Table III. These correction due to nonlinear mechanism are successively [8]

$$\Delta\varphi_{22}^{4,3,3} = -\frac{768}{5} A^2 b_{xyz}\,\Omega + \frac{384}{7} b_{xyz}^2\,\Omega^2 \tag{53}$$

$$\Delta\varphi_{22}^{5,3,4} = -\frac{576}{7} A\,E\,\Delta B\,\Omega + \frac{144}{25}\Delta B^2\,\Omega^2 - 192\,A\,E\,b_{xyz}\,\Phi + \frac{96}{7} b_{xyz}\,\Delta B\,\Omega\,\Phi + \frac{240}{7} b_{xyz}^2\,\Phi^2 \tag{54}$$

$$\Delta\varphi_{22}^{6,4,4} = -\frac{1056}{7} E^2\,\Delta B\,\Phi + \frac{176}{15}\Delta B^2 \Phi^2 \tag{55}$$

where $\Delta B = (3\,B_{zz,zz} - 4\,B_{xz,xz})$. The nonzero components b_{xyz} and $B_{\alpha\beta\gamma\delta}$ stand for these of the dipole–dipole and dipole–dipole-quadrupole hyperpolarizability tensors, respectively. Moreover, Ω and Φ denote the independent components of the permanent octopole and hexadecapole moments. In the case of octaedral molecules, only $\Delta\varphi_{22}^{6,4,4}$ is different from zero and must be considered.

2. *Results and Discussion*

The influence of multipolar polarizabilities has been examined subsequently in several optically isotropic molecules such as CH_4, CD_4, neopentane, CF_4, or SF_6 [4,7–14,17,18]. In this review, our attention is focused on CF_4 for which both Rayleigh [8,13] and ν_1 Raman [17,18] depolarized and isotropic bands have been studied and published by us. In the Rayleigh studies, we measured the $I_\perp(\nu)$ and $I_\parallel(\nu)$ intensities that are scattered by gaseous CF_4 up to 340 cm^{-1}, in

the 2-105 Amagat density range and at 294.5 K. Beyond $150\,\mathrm{cm}^{-1}$, the spectral intensities varies linearly with gas density and are not of CI nature. For the lowest-frequency shifts, a negative contribution due to the three-body processes appears at high pressures. However, we checked that $I_{\perp}(\nu)$ and $I_{\parallel}(\nu)$ are proportional to the density square ρ^2 below $\rho = 40$ Amagat for $\nu < 20\,\mathrm{cm}^{-1}$ and for all the pressure range studied beyond this frequency. Thus, we have been able to deduce the pair contributions $I^p_{\perp}(\nu)$ and $I^p_{\parallel}(\nu)$ to the scattered intensities and the Rayleigh pair depolarization ratio $\eta^p_{\mathrm{exp}}(\nu) = I^p_{\parallel}(\nu)/I^p_{\perp}(\nu)$ given in Fig. 2 up to $150\,\mathrm{cm}^{-1}$. It is noteworthy that η^p_{exp} decreases with ν from 6/7 (expected value of a completely depolarized spectrum) to less than 0.4. For both perpendicular and parallel scattering components, this shows that the first order DID mechanism (for which $\eta^{p\mathrm{th}} = 6/7$) predominates in the lower-frequency domain whereas dipole–quadrupole (DQ) and dipole–octopole (DO) mechanisms (for which $\eta^{p\mathrm{th}} = \frac{9}{23} \approx 0.39$ and $\eta^{p\mathrm{th}} = \frac{22}{63} \approx 0.35$, respectively [33]) predominate for upper frequencies.

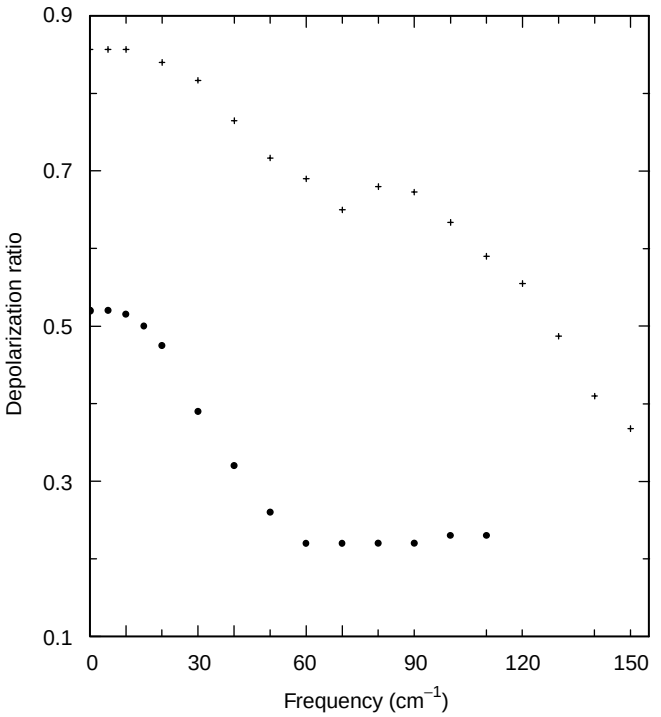

Figure 2. Experimental depolarization ratio $\eta^p_{\mathrm{exp}}(\nu) = I^p_{\parallel}(\nu)/I^p_{\perp}(\nu)$ of the binary Rayleigh band of gaseous CF_4 (+) at 294.5 K. The depolarization ratio for the ν_1 Raman band is also reported (•).

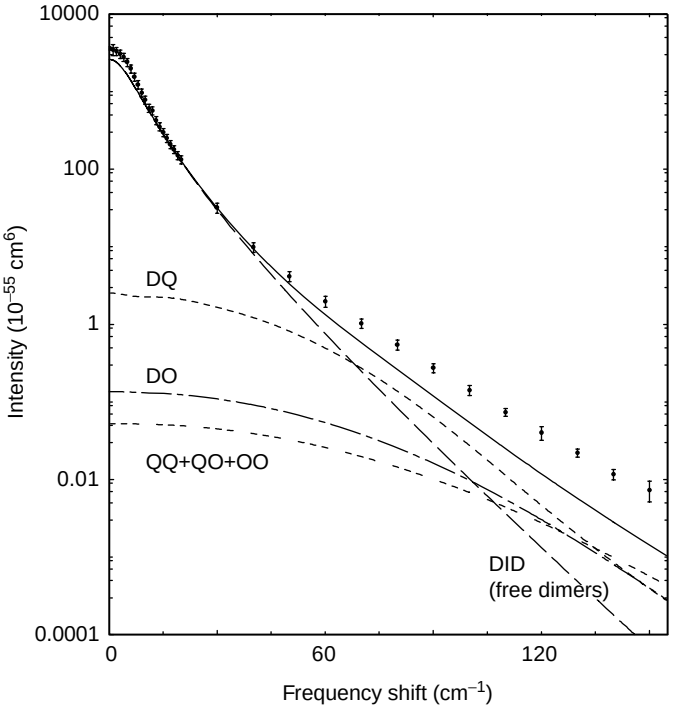

Figure 3. Two-body *depolarized* scattering spectrum for CF_4 gas at 294.5 K. The full circles (•) indicate experimental data with error bars [8]. Theoretical curves are provided for several contributions using $\alpha = 2.93$ Å^3, A = 1 Å, E = 1.5 Å^5: DID (— —), DQ (- - -), DO (— - —), QQ + QO + DO (- - - - - -) and DID + DQ + DO + QQ + QO + OO (———).

a. Anisotropic Scattering. Using Eqs. (35) and (37), the depolarized binary intensities $I_{\text{dep}}(\nu)$ have been deduced directly from $I^p_\perp(\nu)$ and $I^p_\parallel(\nu)$. We calibrated them in absolute units by comparing $I_{\text{dep}}(20\,\text{cm}^{-1})$ with the integrated intensity of the $S_0(0)$ rotational line of gaseous H_2 (taking for the polarizability anisotropy of the latter $\beta = 0.317 \times 10^{-24}$ cm^3 [61] we thus found $I_{\text{dep}}(20\,\text{cm}^{-1}) = (1.33 \pm 0.16) \times 10^{-53}\,\text{cm}^6$). In Fig. 3, these experimental absolute intensities are reported together with their error bars. We equally report in the same figure theoretical contributions due to DID (classical calculation) and dipole–multipole mechanisms for a CF_4 Lennard-Jones potential [62], $\alpha = 2.93$ Å^3 (extrapolated at $\lambda_L = 514.5$ nm from CF_4 refractive index measurements provided in Ref. 63) and a couple of multipolarizability values $(A, E) = (1.0\,\text{Å}^4, 1.5\,\text{Å}^5)$ close to those which has been recently calculated ab initio by Maroulis $(0.97\,\text{Å}^4, 1.15\,\text{Å}^5)$ [64,65]. It is noteworthy that nonlinear origin corrections to the dipole–multipole contributions have been

taken into account by using in Eqs. (53)–(55) the values of b_{xyz}, ΔB, Ω and Φ computed by Maroulis in the same work. For $(A, E) = (1.0\,\text{Å}^4, 1.5\,\text{Å}^5)$, we found that these nonlinear contributions enhance the QQ, QO, and OO contributions by 21%, 10% and 0%, respectively. In Ref. [8], another vector (A, E) was provided $(1.2\,\text{Å}^4, 3.5\,\text{Å}^5)$ which allows a better fit of theoretical and experimental data. Nevertheless as we will see below that at least this E value is not compatible with isotropic spectrum measurements. Moreover, in this depolarized spectrum case, a good agreement between theory and experiment is not necessarily significant. The aforementioned uncertainties on the pure translational contribution (mainly, overlap and exchange effects) shed some doubt on the validity of any fitting procedure in the 50–100-cm^{-1} frequency region, where DID and DQ contributions are of the same order of magnitude. Moreover, for CF_4, several potentials exist that are not all close together. Among available potentials, we found that three ones [47,62,66] provide an integrated intensity of the strong DID contribution to the depolarized spectrum compatible with our measurements. Overall, both integrated intensity and *spectral lineshape* of this purely translational contribution may be significantly affected by the uncertainties concerning the potential. This shows that the presence of a strong purely translational component prevents the depolarized spectrum to be a very good tool for evaluating the dipole–multipole polarizabilities of the globular molecules.

b. Isotropic Scattering. Using the ratio $\eta^p_{\text{exp}}(\nu)$ given in Fig. 2 and the pair depolarized absolute intensities $I_{\text{dep}}(\nu)$ provided in Fig. 3, pair isotropic absolute intensities can be directly deduced from Eqs. (35)–(38). We report them in Fig. 4 together with error bars. The experimental uncertainties are generally substantial. This is mostly due to the fact that in Eq. (38) we subtract two quantities which are close to each other at low frequencies [when $\eta^p_{\text{exp}}(\nu) \approx \frac{6}{7}$] and relatively weak at high frequencies. Nevertheless, the pair isotropic intensities have been measured within satisfactory accuracy in the 50–150-cm^{-1} frequency range and may be compared with theoretical models. In Fig. 4, we also report the theoretical second-order DID and dipole–multipole (DQ, DO, QQ, QO, OO) contributions to the isotropic spectrum for the same potential [62] and the same set (α, A, E) of multipolarizabilities used in Fig. 3. The first remark is that DID contribution is not significant in the frequency range of experimental data. The second remark concerns the discrepancy observed in the higher-frequency range of the isotropic spectrum. We assume that it may be attributed to short-range effects such as overlap and exchange effects, which, in the case of CF_4, are not yet known. The third and most important remark is that the chosen values of A and E allow an acceptable fit of experimental and theoretical spectra below 120 cm^{-1}. Considering the error bars and the mutual competition of the DQ and DO contributions, it is nonetheless obvious that this choice of A and E is not unique. Using a set inversion

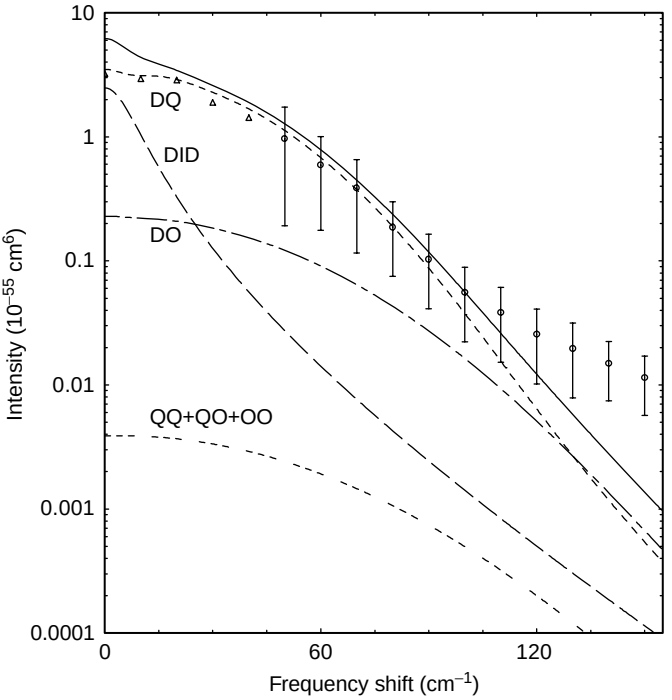

Figure 4. Two-body *isotropic* scattering spectrum for CF_4 gas at 294.5 K. The full circles (•) indicate our experimental data with error bars; triangles (Δ) are just estimated data. Theoretical curves are provided for several contributions using $\alpha = 2.93$ Å^3, $A = 1$ Å^4, $E = 1.5$ Å^5: DID (– – –), DQ (- - -), DO (— - —), QQ+QO+OO (- - - - - -) and DID+DQ+DO+QQ+QO+OO (————).

mathematical approach, it is possible to evaluate the set of all vectors (A, E) such that the theoretical spectrum due to dipole multipole mechanism goes through experimental error bars [67]. For frequencies below 120 cm^{-1}, this set is included in the box defined by $|A| < 1.2$ Å^4 and $|E| < 3.5$ Å^5) (i.e. the maximum values that may be attributed separately to $|A|$ and $|E|$). The value of A is therefore at least 2 times lower than previous experimental estimations of this CF_4 multipolarizability ($A = 2.2$ Å^4 [4,10]). Moreover for a given value of $|A|$, a more restricted interval of confidence is found for $|E|$. For $|A| = 1.2$ Å^4, $|E|$ must be necessarily lower than 0.5 Å^5. Considering the value $A = 0.97$ Å^4 computed by Maroulis [64,65], we get $|E| < 2.75$ Å^5. Conversely, for the $|E| = 1.15$ Å^5 found by Maroulis, we get $0.75 < |A| < 1.15$ Å^5. This shows that ab initio values of Maroulis make theory compatible with experiment. This is fully coherent with the assertion that the isotropic Rayleigh spectrum is due mainly to dipole–multipole contributions. On the other hand, we checked that

the spectral profiles of dipole–multipole contributions are not significantly modified in the 0–150-cm^{-1} frequency domain by the use of another potential among the three ones [47,62,66] compatible with our depolarized spectrum measurements [13]. This is due to the fact (explained above) that the main cause of each rototranslational profile is a rotational stick spectrum (which does not depend on the potential). Indeed, each dipole–multipole contribution may be shifted upward or downward according to the chosen potential (because the latter determines its integrated intensity *via* its convoluted translational part). But for these three potentials, intensity changes in the DQ and DO contributions are less than 20% and corresponding corrections expected for A and E may be evaluated to less than 10%. Therefore at the present time, the study of the isotropic Rayleigh spectrum in absolute units appears to be the most reliable tool for measuring the dipole–multipole components.

B. Linear Centrosymmetric Molecules

1. *Theory*

For linear centrosymmetric molecules such as N_2 and CO_2 we encounter more complicated conditions for observation of CIS scattering than in the case of globular molecules. The polarizability tensor of linear molecules is no longer isotropic and its anisotropy leads to a very strong allowed rotational spectrum. As a result of a pressure broadening mechanism, this allowed spectrum produces substantial intensities even at very high frequencies [68,69]. The excess interaction-induced part of the pair polarizability creates a continuous rototranslational relatively weak but very broad spectral distribution of scattered light. Finally in experiment, both the allowed spectrum and the CIS spectrum, overlap. For depolarized spectra, collision-induced contribution appears to be significant only at very high frequencies. For isotropic intensities, however, the allowed rotational spectrum is composed of one line (Q line), and this creates much better conditions for observation of collision-induced wings.

We briefly discuss, in Cartesian tensor notation, the inductional variations $\Delta\mathbf{A}^{(k)}$ used in our theoretical calculations of collision induced spectra of linear molecules. In the range of intermolecular separations R_{12} where the molecular charge distributions do not overlap $\Delta\mathbf{A}$, up to order R_{12}^{-6}, reads [70–72] as

$$\begin{aligned}\Delta A_{\alpha\beta} = (1+\mathscr{P}^{12})\Big\{&\alpha^{(1)}_{\alpha\gamma}T_{\gamma\delta}(\mathbf{R}_{12})\alpha^{(2)}_{\delta\beta} + \alpha^{(1)}_{\alpha\gamma}T_{\gamma\delta}(\mathbf{R}_{12})\alpha^{(2)}_{\delta\epsilon}T_{\epsilon\phi}(\mathbf{R}_{21})\alpha^{(1)}_{\phi\beta}\\ &+\frac{1}{15}\alpha^{(1)}_{\alpha\gamma}T_{\gamma\delta\epsilon\phi}(\mathbf{R}_{12})E^{(2)}_{\beta,\delta\epsilon\phi} + \frac{1}{15}E^{(2)}_{\alpha,\gamma\delta\epsilon}T_{\gamma\delta\epsilon\phi}(\mathbf{R}_{21})\alpha^{(1)}_{\phi\beta}\\ &-\frac{1}{9}B^{(1)}_{\alpha\beta,\gamma\delta}T_{\gamma\delta\epsilon\phi}(\mathbf{R}_{12})\Theta^{(2)}_{\epsilon\phi} + \cdots\Big\}\end{aligned} \tag{56}$$

where $\boldsymbol{\alpha}$ is the dipole–dipole polarizability tensor of the unperturbated molecule, $\mathbf{E}$ is its dipole–octopole polarizability tensor, $\mathbf{B}$ is the dipole–dipole–quadrupole hyperpolarizability tensor, and $\boldsymbol{\Theta}$ is the permanent quadrupole moment of the molecule; moreover, $\mathscr{P}^{12}$ permutes the indices 1 and 2. The first and second term of inductional polarizability (56) originates, respectively, in the first- and second-order dipole-induced dipole (DID) light scattering mechanism. The third and fourth terms are due to the dipole-induced octopole (DO) mechanism, whereas the last term comes from the permanent quadrupole moment of the molecule and its dipole–dipole–quadrupole hyperpolarizability tensor $\mathbf{B}$.

However, when dealing with molecular rotations for linear molecules, it is very desirable to express $\Delta\,\mathbf{A}^{(k)}$ in the language of spherical harmonics [73]. For linear centrosymmetric molecules all nonzero spherical harmonics coefficients of Eq. (56) for anisotropic scattering $(k = 2)$ are assembled in the Appendix given in Ref. 16 and for isotropic scattering $(k = 0)$, in Ref. 15.

We calculate the pure rotational part of our spectrum taking into account all the light scattering mechanisms described in Eq. (56). Then the resulting spectrum takes the form of the convolution of the rotational and translational parts [see Eqs. (31) and (32)]. We deal numerically with the rotational and translational spectra and their convolution [15,16,36] by methods described in the previous section for optically isotropic molecules.

2. *Results and Discussion*

a. Isotropic Scattering. We have studied the isotropic light scattering from gaseous nitrogen at 295 K and at two densities 41 and 169 Amagat. Two components of the Stokes-side intensities have been measured for frequency shifts up to $700\,\mathrm{cm}^{-1}$ at 90° geometry with incident light parallel $I_{\parallel}(\nu)$ and perpendicular $I_{\perp}(\nu)$ to the scattering plane. The isotropic part of the scattered radiation has been calculated from $I_{\parallel}(\nu)$ and $I_{\perp}(\nu)$ by using Eqs. (35)–(38). The density dependence of the experimental intensities was studied for several frequency shifts. The ratio $I_{\parallel}(450)/I_{\parallel}(60)$ increases linearly with density up to 170 Amagat. From these results, considering that the intensity measured at $\nu = 60\,\mathrm{cm}^{-1}$ was due predominantly to permanent polarizability anisotropy and proportional to the gas density and a function of the local field, it follows that the scattering in the high-frequency part of $I_{\parallel}(\nu)$ is induced by binary mechanisms only. We assume that the same conclusion holds for $I_{\perp}(\nu)$. Therefore in our study we investigate experimentally and theoretically the isotropic spectrum in its binary regime.

We calculate our theoretical isotropic spectrum as a convolution of the rotational stick spectra and the translational spectra. Our rotational stick spectra result from the first- and second-order DID light scattering mechanisms, and from the dipole–octopole (αE) and dipole–dipole–quadrupole ($B\Theta$) multipolar light scattering mechanisms and their cross contributions. We then convolute,

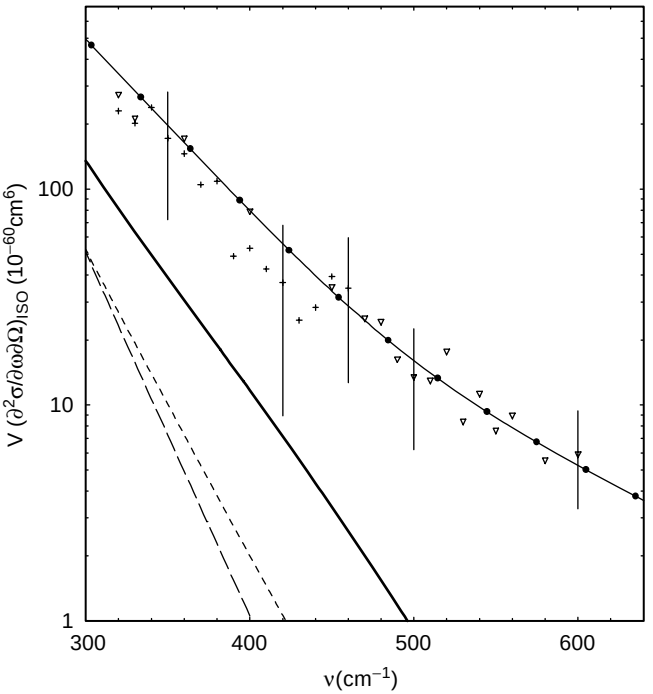

Figure 5. Rototranslational experimental (+, ▽) and theoretical isotropic double-differential cross sections of N_2 at 295 K. Overall theoretical spectrum (———) computed using (E4= −0.69 Å^5 [74]); (- - - -) overall theoretical spectrum computed for (E4= −0.27 Å^5 [75]); (– – –) DID spectrum only. The figure also shows the theoretical spectrum (–•–) computed for $|E4| = 1.5$ Å^5 with an exponential contribution exp(– ν/ν_0) ($\nu_0 = 118$ cm^{-1}) added to represent very short time light scattering mechanisms.

these rotational spectra with translational spectra of Birnbaum–Cohen origin. Figure 5 compares experimental and theoretical isotropic spectra calculated in absolute units. The weak isotropic scattering spectrum originates as the difference of the two, close-in-value, relatively strong "parallel and perpendicular" experimental spectra. This procedure of obtaining the isotropic spectrum involves considerable uncertainty in its values. Because of the very large uncertainty of the experimental isotropic spectrum values at low and very high frequencies, we must analyze the isotropic spectrum in the frequency range 300–600 cm^{-1} only. The theoretical spectrum shown in Fig. 5 was calculated with the use of the molecular multipolar polarizabilities given in the first column of Table IV. In the course of our calculations we found that the high-frequency part of the isotropic spectrum is, as in depolarized scattering [36], due mainly to the components $B^{(0)}_{4044}(R_{12}) = B^{(0)}_{0444}(R_{12})$ [15] of the dipole–induced

TABLE IV
Numerical Values of Nitrogen and Carbon dioxide Multipole Polarizabilities and Permanent Quadrupole Moment Used in Our Calculations[a]

	Nitrogen	Carbon Dioxide
$E_{x,xxx}$	−20.30 [74]	−64.10 [84]
$E_{z,zzz}$	23.88 [74]	176.56 [84]
$B_{x,x,xx}$	−108 [75]	−140 [84]
$B_{x,x,zz}$	62 [75]	79 [84]
$B_{z,z,zz}$	−177 [75]	−305 [84]
$B_{x,z,xz}$	−104 [75]	−205 [84]
θ	−0.9054 [75]	−3.239 [84]
α	11.959 [83][b]	17.626 [84]
γ	4.825 [83][b]	14.271 [84]

[a] All values are in atomic units (a.u). Reference numbers appear in brackets next to the values.
[b] For $\lambda_L = 514.5$ nm

octopole light scattering mechanism with the dipole-octopole tensor anisotropy E4 and the isotropic part α of the linear polarizability involved. These components of $\Delta\mathbf{A}_{(00)}$ induce molecular transitions with selection rules $\Delta J_1 = \pm 4, \Delta J_2 = 0$, and $\Delta J_1 = 0, \Delta J_2 = \pm 4$. The contribution of the components given by the nonlinear part of the pair polarizability to the resulting spectrum is negligible because of their small value for N_2. From our calculations, 5% of the total integrated intensity of the wings of our isotropic nitrogen spectrum originates in the second order DID mechanism and its cross contributions with other light scattering mechanisms. The second-order DID related contributions, however, are located at frequencies up to $350\,\mathrm{cm}^{-1}$ and do not influence the high-frequency rototranslational wings considered here. The high-frequency wings of our theoretical spectrum (above $400\,\mathrm{cm}^{-1}$), however almost totally result from multipolar dipole-induced octopole mechanism (for nitrogen, practically from E4). We found that the high-frequency part of the nitrogen spectrum is mainly associated with the induced dipole–octopole αE light scattering mechanism whereas the influence of the hyperpolarizability and the permanent quadrupole moment term $B\Theta$ is almost insignificant. This observation is similar to the conclusion of Cox and Madden [76] concerning the importance of the αA term and almost negligible significance of $\beta\Theta$ term in their purely interaction-induced spectra of CS_2.

Our theoretical multipolar isotropic spectrum, shown in Fig. 5 and calculated for $\mathrm{E4} = -0.69\,\mathrm{\AA}^5$ [74], lies slightly below the experimental spectrum in the entire experimental frequency range considered. It is generally believed that electron overlap mechanisms strongly contribute to isotropic spectra [73,77]. Then we attribute the abovementioned moderate difference in the theoretical and experimental spectra to overlap effects.

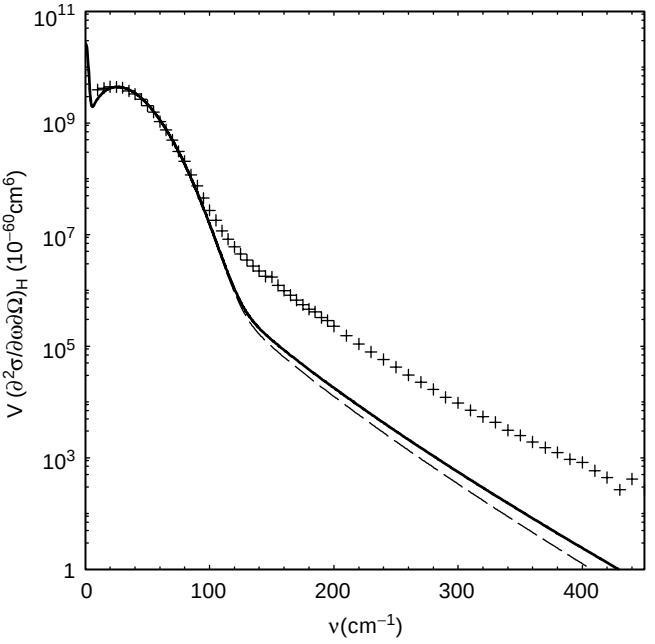

Figure 6. Theoretical and experimental (+ + + +) CO_2 spectra at 23 Amagat and 294.5 K. Theoretical double-differential cross section (- - -) calculated using the first-order DID + the first-order DIO + the first-order BΘ light scattering mechanisms; (———) theoretical double-differential cross section including second-order DID light scattering mechanism.

b. Anisotropic Scattering. We have studied experimentally the anisotropic light scattering from gaseous nitrogen at 295 K and at two densities, 41 and 169 Amagat [36], as well as the anisotropic scattering from carbon dioxide at 294 K and 23 Amagat [16]. In the case of nitrogen, the low-temperature (150 K) spectrum has been also considered. For the depolarized spectrum of nitrogen, second-order quantum-mechanical calculations [68] as well as relaxation matrix considerations [69] show that most of the intensity at relatively large frequency shifts is due to wings of the pressure broadened rotational Raman lines. In this case collision-induced contribution to the depolarized nitrogen spectrum appears to be significant only at very high frequencies. Figure 6 compares the experimental and theoretical depolarized CO_2 spectra. We note that the experimental and theoretical spectra have almost the same shape (slope) but the intensities of the theoretical spectrum at high frequencies are roughly of one order of magnitude smaller than the experimental ones. We attribute this discrepancy to pressure-broadening-allowed rotational Raman lines and overlap effects during CO_2 collisions but, to our knowledge, high-frequency-allowed

rotational Raman spectrum and *numerical* overlap details of the excess pair polarizability are not yet available for CO_2. Obviously, consideration of the next multipole contributions (shorter range than R_{12}^{-6}) could reduce this discrepancy as well. Moreover, Fig. 6 shows that second-order DID CO_2 contributions, although not great in value, visibly improve the comparison between the theoretical and experimental spectra.

V. SCATTERING IN THE RAMAN VIBRATIONAL BANDS OF OPTICALLY ISOTROPIC MOLECULES

A. Theory

For the ν_1 vibration of CF_4, the Raman polarizability tensor of an isolated molecule is isotropic, and, consequently, monomer polarizabilities of Eq. (2) do not contribute to ν_1 depolarized Raman spectral wings. On the other hand, the Raman incremental pair polarizability tensor for the normal vibration ν_1 that takes place in Eq. (2) is [78]

$$ {}_{(\mathrm{RM})}\Delta A_{\alpha\beta} = \frac{\partial \Delta A_{\alpha\beta}}{\partial Q_1^A}\, Q_1^A + \frac{\partial \Delta A_{\alpha\beta}}{\partial Q_1^B}\, Q_1^B \tag{57} $$

where Q_1^p is the normal coordinate for the mode ν_1 and the molecule p. The autocorrelation functions of the isotropic and anisotropic parts of this Raman pair polarizability are provided in Table V for successive multipolar induction operators. In Table V, the F_+ function for the Raman Stokes side of the $\tilde{\nu}_1$ normal vibration refers to [79]

$$ F_+ = \frac{b_{\nu_1}^2}{1 - e^{-[h c \tilde{\nu}_1 / k_B T]}} \tag{58} $$

TABLE V
Coefficients φ_{LL}^{N,j_1,j_2} Involved in Raman Isotropic and Depolarized Light Scattering Correlation Functions $F_{LL}(t) = \sum_{N,j_1,j_2} \varphi_{LL}^{N,j_1,j_2}\, S_N(t)\, R_{j_1}(t)\, R_{j_2}(t)\, F_+$ for Successive Multipolar Induction Operators

Raman CIS	N	j_1	j_2	Isotropic φ_{00}^{N,j_1,j_2}	Depolarized φ_{22}^{N,j_1,j_2}
DID	2	0	0	0	$48\,(\alpha\,\alpha')^2$
DQ	3	0	3	$\frac{160}{7}\,[(\alpha' A)^2 + (\alpha A')^2]$	$\frac{192}{7}\,[(\alpha' A)^2 + (\alpha A')^2]$
DO	4	0	4	$\frac{224}{9}\,[(\alpha' E)^2 + (\alpha E')^2]$	$\frac{220}{9}\,[(\alpha' E)^2 + (\alpha E')^2]$
QQ	4	3	3	$\frac{2816}{189}\,(A A')^2$	$\frac{251{,}648}{945}\,(A A')^2$
QO	5	3	4	$\frac{416}{21}\,[(A E')^2 + (A' E)^2]$	$\frac{9280}{21}\,[(A E')^2 + (A' E)^2]$
OO	6	4	4	$\frac{110}{3}\,(E E')^2$	$\frac{22{,}660}{21}\,(E E')^2$

where $b_{\nu_1} = [h/(8\pi^2 c\,\tilde{\nu}_1)]^{1/2}$ is the zero-point vibrational amplitude of the mode (h being the Planck's constant, c the light velocity, and $\tilde{\nu}_1$ the normal mode frequency in cm^{-1}). Moreover as in Table III, A and E stand for the independent components of the tensors **A** and **E**, whereas each derivative of a (multi)polarizability $\mathscr{Z}$ is defined as $\mathscr{Z}' = \partial\mathscr{Z}/\partial Q_1^p$. It is noteworthy that the latter is related to a corresponding bond length R derivative. For CF_4 with four equivalent bonds this relation has the form [79]

$$\left(\frac{\partial\,\alpha}{\partial Q_1}\right)_{\text{molecule}} = \frac{1}{2\sqrt{m_F}}\left(\frac{\partial\,\alpha}{\partial R}\right)_{\text{molecule}} \tag{59}$$

which may be extended to any multipolarizability, hyperpolarizability, or multipole moment.

As in the Rayleigh case, the pair polarizability results as well from nonlinear light scattering mechanisms (induced by hyperpolarizabilities and permanent multipole moments). For tetrahedral molecules nonlinear mechanisms contribute to some correlation functions listed in Table V—only those related to the depolarized spectrum and governed by double rotational transitions (QQ, QO, and OO). The nonlinear origin corrections $\Delta\varphi_{22}^{N,j_1,j_2}$ which must be added to the linear origin terms φ_{22}^{N,j_1,j_2} of Table V for a tetrahedral molecule are successively [17]

$$\begin{aligned}\Delta\varphi_{22}^{4,3,3} = &-\frac{768}{5}A\,A'\,(b'_{xyz}\,\Omega + b_{xyz}\,\Omega')\\ &+\frac{192}{7}[(b'_{xyz}\,\Omega)^2 + 2\,b_{xyz}\,b'_{xyz}\,\Omega\,\Omega' + (b_{xyz}\,\Omega')^2]\end{aligned} \tag{60}$$

$$\begin{aligned}\Delta\varphi_{22}^{5,3,4} = &-\frac{576}{7}(A'E\,\Delta B\,\Omega' + AE'\,\Delta B'\,\Omega) + \frac{144}{25}[(\Delta B'\,\Omega)^2 + (\Delta B\,\Omega')^2]\\ &-192\left(A'\,E\,b'_{xyz}\,\Phi + A\,E'\,b_{xyz}\,\Phi'\right) + \frac{96}{7}\left(b'_{xyz}\,\Delta B\,\Omega'\,\Phi\right.\\ &\left.+\,b_{xyz}\,\Delta B'\,\Omega\,\Phi'\right) + \frac{240}{7}[(b'_{xyz}\,\Phi)^2 + (b_{xyz}\,\Phi')^2]\end{aligned} \tag{61}$$

$$\begin{aligned}\Delta\varphi_{22}^{6,4,4} = &-\frac{1056}{7}\,E\,E'\,(\Delta B'\,\Phi + \Delta B\,\Phi')\\ &+\frac{88}{15}[(\Delta B'\,\Phi)^2 + 2\,\Delta B\,\Delta B'\,\Phi\,\Phi' + (\Delta B\,\Phi')^2]\end{aligned} \tag{62}$$

where b'_{xyz} and $\Delta B'$ stand for the normal coordinate derivatives of the aforementioned dipole–dipole–dipole and dipole–dipole–quadrupole hyperpolarizability tensors, respectively. Similarly, Ω' and Φ' denote the normal coordinate

derivatives of the permanent octopole and hexadecapole, respectively. For octahedral molecules, both $\Delta\varphi_{22}^{4,3,3}$ and $\Delta\varphi_{22}^{5,3,4}$ terms vanish for symmetry reasons.

Computations of various dipole–multipole contributions have been done by using a procedure similar to that used for Rayleigh spectra. In fact, the main change consists in replacing the coefficients φ_{22}^{N,j_1,j_2} of Table III by these of Table V.

B. Results and Discussion

1. *Experimental and Theoretical Spectra*

Using our experimental setup, CI Raman band intensities of CF_4 were measured at 294.5 K for several densities up to 250 Amagat and for frequency shifts ranging from 3 to 110 cm^{-1} and measured from the center of the ν_1 line of CF_4. Except for $\nu \leq 130\,cm^{-1}$, the intensities increase as the square of the density up to 250 Amagat. This shows that binary interactions predominate in these density and frequency ranges [17]. As shown previously [80], four-body interactions do not contribute to CIS inside a Raman vibrational band. However, a negative contribution due to three-body interactions appears for $\nu \leq 30\,cm^{-1}$ at high densities (50 and 100 Amagat for $\nu = 20$ and $30\,cm^{-1}$, respectively). Therefore, we took off the latter from experimental data in order to get the binary spectra at low frequencies. Moreover, we have checked that in our experiment, leakages and mixing between polarized and depolarized components due to experimental polarization errors do not affect significantly our data. The whole binary spectrum has been calibrated in absolute units from measurements of the depolarized CIS at $\nu = 15\,cm^{-1}$ from the center of the ν_1 band relatively to the integrated intensity of the $S_0(2)$ line of H_2 gas. For the Raman depolarized intensity, we obtained $I_d(15\,cm^{-1}) = (2.03 \pm 0.35)\,10^{-56}\,cm^6$. Then, by using Eqs. (35)–(38) and the values of the Raman experimental depolarization ratio provided in Fig. 2, we got in absolute units both depolarized and isotropic spectra of the light scattered in the vicinity of the ν_1 Raman line of CF_4. These depolarized and isotropic intensities are provided together with their error bars in Figs. 7 (see also Table VI) and 8, respectively. In Figs. 7 and 8, the total theoretical spectra and their successive multipolar contributions are equally reported for a Lennard-Jones potential [62], a couple $(\alpha, \alpha') = (2.93\,\text{Å}^3, 4.00\,\text{Å}^2)$ of dipolar polarizabilities and a set (A, A', E, E') of dipole–multipole polarizabilities provided in Table VI. Contributions of nonlinear origin [Eqs. (60)–(62)] have been taken into account by using ab initio data computed by Maroulis [64,65]. Nevertheless in the case of CF_4, they contribute to less than a few percents to the QQ, QO, and OO intensities and may be neglected. The values of α (used above in the Rayleigh case) and of its bond length R derivative α' (deduced from Raman studies [79,81]) are close to these

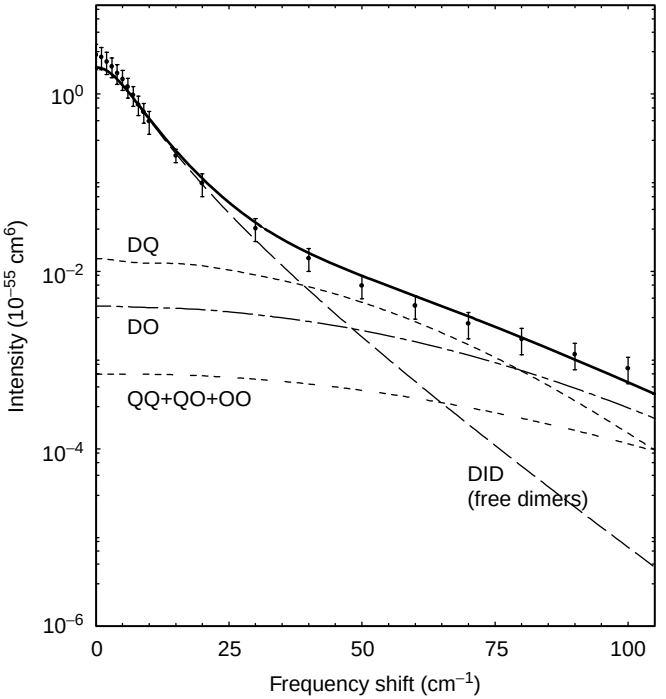

Figure 7. Two-body depolarized scattering Stokes spectrum of the ν_1 Raman band of gaseous CF_4 in absolute units at 294.5 K. Full circles (•) indicate experimental data together with error bars. Theoretical curves (DID — — —, DQ - - - - -, DO — - —, QQ+QO+OO - - - - - -, and total theoretical ———) are computed using a Lennard-Jones potential [62], $\alpha = 2.93$ Å^3, $\alpha' = 4.00$ Å^2, and a set of multipolarizability values provided in Table VI.

computed by Maroulis [64,65] (2.89 Å^3, 3.92 Å^2) and may be regarded with confidence. The values of A and E have been deduced from our Rayleigh measurements (see Figs. 3 and 4) and are also close to these of Maroulis. The values of the bond length R derivatives A' and E' have been estimated according to a fitting procedure applied to both depolarized and isotropic Raman spectra in a frequency range (30–80 cm^{-1}) for which we assume that dipole–multipole mechanisms are predominant.

2. *Discussion*

a. Depolarization Ratio. As can be observed in Fig. 2, Raman depolarization-ratio data measured in the 10–110-cm^{-1} frequency-shift range of the ν_1 Raman band are significantly different from these observed in the Rayleigh band. At low frequencies (10–20 cm^{-1}) the upper Raman value measured is about 0.5

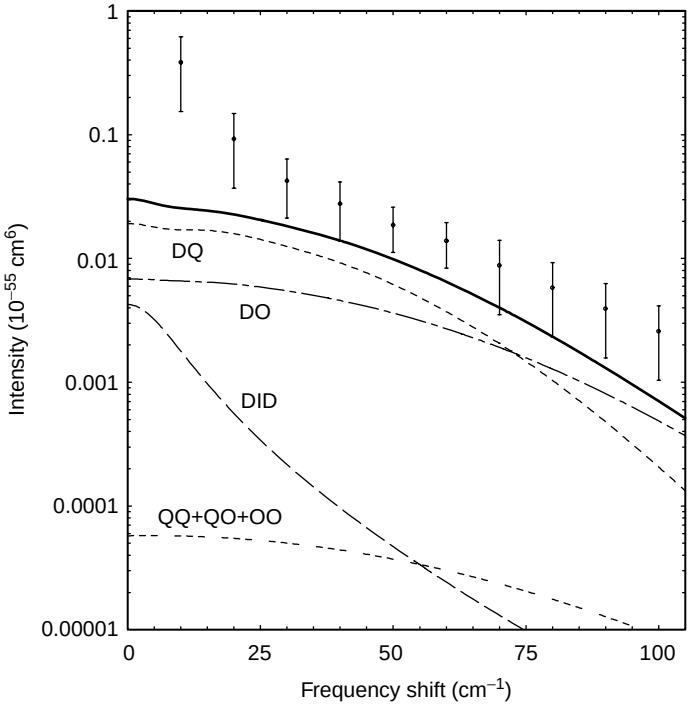

Figure 8. Two-body isotropic scattering Stokes spectrum of the ν_1 Raman band of gaseous CF_4 in absolute units at 294.5 K. Full circles (•) indicate experimental data together with error bars. Theoretical curves (DID — — —, DQ - - - - -, DO — - —, QQ + QO + OO - - - - - -, and total theoretical ———) are computed using a Lennard-Jones potential [62], $\alpha = 2.93$ Å^3, $\alpha' = 4.00$ Å^2, and a set of multipolarizability values provided in Table VI.

TABLE VI
Multipolarizabilities and Their Bond Length R Derivatives for CF_4[a]

Polarizability	Theory	Experiment	CIS spectrum [Ref.]
$\lvert A\rvert$	0.972 Å^4	1. Å^{4b}	Isotropic Rayleigh [13]
$\lvert A'\rvert = \lvert\frac{\partial A}{\partial R}\rvert$	4.09 Å^3	5. Å^{3b}	Raman [17,18]
$\lvert E\rvert$	1.15 Å^5	1.5 Å^{5b}	Isotropic Rayleigh [13]
$\lvert E'\rvert = \lvert\frac{\partial E}{\partial R}\rvert$	5.53 Å^4	$<$ 18 Å^{4b}	Raman [17,18]

[a]Theoretical values were computed ab initio by Maroulis [64,65]. Experimental values were deduced from our CIS experiments [13,18].
[b]Same set of values used in Figs. 7 and 8.

when the corresponding Rayleigh one is almost $\frac{6}{7}(\approx 0.86)$. In the 60–110-cm^{-1} frequency region, $\eta^{p}_{\exp}(\nu) \approx 0.2$, that is, 3 times smaller than the value obtained for the Rayleigh scattering. As DID scattering is depolarized (contrary to multipolar scattering [33]), the aforementioned result may be partly explained by the different value of the DID contribution relatively to the depolarized CIS intensities in the Rayleigh and in the vibrational Raman bands. Indeed, we see from Figs. 3 and 7 that the ratio of the free-dimer DID intensity to the DQ intensity is higher in the Rayleigh spectrum than in the vibrational Raman one by about one order of magnitude, whatever the frequency is. Consequently, the DID intensity and the DQ intensity are equal for a frequency shift of about 40 cm^{-1} in the Raman case instead of about 60 cm^{-1} in the Rayleigh case.

b. Depolarized Spectrum. In the Rayleigh part, in order to make coherent our theoretical model with both depolarized and isotropic spectra, we concluded that the profile of the pure translational component of the depolarized spectrum is affected for $\nu \geq 60$ cm^{-1} by uncertainties related to overlap and exchange effects (not yet known in the case of CF_4) or to the intermolecular potential. However, it can be seen in Fig. 3 that our computed DID spectrum fits well experimental depolarized Rayleigh data until about 40 cm^{-1}. It is a good indication on the reliability of the DID contribution to the depolarized Raman band in this restricted frequency domain. At higher frequencies for the Raman depolarized spectrum, the DQ contribution becomes predominant. Therefore, the restrictions put in the Rayleigh study about the reliability of the depolarized spectrum for measuring dipole–multipole polarizabilities now partly vanish. On the other hand, it can be seen in Figs.7 and 8 that the lack of theoretical isotropic intensity does not concern anymore the depolarized spectrum as in the Rayleigh case (except at highest frequencies) but the isotropic spectrum for all the frequency range scanned. A bigger value of A' could fill this lack of intensity but would involve an excess of theoretical depolarized intensity; the sum DID+DQ remain lower than or equal to every upper error bar limit of the depolarized spectrum only if A' is lower than $A'_{\max} = 6.3$ Å^3. This maximum value is close to the fitted one (5 Å^3) which is itself close to the computed $A' = 4.09$ Å^3 of Maroulis [64,65]. This confirms that the depolarized Raman spectrum allows a good evaluation of the derivative of the dipole–quadrupole polarizability. Nevertheless, using $A' = 5$ Å^3 and a value of E' close to this found by Maroulis (5.53 Å^4), the theoretical depolarized spectrum goes through error bars until 80 cm^{-1} only. Using instead the fitted derivative $E' \approx 18$ Å^4 the theoretical spectrum fits well up to 100 cm^{-1}, whereas this E' value is three times the ab initio calculated one. As the dipole-octopole mechanism is the shortest-range multipolar mechanism considered here, either discrepancy or overstatement make up for the short-range effects that are not considered by our model and may affect spectrum intensities at high frequencies ($\nu \geq 80$ cm^{-1}). Therefore,

the fitted E' value must be regarded as providing an order of magnitude rather than a real estimation.

c. Isotropic Spectrum. Because of the low depolarization ratio in the Raman case, the error bars of the experimental isotropic intensities are much smaller than in the corresponding Rayleigh case. Consequently, the spectrum frequency range provided in Fig. 8 starts from 10 cm^{-1} (instead of 50 cm^{-1} in the Rayleigh experiments). Concerning various theoretical contributions, only DQ and DO contributions must be considered (second-order DID and double rotational contributions may be neglected). As ν tends to zero, the lineshape of the experimental isotropic spectrum deviates from the theoretical one. This discrepancy may be attributed, at least partly, to the vibrational–rotational coupling present in the ν_1 Q line [82]. A similar deviation exists for the highest frequencies scanned, which can be attributed to short-range effects as in the depolarized case. However, in the 30–80-cm^{-1} range, where we assume that multipolar mechanisms are predominant, our theoretical intensities are nearly but not high enough to fit experimental data well. The value of A' for which the DQ intensities remain lower than the upper limit of the experimental error bars in the 30–80-cm^{-1} range becomes 10.5 $\mathring{A}^4$ (2 times our fitted value of A'). The aforementioned rotovibrational coupling of the ν_1 Q line cannot be considered as responsible for this overstatement; its width at half intensity is just several cm^{-1} at a few Amagat values, whereas the effect of coupling decreases with density and with frequency. The influence of the potential must also be dismissed; a potential that would modify dipole–multipole intensities could not allow simultaneous "decrease" of the theoretical depolarized spectrum and "increase" of the theoretical isotropic spectrum in order to make them closer to depolarized and isotropic experiments, respectively. Therefore, the particular sensitivity of the trace-induced isotropic spectrum to short-range interactions appears to be the main cause of the observed discrepancy. Overlap and exchange effects may here play a role, but may molecular frame distortion and the non-point-like size of the CF_4 molecule. However, these effects are not important enough to preclude an evaluation of A' by using both depolarized and isotropic spectra. This evaluation is in good agreement with an ab initio calculation of Maroulis [64,65]. We assume that this result is due to at least two factors: (1) the dipole–quadrupole mechanism (DQ) is predominant from 30 up to 80 cm^{-1} for both depolarized and isotropic spectra; and (2) our theoretical model is correct in this frequency range.

VI. CONCLUSION

It has been shown that multipolar polarizabilities contribute significantly to the collision-induced scattering from fluids composed of linear (N_2, CO_2) or

optically isotropic (CF_4, SF_6) molecules. Several studies concern depolarized scattering in the Rayleigh frequency region. From them, multipolar polarizability constants of globular or linear molecules have been estimated [2–4, 7–12]. However, when depolarized scattering is considered alone, specific effects alter the measurement of multipolar polarizabilities. In particular, the depolarized spectrum includes a strong first-order DID spectrum and/or allowed rotational lines. Because of some inaccuracy of the potential and/or pressure broadening of the rotational lines and/or short-range effects, these contributions cannot be always clearly discriminated from multipolar contributions. On the other hand, these effects do not influence or influence weakly isotropic scattering due to multipolar polarizabilities. Therefore, the isotropic CI Rayleigh spectrum is more adapted to measurements of multipolar polarizabilities than the depolarized spectrum. Analysis of both depolarized and isotropic scattering yields thus a better determination of multipolar polarizability constants. The derivatives of the multipolar polarizabilities may also be deduced from studies related to CI wings of vibrational Raman lines, as it has been shown in recent studies on light scattered in the vicinity of the ν_1 lines of CF_4 and SF_6 [14,17,18]. Like in the Rayleigh case, these first and only works concerning vibrational Raman bands show that it is better to study both depolarized and isotropic components.

In summary, since the early 1980s or so, collision-induced light scattering experiments on molecular fluids have demonstrated that the study of the collision-induced absolute-unit spectra (depolarized and/or isotropic ones) is an useful tool, and up to now the only one, to measure multipolar polarizabilities of molecules.

References

1. G. C. Tabisz and M. N. Neuman, (Eds.), *Collision- and Interaction-Induced Spectroscopy*, Vol. 452 of *NATO ASI Series C: Mathematical and Physical Sciences*, Kluwer Academic, Dordrecht, 1995.
2. A. D. Buckingham and G. C. Tabisz, *Mol. Phys.* **36**, 583 (1978).
3. G. C. Tabisz, in R. F. Barrow, D. A. Long, and J. Sheridan (Eds.), *Molecular Spectroscopy, a* Specialist Periodical Report, Chemical Society, London, 1979, Vol. 6, pp. 136–173.
4. D. P. Shelton and G. C. Tabisz, *Mol. Phys.* **40**, 299 (1980).
5. H. Posch, *Mol. Phys.* **37**, 1059 (1979).
6. H. Posch, *Mol. Phys.* **40**, 1237 (1980).
7. H. Posch, *Mol. Phys.* **46**, 1213 (1982).
8. A. Elliasmine, J.-L. Godet, Y. Le Duff, and T. Bancewicz, *Mol. Phys.* **90**, 147 (1997).
9. F. Barocchi, A. Guasti, M. Zoppi, S. M. El-Sheikh, G. C. Tabisz, and N. Meinander, *Phys. Rev. A* **39**, 4537 (1989).
10. S. M. El-Sheikh and G. C. Tabisz, *Mol. Phys.* **68**, 1225 (1989).
11. U. Bafile, L. Ulivi, M. Z. F. Barocchi, and L. Frommhold, *Phys. Rev. A* **50**, 1172 (1994).
12. N. Meinander, G. C. Tabisz, F. Barocchi, and M. Zoppi, *Mol. Phys.* **89**, 521 (1996).

13. A. Elliasmine, J.-L. Godet, Y. Le Duff, and T. Bancewicz, *Phys. Rev.* **55**, 4230 (1997).
14. J.-L. Godet, Y. Le Duff, R. Rachet, K. Nowicka, and T. Bancewicz, in S.-L. Zhang and B.-F. Zhu (Eds.), *Proc. XVIIth Int. Conf. Raman spectroscopy*, Wiley, New York, 2000, p. 102.
15. T. Bancewicz, V. Teboul, and Y. Le Duff, *Mol. Phys*. **81**, 1353 (1994).
16. V. Teboul, Y. Le Duff, and T. Bancewicz, *J. Chem. Phys*. **103**, 1384 (1995).
17. T. Bancewicz, A. Elliasmine, J.-L. Godet, and Y. Le Duff, *J. Chem. Phys*. **108**, 8084 (1998).
18. J.-L. Godet, A. Elliasmine, Y. Le Duff, and T. Bancewicz, *J. Chem. Phys*. **110**, 1130 (1999).
19. Nonlinear Optics Division, Faculty of Physics, Adam Mickiewicz University, Poznań, Poland, and Laboratoire des Propriétés Optiques des Matériaux et Applications, Université d'Angers, France.
20. S. Kielich, *Nonlinear Molecular Optics*, Nauka, Moscow, 1981.
21. G. Birnbaum (Ed.), *Phenomena Induced by Intermolecular Interactions, NATO ASI Series*, Plenum, New York, 1985.
22. K. L. C. Hunt, in G. Birnbaum (Ed.), *Phenomena Induced by Intermolecular Interactions*, Plenum Press, New York, 1985.
23. L. Frommhold, *Collision-Induced Absorption in Gases*, Cambridge Univ. Press, Dordrecht, 1993.
24. M. S. Brown, S. K. Wang, and L. Frommhold, *Phys. Rev. A* **40**, 2276 (1989).
25. A. De Lorenzi, A. De Santis, R. Frattini, and M. Sampoli, *Phys. Rev. A* **33**, 695 (1986).
26. L. Frommhold, J. D. Poll, and R. H. Tipping, *Phys. Rev. A* **46**, 2955 (1992).
27. S. Kielich, *J. Phys*. **43**, L389 (1982).
28. T. Bancewicz, W. Głaz, and S. Kielich, *Chem. Phys*. **128**, 321 (1988).
29. C. G. Gray and K. E. Gubbins, *Theory of Molecular Fluids*. Vol. 1: *Fundamentals*, Clarendon Press, Oxford, 1984.
30. S. Kielich, *Acta Phys. Polon*. **20**, 433 (1961).
31. W. P. Healy, *J. Phys*. **B7**, (1974).
32. D. A. Varshalovich, A. N. Moskalev, and V. K. Khersonskii, *Kvantovaya Teoria Uglovogo Momenta*, Nauka, 1975.
33. T. Bancewicz, *Chem. Phys. Lett*. **244**, 305 (1995).
34. A. P. Jucis and A. A. Bandzaitis, *Teoria momenta kolichestwa dvizhenia v kvantovoy mekhanike*, Vilnius, 1965 (in Russian).
35. S. Wolfram, The *Mathematica* Book, 3rd ed., Cambridge Univ. Press, Cambridge, UK, 1996.
36. T. Bancewicz, V. Teboul, and Y. Le Duff, *Phys. Rev. A* **46**, 1349 (1992).
37. A. D. Buckingham and G. C. Tabisz, *Opt. Lett*. **1**, 220 (1977).
38. W. Głaz, *Physica* **A148**, 610 (1988).
39. F. Chapeau-Blondeau, V. Teboul, J. Berrue, and Y. Le Duff, *Phys. Lett*. **A173**, 153 (1993).
40. M. H. Proffitt, J. W. Keto, and L. Frommhold, *Can. J. Phys*. **59**, 1459 (1981).
41. B. J. Berne and R. Pecora, *Dynamic Light Scattering*, Wiley, New York, 1976.
42. F. Barocchi and M. Zoppi, in G. Birnbaum (Ed.), *Phenomena Induced by Intermolecular Interactions*, Plenum, New York, 1985.
43. J. deBoer, *Rep. Prog. Phys*. **12**, 305 (1947).
44. L. Frommhold, K. H. Hong, and M. H. Proffitt, *Mol. Phys*. **35**, 665 (1978).
45. M. Chrysos, O. Gaye, and Y. Le Duff, *J. Phys. B* **29**, 583 (1996).
46. F. Rachet, M. Chrysos, C. Guillot-Noël, and Y. Le Duff, *Phys. Rev. Lett*. **84**, 2120 (2000).

47. G. C. Maitland, M. Rigby, E. B. Smith, and W. A. Wakeham, *Intermolecular Forces. Their Origin and Determination*, Clarendon Press, Oxford, 1981.
48. M. Chrysos, O. Gaye, and Y. Le Duff, *J. Chem. Phys*. **105**, 1 (1996).
49. H. B. Levine, *J. Chem. Phys*. **56**, 2455 (1972).
50. A. T. Prengel and W. S. Gornall, *Phys. Rev. A* **13**, 253 (1976).
51. N. Meinander and G. C. Tabisz, *J. Quant. Spectrosc. Radiat. Trans*. **35**, 39 (1986).
52. N. Meinander, in G. C. Tabisz and M. N. Neuman (Eds.), *Collision- and Interaction-Induced Spectroscopy*, Vol. 452 of *NATO ASI Series C: Mathematical and Physical Sciences*, Kluwer Academic, Dordrecht, 1995, p. 507.
53. N. Meinander, G. C. Tabisz, and M. Zoppi, *J. Chem. Phys*. **84**, 3005 (1986).
54. N. Meinander, *Chem. Phys. Lett*. **228**, 295 (1994).
55. A. Bonechi, F. Barocchi, M. Moraldi, C. Biermann, R. Winter, and L. Frommhold, *Phys. Rev. A* **57**, 56 (1998).
56. A. Bonechi, M. Moraldi, and L. Frommhold, *J. Chem. Phys*. **109**, 5880 (1998).
57. C. Ceccherini, M. Moraldi, and L. Frommhold, *J. Chem. Phys*. **111**, 6316 (1999).
58. G. Birnbaum and E. R. Cohen, *Can. J. Phys*. **54**, 593 (1976).
59. A. Borysow, M. Moraldi, and L. Frommhold, *Mol. Phys*. **56**, 913 (1985).
60. T. Bancewicz, *Chem. Phys. Lett*. **213**, 363 (1993).
61. C. Schwartz and R. J. J. LeRoy, *J. Mol. Spectrosc*. **121**, 420 (1987).
62. K. E. MacCormack and W. G. Schneider, *J. Chem. Phys*. **19**, 849 (1951).
63. H. E. Watson and K. L. Ramaswamy, *Proc. Roy. Soc. Lond. A***156**, 144 (1936).
64. G. Maroulis, *Chem. Phys. Lett*. **259**, 654 (1996).
65. G. Maroulis, *J. Chem. Phys*. **105**, 8467 (1996).
66. B. J. Palmer and J. L. Anchell, *J. Phys. Chem*. **99**, 12239 (1995).
67. L. Jaulin, J.-L. Godet, E. Walter, A. Elliasmine, and Y. Le Duff, *J. Phys. A* **30**, 7733 (1997).
68. Y. Fu, A. Borysow, and M. Moraldi, *Phys. Rev. A* **53**, 201 (1996).
69. J. V. Buldyrieva and L. Bonamy, *Phys. Rev. A* **60**, 1 (1999).
70. A. D. Buckingham, *Adv. Chem. Phys* **12**, 107 (1967).
71. S. Kielich, *Proc. Indian Acad. Sci*. (*Chem. Sci*.) **94**, 403 (1985).
72. K. L. C. Hunt, Y. Q. Liang, and S. Sethuraman, *J. Chem. Phys*. **89**, 7126 (1988).
73. L. Frommhold, *Adv. Chem. Phys*. **46**, 1 (1981).
74. I. Cernusak, G. H. F. Diercksen, and A. Sadlej, *Chem. Phys*. **108**, 45 (1986).
75. G. Maroulis and A. J. Thakkar, *J. Chem. Phys*. **88**, 7623 (1988).
76. T. I. Cox and P. A. Madden, *Mol. Phys*. **39**, 1487 (1980).
77. M. S. Brown and L. Frommhold, *Mol. Phys*. **66**, 527 (1989).
78. W. Holzer and Y. Le Duff, *Phys. Rev. Lett*. **32**, 205 (1974).
79. W. F. Murphy, W. Holzer, and H. J. Bernstein, *Appl. Spectrosc*. **23**, 211 (1969).
80. M. Thibeau, A. Gharbi, Y. Le Duff, and V. Sergiescu, *J. de Phys*. **38**, 641 (1977).
81. W. Holzer, *J. Mol. Spectrosc*. **25**, 123 (1968).
82. Y. Le Duff and A. Gharbi, *Phys. Rev. A* **17**, 1729 (1978).
83. G. R. Alms, A. K. Burnham, and W. F. Flygare, *J. Chem. Phys*. **63**, 3321 (1975).
84. G. Maroulis and A. J. Thakkar, *J. Chem. Phys*. **93**, 4164 (1990).

NONSTATIONARY CASIMIR EFFECT AND ANALYTICAL SOLUTIONS FOR QUANTUM FIELDS IN CAVITIES WITH MOVING BOUNDARIES

V. V. DODONOV

Departamento de Física, Universidade Federal de São Carlos, Brazil,
Lebedev Physics Institute of Russian Academy of Sciences
and Moscow Institute of Physics and Technology

CONTENTS

I. INTRODUCTION

Electrodynamics in vacuum or in media with moving boundaries was the subject of numerous studies in the twentieth century. It is sufficient to remember that the famous Einstein paper that gave birth to the relativity theory was entitled "Electrodynamics of moving bodies" [1]. The total number of publications in this field is enormous, since it includes, in particular, such important problems as radiolocation. In this review we confine ourselves to the problem of *cavities* with (ideal) *reflecting* moving boundaries. This means that we consider the fields confined in some limited volume, thus leaving aside the problem of the field propagation in the (semi)infinite space and reflection from single boundaries (as numerous references on this "full space" problem can be found in the literature, e.g., Refs. 2–5).

The plan of the chapter is as follows. In the next section we give a brief historical review of the relevant studies, in the fields of both classical and quantum electrodynamics, providing an extensive list of the known publications. Although we tried to give a more or less complete list, it is clear that some publications have been (undeliberately) omitted. However, we should mention that for decades different groups of physicists and mathematicians performed studies in their own fields of interest, not suspecting the existence of analogous results found in other areas. We hope that our review will serve to help diminish this gap.

It is clear that all results accumulated for several decades cannot be collected in one chapter. Therefore, in the following sections we have decided to emphasize mainly a detailed exposition of our own results concerning the *analytical solutions* for the cavities with *resonantly oscillating* boundaries, since we hope that these solutions could be important for further studies on the problem known as the *nonstationary Casimir effect* or the *dynamical Casimir effect*.

II. BRIEF HISTORY OF STUDIES ON ELECTRODYNAMICS WITH MOVING BOUNDARIES

A. Classical Fields in Cavities with Moving Boundaries

The first exact solution of the wave equation ($c = 1$)

$$\frac{\partial^2 A}{\partial t^2} - \frac{\partial^2 A}{\partial x^2} = 0 \tag{1}$$

in a time-dependent domain $0 < x < L(t)$ [where $L(t)$ is the given law of motion of the right boundary], satisfying the boundary conditions

$$A(0,t) = A(L(t),t) = 0 \tag{2}$$

was obtained by Nicolai [6] for

$$L(t) = L_0(1 + \alpha t) \tag{3}$$

The solution was interpreted in terms of the transverse vibrations of a string with a variable length. A few years later, these results were published [7], and were extended to the case of electromagnetic field. A similar treatment was reported by Havelock [8] in connection with the problem of radiation pressure. About 25 years later, the one-dimensional wave equation in the time-dependent interval interval $0 < x < a + bt$ was considered [9] under the name "Spaghetti problem."

A new wave of interest to the problem of an electromagnetic field in a cavity with moving boundaries arose only in the early 1960s, motivated, in part, by experiments [10] on "field compression," accompanied by frequency multiplication (for 2.3 times) due to multiple reflections of the initial H_{011} wave ($\lambda_{\text{in}} = 10\,\text{cm}$) from the opposite sides of a resonator, one of which was a "plasma piston" moving uniformly with the velocity $v \sim 2 \cdot 10^7$ cm/s. Kurilko [11] studied linearly polarized electromagnetic field between two ideal infinite plates moving with equal constant velocities toward each other. He considered consecutive reflections of the waves from each boundary, writing explicit expressions for the finite timespace intervals, corresponding to zero, one, two, and further reflections. Balazs [12] gave a detailed study of the string problem with the aid of the method similar to that used by Nicolai and Havelock. Besides considering the uniformly moving boundary, he has found an exact solution for $L(t) = (t^2 + 1)^{1/2}$, and presented some graphical method of finding the solution for an arbitrary law of motion $L(t)$. Greenspan [13] studied the one-dimensional string with the uniformly moving right boundary, assuming the boundary condition at the left point in the form $A(0,t) = \sin(\omega t)$. The problem of the "field compression" between two ideal infinite moving walls (the same geometry as in Ref. 11) was studied by Stetsenko [14,15]. An approximate solution for the electromagnetic field in a rectangular waveguide cavity with a uniformly moving boundary was also obtained [16]. In this case one has to solve the equation ($c = 1$)

$$A_{xx} - A_{tt} = \kappa^2 A \tag{4}$$

with the same boundary condition as in (2). The detailed paper by Baranov and Shirokov [17] can be considered, in a sense, as a concluding study of the

one-dimensional problem with a *uniformly moving boundary* (although many publications on this subject have continued to appear). Experiments on *laser cavities* with uniformly moving mirrors have been described [18–22]. In these experiments, the constant velocity of the mirror varied from 7 cm/s [18] to 400 m/s [22].

In short note [23], Askar'yan has pointed out two possible effects of *oscillating* surfaces on the electromagnetic field inside the (laser) resonator cavities. The first effect is the influence of oscillations on the generation and intensity of the laser radiation. It was extensively studied in many experiments, devoted, in particular, to such problems as the generation of optical pulses [24,25], phase locking of laser modes (where the frequencies of the mirror oscillations varied from 50 Hz [26] to 500 kHz [27,28] and 1 MHz [29,30] (see the review in Ref. 31), or modulation of the laser radiation [32,33] (in Ref. 33 the frequencies varied from 17 to 70 kHz). The theory of these phenomena was considered, for example in Refs. 34–36.

The second effect predicted by Askar'yan was the *field amplification* inside the cavity under the parametric resonance condition, when the mirror oscillates at twice the field eigenfrequency. It has not been observed yet, as far as we know, and the main part of the present review is devoted only to the progress in the theoretical treatment of this phenomenon achieved so far.

In 1967, Grinberg [37] proposed a general method of solving the wave equation in the case of an arbitrary law of motion of the boundary, based on expanding the solution over the complete set of "instantaneous modes." Krasil'nikov [38] seems to be the first to give a rather detailed study of the electromagnetic vibrations in a *spherical* cavity with an *oscillating boundary.* The one-dimensional cavity with a *resonantly oscillating* boundary was considered with the aid of the method of characteristics in a 1968 study [39], where it was shown that the energy is "pumped" to the high-frequency modes at the expense of the lower-frequency ones.

A significant contribution was made in a series of papers by Vesnitskii and co-authors. In 1969 [40] he gave an exact solution for the problem of a rectangular waveguide with a uniformly moving lateral wall, specifically, for the equation and the boundary conditions

$$A_{xx} + A_{zz} - A_{tt} = 0, \qquad A|_{x=0} = A|_{x=L(t)} = 0 \tag{5}$$

with $L(t) = L_0(1 + \alpha t)$ (in this case, A is the E_y component of the field of the type H_{n0}). A spherical resonator, whose radius linearly changed with time, was considered in 1971 [41]. A general (although implicit, in some sense) solution of the one-dimensional problem with an arbitrary law of motion of the boundary was given in the same year [42], showing that a complete set of solutions to the problem (1)–(2) can be expressed through the solution of some simple func-

tional equation [see equation (7) in the next subsection]. The solutions of the *inhomogeneous* one-dimensional wave equation for the law of motion $L(t) = L_0(1 + \alpha t)^{\pm 1}$, with an arbitrary inhomogeneity and arbitrary initial conditions, were also given in 1971 [43]. A family of concrete laws of motion admitting simple explicit expressions for the mode functions was found in the framework of the *inverse problem* in Ref. 44. The two-dimensional rectangular membrane with a single uniformly moving boundary was considered 6 years later [45]. The possibility of frequency modulation in the waveguide with a slowly oscillating boundary was also studied [46]. The results obtained by Vesnitskii and co-authors were reviewed in a later publication [47].

Exact solutions for the waveguide with *nonuniformly* moving boundary (problem (5)) have been found by Barsukov and Grigoryan [48,49]. They also considered the electromagnetic resonator with a moving boundary [50]. Similar problems were studied later [51,52]. Periodic solutions of a one-dimensional wave equation with homogeneous conditions on moving boundaries were also considered [53]. Transition processes in one-dimensional systems with moving boundaries were studied in 1982 [54]. Oscillations of a round membrane with a uniformly varying radius were considered later [55]. A nonlinear transformation was applied to solve the inhomogeneous problem of the forced resonance oscillations in a one-dimensional cavity with moving boundaries [56]. The scaling transformation method, which reduces the problem with moving boundaries to that with fixed ones by means of the transformations such as $x \to x/L(t)$, was also considered in [57,58].

In the 1990s, the problem of a vibrating string with moving boundaries was studied in [59] (two supports moving toward each other with constant velocities) and in [60–64] (oscillating supports). The electromagnetic (better to say, massless scalar) field in one-dimensional ideal cavities with periodically moving boundaries were also considered in [65–69]. Analytical solutions for the field in circular waveguides with (linearly) moving boundaries were obtained more recently [70,71]. The "dynamical" field modes in the one-dimensional and spherical cavities with uniformly moving boundaries were found once more time, in 1998 [72]. The same problem for the expanding/contracting ideal spherical cavity, whose radius varies as $R(t) = R_0\sqrt{1 + \alpha t}$, was solved in 2000 [73]. [A family of the laws of motion of the boundary, which includes, in particular, the dependences such as $R(t) = R_0\sqrt{1 + \alpha t + \beta t^2}$, $R(t) = Dt + E + F(At + B)^{-1}$, and their combinations, was considered in the case of the *diffusion-type* equations [74,75], showing that this family admits *exact* solutions of the problem.]

B. Quantum Fields in the Presence of Moving Boundaries

Moore's paper [76] seems to be the first one devoted to the problem of *quantum fields* in cavities mith moving boundaries. It was motivated by the studies of a

more general problem of the particle (in particular, photon) creation in the nonstationary universe [77] and in external intense fields (see, e.g., two books [78,79] and a review [80]), which is closely related to the problem of field quantization in the spaces with nontrivial (e.g., time-dependent) geometry. Considering a model of the "scalar electrodynamics" (when the field depends on a single space coordinate), Moore has found a complete set of solutions to the problem (1)–(2) in the form

$$A_n(x,t) = C_n\{\exp[-i\pi n R(t-x)] - \exp[-i\pi n R(t+x)]\} \tag{6}$$

where function $R(\xi)$ must satisfy the functional equation

$$R(t+L(t)) - R(t-L(t)) = 2 \tag{7}$$

In fact, a quite similar approach was used [6–8] for a *linear* function $L(t)$. Independently, equation (7) was obtained by Vesnitskii [42]. Moore's approach was developed later [78,81,82]. However, the most efforts were applied to the case of a *single* mirror (not necessarily plane) moving with a *relativistic* velocity or with a great acceleration, when the effect of particle production becomes significant [83–100].

The case of two or more boundaries, one of which moves with a *constant relativistic* velocity, was analyzed [101–104] (the case of constant relative acceleration was also considered [105]). For the uniform law of motion of the boundary (3) the solution to Eq. (7), found by many authors cited above, reads (remember that we assume $c = 1$)

$$R_\alpha(\xi) = \frac{2\ln|1+\alpha\xi|}{\ln|(1+v)/(1-v)|}, \quad v = \alpha L_0 \tag{8}$$

Evidently, if $\alpha \to 0$, this function goes to $R_0(\xi) = \xi/L_0$. For an arbitrary non-relativistic law of motion, one can find the solution in the form of the expansion over subsequent time derivatives of the wall displacement. We give it in the form obtained in a 1992 study [106]:

$$R(\xi) = \xi\lambda(\xi) - \frac{1}{2}\xi^2\dot{\lambda}(\xi) + \frac{1}{6}\xi\ddot{\lambda}(\xi)\left[\xi^2 - L^2(\xi)\right] + \cdots, \quad \lambda(\xi) \equiv L^{-1}(\xi) \tag{9}$$

In the special case $L(t) = L_0/(1+\alpha t)$, when $\ddot{\lambda}(\xi) \equiv 0$, Eq. (9) yields another exact solution, $R(\xi) = L_0^{-1}(\xi + \frac{1}{2}\alpha\xi^2)$. Unfortunately, the expansions such as (9) cannot be used in the long-time limit $\xi \to \infty$, since the terms proportional to the derivatives of $\lambda(\xi)$ (which are supposed to be small corrections) become bigger than the unperturbed term $\xi\lambda(\xi)$.

Castagnino and Ferraro [93] have found several solutions of the Moore equation (7) with the aid of the inverse method, which was used earlier by Vesnitskii [44]. In this method, one chooses some reasonable function $R(\xi)$ and determines the corresponding law of motion of the boundary $L(t)$ using the consequence of Eq. (7):

$$\dot{L}(t) = \frac{R'[t - L(t)] - R'[t + L(t)]}{R'[t - L(t)] + R'[t + L(t)]} \tag{10}$$

To solve a differential equation (10) with some simple functions, using $R(\xi)$ is easier (as this can be done numerically) than solving the functional equation (7) for the given function $L(t)$. However, for many simple functions $R(\xi)$, the dependence $L(t)$ appears inadmissible from the point of view of physics (the velocity may occur greater than the speed of light, or some discontinuities may arise). Actually, the cases considered in Ref. 93 correspond to some monotonous displacements of the mirror from the initial to final positions. Typical functions $R(\xi)$ used in that work [93] were some combinations of ξ/L_0 and some trigonometric functions such as $\sin(m\pi\xi/L_0)$. A long list of simple functions $R(\xi)$ (rational, exponential, logarithmic, hyperbolic, trigonometrical, and inverse trigonometrical) and their corresponding functions $L(t)$ was given in Ref. 47. However, no one of these functions can be used in the parametric resonance case. The *asymptotical* solution of the Moore equation in the parametric resonance case $L(t) = L_0[1 + \epsilon \sin(\pi q t/L_0)]$, $q = 1, 2, \ldots,$ was found in other studies [107–110]. For $\epsilon t \gg 1$ it has the form (here $L_0 = 1$)

$$R(t) = t - \frac{2}{\pi q} \operatorname{Im}\{\ln[1 + \zeta + \exp(i\pi q t)(1 - \zeta)]\} \tag{11}$$
$$\zeta = \exp[(-1)^{q+1}\pi q \epsilon t]$$

which clearly demonstrates that the asymptotical mode structure in the resonance case is quite different from the mode structure inside the cavity with unmoving walls. The solution (11) was improved and generalized to the case of *two* vibrating boundaries [111,112]. However, the form of this solution is not very convenient for the calculation of various sums giving the mean numbers of photons, energy, and so on, so a lot of rather sophisticated calculations must be done before the final physical results could be obtained.

One of the first estimations of the number of photons that could be created from *vacuum* in a cavity whose boundary moves with *nonrelativistic* velocity have been performed by Rivlin [113], who considered the parametric amplification of the initial vacuum field oscillations in the framework of the classical approach. He estimated the number of created photons $\mathcal{N} \sim (\epsilon\omega_1 t)^2$, where $\epsilon \sim \delta L/L$ is the relative amplitude of the variation of the distance between the

walls and ω_1 is the fundamental unperturbed field eigenfrequency (provided the frequency of the wall vibrations ω_w is close to $2\omega_1$). A similar estimation was given by Sarkar [114], who used an approximate solution to the Moore equation (7) in the form of the asymptotic series with respect to a small parameter ϵ [115] (such solutions were constructed earlier [17,42]). However, the tremendous numerical values obtained by Sarkar were quite unrealistic, since he used the value of ϵ, which was many orders of magnitude higher than those that can be achieved in the laboratory under real conditions. Moreover, the oversimplified approach of Rivlin and simple perturbative solutions of Sarkar are not valid, in fact, under the resonance conditions, due to the presence of the secular terms (as it always happens for parametric systems). Actually, the structure of the "dynamical" modes in the resonance case is completely different (in the most interesting long-time limit) from the simple standing waves existing in the cavity with unmoving walls. The same is true for the estimation by Askar'yan [23] in the classical case. He evaluated the average work done by the moving wall on the field as $A \sim \overline{\int pv\,dt}$, where $v = v_0 \sin(\omega_w t + \phi)$ is the wall velocity and $p(t)$ is the radiation pressure. Taking the monochromatic dependence $p(t) = p_0 \sin^2(2\omega_1 t)$, he obtained the *linear* dependence on time in the resonance case $\omega_w = 2\omega_1$: $A \sim p_0 v_0 t \sin\phi + \text{const}$. However, these evaluations can serve only as some indication that in the resonance case the energy of the field can grow at the expense of the mechanical work done by the vibrating wall. The real-time dependence can be quite different, since the law $p(t) = p_0 \sin^2(2\omega_1 t)$ holds, in fact, only until $\epsilon\omega_1 t \ll 1$, whereas for larger times the effect of the mode reconstruction must be taken into account. One of the goals of this review is to demonstrate what happens in reality in the resonance case.

Approximate solutions to the Moore equation, such as (9), were used [116] to evaluate corrections to the famous Casimir attractive force between infinite ideal walls [117] (for the reviews on the Casimir effect see, e.g., Ref. 118–121) due to the *nonrelativistic* motion of the walls. The leading term of these corrections turned out to be proportional to the *square of velocity* of the boundary (i.e., of the order of $(v/c)^2$). The Casimir force in the relativistic case was also calculated in [76,78,81,90,91,93,101,103]; it depends in the generic case not only on the instantaneous velocity but also on the whole time dependence $L(t)$ [through the function $R(\xi)$, i.e., on the acceleration and other time derivatives]. The first calculations of the forces acting on the single mirrors moving with *nonrelativistic* velocities due to the vacuum or thermal fluctuations of the field were performed in the framework of the spectral approach (using the fluctuation–dissipation theorem) in Ref. 122 (three-dimensional case, the force proportional to the fifth-order derivative of the coordinate) and in Ref. 123 (one-dimensional model, the force proportional to the third-order derivative of the coordinate). It was mentioned that the force could be significantly amplified under the resonance conditions, either in the *LC*

contour [122] or in the Fabry–Perot cavity [123] (such a possibility was discussed earlier [124]). These studies were later continued in [125–133], assuming that the velocity of the boundary is perpendicular to the surface. The Casimir force between two parallel plates, when their relative velocity is also parallel to the surfaces, was considered by Levitov [134]. Later, the theory of "Casimir friction" was developed [135–139]. Reviews of these approaches can be found in Refs. 140 and 141.

Various quantum effects arising due to the motion of *dielectric boundaries*, including the modification of the Casimir force and creation of photons, in both one and three dimensions, and for different orientations of the velocity vector with respect to the surface, have been studied in detail in the series of papers by Barton and his collaborators [142–148]. In one paper [142] the term *mirror-induced radiation* (MIR) was introduced.

Another term, *nonstationary Casimir effect* (NSCE), was introduced earlier [116] for the class of phenomena caused by the reconstruction of the quantum state of field due to a time dependence of the geometric configuration [149–152]. Its synonym is the term *dynamical Casimir effect*, which became popular after the series of articles by Schwinger [153–157] who tried to explain the phenomenon of *sonoluminescence* by the creation of photons in bubbles with time-dependent radii, oscillating under the action of acoustic pressure in the liquids (see a brief discussion of this subject in Section X).

A possibility of generating the "nonclassical" (in particular, *squeezed*) states of the electromagnetic field in the cavity with moving walls was pointed out in several studies in [106,114,124,158–161]. The dynamical Casimir force has been interpreted as a mechanical signature of the squeezing effect associated with the mirror's motion [123,125] (see also Ref. 162).

It has also been suggested [106,124,159,160] that a significant amount of photons could be created from vacuum even for quite small nonrelativistic velocities of the walls, provided the boundaries of a high-Q cavity perform small oscillations at a frequency proportional to some cavity unperturbed eigenfrequency, due to an accumulation of small changes in the state of the field for a long time. Indeed, using the asymptotical solutions of the Moore equation (11), it was shown [107–110] that the rate of photon generation in each mode becomes constant in the long-time limit, as it is linearly proportional to the product $\epsilon\omega_1$, and that the photons are generated in a wide frequency band whose width grows exponentially fast in time [163]. Other approximate or exact solutions of the Moore equation for the specific periodical time dependences of the cavity dimensions were found by different methods [111,112,164–168], which confirmed the effect of resonance generation of photons.

Moore's approach is based on the decomposition (6) of the field over the mode functions satisfying automatically the (one-dimensional) *wave equation* (1). There exists another approach (proposed in the framework of the classical

problem as far back as in 1967 [37]), when the mode functions are chosen in such a way that they satisfy automatically the time-dependent *boundary conditions* (2), see Eq. (17) (below). In this case it is possible to describe the behavior of the field with the aid of some *effective Hamiltonian*, which is an infinite-dimensional quadratic form of the boson creation/annihilation operators with time-dependent coefficients responsible for the coupling between different modes. Such an approach was considered for the first time (in the quantum case) by Razavy and Terning [169–171] (the case of massive field was also considered by Razavy [172]; see also Ref. 173). However, the resulting infinite set of coupled evolution equations for the annihilation and creation operators turned out to be rather complicated in the generic case. and for this reason they were treated only perturbatively [170]. Later, a similar method was used by Calucci [174], who confined, however, only with the case of adiabatically slow motion of the wall, when no photons could be created (this adiabatic case was studied in detail in 1998 [175]). Essential progress in the development of the Hamiltonian approach (we shall call it also the *instantaneous basis method* or IBM method) was achieved after the papers by Law [176,177], who has demonstrated that the effective Hamiltonian can be significantly simplified under the resonance conditions. Nonetheless, even the reduced coupled equations of motion resulting from the simplified Hamiltonians have been treated for some time either perturbatively (i.e., in the form of the Taylor expansion with respect to the time variable) or numerically (actually, also in the short-time limit corresponding to the initial stage of the process); see the studies for the 1D cavity model [176–181] and for a three-dimensional cavity and a waveguide [182]. The general structure of the effective infinite-dimensional quadratic Lagrangians and Hamiltonians arising in the canonical approach to the dynamical Casimir effect has been analyzed and classified [183–185]. The methods of diagonalization of such Hamiltonians were also considered [186,187].

The first *analytical* solutions describing the field inside the one-dimensional (1D) cavity with resonantly oscillating boundaries have been found in the simplest cases by Dodonov et al. [188–190]. More general solutions have also been obtained [191–193]. They hold for any moment of time (provided the amplitude of the wall vibrations is small enough; this limitation, however, is quite unessential under realistic conditions). Moreover, these solutions enable us not only to calculate the number of photons created from an arbitrary initial state (thus giving, e.g., the temperature corrections) but also to account for the effects of detuning from a strict resonance. Besides, they enable us to calculate the degree of *squeezing* in the field quadrature components, to find the photon distribution function and the energy density distribution inside the cavity, and so on. Therefore, one of the main purposes of this chapter is to give a detailed description of the analytical solutions found in the literature [188–193] and to discuss their physical consequences.

Another goal is to consider the simplest models of the *three-dimensional* cavity, following the scheme given for ideal boundaries [188,189] and for lossy cavities [194,195]. A more detailed study of the quantum properties of the electromagnetic field in rectangular 3D cavities, which takes into account the polarization of the field, was also performed [196,197], but only for the uniform motion of the walls. Periodic motion was considered in 1998 [198], also accounting for the polarization and the influence of all three dimensions, but in the framework of some approximations equivalent to the short-time limit. The case of a three-dimensional rectangular cavity divided in two parts by an ideal mirror, which suddenly disappears, was considered in 1999 [199].

The term *motion induced radiation* was applied to the effect of radiation emission outside the cavity with vibrating walls [200]. Using the spectral approach, Lambrecht et al. [200] showed that the radiation can be essentially enhanced under the resonance conditions (by the orders of magnitude, compared with the case of a single mirror). The problem of the photon generation by a single perfectly reflecting mirror performing a bounded nonrelativistic motion was studied by Maia Neto and others [201,202], who factored in the effects of polarization and found the spectral and angular distributions of the emitted photons. Arbitrary spacetime deformations of a single moving mirror have been treated [203,204] using the path integral approach. The same approach was used in the case of a cavity with deformable perfectly reflecting boundaries [205].

The creation of photons or specific (e.g., squeezed) states of the electromagnetic field due to the motion of some effective mirrors made of the free electrons moving with (ultra)relativistic velocities was studied [206–207]. Another kind of "effective moving mirror" consisting of the electron–hole plasma generated in semiconductors under the action of powerful laser pulses was also suggested [208,209].

The influence of temperature on the dynamical Casimir effect has been evaluated [110,210]; a more detailed analysis was given in the framework of the Hamiltonian approach [211], using the thermofield dynamics [212], and especially by Dodonov and Andreata [192,193]. The energy density distribution inside the cavity under the resonance conditions is no longer uniform; on the contrary, the main part of the energy is concentrated in several sharp peaks that move from one boundary to another, becoming narrower with time. This effect was studied in the framework of numerical calculations [112,164–166,168] (earlier, it was discussed for the classical field [44]). The analytical form of the pulses, including their "fine structure" in the case of initial states different from the vacuum or thermal ones, was also found [193]. A similar pulse structure of radiation emitted from the high-finesse vibrating cavity with partially transparent mirrors has been studied [210,213].

The evolution of *classical* fields in the cavities filled in with media whose dielectric properties vary in time was considered, for example, as far back as in

1966 [214]. Yablonovitch [215] proposed using a medium with a rapidly decreasing in time refractive index (''plasma window'') to simulate the so-called *Unruh effect* [216]: the creation of quanta in an accelerated frame of reference. More rigorous and detailed studies of quantum phenomena in nonstationary (deformed) media have been performed [159,160,217–229]. The case when the dielectric constant changes simultaneously with the distance between mirrors (in one dimension) was also considered [230,231]. Johnston and Sarkar compared the spectra of photons created by the motion of mirrors and by the time variations of the dielectric permeability [232]. An analog of the nonstationary Casimir effect in the superfluid ^{3}He, namely, the friction force on the moving interface between two different phases, was discussed by Volovik [233].

The problem of the interaction between the electromagnetic field created due to the NSCE and various detectors (harmonic oscillators, two-level systems, Rydberg atoms, etc.) placed inside the cavity with moving walls was studied by different methods [188,189,234–238]. It is also discussed in this chapter.

The first experiments on the interaction between the powerful laser radiation and freely suspended light mirrors were reported in two studies in the early 1980s [239,240], where the effect of the optical bistability, similar to that usually observed in the so-called Kerr media, was observed. The first theoretical study of this phenomenon in the cavities whose walls can move under the action of the radiation pressure force appeared in 1985 [241]. This subject has received much attention since 1991 or so in connection with different problems, such as the attenuation or elimination of noise in interferometers [242–253]. This is important, in particular, for the gravitational wave detectors and for the general problem of measuring weak forces acting on a quantum system (see, e.g., Refs. 254 and 255 for more details). Another possible application could be the generation of the so-called ''nonclassical states'' of the field and the mirror itself (when it is also considered as a quantum object) [253,256–258]. The stability of such states, in turn, is closely related to the general problem of *decoherence* in quantum mechanics, and one of the mechanisms that can destroy the coherence of pure quantum superpositions is just the dynamical Casimir effect [259,260]. The backreaction of the dynamical Casimir effect was studied more recently [261]. The influence of fluctuations of the positions of the walls on the field inside the cavity was considered [115,205,262], as was the Brownian motion of the walls due to the field fluctuations [140,263]. The role of the dynamical Casimir effect in the cosmological problems was also studied [264,265].

III. ONE-DIMENSIONAL CAVITY WITH OSCILLATING BOUNDARIES

Let us start with the case of a single-space dimension. Consider a cavity formed by two infinite ideal plates moving in accordance with the prescribed laws

$$x_{\text{left}}(t) = u(t), \quad x_{\text{right}}(t) = u(t) + L(t)$$

where $L(t) > 0$ is the time-dependent length of the cavity. Taking into account only the electromagnetic modes whose vector potential is directed along z axis ("scalar electrodynamics" [76]), one can write down the field operator *in the Heisenberg representation* $\hat{A}(x,t)$ at $t < 0$ (when both the plates were at rest at the positions $x_{\text{left}} = 0$ and $x_{\text{right}} = L_0$) as (we assume $c = \hbar = 1$)

$$\hat{A}_{\text{in}} = 2\sum_{n=1}^{\infty} \frac{1}{\sqrt{n}} \sin \frac{n\pi x}{L_0} \hat{b}_n \exp(-i\omega_n t) + \text{H.c.} \tag{12}$$

where $\hat{b}_n$ means the usual annihilation photon operator and $\omega_n = \pi n/L_0$ (H.c. denotes Hermitian conjugation). The choice of coefficients in Eq. (12) corresponds to the standard form of the field Hamiltonian

$$\hat{H} \equiv \frac{1}{8\pi} \int_0^{L_0} dx \left[\left(\frac{\partial A}{\partial t} \right)^2 + \left(\frac{\partial A}{\partial x} \right)^2 \right] = \sum_{n=1}^{\infty} \omega_n \left(\hat{b}_n^\dagger \hat{b}_n + \frac{1}{2} \right) \tag{13}$$

For $t > 0$ the field operator can be written as

$$\hat{A}(x,t) = 2\sum_{n=1}^{\infty} \frac{1}{\sqrt{n}} [\hat{b}_n \psi^{(n)}(x,t) \ + \ \text{H.c.}] \tag{14}$$

To find the explicit form of functions $\psi^{(n)}(x,t)$, $n = 1, 2, \ldots$, one should take into account that the field operator must satisfy the wave equation (1), the boundary conditions (2) or their generalization

$$A(u(t),t) = A(u(t) + L(t), t) = 0 \tag{15}$$

and the initial condition (12), which is equivalent to

$$\psi^{(n)}(x, t < 0) = \sin \frac{n\pi x}{L_0} \exp(-i\omega_n t) \tag{16}$$

Following the approach in other studies [37,170,174,176,191], we expand the function $\psi^{(n)}(x,t)$ in a series with respect to the *instantaneous basis*:

$$\psi^{(n)}(x, t > 0) = \sum_{k=1}^{\infty} Q_k^{(n)}(t) \sqrt{\frac{L_0}{L(t)}} \sin \left(\frac{\pi k[x - u(t)]}{L(t)} \right), \quad n = 1, 2, \ldots \tag{17}$$

with the initial conditions

$$Q_k^{(n)}(0) = \delta_{kn}, \quad \dot{Q}_k^{(n)}(0) = -i\omega_n \delta_{kn}, \quad k, n = 1, 2, \ldots$$

In this way we satisfy automatically both the boundary conditions (15) and the initial condition (16). Putting expression (17) into the wave equation (1), we can arrive after some algebra at an infinite set of coupled differential equations [180,184,191]

$$\ddot{Q}_k^{(n)} + \omega_k^2(t)Q_k^{(n)} = 2\sum_{j=1}^{\infty} g_{kj}(t)\dot{Q}_j^{(n)} + \sum_{j=1}^{\infty} \dot{g}_{kj}(t)Q_j^{(n)} + \mathcal{O}(g_{kj}^2) \tag{18}$$

where $\omega_k(t) = k\pi/L(t)$, and the time-dependent antisymmetric coefficients $g_{kj}(t)$ read (for $j \neq k$)

$$g_{kj} = -g_{jk} = (-1)^{k-j}\frac{2kj(\dot{L} + \dot{u}\epsilon_{kj})}{(j^2 - k^2)L(t)}, \quad \epsilon_{kj} = 1 - (-1)^{k-j} \tag{19}$$

For $u = 0$ (with the left wall at rest), equations such as (18) and (19) have been derived in [174,177].

If the wall comes back to its initial position L_0 after some time interval T, then the right-hand side (r.h.s.) of Eq. (18) disappears, so at $t > T$ one can write

$$Q_k^{(n)}(t) = \xi_k^{(n)} e^{-i\omega_k(t+\delta T)} + \eta_k^{(n)} e^{i\omega_k(t+\delta T)}, \quad k, n = 1, 2, \ldots \tag{20}$$

where $\xi_k^{(n)}$ and $\eta_k^{(n)}$ are some constant complex coefficients. Consequently, at $t > T$ the initial annihilation operators $\hat{b}_n$ cease to be "physical," because of the contribution of the terms with "incorrect signs" in the exponentials $\exp(i\omega_k t)$. Introducing a new set of "physical" operators $\hat{a}_m$ and $\hat{a}_m^\dagger$, which give the decomposition of the vector potential operator at $t > T$ in the form analogous to (12)

$$\hat{A}(x,t) = \sum_{n=1}^{\infty} \frac{2}{\sqrt{n}} \sin\left(\frac{\pi n x}{L_0}\right)[\hat{a}_n e^{-i\omega_n(t+\delta T)} + \text{H.c.}] \tag{21}$$

one can easily check that the two sets of operators are related by means of the Bogoliubov transformation

$$\hat{a}_m = \sum_{n=1}^{\infty} (\hat{b}_n \alpha_{nm} + \hat{b}_n^\dagger \beta_{nm}^*), \quad m = 1, 2, \ldots \tag{22}$$

with the coefficients

$$\alpha_{nm} = \sqrt{\frac{m}{n}}\,\xi_m^{(n)}, \quad \beta_{nm} = \sqrt{\frac{m}{n}}\,\eta_m^{(n)} \tag{23}$$

The unitarity of the transformation (22) implies the following constraints:

$$\sum_{m=1}^{\infty}(\alpha_{nm}^{*}\alpha_{km}-\beta_{nm}^{*}\beta_{km})=\sum_{m=1}^{\infty}\frac{m}{n}(\xi_{m}^{(n)*}\xi_{m}^{(k)}-\eta_{m}^{(n)*}\eta_{m}^{(k)})=\delta_{nk} \tag{24}$$

$$\sum_{n=1}^{\infty}(\alpha_{nm}^{*}\alpha_{nj}-\beta_{nm}^{*}\beta_{nj})=\sum_{n=1}^{\infty}\frac{m}{n}(\xi_{m}^{(n)*}\xi_{j}^{(n)}-\eta_{m}^{(n)*}\eta_{j}^{(n)})=\delta_{mj} \tag{25}$$

$$\sum_{n=1}^{\infty}(\beta_{nm}^{*}\alpha_{nk}-\beta_{nk}^{*}\alpha_{nm})=\sum_{n=1}^{\infty}\frac{1}{n}(\eta_{m}^{(n)*}\xi_{k}^{(n)}-\eta_{k}^{(n)*}\xi_{m}^{(n)})=0 \tag{26}$$

The mean number of photons in the mth mode equals the average value of the operator $\hat{a}_m^\dagger\hat{a}_m$ in the initial state $|\mathrm{in}\rangle$ (remember that we use the Heisenberg picture), since just this operator has a physical meaning at $t > T$:

$$\begin{aligned}\mathcal{N}_m &\equiv \langle\mathrm{in}|\hat{a}_m^\dagger\hat{a}_m|\mathrm{in}\rangle\\ &=\sum_{n}|\beta_{nm}|^2+\sum_{n,k}\left[\left(\alpha_{nm}^{*}\alpha_{km}+\beta_{nm}^{*}\beta_{km}\right)\langle\hat{b}_n^\dagger\hat{b}_k\rangle+2\mathrm{Re}\left(\beta_{nm}\alpha_{km}\langle\hat{b}_n\hat{b}_k\rangle\right)\right]\\ &=\sum_{n=1}^{\infty}\frac{m}{n}|\eta_m^{(n)}|^2+\sum_{n,k=1}^{\infty}\frac{m}{\sqrt{nk}}(\xi_m^{(n)*}\xi_m^{(k)}+\eta_m^{(n)*}\eta_m^{(k)})\langle\hat{b}_n^\dagger\hat{b}_k\rangle\\ &\quad+2\mathrm{Re}\sum_{n,k=1}^{\infty}\frac{m}{\sqrt{nk}}\eta_m^{(n)}\xi_m^{(k)}\langle\hat{b}_n\hat{b}_k\rangle\end{aligned} \tag{27}$$

The first sum in the right-hand sides of each relationship above describes the effect of the photon creation from vacuum due to the NSCE, while the other sums are different from zero only in the case of a nonvacuum initial state of the field.

To find the coefficients $\xi_k^{(n)}$ and $\eta_k^{(n)}$, one has to solve an infinite set of coupled equations (18) ($k = 1, 2, \ldots$) with time-dependent coefficients; moreover, each equation also contains an infinite number of terms. However, the problem can be essentially simplified, if the walls perform small oscillations at the frequency ω_w close to some unperturbed field eigenfrequency:

$$L(t)=L_0(1+\varepsilon_L\sin[p\omega_1(1+\delta)t]),\quad u(t)=\varepsilon_u L_0\sin[p\omega_1(1+\delta)t+\varphi].$$

Assuming $|\varepsilon_L|, |\varepsilon_u| \sim \varepsilon \ll 1$, it is natural to look for the solutions of equation (18) in the form similar to (20)

$$Q_k^{(n)}(t)=\xi_k^{(n)}e^{-i\omega_k(1+\delta)t}+\eta_k^{(n)}e^{i\omega_k(1+\delta)t} \tag{28}$$

but now we allow the coefficients $\xi_k^{(n)}$ and $\eta_k^{(n)}$ to be *slowly varying functions of time*. The further procedure is well known in the theory of parametrically excited systems [266–268]. First we put expression (28) into equation (18) and neglect the terms $\ddot{\xi}, \ddot{\eta}$ (keeping in mind that $\dot{\xi}, \dot{\eta} \sim \varepsilon$, while $\ddot{\xi}, \ddot{\eta} \sim \varepsilon^2$), as well as the terms proportional to $\dot{L}^2 \sim \dot{u}^2 \sim \varepsilon^2$. Multiplying the resulting equation for Q_k by the factors $\exp[i\omega_k(1+\delta)t]$ and $\exp[-i\omega_k(1+\delta)t]$ and performing averaging over fast oscillations with the frequencies proportional to ω_k (since the functions ξ, η practically do not change their values at the time scale of $2\pi/\omega_k$), one can verify that only the terms with the difference $j-k=\pm p$ survive in the right-hand side. Consequently, for *even* values of p the term $\dot{u}$ in $g_{kj}(t)$ does not make any contribution to the simplified equations of motion; thus only the rate of change of the cavity length $\dot{L}/L_0$ is important in this case. On the contrary, if p is an *odd* number, then the field evolution depends on the velocity of the *center of the cavity* $v_c = \dot{u} + \dot{L}/2$ and does not depend on $\dot{L}$ alone. These *interference effects* were discussed for the short-time limit $\varepsilon\omega_1 t \ll 1$ in Ref. 180 (see also Ref. 200). We assume hereafter that $u=0$ (i.e., that the left wall is at rest), since this assumption does not change anything if p is an even number, whereas one should simply replace $\dot{L}/L_0$ by $2v_c/L_0$ if p is an odd number.

The final equations for the coefficients $\xi_k^{(n)}$ and $\eta_k^{(n)}$ contain only three terms with simple *time-independent* coefficients in the right-hand sides:

$$\frac{d}{d\tau}\xi_k^{(n)} = (-1)^p[(k+p)\xi_{k+p}^{(n)} - (k-p)\xi_{k-p}^{(n)}] + 2i\gamma k\xi_k^{(n)} \tag{29}$$

$$\frac{d}{d\tau}\eta_k^{(n)} = (-1)^p[(k+p)\eta_{k+p}^{(n)} - (k-p)\eta_{k-p}^{(n)}] - 2i\gamma k\eta_k^{(n)} \tag{30}$$

The dimensionless parameters τ (a "slow" time) and γ read ($\varepsilon \equiv \varepsilon_L$)

$$\tau = \frac{1}{2}\varepsilon\omega_1 t, \quad \gamma = \frac{\delta}{\varepsilon} \tag{31}$$

The initial conditions are

$$\xi_k^{(n)}(0) = \delta_{kn}, \quad \eta_k^{(n)}(0) = 0 \tag{32}$$

Note, however, that uncoupled equations (29) and (30) hold only for $k \geq p$. This means that they describe the evolution of *all* the Bogoliubov coefficients only if $p=1$. Then *all* the functions $\eta_k^{(n)}(t)$ are *identically equal to zero* because of the initial conditions (32); consequently, no photon can be created from vacuum. Moreover, in the next section we show that the total number of photons (but not the total energy) is an integral of motion in this specific case.

IV. "SEMIRESONANCE" CASE ($p = 1$)

If $p = 1$, one has to solve the set of equations ($k, n = 1, 2, \ldots$)

$$\frac{d}{d\tau}\xi_k^{(n)} = (k-1)\xi_{k-1}^{(n)} - (k+1)\xi_{k+1}^{(n)} + 2i\gamma k\xi_k^{(n)} \tag{33}$$

An immediate consequence of these equations and the condition $\xi_k^{(n)}(0) = \delta_{kn}$ is the identity

$$\sum_m m\xi_m^{(n)}(\tau)\xi_m^{(k)*}(\tau) \equiv n\delta_{nk} \tag{34}$$

which is simply the unitarity condition of the Bogoliubov transformation in this special case. Taking into account this identity, one can easily verify that the total average number of photons in all modes is conserved in time:

$$\mathscr{N} = \sum_{nkm}\frac{m}{\sqrt{nk}}\xi_m^{(n)*}\xi_m^{(k)}\langle \text{in}|\hat{b}_n^\dagger\hat{b}_k|\text{in}\rangle = \sum_n\langle \text{in}|\hat{b}_n^\dagger\hat{b}_n|\text{in}\rangle \tag{35}$$

A similar phenomenon in the classical case was discussed in Ref. 44, whereas the quantum case was considered in Ref. 176 and especially in Ref. 190. Also, using Eqs. (33) and (34), one can verify that the total energy (normalized by ω_1)

$$\mathscr{E} = \sum_{nkm}\frac{m^2}{\sqrt{nk}}\xi_m^{(n)*}\xi_m^{(k)}\langle \text{in}|\hat{b}_n^\dagger\hat{b}_k|\text{in}\rangle$$

satisfies the simple equation (hereafter overdots mean the differentiation with respect to the dimensionless time τ)

$$\ddot{\mathscr{E}} = 4a^2\mathscr{E} + 4\gamma^2\mathscr{E}(0) - 2\gamma\,\text{Im}(\mathscr{G}_1) \tag{36}$$

where

$$a = \sqrt{1-\gamma^2} \tag{37}$$

$$\mathscr{G}_1 = 2\sum_{n=1}^{\infty}\sqrt{n(n+1)}\langle\hat{b}_n^\dagger\hat{b}_{n+1}\rangle \tag{38}$$

The quantum averaging is performed over the initial state of the field (no matter pure or mixed). The initial values of the total energy and its first derivative (with respect to τ) are given by

$$\mathscr{E}(0) = \sum_{n=1}^{\infty} n\langle\hat{b}_n^\dagger\hat{b}_n\rangle, \quad \dot{\mathscr{E}}(0) = \text{Re}(\mathscr{G}_1) \tag{39}$$

Consequently, the solution to equation (36) can be expressed as

$$\mathscr{E}(\tau) = \mathscr{E}(0) + \frac{2\sinh^2(a\tau)}{a^2}\left[\mathscr{E}(0) - \frac{\gamma}{2}\,\mathrm{Im}(\mathscr{G}_1)\right] + \mathrm{Re}(\mathscr{G}_1)\frac{\sinh(2a\tau)}{2a} \tag{40}$$

One can easily prove that $|\dot{\mathscr{E}}(0)| \le \mathscr{E}(0)$. Thus the total energy grows exponentially when $\tau \gg 1$ (provided $\gamma < 1$), although it can decrease at $\tau \ll 1$, if $\dot{\mathscr{E}}(0) < 0$. Since the total number of photons is constant, such behavior is explained by the effect of pumping the highest modes at the expense of the lowest ones (this effect was also noticed in the classical case [39]).

We see that the total energy can be found without any knowledge of the Bogoliubov coefficients. However, these coefficients are necessary, if one wants to know the distribution of the energy or the mean photon numbers over the modes. To solve the infinite set of equations (33), we introduce the *generating function*

$$X^{(n)}(z,\tau) = \sum_{k=1}^{\infty} \xi_k^{(n)}(\tau) z^k \tag{41}$$

where z is an auxiliary variable. Using the relation $kz^k = z(dz^k/dz)$ one obtains the first-order partial differential equation

$$\frac{\partial X^{(n)}}{\partial \tau} = (z^2 - 1 + 2i\gamma z)\frac{\partial X^{(n)}}{\partial z} + \xi_1^{(n)}(\tau) \tag{42}$$

whose solution satisfying the initial condition $X^{(n)}(0,z) = z^n$ reads as

$$X^{(n)}(z,\tau) = \left[\frac{zg(\tau) - S(\tau)}{g^*(\tau) - zS(\tau)}\right]^n + \int_0^\tau \xi_1^{(n)}(x)\,dx \tag{43}$$

where

$$S(\tau) = \frac{\sinh(a\tau)}{a}, \quad g(\tau) = \cosh(a\tau) + i\gamma S(\tau) \tag{44}$$

Differentiating (43) over z, we find

$$\xi_1^{(n)}(\tau) = \frac{n[-S(\tau)]^{n-1}}{[g^*(\tau)]^{n+1}} \tag{45}$$

Putting this expression into the integral in the right-hand side of equation (43) we arrive at the final form of the generating function

$$X^{(n)}(z,\tau) = \left[\frac{zg(\tau) - S(\tau)}{g^*(\tau) - zS(\tau)}\right]^n - \left[\frac{-S(\tau)}{g^*(\tau)}\right]^n \tag{46}$$

which satisfies automatically the necessary boundary condition $X^{(n)}(\tau, 0) = 0$. The right-hand side of (46) can be expanded into the power series of z with the aid of the formula [see Ref. 269, Vol. 3, Section 19.6, Eq. (16)]

$$(1-t)^{b-c}(1-t+xt)^{-b} = \sum_{m=0}^{\infty} \frac{t^m}{m!}(c)_m F(-m, b; c; x)$$

where $F(a, b; c; x)$ is the Gauss hypergeometric function, and $(c)_k \equiv \Gamma(c+k)/\Gamma(c)$. In turn, the function $(c)_m F(-m, b; c; x)$ with an integer m is reduced to the Jacobi polynomial in accordance with the formula [Ref. 269, Vol. 2, Section 10.8, Eq. (16)]

$$(c)_m F(-m, b; c; x) = m!(-1)^m P_m^{(b-m-c,\, c-1)}(2x-1)$$

Consequently

$$(1-t)^{b-c}(1-t+xt)^{-b} = \sum_{m=0}^{\infty} (-t)^m P_m^{(b-m-c,\, c-1)}(2x-1) \tag{47}$$

and the coefficient $\xi_m^{(n)}(\tau)$ reads

$$\xi_m^{(n)}(\tau) = (-\kappa)^{n-m}\lambda^{n+m} P_m^{(n-m,\, -1)}\left(1-2\kappa^2\right) \tag{48}$$

where

$$\kappa(\tau) = \frac{S}{\sqrt{gg^*}} \equiv \frac{S(\tau)}{\sqrt{1+S^2(\tau)}} \tag{49}$$

$$\lambda(\tau) = \sqrt{g(\tau)/g^*(\tau)} \equiv \sqrt{1-\gamma^2\kappa^2} + i\gamma\kappa, \quad |\lambda| = 1 \tag{50}$$

The form (48) is useful for $n \geq m$. To find a convenient formula in the case of $n \leq m$ we introduce the *two-dimensional* generating function

$$\begin{aligned} X(\tau, z, y) &= \sum_{m=1}^{\infty}\sum_{n=1}^{\infty} z^m y^n \xi_m^{(n)}(\tau) = \sum_{n=1}^{\infty} X^{(n)}(z, \tau) y^n \\ &= \frac{yz}{[g^*(\tau) + yS(\tau)][g^*(\tau) - g(\tau)yz + S(\tau)(y-z)]} \end{aligned} \tag{51}$$

The coefficient at z^m in (51) yields another one-dimensional generating function

$$X_m(\tau, y) = \sum_{n=1}^{\infty} y^n \xi_m^{(n)}(\tau) = y\frac{[g(\tau)y + S(\tau)]^{m-1}}{[g^*(\tau) + yS(\tau)]^{m+1}} \tag{52}$$

Then equation (47) results in the expression

$$\xi_m^{(n)} = (1-\kappa^2)\kappa^{m-n}\lambda^{n+m}P_{n-1}^{(m-n,\,1)}\left(1-2\kappa^2\right) \tag{53}$$

Note that the functions $S(\tau)$, $\cosh(a\tau)$, and $\kappa(\tau)$ are real for any value of γ. For $\gamma > 1$, it is convenient to use, instead of (44), the equivalent expressions in terms of the trigonometrical functions:

$$\tilde{S}(\tau) = \frac{\sin(\tilde{a}\tau)}{\tilde{a}}, \quad \tilde{g}(\tau) = \cos(\tilde{a}\tau) + i\gamma\tilde{S}(\tau), \quad \tilde{a} = \sqrt{\gamma^2-1} \tag{54}$$

In the special case $\gamma = 1$ one has $S(\tau) = \tau$ and $g(\tau) = 1 + i\tau$. In particular,

$$\xi_m^{(n)}(\tau;\gamma=1) = \frac{\tau^{m-n}(1+i\tau)^{n-1}}{(1-i\tau)^{m+1}}P_{n-1}^{(m-n,\,1)}\left(\frac{1-\tau^2}{1+\tau^2}\right) \tag{55}$$

The knowledge of the two-dimensional generating function enables to verify the unitarity condition (25). Consider the product $X^*(\tau, z_1, y_1)X(\tau, z_2, y_2)$, which is a four-variable generating function for the products $\xi_m^{(n)*}\xi_l^{(k)}$. Taking $y_1 = \sqrt{u}\exp(i\varphi)$, $y_2^* = \sqrt{u}\exp(-i\varphi)$ and integrating over φ from 0 to 2π, one obtains a three-variable generating function $\sum z_1^{*m}z_2^l u^n \xi_m^{(n)*}\xi_l^{(n)}$. Dividing it by u and integrating the ratio over u from 0 to 1, one finally arrives at the relation

$$\sum_{n,m,l=1}^{\infty} z_1^{*m}z_2^l\frac{1}{n}\xi_m^{(n)*}\xi_l^{(n)} = -\ln\left(1-z_1^*z_2\right) = \sum_{k=1}^{\infty}\frac{1}{k}\left(z_1^*z_2\right)^k \tag{56}$$

which is equivalent to the special case of (25) for $\eta_m^{(k)} \equiv 0$:

$$\sum_n \frac{1}{n}\xi_m^{(n)*}(\tau)\xi_j^{(n)}(\tau) \equiv \frac{1}{m}\delta_{mj} \tag{57}$$

A. Examples

Suppose that initially there was a single excited mode labeled with an index n. Because of the linearity of the process, one may assume that the mean number of photons in this mode was $\nu_n = 1$. Then the mean occupation number of the m-th mode at $\tau > 0$ equals

$$\mathcal{N}_m^{(n)} = \frac{m}{n}[\xi_m^{(n)}]^2 = \frac{m}{n}[(1-\kappa^2)\kappa^{m-n}P_{n-1}^{(m-n,\,1)}\left(1-2\kappa^2\right)]^2 \tag{58}$$

where κ is given by (49). For example, in the special case $\gamma = 0$ we have

$$\mathcal{N}_m^{(1)} = \frac{m(\tanh\tau)^{2m-2}}{(\cosh\tau)^4}$$
$$\mathcal{N}_m^{(2)} = \frac{m(\tanh\tau)^{2m-4}}{2(\cosh\tau)^4}[(m-1)-(m+1)\tanh^2\tau]^2$$

The maximum of function $\mathcal{N}_m^{(1)}(\tau)$ is achieved at $\sinh\tau_{\max} = \sqrt{(m-1)/2}$. For $m \gg 1$ it equals $\mathcal{N}_m^{(1)}(\tau_{\max}) \approx 4/(me^4)$. For a fixed value of $\tau \gg 1$, the occupation number distribution $\mathcal{N}_m^{(1)}$ reaches its maximum at $m^{(1)}_{\max\mathcal{N}} = \cosh^2\tau$, and $\mathcal{N}^{(1)}_{\max} = \left(e\cosh^2\tau\right)^{-1} \ll 1$. The maximum of the energy distribution is shifted to the right, $m^{(1)}_{\max\mathscr{E}} = 2\cosh^2\tau$, and its value is not decreased with time: $\mathscr{E}^{(1)}_{\max} = 4/e^2$. This explains the exponential growth of the total energy.

Although formula (58) seems asymmetric with respect to the indices m and n, actually the relation

$$\mathcal{N}_m^{(n)} = \mathcal{N}_n^{(m)} \tag{59}$$

holds. To prove it, we calculate the generating function

$$Q(u,v) \equiv \sum_{m,n=1}^{\infty} v^m u^n \mathcal{N}_m^{(n)} \tag{60}$$

It is related to the function $X(z,y)$ (51) as follows:

$$Q(u,v) = v\frac{d}{dv}\int_0^u dr \int_0^{2\pi}\int_0^{2\pi} \frac{d\varphi\, d\psi}{(2\pi)^2} X\left(\sqrt{r}e^{i\varphi}, \sqrt{v}e^{i\psi}\right) X^*\left(\sqrt{r}e^{i\varphi}, \sqrt{v}e^{i\psi}\right)$$

Having performed all the calculations, we arrive at the expression

$$2Q(u,v) = \frac{1+uv-\kappa^2(u+v)}{\{[1+uv-\kappa^2(u+v)]^2 - 4uv(1-\kappa^2)^2\}^{1/2}} - 1 \tag{61}$$

Then (59) is a consequence of the relation $Q(u,v) = Q(v,u)$.

The initial stage of the evolution of $\mathcal{N}_m^{(n)}(\tau)$ does not depend on the detuning parameter γ, since the principal term of the expansion of (58) with respect to τ yields

$$\mathcal{N}_{n\pm q}^{(n)}(\tau \to 0) = \frac{n \pm q}{n}\left[\frac{n(n\pm 1)\cdots(n\pm q\mp 1)}{q!}\right]^2 \tau^{2q}$$

However, the further evolution is sensitive to the value of γ. If $\gamma \leq 1$, then the function $\mathcal{N}_m^{(n)}(\tau)$ has many maxima and minima (especially for large values of m and n), but finally it decreases asymptotically as $mna^4/\cosh^4(a\tau)$. On the contrary, if $\gamma > 1$, then the function $\mathcal{N}_m^{(n)}(\tau)$ is periodic with the period $\pi/\tilde{a}$, and it turns into zero for $\tau = k\pi/\tilde{a}$, $k = 1, 2, \ldots$ (except in the case $m = n$). The magnitude of the coefficient $\mathcal{N}_m^{(n)}(\tau)$ decreases approximately as $\gamma^{-2|m-n|}$ for $\gamma \gg 1$.

Now let us assume for simplicity that $\gamma = 0$. Then Eq. (53) can be represented in the equivalent form:

$$\xi_m^{(n)} = n\frac{(\tanh\tau)^{m-n}}{\cosh^2\tau}(-1)^{n-1}F\left(1-n, m+1; 2; \frac{1}{\cosh^2\tau}\right) \tag{62}$$

If $m \gg n \sim \mathcal{O}(1)$, then $(m)_k \approx m^k$ $(k \leq n)$, so the Gauss hypergeometric function in Eq. (62) can be replaced by the confluent hypergeometric function with a negative integral first index, which is reduced to the associated Laguerre polynomial [269] $L_{n-1}^{(1)}(\mu)$ of the scaled variable $\mu = m/\cosh^2\tau$. Using the approximation $(\tanh\tau)^{2m} \approx \exp(-m/\cosh^2\tau)$ valid for $\tau \gg 1$, we arrive at a simplified expression

$$\mathcal{E}_m^{(n)} = m\mathcal{N}_m^{(n)} = \frac{1}{n}\mu^2 e^{-\mu}[L_{n-1}^{(1)}(\mu)]^2 \tag{63}$$

describing the energy distribution over the modes with large number m.

The fluctuations of the occupation numbers can be calculated with the aid of the formula (again for $\gamma = 0$)

$$\langle\hat{\mathcal{N}}^2\rangle_m(\tau) - \langle\hat{\mathcal{N}}\rangle_m(\tau) = \frac{m^2}{n^2}[\xi_m^{(n)}(\tau)]^4\left[\langle\hat{\mathcal{N}}^2\rangle_n(0) - \langle\hat{\mathcal{N}}\rangle_n(0)\right]$$

which is an immediate consequence of Eq. (57). Consequently, the type of the photon statistics (sub- or super-Poissonian) is conserved. In particular, if the initial mode was in a coherent state, then all other modes will be excited in the coherent states, too.

The assumption on the equidistant eigenmode spectrum can be justified to a certain extent for the longitudinal modes of a Fabry–Perot resonator with perfect mirrors, if the order of interference (the mode number) is high enough. So let us suppose that initially some single mode with $n \gg 1$ was excited. Although the lowest modes are not equidistant in this case, for a limited period of time in the beginning of the process [until $\tau \ll \log(2n)$], the evolution of the chosen mode and its neighbors can be described by the solutions obtained above, since the influence of the "remote" modes becomes essential at sufficiently large times. Then the populations of the modes exhibit strong oscillations, since they

are proportional to the squares of the Jacobi polynomials of large degrees. The asymptotics of these polynomials [see Ref. 269, Eq. 10.14(10)] yields

$$\mathcal{N}_m^{(n)} \approx \frac{2}{n\pi \sin(2\varphi)} \cos^2\left\{(m+n)\varphi - [2|m-n|+1]\frac{\pi}{4}\right\}, \qquad \sin\varphi = \tanh\tau$$

This formula holds provided that $n \gg |m-n| \sim \mathcal{O}(1)$ and $n\sin(2\varphi) \gg 1$. For $\tau \ll 1$ we observe fast oscillations, whose amplitude is modulated with the period π/τ, whereas for $\tau \gg 1$ we have slower periodic variations of $\mathcal{N}_m^{(n)}$ as the function of m with the period $\pi e^{\tau}/2$.

An interesting problem is the field evolution in a cavity that was initially in the equilibrium state at a finite temperature, when the initial occupation numbers were given by the Planck distribution $\nu_n = [\exp(\beta n) - 1]^{-1}$. Let us consider two limit cases. The first one corresponds to the low-temperature approximation $\nu_n = \exp(-\beta n)$. Then the occupation number of the mth mode is merely the coefficient at v^m in the expansion (61) with $u = \exp(-\beta)$. Using the well-known generating function of the Legendre polynomials $P_m(z)$ [Ref. 269, Eq. 10.10(39)], one can obtain the following expression (for $\gamma = 0$):

$$\mathcal{N}_m^{\{\beta\}} = \frac{1}{2}\left(\frac{e^{-\beta} - \rho^2}{1 - e^{-\beta}\rho^2}\right)^m [P_m(x) + P_{m-1}(x)], \quad \rho \equiv \tanh(\tau)$$

$$x = \frac{e^{-\beta}(1-\rho^2)^2 + \rho^2(1-e^{-\beta})^2}{(e^{-\beta} - \rho^2)(1 - e^{-\beta}\rho^2)}$$

In particular, $\mathcal{N}_1^{\{\beta\}} = e^{-\beta}(\cosh\tau)^{-4}(1 - e^{-\beta}\tanh^2\tau)^{-2}$.

In the special case of a cavity filled in with a *high-temperature thermal radiation*, the initial distribution over modes reads $\nu_n(\Theta) = \Theta/n$, where the constant Θ is proportional to the temperature. Then $\mathcal{N}_m^{\{\Theta\}} = \sum_n \nu_n(\Theta)\mathcal{N}_m^{(n)}$. This sum is simply Θ multiplied by the coefficient at v^m in the Taylor series expansion of the function

$$\tilde{Q}(v) = \int_0^1 \frac{du}{u} Q(u,v) = \ln\frac{1 - v\kappa^2(\tau)}{1 - v}$$

Thus we have

$$\mathcal{E}_m^{\{\Theta\}} = m\mathcal{N}_m^{\{\Theta\}} = \Theta(1 - [\kappa(\tau)]^{2m})$$

We see that the resonance vibrations of the wall cause an effective cooling of the lowest electromagnetic modes (provided $|\gamma| < 1$). The total number of quanta and the total energy in this example are formally infinite, due to the equipartition law of the classical statistical mechanics. In reality both these quantities are finite, since $\nu_n(\Theta) < \Theta/n$ at $n \to \infty$ because of the quantum corrections.

V. GENERIC RESONANCE CASE ($p \geq 2$)

If $p \geq 2$, we have $p-1$ pair of *coupled* equations for the coefficients with lower indices $1 \leq k \leq p-1$

$$\frac{d}{d\tau}\xi_k^{(n)} = (-1)^p[(k+p)\xi_{k+p}^{(n)} - (p-k)\eta_{p-k}^{(n)}] + 2i\gamma k\xi_k^{(n)} \tag{64}$$

$$\frac{d}{d\tau}\eta_k^{(n)} = (-1)^p[(k+p)\eta_{k+p}^{(n)} - (p-k)\xi_{p-k}^{(n)}] - 2i\gamma k\eta_k^{(n)} \tag{65}$$

In this case some functions $\eta_k^{(n)}(t)$ are not equal to zero at $t > 0$; thus we have the effect of photon creation from the vacuum.

It is convenient to introduce a new set of coefficients $\rho_k^{(n)}$, whose lower indices run over all integers from $-\infty$ to ∞:

$$\rho_k^{(n)} = \begin{cases} \xi_k^{(n)}, & k > 0 \\ 0, & k = 0 \\ -\eta_{-k}^{(n)}, & k < 0 \end{cases} \tag{66}$$

Then one can verify that equations (29)–(30) and (64)–(65) can be combined in a *single* set of equation ($k = \pm 1, \pm 2, \ldots$) [191]

$$\frac{d}{d\tau}\rho_k^{(n)} = (-1)^p[(k+p)\rho_{k+p}^{(n)} - (k-p)\rho_{k-p}^{(n)}] + 2i\gamma k\rho_k^{(n)} \tag{67}$$

with the initial conditions ($n = 1, 2, \ldots$)

$$\rho_k^{(n)}(0) = \delta_{kn} \tag{68}$$

A remarkable feature of the set of equations (67) is that its solutions satisfy *exactly* the unitarity conditions (24)–(26) (although the coefficients $\xi_k^{(n)}$ and $\eta_k^{(n)}$ introduced via equation (28) have additional phase factors in comparison with the coefficients defined in Eq. (20), these phases do not affect the identities concerned), which can be rewritten as

$$\sum_{m=-\infty}^{\infty} m\rho_m^{(n)*}\rho_m^{(k)} = n\delta_{nk}, \quad n, k = 1, 2, \ldots \tag{69}$$

$$\sum_{n=1}^{\infty} \frac{m}{n}[\rho_m^{(n)*}\rho_j^{(n)} - \rho_{-m}^{(n)*}\rho_{-j}^{(n)}] = \delta_{mj}, \quad m, j = 1, 2, \ldots \tag{70}$$

$$\sum_{n=1}^{\infty} \frac{1}{n}[\rho_m^{(n)*}\rho_{-j}^{(n)} - \rho_j^{(n)*}\rho_{-m}^{(n)}] = 0, \quad m, j = 1, 2, \ldots \tag{71}$$

For example, calculating the derivative $I = (d/d\tau)\sum_{m=-\infty}^{\infty} m\rho_m^{(n)*}\rho_m^{(k)}$ with the aid of Eq. (67) and its complex conjugated counterpart, one can easily verify that $I = 0$. Then the value of the right-hand side of (69) is a consequence of the initial conditions (68). The identities (70) and (71) can be verified in a similar way, if one uses instead of (67) the recurrence relations between the coefficients $\rho_m^{(n)}$ with the same lower index m but with different *upper* indices [see Eqs. (87) and (88)].

Because of the initial conditions (68), the solutions to (67) satisfy the relation

$$\rho_{j+mp}^{(k+np)} \equiv 0 \quad \text{if} \quad j \neq k \tag{72}$$

$$j, k = 0, 1, \ldots, p-1, \quad m = 0, \pm 1, \pm 2, \ldots, \quad n = 0, 1, 2, \ldots$$

Consequently, the nonzero coefficients $\rho_m^{(n)}$ form p independent subsets

$$y_k^{(q,j)} \equiv \rho_{j+kp}^{(j+qp)} \tag{73}$$

$$j = 0, 1, \ldots, p-1, \quad q = 0, 1, 2, \ldots, \quad k = 0, \pm 1, \pm 2, \ldots$$

The subset $y_k^{(q,0)}$ is distinguished, because $y_k^{(q,0)} \equiv 0$ for $k \leq 0$ and the upper index q begins at $q = 1$. One can verify that the functions $y_m^{(n,0)}(\tau)$ with $m \geq 1$ are given by the formulas for $\xi_m^{(n)}(\tau)$ found in the preceding section, provided one replaces τ by $(-1)^p p\tau$ and γ by $(-1)^p\gamma$, whereas $y_m^{(n,0)}(\tau) \equiv 0$ for $m \leq 0$.

In the generic case $j \neq 0$ it is reasonable to introduce a generating function in the form of the *Laurent series* of an auxiliary variable z

$$R^{(n,j)}(z, \tau) = \sum_{m=-\infty}^{\infty} y_m^{(n,j)}(\tau) z^m \tag{74}$$

since the lower index of the coefficient $y_m^{(n,j)}$ runs over all integers from $-\infty$ to ∞. One can verify that the function (74) satisfies the *homogeneous* equation

$$\frac{\partial R^{(n,j)}}{\partial \tau} = \left[\sigma\left(\frac{1}{z} - z\right) + 2i\gamma\right]\left(j + pz\frac{\partial}{\partial z}\right)R^{(n,j)}, \quad \sigma = (-1)^p \tag{75}$$

The solution to (75) satisfying the initial condition $R^{(n,j)}(z, 0) = z^n$ reads as

$$R^{(n,j)}(z, \tau) = z^{-j/p}\left[\frac{zg(p\tau) + \sigma S(p\tau)}{g^*(p\tau) + z\sigma S(p\tau)}\right]^{n+j/p} \tag{76}$$

where the functions $S(\tau)$ and $g(\tau)$ are as defined in (44). The coefficients of the Laurent series (74) can be calculated with the aid of the Cauchy formula

$$y_m^{(n,j)}(\tau) = \frac{1}{2\pi i}\oint_{\mathscr{C}} \frac{dz}{z^{m+1}} R^{(n,j)}(z,\tau) \tag{77}$$

where the closed curve $\mathscr{C}$ rounds the point $z = 0$ in the complex plane in the counterclockwise direction. Making a scale transformation, one can reduce the integral (77) with the integrand (76) to the integral representation of the Gauss hypergeometric function [see Ref. 269, Vol 1, Section 2.1.3]

$$F(a,b;c;x) = \frac{-i\Gamma(c)\exp(-i\pi b)}{2\sin(\pi b)\Gamma(c-b)\Gamma(b)}\oint_1^{(0+)} \frac{t^{b-1}(1-t)^{c-b-1}}{(1-tx)^a}\,dt \tag{78}$$

where $\mathrm{Re}(c-b) > 0$, $b \neq 1, 2, 3, \ldots$, and the integration contour begins at the point $t = 1$ and passes around the point $t = 0$ in the positive direction. After some algebra, one can obtain the expression

$$\begin{aligned} y_m^{(n,j)} = &-\frac{\Gamma(-m-j/p)\Gamma(1+n+j/p)\sin[\pi(m+j/p)]}{\pi\Gamma(1+n-m)} \\ &\times (\sigma\kappa)^{n-m}\lambda^{m+n+2j/p} F\left(n+\frac{j}{p},\, -m-\frac{j}{p};\, 1+n-m;\, \kappa^2\right) \end{aligned} \tag{79}$$

We assume hereafter $\kappa \equiv \kappa(p\tau)$ and $\lambda \equiv \lambda(p\tau)$, the functions $\kappa(x)$ and $\lambda(x)$ being defined as in (49) and (50). Using the known formula

$$\Gamma(-z)\sin(\pi z) = -\frac{\pi}{\Gamma(z+1)} \tag{80}$$

one can eliminate the gamma function of a negative argument:

$$\begin{aligned} y_m^{(n,j)} = &\frac{\Gamma(1+n+j/p)(\sigma\kappa)^{n-m}\lambda^{m+n+2j/p}}{\Gamma(1+m+j/p)\Gamma(1+n-m)} \\ &\times F\left(n+\frac{j}{p},\, -m-\frac{j}{p};\, 1+n-m;\, \kappa^2\right) \end{aligned} \tag{81}$$

The form (81) gives an explicit expression for the coefficient $\xi_{j+pm}^{(j+pn)}$ with $0 \le m \le n$. Moreover, it clearly shows the fulfilment of the initial condition $y_m^{(n,j)}(\tau = 0) = \delta_{mn}$. Transforming the hypergeometric function with the aid of

the formula [269,270]

$$\lim_{c\to -n}\frac{F(a,b;c;x)}{\Gamma(c)}=\frac{(a)_{n+1}(b)_{n+1}x^{n+1}}{(n+1)!}F(a+n+1,b+n+1;n+2;x)$$

($n=0,1,2,\ldots$) and the identity (80), one obtains an equivalent expression

$$y_m^{(n,j)}=\frac{\Gamma(m+j/p)(-\sigma\kappa)^{m-n}\lambda^{m+n+2j/p}}{\Gamma(n+j/p)\Gamma(1+m-n)}\times F\left(m+\frac{j}{p},\,-n-\frac{j}{p};\,1+m-n;\,\kappa^2\right) \tag{82}$$

which gives a convenient form of the coefficient $\xi_{j+pm}^{(j+pn)}$ for $m\geq n$. Formula (79) with negative values of the lower index gives an explicit expression for the nonzero coefficients $\eta_{pk-j}^{(pn+j)}$ ($k\geq 1, n\geq 0$):

$$\eta_{pk-j}^{(pn+j)}=-\frac{\Gamma(k-j/p)\Gamma(1+n+j/p)\sin[\pi(k-j/p)]}{\pi\Gamma(1+n+k)}\times(\sigma\kappa)^{n+k}\lambda^{n-k+2j/p}F\left(n+\frac{j}{p},\,k-\frac{j}{p};\,1+n+k;\,\kappa^2\right) \tag{83}$$

Note that the expressions (81)–(83) are valid for $j=0$, too. In this case they coincide with the formulas obtained in the preceding section. Formulas (81)–(83) immediately give the short-time behavior of the Bogoliubov coefficients at $\tau\to 0$; it is sufficient to put $\kappa\approx p\tau$, $\lambda\approx 1$ and to replace the hypergeometric functions by 1. In this limit the detuning parameter γ drops out of the expressions (in the leading terms of the Taylor expansions).

At $\tau\to\infty$, we have the following asymptotics of the functions $\kappa(p\tau)$ and $\lambda(p\tau)$ (if $\gamma\leq 1$):

$$\kappa\approx 1-\frac{1}{2}S^{-2}(p\tau)\to 1,\quad \lambda\to a+i\gamma,\quad \tau\to\infty$$

Then equation (79) together with the known asymptotics of the hypergeometric function $F(a,b;a+b+1;1-x)$ at $x\ll 1$ [269,270]

$$F(a,b;a+b+1;1-x)=\frac{\Gamma(a+b+1)}{\Gamma(a+1)\Gamma(b+1)}[1+abx\ln(x)+\mathcal{O}(x)] \tag{84}$$

lead to the asymptotical expression for the Bogoliubov coefficients:

$$y_m^{(n,j)}(\tau \gg 1) = \frac{\sin[\pi(m+j/p)]}{\pi(m+j/p)}(a+i\gamma)^{m+n+2j/p}\sigma^{n-m} \times \left[1+\mathcal{O}\left(\frac{mn}{S^2}\ln S\right)\right] \tag{85}$$

For $\gamma < 1$ the correction has an order $mn\tau\exp(-2ap\tau)$, while for $\gamma = 1$ it has an order $mn\ln(\tau)/\tau^2$.

One can verify that the generating function (76) satisfies the recurrence relation

$$\frac{\partial R^{(q,j)}}{\partial\tau} = (j+qp)\{\sigma[R^{(q-1,j)} - R^{(q+1,j)}] + 2i\gamma R^{(q,j)}\} \tag{86}$$

Its immediate consequence is an analogous relation for the Bogoliubov coefficients with the same lower indices:

$$\frac{d}{d\tau}\rho_m^{(n)} = n\{\sigma[\rho_m^{(n-p)} - \rho_m^{(n+p)}] + 2i\gamma\rho_m^{(n)}\} \tag{87}$$

Equation (87) is valid for $n > p$ [when $q \geq 1$ and $j \geq 1$ in (86)], since the coefficients $\rho_m^{(n)}$ are not defined when $n < 0$. However, using the chain of identities

$$R^{(-1,j)}(z) = z^{-j/p}\left[\frac{S+gz}{g^*+Sz}\right]^{j/p-1} = \frac{1}{z}\left(\frac{1}{z}\right)^{j/p-1}\left[\frac{S+g^*/z}{g+S/z}\right]^{1-j/p}$$
$$= \frac{1}{z}[R^{(0,p-j)}(1/z^*)]^* = \frac{1}{z}\sum_{k=-\infty}^{\infty} y_k^{(0,p-j)*}\left(\frac{1}{z}\right)^k = \sum_{k=-\infty}^{\infty} y_{-k-1}^{(0,p-j)*} z^k$$

one can obtain the first $p-1$ recurrence relations

$$\frac{d}{d\tau}\rho_m^{(n)} = n\{\sigma[\rho_{-m}^{(p-n)*} - \rho_m^{(p+n)}] + 2i\gamma\rho_m^{(n)}\}, \quad n = 1, 2, \ldots, p-1 \tag{88}$$

To treat the special case $n = p$ (which corresponds to the distinguished subset with $j = 0$), one should take into account that $R^{(0,0)}(z) \equiv 1$, which means formally that $\rho_m^{(0)} = \delta_{m0}$. So the last recurrence relation reads as

$$\frac{d}{d\tau}\rho_m^{(p)} = p\{-\sigma\rho_m^{(2p)} + 2i\gamma\rho_m^{(p)}\}, \quad m \geq 1$$

(remember that $\rho_m^{(p)} \equiv 0$ for $m \leq 0$). Now one can verify that the unitarity conditions (70) and (71) are the consequencies of the equations (87) and (88).

VI. PHOTON STATISTICS

To evaluate the mean number of photons and the statistical properties of the quantum field created in the cavity at $t > T$, we introduce the Hermitian quadrature component operators

$$\hat{q}_m = \frac{\hat{a}_m + \hat{a}_m^\dagger}{\sqrt{2}}, \quad \hat{p}_m = \frac{\hat{a}_m - \hat{a}_m^\dagger}{i\sqrt{2}}$$

Their variances are defined as

$$U_m = \langle \hat{q}_m^2 \rangle - \langle \hat{q}_m \rangle^2, \quad V_m = \langle \hat{p}_m^2 \rangle - \langle \hat{p}_m \rangle^2$$

whereas the covariance is given by

$$Y_m = \frac{1}{2} \langle \hat{p}_m \hat{q}_m + \hat{q}_m \hat{p}_m \rangle - \langle \hat{p}_m \rangle \langle \hat{q}_m \rangle$$

The average values must be calculated in the state defined *with respect to the initial operators* $\hat{b}_n$ (remember that we use the Heisenberg picture here).

A. Initial Vacuum State

The vacuum state is defined by means of the relations $\hat{b}_n|0\rangle = 0$. In this case, $U_m + V_m = 2\mathcal{N}_m^{(\mathrm{vac})} + 1$, where $\mathcal{N}_m^{(\mathrm{vac})}$ is the mean number of photons created from vacuum in the mth mode. It is given by the single sums over index n in Eq. (27). Initially, $U_m(0) = V_m(0) = \frac{1}{2}$, $Y_m(0) = 0$. Using (22) and assuming for simplicity $\omega_1 = 1$, we obtain the following expressions for $\tau > 0$

$$U_m = \frac{m}{2} \sum_{n=1}^{\infty} \frac{1}{n} \left| \rho_m^{(n)} - \rho_{-m}^{(n)} \right|^2, \quad V_m = \frac{m}{2} \sum_{n=1}^{\infty} \frac{1}{n} \left| \rho_m^{(n)} + \rho_{-m}^{(n)} \right|^2 \tag{89}$$

$$Y_m = \sum_{n=1}^{\infty} \frac{m}{n} \operatorname{Im}[\rho_m^{(n)*} \rho_{-m}^{(n)}] \tag{90}$$

where the coefficients $\rho_{\pm m}^{(n)}$ should be taken at the moment T; thus their argument is $\tau_T \equiv \frac{1}{2}\varepsilon\omega_1 T$. Strictly speaking, the expressions (89) and (90) have physical meanings at those moments of time T when the wall returns to its initial position, that is, for $T = N\pi/[p(1+\delta)]$ with an integer N. Consequently, the argument τ_T of the coefficients $\rho_{\pm m}^{(n)}$ in (89) and (90) assumes

discrete values $\tau^{(N)} = N\varepsilon\pi/[2p(1+\delta)]$. One should remember, however, that something interesting in our problem happens for the values $\tau \sim 1$ (or larger). Then $N \sim \varepsilon^{-1} \gg 1$, and the minimal increment $\Delta\tau \sim \varepsilon$ is so small that τ_T can be considered as a continuous variable (under the realistic conditions, $\varepsilon \leq 10^{-8}$ [189]). For this reason, we omit hereafter the subscript T, writing simply τ instead of τ_T or $\tau^{(N)}$.

Differentiating the right-hand sides of equations (89) and (90) with respect to the "slow time" τ, one can remove the fraction $1/n$ with the aid of the recurrence relations (87) and (88). After that, changing if necessary the summation index n to $n \pm p$, one can verify that almost all terms in the right-hand sides are canceled, and the infinite series are reduced to the finite sums:

$$\left.\begin{matrix}\frac{dU_m}{d\tau}\\ \frac{dV_m}{d\tau}\end{matrix}\right\} = \sigma m \sum_{n=1}^{p-1} \mathrm{Re}([\rho_m^{(p-n)} \mp \rho_{-m}^{(p-n)}][\rho_{-m}^{(n)} \mp \rho_m^{(n)}])$$

$$\frac{dY_m}{d\tau} = \sigma m \sum_{n=1}^{p-1} \mathrm{Im}(\rho_m^{(n)*}\rho_m^{(p-n)*} + \rho_{-m}^{(n)}\rho_{-m}^{(p-n)})$$

Now one should take into account the structure of the coefficients $\rho_m^{(n)}$; they are different from zero provided the difference between the upper index n and the lower one m is some multiple of the number p. If $m = j + pk$ with $j = 1, \ldots, p-1$ and $k = 0, 1, 2, \ldots$, then only the terms with $n = j$ or $n = p - j$ survive in the sums above. Depending on whether $j = p/2$ or $j \neq p/2$, we obtain two different sets of explicit expressions for the derivatives of the (co)variances:

1. If $m = j + pk$ but $j \neq p/2$ (in particular, for all *odd* values of p), then

$$\frac{dU_m}{d\tau} = \frac{dV_m}{d\tau} = 2\sigma m \mathrm{Re}(\rho_m^{(j)}\rho_{-m}^{(p-j)}), \quad \frac{dY_m}{d\tau} = 0 \tag{91}$$

   In this case $Y_m \equiv 0$ and $U_m = V_m = \mathcal{N}_m^{(\mathrm{vac})} + \frac{1}{2}$.

2. A different situation happens in the distinguished modes with the numbers $\mu = p(k + \frac{1}{2})$, $k = 0, 1, 2, \ldots$:

$$\frac{dU_\mu}{d\tau} = -\mu \mathrm{Re}([\rho_\mu^{(p/2)} - \rho_{-\mu}^{(p/2)}]^2), \quad \frac{dV_\mu}{d\tau} = \mu \mathrm{Re}([\rho_\mu^{(p/2)} + \rho_{-\mu}^{(p/2)}]^2) \tag{92}$$

$$\frac{dY_\mu}{d\tau} = \mu\, \mathrm{Im}([\rho_\mu^{(p/2)*}]^2 + [\rho_{-\mu}^{(p/2)}]^2) \tag{93}$$

   We shall call such modes the "principal" ones; they exist only if p is an *even* number. In the strict resonance case ($\gamma = 0$) all the coefficients $\rho_\mu^{(p/2)}$ are real, so $Y_\mu = 0$ and $dU_\mu/d\tau \leq 0$ in the whole interval $0 \leq \tau < \infty$,

resulting in the inequality $U_\mu(\tau) < \frac{1}{2}$, which tells us that the field occurs in the *squeezed* quantum state.

1. *Squeezing in the "Principal" Modes*

Note that the coefficients $\rho_{pm+p/2}^{(pn+p/2)}$ depend on the parameter p only through the dependence of the variable κ on the product $p\tau$ [see Eq. (79) or (81)]. Thus, to study the squeezing properties of the field created as a result of the NSCE (nonstationary Casimir effect) it is sufficient to consider the most important special case of the parametric resonance at the *double* fundamental frequency $2\omega_1$ (i.e., $p = 2$), since the formulas for $p > 2$ can be obtained by a simple rescaling of the "slow time" (for the "principal" modes). In this case, only the odd modes can be excited from the vacuum, and they do exhibit some squeezing.

Using Eqs. (92) and (93), one can immediately find the Taylor expansions of the (co)variances at $\tau \to 0$ (assuming $(-1)!! \equiv 1$):

$$\left.\begin{matrix} U_{2m+1} \\ V_{2m+1} \end{matrix}\right\} = \frac{1}{2} \mp \tau^{2m+1} \left[\frac{(2m-1)!!}{m!}\right]^2 \left[1 \mp \frac{2m+1}{(m+1)^2}\tau + \mathcal{O}(\tau^2)\right] \tag{94}$$

$$Y_{2m+1} = -2\gamma(2m+1)\tau^{2(m+1)} \left[\frac{(2m-1)!!}{m!}\right]^2 + \cdots \tag{95}$$

We see that the U variances are always less than $\frac{1}{2}$ at the initial stage, but the degree of their squeezing rapidly decreases with increase of the number m. Note that the dependence on the detuning parameter γ in the short-time limit appears only in terms of the order of τ^{2m+3} (and higher).

In the opposite limit $\tau \to \infty$ (or $\kappa \to 1$), using Eqs. (92) and (93) and the asymptotics of the Bogoliubov coefficients (85), we obtain *constant* time derivatives

$$\left.\frac{dU_{2m+1}}{d\tau}\right|_{\tau\to\infty} = \frac{16a}{\pi^2(2m+1)} \sin^2\left[\left(m+\frac{1}{2}\right)\phi\right].$$

$$\left.\frac{dV_{2m+1}}{d\tau}\right|_{\tau\to\infty} = \frac{16a}{\pi^2(2m+1)} \cos^2\left[\left(m+\frac{1}{2}\right)\phi\right].$$

$$\left.\frac{dY_{2m+1}}{d\tau}\right|_{\tau\to\infty} = -\frac{8a}{\pi^2(2m+1)} \sin[(2m+1)\phi].$$

where $\phi \equiv \arcsin\gamma$. Consequently, all the (co)variances increase with time linearly, giving the constant photon generation rate in the "principal" (odd) modes

$$\left.\frac{d\mathcal{N}_{2m+1}}{d\tau}\right|_{\tau\to\infty} = \frac{8a}{\pi^2(2m+1)} \tag{99}$$

Equation (99) results in a simple estimation of the mean photon number in the μth mode at $\tau > 1$: $\mathcal{N}_\mu(\tau) \approx a\tau/\mu$.

Since the covariance Y_μ is different from zero if $\gamma \neq 0$, the initial vacuum state of the field is transformed to the *correlated* quantum state [223,271,272]. One should remember, however, that the values of U_μ, V_μ, and Y_μ yield the (co)variances of the field quadratures only at the moment $t = T$ (when the wall stopped oscillating). At the subsequent moments of time the quadrature variances exhibit fast oscillations with twice the frequency of the mode. For example (omitting the mode index), one obtains

$$\sigma_q(t') = U\cos^2(\omega t') + V\sin^2(\omega t') + Y\sin(2\omega t'), \quad t' = t - T$$

Therefore the physical meanings do not have the values U_μ, V_μ, and Y_μ themselves, but rather the *minimal* $\sigma_{\min} \equiv u_\mu$ and *maximal* $\sigma_{\max} \equiv v_\mu$ values of the quadrature variances during the period of fast oscillations [273,274]

$$\left.\begin{matrix} u_\mu \\ v_\mu \end{matrix}\right\} = \frac{1}{2}\left(U_\mu + V_\mu \mp \sqrt{\left(U_\mu - V_\mu\right)^2 + 4Y_\mu^2}\right) \tag{100}$$

Only in the special case of the strict resonane ($\gamma = 0$) do we have $u_\mu = U_\mu$ and $v_\mu = V_\mu$. In the generic case $\gamma \neq 0$, all three (co)variances, U_μ, V_μ, and Y_μ, linearly increase with the interaction time T if $\tau_T \equiv \tau \gg 1$, due to Eqs. (96)–(98). Nonetheless, the *minimal variance* u_μ tends to a *constant* value at $\tau \to \infty$. This is shown in Section VI.B. Examples of explicit time dependences of the coefficients u_μ and v_μ are given in Section VI.C.

2. *Mean Photon Number*

Differentiating the "vacuum" part of sum (27) with respect to τ and performing the summation over the upper index n with the aid of (87) and (88) [remembering that the coefficients $\rho_m^{(n)}$ are different from zero provided the difference $n - m$ is a multiple of p], one can obtain the formula for the photon generation rate from vacuum in each mode ($0 \le j \le p-1$, $q = 0, 1, 2, \ldots$):

$$\begin{aligned} \frac{d}{d\tau}\mathcal{N}_{j+pq}^{(\mathrm{vac})} &= -2\sigma(j+pq)\mathrm{Re}\,[\xi_{j+pq}^{(j)}\eta_{j+pq}^{(p-j)}] \\ &= 2p\sqrt{1-\gamma^2\kappa^2}\,\frac{\sin(\pi j/p)\Gamma(q+j/p)\Gamma(1+q+j/p)\Gamma(2-j/p)}{\pi\Gamma(j/p)\Gamma(q+1)\Gamma(q+2)}\,\kappa^{2q+1} \\ &\quad \times F\left(q+\frac{j}{p}, -\frac{j}{p}; 1+q; \kappa^2\right)F\left(q+\frac{j}{p}, 1-\frac{j}{p}; 2+q; \kappa^2\right) \end{aligned} \tag{101}$$

We see that there is no photon creation in the modes with numbers $p, 2p, \ldots$. In the short-time limit

$$\dot{\mathcal{N}}^{(\mathrm{vac})}_{j+pq} \sim \tau^{2q+1}, \quad \tau \ll 1$$

In the long-time limit the photon generation rate tends to the constant value (if $\gamma < 1$)

$$\frac{d}{d\tau}\mathcal{N}^{(\mathrm{vac})}_{j+pq} = \frac{2ap^2 \sin^2(\pi j/p)}{\pi^2(j+pq)}\left[1 + \mathcal{O}\left(\frac{pq}{S^2}\ln S\right)\right], \quad ap\tau \gg 1 \tag{102}$$

For $q \gg 1$ and for a fixed value of κ, one can simplify the right-hand side of (101) using Stirling's formula for the gamma functions and the easily verified asymptotic formula

$$F(a,b;c;z) \approx (1 - az/c)^{-b}, \quad a, c \gg 1$$

In this case

$$\frac{d}{d\tau}\mathcal{N}^{(\mathrm{vac})}_{j+pq} \approx 2p\sqrt{1-\gamma^2\kappa^2}\,\frac{\sin(\pi j/p)\Gamma(2-j/p)\kappa^{2q+1}}{\pi\Gamma(j/p)q^{2(1-j/p)}(1-\kappa^2)^{1-2j/p}}, \quad q \gg 1 \tag{103}$$

In particular, if $q \gg S^2(p\tau) \gg 1$, then

$$\frac{d}{d\tau}\mathcal{N}^{(\mathrm{vac})}_{j+pq} \approx 2pa\,\frac{\sin(\pi j/p)\Gamma(2-j/p)(S^2/q)^{2(1-j/p)}}{\pi\Gamma(j/p)S^2}\exp(-q/S^2) \tag{104}$$

Comparing (102) and (104), one can conclude that the number of effectively excited modes (i.e., the modes with a time-independent photon generation rate) increases in time exponentially, approximately as $S^2(\tau)/\ln S(\tau)$.

The total number of photons generated from vacuum in all the modes equals

$$\mathcal{N}^{(\mathrm{vac})} = \sum_{m,n=1}^{\infty}\frac{m}{n}|\eta^{(n)}_m|^2 \tag{105}$$

Differentiating (105) with respect to τ and performing the summation over m with the help of Eqs. (66) and (67), one can obtain the formula

$$\frac{d\mathcal{N}^{(\mathrm{vac})}}{d\tau} = 2\sigma\mathrm{Re}\sum_{n=1}^{\infty}\frac{1}{n}\sum_{m=1}^{p} m(p-m)\rho^{(n)*}_{-m}(\tau)\rho^{(n)}_{p-m}(\tau) \tag{106}$$

Evidently, the right-hand side of this equation equals zero in the "semi-resonance" case $p = 1$.

Differentiating equation (106) once again over τ, one can perform the summation over the upper index n with the aid of Eqs. (87) and (88) to obtain a closed expression for the *second derivative* of the total number of "vacuum" photons:

$$\begin{aligned}\frac{d^2}{d\tau^2}\mathcal{N}^{(\mathrm{vac})} &= 2\mathrm{Re}\sum_{m=1}^{p-1} m(p-m)[\xi_m^{(m)}\xi_{p-m}^{(p-m)} + \eta_m^{(p-m)*}\eta_{p-m}^{(m)*}] \\ &= 2\sum_{m=1}^{p-1} m(p-m)\left\{m(p-m)\left[\frac{\kappa}{p}F\left(\frac{m}{p},\,1-\frac{m}{p};\,2;\,\kappa^2\right)\right]^2\right. \\ &\quad \left. +\left(1-2\gamma^2\kappa^2\right)F\left(\frac{m}{p},\,-\frac{m}{p};\,1;\,\kappa^2\right)F\left(\frac{m}{p}-1,\,1-\frac{m}{p};\,1;\,\kappa^2\right)\right\}\end{aligned} \tag{107}$$

In the short-time limit, one obtains

$$\ddot{\mathcal{N}}^{(\mathrm{vac})} = \frac{1}{3}p(p^2-1), \quad |ap\tau| \ll 1 \tag{108}$$

In the long-time limit the formulas (80), (84), and $\sum_{m=1}^{p-1}\sin^2(\pi m/p) = p/2$ lead to another simple expression (provided $p \geq 2$):

$$\ddot{\mathcal{N}}^{(\mathrm{vac})} = \frac{2a^2p^3}{\pi^2}, \quad ap\tau \gg 1, \quad a > 0 \tag{109}$$

Consequently, the total number of photons created from vacuum due to NSCE increases in time quadratically both in the short-time and in the long-time limits (although with different coefficients).

B. Arbitrary Initial Conditions

For an arbitrary initial state of the field, one can write $U_m = U_m^{(\mathrm{vac})} + \Delta U_m$, where $U_m^{(\mathrm{vac})}$ is given by equation (89); similar expressions can be written for V_m and Y_m. The corrections due to the nonvacuum initial states are given by

$$\left.\begin{aligned}\Delta U_m \\ \Delta V_m\end{aligned}\right\} = \mathrm{Re}\sum_{n,j}\frac{m}{\sqrt{nj}}([\rho_m^{(n)} \mp \rho_{-m}^{(n)}]^*[\rho_m^{(j)} \mp \rho_{-m}^{(j)}][\langle\hat{b}_n^\dagger\hat{b}_j\rangle - \langle\hat{b}_n^\dagger\rangle\langle\hat{b}_j\rangle]$$
$$\pm [\rho_m^{(n)} \mp \rho_{-m}^{(n)}][\rho_m^{(j)} \mp \rho_{-m}^{(j)}][\langle\hat{b}_n\hat{b}_j\rangle - \langle\hat{b}_n\rangle\langle\hat{b}_j\rangle]) \tag{110}$$

$$\Delta Y_m = \mathrm{Im}\sum_{n,j}\frac{m}{\sqrt{nj}}([\rho_m^{(n)*}\rho_{-m}^{(j)} - \rho_m^{(j)}\rho_{-m}^{(n)*}][\langle\hat{b}_n^\dagger\hat{b}_j\rangle - \langle\hat{b}_n^\dagger\rangle\langle\hat{b}_j\rangle]$$
$$+ [\rho_m^{(n)}\rho_m^{(j)} - \rho_{-m}^{(n)}\rho_{-m}^{(j)}][\langle\hat{b}_n\hat{b}_j\rangle - \langle\hat{b}_n\rangle\langle\hat{b}_j\rangle]) \tag{111}$$

where the average values such as $\langle \hat{b}_n^\dagger \hat{b}_j \rangle$ are calculated in the initial state. All the corrections disappear in the case of the initial coherent state, $\hat{b}_n|\alpha\rangle = \alpha_n|\alpha\rangle$. If the initial density matrix is *diagonal* in the Fock basis (as happens, e.g., for the Fock or thermal states), then $\langle \hat{b}_n^\dagger \hat{b}_j \rangle = \nu_n \delta_{nj}$ ($\nu_n \geq 0$), and all other average values in (110) and (111) are equal to zero. In this case the double sums are reduced to the single ones:

$$\Delta U_m = m \sum_n \frac{\nu_n}{n} \left|\rho_m^{(n)} - \rho_{-m}^{(n)}\right|^2, \quad \Delta V_m = m \sum_n \frac{\nu_n}{n} \left|\rho_m^{(n)} + \rho_{-m}^{(n)}\right|^2 \tag{112}$$

$$\Delta Y_m = 2m \sum_n \frac{\nu_n}{n} \operatorname{Im}[\rho_m^{(n)*} \rho_{-m}^{(n)}] \tag{113}$$

We see that the initial fluctuations always increase both the variances U_m and V_m (for the diagonal density matrix). However, asymptotically at $\tau \to \infty$ the corrections are bounded for the *physical* initial states having finite total numbers of photons, because the coefficients $|\rho_m^{(n)} \pm \rho_{-m}^{(n)}|^2$ and $\operatorname{Im}[\rho_m^{(n)*} \rho_{-m}^{(n)}]$ do not depend on the summation index n in this limit. For example, if $p = 2$, then

$$\rho_{2m+1}^{(2n+1)}(\tau \gg 1) \approx \frac{2(-1)^m}{\pi(2m+1)} (a + i\gamma)^{m+n+1} \tag{114}$$

$$\rho_{-2m-1}^{(2n+1)}(\tau \gg 1) \approx \frac{2(-1)^m}{\pi(2m+1)} (a + i\gamma)^{n-m} \tag{115}$$

and the exponent n disappears in the sums, because $|a + i\gamma| = 1$. Thus we have in the "principal" μ modes (taking $p = 2$ for the sake of simplicity)

$$\left.\begin{array}{l} \Delta U_\mu^{(\infty)} \\ \Delta V_\mu^{(\infty)} \\ \Delta Y_\mu^{(\infty)} \end{array}\right\} = \frac{8\mathscr{Z}}{\pi^2 \mu} \times \left\{\begin{array}{l} 2\sin^2\left(\frac{\mu\phi}{2}\right) \\ 2\cos^2\left(\frac{\mu\phi}{2}\right) \\ -\sin(\mu\phi) \end{array}\right. \tag{116}$$

where

$$\phi \equiv \arcsin \gamma, \quad \mathscr{Z} = \sum_{k=0}^{\infty} \frac{\nu_{2k+1}}{2k+1}$$

The expressions in (116) are very similar to those in equations (96)–(98). The consequence of Eq. (116) is the important result that in the limit $\tau \to \infty$ the minimal variance u_μ *does not depend* on the initial state of the field inside

the cavity, provided the initial density matrix was diagonal in the Fock basis. Indeed, in this case, combining the equations (96)–(98) and (116), we can write the variances at $\tau \gg 1$ as (we omit the subscript μ)

$$\begin{pmatrix} U(\tau) \\ V(\tau) \\ Y(\tau) \end{pmatrix} = \begin{pmatrix} 2F\sin^2\left(\frac{\chi}{2}\right) + f \\ 2F\cos^2\left(\frac{\chi}{2}\right) + g \\ -F\sin\chi + h \end{pmatrix}, \quad F = \frac{8(a\tau + \mathscr{Z})}{\pi^2\mu}, \quad \chi = \mu\phi \tag{117}$$

The corrections f, g, and h can be found by integrating equations (92) and (93); therefore they *do not depend on the initial state*. At $\tau \to \infty$ these corrections tend to finite limits, so they are much smaller than F. Evidently, $U + V = 2F + f + g$, whereas

$$(U - V)^2 + 4Y^2 = 4F^2 + 4F[(g - f)\cos\chi - 2h\sin\chi] + (f - g)^2 + 4h^2.$$

For $F \gg f, g, h$ we have

$$\sqrt{(U - V)^2 + 4Y^2} = 2F + (g - f)\cos\chi - 2h\sin\chi + \mathcal{O}\left(\frac{1}{F}\right)$$

so the minimal variance $u(\tau)$ (100) tends to the finite limit

$$u(\infty) = f\cos^2\left(\frac{\chi}{2}\right) + g\sin^2\left(\frac{\chi}{2}\right) + h\sin\chi \tag{118}$$

which does not depend on $\mathscr{Z}$, that is on the initial state.

The correction to the mean number of photons in the mth mode for the "diagonal" initial distributions is given by the sum

$$\Delta\mathscr{N}_m = m\sum_n \frac{\nu_n}{n}\left(\left|\rho_m^{(n)}\right|^2 + \left|\rho_{-m}^{(n)}\right|^2\right)$$

It tends to the limit $\Delta\mathscr{N}_\mu^{(\infty)} = 8\mathscr{Z}/(\pi^2\mu)$.

The total number of photons in all the modes equals $\mathscr{N} = \mathscr{N}^{(\mathrm{vac})} + \mathscr{N}^{(\mathrm{cav})}$, where

$$\mathscr{N}^{(\mathrm{cav})} = \mathscr{N}(0) + 2\sum_{m,n,k=1}^{\infty} \frac{m}{\sqrt{nk}}\left[\eta_m^{(n)*}\eta_m^{(k)}\langle\hat{b}_n^\dagger\hat{b}_k\rangle + \mathrm{Re}(\eta_m^{(n)}\xi_m^{(k)}\langle\hat{b}_n\hat{b}_k\rangle)\right] \tag{119}$$

[to obtain this formula, one should use the identity (24)]. Differentiating (119) with respect to τ and performing the summation over m with the help of equations (29), (30), (64), (65), or (67), one can obtain the formula

$$\begin{aligned} \frac{d\mathscr{N}^{(\mathrm{cav})}}{d\tau} &= 2\sigma\sum_{n,k=1}^{\infty}\frac{\langle\hat{b}_n^\dagger\hat{b}_k\rangle}{\sqrt{nk}}\sum_{m=1}^{p} m(p-m)[\rho_{-m}^{(n)*}\rho_{p-m}^{(k)} + \rho_{-m}^{(k)}\rho_{p-m}^{(n)*}] \\ &\quad - 2\sigma\mathrm{Re}\sum_{n,k=1}^{\infty}\frac{\langle\hat{b}_n\hat{b}_k\rangle}{\sqrt{nk}}\sum_{m=1}^{p} m(p-m)[\rho_{-m}^{(n)}\rho_{m-p}^{(k)} + \rho_m^{(n)}\rho_{p-m}^{(k)}] \end{aligned} \tag{120}$$

Using equation (120) and replacing the coefficients $\rho_m^{(n)}$ by their asymptotic values (85), one can obtain the expression

$$\frac{d\mathcal{N}^{(\mathrm{cav})}}{d\tau} = \frac{4ap^2}{\pi^2}\sum_{m=1}^{p-1}\sin^2\left(\frac{\pi m}{p}\right)\sum_{n,k=0}^{\infty}\frac{\sigma^{n+k}}{\sqrt{(m+pn)(m+pk)}} \times \{\langle\hat{b}^\dagger_{m+pn}\hat{b}_{m+pk}\rangle(a+i\gamma)^{k-n} - \sigma\mathrm{Re}[\langle\hat{b}_{m+pn}\hat{b}_{m+pk}\rangle(a+i\gamma)^{k+n+1}]\} \tag{121}$$

which holds provided $ap\tau \gg 1$ and $a > 0$. For the physical initial states the sum in the right-hand side of (121) is finite. This is obvious if a finite number of modes was excited initially. But even if the cavity was initially in a high-temperature thermal state, so that $\langle\hat{b}^\dagger_n\hat{b}_k\rangle = \delta_{nk}\Theta/n$, $\langle\hat{b}_n\hat{b}_k\rangle = 0$, the sum over n, k yields a finite value $\Theta\sum_{n=0}^{\infty}(m+pn)^{-2}$. Consequently, the total number of "nonvacuum" photons increases in time *linearly* at $ap\tau \gg 1$, whereas the total number of quanta generated from vacuum increases *quadratically* in the long time limit.

C. The "Principal Resonance" ($p = 2$)

Many formulas obtained above can be simplified in the special case $p = 2$. In this case there are two subsets of nonzero Bogoliubov coefficients. The first one consists of the coefficients with even upper and lower indices $\xi_{2k}^{(2q)}$ which are reduced to the coefficients $\xi_k^{(q)}$ of the "semiresonance" case. However, since $\eta_{2k}^{(2q)} \equiv 0$, this subset does not contribute to the generation of new photons. The second subset is formed by the "odd" coefficients, which can be written as $[\kappa \equiv \kappa(2\tau)]$

$$\xi_{2m+1}^{(2n+1)} = \frac{\Gamma\left(n+\frac{3}{2}\right)\kappa^{n-m}\lambda^{m+n+1}}{\Gamma\left(m+\frac{3}{2}\right)\Gamma(1+n-m)} \times F\left(n+\frac{1}{2},\, -m-\frac{1}{2};\, 1+n-m;\, \kappa^2\right), \quad n \geq m \tag{122}$$

$$\xi_{2m+1}^{(2n+1)} = \frac{(-1)^{m-n}\Gamma\left(m+\frac{1}{2}\right)\kappa^{m-n}\lambda^{m+n+1}}{\Gamma\left(n+\frac{1}{2}\right)\Gamma(1+m-n)} \times F\left(m+\frac{1}{2},\, -n-\frac{1}{2};\, 1+m-n;\, \kappa^2\right), \quad m \geq n \tag{123}$$

$$\eta_{2k+1}^{(2n+1)} = \frac{(-1)^{k-1}\Gamma\left(k+\frac{1}{2}\right)\Gamma\left(n+\frac{3}{2}\right)\kappa^{n+k+1}\lambda^{n-k}}{\pi\Gamma(2+n+k)} \times F\left(n+\frac{1}{2},\, k+\frac{1}{2};\, 2+n+k;\, \kappa^2\right) \tag{124}$$

It is known [275] that the hypergeometric function $F(a,b;c;z)$ with *half-integral* parameters a,b and an integral parameter c can be expressed in terms of the complete elliptic integrals

$$\mathbf{K}(\kappa)=\int_0^{\pi/2}\frac{d\alpha}{\sqrt{1-\kappa^2\sin^2\alpha}}=\frac{\pi}{2}F\left(\frac{1}{2},\frac{1}{2};\,1;\,\kappa^2\right) \tag{125}$$

$$\mathbf{E}(\kappa)=\int_0^{\pi/2}d\alpha\sqrt{1-\kappa^2\sin^2\alpha}=\frac{\pi}{2}F\left(-\frac{1}{2},\frac{1}{2};\,1;\,\kappa^2\right) \tag{126}$$

In particular

$$\xi_1^{(1)}=\frac{2}{\pi}\lambda(\kappa)\mathbf{E}(\kappa),\quad \eta_1^{(1)}=\frac{2}{\pi\kappa}\left[\tilde{\kappa}^2\mathbf{K}(\kappa)-\mathbf{E}(\kappa)\right] \tag{127}$$

$$\rho_3^{(1)}=\frac{2\lambda^2(\kappa)}{3\pi\kappa}\left[\left(1-2\kappa^2\right)\mathbf{E}(\kappa)-\tilde{\kappa}^2\mathbf{K}(\kappa)\right] \tag{128}$$

$$\rho_{-3}^{(1)}=-\frac{2}{3\pi\kappa^2\lambda(\kappa)}\left[\left(2-\kappa^2\right)\mathbf{E}(\kappa)-2\tilde{\kappa}^2\mathbf{K}(\kappa)\right] \tag{129}$$

where

$$\tilde{\kappa}\equiv\sqrt{1-\kappa^2}=\left[1+S^2(2\tau)\right]^{-1/2} \tag{130}$$

and $\lambda(\kappa)$ is as defined in (50).

The general structure of the coefficients $\rho_\mu^{(1)}$ (we confine ourselves to the case $p=2$) is as follows

$$\rho_{2m+1}^{(1)}=\frac{2\lambda^{m+1}(\kappa)}{\pi\kappa^m}\left[f_m\left(\kappa^2\right)\mathbf{E}(\kappa)+\tilde{\kappa}^2g_m\left(\kappa^2\right)\mathbf{K}(\kappa)\right] \tag{131}$$

$$\rho_{-2m-1}^{(1)}=\frac{2}{\pi\kappa^{m+1}\lambda^m(\kappa)}\left[r_m\left(\kappa^2\right)\mathbf{E}(\kappa)+\tilde{\kappa}^2s_m\left(\kappa^2\right)\mathbf{K}(\kappa)\right] \tag{132}$$

where $f_m(x), g_m(x), r_m(x), s_m(x)$ are the polynomials of the degree m which can be found from the recurrence relations (67).

The photon generation rate from vacuum in the principal cavity mode ($m=1$) reads

$$\frac{d\mathcal{N}_1^{(\mathrm{vac})}}{d\tau}=-2\mathrm{Re}[\eta_1^{(1)}\xi_1^{(1)}]=\frac{8\sqrt{1-\gamma^2\kappa^2}}{\pi^2\kappa}\mathbf{E}(\kappa)\left[\mathbf{E}(\kappa)-\tilde{\kappa}^2\mathbf{K}(\kappa)\right] \tag{133}$$

The average number of photons in the first mode can be obtained by integrating this equation. It is convenient to integrate with respect to the variable κ, taking

into account the relation (for $p = 2$, e.g.)

$$d\kappa = 2\beta\tilde{\kappa}^2 d\tau, \quad \beta = \mathrm{Re}\lambda = \sqrt{1 - \gamma^2\kappa^2}$$

For example, in the case of the quadrature variance U_1, we arrive at the equation

$$\begin{aligned}\frac{dU_1}{d\kappa} = -\frac{2}{\pi^2\tilde{\kappa}^2\kappa^2\beta}\big\{&\big[\kappa^2\big(1 - 2\gamma^2\kappa^2\big) + 1 - 2\beta\kappa\big]\mathbf{E}^2(\kappa) \\ &-2\tilde{\kappa}^2(1 - \beta\kappa)\mathbf{E}(\kappa)\mathbf{K}(\kappa) + \tilde{\kappa}^4\mathbf{K}^2(\kappa)\big\}\end{aligned} \tag{134}$$

Let us consider first the case $\gamma = 0$, when $\beta = 1$. Taking into account the differentiation rules [276]

$$\frac{d\mathbf{K}(\kappa)}{d\kappa} = \frac{\mathbf{E}(\kappa)}{\kappa\tilde{\kappa}^2} - \frac{\mathbf{K}(\kappa)}{\kappa}, \quad \frac{d\mathbf{E}(\kappa)}{d\kappa} = \frac{\mathbf{E}(\kappa) - \mathbf{K}(\kappa)}{\kappa} \tag{135}$$

we may suppose that the factor $\tilde{\kappa}^2$ in the denominator of the right-hand side of Eq. (134) comes from the derivative $d\mathbf{K}/d\kappa$. Thus it is natural to look for the solution in the form

$$U_1 = \frac{2}{\pi^2\kappa}\left[A(\kappa)\mathbf{K}^2(\kappa) + B(\kappa)\mathbf{K}(\kappa)\mathbf{E}(\kappa) + C(\kappa)\mathbf{E}^2(\kappa)\right] \tag{136}$$

where $A(\kappa)$, $B(\kappa)$, and $C(\kappa)$ are some polynomials of κ. Putting the expression (136) into equation (134), we obtain a set of coupled equations for the unknown functions A, B, C. Writing $A(\kappa) = a_0 + A_1(\kappa)$, $B(\kappa) = b_0 + B_1(\kappa)$, and $C(\kappa) = c_0 + C_1(\kappa)$, we determine the constant coefficients a_0, b_0, and c_0 by putting $\kappa = 0$ in that equations. Then we obtain new equations for the functions $A_1(\kappa)$, $B_1(\kappa)$, and $C_1(\kappa)$ and repeat the procedure. After a few steps we arrive at the equations that have obvious trivial solutions $A_n = B_n = C_n = 0$. This confirms our hypothesis on the polynomial structure of the functions $A(\kappa)$, $B(\kappa)$, and $C(\kappa)$ and gives the final answer. The equations for the variances U_μ, V_μ, and so on with $\mu \geq 3$ can be integrated in the same manner; the only difference is that one should write κ^μ instead of κ in the denominator of the expression such as (136). In the generic case $\gamma \neq 0$, we notice that the factor β can appear in the denominator of the expression (134) as a result of differentiating the function $\beta(\kappa)$, since $d\beta/d\kappa = -\gamma^2\kappa/\beta$. Therefore we split each function, A, B, C in the "β-even" and "β-odd" parts such as $A = A_e(\kappa) + \beta(\kappa)A_o(\kappa)$. The equations for the "even" and "odd" coefficients turn out to be independent, and we solve them using the procedure described above.

The results of the integrations are as follows:

$$\mathcal{N}_1^{(\mathrm{vac})}(\kappa) = \frac{2}{\pi^2}\mathbf{K}(\kappa)\left[2\mathbf{E}(\kappa) - \tilde{\kappa}^2\mathbf{K}(\kappa)\right] - \frac{1}{2} \tag{137}$$

$$U_1 = \frac{2}{\pi^2\kappa}\left[\tilde{\kappa}^2(\beta-\kappa)\mathbf{K}^2(\kappa) - 2(\beta-\kappa)\mathbf{K}(\kappa)\mathbf{E}(\kappa) + \beta\mathbf{E}^2(\kappa)\right]$$

$$V_1 = \frac{2}{\pi^2\kappa}\left[2(\beta+\kappa)\mathbf{K}(\kappa)\mathbf{E}(\kappa) - \tilde{\kappa}^2(\beta+\kappa)\mathbf{K}^2(\kappa) - \beta\mathbf{E}^2(\kappa)\right]$$

$$Y_1 = \frac{2\gamma}{\pi^2}\left[\tilde{\kappa}^2\mathbf{K}^2(\kappa) - 2\mathbf{K}(\kappa)\mathbf{E}(\kappa) + \mathbf{E}^2(\kappa)\right]$$

Making the transformation [269,270]

$$\mathbf{K}\left(\frac{1-\tilde{\kappa}}{1+\tilde{\kappa}}\right) = \frac{1+\tilde{\kappa}}{2}\mathbf{K}(\kappa), \quad \mathbf{E}\left(\frac{1-\tilde{\kappa}}{1+\tilde{\kappa}}\right) = \frac{\mathbf{E}(\kappa)+\tilde{\kappa}\mathbf{K}(\kappa)}{1+\tilde{\kappa}}$$

one can rewrite formulas (127) and (137) in the form found for the first time in Ref. 189 (in the special case of $\gamma = 0$). Using the asymptotic expansions of the elliptic integrals at $\kappa \to 1$ [276]

$$\mathbf{K}(\kappa) \approx \ln\frac{4}{\tilde{\kappa}} + \frac{1}{4}\left(\ln\frac{4}{\tilde{\kappa}} - 1\right)\tilde{\kappa}^2 + \cdots$$

$$\mathbf{E}(\kappa) \approx 1 + \frac{1}{2}\left(\ln\frac{4}{\tilde{\kappa}} - \frac{1}{2}\right)\tilde{\kappa}^2 + \cdots$$

one can obtain the formula

$$\mathcal{N}_1^{(\mathrm{vac})}(\tau \gg 1) = \frac{8a}{\pi^2}\tau + \frac{4}{\pi^2}\ln\left(\frac{2}{a}\right) - \frac{1}{2} + \mathcal{O}\left(\tau e^{-4a\tau}\right), \quad a > 0 \tag{138}$$

In the special case of $\gamma = 1$ one can obtain the expansion

$$\mathcal{N}_1^{(\mathrm{vac})}(\tau \gg 1) = \frac{4}{\pi^2}\ln\tau + \frac{12}{\pi^2}\ln 2 - \frac{1}{2} + \mathcal{O}\left(\tau^{-2}\right)$$

If $\gamma > 1$, the number of photons in the principal mode oscillates with the period $\pi/(2\tilde{a})$. For $\gamma \gg 1$ one can write $\kappa \approx \sin(2\tilde{a}\tau)/\tilde{a}$, i.e. $|\kappa| \ll 1$. In this case

$$\mathcal{N}_1^{(\mathrm{vac})} \approx \frac{\kappa^2}{4} \approx \frac{\sin^2(2\tilde{a}\tau)}{4\tilde{a}^2} \ll 1$$

Equation (100) yields the minimal and maximal *invariant variances*

$$u_1 = \frac{2}{\pi^2\kappa}\left[\tilde{\kappa}^2(1-\kappa)\mathbf{K}^2(\kappa) - 2(1-\kappa)\mathbf{K}(\kappa)\mathbf{E}(\kappa) + \mathbf{E}^2(\kappa)\right] \tag{139}$$

$$v_1 = \frac{2}{\pi^2\kappa}\left[2(1+\kappa)\mathbf{K}(\kappa)\mathbf{E}(\kappa) - \tilde{\kappa}^2(1+\kappa)\mathbf{K}^2(\kappa) - \mathbf{E}^2(\kappa)\right] \tag{140}$$

which depend on the detuning parameter γ only implicitly, through the dependence on γ of the function $\kappa(\tau)$. In the short-time limit $\tau \ll 1$ (then $\kappa \approx 2\tau$) we obtain, using the Taylor expansions of the complete elliptic integrals, $u_1 = \frac{1}{2} - \tau + \tau^2 + \cdots$ and $v_1 = \frac{1}{2} + \tau + \tau^2 + \cdots$ in accordance with Dodonov et al. [124]. More precisely

$$\left.\begin{matrix} u_1 \\ v_1 \end{matrix}\right\} = \frac{1}{2}\left(1 \mp \kappa + \frac{1}{2}\kappa^2 \mp \frac{1}{4}\kappa^3 + \frac{7}{32}\kappa^4 + \cdots\right)$$

The minimal variance u_1 monotonously decreases from the value $\frac{1}{2}$ at $t = 0$ to the constant asymptotic value $2/\pi^2$ at $\tau \gg 1$, confirming qualitatively the earlier evaluations [107,110] and giving almost 50% squeezing in the initial vacuum state. The variance of the conjugate quadrature monotonously increases, and for $\tau \gg 1$ it becomes practically linear function of time: $v_1(\tau \gg 1) \approx 16\tau/\pi^2$. The asymptotic minimal value $u_1(\tau = \infty)$ does not depend on γ provided $\gamma \leq 1$ (only the rate of reaching this asymptotic value decreases with γ as $\sqrt{1-\gamma^2}$). In the strongly detuned case, $\gamma > 1$, the minimal variance oscillates as a function of τ (it is always greater than $2/\pi^2$), since in this case the function $\kappa(\tau)$ oscillates between $-\gamma^{-1}$ and γ^{-1}.

The minimal variance does not go to zero when $\tau \to \infty$ because of the *strong intermode interaction*, which results in a high degree of *quantum mixing* for each mode. Since the state originating from the initial vacuum state belongs to the class of *Gaussian* states (see the next subsection), the quantum 'purity' $\chi_m \equiv \mathrm{Tr}\,\hat{\rho}_m^2$ of the mth field mode (described by means of the density matrix $\hat{\rho}_m$) can be expressed in terms of the (co)variances as [277] $\chi_m = [4(U_m V_m - Y_m^2)]^{-1/2}$. Using equations (117) and (118), one can check that for $\tau \gg 1$, $UV - Y^2 = 2Fu(\infty) + \mathcal{O}(1) \sim \tau$. Consequently, the purity factor χ asymptotically goes to zero as $\tau^{-1/2}$. For instance, for $m = 1$, we have (writing simply $\mathbf{K}$ and $\mathbf{E}$ instead of $\mathbf{K}(\kappa)$ and $\mathbf{E}(\kappa)$)

$$\chi_1 = \frac{\pi^2}{4}\kappa\left[4\mathbf{K}\mathbf{E}^3 + 4\tilde{\kappa}^4\mathbf{K}^3\mathbf{E} - 6\tilde{\kappa}^2\mathbf{K}^2\mathbf{E}^2 - \mathbf{E}^4 - \tilde{\kappa}^6\mathbf{K}^4\right]^{-(1/2)} \tag{141}$$

The initial dependence on κ is rather weak: $\chi(\kappa \ll 1) = 1 - \frac{3}{32}\kappa^4 + \cdots$. But when $\kappa \to 1$, χ rapidly goes to zero: $\chi(\tilde{\kappa} \ll 1) \approx (8/\pi^2)[\ln(4/\tilde{\kappa})]^{-1/2}$, with $\mathrm{d}\chi/\mathrm{d}\kappa \to -\infty$.

The expressions for the variances in the modes with numbers $\mu \geq 3$ are rather involved. Here we give only one explicit example—the variance U_3 for $\gamma = 0$:

$$U_3 = \frac{2}{9\pi^2\kappa^3}\left[\tilde{\kappa}^2(1-\kappa)\left(4+10\kappa+9\kappa^2\right)\mathbf{K}^2(\kappa)\right.$$
$$+(1-\kappa)\left(4\kappa^3-14\kappa^2-20\kappa-8\right)\mathbf{K}(\kappa)\mathbf{E}(\kappa)$$
$$\left.+\left(4\kappa^4+6\kappa^3-\kappa^2+6\kappa+4\right)\mathbf{E}^2(\kappa)\right] \tag{142}$$

The Taylor expansion of the right-hand side of (142) coincides with the expansion (94). The asymptotical value at $\tau \to \infty$ equals $U_3(\kappa = 1) = 38/(9\pi^2) \approx 0.43$. We see that the squeezing rapidly disappears with increase of the mode number μ. The variance V_3 can be obtained from (142) by means of a simple substitution $\kappa \to -\kappa$. Therefore, the mean number of photons in the third mode is given by

$$\mathcal{N}_3 = \frac{2}{3\pi^2\kappa^2}\left[\left(3\kappa^2-2\right)\mathbf{K}\left(2\mathbf{E}-\tilde{\kappa}^2\mathbf{K}\right)+2\left(1+\kappa^2\right)\mathbf{E}^2\right]-\frac{1}{2} \tag{143}$$

The second derivative of the total mean number of photons created from vacuum in all the modes (107) takes the form

$$\frac{d^2\mathcal{N}^{(\mathrm{vac})}}{d\tau^2} = \frac{8}{\pi^2\kappa^2}\left[\tilde{\kappa}^4\mathbf{K}^2-2\tilde{\kappa}^2\mathbf{K}\mathbf{E}+\left(1+\kappa^2-2\gamma^2\kappa^4\right)\mathbf{E}^2\right] \tag{144}$$

Integrating this equation with the account of the condition $d\mathcal{N}^{(\mathrm{vac})}/d\tau = 0$ at $\tau = 0$ [which is a trivial consequence of Eq. (106)], we obtain a very simple expression:

$$\mathcal{N}^{(\mathrm{vac})} = \frac{2}{\pi^2}\mathbf{K}(\kappa)[\mathbf{K}(\kappa)-\mathbf{E}(\kappa)] \tag{145}$$

In the limiting cases this formula yields

$$\mathcal{N}^{(\mathrm{vac})}(\tau \ll 1) \approx \tau^2$$
$$\mathcal{N}^{(\mathrm{vac})}(\tau \gg 1) = \frac{8a^2\tau^2}{\pi^2} + \mathcal{O}(\tau), \quad a > 0$$

If $\gamma \gg 1$, then $|\kappa| \ll 1$, but $\gamma^2\kappa^2 \approx \sin^2(2\tilde{a}\tau) \sim \mathcal{O}(1)$. In this case the Taylor expansion of the second derivative yields $\ddot{\mathcal{N}}^{(\mathrm{vac})} = 2\cos(4\tilde{a}\tau) + \mathcal{O}(\gamma^{-2})$. Integrating this equation with account of the initial conditions $\dot{\mathcal{N}}^{(\mathrm{vac})}(0) = \mathcal{N}^{(\mathrm{vac})}(0) = 0$, one obtains $\mathcal{N}^{(\mathrm{vac})} \approx \mathcal{N}_1^{(\mathrm{vac})} \approx \sin^2(2\tilde{a}\tau)/(4\tilde{a}^2)$.

D. Photon Distribution

Now let us turn to the *photon distribution function* (PDF) $f(\mathbf{n}) \equiv \langle\mathbf{n}|\hat{\rho}_m(t)|\mathbf{n}\rangle$, where $|\mathbf{n}\rangle$ is the multimode Fock state, $\mathbf{n} \equiv (n_1, n_2, \ldots)$, and $\hat{\rho}_m(t)$ is the time-dependent density matrix of the mth field mode in the *Schrödinger* picture. Note that all the calculations in the preceding sections were performed in the

framework of the *Heisenberg* picture. Nonetheless, the available information is sufficient to calculate the PDF for the special (but very important) class of *Gaussian* initial states (defined as the states whose density matrices, or wavefunctions, or Wigner functions, are described by some Gaussian exponentials). This class includes coherent, squeezed, and thermal states; in particular, it includes the vacuum state.

The solution is based on two key points. The first one is the statement [170,176,183–185] that the field evolution in a cavity with moving boundaries can be described not only in the Heisenberg picture but, equivalently, in the framework of the Schrödinger picture, with a *quadratic* multidimensional time-dependent Hamiltonian. The second key point is the fact [278,279] that the evolution governed by quadratic Hamiltonians transforms any Gaussian state to another Gaussian state. Knowing these facts, it remains to take into account that the photon distribution function of any Gaussian state is determined completely by the average values of quadratures and by their variances [280,281], which obviously do not depend on the quantum-mechanical representation.

In the most compact form the information on the photon distribution $f(n)$ in some mode (we suppress here the mode index) is contained in the *generating function*

$$G(z) = \sum_{n=0}^{\infty} f(n) z^n$$

For a generic one-mode Gaussian state it can be expressed as [192,280,281]

$$G(z) = [\mathscr{G}(z)]^{-1/2} \exp\left(\frac{1}{D}\left[\frac{z g_1 - z^2 g_2}{\mathscr{G}(z)} - g_0\right]\right) \tag{146}$$

where

$$\mathscr{G}(z) = \frac{1}{4}[(1+z)^2 + 4\big(UV - Y^2\big)(1-z)^2 + 2(U+V)\big(1-z^2\big)] \tag{147}$$

$$D = 1 + 2(U+V) + 4\big(UV - Y^2\big) = 4\mathscr{G}(0)$$

$$g_0 = \langle\hat{p}\rangle^2(2U+1) + \langle\hat{q}\rangle^2(2V+1) - 4\langle\hat{p}\rangle\langle\hat{q}\rangle Y$$

$$g_1 = 2\langle\hat{p}\rangle^2\left(U^2 + Y^2 + U + \frac{1}{4}\right) + 2\langle\hat{q}\rangle^2\left(V^2 + Y^2 + V + \frac{1}{4}\right) - 4\langle\hat{p}\rangle\langle\hat{q}\rangle Y(U+V+1)$$

$$g_2 = 2\langle\hat{p}\rangle^2\left(U^2 + Y^2 - \frac{1}{4}\right) + 2\langle\hat{q}\rangle^2\left(V^2 + Y^2 - \frac{1}{4}\right) - 4\langle\hat{p}\rangle\langle\hat{q}\rangle Y(U+V)$$

In the generic case $f(n)$ is related to the two-dimensional "diagonal" Hermite polynomials [280]:

$$f(n) = \frac{\mathscr{F}_0}{n!} H_{nn}^{\{\mathscr{R}\}}(x, x^*) \tag{148}$$

where

$$\mathscr{F}_0 = f(0) = 2D^{-1/2} \exp\left(\frac{-g_0}{D}\right)$$

$$x = \frac{\sqrt{2}\{(2V-1)\langle\hat{q}\rangle - 2Y\langle\hat{p}\rangle + i[(1-2U)\langle\hat{p}\rangle + 2Y\langle\hat{q}\rangle]\}}{2(U+V) - 4(UV - Y^2) - 1}$$

and 2×2 symmetric matrix $\mathscr{R}$ has the elements

$$\mathscr{R}_{11} = \mathscr{R}_{22}^* = \frac{2}{D}(V - U - 2iY), \quad \mathscr{R}_{12} = \mathscr{R}_{21} = \frac{1}{D}\left[1 - 4\left(UV - Y^2\right)\right]$$

The two-dimensional Hermite polynomials are defined via the expansion [269]

$$\exp\left(-\frac{1}{2}\mathbf{a}\mathscr{R}\mathbf{a} + \mathbf{a}\mathscr{R}\mathbf{x}\right) = \sum_{m,n=0}^{\infty} \frac{a_1^m a_2^n}{m!n!} H_{mn}^{\{\mathscr{R}\}}(x_1, x_2) \tag{149}$$

where $\mathbf{x} = (x_1, x_2)$, $\mathbf{a} = (a_1, a_2)$. The properties of these polynomials were studied in 1994 [281,282]. In particular, they can be expressed as finite sums of the products of the usual (one-dimensional) Hermite polynomials. The corresponding formula for the probabilities reads as [280]

$$f(n) = \mathscr{F}_0 \left(\frac{\Delta}{D}\right)^n \sum_{k=0}^{n} \left(\frac{S}{\Delta}\right)^k \frac{n!}{[(n-k)!]^2 k!} |H_{n-k}(\xi)|^2 \tag{150}$$

where

$$\Delta = \sqrt{(U-V)^2 + 4Y^2}, \quad S = 4\left(UV - Y^2\right) - 1$$

$$\xi = \frac{(2V+1)\langle\hat{q}\rangle - 2Y\langle\hat{p}\rangle + i[(1+2U)\langle\hat{p}\rangle - 2Y\langle\hat{q}\rangle]}{[2D(V - U - 2iY)]^{1/2}}$$

If $\langle\hat{p}\rangle = \langle\hat{q}\rangle = 0$, then the generating function (146) is reduced to $[\mathscr{G}(z)]^{-1/2}$, that is, it has the same structure as the known generating function of the Legendre polynomials $P_n(x)$. In this case, we have the following expression for

the photon distribution in the mth field mode:

$$f_m(n) = \frac{2[(2u_m - 1)(2v_m - 1)]^{n/2}}{[(2u_m + 1)(2v_m + 1)]^{(n+1)/2}} P_n\left(\frac{4u_m v_m - 1}{\sqrt{(4u_m^2 - 1)(4v_m^2 - 1)}}\right) \tag{151}$$

This depends only on the invariant minimal and maximal variances u_m and v_m. Note that the argument of the polynomial in (151) is always *outside* the "traditional" interval $(-1, 1)$ (in particular, this argument is purely imaginary if $2u_m < 1$), being exactly equal to 1 for the "nonprincipal" modes with $u_m = v_m = \mathcal{N}_m + \frac{1}{2}$, when formula (151) transforms to the time-dependent Planck distribution

$$f_m(n; \tau) = \frac{\mathcal{N}_m^n(\tau)}{[\mathcal{N}_m(\tau) + 1]^{n+1}}$$

Only for the "principal" μ modes is the spectrum of photons different from Planck's one because of the squeezing effect.

The function (151) can be simplified in the long-time limit $\tau \gg 1$, when the average number of created photons $\mathcal{N} \equiv \bar{n} \approx (V + U)/2$ exceeds 1. Then the mean-square fluctuation of the photon number has the same order of magnitude as the mean photon number itself, $\sqrt{\sigma_n} \approx \sqrt{2}\mathcal{N}$, and the most significant part of the spectrum corresponds to the values $n \gg 1$. Using the Laplace–Heine asymptotical formula for the Legendre polynomial [283]

$$P_n(z) \approx \frac{\left(z + \sqrt{z^2 - 1}\right)^{n+1/2}}{\sqrt{2\pi n}(z^2 - 1)^{1/4}}, \quad n \gg 1$$

one can simplify (151) for the fixed values of the invariant variances u and v as

$$f(n) \approx \frac{1}{\sqrt{\pi n(v - u)}} \left(\frac{2v - 1}{2v + 1}\right)^{n+1/2} \tag{152}$$

provided the positive difference $v - u$ is not too small. Another approximate formula can be used if $v \gg 1$ but $u \sim 1$:

$$f(n) \approx \frac{\sqrt{2}(2u - 1)^{n/2}}{\sqrt{v}(2u + 1)^{(n+1)/2}} e^{-n/(2v)} P_n\left(\frac{2u}{\sqrt{4u^2 - 1}}\right), \quad n \ll 8v^2 \tag{153}$$

The first and second derivatives of the generating function (146) at $z = 1$ yield the first two moments of the photon distribution (hereafter we suppress subscript m)

$$\bar{n} = \frac{1}{2}(u + v - 1), \quad \sigma_n \equiv \overline{n^2} - (\bar{n})^2 = \frac{1}{4}\left(2u^2 + 2v^2 - 1\right) \tag{154}$$

which result in the Mandel parameter [284]

$$Q \equiv \frac{\sigma_n}{\bar{n}} - 1 = \frac{u^2 + v^2 - u - v + \frac{1}{2}}{u + v - 1} \tag{155}$$

This parameter appears positive for all values of τ, so the photon statistics is super-Poissonian, with strong bunching of photons (the pair creation of photons in the NSCE was discussed elsewhere [142,198,200,213]). In particular,

$$Q_{2m+1}(\tau \to 0) \approx \left[\frac{(m+1)(2m-1)!!}{m!}\right]^2 \frac{\tau^{2m}}{2m+1}, \quad Q_1(0) = 1,$$

whereas $Q_m \approx V_m(\tau) \gg 1$ for $\tau \gg 1$ (if $\gamma \ll 1$).

VII. ENERGY AND FORMATION OF PACKETS

A. Energy Density

The mean value of the energy density operator in one space dimension

$$\hat{W}(x,t) = \frac{1}{8\pi}\left[\left(\frac{\partial \hat{A}}{\partial t}\right)^2 + \left(\frac{\partial \hat{A}}{\partial x}\right)^2\right] \tag{156}$$

at $t \geq T$ equals (hereafter we assume $L_0 = 1$, i.e. $\omega_1 = \pi$)

$$\tilde{W}(x,t) = \pi \sum_{m,j=1}^{\infty} \sqrt{mj}\Big\{\cos[\pi(m+j)x]\mathrm{Re}[\langle \hat{a}_m \hat{a}_j\rangle e^{-i\pi(m+j)t'}] + \frac{1}{2}\cos[\pi(m-j)x][\langle \hat{a}_m^\dagger \hat{a}_j\rangle e^{i\pi(m-j)t'} + \langle \hat{a}_m \hat{a}_j^\dagger\rangle e^{-i\pi(m-j)t'}]\Big\} \tag{157}$$

where the quantum mechanical averaging $\langle\cdots\rangle$ is performed over the initial state of the field (the Heisenberg picture) and $t' \equiv t + \delta T$.

1. Regularization and Casimir's Energy

Because of the commutation relations $[\hat{a}_m, \hat{a}_j^\dagger] = \delta_{mj}$, the series (157) contains the vacuum divergent "diagonal" part with $m = j$:

$$\tilde{W}^{(\mathrm{vac})} = (\pi/2)\sum_{m=1}^{\infty} m \exp(-i\pi m t' + i\pi m t') \tag{158}$$

The recipe for regularizing this divergence was given by Fulling and Davies [81]. One should write the first term in the argument of the exponential in (158) as it stands, but to replace t' in the second term by $t' + i\eta$, $\eta > 0$ (this is the so-called point-splitting method). Then the sum becomes convergent, giving

$$\tilde{W}^{(\mathrm{vac})}(\eta) = (\pi/2)\sum_{m=1}^{\infty} m e^{-m\pi\eta} = (\pi/8)\left[\sinh\left(\frac{\pi\eta}{2}\right)\right]^{-2}$$

The Taylor expansion of this function reads $\tilde{W}^{(\mathrm{vac})}(\eta) = (2\pi\eta^2)^{-1} - \pi/24 + \mathcal{O}(\eta^2)$. According to [81], one should remove the divergent term $(2\pi\eta^2)^{-1}$ and after that proceed to the limit $\eta \to 0$. This limit value gives us the known expression for the one-dimensional negative vacuum Casimir energy [81,117–120] (which does not depend on the coordinate x in the case involved):

$$\tilde{W}^{(\mathrm{Cas})} = \frac{-\pi}{24} \quad \left(\text{or} -\frac{\pi\hbar c}{24L_0^2} \text{ in the dimensional units}\right) \tag{159}$$

Extracting this vacuum energy from $\tilde{W}$, we arrive at the expression

$$\begin{aligned} W \equiv \tilde{W} - \tilde{W}^{(\mathrm{Cas})} = \pi \sum_{m,j=1}^{\infty} \sqrt{mj}\,\mathrm{Re}[\langle \hat{a}_m \hat{a}_j\rangle \cos[\pi(m+j)x] e^{-i\pi(m+j)t'} \\ + \langle \hat{a}_m^\dagger \hat{a}_j\rangle \cos[\pi(m-j)x] e^{i\pi(m-j)t'}] \end{aligned} \tag{160}$$

The same expression (160) can be obtained if one calculates the mean value of the *normally ordered* (with respect to the operators $\hat{a}_n^\dagger$ and $\hat{a}_n$) counterpart of the operator (156) [164]. Then the total energy (without the vacuum part) assumes the usual form

$$\mathscr{E} = \int_0^{L_0} W(x,t)\,dx = \sum_{n=1}^{\infty} \omega_n \langle \hat{a}_n^\dagger \hat{a}_n\rangle \tag{161}$$

which justifies the choice of the normalization in (12) and (21).

Since the initial quantum state was defined with respect to the "in" operators $\hat{b}_n^\dagger$ and $\hat{b}_n$, we must express the "out" operators $\hat{a}_m^\dagger$ and $\hat{a}_m$ in terms of $\hat{b}_n^\dagger$ and $\hat{b}_n$

by means of formula (22). Thus we arrive at the expression containing a combination of the mean values $\langle \hat{b}_n \hat{b}_k \rangle$, $\langle \hat{b}_n^\dagger \hat{b}_k^\dagger \rangle$, $\langle \hat{b}_n^\dagger \hat{b}_k \rangle$, and $\langle \hat{b}_n \hat{b}_k^\dagger \rangle$ calculated in the initial quantum state. For the initial vacuum state defined according to the relations $\hat{b}_n|0\rangle = 0$, $n = 1, 2, \ldots$, the only nonzero mean values are $\langle \hat{b}_n \hat{b}_k^\dagger \rangle = \delta_{nk}$. Then (160) is transformed into the triple sum

$$W_0(x,t) = \pi \sum_{n,m,j=1}^{\infty} \frac{mj}{n} \mathrm{Re}\{\cos[\pi(m-j)x] e^{i\pi(m-j)t'} \rho_{-m}^{(n)} \rho_{-j}^{(n)*} - \cos[\pi(m+j)x] e^{i\pi(m+j)t'} \rho_{-m}^{(n)} \rho_{j}^{(n)*}\} \tag{162}$$

Evidently, $W_0(x,t) = 0$ for $t \leq 0$. For an arbitrary initial state the energy density can be written as a sum of the "vacuum" and "nonvacuum" contributions

$$W = W_0 + W_1, \quad W_1 = \pi \sum_{n,k=1}^{\infty} \frac{1}{\sqrt{nk}} \mathrm{Re}[\langle \hat{b}_n \hat{b}_k \rangle B^{(nk)} + \langle \hat{b}_n^\dagger \hat{b}_k \rangle \tilde{B}^{(nk)}] \tag{163}$$

where

$$B^{(nk)} = \sum_{m,j=1}^{\infty} mj\{\cos[\pi(m+j)x][e^{-i\pi(m+j)t'} \rho_m^{(n)} \rho_j^{(k)} + e^{i\pi(m+j)t'} \rho_{-m}^{(n)} \rho_{-j}^{(k)}] - \cos[\pi(m-j)x][e^{-i\pi(m-j)t'} \rho_m^{(n)} \rho_{-j}^{(k)} + e^{i\pi(m-j)t'} \rho_{-m}^{(n)} \rho_j^{(k)}]\} \tag{164}$$

$$\tilde{B}^{(nk)} = \sum_{m,j=1}^{\infty} mj\{\cos[\pi(m-j)x][e^{-i\pi(m-j)t'} \rho_{-m}^{(n)*} \rho_{-j}^{(k)} + e^{i\pi(m-j)t'} \rho_m^{(n)*} \rho_j^{(k)}] - \cos[\pi(m+j)x][e^{-i\pi(m+j)t'} \rho_{-m}^{(n)*} \rho_j^{(k)} + e^{i\pi(m+j)t'} \rho_m^{(n)*} \rho_{-j}^{(k)}]\} \tag{165}$$

Changing the summation index $j \to -j$ in the first term of (162), we can write

$$W_0(x,t) = -\pi \mathrm{Re} \sum_{n=1}^{\infty} \sum_{m=1}^{\infty} \sum_{j=-\infty}^{\infty} \frac{mj}{n} \cos[\pi(m+j)x] e^{i\pi(m+j)t'} \rho_{-m}^{(n)} \rho_j^{(n)*}$$

Similarly, changing the indices $m \to -m$ or $j \to -j$ in (164) and (165), we can reduce four sums with apparently different summands and the indices running from 1 to ∞ to the unified sums whose two indices run from $-\infty$ to ∞:

$$B^{(nk)} = \sum_{m,j=-\infty}^{\infty} mj \cos[\pi(m+j)x] e^{-i\pi(m+j)t'} \rho_m^{(n)} \rho_j^{(k)}$$

$$\tilde{B}^{(nk)} = \sum_{m,j=-\infty}^{\infty} mj \cos[\pi(m-j)x] e^{i\pi(m-j)t'} \rho_m^{(n)*} \rho_j^{(k)}$$

Now, replacing the cosine function by the sum of two imaginary exponentials, we see that $W(x,t)$ is actually the sum of two identical functions of the light-cone variables:

$$W(x,t) = \frac{\pi}{2}[F(u;\tau) + F(v;\tau)], \quad u = t' + x, \quad v = t' - x \tag{166}$$

where

$$F = F_0 + \sum_{n,k=1}^{\infty} \frac{1}{\sqrt{nk}} \mathrm{Re}[\langle \hat{b}_n \hat{b}_k \rangle F^{(nk)} + \langle \hat{b}_n^\dagger \hat{b}_k \rangle \tilde{F}^{(nk)}] \tag{167}$$

$$F_0(u;\tau) = -\mathrm{Re} \sum_{n=1}^{\infty} \sum_{m=1}^{\infty} \sum_{j=-\infty}^{\infty} \frac{mj}{n} e^{i\pi(m+j)u} \rho_{-m}^{(n)}(\tau) \rho_j^{(n)*}(\tau) \tag{168}$$

$$F^{(nk)}(u;\tau) = \sum_{m=-\infty}^{\infty} \sum_{j=-\infty}^{\infty} mje^{-i\pi(m+j)u} \rho_m^{(n)}(\tau) \rho_j^{(k)}(\tau) \tag{169}$$

$$\tilde{F}^{(nk)}(u;\tau) = \sum_{m=-\infty}^{\infty} \sum_{j=-\infty}^{\infty} mje^{i\pi(m-j)u} \rho_m^{(n)*}(\tau) \rho_j^{(k)}(\tau) \tag{170}$$

The extra argument τ in the preceding expressions is introduced in order to emphasize that the energy density depends not only on the value of the current time variable t [which must satisfy the condition $t > (1+\delta)T$] but also on the moment of time T when the wall stopped moving. It is worth mentioning that the variables t and τ are independent, as are u and τ or v and τ.

Evidently, the double sums (169) and (170) are factorized to the products of independent sums over m and j:

$$F^{(nk)}(u;\tau) = G^{(n)}(u;\tau) G^{(k)}(u;\tau), \quad \tilde{F}^{(nk)}(u;\tau) = G^{(n)*}(u;\tau) G^{(k)}(u;\tau)$$

$$G^{(n)}(u;\tau) = \sum_{m=-\infty}^{\infty} me^{-i\pi mu} \rho_m^{(n)}(\tau) = \frac{i}{\pi} \frac{\partial}{\partial u} \sum_{m=-\infty}^{\infty} e^{-i\pi mu} \rho_m^{(n)}(\tau) \tag{171}$$

The last sum in (171) can be easily expressed in terms of the generating function (74) if one writes $n = j + kp$, $m = j + lp$, and $z = \exp(-i\pi pu)$. Thus we obtain

$$G^{(n)}(u;\tau) = \left. \frac{nz[zg(p\tau) + \sigma S(p\tau)]^{n/p-1}}{[g^*(p\tau) + z\sigma S(p\tau)]^{n/p+1}} \right|_{z=\exp(-i\pi pu)} = nf^{1/2} \Lambda^{n/p} \tag{172}$$

where

$$f(u;\kappa) = |g^*(p\tau) + z\sigma S(p\tau)|^{-4} = \frac{(1-\kappa^2)^2}{[1+\kappa^2+2\sigma\kappa\cos(p\pi u-\varphi)]^2} \tag{173}$$

$$\Lambda = \frac{zg(p\tau)+\sigma S(p\tau)}{g^*(p\tau)+z\sigma S(p\tau)} = e^{i(2\varphi-\pi pu)}\frac{1+\sigma\kappa\exp[i(\pi pu-\varphi)]}{1+\sigma\kappa\exp[i(\varphi-\pi pu)]} \tag{174}$$

$$\kappa = \frac{S(p\tau)}{\sqrt{1+S^2(p\tau)}}, \quad \exp(i\varphi) = \sqrt{1-\gamma^2\kappa^2} + i\gamma\kappa$$

In the "vacuum" contribution (168) we have some asymmetry between the indices m and j, since m runs from 1 to ∞, whereas j runs from $-\infty$ to ∞. This asymmetry can be eliminated if one differentiates both sides of equation (168) with respect to the independent variable τ at a fixed value of u and performs the summation over the superscript n with the aid of the recurrence relations (87) and (88). It is easy to verify that all the summands with $n \geq p$ are canceled, so the infinite series over n can be reduced to the finite sum from 1 to $(p-1)$:

$$\frac{\partial F_0(u;\tau)}{\partial\tau} = -\sigma\mathrm{Re}\sum_{n=1}^{p-1}\sum_{m=1}^{\infty}\sum_{j=-\infty}^{\infty} mj\, e^{i\pi(m+j)u} \times [\rho_{-m}^{(n)}(\tau)\rho_{-j}^{(p-n)}(\tau) + \rho_m^{(p-n)*}(\tau)\rho_j^{(n)*}(\tau)] \tag{175}$$

Changing the summation indices $m \to -m$, $j \to -j$, $n \to p-n$ in the first product inside the square brackets, one can reduce two sums in the right-hand side of (175) to the single series where both the indices m and j run from $-\infty$ to ∞. Moreover, the sums over m and j become completely independent, giving rise to the equation

$$\frac{\partial F_0(u;\tau)}{\partial\tau} = -\sigma\mathrm{Re}\sum_{n=1}^{p-1} G^{(n)}(u;\tau)G^{(p-n)}(u;\tau) \tag{176}$$

where $G^{(n)}(u;\tau)$ is given by (171). As a result of (172), the sum in the right-hand side of (176) is reduced to the sum $\sum_{n=1}^{p-1} n(p-n) = \frac{1}{6}p(p^2-1)$. Introducing the variable $\eta = \exp(2ap\tau)$, we obtain the explicit expression

$$\frac{\partial F_0(u;\eta)}{\partial\eta} = -\frac{(p^2-1)a^4\eta[\eta^2(1+\alpha+\beta)+\alpha-\beta-1]}{12[\eta^2(1+\alpha+\beta)-2\eta(\gamma^2+\beta)+1+\beta-\alpha]^3} \tag{177}$$

where $\alpha = \sigma a\cos(p\pi u)$ and $\beta = \sigma\gamma\sin(p\pi u)$. Integrating (177) with the initial condition $F_0 = 0$ at $\tau = 0$ (or $\eta = 1$), we arrive after some algebra at the simple

expression

$$F_0(u;\kappa) = \mathscr{B}[f(u;\kappa) - 1], \quad \mathscr{B} \equiv \frac{p^2 - 1}{24} \tag{178}$$

where function $f(u;\kappa)$ is given by (176). Finally, we obtain the following expression for the function $F(u;\tau)$ defined by Eq. (166):

$$F = -\mathscr{B} + f(u;\tau)\left\{\mathscr{B} + \sum_{n,k=1}^{\infty} \sqrt{nk}\,\mathrm{Re}[\langle \hat{b}_n \hat{b}_k\rangle \Lambda^{(n+k)/p} + \langle \hat{b}_n^\dagger \hat{b}_k\rangle \Lambda^{(k-n)/p}]\right\} \tag{179}$$

In the special case of the initial states whose density matrix is diagonal in the Fock basis, so that $\langle \hat{b}_n^\dagger \hat{b}_k\rangle = \nu_n \delta_{nk}$ and $\langle \hat{b}_n \hat{b}_k\rangle = 0$ (e.g., the Fock or thermal states; ν_n is the mean number of quanta in the nth mode), the sum in (179) is proportional to the initial total energy $\mathscr{E}_0$ in all the modes (above the Casimir level):

$$F^{(\mathrm{diag})}(u;\tau) = -\mathscr{B} + f(u;\tau)[\mathscr{B} + \mathscr{N}_0] \tag{180}$$

$$\mathscr{N}_0 = \sum_{n=1}^{\infty} n\nu_n = \frac{\mathscr{E}_0}{\pi} \equiv \frac{\mathscr{E}_0}{\hbar\omega_1}$$

B. Packet Formation

Now let us analyze the expressions for the energy density obtained above. For the initial vacuum state we see immediately from equations (173) and (178) that in the generic case the function $W_0(x,t)$ with the fixed value of the "fast time" t has p peaks in the interval $0 \le x \le 1$, whose positions are determined by the equations $\sigma\cos(p\pi u - \varphi) = -1$ and $\sigma\cos(p\pi v - \varphi) = -1$. Obviously, for $t > T$ the energy density is a periodic function of the time variable t, with the period $\Delta t = 1$ if p is an even number and $\Delta t = 2$ if p is odd.

For the even values of the resonance multiplicity p, we have $p/2$ peaks moving (with the light speed) in the positive direction and $p/2$ peaks moving in the negative direction. If p is odd, then the numbers of peaks of each kind differ by 1. All the peaks have the same height

$$W_{\max}^{(\mathrm{vac})} = \frac{2\pi\mathscr{B}\kappa}{(\kappa - 1)^2} = \frac{\pi}{2}\mathscr{B}\left(e^{4p\tau} - 1\right) \tag{181}$$

(in this section the expressions containing τ are related to the special case of the strict resonance $\gamma = 0$), except for some distinguished instants of time when two

peaks moving in the opposite directions merge, forming a peak with double the height.

If $\kappa \to 1$ (i.e., $\tau > 1$ and $\gamma < 1$), then the energy density can be approximated in the vicinity of each peak by the Lorentz-like distribution

$$W^{(\mathrm{vac})}(\delta x) = \frac{W_{\max}^{(\mathrm{vac})}}{\left[1 + \left(2\delta x/\Delta_{1/4}\right)^2\right]^2} \tag{182}$$

where the width

$$\Delta_{1/4} = \frac{2}{p\pi}\frac{1-\kappa}{\sqrt{\kappa}} \approx \frac{4}{p\pi}e^{-2p\tau}$$

of each peak is defined as the double distance between the position of the maximum and the point where the energy density decreases 4 times. One can also introduce the "energy width" of each peak by means of the relation $W_{\max}\Delta_E = \mathscr{E}(\tau)/p$. For $\kappa \to 1$, we obtain

$$\Delta_E \approx \frac{1-\kappa}{2\pi p} \approx (\pi p)^{-1}e^{-2p\tau}$$

Except for narrow regions of the length $\Delta_+ \approx (\pi p)^{-1}\sqrt{1-\kappa} \approx \sqrt{2}(\pi p)^{-1}e^{-p\tau}$ nearby the peaks the "dynamical" energy density is less than its initial vacuum value, in agreement with other results [112,164,165,168] obtained in the framework of different approaches. The minimum values of W_0 far off peak are given by [taking into account the contributions of both the functions $F_0(u)$ and $F_0(v)$]

$$W_{\min} = -4\pi\mathscr{B}\frac{\kappa}{(\kappa+1)^2} = \pi\mathscr{B}\left(e^{-4p\tau} - 1\right) \tag{183}$$

If $\kappa \to 1$, $W_{\min} \to -\pi(p^2-1)/24$. Adding to this expression the initial Casimir energy (159), we obtain the total asymptotical minimum value [164]

$$\tilde{W}_{\min}^{(\mathrm{as})} = \frac{-\pi p^2}{24} \tag{184}$$

For an arbitrary initial state the energy density has, besides the "vacuum" part, the additional terms given in Eq. (179). Since these terms are proportional to the same functions $f(u;\kappa)$ or $f(v;\kappa)$, which determine the structure of the "vacuum" part, the positions of the peaks are not changed (remember that $|\Lambda| = 1$). For the initial states with diagonal density matrices in the Fock basis

(in particular, for the thermal states) all the peaks still have equal heights, increased by the quantity $\Delta W_{\max} = \frac{1}{2}\mathscr{E}_0(1+\kappa)^2/(1-\kappa)^2$, compared with the vacuum case. However, the asymptotical *minimal* value of the energy density at $\kappa \to 1$ does not depend on the initial state, as it is given by formula (184) for all the cases.

If the initial density matrix in the Fock basis has nonzero off-diagonal elements (as occurs, in particular, for any pure state different from the Fock one, e.g., for the coherent states), different terms in the sum (179) can interfere. As a consequence, the peaks acquire some kind of "fine structure." For example, if only the first mode was excited initially in the coherent state $|\alpha\rangle$, $\alpha = |\alpha|\exp(i\psi)$, then for $p = 2$ and $\gamma = 0$ (the strict resonance), we have

$$\Delta W \equiv W - W^{(\mathrm{vac})} = \pi|\alpha|^2 \frac{(1-\kappa^2)^2[\kappa\sin(z+\psi) + \sin(z-\psi)]^2}{[(1-\kappa)^2 + 4\kappa\sin^2 z]^3}$$

where $z \equiv \pi(u - u_*)$ and u_* is the position of the vacuum peak determined above. If $\psi = \pi/2$, then we have the high maximum $\Delta W_{\pi/2}^{\max} = \pi|\alpha|^2(1+\kappa)^2/(1-\kappa)^2$ at $z = 0$. However, if $\psi = 0$, then instead of a maximum, we have the minimum $\Delta W = 0$ at the same point $z = 0$, and the peak is split in two symmetric humps with equal maximal heights $\Delta W_0^{\max} = ([1+\kappa]^2/27\kappa)\Delta W_{\pi/2}^{\max}$ located at the points $\sin z = \pm(1-\kappa)/\sqrt{8\kappa}$. In the intermediate case $0 < \psi < \pi/2$ asymmetric forms of the peaks are observed. If $p > 2$ or several modes were excited initially, the interference between different terms in (179) can result in different heights of the peaks and more complicated fine structures [provided $\langle \hat{b}_n \hat{b}_k \rangle \neq 0$ for some n and k].

If the detuning γ is different from zero, then some deformations of the form of peaks are observed, although the maximal heights are still of the same order of magnitude as in the case $\gamma = 0$, as far as $\gamma \leq 1$. But if the detuning exceeds the critical value $\gamma = 1$, the energy becomes an oscillating function of the "slow time" τ, where the amplitude of oscillations is proportional to approximately $(\gamma^2 - 1)^{-1}$ [191,192]. The peaks become rather wide and low, since the parameter κ is limited by the inequality $\kappa \leq \gamma^{-1}$ if $\gamma > 1$. The illustrations can be found in Ref. 193.

Since the components of the energy-momentum tensor T_{00} and T_{11} are given by similar expressions in the case of single space dimension, the force acting on each wall has the same time dependence as the energy density at the points $x = 0$ and $x = 1$. For the most part of time during the period of field oscillations $2L_0/c$ (where L_0 is the distance between the walls at rest), this force is negative, as it is less than the static Casimir force, with the maximal amplification coefficient p^2. However, the average value of the force over the period is positive because of the creation of real photons inside the cavity.

If the walls possess some small transmission coefficient, then a small part of radiation accumulated inside the cavity can leave it. In this case one could observe sharp pulses of radiation outside the cavity [210], whose amplitudes must be proportional to the heights of the peaks inside the cavity multiplied by the small transmission coefficient. The intensity of these pulses can be significantly increased, if the initial state is different from vacuum and possesses sufficient energy, such as thermal states [210,211] or coherent states. However, to describe the form of the pulses exactly, it is necessary to develop a more general theory that would account for the boundary conditions corresponding to the partially transmitting walls (because the nonzero transmission coefficient can change significantly the pulse shape, just as the nonzero detuning deformed the form of packets in the examples considered above).

C. Total Energy

The total energy (161) of the field inside the cavity (above the initial Casimir level) can be obtained by integrating the density $W(x)$ (166) over x. The contribution of the vacuum [function F_0 in (167)] and 'diagonal' terms (given by the partial sum in (167) over $n = k$) can be calculated with the aid of the formula

$$\int_0^{\pi} \frac{dx}{(a + b\cos x)^2} = \frac{\pi a}{(a^2 - b^2)^{1/2}}$$

To find the contribution of "nondiagonal" terms ($n \neq k$), it is convenient to replace the integration over x by the integration in the complex z plane ($z = \exp[-i\pi p u]$ or $z = \exp[-i\pi p v]$) over the circle $|z| = 1$. One can check that this circle is passed p times when x goes from 0 to 1 (if one takes into account both the u and v contributions). It turns out that the integrals of the "nondiagonal" terms are different from zero if and only if the corresponding integrands in the z plane have simple poles inside the circle $|z| = 1$. This occurs only when $k + n = p$ in the first term inside the square brackets in (179) and $k - n = p$ in the second term inside the same brackets.

Finally we obtain a simple expression

$$\mathscr{E}(\tau) = \mathscr{E}_0 + 2S^2(p\tau)\left[\mathscr{E}_0 + \pi\mathscr{B} + \frac{\gamma\sigma}{2}\mathrm{Im}(\mathscr{G})\right] - \frac{\sigma}{2}S(2p\tau)\mathrm{Re}(\mathscr{G}) \tag{185}$$

where

$$\mathscr{G} = 2\pi\sum_{n=1}^{\infty}\sqrt{n(n+p)}\langle\hat{b}_n^{\dagger}\hat{b}_{n+p}\rangle + \pi\sum_{n=1}^{p-1}\sqrt{n(p-n)}\langle\hat{b}_n\hat{b}_{p-n}\rangle \tag{186}$$

[if $p = 1$, the last sum in (186) should be replaced by zero]. Formula (185) was found for the first time in a different way by Dodonov [191]. In particular, for the initial vacuum state of field we have

$$\mathscr{E}^{(\mathrm{vac})}(\tau) = \frac{p^2 - 1}{12a^2}\sinh^2(pa\tau) \tag{187}$$

The total energy increases exponentially at $\tau \to \infty$, provided $\gamma < 1$. In the special case $\gamma = 0$ such asymptotic behavior of the total energy was obtained also in the frameworks of other approaches in [164–166,177]. Here we have found the explicit dependence of the total energy on time in the whole interval $0 \le \tau < \infty$, as well as a nontrivial dependence on the initial state of field, which is contained in the constant parameter $\mathscr{G}$. This parameter is equal to zero for initial Fock or thermal states of the field. However, in a generic case $\mathscr{G} \neq 0$, and it can affect significantly the total energy, if $\mathscr{E}(0) \gg 1$. Consider, for example, the case $p = 2$. If initially the first mode ($n = 1$) was in the coherent state $|\alpha\rangle$ with $\alpha = |\alpha|e^{i\phi}$, $|\alpha| \gg 1$, and all other modes were not excited, then $\mathscr{E}(0) = |\alpha|^2$, $\mathscr{G} = \alpha^2$, so for $\tau \gg 1$ and $\gamma = 0$ (exact resonance) we have $\mathscr{E}(\tau \gg 1) \approx \frac{1}{4}|\alpha|^2 e^{4\tau}[2 - \cos(2\phi)]$. The maximal value of the energy in this case is 3 times greater than the minimal one, depending on the phase ϕ.

According to (185), the initial stage of the evolution does not depend on the detuning parameter γ for all states that yield $\mathrm{Im}(\mathscr{G}) = 0$, since at $\tau \to 0$ one has

$$\mathscr{E}(\tau) \approx \mathscr{E}(0) - \sigma\mathrm{Re}(\mathscr{G})p\tau + 2\left[\mathscr{E}(0) + \frac{p^2 - 1}{24} + \frac{\gamma\sigma}{2}\mathrm{Im}(\mathscr{G})\right](p\tau)^2 \tag{188}$$

Formula (188) is *exact* in the case of $\gamma = 1$.

If $\gamma > 1$, then one should replace each function $\sinh(ax)/a$ in (185) by its trigonometrical counterpart $\sin(\tilde{a}x)/\tilde{a}$ [see Eq. (54)]. In this case the total energy *oscillates* in time with the period $\pi/(p\tilde{a})$, returning to the initial value at the end of each period. For a large detuning $\gamma \gg 1$ the amplitude of oscillations decrease as γ^{-1} if $\mathrm{Re}\mathscr{G} \neq 0$ and as γ^{-2} otherwise.

Note that the total vacuum and nonvacuum energies increase exponentially with time, if $\gamma < 1$ and $\tau > 1$, whereas the total number of photons increases only as τ^2 and τ, respectively, under the same conditions. The origin of such a great difference in the behaviors of the total energy and the total number of photons becomes clear if one looks at the asymptotic formulas (102)–(104). They show that the rate of photon generation in the mth completely excited mode decreases approximately as $\dot{\mathscr{N}}_m \sim 1/m$ (except the modes whose numbers are multiples of p), so the stationary rate of the *energy* generation $\dot{\mathscr{E}}_m = m\dot{\mathscr{N}}_m$ asymptotically almost does not depend on m. In turn, the number of the effectively excited modes increases in time exponentially. These two

factors lead to the exponential growth of the total energy (see also Ref. 163 in the special case $\gamma = 0$).

VIII. THREE-DIMENSIONAL NONDEGENERATE CAVITY

A. Empty Cavity

Now let us proceed to the three-dimensional case. For definiteness we choose a rectangular cavity with dimensions L_x, L_y, L_z (briefly designated by symbol $\{L\}$). If these dimensions do not depend on time, each field mode is determined by three integers m, n, l, responsible for the eigenfrequency

$$\omega_{mnl} = \pi \left[\left(\frac{m}{L_x}\right)^2 + \left(\frac{n}{L_y}\right)^2 + \left(\frac{l}{L_z}\right)^2 \right]^{1/2} \tag{189}$$

and by two orthogonal directions of polarization. In order to simplify the exposition and to get rid of extra unessential indices, let us consider the case when $L_z \ll L_x \sim L_y$. Then the frequencies with $l \neq 0$ are much greater than those with $l = 0$. It is clear that the interaction between low- and high-frequency modes in the nonstationary case is weak. Consequently, studying the excitation of the *lowest modes*, we may confine ourselves to the case of $l = 0$. Then the only possible polarization of the vector potential is along z axis, so the low-frequency part of the *Heisenberg field operator* at $t < 0$ reads

$$\hat{A}_z(x, y, t < 0) = \sum_{\mathbf{n}} \left(\frac{2\pi}{\omega_{\mathbf{n}}}\right)^{1/2} \psi_{\mathbf{n}}(x, y|\{L\}) \left[\hat{b}_{\mathbf{n}} e^{-i\omega_{\mathbf{n}} t} + \hat{b}^{\dagger}_{\mathbf{n}} e^{i\omega_{\mathbf{n}} t}\right] \tag{190}$$

The difference from the similar expression (12) is that now the suffix n is replaced by its "vector" counterpart $\mathbf{n} = (m, n)$, and the function $\psi_{\mathbf{n}}(x, y|\{L\})$ depends on two space coordinates:

$$\psi_{\mathbf{n}}(x, y|\{L\}) = 2\left(L_x L_y L_z\right)^{-1/2} \sin\frac{m\pi x}{L_x} \sin\frac{n\pi y}{L_y}$$

The coefficients in Eq. (190) are chosen again to correspond to the standard form of the field Hamiltonian (13).

Now let the dimension L_x to depend on time according to the given law $L(t)$. To satisfy the boundary conditions

$$A_z|_{x=0} = A_z|_{x=L(t)} = A_z|_{y=0} = A_z|_{y=L_y} = 0$$

we write the field operator at $t > 0$ in the same functional form (190), but with the time-dependent parameter $L(t)$:

$$\hat{A}_z(x, y, t) = 2\sqrt{\pi} \sum_{\mathbf{n}} \psi_{\mathbf{n}}(x, y|L(t), L_y)\hat{Q}_{\mathbf{n}}(t) \tag{191}$$

In the stationary case the operators $\hat{Q}_{\mathbf{n}}(t)$ coincide with the (coordinate) quadrature components of the field mode operators. Putting (191) into the wave equation

$$\frac{\partial^2 A_z}{\partial t^2} - \Delta A_z = 0$$

we arrive at the equation exactly resembling Eq. (18):

$$\begin{aligned} \ddot{Q}_{\mathbf{k}}^{(\mathbf{n})} + \omega_{\mathbf{k}}^2(t) Q_{\mathbf{k}}^{(\mathbf{n})} &= 2\lambda(t) \sum_{\mathbf{j}} g_{\mathbf{kj}} \dot{Q}_{\mathbf{j}}^{(\mathbf{n})} + \dot{\lambda}(t) \sum_{\mathbf{j}} g_{\mathbf{kj}} Q_{\mathbf{j}}^{(\mathbf{n})} \\ &\quad + \lambda^2(t) \sum_{\mathbf{jl}} g_{\mathbf{jk}} g_{\mathbf{jl}} Q_{\mathbf{l}}^{(\mathbf{n})} \end{aligned} \tag{192}$$

Now $\lambda(t) = \dot{L}(t)/L(t)$, all the indices are "2-vectors," the frequencies are given by Eq. (189) with $l = 0$ and $L(t)$ instead of L_x, and the *constant* numerical coefficients $g_{\mathbf{kj}}$ are given by the integrals

$$g_{\mathbf{kj}} = L \int_0^L dx \int_0^{L_y} dy \int_0^{L_z} dz\, \psi_{\mathbf{j}}(\mathbf{r}|L) \frac{\partial \psi_{\mathbf{k}}(\mathbf{r}|L)}{\partial L}$$

The explicit form of two-dimensional coefficients $g_{\mathbf{kj}}$ is more complicated than a simple formula (19). However, these coefficients remain antisymmetrical: $g_{\mathbf{kj}} = -g_{\mathbf{jk}}$, due to the normalization of functions $\psi_{\mathbf{k}}$,

$$\int_0^{\{L\}} d\mathbf{r}\, \psi_{\mathbf{m}} \psi_{\mathbf{n}} = \delta_{\mathbf{mn}}$$

and due to zero boundary conditions at $x = L$. (Moreover, they do not depend on the cavity dimensions.)

Although we use the same notation as in the 1D case, the operators $\hat{Q}_{\mathbf{n}}(t)$ in Eq. (191) differ from their analogs in a similar decomposition (17). Now $\hat{Q}_{\mathbf{n}}(t)$ means the Hermitian operator coinciding with the ("coordinate") *quadrature component* of the field mode operator.

Suppose for simplicity that the wall oscillates at twice the eigenfrequency of some unperturbed mode

$$L(t) = L_0[1 - \epsilon_L \cos(2\omega_{\mathbf{m}} t)], \quad |\epsilon_L| \ll 1$$

and let us look for the solution to Eq. (192) in the form

$$Q_{\mathbf{k}}(t) = \xi_{\mathbf{k}}(\epsilon_L t)\exp(-i\omega_{\mathbf{k}}t) + \eta_{\mathbf{k}}(\epsilon_L t)\exp(i\omega_{\mathbf{k}}t) \tag{193}$$

[we have omitted "hats" (inverted carets) over operators]. Contrary to the one-dimensional case, now *all the terms* on the right-hand side of Eq. (192) disappear after averaging over fast oscillations, since the spectrum $\omega_{\mathbf{j}}$ *is not equidistant*. Indeed, the first and the second sums on the right-hand side do not contain functions $Q_{\mathbf{k}}$ because of the antisymmetricity of coefficients $g_{\mathbf{kj}}$, whereas the last sum is proportional to $\lambda^2 \sim \epsilon_L^2$. Consequently, after multiplication by the proper exponential functions, the right-hand side will consist of the terms containing the factors such as $\exp(i[\pm\omega_{\mathbf{j}} \pm \omega_{\mathbf{k}} \pm 2\omega_{\mathbf{m}}]t)$ with $\mathbf{j} \neq \mathbf{k}$. After averaging all these terms turn into zero. [Strictly speaking, the frequency spectrum (189) contains the "equidistant subset," corresponding to the indices m, n, l multiplicated by the same integral factors. However, this fact does not change the conclusion, because the "coupling constants" $g_{\mathbf{kj}}$ between such modes are equal to zero.]

Consequently, in the *resonance case* the field problem is reduced [188,189] to that of a one-dimensional parametric oscillator with the time dependence of the eigenfrequency in the form

$$\omega(t) = \omega_0[1 + 2\tilde{\varepsilon}\cos(2\omega_0 t)] \tag{194}$$

where $\omega_0 \equiv \omega_{mn}$ is the unperturbed eigenfrequency of the resonance mode. Here the frequency modulation depth $\tilde{\varepsilon}$ is related to the cavity length modulation depth ϵ_L as follows:

$$\tilde{\varepsilon} = \frac{1}{2}\epsilon_L\left[1 + \left(\frac{nL_0}{mL_y}\right)^2\right]^{-1/2}$$

We use the notation $\tilde{\varepsilon}$ to avoid confusion between the dimensionless modulation parameters in the one-dimensional and three-dimensional cases.

At this point we may abandon the Heisenberg picture and proceed to the Schrödinger representation. Of course, both representations are equivalent, as soon as the field problem has been reduced to studying a finite-dimensional quantum system. However, the most of numerous investigations of the time-dependent quantum oscillator, since Husimi's paper [285], were performed in the Schrödinger picture. So it is natural to use the known results. According to several studies [279,285,286], all the characteristics of the *quantum* oscillator are determined completely by the *complex* solution of the *classical* oscillator equation of motion

$$\ddot{u} + \omega^2(t)u = 0 \tag{195}$$

satisfying the normalization condition

$$\dot{u}u^* - \dot{u}^* u = 2i \tag{196}$$

Let us assume that function $\omega(t)$ takes the constant value ω_0 at $t \leq 0$ and at $t > t_f > 0$. Moreover, it is convenient to choose the initial conditions for u function as follows:

$$u(0) = \frac{1}{\sqrt{\omega_0}}, \quad \dot{u}(0) = i\sqrt{\omega_0} \tag{197}$$

Then the quantum mechanical average number of photons created from the ground state due to the time dependence of the frequency in the interval of time $0 < t < t_f$ is given by the formula

$$\langle n \rangle = \frac{1}{4\omega_0}(|\dot{u}|^2 + \omega_0^2|u|^2) - \frac{1}{2} \tag{198}$$

Looking for the solution of Eq. (195) in the parametric resonance case (194) in the form

$$u(t) = \frac{1}{\sqrt{\omega_0}}\left[\xi(t)e^{i\omega_0 t} + \eta(t)e^{-i\omega_0 t}\right] \tag{199}$$

[the opposite signs in the arguments of the exponential functions in Eqs. (193) and (199) are due to the different representations: the former equation is written in the Heisenberg picture, while the latter – in the Schrödinger one] and using the method of averaging over fast oscillations, one can easily obtain the first-order differential equations for the amplitudes (provided $|\tilde{\varepsilon}| \ll 1$):

$$\dot{\xi} = i\omega_0\tilde{\varepsilon}\eta, \quad \dot{\eta} = -i\omega_0\tilde{\varepsilon}\xi \tag{200}$$

Their solutions satisfying initial conditions (197) (up to the terms of the order of $\tilde{\varepsilon}$) read as [214,287–290]

$$\xi(t) = \cosh(\omega_0\tilde{\varepsilon}t), \quad \eta(t) = -i\sinh(\omega_0\tilde{\varepsilon}t) \tag{201}$$

According to Eqs. (198), (199), and (201), the average number of photons (and the total energy in the cavity) grows in time exponentially:

$$\langle n \rangle = |\eta|^2 = \sinh^2(\omega_0\tilde{\varepsilon}t) \tag{202}$$

It is well known that the initial vacuum state of the oscillator is transformed into the *squeezed vacuum state*, if the frequency depends on time (see, e.g., reviews

in Refs. 223 and 279 and numerous references cited therein). Moreover, looking at Eq. (202), one can immediately recognize the combination $\omega_0\tilde{\varepsilon}t$ as the so-called squeezing parameter. Therefore, the probability of registrating n photons exhibits typical oscillations:

$$\mathscr{P}_{2m} = \frac{[\tanh(\omega_0\tilde{\varepsilon}t)]^{2m}}{\cosh(\omega_0\tilde{\varepsilon}t)} \frac{(2m)!}{(2^m m!)^2}, \quad \mathscr{P}_{2m+1} = 0 \tag{203}$$

This distribution possesses the photon-number variance $\sigma_n = \frac{1}{2}\sinh^2(2\omega_0\tilde{\varepsilon}t)$. Similar formulas for the amount of photons created in a cavity filled with a medium with a time-dependent dielectric permeability (and stationary boundaries) have been found [222]. The quadrature variances change in time as (now $\tau = \tilde{\varepsilon}\omega_0 t$)

$$U = \frac{1}{2}e^{-2\tau}, \quad V = \frac{1}{2}e^{2\tau} \tag{204}$$

An unlimited squeezing can be achieved in this case because of the absence of interaction with other modes.

B. Interaction with a Probe Oscillator inside the Cavity

The situation changes drastically if the field mode is allowed to interact with some detector placed inside the cavity. Following other findings [188,189] we demonstrate the effect in the framework of a simplified model, when a *harmonic oscillator* tuned to the frequency of the resonant mode is placed at the point of maximum of the amplitude mode function $\psi_{mn}(x, y|\{L\})$ in the 3D rectangular cavity.

Assuming the interaction between the oscillator and the field to be described by means of the standard minimal coupling term $-(e/mc)\mathbf{pA}$, we arrive at the following two-dimensional Hamiltonian governing the evolution of the coupled (field oscillator + detector) system:

$$H = \frac{1}{2}\left[P^2 + \omega^2(t)Q^2 + p^2 + \omega_0^2 q^2 - 4\omega_0\kappa pQ\right] \tag{205}$$

Here P, Q are the quadrature components of the field oscillator and p, q are those of the probe oscillator. We neglect the interaction with nonresonant modes, since it is reasonable to suppose that under the resonance conditions their contribution is not essential at $\varepsilon \ll 1$.

In general, the dimensionless coupling coefficient κ must depend on time, due to the decomposition (191). However, since this coefficient is small, its variations of the order of $\varepsilon\kappa$ can be neglected in comparison with the relative variation of the eigenfrequency $\delta\omega/\omega \sim \varepsilon$. So κ is assumed to be constant.

Suppose that the lowest cavity mode is resonant. Then one can evaluate the dimensionless coupling constant as $\kappa \sim (e^2/2\pi mc^2 L)^{1/2}$ (here we return to the dimensional variables). The maximum value of parameter ε is (see the discussion in Section X) $\varepsilon_{\max} \sim \delta_{\max} v_s/2\pi c$, where $\delta_{\max} \sim 0.01$ is the maximal possible relative deformation in the material of the wall, and $v_s \sim 5 \cdot 10^3$ m/s is the sound velocity inside the wall. Then the ratio $\tilde{\varepsilon}/\kappa$ cannot exceed the value $\delta_{\max}\left(mv_s^2 L/8\pi e^2\right)^{1/2} \sim 0.05$ for $L \sim 1$ cm and $m \sim$ the mass of electron (for these parameters $\kappa \sim 2 \cdot 10^{-7}$). Consequently, one may believe that in the real conditions $\tilde{\varepsilon}/\kappa \ll 1$.

In the time-independent case, $\omega(t) = const = \omega_0$, we have two eigenfrequencies

$$\omega_{\pm} = \omega_0(1 \pm \kappa) \tag{206}$$

(provided that $|\kappa| \ll 1$). Let us assume that the wall vibrates exactly at twice the lower frequency ω_-:

$$\omega(t) = \omega_0[1 + 2\tilde{\varepsilon}\cos(2\omega_- t)] \tag{207}$$

Then the lower and upper modes practically do not interact in the limit of $\tilde{\varepsilon} \ll \kappa$.

The Schrödinger equation with Hamiltonian (205) can be solved in the framework of the general theory of multidimensional quantum systems with arbitrary quadratic Hamiltonians, first proposed in 1975 [278] and exposed in detail, for instance, in 1989 [279]. In particular, if both the field and the probe oscillators were initially in their ground states,

$$\psi(Q, q, 0) = \sqrt{\frac{1}{\pi}} \exp\left[-\frac{1}{2}\left(Q^2 + q^2\right)\right] \tag{208}$$

then the wavefunction of the coupled (field + probe oscillator) system at $t > 0$ can be written as [189]

$$\psi(Q, q, t) = \sqrt{\frac{1}{\pi \cosh \mu}} \exp\left(-it - \frac{1}{2}\left[a(t)Q^2 + b(t)q^2 - 2c(t)qQ\right]\right) \tag{209}$$

with the following coefficients:

$$a(t) = 1 + i\tanh\mu e^{-2i\varphi_-} - i\kappa e^{i\Phi}[\tanh\mu e^{-i\Phi}(1 + \tanh\mu \sin\Phi e^{i\varphi}) - \sin\varphi]$$
$$b(t) = 1 - i\tanh\mu e^{-2i\varphi_-} - i\kappa e^{i\Phi}[\tanh\mu e^{-i\Phi}(1 - \tanh\mu \sin\Phi e^{i\varphi}) + \sin\varphi]$$
$$c(t) = \tanh\mu e^{-2i\varphi_-} + i\kappa[1 - \cos\varphi e^{-i\Phi} + i\tanh^2\mu \sin\Phi e^{i(\varphi - 2\Phi)}]$$

Here

$$\Phi = (\omega_+ + \omega_-)t = 2\omega_0 t, \quad \varphi = (\omega_+ - \omega_-)t = 2\omega_0\kappa t = \kappa\Phi$$
$$\mu = \tilde{\varepsilon}\omega_0 t, \quad \Delta = 1 - \cosh\mu\cos\Phi$$

In all the formulas above, the terms of the order of κ^2 were neglected, as well as the terms proportional to $\tilde{\varepsilon}$ (except, of course, the arguments of the hyperbolic functions). Evidently, $\Phi \gg \varphi \gg \mu$. Hereafter we confine our discussion to the most interesting *long-time limit* case, when $\mu \gg 1$. Then all the terms proportional to κ can be neglected, so we can write

$$a(t) = 1 + i\chi, \quad b(t) = 1 - i\chi, \quad c(t) = \chi, \quad \chi = \tanh\mu e^{-2i\varphi_-}$$

Equation (209) shows that the coupled system turns out in a *two-mode squeezed state* at $t > 0$. The properties of this state, as well as of any *Gaussian state* are determined completely by its *covariance matrix*

$$\mathbf{M} = \|\mathscr{M}_{\alpha\beta}\| = \left\| \begin{matrix} \mathbf{M}_{\pi\pi} & \mathbf{M}_{\pi x} \\ \mathbf{M}_{x\pi} & \mathbf{M}_{xx} \end{matrix} \right\|, \qquad \mathscr{M}_{\alpha\beta} = \frac{1}{2}\langle \hat{z}_\alpha \hat{z}_\beta + \hat{z}_\beta \hat{z}_\alpha \rangle$$

where the four-dimensional (in the present case) vector $\mathbf{z}$ is defined as follows: $\mathbf{z} = (\pi, \mathbf{x}) = (P, p, Q, q)$ (evidently, $\langle \mathbf{z} \rangle = 0$ in the case under study). Using the general formulas for multidimensional Gaussian states given elsewhere [279], we have obtained [189] the following explicit expressions for the two-dimensional blocks of matrix $\mathbf{M}$ in the long-time limit $\mu \gg 1$:

$$\mathbf{M}_{\pi\pi} = \frac{1}{2}\cosh^2\mu \left\| \begin{matrix} 1 + \tanh\mu\sin\phi & -\tanh\mu\cos\phi \\ -\tanh\mu\cos\phi & 1 - \tanh\mu\sin\phi \end{matrix} \right\|$$
$$\mathbf{M}_{xx} = \frac{1}{2}\cosh^2\mu \left\| \begin{matrix} 1 - \tanh\mu\sin\phi & \tanh\mu\cos\phi \\ \tanh\mu\cos\phi & 1 + \tanh\mu\sin\phi \end{matrix} \right\|$$
$$\mathbf{M}_{\pi x} = \widetilde{\mathbf{M}}_{x\pi} = \frac{1}{4}\sinh(2\mu) \left\| \begin{matrix} -\cos\phi & -\tanh\mu - \sin\phi \\ \tanh\mu - \sin\phi & \cos\phi \end{matrix} \right\|$$

where $\phi = 2\varphi_-$, and $\widetilde{\mathbf{M}}$ means the transposed matrix. Consequently, there exists a strong correlation between the field and probe oscillators in the long-time limit. For instance, the correlation coefficient between the quadrature components reads as

$$r_{qQ} \equiv \frac{\langle qQ \rangle}{\sqrt{\langle q^2 \rangle \langle Q^2 \rangle}} = \frac{\sinh\mu\cos\phi}{\sqrt{1 + (\sinh\mu\cos\phi)^2}}$$

(If $\phi \approx \pi/2$, this coefficient, as well as other analogous elements of the covariance matrix, does not turn exactly into zero; in such a special case $r_{qQ} \sim \kappa$, due to neglected terms of the order of κ.)

It is clear that the *density matrix* of the probe oscillator [which is obtained from the density matrix of the total system $\rho(Q, q; Q', q') = \psi(Q, q)\psi^*(Q', q')$ by putting $Q = Q'$ and integrating over Q] also has the Gaussian form. Its properties are determined completely by the reduced covariance matrix (it inadvertently coincides with $\mathbf{M}_{xx}$ when $\omega_0 = 1$):

$$\mathbf{M}_{pr} = \frac{1}{2}\cosh^2\mu \begin{Vmatrix} 1 - \tanh\mu\sin\phi & \tanh\mu\cos\phi \\ \tanh\mu\cos\phi & 1 + \tanh\mu\sin\phi \end{Vmatrix} \tag{210}$$

A similar matrix for the field oscillator can be obtained from Eq. (210) by means of changing the sign of parameter μ. As was shown in [280], the photon statistics in Gaussian one-mode states is determined completely by two invariants of the covariance matrix,

$$d = \det\mathbf{M}, \qquad T = \mathrm{Tr}\,\mathbf{M} \tag{211}$$

Evidently, parameter T is twice the energy of quantum fluctuations. The parameter d characterizes the *degree of purity* of the quantum state, due to the relation [277]

$$\mathrm{Tr}\,\hat{\rho}^2 = \frac{1}{2\sqrt{d}} \tag{212}$$

where $\hat{\rho}$ is the statistical operator of the system. The *degree of squeezing*, defined as the minimal possible value of the variance of some quadrature component, normalized by its vacuum value (which is equal to $\hbar/(2m\omega)$ for an oscillator with mass m and frequency ω), is determined jointly by both parameters, T and d, according to the relation [274] [cf. Eq. (100)]

$$s \equiv 2\langle q^2\rangle = T - \sqrt{T^2 - 4d} \tag{213}$$

Both subsystems have identical invariants:

$$T = 4d = \cosh^2\mu$$

so for $\mu \gg 1$ they appear in highly mixed quantum states, with rather moderate degree of squeezing, which tends asymptotically to 50% (cf. the one-dimensional case described in Section VI.C):

$$s = e^{-\mu}\cosh\mu = \frac{1}{2}\left(1 + e^{-2\mu}\right)$$

The average number of quanta in each subsystem equals

$$\langle n\rangle = \frac{1}{2}(T-1) = \frac{1}{2}\sinh^2\mu$$

that is, twice less than in the case of an empty cavity. The variance of the number of quanta (photons) equals

$$\sigma_n \equiv \langle n^2\rangle - \langle n\rangle^2 = \frac{1}{4}\left(2T^2 - 4d - 1\right) = \frac{1}{4}\sinh^2\mu\cosh(2\mu)$$

Mandel's parameter [defined by Eq. (155)] turns out to be much greater than unity for $\mu \gg 1$, indicating that the photon statistics is highly super-Poissonian:

$$\mathscr{Q} \approx \sinh^2(\mu)$$

The photon distribution function can be expressed in terms of the Legendre polynomials, according to the general formula (151)

$$\mathscr{P}_n = \frac{2(iz)^n}{\sqrt{1+3\cosh^2\mu}} P_n(-iz) \tag{214}$$

where

$$z = \frac{\sinh\mu}{\sqrt{1+3\cosh^2\mu}}$$

Actually the right-hand side of Eq. (214) is a polynomial of degree n with respect to the variable z^2, due to the recurrence relation

$$n\mathscr{P}_n = z^2[(2n-1)\mathscr{P}_{n-1} + (n-1)\mathscr{P}_{n-2}]$$

If $\mu \gg 1$, then $z^2 \approx \frac{1}{3}$. The behavior of the distribution function (214) has been shown [189]. Since the argument of the Legendre polynomial is purely imaginary, $\mathscr{P}_n$ has no oscillations, in contradistinction to the vacuum squeezed state.

C. Interaction with a Two-Level Detector

Another model of the detector, which has only two energy levels, has been considered [188]. The most significant features can be described, in the rotating-wave approximation (RWA), in the framework of the following generalization of the Jaynes–Cummings (JC) Hamiltonian:

$$H = a^\dagger a + \frac{1}{2}\Omega\sigma_z + \kappa(a\sigma_+ + a^\dagger\sigma_-) + \frac{\tilde{\varepsilon}}{2}\sin(\omega_w t)[a^2 + \left(a^\dagger\right)^2] \tag{215}$$

The eigenfrequency of the unperturbed mode is assumed $\omega_0 = 1$, Ω is the energy-level difference of the detector, κ and $\tilde{\varepsilon} \ll \kappa$ have the same meaning as above; and $a, a^\dagger$ and $\sigma_+, \sigma_-, \sigma_z$ are the standard photon and spin operators. The wavefunction of the (field + detector) system can be written as

$$\psi(t) = \sum_{n=0}^{\infty} (c_n^{(-)}(t)|n, -\rangle + c_n^{(+)}(t)|n, +\rangle)$$

where the meanings of the symbols are clear. If $\tilde{\varepsilon} = 0$, then the known solution of the JC model reads as [291]

$$c_0^{(-)}(t) = c \tag{216}$$

$$c_{n+1}^{(-)}(t) = a_n \cos\vartheta_n \exp[-itE_n^+] - b_n \sin\vartheta_n \exp[-itE_n^-] \tag{217}$$

$$c_n^{(+)}(t) = a_n \sin\vartheta_n \exp[-itE_n^+] + b_n \cos\vartheta_n \exp[-itE_n^-] \tag{218}$$

where $n = 0, 1, 2, \ldots$, and

$$E_n^{\pm} = n + \frac{1}{2} \pm \lambda_n, \quad \lambda_n = \left[\frac{1}{4}(1-\Omega)^2 + \kappa^2(n+1)\right]^{1/2}$$

$$\tan\vartheta_n = \left(\frac{2\lambda_n - 1 + \Omega}{2\lambda_n + 1 - \Omega}\right)^{1/2}$$

We suppose that initially the system was in the ground state with the only nonzero coefficient $c_0^{(-)}(0) = 1$, and that the frequency of wall's vibrations is close to twice the frequency of the unperturbed mode: $\omega_w = 2 - \nu$. Looking for the solution at $\tilde{\varepsilon} \neq 0$ in the same form (216)–(218), but with time-dependent coefficients, and neglecting the rapidly oscillating terms containing $\exp(2it)$, we get the following equation for the coefficient $c(t)$:

$$\dot{c} = \frac{\sqrt{2}}{4}\tilde{\varepsilon}\{b_1 \sin\vartheta_1 \exp[it(\lambda_1 - \nu)] - a_1 \cos\vartheta_1 \exp[-it(\lambda_1 + \nu)]\}$$

Assuming $\nu = \lambda_1 = [\frac{1}{4}(1-\Omega)^2 + 2\kappa^2]^{1/2}$ and neglecting the terms oscillating with the frequencies of the order of κ, one can check that the infinite system of equations for a_n and b_n is reduced to the following *two* equations:

$$\dot{c} = \frac{\sqrt{2}}{4}\tilde{\varepsilon}\sin\vartheta_1\, b_1, \qquad \dot{b}_1 = -\frac{\sqrt{2}}{4}\tilde{\varepsilon}\sin\vartheta_1\, c$$

Consequently, in the resonance case we have only three nonzero amplitudes:

$$c_0^{(-)} = \cos(\alpha t), \quad c_2^{(-)} = \sin\vartheta_1 \sin(\alpha t) \exp[-itE_1^{(-)}]$$
$$c_1^{(+)} = -\cos\vartheta_1 \sin(\alpha t) \exp[-itE_1^{(-)}]$$

where $\alpha = \sin\vartheta_1\, \tilde{\varepsilon}\sqrt{2}/4$. Only two photons can be created, and the probability of finding the detector in an excited state $\mathscr{P}^{(+)}$ is always less than $\frac{1}{2}$. All the probabilities, in contradistinction to the first example, are periodically oscillating functions of time:

$$\mathscr{P}_1 = \mathscr{P}^{(+)} = \cos^2\vartheta_1 \sin^2(\alpha t), \qquad \mathscr{P}_2 = \sin^2\vartheta_1 \sin^2(\alpha t)$$

It is interesting that the upper level of the detector never can be populated with 100% probability, since $\vartheta_n > 0$ for all values of parameters. For $\Omega = 1$, $\vartheta_n = \pi/4$, and $\mathscr{P}_1 = \mathscr{P}_2 = \mathscr{P}^{(+)} = \frac{1}{2}\sin^2(\tilde{\varepsilon}t/4)$. Large detuning, $1 - \Omega \gg \kappa$, results in increasing $\mathscr{P}^{(+)}_{\max}$, since $\vartheta_1 \to 0$. However, in such a case $\alpha \to 0$, as well, and the applicability of JC-model to the description of the interaction between the detector and field becomes questionable. Recently, a more general model was considered in [238].

IX. INFLUENCE OF DAMPING

The complete theory of the field quantization in media with moving nonideal boundaries is not available at present. The field quantization in spatially inhomogeneous, but *nonabsorbing* dielectrics has been studied [292,293], and the same problem for nonabsorbing media with time-dependent parameters has also been considered [217–219,222]. The case of absorbing media has been analyzed [294–297]. The theory of the field quantization in leaky cavities has been developed [298–300]. However, in all those studies the boundaries were fixed. Because of the complexity of the problem, only a few of the simplest models have been considered up to now in the case of *moving walls*.

For example, one can try, as the first step, to neglect coupling between different field modes inside the cavity. Such an approximation can be justified, for instance, for an adiabatic motion of the cavity walls, when the characteristic mechanical frequency, ω_m, is many orders of magnitude less than the electromagnetic field eigenfrequency, ω_e. However, no new photons can be created under the condition $\omega_m \ll \omega_e$ (and the photon number distribution cannot be changed, as well), since the photon number operator is the adiabatic invariant in this case.

Fortunately, as was shown in the preceding section, the interaction between different field modes can also be neglected in the case of a three-dimensional

cavity with a nonequidistant spectrum of the field eigenfrequencies, under the parametric resonance condition $\omega_m \approx 2\omega_e$. In such a case, one can infer some quantitative information regarding the behavior of the field in the cavity, studying the problem of the parametrically excited oscillator with damping.

The influence of an environment on the parametric amplification was considered in detail, for instance, in Ref. 301, where an explicit coupling with a heat bath consisting of harmonic oscillators was introduced. More general models of the environment were studied, such as, in the framework of the influence functional approach [302], mainly in connection with cosmological problems. It was shown in [299,300,303,304] that the influence of the "modes of the universe" outside the cavity with *fixed mirrors* can be described effectively in the framework of the Heisenberg–Langevin equation of motion for the photon annihilation and creation operators $\hat{a}, \hat{a}^\dagger$. An equivalent description in the Schrödinger picture is achieved in the framework of the "standard master equation" [305–310], whose simplest form reads as

$$\dot{\hat{\rho}} = \frac{i}{\hbar}[\hat{\rho}, \hat{H}] + \frac{\gamma}{2}\left[2\hat{a}\hat{\rho}\hat{a}^\dagger - \hat{a}^\dagger\hat{a}\hat{\rho} - \hat{\rho}\hat{a}^\dagger\hat{a}\right] \tag{219}$$

where $\hat{\rho}$ is the statistical operator of the distinguished field mode, $\hat{H}$ is the Hamiltonian, and the damping coefficient γ absorbs all the details of the loss mechanism, including the transmissivity of the mirror and the coupling between the field and the atoms inside the wall, so that it is proportional to the reciprocal of the dissipation timescale. It was assumed [256,257] that Eq. (219) can be used as well in the case of the *moving mirrors*, with the same value of the damping coefficient as in the case of the fixed boundaries. Following the same line as in Refs. 256 and 257, we also assume that the time evolution of the mixed quantum state of the resonance field mode is governed by a linear master equation (although one cannot exclude the possibility that such an approach is oversimplified; see, e.g., Refs. 311 and 312). However, instead of using an operator equation such as (219), we consider the most general linear equation of the Fokker–Planck type for the *Wigner function* $W(q,p,t)$ [277,308,313] (q,p are the quadrature components of the field mode):

$$\begin{aligned}\frac{\partial W}{\partial t} = {} & \frac{\partial}{\partial q}\left([\gamma_q q - p]W\right) + \frac{\partial}{\partial p}\left([\gamma_p p + \omega^2(t)q]W\right) \\ & + D_{qq}\frac{\partial^2 W}{\partial q^2} + D_{pp}\frac{\partial^2 W}{\partial p^2} + 2D_{qp}\frac{\partial^2 W}{\partial q \partial p}\end{aligned} \tag{220}$$

The coefficients γ_i and $D_{ij} = D_{ji}$ depend on the concrete form of the microscopic interaction between the system involved and an environment [305–308,314]. For example, the simplest models of the damped optical oscillator

with a constant frequency ω_0 yield the following set of coefficients [308,315]

$$\gamma_p = \gamma_q = \pi s(\omega_0)|g(\omega_0)|^2 \tag{221}$$

$$D_{pp} = \omega_0^2 D_{qq} = \gamma_q \mathscr{E}_{eq}(\omega_0), \quad D_{pq} = 0 \tag{222}$$

where $s(\omega)$ is the density of states of the reservoir, $g(\omega_0)$ is the function describing the intensity of coupling between the distinguished oscillator and the reservoir degrees of freedom, and $\mathscr{E}_{\mathrm{eq}}(\omega_0)$ is the equilibrium energy of the oscillator with frequency ω_0 at temperature T:

$$\mathscr{E}_{\mathrm{eq}}(\omega_0) = \frac{1}{2}\hbar\omega_0 \coth\left(\frac{\hbar\omega_0}{2k_B T}\right) \tag{223}$$

Choosing different couplings between the oscillator under study and the reservoir, one can obtain various other sets of the drift and diffusion coefficients [308,314], but all of them must obey the constraint [277,316–319]

$$D_{pp}D_{qq} - D_{qp}^2 \geq \frac{\hbar^2(\gamma_p + \gamma_q)^2}{16} \tag{224}$$

which guarantees an absence of nonphysical solutions violating the uncertainty relations and corresponding to nonpositively definite density matrices. Besides, the coefficients D_{pp} and D_{qq} must be positive. However, it will be shown in this section that in the case of a weak damping, the evolution depends on two combinations of the damping and diffusion coefficients only:

$$\gamma = \frac{1}{2}(\gamma_p + \gamma_q), \quad \mathscr{E}_* = \frac{1}{2\gamma}(D_{pp} + \omega_0^2 D_{qq}) \tag{225}$$

With the fluctuation–dissipation theorem, the diffusion coefficients are proportional to the damping coefficients; therefore, $\mathscr{E}_*$ does not depend on γ, at least up to small corrections of an order of γ^2. The physical meaning of the parameters γ and $\mathscr{E}_*$ is elucidated below; 2γ is the reciprocal energy relaxation time of the cavity due to all possible mechanisms (a real dissipation in the walls and the leakage through the boundaries), namely, $2\gamma = \omega_0/Q$, where Q is the cavity quality factor, whereas $\mathscr{E}_* = \mathscr{E}_{\mathrm{eq}}(\omega_0)$.

Solutions to Eq. (220) with a *constant* frequency and different sets of constant diffusion coefficients were obtained by many authors; they were analyzed in detail in two studies [277,308], where other references can be found. Since Eq. (220) looks like a two-dimensional Schrödinger equation with a quadratic (although non-Hermitian) Hamiltonian, its propagator can be

calculated in the framework of the method of quantum integrals of motion [278]. The explicit form of this propagator in the generic case of time-dependent coefficients can be found in Refs. 277 and 320. Here we only calculate the second order statistical moments and the energy (the number of photons) of the field oscillator.

A. Evolution of the Energy and the Second-Order Moments

The time dependence of the energy and the second-order statistical moments (variances) of the field mode quadrature components, $\sigma_{ab} \equiv \frac{1}{2}\langle ab + ba\rangle - \langle a\rangle\langle b\rangle$, is governed by the equations following from Eq. (220):

$$\dot{\sigma}_{qq} = 2\sigma_{pq} - 2\gamma_q\sigma_{qq} + 2D_{qq} \tag{226}$$

$$\dot{\sigma}_{pq} = \sigma_{pp} - \omega^2(t)\sigma_{qq} - 2\gamma\sigma_{pq} + 2D_{pq} \tag{227}$$

$$\dot{\sigma}_{pp} = -2\omega^2(t)\sigma_{pq} - 2\gamma_p\sigma_{pp} + 2D_{pp} \tag{228}$$

We assume that the oscillator eigenfrequency depends on time as

$$\omega(t) = \omega_0[1 + 2\tilde{\varepsilon}\sin(\Omega t)], \quad \Omega = 2(\omega_0 + \delta), \quad |\delta| \ll \omega_0, \quad |\tilde{\varepsilon}| \ll 1 \tag{229}$$

where ω_0 is the unperturbed field eigenfrequency, and Ω is the frequency of the wall vibrations. Then one could suppose that the damping and diffusion coefficients must depend on time as well. We argue, however, that in the case under study the coefficients γ_a and D_{ab} can be considered as time-independent. For example, let us look at the expressions (221) and (222). In the case of a vibrating cavity, the time variable could enter the coefficients γ_a and D_{ab} through the coupling function $g(\omega_0)$, which can depend on the variable length of the cavity $L(t) = L_0[1 + \xi_L\tilde{\varepsilon}\sin(\Omega t)]$, where ξ_L is a numerical coefficient. Then one could expect a similar time dependence of the coefficients of the Fokker–Planck equations, $\gamma(t) = \gamma_0\left[1 + \xi_\gamma\tilde{\varepsilon}\sin(\Omega t)\right]$, $D(t) = D_0[1 + \xi_D\tilde{\varepsilon}\sin(\Omega t)]$, where ξ_γ and ξ_D are some other numerical coefficients. One should remember, however, that the modulation parameter $\tilde{\varepsilon}$ is very small under the realistic conditions; its absolute value cannot exceed 10^{-8} [188,189]. The set of equations (226)–(228) contains three small dimensionless parameters—$\tilde{\varepsilon}$, δ/ω_0, and γ_0/ω_0—and we are interested in the weak damping case, when these parameters are of the same order of magnitude. Under this condition, the time-dependent parts of the coefficients γ_a and D_{ab} are proportional to the products $\tilde{\varepsilon}\gamma_0/\omega_0 \sim \mathcal{O}(\tilde{\varepsilon}^2) \sim 10^{-16}$, so it seems reasonable to neglect these extremely small terms.

A significant time dependence of the damping and diffusion coefficients could arise in the specific case of an *unstable* reservoir, provided the reservoir oscillators having the frequencies close to ω_0 could be also excited as a result of some resonance processes between the vibrating surface of the wall and the

reservoir. In such a case, the energy of the resonant oscillators would increase in time, resulting in increasing values of the damping and diffusion coefficients [see Eq. (222)]. As a consequence, we would obtain an additional amplification of the energy of the field mode due to the interaction with the reservoir. However, such a model seems unrealistic, since it implies that some distinguished degrees of freedom of the reservoir are practically isolated from the rest of the reservoir. This conjecture contradicts the usual concept of the reservoir consisting of a great number of strongly interacting particles, so that the state of the reservoir is not sensitive to small external perturbations. Therefore, we assume that the only time-dependent coefficient in Eqs. (226)–(228) is $\omega(t)$.

The set of equations (226)–(228) is equivalent to the third-order differential equation for the variance $\sigma_{qq} \equiv \sigma$

$$\frac{d^3\sigma}{dt^3} + 6\gamma\frac{d^2\sigma}{dt^2} + 4\omega^2(t)\frac{d\sigma}{dt} + 4\omega_0(\dot{\omega} + 2\gamma\omega_0)\sigma = 8\gamma\mathscr{E}_* \tag{230}$$

where the coefficients γ and $\mathscr{E}_*$ are given by Eq. (225) (we neglect the terms of the second order with respect to γ, D_{ab}, and $\tilde{\varepsilon}$). To find an approximate explicit solution to Eq. (230) with function $\omega(t)$ given by Eq. (229), we use the well-known method of slowly varying amplitudes, which was exposed, for instance, in three textbooks [266–268] and applied to the quantum parametric oscillator [289,301]. Following this method, we write

$$\sigma_{qq}(t) = A(t) + B(t)\cos(\Omega t) + C(t)\sin(\Omega t) \tag{231}$$

so that the function (231) with $A, B, C = \text{const}$ is an exact solution to Eq. (230) for $\tilde{\varepsilon} = \gamma = \delta = 0$. Supposing that the dimensionless small parameters γ/ω_0 and δ/ω_0 have the same orders of magnitude as the small parameter $\tilde{\varepsilon}$, that is, $\gamma = \tilde{\gamma}\tilde{\varepsilon}\omega_0$, $\delta = \tilde{\delta}\tilde{\varepsilon}\omega_0$, $\tilde{\gamma}, \tilde{\delta} \sim \mathscr{O}(1)$, we assume that the amplitude coefficients A, B, C are functions of the "slow time" $\tau = \tilde{\varepsilon}t$, so that the time derivatives $d^kA/dt^k, d^kB/dt^k, d^kC/dt^k$ are proportional to $\tilde{\varepsilon}^k$ $(k = 1, 2, 3)$. Then we put the function (231) into Eq. (230) and neglect the terms proportional to $\tilde{\varepsilon}^2$ and $\tilde{\varepsilon}^3$. Besides, we perform averaging over fast oscillations with the frequency Ω, in order to eliminate higher harmonics with frequences $m\Omega$, $m = 2, 3, \ldots$, whose amplitudes are proportional to $\tilde{\varepsilon}^{m-1}$ [267,268]. Finally, we arrive at the following set of equations for the slowly varying amplitudes (here the overdot means the derivative with respect to the real time t, and the new parameter $\kappa \equiv \tilde{\varepsilon}\omega_0$ has the dimensionality of frequency, e.g., γ and δ):

$$\dot{A} = -2\gamma A + 2\kappa B + 2\gamma\mathscr{E}_* \tag{232}$$

$$\dot{B} = 2\kappa A - 2\gamma B - 2\delta C \tag{233}$$

$$\dot{C} = 2\delta B - 2\gamma C \tag{234}$$

This system can be easily solved for an arbitrary time dependent function $\gamma(t)$, since the substitution $A(t) = \tilde{A}(t)\exp\left[-2\int\gamma(\tau)\,d\tau\right]$ removes the function $\gamma(t)$ from the homogeneous parts of Eqs. (232)–(234). However, we consider the case of constant coefficients only, because of the physical reasons discussed above.

To simplify the formulas, we assume hereafter $\hbar = \omega_0 = 1$; thence $\Omega = 2$ in the amplitude coefficients. Neglecting small terms of the order of γ/Ω, κ/Ω, and δ/Ω in the amplitude coefficients, one can express the variances σ_{pp} and σ_{pq} as follows:

$$\sigma_{pp}(t) = A(t) - B(t)\cos(\Omega t) - C(t)\sin(\Omega t) \tag{235}$$

$$\sigma_{pq}(t) = C(t)\cos(\Omega t) - B(t)\sin(\Omega t) \tag{236}$$

Then the initial conditions for the set (232)–(234) read as

$$A(0) = \frac{\sigma_{qq}(0) + \sigma_{pp}(0)}{2}, \quad B(0) = \frac{\sigma_{qq}(0) - \sigma_{pp}(0)}{2}, \quad C(0) = \sigma_{pq}(0)$$

Evidently, $A(t)$ coincides with the mean energy to within small corrections of the order of $\tilde{\varepsilon}$, γ, and δ:

$$\mathscr{E}(t) \equiv \frac{\sigma_{pp} + \sigma_{qq}}{2} = A(t)$$

In order to elucidate the meaning of the coefficients B and C, consider the determinant of the invariance matrix [cf. Eq. (211)]:

$$d \equiv \sigma_{pp}\sigma_{qq} - \sigma_{pq}^2 \geq \frac{\hbar^2}{4} \tag{237}$$

Here the last inequality holds due to the Schrödinger–Robertson uncertainty relation [271,279,321,322]. The meaning of the parameter d as the *universal quantum invariant* has also been discussed [323]. The *minimal invariant variance* (100) can be expressed in terms of $\mathscr{E}$ and d as

$$u = \mathscr{E} - \sqrt{\mathscr{E}^2 - d} = \frac{d}{\mathscr{E} + \sqrt{\mathscr{E}^2 - d}} \tag{238}$$

and one can easily verify the relations

$$d = A^2 - B^2 - C^2, \quad u = A - \sqrt{B^2 + C^2} \tag{239}$$

The solutions to Eqs. (232)-(234) read

$$A(t) = A_* + e^{-2\gamma t}[a_0\delta + a_+\kappa e^{2\nu t} + a_-\kappa e^{-2\nu t}] \tag{240}$$

$$B(t) = B_* + e^{-2\gamma t}[a_+\nu e^{2\nu t} - a_-\nu e^{-2\nu t}] \tag{241}$$

$$C(t) = C_* + e^{-2\gamma t}[a_0\kappa + a_+\delta e^{2\nu t} + a_-\delta e^{-2\nu t}] \tag{242}$$

where $\nu = \sqrt{\kappa^2 - \delta^2}$, and

$$a_0 = \frac{1}{\nu^2}[\kappa C(0) - \delta A(0) + \mathscr{E}_*\delta] \tag{243}$$

$$a_\pm = \frac{1}{2\nu^2}\left[\kappa A(0) - \delta C(0) \pm \nu B(0) - \frac{\kappa\gamma\mathscr{E}_*}{\gamma \mp \nu}\right] \tag{244}$$

$$A_* = \frac{\gamma^2 + \delta^2}{\gamma^2 - \nu^2}\mathscr{E}_*, \quad B_* = \frac{\kappa\gamma\mathscr{E}_*}{\gamma^2 - \nu^2}, \quad C_* = \frac{\kappa\delta\mathscr{E}_*}{\gamma^2 - \nu^2}$$

The meanings of the parameters γ and $\mathscr{E}_*$ become clear, if one considers the special case of the oscillator with time-independent coefficients, $\kappa = \delta = \nu = 0$. Then we see that 2γ is the energy relaxation coefficient, so that it can be expressed in terms of the cavity Q factor by means of the relation $2\gamma = \omega_0/Q$. The energy of the oscillator in this special case tends to $\mathscr{E}_*$ as $t \to \infty$, and this value can be identified with the thermodynamic equilibrium oscillator energy $\mathscr{E}_{\rm eq}$ given by Eq. (223) [up to corrections of the order of $(\gamma/\omega_0)^2$] [277,308].

The sign of the difference $\nu - \gamma$ determines the regions of stable and unstable solutions of Eq. (230) in the space of parameters κ, δ, γ (for small values of these parameters). The stable (limited in time) solutions exist for large values of the damping or detuning coefficients, $\nu < \gamma$:

$$\gamma^2 + \delta^2 > \kappa^2 \tag{245}$$

In this case, the final state of the oscillator does not depend on the initial conditions. The asymptotic values of the energy, the d factor, and the minimal invariant variance read

$$\mathscr{E}(\infty) = \frac{\gamma^2 + \delta^2}{\gamma^2 - \nu^2}\mathscr{E}_{\rm eq}, \quad d(\infty) = \frac{\gamma^2 + \delta^2}{\gamma^2 - \nu^2}\mathscr{E}_{\rm eq}^2, \quad u(\infty) = \frac{\sqrt{\gamma^2 + \delta^2}}{\kappa + \sqrt{\gamma^2 + \delta^2}}\mathscr{E}_{\rm eq} \tag{246}$$

At zero temperature, when κ tends to the threshold, the minimal variance u goes to the value $\frac{1}{4}$, which is twice less than in the coherent state.

Above the threshold, that is, in the instability region $\nu > \gamma$, the energy (or the number of photons) increases exponentially for $(\nu - \gamma)t \gg 1$

$$\mathscr{E}(t) = a_+ \kappa e^{2(\nu-\gamma)t} \tag{247}$$

and it depends on the initial conditions through the coefficient a_+. Using Eq. (244) and taking into account the uncertainty relation $d \geq \frac{1}{4}$ (for $\hbar = 1$), one can verify that the coefficient a_+ is bounded from below by a positive value:

$$a_+ > \frac{\kappa\gamma\mathscr{E}_{\text{eq}}}{2\nu^2(\nu - \gamma)}$$

Consider a special case of initial thermal equilibrium state. Then

$$a_\pm^{(\text{eq})} = \frac{\kappa\mathscr{E}_{\text{eq}}}{2\nu(\nu \mp \gamma)}, \quad a_0^{(\text{eq})} = 0, \quad d(0) = \mathscr{E}_{\text{eq}}^2 \tag{248}$$

thus d factor (239) depends on time as

$$d(t) = \frac{\mathscr{E}_{\text{eq}}^2}{\nu(\nu^2 - \gamma^2)}\left[2\kappa^2\gamma e^{-2\gamma t}\sinh(2\nu t) + \kappa^2\nu e^{-4\gamma t} - \nu(\gamma^2 + \delta^2)\right] \tag{249}$$

If $\gamma > 0$ and $(\nu - \gamma)t \gg 1$, then, according to Eq. (238), the minimal variance tends asymptotically to a constant value

$$u_\infty = \frac{\gamma}{\gamma + \nu}\mathscr{E}_{\text{eq}} \tag{250}$$

Consequently, a large squeezing can be achieved even for a high-temperature initial state, if $\nu \gg \gamma$. If $\gamma = 0$, then d does not depend on time, $d \equiv \mathscr{E}_{\text{eq}}^2$, and for $\nu t \gg 1$ the minimal variance goes asymptotically to zero as $u \approx \mathscr{E}_{\text{eq}}(\nu/\kappa)^2 \exp(-2\nu t)$. One should remember, nonetheless, that the solutions indicating the exponential growth of the energy are justified until $t \ll t_2 \sim (\omega_0\tilde{\varepsilon}^2)^{-1}$, since for larger times the neglected second-order terms in Eqs. (230), (232)–(234) could become important. However, the time t_2 is very large under the realistic conditions.

X. DISCUSSION

We have demonstrated a significant progress in our understanding and *quantitative* description of quantum processes in cavities with moving boundaries, achieved 30 years after the pioneer paper by Moore [76] and almost 80 years

after the first papers on *classical electrodynamics* in such cavities by Nicolai and Havelock [6–8]. We have shown that quanta of electromagnetic field can be created from vacuum in a cavity with vibrating walls *under the resonance condition* (and cannot be generated for nonresonance nonrelativistic laws of boundary motion, in particular, in the case of a large detuning from the resonance), and the quantum state of field exhibits the "nonclassical" properties.

The possibility of observing the effect depends crucially on the achievable values of the wall displacement amplitude. For the cavity dimensions of the order of $1 \div 100$ centimeters, the resonance frequency ω_0/π varies from 30 GHz to 300 MHz. It is difficult to imagine that the wall could be forced to oscillate as a whole at such a high frequency. Rather, one could think of the oscillations on the *surface* of the cavity wall. In such a case one has to find a way of exciting a sufficiently strong standing acoustic wave at frequency $\omega_w = 2\omega_0$ inside the wall. The amplitude a of this wave (coinciding with the amplitude of oscillations of the free surface) is connected to the relative deformation amplitude δ inside the wall as $\delta = \omega_w a/v_s$, where v_s is the sound velocity. Since the usual materials cannot bear the deformations exceeding the value $\delta_{\max} \sim 10^{-2}$ [324], the maximal possible velocity of the boundary appears $v_{\max} \sim \delta_{\max} v_s \sim 50$ m/s (independent on the frequency). Thus the maximal dimensionless displacement $\varepsilon = a/L_0$ is $\varepsilon_{\max} \sim (v_s/2\pi c)\delta_{\max} \sim 3 \times 10^{-8}$ for the lowest mode with the frequency $\omega_0 \sim c\pi/L_0$. It also does not depend on the frequency. Consequently, the maximal rate of photon generation in the principal mode of a 1D cavity can be estimated as

$$\left(\frac{d\mathscr{P}_1}{dt}\right)_{\max} = \frac{4}{\pi^2}\frac{v_s}{c}\delta_{\max}\frac{\omega_1}{2\pi} \sim 6 \times 10^{-8}\frac{\omega_1}{2\pi} \tag{251}$$

It is proportional to the frequency. For $\omega_1/2\pi = 10$ GHz (corresponding to a distance between the plates of the order of several centimeters) we get 600 photons/s.

This number can be significantly increased in a 3D cavity, according to the exponential law (202). For the same frequency $\omega_0/2\pi = 10$ GHz, the maximal value of parameter $\mu = \gamma\omega_0 t$ equals $\mu_{\max} \sim 600t$, time t being expressed in seconds. Even if the amplitude of the vibrations were 100 times less than the maximal possible value, in $t = 1$ s one could get about $\sinh^2(6) \approx 4 \times 10^4$ photons in an empty cavity. Obviously, the concrete shape of a 3D cavity is not important. The significant requirements are (1) the nondegenerate character of the eigenfrequency spectrum and (2) the condition of the parametric resonance between the oscillating wall and some electromagnetic mode. The *total* energy of photons created in the 1D cavity is approximately the same as in the three-dimensional case. The difference is that in the 1D case this energy is spread over many interacting modes, resulting in moderate numbers of quanta in each mode.

The rate of photon generation in the mth (odd) mode of the 1D cavity is approximately m times less than in the principal mode with $m = 1$ (in the asymptotical regime).

To create the abovementioned 600 or 4×10^4 photons, one should vibrate the wall for no less than 1 s. The necessary Q factor of the cavity must be $Q \sim 3 \times 10^{10}$. This value was achieved in experiments in 1990 [325]. An unsolved problem is how to excite the high-frequency surface vibrations with a sufficiently large amplitude. One could think, for instance, of using some kind of piezo effect. This method was successfully applied in early experiments devoted to solving the mode-locking and pulse production problems in lasers with the aid of vibrating mirrors. Displacements of the mirror from 0.1 to 0.7 μm at the frequency 500 kHz have been achieved [27,28]. In 1966 [24] resonance vibrations of the mirror in a laser with a length of 250 cm (i.e., at a frequency about 100 MHz) were excited with the aid of a quartz transducer. However, for our purposes the frequency 100 MHz is too small, since the parameter μ becomes 100 times less, compared to the estimations given above (remember that $\varepsilon_{\max}$ does not depend on the frequency).

Fortunately, the results of recent studies [192,210–212] show that the influence of temperature is not as significant as it might appear at first glance. Moreover, in certain situations the initial temperature fluctuations could be used to amplify the effect [211]. However, the resonance requirements are rather hard; for values of frequency $\omega \sim 10^{10}$ Hz and maximal possible modulation parameter $\varepsilon \sim 10^{-8}$, the admissible detuning should not exceed 100 Hz during the whole time interval ~ 1 s, necessary to accumulate the resonance effect.

One of the reasons for the studies on the dynamical Casimir effect was Schwinger's hypothesis [153–157] that this effect could explain the *sonoluminescence* phenomenon, specifically, the emission of bright short pulses of the visible light from the gas bubbles in the water, when the bubbles pulsate because of the pressure oscillations in a strong standing acoustic wave. (Several reviews and numerous references related to this effect are available, [121,326–328].) There are several publications [329–331], whose authors considered the models giving tremendous numbers of photons that could be produced even in the visible range as a result of the fast motion of the boundaries. However, analysis of these models shows that they are based on such laws of motion of the boundaries that imply the superluminal velocities, so they are not realistic.

Although the results of this chapter, which were obtained in the framework of simplified one-dimensional and three-dimensional models, cannot be applied directly to the analysis of the sonoluminescence problem, they are not in favor of Schwinger's hypothesis. The main difficulty is connected with quite different timescales of the phenomena. The accumulation of the "dynamical Casimir energy" is a very slow process, which needs a great number of wall oscillations, whereas the sonoluminescence pulses (containing up to 10^7 photons) have the

duration of the order of picoseconds. Moreover, the wall oscillations must be in extremely finely tuned resonance with the field eigenfrequencies, since the detuning $\delta > \varepsilon$ completely destroys the energy growth [191]. In particular, if the frequency of the wall oscillations $\omega_{\rm wall}$ is much less than the minimal field eigenfrequency ω_1, then the field variation is adiabatic, and the mean number of created photons is proportional to [189] $\varepsilon^2(\omega_{\rm wall}/\omega_1)^4 \ll 1$. These features survive in the three-dimensional model considered in this chapter, too. Therefore, it is difficult to believe that very specific conditions of the parametric resonance described above could arise naturally in the sonoluminescence case. For other discussions of the problem see, for example, Ref. 332 and the contributions in Ref. 333.

Actually, the main obstacle to producing the "Casimir light" is the very low ratio of the wall velocity to the speed of light in laboratory experiments. If the velocity of the boundary were of the order of c, then a sufficient number of photons could be created from vacuum practically for any law of motion. For the nonrelativistic velocities, the only possibility is to accumulate the effect gradually under the resonance conditions. Nonetheless, perhaps, the experimental situation could be improved in the case of using some kinds of "effective mirrors," such as the layers made of the electron–hole plasma [209], or some others. Therefore, we cannot exclude a possibility that in a not very remote future one could assist a show of "quantum magics," when some "quantum magician" takes an empty box, then shakes it well, opens it, and an astonished audience sees a large number of photons that have appeared "from nothing" as a result of the nonstationary Casimir effect.

Acknowledgments

I would like to thank my coauthors V. I. Man'ko, A. B. Klimov, and M. A. Andreata for the long-term fruitful collaboration. Also, I would like to express my sincere gratitude to Prof. S. S. Mizrahi and the Physics Department of the Federal University of São Carlos, since this review could not be written without their great support and help.

References

1. A. Einstein, *Ann. Phys.* (Leipzig) **17**, 891 (1905).
2. U. I. Frankfurt and A. N. Frank, *Optics of Moving Bodies*, Nauka, Moscow, 1972.
3. L. A. Ostrovskii, *Usp. Fiz. Nauk* **116**, 315 (1975).
4. K. S. Kunz, *J. Appl. Phys.* **51**, 873 (1980).
5. B. M. Bolotovskii and S. N. Stolyarov, *Usp. Fiz. Nauk* **159**, 155 (1989) [*Sov. Phys.—Uspekhi* **32**, 813 (1989)].
6. E. L. Nicolai, *Ann. Petrograd. Polytechn. Inst.* **28**, 273 (1921) [reproduced in E. L. Nicolai, *Trudy po Mekhanike*, GITTL, Moscow, 1955, pp. 329–343 (in Russian)].
7. E. L. Nicolai, *Phil. Mag.* **49**, 171 (1925).
8. T. H. Havelock, *Phil. Mag.* **47**, 754 (1924).

9. G. F. Carrier, *Am. Math. Monthly* **56**, 669 (1949).
10. O. G. Zagorodnov, Y. B. Fainberg, A. M. Egorov, and L. I. Bolotin, *Zh. Tekhnicheskoi Fiziki* **31**, 297 (1961) [*Sov. Phys.—Tech. Phys.* **6**, 212 (1961)].
11. V. I. Kurilko, *Zh. Tekhnicheskoi Fiziki* **30**, 504 (1960) [*Sov. Phys.—Tech. Phys.* **5**, 473 (1960)].
12. N. L. Balazs, *J. Math. Anal. Appl.* **3**, 472 (1961).
13. H. P. Greenspan, *J. Math. Anal. Appl.* **6**, 339 (1963).
14. O. A. Stetsenko, *Izvestiya VUZ—Radiotekhnika* **6**, 695 (1963).
15. O. A. Stetsenko, *Izvestiya VUZ—Radiotekhnika* **6**, 701 (1963).
16. O. A. Stetsenko, *Izvestiya VUZ—Radiofizika* (*Sov. Phys. Radiophys. & Quant. Electron.*) **7**, 71 (1964).
17. R. I. Baranov and Yu. M. Shirokov, *Zh. Eksper. Teor. Fiz.* **53**, 2123 (1967) [*Sov Phys.—JETP* **26**, 1199 (1968)].
18. P. W. Smith, *Appl. Phys. Lett.* **10**, 51 (1967).
19. T. H. Peek, P. T. Bolwijn, and C. T. Alkemade, *Phys. Lett. A* **24**, 128 (1967).
20. V. K. Klinkov and C. K. Mukhtarov, *Dokl. Akad. Nauk SSSR* **207**, 817 (1972) [*Sov. Phys.—Doklady* **17**, 1163 (1973)].
21. M. M. Makogon, *Optika i Spektrosk.* **38**, 620 (1975) [*Opt. Spectrosc.* **38**, 351 (1975)].
22. S. P. Anokhov, G. A. Galich, V. I. Kravchenko, and Y. I. Khanin, *Opt. Commun.* **25**, 384 (1978).
23. G. A. Askar'yan, *Zh. Eksp. Teor. Fiz.* **42**, 1672 (1962) [*Sov. Phys.—JETP* **15**, 1161 (1962)].
24. W. C. Henneberger and H. J. Schulte, *J. Appl. Phys.* **37**, 2189 (1966).
25. M. H. Ober, M. Hofer, and M. E. Fermann, *Opt. Lett.* **18**, 367 (1993).
26. A. Bambini and P. Burlamacchi, *J. Appl. Phys.* **39**, 4864 (1968).
27. V. I. Voronov and Yu. E. Pol'skiy, *Pribory i Tekhnika Eksperimenta* [*Sov. Phys.— Instrum. Exp. Techniques*] No. 6, 174 (1970).
28. V. I. Voronov and Yu. E. Pol'skiy, *Radiotekhnika i Elektronika* **18**, 1434 (1973).
29. E. A. Gerber and E. R. Ahlstrom, *J. Appl. Phys.* **35**, 2546 (1964).
30. E. A. Gerber and E. R. Ahlstrom, *IEEE J. Quantum Electron.* **5**, 403 (1969).
31. J. P. Bernardin and N. M. Lawandy, *Opt. Commun.* **94**, 445 (1992).
32. J. T. Ruscio, *IEEE J. Quantum Electron.* **QE1**, 182 (1965).
33. G. N. Belova, *Akust. Zh.* **17**, 365 (1971) [*Sov. Phys.—Acoustics* **17**, 309 (1972)].
34. F. Bodem, *Z. Naturforsch. A* **33**, 914 (1978).
35. L. S. Kornienko, E. G. Lariontsev, and V. A. Sidorov, *Kvantovaya Elektronika* **7**, 1213 (1980) [*Sov. J. Quant. Electron.* **10**, 695 (1980)].
36. S. Longhi and P. Laporta, *Phys. Rev. A* **60**, 4016 (1999).
37. G. A. Grinberg, *Prikladnaya Matematika i Mekhanika* **31**, 193 (1967) [*Sov. J. Appl. Math. Mech.* **31**, 215 (1967)].
38. V. N. Krasil'nikov, in *Problems of Difraction and Wave Propagation*, Leningrad State Univ., 1968, Vol. 8, p. 43 (in Russian).
39. V. N. Krasil'nikov and A. M. Pankratov, in *Problems of Difraction and Wave Propagation*, Leningrad State Univ., 1968, Vol. 8, p. 59 (in Russian).
40. A. I. Vesnitskii, *Izvestiya VUZ—Radiofizika* (*Sov. Phys. – Radiophys. Quant. Electron.*) **12**, 935 (1969).
41. A. I. Vesnitskii and A. V. Kostrov, *Izvestiya VUZ—Radiofizika* (*Sov. Phys.—Radiophys. Quant. Electron.*) **14**, 754 (1971).

42. A. I. Vesnitskii, *Izvestiya VUZ—Radiofizika* (*Sov. Phys.—Radiophys. Quant. Electron.*) **14**, 1432 (1971).
43. A. I. Vesnitskii, *Izvestiya VUZ—Radiofizika* (*Sov. Phys.—Radiophys. Quant. Electron.*) **14**, 1531 (1971).
44. A. I. Vesnitskii, *Izvestiya VUZ—Radiofizika* (*Sov. Phys.—Radiophys. Quant. Electron.*) **14**, 1538 (1971).
45. B. P. Borisov and A. I. Vesnitskii, *Prikladnaya Mekhanika* (*Sov. Appl. Mech.*) **XIII**(3), 57 (1977).
46. V. P. Boldin and A. I. Vesnitskii, *Radiotekhnika i Elektronika* (*Sov. Phys.—Radio Eng. Electron. Phys.*) **23**, 1657 (1978).
47. A. I. Vesnitskii and A. I. Potapov, in *Mathematical Methods of the Theory of Vibrations*, Vol. 13, *Dynamics of Systems Series*, Gorky State Univ. Gorky, 1978, p. 38 (in Russian).
48. K. A. Barsukov and G. A. Grigoryan, *Izvestiya VUZ—Radiofizika* **19**, 280 (1976) [*Sov. Phys.—Radiophys. Quant. Electron.* **19**, 194 (1976)].
49. K. A. Barsukov and G. A. Grigoryan, *Izvestiya VUZ—Radiofizika* (*Sov. Phys.—Radiophys. Quant. Electron.*) **19**, 603 (1976).
50. K. A. Barsukov and G. A. Grigoryan, *Radiotekhnika i Rlektronika* **21**, 57 (1976) [*Sov. Phys.—Radio Eng. Electron. Phys.* **21**, 46 (1976)].
51. E. L. Bartashevsky and V. M. Korchinsky, *Radiotekhnika i Rlektronika* **24**, 248 (1979).
52. E. L. Bartashevsky and V. M. Korchinsky, *Radiotekhnika i Rlektronika* **27**, 2367 (1982).
53. A. V. Balandin, A. I. Vesnitskii, and G. A. Utkin, in *Differential and Integral Equations*, Vol. 4, Gorky State Univ. Gorky, 1980, p. 84 (in Russian).
54. A. I. Vesnitskii and A. I. Potapov, in *Numerical Methods of Studies of Dynamical Systems*, *Dynamics of Systems* series, Gorky State Univ., Gorky, 1982, p. 49 (in Russian).
55. B. P. Borisov and A. I. Vesnitskii, in *Stability, Autovibrations and Stochasticity*, *Dynamics of Systems* series, Gorky State Univ., Gorky, 1985, p. 104 (in Russian).
56. T. G. Vesnitskaya and A. I. Vesnitskii, *Zhurn. Tekhnicheskoi Fiziki* **55**, 2312 (1985) [*Sov. Phys.—Tech. Phys.* **30**, 1373 (1985)].
57. H. E. Wilhelm *J. Appl. Phys.* **64**, 1652 (1988).
58. H. E. Wilhelm and M. A. Hasan, *Archiv für Elektrotechnik* **72**, 165 (1989).
59. Y. M. Ram and J. Caldwell, *J. Sound Vibr.* **194**, 35 (1996).
60. J. Cooper, *J. Math. Anal. Appl.* **174**, 67 (1993).
61. J. Dittrich, P. Duclos, and P. Šeba, *Phys. Rev. E* **49**, 3535 (1994).
62. M. Yamaguchi, *J. Diff. Equations* **135**, 1 (1997).
63. M. Yamaguchi, in *Dynamical Systems and Differential Equations*, *Discrete Contin. Dynam. Systems*, Springfield, MO, 1996, additional Vol. II, 303 (1998).
64. M. Yamaguchi and H. Yoshida, in *Operator Theory and Its Applications*, Winnipeg, MB, 1998; *Fields Inst. Commun.* **25**, 565 (2000).
65. J. Cooper, *IEEE Trans. Antennas Prop.* **41**, 1365 (1993).
66. J. Dittrich, P. Duclos, and N. Gonzalez, in D. V. Shirkov, D. I. Kazakov, and A. A. Vladimirov (Eds.), *Problems of Quantum Field Theory*, *Proc. 10th Int. Conf.* (Alushta, Crimea, May 1996), JINR, Dubna, 1996, p. 166.
67. J. Dittrich, P. Duclos, and N. Gonzalez, *Rev. Math. Phys.* **10**, 925 (1998).
68. N. Gonzalez, *J. Math. Anal. Appl.* **228**, 51 (1998).
69. R. de la Llave and N. P. Petrov, *Phys. Rev. E* **59**, 6637 (1999).

70. L. Gaffour and G. Grigorian, *J. Electromagn. Waves Appl.* **10**, 97 (1996).
71. L. Gaffour, *J. Electromagn. Waves Appl.* **10**, 757 (1996).
72. Y. Dolinsky and T. Elperin, *J. Appl. Phys.* **83**, 5644 (1998).
73. V. E. Mkrtchian and R. von Baltz, *J. Math. Phys.* **41**, 1956 (2000).
74. G. A. Grinberg, *Prikladnaya Matematika i Mekhanika* **33**, 269 (1969) [*Sov. J. Appl. Math. Mech.* **33**, 251 (1969)].
75. G. A. Grinberg and V. A. Koss, *Prikladnaya Matematika i Mekhanika* **35**, 759 (1971) [*Sov. J. Appl. Math. Mech.* **35**, 711 (1971)].
76. G. T. Moore, *J. Math. Phys.* **11**, 2679 (1970).
77. L. Parker, *Phys. Rev. Lett.* **21**, 562 (1968).
78. N. D. Birrell and P. C. W. Davies, *Quantum Fields in Curved Space*, Cambridge Univ. Press, Cambridge, UK, 1982.
79. A. A. Grib, S. G. Mamaev, and V. M. Mostepanenko, *Vacuum Quantum Effects in Intense Fields*, Energoatomizdat, Moscow, 1988 (in Russian).
80. A. I. Nikishov and V. I. Ritus, in V. L. Ginzburg (ed.), *Issues in Intense-Field Quantum Electrodynamics*, *Proc. Lebedev Physics Inst.*, Vol. 168, Nova Science, New York, 1987.
81. S. A. Fulling and P. C. W. Davies, *Proc. Roy. Soc. Lond.* **A348**, 393 (1976).
82. A. Hosoya, *Prog. Theor. Phys.* **61**, 280 (1979).
83. B. S. DeWitt, *Phys. Rep.* **19**, 295 (1975).
84. P. Candelas and D. Deutsch, *Proc. Roy. Soc. Lond.* **A354**, 79 (1977).
85. P. C. W. Davies and S. A. Fulling, *Proc. Roy. Soc. Lond.* **A356**, 237 (1977).
86. M. Horibe, *Prog. Theor. Phys.* **61**, 661 (1979).
87. K. Oku and Y. Tsuchida, *Prog. Theor. Phys.* **62**, 1756 (1979).
88. V. P. Frolov and E. M. Serebriany, *J. Phys. A* **12**, 2415 (1979).
89. V. P. Frolov and E. M. Serebriany, *J. Phys. A* **13**, 3205 (1980).
90. L. H. Ford and A. Vilenkin, *Phys. Rev. D* **25**, 2569 (1982).
91. Yu. M. Sinyukov, *J. Phys. A* **15**, 2533 (1982).
92. W. R. Walker and P. C. W. Davies, *J. Phys. A* **15**, L477 (1982).
93. M. Castagnino and R. Ferraro, *Ann. Phys.* (NY) **154**, 1 (1984).
94. W. R. Walker, *Phys. Rev. D* **31**, 767 (1985).
95. R. D. Carlitz and R. S. Willey, *Phys. Rev. D* **36**, 2327 (1987).
96. A. C. Ottewill and S. Takagi, *Prog. Theor. Phys.* **79**, 429 (1988).
97. A. I. Nikishov and V. I. Ritus, *Zh. Eksper. Teor. Fiz.* **108**, 1121 (1995) [*JETP* **81**, 615 (1995)].
98. V. I. Ritus, *Zh. Eksper. Teor. Fiz.* **110**, 526 (1996) [*JETP* **83**, 282 (1996)].
99. V. Frolov and D. Singh, *Class. Quant. Grav.* **16**, 3693 (1999).
100. W. G. Anderson and W. Israel, *Phys. Rev. D* **60**, 084003 (1999).
101. M. Bordag, G. Petrov, and D. Robaschik, *Yad. Fiz.* **39**, 1315 (1984) [*Sov. J. Nucl. Phys.* **39**, 828 (1984)].
102. G. Petrov, *Bulg. J. Phys.* **12**, 355 (1985).
103. M. Bordag, F.-M. Dittes, and D. Robaschik, *Yad. Fiz.* **43**, 1606 (1986) [*Sov. J. Nucl. Phys.* **43**, 1034 (1986)].
104. G. Petrov, *Rev. Roum. Phys.* **34**, 453 (1989).
105. H. Beyer and J. Nitsch, *Found. Phys.* **20**, 459 (1990).

106. V. V. Dodonov, A. B. Klimov and V. I. Man'ko, in V. I. Man'ko and M. A. Markov (Eds.), *Theory of the Interaction of Multilevel Systems with Quantized Fields*, *Proc. Lebedev Phys. Inst.*, Vol. 208, Nauka, Moscow, 1992, p. 105 (translated by Nova Science, New York, 1996, as Vol. 209, p. 1).
107. V. V. Dodonov and A. B. Klimov, *Phys. Lett. A* **167**, 309 (1992).
108. V. V. Dodonov and A. B. Klimov, *J. Sov. Laser Res.* **13**, 230 (1992).
109. A. B. Klimov and V. V. Dodonov, in D. Han, Y. S. Kim, and V. I. Man'ko (eds.), *Proc. 2 Int. Workshop on Squeezed States and Uncertainty Relations* (Moscow, May 25–29, 1992), NASA Conf. Publication 3219, NASA, Greenbelt, MD, 1993, p. 415.
110. V. V. Dodonov, A. B. Klimov, and D. E. Nikonov, *J. Math. Phys.* **34**, 2742 (1993).
111. D. A. R. Dalvit and F. D. Mazzitelli, *Phys. Rev. A* **57**, 2113 (1998).
112. D. A. R. Dalvit and F. D. Mazzitelli, *Phys. Rev. A* **59**, 3049 (1999).
113. L. A. Rivlin, *Kvantovaya Elektronika* **6**, 2248 (1979).
114. S. Sarkar, in E. R. Pike and H. Walther (Eds.), *Photons and Quantum Fluctuations*, Hilger, Bristol, 1988, p. 151.
115. S. Sarkar, *J. Phys. A* **21**, 971 (1988).
116. V. V. Dodonov, A. B. Klimov, and V. I. Man'ko, *Phys. Lett. A* **142**, 511 (1989).
117. H. B. G. Casimir, *Proc. Kon. Ned. Akad. Wetenschap* **51**, 793 (1948).
118. G. Plunien, B. Müller, and W. Greiner, *Phys. Rep.* **134**, 87 (1986).
119. P. W. Milonni, *The Quantum Vacuum: An Introduction to Quantum Electrodynamics*, Academic, San Diego, 1994.
120. V. M. Mostepanenko and N. N. Trunov, *The Casimir Effect and Its Applications*, Clarendon, Oxford, 1997.
121. S. K. Lamoreaux, *Am. J. Phys.* **67**, 850 (1999).
122. V. B. Braginsky and F. Y. Khalili, *Phys. Lett. A* **161**, 197 (1991).
123. M. T. Jaekel and S. Reynaud, *J. Phys.* (Paris) *I* **2**, 149 (1992).
124. V. V. Dodonov, A. B. Klimov, and V. I. Man'ko, *Phys. Lett. A* **149**, 225 (1990).
125. M. T. Jaekel and S. Reynaud, *Quant. Opt.* **4**, 39 (1992).
126. M. T. Jaekel and S. Reynaud, *Phys. Lett. A* **167**, 227 (1992).
127. M. T. Jaekel and S. Reynaud, *Phys. Lett. A* **172**, 319 (1993).
128. M. T. Jaekel and S. Reynaud, *J. Phys.* (Paris) *I* **3**, 1093 (1993).
129. C. Eberlein, *J. Phys.* (Paris) *I* **3**, 2151 (1993).
130. P. A. Maia Neto and S. Reynaud, *Phys. Rev. A* **47**, 1639 (1993).
131. P. A. Maia Neto, *J. Phys. A* **27**, 2167 (1994).
132. P. A. Maia Neto and L. A. S. Machado, *Braz. J. Phys.* **25**, 324 (1995).
133. A. B. Matsko, E. A. Zubova, and S. P. Vyatchanin, *Opt. Commun.* **131**, 107 (1996).
134. L. S. Levitov, *Europhys. Lett.* **8**, 499 (1989).
135. J. S. Hoye and I. Brevik, *Physica A* **181**, 413 (1992).
136. J. S. Hoye and I. Brevik, *Physica A* **196**, 241 (1993).
137. V. E. Mkrtchian, *Phys. Lett. A* **207**, 299 (1995).
138. J. B. Pendry, *J. Phys. Condensed Matter* **9**, 10301 (1997).
139. A. I. Volokitin and B. N. J. Persson, *J. Phys. Condensed Matter* **11**, 345 (1999).
140. M. T. Jaekel and S. Reynaud, *Rep. Prog. Phys.* **60**, 863 (1997).

141. M. Kardar and R. Golestanian, *Rev. Mod. Phys.* **71**, 1233 (1999).
142. G. Barton and C. Eberlein, *Ann. Phys.* (NY) **227**, 222 (1993).
143. G. Barton and A. Calogeracos, *Ann. Phys.* (NY) **238**, 227 (1995).
144. A. Calogeracos and G. Barton, *Ann. Phys.* (NY) **238**, 268 (1995).
145. G. M. Salamone and G. Barton, *Phys. Rev. A* **51**, 3506 (1995).
146. G. Barton, *Ann. Phys.* (NY) **245**, 361 (1996).
147. G. Barton and C. A. North, *Ann. Phys.* (NY) **252**, 72 (1996).
148. R. Gütig and C. Eberlein, *J. Phys. A* **31**, 6819 (1998).
149. V. I. Man'ko, in M. Bertolotti and E. R. Pike (Eds.), *Proc. Eur. Conf. Optics, Optical Systems and Applications* "ECOOSA 90—Quantum Optics," Rome, 1990, IOP Conf. Proc. 115, Institute of Physics, Bristol, 1991, p. 39.
150. V. I. Man'ko, *J. Sov. Laser Res.* **12**, 383 (1991).
151. V. V. Dodonov, O. V. Man'ko, and V. I. Man'ko, in M. A. Markov (Ed.), *Squeezed and Correlated States of Quantum Systems*, *Proc. Lebedev Physics Inst.*, Vol. 200, Nauka, Moscow, 1991, p. 155 (translated by Nova Science, New York, 1993, as Vol. 205, p. 163).
152. V. I. Man'ko, in P. Tombesi and D. F. Walls (Eds.), *Quantum Measurements in Optics*, Plenum, New York, 1992, NATO ASI Series B, Physics, Vol. 282, p. 239.
153. J. Schwinger, *Proc. Natl. Acad. Sci. (USA)* **90**, 958 (1993).
154. J. Schwinger, *Proc. Natl. Acad. Sci. (USA)* **90**, 2105 (1993).
155. J. Schwinger, *Proc. Natl. Acad. Sci. (USA)* **90**, 4505 (1993).
156. J. Schwinger, *Proc. Natl. Acad. Sci. (USA)* **90**, 7285 (1993).
157. J. Schwinger, *Proc. Natl. Acad. Sci. (USA)* **91**, 6473 (1994).
158. V. V. Dodonov, A. B. Klimov, and V. I. Man'ko, in V. V. Dodonov and V. I. Man'ko (Eds.), *Group Theoretical Methods in Physics, Proc. XVIII Int. Colloquium* (Moscow, June 1990), *Lecture Notes in Physics*, Vol. 382, Springer, Berlin, 1991, p. 450.
159. V. V. Dodonov, A. B. Klimov and V. I. Man'ko, *J. Sov. Laser Res.* **12**, 439 (1991).
160. V. V. Dodonov, A. B. Klimov, and D. E. Nikonov, in D. Han, Y. S. Kim, and W. Zachary (Eds.), *Proc. Workshop on Squeezed States and Uncertainty Relations* (College Park, March 1991), NASA Conf. Publication **3135**, NASA, Greenbelt, MD, 1992, p. 199.
161. S. Sarkar, *Quant. Opt.* **4**, 345 (1992).
162. S. Weigert, *Phys. Lett. A* **214**, 215 (1996).
163. A. B. Klimov and V. Altuzar, *Phys. Lett. A* **226**, 41 (1997).
164. C. K. Law, *Phys. Rev. Lett.* **73**, 1931 (1994).
165. C. K. Cole and W. C. Schieve, *Phys. Rev. A* **52**, 4405 (1995).
166. O. Méplan and C. Gignoux, *Phys. Rev. Lett.* **76**, 408 (1996).
167. L.-P. Fu, C. K. Duan, and G.-C. Guo, *Phys. Lett. A* **234**, 163 (1997).
168. Y. Wu, K. W. Chan, M.-C. Chu, and P. T. Leung, *Phys. Rev. A* **59**, 1662 (1999).
169. M. Razavy and J. Terning, *Lett. Nuovo Cim.* **41**, 561 (1984).
170. M. Razavy and J. Terning, *Phys. Rev. D* **31**, 307 (1985).
171. M. Razavy, *Hadronic J.* **8**, 153 (1985).
172. M. Razavy, *Lett. Nuovo Cim.* **37**, 449 (1983).
173. M. Reuter and C. T. Hill, *Ann. Phys.* (NY) **195**, 190 (1989).
174. G. Calucci, *J. Phys. A* **25**, 3873 (1992).

175. M. Janowicz, *Phys. Rev. A* **57**, 4784 (1998).
176. C. K. Law, *Phys. Rev. A* **49**, 433 (1994).
177. C. K. Law, *Phys. Rev. A* **51**, 2537 (1995).
178. A. V. Chizhov, G. Schrade, and M. S. Zubairy, *Phys. Lett. A* **230**, 269 (1997).
179. J.-Y. Ji, H.-H. Jung, J.-W. Park, and K.-S. Soh, *Phys. Rev. A* **56**, 4440 (1997).
180. J.-Y. Ji, H.-H. Jung, and K.-S. Soh, *Phys. Rev. A* **57**, 4952 (1998).
181. J.-Y. Ji and K.-S. Soh, *J. Kor. Phys. Soc.* **33**, S490 (1998).
182. J.-Y. Ji, K.-S. Soh, R.-G. Cai, and S. P. Kim, *J. Phys. A* **31**, L457 (1998).
183. H. Johnston and S. Sarkar, *J. Phys. A* **29**, 1741 (1996).
184. R. Schützhold, G. Plunien, and G. Soff, *Phys. Rev. A* **57**, 2311 (1998).
185. G. Plunien, R. Schützhold, and G. Soff, in M. Bordag (Ed.), *The Casimir Effect Fifty Years Later*, *Proc. 4th Workshop on Quantum Field Theory under the Influence of External Conditions* (Leipzig, Germany, Sept. 14–18 1998), World Scientific, Singapore, 1999, p. 133.
186. Y. Wu, M.-C. Chu, and P. T. Leung, *Phys. Rev. A* **59**, 3032 (1999).
187. X.-X. Yang and Y. Wu, *J. Phys. A* **32**, 7375 (1999).
188. V. V. Dodonov, *Phys. Lett. A* **207**, 126 (1995).
189. V. V. Dodonov and A. B. Klimov, *Phys. Rev. A* **53**, 2664 (1996).
190. V. V. Dodonov, *Phys. Lett. A* **213**, 219 (1996).
191. V. V. Dodonov, *J. Phys. A* **31**, 9835 (1998).
192. V. V. Dodonov and M. A. Andreata, *J. Phys. A* **32**, 6711 (1999).
193. M. A. Andreata and V. V. Dodonov, *J. Phys.* A **33**, 3209 (2000).
194. V. V. Dodonov, *Phys. Lett. A* **244**, 517 (1998).
195. V. V. Dodonov, *Phys. Rev. A* **58**, 4147 (1998).
196. R. Jáuregui, C. Villarreal and S. Hacyan, *Mod. Phys. Lett. A* **10**, 619 (1995).
197. C. Villarreal, S. Hacyan, and R. Jáuregui, *Phys. Rev. A* **52**, 594 (1995).
198. D. F. Mundarain and P. A. Maia Neto, *Phys. Rev. A* **57**, 1379 (1998).
199. M. A. Cirone and K. Rzążewski, *Phys. Rev. A* **60**, 886 (1999).
200. A. Lambrecht, M.-T. Jaekel, and S. Reynaud, *Phys. Rev. Lett.* **77**, 615 (1996).
201. P. A. Maia Neto and L. A. S. Machado, *Phys. Rev. A* **54**, 3420 (1996).
202. J. P. F. Mendonça, P. A. Maia Neto, and F. I. Takakura, *Opt. Commun.* **160**, 335 (1999).
203. R. Golestanian and M. Kardar, *Phys. Rev. Lett.* **78**, 3421 (1997).
204. F. Miri and R. Golestanian, *Phys. Rev. A* **59**, 2291 (1999).
205. R. Golestanian and M. Kardar, *Phys. Rev. A* **58**, 1713 (1998).
206. V. V. Kulagin and V. A. Cherepenin, *Pis'ma ZhETF* **63**, 160 (1996) [*JETP Lett.* **63**, 170 (1996)].
207. V. V. Kulagin and V. A. Cherepenin, *Laser Phys.* **7**, 131 (1997).
208. Y. E. Lozovik, V. G. Tsvetus, and E. A. Vinogradov, *Pis'ma ZhETF* **61**, 711 (1995) [*JETP Lett.* **61**, 723 (1995)].
209. Y. E. Lozovik, V. G. Tsvetus, and E. A. Vinogradov, *Phys. Scripta* **52**, 184 (1995).
210. A. Lambrecht, M.-T. Jaekel, and S. Reynaud, *Europhys. Lett.* **43**, 147 (1998).
211. G. Plunien, R. Schützhold, and G. Soff, *Phys. Rev. Lett.* **84**, 1882 (2000).
212. J. Hui, Q. Y. Shi, and J. S. Wu, *Phys. Lett. A* **268**, 174 (2000).
213. A. Lambrecht, M.-T. Jaekel, and S. Reynaud, *Eur. Phys. J. D* **3**, 95 (1998).

214. A. Yariv, *IEEE J. Quant. Electron.* **QE2**, 30 (1966).
215. E. Yablonovitch, *Phys. Rev. Lett.* **62**, 1742 (1989).
216. W. G. Unruh, *Phys. Rev. D* **14**, 870 (1976).
217. Z. Bialynicka-Birula and I. Bialynicki-Birula, *J. Opt. Soc. Am. B* **4**, 1621 (1987).
218. A. A. Lobashov and V. M. Mostepanenko, *Teor. Mat. Fiz.* **86**, 438 (1991) [*Theor. Math. Phys.* **86**, 303 (1991)].
219. A. A. Lobashov and V. M. Mostepanenko, *Teor. Mat. Fiz.* **88**, 340 (1991) [*Theor. Math. Phys.* **88**, 913 (1991)].
220. V. V. Dodonov, T. F. George, O. V. Man'ko, C. I. Um, and K. H. Yeon, *J. Sov. Laser Res.* **13**, 219 (1992).
221. V. V. Hizhnyakov, *Quant. Opt.* **4**, 277 (1992).
222. V. V. Dodonov, A. B. Klimov, and D. E. Nikonov, *Phys. Rev. A* **47**, 4422 (1993).
223. V. V. Dodonov and V. I. Man'ko, in M. Evans and S. Kielich (Eds.), *Modern Nonlinear Optics*, Part 3, *Advances in Chemical Physics* series, Vol. LXXXV, Wiley, New York, 1994, p. 499.
224. T. Okushima and A. Shimizu, *Jpn. J. Appl. Phys.* **34**, 4508 (1995).
225. M. Artoni, A. Bulatov, and J. Birman, *Phys. Rev. A* **53**, 1031 (1996).
226. M. Cirone, K. Rzążewski, and J. Mostowski, *Phys. Rev. A* **55**, 62 (1997).
227. M. Artoni, A. Bulatov, and B. D. Seery, *Phys. Rev. A* **58**, 3345 (1998).
228. J. B. Pendry, *J. Mod. Opt.* **45**, 2389 (1998).
229. C. Eberlein, *J. Phys. A* **32**, 2583 (1999).
230. H. Saito and H. Hyuga, *J. Phys. Soc. Jpn.* **65**, 1139 (1996).
231. H. Saito and H. Hyuga, *J. Phys. Soc. Jpn.* **65**, 3513 (1996).
232. H. Johnston and S. Sarkar, *Phys. Rev. A* **51**, 4109 (1995).
233. G. E. Volovik, *JETP Lett.* **63**, 483 (1996).
234. C. K. Law, S.-Y. Zhu, and M. S. Zubairy, *Phys. Rev. A* **52**, 4095 (1995).
235. R. Jáuregui and C. Villarreal, *Phys. Rev. A* **54**, 3480 (1996).
236. T. Taneichi and T. Kobayashi, *J. Phys. Soc. Jpn.* **67**, 1594 (1998).
237. M. Janowicz, *Phys. Rev. A* **57**, 5016 (1998).
238. A. M. Fedotov, N. B. Narozhny, and Y. E. Lozovik, *Phys. Lett. A* **274**, 213 (2000).
239. A. Dorsel, J. D. McCullen, P. Meystre, E. Vignes, and H. Walther, *Phys. Rev. Lett.* **51**, 1550 (1983).
240. A. Cozzini, F. Maccarrone, F. Mango, I. Longo, and S. Barbarino, *J. Opt. Soc. Am. B* **2**, 1841 (1985).
241. P. Meystre, E. M. Wright, J. D. McCullen, and E. Vignes, *J. Opt. Soc. Am. B* **2**, 1830 (1985).
242. S. Solimeno, F. Barone, C. DeLisio, L. DiFiore, L. Milano, and G. Russo, *Phys. Rev. A* **43**, 6227 (1991).
243. A. Luis and L. L. Sanchez-Soto, *Phys. Rev. A* **45**, 8228 (1992).
244. C. Fabre, M. Pinard, S. Bourzeix, A. Heidmann, E. Giacobino, and S. Reynaud, *Phys. Rev. A* **49**, 1337 (1994).
245. K. Jacobs, P. Tombesi, M. J. Collett, and D. F. Walls, *Phys. Rev. A* **49**, 1961 (1994).
246. S. Mancini and P. Tombesi, *Phys. Rev. A* **49**, 4055 (1994).
247. A. Heidmann and S. Reynaud, *Phys. Rev. A* **50**, 4237 (1994).

248. M. Pinard, C. Fabre, E. Giacobino, A. Heidmann, and S. Reynaud, *Ann. Physique* (Paris) **20**, 133 (1995).
249. A. Heidmann, Y. Hadjar, and M. Pinard, *Appl. Phys. B* **64**, 173 (1997).
250. K. Jacobs, I. Tittonen, H. M. Wiseman, and S. Schiller, *Phys. Rev. A* **60**, 538 (1999).
251. M. Pinard, Y. Hadjar, and A. Heidmann, *Eur. Phys. J. D* **7** 107 (1999).
252. P. F. Cohadon, A. Heidmann, and M. Pinard, *Phys. Rev. Lett.* **83**, 3174 (1999).
253. C. Brif and A. Mann, *J. Opt. B* **2**, 53 (2000).
254. A. F. Pace, M. J. Collett, and D. F. Walls, *Phys. Rev. A* **47**, 3173 (1993).
255. M. F. Bocko and R. Onofrio, *Rev. Mod. Phys.* **68**, 755 (1996).
256. S. Mancini, V. I. Man'ko, and P. Tombesi, *Phys. Rev. A* **55**, 3042 (1997).
257. S. Bose, K. Jacobs, and P. L. Knight, *Phys. Rev. A* **56**, 4175 (1997).
258. S.-B. Zheng, *Quantum Semiclass. Opt.* **10**, 657 (1998).
259. D. A. R. Dalvit and P. A. Maia Neto, *Phys. Rev. Lett.* **84**, 798 (2000).
260. P. A. Maia Neto and D. A. R. Dalvit, *Phys. Rev.* A **62**, 042103 (2000).
261. Y. Nagatani and K. Shigetomi, *Phys. Rev. A* **62**, 022117 (2000).
262. L. H. Ford and N. F. Svaiter, *Phys. Rev. D* **58**, 065007 (1998).
263. G. Gour and L. Sriramkumar, *Found. Phys.* **29**, 1917 (1999).
264. C. Anastopoulos, *J. Math. Phys.* **41**, 617 (2000).
265. I. Brevik, K. A. Milton, S. D. Odintsov, and K. E. Osetrin, *Phys. Rev. D* **62**, 064005 (2000).
266. W. H. Louisell, *Coupled Mode and Parametric Electronics*, Wiley, New York, 1960.
267. L. D. Landau and E. M. Lifshitz, *Mechanics*, Pergamon, Oxford, 1969.
268. N. N. Bogoliubov and Y. A. Mitropolsky, *Asymptotic Methods in the Theory of Non-Linear Oscillations*, Gordon & Breach, New York, 1985.
269. A. Erdélyi (Ed.), *Bateman Manuscript Project, Higher Transcendental Functions*, McGraw-Hill, New York, 1953.
270. M. Abramowitz and I. A. Stegun (Eds.), *Handbook of Mathematical Functions*, Dover, New York, 1972.
271. V. V. Dodonov, E. V. Kurmyshev, and V. I. Man'ko, *Phys. Lett. A* **79**, 150 (1980).
272. V. V. Dodonov, A. B. Klimov, and V. I. Man'ko, in M. A. Markov (Ed.), *Squeezed and Correlated States of Quantum Systems*, *Proc. Lebedev Physics Inst.*, Vol. 200, Nauka, Moscow, 1991, p. 56 (Nova Science, New York, 1993, Vol. 205, p. 61).
273. A. Lukš, V. Peřinova, and Z. Hradil, *Acta Phys. Polon. A* **74**, 713 (1988).
274. V. V. Dodonov, V. I. Man'ko, and P. G. Polynkin, *Phys. Lett. A* **188**, 232 (1994).
275. A. P. Prudnikov, Y. A. Brychkov, and O. I. Marichev, *Integrals and Series. Additional Chapters*, Nauka, Moscow, 1986.
276. I. S. Gradshtein and I. M. Ryzhik, *Tables of Integrals, Series and Products*, Academic, New York, 1994.
277. V. V. Dodonov and V. I. Man'ko, in A. A. Komar (Ed.), *Group Theory, Gravitation and Elementary Particle Physics*, *Proc. Lebedev Physics Inst.*, Vol. 167, Nova Science, New York, 1987, pp. 7–101.
278. V. V. Dodonov, I. A. Malkin, and V. I. Man'ko, *Int. J. Theor. Phys.* **14**, 37 (1975).
279. V. V. Dodonov and V. I. Man'ko, *Invariants and the Evolution of Nonstationary Quantum Systems*, *Proc. Lebedev Physics Inst.*, Vol. 183, Nova Science, New York, 1989.
280. V. V. Dodonov, O. V. Man'ko, and V. I. Man'ko, *Phys. Rev. A* **49**, 2993 (1994).

281. V. V. Dodonov and V. I. Man'ko, *J. Math. Phys.* **35**, 4277 (1994).
282. V. V. Dodonov, *J. Phys. A* **27**, 6191 (1994).
283. G. Szegö, *Orthogonal Polynomials*, American Mathematical Society, New York, 1959.
284. L. Mandel, *Opt. Lett.* **4**, 205 (1979).
285. K. Husimi, *Prog. Theor. Phys.* **9**, 381 (1953).
286. V. V. Dodonov and V. I. Man'ko, *Phys. Rev. A* **20**, 550 (1979).
287. W. H. Louisell, A. Yariv, and A. E. Siegman, *Phys. Rev.* **124**, 1646 (1961).
288. H. Takahasi, in A. V. Balakrishnan, (Ed.), *Advances in Communication Systems. Theory and Applications*, Vol. 1, Academic, New York, 1965, pp. 227–310.
289. M. T. Raiford, *Phys. Rev. A* **2**, 1541 (1970).
290. V. V. Dodonov, V. I. Man'ko, and V. N. Rudenko, *Pis'ma Zh. Exper. Teor. Fiz.* **36**, 53 (1982) [*Sov. Phys. JETP Lett.* **36**, 63 (1982)].
291. W. H. Louisell, *Radiation and Noise in Quantum Electronics*, McGraw-Hill, New York, 1964.
292. R. J. Glauber and M. Lewenstein, *Phys. Rev. A* **43**, 467 (1991).
293. A. Tip, *Phys. Rev. A* **56**, 5022 (1997).
294. R. Matloob, R. Loudon, S. M. Barnett, and J. Jeffers, *Phys. Rev. A* **52**, 4823 (1995).
295. R. Matloob and R. Loudon, *Phys. Rev. A* **53**, 4567 (1996).
296. T. Gruner and D.-G. Welsch, *Phys. Rev. A* **53**, 1818 (1996).
297. T. Gruner and D.-G. Welsch, *Phys. Rev. A* **54**, 1661 (1996).
298. K. Ujihara, *Phys. Rev. A* **12**, 148 (1975).
299. J. Gea-Banacloche, N. Lu, L. M. Pedrotti, S. Prasad, M. O. Scully, and K. Wódkiewicz, *Phys. Rev. A* **41**, 369 (1990).
300. L. Knöll, W. Vogel, and D.-G. Welsch, *Phys. Rev. A* **43**, 543 (1991).
301. M. T. Raiford, *Phys. Rev. A* **9**, 2060 (1974).
302. M. Hotta, I. Joichi, S. Matsumoto, and M. Yoshimura, *Phys. Rev. D* **55**, 4614 (1997).
303. M. J. Collett and C. W. Gardiner, *Phys. Rev. A* **30**, 1386 (1984).
304. H. J. Carmichael, *J. Opt. Soc. Am. B* **4**, 1588 (1987).
305. H. Haken, *Rev. Mod. Phys.* **47**, 67 (1975).
306. E. B. Davies, *Quantum Theory of Open Systems*, Academic, London, 1976.
307. H. Spohn, *Rev. Mod. Phys.* **52**, 569 (1980).
308. H. Dekker, *Phys. Rep.* **80**, 1 (1981).
309. C. W. Gardiner and M. J. Collett, *Phys. Rev. A* **31**, 3761 (1985).
310. C. W. Gardiner, A. S. Parkins, and M. J. Collett, *J. Opt. Soc. Am. B* **4**, 1683 (1987).
311. P. T. Leung, S. Y. Liu, and K. Young, *Phys. Rev. A* **49**, 3057 (1994).
312. E. S. C. Ching, P. T. Leung, A. Maassen van den Brink, W. M. Suen, S. S. Tong, and K. Young, *Rev. Mod. Phys.* **70**, 1545 (1998).
313. M. Hillery, R. F. O'Connell, M. O. Scully, and E. P. Wigner, *Phys. Rep.* **106**, 121 (1984).
314. V. V. Dodonov, O. V. Man'ko, and V. I. Man'ko, *J. Russ. Laser Res.* **16**, 1 (1995).
315. R. J. Glauber, in R. J. Glauber (Ed.), *Proc. Int. School of Physics "Enrico Fermi"*, Academic, New York, 1969, Vol. XLII, p. 15.
316. V. V. Dodonov and V. I. Man'ko, in M. A. Markov, V. I. Man'ko, and A. E. Shabad (Eds.), *Group Theoretical Methods in Physics, Proc. 2nd Int. Seminar* (Zvenigorod, 1982), Harwood Academic, New York, 1985, Vol. 1, p. 705.

317. A. Barchielli, *Nuovo Cim. B* **74**, 113 (1983).
318. H. Dekker and M. C. Valsakumar, *Phys. Lett. A* **104**, 67 (1984).
319. A. Săndulescu and H. Scutaru, *Ann. Phys.* (NY) **173**, 277 (1987).
320. V. V. Dodonov and V. I. Man'ko, *Physica A* **94**, 403 (1978).
321. E. Schrödinger, *Ber. Kgl. Akad. Wiss. Berlin* **24**, 296 (1930).
322. H. P. Robertson, *Phys. Rev.* **35**, 667 (1930).
323. V. V. Dodonov, *J. Phys. A* **33**, 7721 (2000).
324. D. E. Gray (Ed.), *American Institute of Physics Handbook*, McGraw-Hill, New York, 1972.
325. G. Rempe, F. Schmidt-Kaler, and H. Walther, *Phys. Rev. Lett.* **64**, 2783 (1990).
326. J. D. N. Cheeke, *Can. J. Phys.* **75**, 77 (1997).
327. B. P. Barber, R. A. Hiller, R. Löfsted, S. J. Putterman, and K. R. Weninger, *Phys. Rep.* **282**, 65 (1997).
328. *Acoustic Cavitation and Sonoluminescence*, special issue of *Phil. Trans. A* **357**(1751) (1999).
329. E. Sassaroli, Y. N. Srivastava, and A. Widom, *Phys. Rev. A* **50**, 1027 (1994).
330. C. Eberlein, *Phys. Rev. A* **53**, 2772 (1996).
331. C. Eberlein, *Phys. Rev. Lett.* **76**, 3842 (1996).
332. R. Esquivel-Sirvent, R. Jáuregui, and C. Villarreal, *Phys. Rev. A* **56**, 2463 (1997).
333. M. Bordag (Ed.), *The Casimir Effect Fifty Years Later, Proc. 4th Workshop on Quantum Field Theory under the Influence of External Conditions* (Leipzig, Germany, Sept. 14–18, 1998), World Scientific (Singapore, 1999).

QUANTUM MULTIPOLE RADIATION

ALEXANDER S. SHUMOVSKY

Physics Department, Bilkent University, Bilkent, Ankara, Turkey

There are some points which are as dark as ever. But we have so much that it will be our own fault if we cannot get the rest.

—Sir Arthur Conan Doyle, *The Second Stain*

CONTENTS

I. INTRODUCTION

> Before we start to investigate that, let us try to realize what we do know, so as to make the most of it, and to separate the essential from the accidental.
>
> —Sir Arthur Conan Doyle, *The Priory School*

Since the pioneering paper by Dirac [1], the formalism of quantum electrodynamics (QED) has been based on the use of the photon creation and annihilation operators, forming a representation of the Weyl–Heisenberg algebra, and on the notion of the electromagnetic vacuum state [2–4]. As far as a denumerable set of Fock number states can be generated from the vacuum state by successive action of the creation operator, one can choose to interpret the electromagnetic vacuum as a ''physical system'' ready for support of any electromagnetic radiation.

It is not heretical to consider the electromagnetic vacuum as a ''physical system.'' In fact, it manifests some physical properties and is responsible for a number of important effects. For example, the field amplitudes continue to oscillate in the vacuum state. These zero-point oscillations cause the spontaneous emission [1], the natural linebreadth [5], the Lamb shift [6], the Casimir force between conductors [7], and the quantum beats [8]. It is also possible to generate quantum states of electromagnetic field in which the amplitude fluctuations are reduced below the symmetric quantum limit of zero-point oscillations in one quadrature component [9].

In spite of the great success of QED, there still are a number of unclear principal problems [10–15]. Leaving aside the detailed discussion of foundations of QED, we shall concentrate here on the problems of localization of photons and quantum phase of electromagnetic radiation, which have attracted a great deal of interest.

The point is that the photon creation and annihilation operators are defined in QED as nonlocal objects. In other words, the photon number operator gives the total number of photons in the volume of quantization without specification of their spacetime location [14,15]. Moreover, it has been proved by Newton and Wigner [16] that no position operator can exist for the photon. There is a widespread belief that the maximum precise localization appears in the form of

a wavefront [17]. At the same time, the specific falloff of the photon energy density and of the photodetection rate can be interpreted as the photon localization in space [18,19].

Perhaps the most evident and bright example of photon localization is provided by the photodetection process, when a photon is transformed into electronic signal in the sensitive element of the detecting device [20]. Such a localization is usually described in the operational way (in terms of what can be measured by a macroscopic detector) through the use of the so-called configuration number operator, determining the number of photons in the cylindrical volume $\sigma c\,\Delta t$, where σ denotes the area of the sensitive element, c is the light velocity, and Δt is the detector exposition time [14,20]. Other interesting examples are provided by the localization in photonic crystals [21] and by the emission and absorption of radiation by atoms and molecules [22].

We now stress that, in the usual treatment of photon localization, the radiation field is considered as though it consist of the *plane waves of photons* [14–20]. In reality, the radiation emitted by the atomic transitions corresponds to the *multipole photons* [23] represented by the quantized spherical waves [2].

Although the classical plane and spherical waves are equivalent in the sense that they both form complete orthogonal sets of solutions of the homogeneous Helmholtz wave equation [24,25], there is a strong qualitative difference between the two quantum representations. The plane waves of photons correspond to the running-wave solutions of the homogeneous Helmholtz wave equation in a large but finite cubic cavity with periodic boundary conditions [1,2,14,15]. This choice of the boundary conditions corresponds to the translational symmetry of solutions and leads to the states of photons with given linear momentum [3,10,11]. In turn, the solution of the homogeneous Helmholtz wave equation in terms of spherical waves assumes the existence of a singular point, corresponding to an atom (source or absorber of radiation) whose size is small with respect to the wavelength [24–26]. In this case, the boundary conditions correspond to the rotational symmetry and lead to the states of photons with given angular momentum [2,4,27]. Since the components of linear and angular momenta do not commute, the two representations of quantum electromagnetic field correspond to physical quantities that cannot be measured at once.

The simplest way to show the principal difference between the representations of plane and multipole photons is to compare the number of independent quantum operators (degrees of freedom), describing the monochromatic radiation field. In the case of plane waves of photons with given wavevector $\vec{k}$ (energy and linear momentum), there are only two independent creation or annihilation operators of photons with different polarization [2,14,15]. It is well known that QED (quantum electrodynamics) interprets the polarization as given spin state of photons [4]. The spin of photon is known to be 1, so that there are three possible spin states. In the case of plane waves, projection of spin on the

direction of $\vec{k}$ is forbidden because of the translational invariance, and hence only two transversal polarizations are allowed [4].

In turn, the monochromatic multipole photons are described by the scalar wavenumber k (energy), parity (type of radiation either electric or magnetic), angular momentum $j = 1, 2, \ldots$, and projection $m = -j, \ldots, j$ [2,26,27]. This means that even in the simplest case of monochromatic dipole $(j = 1)$ photons of either type, there are three independent creation or annihilation operators labeled by the index $m = 0, \pm 1$. Thus, the representation of multipole photons has much physical properties in comparison with the plane waves of photons. For example, the third spin state is allowed in this case and therefore the quantum multipole radiation is specified by three different polarizations, two transversal and one longitudinal (with respect to the radial direction from the source) [27,28]. In contrast to the plane waves of photons, the projection of spin is not a quantum number in the case of multipole photons. Therefore, the polarization is not a global characteristic of the multipole radiation but changes with distance from the source [22].

Another very important difference between the plane and multipole photons consists in the character of zero-point oscillations of the field strengths [29]. We shall show here that, unlike the former case with spatially homogeneous zero-point oscillations, the multipole vacuum noise strongly depends on the distance from the singular point (atom). It is not an unexpected result. In fact, zero-point oscillations reflect the structure of the electromagnetic vacuum state, which, in turn, depends on the boundary conditions for the homogeneous Helmholtz wave equation [3]. Let us note in this connection that the possible influence of an atom on the electromagnetic vacuum state in the absence of radiation has been discussed in QED for a long time [30,31]. It should be stressed that the spatial inhomogeneity of the multipole vacuum noise can be very important for prognosis of experiments with trapped atoms [32] and single-atom laser [33], especially in the engineered entanglement in the atom–photon systems [32].

We now note that, since the 1990s entanglement has been recognized as one of the most fundamental features of quantum systems as well as an important tool of quantum communication and information processing [34]. One of the promising ways in the engineered entanglement is represented by the so-called two-photon polarization entanglement (see Sec. 12.14 in Ref. 14). In this case, the cascade decay of an atomic transition leads to the creation of two entangled photons with different polarizations and different directions of propagation. Therefore, an adequate estimation of the vacuum noise in atom–photon interactions seems to be of great importance.

While the simplified picture based on the model of plane waves of photons, neglecting the presence of sources and absorbers, is incapable of describing the photon localization, we show here that the use of the rich physical properties of multipole photons leads to an adequate description of localization in the atom–

field interaction processes as well as in conventional photodetection. We note that the causal relation between the boundary conditions for the homogeneous Helmholtz wave equation and photon localization has been discussed since the late 1990s [19,22,29,35].

The representation of multipole photons is also useful in the investigation of the quantum phase problem [36]. In the pioneering paper [1] on the quantization of electromagnetic field, Dirac first postulated the existence of a Hermitian phase operator defined by the polar decomposition of the annihilation operator and conjugated to the photon number operator. Later it was realized that the Dirac's phase operator cannot be considered as a properly defined Hermitian operator, describing the quantum phase properties of electromagnetic radiation (for reviews, see Refs. 14 and 37–40). In particular, Susskind and Glogower [41] emphasized that the main difficulty in the correct definition of the phase operator arises because the spectrum of the number operator is bounded from below. An extension of the eigenvalue spectrum to negative values allows for the correct mathematical construction of the Hermitian phase operator [42,43], which leads to nonphysical states. An attempt to use the cosine and sine of the phase operators rather than the quantum phase operator has also been discussed [44].

A way to overcome the difficulties in the definition of the Hermitian phase operator has been proposed by Pegg and Barnett [40,45]. Their method is based on a contraction of the infinite-dimensional Hilbert–Fock space of photon states $\mathscr{H}$. Within this method, the quantum phase variable is determined first in a finite s-dimensional subspace of $\mathscr{H}$, where the polar decomposition is allowed. The formal limit $s \to \infty$ is taken only after the averages of the operators, describing the physical quantities, have been calculated. Let us stress that any restriction of dimension of the Hilbert–Fock space of photons is equivalent to an effective violation of the algebraic properties of the photon operators and therefore can lead to an inadequate picture of quantum fluctuations [46].

Perhaps, the most important result in the field of quantum phase problem was obtained by Mandel et al. [47] within the framework of the operational approach. According to their analysis, *there is no unique quantum phase variable, describing universally the measured phase properties of light*. This very strong statement has obtained a totally convincing confirmation in a number of experiments [47,48]. The results of the operational approach can be interpreted with the aid of the method based on the special quasiprobability distribution functions [49].

Generally speaking, the quantum phase variables can be divided into two classes. First, we have the pure operational phases that are completely determined by the scheme of measurement. This has no contradiction with the existence of an intrinsic quantum-dynamical variable responsible for the phase properties of light [50]. In addition, there might be some *inherent* quantum

phases related to the quantum properties of photons. Since any photon can be specified by its energy, angular momentum, and/or linear momentum, the inherent phase should be determined by either the angular or linear momenta, as the energy is a scalar. The former is connected with the spin states and hence, with the polarization of radiation field. The latter can lead to some "geometric" phase, which, for example, can be measured as the phase difference between two plane waves emitted by one source in opposite directions.

It is well known that the angular momentum of a quantum mechanical system is specified by a representation of the $SU(2)$ algebra. If the corresponding enveloping algebra contains a uniquely defined scalar (the Casimir operator), the polar decomposition of the angular momentum can be obtained [51]. This polar decomposition determines a dual representation of the $SU(2)$ algebra expressed in terms of so-called phase states [51]. In particular, the Hermitian operator of the $SU(2)$ quantum phase can be constructed [51].

Although the angular momentum of quantum multipole radiation is well defined in terms of the multipole photon operators of creation and annihilation, the direct polar decomposition of the corresponding $SU(2)$ subalgebra in the Weyl–Heisenberg algebra is impossible. The point is that this $SU(2)$ subalgebra has no isotype representation [52]. This means that the Casimir operator (scalar) cannot be uniquely determined in the whole Hilbert–Fock space of photon states. Hence, the quantum phase of the angular momentum of multipole photons cannot be determined by a method proposed [51] as valid for the quantum mechanical systems.

An approach focused on overcoming this difficulty has been developed [36,46,53,54]. The main idea, which seems to be a very natural one, is to consider the radiation of a given quantum source (atom or molecule) rather than a source-free electromagnetic field represented by the plane waves. Even in the classical picture, the multipole radiation can be determined completely only if the source functions, describing a local source at the origin, are known [25]. Within the quantum picture where the atom–field interaction is described in terms of the perturbation theory [26], we can take into account the source dependence of radiation using the conservation laws. In particular, the conservation of angular momentum in the process of radiation [26] permits us first to define the $SU(2)$ quantum phase of the atomic transition, following the method by Vourdas [51], an then to construct an operator complement of the atomic cosine and sine operators with respect to the integrals of motion in the whole atom–field system [36].

Many attempts have been made to define the quantum phase of light via the angular momentum (e.g., see Ref. 55 and references cited therein). The new element of our approach [36,46,53,54] is that we determine the quantum phase of radiation via the quantum phase of the angular momentum of its source.

Let us stress that the electromagnetic vacuum state has no phase at all. This is the same as saying that the vacuum state is degenerated with respect to the phase or that the phase is distributed uniformly over the vacuum [14,15]. The degeneration is taken off in the process of creation of the photon by atomic transition. Thus, it seems quite logic to assume that the inherent quantum phase of photons is generated by the source [36,46]. Definitely, this is not an unusual assumption. Actually, the classical amplitudes of the multipole field are completely determined by the source functions, describing the charge density, current density, and magnetization [25]. Hence, the multipole photon operators, which are obtained by the quantization of classical amplitudes [1,2], are also specified by the source [56].

We also note that, in contrast to the Pegg–Barnett formalism [45], we consider an extended space of states, including the Hilbert–Fock state of photons as well as the space of atomic states [36,46,53,54]. The quantum phase of radiation is defined, in this case, by mapping of corresponding operators from the atomic space of states to the whole Hilbert–Fock space of photons. This procedure does not lead to any violation of the algebraic properties of multipole photons and therefore gives an adequate picture of quantum phase fluctuations [46].

We provide here a review of investigations of the photon localization and quantum phase problems based on the use of the representation of multipole photons. Section II presents a general consideration of the field quantization. In particular, we compare the zero-point oscillations of the plane and multipole waves of photons and show that the vacuum noise is concentrated in some vicinity of atoms. In Section III we discuss the atom–field interaction leading to the multipole radiation and consider the $SU(2)$ quantum phase representation of atomic variables. Here we also discuss a connection between the $SU(2)$ quantum phase states and entanglement phenomenon. In Section IV we describe the quantum phase of multipole radiation caused by the angular momentum conservation in the process of radiation. We compare this approach with the Pegg–Barnett formalism and with Mandel's operational approach. In Section V we consider the quantum polarization properties of multipole radiation. Then, in Section VI, we discuss the photon localization, quantum measurements, and causality. To simplify the reading, we supplement each section by a brief summary. A general conclusion and the implications of this work are presented in Section VII.

II. QUANTUM MULTIPOLE FIELD

> We must not think of the things that we could do with, but only of the things we can't do without.
>
> —Jerome K. Jerome, *Three Men in a Boat*

A. Classical Electromagnetic Field

An arbitrary free classical electromagnetic field is described by the vector potential $\vec{\mathscr{A}}(\vec{r})$, which obeys the wave equation [14,24,25]

$$\nabla^2 \vec{\mathscr{A}} - \frac{1}{c^2}\frac{\partial^2 \vec{\mathscr{A}}}{\partial t^2} = 0 \tag{1}$$

and Coulomb gauge condition

$$\vec{\nabla} \cdot \vec{\mathscr{A}} = 0 \tag{2}$$

The field strengths are then defined as follows:

$$\vec{\mathscr{E}} = -\frac{1}{c}\frac{\partial \vec{\mathscr{A}}}{\partial t}, \qquad \vec{\mathscr{B}} = \vec{\nabla} \times \vec{\mathscr{A}} \tag{3}$$

Equation (1) can be solved by separation of variables [24]:

$$\vec{\mathscr{A}}(\vec{r}, t) = \sum_{\ell} q_\ell(t)\vec{u}_\ell(\vec{r}) \tag{4}$$

Employing (1) then gives the homogeneous Helmholtz wave equations of the form

$$\begin{aligned} \frac{d^2 q_\ell}{dt^2} + \omega_\ell^2 q_\ell &= 0 \\ \nabla^2 \vec{u}_\ell + \frac{\omega_\ell^2}{c^2}\vec{u}_\ell &= 0 \end{aligned} \tag{5}$$

where ω_ℓ are some constants, arising from the separation of variables [24]. Solution of the first equation in (5) gives the harmonic time dependence $q_\ell = \exp(\pm i\omega_\ell t)$. Because of the harmonic time dependence in (4), it is customary to represent the vector potential in terms of the positive and negative frequency parts:

$$\vec{\mathscr{A}}(\vec{r}) = \vec{A}(\vec{r}) + \vec{A}^*(\vec{r}) \tag{6}$$

where $\vec{A} \sim \exp(-i\omega t)$.

The energy density of the field is

$$W(\vec{r}) = \frac{1}{16\pi}[\vec{\mathscr{E}}^*(\vec{r}) \cdot \vec{\mathscr{E}}(\vec{r}) + \vec{\mathscr{B}}^*(\vec{r}) \cdot \vec{\mathscr{B}}(\vec{r})] \tag{7}$$

In turn, the flux of energy is given by the real part of the complex Poynting vector

$$\vec{S}(\vec{r}) = \frac{1}{8\pi}\vec{E}(\vec{r}) \times \vec{B}^*(\vec{r}) \tag{8}$$

where, according to (3), we obtain

$$\vec{E}(\vec{r}) = -ik\vec{A}(\vec{r}), \quad \vec{B}(\vec{r}) = \vec{\nabla} \times \vec{A}(\vec{r})$$

The angular momentum density of the field has the form [25]

$$\vec{M}(\vec{r}) = \frac{1}{4\pi c}\vec{r} \times [\vec{\mathscr{E}}(\vec{r}) \times \vec{\mathscr{B}}(\vec{r})] \tag{9}$$

One possible solution of the first equation in (5), corresponding to the plane waves, traveling along the z axis and having the same amplitude and phase everywhere [24], has the form [14,24,25]

$$\vec{u}_\ell(\vec{r}) = \sum_\ell \sum_{\sigma=x,y} \vec{e}_{\ell\sigma} e^{i\vec{k}_\ell \cdot \vec{r}} a_{\ell\sigma} + \text{c.c} \tag{10}$$

(where c.c. denotes complex conjugates). Here $a_{\ell\sigma}$ are the complex field amplitudes, $\vec{e}_{x,y}$ are the unit vectors of polarization which, due to the Coulomb (guage) condition (2), obey the relation

$$\forall \ell \quad \vec{e}_{x,y} \cdot \vec{k}_\ell = 0 \tag{11}$$

and $k_\ell^2 = \omega_\ell^2/c^2$. Employing (3), (6), and (10) then gives

$$\begin{aligned} E_x(\vec{r}) &= i\sum_k kA_{kx}(\vec{r}) = B_y(\vec{r}) \\ E_y(\vec{r}) &= i\sum_k kA_{ky}(\vec{r}) = -B_x(\vec{r}) \end{aligned} \tag{12}$$

To simplify the notations, we omit the index ℓ here. According to (10), we have

$$A(\vec{r}) = \sum_k \gamma_k \sum_{\sigma=x,y} \vec{e}_{k\sigma} e^{i\vec{k}\cdot\vec{r}} a_{k\sigma} e^{-i\omega t} \tag{13}$$

where γ_k is the normalization factor. Another possible solution of the homogeneous Helmholtz wave equation (5) convenient for electromagnetic boundary-value problems possessing spherical symmetry properties is provided

by the spherical waves [24,25]. In this case, it is supposed that there is a singular point at the origin, corresponding to a localized source distribution or to an absorber (in the case of incoming spherical waves).

In the spherical coordinates $x = r\sin\theta\cos\phi$, $y = r\sin\theta\sin\phi$, and $z = r\cos\theta$, the second equation in (5) takes the form [24]

$$\frac{\partial^2 u_\ell}{\partial r^2} + \frac{2}{r}\frac{\partial u_\ell}{\partial r} + \frac{1}{r^2\sin\theta}\frac{\partial}{\partial\theta}\left(\sin\theta\frac{\partial u_\ell}{\partial\theta}\right) + \frac{1}{r^2\sin^2\theta}\frac{\partial^2 u_\ell}{\partial\phi^2} + \frac{\omega_\ell^2}{c^2}u_\ell = 0 \tag{14}$$

A corresponding solution can be found by the separation of variables $u = R(r)\Theta(\theta)\Phi(\phi)$ in the mode function in (5), which yields the following set of ordinary differential equations [24]:

$$\begin{aligned} \frac{d^2R}{dr^2} + \frac{2}{r}\frac{dR}{dr} + \left[\frac{\omega^2}{c^2r^2} - j(j+1)\right]R = 0 \\ \frac{1}{\sin\theta}\frac{d}{d\theta}\left(\sin\theta\frac{d\Theta}{d\theta}\right) + \left[j(j+1) - \frac{m^2}{\sin^2\theta}\right]\Theta = 0 \\ \frac{d^2\Phi}{d\phi^2} + m^2\Phi = 0 \end{aligned} \tag{15}$$

The solution of these equations is represented by certain combinations of spherical Bessel or Hankel functions and spherical harmonics [24–26].

To establish contact with the quantum picture, consider the so-called helicity basis [27]

$$\vec{\chi}_\pm = \mp\frac{\vec{e}_x \pm i\vec{e}_y}{\sqrt{2}}, \quad \vec{\chi}_0 = \vec{e}_z \tag{16}$$

It is clear that $\{\vec{\chi}_\mu\}$ formally coincide with the three states of spin 1 of a photon. Therefore, one can choose to interpret $\vec{\chi}_\pm$ as the unit vectors of circular polarization with either positive or negative helicity, while $\vec{\chi}_0$ gives the linear polarization in the z direction [27]. We note here that to within the sign at $\vec{\chi}_\pm$ the helicity basis (16) coincides with the so-called polarization basis frequently used in optics [57].

In the basis (16), any vector $\vec{\mathscr{A}}$ can be expanded as follows:

$$\vec{\mathscr{A}} = \sum_{\mu=-1}^{1}(-1)^\mu\,\vec{\chi}_{-\mu}\mathscr{A}_\mu$$

In this basis, for the positive-frequency part of the vector potential in (6) we get [2,24–27]

$$\vec{A}_\lambda(\vec{r}) = \sum_k \sum_\mu \sum_j \sum_{m=-j}^{j} (-1)^\mu \vec{\chi}_{-\mu} V_{\lambda kjm\mu}(\vec{r}) a_{\lambda kjm} e^{-i\omega t} \tag{17}$$

Here $\lambda = E, M$ denotes the type of radiation, either electric or magnetic, index j takes the values 1, 2, . . . , and index $m = -j, \ldots, j$. The complex field amplitudes are defined in terms of the source functions, describing the local distribution of current and intrinsic magnetization [25]. The mode functions in (17) can be represented in the following form [2,26,27]:

$$\begin{aligned} V_{Ekjm\mu} &= \gamma_{Ekj}[\sqrt{j} f_{j+1}(kr)\langle 1, j+1, \mu, m-\mu | jm\rangle Y_{j+1,m-\mu}(\theta\phi) \\ &\quad - \sqrt{j+1} f_{j-1}(kr)\langle 1, j-1, \mu, m-\mu | jm\rangle Y_{j-1,m-\mu}(\theta, \phi)] \\ V_{Mkjm\mu} &= \gamma_{Mkj} f_j(kr)\langle 1, j, \mu, m-\mu | jm\rangle Y_{jm}(\theta, \phi) \end{aligned} \tag{18}$$

Here $\gamma_{\lambda kj}$ is the normalization constant, $\langle \cdots | jm\rangle$ denotes the Clebsch–Gordon coefficient, and $Y_{\ell m}$ is the spherical harmonics. The radial contribution into the mode functions (18) depends on the boundary conditions as follows [24]

$$f_\ell(kr) = \begin{cases} h_\ell^{(1)}(kr), & \text{outgoing spherical wave} \\ h_\ell^{(2)}(kr), & \text{incoming spherical wave} \\ j_\ell(kr), & \text{standing spherical wave} \end{cases} \tag{19}$$

where $h_\ell^{(1,2)}$ denotes the spherical Hankel function of the first and second kinds, respectively, and j_ℓ is the spherical Bessel function [24,25].

Unlike the case of plane waves of photons, the multipole field (18) propagates as a uniformly expanding spherical shell rather than propagates along a given direction of $\vec{k}$. Instead of the symmetry relations (12), for the spherical waves of photons we get the following reciprocity relations [2,27]:

$$\begin{aligned} \vec{E}_{Ekjm} &= \vec{B}_{Mkjm} = ik\vec{A}_{Ekjm} \\ \vec{E}_{Mkjm} &= -\vec{B}_{Ekjm} = ik\vec{A}_{Mkjm} \end{aligned} \tag{20}$$

B. Quantum Electromagnetic Field

The canonical quantization of the field has introduced by Dirac [1] (see also Refs. 2–4,10,11,14,15,26,27) is provided by the substitution of the photon operators, forming a representation of the Weyl–Heisenberg algebra, into the

expression for the vector potential instead of the complex field amplitudes. For example, in the case of plane waves, described by the positive-frequency part of the vector potential (13), we get the following operator construction

$$A(\vec{r}) = \sum_{k} \sum_{\sigma=x,y} \sqrt{\frac{2\pi\hbar c}{kV}} \vec{e}_{k\sigma} e^{i\vec{k}\cdot\vec{r}} a_{k\sigma} \tag{21}$$

where V is the volume of quantization, which is supposed to be a large cubic box with periodical boundary conditions. Here the harmonic time dependence is included into the photon operators that obey the commutation relations

$$[a_{k\sigma}, a^{+}_{k'\sigma'}] = \delta_{kk'}\delta_{\sigma\sigma'} \tag{22}$$

As a result of the translational symmetry along the z direction, the plane waves of photons, described by (21) and (22), correspond to the states of the radiation field with given linear momentum

$$\vec{P} = \sum_{k\sigma} \hbar\vec{k} a^{+}_{k\sigma} a_{k\sigma}$$

where $\vec{k} = k\vec{e}_z$.

The multipole electromagnetic field "can be quantized in much the same way as plane waves" [2]. We have to subject the complex field amplitudes in the expansion (17) to the Weyl–Heisenberg commutation relations of the form

$$[a_{\lambda kjm}, a^{+}_{\lambda' k' j' m'}] = \delta_{\lambda\lambda'}\delta_{kk'}\delta_{jj'}\delta_{mm'} \tag{23}$$

Then, the positive-frequency part of the operator vector potential of the multipole radiation of a given type λ takes the form [2,27]

$$\vec{A}_{\lambda}(\vec{r}) = \sum_{k} \sum_{\mu} \sum_{j} \sum_{m=-j}^{j} (-1)^{\mu} \vec{\chi}_{-\mu} V_{\lambda kjm\mu}(\vec{r}) a_{\lambda kjm} \tag{24}$$

where the harmonic time dependence is again included into the definition of the photon operators of creation and annihilation. In the case of standing waves of photons in an ideal spherical cavity of volume V, the normalization factors in (18) take the form [2,27]

$$\gamma_{Ekj} = \sqrt{\frac{2\pi\hbar c}{kV(2j+1)}}$$

$$\gamma_{Mkj} = \sqrt{\frac{2\pi\hbar c}{kV}}$$

Within the quantum picture, the Clebsch–Gordon coefficients in (18) represent the vector addition of the spin and orbital parts of the total angular momentum of the field [2]. The indices j and m in (23) and (24) correspond to the angular momentum and projection of angular momentum on the quantization axis. The electric-type multipole radiation is interpreted as having the parity of state $(-1)^{j+1}$, while the magnetic-type multipole radiation is specified by the states with parity $(-1)^{j}$. Because of the spherical symmetry of solutions (17)–(19), the representation of spherical waves of photons (23)–(24) corresponds to the states of quantum multipole field with given angular momentum. Since the components of the linear and angular momenta do not commute with each other, the two representations (21)–(22) and (23)–(24) are different in principle. They correspond to the physical observables that cannot be measured simultaneously.

For both the plane and multipole waves of photons, the vacuum state can be defined by the stability condition in the same way [3,4]:

$$\begin{aligned} \forall k, \sigma \quad & a_{k\sigma}|0\rangle = 0 \\ \forall \lambda, k, j, m \quad & a_{\lambda kjm}|0\rangle = 0 \end{aligned} \tag{25}$$

Then, the corresponding Fock number states are defined as follows

$$\begin{aligned} |n_{k\sigma}\rangle &= \frac{(a^{+}_{k\sigma})^{n}_{k\sigma}}{\sqrt{n_{k\sigma}!}}|0\rangle \\ |n_{\lambda kjm}\rangle &= \frac{(a^{+}_{\lambda kjm})^{n}_{\lambda kjm}}{\sqrt{n_{\lambda kjm}}}|0\rangle \end{aligned} \tag{26}$$

where $n \geq 0$ is an integer.

As can be seen from the equations (21)–(22) and (23)–(24), there is an essential difference between the representations of plane and multipole waves of photons. In particular, a monochromatic plane wave of photons is specified by only two different quantum numbers $\sigma = x, y$, describing the linear polarization in Cartesian coordinates. In turn, the monochromatic multipole photons are described by much more quantum numbers. Even in the simplest case of the electric dipole radiation when $\lambda = E$ and $j = 1$, we have three different states of multipole photons in (23) with $m = 0, \pm 1$. Besides that, the plane waves of photons have the same polarization σ everywhere, while the states of multipole photons have given m. It is seen from (24) that, in this case, the polarization described by the spin index μ can have different values at different distances from the singular point. In Section V we discuss the polarization properties of the multipole radiation in greater detail.

A more profound difference between the two representations can be traced in the properties of the zero-point oscillations. In fact, the energy operators

obtained by quantization of (7) in the plane and spherical wave representations have the form [26–59]

$$H_{(\text{plane})} = \sum_{k,\sigma} \hbar\omega_k \left(a^{+}_{k\sigma} a_{k\sigma} + \frac{1}{2} \right)$$

$$H_{(\text{multi})} = \sum_{k} \hbar\omega_k \sum_{\lambda,j,m} \left(a^{+}_{\lambda jm} a_{\lambda jm} + \frac{1}{2} \right)$$

Thus, the energies of the vacuum state are

$$H^{(\text{vac})}_{(\text{plane})} = \sum_{k,\sigma} \frac{\hbar\omega_k}{2} = \sum_{k} \hbar\omega_k$$

$$H^{(\text{vac})}_{(\text{multi})} = \sum_{k} \hbar\omega_k \sum_{\lambda,j,m} \frac{1}{2} = \sum_{k} \hbar\omega_k \left(\sum_{j} (2j+1) \right) \tag{27}$$

According to the definition of k, both expressions give an infinite energy and, at first sight, cannot be compared with each other. In fact, this infinity is inessential because of the following reason. The contribution of zero-point oscillations can be observed only via measurement which implies an averaging of physical quantities over a finite "volume of detection" and exposition time of detector. Such an averaging plays a part of filtration leading to a selection of a certain finite transmission frequency band [58]. It is then seen that, even if the filtration process leads to separation of the dipole photons only, the second term in (27) exceeds the first one 3 times. From the physical point of view, this result is caused by the more number of quantum degrees of freedom in the case of multipole photons.

Much more interesting and important result can be obtained from the consideration of the spatial properties of the vacuum fluctuations. The simplest example is provided by the calculation of vacuum average of the squared electric field strength [58,59]

$$W(\vec{r}) = \langle 0|\vec{\mathscr{E}} \cdot \vec{\mathscr{E}}|0\rangle = k^2 \langle 0|\vec{\mathscr{A}} \cdot \vec{\mathscr{A}}|0\rangle$$

obtained from (6) by the canonical quantization of the field. It follows from the definition of the vacuum state (25) that this expression can be put into the form

$$W(\vec{r}) = k^2 \langle 0|[\vec{A}, \vec{A}^{+}]|0\rangle = k^2 [\vec{A}, \vec{A}^{+}]$$

independent of the type of representation. Consider first the monochromatic plane waves of photons. Using (21) together with the commutation relations

(22), we get

$$W^{(\text{plane})}(\vec{r}) = W^{(\text{plane})} = \sum_{k,\sigma} \frac{\hbar\omega_k}{2V}, \quad \omega_k = kc \tag{28}$$

Here V has the same meaning as in (21). Thus, the zero-point fluctuations of the electric field strength of plane waves have the same magnitude at any space point. By construction, (28) describes the zero-point fluctuations *in empty space*.

In turn, employing the representation (23)–(24) then gives for (27) in the case of multipole photons the following equation:

$$W^{(\text{multi})}(\vec{r}) = k^2 \sum_{\lambda=E,M} \sum_{\mu} \sum_{k,j,m} |V_{\lambda kjm\mu}(\vec{r})|^2 \tag{29}$$

It is seen from the definition of the mode functions (18) and (19) that, in contrast to (28), the zero-point oscillations of the electric field strength of multipole photons manifest the *spatial inhomogeneity.*

For simplicity, we can compare the monochromatic contributions into (28) and (29) at the same k and V. Then

$$W_k^{(\text{plane})} = \sum_{\sigma=1,2} \frac{\hbar kc}{2V}$$

and

$$\begin{aligned} W_k^{(\text{multi})}(\vec{r}) = \sum_{jm\mu} \frac{2\pi\hbar kc}{V} & \\ \times \Bigg[\Bigg| \sqrt{\frac{j}{2j+1}} f_{j+1}(kr) \langle 1, j+1, \mu, m-\mu | 1m \rangle Y_{j+1,m-\mu} & \\ - \sqrt{\frac{j+1}{2j+1}} f_{j-1}(kr) \langle 1, j-1, \mu, m-\mu | 1m \rangle Y_{j-1,m-\mu} \Bigg|^2 & \\ + |f_j(kr) \langle 1, j, \mu, m-\mu | 1m \rangle Y_{j,m-\mu}|^2 \Bigg] & \end{aligned}$$

Since $Y_{\ell,m-\mu} \sim e^{i(m-\mu)\phi}$, this form is independent of the azimuthal angle ϕ. Moreover, it is a straightforward matter to arrive at the conclusion that

$$W_k^{(\text{multi})}(\vec{r}) = W_k^{(\text{multi})}(r)$$

(see discussion in Section V.C).

Consider first the case of standing spherical waves in an ideal spherical cavity when, according to (19)

$$f_\ell(kr) = \sqrt{\frac{\pi}{2kr}} J_{\ell+1/2}(kr)$$

We stress here that, in the quantum theory of radiation, exactly the standing spherical waves are usually considered [2,27]. Unlike the outgoing and incoming spherical waves of photons, this choice does not lead to the divergence of the vector potential at $r \to 0$. Taking into account the properties of Bessel functions $J_j(x)$, it is easily seen that the principal contribution into $W^{(\mathrm{multi})}$ in vicinity of the singular point (atom) comes from $J_{1/2}(kr)$, corresponding to the electric dipole radiation. The radial dependence of $W^{(\mathrm{multi})}$ at fixed k and $j = 1$ is shown in Fig. 1. It is seen that the vacuum fluctuations are concentrated near atoms where their level can strongly exceed that calculated within the framework of the model of plane waves.

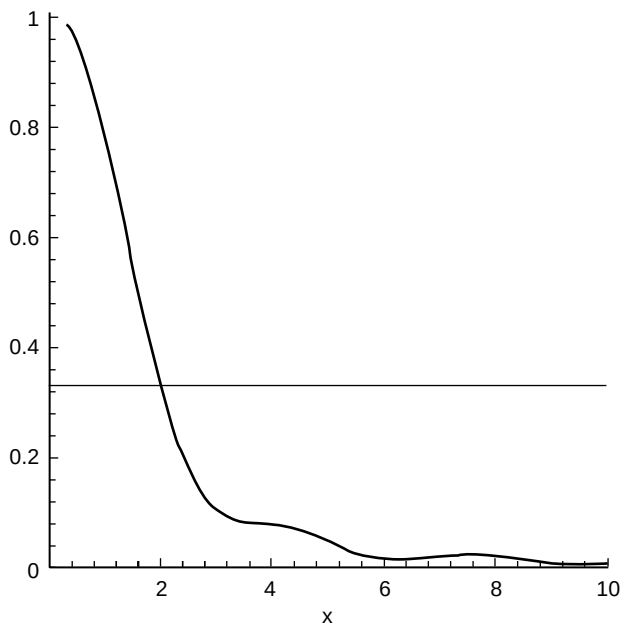

Figure 1. Contribution into the zero-point oscillations (29) from the terms with $j = 1$ in the case of an ideal spherical cavity as a function of $x = kr$; (b) the level (28) is shown by the straight line.

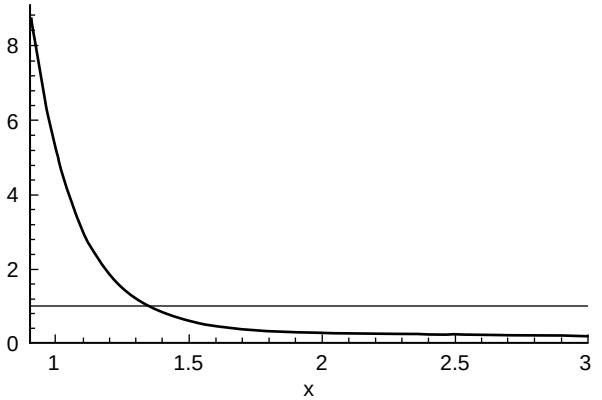

Figure 2. Contribution into (29) from the term $j = 1$ for outgoing spherical waves outside the atom with radius $r_a = 1$ in arbitrary units. The straight line shows the level of $W_k^{(\mathrm{plane})}$.

The case of outgoing and incoming spherical waves can be examined under the standard assumption that the atom located at the origin has a finite size that permits us to avoid the divergence at $kr \to 0$. It is seen that, in some small vicinity of the atom, the zero-point oscillations, corresponding to the multipole field in an infinite space, strongly exceed those in the ideal spherical cavity (see Fig. 2).

It should be stressed that the preceding results were obtained under the assumption that the atom exists only at the origin, no matter whether we use it as an emitter or absorber of radiation. In other words, the spatial inhomogeneity of the zero-point oscillations in (29) reflects the existence of the singular point that, in fact, is the boundary condition for the homogeneous Helmholtz wave equation (5). It is possible to say that the electromagnetic vacuum state "feels" the presence of an atom at the origin and is ready to support any radiation (with all possible λ, j, and m) either outgoing or incoming. This is not an astonishing result. The influence of the electromagnetic vacuum state by the presence of an atom has been discussed in quantum electrodynamics for a long time [7,30,31]. The new result here is that the zero-point oscillations are concentrated in some vicinity of atoms where their levels can exceed the standard level (28), which is usually considered.

The point is that the zero-point oscillations are responsible for the so-called shot noise [14,15], determining the quantum limit of uncertainty in different optical measurements. The preceding result shows that the presence of an atom causes the increase of shot noise and hence a deterioration of the quantum limit of precision of measurements, at least, in some vicinity of the atom [22,29]. We discuss this effect in more details in Section VI.

C. Summary

1. Although the monochromatic plane waves of photons are described by only two quantum numbers, specifying the polarization, the monochromatic multipole waves of photons have much more quantum degrees of freedom: the type of radiation (parity) $\lambda = E, M$ and the angular momentum $j \geq 1$ and its projection $m = -j, \ldots, j$.
2. The zero-point oscillations of the energy density of plane waves of photons have the same magnitude everywhere. In contrast, those calculated in the presence of a singular point (source or absorber) manifest spatial inhomogeneity. Precisely, the vacuum noise is concentrated in some vicinity of the singular point.

III. ATOM–FIELD INTERACTION

"Well! I've often seen a cat without a grin", thought Alice; "but a grin without a cat! It's the most curious thing I ever saw in all my life".

—Lewis Carroll, *Alice's Adventures in Wonderland*

A. Multipole Jaynes–Cummings Model

In the previous section, the classical and quantum electromagnetic fields were considered as absolutely free sourceless objects. This picture follows from the existence of nontrivial solutions of the homogeneous Helmholtz wave equation (5). In some textbooks, this mathematical fact is interpreted as the claim of the following type: *the electromagnetic field can exist in the absence of any charge* (e.g., see Ref. 60). At the same time, as we know, no one has ever observed photons that had not been created by a source. According to the quantum picture, the electromagnetic vacuum state contains unborn photons of all possible types. They are extracted from this state in the form of overvacuum excitations (waves) in the process of source–photon interaction, leading to the photon generation. The observable properties of real photons are governed by this interaction, which causes the success of conventional [23,61] and correlation [62,63] spectroscopy. Rephrasing Lewis Carroll's *Alice's Adventures in Wonderland*, it is possible to say that the source is similar to Cheshire Cat, creating grin which propagates in spacetime (see Fig. 3).

The simplest quantum source of photons is the atomic transition, creating, according to the selection rules, multipole photons. The simplest model of the interaction of an atom with the electromagnetic radiation is associated with the notion of so-called two-level atom [64]. In fact, this model originates from the famous study of radiation kinetics by Einstein [65]. With the development of laser, the notion of two-level atom entered firmly into the practice of quantum optics. The fact is that, using lasers as sources of electromagnetic radiation, one

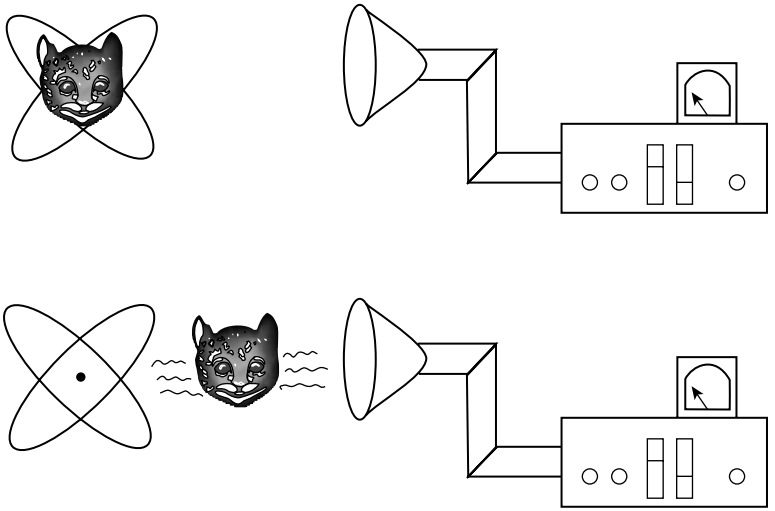

Figure 3. Transmission of information from atom to detector as propagation of the grin of a Cheshire cat. In the upper picture, the atom keeps information about excited level (cat's grin). In the lower picture, the atom hands this information to a photon, propagating to a detector.

can act on the atom with field having frequency very close to the transition frequency between any pair of levels. In this case, the influence of the other levels can be ignored, and one need the consider only a two-level atom (in general, an atom with a finite number of levels) [64]. On the other hand, the use of high-quality cavities has the consequence that an atom in such a cavity interacts with only one or very few modes of the field quantized in the volume of the cavity [32,33,66].

The branch of quantum optics studying the processes of interaction of one or a few atoms with the quantized cavity modes is usually called *cavity quantum electrodynamics* (cavity QED). The theoretical concepts of cavity QED are based in the first place on investigation of the Jaynes–Cummings model [67] and its generalizations (for a review, see Ref. 68). The reason for this is that the model describes fairly well the physical processes under consideration and at the same time admits an exact solution.

In the usual formulation of the Jaynes–Cummings model, the atom is considered as though it consisted of two nondegenerated levels [67] . In contrast, the radiative transitions in real atoms occur between the states with given angular quantum numbers $|j,m\rangle \to |j',m'\rangle$ such that $j > j' \geq 0$ [23,26,61]. This means that, at least the upper level, is degenerated with respect to the quantum number m $(-j \leq m \leq j)$. For example, in the simplest case of the electric dipole transition between the states $|j=1, m=0, \pm 1\rangle$ and

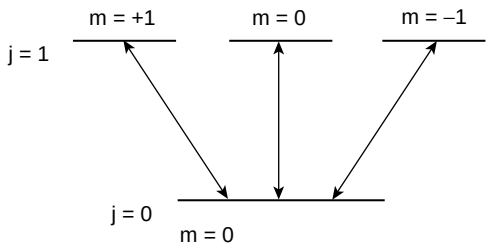

Figure 4. Scheme of transitions between the triple degenerated excited state $|j = 1, m = 0, \pm 1\rangle$ and ground state $|j' = 0, m = 0\rangle$ in a two-level atom with the dipole transition.

$|j' = 0, m' = 0\rangle$, the excited state is triple degenerated (see Fig. 4). The corresponding generalization of the Jaynes–Cummings model has been discussed [36,53]. Similar models have been considered in different problems of interaction of quantum light and matter [69].

Interaction between a single atom and a radiation field is usually considered within the framework of perturbation theory using the following Hamiltonian [26,64]

$$H = H_0 + \frac{1}{2m_e}\left(\vec{p} - \frac{e}{c}\vec{A}\right)^2 \tag{30}$$

where H_0 describes the unperturbed atom and field and the rest is written for the interaction between a single spinless electron with charge e, mass m_e, momentum p, and free electromagnetic field described by the vector potential $\vec{A}$. Following earlier observations [36,53], consider a two-level atom with the electric dipole transition between the triple-degenerated excited atomic state with $j = 1$ and nondegenerated ground state with $j' = 0$. The atom is supposed to be located at the center of an ideal spherical cavity. The coupling constant of the atom–field interaction can be found by calculating the matrix element [26,27]

$$-\frac{e}{2m_e c}\langle 0, 0|\vec{p}\cdot\vec{A} + \vec{A}\cdot\vec{p}|1, m\rangle = ik_0\langle 0, 0|\vec{d}\cdot\vec{A}|1, m\rangle \tag{31}$$

obtained from (30). The A^2 term is excluded because of the use of the so-called rotating-wave approximation [64]. Here $\vec{d} = e\vec{r}$ is the dipole moment and $\vec{A}(\vec{r})$ is the operator vector potential (24) with the radial dependence of the mode functions (18) described by $f_\ell(kr) = j_\ell(kr)$ in (19) due to the choice of the boundary conditions.

Assuming the central symmetry of atomic field and taking into account the fact that the spin state of an atom does not change under the electric dipole

transition [27,61], we can represent the atomic states in (31) as

$$|1,m\rangle = \mathscr{R}_1(kr)Y_{1m}(\theta,\phi), \quad |0,0\rangle = \mathscr{R}_0(kr)Y_{00}(\theta,\phi)$$

where $\mathscr{R}_\ell$ is the radial part of the atomic wave function. Then, representing the dipole moment $\vec{d}$ in the helicity basis (16) and carrying out the calculations of integrals in (31) over the atomic volume, we get

$$\forall m \quad g \equiv k_0\langle 1,m|\vec{d}\cdot\vec{A}|0,0\rangle = k_0 D\sqrt{\frac{3\hbar c}{10kR}} \tag{32}$$

where

$$D = e\int_0^{r_a} drr^3 f_1(kr)f_0(kr)$$

is the effective dipole factor. Here R and r_a denote the cavity and atomic radii respectively and k is the wave number, describing the cavity field.

Taking into account the explicit form of spherical Bessel functions [70]

$$\begin{aligned} j_0(kr) &= \frac{\sin kr}{kr}, \\ j_2(kr) &= \frac{3-(kr)^2}{(kr)^3}\sin kr - \frac{3\cos kr}{(kr)^2} \end{aligned} \tag{33}$$

we note that, owing to the structure of the mode functions (18), all other radial functions do not contribute (24). Assuming that the atom is a point-like object (in fact, very small with respect to the wavelength of radiation field), we get

$$\lim_{kr\to 0} j_0(kr) = 1, \quad \lim_{kr\to 0} j_2(kr) = 0$$

Using the properties of the Clebsch–Gordon coefficients [71] and spherical harmonics [70], for the mode functions (18) in this limit we get

$$V_{Ek1m}(0) \sim -\delta_{m\mu}$$

Inserting this into (24), we obtain

$$\vec{A}_{Ek1}(0) = -\sqrt{\frac{\hbar c}{3kV}}\sum_{m=-1}^{1}(-1)^\mu\,\vec{\chi}_{-\mu}a_{Ek1m}\delta_{m\mu}$$

This means that the electric dipole transition $|1,m\rangle \to |0,0\rangle$ creates a photon with spin state (polarization) $\mu = m$. However, the picture of the polarization

changes with the distance from the atom because of the position dependence of the mode functions (18).

Thus, the Jaynes–Cummings Hamiltonian for the electric dipole transition can be written as follows [36,53]:

$$
\begin{aligned}
H &= H_0 + H_{\text{int}} \\
H_0 &= \sum_{m=-1}^{1} \{\omega a^{+}_{E1m} a_{E1m} + \omega_0 R_{mm}\} \\
H_{\text{int}} &= g \sum_{m=-1}^{1} \{R_{mg} a_{E1m} + a^{+}_{E1m} R_{gm}\}
\end{aligned}
\tag{34}
$$

Here $\omega_0 = \hbar k_0 c$ and $\omega = \hbar k c$ are the energies of the atomic transition and cavity field, respectively, and the atomic operators are defined as follows:

$$
R_{mg} = |1, m\rangle\langle 0, 0|, \quad R_{mm'} = |1, m\rangle\langle 1, m'| \tag{35}
$$

The first term in (34) describes the energy of the free cavity field and atom, while the second term gives the energy either of the transition $|1, m\rangle \to |0, 0\rangle$ with generation of the multipole photon or of the transition $|0, 0\rangle \to |1, m\rangle$ accompanied by the absorption of corresponding electric dipole photon.

Generalizations of the Jaynes–Cummings model (34) in the case of quadrupole and other high-order multipole transitions can be constructed in the same way.

B. The $SU(2)$ Atomic Phase States

In the model Hamiltonian (34), the excited atomic state is specified by the following three orthogonal states:

$$
|1, 1\rangle, \quad |1, 0\rangle, \quad |1, -1\rangle \tag{36}
$$

On this basis, we can construct a representation of the $SU(2)$ algebra with the following generators [53,54]

$$
\begin{aligned}
J_z &= R_{++} - R_{--} \\
J_+ &= \sqrt{2}(R_{+0} + R_{0-}) \\
J_- &= \sqrt{2}(R_{0+} + R_{-})
\end{aligned}
\tag{37}
$$

which obey the standard commutation relations

$$
[J_+, J_-] = 2J_z, \quad [J_z, J_\pm] = \pm J_\pm \tag{38}
$$

The enveloping algebra of (37)–(38) contains the uniquely defined Casimir operator

$$\mathbf{J}^2 = 2\sum_{m=-1}^{1} R_{mm} \equiv 2 \times \mathbf{1} \tag{39}$$

where

$$\mathbf{1} = |1,1\rangle\langle 1,1| + |1,0\rangle\langle 1,0| + |1,-1\rangle\langle 1,-1|$$

is the unit operator in the space spanned by the basis (36).

The existence of (39) permits us to use the method, proposed by Vourdas [51], to construct the dual representation of the $SU(2)$ algebra (37)–(38). Following [51], we represent the lowering and rising operators in (37) as

$$J_+ = J_r\varepsilon, \quad J_- = \varepsilon^+ J_r \tag{40}$$

where J_r is the Hermitian "radial" operator and ϵ is the unitary

$$\varepsilon\varepsilon^+ = \mathbf{1}$$

"exponential of the phase" operator. The terminology here is borrowed from complex calculus. It is clear that the phase variable here describes the azimuth of the angular momentum of the excited atomic state. Equations (40) can now be done in a straightforward manner to yield

$$\begin{aligned} J_r &= \sqrt{2}(\mathbf{1} - R_{--}) \\ \varepsilon &= R_{+0} + R_{0-} + e^{i\psi}R_{-+} \end{aligned} \tag{41}$$

where ψ is an arbitrary real parameter describing the so-called atomic reference phase [53,54]. It is clear that ϵ is a Coxeter-type operator [72] because

$$\varepsilon^3 = e^{i\psi} \times \mathbf{1}$$

In analogy to complex calculus, we can now define the cosine and sine of the atomic $SU(2)$ phase operators [36]

$$C_a = \frac{\varepsilon + \varepsilon^+}{2}, \quad S_a = \frac{\varepsilon - \varepsilon^+}{2i} \tag{42}$$

such that

$$C_a^2 + S_a^2 = \mathbf{1} \tag{43}$$

and

$$[C_a, S_a] = 0 \tag{44}$$

Following [51], we now introduce the dual representation of the $SU(2)$ algebra (37)–(38). Consider first the eigenstates of the exponential operator in (41):

$$\varepsilon|\phi_m\rangle = e^{i\phi_m}|\phi_m\rangle \tag{45}$$

It is a straightforward matter to arrive at the relations [46]

$$|\phi_m\rangle = \frac{1}{\sqrt{3}}\sum_{m'=-1}^{1} e^{-im'\phi_m}|1, m\rangle, \quad \phi_m = \frac{2m\pi - \psi}{3} \tag{46}$$

where m acquires the values 0 and ± 1 as above. It is easily seen that the so-called phase states [51] (45) determine the basis dual to (36) [46]. In particular

$$\sum_{m=-1}^{1} |\phi_m\rangle\langle\phi_m| = \mathbf{1}$$

Then, the atomic $SU(2)$ quantum phase operator can be defined as follows:

$$\hat{\phi} = \sum_{m=-1}^{1} \phi_m|\phi_m\rangle\langle\phi_m| = -\frac{\psi}{3}\mathbf{1} - \frac{2i\pi}{3\sqrt{3}}(e^{-i\psi/3}\epsilon - e^{i\psi/3}\epsilon^{+}) \tag{47}$$

In turn, the cosine and sine operators (42) can be represented as the functions

$$C_a = \cos\hat{\phi}, \quad S_a = \sin\hat{\phi}$$

of the operator (47). Then, the dual representation of the atomic $SU(2)$ algebra (37) is provided by the following generators:

$$\begin{aligned} J_z^{(\phi)} &= \sum_m m|\phi_m\rangle\langle\phi_m| \\ J_+^{(\phi)} &= \sum_m \sqrt{2 - m(m+1)}|\phi_{m+1}\rangle\langle\phi_m| \\ J_-^{(\phi)} &= \sum_m \sqrt{2 - m(m-1)}|\phi_{m-1}\rangle\langle\phi_m| \end{aligned} \tag{48}$$

Similar results can be obtained for an arbitrary atomic multipole transition in much the same way as above. For example, in the case of the excited atomic

state with $j = 2$, the representation of the $SU(2)$ algebra takes the form

$$J_+ = \sqrt{2}|2\rangle\langle 1| + \sqrt{3}|1\rangle\langle 0| + \sqrt{3}|0\rangle\langle -1| + \sqrt{2}|-1\rangle\langle -2|$$
$$J_- = \sqrt{2}|1\rangle\langle 2| + \sqrt{3}|0\rangle\langle 1| + \sqrt{3}|-1\rangle\langle 0| + \sqrt{2}|-2\rangle\langle -1|$$
$$J_z = 2|2\rangle\langle 2| + |1\rangle\langle 1| - |-1\rangle\langle -1| - 2|-2\rangle\langle -2|$$

where $|n\rangle \equiv |m = n\rangle$. The corresponding exponential of the phase operator is

$$\varepsilon = |2\rangle\langle 1| + |1\rangle\langle 0| + |0\rangle\langle -1| + |-1\rangle\langle -2| + e^{i\psi}|-2\rangle\langle 2|$$

In this case, the eigenvalues of the phase variable take the following five independent values:

$$\phi_m = \frac{\psi + 2m\pi}{5}, \quad m = 2, 1, \ldots, -2$$

In the general case of an arbitrary integer $j \geq 1$, the number of independent eigenvalues of the phase variable ϕ_m is $(2j + 1)$.

C. EPR Paradox and Entanglement

The preceding formalism of $SU(2)$ phase states can be used in a number of problems of quantum physics. As an illustrative example of great importance, consider the so-called Einstein–Podolsky–Rosen (EPR) paradox [73] (see also discussions in Refs. 14, 15, 74, and 75). The EPR paradox touches on the conceptual problems of reality and locality and existence of hidden variables in quantum physics as well as the more technological aspects of quantum cryptography [34].

In the original EPR gedanken experiment [73], a two-component system, consisting of two spin-$\frac{1}{2}$ particles, is considered. Up to some time t_0, these particles are taken to be in a bounded state of zero angular momentum. At t_0, the binding is taken off without any disturbance of the spin states. Then, the separated particles move off in the opposite directions. Since the particles are in the common quantum state, the measurement of one chosen variable of particle 1, moving "to the left," completely determines the outcome of a measurement of corresponding variable of particle 2, moving "to the right."

Before making the measurement, the system is supposed to be in the EPR state, which is also called the *entangled state*. It is described by the wavefunction of the form

$$|\Psi_{\pm}^{(\mathrm{EPR})}\rangle = \frac{1}{\sqrt{2}}(|\uparrow_L\downarrow_R\rangle \pm |\downarrow_L\uparrow_R\rangle) \tag{49}$$

Here $|\updownarrow_{L,R}\rangle$ denotes the spinup or spindown state of the left or right particle. The two state vectors in the right-hand side of (49) form a basis of the corresponding Hilbert space in which we can define the representation of the $SU(2)$ algebra by the following generators

$$\begin{aligned} J_+ &= |\uparrow_L\downarrow_R\rangle\langle\downarrow_L\uparrow_R| \\ J_- &= |\downarrow_L\uparrow_R\rangle\langle\uparrow_L\downarrow_R| \\ J_z &= \frac{1}{2}(|\uparrow_L\downarrow_R\rangle\langle\uparrow_L\downarrow_R| - |\downarrow_L\uparrow_R\rangle\langle\downarrow_L\uparrow_R|) \end{aligned} \tag{50}$$

so that these operators obey the commutation relations (38) as well as the condition (39). Hence, the operators (47) admit a polar decomposition of the form discussed in the previous subsection. In particular, the exponential of the $SU(2)$ phase operator (41) takes the form

$$\varepsilon = |\uparrow_L\downarrow_R\rangle\langle\downarrow_L\uparrow_R| + e^{i\psi}|\downarrow_L\uparrow_R\rangle\langle\uparrow_L\downarrow_R| \tag{51}$$

where ψ is again an arbitrary real reference phase. The $SU(2)$ phase states of the type of (45), and (46) which are defined to be the eigenstates of the operator (51), have the form

$$|\phi_\sigma\rangle = \frac{1}{\sqrt{2}}(|\uparrow_L\downarrow_R\rangle + e^{i\phi_\sigma}|\downarrow_L\uparrow_R\rangle) \tag{52}$$

where

$$\phi_\sigma = \frac{\psi}{2} + \sigma\pi, \quad \sigma = 0, 1$$

It is now easily seen that, at $\psi = 0$, the $SU(2)$ phase states (52) coincide with the EPR states (49). Thus, the EPR states can be interpreted as the eigenstates of the exponential of the phase operator (51) of the $SU(2)$ algebra (50). The corresponding quantum phase operator takes the form

$$\hat{\phi} = \frac{\psi + \pi}{2} \times \mathbf{1} - \frac{\pi}{2} e^{-i\psi/2}\varepsilon \tag{53}$$

where

$$\mathbf{1} \equiv |\uparrow_L\downarrow_R\rangle\langle\uparrow_L\downarrow_R| + |\downarrow_L\uparrow_R\rangle\langle\downarrow_L\uparrow_R|$$

By construction, the operator (53) describes the relative phase between the two EPR states (49).

There are many different physical realizations of the EPR or entangled states in optics and condensed-matter physics. For example, the creation of two photons with different helicities by a single atom in the process of cascade

decay of transition of the type $j - j' = 0$ leads to the polarization-entangled state of the photons, leaving the atom in opposite directions (e.g., see Section 12.14.1 in Ref. 14).

Another important example of entanglement is provided by the system of two 2-level atoms in an optical resonator [76]. Such a system can be described by the following Jaynes–Cummings Hamiltonian:

$$\begin{aligned} H &= H_0 + H_{\text{int}} \\ H_0 &= \sum_{f=1,2} \omega_f |e_f\rangle\langle e_f| + \omega a^+ a \\ H_{\text{int}} &= \sum_{f=1,2} i\gamma_f (|e_f\rangle\langle g_f| a - a^+ |g_f\rangle\langle e_f|) \end{aligned} \tag{54}$$

Here index f denotes the atom in the cavity, $|e_f\rangle$ ($|g_f\rangle$) is the excited (ground) state of the corresponding atom, γ_f is the atom–field coupling constant, and the operators a^+ and a describe the cavity photons. Among the eigenstates of (54)

$$\begin{aligned} |\psi_0\rangle &= \frac{1}{\sqrt{\gamma_1^2 + \gamma_2^2}} (\gamma_1 |0; g_1; e_f\rangle - \gamma_2 |0; e_1; g_2\rangle) \\ |\psi_\pm\rangle &= \frac{1}{\sqrt{2}} \left(|1; g_1; g_2\rangle \pm \frac{i}{\sqrt{\gamma_1^2 + \gamma_2^2}} (\gamma_2 |0; g_1; e_2\rangle + \gamma_1 |0; e_1; g_2\rangle) \right) \end{aligned} \tag{55}$$

there is a maximally entangled atomic state $|\psi_0\rangle$, which, under the assumption that $\gamma_1 = \gamma_2$, takes the form

$$\begin{aligned} |\psi_0\rangle &= |0\rangle \otimes |\psi_{\text{ent}}\rangle \\ |\psi_{\text{ent}}\rangle &= \frac{1}{\sqrt{2}} (|g_1; e_2\rangle - |e_1; g_2\rangle) \end{aligned} \tag{56}$$

similar to EPR state (49). In the above formulas we use the following notations:

$$\begin{aligned} |0; e_f; g_{f' \neq f}\rangle &= |0\rangle_{\text{field}} \otimes |e_f\rangle \otimes |g_{f'}\rangle \\ |1; g_1; g_2\rangle &= |1\rangle_{\text{field}} \otimes |g_1\rangle \otimes |g_2\rangle \end{aligned}$$

To establish contact with the $SU(2)$ phase states, we can consider the following representation of generators of the atomic $SU(2)$ algebra

$$\begin{aligned} J_+ &= |e_1\rangle\langle e_2| \\ J_- &= |e_2\rangle\langle e_1| \\ J_z &= \frac{1}{2} (|e_1\rangle\langle e_1| - |e_2\rangle\langle e_2| \end{aligned}$$

similar to (50). Then, the exponential of the phase operator takes the form (for simplicity, we put here $\psi = 0$)

$$\varepsilon = |e_1\rangle\langle e_2| + |e_2\rangle\langle e_1|$$

It is now seen that the maximally entangled atomic state in (55) is again the $SU(2)$ quantum phase state.

An interesting example of entanglement in condensed matter is represented by the formation of Cooper pairs in conventional superconductors. It is well known that the electron–phonon interaction in metals can lead to formation of collective quantum states of paired electrons with opposite spins and linear momenta [77]. In the simplest quasispin form, the system can be specified by the Hamiltonian [78,79]

$$H = \sum_p E_p \sigma_p^z - \sum_{p,p'} J_{pp'} \sigma_p^- \sigma_{p'}^+ \tag{57}$$

where E_p denotes the energy spectrum depending on the momentum p of electrons, $J_{pp'}$ is the effective coupling constant, and the Pauli operators

$$\sigma_p^- = \begin{pmatrix} 0 & 1 \\ 0 & 0 \end{pmatrix}, \quad \sigma_p^+ = \begin{pmatrix} 0 & 0 \\ 1 & 0 \end{pmatrix}, \quad \sigma_p^z = \frac{1}{2}\begin{pmatrix} 1 & 0 \\ 0 & -1 \end{pmatrix}$$

correspond to the pairs of electrons with opposite spins and momenta. Since the Pauli operators obey the commutation relations

$$[\sigma_p^-, \sigma_{p'}^+] = 2\sigma_p^z \delta_{pp'}, \quad [\sigma_p^z, \sigma_{p'}^\mp] = \pm\sigma_p^\mp \delta_{pp'}$$

which coincide with (38); by performing an analysis similar to that described in previous subsection, we get

$$\varepsilon_p = \sigma_p^- + e^{i\psi}\sigma_p^+$$

This is the $SU(2)$ exponential of the phase operator similar to (41) defined for each p.

It is also known that, in the so-called thermodynamic limit, when the number of electrons tends to infinity at constant density, the state of the system with the quasispin Bardeen-Cooper-Shriefer (BCS) Hamiltonian (57) is the eigenstate of the trial Hamiltonian, in which the interaction part of (57) is changed by the operator [79]

$$H_{\text{int}} = -T_c \sum_p (\sigma_p^- \Delta + \sigma_p^+ \Delta^* - |\Delta|^2)$$

where T_c is some constant related to $J_{pp'}$ in (57) and Δ is the complex parameter, characterizing the gap in the spectrum of eigenenergy and depending on the temperature. Thus, at $\psi = -2 \arg \Delta$, the superconducting state (the eigenstate of ε_p) is the $SU(2)$ quantum phase state, describing entangled electrons with opposite spins and momenta (Cooper pair). Therefore, the phase transition into the superconducting state can be interpreted as the creation of collective entangled state of electrons.

D. Summary

1. For the electric dipole radiation described by the Jaynes–Cummings Hamiltonian (34), the polarization of photons at $kr \to 0$ is defined by the quantum number $m = 0, \pm 1$, describing the excited atomic state.
2. For any atomic multipole transition, the excited state can be described in terms of the dual representation of corresponding $SU(2)$ algebra, describing the azimuthal quantum phase of the angular momentum. In particular, the exponential of the phase operator and phase states can be constructed. The quantum phase variable has a discrete spectrum with $(2j + 1)$ different eigenvalues.
3. In a special case of $j = \frac{1}{2}$, the eigenstates of the exponential of the phase operator coincide with the EPR (entangled) states, which can be interpreted as the $SU(2)$ phase state.

IV. QUANTUM PHASE OF MULTIPOLE RADIATION

> No, my dear Watson, the two events are connected – must be connected. It is for us to find the connection.
>
> —Sir Arthur Conan Doyle, *The Second Stain*

A. Conservation of Angular Momentum in the Process of Radiation

We now turn to the problem of the $SU(2)$ quantum phase of multipole radiation. As a particular example of some considerable interest, we investigate the electric dipole field. All other types of the multipole radiation can be considered in the same way.

In Section III.B, we introduced the atomic quantum phase states through the use of the representation of the $SU(2)$ algebra (37) and dual representation (48), corresponding to the angular momentum of the excited atomic state. The multipole radiation emitted by atoms carries the angular momentum of the excited atomic state and can also be specified by the angular momentum [2,26,27]. The bare operators of the angular momentum of the electric dipole

radiation have the form

$$
\begin{aligned}
M_+ &= \sqrt{2}(a_+^+ a_0 + a_0^+ a_-) \\
M_- &= \sqrt{2}(a_0^+ a_+ + a_-^+ a_0) \\
M_z &= \sum_{m=-1}^{1} m a_m^+ a_m
\end{aligned}
\tag{58}
$$

This result can be obtained by canonical quantization of the components of classical angular momentum (9) [2]. Hereafter in this section we use the following notation:

$$a_m \equiv a_{Ek1m}$$

Taking into account the commutation relations (23), it is easy to check that

$$[M_+, M_-] = 2M_z, \quad [M_z, M_\pm] = \pm M_\pm \tag{59}$$

so that the operators (58) form a representation of the $SU(2)$ subalgebra in the Weyl–Heisenberg algebra (18) of the electric dipole photons.

The electric dipole photons, as well as the operators (58), are defined in the Hilbert space

$$\mathscr{H}_{\text{field}} = \bigotimes_{m=-1}^{1} \mathscr{H}_m \tag{60}$$

where each subspace $\mathscr{H}_m$ is spanned by the countable set of Fock vectors $|n_m\rangle$ $(n_m = 0, 1, 2, \ldots)$, which obey the orthogonality condition

$$\langle n'_{m'} | n_m \rangle = \delta_{nn'} \delta_{mm'}$$

and the completeness condition

$$\bigotimes_{m=-1}^{1} \sum_{n_m=0}^{\infty} |n_m\rangle\langle n_m| = \mathbf{1} \tag{61}$$

Here $\mathbf{1}$ is the unit operator, acting in (60). Unlike (39)

$$M^2 = M_z^2 + M_+ M_- - M_z \neq \mathbf{1}$$

in the whole Hilbert space (60). In other words, there is no isotype representation [52] of (58) in (60). Therefore, the polar decomposition of the

$SU(2)$ subalgebra (58) in the Weyl–Heisenberg algebra of electric dipole photons cannot be constructed in the way discussed in Section III.B.

At the same time, we know that the photons carry information obtained from the atom in the process of generation. This information is transmitted through the conservation laws. In particular, the photon carries the angular momentum of the excited state because

$$[(J_\alpha + M_\alpha, H] = 0 \tag{62}$$

Here J_α denotes the atomic $SU(2)$ generators (37) with $\alpha = z, \pm, M_\alpha$ is the component of the field angular momentum operator (58), and H is the Jaynes–Cummings model Hamiltonian (34).

Since the atomic $SU(2)$ quantum phase, discussed in Section III.B, is defined by the angular momentum of the excited atomic state, the conservation law (62) can be used to determine the field counterpart of the exponential of the phase operator (41) and other operators referred to the $SU(2)$ quantum phase [36,46]. For example, it is easily seen that the operator

$$\varepsilon_{\text{rad}} = a_+^+ a_0 + a_0^+ a_- + a_-^+ a_+ \tag{63}$$

complements the atomic exponential of the phase operator (41) (at $\psi = 0$) with respect to the integral of motion:

$$[(\varepsilon_a + \varepsilon_{\text{rad}}), H] = 0 \tag{64}$$

The operator (63) can be considered as the result of "mapping" of the atomic exponential of the $SU(2)$ phase operator (41) on the field variables through the use of the integral of motion (64). Unlike (41), it is not unitary

$$\varepsilon_{\text{rad}} \varepsilon_{\text{rad}}^+ \neq \mathbf{1}$$

but it is a normal operator

$$[\varepsilon_{\text{rad}}, \varepsilon_{\text{rad}}^+] = 0$$

commuting with the total number of photons

$$[\varepsilon_{\text{rad}}, \sum_m a_m^+ a_m] = 0 \tag{65}$$

In the same way, it is easy to show that the operator constructions $\varepsilon_{\text{rad}} + \varepsilon_{\text{rad}}^+$ and $-i(\varepsilon_{\text{rad}} - \varepsilon_{\text{rad}}^+)$ complement the atomic cosine and sine of the $SU(2)$ phase operators (42) with respect to the integrals of motion with the atom–field Hamiltonian (34).

B. Dual Representation of Dipole Photons

We now turn to the construction of the dual representation of the photon operators, providing the field counterpart of the $SU(2)$ phase representation of the atomic variables. It is easily seen that the atomic exponential of the $SU(2)$ phase operator (41) takes [in the representation of dual states (46)] the following diagonal form

$$\varepsilon_a^{(\phi)} = \sum_{m=-1}^{1} e^{i\phi_m} |\phi_m\rangle\langle\phi_m| \tag{66}$$

where ϕ_m takes the values (46) (hereafter we put $\psi = 0$ without loss of generality). Thus, the dual representation of the atomic operators leads to the diagonal form of the exponential of the phase operator.

In turn, the field operator (63), representing the field counterpart of (41), can be diagonalized by the following Bogolubov-type [80] canonical transformation [46]

$$\begin{aligned} a_m &= \frac{1}{\sqrt{3}} \sum_{m'=-1}^{1} e^{-im'\phi_m} \mathbf{a}_{m'} \\ \mathbf{a}_m &= \frac{1}{\sqrt{3}} \sum_{m'=-1}^{1} e^{im'\phi_m} a_{m'} \end{aligned} \tag{67}$$

which has the form of finite Fourier transformation with ϕ_m defined in (46). It follows from the commutation relations (23) that

$$[\mathbf{a}_m, \mathbf{a}_{m'}^+] = \delta_{mm'} \tag{68}$$

Hence, the operators $\mathbf{a}$ in (67) also form a representation of the Weyl–Heisenberg algebra of the electric dipole photons. Employing this transformation (67) then gives the diagonal representation of the operator (63)

$$\varepsilon_{\text{rad}}^{(\phi)} = \sum_{m=-1}^{1} e^{i\phi_m} \mathbf{a}_m^+ \mathbf{a}_m \tag{69}$$

similar to (66). It is now a straightforward matter to arrive at the integral of motion:

$$[(\varepsilon_a^{(\phi)} + \varepsilon_{\text{rad}}^{(\phi)}), H] = 0 \tag{70}$$

By construction, it corresponds to (64) in the dual representation of the dynamical variables for the atom and radiation field. This integral of motion reflects the fact that the $SU(2)$ phase information is also transmitted from the

atom to photon in the process of generation. In other words, the integral of motion (70) is responsible for the mapping of the atomic $SU(2)$ phase on the field variables. Therefore, one can choose to interpret $\mathbf{a}_m$ and $\mathbf{a}_m^+$ in the canonical transformation (67) as the annihilation and creation operators of the electric dipole photons *with given radiation phase* [46].

As can be seen from the transformation (67), the operators $\mathbf{a}_m$ obey the same stability condition (25) as a_m

$$\forall m, m' \quad a_m|0\rangle = \mathbf{a}_{m'}|0\rangle = 0 \tag{71}$$

where the dipole vacuum state is defined as follows:

$$|0\rangle \equiv \bigotimes_{m=-1}^{1} |0_m\rangle$$

Hence, the creation operators $\mathbf{a}_m^+$ in (67) can be used to generate the Fock number states in the "phase representation"

$$|\nu_m\rangle = \frac{1}{\sqrt{\nu_m!}}(\mathbf{a}_m^+)^{\nu_m}|0\rangle \tag{72}$$

such that

$$\mathbf{a}_m^+\mathbf{a}_m|\nu_m\rangle = \nu_m|\nu_m\rangle, \quad \nu_m = 0, 1, \ldots$$

and

$$\langle\nu_m|\nu'_{m'}\rangle = \delta_{mm'}\delta_{\nu\nu'}, \qquad \bigotimes_{m=-1}^{1}\sum_{\nu_m}|\nu_m\rangle\langle\nu_m| = \mathbf{1}$$

The unit operator here coincides with (61). Thus, the states (72) form a basis in the Hilbert space (60) dual to the basis of conventional number states $|n_m\rangle$. In analogy to the atomic phase states (46), we call (72) the *radiation phase states* of the electric dipole photons. It follows from (69) that the radiation phase states (72) are the eigenstates of the operator $\varepsilon_{\text{rad}}^{(\phi)}$:

$$\varepsilon_{\text{rad}}^{(\phi)}|\nu_m\rangle = \nu_m e^{i\phi_m}|\nu_m\rangle \tag{73}$$

In contrast to the relation (45), the eigenvalues of $\varepsilon_{\text{rad}}^{(\phi)}$ in (73) contain, in addition to the exponential, a factor of ν_m, describing the number of photons in a given radiation phase state. Thus, this is an non-normalized exponential of the phase operator.

The preceding results lead to the conclusion that the radiation phase states (72) are dual to the conventional Fock number states $|n_m\rangle$. In turn, the operators (67) form the representation of the Weyl–Heisenberg algebra of the electric dipole photons dual to the operators a_m and a_m^+ [46].

Although the canonical transformation (67) has the very simple form of the finite Fourier transformation, the connection between the conventional number states and the radiation phase states (72) is not simple:

$$|\nu_m\rangle = \sqrt{\frac{\nu_m!}{3^{\nu_m}}} \sum_{n_0=0}^{\nu_m} \sum_{n_+=0}^{\nu_m-n_0} \frac{\exp[(i(\nu_m - n_0 - 2n_+)\phi_m]}{\sqrt{n_0! n_+! (\nu_m - n_0 - n_+)!}} \times |n_+; n_0; \nu_m - n_0 - n_+\rangle \tag{74}$$

It is interesting that the "dual" coherent states

$$|\alpha^{(a)}\rangle = \prod_m D_m^{(a)}(\alpha^{(a)})|0\rangle$$
$$|\alpha^{(\mathbf{a})}\rangle = \prod_m D^{(\mathbf{a})}(\alpha^{(\mathbf{a})})|0\rangle$$

are equivalent up to the following transformation of the parameters:

$$\alpha_{m'}^{(a)} = \frac{1}{\sqrt{3}} \sum_m e^{-im'\phi_{m'}} \alpha_m^{(\mathbf{a})}$$
$$\alpha_{m'}^{(\mathbf{a})} = \frac{1}{\sqrt{3}} \sum_m e^{im\phi_{m'}} \alpha_m^{(a)}$$

similar to the canonical transformation (67). Here

$$D_m^{(a)} = \exp(\alpha_m^{(a)} a_m^+ - \text{H.c.})$$
$$D_m^{(\mathbf{a})} = \exp(\alpha_m^{(\mathbf{a})} \mathbf{a}_m^+ - \text{H.c.})$$

are the "dual" Glauber displacement operators [81] (H.c. denotes Hermitian conjugation). If we consider, as an example, the state $|\alpha_+; 0; 0\rangle$ of the electric dipole radiation with only one component $m = +1$, we will see that it is represented by the dual coherent state

$$\bigotimes_m |\alpha_m^{(\mathbf{a})}\rangle, \quad \alpha_m^{(\mathbf{a})} = \frac{1}{\sqrt{3}} \alpha_+^{(a)} e^{i2m\pi/3}$$

in which all the three "phase" components of the electric dipole radiation are in the coherent states.

The dual representation of the photon operators (67) reflects the transmission of "phase information" from the atomic transition to the radiation field via the integral of motion (70). This statement can be illustrated with the aid of the Jaynes–Cummings model (34). Employing the atomic phase states (46), we can introduce the dual representation of the atomic operators (35) as follows:

$$R^{(\phi)}_{mm'} \equiv |\phi_m\rangle\langle\phi_{m'}|, \quad R^{(\phi)}_{mg} \equiv |\phi_m\rangle\langle g| \tag{75}$$

Then, the simultaneous use of the dual representation of the atomic operators (75) and the canonical transformation of photon operators (67) leads to the following form of the Jaynes–Cummings Hamiltonian (34):

$$\begin{aligned} H^{(\phi)} &= H^{(\phi)}_0 + H^{(\phi)}_{\text{int}} \\ H^{(\phi)}_0 &= \sum_{m=-1}^{1} [\omega \mathbf{a}^+_m \mathbf{a}_m + \omega_0 R^{(\phi)}_{mm}] \\ H^{(\phi)}_{\text{int}} &= +g(R^{(\phi)}_{mg}\mathbf{a}_m + \mathbf{a}^+_m R^{(\phi)}_{gm})] \end{aligned} \tag{76}$$

which has exactly the same operator structure as (34) in the dual representation [46]. Since the dual atomic operators (75) describe the transition between the atomic phase states and ground state, and the operators $\mathbf{a}_m$ and $\mathbf{a}^+_m$ determine the annihilation and creation of photons with given radiation phase, the interaction term in (76) *describes the transmission of the quantum phase information from the atom to photons.*

We now note that the quantum phase in the Jaynes–Cummings model has been examined in a huge number of papers (for reviews, see Refs. 39 and 68). Most of them are based on the approach proposed in the pioneering paper by Dirac [1] and developed by a number of authors. Among the principal contributions to the field, the Pegg–Barnett approach [45] should be mentioned as the currently most popular. The main idea of the approach consists in defining the quantum phase operator first in a finite s-dimensional subspace of the infinite-dimensional Hilbert space $\mathscr{H}_{\text{field}}$ with subsequent formal limit transition $s \to \infty$, which is taken only after the averages have been calculated. In contrast, we consider the extended space of states $\mathscr{H}_a \otimes \mathscr{H}_{\text{field}}$ in which the quantum phase of radiation is defined *by mapping of corresponding atomic operators from* $\mathscr{H}_a$ *into the whole Hilbert space* $\mathscr{H}_{\text{field}}$ *(60), using the conservation of angular momentum*. In view of the dual form of the Jaynes–Cummings Hamiltonian (76), it is possible to say that the radiation phase is expressed in terms of what *can be generated* by a given quantum source.

So far our observations have been applied only to electric dipole radiation. It is straightforward to find the general form of the canonical transformation (67)

in the same way as above. In the case of an arbitrary monochromatic pure (λ, j)-pole radiation, we get [46]

$$\mathbf{a}_{\lambda kjm} = \frac{1}{\sqrt{2j+1}} \sum_{m'=-j}^{j} e^{im'\phi_{jm}} a_{\lambda kjm'}, \quad \phi_{jm} = \frac{2\pi m}{2j+1} \tag{77}$$

Here we again put $\psi = 0$.

C. Structure of Radiation Phase

We now examine the spectrum of radiation phase constructed in the preceding subsection. Consider the state

$$|\phi^{(\mathrm{rad})}\rangle = \bigotimes_{m=-1}^{1} |\nu_m\rangle \tag{78}$$

where $|\nu_m\rangle$ is the radiation phase state (72). It is clear that (78) is the eigenstate of the operator (73). Since the operator (73) commute with the total number of photons

$$N = \sum_{m=-1}^{1} a_m^+ a_m = \sum_{m=-1}^{1} \mathbf{a}_m^+ \mathbf{a}_m$$

the eigenstates and eigenvalues of $\varepsilon_{\mathrm{rad}}^{(\phi)}$ can be specified by the index

$$n = \sum_{m=-1}^{1} \nu_m$$

describing the total number of photons in a given state (72) and (74) and by an additional index ℓ, describing a given distribution of n photons over the three independent phase components of the electric dipole radiation in (72) and (74). The total number of possible different values of ℓ, corresponding to a given n, is clearly

$$\frac{1}{2}(n+2)(n+1)$$

Then

$$\varepsilon_{\mathrm{rad}}^{(\phi)} |\phi_{n\ell}^{(\mathrm{rad})}\rangle = e^{i\varphi_{n\ell}} \kappa_{n\ell} |\phi_{n\ell}^{(\mathrm{rad})}\rangle \tag{79}$$

where $|\phi_{n\ell}^{(\mathrm{rad})}\rangle$ denotes the state (78) at given n and ℓ. The modulus of the eigenstates in (79) is determined as

$$\begin{aligned}\kappa_{n\ell}^2 = \langle\phi_{n\ell}^{(\mathrm{rad})}|\varepsilon_{\mathrm{rad}}^{(\phi)}(\varepsilon_{\mathrm{rad}}^{(\phi)})^+|\phi_{n\ell}^{(\mathrm{rad})}\rangle &= \sum_{mm'} \nu_m \nu'_m e^{i(m-m')2\pi/3} \\ &= \sum_m \nu_m^2 - (\nu_+\nu_0 + \nu_0\nu_- + \nu_-\nu_+) \\ &= n^2 + 2(\nu_+^2 + \nu_-^2) - 3n(\nu_+ + \nu_-) + 3\nu_+\nu_-\end{aligned} \tag{80}$$

In turn, for the "phase eigenvalues" $\varphi_{n\ell}$ in (79), we get [46]

$$\tan\phi = \frac{\sqrt{3}(\nu_+ - \nu_-)}{2\nu_0 - (\nu_+ + \nu_-)} \tag{81}$$

Taking into account the physical meanings of the atomic operators (41) and (66) and the integrals of motion (64), we can consider the field operators (63) and (69) as the nonnormalized exponential operators of the radiation phase, which, by construction, is the $SU(2)$ phase of the multipole (electric dipole) radiation. By performing a similar analysis to that described in Section III.B, we can define the cosine and sine operators of the radiation phase as follows [36]

$$C_{\mathrm{rad}} = K(\varepsilon_{\mathrm{rad}} + \varepsilon_{\mathrm{rad}}^+), \quad S_{\mathrm{rad}} = -iK(\varepsilon_{\mathrm{rad}} + \varepsilon_{\mathrm{rad}}^+) \tag{82}$$

where K is the normalization coefficient determined from the natural condition

$$\langle C_{\mathrm{rad}}^2 + S_{\mathrm{rad}}^2\rangle = 1 \tag{83}$$

where $\langle\cdots\rangle$ is the averaging over the states of the electric dipole radiation under consideration. It is clear that C_{rad} and S_{rad} are commuting Hermitian operators so that corresponding physical quantities can be measured at once. In the dual representation provided by the canonical transformation (67), the operators (82) take the diagonal form

$$\begin{aligned}C_{\mathrm{rad}}^{(\phi)} &= K\sum_{m=-1}^{1} \mathbf{a}_m^+\mathbf{a}_m \cos\phi_m \\ S_{\mathrm{rad}}^{(\phi)} &= K\sum_{m=-1}^{1} \mathbf{a}_m^+\mathbf{a}_m \sin\phi_m\end{aligned} \tag{84}$$

Therefore, averaging over the phase states (78), we get

$$\langle \phi_{n\ell}^{(\mathrm{rad})} | C_{\mathrm{rad}}^{(\phi)} | \phi_{n\ell}^{(\mathrm{rad})} \rangle = 2\kappa_{n\ell} \cos \varphi_{n\ell}$$
$$\langle \phi_{n\ell}^{(\mathrm{rad})} | S_{\mathrm{rad}}^{(\phi)} | \phi_{n\ell}^{(\mathrm{rad})} \rangle = 2\kappa_{n\ell} \sin \varphi_{n\ell}$$

According to the condition (83), we obtain

$$K = \frac{1}{2\kappa_{n\ell}}$$

in this case. Hence, the radiation phase states (78) are the eigenstates of the operators (84), which, because of their structure, can be interpreted as the cosine and sine of the radiation phase operators. It is interesting that the eigenvalues of the radiation phase variable defined by (81) belong to the interval $(0, 2\pi)$ and form a discrete set for any finite number of photons n and

$$\ell = 1, 2, \ldots, \frac{(n+1)(n+2)}{2}$$

The first few eigenvalues are shown in Table I and Fig. 5.

It is not difficult to see that the vacuum averages of the operators (84) have the form

$$\langle 0 | C_{\mathrm{rad}}^{(\phi)} | 0 \rangle = \langle 0 | S_{\mathrm{rad}}^{(\phi)} | 0 \rangle = 0$$

TABLE I
List of Eigenvalues (81)[a]

$n = 1$	$\epsilon^{(1)} = 1$	$\varphi^{(1)} = 2\ell\pi/3$
$n = 2$	$\epsilon^{(2)} = 2$	$\varphi^{(2)} = 2\ell\pi/3$
	$\epsilon^{(2)} = 1$	$\varphi^{(2)} = (2\ell + 1)\pi/3$
$n = 3$	$\epsilon^{(3)} = 3$	$\varphi^{(3)} = 2\ell\pi/3$
	$\epsilon^{(3)} = \sqrt{3}$	$\phi^{(3)} = \pm(\pi/2 + \ell\pi/3)$
$n = 4$	$\epsilon^{(4)} = 4$	$\varphi^{(4)} = 2\ell\pi/3$
	$\epsilon^{(4)} = \sqrt{7}$	$\varphi^{(4)} = \pm\tan^{-1}(\sqrt{3}/5) + 2\ell\pi/3$
	$\epsilon^{(4)} = 2$	$\varphi^{(4)} = (2\ell + 1)\pi/3$
	$\epsilon^{(4)} = 1$	$\varphi^{(4)} = 2\ell\pi/3$
$n = 5$	$\epsilon^{(5)} = 5$	$\varphi^{(5)} = 2\ell\pi/3$
	$\epsilon^{(5)} = \sqrt{13}$	$\varphi^{(5)} = \tan^{-1}(\sqrt{3}/7) \pm 2\ell\pi/3$
		$\varphi^{(5)} = \pm\tan^{-1}(\sqrt{3}/7) + 2\ell\pi/3$
	$\epsilon^{(5)} = \sqrt{7}$	$\varphi^{(5)} = \pm\tan^{-1}(\sqrt{3}/5) + \pi + 2\ell\pi/3$
	$\epsilon^{(5)} = 2$	$\varphi^{(5)} = 2\ell\pi/3$
	$\epsilon^{(5)} = 1$	$\varphi^{(5)} = (2\ell = 1)\pi/3$

[a]Here $\ell = 0, \pm$.

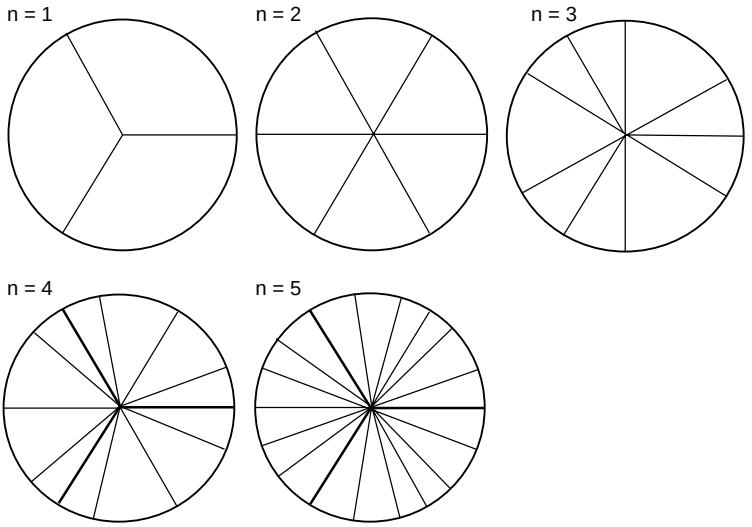

Figure 5. The structure of eigenvalues (80)–(81) corresponding to the phase states with $n = 1, \ldots, 5$ photons. The bold lines correspond to the double-degenerated eigenstates.

while the vacuum variances

$$\langle 0|(\Delta C_{\text{rad}}^{(\phi)})^2|0\rangle = \langle 0|(\Delta S_{\text{rad}}^{(\phi)})^2|0\rangle = \frac{1}{2}$$

Hence, as all one can expect, the vacuum distribution of the radiation phase is uniform.

Now consider the electric dipole radiation with coherent components $m = \pm 1$, while the component $m = 0$ is in the vacuum state:

$$|\alpha\rangle = |\alpha_+\rangle \otimes |0\rangle \otimes |\alpha_-\rangle \tag{85}$$

at $|\alpha_+| = |\alpha_-| \equiv |\alpha|$. In this case, the condition (83) gives

$$K = \frac{1}{\sqrt{4|\alpha|^2(2 + |\alpha|^2)}}$$

so that

$$\begin{aligned} \langle C_{\text{rad}}^{(\phi)}\rangle &= \frac{|\alpha|}{\sqrt{2 + |\alpha|^2}} \cos \Delta_{+-} \\ \langle S_{\text{rad}}^{(\phi)}\rangle &= \frac{|\alpha|}{\sqrt{2 + |\alpha|^2}} \sin \Delta_{+-} \end{aligned} \tag{86}$$

where

$$\Delta_{+-} \equiv \arg\alpha_+ - \arg\alpha_-$$

One can see that at $|\alpha| \to \infty$ we get

$$\langle C_{\text{rad}}^{(\phi)})\rangle \to \cos\Delta_{+-}, \quad \langle S_{\text{rad}}^{(\phi)})\rangle \to \sin\Delta_{+-}$$

so that in the classical limit of infinitely many coherent photons the operators (113) define the cosine and sine of the phase difference between the two components of the radiation field (85). In turn, for the variances we get

$$\langle 0|(\Delta C_{\text{rad}}^{(\phi)})^2|0\rangle = \langle 0|(\Delta S_{\text{rad}}^{(\phi)})^2|0\rangle = \frac{2+\cos\Delta_{+-}}{2(2+|\alpha|^2)} \tag{87}$$

Here the right-hand side tends to zero when $|\alpha| \to \infty$. Hence, the radiation phase has the natural classical limit.

At first sight, Eq. (87) gives wrong limit at $|\alpha| \to 0$:

$$\lim_{|\alpha|\to 0}\langle 0|(\Delta C_{\text{rad}}^{(\phi)})^2|0\rangle = \lim_{|\alpha|\to 0}\langle 0|(\Delta S_{\text{rad}}^{(\phi)})^2|0\rangle = \frac{2+\cos\Delta_{+-}}{4} \tag{88}$$

In fact, this is an illusory contradiction. Because of the degeneration of the vacuum state with respect to the phase difference, the limit transition $|\alpha| \to 0$ should imply the averaging over all possible $\Delta \in (0, 2\pi)$, which leads to the natural value of the vacuum variances.

Now consider the case when $|\alpha_+| \neq |\alpha_-|$ in the state (85). Then, instead of (86) and (87), we get

$$\begin{aligned}\langle C_{\text{rad}}^{(\phi)})\rangle &= \frac{\cos\Delta_{+-}}{\sqrt{1+|\alpha_+|^{-2}+|\alpha_-|^{-2}}}\\ \langle S_{\text{rad}}^{(\phi)})\rangle &= \frac{\sin\Delta_{+-}}{\sqrt{1+|\alpha_+|^{-2}+|\alpha_-|^{-2}}}\end{aligned} \tag{89}$$

and

$$\begin{aligned}\langle(\Delta C_{\text{rad}}^{(\phi)})^2\rangle &= \langle(\Delta S_{\text{rad}}^{(\phi)})^2\rangle\\ &= \frac{|\alpha_+|^2+|\alpha_-|^2+|\alpha_+||\alpha_-|\cos\Delta_{+-}}{2(|\alpha_+|^2+|\alpha_-|^2+|\alpha_+|^2|\alpha_-|^2)}\end{aligned}$$

respectively. Examine now the averages (89) and variance (90) as a function of $|\alpha_+|$ at fixed $|\alpha_-|$ [54]. We obtain

$$\begin{cases} \langle C_{\text{rad}}^{(\phi)}\rangle \to 0 \\ \langle S_{\text{rad}}^{(\phi)}\rangle \to 0 \\ \langle 0|(\Delta C_{\text{rad}}^{(\phi)})^2|0\rangle \to \frac{1}{2} \\ \langle 0|(\Delta S_{\text{rad}}^{(\phi)})^2|0\rangle \to \frac{1}{2} \end{cases} \tag{91}$$

because the operators (84) define properties of the relative phase (phase difference between the components) which does not exist when only component $m = -1$ is emitted. It is seen that, under the condition

$$|\alpha_+||\alpha_-| < \cos\Delta_{+-} \leq 1 \tag{92}$$

which can be realized in the strong quantum case of very low intensities, the value of the variances (90) can exceed the vacuum limit of $\frac{1}{2}$. The maximum in (90) is achieved at

$$|\alpha_+| = |\alpha_-| \times \frac{\sqrt{|\alpha_-|^4 + (1 + |\alpha_-|^2)\cos\Delta_{+-}} - |\alpha_-|^2}{(1 + |\alpha_-|^2)\cos\Delta_{+-}}$$

The dependence of the variances (90) on $|\alpha_+|$ at fixed $|\alpha_-|$ is shown in Fig. 6. The qualitative explanation of this effect of strong increase of quantum fluctuations in the low-intensity limit is based on the consideration of the probability to have a given phase difference Δ_{+-}. At $|\alpha_+| = 0$, there is a uniform probability distribution in the system, causing the limit relations (91). Creation of very few photons of the mode $m = +1$ leads to the formation of some domains with almost equal probabilities having phase differences Δ_{+-} and $\Delta_{\pm} + \pi$. So, it looks like a "phase bunching" (for the bunching of photons, see Refs. 14 and 15). Further increase of $|\alpha_+|$ leads to formation of a more or less sharp probability distribution that cannot reach the δ-function shape because the variances (90) achieve the saturation described by the expression

$$\lim_{|\alpha_+|\to\infty} \langle C_{\text{rad}}^{(\phi)}\rangle = \lim_{|\alpha_+|\to\infty} \langle S_{\text{rad}}^{(\phi)}\rangle = \frac{1}{2(1 + |\alpha_-|^2)}$$

which coincides with the classical limit only if $|\alpha_-| \to \infty$ as well. This means that the presence of one quantum component in the coherent state (85) leads to quantum phase fluctuations.

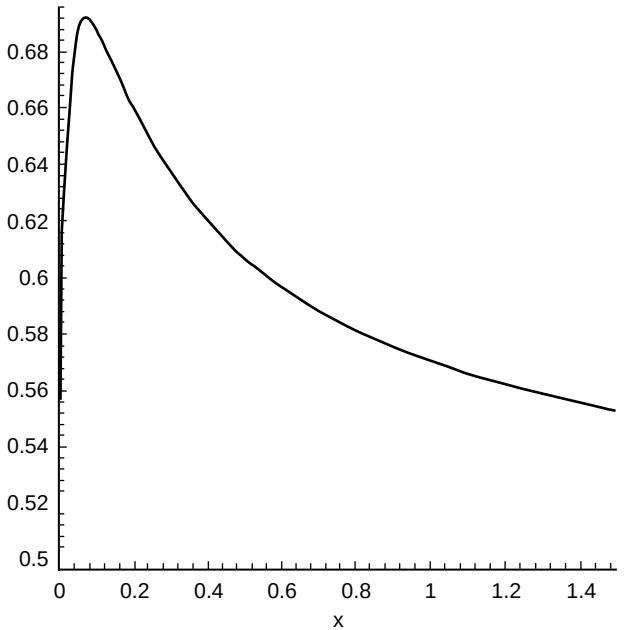

Figure 6. The dependence of variances (90) on $|\alpha_+|$ at fixed $|\alpha_-| = 0.275$ and $\Delta_{+-} = \pi/6$.

Using the standard representation of Glauber coherent states in terms of the number states of photons [14,81]

$$|\alpha\rangle = e^{-|\alpha|^2/2} \sum_{n=0}^{\infty} \frac{\alpha^n}{\sqrt{n!}} |n\rangle$$

and making use of the relation (74), we can represent the coherent state (85) in the following way

$$|\alpha_+; 0; \alpha_-\rangle = \prod_{m=-1}^{1} e^{-i|\alpha_m^{(\mathbf{a})}|^2/2} \sum_{\nu_m=0}^{\infty} \frac{(\alpha_m^{(\mathbf{a})})^{\nu_m}}{\sqrt{\nu_m}} |\nu_m\rangle$$

where the parameters $\alpha_m^{(\mathbf{a})}$ have been defined at the end of Section IV.A. Assume that $|\alpha_+| = |\alpha_-| \equiv |\alpha|$. Then

$$\sum_m |\alpha_m^{(\mathbf{a})}|^2 = 2|\alpha|^2$$

and the probability of observing the radiation field in a given phase state (72), (74) is

$$|\langle \nu_+; \nu_0; \nu_- | \alpha_+; 0; \alpha_- \rangle|^2 = e^{-2|\alpha|^2} \left(\frac{2}{3}\right)^n \frac{|\alpha|^{2n}}{\nu_+! \nu_0! \nu_-!} \prod_{m=-1}^{1} \left[1 + \cos\left(\Delta_{+-} - \frac{2m\pi}{3}\right)\right]^{\nu_m} \tag{93}$$

where $n = \sum_m \nu_m$. It is easily seen that this probability tends to zero when $|\alpha| \to 0$ or $|\alpha| \to \infty$. This means that the eigenvalues of the radiation phase are distributed uniformly over the interval $(0, 2\pi)$ in the vacuum state as well as in the classical limit of high-intensity coherent state. Between these two extrema, the probability (93) has a maximum, which can be considerably high. It is interesting that the position of the maximum is completely determined by the mean number of photons $|\alpha_{\max}|^2 = n$, while the magnitude also depends on the phase difference Δ_{+-} (see Fig. 7).

Let us now calculate the probability to have a given value of the radiation phase in the coherent state under consideration. Consider, for example, the eigenvalue of the radiation phase $\varphi = 2\pi/3$. Employing equations (80) and (81) then gives the following properties of the states corresponding to this radiation phase:

$$n - 3\nu_- = \kappa_n \qquad \nu_+ = n - 2\nu_- \qquad \nu_0 = \nu_-$$

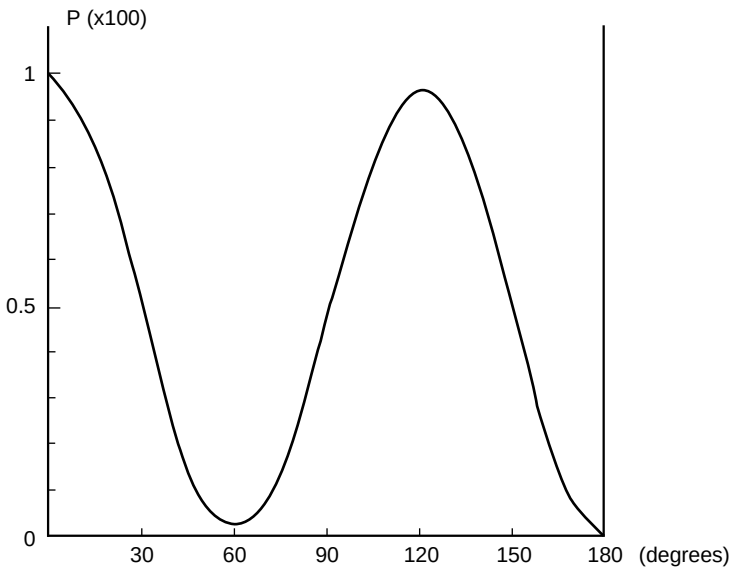

Figure 7. Probability (93) versus Δ_{+-}.

It is easy to see that the states obeying these conditions have the following structure:

$$|n_p - 2k_p; k_p; k_p\rangle \tag{94}$$

where p is an integer and for each $n_p = 3p, 3p-1, 3p-2$ the numbers k_p take the values $k_p = 0, 1, \ldots, p-1$. For example, at $n_p = 10$, we get $p = 4$ and $n_p = 3p - 2$, while the states (94) are

$$|10; 0; 0\rangle, \quad |8; 1; 1\rangle, \quad |6; 2; 2; \rangle, \quad |4; 3; 3\rangle$$

Consider first the states $|n_p; 0; 0\rangle$ in (94). Then, the probability (93) takes the value

$$\begin{aligned}\mathscr{P}_{n_p} &\equiv |\langle n_p; 0; 0|\alpha_+; 0; \alpha_-\rangle|^2 \\ &\quad \times e^{-2|\alpha|^2}\left(\frac{2}{3}\right)^{n_p}\frac{|\alpha|^{2n_p}}{n_p!}\left[1 + \cos\left(\Delta_{+-} - \frac{2\pi}{3}\right)\right]^{n_p}\end{aligned}$$

It is then clear that $\mathscr{P}_{n_p}$ reaches its maximum at $\Delta_{+-} = 2\pi/3$. Then, the total probability to have the phase states $|n_p; 0; 0\rangle$ is

$$\mathscr{P} = \sum_{n_p=1}^{\infty}\mathscr{P}_{n_p} = e^{-2|\alpha|^2/3} - e^{-2|\alpha|^2} \geq 0 \tag{95}$$

(see Fig. 8). It is clear that this function $\mathscr{P}$ gives the lower bond of the total probability to observe the radiation phase $\varphi = 2\pi/3$ in the coherent state under consideration. The contribution of the other states (94) can be calculated in the same way.

D. Radiation Phase in Jaynes–Cummings Model

To illustrate the exchange of the phase information between the atomic transition and the multipole field, consider the electric dipole Jaynes–Cummings model (34). Assume that the field consists of two circularly polarized components in a coherent state each. The atom is supposed to be initially in the ground state. Then, the time-dependent wave function of the system has the form [53]

$$\begin{aligned}|\Psi(t)\rangle &= \sum_{n_+,n_-} P(n_+, n_-)[\cos(g\sqrt{nt})|0, 0\rangle \\ &\quad + (\alpha_+|1, 1\rangle + \alpha_-|1, -1\rangle)\xi(n_+, n_-)]|n_+n_-\rangle\end{aligned} \tag{96}$$

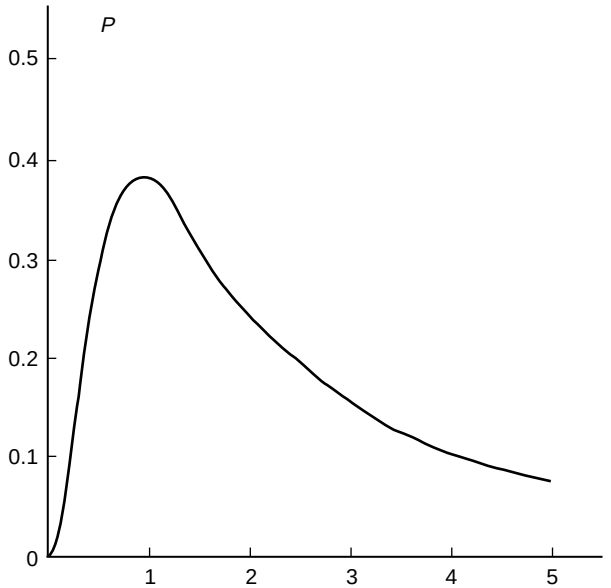

Figure 8. Lower estimate of the probability to have the radiation phase $\varphi = 2\pi/3$ as a function of $|\alpha|^2$ at $\Delta_{+-} = 2\pi/3$.

where $|n_m\rangle$ denotes the Fock number state with n_m photons with the quantum number m; $|1, m\rangle$ and $|0, 0\rangle$ are the excited and ground atomic states, respectively; g is the coupling constant in (34), $n = n_+ n_-$

$$P(n_+, n_-) = e^{-(|\alpha_+|^2 - |\alpha_-|^2)/2} \frac{\alpha_+^{n_+} \alpha_-^{n_-}}{\sqrt{n_+! n_-!}}$$

and

$$\xi(n_+, n_-) = \frac{\sin(gt\sqrt{n+1})}{\sqrt{n+1}} e^{-i(n+1)\omega t}$$

Then, the mean values of the operators (82), describing the cosine and sine of the radiation phase, take the form

$$\langle C_{\text{rad}} \rangle_t = \sqrt{\frac{|\alpha_+|^2 |\alpha_-|^2}{|\alpha_+|^2 |\alpha_-|^2 + |\alpha_+|^2 |\alpha_-|^2}} \frac{\langle a_+^+ a_+ + a_-^+ a_- \rangle_t}{|\alpha_+|^2 + |\alpha_-|^2} \cos \Delta_{+-}$$

$$\langle S_{\text{rad}} \rangle_t = \sqrt{\frac{|\alpha_+|^2 |\alpha_-|^2}{|\alpha_+|^2 |\alpha_-|^2 + |\alpha_+|^2 |\alpha_-|^2}} \frac{\langle a_+^+ a_+ + a_-^+ a_- \rangle_t}{|\alpha_+|^2 | + \alpha_-|^2} \sin \Delta_{+-} \qquad (97)$$

Here

$$\langle a_+^+ a_+ + a_-^+ a_- \rangle_t = |\alpha_+|^2 + |\alpha_-|^2 - \sum_{n_+,n_-=0}^{\infty} |P(n_+, n_-)|^2 \sin^2 gt\sqrt{n_+ + n_-}$$

and $\Delta_{+-} \equiv \arg\ \alpha_+ - \arg\ \alpha_-$. Thus, the averages (97) describe the Rabi oscillations of cosine and sine of the phase difference between the two coherent components of the field. Corresponding variances have the form

$$\begin{aligned} \langle (\Delta C_{\text{rad}})^2 \rangle_t &= \frac{\langle a_+^+ a_+ + a_-^+ a_- \rangle_t}{|\alpha_+|^2 + |\alpha_-|^2} [\langle (\Delta C_{\text{rad}})^2 \rangle_0 + \beta_C Q] \\ \langle (\Delta S_{\text{rad}})^2 \rangle_t &= \frac{\langle a_+^+ a_+ + a_-^+ a_- \rangle_t}{|\alpha_+|^2 + |\alpha_-|^2} [\langle (\Delta S_{\text{rad}})^2 \rangle_0 + \beta_S Q] \end{aligned} \tag{98}$$

Here

$$\begin{aligned} \langle (\Delta C_{\text{rad}})^2 \rangle_0 &= \frac{1}{2} \cos\ \Delta_{+-} \\ \langle (\Delta S_{\text{rad}})^2 \rangle_0 &= \frac{|\alpha|^2 + |\alpha_-|^2 - |\alpha_+||\alpha_-|}{|\alpha|^2 + |\alpha_-|^2 + |\alpha_+||\alpha_-|} \cos \Delta_{+-} \end{aligned}$$

and

$$\begin{aligned} \beta_C &= \frac{|\alpha_+||\alpha_-|}{(|\alpha|^2 + |\alpha_-|^2 + |\alpha_+||\alpha_-|)(|\alpha|^2 + |\alpha_-|^2 + |\alpha_+||\alpha_-|)} \cos^2 \Delta_{+-} \\ \beta_C &= \frac{|\alpha_+||\alpha_-|}{(|\alpha|^2 + |\alpha_-|^2 + |\alpha_+||\alpha_-|)(|\alpha|^2 + |\alpha_-|^2 + |\alpha_+||\alpha_-|)} \sin^2 \Delta_{+-} \end{aligned}$$

In (98), Q is the Mandel factor [14], describing the deviation of the photon statistics from the Poisson distribution for the total intensity:

$$Q = \frac{\langle [\Delta(a_+^+ a_+ + a_-^+ a_-)]^2 \rangle - \langle (a_+^+ a_+ + a_-^+ a_-) \rangle}{\langle (a_+^+ a_+ + a_-^+ a_-) \rangle}$$

It is seen that the time-averaged Mandel Q factor is always positive, which shows the super-Poissonian number distribution for the total field.

Since $\langle C_{\text{rad}} \rangle_t$ and $\langle (\Delta C_{\text{rad}})^2 \rangle_t$ can be transformed into $\langle S_{\text{rad}} \rangle_t$ and $\langle (\Delta S_{\text{rad}})^2 \rangle_t$, respectively, by the change of phase difference

$$\Delta_{+-} \to \Delta_{+-} + \frac{k\pi}{2}$$

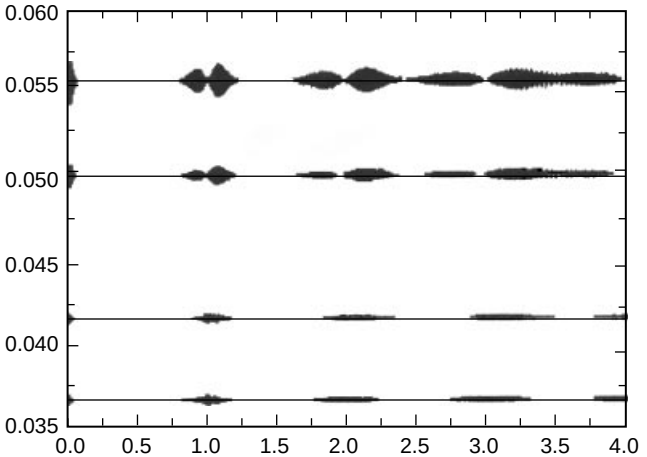

Figure 9. Rabi oscillations of the variance of the field cosine operator as a function of scaled time $t_s = gt/(2\pi\sqrt{n_+ + n_-})$ at $n_\pm = 25$ and $g = 1$. Graphs from top to bottom correspond to the relative phase $\Delta_{+-} = 0°, 45°, 75°, 90°$, respectively.

it suffices to examine only one pair of these functions. In Fig. 9, the Rabi oscillations of the variance $\langle(\Delta C_{\text{rad}})^2\rangle_t$ are shown as a function of time for different Δ_{+-}. At small Δ_{+-}, the collapse and revival picture of Rabi oscillations behaves quite typically for the Jaynes–Cummings model [68], while the increase of Δ_{+-} leads to a confluence of the nearest revivals. The Rabi oscillations of $\langle C_{\text{rad}}\rangle_t$ have similar behavior.

It should be emphasized that the system under consideration completely describes the process of transmission of the phase information between the field and the atom. Initially the atom is in the ground state with the angular momentum 0 and has no $SU(2)$ atomic phase at all. Absorption of photons induces an atomic phase that coincides with the phase difference between the two coherent components of the field. This can be concluded from a direct calculation of the expectation value of the atomic cosine operator (43) over the state (96):

$$\langle C_a\rangle_t = \sum_{n_+,n_-=0}^{\infty} |P(n_+,n_-)|^2 \frac{\sin^2(gt\sqrt{n+1})}{n+1} \cos\Delta_{+-}$$

This again clearly demonstrates the one-to-one correspondence between the atomic $SU(2)$ phase and the radiation phase.

Let us also stress that, according to (98), the variances of the cosine and sine of the radiation phase can be measured in the same way as the Mandel Q factor.

E. Radiation Phase and Pegg–Barnett Quantum Phase

Following [54], let us compare the quantum statistical behavior of the radiation phase, constructed in Sections IV.A–IV.D and that obtained within the Pegg–Barnett approach [45], which has received a lot of attention since the early 1990s years and has led to many important results (for a review, see Refs. 39 and 40). We use here the form of the Pegg–Barnett approach considered in Ref. 82. The point is that Ref. 82 deals with a generalization of the Pegg–Barnett approach to the case of two circularly polarized modes. Then, the phase distribution over the phases of two circularly polarized modes is determined as

$$P_\psi = |\langle \phi_+, \phi_- | \psi \rangle|^2$$

where $|\phi_+, \phi_-\rangle$ is the Susskind–Glogower phase state [41] and $|\psi\rangle$ is the state of the radiation field. To establish the connection with the results already obtained in this section, suppose that

$$|\psi\rangle = |\alpha_+\rangle \otimes |0_0\rangle \otimes |\alpha_-\rangle \tag{99}$$

Since the formalism of the radiation phase is focused on the phase difference between the components, we need to use the distribution function for the relative phase

$$\phi = \phi_+ - \phi_-$$

We use here the notations of Refs. 54 and 82. Referring to the procedure suggested in Refs. 82 and 83 to cast the range of ϕ into 2π range from 4π range, we take

$$P_{2\pi} = \sum_{n=0}^{\infty} |\langle \phi^{(n)} | \psi \rangle|^2$$

where

$$|\phi^{(n)}\rangle = \frac{1}{\sqrt{2\pi}} \sum_{n_+=0}^{n} e^{i\phi n_+} |n_+\rangle \otimes |0_0\rangle \otimes |n - n_+\rangle$$

Using this distribution function, one can calculate the mean value of any function $F(\phi)$ of the relative phase as follows [82]:

$$\langle F(\phi) \rangle = \int_{-\pi}^{\pi} d\phi P_{2\pi}(\phi) F(\phi)$$

In the case under consideration, the relative phase represents the phase difference between the two circularly polarized components in coherent state. Then, for the Pegg–Barnett cosine of the relative phase, we get

$$\langle \cos \phi_{\mathrm{PB}} \rangle = e^{(|\alpha_+|^2+|\alpha_-|^2)} \sum_{n_\pm=0}^{\infty} \frac{|\alpha_+|^{2n_+}|\alpha_-|^{2n_-}}{n_+!n_-!} \times \frac{\mathrm{Re}(\alpha_+\alpha_-^*)}{\sqrt{(n_+ + 1)(n_- + 1)}} \tag{100}$$

In turn, the average of the squared cosine takes the form

$$\langle \cos^2 \phi_{\mathrm{PB}} \rangle = \frac{1}{2} + \frac{e^{(|\alpha_+|^2+|\alpha_-|^2)}}{2} \sum_{n_\pm=0}^{\infty} \frac{|\alpha_+|^{2n_+}|\alpha_-|^{2n_-}}{n_+!n_-!} \times \frac{\mathrm{Re}(\alpha_+\alpha_-^*)}{\sqrt{(n_+ + 2)(n_+ + 1)(n_- + 2)(n_- + 1)}} \tag{101}$$

Here ϕ_{PB} denotes the Pegg–Barnett quantum phase operator [45]. These expressions can be now compared with the results (89) and (90) for the radiation cosine and its variance. To clarify the difference between the two approaches, we represent (89) and (90) in the same manner as (100) and (101) [54]:

$$\langle C_{\mathrm{rad}}^{(\phi)} \rangle = e^{(|\alpha_+|^2+|\alpha_-|^2)} \sum_{n_\pm=0}^{\infty} \frac{|\alpha_+|^{2n_+}|\alpha_-|^{2n_-}}{n_+!n_-!} \times \frac{\mathrm{Re}(\alpha_+\alpha_-^*)}{\sqrt{|\alpha_+|^2 + |\alpha_-|^2 + |\alpha_+|^2|\alpha_-|^2}} \tag{102}$$

and

$$\langle (C_{\mathrm{rad}}^{(\phi)})^2 \rangle = \frac{1}{2} + \frac{\langle C_{\mathrm{rad}}^{(\phi)} \rangle}{2\sqrt{|\alpha_+|^2 + |\alpha_-|^2 + |\alpha_+|^2|\alpha_-|^2}} + \frac{[\mathrm{Re}(\alpha_+\alpha_-^*)]^2}{2(|\alpha_+|^2 + |\alpha_-|^2 + |\alpha_+|^2|\alpha_-|^2)} \sum_{n_\pm+0}^{\infty} \frac{|\alpha_+|^{2n_+}|\alpha_-|^{2n_-}}{n_+!n_-!} \tag{103}$$

One can easily see that each term in the sums in Eqs. (100) and (101) has different normalization, while in Eqs. (102) and (103) all the terms have the same normalization factor related to our choice of the constant K in (82) and (83). In addition, Eq. (103) contains an extra term proportional to $\langle C_{\mathrm{rad}}^{(\phi)} \rangle$. This term comes from the vacuum fluctuations related to the mode $m = 0$. This causes a striking difference when one of the modes $m = \pm 1$ is in the quantum

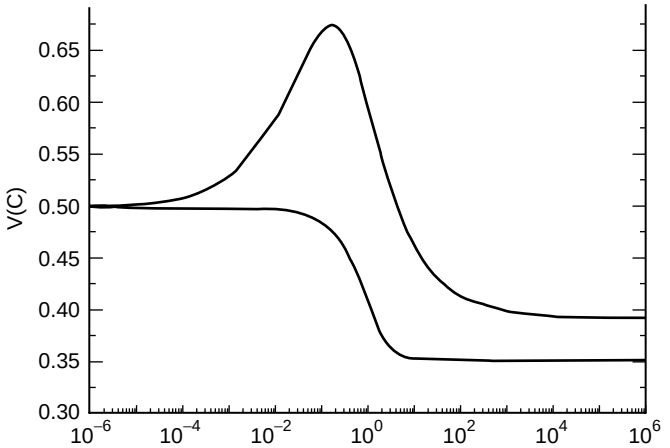

Figure 10. Variance of cosine. The lower curve represents the Pegg–Barnett cosine; the upper curve, the radiation phase cosine. Both curves are drawn at $\Delta_{+-} = 0$ and $I_{-} = 0.275$.

domain. Specifically, the existence of the "phase bunching" discussed in Section IV.C is caused just by this term. At the same time, both approaches show the saturation of the variances when one of the intensities tends to infinity while the second is kept constant (Fig. 10). It is seen that the quantum fluctuations of the phase difference between the two circularly polarized coherent fields with different helicity calculated with the aid of the radiation phase always exceed those calculated within the Pegg–Barnett approach.

This fact can be explained in the following way. The cutoff of the Hilbert space, which is a distinctive feature of the Pegg–Barnett approach [45], leads to an effective change of the algebraic properties of the photon operators. In fact, such a cutoff of the Fock basis leads to the definition of the unit operator, which can be considered as some approximation of the Casimir operator of the $SU(2)$ subalgebra, describing the angular momentum of radiation, but only in a particular subspace of the Hilbert space of photons. Existence of the unit operator makes it possible to perform direct polar decomposition and determine the corresponding quantum phase properties. This can be clearly traced in Ref. 84. At the same time, the cutoff procedure reduces the algebraic properties of photons responsible for the quantum fluctuations. The limit taken in the Pegg–Barnett approach after the calculation of all expectation values cannot completely restore these properties, which are especially important in the quantum domain.

Unlike the Pegg–Barnett approach, the definition of the radiation phase is based on the conservation laws for electromagnetic radiation and canonical

transformation (67), which does not disturb the Weyl–Heisenberg algebra of the photon operators.

F. Radiation Phase and Mandel's Operational Approach

We now note that the operators (69) and (84) introducing the radiation phase are defined in terms of *bilinear* forms in the photon operators. At first glance, such a definition runs counter to the original idea by Dirac to determine the Hermitian quantum phase via *linear* forms in the photon operators [1] (see also Refs. 38, 42, and 44). Leaving aside Dirac's problem of existence of a Hermitian quantum phase variable of a harmonic oscillator, we should emphasize that the use of bilinear forms seems to be quite reasonable from the physical point of view. It can be argued in the following way:

1. The phase information is transmitted from the quantum source (atom) to photons via the conservation laws. In fact, only three physical quantities are conserved in the process of radiation: energy, linear momentum, and angular momentum [26]. All of them are represented by the bilinear forms in the photon operators.
2. The detection process is also based on the transmission of energy, linear momentum, and/or angular momentum from the photons to a detecting device [14]. In other words, the Hermitian bilinear forms in (84) corresponds to what can be emitted by the source and detected by a photodetector.

Let us stress that the operational definition of the quantum phase of radiation [47] is also based on the use of bilinear forms in the photon operators. In the simplest form, the idea of the operational approach to the phase difference can be illustrated with the aid of the two-port interferometer shown in Fig. 11 (see Refs. 14 and 47 for more detailed discussion). The two incident monochromatic (or quasimonochromatic) light beams are combined by a symmetric beamsplitter oriented at 45° to each beam. The resultant intensities emerging from each output port are measured by the two photodetectors connected with a "comparator" (computer) as in the Hanbury–Brown–Twiss interferometer [85] (also see Refs. 14, 15, and 86). Following Noh et al. [47], we denote by a_1 and a_2 the photon annihilation operators, describing the field at the two input ports, and by a_3 and a_4 the corresponding operators at the two output ports. Then

$$a_3 = ta_1 + r'a_2$$
$$a_4 = ra_1 + t'a_2$$

where t and r denote the complex-amplitude transmittance and reflectance from one side of the beamsplitter and r' and t' from the other side. The number of

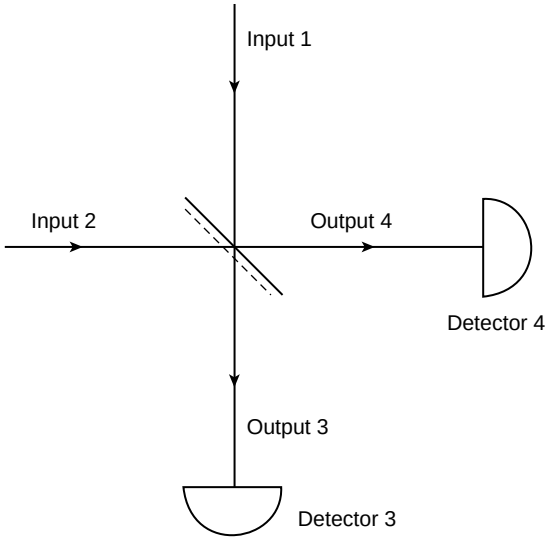

Figure 11. Outline of the scheme of two-part interferometer.

photons in the output modes is defined as follows

$$\hat{n}_3 = |t|^2\hat{n}_1 + |r|^2\hat{n}_2 + t^* r' a_1^+ a_2 + t r'^* a_2^+ a_1$$
$$\hat{n}_4 = |r|^2\hat{n}_1 + |t|^2\hat{n}_2 + t' r^* a_1^+ a_2 + r t'^* a_2^+ a_1$$

where $\hat{n}_\ell \equiv a_\ell^+ a_\ell$. It is clear that

$$\hat{n}_4 - \hat{n}_3 = \exp[i \arg r - \arg r')]a_2^+ a_1 + \exp[i(\arg t' - \arg t)]a_1^+ a_2$$

Hence, the sine and cosine of the phase difference between the two output beams can be defined as follows [47]

$$S_M = K_1(\exp[i(\arg r - \arg t')]a_2^+ a_1 + \exp[i(\arg t' - \arg r)]a_1^+ a_2)$$
$$C_M = iK_2(\exp[i(\arg r - \arg t')]a_2^+ a_1 - \exp[i(\arg t' - \arg r)]a_1^+ a_2)$$

where K_1 and K_2 are some constants. It is clear that, apart from the exponential factors caused by the measuring device, these equations for S_M and C_M have the operator structure similar to the cosine and sine operators of the radiation phase (82). Of course, the operational definition by Mandel et al. [47] discussed above does not take into consideration the third component of the multipole radiation. Therefore, the operators (104) do not commute with each other.

From the preceding discussion, one can conclude that the method of radiation phase, defining the quantum phase variable in terms of what can be emitted by the source, complements the operational phase, which deals with what can be measured in a real experiment.

G. Phase Properties of Radiation in Fabry-Pérot Resonator

Our consideration so far have applied to photons in an ideal spherical cavity. Consider now the very important case of interaction between a single atom with electric dipole transition and cavity field in the case of Fabry–Perot resonator formed by two parallel ideal reflecting mirrors. In this case, the cavity field can consist only of the photons propagating along the axis of resonator (z axis) because all other photons should leave the space limited by the mirrors. This means that the cavity photons have well-defined direction and therefore are in a state with given linear momentum (21)–(22). Hence, the radiation emitted by the electric dipole transition consists of the two modes with $m = \pm 1$, while the radiation of the third mode $m = 0$ is forbidden. In this case, the photons with given helicity can be represented in terms of linearly polarized photons as follows [27];

$$a_\mu = \mp \frac{a_x \pm i a_y}{\sqrt{2}}, \quad \mu = \pm 1 \tag{104}$$

Since the atom–field interaction in the Fabry-Perot resonator is allowed for the two electric dipole transitions

$$|1, \pm 1\rangle \to |0, 0\rangle$$

the interaction term in the electric dipole Jaynes–Cummings Hamiltonian (34) takes the form

$$H_{\text{int}} = g \sum_{\mu=\pm 1} (R_{\mu g} a_\mu + a_\mu^+ R_{g\mu}) \tag{105}$$

Then, the representation of the $SU(2)$ algebra corresponding to the excited state in (105) takes the form

$$\begin{aligned} J_z &= \frac{R_{++} - R_{+-})}{2} \\ J_+ &= R_{+-} \\ J_- &= R_{-+} \end{aligned} \tag{106}$$

similar to (50). Then, the exponential of the atomic $SU(2)$ phase operator takes the form

$$\varepsilon = R_{+-} + e^{i\psi} R_{-+} \tag{107}$$

such that

$$\varepsilon\varepsilon^{+} = R_{++} + R_{--} = \mathbf{1}$$

and

$$\varepsilon^{2} = e^{i\psi}\mathbf{1}$$

Here again ψ denotes an arbitrary reference phase. The atomic cosine and sine of the phase operators (42) are defined in the case under consideration as follows:

$$\begin{aligned} C &= (R_{+-}e^{-i\psi/2} + R_{-+}e^{i\psi/2})\cos\frac{\psi}{2} = \varepsilon e^{-i\psi/2}\cos\frac{\psi}{2} \\ S &= (R_{+-}e^{-i\psi/2} + R_{-+}e^{i\psi/2})\sin\frac{\psi}{2} = \varepsilon e^{-i\psi/2}\sin\frac{\psi}{2} \end{aligned} \tag{108}$$

It is clear that these are commuting Hermitian operators.

In analogy to (45) and (46), we can define the atomic phase states as follows:

$$|\phi_\mu\rangle = \frac{1}{\sqrt{2}}(|1,+1\rangle + e^{i\phi_\mu}|1,-1\rangle) \tag{109}$$

where

$$\phi_\mu = \frac{\psi + (1-\mu)\pi}{2}, \quad \mu = \pm 1 \tag{110}$$

It is seen that, apart from a factor of $e^{i\psi/2}$, the states (110) formally coincide with the EPR states (49). It is clear that the operator (107) is represented in terms of states (109) in the diagonal form

$$\varepsilon = \sum_{\mu=\pm 1} e^{i\phi_\mu}|\phi_\mu\rangle\langle\phi_\mu| \tag{111}$$

[cf. (66)].

Following the approach discussed in Section IV.A, we note that the field counterpart of (106) is provided by the operators

$$\begin{aligned} M_z &= \frac{a_+^+a_+ - a_-^+a_-}{2} \\ M_+ &= a_+^+a_- \\ M_- &= a_-^+a_+ \end{aligned} \tag{112}$$

which form the representation of the $SU(2)$ subalgebra in the Weyl–Heisenberg algebra of photons. As in (58), this is not an isotype representation. In analogy to (63), we introduce the field counterpart of (107)

$$\varepsilon_{\text{rad}} = a_+^+ a_- + e^{i\psi} a_-^+ a_+ \tag{113}$$

It is easy to verify that (113) complements the atomic operator (107) with respect to the integral of motion with the Jaynes–Cummings Hamiltonian (34) with the interaction term of the form (105). In analogy to (82), we introduce the cosine and sine of the radiation phase operators:

$$\begin{aligned} C_{\text{rad}} &= K(\varepsilon_{\text{rad}}^+ + \varepsilon_{\text{rad}}) = 2Ke^{-i\psi/2}\varepsilon_{\text{rad}} \cos\frac{\psi}{2} \\ S_{\text{rad}} &= iK(\varepsilon_{\text{rad}}^+ - \varepsilon_{\text{rad}}) = 2Ke^{-i\psi/2}\varepsilon_{\text{rad}} \sin\frac{\psi}{2} \end{aligned} \tag{114}$$

such that

$$[C_{\text{rad}}, S_{\text{rad}}] = 0$$

and

$$[(C + C_{\text{rad}}), H] = [(S + S_{\text{rad}}), H] = 0$$

Then, the condition (83) takes the form

$$\langle C_{\text{rad}}^2 + S_{\text{rad}}^2 \rangle = 4K^2 e^{-i\psi} \langle \varepsilon_{\text{rad}}^2 \rangle = 1 \tag{115}$$

In analogy to (66), the operator (113) is diagonalized by the canonical transformation of the form

$$\begin{aligned} a_\mu &= \frac{1}{\sqrt{2}} \sum_{\mu'=\pm 1} e^{-i(1-\mu')\phi_\mu/2} \mathbf{a}_{\mu'} \\ \mathbf{a}_\mu &= \frac{1}{\sqrt{2}} \sum_{\mu'=\pm 1} e^{i(1-\mu')\phi_\mu/2} a_\mu \end{aligned} \tag{116}$$

where ϕ_μ is the phase variable (110).

Taking into account the equation (104), expressing the photons with given helicity in terms of linearly polarized photons, it is easily seen from (116) that we get

$$\mathbf{a}_+ = -a_x E^{i\psi/2}, \quad \mathbf{a}_- = -ia_y e^{-i\psi/2}$$

Hence, the dual representation of the photon operators (104) with given helicity coincides, apart from certain unimportant factors, with the photon operators with given linear polarization. In the representation (116), the operators (113) and (114) take the diagonal form

$$\begin{aligned}
\varepsilon_{\text{rad}}^{(\phi)} &= \sum_{\mu=\pm 1} e^{i\phi_\mu} \mathbf{a}_\mu^+ \mathbf{a}_\mu \cos\frac{\psi}{2} \\
C_{\text{rad}}^{(\phi)} &= 2k \sum_{\mu=\pm 1} \mathbf{a}_\mu^+ \mathbf{a}_\mu \cos\phi_\mu \cos\frac{\psi}{2} \\
S_{\text{rad}}^{(\phi)} &= 2k \sum_{\mu=\pm 1} \mathbf{a}_\mu^+ \mathbf{a}_\mu \sin\phi_\mu \cos\frac{\psi}{2}
\end{aligned} \tag{117}$$

where the phase variable ϕ_μ is defined in (110). Since the condition (115) can now be done in a straightforward manner to yield

$$K = \frac{1}{2\cos(\psi/2)\sqrt{\langle(\mathbf{a}_+^+\mathbf{a}_+ - \mathbf{a}_-^+\mathbf{a}_-)^2\rangle}} \tag{118}$$

the expressions for cosine and sine operators in (117) take the form

$$\begin{aligned}
C_{\text{rad}}^{(\phi)} &= \frac{\sum_\mu \mathbf{a}_\mu^+ \mathbf{a}_\mu \cos\phi_\mu}{\sqrt{\langle(\sum_\mu \mu \mathbf{a}_\mu^+ \mathbf{a}_\mu)^2\rangle}} \\
S_{\text{rad}}^{(\phi)} &= \frac{\sum_\mu \mathbf{a}_\mu^+ \mathbf{a}_\mu \sin\phi_\mu}{\sqrt{\langle(\sum_\mu \mu \mathbf{a}_\mu^+ \mathbf{a}_\mu)^2\rangle}}
\end{aligned} \tag{119}$$

This representation explicitly manifests the structure of the cosine and sine operators in terms of cosine and sine of phase variable (110).

In analogy to (72) and (74) we now construct the dual Fock number states

$$\begin{aligned}
|\nu_\mu\rangle &= \frac{(\mathbf{a}_\mu^+)^{\nu_\mu}}{\sqrt{\nu_\mu!}}|0\rangle \\
&= \sum_{k=0}^{\nu_\mu} \sqrt{\frac{\nu_\mu!}{2^{\nu_\mu} k!(\nu_\mu - k)!}}(-1)^{\nu_\mu - k}|k\rangle_+ \otimes |\nu_\mu - k\rangle_-
\end{aligned} \tag{120}$$

Here ν_μ is an integer such that

$$\mathbf{a}_\mu^+ \mathbf{a}_\mu |\nu_\mu\rangle = \nu_\mu |\nu_\mu\rangle$$

and the states in the right-hand side correspond to the photons with given helicity. It is easy to show that the states (120) obey the orthonormality and completeness conditions.

Following the method described in Section IV.C, we introduce the state

$$|\phi^{(\mathrm{rad})}\rangle = \bigotimes_{\mu=\pm 1} |\nu_\mu\rangle \tag{121}$$

[see (78)], which can be interpreted as the radiation phase state in the resonator under consideration. For a given total number of photons $n = \sum_\mu \nu_\mu$, there are $n+1$ different phase states with degenerated "eigenphase":

$$\varphi_{n\ell} = \frac{\psi}{2} + 2\ell\pi, \quad \ell = 1, \ldots, n+1$$

This result is obtained by analogy with (79)–(81). Thus, unlike the case of spherical cavity, the spectrum of the $SU(2)$ phase of photons in the Fabry–Perot resonator is trivial.

To complete the comparison with the previous results obtained in Sections IV.C and IV.E, let us average the cosine operator in (114) over the states with two circularly polarized coherent modes $|\alpha_+, \alpha_-\rangle$. We get

$$\langle C_{\mathrm{rad}}\rangle = \frac{2|\alpha_+||\alpha_-|\cos(\Delta_{+-} + \psi/2)}{\sqrt{|\alpha_+|^2 + |\alpha_-|^2 + 4|\alpha_+|^2|\alpha_-|^2\cos^2(\Delta_{+-} + \psi/2)}}\cos\frac{\psi}{2} \tag{122}$$

It is clear that

$$\langle C_{\mathrm{rad}}\rangle \to 0$$

in the "vacuum limit" $|\alpha_\pm| \to 0$ independent of ψ, and

$$\langle C_{\mathrm{rad}}\rangle \to \cos\frac{\psi}{2}$$

in the classical limit $|\alpha_\pm| \to \infty$. The behavior of corresponding variance is shown in Figs. 12 and 13 in the cases of $|\alpha_+| = |\alpha_-| \equiv |\alpha|$ and fixed $|\alpha_-|$ respectively. It is seen, that the variance shows the "normal" behavior and that the "phase bunching," discussed in Section IV.C, does not exist in the case under consideration. In contrast to (90), the presence of the component $\mu = -1$ in the quantum state $(|\alpha_-|^2 \ll 1)$ leads to the decrease of fluctuations.

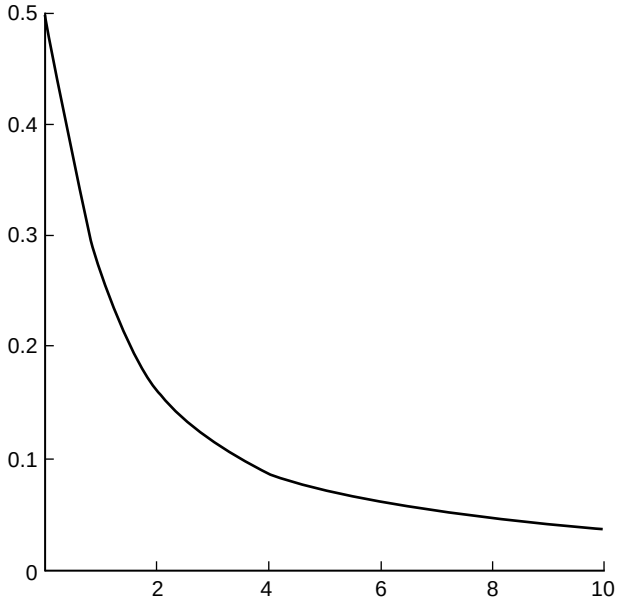

Figure 12. Variance of the cosine of radiation phase (119) in the two-mode coherent state at $|\alpha_+|^2 = |\alpha_-|^2 = |\alpha|^2$ versus $|\alpha|^2$.

H. Summary

1. There is no isotype representation of the $SU(2)$ subalgebra, describing the angular momentum of radiation, in the Weyl–Heisenberg algebra of photons. Therefore, the $SU(2)$ quantum phase of angular momentum of radiation field cannot be constructed in the same way as that of a quantum-mechanical system with a finite number of degrees of freedom.
2. At the same time, the conservation of angular momentum in the process of radiation makes it possible to map the atomic phase variable into the field variables via corresponding integrals of motion.
3. The Weyl–Heisenberg algebra of multipole photons allows the dual representation in which we deal with the photons with given radiation phase (the $SU(2)$ phase of angular momentum) instead of standard photons with given projection of the angular momentum.
4. Through the use of the dual representations of the atomic and field operators, it is possible to construct an equivalent form of the Jaynes–Cummings Hamiltonian, describing the exchange of the ‘‘phase information’’ between the atom and radiation field.

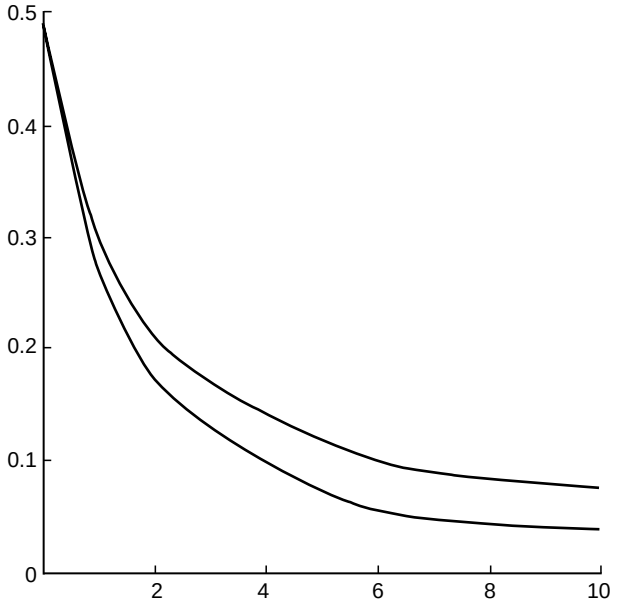

Figure 13. Variance of the cosine of radiation phase (119) in the two-mode coherent state as a function of $|\alpha_+|^2$ at fixed $|\alpha_-|^2 = 0.1$, respectively.

5. The radiation phase of multipole photons has discrete spectrum in the interval $(0, 2\pi)$. In the classical limit of high-intensity coherent field, the eigenvalues of the radiation phase are distributed uniformly over $(0, 2\pi)$.
6. The quantum fluctuations of the radiation phase manifest qualitative difference from those calculated within the Pegg–Barnett approach. In particular, the "phase bunching" effect can be observed for a multipole radiation in a spherical cavity in the quantum domain of low intensity. This effect does not occur in a linear cavity (Fabry–Perot resonator).
7. Our approach, leading to the definition of the radiation phase, is the natural complement of Mandel's operational approach. The radiation phase is defined in terms of what can be transmitted from a quantum mechanical system to photon and vice versa.

V. POLARIZATION PROPERTIES OF MULTIPOLE RADIATION

It is not really difficult to construct a series of inferences, each depends upon its predecessor and each simple in itself.

—Sir Arthur Conan Doyle, *The Dancing Men*

A. Polarization of Classical Field

In previous sections, we considered the polarization as a formal property of either plane or spherical waves of photons described by the corresponding index in the expansion (13) and (17). In this Section, we examine the quantum properties of polarization in more details. In particular, we show that the radiation phase of electric dipole radiation formally coincides with the inherent quantum phase of polarization which is the $SU(2)$ phase of spin of photons.

It is well known that the polarization measurements play an important role in optics and spectroscopy [87]. The description usually given of the polarization is a classical one, defining the polarization as a measure of *transversal anisotrophy* of the plane electromagnetic waves [57]. It is based on the fact that the field strengths (11) have only two symmetric spatial components. At the same time, these complex components may have different magnitudes and phases. The quantitative description of polarization is provided by the so-called polarization matrix with the elements [14,57]

$$P_{\sigma\sigma'} = E^*_\sigma(\vec{r})E_{\sigma'}(\vec{r}) \tag{123}$$

Here $E_\sigma(\vec{r})$ denotes the component of the positive-frequency part of the classical electric field strength. For monochromatic plane waves, in view of (13) we get

$$P_{\sigma\sigma'} = \gamma^2 a^*_{k\sigma} a_{k\sigma'} \tag{124}$$

By definition [14,25,57], the diagonal elements in (26) and (27) give the contribution of the corresponding spatial components of the radiation field into the energy density, while the off-diagonal elements give the "phase" information concerning the phase difference between the components.

The polarization matrix (124) can also be represented in the helicity basis (16) at $\vec{\chi}_0 = \vec{k}/k$ as follows

$$P_{\mu\mu'} = \gamma^2 a^*_{k\mu} a_{k\mu'} \tag{125}$$

where $\mu, \mu' = \pm 1$ and

$$a_{k\pm} = \mp \frac{a_{kx} \pm i a_{ky}}{\sqrt{2}} \tag{126}$$

It is seen from (123)–(125) that P is the Hermitian (2×2) matrix. In spite of the position dependence of the mode functions in (13), the elements of (124) and (125) have the same value everywhere. This means that the polarization is the global property of classical plane waves.

In contrast to the plane waves, the field strengths of the multipole radiation can have any direction. In fact, the electric multipole radiation obey the condition $\vec{\mathscr{B}} \cdot \vec{r} = 0$, while it can have nonzero longitudinal component ($\vec{\mathscr{E}} \cdot \vec{r} \neq 0$) of the electric field strength [25]. In other words, this is the *transversal magnetic radiation*. In turn, the magnetic multipole field is characterized by the relations

$$\vec{\mathscr{E}} \cdot \vec{r} = 0, \quad \vec{\mathscr{B}} \cdot \vec{r} \neq 0$$

Hence, the polarization of either multipole radiation should be specified by the spatial anisotrophy of the field strengths rather than the transversal anisotrophy as in the case of plane waves [28,46,54,88]. Thus, the polarization of the classical multipole field should be described by bilinear forms in all three components of the field strengths which leads to the Hermitian (3×3) matrix with the elements [28,46]

$$P^{(E)}_{\mu\mu'}(\vec{r}) = E^*_\mu(\vec{r})E_\mu(\vec{r}), \quad \mu, \mu' = \pm 1, 0 \tag{127}$$

Here we again consider a monochromatic radiation field. Let us stress that this expression describes the spatial anisotrophy of the electric field and therefore specifies the polarization of the electric multipole radiation. In the case of magnetic multipole radiation, the spatial anisotrophy of magnetic induction can be described by the following polarization matrix [89]:

$$P^{(M)}_{\mu\mu'}(\vec{r}) = B^*_\mu(\vec{r})B_{\mu'}(\vec{r}) \tag{128}$$

Now consider the monochromatic multipole field with given λ and j. Exactly this field is emitted by an atomic transition. Employing (21) and (17) then gives

$$\begin{aligned} P^{(E)}_{\mu\mu'} &= k^2 \sum_{mm'} V^*_{Ekjm\mu}(\vec{r})V_{Ekjm'\mu'}(\vec{r})a^*_{Ekjm\mu}a_{Ekjm'\mu'} \\ P^{(M)} &= k^2 \sum_{mm'} V^*_{Ekjm\mu}(\vec{r})V_{Ekjm'\mu'}(\vec{r})a^*_{Mkjm\mu}a_{Mkjm'\mu'} \end{aligned} \tag{129}$$

Thus, the difference between $P^{(E)}$ and $P^{(M)}$ lies in the definition of the complex field amplitudes, while the position dependence is described in the same way. Within the classical picture, these amplitudes are defined differently in terms of the source functions [25]. For example, if the source of radiation is represented by the harmonically varying current $\vec{J}(\vec{r})$ and intrinsic magnetization $\vec{\mathscr{M}}(\vec{r})$, the field amplitudes for the electric radiation are determined by the integral of the function

$$\left(\vec{\mathscr{M}} + \frac{1}{ck^2}\vec{\nabla} \times \vec{J}\right)$$

over the volume of the source localization, while those for the magnetic radiation by the integrals of

$$\left(\frac{\vec{J}}{c} + \vec{\nabla} \times \vec{\mathscr{M}}\right)$$

It should be mentioned here that the quantum multipole radiation, defined in terms of the source, has also been considered [56].

In direct analogy to the case of plane waves, the diagonal elements of (129) describe the contribution of the components of the field strengths into the energy density. The off-diagonal elements give the "phase information" about the phase differences between the spatial components with different polarization. Unlike the plane waves, there are three phase differences [46,54]:

$$\Delta_{\mu\mu'}(\vec{r}) = \arg A_{E\mu}(\vec{r}) - \arg A_{E\mu'}(\vec{r})$$

In view of the evident equality

$$\Delta_{+0} + \Delta_{0-} + \Delta_{+} = 0$$

valid at any point $\vec{r}$, only two of the phase differences $\Delta_{\mu\mu'}$ are independent.

In contrast to (124) and (125), the polarization matrix (129) of either multipole radiation depend on the position with respect to the source (origin). Since the component $A_{\mu=0}$ vanishes at far distance much faster than do the two transversal components, the polarization in the so-called far zone $(kr \gg 1)$ is similar to that of the plane waves.

In addition to the Hermitian polarization matrix with complex elements, the spatial anisotrophy of the electromagnetic field can be described by an equivalent set of real Stokes parameters [14,57].

The classical Stokes parameters of plane waves are usually defined in the linear polarization basis as follows:[1]

$$\begin{aligned}
s_0^{(\text{plane})} &= |\vec{e}_x \cdot \vec{E}|^2 + |\vec{e}_y \cdot \vec{E}|^2 \\
s_1^{(\text{plane})} &= |\vec{e}_x \cdot \vec{E}|^2 - |\vec{e}_y \cdot \vec{E}|^2 \\
s_2^{(\text{plane})} &= 2\,\text{Re}[(\vec{e}_x \cdot \vec{E}^*)(\vec{e}_y \cdot \vec{E})] \\
s_3^{(\text{plane})} &= 2\text{Im}\,[(\vec{e}_x \cdot \vec{E}^*)(\vec{e}_y \cdot \vec{E})]
\end{aligned} \tag{130}$$

[1]Unfortunately, there is no uniform notation for the Stokes parameters. Our notation is that of Ref. 57.

In the helicity basis (16) we get

$$
\begin{aligned}
s_0^{(\mathrm{plane})} &= |E_-|^2 + |E_+|^2 \\
s_1^{(\mathrm{plane})} &= -2\,\mathrm{Re}(E_+^* E_-) \\
s_2^{(\mathrm{plane})} &= 2\,\mathrm{Im}(E_+^* E_-) \\
s_3^{(\mathrm{plane})} &= |E_-|^2 - |E_+|^2
\end{aligned}
\tag{131}
$$

where $E_\mu \equiv \vec{\chi}_\mu \cdot \vec{E}$. It is clear that the parameter $s_0^{(\mathrm{plane})}$ measures the relative intensity of the wave. At the same time, the expressions (130) and (131) show a rearrangement of the roles of the Stokes parameters with respect to the two bases. The parameter $s_1^{(\mathrm{plane})}$ in (130) gives the preponderance of the x-linear polarization over the y-linear polarization, while in (131) it concerns the phase difference between the two components with opposite helicities. The parameter $s_2^{(\mathrm{plane})}$ in (130) gives the cosine of the phase difference between the linearly polarized components, while in (131) it gives the sine of the phase difference between the circular polarized components. In turn, the parameter $s_3^{(\mathrm{plane})}$ in (48) specifies the sine of the phase difference in the Cartesian basis with linear polarizations, while in (131) it gives the preponderance of polarization with negative helicity over positive helicity.

Now consider the set of classical Stokes parameters of the monochromatic pure (λ, j)-pole radiation. Since the polarization, in this case, is described by the Hermitian (3×3) matrix (127), the set should consist of nine Stokes parameters because all three spatial components of the field strength contribute into polarization [46]. For definiteness, let us consider the electric-type radiation. To establish a contact with the previous result (131), we choose the set of Stokes parameters as follows [46]:

$$
\begin{aligned}
s_0^{(\mathrm{multi})}(\vec{r}) &= \sum_\mu |E_\mu|^2 \\
s_1^{(\mathrm{multi})}(\vec{r}) &= -2\,\mathrm{Re}(E_+^* E_0 + E_0^* E_- + E_-^* E_+) \\
s_2^{(\mathrm{multi})}(\vec{r}) &= 2\,\mathrm{Im}(E_+^* E_0 + E_0^* E_- + E_-^* E_+) \\
s_3^{(\mathrm{multi})}(\vec{r}) &= |E_-|^2 - |E_+|^2 \\
s_4^{(\mathrm{multi})}(\vec{r}) &= |E_+|^2 + |E_-|^2 - 2|E_0|^2 \\
s_5^{(\mathrm{multi})}(\vec{r}) &= -2\,\mathrm{Re}(E_+^* E_-) \\
s_6^{(\mathrm{multi})}(\vec{r}) &= 2\mathrm{Im}(E_+^* E_-) \\
s_7^{(\mathrm{multi})}(\vec{r}) &= -2\,\mathrm{Re}(E_0^* E_+) \\
s_8^{(\mathrm{multi})}(\vec{r}) &= 2\,\mathrm{Im}(E_0^* E_+)
\end{aligned}
\tag{132}
$$

These parameters have very simple physical meanings. The parameter s_0 measures the contribution of all three components into the energy density. The parameters $s_{1,2,5,6,7,8}$ give the phase information about the phase differences between the circular and linear polarized components. The parameter s_3 gives the preponderance of negative helicity over positive helicity and the parameter s_4 gives the preponderance of transversal circular polarization over linear (radial) polarization. Unlike (131), the multipole Stokes parameters (132) describe the *local properties of polarization* due to the position dependence of the mode functions (18). It is clear that, at far distances $(kr \gg 1)$ when E_0 is negligibly small in comparison with $E_\pm$, the set (132) formally coincides with (131) because

$$\begin{cases} s_1^{(\text{multi})} \longrightarrow s_5^{(\text{multi})} \propto s_1^{(\text{plane})} \\ s_2^{(\text{multi})} \longrightarrow s_6^{(\text{multi})} \propto s_2^{(\text{plane})} \\ s_4^{(\text{multi})} \longrightarrow s_0^{(\text{multi})} \propto s_0^{(\text{plane})} \end{cases}$$

and

$$\begin{cases} s_7^{(\text{multi})} \longrightarrow 0 \\ s_8^{(\text{multi})} \longrightarrow 0 \end{cases}$$

in this limit.

B. Polarization of Quantum Radiation

The quantum counterpart of the polarization matrices can be constructed in direct analogy to the field quantization [90]. We have to subject the field amplitudes in (124), (125), and (129) to the Weyl–Heisenberg commutation relations (22) and (23) respectively. Thus, we get the operator matrices of polarization of the multipole radiation of the form

$$\begin{aligned} \hat{P}^{(E,n)}_{\mu\mu'} &= k^2 \sum_{mm'} V^*_{Ekjm\mu}(\vec{r}) V_{Ekjm'\mu'}(\vec{r}) a^+_{Ekjm\mu} a_{Ekjm'\mu'} \\ \hat{P}^{(M,n)}_{\mu\mu'} &= k^2 \sum_{mm'} V^*_{Ekjm\mu}(\vec{r}) V_{Ekjm'\mu'}(\vec{r}) a^+_{Mkjm} a_{Mkjm'} \end{aligned} \tag{133}$$

These are the Hermitian (3×3) matrices with the operator elements defined in terms of the normal order of the creation and annihilation photon operators.

To clarify the structure of (133) and establish a contact with previous results for the radiation phase, consider the bare operator form of $\hat{P}^{(E,n)}$ in (133) in the case of the electric dipole radiation in a spherical cavity. The bare operator

structure is provided by the limit $kr \to 0$ in the mode functions (18). This means that we consider the polarization of radiation directly near a source. Using the properties of spherical Bessel functions discussed in Section III.A, we get [28,46]

$$\hat{P}^{(E,n)}_{mm'} = \gamma_{E1} a^{+}_{Ek1m} a_{Ek1m'} \tag{134}$$

where γ_{E1} is an unimportant normalization factor.

Now consider the set of Stokes operators that can be obtained by canonical quantization of (132). On the other hand, the Stokes operators should by definition represent the complete set of independent Hermitian bilinear forms in the photon operators of creation and annihilation. It is clear that such a set is represented by the generators of the $SU(3)$ subalgebra in the Weyl–Heisenberg algebra of electric dipole photons. The nine generators have the form [46]

$$\begin{array}{ccc} (a^{+}_{+}a_{+} - a^{+}_{0}a_{0}) & (a^{+}_{0}a_{0} - a^{+}_{-}a_{-}) & (a^{+}_{-}a_{-} - a^{+}_{+}a_{+}) \\ \frac{1}{2}(a^{+}_{+}a_{0} + a^{+}_{0}a_{+}) & \frac{1}{2}(a^{+}_{0}a_{-} + a^{+}_{-}a_{0}) & \frac{1}{2}(a^{+}_{-}a_{+} + a^{+}_{+}a_{-}) \\ \frac{1}{2i}(a^{+}_{+}a_{0} - a^{+}_{0}a_{-}) & \frac{1}{2i}(a^{+}_{0}a_{-} - a^{+}_{-}a_{0}) & \frac{1}{2i}(a^{+}_{-}a_{+} - a^{+}_{+}a_{-}) \end{array} \tag{135}$$

and only eight of them are independent. To simplify the notations we omit here the indexes E, k, and $j = 1$. To get the set of Stokes operators, we have to use the generators (135) or independent linear combinations of this generators together with the operator

$$S_0 = \sum_{m=-1}^{1} a^{+}_{m} a_{m} \tag{136}$$

describing the total number of multipole photons. It seems to be logical to choose the rest of the set of Stokes operators as follows [46]

$$\begin{aligned} S_1 &= (\varepsilon_{\text{rad}} + \varepsilon^{+}_{\text{rad}}) \\ S_2 &= i(\varepsilon^{+}_{\text{rad}} - \varepsilon_{\text{rad}}) \\ S_3 &= a^{+}_{+}a_{+} - a^{+}_{-}a_{-} \\ S_4 &= a^{+}_{+}a_{+} + a^{+}_{-}a_{-} - 2a^{+}_{0}a_{0} \\ S_5 &= (a^{+}_{+}a_{0} + a^{+}_{0}a_{+}) \\ S_6 &= i(a^{+}_{0}a_{+} - a^{+}_{+}a_{0}) \\ S_7 &= (a^{+}_{0}a_{-} + a^{+}_{-}a_{0}) \\ S_8 &= i(a^{+}_{-}a_{0} - a^{+}_{0}a_{-}) \end{aligned} \tag{137}$$

Here the operator ε_{rad} is as defined in (63). Thus, the operators S_1 and S_2 in (137) coincide, apart from a normalization factor, with the cosine and sine of the radiation phase operators (82). It seems to be natural. By construction, the operators S_1 and S_2 give the phase information about the phase differences $\Delta_{\mu\mu'}$ defined in the previous subsection.

Additional phase information is provided by the operators S_6–S_8 in (137). To clarify the physical meaning of the phase-dependent operators in (137), let us average them over the two-mode coherent state (85) at $|\alpha_+| = |\alpha_-| \equiv |\alpha|$. We get

$$\langle S_\ell \rangle = \begin{cases} 2|\alpha|^2 & \text{at} \quad \ell = 0, 3 \\ 2|\alpha|^2 \cos \Delta_{+-} & \text{at} \quad \ell = 1 \\ 2|\alpha|^2 \sin \Delta_{+-} & \text{at} \quad \ell = 2 \\ 0 & \text{otherwise} \end{cases} \tag{138}$$

Here

$$\Delta_{+-} \equiv \arg \alpha_+ - \arg \alpha_-$$

as in Section IV.C. It is seen that the first two averages in (138) formally coincide with the conventional phase-dependent Stokes parameters defined in the helicity basis (131) [25,57]. Hence, the Stokes operators S_1 and S_2 give the cosine and sine of the radiation phase while the operators S_5–S_8 give the cosine and sine of the phase differences $\Delta_0\pm$ between the linear and one of the circular polarizations. Since

$$[S_1, S_2] = 0, \qquad [S_1, S_0] = [S_2, S_0] = 0 \tag{139}$$

the operators S_1 and S_2 form the Cartan algebra in the $SU(3)$ subalgebra (135) of the Weyl–Heisenberg algebra of multipole photons.

The remaining Stokes operators S_0, S_3, and S_4 in (133) and (134) also have simple physical meaning. In fact, S_0 describes the total number of photons (intensity), S_3 gives the preponderance of positive helicity over negative helicity, and S_4 defines the preponderance of transversal circular polarization over longitudinal linear polarization.

In spite of the formal coincidence between the Stokes parameters (138) and those obtained by quantization of (131) and further averaging over the coherent state (85), there is also a essential difference. Consider, for example, the variances of the Stokes operators S_1 and S_2 in (137):

$$\begin{aligned} \langle (\Delta S_1)^2 \rangle &= 2|\alpha|^2 (2 + \cos \Delta_{+-}) \\ \langle (\Delta S_2)^2 \rangle &= 2|\alpha|^2 (2 - \cos \Delta_{+-}) \end{aligned} \tag{140}$$

In turn, the variances of the corresponding Stokes operators describing the phase properties of plane waves of photons in the two-mode coherent state (85) have the form

$$\langle(\Delta S_1)^2\rangle = \langle(\Delta S_2)^2\rangle = 2|\alpha|^2 \tag{141}$$

Hence, the quantum fluctuations of the physical quantities, describing the phase information in the Stokes parameters are much stronger in the case of multipole radiation in comparison with the case of plane waves of photons. Moreover, they are qualitatively different because of the phase dependence in (140).

One more difference follows from the fact that, because of condition (139), the physical quantities described by S_1 and S_2 in (137) can be measured at once. At the same time, the operators, obtained by quantization of S_1, S_2, and S_3 in (131), form a representation of the $SU(2)$ algebra that excludes the possibility of simultaneous measurement of corresponding physical quantities.

C. Spatial Properties of Polarization

Our consideration of polarization so far has applied to the bare operator forms, corresponding to the normal-ordered polarization matrix and Stokes operators at the source location when $r \to 0$. In reality, (133) describes the position-dependent operator polarization matrix of the multipole radiation. In addition to the normal-ordered form of the operator polarization matrix (133), one can define the antinormal form:

$$\begin{aligned}
\hat{P}^{(E,an)}_{\mu\mu'} &= k^2 \sum_{mm'} V^*_{Ekjm\mu}(\vec{r}) V_{Ekjm'\mu'}(\vec{r}) a_{Ekjm'}\, a^+_{Ekjm} \\
\hat{P}^{(M,an)}_{\mu\mu'} &= k^2 \sum_{mm'} V^*_{Ekjm\mu}(\vec{r}) V_{Ekjm'\mu'}(\vec{r}) a_{Mkjm'\mu'}\, a^+_{Mkjm\mu}
\end{aligned} \tag{142}$$

It is seen that, in view of the commutation relations (23), the difference

$$P^{(0)}_{\mu\mu'}(\vec{r}) = \hat{P}^{(\lambda,an)}_{\mu\mu'} - \hat{P}^{(\lambda,n)}_{\mu\mu'} = k^2 \sum_{m} V^*_{Ekjm\mu}(\vec{r}) V_{Ekjm\mu'}(\vec{r}) \tag{143}$$

defines the zero-point or vacuum oscillations of the components of the polarization of either multipole field [22,91]. In fact, the matrix elements of $P^{(0)}$ in (143) coincide with the commutators of the type

$$[A_{\lambda kjm\mu}, A^+_{\lambda kjm'\mu'}]$$

The trace of (143) coincides, apart from an unimportant factor, with the zero-point fluctuations of energy (29).

It is seen from (143) that the vacuum polarization matrix is independent of index λ, describing the type of the multipole field. This seems to be natural, because the vacuum properties are affected by the presence of the singular point (atom) without respect to the type of radiation that might be emitted.

A similar object can be constructed in the case of plane waves of photons. In analogy to (133) and (142), we can construct the quantum counterpart of (123) and corresponding antinormal operator polarization matrix. Then, using the commutation relations (22) and definition (143), we get

$$P^{(0)}_{\text{plane}} = \frac{2\pi\hbar\omega_k}{V}\begin{pmatrix} 1 & 0 \\ 0 & 1 \end{pmatrix} \tag{144}$$

In contrast to (143), this is a diagonal matrix independent of the spatial variables. Hence, in exactly the same way as with the zero-point oscillations of energy density, the vacuum fluctuations of polarization in empty space has the global nature, while those in the presence of the singular point manifest certain spatial inhomogeneity.

It is intuitively clear that the spatial properties of the vacuum noise of polarization described by (143) should be determined by the distance r from the source independently of the spherical angles θ and ϕ. In fact, all directions from the singular point should be equivalent in the absence of radiation. It is possible to say that the multipole vacuum state is degenerated with respect to the directions from the source or is invariant under rotations about an arbitrary axis, passing through the source. This degeneration is offset by the generation of radiation of a given type λ and with given j and m, which causes the characteristic radiation pattern [25].

Consider first the polar direction when $\theta = 0$ in (18). Then, due to the known property of spherical harmonics [70]

$$Y_{j\pm 1, m-\mu}(0, \phi) = \sqrt{\frac{2(j \pm 1) + 1}{4\pi}}\delta_{m\mu}$$

the mode functions in (19) are independent of the spherical angle ϕ. Consider pure electric multipole radiation with given j. Then, the corresponding polarization matrix in (33) takes the form

$$P^{(E,n)}_{\mu\mu'}(r, 0, \phi) = k^2 \mathscr{F}^*_{j\mu}(r)\mathscr{F}_{j\mu'}(r) a^+_{Ej\mu} a_{Ej\mu'} \tag{145}$$

where

$$\begin{aligned}\mathscr{F}_{j\mu}(r) &\equiv V_{Ejm\mu}(r,0,\phi)\delta_{m\mu}\\ &= \sqrt{\frac{\hbar c}{2kV(2j+1)}}\,[\sqrt{j(2j+3)}f_{j+1}(kr)\langle 1,j+1,\mu,0|j\mu\rangle\\ &\quad - \sqrt{(j+1)(2j-1)}f_{j-1}(kr)\langle 1,j-1,\mu,0|j\mu\rangle]\end{aligned}$$

It is seen that the photon operators with $|m| \geq 2$ do not contribute to the polarization of radiation in the polar direction even if $j \geq 2$. It is straightforward to calculate the elements of the vacuum polarization matrix (143) at $\theta = 0$:

$$P^{(0)}_{\mu\mu'}(r,0,\phi) = k^2 \sum_{j=1}^{\infty} |\mathscr{F}^*_{j\mu}(r)|^2 \delta_{\mu\mu'} \tag{146}$$

Thus, the vacuum noise of polarization in the polar direction is represented by the diagonal matrix. Since the vacuum noise of polarization is supposed to be independent of the direction in the space, the matrix (143) can be put into the form (146) by a proper transformation of the reference frame spanned by the base vectors (16). We have

$$U(\vec{r})P^{(0)}(\vec{r})U^+(\vec{r}) = \mathscr{P}^{(0)}(r), \qquad U^+(\vec{r})U(\vec{r}) = \mathbf{1} \tag{147}$$

As a result of this transformation, $\vec{\chi}_0(\vec{r}) \to \vec{r}/r$. Here

$$\mathscr{P}^{(0)}(r) = \begin{pmatrix} P_T(r) & 0 & 0 \\ 0 & P_L(r) & 0 \\ 0 & 0 & P_T(r) \end{pmatrix} \tag{148}$$

and

$$P_T(r) = k^2 \sum_{j=1}^{\infty} |\mathscr{F}_{j\pm}(r)|^2, \qquad P_L(r) = k^2 \sum_{j=1}^{\infty} |\mathscr{F}_{j0}(r)|^2$$

The element P_T describes the vacuum noise of transversal (with respect to $\vec{r}$) circular polarizations with positive and negative helicity, while P_L gives the zero-point oscillations of linear polarization in the longitudinal direction (along $\vec{r}$). The explicit form of the unitary transformation (147) is

$$U_{\mu\mu'} = \frac{D_{\mu\mu'} + (1 - D_{\mu\mu})\delta_{\mu\mu'}}{\sqrt{1 + \sum_{\nu\neq\mu} |D_{\mu\nu}|^2}} \tag{149}$$

Here $D_{\mu\mu'}(\vec{r})$ is expressed in terms of the elements of matrices (143) and (148) as follows

$$
\begin{aligned}
D_{+0} &= \frac{1}{F_+}[P^{(0)}_{--}(P_T - P^{(0)}_{++}) + |^{(0)}P_{+-}|^2] \\
D_{+-} &= -\frac{1}{F_+}[P^{(0)}_{0-}(P_T - P^{(0)}_{++}) + P^{(0)*}_{+0}P^{(0)}_{+-}] \\
D_{0+} &= \frac{1}{F_0}[P^{(0)}_{--}(P_L - P^{(0)}_{00}) + |P^{(0)}_{0-}|^2] \\
D_{0-} &= -\frac{1}{F_0}[P^{(0)}_{+-}(P_L - P^{(0)}_{00}) + P^{(0)}_{+0}P^{(0)}_{0-}] \\
D_{-+} &= \frac{1}{F_-}[P^{(0)*}_{+0}(P_T - P^{(0)}_{--}) + P^{(0)}_{0-}P^{(0)*}_{+-}] \\
D_{-0} &= -\frac{1}{F_-}[P^{(0)}_{++}(P_T - P^{(0)}_{--}) + |P^{(0)}_{+-}|^2]
\end{aligned}
$$

where

$$
\begin{aligned}
F_+ &= (P^{(0)*}_{+0}P^{(0)}_{--} - P^{(0)*}_{+-}P^{(0)}_{0-}) \\
F_0 &= (P^{(0)}_{+0}P^{(0)}_{--} - P^{(0)*}_{0-}P^{(0)}_{+-}) \\
F_- &= (P^{(0)}_{+-}P^{(0)*}_{+0} - P^{(0)}_{0-}P^{(0)}_{++})
\end{aligned}
$$

It follows from the structure of (148) that the vacuum noise of transversal (with respect to $\vec{r}$) polarization described by P_T is independent of helicity. At the same time, the transversal and longitudinal vacuum noises show different behavior as functions of distance (see discussion at the end of Section II).

To illustrate the spatial properties of the polarization of multipole radiation, consider the normal-ordered operator polarization matrix (133) in the case of monochromatic electric-type pure j-pole radiation. Assume that the radiation field is in a single-photon state $|1_m\rangle$ with given m. Then, the average of (133) takes the form

$$
\langle \hat{P}^{(E,n)}_{\mu\mu'}(\vec{r})\rangle = k^2 V^*_{Ekjm\mu}(\vec{r})V_{Ekjm\mu'}(\vec{r})
$$

It is seen that the state with given m contributes to the polarization with different μ. For variances of the elements of the polarization matrix, we get

$$
\begin{aligned}
\langle[\Delta\hat{P}^{(E,n)}_{\mu\mu'}(\vec{r})]^2\rangle &\equiv \langle \hat{P}^{(E,n)2}_{\mu\mu'}\rangle - \langle \hat{P}^{(E,n)}_{\mu\mu'}\rangle^2 \\
&= k^4 V^*_{Ekjm\mu}V_{Ekjm\mu'}\sum_{m'\neq m} V^*_{Ekjm'\mu}V_{Ekjm'\mu'}
\end{aligned}
$$

It is also seen that the vacuum fluctuations of the field with $m' \neq m$ contribute to the quantum noise of polarization of the mode with given m. Similar results can be obtained for the position dependent Stokes operators obtained from (132) by canonical quantization.

D. Operator Polarization Matrix in the Proper Frame

We saw that an appropriate choice of a local reference frame leads to the diagonal representation (148) of the vacuum polarization matrix (142). The use of the unitary transformation (147) allows the operator polarization matrix (142) to be cast into the form

$$\mathscr{P}^{(E,n)}(\vec{r}) = U(\vec{r})P^{(E,n)}(\vec{r})U^{+}(\vec{r}) \tag{150}$$

where

$$\mathscr{P}^{(E,n)}_{\mu\mu'}(\vec{r}) = k^2 \mathscr{A}^{+}_{Ekj\mu}(\vec{r})\mathscr{A}_{Ekj\mu'}(\vec{r}) \tag{151}$$

and

$$\mathscr{A}_{Ekj\mu}(\vec{r}) = \sum_{\mu'=-1}^{1} U^{*}_{\mu\mu'}(\vec{r}) \sum_{m=-j}^{j} V_{Ekjm\mu'}(\vec{r}) a_{Ekjm} \tag{152}$$

Similar representation can be constructed for the magnetic-type operator polarization matrix in (142) as well.

It is clear that, in view of (22), the operators (152) obey the commutation relations

$$[\mathscr{A}_{\lambda kj\mu}(\vec{r}), \mathscr{A}^{+}_{\lambda' k' j' \mu'}(\vec{r})] = \delta_{\lambda\lambda'}\,\delta_{kk'}\,\delta_{jj'}\,\delta_{\mu\mu'} \times \begin{cases} P_T(r) & \text{at} \quad \mu = \pm 1 \\ P_L(r) & \text{at} \quad \mu = 0 \end{cases} \tag{153}$$

Here $P_{\mu=\pm} \equiv P_T$ and $P_{\mu=0} \equiv P_L$ are the matrix elements of the diagonal vacuum polarization matrix (148). The representation of the Stokes operators in the proper frame can be constructed in the same way.

We now note that the only difference between (153) and commutation relations (23) is the presence of position-dependent factors in the right-hand side of (153). It seems to be quite tempting to introduce the normalized local operators

$$b_{\lambda kj\mu}(\vec{r}) = \frac{\mathscr{A}_{\lambda kj\mu}(\vec{r})}{\sqrt{P_\mu(\vec{r})}} \tag{154}$$

which obey the standard Weyl–Heisenberg commutation relations

$$[b_{\lambda kj\mu}(\vec{r}), b^{+}_{\lambda' k' j' \mu'}(\vec{r})] = \delta_{\lambda\lambda'}\delta_{kk'}\delta_{jj'}\delta_{\mu\mu'} \tag{155}$$

at any point $\vec{r}$. Hence, the local transformation (152), representing the components of the operator vector potential in the proper frame, can be interpreted as a local Bogolubov canonical transformation [80], conserving the commutation relations. In fact, Eqs. (152) and (154) describe the transformation of global multipole photon operators $a_{\lambda kjm}$ with given $m = -j, \ldots, j$ into the local photon operators $b_{\lambda kj\mu}(\vec{r})$ with given polarization $\mu = 0, \pm 1$ at any point of the space.

Due to the form of the operator polarization matrix (142) and corresponding Stokes operators, the polarization, defined to be the spin state of photons [4,27], is not a global property of the quantum multipole radiation. Any atomic transition emits photons with given quantum number m, which yields, in view of (18), (24), and (142), the polarization of all three types depending on the distance from the atom. The structure of (152) and (154) just shows us how the photons with different m contribute into the polarization at an arbitrary point $\vec{r}$. Using the operators (154), we can construct, for example, the local bare operator representation of the polarization matrix (142) as follows

$$p^{(E,n)}_{\mu\mu'}(\vec{r}) = b^{+}_{Ekj\mu}(\vec{r}) b_{Ekj\mu'}(\vec{r}) \tag{156}$$

as well as of the Stokes operators:[2]

$$\begin{aligned}
S_0(\vec{r}) &= \sum_{\mu} b^{+}_{\mu}(\vec{r}) b_{\mu}(\vec{r}) \\
S_1(\vec{r}) &= \overline{\varepsilon}(\vec{r}) + \overline{\varepsilon}^{+}(\vec{r}) \\
S_2(\vec{r}) &= -i(\overline{\varepsilon}(\vec{r}) - \overline{\varepsilon}^{+}(\vec{r})) \\
S_3(\vec{r}) &= b^{+}_{+}(\vec{r}) b_{+}(\vec{r}) - b^{+}_{-}(\vec{r}) b_{-}(\vec{r}) \\
S_4(\vec{r}) &= b^{+}_{+}(\vec{r}) b_{+}(\vec{r}) + b^{+}_{-}(\vec{r}) b_{-}(\vec{r}) - 2 b^{+}_{0}(\vec{r}) b_{0}(\vec{r}) \\
S_5(\vec{r}) &= (b^{+}_{+}(\vec{r}) b_{0}(\vec{r}) + b^{+}_{0}(\vec{r}) b_{+}(\vec{r})) \\
S_6(\vec{r}) &= -i(b^{+}_{+}(\vec{r}) b_{0}(\vec{r}) - b^{+}_{0}(\vec{r}) b_{+}(\vec{r})) \\
S_7(\vec{r}) &= (b^{+}_{0}(\vec{r}) b_{-}(\vec{r}) + b^{+}_{-}(\vec{r}) b_{0}(\vec{r})) \\
S_8(\vec{r}) &= -i(b^{+}_{0}(\vec{r}) b_{-}(\vec{r}) - b^{+}_{-}(\vec{r}) b_{0}(\vec{r}))
\end{aligned} \tag{157}$$

where

$$\overline{\varepsilon}(\vec{r}) \equiv b^{+}_{+}(\vec{r}) b_{0}(\vec{r}) + b^{+}_{0}(\vec{r}) b_{-}(\vec{r}) + b^{+}_{-}(\vec{r}) b_{+}(\vec{r}) \tag{158}$$

[2]Hereafter we omit all unimportant indices.

It is seen that (157) has the operator structure and algebraic properties similar to those of (136)–(137). At $r \to 0$, the set (157) exactly coincides with (136)–(137). Due to the commutation relations (155), the operators (157) have the same algebraic properties as do (136)–(137) at any given point. In particular, we can construct the local representation of the radiation phase operators in the same way as in Section IV, using the operator (158) instead of (63). By construction, this gives us the $SU(2)$ quantum phase of spin or polarization with the properties described in Section IV.C.

Let us stress a very important difference between the representations of Stokes operators (137) and (157). If the former is valid only for the electric dipole photons, the latter describes an arbitrary multipole radiation with any λ and j. The similarity in the operator structure and quantum phase properties is caused by the same number of degrees of freedom defining the representation of the $SU(2)$ subalgebra in the Weyl–Heisenberg algebra.

E. Summary

1. The polarization is described by a bilinear forms in the field components corresponding to the spin states of photons. In general, the polarization is defined by nine physical parameters (operators, in the quantum picture). In the case of plane waves of photons when only two spin states are allowed, the polarization is specified by only four parameters (operators).
2. The set of Stokes operators in the general case corresponds to a representation of the $SU(3)$ subalgebra in the Weyl–Heisenberg algebra of photons. In the case of plane waves of photons, it reduces to the representation of the $SU(2)$ subalgebra.
3. The $SU(2)$ quantum phase of spin (polarization) of photons described in a proper reference frame coincides with the radiation phase of electric dipole radiation discussed in Section IV.

VI. MEASUREMENT, LOCALITY, AND CAUSALITY

> And then he would have lost sight of the mark he had made on the wall, where the nail was to go in, and each had to get up on the chair, besides him, and see if we could find it; and we would each discover it in a different place, and he would call us all fools, one after another, and tell us to get down. And he would take the rule, and re-measure, and find that he wanted half thirty one and three-eights inches from the corner, and try to do it in his head, and go mad.
>
> —Jerome K. Jerome, *Three Men in a Boat*

A. Measurement and Photon Localization

It was indicated in Section I that, although the photon operators refer to the radiation field *in all space*, it looks tempting to interpret the electronic signal

registered by a photodetector as due to a photon localization in a vicinity of the sensitive area of this detector. The corresponding operational definition of localization has been done by Mandel [20] (see also Refs. 14, 15, and 92). It is based on the consideration of a plane wave of photons, being absorbed by the sensitive area s of photodetector during some finite time $\Delta\tau$. Then, it is logical to interpret this process as a measurement of photons located in a cylindrical volume $\mathscr{V} = s \cdot (\Delta\tau)$ (Fig. 14).

Following [14], we introduce a photon absorption operator at the point $\vec{r}$ at time t as follows:

$$\vec{a}(\vec{r}, t) = \gamma \sum_{k,\sigma}{}' \vec{e}_{k\sigma} a_{k\sigma} e^{i(\vec{k}\cdot\vec{r} - kct)} \tag{159}$$

Here γ is the normalization factor, $a_{k\sigma}$ are the operators (21)–(22), and summation is taken over a finite set of modes to which the detector responds. The so-called *configuration space number operator* [14] is defined by the relation

$$\begin{aligned} \mathscr{N}(\mathscr{V}, t) &= \int_{\mathscr{V}} \vec{a}'(\vec{r}, t) \cdot \vec{a}(\vec{r}, t) d^3 r \\ &= \gamma^2 \sum_{k,\sigma} \sum_{k',\sigma'} \vec{e}_{k\sigma} \cdot \vec{e}_{k'\sigma'} e^{-i(\vec{k}-\vec{k}')\cdot\vec{r}} e^{i(k-k')ct} a^{+}_{k\sigma} a_{k'\sigma'} \end{aligned} \tag{160}$$

where the integral is taken over the volume of photon localization. The operators (159) and (160) obey the following commutation relations [14]

$$[\mathscr{N}(\mathscr{V}, t), \mathscr{N}(\mathscr{V}', t)] = 0 \tag{161}$$

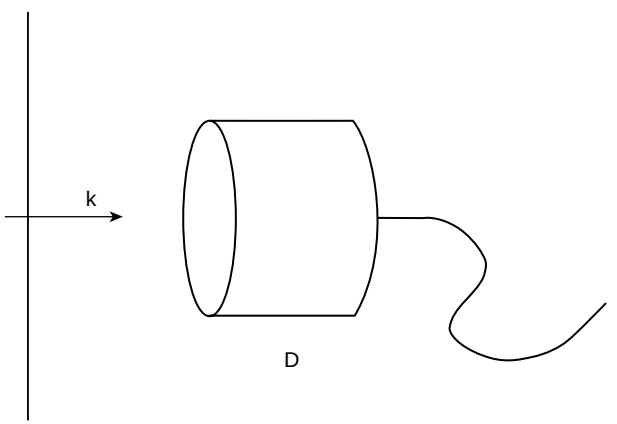

Figure 14. Photodetection and region of localization.

and

$$[\vec{a}(\vec{r},t), \mathcal{N}(\mathscr{V},t)] \approx \begin{cases} -\vec{a}(\vec{r},t) & \text{if} \qquad \vec{r} \in \mathscr{V} \\ 0 & \text{otherwise} \end{cases} \tag{162}$$

Let us stress that (162) has an approximate sense.

There is a principal difference that complicates the direct use of the operation approach to the problem of localizing photons in the case of multipole radiation. The point is that the multipole photons are in a state with given angular momentum and therefore they have no well-defined direction of propagation. In view of the wave–particle dualism, one can say that the multipole photons emitted by a point-like quantum source propagate as outgoing spherical waves. Definitely, these photons are localized initially inside the source.

Consider a model of Hertz-type experiment on emission and detection of a multipole photon in the system of two identical atoms separated by a distance d. If we assume that a photon is first emitted by the atom 1 (source) and then absorbed by the atom 2 (detector), it is most natural to consider the field as a superposition of outgoing and incoming spherical waves focused on the source and detector, respectively (Fig. 15). This superposition should obey the boundary conditions for the real radiation field. Then, in analogy to (159) and (160), one can construct a configuration space photon number operator via the integration of the corresponding local operator over the spherical volume of radius $c\,\Delta\tau$, surrounding the detecting atom. Here $\Delta\tau$ is again the detection time.

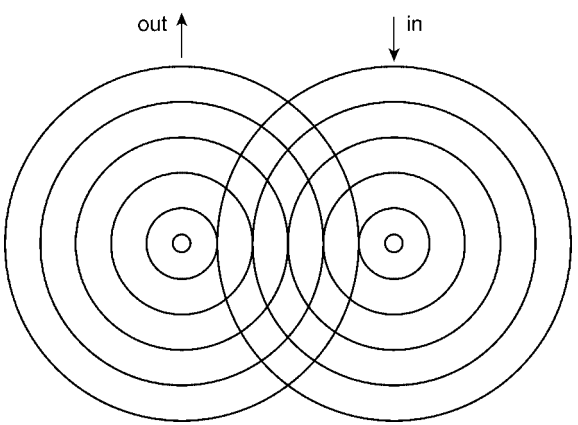

Figure 15. The scheme of two-atom Hertz experiment.

Considering into account that (159) is simply the positive-frequency part of the vector potential (21), we can introduce the multipole photon absorption operator as follows

$$\vec{\mathbf{a}}(\vec{r},t) = \sum_{\mu}(-1)^{\mu}\vec{\chi}_{-\mu}\sum_{\lambda kjm}{}' V_{\lambda kjm\mu}(\vec{r})e^{-ikc}a_{\lambda kjm}$$

which coincides with (24) apart from the fact that the sum is taken over the modes allowed by the selection rules. Here the mode function is defined by Eq. (18) with the radial part (19) corresponding to the incoming spherical wave. Then, the configuration space multipole photon number operator takes the form

$$\mathbf{N}(\mathscr{V},t) = \int_{\mathscr{V}} \vec{\mathbf{a}}^{+}(\vec{r},t)\cdot\vec{\mathbf{a}}(\vec{r},t)\,d^3r$$

similar to (162). Here the volume of detection is

$$\mathscr{V} = \frac{4\pi}{3}[(c\Delta\tau)^3 - r_a^3]$$

where r_a is the atomic radius. We have to exclude the "volume of generation" occupied by the atom to avoid the divergence at $r \to 0$ in the case of outgoing and incoming spherical waves of photons. By virtue of the transformation (152), we can rewrite it as

$$\mathbf{N}(\mathscr{V},t) = \int_{\mathscr{V}} \vec{\mathscr{A}}^{+}(\vec{r},t)\cdot\vec{\mathscr{A}}(\vec{r},t)\,d^3r \tag{163}$$

where the definition of the components of $\vec{\mathscr{A}}$ differs from (152) by summation over all allowed modes.

Taking into account the properties of spherical harmonics [70], Clebsch–Gordon coefficients [71], and spherical Bessel and Hankel functions [70], it is possible to show that the mode functions in (18) obey the following condition of symmetry:

$$V_{\lambda kj,-m,-\mu}(\vec{r}) = (-1)^{m+j-\mu}V^{*}_{\lambda kjm\mu}(\vec{r})$$

Then, it can be easily seen that the commutation relation (161) is valid for the operators $\mathbf{N}$ as well:

$$[\mathbf{N}(\mathscr{V},t),\mathbf{N}(\mathscr{V}',t)] = 0$$

The commutation relation corresponding to (162) is less simple. It can be proven as an approximate one.

Thus, the picture of measurement in the atom–detector system of two identical atoms is compatible with Mandel's operational approach to the photon localization. For example, the multipole photon statistics in finite volume can be examined in the same way as in Refs. 14 and 20. The commutators for different t can also be constructed in analogy to Ref. 20.

Nevertheless, there is one important difference. The point is that the zero-point oscillations of the multipole field are concentrated in a vicinity of the atoms, where they can strongly exceed the level calculated in the model of plane waves in empty space (see Section II.B). If the atomic separation is large in comparison to the wavelength, then a major contribution into the vacuum noise of measurement comes from the presence of the detecting atom. At the intermediate and short distances, the vacuum noise in the vicinity of the detecting atom is increased because of the influence of the source atom via the superposed zero-point oscillations of outgoing and incoming spherical waves. Since the vacuum noise influences the precision of measurements [14,15,58,59,86], this fact seems to be very important, especially for the experiments with trapped Ridberg atoms, which are usually separated by distances corresponding to the intermediate and even near zone [32,66].

Now consider the measurement of monochromatic plane photons by a photodetector shown in Fig. 14. At far distances, the photons are specified by a unique wave vector $\vec{k}$. Mandel's localization of photons in the vicinity of the sensitive area σ assumes that the wave converges to σ. This means that there is a variety of directions of the wavevectors near σ (Fig. 16). This picture can be described by a proper expansion over spherical waves. In view of the discussion

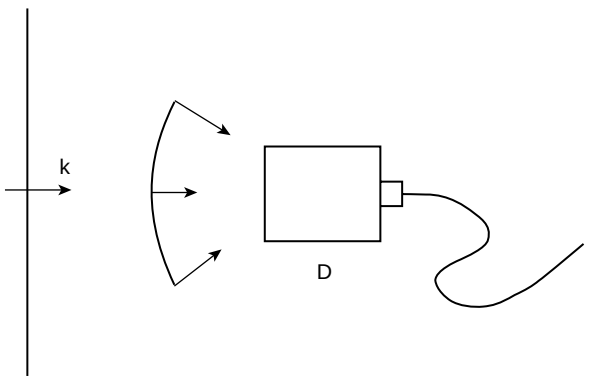

Figure 16. Absorption of radiation by photodetector.

above, it should lead to an increase of the vacuum noise of measurement over the level of plane waves as well.

B. Causality in the Two-Atom Hertz Experiment

In the previous subsection, we considered the field emitted by one atom and then absorbed by another atom as a superposition of outgoing and incoming spherical waves of multipole photons. This wave picture completely eliminates an inquiry concerning the trajectory of photons between the atoms. In fact, the path of a particle in quantum mechanics is not a well-defined notion. The most that we can state about the path of a quantum particle in many cases is that it is represented by a nondifferentiable, statistically self-similar curve [93]. For example, the path of a tunneling electron and time spending in the barrier are not still defined unambiguously [94]. Moreover, some experiments on photonic tunneling and transmission of information show the possibility of superluminal motion of photons inside an opaque barrier [95].

We now note that, according to the principles of quantum theory, not the path, but causality in the transmission of information from one object to another is important [3,10–13,31]. In the Hertz experiment with two atoms separated by empty space, this means that the detecting atom cannot be excited earlier than in d/c seconds after the emission of a photon by the first atom. Here d denotes the interatomic distance. Such a causality has been proven recently by Kaup and Rupasov [96]. Here we briefly discuss their proof.

In the model experiment under consideration, the field is represented by the outgoing and incoming spherical waves of photons, which are specified by a continuous distribution of k or of $\omega = ck$. Assume that the two identical atoms are the two-level atoms of the type of (34) with the electric dipole transition. Because of the simple geometry of the problem (Fig. 17), it can be considered as a quasiunidimensional integrable system [69]. The effective spatial dependence of the photon operators can be introduced with the aid of the Fourier transformation

$$c_m(x) = \int_{-\infty}^{\infty} \frac{d\omega}{2\pi} e^{i(\omega-\omega_0)x} a_m(\omega) \tag{164}$$

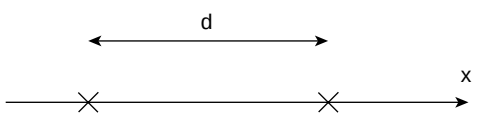

Figure 17. Effective geometry of the model. The x axis corresponds to the quasi-one-dimensional time-dependent wavefunction.

where $a_m(\omega) \equiv a_{E1km}$ and ω_0 is the frequency of the atomic transition. According to (23), the operators obey the commutation relations

$$[c_m(x), c^+_{m'}(x')] = \delta_{mm'}\delta(x - x') \tag{165}$$

In analogy to (34), the Hamiltonian of the system under consideration can be represented as follows:

$$\begin{aligned} H &= H_0 + H_{\text{int}} + \omega_0 N \\ H_0 &= -i \sum_m \int_{-\infty}^{\infty} c^+_m(x) \left(\frac{d}{dx} c_m(x) \right) dx \\ H_{\text{int}} &= \sqrt{\eta} \sum_m \sum_{f=1,2} \int_{-\infty}^{\infty} [R^{(f)}_{mg} c_m(x) + c^+_m(x) R^{(f)}_{gm}] \delta(x - x_f)\, dx \\ N &= \sum_m \left[\sum_f R^{(f)}_{mm} + \int_{-\infty}^{\infty} c^+_m(x) c_m(x) dx \right] \end{aligned} \tag{166}$$

Here $\sqrt{\eta}$ denotes the coupling constant, index $f = 1, 2$ denotes the atoms, x_f is the atomic position along the x axis (see Fig. 17), and the operator N describes the total number of excitations in the system. It is clear that

$$[N, H] = 0 \tag{167}$$

Using the notation of Section III.A, we define the ground state of the system

$$|\text{Ground}\rangle = |j' = 0, m' = 0\rangle_{f=1} \otimes |j' = 0, m' = 0\rangle_{f=2} \otimes |0\rangle$$

as the state of two unexcited atoms and vacuum field.

Assume that the first atom is initially excited into one of the sublevels of the excited state with a given probability:

$$\begin{aligned} |\text{in}\rangle &= \sum_m p_m R^{(1)}_{mg} |\text{ground}\rangle \\ \sum_m |p_m|^2 &= 1 \end{aligned} \tag{168}$$

Then, the Schrödinger time evolution is described by the wavefunction

$$|\Psi(t)\rangle = e^{-iHt} |\text{in}\rangle \tag{169}$$

Let us denote by $|\zeta\rangle$ the eigenstates of the Hamiltonian (166):

$$H|\zeta\rangle = E|\zeta\rangle \tag{170}$$

Here, in general, ζ is a complex parameter. Then, the wavefunction (169) can be represented in the following way:

$$|\Psi(t)\rangle = \int_{-\infty}^{\infty} \frac{d\zeta}{2\pi} L(\zeta) e^{-iEt} |\text{in}\rangle \tag{171}$$

To find the eigenstates $|\zeta\rangle$ and eigenvalues E in (170), we now note that, because of the initial condition (168), the states with single excitation only are allowed in the system. These states, in general, can be chosen as follows:

$$|\zeta\rangle = \sum_m \left[\sum_f \xi_m^{(f)}(\zeta) R_{mg}^{(f)} + \int_{-\infty}^{\infty} e^{i\zeta x} f_m(\zeta, x) c_m^+(x) dx \right] |\text{ground}\rangle \tag{172}$$

Employing (170) then gives the following set of equations for unknown functions $f_m(\zeta, x)$ and $\xi_m^{(f)}(\zeta)$:

$$\begin{aligned} i\frac{d}{dx}[e^{i\zeta x} f_m(\zeta, x)] + E e^{i\zeta x} f_m(\zeta, x) &= \sqrt{\eta} \sum_f \xi_m^{(f)} \delta(x - x_f) \\ \sqrt{\eta} \int e^{i\zeta x} f_m(\zeta, x) \delta(x - x_f) &= E \xi_m^{(f)}(\zeta) \end{aligned} \tag{173}$$

It is seen that the first equation in (173) gives formally a nonphysical discontinuity at $x \to x_f$. To avoid this, we have to consider the finite-size atoms and change $\delta(x - x_f)$ by a smooth distribution function $u(x, x_f)$, then solve the equations, and after that to put $u(x, x_f) = \delta(x - x_f)$. We get

$$\begin{aligned} f_m(\zeta, x) &= \prod_{f=1,2} \frac{\zeta - i(\eta/2) sgn(x - x_f)}{\zeta + i\eta/2} \\ \xi_m^{(1)} &= \frac{\sqrt{\eta}}{\zeta + i\eta/2} e^{i\zeta x_1} \\ \xi_m^{(2)} &= \frac{\zeta - i\eta/2}{\zeta + i\eta/2} \frac{\sqrt{\eta}}{\zeta + i\eta/2} e^{i\zeta x_2} \end{aligned} \tag{174}$$

where

$$sgn(x - x_f) = \begin{cases} 1 & \text{at} \quad x > x_f \\ -1 & \text{at} \quad x < x_f \\ 0 & \text{at} \quad x = x_f \end{cases}$$

and $E = \zeta$, which is real. Thus, the function (172) is completely defined.

Since any two states (172) obey the orthogonality condition

$$\langle\zeta|\zeta'\rangle = 2\pi\delta(\zeta - \zeta')$$

and, in view of (171) the initial state can be expanded in the following way

$$|\text{in}\rangle = \int \frac{d\zeta}{2\pi} L(\zeta)|\zeta\rangle$$

and for the coefficients in (172) we get

$$L(\zeta) = \langle\zeta|\text{in}\rangle = \frac{\sqrt{\eta}}{\zeta - i\eta/2}$$

Finally, for the function (172), describing the time evolution of the system, we get

$$|\Psi(t)\rangle = \sum_m p_m \int_{-\infty}^{\infty} \frac{d\zeta}{2\pi} \frac{\sqrt{\eta}}{\zeta - i\eta/2} e^{-i\zeta t}|\zeta\rangle \tag{175}$$

This wavefunction can be used to calculate the evolution of any physical quantity in the system under consideration. To prove the causality, we now have to calculate the time-dependent expectation value

$$\langle R^{(2)}_{mm}\rangle_t = |p_m|^2 \left| \int \frac{d\zeta}{2\pi} \frac{\eta}{(\zeta + i\eta/2)^2} e^{-i\zeta(t-d/c)} \right|^2 \tag{176}$$

describing the evolution of population of corresponding sublevel of the detecting atom. It is now a straightforward matter to arrive at the following result

$$\langle R^{(2)}_{mm}\rangle = |p_m|^2 \times \begin{cases} 0 & 0 \le t \le \frac{d}{c} \\ \eta^2\left(t - \frac{d}{c}\right)^2 e^{-\sqrt{\eta}(t-d/c)} & t > \frac{d}{c} \end{cases} \tag{177}$$

(see Fig. 18). It is seen that this average shows the causal behavior.

C. Polarization Measurements

Instead of discussing the well-known methods of polarization measurements [87], we now turn our attention to the fluctuations in the measurement of the

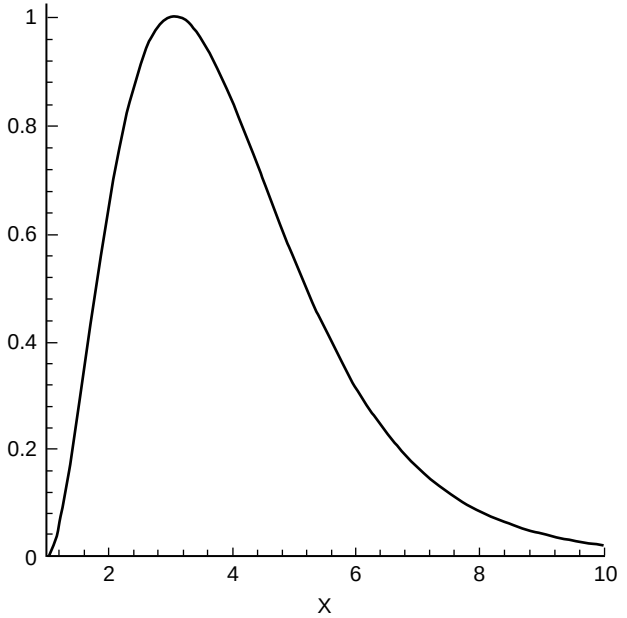

Figure 18. Time dependence of the mean population of the excited level of the detecting atom.

parameters of polarization. Following [97], consider first a fully polarized coherent plane wave in the weak quantum limit. To measure the Stokes parameters, one can use the six-port scheme shown in Fig. 19, which reflects the principal ideas of Mandel's operational approach to phase measurements [47]. A similar scheme has been analyzed [98]. The beam whose polarization is to be measured is first split by the non-polarizing beamsplitter BS_1. One of the output beams is sent to a polarizing beamsplitter PBS_1, which defines two linearly polarized orthogonal polarization eigenmodes labeled by $i = 1,2$. Then, the intensities I_1 and I_2 are measured by the photodetectors. The other output beam from BS_1 is further split at BS_2 with the purpose of simultaneous measuring the sine and cosine of the phase difference between the polarized components of the field. One of the output beams from BS_2 is analyzed with PBS_2, which is oriented at 45° with respect to the axes $i = 1,2$ defined by PBS_1. The other output beam from BS_2 goes through a quarter-wave plate whose fast and slow axes are aligned along the $i = 1,2$ directions. This beam is then analyzed at PBS_3, whose axes are aligned with PBS_2.

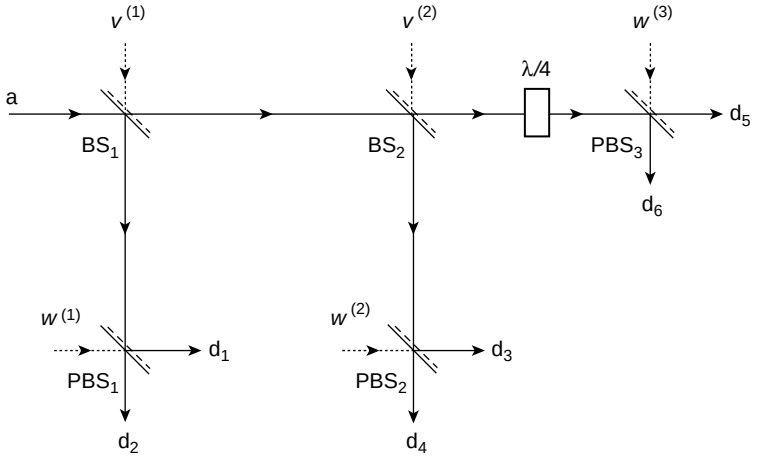

Figure 19. The experimental setup for measurement of the Stokes parameters.

Consider first the measurement of the classical field. Then, for 50% nonpolarizing beamsplitters, the detectors $d_1, \ldots d_6$ measures the intensities

$$
\begin{aligned}
I_1 &= \frac{1}{2}|E_1|^2 \\
I_2 &= \frac{1}{2}|E_2|^2 \\
I_3 &= \frac{1}{4}(|E_1|^2 + |E_2|^2) + 2|E_1|^2|E_2|^2 \cos\Delta \\
I_4 &= \frac{1}{4}(|E_1|^2 + |E_2|^2) - 2|E_1|^2|E_2|^2 \cos\Delta \\
I_5 &= \frac{1}{4}(|E_1|^2 + |E_2|^2) + 2|E_1|^2|E_2|^2 \sin\Delta \\
I_5 &= \frac{1}{4}(|E_1|^2 + |E_2|^2) - 2|E_1|^2|E_2|^2 \sin\Delta
\end{aligned} \tag{178}
$$

Where I_ℓ denotes the intensity measured by the detector d_ℓ. From these relations, the classical Stokes parameters (130) can be found as

$$
\begin{aligned}
s_0^{(\text{plane})} &= I_1 + I_2, \qquad & s_1^{(\text{plane})} &= I_1 - I_2 \\
s_2^{(\text{plane})} &= I_2 - I_4, \qquad & s_4^{(\text{plane})} &= I_5 - I_6
\end{aligned} \tag{179}
$$

were $1 \leftrightarrow x$ and $2 \leftrightarrow y$. Having defined our measurement in the classical domain, we next look at the quantum case when the unused ports in the beamsplitters are considered as input for vacuum fields [14]. These vacuum fields are indicated in Fig. 19 by v_ℓ and w_ℓ for BS and PBS, respectively.

The photon annihilation operators associated with the field at the output arms of PBS_1 are related to those at the input through

$$d_1 = ra_1 + tv_1^{(1)}, \qquad d_2 = ra_2 + tc_2^{(1)} \tag{180}$$

where $r = i/\sqrt{2}$ and $t = 1/\sqrt{2}$ are the field reflection and transmission coefficients, respectively, and $v_\ell^{(1)}$ describes the polarized vacuum field in the ℓ direction entering through the vacuum port of BS_1 (cf. Section 4.6). The vacuum fields $w^{(k)}$ $(k = 1, 2, 3)$ do not couple with the measured field operators since they are orthogonal to them.

In analogy to the classical definition of the angular functions

$$\sin\theta = 2\frac{\sqrt{I_1 I_2}}{I_1 + I_2}, \qquad \cos\theta = \frac{I_1 - I_2}{I_1 + I_2}$$

where θ is related to the ellipticity angle [87], we define the operators [97]

$$S_\theta = 2\frac{\sqrt{n_1 n_2}}{n_1 + n_2}, \quad C_\theta = \frac{n_1 - n_2}{n_1 + n_2} \tag{181}$$

Here

$$n_\ell \equiv d_\ell^+ d_\ell, \quad \ell = 1, 2$$

are the photon number operators for the fields measured at the detectors 1 and 2. From the Weyl–Heisenberg commutation relations for the photon operators, we get

$$[S_\theta, C_\theta] = 0 \tag{182}$$

so that these two quantities can be measured at once. It is also seen that

$$S_\theta^2 + C_\theta^2 = \mathbf{1}$$

On the other hand, at the output ports of PBS_2 and PBS_3, the field operators are

$$\begin{aligned}
d_3 &= \frac{1}{\sqrt{2}}[(tr(a_1 + a_2) + r^2(v_1^{(1)} + v_2^{(1)}) + t(v_1^{(2)} + v_2^{(2)})] \\
d_4 &= \frac{-1}{\sqrt{2}}[tr(a_1 - a_2) + r^2(v_1^{(1)} - v_2^{(1)}) + t(v_1^{(2)} - v_2^{(2)})] \\
d_5 &= \frac{1}{\sqrt{2}}[r^2(ia_1 + a_2) + tr(iv_1^{(1)} + v_2^{(1)}) + r(iv_1^{(2)} + v_2^{(2)}] \\
d_6 &= \frac{-1}{\sqrt{2}}[r^2(ia_1 - a_2) + tr(iv_1^{(1)} - v_2^{(1)}) + r(iv_1^{(2)} - v_2^{(2)}]
\end{aligned} \tag{183}$$

Then, in analogy to the classical functions

$$\cos\Delta = \frac{I_3 - I_4}{\sqrt{(I_3 - I_4)^2 + (I_5 - I_6)^2}}$$
$$\sin\Delta = \frac{I_5 - I_6}{\sqrt{(I_3 - I_4)^2 + (I_5 - I_6)^2}}$$

we get the operators

$$C_\Delta = \frac{n_3 - n_4}{\sqrt{(n_3 - n_4)^2 + (n_5 - n_6)^2}}$$
$$S_\Delta = \frac{n_5 - n_6}{\sqrt{(n_3 - n_4)^2 + (n_5 - n_6)^2}} \tag{184}$$

such that

$$[C_\Delta, S_\Delta] = 0$$

Here n_ℓ denotes the number operators constructed from the photon operators (183).

It is now a straightforward matter to calculate the variances of the operators (181) and (184) [97]. In particular, it is possible to show that the quantum fluctuations imply the uncertainty relations

$$\langle(\Delta S_2^{(\text{plane})})^2\rangle\langle(\Delta C_\Delta)^2\rangle \geq \frac{1}{4}\langle S_\Delta\rangle$$
$$\langle(\Delta S_2^{(\text{plane})})^2\rangle\langle(\Delta S_\Delta)^2\rangle \geq \frac{1}{4}\langle C_\Delta\rangle \tag{185}$$

similar, in some sense, to the Susskind–Glogower uncertainty relations [41] and those of the operational definition of quantum phase [47]. Here $S_2^{(\text{plane})}$ is the Stokes operator obtained by the quantization of the Stokes parameter $s_2^{(\text{plane})}$ in (179).

D. Nondemolition Polarization Measurement

In the preceding subsection, we discussed the polarization measurement through the use of the detection of the field variables done by photocounting techniques, which are field-destructive. As a result, successive measurements of the field variables yield different results. It seems to be tempting to use the measurement schemes avoiding backward action of the detecting device on the detected

observable. Such a measurement is usually called a *quantum nondemolition measurement* [99]. Here, following our results [100], we discuss the possibility of quantum nondemolition measurement of polarization of the electromagnetic field via the Aharonov–Bohm effect [101].

First, we note that the standard photodetection is a *local* measurement of the field variables (intensities). At the same time, the Aharonov–Bohm effect represents a *topological* measurement referred to the properties of vector potential along some loop. In the usual form, the Aharonov–Bohm effect deals with static or slowly time-varying magnetic fields [101]. The effect consists in the appearance of a persistent current in a metallic loop over which the magnetic flux passes. This current is a periodic function of magnetic flux with the period of flux quantum hc/e. Besides that, certain resistance oscillations in the loop incorporated into an external circuit with the same period can occur.

An important case of varying magnetic field has been considered by Aronov et al. [102] under the assumption that the space-dependent time-varying electromagnetic field produces static electron energy minibands in the loop. These minibands have been suggested to appear due to electron motion in a time-averaged electrostatic potential periodic with coordinate along the loop circumference, produced by the square of time-varying electric field [103]. However, in the quantum case, an electron reflection forms an oscillating potential causes time-dependent phase shifts, resulting in an effective chaotization of the phase of electron wavefunction, except at energy multiples of $\hbar\omega$, where ω is the field frequency.

In our papers [100], we considered the case of optical frequencies $\omega > \Delta E/\hbar$, where ΔE is the width of the electron conduction band of the metal. Under this condition, the elastic scattering of electrons is prohibited if the separation between the conduction and higher nonoccupied bands of a metal is larger than $\hbar\omega$. In this case, the magnetic component of electromagnetic field represents the main source of the electron wavefunction phase shift. The effect of oscillating magnetic field results in the modulation of the electron transmission amplitude between the parts of the loop. As a result of the quantum interference of electron waves in oscillating potential, the dependence of the loop resistance of the time-varying field amplitude manifests a non-monotone character.

The geometry of the experiment assumes that the magnetic field oscillates along the axis orthogonal to the plane of the loop circumference and passing through its center. An example is provided by a small metallic ring surrounding an optical fiber. In this case, the largest contribution to the conductance oscillations comes from the TE_{01} mode of the fiber field [100] (about the fiber modes; see Ref. 104). Definitely, such a measurement does not perturb the quantum state of the fiber mode. Another example is provided by the magnetic dipole radiation, when a longitudinal oscillating magnetic field can be observed,

at least in some vicinity of the source. In the case of radioband frequencies, this vicinity seems to be extended enough to make a macroscopic measurement. As a powerful localized source of such a radiation the radioband Dicke superradiance [105] can be used. The geometry of the experiment is simplified, in this case, by a characteristic sharp radiation pattern of superradiance [64].

To make necessary estimations, consider a one-dimensional loop in a tight-binding approximation with two transmittance amplitudes t_1 and t_2 at the points A and B, connecting two parts of the ring (see Fig. 20). It is supposed that $t_1, t_2 \ll t_0$, the hopping amplitude between the nearest points inside the upper and lower parts of the ring. The system under consideration is described by the Hamiltonian [100]

$$H = -t_0 \sum_n (a_n^+ a_{n+1} + b_n^+ b_{n+1}) + \text{H.c.} + H_{\text{int}}$$

$$H_{\text{int}} = -t_1 a_{n_1}^+ b_{n_1} e^{i\alpha_1} - t_2 a_{n_2}^+ b_{n_2} e^{i\alpha_2} + \text{H.c.} \tag{186}$$

where a, b are the *electron* (not photon) annihilation operators. The phases of transmission amplitudes at the contraction points n_i are

$$\alpha_i = \alpha_i^0 + A_i \sin(\omega t + \delta_i)$$

where α_i^0 accounts for the effect of a static magnetic field applied perpendicular to the plane of the ring

$$\alpha_1^0 - \alpha_2^0 = \frac{2\pi\Phi_S}{\Phi_0}, \qquad \Phi_s = \int \vec{B} \cdot d\vec{S}, \qquad \Phi_0 = \frac{hc}{e}$$

while A_i are the amplitudes of high-frequency field at corresponding points.

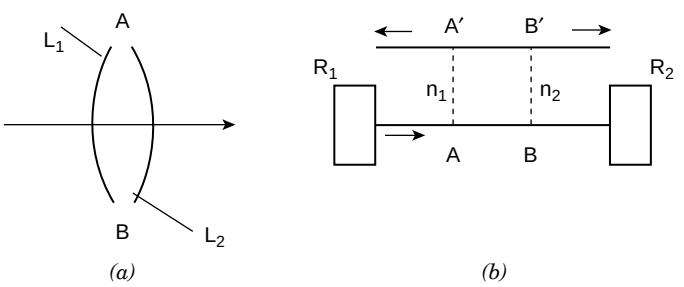

Figure 20. The scheme of one-dimensional Aharonov–Bohm loop, surrounding the direction of propagation of a longitudinal mode and weakly coupled at points A and B with the external leads L_1 and L_2 [(a) and (b)]. (d) The model of an ac normal-metal interferometer. R_1 and R_2 are the thermal reservoirs held at voltages $\pm V/2$, respectively.

The model with the Hamiltonian (186) can be solved exactly [100]. It is a straightforward matter to arrive at the following relation for the current

$$J = \int_0^{\pi} \frac{dk}{2\pi} W_0 \left[\frac{W_k}{W_0 + W_k} + \frac{W_{-k}}{W_0 + W_{-k}} \right] \times \left[f_0\left(\epsilon_k - \frac{eV}{2}\right) - f_0\left(\epsilon_k + \frac{eV}{2}\right) \right] \tag{187}$$

Here $f_0(\cdot)$ denotes the equilibrium distribution function of electrons, $\epsilon_k = -2t_0 \cos k$, $W_{\pm k}$ is the forward $(+k)$ or backward $(-k)$ scattering probability, and V is the voltage. Then, the conductance G can be found from (187) as follows:

$$G = \frac{dJ}{dV} \tag{188}$$

It follows from (187) that the dependence of G on the phase α and on the electromagnetic field amplitude leads to two different effects. First, the oscillatory dependence $G(\Phi_S)$ is the standard mesoscopic interference effect similar to that in static electron interferometer [101]. Another type of oscillating dependence $G(A)$ is completely caused by the time-varying field. The dependence of the conductance on the field intensity P is shown in Fig. 21.

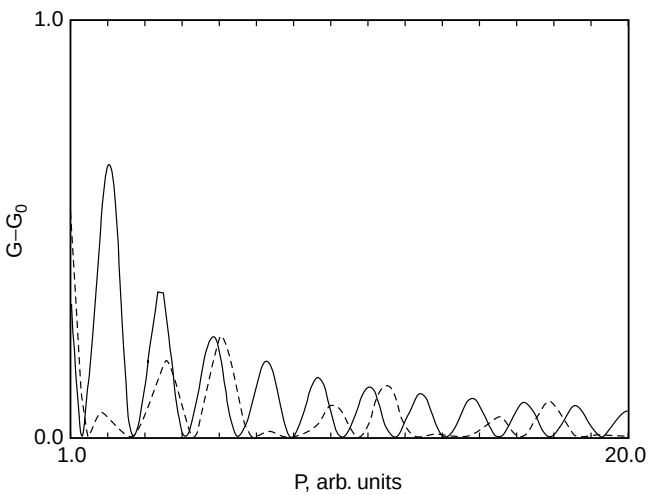

Figure 21. Direct-current conductance of the loop versus square root of ac power: solid line, $A_1 : A_2 = 1 : 1$; dotted line, $A_1 : A_2 = 1 : 2$. Change in the conductance is normalized with respect to static conductance oscillation amplitude.

The observation of such oscillations requires temperatures low enough to allow the phase-breaking length of electron scattering ℓ_ϕ to exceeds the circumference of the ring L. For the loop size of the order of $L = 1\,\mu\text{m}$, which is technically reasonable, the condition $\ell_\phi > L$ is valid at $T \leq 1\,\text{K}$.

At $L = 1\,\mu\text{m}$, the measurement can be done at the magnetic field $B \sim 10^{-7}\,\text{T}$, which corresponds to the oscillating power $P \sim 10^{-3}\,\text{W}$ [100]. This seems to be not very high. Estimated in a different way as a minimum number of optical photons transmitted through the loop, the field should contain $n \sim 1/\alpha \sim 137$ photons, where $\alpha \equiv e^2/\hbar c$ is the fine-structure constant. This estimation corresponds either to an optical soliton propagating through the fiber [104] or to the superradiant pulse in the radioband superradiance [105].

Thus, the linearly polarized longitudinal component of electromagnetic radiation arising in corresponding geometry (fiber or localized source) can be measured in nondemolition way with the aid of the Aharonov–Bohm effect at optical frequencies.

E. Summary

1. Localization of multipole photons at generation and absorption by an atom, described in terms of outgoing or incoming waves of photons, is compatible with Mandel's conception of localization.
2. The photon localization at detection leads to a strong increase of the vacuum noise in a certain vicinity of a detector (atom or active area of photodetector).
3. The two-atom scheme of the Hertz experiment with multipole photons, in which the radiation field is described by a superposition of outgoing and incoming waves focused on the emitting and detecting atoms respectively, obeys the causality principle even though the path of detecting photons is indefinite.
4. The quantum fluctuations of polarization can be measured in the multiport six-detector scheme similar to that proposed by Mandel for the phase measurements.
5. The linear polarization of longitudinal component of electromagnetic field caused by a characteristic geometry of the system (cylindrical geometry in an optical fiber or spherical in the case of field generated by a local source) can be measured in a nondemolition way with the aid of the Aharonov–Bohm effect.

VII. CONCLUSION

Every problem becomes very childish when once it is explained to you.

—Sir Arthur Conan Doyle, *The Dancing Men*

In this chapter we have reviewed some results concerning the quantum multipole radiation. Although the representation of quantum electromagnetic radiation in terms of spherical waves of photons known since the first edition in 1936 of the famous book by Heitler on quantum theory of radiation [2], where this subject is discussed in the Appendix, this representation is not a widespread one. The spherical waves of photons are considered in very few advanced monographs on quantum optics [26]. The brilliant encyclopedic monographs [14,15] just touch on the subject.

At the same time, the quantum multipole radiation is precisely what the atomic transitions between the states with given angular momenta emit. The states of multipole (spherical) photons are specified by given angular momentum and projection of the angular momentum, while the spin state (polarization) is changed in spacetime. On the contrary, the common representation of plane waves of photons is specified by a given linear momentum and polarization everywhere. This difference reflects the boundary conditions used in the canonical quantization of the free electromagnetic field [2].

It was shown in Section I that the clear-cut distinction between the symmetry properties of plane and spherical waves leads to a qualitative difference in the zero-point oscillations. While the former are homogeneous in space (along the direction of propagation), the latter concentrate in a certain vicinity of a local source (atom) where they may exceed the level calculated in the model of plane waves. Although the result is simple in itself, to our knowledge, it was indicated for the first time in 1999 [46] and then discussed later [22,29]. Since the zero-point oscillations define the quantum limit of precision of measurements of corresponding physical quantity [14,15,99], this result seems to be very important. The estimations based on the results of Section II.B show that the zero-point oscillations exceed the conventional level provided by the representation of plane waves at the distances $r \leq 0.2\lambda$, where λ is the wavelength. Within the standard classification, it corresponds to the so-called intermediate zone. Let us stress that this distance is of the order of the typical interatomic separation in experiments with trapped Ridberg atoms [32].

One of the major trends of current research is the study of transmission of ‘‘information’’ between the atom and photons in the process of emission and absorption. In particular, the conservation of angular momentum provides the transmission of the ‘‘quantum phase information’’ in the atom–field system. The atomic quantum phase can be constructed as the $SU(2)$ phase of the angular momentum of the excited atomic state (Section III). It is shown that this phase has very close connection with the EPR paradox and entangled states in general. Via the integrals of motion, it is mapped into the Hilbert space of multipole photons (Section IV.A). This mapping is adequately described by the dual representation of multipole photons, constructed in another study [46] (see also Section IV.B, below). Instead of the quantum number m, corresponding to the

projection of angular momentum, these photons are specified by the quantum phase index. The spectrum of corresponding quantum (radiation) phase is discrete and lies in the interval $(0, 2\pi)$. In the classical limit provided by the high-intensity coherent multipole radiation, the eigenvalues of the radiation phase are distributed uniformly over this interval. By construction, the radiation phase is complementary to Mandel's operational phase [47]. It defines the quantum phase in terms of *what can be generated* by a quantum local source. In the quantum limit of weak intensity, the behavior of radiation and the Pegg–Barnett [45] quantum phases are completely different. They are caused by the specific truncation procedure used within the Pegg–Barnett approach, which leads to an effective violation of the Weyl-Heisenberg algebra of photons.

The radiation phase is closely related to the polarization of the multipole field. In contrast to the plane waves, the polarization of multipole radiation is specified by three orthogonal directions of the field oscillations or by three allowed spin states of photons [28]. Therefore, the polarization is described by the (3×3) Hermitian matrix of polarization (operator matrix, in the quantum case) (Sections V.A and V.B). This general form of the polarization matrix gives in the limit the standard case of (2×2) matrix in the representation of plane waves. The set of multipole Stokes operators corresponds to a representation of the $SU(3)$ subalgebra in the Weyl–Heisenberg algebra of photons. The Cartan algebra of this $SU(3)$ subalgebra corresponds to the representation of the radiation phase in the case of the angular momentum $j = 1$. Thus, the polarization of multipole radiation has a certain inherent quantum phase that, in some important cases, can be interpreted as the phase difference between the components with different polarization (Section V.B). The quantum properties of polarization can be measured with the aid of a multiport scheme [97] (Section VI.C).

The polarization and quantum phase properties of multipole photons change with the distance from the source. This dependence can be adequately described with the aid of the local representation of the photon operators proposed in Ref. 91 and discussed in Section V.D. In this representation, the photon operators of creation and annihilation correspond to the states with given spin (polarization) at any point. This representation may be useful in the quantum near-field optics. As we know, so far near-field optics is based mainly on the classical picture of the field [106].

The local representation of multipole photons is compatible with the Mandel operational definition of photon localization [20]. In addition to the localization at photodetection, it permits us to describe a complete Hertz-type experiment with two identical atoms used as the emitter and detector (Section VI.A). Although the photon path is undefined from the quantum-mechanical point of view, the measurement process in such a system obeys the causality principle (Section IV.B). The two-atom Hertz experiment can be realized for the trapped

Ridberg atoms. Let us stress that such a measurement is closely connected with the problem of atomic entanglement discussed in Ref. 76.

The standard measurement of different properties of quantum electromagnetic radiation is based on the photodetection, which is field destructive. Following our consideration of the possibility of the Aharonov–Bohm effect at optical frequencies [100], we propose here a new nondemolition method of polarization measurement in which the linearly polarized longitudinal mode of the field is detected without any perturbation of its quantum state (Section VI.D). The estimation of physical conditions shows that such a measurement can be done either for the photons propagating through the fiber, or for the superradiant photons in radioband frequencies.

In this review, we relied to a large extent on our own results. We believe, however, that this chapter covers a number of topics important for quantum optics, and that the reported results may stimulate an interest in further investigations. Success in the field of quantum optics has convicingly shown that developments in optics have very often had a direct influence on other fields, both pure and applied.

Acknowledgments

A number of reported results were obtained together with my colleagues O. Aytur, T. Hakioğlu, A. A. Klyachko, and B. Tanatar and students Ö. E. Müstecaplıoğlu, M. Ünsal, and M. A. Can, whom I would like to thank for fruitful collaboration. I wish to express a deep gratitude to A. Bandilla, H.-D. Doebner, J. H. Eberly, E. Kapuscik, P. L. Knight, P. Kumar, A. Miranowicz, H. Paul, V. I. Rupasov, A. Vourdas, H. Walther, K. Wodkiewicz, and A. Wuensche for stimulating discussions. Finally, I am grateful to my wife, Natalia Shumovsky, and Dr. A. I. Degtyarev, who helped me a lot in preparing a readable text.

References

1. P. A. M. Dirac, *Proc. Roy. Soc. Lond. A* **114**, 243, 710 (1927).
2. W. Heitler, *The Quantum Theory of Radiation*, Oxford Univ. Press, New York, 1954.
3. N. N. Bogoliubov and D.V. Shirkov, *Introduction to the Theory of Quantum Fields*, Wiley, New York, 1980.
4. V. B. Berestetskii, E. M. Lifshitz, and L. P. Pitaevskii, *Quantum Electrodynamics*, Pergamon, Oxford, 1982.
5. V. Weisskopf and E. P. Wigner, *Z. Phys.* **63**, 54 (1930); **65**, 18 (1930).
6. W. E. Lamb Jr. and R. C. Retherford, *Phys. Rev.* **72**, 241 (1947).
7. H. B. G. Casimir, *J. de Chem. Physique* **46**, 407 (1949); H. B. G. Casimir and D. Polder, *Phys. Rev.* **73**, 360 (1948).
8. W. W. Chow, M. O. Scully, and J. O. Stoner Jr., *Phys. Rev. A* **11**, 1380 (1975); R. M. Herman, H. Groth, R. Kornblith, and J. H. Eberly, *Phys. Rev. A* **11**, 1389 (1975).
9. D. Stoler, *Phys. Rev. D* **1**, 3217 (1970); H. P. Yuen, *Phys. Rev. A* **13**, 2226 (1976); D. F. Walls, *Nature* **106**, 141 (1983); R. Loudon and P. Knight, *J. Mod. Optics* **34**, 709 (1987).
10. H. A. Kramers, *Quantum Mechanics*, North-Holland, Amsterdam, 1985.
11. E. A. Power, *Introductory Quantum Electrodynamics*, Longman, London, 1964.

12. I. Bialynicki-Birula and Z. Bialanicka-Birula, *Quantum Electrodynamics*, Pergamon, Oxford, 1976.
13. M. W. Evans and J.-P. Vigier, *The Engimatic Photon*, Vols. 1, 2, Kluwer, Dordrecht, 1994; M. W. Evans, J.-P. Vigier, S. Roy, S. Jeffers, and G. Hunter, *The Engimatic Photon*, Vols. 3, 4, Kluwer, Dordrecht, 1997.
14. L. Mandel and E. Wolf, *Optical Coherence and Quantum Optics*, Cambridge Univ. Press, New York, 1995.
15. M. O. Scully and M. S. Zubairy, *Quantum Optics*, Cambridge Univ. Press, New York, 1997.
16. T. D. Newton and E. P. Wigner, *Rev. Mod. Phys.* **21**, 400 (1949).
17. R. Acharya and E. C. G. Sudarshan, *J. Math. Phys.* **1**, 532 (1960).
18. I. Bialynicki-Birula, *Acta Phys. Pol. A* **86**, 97 (1994).
19. I. Bialynicki-Birula, *Phys. Rev. Lett.* **80**, 5247 (1998).
20. L. Mandel, *Phys. Rev.* **144**, 1071 (1966).
21. S. John, *Phys. Rev. Lett.* **58**, 2486 (1987).
22. A. S. Shumovsky, in *Electronic Proc. 7th Central Eur. Workshop on Quantum Optics* April 28–May 1, 2000, available at http://optics.szfki.kfki.hu/cewqo2000.
23. E. U. Condon and G. H. Shortley, *The Theory of Atomic Spectra*, Cambridge Univ. Press, New York, 1987.
24. H. Bateman, *The Mathematical Analysis of Electric and Optical Wave-Motion* Dover, New York, 1955.
25. J. D. Jackson, *Classical Electrodynamics*, Wiley, New York, 1978.
26. C. Cohen-Tannouji, J. Dupont-Roc, and G. Grinberg, *Atom-Photon Interaction*, Wiley, New York, 1992.
27. A. S. Davydov, *Quantum Mechanics*, Pergamon, Oxford, 1976.
28. A. S. Shumovsky and Ö. E. Müstecaplıoğlu, *Phys. Rev. Lett.* **80**, 1202 (1998).
29. A. S. Shumovsky, *lanl e-print* quantum-ph/0007109.
30. P. W. Milony, *The Quantum Vacuum*, Academic, San Diego, 1994.
31. G. Compagno, R. Pasante, and F. Persico, *Atom-field Interaction and Dressed Atoms*, Cambridge Univ. Press, Cambridge, UK, 1995.
32. S. Haroche, *AIP Conf. Proc.* Vol. 464, Issue 1, p. 45 (1999); J. M. Raimond, E. Hagley, X. Maitre, G. Nogues, C. Wunderlich, M. Brune, and S. Haroshe, in *AIP Conf. Proc.* Vol. 477, Issue 1, p. 209 (1999).
33. M. Weidinger, B. T. H. Varcoe, R. Heerlein, and H. Walther, *Phys. Rev. Lett.* **82**, 3795 (1999).
34. A. K. Ekert, *Phys. Rev. Lett.* **67**, 661 (1991); C. H. Benett and S. J. Wiesner, *Phys. Rev. Lett.* **69**, 2881 (1992); C. H. Benett, G. Brassard, C. Crepeau, R. Jozza, A. Peres, and W. K. Wootters, *Phys. Rev. Lett.* **70**, 1895 (1993); D. Bouwmeester, J.-W. Pan, K. Mattle, M. Eibl, H. Weinfürter, and A. Zeilinger, *Nature* **390**, 575 (1997); D. Boschi, S. Branca, F. De Martini, L. Hardy, and S. Popescu, *Phys. Rev. Lett.* **80**, 1121 (1998); J.-W. Pan, D. Bowmeester, H. Weinfürter, and A. Zeilinger, *Phys. Rev. Lett.* **80**, 3891 (1998).
35. C. Adlard, E. P. Pike, and S. Sarkar, *Phys. Rev. Lett.* **79**, 1583 (1997).
36. A. S. Shumovsky, *Opt. Commun.* **136**, 219 (1997).
37. *Physica Scripta T* **48**, special issue (1995).
38. R. Lynch, *Phys. Rep.* **256**, 367 (1995).
39. R. Tanaś, A. Miranowicz, and T. Gantsog, *Prog. Opt.* **35**, 1 (1996).

40. D. T. Pegg and S. M. Barnett, *J. Mod. Opt.* **44**, 225 (1997).
41. L. Susskind and J. Glogower, *Physics* **1**, 49 (1964).
42. S. M. Barnett and D. T. Pegg, *J. Phys. A* **19**, 3849 (1986).
43. A. Lukš and V. Perinova, *Czech. J. Phys. A* **41**, 1205 (1991).
44. W. H. Louisell, *Phys. Lett.* **7**, 60 (1963); P. Carruthers and M. Nieto, *Rev. Mod. Phys.* **40**, 411 (1968).
45. D. T. Pegg and S. M. Barnett, *Europhys. Lett.* **6**, 483 (1988); S. M. Barnett and D. T. Pegg, *J. Mod. Opt.* **36**, 7 (1989); D. T. Pegg and S. M. Barnett, *J. Mod. Opt.* **39**, 2121 (1992).
46. A. S. Shumovsky, *J. Phys. A* **32**, 6589 (1999).
47. J. W. Noh, A. Fougères, and L. Mandel, *Phys. Rev. Lett.* **67**, 1426 (1991); J. W. Noh, A. Fougères, and L. Mandel, *Phys. Rev. A* **45**, 242 (1992).
48. A. Fougères, J. R. Torgerson, and L. Mandel, *Optics Commun.* **105**, 199 (1994); J. R. Torgerson and L. Mandel, *Phys. Rev. Lett.* **76**, 3939 (1996); J. R. Torgerson and L. Mandel, *Optics Commun.* **133**, 153 (1997).
49. A. Bandilla and H. Paul, *Ann. Phys.* (Leipzig) **23**, 323 (1969); W. P. Schleih, A. Bandilla, and H. Paul, *Phys. Rev. A* **45**, 6652 (1992); M. Freyberger, K. Vogel, and W. P. Schleih, *Phys. Lett. A* **176**, 41 (1993); U. Leonhardt and H. Paul, *Phys. Rev. A* **47**, R2460 (1993).
50. B.-G. Englert and J. Wodkiewicz, *Phys. Rev. A* **51**, R266 (1995).
51. A. Vourdas, *Phys. Rev. A* **41**, 1653 (1990).
52. J.-P. Serre, *Linear Representations of Finite Groups*, Springer, New York, 1977.
53. A. S. Shumovsky and Ö. E. Müstecaplıoğlu, *Phys. Lett. A* **235**, 438 (1997); A. S. Shumovsky and Ö. E. Müstecaplıoğlu, in G. Hunter, S. Jeffers, and J.-P. Vigier (Eds.), *Causality and Locality in Modern Physics*, Kluwer, Dordrecht, 1998.
54. A. S. Shumovsky and Ö. E. Müstecaplıoğlu, *J. Mod. Opt.* **45**, 619 (1998); A. S. Shumovsky and Ö. E. Müstecaplıoğlu, *Opt. Commun.* **146**, 124 (1998).
55. J. M. Levi-Leblond, *Ann. Phys.* (NY) **101**, 319 (1979); S. M. Barnett and D. T. Pegg, *Phys. Rev. A* **41**, 3427 (1990); L. L. Sanchez-Soto and A. Luis, *Optics Commun.* **105**, 84 (1994); A. Lukš and V. Perinova, *Quantum Opt.* **6**, 125 (1994).
56. I. C. Koo and J. H. Eberly, *Phys. Rev. A* **14**, 2174 (1976).
57. M. Born and E. Wolf, *Principles of Optics*, Pergamon, Oxford, 1970.
58. W. H. Louisell, *Radiation and Noise in Quantum Electronics*, McGraw-Hill, New York, 1964.
59. R. Loudon, *The Quantum Theory of Light*, Oxford Univ. Press, New York, 1973.
60. L. D. Landau and E. M. Lifshitz, *The Classical Theory of Fields*, Pergamon, Oxford, 1975.
61. G. Herzberg, *Atomic Spectra and Atomic Structure*, Dover, New York, 1944; C. E. Moore, *Atomic Energy Levels* (U.S. National Bureau of Standards, Washington DC, 1971); J. M. Hollas, *Modern Spectroscopy*, Wiley, New York, 1996.
62. B. Crosignani, P. Di Porto, and M. Bertolotti, *Statistical Properties of Scattered Light*, Academic, New York, 1975; B. E. A. Saleh, *Photoelectron Statistics with Applications to Spectroscopy and Communications*, Springer, Berlin, 1978; J. Peřrina, *Quantum Statistics of Linear and Nonlinear Optical Phenomena*, Reidel, Dordrecht, 1984; N. N. Bogolubov, A. S. Shumovsky, and V. I. Yukalov (Eds.), *Interaction of Electromagnetic Field with Condensed Matter*, World Scientific, Singapore, 1990; A. S. Shumovsky, in T. Hakiioğlu and A. S. Shumovsky (Eds.), *Quantum Optics and Spectroscopy of Solids*, Kluwer, Dordrecht, 1997.

63. A. S. Shumovsky and B. Tanatar, *Phys. Rev. A* **48**, 4735 (1993); Ö. E. Müstecaplıoğlu and A. S. Shumovsky, *Appl. Phys. Lett.* **70**, 3489 (1997); Ö. E. Müstecaplıoğlu and A. S. Shumovsky, *Phys. Rev. B* **60**, 3970 (1999).

64. A. Allen and J. H. Eberly, *Optical Resonance and Two-Level Atoms*, Wiley, New York, 1975.

65. A. Einstein, *Z. Phys.* **18**, 121 (1917).

66. D. Meschede, H. Walther, and G. Muller, *Phys. Rev. Lett.* **54**, 551 (1985); S. Haroche and J. M. Raimond, in D. Bates and B. Bederson (Eds.), *Advances in Atomic and Molecular Physics*, Vol. 20, Academic, New York, 1985; G. Rempe, H. Walther, and N. Klein, *Phys. Rev. Lett.* **58**, 353 (1987); E. R. Pike and H. Walther (Eds.), *Photons and Quantum Fluctuations*, Hilger, Bristol, 1988; M. O. Scully, B.-G. Englert, and H. Walther, *Nature* **351**, 111 (1991); G. Raithel, O. Benson, and H. Walther, *Phys. Rev. Lett.* **72**, 3506 (1995); H. Walther, in T. Hakioğlu and A. S. Shumovsky (Eds.), *Quantum Optics and the Spectroscopy of Solids*, Kluwer, Dordrecht, 1997.

67. E. T. Jaynes and F. W. Cummings, *Proc. IEEE* **51**, 89 (1963).

68. H. I. Yoo and J. H. Eberly, *Phys. Rep.* **118**, 239 (1985); F. L. Kien and A. S. Shumovsky, *Int. J. Mod. Phys. B* **5**, 2287 (1991); R. Shore and P. L. Knight, *J. Mod. Optics* **40**, 1195 (1993); E. I. Aliskenderov, A. S. Shumovsky, and H. T. Dung, *Phys. Part. Nucl.* **24**, 177 (1993).

69. V. I. Rupasov, *JETP Lett.* **36**, 142 (1982); V. I. Rupasov, *Sov. Phys. JETP* **56**, 989 (1982); V. I. Rupasov and V. I. Yudson, *Sov. Phys. JETP* **60**, 927 (1984); V. I. Rupasov and M. Singh, *Phys. Rev. Lett.* **77**, 338 (1996); V. I. Rupasov and M. Singh, *Phys. Rev. A* **54**, 3614 (1996).

70. I. S. Gradshtein and I. M. Ryzhik, *Table of Integrals, Series, and Products*, Academic, Boston, 1994.

71. D. M. Brink and G. R. Satchler, *Angular Momentum*, Clarendon, Oxford, 1993.

72. H. S. M. Coxeter and W. O. J. Moser, *Generators and Relations for Discrete Groups*, Springer, Berlin, 1965.

73. A. Einstein, B. Podolsky, and N. Rosen, *Phys. Rev.* **47**, 777 (1935).

74. D. Bohm, *Quantum Theory*, Prentice-Hall, Englewood Cliffs, NJ, 1951.

75. J. S. Bell, *Physics* **1**, 195 (1964); J. S. Bell, *Rev. Mod. Phys.* **38**, 447 (1966).

76. M. B. Plenio, S. F. Huelga, A. Beige, and P. L. Knight, *Phys. Rev. A* **59**, 2468 (1999).

77. H. Frölich, *Phys. Rev.* **79**, 845 (1950); J. Bardeen, L. N. Cooper, and J. R. Schrieffer, *Phys. Rev.* **108**, 1175 (1957); N. N. Bogolubov, *Sov. Phys. JETP* **7**, 41 (1958); J. R. Schrieffer, *Superconductivity*, Benjamin, New York, 1964.

78. P. W. Anderson, *Phys. Rev.* **110**, 985 (1958).

79. W. Thirring, *Comm. Math. Phys.* **7**, 181 (1968); N. N. Bogolubov Jr., B. I. Sadovnikov, and A. S. Shumovsky, *Mathematical Methods of Statistical Mechanics of Model Systems*, CRC Press, Boca Raton, FL, 1994.

80. N. N. Bogolubov, A. M. Kurbatov, and A. S. Shumovsky (Eds.), *N. N. Bogolubov Selected Works*, Part II, *Quantum and Classical Statistical Mechanics*, Gordon & Breach, New York, 1991.

81. R. J. Glauber, *Phys. Rev.* **131**, 2766 (1963); E. C. G. Sudarshan, *Phys. Rev. Lett.* **10**, 277 (1963).

82. A. Luis, A. L. L. Sanchez-Soto, and R. Tanaś, *Phys. Rev. A* **51**, 1634 (1995).

83. Ts. Gantsog and R. Tanaś, *J. Mod. Optics* **38**, 1537 (1991).

84. T. Hakioğlu, *J. Phys. A* **31**, 707 (1998).

85. R. Hanbury-Brown and R. Q. Twiss, *Phil. Mag.* **45**, 663 (1954); H. Hanbury-Brown and R. Q. Twiss, *Nature* **178**, 1046 (1956); H. Hanbury-Brown and R. Q. Twiss, *Proc. Roy. Soc. A* **242**, 300 (1957); R. Hanbury-Brown, *The Intensity Interferometer*, Taylor & Fancis, London, 1974.

86. W. Vogel and D.-G. Welsch, *Lectures on Quantum Optics*, Akademic, Verlag, Berlin, 1994.

87. R. M. A. Azzam and N. M. Bashara, *Ellipsometry and Polarized Light*, North-Holland, Amsterdam, 1987; D. S. Kliger, J. W. Lewis, and C. E. Randal, *Polarized Light in Optics and Spectroscopy*, Academic, New York, 1990; S. Huard, *Polarization of Light*, Wiley, New York, 1996; C. Brosseau, *Fundamentals of Polarized Light*, Wiley, New York, 1998.

88. A. S. Shumovsky, *Laser Phys.* **9**, 26 (1999); A. S. Shumovsky, Ö. E. Müstecaplıoğlu, and M. Ünsal, *Laser Phys.* **10**, 31 (2000).

89. E. Wolf, *Nuovo Cimento* **12**, 884 (1954).

90. J. M. Jauch and F. Rohrlich, *The Theory of Photons and Electrons* (Addison-Wesley, Reading, MA, 1959).

91. A. S. Shumovsky and A. A. Klyachko, *Laser Phys.* **11**, 57 (2001).

92. R. J. Cook, *Phys. Rev. A* **25**, 2164 (1982); R. J. Cook, in L. Mandel and E. Wolf (Eds.), *Coherence and Quantum Optics*, Vol. V, (Plenum, New York, 1984; E. R. Pike and S. Sarkar, in E. R. Pike and S. Sarkar (Eds.), *Frontiers in Quantum Optics*, Hilger, Bristol, 1986.

93. R.P Feynman and A. R. Hibbs, *Quantum Mechanics and Path Integrals* McGrow-Hill, New York, 1965.

94. E. H. Haug and J. A. Støvneng, *Rev. Mod. Phys.* **61**, 917 (1989); R. Landauer, *Nature* **341**, 567 (1989); R. Landauer and Th. Martin, *Rev. Mod. Phys.* **66**, 217 (1994).

95. A. Ranfagni, D. Mugnai, P. Fabeni, and G. Pazzi, *Appl. Phys. Lett.* **58**, 774 (1991); A. Enders and G. Nimitz, *J. Phys.* (*France*) *I* **2**, 1693 (1992); A. Ranfagni, P. Fabeni, G. Pazzi, and D. Mugnai, *Phys. Rev. E* **48**, 1453 (1993); C. Spielmann, R. Szipöcs, A. Stingl, and F. Kraus, *Phys. Rev. Lett.* **73**, 2308 (1994); D. Mugnai, A. Ranfagni, and R. Ruggeri, *Phys. Rev. Lett.* **84**, 4830 (2000).

96. D. Kaup and V. I. Rupasov, *J. Phys. A* **29**, 6911 (1996).

97. T. Hakioğlu, A. S. Shumovsky, and O. Aytur, *Phys. Lett. A* **194**, 304 (1994).

98. A. Zuchetti, W. Vogel, and D.-G. Welsch, *Phys. Rev. A* **54**, 856 (1996).

99. V. B. Braginsky, Y. I. Vorontsov, and F. I. Khalili, *Sov. Phys. JETP* **46**, 705 (1977); C. M. Caves, K. S. Thorn, R. W. D. Drever, V. D. Sandberg, and M. Zimmerman, *Rev. Mod. Phys.* **52**, 341 (1980); V. B. Braginsky and F. I. Khalili, *Quantum Measurement*, Cambridge Univ. Press, New York, 1992.

100. I. O Kulik and A. S. Shumovsky, *Appl. Phys. Lett.* **69**, 2779 (1996); I. O Kulik and A. S. Shumovsky, in G. Hunter, S. Jeffers, and J.-P. Vigier (Eds.), *Causality and Locality in Modern Physics*, Kluwer, Dordrecht, 1998.

101. Y. Aharonov and D. Bohm, *Phys. Rev.* **115**, 485 (1959); M. Peshkin and A. Tonomura, *The Aharonov-Bohm Effect*, Springer Verlag, Berlin, 1989; B. L. Altshuler, P. A. Lee, and R. A. Webb (Eds.), *Mesoscopic Phenomena in Solids*, North Holland, Amsterdam, 1991.

102. I. E. Aronov, E. N. Bogachek, and I. V. Krive, *Phys. Lett. A* **164**, 331 (1992); I. E. Aronov, A. Grincwajg, M. Jonson, R. I. Shekhter, and E. N. Bogachek, *Solid State Commun.* **91**, 75 (1994).

103. V. Chandrasekhar, R. A. Webb, M. J. Brady, M. B. Ketchen, W. J. Gallagher, and A. Kleinsasser, *Phys. Rev. Lett.* **70**, 2020 (1991).

104. G. Agrawal, *Nonlinear Fiber Optics*, Academic, Boston, 1989.

105. Yu. Kiselev, A. Prutkoglyad, A. Shumovsky, and V. Yukalov, *Sov. Phys. JETP* **94**, 344 (1988); Yu. F. Kiselev, A. S. Shumovsky, and V. I. Yukalov, *Mod. Phys. Lett. B* **3**, 1149 (1989).

106. D. W. Pohl and D. Courjon (Eds.), *Near Field Optics*, Kluwer, Dordrecht, 1993.

NONLINEAR PHENOMENA IN QUANTUM OPTICS

JIŘÍ BAJER, MILOSLAV DUŠEK, JAROMÍR FIURÁŠEK, ZDENĚK HRADIL, ANTONÍN LUKŠ, VLASTA PEŘINOVÁ, AND JAROSLAV ŘEHÁČEK

Department of Optics, Palacký University, Olomouc, Czech Republic

JAN PEŘINA

Department of Optics, Palacký University and Joint Laboratory of Optics of Palacký University and the Academy of Sciences of the Czech Republic, Czech Republic

ONDŘEJ HADERKA, MARTIN HENDRYCH, AND JAN PEŘINA, JR.

Joint Laboratory of Optics of Palacký University and the Academy of Sciences of the Czech Republic, Olomouc, Czech Republic

NOBUYUKI IMOTO AND MASATO KOASHI

CREST Research Team for Interacting Carrier Electronics, School of Advanced Sciences, The Graduate University for Advanced Studies (SOKEN), Hayama, Kanagawa, Japan

ADAM MIRANOWICZ

CREST Research Team for Interacting Carrier Electronics, School of Advanced Sciences, The Graduate University for Advanced Studies (SOKEN), Hayama, Kanagawa, Japan and Nonlinear Optics Division, Institute of Physics, Adam Mickiewicz University, Poznań, Poland

CONTENTS

I. INTRODUCTION

In this chapter we provide a review of nonlinear phenomena in quantum optics, giving an overview of scientific activities in quantum optics at the Natural Science Faculty of Palacký University in Olomouc (Czech Republic). Contributions of various authors are included in this chapter as sections and names of the corresponding authors are given after the section titles in brackets. The first section is devoted to quantum and classical methods to obtain photon statistics in higher-harmonics generation, including a method of classical trajectories. It is followed by a discussion of photon bunching and antibunching of nonstationary fields. The chapter continues with a discussion of methods for reconstruction of quantum states. The following part of the chapter deals with the process of frequency downconversion with pulses, Zeno and anti-Zeno effects based on optical parametric processes, Raman nonlinear couplers as switching elements and sources of nonclassical light for optoelectronics and photonics, and quantum cryptography. Finally, quantum spatial propagation of a two-mode squeezed light in a cubically behaved quadratic medium is treated as another feature of a two-field squeezed steady-state light, and this approach is compared with the conventional one.

II. QUANTUM, CLASSICAL, AND SEMICLASSICAL ANALYSES OF PHOTON STATISTICS IN HARMONIC GENERATION (*J. BAJER and A. MIRANOWICZ*)

A. Introduction

Harmonic generation is one of the earliest discovered and studied nonlinear optical processes. For 40 years, since the first experimental demonstration of

second-harmonic generation (SHG) by Franken and co-workers [1] followed by its rigorous theoretical description by Bloembergen and Pershan [2], harmonic generation has unceasingly attracted much attention [3]. In particular, harmonic generation has been applied as a source of nonclassical radiation (see Refs. 4 and 5 for a detailed account and bibliography). It was demonstrated that photon antibunched and sub-Poissonian light [6,7], as well as second- [8] and higher-order [9,10] squeezed light, can be produced in SHG. In experimental schemes, second-harmonic generation is usually applied for the sub-Poissonian and photon antibunched light production, whereas second-subharmonic generation (also referred to as *two-photon downconversion*) is used for the squeezed-light generation [4,11]. Nonclassical effects in higher-harmonic generation have also been investigated, including sub-Poissonian photocount statistics [5,7,12,13], squeezing [5,14,15], higher-order squeezing [16,17] according to the Hong–Mandel definition [9], or higher-power-amplitude squeezing [18,17] based on Hillery's concept [10]. In this contribution, we will study photocount statistics of second- and higher-harmonic generations with coherent light inputs.

Photocount noise of the observed statistics can simply be described by the (quantum) *Fano factor* [19]

$$F^{\mathrm{Q}} \equiv \frac{\langle (\Delta\hat{n})^2 \rangle}{\langle \hat{n} \rangle} = \frac{\langle \hat{n}^2 \rangle - \langle \hat{n} \rangle^2}{\langle \hat{n} \rangle} \tag{1}$$

where $\langle \hat{n} \rangle$ is the (ensemble) mean number of detected photons and $\langle (\Delta\hat{n})^2 \rangle$ is the variance of photon number. We also analyze the global (quantum) Fano factor defined to be [20]

$$F^{\mathrm{G}} \equiv \frac{\langle\langle (\Delta\hat{n})^2 \rangle\rangle}{\langle\langle \hat{n} \rangle\rangle} = \frac{\langle\langle \hat{n}^2 \rangle\rangle - \langle\langle \hat{n} \rangle\rangle^2}{\langle\langle \hat{n} \rangle\rangle} \tag{2}$$

where the mean values $\langle\langle \hat{n}^k \rangle\rangle$ are obtained by the ensemble and time averaging;

$$\langle\langle \hat{n}^k \rangle\rangle = \lim_{T\to\infty} \frac{1}{T} \int_0^T \langle \hat{n}^k(t) \rangle \, dt \tag{3}$$

In the classical trajectory approach, the Fano factor is defined to be

$$F^{\mathrm{S}} \equiv \frac{\overline{(\Delta n)^2}}{\bar{n}} = \frac{\overline{n^2} - \bar{n}^2}{\bar{n}} \tag{4}$$

as a semiclassical analog of the quantum Fano factor. The mean values $\overline{n^k}$ in Eq. (4) are obtained by averaging over all classical trajectories, as will be discussed in detail in Sections II. B and II. C.

Coherent (ideal laser) light has Poissonian photon-number distribution thus described by the unit Fano factor. For $F < 1$, the light is referred to as light *sub-Poissonian* since its photocount noise is smaller than that of coherent light with the same intensity. Whereas for $F > 1$, the light is called *super-Poissonian* with the photocount noise higher than that for coherent light.

We shall compare different descriptions of photon-number statistics in harmonic generation within quantum, classical and semiclassical approaches. First, we will study the exact quantum evolution of the harmonic generation process by applying numerical methods including those of Hamiltonian diagonalization and global characteristics. As a brief introduction, we will show explicitly that harmonic generation can, indeed, serve as a source of nonclassical light. Then, we will demonstrate that the quasistationary sub-Poissonian light can be generated in these quantum processes under conditions corresponding to the so-called no-energy-transfer regime known in classical nonlinear optics. By applying method of classical trajectories, we will demonstrate that the analytical predictions of the Fano factors are in good agreement with the quantum results. On comparing second- [21], third- [22] and higher- [23] harmonic generations in the no-energy-transfer regime, we will show that the highest noise reduction is achieved in third-harmonic generation with the Fanofactor of the third harmonic equal to $F_3^{\mathrm{Q}} \approx F_3^{\mathrm{S}} = \frac{13}{16}$.

B. Second-Harmonic Generation

1. *Quantum Analysis*

The quantum process of second-harmonic generation (SHG) can be described by the following interaction Hamiltonian [4,5]:

$$\hat{H} = \hbar g\left(\hat{a}_1^2\hat{a}_2^\dagger + \hat{a}_1^{\dagger 2}\hat{a}_2\right) \tag{5}$$

where $\hat{a}_1$ and $\hat{a}_2$ denote annihilation operators of the fundamental and second-harmonic modes, respectively; g is a nonlinear coupling parameter. The Hamiltonian (5) describes a process of absorption of two photons at frequency ω_1 and simultaneous creation of a new photon at the harmonic frequency $\omega_2 = 2\omega_1$, together with the inverse process. Unfortunately, no exact solution of quantum dynamics of the model, described by (5), can be found. Thus, various analytical approximations or numerical methods have to be applied in the analysis of the conversion efficiency, quantum noise statistics, or other characteristics of the process [5]. Because of mathematical complexity of the problem, the investigations of nonclassical effects in harmonic generation have usually been restricted to the regime of short interactions (short optical paths or short times). Theoretical predictions of quantum parameters (including the Fano factor or, equivalently, the Mandel Q-parameter) were obtained

under the short time approximation only [4,5,13]. This is a physically sound approximation in case of weak nonlinear coupling of optical fields. The Fano factors under the short-time approximation (i.e., for $gt \ll 1$) for coherent inputs $\alpha_1 = r_1 \exp(i\phi_1)$ and $\alpha_2 = r_2 \exp(i\phi_2)$ are given by the expansions (for $r_1, r_2 \neq 0$)

$$\begin{aligned} F_1^{\mathrm{Q}} &= 1 - 4\sin\theta\, r_2 gt \\ &\quad + \left\{4r_1^{-2}r_2^2 - 2r_1^2 + 8[2+\cos(2\theta)]r_2^2\right\}(gt)^2 + \mathcal{O}\{(gt)^3\} \\ F_2^{\mathrm{Q}} &= 1 - \frac{16}{3}\sin\theta\, r_1^2 r_2 (gt)^3 \\ &\quad + \frac{4}{3}\left\{2r_2^2 + 16r_1^2r_2^2 - [4+3\cos(2\theta)]r_1^4\right\}(gt)^4 + \mathcal{O}\{(gt)^5\} \end{aligned} \tag{6}$$

where $\theta = 2\phi_1 - \phi_2$ and $\mathcal{O}\{x\}$ denotes the order of magnitude. Equation (6) determines whether the generation of harmonics ($\omega + \omega \to 2\omega$) or subharmonics ($2\omega \to \omega + \omega$) occurs. It also determines the sub-Poissonian or super-Poissonian photon-number statistics of light generated during the short-time interactions. For spontaneous SHG process (i.e., for $r_2 = 0$), the well-known expansions for the quantum Fano factors are

$$\begin{aligned} F_1^{\mathrm{Q}} &= 1 - 2(r_1 gt)^2 + \frac{4}{3}r_1^2\left(3r_1^2+1\right)(gt)^4 + \mathcal{O}\{(gt)^6\} \\ F_2^{\mathrm{Q}} &= 1 - \frac{4}{3}(r_1 gt)^4 + \frac{4}{45}r_1^4\left(36r_1^2+17\right)(gt)^6 + \mathcal{O}\{(gt)^8\} \end{aligned} \tag{7}$$

or, equivalently, for the normally ordered photon-number variances [4,6,7]:

$$\begin{aligned} \langle :(\Delta\hat{n}_1)^2: \rangle &\equiv \langle (\Delta\hat{n}_1)^2\rangle - \langle \hat{n}_1\rangle = -2r_1^4(gt)^2 + \mathcal{O}\{(gt)^4\} \\ \langle :(\Delta\hat{n}_2)^2: \rangle &\equiv \langle (\Delta\hat{n}_2)^2\rangle - \langle \hat{n}_2\rangle = -\frac{4}{3}r_1^8(gt)^6 + \mathcal{O}\{(gt)^8\} \end{aligned} \tag{8}$$

It is seen that the photon-number statistics of fundamental mode exhibits, in the short-time regime, much stronger sub-Poissonian behavior than that of harmonic mode.

For longer interaction times ($gt > 1$), there are no exact analytical solutions, thus the numerical analysis has to be applied. We have used two methods to study the quantum dynamics: (1) the well-known Hamiltonian diagonalization proposed by Walls and Barakat [24] and (2) the method of global characteristics based on manipulation with spectra [20]. These methods can be applied for arbitrary initial photon statistics. Nevertheless, for the purpose of our chapter, we restrict our analysis to the initial coherent fields solely. Owing to computa-

tional difficulties, the results can be obtained for small numbers of interacting photons only. The analysis of about 100 interacting photons reaches practically the computational capabilities of the standard mathematical software.

Analysis of a typical evolution of the Fano factors $F^{Q}_{1,2}$, such as presented in Fig. 1a, leads to the conclusion that after initial short-time ($gt < 1$) relaxations in both modes, a strongly super-Poissonian ($F^{Q}_{1,2} \gg 1$). This behavior occurs for the majority of initial coherent states $|\alpha_1\rangle$ and $|\alpha_2\rangle$ except a certain set of initial

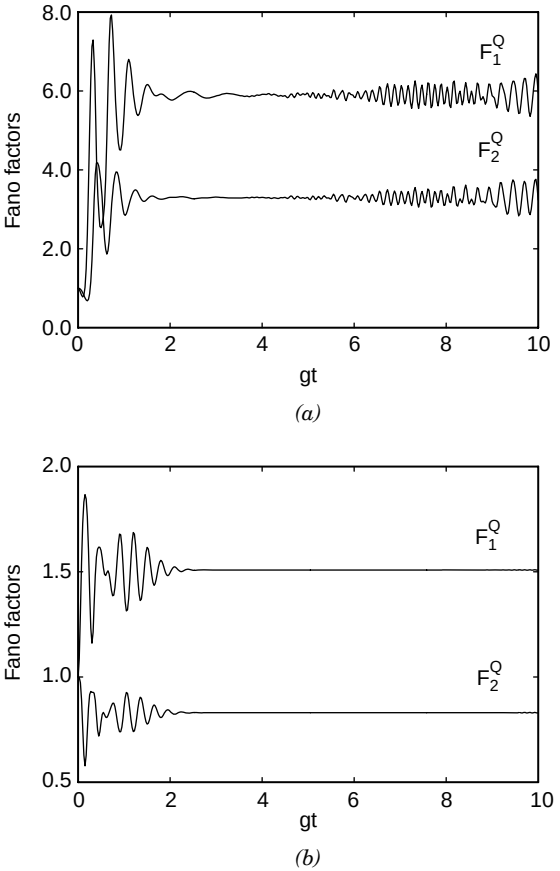

Figure 1. Fano factors of the fundamental, F^{Q}_{1}, and the second-harmonic mode, F^{Q}_{2}, in the long-time interaction for initial coherent states with real amplitudes (a) $\alpha_1 = 6, \alpha_2 = 1$, and (b) $\alpha_1 = 6, \alpha_2 = 3$. Case a is a typical example of super-Poissonian behavior in both modes outside the no-energy-transfer regime. In case b, the harmonic mode exhibits stable sub-Poissonian statistics with $F^{Q}_{2} \simeq 0.83$. It is a charactersitc example of the sub-Poissonian behavior within the no-energy-transfer regime along the line $|\alpha_1| = 2|\alpha_2|$.

states concentrated along the line $|\alpha_1| = 2|\alpha_2| > 0$ and $\theta \simeq 0$ (see Fig. 1b). The same conclusion can be drawn by analyzing the global Fano factors $F^{\mathrm{G}}_{1,2}$. We find that the global Fano factor of the harmonic mode remains independent of amplitude $|\alpha_k|$ and equal to $F^{\mathrm{G}}_2 = 0.83 < 1$ along the line $|\alpha_1| = 2|\alpha_2|$ (see Figs. 2 and 3). As depicted in Fig. 1b, when the initial relaxation oscillations fade out, the harmonic mode remains sub-Poissonian for a long interaction time interval. In the classical theory of SHG, this case is referred to as the *no-energy-transfer regime* [25], because of the conservation of energy in every mode. We have found a quantum analog of this regime for coherent inputs with amplitudes satisfying the conditions: $|\alpha_1| = 2|\alpha_2|$ and $\theta \simeq 0$.

By analyzing Figs. 2 and 3, an intriguing question arises: Why does the harmonic-field photocount statistics in the no-energy-transfer regime remain sub-Poissonian with the Fano factor almost independent of the interaction time $gt > 1$? This behavior can be understood better by plotting the Husimi Q function. Let us have a look at the snapshots of typical evolution of Q functions for both modes at six time moments $gt = 0, 0.5, \ldots, 2.5$ with initial amplitudes $\alpha_1 = 6, \alpha_2 = 3$ (Fig. 4). These results were obtained numerically and represent the exact quantum solution of the model (5). One can observe how the cross-sections of the Q-functions change from circles (for initially coherent fields)

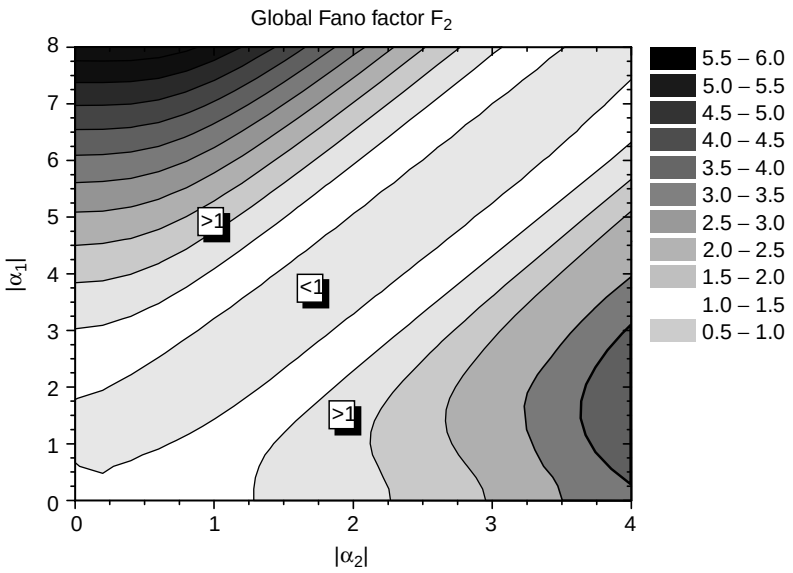

Figure 2. Global Fano factor, F^{G}_2, of the second-harmonic mode as a function of the initial coherent state amplitudes α_1 and α_2 with $\theta = 0$. It is seen that the harmonic mode exhibits globally sub-Poissonian behavior ($F^{\mathrm{G}}_2 < 1$) near the diagonal $|\alpha_1| = 2|\alpha_2|$ and $\theta = 0$.

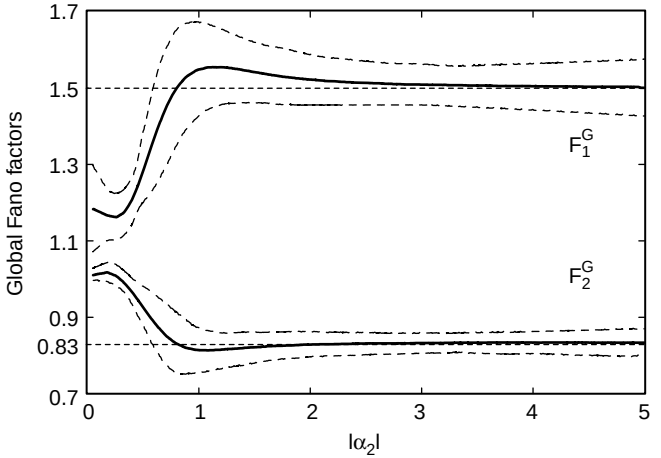

Figure 3. Global Fano factors F_1^G and F_2^G along the line $|\alpha_1| = 2|\alpha_2|$ for $\theta = 0$. Dotted lines denote the RMS deviation of oscillations in the long-time interaction. It's seen that the harmonic mode exhibits globally sub-Poissonian behavior.

through crescents into rings. We note that both modes have relatively small photon-number variances and small Fano factors, $F_1^Q \approx 1.50$ and $F_2^Q \approx 0.83$ [see also Fig. 1b]. The ring shapes, once formed, are very stable. So, not only the Fano factors, but the entire quantum states become stationary.

The Q functions are very wide, thus no linearization of the quantum problem is possible and no pure quantum technique can be used for estimation of the observed values $F_1^Q \approx 1.50$ and $F_2^Q \approx 0.83$. However, good quantitative explanation of these numerical values can be obtained by the method of classical trajectories as will be shown in Section II.B.

Our discussion is focused on photon-number statistics rather than squeezing or other phase-related properties. Nevertheless, by analyzing the Q-function evolution presented in Fig. 4, we can draw the conclusion that squeezing cannot be observed for initial coherent fields at interaction times exceeding the relaxation time. In fact, the quadrature squeezing variances ($k = 1, 2$)

$$S_k^Q \equiv \langle(\Delta\hat{X}_k)^2\rangle = \langle[\Delta(\hat{a}_k e^{-i\theta} + \hat{a}_k^\dagger e^{i\theta})]^2\rangle \tag{9}$$

are monotonically rising from the standard shot-noise-limit ($S_k^Q = 1$) to much more noisy state with the saturated quadrature variances

$$\begin{aligned} S_1^Q &= 1 + 8r^2 \gg 1 \\ S_2^Q &= 1 + 2r^2 \gg 1 \end{aligned} \tag{10}$$

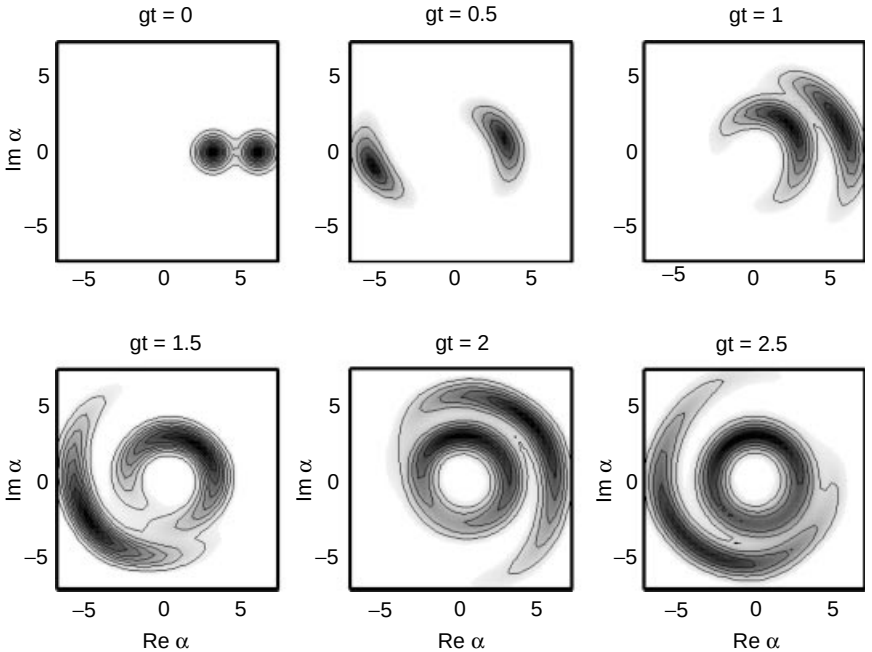

Figure 4. Quantum evolution of the Q function for the fundamental (outer contour plots) and the second-harmonic mode (inner plots) at six time moments for initial coherent states with $\alpha_1 = 6, \alpha_2 = 3, \theta = 0$. Solution obtained by quantum numerical method.

It is evident that the no-energy-transfer regime is not useful for the quadrature squeezing generation.

2. *Classical Analysis*

Complete quantum solution of the model given by Hamiltonian (5) can be found by applying sophisticated numeric methods on a fast computer only. However, since we are interested in a special type of solution for strong fields, we can adopt approximate classical and semiclassical methods to obtain some analytical results.

In analogy with Eq. (5), the classical model of SHG can be described by

$$\mathscr{H} = g[\alpha_1^2\alpha_2^* + (\alpha_1^*)^2\alpha_2] \tag{11}$$

where α_1 and α_2 are complex amplitudes of the fundamental and second-harmonic modes, respectively, and g is a nonlinear coupling parameter. The exact solution of the model, described by (11), is well-known [26]. The solution

is periodic and can be written in terms of the Jacobi elliptic function. A few special cases (e.g., the phase-matched second-harmonic generation) have monotonous solution described by hyperbolic functions. The classical solution is a good approximation for strong fields, for which gives correct predictions of the output light intensities and frequency conversion efficiency. Unfortunately, it cannot be used to describe the photocount noise and other statistical properties of generated light. Now, we will summarize some classical results, which we will use in the method of classical trajectories.

The Hamiltonian (11) for the classical SHG leads to the following system of complex differential equations [26]

$$\begin{aligned} \dot{\alpha}_1 &= -2ig\alpha_1^*\alpha_2 \\ \dot{\alpha}_2 &= -ig\alpha_1^2 \end{aligned} \tag{12}$$

One obtains, after substitution of $\alpha_k = r_k e^{i\phi_k}$, a new system of real equations for the amplitudes and phases:

$$\begin{aligned} \dot{r}_1 &= -2r_1 r_2 \sin\theta \\ \dot{r}_2 &= r_1^2 \sin\theta \\ \dot{\theta} &= \left(\frac{r_1^2}{r_2} - 4r_2\right)\cos\theta \end{aligned} \tag{13}$$

where $\theta = 2\phi_1 - \phi_2$. The system has two integrals of motion: $E = r_1^2 + 2r_2^2 = n_1 + 2n_2$ and $\Gamma = r_1^2 r_2 \cos\theta$. By extracting r_1 and θ from Eq. (13), we get the following equation for r_2:

$$(r_2\dot{r}_2/g)^2 + \Gamma^2 = r_2^2(E - 2r_2^2)^2 \tag{14}$$

or even in simpler form for the intensity $n_2 = r_2^2$:

$$\left(\frac{\dot{n}_2}{2g}\right)^2 + \Gamma^2 = n_2(E - 2n_2)^2 \tag{15}$$

Separation of t and n_2 leads to the equation

$$2g\,dt = \frac{dn_2}{\sqrt{n_2(E - 2n_2)^2 - \Gamma^2}} \tag{16}$$

which can be rewritten as

$$4g\,dt = \frac{dn_2}{\sqrt{(a - n_2)(b - n_2)(n_2 - c)}} \tag{17}$$

where the numbers a, b, c are the roots of cubic equation $n_2(E - 2n_2)^2 - \Gamma^2 = 0$. For $c \leq u \leq b < a$, the solution of Eq. (17) reads as

$$\int_c^u \frac{dx}{\sqrt{(a-x)(b-x)(x-c)}} = \frac{2}{\sqrt{a-c}} \operatorname{asn}\left(\sqrt{\frac{u-c}{b-c}}, k\right) \tag{18}$$

in terms of the inverse Jacobi elliptic function, $\operatorname{asn}(x, k)$, with parameter $k = \sqrt{\frac{b-c}{a-c}}$. Finally, the inversion of (18), gives the required solution

$$n_2(t) = c + (b-c)\operatorname{sn}^2[2g\sqrt{a-c}(t-t_0), k] \tag{19}$$

where $\operatorname{sn}(u, k)$ is the Jacobi elliptic function with the same parameter k. Solution (19) can be simplified in special cases. In particular, the well-known elementary solution is obtained for second-harmonic generation from vacuum, where $r_1(0) = r$ and $r_2(0) = 0$. In this case $k = 1$ and the Jacobi elliptic function simplifies to hyperbolic tangent. Thus, the solution reads as

$$\begin{aligned} r_1(t) &= r\cosh(\sqrt{2}rgt) \\ r_2(t) &= \frac{r}{\sqrt{2}}\tanh(\sqrt{2}rgt) \end{aligned} \tag{20}$$

and $\theta(t) = \pi/2$. Subharmonic generation does not occur in this classical model, since for $r_1(0) = 0$ and $r_2(0) = r$ implies that $r_1(t) = 0,\ r_2(t) = r$ for any evolution time t. Another important special case of solution (19) can be obtained for the initial zero phase difference, $\theta(0) = 0$, and the initial amplitudes satisfying $r_1(0) = 2r$ and $r_2(0) = r$. Here, $E = 6r^2,\ \Gamma = 4r^3,\ a = 4r^2,\ b = c = r^2,\ k = 0$ and Jacobi elliptic function simplifies to trigonometric sinus. Finally, this elementary solution reads as

$$\begin{aligned} \alpha_1(t) &= 2re^{-2irgt} \\ \alpha_2(t) &= re^{-4irgt} \end{aligned} \tag{21}$$

which corresponds to the no-energy-transfer regime, in which energy is conserved in every mode. Phase trajectories of that solution are presented in Fig. 5a. The slightly perturbed solution in the no-energy-transfer regime can also be approximated by $k \approx 0$ and elementary function sinus with small amplitude $(b - c) \approx 0$ (see Fig. 5b,c).

3. *Classical Trajectory Analysis*

The answer to our question concerning the origin of sub-Poissonian behavior can be found by the method of classical trajectories. The method is very general.

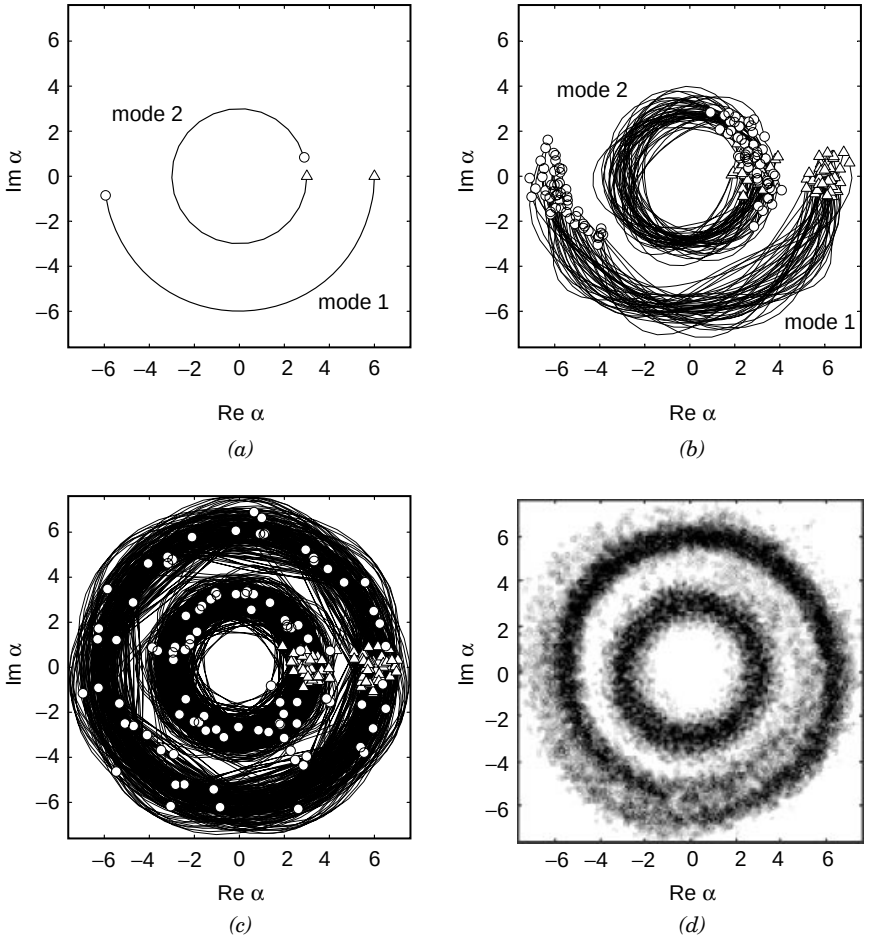

Figure 5. Classical trajectories of the fundamental and second-harmonic modes in the no-energy-transfer regime for $\alpha_1 = 6$ and $\alpha_2 = 3$: (a) classical evolution according to Eq. (19) for $0 < gt < 0.5$; (b) 50 random trajectories out of 10,000 trajectories used in the simulations for $0 < gt < 0.5$; (c) same as in (b), but for $0 < gt < 5$; (d) snapshot of the Q function, obtained from 10,000 random trajectories at time $gt = 5.0$. Triangles denote starting points ($gt = 0$) of the trajectories, and circles are their ends.

It can be applied in the analysis of almost every nonlinear quantum process. Even external pumping and energy losses can be easily described. In the classical trajectory approach to SHG [27], deterministic solutions of the classical SHG are used, while quantum noise of initial fields is artificially simulated by Gaussian distribution. One can study the time evolution of the bunch of

trajectories like the evolution of quantum distributions. This semiclassical method can often shed some light on complicated quantum dynamics. For strong inputs, where the quantum noise can be assumed small, the method gives surprisingly good results.

According to the classical trajectory method, one assumes that the input stochastic amplitudes are of the form

$$\begin{aligned} \alpha_1 &= r_1 + x_1 + iy_1 \\ \alpha_2 &= r_2 + x_2 + iy_2 \end{aligned} \tag{22}$$

where r_k are coherent complex amplitudes, whereas x_k and y_k are real and mutually independent Gaussian stochastic quantities with identical variances

$$\sigma^2 = \frac{1}{4} \ll r_k^2. \tag{23}$$

By analogy with our quantum analysis, we calculate the semiclassical Fano factor, defined by Eq. (1.4), and quadrature squeezing variance

$$S_k^{\mathrm{S}} \equiv \overline{(\Delta X_k)^2} = \overline{[\Delta(\alpha_k \mathrm{e}^{-i\theta} + \alpha_k^* \mathrm{e}^{i\theta})]^2} \tag{24}$$

as counterparts of quantum parameters (1) and (9), respectively. By applying the method of classical trajectories with the noise variance given by Eq. (23), we find the semiclassical quadrature squeezing and Fano factor given by

$$\begin{aligned} S_k^{\mathrm{S}} &= 4\sigma^2 = 1 \\ F_k^{\mathrm{S}} &\approx 4\sigma^2 = 1 \end{aligned} \tag{25}$$

respectively. According to the method described above, one needs to solve thousands of the classical SHG trajectories. The mean values are simply obtained by averaging over all these trajectories. In Fig. 6, we have presented graphically snapshots in a selected time interval of all complex solutions in phase space. These clouds of points naturally correspond to the Q functions in the quantum picture (see Fig. 4). We have found that this semiclassical method gives the results surprisingly similar to the quantum results even for relatively weak fields! This very good agreement is clearly seen by comparing Figs. 4 and 6, where the initial amplitudes are chosen to be $\alpha_1 = 6$, $\alpha_2 = 3$. The patterns given by 50 random trajectories out of the total number of 10,000 analyzed trajectories are shown in Fig. 5b in the time interval $gt \in (0, 0.5)$ and Fig. 5c in $gt \in (0, 5)$. The final snapshot of the "cloud" ring at $gt = 5$ is given in Fig. 5d.

The method of classical trajectories can be used not only numerically (Figs. 5 and 6) but also analytically in special cases. For example, the evolution of

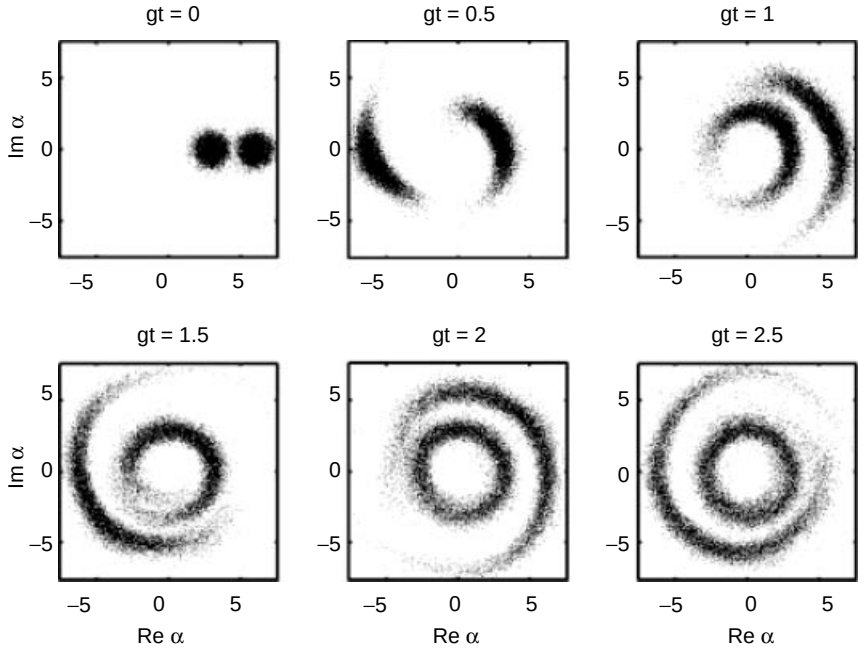

Figure 6. Classical trajectory simulation of quantum evolution of the Q function for the same initial conditions and interaction times as in Fig. 4. In our simulation 10,000 trajectories were calculated.

low-noise fields in the no-energy-transfer regime can be found analytically in the first approximation with the solution given by elementary trigonometric functions. To show this, let us analyze integrals of motions. On assuming the initial amplitudes of the forms $\alpha_1 = 2r + x_1 + iy_1$ and $\alpha_2 = r + x_2 + iy_2$, the integrals of motion can be expressed in the form of successive corrections

$$\begin{aligned} E &= 6r^2 + \Delta E_1 + \Delta E_0 \\ \Gamma &= 4r^3 + \Delta\Gamma_2 + \Delta\Gamma_1 + \Delta\Gamma_0 \end{aligned} \tag{26}$$

where we denote $\Delta E_1 = 4r(x_1 + x_2)$, $\Delta E_0 = x_1^2 + y_1^2 + 2(x_2^2 + y_2^2)$, and $\Delta\Gamma_2 = 4r^2(x_1 + x_2)$, $\Delta\Gamma_1 = r(x_1^2 - y_1^2 + 4x_1x_2)$ and $\Delta\Gamma_0 = x_2(x_1^2 - y_1^2) + 2x_1y_1y_2$. By substituting $n_2 = E/6 + \epsilon$, where ϵ is a small correction, and after omitting the cubic term $2\epsilon^3$, we find that the denominator in Eq. (16) can be approximated by the quadratic function

$$n_2(E - 2n_2)^2 - \Gamma^2 \approx 2E(A^2 - \epsilon^2) \tag{27}$$

Now, we can perform integration of these elementary functions leading to the simple result

$$n_2(t) = r^2 + B + A\cos\Omega gt \tag{28}$$

where $\Omega = \sqrt{8E}$, $A = \frac{2}{3}r\sqrt{(x_1 - 2x_2)^2 + 3(y_1^2 + y_2^2)}$ and $B = \frac{2}{3}r(x_1 + x_2)$ We get a similar result

$$n_1(t) = E - 2n_2 = 4r^2 + 4B - 2A\cos\Omega gt \tag{29}$$

for the fundamental (or subharmonic) mode. Both solutions are constant functions weakly perturbed by harmonic function. The evolution in phase space can be understood clearly by analyzing Figs. 5 and 6. Because of the frequency dispersion $\Omega(\{x_k, y_k\})$ (see Fig. 5b,c), different trajectories are drifting variously and create a crescent-shaped cloud in phase space, which develops later into a full ring as seen in Figs. 5 and 6. One has to perform the averaging of solutions to calculate the required statistical moments. We find $\overline{n}_1 = 4r^2$, $\overline{n}_2 = r^2$, and

$$\begin{aligned} \overline{n_1^2} &= 16r^4 + 16\overline{B^2} + 2\overline{A^2} \\ \overline{n_2^2} &= r^4 + \overline{B^2} + \frac{1}{2}\overline{A^2} \end{aligned} \tag{30}$$

where $\overline{B} = 0, \overline{A^2} = \frac{44}{9}r^2\sigma^2 = \frac{11}{9}r^2, \overline{B^2} = \frac{8}{9}r^2\sigma^2 = \frac{2}{9}r^2$ and $\overline{\cos^2\Omega gt} = \frac{1}{2}$. Finally, we arrive at the semiclassical Fano factors given by simple rational numbers:

$$\begin{aligned} F_1^{\mathrm{S}} &= \frac{1}{r^2}\left(4\overline{B^2} + \frac{1}{2}\overline{A^2}\right) = \frac{3}{2} \\ F_2^{\mathrm{S}} &= \frac{1}{r^2}\left(\overline{B^2} + \frac{1}{2}\overline{A^2}\right) = \frac{5}{6} \end{aligned} \tag{31}$$

By analyzing Figs. 1b and 3 as well as Tables I and II, we conclude that our estimations (31) are in very good agreement with those values of Fano factors obtained by the quantum numerical analysis of Section II.B.

C. Higher-Harmonic Generation

1. *Quantum Analysis*

In this section, we will generalize our results of Section II. B to describe the processes of the Nth-harmonic generation. Again, we will focus on predictions of the sub-Poissonian photon-number statistics.

TABLE I
Quasistationary Values of the Quantum Fano Factors F_1^Q and their Semiclassical Approximations F_1^S, Given by Eq. (54), for the Fundamental Mode in Nth-Harmonic Generation with $N = 1 - 5$ in No-Energy-Transfer Regime[a]

N	F_1^Q	F_1^S	$(F_1^Q\text{-}F_1^S)/F_1^Q$
1	1	1	0
2	1.5029291	$\frac{3}{2}$	0.0020
3	1.8202032	$\frac{29}{16}$	0.0042
4	2.0323293	$\frac{101}{50}$	0.0061
5	2.1830414	$\frac{13}{6}$	0.0075

[a]The values of F_1^Q are calculated for $r = r_N = 5$.

TABLE II
Same as in Table I, but for the Nth-Harmonic Mode; F_N^S Calculated From Eq. (155)

N	F_N^Q	F_N^S	$\lvert F_N^Q - F_N^S\rvert/F_N^Q$
1	1	1	0
2	0.83228800	$\frac{5}{6}$	0.0013
3	0.81125970	$\frac{13}{16}$	0.0015
4	0.81924902	$\frac{41}{50}$	0.00092
5	0.8333127	$\frac{5}{6}$	0.000026

Processes of the Nth-harmonic or subharmonic generation can be described by the conventional interaction Hamiltonian [5]

$$\hat{H} = \hbar g\left(\hat{a}_1^N \hat{a}_N^\dagger + \hat{a}_1^{\dagger N} \hat{a}_N\right) \tag{32}$$

for $N = 2, 3, \ldots$. In (32), $\hat{a}_1$ and $\hat{a}_N$ denote annihilation operators of the fundamental and Nth-harmonic modes, respectively, and g is a nonlinear coupling parameter. For short evolution times, the following approximation of the quantum Fano factors can be obtained for the fundamental mode [13]

$$F_1^{\mathrm{Q}} = 1 - 2N(N-1)r_1^{N-2} r_2 \sin\theta\, gt + \mathcal{O}\{(gt)^2\} \tag{33}$$

with $N = 2, 3, \ldots$, and for higher harmonics:

$$\begin{aligned} F_3^{\mathrm{Q}} &= 1 - 36 r_1^3 r_2 \left(r_1^2 + 2\right) \sin\theta\, (gt)^3 + \mathcal{O}\{(gt)^4\} \\ F_4^{\mathrm{Q}} &= 1 - 64 r_1^4 r_2 (17 + 12 r_1^2 + 2 r_1^4) \sin\theta\, (gt)^3 + \mathcal{O}\{(gt)^4\} \end{aligned} \tag{34}$$

where r_k are input amplitudes, and $\theta = N\phi_1 - \phi_N$ is the input phase mismatch. For spontaneous harmonic generation (i.e., for $r_N = 0$), Eqs. (33)–(34) simplify to the formulas derived by Kozierowski and Kielich [14]. This analysis shows the possibility of sub-Poissonian light generation in short-time regime under the proper phase condition.

On testing different coherent input amplitudes and phases in order to minimize the Fano factor for long interaction times, we have discovered a regime for which the harmonic field exhibits the quasistationary sub-Poissonian photocount noise. The regime occurs if the ratio of amplitudes $|\alpha_1|$ and $|\alpha_N|$ is equal to N, and phases are related by $N\phi_1 = \phi_N$. As described in Section II. B for SHG, this is a quantum analog of the no-energy-transfer regime [25] known from classical nonlinear optics as an evolution exhibiting the no-energy transfer between the interacting modes. The intensities of both modes remain quasi-stationary during the interaction. Obviously, in quantum analysis some small energy fluctuations between modes are observed as a consequence of vacuum fluctuations. However, the influence of energy fluctuations can be neglected for strong fields.

For better comparison of theoretical predictions for different-order processes, we have plotted the quantum Fano factors for both interacting modes in the no-energy-transfer regime with $N = 2 - 5$ and $r = 5$ in Fig. 7. One can see that all curves start from $F^{\mathrm{Q}}_{1,N}(0) = 1$ for the input coherent fields and become quasi-stationary after some relaxations. The quantum and semiclassical Fano factors coincide for high-intensity fields and longer times, specifically for $t \geq 50/(\bar{\Omega}g)$, where $\bar{\Omega}$ will be defined later by Eq. (54). In Fig. 17, we observe that all fundamental modes remain super-Poissonian $[F^{\mathrm{Q}}_1(t) > 1]$, whereas the Nth harmonics become sub-Poissonian $(F^{\mathrm{Q}}_N(t) < 1)$. The most suppressed noise is observed for the third harmonic with the Fano factor $F^{\mathrm{Q}}_3 \approx 0.81$. In Fig. 7, we have included the predictions of the classical trajectory method (plotted by dotted lines) to show that they properly fit the exact quantum results (full curves) for the evolution times $t \geq 50/(\bar{\Omega}g)$. The small residual differences result from the fact that the amplitude r was chosen to be relatively small ($r = 5$). This value does not precisely fulfill the condition $r \gg 1$. We have taken $r = 5$ as a compromise between the asymptotic value $r \to \infty$ and computational complexity to manipulate the matrices of dimensions 1000×1000. Unfortunately, we cannot increase amplitude r arbitrary due to computational limitations.

Numerical values of the quantum Fano factors in comparison to their semiclassical approximations for the fundamental mode, given by Eq. (56), are presented in their dependence on N in Table I and Fig. 8a. Analogously, those values for harmonics are presented in Fig. 8b and Table II as calculated by the numerical quantum method and from analytical semiclassical formula (57). It is seen that the approximate predictions of the Fano factors, according to (56)

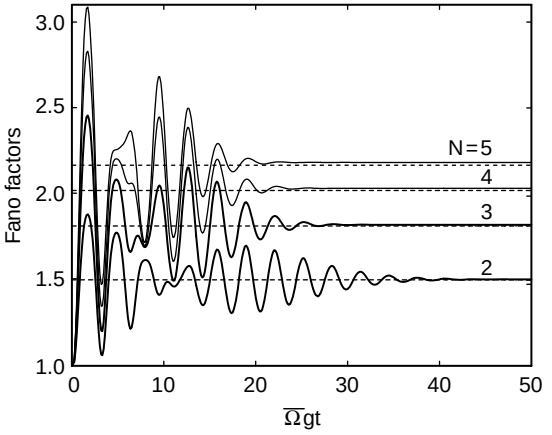

(a)

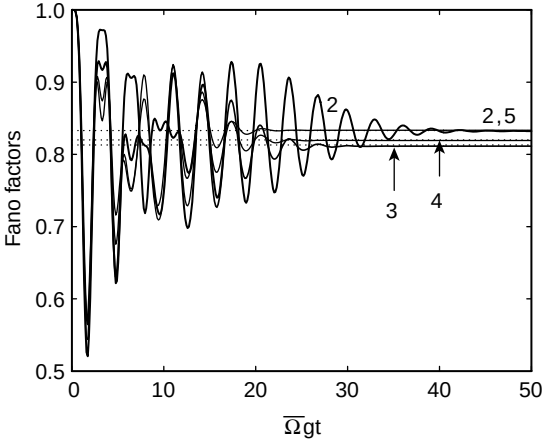

(b)

Figure 7. Time evolution of the exact quantum Fano factors: (a) $F_1^{\mathrm{Q}} = F_1^{\mathrm{Q}}(N)$ for the fundamental mode and (b) F_N^{Q} for the harmonic mode in Nth-harmonic generation for $N = 2$ (thickest curve), 3, 4 and 5 (thinnest curve). Time t is rescaled with frequency $\bar{\Omega}$, given by (52), and coupling constant g. The harmonic mode amplitude is $r = r_N = 5$. The dotted lines correspond to the semiclassical Fano factors, given by (54) and (55). It is seen that the fundamental mode is super-Poissonian, whereas the harmonic mode is sub-Poissonian for all nonzero evolution times.

and (57), fit very well the values obtained by applying the numerical quantum method. In fact, the differences between the approximate and exact values are hardly visible on the scale of Fig. 8. Nevertheless, some small ($< 1\%$) differences in $F_{1,N}^{\mathrm{Q}}$ (see Tables I and II) can be explained by the fact that the value of r for numerical analysis was chosen too small.

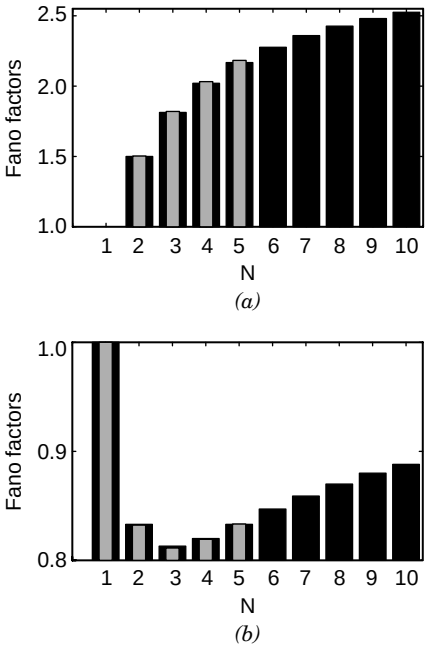

Figure 8. Semiclassical (solid bars) and quantum (dithered bars) Fano factors versus order N of harmonic generation for (a) fundamental and (b) Nth-harmonic modes in the quasistationary no-energy-transfer regime. Panels (a) and (b), for $N = 1 - 5$, correspond to Tables I and II, respectively. It is seen that the quantum results are well fitted by the semiclassical Fano factors. According to both analyses, the third-harmonic mode has the most suppressed photocount noise.

2. *Classical Analysis*

Our classical analysis of higher-harmonic generation follows the same method as described in Sect. II. B. The classical model of the Nth-harmonic generation can be described by

$$\mathscr{H} = g\left[\alpha_1^N \alpha_N^* + (\alpha_1^*)^N \alpha_N\right] \tag{35}$$

which in a special case of $N = 2$ goes over into Eq. (11). In Eq. (35), α_1 (α_N) is the complex amplitude of the fundamental (Nth-harmonic) mode. The Hamiltonian (35) leads to the pair of complex differential equations [26]

$$\begin{aligned} \dot{\alpha}_1 &= -\mathrm{i}gN\alpha_1^{*N-1}\alpha_N \\ \dot{\alpha}_N &= -\mathrm{i}g\alpha_1^N \end{aligned} \tag{36}$$

On introducing real amplitudes and phases, $\alpha_k = r_k e^{i\phi_k}$, (36) can be transformed into a system of three real equations:

$$\begin{aligned}\dot{r}_1 &= -gNr_1^{N-1} r_N \sin\theta \\ \dot{r}_N &= g r_1^N \sin\theta \\ \dot{\theta} &= g\left(\frac{r_1^N}{r_N} - N^2 r_1^{N-2} r_N\right)\cos\theta\end{aligned} \tag{37}$$

where $\theta = N\phi_1 - \phi_N$ is the phase mismatch. Equations (37) have two integrals of motion:

$$\begin{aligned}E &= r_1^2 + Nr_N^2 = n_1 + Nn_N \\ \Gamma &= r_1^N r_N \cos\theta\end{aligned} \tag{38}$$

On extraction of r_1 and θ from Eq. (37), we find an equation for the amplitude r_N:

$$\left(\frac{r_N \dot{r}_N}{g}\right)^2 + \Gamma^2 = r_N^2 \left(E - Nr_N^2\right)^N \tag{38}$$

or its simpler form for the intensity $n_N = r_N^2$:

$$\left(\frac{\dot{n}_N}{2g}\right)^2 = n_N (E - Nn_N)^N - \Gamma^2 \tag{40}$$

The general solution for $n_N(t)$ is a periodic function oscillating between the values $n_{\min}$ and $n_{\max}$. The solution can be given in terms of the Jacobi elliptic functions for $N = 2$ and $N = 3$, and in terms of hyperelliptic functions for $N > 3$.

One elementary solution of set of Eqs. (37) is obtained for the zero initial phase mismatch $\theta = 0$ and the initial amplitudes satisfying the condition $r_1 = Nr_N$. The solution reads as

$$\begin{aligned}\alpha_1(t) &= r_1 \exp\left(-igtr_1^{N-1}\right) \\ \alpha_N(t) &= r_N \exp\left(-iNgtr_1^{N-1}\right)\end{aligned} \tag{41}$$

which corresponds to the no-energy-transfer regime, since the amplitude and energy in both the interacting modes remain constant $n_1(t) = |\alpha_1(t)|^2 = r_1^2$ and $n_N(t) = |\alpha_N(t)|^2 = r_N^2$ [25].

3. *Classical Trajectory Analysis*

The results of Section II.C can be used in the method of classical trajectories in analogy with the technique described in Section II. B. We need to express the trajectories in their dependence on small noise parameters x_k and y_k. The integrals of motion, given by (38), can be expressed in a form of corrections in successive powers of large r:

$$E = N(N+1)r^2 + \Delta E_1 + \Delta E_0 \tag{42}$$

where

$$\begin{aligned} \Delta E_1 &= 2N(x_1 + x_N)r \\ \Delta E_0 &= x_1^2 + y_1^2 + N\left(x_N^2 + y_N^2\right) \end{aligned} \tag{43}$$

and

$$\Gamma = N^N r^{N+1} + \Delta\Gamma_N + \Delta\Gamma_{N-1} + \Delta\Gamma_{N-2} + \cdots \tag{44}$$

where

$$\begin{aligned} \Delta\Gamma_N &= (x_1 + x_N)(Nr)^N \\ \Delta\Gamma_{N-1} &= \left[\frac{N-1}{2}\left(x_1^2 - y_1^2\right) + N(x_1 x_N + y_1 y_N)\right](Nr)^{N-1} \end{aligned} \tag{45}$$

The lower-order terms $\Delta\Gamma_{N-2}$, $\Delta\Gamma_{N-3}, \ldots$ can be neglected in further considerations. On assumption of high-intensity fields ($r \gg 1$), we can substitute

$$n_N = \frac{E}{N(N+1)} + \epsilon \tag{46}$$

where ϵ is a small correction of stationary value. Then, the right-hand side of (40) can be rewritten as

$$n_N(E - Nn_N)^N - \Gamma^2 \approx \frac{N^N}{2(N+1)^{N-2}} E^{N-1}\left(A^2 - \epsilon^2\right) \tag{47}$$

on omission of higher-order terms involving $\epsilon^3, \epsilon^4, \ldots$. One arrives at the simple equation

$$\left(\frac{\dot{\epsilon}}{2g}\right)^2 = \frac{N^N}{2(N+1)^{N-2}} E^{N-1}\left(A^2 - \epsilon^2\right) \tag{48}$$

Thus, the solution of (40) reads as

$$n_N(t) = r^2 + B + A \sin \Omega g t \tag{49}$$

where the frequency Ω is given by

$$\Omega = \sqrt{\frac{2N^N E^{N-1}}{(N+1)^{N-2}}} \tag{50}$$

and

$$\begin{aligned} A &= \frac{r}{N+1}\sqrt{4(x_1 - Nx_N)^2 + 2N(N+1)(y_1 - y_N)^2} \\ B &= \frac{\Delta E_1}{N(N+1)} = \frac{2}{N+1} r(x_1 + x_N) \end{aligned} \tag{51}$$

From (38), a result similar to that from (49) is obtained for the fundamental mode:

$$n_1(t) = E - Nn_N(t) = N^2 r^2 + N^2 B - NA \sin \Omega g t \tag{52}$$

It is seen that both solutions (49) and (52) are given in a form of large constants weakly perturbed by harmonic function.

Now, on applying the classical trajectory method, one should perform averaging over all solutions (49) and (52) to calculate the required statistical moments. Here, we calculate the first and second-order field intensity moments necessary for determination of the Fano factors. The mean intensities of the fundamental and harmonic modes are simply given by $\bar{n}_1 = N^2 r^2$ and $\bar{n}_N = r^2$, respectively. The second-order moments of field intensity are found to be

$$\begin{aligned} \overline{n_1^2} &= N^4 r^4 + N^4 \overline{B^2} + \frac{1}{2} N^2 \overline{A^2} \\ \overline{n_N^2} &= r^4 + \overline{B^2} + \frac{1}{2}\overline{A^2} \end{aligned} \tag{53}$$

in terms of $\overline{A^2} = r^2(2N^2 + N + 1)/(N+1)^2$ and $\overline{B^2} = 2r^2/(N+1)^2$. We note that $\bar{B}$ vanishes. The term $\overline{\sin^2 \Omega g t}$ can simply be estimated with $\frac{1}{2}$ for sufficiently long time t, when $n_k(t)$ and $F_k^{\mathrm{Q}}(t)$ become quasistationary. The relaxation in $n_k(t)$ and $F_k^{\mathrm{Q}}(t)$ is observed for short times t, due to the presence of harmonic sine function and residual phase synchronization. The mean value of the frequency (50), given by

$$\bar{\Omega} \approx \sqrt{2N(N+1)}(Nr)^{N-1} \tag{54}$$

enables estimation of the oscillation period $T_{\mathrm{osc}} = 2\pi/\overline{\Omega}$, whereas the standard deviation

$$\Delta\Omega \approx \sqrt{2N(N+1)}N^{N-1}r^{N-2}\frac{N-1}{N+1} \tag{55}$$

determines the duration $T_{\mathrm{rel}} = 2\pi/\Delta\Omega$ of relaxation. By comparing the characteristic times T_{osc} and T_{rel}, one finds that the evolution time can be scaled by $\tau = \bar{\Omega}gt$ to synchronize optimally the oscillations of the exact quantum solutions for different N. These synchronized oscillations of the Fano factors are clearly presented in Fig. 7.

Finally, we arrive at the semiclassical Fano factors

$$F_1^{\mathrm{S}} = \frac{1}{2}\frac{6N^2+N+1}{(N+1)^2} \tag{56}$$

$$F_N^{\mathrm{S}} = \frac{1}{2}\frac{2N^2+N+5}{(N+1)^2} \tag{57}$$

which are the compact-form analogs of the quantum Fano factors. The semiclassical Fano factors for the fundamental and higher harmonics for various values of N are listed in Tables I and II, and plotted in Fig. 7a and b, respectively.

Our solutions (56) and (57) reduce to the results derived in Ref. 21 for $N = 2$, and those of Ref. 22 for $N = 3$. By analyzing (57), we find that higher harmonics evolve into quasistationary sub-Poissonian states ($F_N^{\mathrm{S}} < 1$) for any $N > 1$. Except for second harmonic, the photocount noise reduction in higher harmonics becomes less effective with increasing N. Thus, the deepest noise reduction occurs for the third harmonic as described by the Fano factor $F_3^{\mathrm{S}} = \frac{13}{16} = 0.8125$. The photocount noise reductions for the second and fifth harmonics are predicted to be the same, although the quantum analysis (see Table II) reveals that they differ slightly ($< 1\%$). As comes from (56), the fundamental mode has solely the super-Poissonian photocount statistics ($F_1^{\mathrm{S}} > 1$) with noise monotonically growing in N for the no-energy-transfer regime. For $N = 1$, the process is linear and no change in the photon statistics occurs. The interacting modes remain coherent with the unit Fano factors for both modes. It is worth noting that qualitatively different photocount statistics of the fundamental mode is observed in the short-interaction regime as given by Eqs. (6) and (33)–(34).

We have shown, in agreement with the results presented in Ref. 21, that the method of classical trajectories gives very good predictions in the case of strong-field interactions (i.e., for the photon numbers larger than 10). The calculation speed of the method does not depend on numbers of interacting

photons. But a better approximation is achieved with the increasing number of photons. Thus, the method is very fast and significantly simplifies the tedious exact quantum calculations.

D. Conclusion

We have presented quantum, classical and semiclassical descriptions of second- and higher harmonic generations. We have demonstrated that these processes can be a source of sub-Poissonian light. On testing different coherent input amplitudes and phases in order to minimize the Fano factor, we have discovered a quantum regime for which the long-interaction output is generated with the quasi-stationary sub-Poissonian photocount noise [21–23]. The regime occurs if the initial coherent state amplitudes are related by $|\alpha_1| = N|\alpha_N|$ and $\mathrm{Arg}(\alpha_N) \simeq N\mathrm{Arg}(\alpha_1)$. This is a quantum analog of the no-energy-transfer regime [25] known in classical nonlinear optics as an evolution exhibiting no-energy transfer between the interacting modes. The intensities of both modes remain quasiconstant in time during the interaction. Obviously, in a quantum analysis some small energy fluctuations between modes are observed as a consequence of vacuum fluctuations. However, the influence of energy fluctuations can be neglected for strong fields.

We have proved that in the no-energy-transfer regime, the fundamental mode evolves into a quasistationary state with the super-Poissonian ($F_1^{\mathrm{Q}} > 1$) photocount statistics, whereas the Nth harmonic goes over into a sub-Poissonian ($F_N^{\mathrm{Q}} < 1$) quasistationary state. We have found that the most suppressed photocount noise is obtained for the third harmonic as described by the quantum Fano factor $F_3^{\mathrm{Q}} = 0.811\ldots$. Good analytical predictions of the quantum Fano factors for both the fundamental and harmonic modes ($F_3^{\mathrm{S}} = \frac{13}{16} = 0.8125$) were obtained under the semiclassical approximation in the strong-field limit.

III. PHOTON BUNCHING AND ANTIBUNCHING EFFECTS IN NONSTATIONARY FIELDS (*A. MIRANOWICZ, J. BAJER, M. KOASHI, and N. IMOTO*)

A. Introduction

In the 1950s, Hanbury-Brown and Twiss [28] carried out the fundamental measurements of photon-number correlations demonstrating that photons of classical light exhibit a tendency to distribute themselves preferentially in bunches rather than at random. This effect was coined the *photon bunching* (PB). The Hanbury-Brown and Twiss experiments have triggered theoretical and experimental search for light exhibiting effect opposite to PB, namely, the so-called *photon antibunching* (PAB). It was first observed in the process of resonance fluorescence from an atom by Kimble et al. [29] only 20 years after the first demonstration of PB [28]. Subsequent generations of PAB in resonance

fluorescence were reported in Ref. 30. Antibunched light was also generated in other processes, including parametric downconversion [31], degenerate [32] and nondegenerate [33] parametric amplification, or destructive two-photon interference [34]. Analysis of PB and PAB effects in nonlinear optical systems has been one of the hot topics of quantum optics for several decades [35–38].

It is a well known fact, that the PAB of stationary fields is one of the manifestations of nonclassical properties of light. PAB cannot be understood within the classical field theory describing light as a wave. But, on the other hand, it has a simple interpretation in particle (photon) models by the rise of the joint probability of two detected particles upon the increase of their time separation τ close to zero.

In this chapter we would like to address the following question: how to describe PB and PAB in non-stationary fields in a way closest to the original photodetection interpretation of the effect in stationary field regime, having a guarantee that the PAB cannot occur for classical light. PAB of non-stationary fields has already been analyzed theoretically in various nonlinear optical models [39–44]. Here, we show that the approaches developed for stationary fields, when applied directly to analyze the non-stationary fields, are by no means unique and might lead to self-contradictory predictions [45]. And what is more counterintuitive, we will show that, in some cases, the standard definitions do not exclude the possibility of observation of the PAB artifacts in classical nonstationary fields [46].

The *classical light* is usually defined [35,36] to be one for which the Glauber-Sudarshan P function, namely, the weight factor in the coherent state representation of the density matrix

$$\hat{\rho} = \int d^2\{\alpha_j\} P(\{\alpha_j\}) |\{\alpha_j\}\rangle\langle\{\alpha_j\}| \tag{58}$$

is a probability distribution, that is, nonnegative and cannot be more singular than the Dirac δ function. Otherwise, the state is nonclassical. In Eq. (58), the compact notation for the multimode field is used, where the argument $\{\alpha_j\}$ stands for $(\alpha_1, \alpha_2, \ldots)$.

To test various definitions of photon antibunching, we analyze a parametric frequency conversion—a process of exchanging photons between signal and idler optical modes of different frequencies. It is one of the most fundamental models in quantum optics both from theoretical and experimental viewpoints. The model has been successfully applied to describe various optical phenomena. In particular, wave mixing and beamsplitting [36,47], Raman scattering [36,48], a two-level atom driven by a single-mode electromagnetic field [49] or, by straightforward generalization, coherent or incoherent spontaneous emission from a system of N two-level atoms [50]. There have been great advances in the

construction of frequency converters since the late 1950s. The frequency conversion devices are based on the coupling of light waves in, for instance, nonlinear dielectric crystals such as KDP, $LiNbO_3$, or $LiIO_3$ [51]. A simple quantum description of the parametric frequency conversion was given by Louisell [52]. The remarkable property of the Louisell model is the classical-like evolution or, explicitly, the conservation of quasidistributions along classical trajectories as was predicted by Glauber [53] and experimentally observed by Huang and Kumar [54] for initial quantum states. Our interest in the frequency conversion comes from this conservation of the initial (classical or quantum) character of the fields during the process.

This paper is organized as follows. In Section II.B, we give a short account of the most popular definitions of PAB and we propose a generalized definition. In Section II.C, we briefly review the parametric frequency converter model and Glauber's theorem useful for our analysis of PAB. In Section II.D, we show discrepancies between three definitions of PAB for quantum nonstationary fields. In Section III.E, we show that there are classical non-stationary fields exhibiting apparently PAB according to the standard definitions.

B. Criteria for Photon Antibunching

The central role in definitions of PAB in a single-mode radiation field plays the intensity correlation function [55]

$$G^{(2)}(t,t+\tau) = \langle \mathscr{T} : \hat{n}(t)\hat{n}(t+\tau) : \rangle = (\alpha c S)^{-2} P_2(t,t+\tau) \tag{59}$$

where $\hat{n}(t)$ denotes the photon-number density operator, and products of the operators are written in normal order (: :) and in time order ($\mathscr{T}$). As was proved by Glauber [55], $G^{(2)}(t,t+\tau)$ is directly related to the joint detection probability, $P_2(t,t+\tau)$, of detecting two photons, one at time t and another at time $(t+\tau)$, by photodetector of quantum efficiency α with photocathode of area S. In Eq. (59), c denotes the light velocity; the space coordinates are suppressed and only one photodetector is assumed.

Different normalizations of $G^{(2)}(t,t+\tau)$ can be applied in the analysis of photon-number correlations. Here, we analyze the normalized two-time second-order intensity correlation functions defined as

$$\begin{aligned} g_{\mathrm{I}}^{(2)}(t,t+\tau) &= \frac{G^{(2)}(t,t+\tau)}{[G^{(1)}(t)]^2} \\ g_{\mathrm{II}}^{(2)}(t,t+\tau) &= \frac{G^{(2)}(t,t+\tau)}{G^{(1)}(t)G^{(1)}(t+\tau)} \\ g_{\mathrm{III}}^{(2)}(t,t+\tau) &= \frac{G^{(2)}(t,t+\tau)}{\sqrt{G^{(2)}(t,t)G^{(2)}(t+\tau,t+\tau)}} \end{aligned} \tag{60}$$

where $G^{(1)}(t) = \langle n(t)\rangle = \langle \widehat{a}^\dagger(t)\widehat{a}(t)\rangle$ is the light intensity. Yet another definition can be obtained if the correlation function $g^{(2)}_{\rm III}(t, t+\tau)$ can be replaced by the so-called correlation coefficient [56]

$$\bar{g}^{(2)}_{\rm III}(t, t+\tau) \equiv \frac{{\rm Cov}\{\hat{n}(t), \hat{n}(t+\tau)\}}{\sigma\{\hat{n}(t)\}\sigma\{\hat{n}(t+\tau)\}} = \frac{\bar{G}^{(2)}(t, t+\tau)}{\sqrt{\bar{G}^{(2)}(t,t)\bar{G}^{(2)}(t+\tau, t+\tau)}} \tag{61}$$

where $\bar{G}^{(2)}(t, t+\tau) \equiv G^{(2)}(t, t+\tau) - G^{(1)}(t)G^{(1)}(t+\tau)$ is the covariance in time and normal order, and $\sigma\{\hat{n}(t)\} = \sqrt{\bar{G}^{(2)}(t,t)}$ is the standard deviation. The correlation coefficient has well-known properties and simple geometrical interpretation applied in probability theory and mathematical statistics [56].

The *photon antibunching* according to the jth ($j = {\rm I, II, III}$) definition occurs if the normalized intensity correlation function $g^{(2)}_j(t, t+\tau)$ increases from its initial value at $\tau = 0$;

$$\Delta g_j(t, t+\tau) \equiv g^{(2)}_j(t, t+\tau) - g^{(2)}_j(t,t) > 0 \tag{62}$$

The *photon bunching* occurs for decreasing correlation function $g^{(2)}_j(t, t+\tau)$, whereas *photon unbunching* takes place if $g^{(2)}_j(t, t+\tau)$ is locally constant. Alternatively, on assumption that $g_j(t, t+\tau)$ is a well-behaved function of τ, the PAB according to the jth definition occurs if the lowest-order (say, n_0) nonvanishing derivative of $g^{(2)}_j(t, t+\tau)$ [or $\Delta g_j(t, t+\tau)$] is positive at $\tau = 0$, i.e., exists such $n_0 \geq 1$ that

$$\gamma_j(t) \equiv \gamma^{(n_0)}_j(t) = \frac{\partial^{n_0}}{\partial\tau^{n_0}} g^{(2)}_j(t, t+\tau)\bigg|_{\tau=0} > 0 \tag{63}$$

if the derivatives $(\partial/\partial\tau)^n g^{(2)}_j(t, t+\tau)$ vanish at $\tau = 0$ for $n = 1, \ldots n_0 - 1$. The field exhibits PB if the lowest-order nonvanishing derivative, $\gamma_j(t)$, is negative. If the derivatives of all orders vanish, $\gamma_j(t) = 0$, the field is said to be unbunched. In the Sections III.D and III.E, we will use both parameters $\gamma_j(t)$ and correlation functions $\Delta g_j(t, t+\tau)$ to analyze PB and PAB effects in a model of frequency conversion.

Both Def. I (see Ref. 36 and references cited therein) and Def. II (see, e.g., Ref. 37) have been applied to analyze PAB of nonstationary light generated in various nonlinear optical processes. In particular, analysis of PAB in *nonstationary* light has been studied by, for instance Singh [43] and Feng et al. [44] with the help of Def. I, and by, for instance, Kryszewski and Chrostowski [39], Srinivasan and Udayabaskaran [40], Dung et al. [41], and Aliskenderov et al. [42] by applying Def. II.

For stationary fields, namely, fields satisfying the property $G^{(2)}(t, t+\tau) = G^{(2)}(\tau)$, Defs. I–III are equivalent up to τ-independent function. In Section III.D, we will show that the predictions of PAB according to Defs. I–III can be essentially different for nonstationary fields, even though they coincide in stationary fields. Differences between various approaches to PAB result from the normalization functions of $G^{(2)}(t, t+\tau)$, which for Def. I is independent of τ, whereas in cases of Defs. II and III, the normalizations are τ-dependent but in two not equivalent ways for nonstationary fields.

The Cauchy-Schwarz inequality,

$$\left[G^{(2)}(t, t+\tau)\right]^2 \leq G^{(2)}(t, t) G^{(2)}(t+\tau, t+\tau) \tag{64}$$

must be fulfilled for any classical field. Thus, the violation of inequality (64) can reflect the corpuscular nature of light and can serve as a criterion of PAB. All definitions of the PAB effect for stationary fields are based on the Cauchy–Schwarz inequality. However, for non-stationary fields, PAB according to Defs. I and II does not imply violation of the Cauchy-Schwarz inequality (64). In Section III.E, we will give examples of classical nonstationary fields exhibiting apparently PAB according to Defs. I and II. By contrast, PAB according to Def. III occurs for nonclassical fields only, independent of the stationary field condition. This conclusion is readily obtained by comparing the form of the correlation functions $g^{(2)}_{\mathrm{III}}(t, t+\tau)$ with the Cauchy–Schwarz inequality, given by (64).

C. Model for Testing Photon Antibunching

We will test different approaches to PB and PAB in a process of parametric frequency conversion. The model can be described by the interaction Hamiltonian [52]:

$$\hat{H}_{\mathrm{int}} = \hbar\kappa \hat{a}_a \hat{a}_{\mathrm{b}}^{\dagger} \exp\left(\mathrm{i}\ \Delta\omega t\right) + \mathrm{H.c.} \tag{65}$$

where $\Delta\omega = \omega_L + \omega_b - \omega_a$, and $\hat{a}_{a,b}$ are the annihilation operators for the signal (with subscript a) and idler (subscript b) modes; κ is the real coupling constant (H.c. denotes Hermitian conjugation). For simplicity, we analyze only the resonance case for $\Delta\omega = 0$. One can interpret the process described by Eq. (65) as the conversion of frequency ω_a to ω_b assisted by intensive classical light of frequency ω_L. Thus, instead of exact quantum Hamiltonian describing the three-photon interaction, $\hat{H}_{\mathrm{int}} = \hbar\kappa' \hat{a}_L \hat{a}_a \hat{a}_b^{\dagger} + \mathrm{H.c.}$, we use its approximation given by (65), where the amplitude of classical light is included in the coupling constant $\kappa = \kappa' \langle \hat{a}_L \rangle = \kappa' \alpha_L$. Model given by Eq. (65) can be realized by a beamsplitter.

The solutions of the Heisenberg equation of motion for the signal and idler modes are [52]

$$\hat{a}_j(t) = \cos\left(\kappa t\right) \hat{a}_j - i \sin\left(\kappa t\right) \hat{a}_k \tag{66}$$

where $\hat{a}_j \equiv \hat{a}_j(0)$, $j = a, b$ and $k = b, a$, respectively. According to Glauber's theorem [53], the two-mode Glauber–Sudarshan P function can be given by

$$P(\alpha_a, \alpha_b, t) = P\{\alpha_a(-t), \alpha_b(-t), 0\} \tag{67}$$

where

$$\alpha_j(t) = \cos(\kappa t)\alpha_j - i\sin(\kappa t)\alpha_k \tag{68}$$

are the solutions of classical equations of motion for the frequency converter [52]. The two-mode P function remains constant along classical trajectories $\alpha_j(t)$. In other words, if both the signal and idler modes are initially quantum (classical), then they will preserve their original quantum (classical) character for the whole evolution. This property was experimentally verified by Huang and Kumar [54].

In the following sections, we will analyze PAB in quantum and, then, classical nonstationary fields generated by this model.

D. Photon Correlations in Quantum Fields

Let us analyze the parametric frequency conversion of the signal and idler modes initially in Fock states with photon numbers N_a and N_b, respectively. By applying Eq. (67), we readily find the evolution of the two-mode Glauber–Sudarshan P-function

$$P(\alpha_a, \alpha_b, t) = \frac{1}{\pi^2}\prod_{j=a,b}\frac{N_j!}{(2N_j)!}\frac{\exp(r_j^2)}{r_j}\left(\frac{\partial}{\partial r_j}\right)^{2N_j}\delta(r_j)\bigg|_{r_j=|\alpha_j(-t)|} \tag{69}$$

via derivatives of the Dirac δ function of the classical solutions, given by Eq. (68). It is seen that the P function remains singular evolving along classical trajectories. Thus, the field is nonclassical for arbitrary evolution times.

Here, we analyze all cases for which the three definitions of PAB might not be equivalent for some evolution times. These cases are listed in Table III with examples of the nonclassical signal fields presented graphically in Fig. 9 for the parameters γ_j and in Fig. 10 for the correlations Δg_j. We refer to these ordinal numbers of the cases throughout the chapter. In particular, they are given in the upper part of the figures. We present correlation functions for the signal mode only. Thus, we can consequently omit subscript a in correlation functions: $G^{(2)}(t_1, t_2) \equiv G_a^{(2)}(t_1, t_2)$, $g_j^{(2)} \equiv g_{j,a}^{(2)}$, and $\Delta g_j \equiv \Delta g_{j,a}$ for $j = \mathrm{I}, \mathrm{II}, \mathrm{III}$. Because of the symmetry of the solutions (66) for $j = a, b$, one can deduce the explicit expressions for the idler mode simply by interchanging the subscripts. Exact analytical solutions for the normalized correlation functions $g_j^{(2)}(t, t+\tau)$

TABLE III
All Possible Predictions of Photon Bunching and Antibunching of Quantum Fields According to Defs. I, II, and III [a]

Case	Def. I	Def. II	Def. III	Examples
1	Bunching	Bunching	Bunching	$\kappa t \in \left(\pi - f\{\frac{3}{5}\}, \pi\right)'$
2	Antibunching	Bunching	Bunching	$\kappa t \in \left(\pi - f\{\frac{1}{3}\}, \pi\right)''$
3	Bunching	Antibunching	Bunching	$\kappa t \in \left(0,\ f\{\frac{1}{3}\}\right)''$
4	Antibunching	Antibunching	Bunching	$\kappa t \in \left(0,\ f\{\frac{1}{5}\}\right)'$
5	Bunching	Bunching	Antibunching	$\kappa t \in \left(f\{-\frac{3}{5}\}, \frac{\pi}{2}\right)'$
				$\kappa t \in \left(\pi - f\{\frac{1}{3}\}, \pi - f\{\frac{3}{5}\}\right)'$
				$\kappa t \in \left(f\{-\frac{1}{3}\}, \frac{\pi}{2}\right)''$
6	Antibunching	Bunching	Antibunching	$\kappa t \in \left(\pi - f\{-\frac{1}{5}\}, \pi - f\{\frac{1}{3}\}\right)'$
				$\kappa t \in \left(\pi - f\{-\frac{1}{3}\}, \pi - f\{\frac{1}{3}\}\right)''$
7	Bunching	Antibunching	Antibunching	$\kappa t \in \left(f\{\frac{1}{3}\}, f\{-\frac{1}{5}\}\right)'$
				$\kappa t \in \left(f\{\frac{1}{3}\}, f\{-\frac{1}{3}\}\right)''$
8	Antibunching	Antibunching	Antibunching	$\kappa t \in \left(f\{\frac{3}{5}\}, f\{\frac{1}{3}\}\right)'$
				$\kappa t \in \left(\frac{\pi}{2}, \pi - f\{-\frac{1}{5}\}\right)'$
				$\kappa t \in \left(\frac{\pi}{2}, \pi - f\{-\frac{1}{3}\}\right)''$

[a] Signal and idler modes are initially in Fock states with (1) $N_a = 2$, $N_b = 1$ (marked by prime) and (2) $N_a = 3$, $N_b = 1$ (double prime). Here, $f\{x\} \equiv \frac{1}{2}\arccos(x)$.

($j = \mathrm{I}, \mathrm{II}, \mathrm{III}$) were obtained in Ref. 45 for arbitrary initial Fock states. However, for the purpose of our presentation, it is sufficient to analyze only two special cases.

If the initial signal mode is in Fock state with $N_a = 2$, and idler mode in Fock state with $N_b = 1$, the Taylor expansions of the correlation functions $\Delta g_j(t, t+\tau)$ are

$$\Delta g_{\mathrm{I}}(t, t+\tau) = \frac{-1 + 3\cos(2\kappa t)}{\langle n_a(t)\rangle^2} \sin(2\kappa t)(\kappa\tau) + \mathcal{O}(\tau^2)$$

$$\Delta g_{\mathrm{II}}(t, t+\tau) = \frac{1 + 5\cos(2\kappa t)}{\langle n_a(t)\rangle^3} \sin(2\kappa t)(\kappa\tau) + \mathcal{O}(\tau^2)$$

$$\Delta g_{\mathrm{III}}(t, t+\tau) = 2\sec^2(\kappa t)\frac{3 - 5\cos(2\kappa t)}{[5 - 3\cos(2\kappa t)]^2}(\kappa\tau)^2 + \mathcal{O}(\tau^3) \tag{70}$$

where the mean photon number is $\langle n_a(t)\rangle = \frac{1}{2}[3 + \cos(2\kappa t)]$; and $\mathcal{O}(\tau^k) \equiv \mathcal{O}(\{\kappa\tau\}^k)$ denotes the order of magnitude. The discrepancies between Defs. I, II, and III are well pronounced both analytically and graphically in Fig. 9a with the help of the parameters γ_j and in Fig. 10 directly in terms of the correlation functions $\Delta g_j(t, t+\tau)$ ($j = 1, 2, 3$). During the evolution of initial Fock states $|N_a, N_b\rangle = |2, 1\rangle$ almost all (except cases 2 and 3) are observed. The remaining

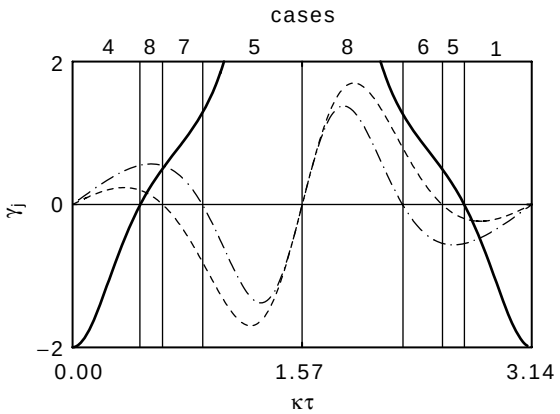

(a)

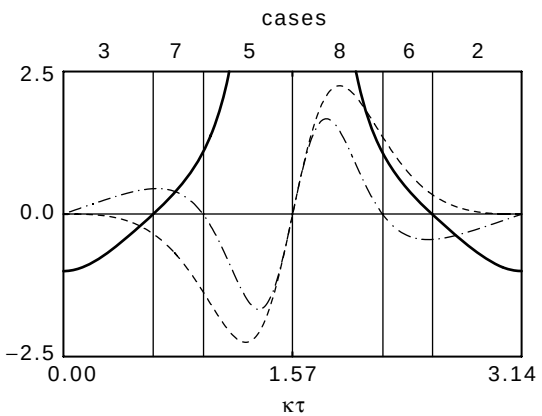

(b)

Figure 9. Quantum field evolution of the parameters $\gamma_{\mathrm{I}}(t)$ (dashed lines), $\gamma_{\mathrm{II}}(t)$ (dot–dash) and $\gamma_{\mathrm{III}}(t)$ (solid). Initially, both signal and idler modes are in Fock states with (a) $N_a = 2, N_b = 1$ and (b) $N_a = 3, N_b = 1$.

two cases can be found, for example, in the signal field evolution of the initial Fock states $|N_a, N_b\rangle = |3, 1\rangle$. Here, we obtain

$$\Delta g_{\mathrm{I}}(t, t+\tau) = -\frac{6\sin^2(\kappa t)}{\langle n_a(t)\rangle^2}\sin(2\kappa t)(\kappa\tau) + \mathcal{O}(\tau^2)$$

$$\Delta g_{\mathrm{II}}(t, t+\tau) = 3\frac{1+3\cos(2\kappa t)}{\langle n_a(t)\rangle^3}\sin(2\kappa t)(\kappa\tau) + \mathcal{O}(\tau^2)$$

$$\Delta g_{\mathrm{III}}(t, t+\tau) = \frac{1-3\cos(2\kappa t)}{[3-\cos(2\kappa t)]^2}\sec^2(\kappa t)\,(\kappa\tau)^2 + \mathcal{O}(\tau^3) \tag{71}$$

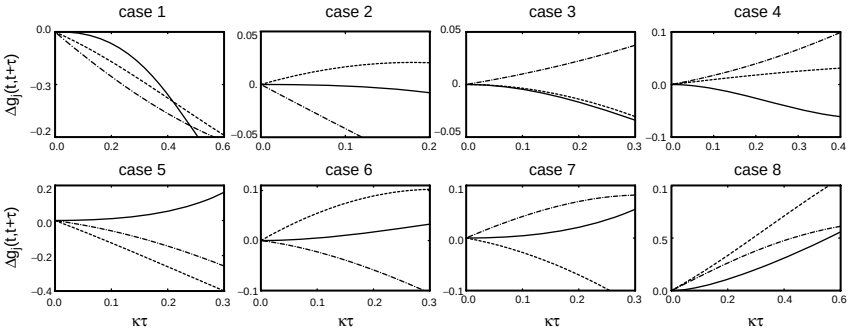

Figure 10. Illustration of eight different predictions of photon antibunching of quantum fields, corresponding to the cases analyzed in Table III and Fig. 9. The two-time signal-mode correlation functions $\Delta g_{\mathrm{I}}(t, t+\tau)$ (dashed curves), $\Delta g_{\mathrm{II}}(t, t+\tau)$ (dot–dashed), and $\Delta g_{\mathrm{III}}(t, t+\tau)$ (solid) are plotted in their dependence on the rescaled time separation $\kappa\tau$ for fixed values of the evolution time: (case 1) $\kappa t = 2.8$, (2) $\kappa t = 2.6$, (3) $\kappa t = 0.1$, (4) $\kappa t = 0.1$, (5) $\kappa t = 1.0$, (6) $\kappa t = 2.3$, (7) $\kappa t = 0.7$, and (8) $\kappa t = 1.8$. Signal and idler modes are initially in Fock states with $N_a = 3$ and $N_b = 1$ in cases 2 and 3, or with $N_a = 2$ and $N_b = 1$ in all other cases.

where $\langle n_a(t)\rangle = 2 + \cos(2\kappa t)$. The evolution of the parameters γ_j, given by the expansion coefficients in (71) are presented in Fig. 9b. We find six out of eight different predictions, including cases 2 and 3 not observed in the evolution of $|N_a, N_b\rangle = |2, 1\rangle$. The latter two cases are also presented in Fig. 10 in a standard way for the correlation functions evolving with the time separation τ for fixed values of time t. The values of evolution times t given in Table III are calculated from (70) and (71).

In conclusion, during the evolution of the nonclassical signal field in the parametric frequency converter, one observes that both PB and PAB effects from Defs. I–III can be accompanied, for some evolution times, with the same or different correlations of photons derived from other two definitions. We have given examples of all these cases in Figs. 9 and 10, and Table III.

E. Photon Correlations in Classical Fields

If the initial modes are in a superposition of coherent states (with amplitudes α_{j0}, where $j = a, b$) and chaotic fields (with intensities $\langle n_{\mathrm{ch},j}\rangle$), then the evolution of the frequency converter is described by the following Glauber–Sudarshan P function

$$P(\alpha_a, \alpha_b, t) = \frac{1}{\pi^2} \prod_{j=a,b} \frac{1}{\langle n_{\mathrm{ch},j}\rangle} \exp\left(-\frac{|\alpha_j(-t) - \alpha_{j0}|^2}{\langle n_{\mathrm{ch},j}\rangle}\right) \tag{72}$$

evolving along the classical solutions, given by Eq. (68). The P function (72) is a product of regular and positive Gaussian functions, thus describing explicitly the classical behavior of the idler and signal fields during the whole process of frequency conversion. Here, we analyze two special cases of these classical fields.

First, for simplicity, we assume that the mean photon numbers of chaotic photons in both modes are the same $\langle n_{\mathrm{ch},a}\rangle = \langle n_{\mathrm{ch},b}\rangle \equiv \langle n_{\mathrm{ch}}\rangle$ and the initial coherent amplitudes α_{j0} are real. We find

$$\begin{aligned}
\Delta g_{\mathrm{I}}(t,t+\tau) &= -2\langle n_a(t)\rangle^{-2}\{\langle n_{\mathrm{ch}}\rangle + \langle n_a(t)\rangle\}N_{-}\sin(2\kappa t)(\kappa\tau) + \mathcal{O}(\tau^2)\\
\Delta g_{\mathrm{II}}(t,t+\tau) &= 2\langle n_a(t)\rangle^{-3}\langle n_{\mathrm{ch}}\rangle\langle n_{\mathrm{coh},a}(t)\rangle N_{-}\sin(2\kappa t)(\kappa\tau) + \mathcal{O}(\tau^2)\\
\Delta g_{\mathrm{III}}(t,t+\tau) &= -\{G^{(2)}(t,t)(\langle n_{\mathrm{ch}}\rangle + 2N_{+}) - 4N_{-}^2\langle n_{\mathrm{ch}}\rangle\sin^2(2\kappa t)\}\\
&\quad\times\langle n_{\mathrm{ch}}\rangle[G^{(2)}(t,t)]^{-2}(\kappa\tau)^2 + \mathcal{O}(\tau^3) \le 0
\end{aligned} \tag{73}$$

where $N_{\pm} = \frac{1}{2}(\alpha_{a0}^2 \pm \alpha_{b0}^2)$. The time-dependent mean intensity of the signal mode is given by $\langle n_a(t)\rangle = \langle n_{\mathrm{ch}}\rangle + \langle n_{\mathrm{coh},a}(t)\rangle$, where $\langle n_{\mathrm{coh},a}(t)\rangle = \alpha_{a0}^2\cos^2(\kappa t) + \alpha_{b0}^2\sin^2(\kappa t)$ is the time-dependent intensity of input coherent fields, and $\langle n_{\mathrm{ch}}\rangle$ is the initial intensity of chaotic field. Moreover, $G^{(2)}(t,t) = \langle n_{\mathrm{coh},a}(t)\rangle^2 + 4\langle n_{\mathrm{ch}}\rangle\langle n_{\mathrm{coh},a}(t)\rangle + 2\langle n_{\mathrm{ch}}\rangle^2$ is the single-time correlation function. In expansion (73), similar to Eq. (71), the first τ derivative of $g_{\mathrm{III}}^{(2)}(t,t+\tau)$ vanishes at $\tau = 0$. Expansions (73) have simple interpretation. The correlation function $\Delta g_{\mathrm{III}}(t,t+\tau)$ is never positive; thus PAB according to Def. III cannot be observed. On the contrary, both $\Delta g_{\mathrm{I}}(t,t+\tau)$ and $\Delta g_{\mathrm{II}}(t,t+\tau)$ oscillate between negative and positive values; therefore, PAB according to Defs. I and II is apparently not prohibited. Surprisingly, predictions of Defs. I and II are opposite. As comes from Eq. (73), $\Delta g_{\mathrm{I}}(t,t+\tau)$ and $\Delta g_{\mathrm{II}}(t,t+\tau)$ have opposite signs and the same time-dependent function. Our conclusion is supported by graphical representations of the parameters γ_j in Fig. 11a and $\Delta g_j(t,t+\tau)$ in Fig. 12 (cases 2 and 3) for the initial condition

$$\rho_1(0) = \rho\{\alpha_a^2 = \langle n_{\mathrm{ch},a}\rangle = \langle n_{\mathrm{ch},b}\rangle = 1, \alpha_b = 0, t = 0\}. \tag{74}$$

Whenever PB is predicted according to one of Defs. I and II, it must be accompanied by the classical-field PAB artifact according to the other.

As the second example, we analyze another special case of the field (72), evolving in a way opposite the field evolution under initial condition (74). Let the signal mode is initially coherent (with real amplitude α_{a0}), whereas the idler mode is chaotic (with the mean photon number $\langle n_{\mathrm{ch},b}\rangle$). We obtain the following

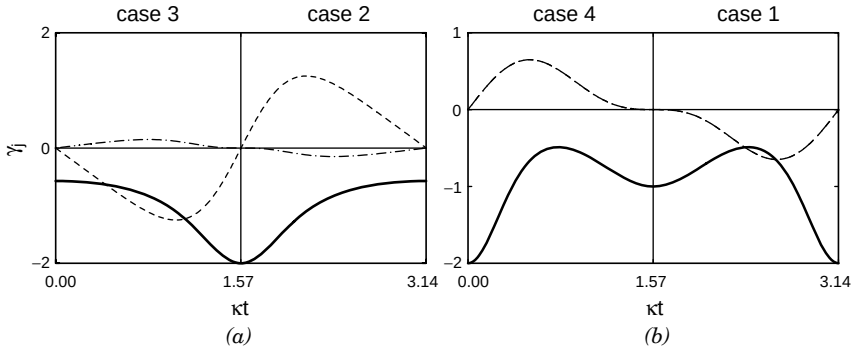

Figure 11. Clasical-field evolution of the parameters $\gamma_j(t)$ for initial superpositions of coherent state with thermal field: (a) $\rho_1(0)$ and (b) $\rho_2(0)$ given by Eqs. (74) and (76), respectively. Labels are the same as in Fig. 9.

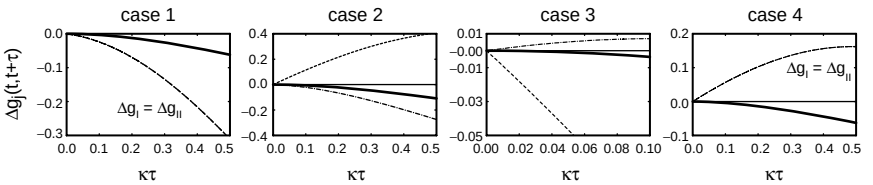

Figure 12. Illustration of all four possible different predictions of PB and the PAB artifacts for classical fields as listed in Table III. Initial conditions are given by Eqs. (74) and (76): (case 1) $\rho_2(0)$ at $\kappa t = 2$; (case 2) $\rho_1(0)$ at $\kappa t = 2$; (case 3) $\rho_1(0)$ at $\kappa t = 0.6$, and (case 4) $\rho_2(0)$ at $\kappa t = 0.4$. Evolution times κt are chosen with the help of Fig. 11. Labels and notation are the same as in Fig. 10.

power expansions of the normalized correlations $\Delta g_j(t, t+\tau)$ are

$$\begin{aligned}
\Delta g_{\mathrm{I}}(t, t+\tau) &= 2\left\{[2y\cot(\kappa t) - x\tan(\kappa t)]\langle n_a(t)\rangle - xy\tan(\kappa t)\right\} \\
&\quad \times \ \langle n_a(t)\rangle^{-2}(\kappa\tau) + \mathcal{O}(\tau^2) \\
\Delta g_{\mathrm{II}}(t, t+\tau) &= 4x^2 y\csc(2\kappa t)\langle n_a(t)\rangle^{-3}(\kappa\tau) + \mathcal{O}(\tau^2) \\
\Delta g_{\mathrm{III}}(t, t+\tau) &= -\frac{2\alpha_{a0}^2\langle n_{\mathrm{ch},b}\rangle(x^2+2y^2)}{(x^2+4xy+2y^2)^2}(\kappa\tau)^2 + \mathcal{O}(\tau^3) \leq 0
\end{aligned} \tag{75}$$

in terms of the mean signal mode intensity, $\langle n_a(t)\rangle = x + y$, where $x = \alpha_{a0}^2 \cos^2(\kappa t)$ and $y = \langle n_a(t)\rangle - x$. The short-time solution (75) reveals non-positive character of $\Delta g_{\mathrm{III}}(t, t+\tau)$, thus excluding the possibility of PAB according to

Def. III. By contrast, both $\Delta g_{\mathrm{I}}(t, t+\tau)$ and $\Delta g_{\mathrm{II}}(t, t+\tau)$ change their signs during evolution. On further assumption of equal initial intensities of the signal and idler modes, namely

$$\rho_2(0) = \rho\left\{\alpha_a^2 = \langle n_{\mathrm{ch},b}\rangle > 0, \alpha_b = \langle n_{\mathrm{ch},a}\rangle = 0, t = 0\right\} \tag{76}$$

we find that the normalized correlation functions $g_{\mathrm{I}}^{(2)}(t_1, t_2) = g_{\mathrm{II}}^{(2)}(t_1, t_2)$, and $g_{\mathrm{III}}^{(2)}(t_1, t_2)$ are independent of the initial intensities. Equations (75) reduce to

$$\Delta g_{\mathrm{I}}(t, t+\tau) = \Delta g_{\mathrm{II}}(t, t+\tau) = \cos^2(\kappa t)\sin(2\kappa t)\,(\kappa\tau) + \mathcal{O}(\tau^2) \tag{77}$$

$$\Delta g_{\mathrm{III}}(t, t+\tau) = -\frac{1 + 4\sin^2(\kappa t) + 3\cos^2(2\kappa t)}{2[2 - \cos^4(\kappa t)]^2}(\kappa\tau)^2 + \mathcal{O}(\tau^3) \leq 0 \tag{78}$$

Evidently, the solution (77) takes positive values at some evolution times. We conclude that the classical field PAB artifact according to Def. I occurs whenever it exists according to Def. II for the signal under the initial condition (76). These results are graphically represented in Fig. 11b and Fig. 12 (cases 1 and 4). It is worth comparing solution (77) with Eqs. (73) for $\Delta g_{\mathrm{I}}(t, t+\tau)$ and $\Delta g_{\mathrm{II}}(t, t+\tau)$, describing their opposite (out-of-phase) behavior (see Fig. 11a).

Table IV summarizes our investigations of PB effects in classical fields. By virtue of the Cauchy–Schwarz inequality, PAB according to Def. III cannot occur for classical fields, thus cases 5–7 in Table IV are excluded. However, the remaining cases 1–4 are observed in the evolution of classical fields as presented in Figs. 11 and 12. The classical PAB apparently exists according to both Defs. I and II.

PAB of classical fields can only be an artifact. So, it seems necessary to modify the conventional definitions in a nonstationary regime. For instance, one

TABLE IV
Same as Table III but Examples are Given for Classical Fields[a]

Case	Δg_{I} (Def. I)	Δg_{II} (Def. II)	Δg_{III} (Def. III)	Examples
1	Negative (bunching)	Negative (bunching)	Negative (bunching)	$\kappa t \in (\frac{\pi}{2}, \pi)''$
2	Positive	Negative (bunching)	Negative (bunching)	$\kappa t \in (\frac{\pi}{2}, \pi)'$
3	Negative (bunching)	Positive	Negative (bunching)	$\kappa t \in (0, \frac{\pi}{2})'$
4	Positive	Positive	Negative (bunching)	$\kappa t \in (0, \frac{\pi}{2})''$
5	Negative (bunching)	Negative (bunching)	Positive	Forbidden
6	Positive	Negative (bunching)	Positive	Forbidden
7	Negative (bunching)	Positive	Positive	Forbidden
8	Positive	Positive	Positive	Forbidden

[a]Signal and idler modes are initially described by Eq. (74) (marked by prime) or Eq. (76) (double prime).

can add an extra condition, which guarantees the nonclassical character of the field but keeping the original inequalities unchanged. Nevertheless, the problem of the unique description of PAB in nonstationary case would remain in the conventional definitions. On the contrary, these problems do not arise in the generalized approach to PAB (Def. III), where the Cauchy–Schwarz inequality is applied directly without any further assumptions.

F. Conclusion

We have generalized the concept of PB and PAB to describe nonstationary fields. The definition is based on the two-time second-order intensity correlation function $G^{(2)}(t_1, t_2)$ normalized by the square root of single-time second-order intensity correlations at two moments t_1 and t_2. This is contrary to the standard approaches to PAB, where the two-time correlation $G^{(2)}(t_1, t_2)$ is normalized by either (1) the single-time first-order intensity correlations at two moments, or (2) functions independent of the time separation $\tau = t_2 - t_1$. In a special case, when a field is stationary the generalized definition is equivalent to the standard definitions. However, as we have shown, the predictions of PAB according to these three approaches might be different for nonstationary fields. As an example, we have analyzed evolution of the signal mode during the parametric frequency conversion of initial Fock states and have found all (i.e., eight) possible different cases, when PAB (and also PB) effect according to one definition can be accompanied by arbitrary photon correlation effects according to other two definitions. One may conclude that the three definitions describe distinct quantum nonstationary phenomena.

The generalized definition of PAB was proposed on the basis of the Cauchy–Schwarz inequality without any assumptions concerning properties of the fields. Whereas the standard definitions come from the Cauchy–Schwarz inequality under stationary-field condition. Thus, PAB according to the generalized definition cannot occur for classical fields. However, as we have shown in the parametric frequency converter with classical initial conditions, the classical nonstationary fields possibly exhibit PAB artifacts according to the standard definitions without violating any classical inequalities.

IV. MAXIMUM-LIKELIHOOD PHASE RECONSTRUCTION (*J. ŘEHÁČEK, Z. HRADIL, O. HADERKA, and M. HENDRYCH*)

There is no doubt that the concept of phase has turned out to be useful in the classical theory. Phase measurements in the domain of classical wave optics are well established and belong to the most precise measurement schemes currently available. It is natural that many attempts have been made to translate this concept to the language of quantum theory. Quantum phase, however,

encountered theoretical difficulties when an adequate quantum theory was constructed [57–62].

There are several concepts for the description of phase in quantum theory at present. Some of them are accenting the theoretical aspects, other the experimental ones. Quantization based on the correspondence principle leads to the formulation of operational quantum phase concepts. For example, the well-known operational approach formulated by Noh et al. [63,64] is motivated by the correspondence principle in classical wave theory. Further generalization may be given in the framework of quantum estimation theory. The prediction may be improved using the maximum-likelihood estimation. The optimization of phase inference will be pursued in the following.

Phase measurements do not belong to the category of conventional measurements since a Hermitian phase operator does not exist. What is usually measured in practice is energy, and various phase sensitive devices (interferometers, etc.) are used to transform phase shifts into variations of output energies. Because of the statistical nature of quantum theory the resulting relationship between the measured quantities and the parameters of interest is not deterministic. This sort of indirect inferences is usually called estimation. The scheme of an estimation procedure is the following

$$\rho \rightarrow \boxed{\begin{array}{c}\text{true phase}\\ \text{shift}\quad \bar{\theta}\end{array}} \rightarrow \rho(\bar{\theta}) \rightarrow \boxed{\text{detection}} \rightarrow \mathbf{v} = \{v_1 \cdots v_n\} \rightarrow$$
$$\rightarrow \boxed{\text{estimation}} \rightarrow \theta(\mathbf{v}) \tag{81}$$

Here ρ is the known initial density matrix, $\mathbf{v}$ is a set of outcomes of the given measurement, and θ is our phase estimate based on the measured data $\mathbf{v}$. The true phase shift inside the interferometer $\bar{\theta}$, which is a nonfluctuating parameter controlled by the experimentalist, should be carefully distinguished from the phase estimate θ, which is (usually) a random quantity. Hereafter, the latter is denoted by θ.

To proceed some measure of error of estimation is needed. The error is quantified with the help of the "cost function." The choice of the cost function depends on the given problem. Two most often used cost functions are as follows:

$$C(\theta,\bar{\theta}) \begin{cases} (\theta-\bar{\theta})^2 & \text{least-square fit} \\ -\delta(\theta-\bar{\theta}) & \text{maximum likelihood} \end{cases} \tag{82}$$

According to the well-known Bayes theorem, the posterior probability distribution of an estimate reads as

$$p(\bar{\theta}|\mathbf{v}) \propto p(\mathbf{v}|\bar{\theta})z(\bar{\theta}) \tag{83}$$

where $p(\mathbf{v}|\bar{\theta})$ is the probability of the occurrence of the outcome $\mathbf{v}$ provided that the true phase shift is $\bar{\theta}$,

$$p(\mathbf{v}|\bar{\theta}) = \mathrm{Tr}\{\rho(\theta)|\mathbf{v}\rangle\langle\mathbf{v}|\} \tag{84}$$

and $z(\bar{\theta})$ quantifies our prior knowledge of unknown phase shift $\bar{\theta}$. In absence of any information the uniform prior distribution or a prior distribution invariant with respect to a certain class of transformations can be chosen. In the following the uniform prior distribution is used.

After detection of data $\mathbf{v}$ the risk of a particular phase estimate θ can be defined in the following way

$$r(\theta|\mathbf{v}) = \int C(\theta, \bar{\theta}) p(\bar{\theta}|\mathbf{v})\, d\bar{\theta} \tag{85}$$

The best strategy then consist in minimizing the overall risk. This is done by choosing the phase estimate having minimum risk (85)

$$\theta(\mathbf{v}) = \arg\{\min_{\theta} r(\theta|\mathbf{v}\} \tag{86}$$

Using "δ peaked" cost function (82) and posterior distribution (83) in Eq. (85), we obtain $r(\theta|\mathbf{v}) = -p(\theta|\mathbf{v})$. Minimizing risk (85) is therefore equivalent to maximizing the likelihood function

$$\mathscr{L} \equiv p(\theta|\mathbf{v}) \propto p(\mathbf{v}|\theta) \tag{87}$$

Equation (87) is a nice demonstration of the maximum-probability principle. After registration of data the estimate of the unknown parameter is chosen, which would give rise to the observed data with greatest probability. This principle is very general and maximum-likelihood (ML) estimation as well as many other reconstruction methods (maximum entropy, etc.) follow from this principle [65].

A. Quantum Phase Estimation

First, let us show that the operational phase concepts can naturally be embedded in the general scheme of quantum estimation theory [66,67] as was done by Hradil, Zawisky, and others [68–71]. Let us consider the eight port homodyne detection scheme [63,72] with four output channels numbered by indices 3,4,5,6, where the actual values of intensities are registered in each run. Assume that these values fluctuate in accordance with some statistics. The mean intensities are modulated by a phase parameter $\bar{\theta}$

$$\begin{aligned} \bar{n}_{3,4} &= \frac{N}{2}(1 \pm V\cos\bar{\theta}) \\ \bar{n}_{5,6} &= \frac{N}{2}(1 \pm V\sin\bar{\theta}) \end{aligned} \tag{88}$$

where N is the total intensity and V is the visibility of the interference fringes. This device is equivalent to a Mach–Zehnder interferometer, when the measurement is performed with zero and $\pi/2$ auxiliary phase shifters. In this case, data are not obtained simultaneously, but are collected during repeated experiments. Provided that a particular combination of outputs $\{n_3, n_4, n_5, n_6\}$ has been registered, the phase shift can be inferred. The point estimators of phase corresponding to the ML estimation will be used here [73,74]. In accordance with the ML approach [75], the sought-after phase shift is given by the value, which maximizes the likelihood function (87).

Now, let us assume that the phase-sensitive device operates with a Gaussian signal with phase-insensitive noise. This is only an approximation to the real situation since realistic signals are discrete. Under such approximation the likelihood function corresponding to the detection of given data reads as

$$\mathscr{L} \propto \exp\left\{-\frac{1}{2\sigma^2}\sum_{i=3}^{6}[n_i - \bar{n}_i]^2\right\} \tag{89}$$

Here the variance σ^2 represents the phase-insensitive noise of each channel. The sampling of intensities may serve for an estimation of phase shift and the visibility simultaneously. Likelihood function (89) is maximized on the physically allowed space of parameters $V \leq 1$ by the following phase and visibility:

$$e^{i\theta} = \frac{n_3 - n_4 + i(n_5 - n_6)}{\sqrt{(n_3 - n_4)^2 + (n_5 - n_6)^2}} \tag{90}$$

$$V = \min\left(2\frac{\sqrt{(n_3 - n_4)^2 + (n_5 - n_6)^2}}{\sum_{i=3}^{6} n_i}, 1\right) \tag{91}$$

Notice that the prediction of Gaussian theory (90) coincides with the operational quantum phase of Noh, Fougèeres, and Mandel (NFM) [64]. This means that NFM phase concept can be thought of as a special case of ML phase estimation — ML estimation for Gaussian signals. This also means that NFM phase prediction should be optimum only for signals represented by continuous Gaussian signal with phase-independent and symmetric noises.

Since realistic signals are discrete, the phase prediction can be optimized by considering the actual statistics of the experiment. This can be demonstrated on the case of Poissonian signals. These are frequently encountered in laboratories as lasers and thermal sources of particles (like neutrons) are Poissonian.

Assume the Poissonian statistics of an ideal laser. ML estimation based on the Poissonian likelihood function

$$\mathscr{L} \propto \prod_{i=3}^{6} \bar{n}_i^{n_i} e^{-\bar{n}_i} \tag{92}$$

gives optimum values for phase shift and visibility

$$e^{i\theta} = \frac{1}{V}\left[\frac{n_4 - n_3}{n_4 + n_3} + i\frac{n_6 - n_5}{n_6 + n_5}\right] \tag{93}$$

$$V = \sqrt{\left(\frac{n_4 - n_3}{n_4 + n_3}\right)^2 + \left(\frac{n_6 - n_5}{n_6 + n_5}\right)^2} \tag{94}$$

provided the estimated visibility (94) is smaller than unity. In the opposite case it is necessary to maximize the likelihood function (92) on the boundary ($V = 1$) of the physically allowed region of the parameter space numerically. Relations (93) and (94) provide a correction of the Gaussian theory with respect to Poissonian signals.

The apparent difference between inferred phases (90) and (93) represents the theoretical background of the presented treatment. The principles of inference together with two different assumptions about the nature of the signal give rise to two different phase estimates. One may wonder whether the improvement of phase inference gained by taking the correct statistics of the experiment into account is worth of giving up the simple NFM formalism and resorting to numerical methods. Could the optimization of the information yield from detected data lead to a significant increase of the accuracy of phase fitting?

The difference between (90) and (93) can be tested in a controlled phase measurement. The phase difference may be adjusted to a certain value and estimated independently using both the methods (90) and (93) in repeated experiments. The efficiency of both methods is then compared by evaluation of confidence intervals. Since any imperfections of the detection scheme will smooth the differences, it is questionable whether both the schemes can be experimentally distinguished. This idea will be pursued in the following sections.

To compare two or more phase estimators, some measure of the estimation error is needed. Dispersion defined by the relation

$$\sigma^2 = 1 - \left|\langle e^{i\theta}\rangle\right|^2 \tag{95}$$

can well be used. Here the average is taken over posterior phase distribution of the corresponding phase estimator.

The evaluation of the average quadratic cost (95) is not the only way to compare efficiencies of different estimation procedures. Another possibility is to

use the rectangular cost function

$$C(\theta - \bar{\theta}) = \begin{cases} -1 & |\theta - \bar{\theta}| \leq \Delta\theta \\ 0 & |\theta - \bar{\theta}| > \Delta\theta \end{cases} \tag{96}$$

The averaged rectangular cost $\langle C(\theta - \bar{\theta})\rangle$ measures how many times an estimate falls within the chosen window $\Delta\theta$ spanning around the true phase $\bar{\theta}$ The difference

$$\Delta E = \langle C(\theta - \bar{\theta})\rangle_{\text{Gauss}} - \langle C(\theta - \bar{\theta})\rangle_{\text{Poiss}} \tag{97}$$

then measures how much is the Poissonian prediction better than the Gaussian one. If this quantity is found to be positive, the ML estimation is better than its NFM counterpart.

Although the dispersion (95) and ΔE cannot be calculated explicitly for arbitrary input intensity N, it is possible to analyze the limit cases [71]. Obviously, both the predictions (90) and (93) will coincide provided that there is almost no information available in the low-field limit $N \to 0$. Not so obvious is the fact that both predictions will coincide also in the high-energy limit $N \gg 1$ provided the visibility is low $V \to 0$. To see this, let us compare the asymptotic dispersion of the NFM estimator

$$\sigma_G^2 \approx \frac{1}{V^2} N^{-1} + O\left(\frac{1}{N^2}\right) \tag{98}$$

with the asymptotic expression for the Cramér–Rao lower bound (CRLB) on the dispersion of any estimator:

$$\sigma_{\text{CRLB}}^2 = \frac{V^2 - 1 - \frac{1}{4}V^4 \sin^2 2\bar{\theta}}{V^2 - 1 - \frac{1}{2}V^2 \sin^2 2\bar{\theta}} V^{-2} N^{-1} + O\left(\frac{1}{N^2}\right) \tag{99}$$

In the limit of low visibility both expressions become identical. Therefore NFM theory is optimal in this limit case [76].

Asymptotic expressions for various phase estimators in the opposite limit of high visibility $V \approx 1$ are given in Table V where u-ML is the phase prediction given by Eq. (93), that is, one accepts possible unphysical inferred visibilities $V > 1$, and ML(1) is the phase prediction obtained by putting $V = 1$ in the likelihood function (92) and maximizing it only with respect to phase (maximization on the boundary of the physical space of parameters).

Notice that uncertainty of all the estimators scales as $1/\sqrt{N}$, which is the standard quantum limit. Best-known proposed phase measurements scale as $1/N$ [77,78], but these methods necessitate the use of exotic quantum states of

TABLE V
Asymptotic Dispersions and Overall Quadratic Costs of Various Phase Estimators[a]

Estimator	σ^2	$\bar{C} \equiv \int \sigma^2 d\bar{\theta}$
NFM	$1/N$	$2\pi/N$
u-ML	$(1+\cos^2 2\bar{\theta})/2N$	$\frac{3}{2}\pi/N$
ML	$\approx (1+0.5\ \cos^2\bar{\theta})/2N$	$\approx \frac{5}{4}\pi/N$
ML (1)	$1/2N$	π/N
CRLB	$1/2N$	π/N

[a]*Key*: u-ML — unconstrained ML estimation; ML(1) — single-parameter ML estimation. For comparison, CRLB is shown.

light, which are still not readily available in laboratories. Notice that by taking physical constraints into account the accuracy of phase fitting is improved.

Single-parameter ML estimator outperforms all the other studied estimators. It attains the CRLB and hence is optimum. This optimum evaluation of measured data yields a phase prediction whose uncertainty is reduced by a factor of $\sqrt{2}$, that is, by about 70%, in comparison with the semiclassical NFM theory. However, some caution is necessary when the actual visibility is less then one or fluctuates. In this case, using $V = 1$ in the likelihood function (92) leads to biased phase predictions. For large intensities the bias might spoil the estimation [71].

B. Experiments

The performance of the Gaussian and Poissonian phase estimators have been determined in a series of experiments utilizing two principal sources of particles: laser light [71] and a beam of thermal neutrons [70]. The main goal of the experiments was to compare the optimum phase prediction with the NFM semiclassical theory in the (quantum) regime of only a few input particles. As a side result, the theoretical asymptotic uncertainties given in Table V were tested in a real experiment.

The dispersions (95) of the NFM (or equivalently Gaussian) and ML phase estimators found in experiments with light are shown in Fig. 13. The true phase was fixed at $\bar{\theta} = \pi/3$. The number of detected quadruples $\{n_3, n_4, n_5, n_6\}$ used for the calculation of the dispersions varied from 1000 samples for the input mean number of photons $N = 60$ to more than $100,000$ samples for $N = 0.1$. The error bars corresponding to these finite numbers of samples are the result of numerical simulation. The visibility during the experiments was better than 99.6%.

The most distinct (absolute) difference between the dispersions of the ML and NFM estimators is seen for the input mean number of photons $N \approx 7.5$. For

even weaker signals, both estimators become "equally bad." In the opposite limit of a strong signal the difference decreases from the vanishing of both dispersions simultaneously.

The ML estimator was found to be significantly more accurate (by many standard deviations) than its NFM semiclassical counterpart. This was confirmed by evaluating the difference of the rectangular costs (97), see Fig. 14. ΔE was calculated using 7500 experimental samples measured in experiment with $N = 10$ photons and visibility of 99.6%. The chosen input energy roughly fits the maximum seen in Fig. 13. Standard deviation corresponding to 7500 measured samples is shown in Fig. 14 as error bars for each phase window.

A significant difference between the effectiveness of semiclassical and optimal treatments is apparent in Fig. 14. The optimal treatment provides an improvement in estimation procedure, and the difference is more than 10 standard deviations beyond the statistical error. High stability and visibility of interference fringes in the optical interferometer along with a high repetition rate of pulsed lasers made the improvement of the NFM phase prediction more evident than in a similar comparison that had been done with thermal neutrons [70] (see Fig. 15).

An experimental comparison of three phase estimations—NFM, unconstrained ML, and ML estimators—in the asymptotic regime is shown in Fig. 16. The experiment was done with photons. For comparison, the theoretical values of dispersions given in Table V are also shown. Several important

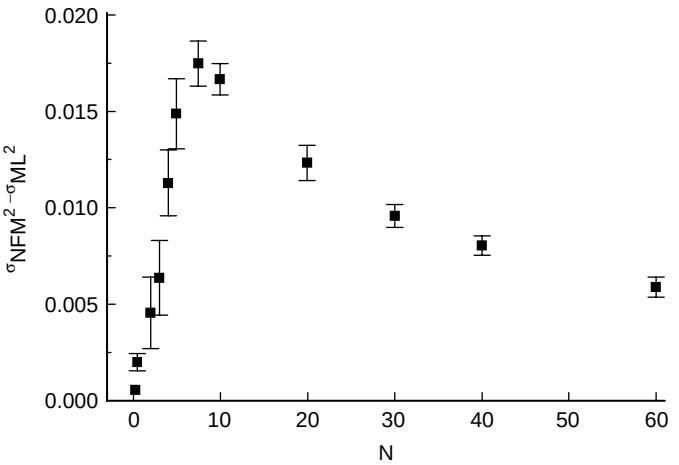

Figure 13. The experimentally observed difference between dispersions of the NFM and ML estimators as a function of the input mean number of photons N for fixed true phase $\bar{\theta} = \pi/3$. Error bars corresponding to 68% confidence intervals are shown.

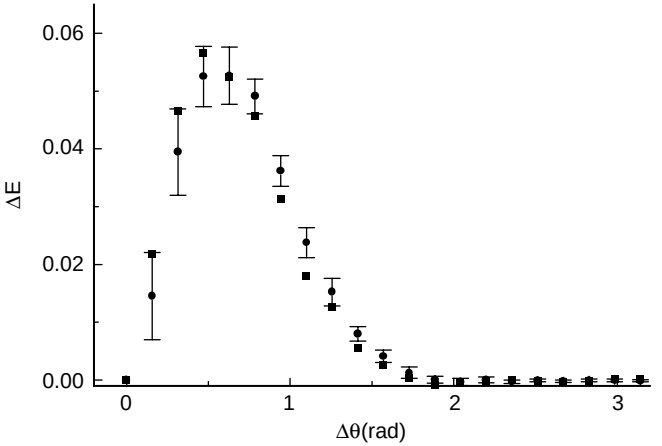

Figure 14. Experimentally obtained ΔE (squares) compared to theoretical values (circles). Error bars corresponding to 7500 measured samples are shown. $N = 10$ photons.

conclusions can be drawn from Fig. 16. (i) We can see that the uncertainty of the constrained ML estimation is definitely below the uncertainty of the unconstrained estimation in agreement with theory presented in Table V. This means that insisting on the physical constraints (here non-negativity of the intensity) is important not only for the sake of interpretation, but it also makes the estimation more efficient. Of course, both ML estimations beat the phase resolution of the semiclassical NFM theory. (ii) The observed values of dispersion exhibit a systematic error. The additional noise above the theoretical uncertainty is caused by inherent phase fluctuations in the experimental setup, and their magnitude can be estimated from Fig. 16 as 0.020 ± 0.003 rad. This value is in an excellent agreement with the value 0.019 rad obtained by an independent method. Hence our statistically motivated evaluation of experimental data can be used for inferring the amount of fluctuations, and therefore it provides an independent and nontrivial way for calibrating an interferometer. Moreover, a slightly different sensitivity of different phase estimators to various parameters of the setup makes it possible, at least in principle, to distinguish between different sources of phase noise.

A precise analysis of the noise is not the only merit of the phase estimation. Since phase detection represents an indirect measurement, it could serve as the simplest example of quantum tomography. Similar treatment inspired by the ML estimation may be applied to the reconstruction of a generic quantum state, namely that of entangled qubits.

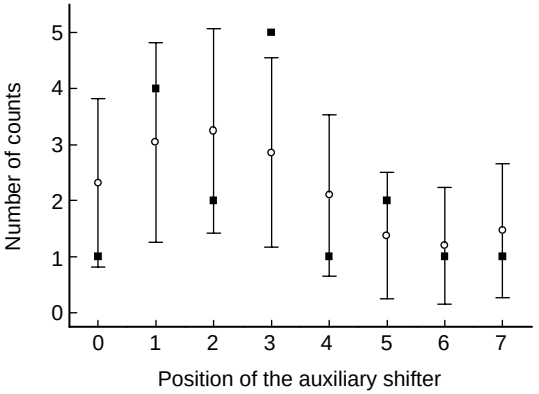

(a)

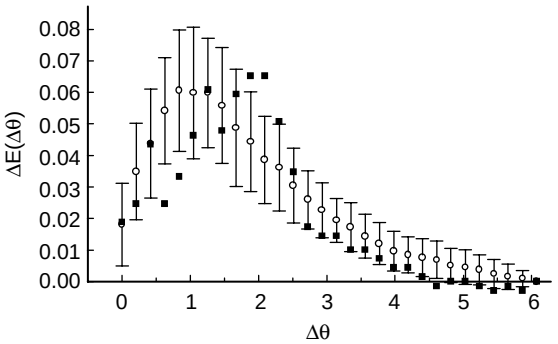

(b)

Figure 15. (a) Detected intereference fringe in ordinary channel as mean of 690 single measuremens (○) and error bars corresponding to the Poissonian detection statistics. The mean number $N = 8.54$ of incoming neutrons was asymmetrically split between the ordinary ($N_o = 2.21$) and extraordinary ($N_h = 6.33$) channels. The average visibility was about 31%. A typical single detection denoted by full squares is shown as an example. (b) Experimentally obtained ΔE denoted by full squares are compared with theoretical prediction denoted by corresponding mean values (○) and eror bars for 690 samples.

V. FREQUENCY PARAMETRIC DOWNCONVERSION WITH PULSED FIELDS (*J. PEŘINA, JR.*)

The process of spontaneous parametric downconversion has been studied extensively [79,80] for cw (continuous-wave) pump lasers over the last decades. A great deal of attention has been paid to the process of spontaneous parametric

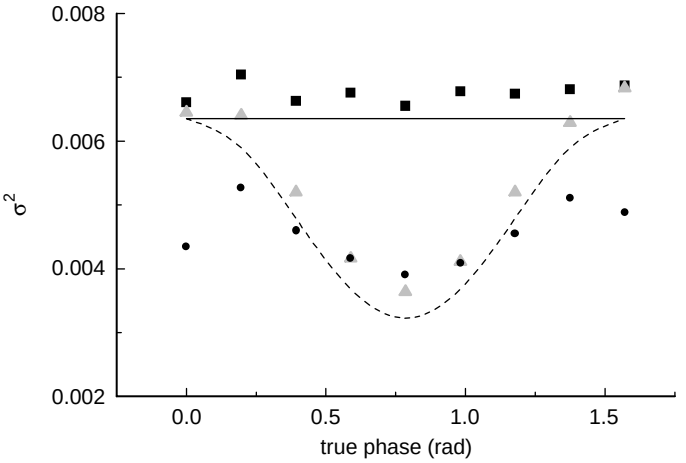

Figure 16. Asymptotic dispersions of the NFM estimator; theory (solid line) and experimentally obtained values (squares). Asymptotic dispersions of the unconstrained ML estimator; theory (dashed line) and experimentally obtained values (triangles). Experimentally obtained dispersions of the ML estimation on the physical space of parameters (circles). The corresponding input mean number of photons and the estimated visibility were $N = 160$ and $V = 99.2\%$, respectively.

downconversion pumped by femtosecond pulses. Pairs of downconverted photons generated from ultrashort pump pulses may be synchronized in time and create optical fields with more than two mutually entangled photons this way [81,82]. Such fields have already been successfully used when observing quantum teleportation [83] and generating GHZ (Greenberger-Horne-Zeilinger) states [84–86]. The basic theoretical model of spontaneous parametric downconversion process pumped by an (ultrashort) Gaussian pulse has been developed in [87–89].

The process of spontaneous parametric downconversion is described by the following interaction Hamiltonian [79]:

$$\hat{H}_{\text{int}}(t) = \int_{-L}^{0} dz\, \chi^{(2)} E_p^{(+)}(z,t) \hat{E}_1^{(-)}(z,t) \hat{E}_2^{(-)}(z,t) + \text{H.c.} \tag{100}$$

where $\chi^{(2)}$ is the second-order susceptibility, $E_p^{(+)}$ denotes the positive-frequency part of the electric field amplitude of the pump field, and $\hat{E}_1^{(-)}$ ($\hat{E}_2^{(-)}$) is the negative-frequency part of the electric field operator of downconverted field 1 (2). The nonlinear crystal extends from $z = -L$ to $z = 0$. The symbol H.c. means Hermitian conjugate.

Second-order perturbational theory then provides the entangled two-photon state $|\psi^{(2)}(0, t_0)\rangle$ for times t_0 sufficiently long so that the nonlinear interaction is

complete in the form [90]:

$$|\psi^{(2)}(0,t_0)\rangle = C_\psi \int_{-L}^{0} dz \sum_{k_p}\sum_{k_1}\sum_{k_2} \mathscr{E}_p^{(+)}(0,\omega_{k_p}-\omega_p^0)\hat{a}_1^\dagger(k_1)\hat{a}_2^\dagger(k_2)\exp[i(k_p-k_1 - k_2)z]\delta(\omega_{k_p}-\omega_{k_1}-\omega_{k_2})\exp[i(\omega_{k_1}+\omega_{k_2})t]|\text{vac}\rangle, \tag{101}$$

where C_ψ is a constant. The symbol $\mathscr{E}_p^{(+)}(0,\omega_{k_p}-\omega_p^0)$ denotes the positive-frequency part of the envelope of the pump beam electric field amplitude at the output plane of the crystal; k_p stands for the wavevector of a mode in the pump beam, and ω_p^0 is the central frequency of the pump beam. The symbol $\hat{a}_1^\dagger(k_1)$ ($\hat{a}_2^\dagger(k_2)$) represents the creation operator of the mode with wave vector k_1 (k_2) and frequency ω_{k_1} (ω_{k_2}) in the downconverted field 1 (2); $|\text{vac}\rangle$ denotes a multimode vacuum state. The symbol δ means the Dirac δ function.

A. Properties of One-Photon Fields

The mean number of photons N_j in downconverted field j is given as follows:

$$N_j(\tau) = \langle\psi^{(2)}(0,t_0)|\hat{E}_j^{(-)}(0,t_0+\tau)\hat{E}_j^{(+)}(0,t_0+\tau)|\psi^{(2)}(0,t_0)\rangle \tag{102}$$

The positive-frequency part of the electric field operator $\hat{E}_j^{(+)}$ has the form

$$\hat{E}_j^{(+)}(z_j,t_j) = \sum_{\nu_j} e_j(\nu_j)\hat{a}_j(\nu_j)\exp[ik_j^v(\omega_j^0+\nu_j)z_j - i(\omega_j^0+\nu_j)t_j] \tag{103}$$

and $e_j(\nu_j)$ denotes the amplitude per photon of the mode with the frequency $\omega_j^0+\nu_j$ (ω_j^0 stands for the central frequency of mode j); k_j^v means a wavevector in vacuum in the jth field. Substituting Eqs. (101) and (103) into Eq. (102), we arrive at the expression for N_j in the form [91]

$$N_j(\tau) = \frac{(2\pi)^2|C_{N_j}|^2}{|D|}\int_{-L}^{0} dz|\mathscr{E}_p^{(+)}(0,\tau-D_{pj}z)|^2 \tag{104}$$

in which

$$\begin{aligned} D_{pj} &= \frac{1}{v_p}-\frac{1}{v_j} = \Lambda + (-1)^j\frac{D}{2}, \quad j=1,2 \\ \Lambda &= \frac{1}{v_p}-\frac{1}{2}\left(\frac{1}{v_1}+\frac{1}{v_2}\right) \\ D &= \frac{1}{v_1}-\frac{1}{v_2} \end{aligned} \tag{105}$$

The symbol $\mathscr{E}_p^{(+)}(0,t)$ denotes the positive-frequency part of the envelope of the pump-field amplitude at the output plane of the crystal; C_{N_j} is a constant. The relation $\int_{-\infty}^{\infty} d\tau N_1(\tau) = \int_{-\infty}^{\infty} d\tau N_2(\tau)$ reflects the fact that photons are in the nonlinear process generated in pairs.

The time dependence of $N_j(\tau)$ in Eq. (104) resembles that of the pump field, if $D_{pj}L \ll \tau_{\text{char}}$ (τ_{char} is a characteristic time of the change of pump-field intensity). This means that one-photon multimode Fock-state fields with a given mean-photon-number time dependence can be generated for suitably chosen pump-field-intensity profiles. For instance, if the pump field consists of two femtosecond pulses of the same duration and one has no chirp whereas the other one is highly chirped, the overall pump field as well as $N_j(t)$ have a peaked structure (see Fig. 17).

The spectrum S_j of downconverted field j,

$$S_j(\nu_j) = \langle \psi^{(2)}(0,t_0)|e_j^*(\nu_j)\hat{a}_j^\dagger(\nu_j)e_j(\nu_j)\hat{a}_j(\nu_j)|\psi^{(2)}(0,t_0)\rangle \tag{106}$$

can be expressed as a function of the pump pulse spectrum:

$$S_j(\nu_j) = |C_{S_j}(\nu_j)|^2 \int_{-\infty}^{\infty} d\nu_p \left|\mathscr{E}_p^{(+)}(0,\nu_p)\right|^2 L^2 \text{sinc}^2\left[\frac{L}{2}\left(D_{p\,3-j}\nu_p - D\nu_j\right)\right] \tag{107}$$

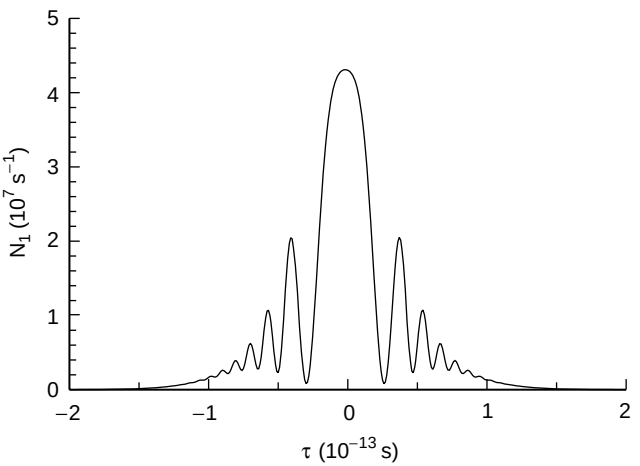

Figure 17. Mean number of photons $N_1(\tau)$ of the signal field; $\tau_1 = 1 \times 10^{-13}$ s, $\tau_2 = 0.5 \times 10^{-13}$ s, $a_1 = 0$, $a_2 = 10$, $\zeta_1 = \zeta_2 = 1$, $L = 0.05$ mm, $\phi = 0$ rad, $\theta = 0$ s, $|C_{N_1}|^2 = 1$ m^{-2} (after Ref. 91). Values of the inverse group velocities appropriate for the BBO crystal with type interaction at the pump wavelength $\lambda_p = 413$ mm ($\lambda_p = 397.5$ nm) and at the downconversion wavelengths $\lambda_1 = \lambda_2 = 826$ nm ($\lambda_1 = \lambda_2 = 795$nm) are used in Figs. 1, 2, and 5 (4).

where

$$\mathscr{E}_p^{(+)}(0,\nu_p) = \frac{1}{2\pi}\int_{-\infty}^{\infty} dt\, \mathscr{E}_p^{(+)}(0,t)\exp(i\nu_p t) \tag{108}$$

$\mathrm{sinc}(x) = \sin(x)/x$, and $C_{S_j}(\nu_j)$ is a constant. The spectrum of a downconverted field is obtained as a convolution of the pump pulse spectrum with a function (sinc^2) characterizing phase matching of the interacting fields in the nonlinear crystal. If the pump field spectrum $|\mathscr{E}_p^{(+)}(0,\nu_p)|^2$ has a peaked structure, oscillations in the spectrum $S_j(\nu_j)$ occur for longer crystals (see Fig. 18). Oscillations in the spectrum $S_j(\nu_j)$ do not occur for shorter crystals, because a peaked structure of the pump pulse spectrum $|\mathscr{E}_p^{(+)}(0,\nu_p)|^2$ is smoothed out by the wide sinc^2 function in Eq. (107).

A downconverted field in multimode Fock state with a required spectrum S_j can be generated if the pump-field spectrum $|\mathscr{E}_p^{(+)}(0,\nu_p)|^2$ is suitably chosen. A suitable pump-pulse spectrum is provided by the inverse formula to that in Eq. (107). If $|D_{p1}| \geq |D_{p2}|$, the spectrum S_1 can be expressed in terms of the spectrum S_2 [91]. The obtained relation is a consequence of entanglement of photons emerging during their generation and shows how photons in modes of the downconverted fields are correlated.

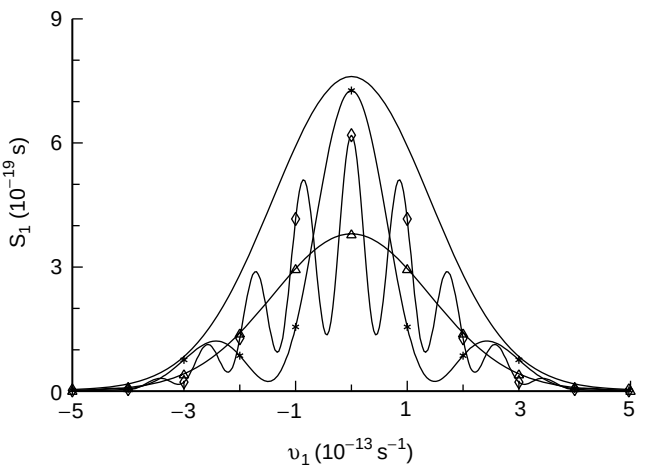

Figure 18. Spectrum $S_1(\nu_1)$ of the signal field for various values of the delay ϑ; $\vartheta = 0$ s (solid curve without symbols), $\vartheta = 3\times10^{-13}$ s ($*$), $\vartheta = 10\times10^{-13}$ s ($\diamond$), and $\vartheta = 50\times10^{-13}$ s ($\triangle$); $\tau_1 = \tau_2 = 1\times10^{-13}$ s, $a_1 = a_2 = 0$, $\zeta_1 = \zeta_2 = 1$, $L = 10$ mm, $\phi = 0$ rad, and $|C_{S_1}|^2 = 1$ m^{-2} (after Ref. 91).

B. Properties of Two-Photon Fields

Two-photon properties of downconverted fields are studied in coincidence-count measurements. Such measurements are conveniently described in terms of a two-photon amplitude $\mathscr{A}_{12}$ defined as follows:

$$\mathscr{A}_{12}(\tau_1, \tau_2) = \langle \text{vac}|\hat{E}_1^{(+)}(0, t_0 + \tau_1)\hat{E}_2^{(+)}(0, t_0 + \tau_2)|\psi^{(2)}(0, t_0)\rangle \tag{109}$$

Using the state $|\psi^{(2)}(0, t_0)\rangle$ given in Eq. (101), we arrive at the expression ($\omega_1^0 = \omega_2^0$ is assumed)

$$\mathscr{A}_{12}(T_0, \tau) = C_{\mathscr{A}} \frac{1}{|D|} \exp(-2i\omega_1^0 T_0) \operatorname{rect}\left(\frac{\tau}{DL}\right) \mathscr{E}_p^{(+)}\left(0, \frac{\Lambda}{D}\tau + T_0\right) \tag{110}$$

$\tau = \tau_1 - \tau_2$ and $T_0 = (\tau_1 + \tau_2)/2$. The symbol rect means the rectangular function ($\operatorname{rect}(x) = 1$ for $0 < x < 1$, $\operatorname{rect}(x) = 0$ otherwise); $C_{\mathscr{A}}$ is a constant.

We further consider one of typical interferometric configurations, the polarization analog of the Hong–Ou–Mandel interferometer. Its scheme is shown in Fig. 19. Assuming type II parametric downconversion, two mutually perpendicularly polarized photons occur at the output plane of the crystal. They propagate through a birefringent material (with group velocities g_1 and g_2) of a variable length l and then hit a 50/50% beamsplitter. The coincidence-count rate R_c is then given by the number of simultaneously detected photons at both detectors D_A and D_B in a given time interval. Analyzers rotated by 45 degrees with respect to ordinary and extraordinary polarization directions of the nonlinear crystal enable quantum interference between two paths leading to a coincidence count; either a photon from field 1 is detected by the detector D_A and a photon from field 2 by the detector D_B or vice versa. The normalized

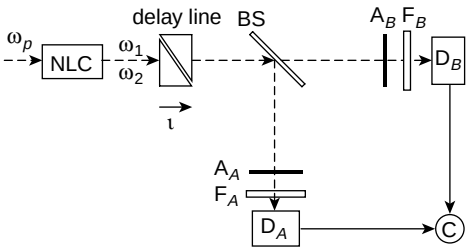

Figure 19. Sketch of the polarization analog of the Hong–Ou–Mandel interferometer: pump pulse at the frequency ω_p generates in the nonlinear crystal NLC downconverted photons at the frequencies ω_1 and ω_2. They propagate through a delay line of the length l and are detected at the detectors D_A and D_B; BS denotes a beamsplitter, A_A and A_B are analyzers, F_A and F_B are frequency filters, and C means a coincidence device.

coincidence-count rate R_n in this setting and for the two-photon amplitude $\mathscr{A}_{12}$ given in Eq. (110) can be expressed as follows ($D > 0$ is assumed [91]):

$$R_n(l) = 1 - \rho(l) \tag{111}$$

where

$$\rho(l) = \frac{|C_{\mathscr{A}}|^2}{2R_0 D^2} \int_{-DL/2+|\Delta\tau_l|}^{DL/2-|\Delta\tau_l|} d\tau \int_{-\infty}^{\infty} dT_0 \times \mathrm{Re}\left\{ \mathscr{E}_p^{(+)}\left(0, \frac{\Lambda}{D}\tau + T_0\right) \mathscr{E}_p^{(-)}\left(0, -\frac{\Lambda}{D}\tau + T_0\right) \right\} \tag{112}$$

and

$$R_0 = \frac{|C_{\mathscr{A}}|^2}{2D^2} \int_0^{DL} d\tau \int_{-\infty}^{\infty} dT_0 \left| \mathscr{E}_p^{(+)}\left(0, \frac{\Lambda}{D}\tau + T_0\right) \right|^2 \tag{113}$$

The symbol Re means real part, $\Delta\tau_l = \tau_l - DL/2$ and $\tau_l = (1/g_2 - 1/g_1)/l$.

The interference term $\rho(l)$ given in Eq. (112) is nonzero only in the interval $0 \le \tau_l \le DL$ for an arbitrary pump field. The interference pattern has the shape of a dip of the width DL. The change of envelope of the pump field leads only to a small modification of this shape. On the other hand, internal structure of the pump field may result in the occurrence of peaks at the bottom of the dip [91]. This behavior is well understood from the general relation between the shape of the two-photon amplitude and the profile of the interference pattern (for details, see Ref. 90).

The coincidence-count interference pattern has already been measured for a Gaussian pump pulse and for the downconverted fields being filtered by narrow frequency filters [88,92].

C. Effects of Dispersion in the Polarization Analog of the Hong–Ou–Mandel Interferometer

The wavevectors $k_p(\omega_{k_p})$, $k_1(\omega_{k_1})$, and $k_2(\omega_{k_2})$ of the pump, signal, and idler beams in the nonlinear crystal can be expressed in the following form including material dispersion up to the second order [90]:

$$k_j(\omega_{k_j}) = k_j^0 + \frac{1}{v_j}(\omega_{k_j} - \omega_j^0) + \frac{D_j}{4\pi}(\omega_{k_j} - \omega_j^0)^2, \quad j = p, 1, 2 \tag{114}$$

$k_j^0 = k_j(\omega_j^0)$. The symbol D_j stands for second-order dispersion coefficient of field j. Wave vectors of the down-converted beams in a dispersive material outside the crystal can be expressed similarly.

The coincidence-count rate $R_n(\tau_l)$ forms a triangular dip of width DL with the visibility 1 for cw pumping [79]. An ultrashort pump pulse of duration τ_{Di} leads to a loss of visibility but the width of the dip remains unchanged [88]. The shorter the pump pulse duration the smaller the values of visibility. Increasing values of the chirp parameter a_i lead to a reduction of visibility but the width of the dip does not change.

Second-order dispersion in the pump beam broadens the pump pulse. As a result, an increase in the second-order dispersion parameter D_p causes an increase of visibility, but no change in the width of the dip. Second-order dispersion in the downconverted beams leads to a broadening of the dip, as well as asymmetry and oscillations at its borders.

Second-order dispersion in an optical material (d_1 and d_2 are second-order dispersion parameters of the signal and idler beams in the material) through which downconverted photons propagate leads to asymmetry of the dip. The dip is particularly stretched to larger values of l (see Fig. 20) as a consequence of the deformation and lengthtening of the two-photon amplitude $A_{12,l}$ in a dispersive material. The higher the difference $d_1 - d_2$ of the dispersion parameters, the higher the asymmetry and the wider the dip; moreover its minimum is shifted further to smaller values of l (see Fig. 20).

Asymmetry of the dip caused by second-order dispersion in an optical material through which downconverted photons propagate can be suppressed

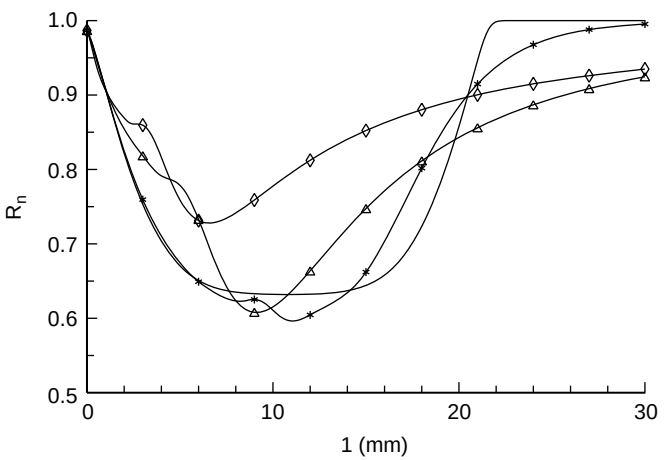

Figure 20. Coincidence-count rate $R_n(l)$ for various values of the second-order dispersion parameter $d = d_1 - d_2$ of an optical material (the material for the delay line is assumed to be quartz [91,90]); $d = 0$ s^2/mm (plain curve), $d = 1 \times 10^{-26}$ s^2/mm $(*)$, $d = 5 \times 10^{-26}$ s^2/mm ($\triangle$), and $d = 1 \times 10^{-25}$ s^2/mm ($\diamond$); $\tau_{D_i} = 1.55 \times 10^{-13}$ s, $L = 3$ mm, and $\sigma_1 = \sigma_2 = 50$ nm; values of the other parameters are zero (after Ref. 90).

under the following conditions; either the magnitude of second-order dispersion in the path of the first photon (given by $d_1 l$) equals that of the second photon (given by $d_2 l$) or the pump pulse duration has to be sufficiently long (in the cw regime). Dispersion cancellation has its origin in the entanglement of the photons, specifically, in the fact that the permitted values of the frequency ω_1 and the frequency ω_2 are governed by the relation $\delta(\omega_p - \omega_1 - \omega_2)$, where ω_p lies within the pump pulse spectrum.

D. Interference of Two Entangled Two-Photon Fields in the Polarization Analog of the Hong–Ou–Mandel Interferometer

We assume that the overall pump field consists of two partially overlapping ultrashort pulses (their mutual delay is denoted as ϑ). Then the overall down-converted field can be considered as composed of two partially overlapping two-photon fields that are mutually coherent and interfere. Interference between two entangled two-photon fields has its origin in the mutual coherence of the pump pulses.

The fourth-order interference pattern in the polarization analog of the Hong–Ou–Mandel interferometer behaves as follows. The visibility V of the coincidence-count pattern (coincidence-count dip [79]) as a function of the delay ϑ is shown in Fig. 21. For $\vartheta = 0$ s the entangled two-photon fields completely overlap, so in fact, there is only one entangled two-photon field with a given visibility. As the delay ϑ increases, two entangled two-photon fields are gradually formed at the output plane of the crystal. When the delay ϑ increases,

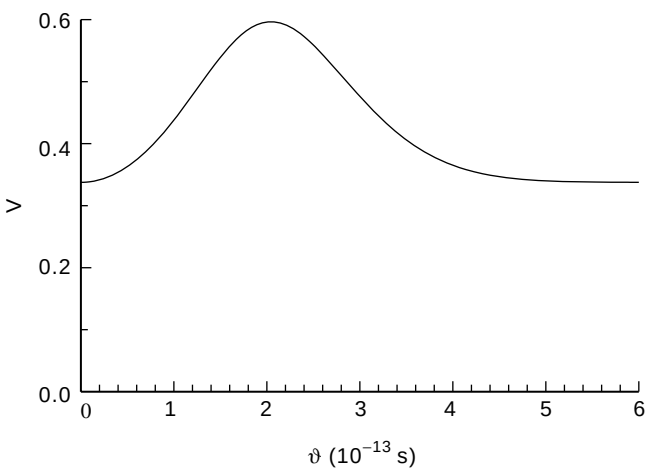

Figure 21. Visibility $V\,[V = (R_{n,\max} - R_{n,\min})/(R_{n,\max} + R_{n,\min})]$ as a function of the delay ϑ; $\tau_1 = \tau_2 = 1 \times 10^{-13}$ s, $a_1 = a_2 = 0$, $\zeta_1 = \zeta_2 = 1$, $L = 1.5$ mm, $\phi = 0$ rad, and $|C_{\mathscr{A}}|^2 = 10$ m^{-2} (after Ref. 91).

the overlap of the two entangled two-photon fields becomes smaller and higher values of the visibility V occur. This means that distinguishability of the signal and idler photons decreases with increasing ϑ because the higher the visibility the lower the distinguishability of the signal and idler photons [88]. For greater values of ϑ, the visibility V decreases. When the pump pulses are delayed so much that they do not overlap, there are two nonoverlapping downconverted fields and the visibility V is back to the value appropriate for $\vartheta = 0\,\mathrm{s}$. The increase of the visibility V caused by partially overlapped entangled two-photon fields might be useful in various multiparticle experiments for which high visibilities are required.

E. Absorption of Entangled Multiphoton Fields

Multiphoton absorption cross sections as functions of entanglement times and path delayes reflect quantum correlations among the optical fields constituting an entangled state [93,94]. There may occur entanglement-induced multiphoton transparency—the value of absorption cross section drops to zero for some values of entanglement times and path delayes (see Fig. 22 for entangled three-photon absorption cross section).

The dependence of multiphoton absorption cross sections on entanglement times and path delayes may, in principle, be used for the determination of spectrum and dipol moments of the absorbing material (for two-photon (three-photon) absorption, see Ref. 95 (Ref. 94).

The process of spontaneous parametric downconversion generates photons in mutually entangled multimode Fock states. Properties of such states depend strongly on the pump pulse characteristics; that is, entangled states with prescribed properties can be generated. The single-photon fields composing an entangled state are correlated in sharp time windows and this correlation is responsible both for a typical triangular dip in the Hong–Ou–Mandel interferometer and suppression of dispersion effects in dispersive materials. It also leads to entanglement-induced transparency. Properties of entangled fields are also conveniently applied in quantum cryptography [96] and metrology [97], as well as in experiments testing quantum theory.

VI. QUANTUM ZENO EFFECT IN FREQUENCY DOWNCONVERSION (*J. ŘEHÁČEK and J. PEŘINA*)

In quantum optics a downconversion process may be visualized as the decay of a pump photon into a pair of signal and idler photons of lower frequency. Provided the pumping remains not depleted and phase matching takes place, the energy of the spontaneously downconverted light monotonically increases and that of the pump beam monotonically decreases. From this point of view the downconversion process may be regarded as the decay process of an unstable

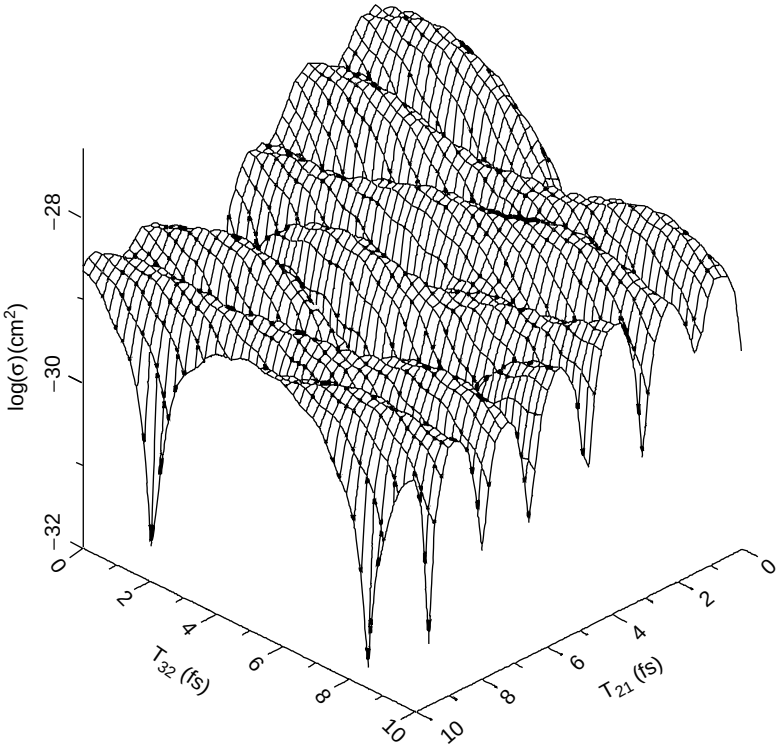

Figure 22. Entangled three-photon absorption cross section $\sigma(T_{21}, T_{32})$ for the transition $1s \to 4f$ in atomic hydrogen; the state $4f$ is assumed to be Lorentzian broadened with the lifetime 10^{-6} s; $\hbar\omega_1^0 = 4$ eV, $\hbar\omega_2^0 = \hbar\omega_3^0 = 4.37$ eV, $\theta_3 = 10$ fs, $A_{e2} = A_{e3} = 10^{-10}$ m^2; log denotes a decadic logarithm (after Ref. 94).

system. It is well known that frequent monitoring of a quantum system leads to inhibition of its evolution. This phenomenon is called the *quantum Zeno effect* (QZE) [98,99]. QZE has been studied in variety of physical systems including truly unstable systems and systems with finite recurrence time. For an excellent overview, see Ref. 100. Nonlinear optical systems are especially suitable for the analysis of QZE. Well-established methods of quantum optics can be used to deepen insight into this interesting phenomenon. Nonlinear optical realizations are also promising in view of possible future experiments. In the following paragraphs we will focus on QZE in frequency downconversion. Downconversion of light has already proved to be an invaluable tool in many fundamental experiments confirming quantum theory and extending the understanding of nature at the quantum level. This is true also for the study of QZE.

A. Pulsed Observations

A thought experiment has been suggested [101] in which it is possible to determine the place where the conversion of the pump photon took place inside the nonlinear crystal. The idea goes as follows. The nonlinear crystal is transversely cut in N pieces, which are then carefully aligned so that the signal and pump photons, leaving, say, the kth slice become the input signal and pump photons to the $(k+1)$th slice of the crystal (see Fig. 23). The idler photons, on the other hand, are removed after each slice, thus allowing for a future measurement to be performed on them. By increasing the number of slices, the actual position of birth of the signal and idler photons becomes more certain. Each piece of crystal will be described by the effective interaction Hamiltonian

$$H_{\mathrm{I}} = \Gamma(a_s^\dagger a_i^\dagger + a_s a_i), \qquad \hbar = c = 1 \tag{115}$$

where Γ is nonlinear coupling constant (proportional to the second-order susceptibility), and we assume that the strong pump beam is unaffected by the decay and can be treated in classical terms. We also assume that the process is perfectly phase-matched:

$$\Delta \equiv (\mathbf{k_p} - \mathbf{k_s} - \mathbf{k_i})_z = 0 \tag{116}$$

Here axes z is chosen along the direction of propagation. We adhere to the natural units $\hbar = c = 1$ hereafter. First recall the unobserved dynamics of a *weakly* nonlinear downconvertor. The probability of the emission of one signal photon in one crystal of length L is approximately

$$P_s(1) \approx \langle a_s'^\dagger a_s' \rangle \approx (\Gamma L)^2 \tag{117}$$

It is this short-time quadratic region that makes it possible to suppress the decay by repeated measurements. Such monitoring will be done as shown in Fig. 23. With this modification, the moment of emission can be inferred with accuracy $\delta L = L/N$ without disturbing the signal photons. Now, the probability of having

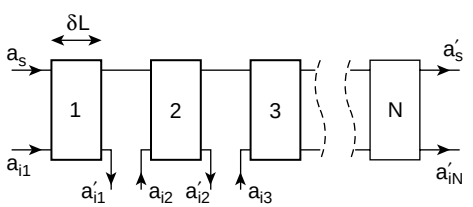

Figure 23. Scheme devised to infer the moment of emission of a signal downconverted photon.

one signal photon in the cascade becomes inverse proportional to the number of pieces:

$$\tilde{P}_s(1) \approx \langle a'^{\dagger}_s a'_s \rangle \approx \frac{(\Gamma L)^2}{N} \tag{118}$$

This is clearly manifestation of QZE. If the accuracy of the observation is increased by increasing N, the probability of the emission decreases at the same rate. In agreement with the Misra-Sudarshan theorem [99], the decay of pump photons is completely suppressed in the limit of very frequent monitoring $N \to \infty$. Further insight into the effect can be gained by rewriting Eqs. (117) and (118) in terms of uncertainty δL:

$$P_s(1) \approx N^2(\Gamma\delta L)^2, \qquad \tilde{P}_s(1) \approx N(\Gamma\delta L)^2 \tag{119}$$

We may say that for the unobserved system the emission is a cooperative effect of the N parts, whereas for the observed system we have an ordinary spontaneous emission from the N pieces. More to this, for the unobserved case the N emitters are stimulated by the same vacuum, imparting phase correlations between them. On the observed system the pieces are influenced by different and statistically independent vacuum fields leading to mutually incoherent emissions.

B. Continuous Monitoring—Kerr Interaction

The idea of considering the continuous interaction with an external agent as a sort of "steady gaze" at the system goes back to Kraus [102] and has recently been revived in relation with QZE [103]. Schulman [104], in particular, has even provided a quantitative relation between QZE produced by pulsed measurements (in the sense of the discussion in Ref. 99) and continuous observation (in the sense discussed below) performed by an external system.

Continuous observation offers distinct advantages for practical realization, since the strength of the observation can be controlled by a more accessible parameter than N, e.g. an intensity. Instead of dividing the crystal into pieces, let us assume another nonlinear interaction of the Kerr type between the idler mode and an auxiliary mode b (see Fig. 24). We replace (115) by the interaction Hamiltonian

$$H_{\mathrm{I}} = \Gamma(a_s^{\dagger}a_i^{\dagger} + a_s a_i) + \kappa a_i^{\dagger} a_i b^{\dagger} b \tag{120}$$

Now the information concerning the moment of emission of the signal photon is contained in the phase of the mode b, where the phase of the field b is proportional to the length covered by the idler photon since it has been emitted.

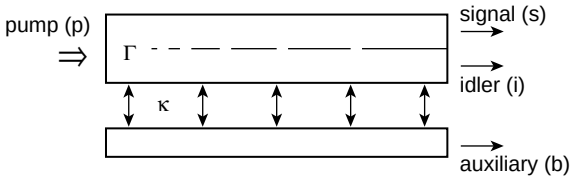

Figure 24. Downconversion process coupled to an auxiliary mode b.

The instant of emission of the signal photon can then be inferred by a phase-dependent measurement on the output field b.

Assuming weak nonlinearity as before we easily get the probability of emitting one signal photon,

$$\tilde{P}_s(1) \approx (\Gamma L)^2 \langle\varphi| \left[\frac{\sin(\kappa L b^\dagger b/2)}{\kappa L b^\dagger b/2}\right]^2 |\varphi\rangle \tag{121}$$

where $|\varphi\rangle$ is the initial state of the auxiliary mode b. One can see that the probability of emission of the signal photon is always less than or equal to the probability of the unobserved case (117), and it depends on the choice of the input state $|\varphi\rangle$ of the auxiliary field b. On the other hand, the accuracy of the inference of the emission time of the signal photon also depends strongly on the choice for $|\phi\rangle$. Two extreme cases can be recognized. In the limit when $|\varphi\rangle$ tends to vacuum state the probability (121) tends to that of the unobserved system (117). However, in this limit the phase of the field b is completely uncertain and the inference of the moment of the emission fails to give any meaningful information. In order to have a precise measurement of the phase shift a field $|\varphi\rangle$ with strong intensity is needed. However, in the limit of an intense field b, the probability (121) tends to zero and the emission is again prohibited.

This can be again interpreted in terms of QZE. Although the influence of the measuring apparatus (here mode b) cannot be described by a projection postulate in the sense of von Neumann, the evolution of the system is hindered in a way that is reminiscent of QZE. In contrast to previous "discrete" scheme, strength rather than frequency of observation is relevant here. It is interesting to notice that similarly to the discrete case, the suppression of the downconversion process can again be traced to the change of the phase relations between the interacting fields. Photon-number measurements based on Kerr-like interactions do not disturb the photon number of the measured system. However they affect its phase, and the frequency downconversion is very sensitive to the phase relations between the signal and idler beams. This dynamical explanation of the QZE will be studied in Section VI.D in greater detail.

C. Inverse Zeno Effect in Downconversion

In a dynamical explanation of QZE the inhibition of the original evolution is not a mandatory consequence. For instance, it has been shown in [105,106] that provided the phase matching condition is not fulfilled in the process of downconversion, the observation may, on the contrary, enhance the emission for a properly chosen N (inverse Zeno effect).

Let us consider once again a nonlinear medium cut into N pieces (Fig. 23). But now assume that the geometry of the original nonlinear process was such that the phase matching condition was not satisfied. The phase mismatch Δ can be accounted for by changing the interaction Hamiltonian to

$$H_{\mathrm{I}} = \Gamma(a_s^\dagger a_i^\dagger e^{-i\Delta t} + a_s a_i e^{i\Delta t}) \tag{122}$$

It is well known that mismatched nonlinear processes are always less effective than perfectly matched ones. One might wonder what will happen if a phase mismatched process is further disturbed by repeated measurements. Straightforward calculation gives the simple expression

$$\tilde{P}_s(1) \approx (\Gamma L)^2 \frac{1}{N}\left[\frac{\sin(\Delta L/2N)}{\Delta L/2N}\right] \tag{123}$$

for the probability of emitting one signal photon in the limit of weak nonlinearity. Notice that two opposite tendencies compete in Eq. (123). There is inhibition of emission due to the $1/N$ term. In the absence of mismatch it gives rise to QZE. Besides, there is a second effect due to the term in brackets that influences in the opposite direction. It tends to one in the limit of accurate observation. In this limit, however, the term $1/N$ will prevail. But before reaching this limit a question arises as to whether the combination of the two mentioned effects improves the emission in comparison with unobserved phase-mismatched process [obtained by putting $N = 1$ in Eq. (123)]. This would be a manifestation of the inverse Zeno effect (IZE). The rigorous answer can be obtained by comparing the original asymptotic exponential decay law with the exponential decay law forced by the repeated measurements [100,107]. It turns out that if $\Delta > \sqrt{3}\Gamma$ IZE is possible. The maximum emission rate results for N set to the nearest integer to $0.429\Delta L$; let us call this integer $N_{\max}$. The Zeno/inverse Zeno interplay shows up nicely in Fig. 25. It has an appealing explanation in terms of destructive and constructive interference of subsequent emissions inside the nonlinear crystal [101,105,106]. We have already seen that the emission in the unobserved case results from the coherent superpositions of probability amplitudes originated in each part of the crystal. As a result of phase mismatch, this interference is partially or completely destructive depending on

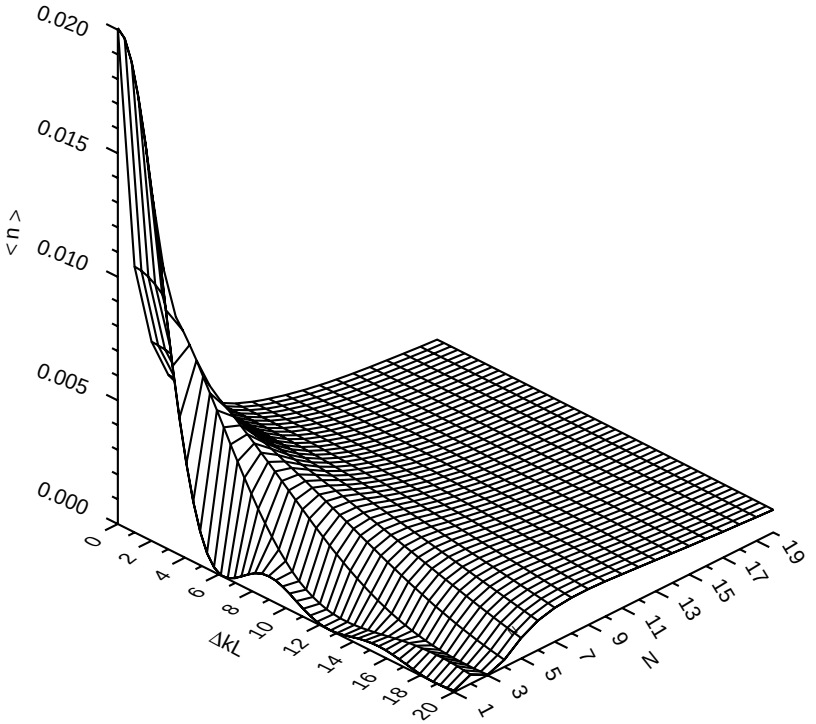

Figure 25. Interplay between the frequency of observations and phase mismatch. The mean number of signal photons $\langle n \rangle \equiv \langle n_s \rangle$ behind N nonlinear crystals is shown for various nonlinear mismatches $\Delta k \equiv \Delta$; $\Gamma = \sqrt{2}/10$; $L = 1$ (arbitrary units).

ΔL. After interrupting N times the idler mode, $N < N_{\max}$, the loss of coherence prevents this destructive interference and the probability of emission increases. But the mutual incoherence of the N emitters prevents also constructive interference and probability (123) is always less than it would be in the unobserved and phase-matched case (117).

If the original interference is destructive, the emission probability can be increased by repeated measurements (IZE). But this has a limit, since it is not possible to convert destructive interference into constructive interference by these means.

D. Continuous Monitoring—Linear Interaction

In Section VI.B a Kerr interaction has been used to extract some information about the time of the emission of signal photon. One may wonder what will happen if the Kerr interaction is replaced by a simpler one, for instance, by

simple linear exchange of energy between the idler and auxiliary modes. At first sight it might seem that linear interaction cannot give rise to a similar effect since only the output fields are accessible to measurement in the experimental setup in Fig. 24, and no relevant information is readily available in mode b about the place where the signal and idler photons are created. In this sense, no bona fide measurement is being performed on the fields by auxiliary mode. This point is discussed by Nakazato et al. [108] in connection with the experiment performed by Itano et al. [109]. Nevertheless, it is still possible (and useful) to speak about QZE in the more general sense given above. The exposition presented closely follows Ref. 110.

A downconversion process linearly coupled to an auxiliary mode b can be modeled by the following interaction Hamiltonian

$$H_I = \Gamma a_s^\dagger a_i^\dagger e^{i\Delta t} + \kappa a_i^\dagger b + \text{H.c.} \tag{124}$$

where κ is strength of the linear coupling. A possible realization of the Hamiltonian (124) could be a waveguide made of nonlinear material coupled to a linear waveguide, such as by means of evanescent waves [111].

First let us see how the linear coupling influences the dynamics of a phase matched process. To this end it is convenient to use "dressed modes." If $\Delta = 0$, the Hamiltonian (124) can be rewritten in terms of dressed modes as follows

$$H_I = \frac{\Gamma}{\sqrt{2}} a_s^\dagger c^\dagger e^{i\kappa t} + \frac{\Gamma}{\sqrt{2}} a_s^\dagger d^\dagger e^{-i\kappa t} + \text{H.c.}, \qquad (\Delta = 0) \tag{125}$$

where the operators of the dressed modes are simply linear combinations of the old operators,

$$\begin{aligned} c &= \frac{a_i + b}{\sqrt{2}} \\ d &= \frac{a_i - b}{\sqrt{2}} \end{aligned} \tag{126}$$

By comparing the Hamiltonian (125) with the Hamiltonian of a phase-mismatched process (122), one immediately sees that the coupling and the phase mismatch influence the downconversion process in a similar way. The coupling of the idler mode a_i with the auxiliary mode b yields two dressed modes c and d the pump photon can decay to. They are completely decoupled and due to their energy shift exhibit a phase mismatch $\pm\kappa$. Since the phase mismatch effectively shortens the time during which a fixed phase relation holds between the interacting beams, the amount of converted energy is smaller than in the ideal case of a perfectly phase-matched interaction. A strong linear

coupling then makes the subsequent emissions of converted photons interfere destructively and the nonlinear interaction is frozen.

There is an intuitive explanation of this behavior; since the linear coupling changes the phases of the amplitudes of the interacting modes, the constructive interference yielding exponential increase of the converted energy is destroyed, and downconversion becomes frozen. In this respect the disturbances caused by the linear coupling and by frequently repeated measurements are similar and we can interpret the phenomenon as QZE in the following sense: by increasing the coupling with the auxiliary mode, one performs a better "observation" of the idler mode and therefore of the "decay" of the pump. The hindering of the evolution results. We should mention that a more general definition of QZE has been given [100], which better fits into the present context than the original more stringent one given, for example, in Ref. 99.

The interpretation given in the preceding paragraph is strengthen by the fact that linear interaction can yield a kind of IZE under conditions similar to that discussed in Section VI.C. We shall show that when both linear coupling and phase mismatch are present in the process, the linear coupling can, rather surprisingly, compensate for the phase mismatch and vice versa, so that the probability of emission of the signal and idler photons can almost return back to its undisturbed value.

We start from the equations of motion generated by the full interaction Hamiltonian (124)

$$\begin{aligned} \dot{a}_s &= -i\Gamma a_i^\dagger e^{i\Delta t} \\ \dot{a}_i &= -i\Gamma a_s^\dagger e^{i\Delta t} - i\kappa b, \qquad (\Delta \neq 0, \kappa \neq 0) \\ \dot{b} &= -i\kappa a_i \end{aligned} \tag{127}$$

Although it is easy to write down the explicit solution of the system (127), here we shall provide only a qualitative discussion of the solution. The main features are then best demonstrated with the help of a figure. Eliminating idler and auxiliary mode variables from Eq. (127) we get a differential equation of the third order for the annihilation operator of the signal mode. Its characteristic polynomial (on substitution $a_s(t)$=$a_s(0)\exp(i\lambda t)$)

$$\lambda^3 + 2\Delta\lambda^2 + (\Delta^2 - \kappa^2 + \Gamma^2)\lambda + \Delta\Gamma^2, \quad \kappa \neq 0 \tag{128}$$

is recognized as a cubic polynomial in λ with real coefficients. An oscillatory behavior of the signal mode occurs only provided the polynomial (128) has three real roots (causus irreducibilis); thus, its determinant D must obey the condition $D < 0$. The case $\Delta \gg \Gamma$ is of main interest here. The resulting intervals are

$$\begin{aligned} &\text{Hyperbolic behavior:} \quad \kappa \in \langle \Delta - \sqrt{2}\Gamma, \Delta + \sqrt{2}\Gamma \rangle \\ &\text{Oscillatory behavior:} \quad \kappa \in \langle 0, \Delta - \sqrt{2}\Gamma) \cup (\Delta + \sqrt{2}\Gamma, \infty) \end{aligned} \tag{129}$$

In the absence of linear coupling the downconverted light shows oscillations and the overall effectiveness of the nonlinear process is small owing to the presence of strong phase mismatch $\Delta \gg \Gamma$. However, as we switch on the coupling between the idler and the auxiliary mode, the situation changes. By increasing the strength of the coupling the period of the oscillations gets longer and its amplitude gets larger. When κ becomes larger than $\Delta - \sqrt{2}\Gamma$, the oscillations are no longer seen and the intensity of the signal beam starts to grow monotonically. We can say that in this regime the initial nonlinear mismatch has been compensated by the coupling.

The interplay between nonlinear mismatch and linear coupling is illustrated in Fig. 26. A significant production of signal photons is a clear manifestation of IZE. In correspondence with the observations in other studies [105,106] (Section VI.C), such IZE occurs only provided a substantial phase mismatch is introduced in the process of downconversion. It is worthwhile to compare the interesting behavior seen in Fig. 26 with QZE and IZE observed in a sliced nonlinear crystal (Fig. 25). It can be seen that the coupling parameter κ here plays a role similar to the number of slices N, into which the crystal is cut in the latter scheme. Moreover, the sharpness of the "observation" (κ or N), at which a maximum output intensity occurs, is approximately a linear function of the introduced phase mismatch in both schemes. There are, however, also some points of difference. For example, the maximum output intensity obtainable for

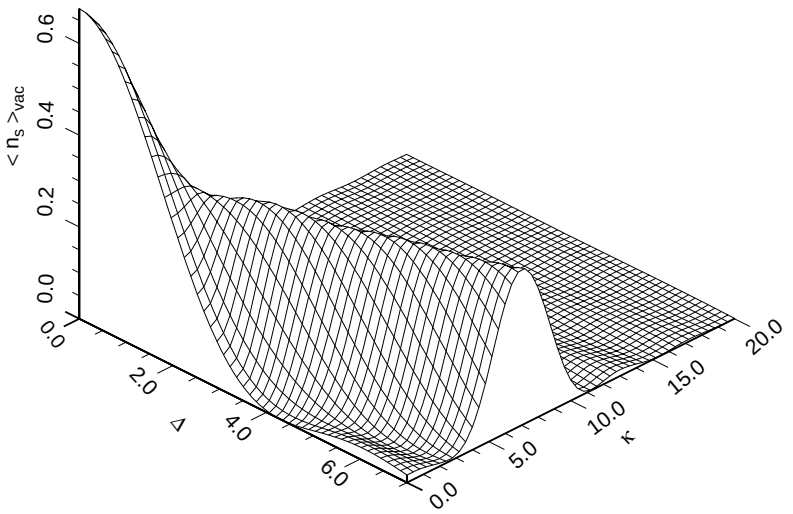

Figure 26. Interplay between linear coupling and phase mismatch. The mean number of signal photons $\langle n_s \rangle$ behind the nonlinear medium of length $L = 1.5$ is shown versus strength κ of linear coupling and nonlinear mismatch Δ ($\Gamma = 0.5$).

a given Δ by slicing the crystal decreases with increasing phase mismatch Δ [106]. On the other hand, no matter how strong the mismatch is, it can always be removed with the help of a suitable linear coupling (and vice versa). This difference is due to the $1/N$ scaling of intensities of output light generated by a process under observation [101,105,106]. An analogous factor is missing here.

Several intuitive explanations of IZE seen in Fig. 26 are at hand. From the point of view of constructive and destructive interference one can say that since the linear coupling effectively changes the phase relations among interacting modes, the destructive interference of subsequent pump photon decays caused by phase mismatch is suppressed in the same way as the constructive interference has been suppressed in the case of perfectly matched interaction.

Figure 26 can also be interpreted in a quantitative way in analogy with the dressed state description of interaction of atoms with intense light [112]. In terms of the dressed modes c and d of Eq. (126), if $\Delta \neq 0$, in place of the Hamiltonian (125), one gets

$$H_I = \frac{\Gamma}{\sqrt{2}} a_s^\dagger c^\dagger e^{i(\Delta+\kappa)t} + \frac{\Gamma}{\sqrt{2}} a_s^\dagger d^\dagger e^{i(\Delta-\kappa)t} + \text{H.c.} \tag{130}$$

The energy scheme implied by Hamiltonian (125) is shown in Fig. 27. Under the influence of the coupling with the auxiliary mode b the mismatched downconversion splits into two dressed energy–shifted interactions. It is apparent that when $\kappa = \pm\Delta$ one of the two interactions becomes resonant. The other one is "counterrotating" and acquires a phase mismatch 2Δ, yielding oscillations. Also, the amplitude of such oscillations decreases as Δ^{-2} and the mode output becomes negligible compared to the other one. The linear coupling to an auxiliary mode compensates for the phase mismatch up to a change in the effective nonlinear coupling strength $\Gamma \to \Gamma/\sqrt{2}$.

To summarize, the statement "the downconversion process is mismatched" means that the nonlinear process is out of resonance in the sense that the momentum of the decay products (signal and idler photons) differs from the

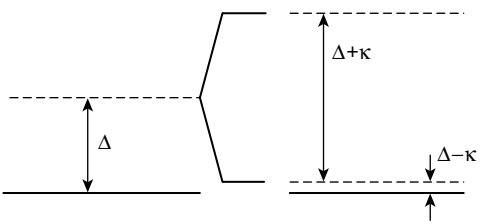

Figure 27. Energy scheme of a mismatched downconversion process subject to linear coupling. The bottom solid lines denote a resonant process.

momentum carried by the pump photon before the decay took place. When the linear interaction is switched on, the system gets "dressed" and the energy spectrum changes. A careful adjustment of the coupling strength κ then makes it possible to tune the nonlinear interaction back to resonance. In this way the probability of pump photon decay can be greatly enhanced. This occurs when $\kappa \simeq \pm\Delta$ and explains why IZE takes place along the line $\kappa = \Delta$ in Fig. 26.

In a certain sense, QZE is a consequence of the new dynamical features introduced by the coupling with an external agent that (through its interaction) "looks closely" at the system. When this interaction can be effectively described as a projection operator in the sense of von Neumann, we obtain the usual formulation of the QZE in the limit of very frequent measurements. In general, the description in terms of projection operators may not apply, but the dynamics can be modified in a way that is strongly reminiscent of QZE. Examples of the type analyzed here advocate a broader definition of quantum Zeno effect.

VII. QUANTUM STATISTICS OF LIGHT PROPAGATING IN RAMAN COUPLERS (*J. FIURÁŠEK and J. PEŘINA*)

A. Introduction

Attention has increasingly been paid to the propagation of light in nonlinear optical couplers, devices formed from two (or more) closely lying waveguides, whose guided modes are thus mutually linearly coupled by means of evanescent waves. Moreover, some nonlinear optical processes are active in the cores of the waveguides. Nonlinear couplers can serve as efficient ultrafast all optical switches [113–115] or logical gates [116,117].

Quantum description of the light propagation in the couplers allows investigation of the generation of nonclassical light in such devices. The nonlinear processes considered in this context include degenerate [113,118,119] and nondegenerate [114,120–122] parametric downconversion, Kerr effect [123,124], and Raman and Brillouin scattering [125–128]. Various configurations were investigated, including symmetric (nonlinear processes are in operation in both the waveguides) and asymmetric ones (one of the waveguides is linear) as well as codirectional and contradirectional propagation. In connection with the latter case quantum consistent input–output description was developed [129]. It was shown that squeezed light as well as light with sub–Poissonian photocount distribution can be generated in single modes or compound modes composed of two modes depending on the type of nonlinear interaction. Influence of various phase mismatches has been discussed [118, 126]. The quantum phase of optical fields propagating in nonlinear couplers has been studied [130,131]. For reviews, see Refs. 132 and 133.

In this contribution we focus on nonlinear couplers operating by means of Raman scattering [125–128]. This nonlinear process was thoroughly studied in

quantum optics, and several models were considered. In the simplest description one assumes strong coherent laser pumping and broad reservoir of phonon modes that are elliminated in Wigner–Weisskopf approximation [134–136]. A more complicated model includes one effective phonon mode [137,138], possibly coupled to reservoir. This allows for investigation of the quantum statistics and dynamics of the phonon field. Fully quantum treatment including laser modes can be found in Ref. 139.

B. Quantum Dynamics of Raman Couplers

We investigate the spatial evolution of the optical fields propagating in the Raman coupler depicted in Fig. 28. Working in the Heisenberg picture, we solve a set of Heisenberg–Langevin equations for the z-dependent field operators. It is convenient to employ momentum operator $\hat{G}$ rather than Hamiltonian $\hat{H}$ to describe the operation of the coupler because this approach allows us to take dispersion into account.

1. *Heisenberg–Langevin Equations*

The momentum operator $\hat{G}$ corresponding to the Raman coupler shown in Fig. 28 reads as [125]

$$\begin{aligned}\hat{G} = &\sum_{j=L_1,S_1,A_1,V_1} \hbar k_j \hat{a}_j^\dagger \hat{a}_j + \sum_{j=L_2,S_2,A_2,V_2} \hbar k_j \hat{a}_j^\dagger \hat{a}_j \\ &+ \sum_{k=1,2} [\hbar \tilde{g}_{A_k} \hat{a}_{L_k} \hat{a}_{V_k} \hat{a}_{A_k}^\dagger + \hbar \tilde{g}_{S_k} \hat{a}_{L_k} \hat{a}_{V_k}^\dagger \hat{a}_{S_k}^\dagger + \text{H.c.}] \\ &+ [\hbar \kappa_S \hat{a}_{S_1} \hat{a}_{S_2}^\dagger + \hbar \kappa_A \hat{a}_{A_1} \hat{a}_{A_2}^\dagger + \text{H.c.}]\end{aligned} \tag{131}$$

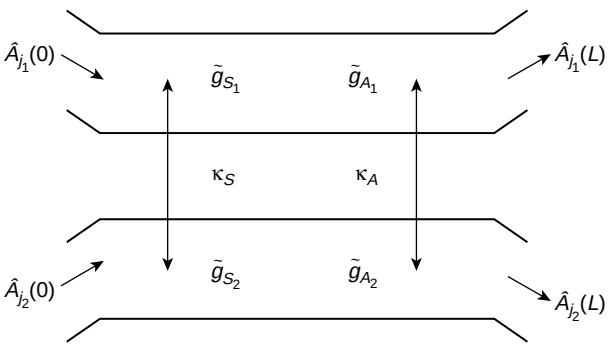

Figure 28. Sketch of the nonlinear Raman coupler formed from two waveguides of the length L.

Here H.c. denotes Hermitian conjugation; $\hat{a}_j^\dagger$ and $\hat{a}_j$ are creation and annihilation operators of laser (L), Stokes (S), anti-Stokes (A), and vibration (V) modes in the first (1) and second (2) waveguides. We can see that momentum operator (131) consists of a sum of three different parts. The first is the momentum operator of the free fields, k_j are propagation constants of the guided modes. The second part of $\hat{G}$ describes nonlinear scattering in the cores of first and second waveguides, $\tilde{g}_{S_j}$ and $\tilde{g}_{A_j}$, $j = 1, 2$ are nonlinear Stokes and anti-Stokes coupling constants characterizing intensity of Stokes and anti-Stokes processes, respectively. Finally the third term, which typically appears if we study couplers, represents linear coupling of Stokes and anti-Stokes modes in both the waveguides, and κ_S and κ_A are the corresponding linear coupling constants.

In the Heisenberg picture one has to solve a set of ordinary differential equations for creation and annihilation operators,

$$i\hbar \frac{d\hat{a}_j}{dz} = [\hat{G}, \hat{a}_j] \tag{132}$$

Here $[,]$ denotes commutator. All operators fulfill standard boson-type commutation rules

$$[\hat{a}_i, \hat{a}_j] = 0, \quad [\hat{a}_i^\dagger, \hat{a}_j^\dagger] = 0, \quad [\hat{a}_i, \hat{a}_j^\dagger] = \delta_{ij} \tag{133}$$

We assume strong coherent pumping of laser modes and replace the operators $\hat{a}_{L_j}$ with corresponding complex amplitudes $\alpha_{L_j} \exp(ik_{L_j} z)$. To simplify the notation, we define new parameters $g_{S_j,A_j} = \alpha_{L_j} \tilde{g}_{S_j,A_j}$, $j = 1, 2$.

To remove fast oscillations we work in the interaction picture introducing new operators $\hat{A}_j = \hat{a}_j(z) \exp(-ik_j z)$. The damping of vibration modes is modelled as coupling of each vibration mode to the broad reservoir of harmonic oscillators in thermal equilibrium [140]. The two important parameters are damping constants γ_{V_j} and mean number of chaotic phonons $\langle n_{V_j} \rangle$, $j = 1, 2$. Finally we arrive at [127] the following:

$$\begin{aligned}
\frac{d\hat{A}_{S_1}}{dz} &= ig_{S_1} e^{i\Delta k_{S_1} z} \hat{A}_{V_1}^\dagger + i\kappa_S^* e^{-i\Delta K_S z} \hat{A}_{S_2} \\
\frac{d\hat{A}_{A_1}}{dz} &= ig_{A_1} e^{i\Delta k_{A_1} z} \hat{A}_{V_1} + i\kappa_A^* e^{-i\Delta K_A z} \hat{A}_{A_2} \\
\frac{d\hat{A}_{V_1}}{dz} &= -\gamma_{V_1} \hat{A}_{V_1} + ig_{S_1} e^{i\Delta k_{S_1} z} \hat{A}_{S_1}^\dagger + ig_{A_1}^* e^{-i\Delta k_{A_1} z} \hat{A}_{A_1} + \hat{L}_{V_1}(z)
\end{aligned} \tag{134}$$

Equations for other operators can be obtained from the symmetry and by Hermitian conjugation. Operators of Langevin forces $\hat{L}_{V_j}$ ensure the validity of

commutation relations (133) for all z and they fulfill Markoffian properties [140]

$$\begin{aligned}&\langle \hat{L}_{V_i}(z)\rangle = 0, \quad \langle \hat{L}_{V_i}(z_1)\hat{L}_{V_j}(z_2)\rangle = 0, \quad \langle \hat{L}^\dagger_{V_i}(z_1)\hat{L}^\dagger_{V_j}(z_2)\rangle = 0\\ &\langle \hat{L}^\dagger_{V_i}(z_1)\hat{L}_{V_j}(z_2)\rangle = 2\gamma_{V_i}\langle n_{V_i}\rangle\delta(z_1 - z_2)\delta_{ij}, \quad i,j = 1,2\end{aligned} \tag{135}$$

Various phase mismatches appearing in (134) are defined as follows:

$$\begin{aligned}\Delta K_S &= k_{S_1} - k_{S_2}, & \Delta K_A &= k_{A_1} - k_{A_2}\\ \Delta k_{S_j} &= k_{L_j} - k_{V_j} - k_{S_j}, & \Delta k_{A_j} &= k_{L_j} + k_{V_j} - k_{A_j}\end{aligned} \tag{136}$$

The actual values of these phase mismatches depend on the dispersion of the waveguides forming the coupler.

The set of equations (134) and related ones separates into two independent subsets, one for $\hat{A}^\dagger_{S_1}$, $\hat{A}_{A_1}$, $\hat{A}_{V_1}$, $\hat{A}^\dagger_{S_2}$, $\hat{A}_{A_2}$, $\hat{A}_{V_2}$ and the other for their Hermitian conjugates. It is useful to take advantage of matrix formalism and to rewrite (134) to the compact form [127,128]

$$\frac{d}{dz}\hat{\mathbf{A}}(z) = \mathbf{M}(z)\hat{\mathbf{A}}(z) + \hat{\mathbf{L}}(z) \tag{137}$$

here $\hat{\mathbf{A}}$ and $\hat{\mathbf{L}}$ are column vectors

$$\hat{\mathbf{A}} = \left(\hat{A}^\dagger_{S_1}, \hat{A}_{A_1}, \hat{A}_{V_1}, \hat{A}^\dagger_{S_2}, \hat{A}_{A_2}, \hat{A}_{V_2}\right)^T, \quad \hat{\mathbf{L}} = \left(0, 0, \hat{L}_{V_1}, 0, 0, \hat{L}_{V_2}\right)^T$$

and the elements of matrix $\mathbf{M}(z)$ can be determined from (134). We can write the generic solution of (137) as

$$\hat{\mathbf{A}}(z) = \mathbf{F}(z)\hat{\mathbf{A}}(0) + \mathbf{F}(z)\int_0^z \mathbf{F}^{-1}(z')\hat{\mathbf{L}}(z')\,dz' \tag{138}$$

We have introduced the matrix of the fundamental solution $\mathbf{F}(z)$, which is the solution of the homogeneous equation

$$\frac{d}{dz}\mathbf{F}(z) = \mathbf{M}(z)\mathbf{F}(z), \qquad \mathbf{F}(0) = \mathbf{E} \tag{139}$$

Here $\mathbf{E}$ is the identity matrix. $\mathbf{F}(z)$ can be expressed in a simple form if $\mathbf{M}$ does not depend on z, or if one can transform (134) to a system with constant coefficients [127], then $\mathbf{F}(z) = \exp(\mathbf{M}z)$.

2. *Dynamic Regimes of the Coupler*

If all phase matching conditions are fulfilled, that is, all phase mismatches are zero, then the dynamics of the coupler is fully characterized by the eigenvalues

Λ_j of the matrix $\mathbf{M}$, which does not depend on z. Positive or negative real parts of the eigenvalues correspond to exponential amplification or attenuation and imaginary parts give the period of oscillations.

Simple analytical results can be obtained for asymmetric configuration when the nonlinear scattering takes place only in the first waveguide and damping is neglected. One eigenvalue is zero, $\Lambda_5 = 0$, the others are roots of biquadratic equation

$$\Lambda_j = \pm\frac{1}{2}\left(\sqrt{p+2q} \pm \sqrt{p-2q}\right) \tag{140}$$

where

$$\begin{aligned} p &= |g_{S_1}|^2 - |g_{A_1}|^2 - |\kappa_S|^2 - |\kappa_A|^2 \\ q^2 &= |\kappa_S|^2|\kappa_A|^2 + |\kappa_S|^2|g_{A_1}|^2 - |\kappa_A|^2|g_{S_1}|^2 \end{aligned} \tag{141}$$

The influence of coupling constants on the dynamic properties of the coupler can be deduced from (140). The following qualitative classification is valid [127]:

1. $q^2 < 0$—anti-Stokes scattering is weakened by linear coupling κ_A. Simultaneously the nonlinear Stokes interaction is stronger than Stokes linear coupling, $|\kappa_S| < |g_{S_1}|$, which enables amplification due to Stokes scattering. Two roots are real and two are purely imaginary.
2. $q^2 > 0$, $p > 0$, $p^2 > 4q^2$— Stokes scattering dominates, $|g_{S_1}| > |g_{A_1}|$, and the linear coupling is weak; all four roots are real.
3. $q^2 > 0$, $p < 0$, $p^2 > 4q^2$— strong Stokes linear coupling suppresses the amplification, all four roots are purely imaginary.
4. $q^2 > 0$, $p^2 < 4q^2$— the interplay of Stokes and anti-Stokes linear coupling allows for amplification, all four roots are complex.

Since the amplification is accompanied by exponential increase of noise transferred from the phonon reservoirs, the oscillating dynamics of region 3 is optimal for the generation of nonclassical states of light in the coupler.

The region of oscillatory dynamics further reduces when the damping of vibration modes is taken into account. An analysis based on Hurwitz criterion reveals that exponential amplification takes place for almost all values of the parameters except for a class of special configurations meeting [127]

$$\begin{aligned} &|\kappa_S| = |\kappa_A| = \kappa, \quad |g_{S_2}| = c|g_{S_1}|, \quad |g_{A_2}| = c|g_{A_1}| \\ &\arg\left(\kappa_S\kappa_A g_{S_1} g_{A_1} g_{S_2}^* g_{A_2}^*\right) = \pi, \quad |g_{S_j}| < |g_{A_j}| \end{aligned} \tag{142}$$

where $c \geq 0$ is an arbitrary nonnegative real number. Damping constants of vibration modes γ_{V_1} and γ_{V_2} are arbitrary and perfect phase matching is assumed.

The phase mismatches can alter the dynamics significantly [126,127] and they can either support or suppress the amplification. Their influence depends in complex manner on the coupling parameters and damping constants of the coupler.

C. Quantum Statistical Properties of Light

1. *Generalized Superposition of Coherent Signal and Quantum Noise*

The linearization of the Heisenber–Langevin equations (134) allows us to treat the quantum statistical properties of light within the framework of generalized superposition of coherent signal and quantum noise [140]. Quantum states belonging to this class are also called Gaussian states, because the quasi-distributions (phase-space representations of the quantum state) have Gaussian form. Similarly, the normal characteristic function is Gaussian:

$$\begin{aligned} C_{\mathcal{N}}(\{\beta_j\}, z) = \exp\Bigg\{ & \sum_j \left[-B_j(z)|\beta_j|^2 + \left(\frac{1}{2} C_j(z)\beta_j^{*2} + \text{c.c.} \right) \right] \\ & + \sum_j \sum_{k>j} [D_{jk}(z)\beta_j^*\beta_k^* + \bar{D}_{jk}(z)\beta_j\beta_k^* + \text{c.c.}] \\ & + \sum_j [\beta_j \xi_j^*(z) - \text{c.c.}] \Bigg\} \end{aligned} \tag{143}$$

(where c.c. = complex conjugates). The sum is performed over all modes taking part in the interaction. The complex amplitudes $\xi_j(z)$ and noise parameters $B_j, C_j, D_{jk}, \bar{D}_{jk}$ are defined as [140]

$$\xi_j(z) = \langle \hat{A}_j(z) \rangle \tag{144}$$

$$\begin{aligned} B_j(z) &= \langle \Delta\hat{A}_j^\dagger(z)\Delta\hat{A}_j(z) \rangle, \quad D_{jk}(z) = \langle \Delta\hat{A}_j(z)\Delta\hat{A}_k(z) \rangle \\ C_j(z) &= \langle \Delta\hat{A}_j(z)\Delta\hat{A}_j(z) \rangle, \quad \bar{D}_{jk}(z) = -\langle \Delta\hat{A}_j^\dagger(z)\Delta\hat{A}_k(z) \rangle \end{aligned} \tag{145}$$

where $\Delta\hat{A}_j(z) = \hat{A}_j(z) - \langle \hat{A}_j(z) \rangle$.

To calculate complex amplitudes and noise functions we insert the solution (138) to (144) and (145), perform the averages using (135), and evaluate the resulting integrals [127,135,141]. The amplitudes and noise coefficients at given z depend on the initial values $\xi_j(0)$, $B_j(0), C_j(0)$ and mean numbers of chaotic phonons $\langle n_{V_j} \rangle$. Usually the input modes are not correlated, hence $D_{jk}(0) = \bar{D}_{jk}(0) = 0$.

The photon-number operator of the jth mode reads as $\hat{n}_j = \hat{A}_j^\dagger \hat{A}_j$, and in case of multimode field we introduce the total photon-number operator $\hat{n} = \sum_j \hat{n}_j$. The photon-number statistics can be conveniently characterized by reduced factorial moments (RFMs) of the kth order

$$\mathrm{RFM} = \frac{\langle : \hat{n}^k : \rangle}{\langle n \rangle^k} - 1 \tag{146}$$

where : : denotes normal ordering. Explicit formulas for RFM of Gaussian states can be found in Ref. 140. The negative value of the second RFM indicates violation of classical statistical inequalities and such nonclassical state of light is called sub-Poissonian because the photon-number variance is lower than mean number of photons.

Let us now turn to squeezed light. We define quadrature components of single and compound modes;

$$\begin{aligned} \hat{p}_j &= -i(\hat{A}_j - \hat{A}_j^\dagger), & \hat{q}_j &= \hat{A}_j + \hat{A}_j^\dagger \\ \hat{p}_{jk} &= \hat{p}_j + \hat{p}_k, & \hat{q}_{jk} &= \hat{q}_j + \hat{q}_k \end{aligned}$$

Squeezing occurs if one of the quadrature variances $\langle (\Delta\hat{p})^2 \rangle$, $\langle (\Delta\hat{q})^2 \rangle$ is below the coherent state level. A more general definition deals with single and compound mode principal squeeze variances λ_j and λ_{jk} [140]

$$\begin{aligned} \lambda_j(z) &= 1 + 2[B_j(z) - |C_j(z)|], \\ \lambda_{jk}(z) &= 2\{1 + B_j(z) + B_k(z) - 2\mathrm{Re}[\bar{D}_{jk}(z)] - |C_j(z) + C_k(z) + 2D_{jk}(z)|\} \end{aligned} \tag{147}$$

Single-mode squeezing occurs when $\lambda_j < 1$ and compound mode is squeezed if $\lambda_{jk} < 2$. Yet more general definition of the squeezing is possible, the so-called generalized squeezing [128,142]. The generalized squeeze variance λ_G is related to the lowest eigenvalue of the matrix defining the quadratic form in the exponent on the right-hand side of Eq. (143) [128,142].

The structure of the interaction implies that if $C_j(0) = 0$, then $C_j(z) = 0$ and either $D_{jk}(z) = 0$ or $\bar{D}_{jk}(z) = 0$ for all j. This means that nonclassical light cannot be generated in single modes. Photocount distribution of single modes is super–Poissonian and no squeezing occurs. Thus the focus is on compound modes that can exhibit various nonclassical properties.

2. *Squeezing of Light in the Coupler*

Because of the linearity of Heisenberg–Langevin equations, the squeezing does not depend on the initial complex amplitudes of optical modes. Squeezed light

can be generated in compound modes composed of Stokes and anti-Stokes modes; also, the compound photon–phonon mode consisting of Stokes and vibration modes can exhibit suppression of the quadrature fluctuations below the coherent state level.

If damping of vibration modes is negligible, then the evolution governed by Heisenberg equations (134) is unitary and input pure multimode state remains pure during the propagation. In particular, input multimode coherent state evolves to pure multimode Gaussian state. Such minimum-uncertainty states are either coherent or nonclassical, exhibiting multimode generalized squeezing [143]. In the latter case, there exists a quadrature formed by linear combinations of the quadratures of all six involved modes, whose variance falls below the coherent state level. Of course, the unitary evolution is also optimal for the generation of the two-mode squeezing in compound Stokes and anti-Stokes modes.

Usually, however, the damping of vibration modes is significant, the evolution is not unitary, input pure Gaussian state evolves into mixed state and the uncertainty increases as the noise is transferred from the reservoir to the optical modes. It turns out that the special configurations (142) exhibiting oscillatory dynamics and no amplification are optimal for the squeezed-light generation in the initial stage of the interaction [127,128].

An example of principal squeeze variances of compound mode (S_1, A_1) is given in Fig. 29 for three different asymmetric configurations. When $\gamma_{V_1} = 0$ (no damping) we have maximal squeezing and periodic dependence on z, whereas for $\gamma_{V_1} = 2.5$ the oscillations are damped and λ reaches some asymptotic value. Figure 29 also illustrates that nonzero mean number of chaotic phonons makes the squeezing less pronounced.

3. *Sub-Poissonian Light Generation*

It holds for the class of fields with Gaussian quasidistributions that the sub-Poissonian photon-number statistics are closely related to the squeezing. More precisely, the occurrence of generalized squeezing is necessary in order to reduce photon-number fluctuations below the coherent state level [143]. Such reduction can be achieved by properly adjusting the coherent components $\xi_j(0)$ of the input modes. In this way we can control the position of the noise ellipsoid in the phase space and distribute the quantum fluctuations in such a way that the photon-number variance is reduced below the mean photon number [143]. Sub-Poissonian light can be generated in compound (Stokes, anti-Stokes) modes. An example is given in Fig. 30, which illustrates typical behavior of the second RFM of the compound mode (S_1, A_1). The regions of sub-Poissoninan statistics appear in the initial stage of the interaction and for larger z the light becomes super-Poissonian. The noise from phonon reservoir can strongly reduce the nonclassical behavior. Cooling of the coupler can reduce the mean number of

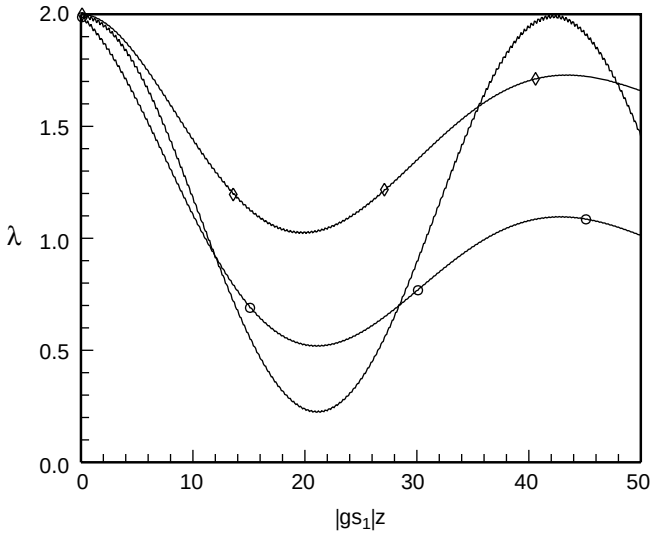

Figure 29. Principal squeeze variance λ for mode (S_1, A_1); $\gamma_{V_1} = 0, \langle n_{V_1} \rangle = 0\,(-)$; $\gamma_{V_1} = 2.5, \langle n_{V_1} \rangle = 0\,(\circ)$; $\gamma_{V_1} = 2.5, \langle n_{V_1} \rangle = 1\,(\diamond)$; $gs_1 = 1, g_{A_1} = 2$, $\kappa_S = \kappa_A = 10, B_{V_1}(0) = 0$, and other parameters are zero. All optical modes are initially in coherent states.

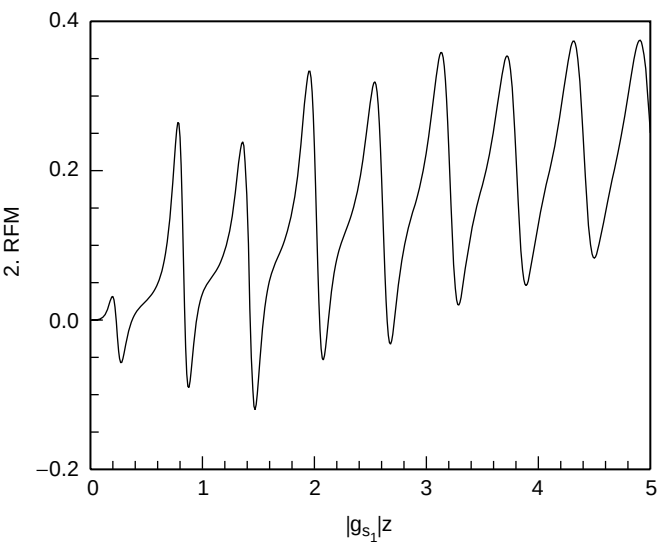

Figure 30. The second RFM for the mode (S_2, A_1); $\kappa_S = \kappa_A = 5$, $g_{S_1} = i, g_{A_1} = 2i, \gamma_{V1} = 0.5$, $B_{V_1}(0) = \langle n_V \rangle = 0, \xi_{S_1} = 0.5, \xi_{S_2} = i, \xi_{A_1} = 2, \xi_{A_2} = i$ and the other parameters are zero. Fields are initially coherent.

chaotic phonons $\langle n_{V_j} \rangle$, thus enhancing the desired suppression of photon-number fluctuations [127].

D. Summary

The nonlinear optical couplers are emerging as promising devices for the controlled generation and transfer of nonclassical states of light, which may find broad applications in optical communication systems. Several types of nonlinear optical processes have been considered in this context and greatest attention has been paid to couplers based on degenerate or nondegenerate parametric downconversion. However, second-order processes require noncentrosymmetric media and it need not be easy to fabricate couplers with sufficient second-order nonlinear susceptibility. Therefore, couplers based on Raman scattering may represent an alternative to the couplers operating by means of downconversion. We have seen that the Raman coupler is capable of generating squeezed light as well as light with sub-Poissonian statistics. The transfer of noise from phonon reservoir to optical modes can spoil the nonclassical features, but this unwanted effect can be minimized if the coupler is properly designed and the amplification leading to inevitable increase of noise is avoided.

VIII. QUANTUM CRYPTOGRAPHY (*O. HADERKA, M. HENDRYCH, and M. DUŠEK*)

For ages people have wished to find a way to communicate in secrecy so as to allow nobody to overhear their messages. This wish or desire may come true with the aid of cryptography. *Cryptography* may be defined as the art of writing and deciphering messages in code.

The use of cryptography in everyday life has grown enormously since the 1980s. The outburst of electronic communications between banks, state agencies, and various institutions handling private data, as well as the fast development of e-commerce on the Internet, has lead to a huge increase of demand for secure cryptographic methods and devices. Today most of cryptographic tasks are solved with the help of cryptosystems [144] that rely on computational complexity, such as on the difficulty in factoring large numbers. However, advances in mathematical algorithms and computing power compromise the security of these methods, which is maintained by continual lengthening of cryptographic keys. Classical cryptography also faces an increasingly serious menace arising from the construction of quantum computers. Algorithms capable of breaking public-key ciphers have already been developed [145]. Although the construction of a practical device is still hypothetical, experimental advances are very rapid. Another threat to classical systems comes from single-purpose massively parallel optoelectronic devices [146].

In contrast to classical cryptographic methods, the security of quantum cryptography is based on the fundamental laws of physics. It is guaranteed by the Heisenberg uncertainty principle and is independent of any mathematical or technological developments.

The first prototype of quantum cryptographic apparatus came into existence around 1990 [147]. In the meantime, quantum cryptography has become a well-known technique of communication in a provably secure way, and together with an intensive research in the field of quantum computers it has given rise to a whole new branch of science: quantum information theory [148]. Viewed from this perspective, quantum cryptography today is only a subset of a broad field of quantum communications that also include quantum teleportation, quantum dense coding, quantum error-correcting codes, and quantum data compression.

The purpose of this review is to give an overview of both theoretical and experimental achievements in the field with a focus on recent developments.

A. Cryptographic Tasks

Current classical cryptographic methods are used to solve a number of tasks. One of the most important ones is *secure message exchange*, which allows two parties to communicate in such a way that their messages are unintelligible to any third party. An unconditionally secure method that enables to achieve this goal is the so-called Vernam cipher [149], or a one-time pad, which was invented in 1917. The principle of this cipher is that addition of a string of random bits, called the "key," to a message, renders the resulting string also completely random. For this cipher to be unconditionally secure, three requirements must be satisfied: (1) the key must be as long as the message, (2) it must be purely random, and (3) it may be used once and only once. The only way to reveal the contents of the original message is to subtract the key. Thus the task of secure message exchange can be reduced to the problem of secure distribution of the cryptographic key.

Other tasks challenging cryptographers include mutual identification, secret sharing, and multiparty computations. The goal of *mutual identification* is for individual parties to assure each other of their identities. *Secret sharing* is a method that enables us to split a secret string, such as a vault password, into several shares in such a way that individual shares contain absolutely no information about the secret, however, certain minimal subsets of the shares, pieced together, can recover the original secret. *Multiparty computations* allow two or more parties to perform a common computation without disclosing the input data of individual participants. After each party submits its input, every participant learns the output, computed from the inputs, without learning the inputs of the others, except those inferable from the output. This can be used, such as for voting ballots.

It should be mentioned that all these tasks can be solved classically, but they suffer either from the key-distribution problem or from the absence of an unconditional security proof, and therefore from vulnerability to future decrypting techniques, quantum or classical.

On the other hand, quantum physics enables us to design a cryptographic primitive, which resolves at least part of the tasks mentioned above. This primitive is called *quantum key distribution*.

B. The Principle

The quantum key distribution (QKD) procedure allows two parties to establish a common random secret key. It takes advantage of the fact that quantum mechanics does not allow us to distinguish nonorthogonal states with certainty. The security of QKD is guaranteed by their overlap.

Within the framework of classical physics, information encoded into a property of a classical object, can be acquired without affecting the state of the object. However, if information is encoded into a property of a quantum object, any attempt to discriminate its nonorthogonal states inevitably changes the original state with a nonzero probability. And since eavesdropping is also governed by the laws of quantum mechanics, these changes cause errors in transmissions and reveal the eavesdropper.

An eavesdropper could also try to amplify the signal and split off its part, however, cloning of quantum states is also forbidden by quantum principles [150]. Thus QKD cannot prevent from eavesdropping, but it enables legitimate users to discover it. If any eavesdropping is detected, the key is simply thrown away and a new one is generated. No leakage of information occurs, since the key is just a random sequence.

1. Communication Protocol BB84

The first QKD protocol was proposed by C. H. Bennett and G. Brassard in 1984 [151] (therefore the acronym BB84), following the first ideas by S. Wiesner [152]. At present time this protocol has been best elaborated, both theoretically and experimentally. The properties that may be employed to encode information are, for example, polarization of photons, phase, or quantum correlations (entanglement) of quantum systems. How does this protocol work? Let us first describe a system, where information is encoded into linear polarizations of photons:

At the beginning, the two parties that wish to communicate, traditionally called Alice and Bob, agree on two polarization bases mutually rotated by 45°, and determine which polarization in each basis corresponds to a logical 1 and 0; for instance,

$$\begin{array}{llll} \text{Base } + : & \updownarrow = 0 & \leftrightarrow = 1 \\ \text{Base } \times : & \nwarrow\!\!\!\searrow = 0 & \swarrow\!\!\!\nearrow = 1 \end{array}$$

Then Alice generates random bits, chooses randomly between the two polarization bases, and sends photons with corresponding polarizations to Bob. Bob also chooses randomly (and independently of Alice) his detection bases, namely, the orientation of his polarization analyzer. The two outputs of the analyzer are fed to detectors. One detector corresponds to a "1", the other to a "0". Next, Alice and Bob tell each other through a public channel (computer network, telephone, etc.), which bases they used for individual photons. Note that they communicate *bases only*, not particular polarizations of photons. They keep only those bits when their bases coincided. In those cases their bits should be identical as the results of Bob's measurements are deterministic. Thus they obtain a shared key. When they used different bases, the outcomes of Bob's measurements are random, and are discarded. Afterward Alice and Bob "sacrifice" a random part of this sequence by publicly comparing it. Their strings should be identical; possible differences reveal an eavesdropper's activity. The disclosed part of the key must be thrown away and cannot be used for any other purposes. The whole procedure is summarized in the following table:

(1)	0	1	1	0	1	1	0	0	1	0	1	1	0	0	1
(2)	×	+	×	+	+	+	+	+	×	×	+	×	×	×	+
(3)	⤡	↔	⤢	↕	↔	↔	↕	↕	⤢	⤡	↔	⤢	⤡	⤡	↔
(4)	+	×	×	+	+	×	×	+	×	+	×	×	×	×	+
(5)	1		1		1	0	0	0		1	1	1		0	1
(6)	+		×		+	×	×	+		+	×	×		×	+
(7)			OK		OK			OK				OK		OK	OK
(8)			1		1			0				1		0	1
(9)					1									0	
(10)					OK									OK	
(11)			1					0				1			1

A. Quantum distribution:
   (1) Random bits generated by Alice
   (2) Polarization bases randomly chosen by Alice
   (3) Polarizations of photons sent by Alice
   (4) Random orientations of Bob's polarization analyzer
   (5) Bits obtained by Bob (blank spaces mean that the photon was lost)

B. Public discussion:
   (6) Bob announces his polarization bases
   (7) Alice announces coincidences of their bases
   (8) Random shared sequence of bits (in the absence of an eavesdropper and noise, these bits must be identical with the bits sent by Alice)

C. Test for eavesdropping:
   (9) Bob picks a random part of his bits and makes them public in order to detect eavesdropping
   (10) Alice checks these bits and informs Bob if they are correct (eavesdropping would have caused errors)
   (11) Secret bits shared by Alice and Bob—the key

2. *Eavesdropping on Quantum States*

Let us suppose that two parties, Alice and Bob, want to interchange a secret key by means of a channel which is accessible to a third party, eavesdropper, traditionally called Eve. Eve is allowed to use all the power of quantum mechanics. What happens if Eve is listening? First, we should realize that classical eavesdropping is out of the question. Eve simply cannot draw out a small part of the signal. Since a single particle is used for each bit, she can get either nothing or the whole particle. In the latter case the particle is lost for Bob and the corresponding bit is not contained in the key (some loss is tolerated). Eve cannot even copy (or clone) the quantum state of the particle [150]. The simplest reasonable Eve's strategy is to use a measuring device, similar to that of Bob, to measure the polarization of incoming photons, and resend each bit again to Bob with the help of a device similar to Alice's. If Eve chooses the "wrong" polarization basis for her measuring and preparation apparatuses (i.e., different from Alice's and Bob's ones), she inevitably changes the polarization state of the photon and then there is a nonzero probability that Bob gets a result different from the original Alice's bit. These differences enable Alice and Bob to disclose Eve.

Of course, Eve may use some more sophisticated measurements (e.g., such that does not swallow up the original photon). However, it can be shown that the resultant effect is qualitatively the same (see Section VIII.D). In general any interaction modifies the states of a photon.

Eve is assumed to know the types of bases Alice and Bob use. This is why Alice and Bob must alternate randomly and independently between two conjugated bases (e.g., polarization bases rotated by 45°). Now, even if Eve has known the bases, she could hit the right one only in 50% of cases on average. Thus continual eavesdropping using the described strategy causes a 25% error rate. By comparing part of transmitted bits, Alice and Bob can estimate the error rate and detect Eve's activity.

Note that Eve could also modify the "auxiliary" information transmitted through the classical open channel. For example, she can cut both channels and pretend to be Bob in front of Alice. Therefore *authentication* of the messages sent over the open channel is necessary [144,153]. The recipient must be able to check that the message has come from the "proper" sender and that it has not

been modified. This requires of Alice and Bob to share a small amount of secret information (an authentication password) at the beginning. After each transmission, this password is replaced by a new one, obtained from the transmitted sequence. Therefore, the QKD cryptosystem works rather as an "expander" of shared secret information.

In any real apparatus, there is noise which may also cause errors. Therefore, some small amount of errors have to be tolerated. Of course, it is possible to correct errors by standard *error correction* procedures [147,154]. Nevertheless, we cannot exclude the possibility that the errors are due to Eve and not due to "technological" noise. Fortunately, the amount of information, which could have leaked out to Eve, can be estimated from the error rate for a large class of eavesdropping strategies [147,155,156]. To minimize Eve's information, a *privacy amplification* procedure can be applied to the key at the cost of its shortening [147,157]. Finding the limit of the amount of information that Eve can obtain for the most general attack allowed by quantum mechanics is the cornerstone of the efforts to provide the ultimate security proof of quantum cryptography (see Section VIII.D).

3. *Other Communication Protocols*

Besides BB84, other protocols were designed. The B92 protocol [158] uses only two nonorthogonal states. A strong reference pulse is used to prevent an eavesdropper from misusing vacuum states on a lossy quantum channel. The same trick may be used to enhance the security of BB84 — this protocol is known as the "4 + 2 protocol" [159]. In the six-state protocol, three nonorthogonal bases are used [160]. Although the latter protocols offer security improvements compared to BB84, they have not attracted the attention of experimentalists yet.

Another class of QKD protocols is based on entangled quantum systems [162]. Both Alice and Bob receive one member of a pair of particles obtained from the parametric downconversion process [161]. These particles feature nonclassical properties; results of suitably chosen measurements on the particles exhibit, even when spatially separated, correlations that cannot be explained by any classical theory consistent with local realism. When Alice and Bob decide to establish a key, they perform independent measurements in randomly chosen bases (from a given nonorthogonal set), and using a public channel they arrive at a secret shared key in a way similar to BB84. Later developments showed a way to improve the security of this protocol by means of the so-called entanglement purification techniques [163].

We note that also protocols using orthogonal states have been designed [164]. Superpositions of quantum states are employed. A superposition is divided into parts, which are sent separately with a time delay larger than the time distance

between Alice and Bob. This requirement, however, makes such schemes difficult to implement.

There have also been a number of other, more or less, exotic proposals.

C. Quantum Cryptographic Methods in Practice

The quantum communication protocols described above may be used to implement quantum counterparts to the classical solutions of cryptographic tasks mentioned in Section VIII.A. Until now most of the efforts were devoted to a quantum solution of the key-distribution problem, which may readily be applied to secure message exchange or can be used as a building block for different cryptographic schemes.

1. Quantum Key Distribution

The first QKD prototype operated over a distance of 32 cm in free space [147]. Since then, experimental techniques have undergone a tremendous progress and today QKD systems at almost a commercial level are offered [165]. A number of problems must have been solved. Communication distance has reached several tens of kilometers in optical fibers [166–169]. Also, free-space systems are being developed with earth–satellite communication on mind [170]. It should be noted that only a few systems presented until now have exhibited parameters that would ensure a secure key generation.

Two main conceptions of QKD apparatuses have been followed. Until late 1990s, most of the attention was devoted to the construction of QKD devices, which used dim laser pulses as the source of photons. Pulses from a laser diode are attenuated down below one photon per pulse. Since laser pulses exhibit Poissonian statistics in photon-number distribution, this unavoidably results in a nonnegligible fraction of vacuum and multiphoton pulses.[1] Bit values are encoded into polarization states of the laser pulses [167,170,171] or into phase differences in a large Mach–Zehnder interferometer [165,166,168, 169]. The former method requires stabilization of polarization over the communication distance, which is achieved by active stabilization. It was shown that it is possible to operate such a system in field conditions over a distance of 23 km [167]. The interferometric method achieves the stabilization of the Mach–Zehnder interferometer over the communication distance by splitting the interferometer into two unbalanced interferometers and by using time-multiplexing over a single transmission fiber. This method has been successfully applied over 46 km in the field [168]. While polarization measurements are more precise than phase interferometry, the latter method seems to gain more

[1]For instance, when pluses are attenuated to 0.1 photon per pulse, then 90.5% pulses contain no photons at all, 9% of pulses contain exactly one photon, and only 0.5% of pulses contain two or more photons.

popularity amongst experimentalists after the development of highly stable interferometric schemes employing Faraday mirrors [165,169]. Error rates below one percent are achievable. The main obstacles both these methods face are attenuation in optical fibers, and low efficiency and high noise level in currently available detectors. These factors result in a serious limitation of the secure transmission distance.

Free-space QKD also advances at a rapid pace. Filtering of the stray light is achieved by means of carefully adjusted telescopes and by tight spectral and time filtering. It was shown that under good atmospheric conditions, QKD is feasible up to 1.6 km [170], a distance approaching the effective turbulent atmospheric thickness in a surface–satellite path. Observed error rates were around 5% and 3% by day and night, respectively.

Interest in correlated photon pairs has been revived, although the original Ekert proposal originated in 1991 [162]. It was shown that the entanglement can be preserved over large distances [172]. To discover an eavesdropper, the communication protocol can either test the Bell inequalities [162,173,174], or a variant of the BB84 can be applied [173,175]. Both energy–time [162,174] and polarization [173,176,177] entanglements have been used. A novel source of entangled photons brings cryptography with correlated photons closer to applications [174,178]. At the present experimental level, error rates fall only slightly below 10% at communication distances approaching 10 km.

Another way to employ correlated photons pairs in quantum cryptography has been suggested [179,180]. The idea is to take advantage of the fact that in the downconversion process photons are always created as in pairs. Performing a photon-number measurement in one of the beams, only single-photon states can be selected in the other beam. Such a source would not only extend the distance limit of secure QKD, but it would also conform with the ultimate security proof which was derived under the assumption that single-photon states are used [181]. A more detailed investigation [182] shows that even though physical imperfections in real experiments keep such sources far from single photons, they still offer certain benefits compared to dim laser pulses.

The development of QKD also stimulated the construction of high-quality random-number generators [183]. This is an important question, because to preserve the level of security, Alice's and Bob's choices of encoding and measurement bases and bit values must be truly random. Quantum generators based on the division of a weak photon flux at a beamsplitter seem to accomplish this task.

2. *Quantum Identification*

Attempts have been made to build a quantum identification system [184] by first implementing another cryptographic primitive, the so-called bit commitment [185]. This task, however, has been proved impossible to implement in a secure way [186].

Later a secure solution of this task was found. It combines a classical three-step identification procedure with QKD [187]. The identification procedure uses random sequences which are used just once, and the QKD procedure supplies the users with new key material. Moreover, the identification procedure may easily be incorporated into the public discussion within the QKD, which substantially simplifies the system.

Other ways to solve mutual identification were proposed using correlated particles [188,189]. Here again, modifications of the QKD procedure are used. In the latter case, a third communicating party, "trusted arbitrator," is required.

3. *Quantum Secret Sharing*

A theoretical proposal of how to implement secret sharing in a quantum way was proposed in [190]. This method uses three-particle quantum entanglement of Greenberger–Horne–Zeilinger states, which, however, have not neatly been produced in the laboratory yet. Later a modification of the secret sharing protocol was developed, which expediently utilizes the entanglement of EPR photon pairs, and which is already within the reach of today's technologies [191]. This task has already been implemented experimentally, too [192].

4. *Multiparty Computations*

The hope for secure quantum implementation of multiparty computations using a cryptographic primitive, called "oblivious transfer" [193], was dashed together with the bit commitment [186]. Until now, no other solution has been published.

D. Security

Provided that quantum theory is a right description of our physical world, quantum cryptography offers, in principle, unconditional security. However, there are several problems in practice. First, each real apparatus and transmission line exhibit losses, imperfections, and misalignments. This results in nonzero error rates during transmissions even in the absence of an eavesdropper. The unconditional security is imperiled. Second, there is no easy-to-use single-particle carrier in the optical domain where naturally quantum cryptography is likely to be employed. The sources used until now suffer from a certain content of vacuum or multiphoton states, both of which open security risks. Multiphoton events can in principle be identified by Eve, and she can eavesdrop on them by splitting and diverting part of the signal without risking disclosure. Vacuum states, on the other hand, can be used for manipulations that can hide the consequences of eavesdropping.

These actualities force communicating parties to undertake steps (privacy amplification [147,157]) to eliminate information possibly leaked to an eavesdropper. Since it is impossible to discriminate between errors caused by

technology and by eavesdropping, legitimate users must attribute all the errors to Eve's activity. To estimate the amount of Eve's knowledge from the detected error rate, one has to consider possible eavesdropping strategies; not only those technologically possible today but all strategies possible in principle. The intercept/resend attack, described in Section VIII.B, was investigated in detail first [147,194–196]. Then more general attacks on single quantum bits (qubits) — such that Eve could use positive-operator-valued measurement (POVM)— were considered [194,155]. Other generalizations of eavesdropping strategies "enable" Eve to use "probes" interacting with information carriers. These probes could be stored and measured (by POVM) later — after the announcement of Alice's and Bob's bases [156]. The next step has covered the so-called collective and coherent attacks. In these cases it is supposed that an eavesdropper can carry out measurements not only on individual qubits but also on the key as a whole by means of collective measurement on nonentangled probes corresponding to individual qubits (collective attack), or by means of an unrestricted, arbitrarily complex "common" probe (coherent or joint attack) [197]. Proofs of security of the BB84 scheme against the most general attack, even in the presence of noise, have finally been obtained [181,198]. It was shown that if the technological error rate does not exceed a certain limit, quantum key distribution can still be unconditionally secure.

However, all the proofs mentioned in the previous paragraph are idealized in the following sense. A proof of security is independent of the physical implementation of signal states as long as they have the correct overlap probabilities and if the recipient is able to detect exactly the same set of states as are sent. But the latter condition represents a serious difficulty in practice. Real detectors are usually not able to distinguish the number of impinging particles. It could be overcome by sending quantum states of exactly one particle. Unfortunately, it is also a hard technological problem. If Alice cannot guarantee one-photon signals and Bob's detectors just either fire or they do not fire, an eavesdropper can split and read some signals without the recipient detecting it. The difficulties implied, for example, by the use of weak coherent states in combination with lossy lines have been pointed out and their various aspects have been discussed [159,180,195,199,200]. This subject has been further analyzed [179,180,182], where bounds on coverable distances were given. Positive security proofs for individual attacks for sufficiently short distances taking account of realistic signals have been given [180]. It has been shown that with the best current technology (transmission line made of optical fiber at 1550 nm, Ge or InGaAs avalanche detectors, and weak laser pulses as a source of quantum state carriers), the distance allowing secure QKD is limited to about 25 km. The hope for extending this range above 120 km by using a source based on postselection from correlated photon pairs has been weakened when a more realistic treatment found a limit of about 55 km

achievable with present laboratory skills [182]. There is also some work in progress on the positive security proof for the case of coherent attacks [201]. On the other hand, the eavesdropping attacks which may undermine the secrecy of the key for setups exceeding these secure distances, are still quite complicated. The eavesdropper needs perform a nondemolition measurement of the total photon number in the signal state, then she has to split off one photon providing a multiphoton signal has occurred, store that photon, and then, finally, measure it after the public discussion.

E. Prospects

It is clearly apparent that quantum cryptography is now ready to offer efficient and user-friendly systems providing an unprecedented level of security. While classical methods are still safe enough for short-lifetime encryption, quantum cryptography may prove valuable when thinking with longer prospects. The development of quantum computers can play a significant role in speeding up the increase of the need for QKD in the IT (information technology) market.

Still there is a lot to be done. While the security of single-photon methods is already quite well defined, the security of cryptography with correlated pairs is much less understood. It would also be useful to perform a rigorous analysis of what is the optimum protocol. QKD itself is now well elaborated, but its further propagation to other areas of cryptography (or discovery of another quantum primitive) still stands ahead.

Theoretical progress will no doubt be immediately followed by experimental advances. The development of new technologies can extend the limit of secure communication. Mainly detectors in the 1550-nm fiber-optic communication window require a big improvement. Any reduction of the fiber attenuation would also greatly contribute to extending the communication range.

It should be stressed that future practical applications of quantum cryptography are by far not the only benefit of this area of research. As already mentioned, a whole new field has been stimulated, which has helped us better understand the nature. It is believed that this resource is still far from being exhausted.

IX. CUBIC BEHAVIOR OF IMPEDED SECOND-HARMONIC GENERATION (*V. PEŘINOVÁ and A. LUKŠ*)

The phase mismatch which impedes the second-harmonic generation leads also to the cascading of quadratic nonlinearities and the induced phase shift. This effect has been used in continuous-wave optical devices and much effort has been devoted to the classical description of light propagation. We address the quantum theory of steady-state propagation of light and compare this formalism

with the conventional modal quantum description, which seems, however, to be more appropriate for the propagation of light pulses in the impeded second-harmonic generation.

A. Introduction

The power-dependent self-phase modulation is useful for all-optical switching and emerging applications [202]. The self-phase modulation as a cubic nonlinear effect was previously large enough to screen the fact that also quadratic nonlinear effect may contribute to the origin of a Kerr-like property. This occurs in the nearly phase-matched second-harmonic generation and other parametric processes [203,204]. Other intensity-dependent effects known to take place in a Kerr medium can also be present in a quadratic medium [205–207]. Interestingly, one of these is the soliton formation. The bistability due to cascaded quadratic nonlinearities was demonstrated experimentally [208]. Thorough studies go beyond the Kerr-like properties of a quadratic medium; for example, chaotic behavior of the ring cavity has been derived [209].

The study of self-phase modulation of one wave may not neglect the statistical properties of the quantum phase. The study of statistical properties of the quantum phase in the situation of self-phase modulation of one wave has a long tradition. To the investigation of the propagation in the Kerr medium including the Kerr nonlinear devices, the nonlinear oscillator model has been applied (see Ref. 210 and references cited therein). The work has been reviewed laying the emphasis on properties of the nonlinear phase shift such as a generation of superposition states.

A coherent phase shift has been treated as a transient effect or a short-time behavior. Therefore, only a few papers have been devoted to the quantitative study of coherent phase shift in which they have used mean phase [211] or the preferred phase [212–214] to characterize this shift. The quantum statistical approach developed in that work is relevant to the coherent phase shift due to cascading of quadratic nonlinearities.

The propagation of light in a quadratic medium has been investigated from the quantum optical viewpoint [215]. It has been taken into account that in noncentrosymmetric crystals, the role of the tensor of macroscopic susceptibility is much greater than in the Kerr-like media, whose cubic susceptibility tensor is isotropic; that is, the tensorial character of mismatch must be included in the formulas for the normally ordered quadrature variances of the second-harmonic and fundamental fields [215]. A simplified treatment of the second-harmonic generation is restricted to some polarization components of some interacting modes and uses the appropriate components of the susceptibility tensor. Immense effort was devoted to the study of the quantum behavior of the phase-matched second-harmonic generation in the very early days of quantum optics (see Ref. 216 for other references). Near the phase-matching angle of the

codirectional propagation, the efficiency of the mode conversion is lowered. But a Kerr-like behavior results in the fundamental mode [203,204]. The joint phase distribution of the two modes has demonstrated that in the phase-matched case the initial two-mode coherent state with the vacuum in the second-mode component does not exhibit any quantum phase shift in the fundamental mode [217]. In contrast, Ref. 218 presents the fundamental-mode Q function, which, by its peak, indicates that a quantum phase shift occurs on the assumption of the phase mismatch. In Ref. 217 the canonical phase distribution has been determined; however, the figures in Ref. 218 are not far from the phase distribution derived out of the Q function. Although these papers studied the coherent phase shift, they have not expressed its behavior in terms of the mean phase or the preferred phase, as they were devoted to the nonlinear effects in general. Special interest in the cascading effect is reflected in Ref. 219–222. These papers have used the method of linearization around the classical solutions to determine the quantum progression and they have predicted quantum noise reduction as well as the squeezing of a quadrature. The principal squeezing variance and the phase of expectation value of the annihilation operator in the fundamental mode have been determined [223,224] using a perturbative method. The effective Kerr-type nonlinearity has been demonstrated by the induced quantum phase shift and the principal squeezing behavior.

The phase-matched second-harmonic generation can be achieved artificially by a periodic poling of the nonlinear susceptibility (quasiphase matching). For the optimization of the cascading effect, the periodicity could be chosen appropriately. Quasiphase matching in fibers, waveguides, and semiconductors can allow one to realize compact and integrable squeezing devices [225].

Besides the phase of the fundamental mode, strictly speaking, the preferred phase, many other characteristics have been studied in [226]. Because a large mismatch was chosen, they have lacked any trend, but an interesting oscillatory behavior has been discovered for the initial two-mode coherent state. Within each period, the phase-matched second-harmonic and second-subharmonic generation processes can be prepared. The model of an ideal Kerr-like medium [223] have been considered for a comparison with cascaded quadratic nonlinearities. It follows that these nonlinearities exhibit not only self-phase modulation in the fundamental mode but also a cross-phase modulation of the modes that can be considered for a nondemolition measurement.

B. Macroscopic Approach to Propagation

In the exposition of various macroscopic theories of electromagnetic field in dispersive media [227–229], limitations and possibilities of narrow-bandwidth quantum fields were considered. Such quantum fields are common in the study of quantum solitons. Similar quantum fields are derived in the study of paraxial propagation [230,231]. We will present partial differential equations for these

fields and specify the equal-time commutation relations. Such differential equations can be solved only by the renormalization, if possible, but we will not even try the renormalization or prove the impossibility thereof [227,232].

As usual in this situation, we will use the linearization around a classical solution. We will consider a classical solution in terms of the elliptic functions. Since the classical solution describes a steady-state field, we will find a steady-state solution of linearized quantum equations. To this end we will find the state of the field, which is an eigenstate of an appropriate quadratic Hamiltonian to the classical solution using the generalized approach of Deutsch and Garrison [230], namely, the ansatz that the eigenstate will be a functionally squeezed vacuum, generalized to the assumption that the eigenstate is a Bogolubov transformed vacuum.

Generalizing somewhat the approach of Deutsch and Garrison [230,231], we consider (non-Hermitian) envelope field operators $\hat{\psi}_j(z,t)$, $j = 1,2$, with the property

$$\begin{aligned}[\hat{\psi}_j(z,t), \hat{\psi}_k^\dagger(z',t)] &= \delta_{jk}\delta(z-z')\hat{1} \\ [\hat{\psi}_j(z,t), \hat{\psi}_k(z',t)] &= \hat{0}, \quad j,k = 1,2 \end{aligned} \tag{148}$$

In the application to the optical field, the vector potential (or the electric field in the lowest order) corresponding to carrier plane waves of given frequencies ω_j, wavenumbers k_j, and polarizations $\boldsymbol{\varepsilon}_j$

$$\hat{\mathbf{E}}^{(+)}_{\omega_1,\omega_2}(z,t) = \sum_{j=1}^{2} \boldsymbol{\varepsilon}_j \left(\frac{2\pi\hbar\omega_j}{An^2(\omega_j)}\right)^{1/2} \hat{\psi}_j(z,t) \tag{149}$$

where A is the beam area, $n(\omega_j)$ is a dispersive index of refraction, ω_1 is the fundamental frequency, ω_2 is the second-harmonic frequency, $\omega_2 = 2\omega_1$, $|k_j| = \omega_j n(\omega_j)/c$, $j = 1,2$, $k_1 > 0$, and $k_2 > 0$ or $k_2 < 0$ for the directional or contradirectional propagation, respectively. For the effective interaction of the two waves, the total Hamiltonian can be written as

$$\hat{H} = \hat{H}_{\text{env}} + \hat{H}_{\text{int}} \tag{150}$$

with

$$\hat{H}_{\text{env}} = -\frac{\mathrm{i}\hbar}{2}\int \sum_{j=1}^{2} \frac{\omega_j}{k_j}\left[\hat{\psi}_j^\dagger(z,t)\frac{\partial}{\partial z}\hat{\psi}_j(z,t) - \frac{\partial}{\partial z}\hat{\psi}_j^\dagger(z,t)\hat{\psi}_j(z,t)\right] dz \tag{151}$$

$$\hat{H}_{\text{int}} = -\hbar c \int [g^* \hat{\psi}_1^{\dagger 2}(z,t)\hat{\psi}_2(z,t) + \text{H.c.}]\, dz \tag{152}$$

where $\hat{H}_{\text{env}}$ is the Hamiltonian governing the free evolution of the envelope and $\hat{H}_{\text{int}}$ is the interaction Hamiltonian. In the spacetime Heisenberg picture with smoothed and slowly varying field operators

$$\hat{\Psi}_j(z,t) = \hat{\psi}_j(z,t)\exp\left[-i(k_j z - \omega_j t)\right], \quad j = 1,2 \tag{153}$$

the equations of motion for these operators read as

$$\frac{\partial}{\partial t}\hat{\Psi}_j(z,t) = -\frac{i}{\hbar}[\hat{\Psi}_j(z,t), \hat{H}_{\text{slow}}], \quad j = 1,2 \tag{154}$$

where the total Hamiltonian

$$\hat{H}_{\text{slow}} = \hat{H}_{\text{env}}^{(\text{slow})} + \hat{H}_{\text{int}}^{(\text{slow})} \tag{155}$$

should be understood as dependent on $\hat{\Psi}_j(z,t)$, with

$$\hat{H}_{\text{env}}^{(\text{slow})} = \hat{H}_{\text{env}}\Big|_{\hat{\psi}_j(z,t)\to\hat{\Psi}_j(z,t)} \tag{156}$$

$$\hat{H}_{\text{int}}^{(\text{slow})} = -\hbar c\int[g^*\hat{\Psi}_1^{\dagger 2}(z,t)\hat{\Psi}_2(z,t)\exp(i\Delta k\, z) + \text{H.c.}]\,\mathrm{d}z \tag{157}$$

with the phase mismatch Δk given by $\Delta k = k_2 - 2k_1$. Here $\hat{H}_{\text{env}}^{(\text{slow})}$ is the envelope Hamiltonian and $\hat{H}_{\text{int}}^{(\text{slow})}$ is the interaction Hamiltonian. If we adopt the spatial and temporal Heisenberg pictures gradually, we encounter the virtual carrier wave Hamiltonian

$$\hat{H}_{\text{c}} = \hbar\int\sum_{j=1}^{2}\omega_j\hat{\psi}_j^{\dagger}(z,t)\hat{\psi}_j(z,t)\,dz \tag{158}$$

Equations (154) can be written in the form

$$\begin{aligned}\left[\frac{n(\omega_1)}{c}\frac{\partial}{\partial t} + \frac{\partial}{\partial z}\right]\hat{\Psi}_1(z,t) &= 2\mathrm{i}n(\omega_1)g^*\hat{\Psi}_1^{\dagger}(z,t)\hat{\Psi}_2(z,t)\exp(i\Delta k\, z),\\ \left[\frac{k_2}{|k_2|}\frac{n(\omega_2)}{c}\frac{\partial}{\partial t} + \frac{\partial}{\partial z}\right]\hat{\Psi}_2(z,t) &= i\frac{k_2}{|k_2|}n(\omega_2)g\hat{\Psi}_1^2(z,t)\exp(-i\Delta k\, z).\end{aligned} \tag{159}$$

Let us remark that the coefficients $n(\omega_j)$ on the right-hand sides in (159) need not be present in other versions of macroscopic theory. Let us replace Eq. (159) with corresponding classical equations for $\bar{\Psi}_j(z,t), j = 1,2$. The solution will be given later. Introducing the quantum corrections

$$\delta\hat{\Psi}_j(z,t) = \hat{\Psi}_j(z,t) - \bar{\Psi}_j(z,t)\hat{1}, \quad j = 1,2 \tag{160}$$

we arrive at the linearized equations:

$$\left[\frac{n(\omega_1)}{c}\frac{\partial}{\partial t}+\frac{\partial}{\partial z}\right]\delta\hat{\Psi}_1(z,t) = 2in(\omega_1)g^*[\bar{\Psi}_2(z,t)\delta\hat{\Psi}_1^\dagger(z,t) + \bar{\Psi}_1^*(z,t)\delta\hat{\Psi}_2(z,t)]\exp(i\Delta k\, z)$$

$$\left[\frac{k_2}{|k_2|}\frac{n(\omega_2)}{c}\frac{\partial}{\partial t}+\frac{\partial}{\partial z}\right]\delta\hat{\Psi}_2(z,t) = 2\mathrm{i}\frac{k_2}{|k_2|}n(\omega_2)g\bar{\Psi}_1(z,t)\delta\hat{\Psi}_1(z,t) \times \exp(-i\Delta k\, z) \tag{161}$$

These equations can be obtained as the equations of motion if we make the replacement $\hat{\Psi}_j(z,t)$ by $\delta\hat{\Psi}_j(z,t)$ in (151) and consider, instead of $\hat{H}_{\mathrm{int}}^{(\mathrm{slow})}$, the quadratic Hamiltonian

$$\hat{H}_{\mathrm{int}}^{(2\,\mathrm{slow})} = -\hbar c\int_0^L \Big\{g^*[\bar{\Psi}_2(z,t)\delta\hat{\Psi}_1^{\dagger 2}(z,t) + 2\bar{\Psi}_1^*(z,t)\delta\hat{\Psi}_1^\dagger(z,t)\delta\hat{\Psi}_2(z,t)] \times \exp(i\Delta k\, z) + \mathrm{H.c.}\Big\}\, dz \tag{162}$$

We denote the envelope Hamiltonian after this replacement by a new notation,

$$\hat{H}_{\mathrm{env}}^{(\mathrm{slow})}\big|_{\hat{\Psi}_j(z,t)\to\delta\hat{\Psi}_j(z,t)} = \hat{H}_{\mathrm{env}}^{(2\,\mathrm{slow})} \tag{163}$$

We rewrite the Hamiltonian (162) in the form

$$\hat{H}_{\mathrm{int}}^{(2\,\mathrm{slow})} = \int\Big[H_{12}(z,t)\delta\hat{\Psi}_1^\dagger(z,t)\delta\hat{\Psi}_2(z,t) + H_{21}(z,t)\delta\hat{\Psi}_2^\dagger(z,t)\delta\hat{\Psi}_1(z,t)\Big]\, dz + \left[\frac{1}{2}\int I_{11}(z,t)\delta\hat{\Psi}_1^{\dagger 2}(z,t)\,\mathrm{d}z + \mathrm{H.c.}\right] \tag{164}$$

where

$$\begin{aligned} H_{12}(z,t) &= -\hbar c 2g^*\bar{\Psi}_1^*(z,t)\exp(i\Delta k\, z)\\ H_{21}(z,t) &= [H_{12}(z,t)]^*\\ I_{11}(z,t) &= -\hbar c g^*\bar{\Psi}_2(z,t)\exp(i\Delta k\, z) \end{aligned} \tag{165}$$

The method of linearization is useful in the case where a displaced two-field squeezed or unsqueezed vacuum state $|\{\bar{\Psi}_1,\bar{\Psi}_2\}\rangle_{\{\xi_{11},\xi_{12},\xi_{22}\}}$ is the initial state (for $t=0$)

$$|\{\bar{\Psi}_1,\bar{\Psi}_2\}\rangle_{\{\xi_{11},\xi_{12},\xi_{22}\}} = \hat{D}[\bar{\Psi}_1,\bar{\Psi}_2]|0\rangle_{\{\xi_{11},\xi_{12},\xi_{22}\}} \tag{166}$$

or

$$|\{\bar{\Psi}_1,\bar{\Psi}_2\}\rangle = \hat{D}[\bar{\Psi}_1,\bar{\Psi}_2]|0\rangle \tag{167}$$

where $\hat{D}[\bar{\Psi}_1, \bar{\Psi}_2]$ is a displacement operator

$$\hat{D}[\bar{\Psi}_1, \bar{\Psi}_2] = \exp\left\{\int \sum_{j=1}^{2} [\bar{\Psi}_j(z)\hat{\Psi}_j^\dagger(z) - \bar{\Psi}_j^*(z)\hat{\Psi}_j(z)]\,\mathrm{d}z\right\} \tag{168}$$

and $|0\rangle_{\{\xi_{11},\xi_{12},\xi_{22}\}}$ is a two-field squeezed vacuum state

$$|0\rangle_{\{\xi_{11},\xi_{12},\xi_{22}\}} = \hat{S}[\xi_{11}, \xi_{12}, \xi_{22}]|0\rangle \tag{169}$$

with the two-field squeezing operator

$$\begin{aligned}\hat{S}[\xi_{11}, \xi_{12}, \xi_{22}] = \exp\Big\{\frac{1}{2}\int &[\xi_{11}(z)\hat{\Psi}_1^{\dagger 2}(z) + 2\xi_{12}(z)\hat{\Psi}_1^\dagger(z)\hat{\Psi}_2^\dagger(z) \\ &+ \xi_{22}(z)\hat{\Psi}_2^{\dagger 2}(z)]\,\mathrm{d}z - \mathrm{H.c.}\Big\}\end{aligned} \tag{170}$$

It is easy to see that a statistical use of the operators (160) is possible

$$|\{\bar{\Psi}_1, \bar{\Psi}_2\}\rangle_{\{\xi_{11},\xi_{12},\xi_{22}\}} = \hat{S}^{(2)}[\xi_{11}, \xi_{12}, \xi_{22}]|\{\bar{\Psi}_1, \bar{\Psi}_2\}\rangle \tag{171}$$

where

$$\hat{S}^{(2)}[\xi_{11}, \xi_{12}, \xi_{22}] = \hat{D}[\bar{\Psi}_1, \bar{\Psi}_2]\hat{S}[\xi_{11}, \xi_{12}, \xi_{22}]\hat{D}^\dagger[\bar{\Psi}_1, \bar{\Psi}_2] \tag{172}$$

$$\begin{aligned}= \exp\Big\{\frac{1}{2}\int &[\xi_{11}(z)\delta\hat{\Psi}_1^{\dagger 2}(z) + 2\xi_{12}(z)\delta\hat{\Psi}_1^\dagger(z)\delta\hat{\Psi}_2^\dagger(z) \\ &+ \xi_{22}(z)\delta\hat{\Psi}_2^{\dagger 2}(z)]\,dz - \mathrm{H.c.}\Big\}\end{aligned} \tag{173}$$

The action of the two-field squeezing operator can be as follows

$$\delta\hat{\tilde{\Psi}}_j(z) \equiv \hat{S}^{(2)\dagger}[\xi_{11}, \xi_{12}, \xi_{22}]\delta\hat{\Psi}_j(z)\hat{S}^{(2)}[\xi_{11}, \xi_{12}, \xi_{22}] \tag{174}$$

$$= \sum_{k=1}^{2}\Big[\mu_{kj}^*(z)\delta\hat{\Psi}_k(z) - \nu_{kj}(z)\delta\hat{\Psi}_k^\dagger(z)\Big], \quad j = 1, 2 \tag{175}$$

where $\mu_{jk}(z) \equiv \mu_{jk}(\xi_{11}(z), \xi_{12}(z), \xi_{22}(z))$, $\nu_{jk}(z) \equiv \nu_{jk}(\xi_{11}(z), \xi_{12}(z), \xi_{22}(z))$ may be simply expressed only when arranged in matrices. The formula (175) can be simplified, since $\mu_{kj}^*(z) = \mu_{jk}(z)$, $\nu_{kj}(z) = \nu_{jk}(z)$. The matrix $(\mu_{jk}(z))$ is positive definite. For the general form, it holds that [233]

$$\sum_{l=1}^{2}(\mu_{jl}\mu_{kl}^* - \nu_{jl}\nu_{kl}^*) = \delta_{jk} \tag{176}$$

$$\sum_{l=1}^{2}(\mu_{jl}\nu_{kl} - \nu_{jl}\mu_{kl}) = 0, \quad j = 1, 2, k = 1, 2 \tag{177}$$

We assume that the amplitudes of the displacement are $\bar{\Psi}_j(z) \equiv \bar{\Psi}_j(z,0)$ initially, and, for $t \geq 0$, we have the amplitudes $\bar{\Psi}_j(z) \equiv \bar{\Psi}_j(z,t)$ given as classical solutions of the classical equations such that

$$\bar{\Psi}_j(z,t)\big|_{t=0} = \bar{\Psi}_j(z,0), \quad j = 1,2 \tag{178}$$

Adopting the slowly varying operator picture, we are interested in the temporal evolution of the operators $\delta\hat{\Psi}_j(z,t), j = 1,2$, or in the solutions of the equations (161). The squeeze parameters $\xi_{11}, \xi_{12}, \xi_{22}$ do not then vary. In the calculation of statistics we can express $\hat{\Psi}_j(z,t)$ from the relation (160); that is, we always consider the amplitudes of displacement $\bar{\Psi}_j(z,t)$ that correspond to the time at which one of the statistics is calculated.

Adopting the interaction picture, we are concerned with the temporal evolution of the squeeze parameters $\xi_{11} \equiv \xi_{11}(z,t)$, $\xi_{12} \equiv \xi_{12}(z,t)$, $\xi_{22} \equiv \xi_{22}(z,t)$. The quantum fluctuation of the displaced state continues to undergo the two-field squeezing transformation. The state $|\Phi\rangle$ evolves by the Schrödinger equation

$$\frac{\partial}{\partial t}|\Phi\rangle = -\frac{\mathrm{i}}{\hbar}(\hat{H}_{\mathrm{env}}^{(2\,\mathrm{slow})} + \hat{H}_{\mathrm{int}}^{(2\,\mathrm{slow})})|\Phi\rangle \tag{179}$$

In the calculation of statistics we again express $\bar{\Psi}_j(z,t)$ from the relation (160), where nevertheless $\delta\hat{\Psi}_j(z,t) = \delta\hat{\Psi}_j(z,0)$ for all time (they do not vary).

Following Deutsch and Garrison [230] we are interested (in such an interaction picture) in an initial state that does not vary any more, or does so that only its unimportant overall factor varies. The amplitude of its displacement is given by the classical solution being of the same property, namely, a solution of the classical equations (corresponding to) (159), from which the differential operator $\partial/\partial t$ and its factor have been left out, let us say $\bar{\Psi}_j(z,t) = \bar{A}_j(z)$, $j = 1,2$ independent of t. We are therefore concerned with the two-field squeezed vacuum state which is an eigenstate

$$(\hat{H}_{\mathrm{env}}^{(2\,\mathrm{slow})} + \hat{H}_{\mathrm{int}}^{(2\,\mathrm{slow})})|\Phi\rangle_{\mathrm{ss}} = \lambda|\Phi\rangle_{\mathrm{ss}} \tag{180}$$

We will omit the subscript ss in what follows.

Recalling that the operators are replaced by the mean complex amplitudes, we observe that equations (159) become

$$\frac{d}{dz}\bar{A}_1(z) = i2g^*\bar{A}_1^*(z)\bar{A}_2(z)\exp(i\Delta kz) \tag{181}$$

$$\frac{d}{dz}\bar{A}_2(z) = ig\bar{A}_1^2(z)\exp(-i\Delta kz) \tag{182}$$

We may consider the solution in the form

$$\bar{A}_j(z) = \bar{\rho}_j(z)\exp[i\bar{\varphi}_j(z)], \quad j = 1, 2 \tag{183}$$

where

$$\bar{\rho}_1(z) = \sqrt{W}u(-|g|\sqrt{2W}z), \qquad \bar{\rho}_2(z) = \sqrt{\frac{W}{2}}v(-|g|\sqrt{2W}z) \tag{184}$$

with

$$W = |\bar{A}_1(0)|^2 + 2|\bar{A}_2(0)|^2 \tag{185}$$

and [234]

$$v(\zeta) = \sqrt{v_a^2 + (v_b^2 - v_a^2)\,\mathrm{sn}^2[\sqrt{v_c^2 - v_a^2}(\zeta + \zeta_0), \gamma]}$$

$$u(\zeta) = \sqrt{1 - v_a^2 - (v_b^2 - v_a^2)\,\mathrm{sn}^2[\sqrt{v_c^2 - v_a^2}(\zeta + \zeta_0), \gamma]} \tag{186}$$

$v_a^2 \le v_b^2 \le v_c^2$ are the roots of the cubic equation

$$v^2(1 - v^2)^2 - \left\{\Gamma - \frac{\Delta s}{2}[v^2 - [v(0)]^2]\right\}^2 = 0 \tag{187}$$

$$\Delta s = \frac{\Delta k}{|g|\sqrt{2W}}, \quad \Gamma = \frac{1}{W}\sqrt{\frac{1}{2W}}\left[\frac{g}{|g|}\bar{A}_1^2(0)\bar{A}_2^*(0) + \text{c.c.}\right] \tag{188}$$

$$[v(0)]^2 = \frac{2}{W}|\bar{A}_2(0)|^2 \tag{189}$$

ζ_0 is determined by the initial "mean" complex amplitudes $\bar{A}_j(0), j = 1, 2$, and

$$\gamma = \sqrt{\frac{v_b^2 - v_a^2}{v_c^2 - v_a^2}} \tag{190}$$

The phases are

$$\bar{\varphi}_1(z) = \bar{\varphi}_1(0) + 2\int_0^z \frac{1}{|\bar{A}_1(z')|^2}\left[W\sqrt{2W}|g|\Gamma_{\Delta s} - \Delta k|\bar{A}_2(z')|^2\right]dz'$$

$$\bar{\varphi}_2(z) = \bar{\varphi}_2(0) + \int_0^z \frac{1}{|\bar{A}_2(z')|^2}\left[W\sqrt{2W}|g|\Gamma_{\Delta s} - \Delta k|\bar{A}_2(z')|^2\right]dz' \tag{191}$$

where

$$\Gamma_{\Delta s} = \Gamma + \frac{\Delta k}{|g|W\sqrt{2W}}|A_2(0)|^2 \tag{192}$$

On the substitution from the definition (171), we see that $\xi_{11}(z)$, $\xi_{12}(z)$, $\xi_{22}(z)$, and λ should be solutions of the equation

$$\hat{S}^{(2)\dagger}[\xi_{11},\xi_{12},\xi_{22}](\hat{H}_{\text{env}}^{(2\,\text{slow})}+\hat{H}_{\text{int}}^{(2\,\text{slow})})\hat{S}^{(2)}[\xi_{11},\xi_{12},\xi_{22}]|\{\bar{\Psi}_1,\bar{\Psi}_2\}\rangle=\lambda|\{\bar{\Psi}_1,\bar{\Psi}_2\}\rangle \tag{193}$$

Applying the operators $\delta\hat{\Psi}_j(z)$, $j=1,2$, to both the sides of (193) and taking into account that

$$\begin{aligned}\lambda\delta\hat{\Psi}_j(z)|\{\bar{\Psi}_1,\bar{\Psi}_2\}\rangle=0=\hat{S}^{(2)\dagger}[\xi_{11},\xi_{12},\xi_{22}](\hat{H}_{\text{env}}^{(2\,\text{slow})}+\hat{H}_{\text{int}}^{(2\,\text{slow})})\\ \times\hat{S}^{(2)}[\xi_{11},\xi_{12},\xi_{22}]\delta\hat{\Psi}_j(z)|\{\bar{\Psi}_1,\bar{\Psi}_2\}\rangle,\quad j=1,2\end{aligned} \tag{194}$$

we rewrite the eigenvalue problem in the λ-independent form

$$\begin{aligned}&[\hat{S}^{(2)\dagger}[\xi_{11},\xi_{12},\xi_{22}](\hat{H}_{\text{env}}^{(2\,\text{slow})}+\hat{H}_{\text{int}}^{(2\,\text{slow})})\hat{S}^{(2)}[\xi_{11},\xi_{12},\xi_{22}],\delta\hat{\Psi}_j(z)]|\{\bar{\Psi}_1,\bar{\Psi}_2\}\rangle\\ &\quad=0=\hat{\tilde{C}}_j^{(2)}|\{\bar{\Psi}_1,\bar{\Psi}_2\}\rangle,\quad j=1,2,\end{aligned} \tag{195}$$

where the commutators $\hat{\tilde{C}}_j^{(2)}$ are

$$\begin{aligned}\hat{\tilde{C}}_j^{(2)}=&\frac{\mathrm{i}\hbar}{2}\Big\{-\sum\mu_{jl}\frac{\omega_l}{k_l}\frac{\partial}{\partial z}[\nu_{ml}\delta\hat{\Psi}_m^\dagger(z)]-\sum\mu_{jl}\frac{\partial}{\partial z}\left[\frac{\omega_l}{k_l}\nu_{ml}\delta\hat{\Psi}_m^\dagger(z)\right]\\ &+\sum\nu_{jl}\frac{\partial}{\partial z}\left[\frac{\omega_l}{k_l}\mu_{ml}\delta\hat{\Psi}_m^\dagger(z)\right]+\sum\nu_{jl}\frac{\omega_l}{k_l}\frac{\partial}{\partial z}[\mu_{ml}\delta\hat{\Psi}_m^\dagger(z)]\Big\}\\ &+\sum\mu_{jk}H_{kl}\nu_{ml}\delta\hat{\Psi}_m^\dagger(z)+\sum\nu_{jk}H_{lk}\mu_{ml}\delta\hat{\Psi}_m^\dagger(z)\\ &-\sum\nu_{jk}I_{kl}^*\nu_{ml}\delta\hat{\Psi}_m^\dagger(z)-\sum\mu_{jk}I_{kl}\mu_{ml}\delta\hat{\Psi}_m^\dagger(z)\\ &+\frac{\mathrm{i}\hbar}{2}\Big\{\sum\mu_{jl}\frac{\omega_l}{k_l}\frac{\partial}{\partial z}[\mu_{ml}^*\delta\hat{\Psi}_m(z)]+\sum\mu_{jl}\frac{\partial}{\partial z}\left[\frac{\omega_l}{k_l}\mu_{ml}^*\delta\hat{\Psi}_m(z)\right]\\ &-\sum\nu_{jl}\frac{\partial}{\partial z}\left[\frac{\omega_l}{k_l}\nu_{ml}^*\delta\hat{\Psi}_m(z)\right]-\sum\nu_{jl}\frac{\omega_l}{k_l}\frac{\partial}{\partial z}[\nu_{ml}^*\delta\hat{\Psi}_m(z)]\Big\}\\ &-\sum\mu_{jk}H_{kl}\mu_{ml}^*\delta\hat{\Psi}_m(z)-\sum\nu_{jk}H_{lk}\nu_{ml}^*\delta\hat{\Psi}_m(z)\\ &+\sum\nu_{jk}I_{kl}^*\mu_{ml}^*\delta\hat{\Psi}_m(z)+\sum\mu_{jk}I_{kl}\nu_{ml}^*\delta\hat{\Psi}_m(z),\quad j=1,2\end{aligned} \tag{196}$$

with $\sum\equiv\sum_{l=1}^2\sum_{m=1}^2$ or $\sum\equiv\sum_{k=1}^2\sum_{l=1}^2\sum_{m=1}^2$, according to which subscripts repeat and $H_{11}\equiv H_{22}\equiv H_{12}\equiv I_{21}\equiv I_{22}\equiv 0$. For a simple generalization of the Deutsch–Garrison technique to be feasible, it is needed that the commutators do not comprise the derivatives $(\partial/\partial z)\delta\hat{\Psi}_j^\dagger(z)$, $j=1,2$. This happens when neither dispersion nor contradirectional propagation need be taken into account.

The eigenvalue condition requires that the coefficients at $\delta\hat{\Psi}_j^\dagger(z)$, $j = 1, 2$, vanish, yielding the desired propagation equations

$$\sum\left(\mu_{jl}\frac{d}{dz}\nu_{kl} - \nu_{jl}\frac{d}{dz}\mu_{kl}\right) = \frac{i}{\hbar}\frac{n(\omega)}{c}\sum(-\mu_{jl}H_{lm}\nu_{km} - \nu_{jl}H_{ml}\mu_{km} + \nu_{jl}I_{lm}^*\nu_{km} + \mu_{jl}I_{lm}\mu_{km}), \quad j,k = 1,2 \tag{197}$$

where $\sum \equiv \sum_{l=1}^2$ or $\sum \equiv \sum_{l=1}^2 \sum_{m=1}^2$ according to which subscripts repeat. Taking into account that

$$\sum\left(\mu_{jl}\frac{d}{dz}\nu_{kl} - \nu_{jl}\frac{d}{dz}\mu_{kl}\right) = \sum\left(\frac{d\nu_{jl}}{dz}\mu_{kl} - \frac{d\mu_{jl}}{dz}\nu_{kl}\right) \tag{198}$$

we may give the propagation equations (197) a manifestly symmetric form; the left-hand sides are

$$\frac{1}{2}\sum\left[\left(\mu_{jl}\frac{d}{dz}\nu_{kl} - \nu_{jl}\frac{d}{dz}\mu_{kl}\right) + \left(\frac{d\nu_{jl}}{dz}\mu_{kl} - \frac{d\mu_{jl}}{dz}\nu_{kl}\right)\right] \tag{199}$$

Three of these equations suffice, $j = 1, 2$, $k = \begin{cases} 1,2 & \text{for} \quad j = 1 \\ 2 & \text{for} \quad j = 2 \end{cases}$. The particular form of the two-field squeezing of a state presents a restriction. Such two-field squeezed states provide a solution (an eigenstate) only when one may get rid also of the derivatives $(\partial/\partial z)\delta\hat{\Psi}_j^\dagger(z)$, $j = 1, 2$. But this is possible only in case the propagation velocities are of the same magnitude and direction. No generalization of the form (170) is considered in this section.

In order to solve these equations, we consider classical corrections $\delta A_j(z)$, $j = 1, 2$, and the equations

$$\frac{d}{dz}\delta A_j(z) = -\frac{i}{\hbar}\sum_{k=1}^{2}[H_{jk}(z)\delta A_k(z) + I_{jk}(z)\delta A_k^*(z)] \tag{200}$$

We write down the solutions in the form

$$\delta A_j(z) = \sum_{k=1}^{2}[\mu_{kj}^{(g)*}(z)\delta A_k(0) - \nu_{kj}^{(g)}(z)\delta A_k^*(0)] \tag{201}$$

where the matrix elements $\mu_{jk}^{(g)}(z)$ and $\nu_{jk}^{(g)}(z)$ have the properties (176) and (177). According to an important theorem on the polar decomposition, there is a unitary matrix $(u_{jk}(z))$ such that the elements

$$\mu_{jk} = \sum_{l=1}^{2} u_{lj}^*\mu_{lk}^{(g)}, \quad j,k = 1,2 \tag{202}$$

form a positive definite Hermitian matrix. It can be proved that the elements

$$\nu_{jk} = \sum_{l=1}^{2} u_{lj}^{*} \nu_{lk}^{(g)}, \quad j,k = 1,2 \tag{203}$$

form a symmetric matrix, and that the elements μ_{jk}, ν_{jk} together obey the equations (197). Let us remind the reader that we assume the equal propagation velocities.

It has been proved that, on this assumption, we obtain the simpler statistics–the single-point ones—the same as in the framework of the usual problem formulation, which follows. It is understood that the linearization can be used in both the formulations to make a comparison "fair" and transparent.

C. Modal Approach

We may consider the normalized wavefunctions $\phi_{j\text{in}}(z)$ and $\phi_{j\text{out}}(z)$, which are different from zero in the infinite intervals $(-\infty, 0]$, $[L, \infty)$, respectively, for $j = 1$ and on the same condition for $j = 2$ and the codirectional propagation and with the obvious exchange of the infinite intervals for $j = 2$ and the contradirectional propagation. We may introduce the annihilation operators

$$\begin{aligned} \hat{A}_{j\text{in}} &= \int \phi_{j\text{in}}(z) \hat{\Psi}_j(z,0)\, dz \\ \hat{A}_{j\text{out}} &= \int \phi_{j\text{out}}(z) \hat{\Psi}_j(z,0)\, dz \end{aligned} \tag{204}$$

In order to complete the description of propagation, let us assume that in front of the nonlinear crystal it holds that

$$\bar{\Psi}_j(z,t) = \bar{A}_j(0) \phi_{j\text{in}}^{*}(z), \quad j = 1,2, z \le 0, \text{ all } t \tag{205}$$

Further it holds that

$$\xi_{11}(z) = \xi_{12}(z) = \xi_{22}(z) = 0, \quad z \le 0 \tag{206}$$

In other words, the input field is in a displaced unsqueezed vacuum state. On choosing a positive wavefunction and adopting the *unit of length* such that

$$\int \phi_{j\text{in}}(z)\, dz = \int \phi_{j\text{out}}(z)\, dz = 1, \quad j = 1,2 \tag{207}$$

the result of integration of the decomposition (160) according to (204) (introducing $\delta\hat{A}_{j\text{in}}$, $\delta\hat{A}_{j\text{out}}$) will be simple and the mean complex amplitudes will

remain unchanged. Behind the nonlinear crystal it holds that

$$\bar{\Psi}_j(z,t) = \bar{A}_j(L)\phi^*_{j\text{out}}(z), \quad j = 1,2, \quad z \geq L, \text{ all } t \tag{208}$$

Further it holds there that

$$\xi_{11}(z), \xi_{12}(z), \xi_{22}(z), z \geq L \tag{209}$$

are determined by $\mu_{jk}(L)$ and $\nu_{jk}(L)$. We may integrate also the relation (175), which characterizes the squeezing and introduce $\delta\hat{A}_{j\text{out}}$. The use of the wavefunctions $\phi_{j\text{in}}$, $\phi_{j\text{out}}$ is possible, but the connection with the modal approach that follows still stays partial.

The preceding analysis has been appropriate to the study of propagation and to the study of continuous-wave optical processes and devices. For comparison, we will review a simpler approach that can be rather securely applied to the interaction of pulsed light fields, but that had better not to be used for study of propagation problems. The modal approach consists in considering annihilation operators $\hat{A}_j(z)$, $j = 1,2$, related to the pulses centered at the frequencies ω_j, $j = 1,2$. It is assumed that these operators obey the quasiclassical equations

$$\begin{aligned} \frac{d}{dz}\hat{A}_1(z) &= i2g^*\hat{A}_1^\dagger(z)\hat{A}_2(z)\exp(i\Delta k\, z) \\ \frac{d}{dz}\hat{A}_2(z) &= i\frac{k_2}{|k_2|}g\hat{A}_1^2(z)\exp(-i\Delta k\, z) \end{aligned} \tag{210}$$

where the phase mismatch Δk is given by

$$\Delta k = k_2 - 2k_1 \tag{211}$$

and that they fulfill the initial conditions for the codirectional propagation

$$\hat{A}_1(z)_{|z=0} = \hat{A}_1(0), \quad \hat{A}_2(z)_{|z=0} = \hat{A}_2(0) \tag{212}$$

and the boundary conditions for the contradirectional propagation

$$\hat{A}_1(z)_{|z=0} = \hat{A}_1(0), \quad \hat{A}_2(z)_{|z=L} = \hat{A}_2(L) \tag{213}$$

In the latter case $\Delta k \ll 0$. From the Eq. (210) it can be derived that

$$\frac{d}{dz}\left[\hat{A}_1^\dagger(z)\hat{A}_1(z) + 2\frac{k_2}{|k_2|}\hat{A}_2^\dagger(z)\hat{A}_2(z)\right] = \hat{0} \tag{214}$$

We consider the input field operators at $z = 0$ for the mode of the frequency ω_1 and the input ones at $z = 0$ or $z = L$ for the mode of the frequency ω_2 according to whether the propagation is co- or contradirectional, respectively. Further we consider the output field operators at $z = L$ for the mode of the frequency ω_1 and the output ones at $z = L$ or $z = 0$ for the mode of the frequency ω_2 according to the direction of propagation. We assume the ordinary commutation relations in cases $k_2 \gtrless 0$

$$\begin{aligned}[\hat{A}_{1\mathrm{in}}, \hat{A}^{\dagger}_{1\mathrm{in}}] &= [\hat{A}_{2\mathrm{in}}, \hat{A}^{\dagger}_{2\mathrm{in}}] = \hat{1} \\ [\hat{A}_{1\mathrm{in}}, \hat{A}_{2\mathrm{in}}] &= [\hat{A}_{1\mathrm{in}}, \hat{A}^{\dagger}_{2\mathrm{in}}] = \hat{0}\end{aligned} \tag{215}$$

where $\hat{A}_{1\mathrm{in}}$, $\hat{A}_{2\mathrm{in}}$ are understood in the sense of the relations (the codirectional case)

$$\hat{M}_{\mathrm{in}} = M\big(\hat{A}_1(0), \hat{A}_2(0)\big) \tag{216}$$

and (the contradirectional case)

$$\hat{M}_{\mathrm{in}} = M\big(\hat{A}_1(0), \hat{A}_2(L)\big) \tag{217}$$

The system of equations (210) does not admit a closed analytical solution. The approximations according to Ref. 215 have been extended to the contradirectional propagation in Ref. 224. We rewrite the initial problem (210) and (212) and the boundary problem (210) and (213) as integral equations for $\hat{A}_j(z)$, $j = 1, 2$;

$$\hat{A}_1(z) = \hat{A}_1(0) + i2g^{\star} \int_0^z \hat{A}_1^{\dagger}(z')\hat{A}_2(z') \exp(\mathrm{i}\Delta k\, z')\, dz', \quad k_2 \gtrless 0 \tag{218}$$

$$\hat{A}_2(z) = \hat{A}_2(0) + ig \int_0^z \hat{A}_1^2(z') \exp(-i\Delta k\, z')\, dz', \quad k_2 > 0 \tag{219}$$

$$\hat{A}_2(z) = \hat{A}_2(L) + ig \int_z^L \hat{A}_1^2(z') \exp(-i\Delta k\, z')\, dz', \quad k_2 < 0 \tag{220}$$

We solve the joint equations (218), (219) for $k_2 > 0$ or (218), (220) for $k_2 < 0$ by the iterative method, and in the resulting series, we restrict ourselves to terms up to second order in z except the z factors that go together with Δk. We denote by $\hat{J}_3(z)$ the ideal consisting of all formal operator series that start with the order z^3. Thus we obtain that

$$\hat{A}_{j\mathrm{out}} \equiv \hat{A}^{(\mathrm{appr})}_{j\mathrm{out}} = \hat{A}_{j\mathrm{in}} + L\hat{a}_{j1}(\Delta k\, L) + L^2 \hat{a}_{j2}(\Delta k\, L) \quad \mathrm{mod}\ \hat{J}_3(L) \tag{221}$$

where

$$L\hat{a}_{11}(\Delta k L) = 2K_1(L)\hat{A}^\dagger_{1\text{in}}\hat{A}_{2\text{in}}$$
$$L^2\hat{a}_{12}(\Delta k L) = -4K_{12}(L)\hat{A}_{1\text{in}}\hat{A}^\dagger_{2\text{in}}\hat{A}_{2\text{in}} + 2K_{12}(L;k_2)\hat{A}^\dagger_{1\text{in}}\hat{A}^2_{1\text{in}} \tag{222}$$
$$L\hat{a}_{21}(\Delta k L) = K_2(L)\hat{A}^2_{1\text{in}}$$
$$L^2\hat{a}_{22}(\Delta k L) = 4K_{21}(L)\left(\hat{A}^\dagger_{1\text{in}}\hat{A}_{1\text{in}} + \frac{1}{2}\hat{1}\right)\hat{A}_{2\text{in}} \tag{223}$$

with

$$K_1(z) = \frac{g^\star}{\Delta k}[\exp(i\Delta k z) - 1]$$
$$K_2(z) = -\frac{g}{\Delta k}[\exp(-i\Delta k z) - 1] \tag{224}$$
$$K_{12}(z) = |g|^2\left\{-i\frac{z}{\Delta k} + \frac{1}{(\Delta k)^2}[\exp(i\Delta k z) - 1]\right\}$$
$$K_{21}(z) = |g|^2\left\{i\frac{z}{\Delta k} + \frac{1}{(\Delta k)^2}[\exp(-i\Delta k z) - 1]\right\} \tag{225}$$

and

$$K_{12}(L;k_2) = \text{Re}[K_{12}(L)] + i\frac{k_2}{|k_2|}\text{Im}[K_{12}(L)] \tag{226}$$

The notation $A \equiv B \bmod C$ means that the difference $A - B$ belongs to the set C.

It can be verified that

$$[\hat{A}^{(\text{appr})}_{1\text{out}}, \hat{A}^{(\text{appr})\dagger}_{1\text{out}}] \equiv [\hat{A}^{(\text{appr})}_{2\text{out}}, \hat{A}^{(\text{appr})\dagger}_{2\text{out}}] \equiv \hat{1} \mod \hat{J}_3(L)$$
$$[\hat{A}^{(\text{appr})}_{1\text{out}}, \hat{A}^{(\text{appr})}_{2\text{out}}] \equiv [\hat{A}^{(\text{appr})}_{1\text{out}}, \hat{A}^{(\text{appr})\dagger}_{2\text{out}}] \equiv \hat{0} \mod \hat{J}_3(L) \tag{227}$$

While for $k_2 > 0$ these relations are usual in the Heisenberg picture, for $k_2 < 0$ it is a new result, although very weak.

In the codirectional case, the description is standard and the unitary progression operator can be found as the solution to the initial problem

$$\frac{d}{dz}\hat{U}(z) = \frac{i}{\hbar}\hat{U}(z)\hat{G}(z) \tag{228}$$

where $\hat{G}(z)$ is a generator of the spatial progression having units of momentum [235]

$$\hat{G}(z) \equiv \hat{G}_{\text{int}}(z) = \hbar\left[g^* \hat{A}_1^{\dagger 2}(z)\hat{A}_2(z)\exp(i\Delta k\, z) + \text{H.c.}\right] \tag{229}$$

and

$$\hat{U}(z)_{|z=0} = \hat{1} \tag{230}$$

The role of the system (218)–(219) is played here by a single integral equation:

$$\hat{U}(z) = \hat{1} + \frac{\mathrm{i}}{\hbar}\int_0^z U(z')\hat{G}(z')\, dz' \tag{231}$$

Using the iterative method, we can found $\hat{U}_{\text{appr}}(L)$ such that

$$\hat{U}(L) \equiv \hat{U}_{\text{appr}}(L) \mod \hat{J}_3(L) \tag{232}$$

Exploiting the operator $\hat{U}(L)$, we expect the output operators to be in the form

$$\hat{M}_{\text{out}} = \hat{U}^\dagger(L)\hat{M}_{\text{in}}\hat{U}(L) \tag{233}$$

providing

$$\hat{M}_{\text{out}} = M\big(\hat{A}_1(L), \hat{A}_2(L)\big) \tag{234}$$

If we were lucky enough to have in hand the relation (233) with an appropriate unitary operator $\hat{U}(L)$ also in the contradirectional case, this would yield

$$\hat{M}_{\text{out}} = M\big(\hat{A}_1(L), \hat{A}_2(0)\big) \tag{235}$$

In particular,

$$\hat{A}_{j\text{out}} = \hat{U}^\dagger(L)\hat{A}_{j\text{in}}\hat{U}(L) \tag{236}$$

This is valid in descriptions of lossless linear and nonlinear processes which lead to a linear system similar to (218)–(220). We will show that in the co- and contradirectional cases, the relation

$$\hat{A}_{j\text{out}} \equiv \hat{U}^\dagger_{\text{appr}}(L)\hat{A}_{j\text{in}}\hat{U}_{\text{appr}}(L) \mod \hat{J}_3(L) \tag{237}$$

holds. Here $\hat{U}_{\text{appr}}(L)$ entering the congruence (232) for $k_2 < 0$ will be derived by the following method. Introducing $\hat{u}_1(\Delta k L)$ and $\hat{u}_2(\Delta k L)$, we express

$$\hat{U}_{\text{appr}}(L) = \hat{1} + L\hat{u}_1(\Delta k L) + L^2\hat{u}_2(\Delta k L) \tag{238}$$

where $\hat{u}_1^\dagger(\Delta k L) = -\hat{u}_1(\Delta k L)$.

Setting $\hat{M}_{\text{in}} = \hat{1}$, we obtain $\hat{M}_{\text{out}} = \hat{1}$ for all L and hence

$$\text{Re}[\hat{u}_2(\Delta k L)] = \frac{1}{2}\hat{u}_1^2(\Delta k L) \tag{239}$$

where $\hat{u}_1(\Delta k L)$ is the same as in the codirectional case

$$L\hat{u}_1(\Delta k L) = K_1(L)\hat{A}_{1\text{in}}^{\dagger 2}\hat{A}_{2\text{in}} + K_2(L)\hat{A}_{1\text{in}}^2\hat{A}_{2\text{in}}^\dagger \tag{240}$$

Now we introduce the operators $\hat{m}_1(\Delta k L)$ and $\hat{m}_2(\Delta k L)$ and assume that $\hat{M}_{\text{out}}$ has the form

$$\hat{M}_{\text{out}} \equiv \hat{M}_{\text{in}} + L\hat{m}_1(\Delta k L) + L^2\hat{m}_2(\Delta k L) \quad \text{mod } \hat{J}_3(L) \tag{241}$$

in order to determine the anti-Hermitian part $i\,\text{Im}[\hat{u}_2(\Delta k L)]$. From Eq. (233) reduced modulo the ideal $\hat{J}_3(L)$, we obtain the equation

$$-i\big[\hat{M}_{\text{in}}, \text{Im}[\hat{u}_2(\Delta k L)]\big] = \frac{1}{2}[[\hat{M}_{\text{in}}, \hat{u}_1(\Delta k L)], \hat{u}_1(\Delta k L)] - \hat{m}_2(\Delta k L) \tag{242}$$

Let us consider particularly

$$\hat{M}(z) = \hat{A}_1(z),\ \hat{A}_1^\dagger(z),\ \hat{A}_2(z),\ \hat{A}_2^\dagger(z) \tag{243}$$

which on the substitution into (242) enables us to determine

$$\begin{aligned} iL^2\text{Im}[\hat{u}_2(\Delta k L)] &= [K_{21}(L) - K_{12}(L)] \\ &\quad \times \left\{2\left[\hat{A}_{1\text{in}}^\dagger\hat{A}_{1\text{in}} + \frac{1}{2}\hat{1}\right]\hat{A}_{2\text{in}}^\dagger\hat{A}_{2\text{in}} - \frac{k_2}{2|k_2|}\hat{A}_{1\text{in}}^{\dagger 2}\hat{A}_{1\text{in}}^2\right\} \end{aligned} \tag{244}$$

The relation (244) can be simplified as $k_2 < 0$. It can be verified in an appropriate way that it holds also in the codirectional case where $k_2 > 0$.

D. Floquet Theory

We will demonstrate a quantum counterpart of the well-known classical Kerr-like behavior for the cascaded second-order nonlinearities. We restrict our

treatment of this effect to the case of codirectional propagation. Although clasical optics predicts that the oscillations will be superposed on the Kerr-like trend, quantum optics represents a suitable decomposition. According to the Floquet theorem, there exists the decomposition [223]

$$\hat{U}(z) = \hat{U}_{\text{nonpri}}(z)\hat{U}_{\text{pri}}(z) \tag{245}$$

where $\hat{U}_{\text{nonpri}}(z)$ is a nonperiodic unitary operator and $\hat{U}_{\text{pri}}(z)$ is a periodic unitary operator. These are given by the relations

$$\hat{U}_{\text{nonpri}}(z) = \left[\hat{U}\left(\frac{2\pi}{\Delta k}\right)\right]^{(\Delta k/2\pi)z}$$
$$\hat{U}_{\text{pri}}(z) = \hat{U}^{\dagger}_{\text{nonpri}}(z)\hat{U}(z) \tag{246}$$

and have the properties

$$\hat{U}_{\text{nonpri}}(z)\big|_{z=0} = \hat{1}, \quad \hat{U}_{\text{pri}}\left(z + \frac{2\pi}{\Delta k}\right) = \hat{U}_{\text{pri}}(z) \tag{247}$$

Up to the second order the second relation in (246) yields

$$\hat{U}_{\text{pri}}(z) = \hat{1} + z\hat{u}_1(\Delta k\, z) + z^2\hat{u}_{2\text{pri}}(\Delta k\, z) \quad \text{mod} \quad \hat{J}_3(z) \tag{248}$$

where

$$\hat{u}_{2\text{pri}}(\Delta k\, z) = \hat{u}_2(\Delta k\, z) - \frac{2\pi}{\Delta k\, z}\hat{u}_2(2\pi) \tag{249}$$

The manipulations with the first relation in (246) are very simple, because the operator $\hat{u}_1(2\pi) = \hat{0}$. In the approximation exact up to the second order, we obtain that

$$\hat{U}_{\text{nonpri}}(z) \equiv \hat{1} + z^2\hat{u}_{2\text{nonpri}}(\Delta k\, z) \quad \text{mod}\, \hat{J}_3(z) \tag{250}$$

where

$$\begin{aligned} z^2\hat{u}_{2\text{nonpri}}(\Delta k\, z) &= z\frac{2\pi}{\Delta k\, z}\hat{u}_2(2\pi) \\ &= \mathrm{i}|g|^2\frac{z}{\Delta k}[\hat{A}_1^2(0)\hat{A}_2^{\dagger}(0), \hat{A}_1^{2\dagger}(0)\hat{A}_2(0)] \end{aligned} \tag{251}$$

Compare also (244). On introducing the photon-number operators $\hat{n}_j(z) = \hat{a}_j^{\dagger}(z)\hat{a}_j(z)$, we observe that the complicated commutator in (251) is of the form

$$-\hat{n}_1(0)[\hat{n}_1(0) - \hat{1}] + 4\left[\hat{n}_1(0) + \frac{1}{2}\hat{1}\right]\hat{n}_2(0) \tag{252}$$

This is reminiscent of the interaction Hamiltonian for a nonlinear medium where mode 1 has the Kerr property, unlike mode 2, which is a linear oscillator and there is a nonlinear intensity coupling between these modes.

E. Conclusion

In this section we have studied the cascaded quadratic processes with an input two-mode coherent state in order to characterize the quantum phase shift. We have assumed the steady-state fields and illustrated this situation by the Deutsch–Garrison technique. To fit in the framework of such a technique, we perform a linearization around a classical solution. Further we have adopted the traditional approach to the propagation. We have determined a z-dependent unitary progression operator of the two-mode system in the Schrödinger picture by direct integration. We have compared the results in the large-mismatch limit with a model of an ideal Kerr-like medium, whose properties are effectively those of the cascaded quadratic nonlinearities.

Acknowledgments

This work was supported by the Ministry of Education of Czech Republic (Projects VS96028, CEZ J14/98 and LN00A015), Grant Agency of Czech Republic (Project 202/00/0142), Japan Science and Technology Corporation (JST-CREST), and Czech National Security Authority (Project 19982003012).

References

1. P. A. Franken, A. E. Hill, C. W. Peters, and G. Weinreich, *Phys. Rev. Lett.* **7**, 118 (1961); M. Bass, P. A. Franken, J. F. Ward, and G. Weinreich, *Phys. Rev. Lett.* **9**, 446 (1962).
2. N. Bloembergen and P. S. Pershan, *Phys. Rev.* **128**, 606 (1962); J. A. Armstrong, N. Bloembergen, J. Ducuing, and P. S. Pershan, *Phys. Rev.* **127**, 1918 (1962); N. Bloembergen, *Nonlinear Optics*, Benjamin, New York, 1965.
3. S. Youn, S. Choi, P. Kumar, and R. Li, *Opt. Lett.* **21**, 1597 (1996); R. Li, S. Choi, Ch. Kim, and P. Kumar, *Phys. Rev. A* **51**, 3429 (1995); E. Sidick, A. Knoesen, and A. Dienes, *J. Opt. Soc. Am. B* **12**, 1704 (1995); N. C. Kothari and X. Carlotti, *Opt. Soc. Am. B* **5**, 756 (1988).
4. L. Mandel and E. Wolf, *Optical Coherence and Quantum Optics*, Cambridge Univ. Press, Cambridge, UK, 1995, Chaps. 12.10 and 14.9.
5. J. Peřina, *Quantum Statistics of Linear and Nonlinear Optical Phenomena*, Kluwer, Dordrecht, 1991, Chap. 10.
6. M. Kozierowski and R. Tanaś, *Opt. Commun.* **21**, 229 (1977).
7. S. Kielich, M. Kozierowski, and R. Tanaś, in L. Mandel and E. Wolf (Eds.), *Coherence and Quantum Optics*, Vol. IV, Plenum, New York, 1978, p. 511.
8. L. Mandel, *Opt. Commun.* **42**, 437 (1982).
9. C. K. Hong and L. Mandel, *Phys. Rev A* **32**, 974 (1982).
10. M. Hillery, *Opt. Commun.* **62**, 135 (1987).
11. J. Peřina, Z. Hradil, and B. Jurčo, *Quantum Optics and Fundamentals of Physics*, Kluwer, Dordrecht, 1994, Chap. 8.5; H. A. Bachor, *A Guide to Experiments in Quantum Optics*, Wiley, Weinheim, 1998, Chap. 9.

12. Y. P. Malakyan, *Opt. Commun.* **86**, 423 (1991).
13. J. Bajer and J. Peřina, *Opt. Commun.* **92**, 99 (1992).
14. M. Kozierowski and S. Kielich, *Phys. Lett.* **94**, 213 (1983).
15. J. Bajer, T. Opatrný, and J. Peřina, *Quantum Opt.* **6**, 403 (1994).
16. M. Kozierowski, *Phys. Rev. A* **34**, 3474 (1986).
17. S. D. Du, C. D. Gong, *Phys. Rev. A* **48**, 2198 (1993).
18. Y. B. Zhan, *Phys. Rev. A* **46**, 686 (1992).
19. U. Fano, *Phys. Rev.* **72**, 26 (1947).
20. O. Haderka, J. Bajer, and J. Peřina, *Quantum Semiclass. Opt.* **8**, 1159 (1996).
21. J. Bajer, O. Haderka, and J. Peřina, *J. Opt. B: Quantum Semiclass. Opt.* **1**, 529 (1999).
22. J. Bajer, O. Haderka, J. Peřina, and A. Miranowicz, *Czech. J. Phys.* **50**, 717 (2000).
23. J. Bajer and A. Miranowicz, *J. Opt. B: Quantum Semiclass. Opt.* **2**, L10 (2000).
24. D. Walls and R. Barakat, *Phys. Rev. A* **1**, 446 (1970).
25. H. Paul, *Nichtlineare Optik II*, Academie, Berlin, 1973, p. 16; A. Bandilla, G. Drobný, and I. Jex, *Opt. Commun.* **128**, 353 (1996); G. Drobný, A. Bandilla, and I. Jex, *Phys. Rev. A* **55**, 78 (1997).
26. R. W. Boyd, *Nonlinear Optics*, Academic Press, 1991, p. 78; A. Bandilla, G. Drobný, and I. Jex, *Opt. Commun.* **156**, 112 (1998).
27. S. P. Nikitin and A. V. Masalov, *Quantum. Opt.* **3**, 105 (1991); G. J. Milburn, *Phys. Rev. A* **33**, 674 (1986).
28. R. Hanbury Brown and R. Q. Twiss, *Nature* (London) **177**, 23 (1956); *Proc. Roy. Soc. Lond.* **A242**, 300 (1957); ibid. **A243**, 291 (1957).
29. H. J. Kimble, M. Dagenais, and L. Mandel, *Phys. Rev. Lett.* **39**, 691 (1977).
30. F. Diedrich and H. Walther, *Phys. Rev. Lett.* **58**, 203 (1987); T. Basché, W. E. Moerner, M. Orrit, and H. Talon, *Phys. Rev. Lett.* **69**, 1516 (1992); W. M. Itano, J. C. Berquist, and D. J. Wineland, *Phys. Rev. A* **38**, 559 (1988); T. W. Hodapp, M. A. Finn, and G. W. Greenlees, *Phys. Rev. A* **41**, 2698 (1990); ibid. **46**, 4234 (1992); G. Rempe, R. J. Thompson, and H. J. Kimble, *Phys. Scripta* **T51**, 67 (1994); M. Schubert, I. Siemers, R. Blatt, W. Neuhauser, and P. E. Toschek, *Phys. Rev. Lett.* **68**, 3016 (1992); *Phys. Rev. A* **52**, 2994 (1995).
31. J. G. Walker and E. Jakeman, *Opt. Acta* **32**, 1303 (1985); J. G. Rarity, P. R. Tapster, and E. Jakeman, *Opt. Commun.* **62**, 201 (1987).
32. M. Koashi, K. Kono, T. Hirano, and M. Matsuoka, *Phys. Rev. Lett.* **71**, 1164 (1993).
33. K. Kono, M. Koashi, T. Hirano, and M. Matsuoka, *Opt. Commun.* **127**, 237 (1996).
34. M. Koashi, M. Matsuoka, and T. Hirano, *Phys. Rev A* **53**, 3621 (1996).
35. L. Mandel and E. Wolf, *Optical Coherence and Quantum Optics*, Cambridge Univ. Press, Cambridge, UK, 1995, Chap. 11; L. Mandel, *Phys. Scripta* **T12**, 34 (1986).
36. J. Peřina, *Quantum Statistics of Linear and Nonlinear Optical Phenomena*, 2nd ed., Kluwer, Dordrecht, 1991, Chap. 4; J. Peřina, Z. Hradil, and B. Jurčo, *Quantum Optics and Fundamentals of Physics*, Vol. 63 of *Fundamental Theories of Physics*, Kluwer, Dordrecht, 1994, Chap 4.
37. M. C. Teich and B. E. A. Saleh, in E. Wolf (Ed.), *Progress in Optics*, Vol. 26, Elsevier, Amsterdam, 1988, p. 1; *Physics Today* **6**, 26 (1990).
38. D. F. Walls, *Science Progress* **74**, 291 (1990); D. F. Smirnov and A. S. Troshin, *Usp. Fiz. Nauk* **153**, 233 (1987) [*Sov. Phys. Usp.* **30**, 851 (1987)]; G. Leuchs, in G. T. Moore and M. O. Scully (Eds.), *Frontiers of Nonequilibrium Statistical Physics*, Plenum, New York, 1986, p. 329; H. Paul, *Rev. Mod. Phys.* **54**, 1061 (1982); R. Loudon, *Phys. Bull.* **1**, 21 (1976).
39. S. Kryszewski and J. Chrostowski, *J. Phys. A* **10**, L261 (1977).

40. S. K. Srinivasan and S. Udayabaskaran, *Optica Acta* **26**, 1535 (1979).
41. H. T. Dung, A. S. Shumovsky, and N. N. Bogolubov Jr., *Opt. Commun.* **90**, 322 (1992).
42. E. I. Aliskenderov, H. T. Dung, and L. Knöll, *Phys. Rev. A* **48**, 1604 (1993).
43. S. Singh, *Opt. Commun.* **44**, 254 (1983).
44. L.-Y. Feng, F. Qian, and L.-B. Deng, *J. Mod. Opt.* **41**, 431 (1998).
45. A. Miranowicz, J. Bajer, H. Matsueda, M. R. B. Wahiddin, and R. Tanaś, *J. Opt. B: Quantum Semiclass. Opt.* **1**, 511 (1999); A. Miranowicz, J. Bajer, A. Ekert, and W. Leoński, *Acta Phys. Slov.* **47**, 319 (1997).
46. A. Miranowicz, H. Matsueda, J. Bajer, M. R. B. Wahiddin, and R. Tanaś, *J. Opt. B: Quantum Semiclass. Opt.* **1**, 603 (1999).
47. A. Yariv, *Quantum Electronics*, 3rd ed., Wiley, New York, 1989.
48. A. Miranowicz and S. Kielich, in M. Evans and S. Kielich (Eds.), *Modern Nonlinear Optics*, Prigogine and Rice Seies., Vol. 85/3, Wiley, New York, 1994, p. 531.
49. W. J. Mielniczuk and J. Chrostowski, *Phys. Rev. A* **23**, 1382 (1981).
50. D. F. Walls and R. Barakat, *Phys. Rev. A* **1**, 446 (1970).
51. V. G. Dmitriev, G. G. Gurzadyan, and D. N. Nikogosyan, *Handbook of Nonlinear Optical Crystals*, Springer, Berlin, 1999.
52. W. Louisell, *Radiation and Noise in Quantum Electronics*, McGraw-Hill, New York, 1964, p. 274.
53. R. J. Glauber, *Phys. Lett.* **21**, 650 (1966); L. Mišta, *Czech. J. Phys. B* **19**, 443 (1969).
54. J. Huang and P. Kumar, *Phys. Rev. Lett.* **68**, 2153 (1992).
55. R. J. Glauber, *Phys. Rev.* **130**, 2529 (1963); ibid. **131**, 2766 (1963).
56. M. A. Berger, *An Introduction to Probability and Stochastic Processes*, Springer, New York, 1993; Y. G. Sinay, *Probability Theory*, Springer, Berlin, 1992; A. N. Shiryayev, *Probability*, Springer, New York, 1984.
57. M. M. Nieto, *Phys. Scripta T* **48**, 5 (1993).
58. A. Royer, *Phys. Rev. A* **53**, 70 (1996).
59. P. Carruthers and M. M. Nieto, *Rev. Mod. Phys.* **40**, 411 (1968).
60. A. Lukš and V. Peřinová, *Quantum Opt.* **6**, 125 (1994).
61. V. Peřinová, A. Lukš, and J. Peřina, *Phase in Optics*, World Scientific, Singapore, 1998.
62. A. Luis and L. L. Sánchez-Soto, in E. Wolf (Ed.), *Progress in Optics*, Vol. 41, Elsevier, Amsterdam, p. 421.
63. J. W. Noh, A. Fougères, and L. Mandel, *Phys. Rev. A* **45**, 424 (1992).
64. J. W. Noh, A. Fougères, and L. Mandel, *Phys. Rev. Lett.* **71**, 2579 (1993).
65. R. Frieden, in C. R. Smith and W. T. Grandy, Jr. (Eds.), *Maximum-Entropy and Bayesian Methods in Inverse Problems*, Reidel, Dordrecht, 1985, p. 134.
66. C. W. Helstrom, *Quantum Detection and Estimation Theory*, Academic, New York, 1976.
67. K. R. W. Jones, *Ann. of Phys.* **207**, 140 (1991).
68. Z. Hradil et al., *Phys. Rev. Lett.* **76**, 4295 (1996).
69. M. Zawisky et al., *J. Phys. A: Math. Gen.* **31**, 551 (1998).
70. J. Řeháček, Z. Hradil, M. Zawisky, S. Pascazio, H. Rauch, and J. Peřina, *Phys. Rev. A* **60**, 473 (1999).
71. J. Řeháček, Z. Hradil, M. Dušek, O. Haderka, and M. Hendrych, *J. Opt. B: Quantum Semiclass. Opt.* **2**, 237 (2000).

72. J. W. Noh, A. Fougères, and L. Mandel, *Phys. Rev. Lett.* **67**, 1426 (1991).
73. A. S. Lane, S. L. Braunstein, and C. M. Caves, *Phys. Rev. A* **47**, 1667 (1993).
74. Z. Hradil, *Phys. Rev. A* **55**, R1561 (1997).
75. M. G. Kendall and A. Stuart, *Advanced Theory of Statistics*, Charles Griffin, London, 1961, Vol. 2.
76. J. F. Walkup and J. W. Goodman, *J. Opt. Soc. Am.* **63**, 399 (1973).
77. B. Yurke, S. L. McCall, and J. R. Klauder, *Phys. Rev. A* **33**, 4033 (1986).
78. M. J. Holland and K. Burnett, *Phys. Rev. Lett.* **71**, 1355 (1993).
79. L. Mandel and E. Wolf, *Optical Coherence and Quantum Optics*, Cambridge Univ. Press, Cambridge, UK, 1995, Sec. 22.4 and references cited therein.
80. J. Peřina, Z. Hradil, and B. Jurčo, *Quantum Optics and Fundamentals of Physics*, Kluwer, Dordrecht, 1994, Sec. 8.6 and references cited therein.
81. M. Zukowski, A. Zeilinger, M. A. Horne, and A. K. Ekert, *Phys. Rev. Lett.* **71**, 4287 (1993).
82. J.-W. Pan and A. Zeilinger, *Phys. Rev. A* **57**, 2208 (1998).
83. D. Bouwmeester, J.-W. Pan, K. Mattle, M. Eibl, H. Weinfurter, and A. Zeilinger, *Nature* **390**, 575 (1997).
84. D. M. Greenberger, M. A. Horne, A. Shimony, and A. Zeilinger, *Am. J. Phys.* **58**, 1131 (1990).
85. D. Bouwmeester, J.-W. Pan, M. Daniell, H. Weinfurter, and A. Zeilinger, *Phys. Rev. Lett.* **82**, 1345 (1999).
86. J. G. Rarity and P. R. Tapster, *Phys. Rev. A* **59**, R35 (1999).
87. T. E. Keller and M. H. Rubin, *Phys. Rev. A* **56**, 1534 (1997).
88. G. Di Guiseppe, L. Haiberger, F. De Martini, and A. V. Sergienko, *Phys. Rev. A* **56**, R21 (1997).
89. W. P. Grice, I. A. Walmsley, *Phys. Rev. A* **56**, 1627 (1997).
90. J. Peřina, Jr., A. V. Sergienko, B. M. Jost, B. E. A. Saleh, and M. C. Teich, *Phys. Rev. A* **59**, 2359 (1999).
91. J. Peřina, Jr., *Eur. Phys. J. D* **7**, 235 (1999).
92. W. P. Grice, R. Erdmann, I. A. Walmsley, D. Branning, *Phys. Rev. A* **57**, R2287 (1998).
93. H.-B. Fei, B. M. Jost, S. Popescu, B. E. A. Saleh, and M. C. Teich, *Phys. Rev. Lett.* **78**, 1679 (1997).
94. J. Peřina, Jr., B. E. A. Saleh, and M. C. Teich, *Phys. Rev. A* **57**, 3972 (1998).
95. B. E. A. Saleh, B. M. Jost, H.-B. Fei, and M. C. Teich, *Phys. Rev. Lett.* **80**, 3483 (1998).
96. A. Ekert, *Phys. Rev. Lett.* **67**, 661 (1991).
97. A. Migdall, *Physics Today* **1**, 41 (1999).
98. A. Beskow and J. Nilsson, *Arkiv für Fysik* **34**, 561 (1967); L. A. Khalfin, *Zh. Eksp. Teor. Fiz. Pis. Red.* **8**, 106 (1968) [*JETP Lett.* **8**, 65 (1968)]; L. Fonda, G. C. Ghirardi, A. Rimini, and T. Weber, *Nuovo Cim.* **A15**, 689 (1973); **A18**, 805 (1973).
99. B. Misra and E. C. G. Sudarshan, *J. Math. Phys.* **18**, 756 (1977).
100. P. Facchi and S. Pascazio, in E. Wolf (Ed.), *Progress in Optics*, Vol. 42, Elsevier, Amsterdam, (in press).
101. A. Luis and J. Peřina, *Phys. Rev. Lett.* **76**, 4340 (1996).
102. K. Kraus, *Found. Phys.* **11**, 547 (1981).
103. E. Mihokova, S. Pascazio, and L. S. Schulman, *Phys. Rev.* **A56**, 25 (1997).
104. L. S. Schulman, *Phys. Rev.* **A57**, 1059 (1998).

105. A. Luis and L. L. Sánchez–Soto, *Phys. Rev. A* **57**, 781 (1998).
106. K. Thun and J. Peřina, *Phys. Lett. A* **249**, 363 (1998).
107. P. Facchi, H. Nakazato, and S. Pascazio, e-print archive, quant-ph/0006094.
108. H. Nakazato, M. Namiki, S. Pascazio, and H. Rauch, *Phys. Lett. A* **217**, 203 (1996).
109. W. H. Itano, D. J. Heinzen, J. J. Bollinger, and D. J. Wineland, *Phys. Rev. A* **41**, 2295 (1990).
110. J. Řeháček, J. Peřina, P. Facchi, S. Pascazio, and L. Mišta, Jr., *Phys. Rev. A* **62**, 013804 (2000).
111. A. Yariv and P. Yeh, *Optical Waves in Crystals*, Wiley, New York, 1984.
112. S. Pascazio and P. Facchi, *Acta Phys. Slovaca* **49**, 557 (1999); P. Facchi and S. Pascazio, *Phys. Rev. A* **62**, 023804 (2000).
113. G. Assanto, A. Laureti-Palma, C. Sibilia, and M. Bertolotti, *Opt. Commun.* **110**, 599 (1994).
114. J. Janszky, C. Sibilia, M. Bertolotti, P. Adam, and A. Petak, *Quant. Semiclass. Opt.* **7**, 509 (1995).
115. S. J. Lee, J. B. Khurgin and Y. J. Ding, *Opt. Commun.* **139**, 63 (1997).
116. C. C. Yang, *Opt. Lett.* **16**, 1641 (1991).
117. H. Hatami-Hanza and P. L. Chu, *Opt. Commun.* **124**, 90 (1996).
118. J. Peřina and J. Peřina, Jr., *Quantum Semiclass. Opt.* **7**, 863 (1995).
119. J. Peřina and J. Peřina, Jr., *J. Mod. Opt.* **43**, 1951 (1996).
120. J. Herec, *Acta Phys Slovaca* **49**, 731 (1999).
121. L. Mišta, Jr., J. Herec, V. Jelínek, J. Řeháček, and J. Peřina, *J. Opt. B.: Quant. Semiclass. Opt. 2*, 726 (2000); e-print quant-ph 0004070.
122. M. S. Abdalla, F. A. A. El-Orany, and J. Peřina, *J. Mod. Opt.* **47**, 1055 (2000).
123. A. Chefles and S. M. Barnett, *J. Mod. Opt.* **43**, 709 (1996).
124. N. Korolkova and J. Peřina, *Opt. Commun.* **136**, 135 (1997).
125. J. Peřina, Jr. and J. Peřina, *Quantun. Semiclass. Opt.* **9**, 443 (1997).
126. J. Fiurášek and J. Peřina, *Acta Phys. Slovaca* **48**, 361 (1998).
127. J. Fiurášek and J. Peřina, *J. Mod. Opt.* **46**, 1255 (1999).
128. J. Fiurášek and J. Peřina, *J. Opt. B: Quantum Semiclass. Opt.* **2**, 10 (2000).
129. A. Luis and J. Peřina, *Quantum. Semiclass. Opt.* **8**, 39 (1996).
130. L. Mišta, Jr., J. Řeháček, and J. Peřina, *J. Mod. Opt.* **45**, 2269 (1998).
131. J. Fiurášek, J. Křepelka, and J. Peřina, *Opt. Commun.* **167**, 115 (1999).
132. J. Peřina Jr. and J. Peřina, in E. Wolf (Ed.), *Progress in Optics*, Vol. 41, Elsevier, Amsterdam, 2000, p. 361.
133. J. Fiurášek and J. Peřina, in J. Peřina (Ed.), *Coherence and Statistics of Photons and Atoms*, Wiley, New York, 2001, p. 65.
134. J. Peřina, *Opt. Acta* **28**, 325 (1981); ibid. 1529 (1981).
135. M. Kárská and J. Peřina, *J. Mod. Opt.* **37**, 195 (1990).
136. A. V. Chizhov, J. W. Haus, and K. C. Yeong, *Phys. Rev. A* **52**, 1698 (1995).
137. A. Pieczonková, *Opt. Acta* **29**, 1509 (1982).
138. A. V. Chizhov, J. W. Haus, and K. C. Yeong, *J. Opt. Soc. Am. B* **14**, 1541 (1997).
139. P. Szlachetka, S. Kielich, J. Peřina, and V. Peřinová, *J. Phys. A* **12**, 1921 (1979).
140. J. Peřina, *Quantum Statistics of Linear and Nonlinear Optical Phenomena*, Kluwer, Dordrecht, 1991, Chap. 9.

141. J. Peřina and J. Křepelka, *J. Mod. Opt.* **38**, 2137 (1991).
142. R. Simon, N. Mukunda, and B. Dutta, *Phys. Rev. A* **49**, 1567 (1994).
143. J. Fiurášek and J. Peřina, *Phys. Rev. A* **61**, 033808 (2000).
144. For references on classical cryptography see, e.g., D. R. Stinson, *Cryptography: Theory and Practice*, CRC Press, Boca Raton, FL, 1995.
145. P. W. Shor, in S. Goldwasser (Ed.), *Proc. 35th Ann. Symp. Found. Comp. Sci.*, IEEE, Los Alamitos, CA, 1994.
146. A. Shamir, paper presented at Int. Conf. Theor. Appl. Crypt. Techniques, Prague, 1999; available at http://jya.com/twinkle.eps.
147. C. H. Bennett, F. Besette, G. Brassard, L. Salvail, and J. Smolin, *J. Crypt.* **5**, 3 (1992).
148. For a review, see C. H. Bennett and P. W. Shor, *IEEE Trans. Inform. Theory* **44**, 2724 (1992).
149. G. S. Vernam, *J. Am. Ins. Elect. Eng.* **45**, 109 (1926).
150. W. K. Wootters and W. H. Zurek, *Nature* **299**, 802 (1982).
151. C. H. Bennett and G. Brassard, *Proc. IEEE Int. Conf. Computers, Systems, and Signal Processing, Bangalore, India*, IEEE, New York, 1984, p. 175.
152. S. Wiesner, *SIGACT News* **15**, 78 (1983).
153. M. N. Wegman and J. L. Carter, *J. Comput. Syst. Sci.* **22**, 265 (1981).
154. G. Brassard and L. Salvail, in *Advances in Cryptology: Proc. of Crypto '93*, Vol. 765, *Lecture Notes in Comput. Science*, Springer-Verlag, Berlin, 1994, p. 410.
155. N. Lütkenhaus, *Phys. Rev. A* **54**, 97 (1996).
156. C. Fuchs, N. Gisin, R. B. Griffits, C.-S. Niu, and A. Peres, *Phys. Rev. A* **56**, 1164 (1997).
157. C. H. Bennett, G. Brassard, C. Crépeau, and U. M. Maurer, *IEEE Trans. Inform. Theor.* **41**, 1915 (1995).
158. C. H. Bennett, *Phys. Rev. Lett.* **68**, 3121 (1992).
159. B. Huttner, N. Imoto, N. Gisin, and T. Mor, *Phys. Rev. A* **51**, 1863 (1995).
160. D. Bruss, *Phys. Rev. Lett.* **81**, 3018 (1998).
161. See, e.g., D. F. Walls and G. J. Milburn, *Quantum Optics*, Springer, Berlin, 1995, Chap. 5.
162. A. Ekert, *Phys. Rev. Lett.* **67**, 661 (1991).
163. D. Deutch, A. K. Ekert, R. Jozsa, C. Macchiavello, S. Popescu, and A. Sanpera, *Phys. Rev. Lett.* **77**, 2818 (1996).
164. L. Goldenberg and L. Vaidman, *Phys. Rev. Lett.* **75**, 1239 (1995); A. Peres, *Phys. Rev. Lett.* **77**, 3264 (1996); L. Goldenberg and L. Vaidman, *Phys. Rev. Lett.* **77**, 3265 (1996); M. Koashi and N. Imoto, *Phys. Rev. Lett.* **79**, 2383 (1997).
165. G. Ribordy, J.-D. Gautier, N. Gisin, O. Guinnard, and H. Zbinden, *J. Mod. Opt.* **47**, 517 (2000).
166. C. Marand and P. D. Townsend, *Opt. Lett.* **20**, 1695 (1995).
167. A. Muller, H. Zbinden, and N. Gisin, *Europhys. Lett.* **33**, 335 (1996).
168. R. J. Hughes, G. G. Luther, G. L. Morgan, C. G. Peterson, and C. Simmons, *Lecture Notes Comput. Sci.* **1109**, 329 (1996).
169. M. Bourennane, D. Ljunggren, A. Karlsson, P. Jonsson, A. Hening, and J. P. Ciscar, *J. Mod. Opt.* **47**, 563 (2000).
170. W. T. Buttler, R. J. Hughes, S. K. Lamoreaux, G. L. Morgan, J. E. Nordholt, and C. G. Peterson, *Phys. Rev. Lett.* **84**, 5652 (2000).
171. J. D. Franson and B. C. Jacobs, *Electron. Lett.* **31**, 232 (1995).

172. P. R. Tapster, J. G. Rarity, and P. C. M. Owens, *Phys. Rev. Lett.* **73**, 1923 (1994); W. Tittel, J. Brendel, H. Zbinden, and N. Gisin, *Phys. Rev. Lett.* **81**, 3563 (1998); G. Weihs, T. Jennewein, Ch. Simon, H. Weinfurter, and A. Zeilinger, *Phys. Rev. Lett.* **81**, 5039 (1998).

173. T. Jennewein, Ch. Simon, G. Weihs, H. Weinfurter, and A. Zeilinger, *Phys. Rev. Lett.* **84**, 4729 (2000).

174. W. Tittel, J. Brendel, H. Zbinden, and N. Gisin, *Phys. Rev. Lett.* **84**, 4737 (2000).

175. C. H. Bennett, G. Brassard, and N. D. Mermin, *Phys. Rev. Lett.* **68**, 557 (1992).

176. A. V. Sergienko, M. Atatüre, Z. Walton, G. Jaeger, B. E. A. Saleh, and M. C. Teich, *Phys. Rev. A* **60**, R2622 (1999).

177. D. S. Naik, C. G. Peterson, A. G. White, A. J. Berglund, and P. G. Kwiat, *Phys. Rev. Lett.* **84**, 4733 (2000).

178. J. Brendel, N. Gisin, W. Tittel, and H. Zbinden, *Phys. Rev. Lett.* **82**, 2594 (1999).

179. G. Brassard, N. Lütkenhaus, T. Mor, and B. C. Sanders, *Phys. Rev. Lett.* **85**, 1330 (2000).

180. N. Lütkenhaus, *Phys. Rev. A* **61**, 052304 (2000).

181. D. Mayers, in *Advances in Cryptology, Proc. Crypto '96*, Springer, Berlin, 1996, p. 343; Los Alamos e-print archive quant-ph/9606003; D. Mayers, *Unconditional Security in Quantum Cryptography*, Los Alamos e-print archive quant-ph/9802025v4 (1998).

182. O. Haderka and J. Peřina, Jr., *Proc. 12th Czech-Slovak-Polish Optical Conf.* (Velké Losiny, Czech Republic, Sept. 2000); in *Proc. SPIE*, Vol. 4356, Bellingham, 2001, p. 61.

183. A. Stefanov, N. Gisin, O. Guinnard, L. Guinnard, and H. Zbinden, *J. Mod. Optics* **47**, 595 (2000); T. Jennewein, U. Achleitner, G. Weihs, H. Weinfurter, and A. Zeilinger, *Rev. Sci. Instrum.* **71**, 1675 (2000); J. Soubusta, O. Haderka, and M. Hendrych, *Proc. 12th Czech-Slovak-Polish Optical Conf.* (Velké Losiny, Czech Republic, Sept. 2000), in *Proc. SPIE*, Vol. 4536, Bellingham, 2001, p. 54.

184. C. Crépeau and L. Salvail, in L. C. Guillon and J. J. Quisquater (Eds.), *Advances of Cryptology: Proc. Eurocrypt '95*, Springer-Verlag, New York, 1995, p. 133.

185. G. Brassard, C. Crépeau, R. Jozsa, and D. Langlois, *Proc. 34th Ann. IEEE Symp. Found. Comp. Sci.* 362 (1993).

186. D. Mayers, *Phys. Rev. Lett.* **78**, 3410 (1997); H.-K. Lo and H. F. Chau, *Phys. Rev. Lett.* **78**, 3410 (1997).

187. M. Dušek, O. Haderka, and M. Hendrych, *Acta Phys. Slov.* **48**, 169 (1998); M. Dušek, O. Haderka, M. Hendrych, and R. Myška, *Phys. Rev. A* **60**, 149 (1999).

188. H. Barnum, *Quantum Secure Identification Using Entanglement and Catalysis*, Los Alamos e-print archive quant-ph/9910072 (1999).

189. D. Ljunggren, M. Bourennane, and A. Karlsson, *Phys. Rev. A* **62**, 022305 (2000).

190. M. Hillery, V. Bužek, and A. Berthiaume, *Phys. Rev. A* **59**, 1829 (1999); M. Hillery and V. Bužek, *Acta Phys. Slov.* **49**, 533 (1999).

191. A. Karlsson, M. Koashi, and N. Imoto, *Phys. Rev. A* **59**, 162 (1999).

192. W. Tittel, H. Zbinden, and N. Gisin, *Quantum Secret Sharing Using Pseudo-GHZ states*, Los Alamos e-print archive quant-ph/9912035 (1999).

193. C. H. Bennett, G. Brassard, C. Crépeau, and M.-H. Skubiszewska, in *Advances in Cryptology: Proc. Crypto '91*, Springer, New-York, 1992, p. 361.

194. A. Ekert, B. Huttner, G. M. Palma, and A. Peres, *Phys. Rev. A* **50**, 1047 (1994).

195. H. P. Yuen, *Quantum Semiclass. Opt.* **8**, 939 (1996).

196. B. Huttner and A. K. Ekert, *J. Mod. Opt.* **41**, 2455 (1994).

197. E. Biham and T. Mor, *Phys. Rev. Lett.* **78**, 2256 (1997); E. Biham and T. Mor, *Phys. Rev. Lett.* **79**, 4034 (1997); E. Biham, M. Boyer, G. Brassard, J. van de Graaf, and T. Mor, *Security of Quantum Key Distribution against All Collective Attacks*, Los Alamos e-print archive quant-ph/9801022 (1998).
198. H.-K. Lo and H. F. Chau, *Science* **283**, 2050 (1999).
199. M. Dušek, O. Haderka, and M. Hendrych, *Opt. Commun.* **169**, 103 (1999).
200. M. Dušek, M. Jahma, and N. Lütkenhaus, *Phys. Rev. A* **62**, 022306 (2000).
201. H. Inamori, N. Lütkenhaus, and D. Mayers, to be published.
202. G. J. Stegeman and A. Miller, in J. E. Midwinter (Ed.), *Photonics in Switching*, Vol. I, *Background and Components*, Academic, Boston, 1993, p. 81.
203. J.-M. R. Thomas and J.-P. E. Taran, *Opt. Commun.* **4**, 329 (1972).
204. R. De Salvo, D. J. Hagan, M. Sheik-Bahae, G. Stegeman, and E. W. Van Stryland, *Opt. Lett.* **17**, 28 (1992).
205. G. I. Stegeman, M. Sheik-Bahae, E. Van Stryland, and G. Assanto, *Opt. Lett.* **18**, 13 (1993).
206. C. Sibilia, A. Re, E. Fazio, and M. Bertolotti, *J. Opt. Soc. Am. B* **13**, 1151 (1996).
207. A. Kobyakov and F. Lederer, *Phys. Rev. A* **54**, 3455 (1996).
208. A. G. White, J. Mlynek, and S. Schiller, *Europhys. Lett.* **35**, 425 (1996).
209. A. Re, C. Sibilia, E. Fazio, and M. Bertolotti, *J. Mod. Opt.* **42**, 823 (1995).
210. V. Peřinová and A. Lukš, in E. Wolf (Ed.), *Progress in Optics*, Vol. XXXIII, Elsevier Science, Amsterdam, 1994, p. 129.
211. Ts. Gantsog and R. Tanaś, *J. Mod. Opt.* **38**, 1021 (1991).
212. A. Lukš and V. Peřinová, *Czech. J. Phys.* **41**, 1205 (1991).
213. A. Lukš and V. Peřinová, *J. Phys. A: Math. Gen.* **29**, 4665 (1996).
214. V. Peřinová, A. Lukš, and J. Křepelka, *Quantum Semiclass. Opt.* **9**, 1 (1997).
215. S. Kielich, R. Tanaś, and R. Zawodny, *J. Mod. Opt.* **34**, 979 (1987).
216. J. Peřina, *Quantum Statistics of Linear and Nonlinear Optical Phenomena*, 2nd ed., Kluwer, Dordrecht, 1991, p. 275.
217. R. Tanaś, Ts. Gantsog, and R. Zawodny, *Opt. Commun.* **83**, 278 (1991).
218. S. P. Nikitin and A. V. Masalov, *Quantum Opt.* **3**, 105 (1991).
219. R.-D. Li and P. Kumar, *Opt. Lett.* **18**, 1961 (1993).
220. Z. Y. Ou, *Phys. Rev. A* **49**, 2106 (1994).
221. R. D. Li and P. Kumar, *Phys. Rev. A* **49**, 2157 (1994).
222. A. Berzanskis, K.-H. Feller, and A. Stabinis, *Opt. Commun.* **118**, 438 (1995).
223. V. Peřinová and A. Lukš, *Acta Phys. Slov.* **35**, 395 (1995).
224. V. Peřinová, A. Lukš, J. Křepelka, C. Sibilia, and M. Bertolotti, *J. Mod. Opt.* **43**, 13 (1996).
225. L. Noirie, P. Vidaković, and J. A. Levenson, *J. Opt. Soc. Am. B* **14**, 1 (1997).
226. V. Peřinová, A. Lukš, and J. Křepelka, *Quantum Semiclass. Opt.* **10**, 375 (1998).
227. I. Abram and E. Cohen, *Phys. Rev. A* **44**, 500 (1991).
228. P. D. Drummond, *Phys. Rev. A* **42**, 6845 (1990).
229. P. D. Drummond, in M. Evans and S. Kielich (Eds.), *Modern Nonlinear Optics*, Part 3, Wiley, New York, 1994, p. 379.

230. I. H. Deutsch and J. C. Garrison, *Opt. Commun.* **86**, 311 (1991).
231. I. H. Deutsch and J. C. Garrison, *Phys. Rev. A* **43**, 2498 (1991).
232. I. Abram and E. Cohen, *J. Mod. Opt.* **41**, 847 (1994).
233. V. Peřinová, J. Křepelka, J. Peřina, A. Lukš, and P. Szłachetka, *Optica Acta* **33**, 15 (1986).
234. J. A. Armstrong, N. Bloembergen, J. Ducuing, and P. S. Pershan, *Phys. Rev.* **127**, 1918 (1962).
235. V. Peřinová, J. Křepelka, A. Lukš, C. Sibilia, and M. Bertolotti, *J. Mod. Opt.* **38**, 2429 (1991).

A QUANTUM ELECTRODYNAMICAL FOUNDATION FOR MOLECULAR PHOTONICS

DAVID L. ANDREWS

School of Chemical Sciences, University of East Anglia, Norwich, United Kingdom

PHILIP ALLCOCK

Department of Physics, University of Bath, Bath, United Kingdom

CONTENTS

I. INTRODUCTION

Molecular photonics has come of age at the threshold of the new millennium. With the main principles of molecule–photon interaction generally well understood, and with laser science mature, it is a field in which we are now witnessing an unparalleled advancement in science and technology, and the realisation of many new and exciting applications. It is nonetheless a field in which the gulf between the two disciplines of chemistry and optics, which represent its molecular and photonic heritage, demands a conceptual and mathematical bridge of sufficient strength to support its progeny. At one extreme, the chemists and materials scientists whose work is increasingly directed toward the devising, synthesis, and characterization of novel photonic materials, need a framework that can accommodate and relate to their insights into the relationships between molecular quantum mechanics, structure, and optical properties. At the other, laser physicists and optical engineers need a vehicle for the furtherance of theory in a form that can reveal the detailed format of the quantum optical parameters that relate to particular materials.

As a theory that addresses the full extent of its molecular photonics remit with the equitable rigour of quantum mechanics, quantum electrodynamics is undoubtedly the tool of choice for this demanding task. In a previous review, one of us has delineated the development of a quantum electrodynamical framework for the generation of optical harmonics in molecular systems [1]. The present work has a rather different focus and is intended to supplement that review, making reference to it but expanding its remit and elaborating on different topics. Theory is cast in a form suitable to address any condensed-phase system of independent atoms or molecules, for example liquids, solutions, molecular crystals, or mesoscopically more intricate structures such as membranes. Among other things, this present work focuses on a number of more recent topical issues such as the quantum-optical basis for dissipative and refractive effects, the role of permanent dipole moments, resonance damping, and time-reversal symmetry. Attention is also drawn to a new diagram-based calculational device that appears to offer significant advantages over the traditional time-ordered diagrammatic methods.

II. FOUNDATIONS

To fully develop the photonic and material components of quantum-optical response invites the application of quantum electrodynamics (QED). The defining characteristic of this theory is that it addresses every optical interaction in terms of a closed dynamical system where light and matter are treated on an equal footing, each component addressed with full quantum-mechanical rigor. It is a theory whose predictions have been tested to a higher degree of precision

than any other in modern physics, and that remains unchallenged by the most sophisticated experimental measurements [2]. Even in the noncovariant form commonly employed for dealing with the optical interactions of conventional matter, QED accommodates retardation features associated with the finite time of signal propagation. The success of QED in leading to the correct form of the Casimir–Polder interaction, for example, owes its origin to this intrinsic property of its formulation [3–6]. Indeed, it has recently been shown that even the application of properly retarded *classical* electrodynamics produces results of significantly different form [7]. In the subjects to be described below, retardation effects are not specifically at issue—and the advantages of a QED foundation, which we shall highlight, are entirely independent of such features. The need to apply QED in order to properly accommodate retardation features in the quantum optics of nanostructures has nonetheless been demonstrated by Chernyak and Mukamel [8]. The interested reader may also find another body of work on resonance energy transfer and cooperative absorption, in which we have described several processes where retardation is a highly significant factor. The primary references to such work can be found elsewhere in reviews of that subject area [9,10].

The familiar semiclassical basis for optical calculations has been compared to the QED method previously [1]. Some of its shortcomings in connection with nonlinear optics and electro-optics have recently been highlighted [11]. Not surprisingly, the semiclassical theory is inconsistent with the general principles of quantum optics, allowing for example the detection of a single photon by two different detectors [12]. The semiclassical invocation of an electric polarization as the oscillating moment of a radiating dipole, coupled with the electric field vector of the ensuing radiation, generally casts the signal amplitude in the form of a sum of contributions associated with physically distinct processes—when it is a fundamental violation of the superposition principle to summarize the amplitudes of transitions between nonidentical sets of initial and final radiation states. Again, the semiclassical polarization formalism does not allow the full incorporation of magnetic and diamagnetic interactions. For example, in a general three-wave interaction mediated by a species that supports $E1^2M1$ (two electric dipoles, one magnetic dipole) but not $E1^3$ channels, the magnetic dipole interaction in the former can be associated with each of the three waves, yet for obvious reasons only two are accommodated in the electric polarization. It has also been remarked that outside of QED there is no formal basis for establishing the gauge transformations that underpin the familiar multipolar description of optical interactions [13,14a,b].

The definitive molecular formulation of quantum electrodynamics established by Power [3] and Craig and Thirunamachandran [15] forms the primary basis for the theory developed below (see also Dalton et al. [16]). This framework provides for direct calculation of the tensor parameters involved in

linear and nonlinear optical interactions, which naturally emerge from the derivation of observables such as signal intensities. The starting point for such calculations is the QED Hamiltonian for the dynamical system, wherein matter is conventionally described in terms of individual components with distinct electronic integrity and overall electrical neutrality. In the following text we cast theory in a form suitable to address any condensed-phase system of independent atoms or molecules, for example, liquids, solutions, molecular crystals, or even mesoscopically more intricate structures such as membranes. The theory can also be applied to subunits such as ions or chromophores, assuming that it is the transitions in these that dominate the optical response of the medium, so that each ion or chromophore can be treated as the optical representative of a local environment that is itself electrically neutral. For simplicity, the term *molecules* is used here as an umbrella term for the distinct optical units labeled ξ. In multipolar form the system Hamiltonian may then be represented as follows;

$$H = H_{\text{rad}} + \sum_{\xi} H_{\text{mol}}(\xi) + \sum_{\xi} H_{\text{int}}(\xi) \tag{1}$$

Here H_{rad} is the Hamiltonian for the radiation field *in vacuo*, H_{mol} the field-free Hamiltonian for molecule ξ, and H_{int} is a term representing molecular interaction with the radiation. It is worth emphasising that the basic simplicity of Eq. (1) specifically results from adoption of the multipolar form of light-matter interaction. This is based on a well-known canonical transformation from the minimal-coupling interaction [17–21]. The procedure results in precise cancellation from the system Hamiltonian of all Coulombic terms, save those intrinsic to the Hamiltonian operators for the component molecules; hence no terms involving intermolecular interactions appear in Eq. (1).

An important implication of developing theory from the full QED Hamiltonian is that neither the eigenstates of H_{rad} nor those of $H_{\text{mol}}(\xi)$ are stationary states for the system described by it. Thus the presence of the radiation field modifies the form of the molecular wavefunctions, and equally the presence of matter modifies the form of the radiation wavefunctions. Since the Hamiltonian remains the same irrespective of the state of the system, then even when no light is present the coupling still effects a modification of the molecular wavefunctions. This is, for example, manifest in the occurrence of spontaneous emission (luminescence) from isolated molecules in excited states, the lifting of degeneracy between the $2^2S_{1/2}$ and $2^2P_{1/2}$ states of atomic hydrogen (the Lamb shift), also the Casimir force between conducting plates, and yet again the corrections responsible for what was once considered the "anomalous" magnetic moment of the electron.

We now consider the detailed nature of the terms in the QED Hamiltonian. The simplest to deal with is the middle term, which denotes a sum of the normal

nonrelativistic Schrödinger operators $H_{\mathrm{mol}}(\xi)$ for each molecule, the operator counterparts of their classical energies, which need no further elaboration. Equally, the radiation field term H_{rad} is the operator equivalent of the classical expression for electromagnetic energy—which, recalling the relation $c^2 = 1/(\mu_0\varepsilon_0)$ between the vacuum electric susceptibility ε_0 and magnetic permeability μ_0, is expressible as

$$H_{\mathrm{rad}} = \frac{1}{2}\int [\varepsilon_0 \mathbf{e}^{\perp 2}(\mathbf{r}) + \mu_0^{-1}\mathbf{b}^2(\mathbf{r})]\,\mathrm{d}^3\mathbf{r} \tag{2}$$

Here $\mathbf{e}^{\perp}$ is the fundamental transverse microscopic electric field operator and $\mathbf{b}$ is the corresponding magnetic field operator. The superscript on the electric field operator designate its transverse character with respect to the direction of propagation, redundant in the case of the magnetic field as it is intrinsically transverse, namely, divergence-free, since it arises from the curl of a vector potential field $\mathbf{a}(\mathbf{r})$. Since the electric field also derives from $\mathbf{a}(\mathbf{r})$, we concentrate first on the second-quantized form of this vector potential, which is cast in terms of a summation over radiation modes as follows:

$$\mathbf{a}^{\perp}(\mathbf{r}) = \sum_{\mathbf{k},\lambda}\left(\frac{\hbar}{2V\omega\varepsilon_0}\right)^{1/2}[\mathbf{e}_{\mathbf{k}}^{(\lambda)}a_{\mathbf{k}}^{(\lambda)}e^{i\mathbf{k}\cdot\mathbf{r}} + \bar{\mathbf{e}}_{\mathbf{k}}^{(\lambda)}a_{\mathbf{k}}^{\dagger(\lambda)}e^{-i\mathbf{k}\cdot\mathbf{r}}] \tag{3}$$

Here V denotes the quantization volume, and $\mathbf{e}_{\mathbf{k}}^{(\lambda)}$ is the unit polarization vector for the radiation mode characterized by wavevector $\mathbf{k}$, polarization λ and circular frequency $\omega = c|\mathbf{k}|$; where it appears, an overbar denotes complex conjugation. The polarization vector is considered a complex quantity specifically to admit the possibility of circular or elliptical polarizations. Associated with each mode $(\mathbf{k},\lambda)$ are a Hermitian conjugate pair of photon annihilation and creation operators, $a_{\mathbf{k}}^{(\lambda)}$ and $a_{\mathbf{k}}^{\dagger(\lambda)}$, respectively, which operate eigenstates of H_{rad} with $m(\mathbf{k},\lambda)$ photons (m being the mode occupation number) as follows

$$a_{\mathbf{k}}^{(\lambda)}|m(\mathbf{k},\lambda)\rangle = \sqrt{m}|(m-1)(\mathbf{k},\lambda)\rangle \tag{4}$$

$$a_{\mathbf{k}}^{\dagger(\lambda)}|m(\mathbf{k},\lambda)\rangle = \sqrt{(m+1)}|(m+1)(\mathbf{k},\lambda)\rangle \tag{5}$$

reducing the number of $(\mathbf{k},\lambda)$ photons by one in the former case and increasing it by one in the latter. We note in passing that these operators are not *form-invariant*, meaning that although the same symbols are used in connection with field expansions in the minimal coupling formalism, the operators themselves differ as from those we employ for multipolar coupling, as the radiation states on which they operate also differ when matter is present [22].

Our efforts will be repaid if we take pause to examine the properties of the vector potential, and thereby also its derivative fields. The vector potential is self-evidently Hermitian, as befits the status of the field it represents. Its parity with respect to space-inversion is odd, since P operation reverses the sign of $\mathbf{r}$, $\mathbf{e}$, and $\mathbf{k}$. Its character with respect to time-inversion T, which is also of interest, is less self-evident. First, this operation gives

$$\mathbf{a}^{\perp}(\mathbf{r}) \xrightarrow{T} \sum_{\mathbf{k},\lambda} \left(\frac{\hbar}{2V\omega\varepsilon_0}\right)^{1/2} [\bar{\mathbf{e}}_{-\mathbf{k}}^{(\lambda)} a_{-\mathbf{k}}^{(\lambda)} e^{i(-\mathbf{k}\cdot\mathbf{r})} + \mathbf{e}_{-\mathbf{k}}^{(\lambda)} a_{-\mathbf{k}}^{\dagger(\lambda)} e^{-i(-\mathbf{k}\cdot\mathbf{r})}]$$

since it reverses the sign of $\mathbf{k}$ and complex conjugates all numbers. Then, since the sum over the dummy variable $\mathbf{k}$ extends in all directions, it is convertible to a sum over $-\mathbf{k}$, and using the permissible relation $\bar{\mathbf{e}}_{-\mathbf{k}}^{(\lambda)} = -\mathbf{e}_{\mathbf{k}}^{(\lambda)}$ [23,24], we obtain the result that $\mathbf{a}^{\perp}(\mathbf{r})$ is also of odd parity in time. Now, using the source-free result

$$\mathbf{e}(\mathbf{r}) = -\frac{\partial \mathbf{a}(\mathbf{r})}{\partial t} \tag{6}$$

implemented in the interaction picture where time features explicitly [compare with the later equations (30)–(32)], we obtain the following expression for the electric field operator:

$$\mathbf{e}^{\perp}(\mathbf{r}) = i \sum_{\mathbf{k},\lambda} \left(\frac{\hbar\omega}{2V\varepsilon_0}\right)^{1/2} [\mathbf{e}_{\mathbf{k}}^{(\lambda)} a_{\mathbf{k}}^{(\lambda)} e^{i\mathbf{k}\cdot\mathbf{r}} - \bar{\mathbf{e}}_{\mathbf{k}}^{(\lambda)} a_{\mathbf{k}}^{\dagger(\lambda)} e^{-i\mathbf{k}\cdot\mathbf{r}}] \tag{7}$$

Equally, from

$$\mathbf{b}(\mathbf{r}) = \text{curl } \mathbf{a}(\mathbf{r}) \tag{8}$$

we have a magnetic field given by

$$\mathbf{b}(\mathbf{r}) = i \sum_{\mathbf{k},\lambda} \left(\frac{\hbar\omega\mu_0}{2V}\right)^{1/2} [\mathbf{b}_{\mathbf{k}}^{(\lambda)} a_{\mathbf{k}}^{(\lambda)} e^{i\mathbf{k}\cdot\mathbf{r}} - \bar{\mathbf{b}}_{\mathbf{k}}^{(\lambda)} a_{\mathbf{k}}^{\dagger(\lambda)} e^{-i\mathbf{k}\cdot\mathbf{r}}] \tag{9}$$

where the complex unit vector $\mathbf{b}_{\mathbf{k}}^{(\lambda)}$ is defined as

$$\mathbf{b}_{\mathbf{k}}^{(\lambda)} = \hat{\mathbf{k}} \times \mathbf{e}_{\mathbf{k}}^{(\lambda)} \tag{10}$$

Again, both the electric and magnetic fields are obviously of Hermitian character. What also emerges from the route of their derivation through Eqs. (3), (6), and

(8) is that the electric field operator is of odd parity with respect to space, and even parity with respect to time; the magnetic field operator is of even parity with respect to space and odd with respect to time.

Employing the preceding field operator expansions enables the radiation Hamiltonian (2) to be recast in a form that more readily identifies its own quantum properties, explicitly featuring the photon creation and annihilation operators:

$$H_{\text{rad}} = \sum_{\mathbf{k},\lambda} \left(a_{\mathbf{k}}^{\dagger(\lambda)} a_{\mathbf{k}}^{(\lambda)} + \frac{1}{2} \right) \hbar\omega \tag{11}$$

The $\frac{1}{2}\hbar\omega$ associated with each radiation mode is the energy associated with the familiar vacuum fluctuations, the origin of spontaneous emission and self-energy corrections. The eigenstates $|m(\mathbf{k},\lambda)\rangle$ of H_{rad} are number states; states that more closely model the coherence and other properties of laser light will be introduced later.

To complete the definitions of the terms in Eq. (1), the full expression for the interaction Hamiltonian $H_{\text{int}}(\xi)$, before multipolar decomposition, can be written as follows

$$\begin{aligned} H_{\text{int}}(\xi) = {} & -\varepsilon_0^{-1} \int \mathbf{p}^{\perp}(\xi,\mathbf{r}) \cdot \mathbf{d}^{\perp}(\mathbf{r})\, d^3\mathbf{r} - \int \mathbf{m}(\xi,\mathbf{r}) \cdot \mathbf{b}(\mathbf{r}) d^3\mathbf{r} \\ & + \frac{1}{2} \int\int O_{ij}(\xi,\mathbf{r},\mathbf{r}') b_i(\mathbf{r}) b_j(\mathbf{r})\, d^3\mathbf{r}\, d^3\mathbf{r}' \end{aligned} \tag{12}$$

where $\mathbf{p}^{\perp}(\xi,\mathbf{r})$ is the transverse electric polarization vector field, $\mathbf{m}(\xi,\mathbf{r})$ is the magnetization vector field, and $\mathbf{O}(\xi,\mathbf{r},\mathbf{r}')$ is the diamagnetization tensor associated with molecule ξ. Each has a multipolar expansion (see, e.g., Refs. 20 and 21) leading to an infinite series of terms, the leading contributions of which provide the leading terms of $H_{\text{int}}(\xi)$ as follows:

$$H_{\text{int}}(\xi) = -\varepsilon_0^{-1} \mu(\xi) \cdot \mathbf{d}^{\perp}\big(\mathbf{R}_{\xi}\big) - \varepsilon_0^{-1} Q_{ij}(\xi) \nabla_i d_j^{\perp}\big(\mathbf{R}_{\xi}\big) - \mathbf{m}(\xi) \cdot \mathbf{b}\big(\mathbf{R}_{\xi}\big) - \cdots \tag{13}$$

Here $\boldsymbol{\mu}(\xi)$ is the electric dipole (E1) operator for molecule ξ located at position $\mathbf{R}_{\xi}$, $Q_{ij}(\xi)$ is the corresponding electric quadrupole (E2) operator, and $\mathbf{m}(\xi)$ is the magnetic dipole (M1) operator. The diamagnetization does not contribute to this order of approximation. We also recognize in Eqs. (12) and (13) the microscopic transverse displacement electric field, $\mathbf{d}^{\perp}$, whose quantum operator form will be discussed in the next section. Explicit expressions for the components of the

leading molecular multipoles are as follows

$$\mu_i(\xi) = \sum_{\alpha(\xi)} e_\alpha (\mathbf{q}_{\alpha(\xi)} - \mathbf{R}_\xi)_i \tag{14}$$

$$Q_{ij}(\xi) = \frac{1}{2}\sum_{\alpha(\xi)} e_\alpha \left[(\mathbf{q}_{\alpha(\xi)} - \mathbf{R}_\xi)_i (\mathbf{q}_{\alpha(\xi)} - \mathbf{R}_\xi)_j - \frac{1}{3}|\mathbf{q}_{\alpha(\xi)} - \mathbf{R}_\xi|\delta_{ij} \right] \tag{15}$$

$$m_i(\xi) = \frac{1}{2}\sum_{\alpha(\xi)} e_\alpha [(\mathbf{q}_{\alpha(\xi)} - \mathbf{R}_\xi) \times \dot{\mathbf{q}}_{\alpha(\xi)}]_i \tag{16}$$

where summations are taken over each constituent particle $\alpha(\xi)$ of charge e_α and position vector $\mathbf{q}_\alpha$. In passing it may be noted that employment of the traceless form of the electric quadrupole and higher-order multipoles is consistent with the divergence-free character of the electric displacement field on which the gradient operator, ∇, acts in Eq. (13). In general, each electric multipole (En) is time-even and carries a $(-1)^n$ signature for space inversion; the corresponding magnetic multipole (Mn) is time-odd and has $(-1)^{n-1}$ space parity. Hence the time-even, space-even nature of H_{int} is secure.

The electric dipole term in (13) normally represents the strongest coupling between matter and radiation and is sufficient for the majority of cases, in which the electronic excitations of molecules are restricted to regions significantly smaller than the wavelengths of the radiation engaged. The electric quadrupole and magnetic dipole terms together are then smaller by a factor typically of the order of the fine structure constant $\alpha = \frac{1}{137}$. The leading diamagnetisation contribution is of the order α^2, and thus comes into play at the same level as electric octupole and magnetic quadrupole interactions. Although in many quantum optical calculations the detailed, multipolar form of the coupling is deemed largely irrelevant, the spatial and temporal symmetries depend crucially on the multipoles involved, as do the magnitudes of the corresponding coupling constants.

III. MEDIA CORRECTIONS

The development of the quantum field theory so far has been cast in a form most directly suited for applications in which the material part of the system comprises only those molecules or optical centers involved in the interactions of interest, with no other matter present. More generally in condensed-phase materials, such centers are surrounded by other atoms or molecules whose electronic properties modify the fields experienced (and produced) by those optical centers. To take account of such influences, we introduce the microscopic displacement electric field $\mathbf{d}$. This arises as a direct consequence of working within the multipolar

formalism and is related to the fundamental electric field **e** and microscopic polarization field **p** by

$$\mathbf{d}^{\perp} = \varepsilon_0 \mathbf{e}^{\perp} + \mathbf{p}^{\perp} \tag{17}$$

At this stage the molecular and optical properties are neatly entwined. In its semiclassical macroscopic counterpart, Eq. (17) is termed a *material* equation because of its engagement of a bulk polarization **P**; the microscopic and bulk polarisations are, for simple cubic systems, related through the succinct expression

$$\frac{\mathbf{P}}{3} = \mathbf{p} \tag{18}$$

It is common practice in the semiclassical formalism to incorporate all the ensuing material-induced (Lorentz) field corrections as an integral part of the optical susceptibilities in an ad hoc manner. In using quantum field theory, and considering all interactions to occur through the exchange of transverse photons, it is not necessary to modify the corresponding molecular polarizabilities, if the field operators take full account of the light propagation environment. Then all matter-induced corrections are carried with the displacement field, and the appropriately modified operator automatically accommodates the local field or media effects.

The nature of media effects relates to the fact that, since the microscopic displacement field is the net field to which molecules of the medium are exposed, it corresponds to a fundamental electric field dynamically "dressed" by interaction with the surroundings. The quantized radiation is in consequence described in terms of "dressed photons" or *polaritons*. A full and rigorous theory of dressed optical interactions using noncovariant molecular quantum electrodynamics is now available [25–27], and its application to energy transfer processes has been delineated in detail [10]. In the present context its deployment leads to a modification of the quantum operators for the auxiliary fields $\mathbf{d}^{\perp}$ and **h**, which fully account for the influence of the medium—the fundamental fields of course remain unchanged. Expressions for the local displacement electric and the auxiliary magnetic field operators [27], correct for all microscopic interactions, are then as follows

$$\mathbf{d}^{\perp}(\mathbf{r}) = i \sum_{\mathbf{k},\lambda,m} \left(\frac{\hbar v_g^{(m)} \omega_k^{(m)} \varepsilon_0}{2cVn(\omega_k^{(m)})} \right)^{1/2} \left(\frac{\{n(\omega_k^{(m)})\}^2 + 2}{3} \right) \times [\mathbf{e}_{\mathbf{k}}^{(\lambda)} P_{\mathbf{k},m}^{(\lambda)} e^{i(\mathbf{k}\cdot\mathbf{r})} - \bar{\mathbf{e}}_k^{(\lambda)} P_{k,m}^{\dagger(\lambda)} e^{-i(\mathbf{k}\cdot\mathbf{r})}] \tag{19}$$

$$\mathbf{h}^{\perp}(\mathbf{r}) = i \sum_{\mathbf{k},\lambda,m} \left(\frac{\hbar v_g^{(m)} \omega_k^{(m)} n(\omega_k^{(m)})}{2\mu_0 cV} \right)^{1/2} [\mathbf{b}_{\mathbf{k}}^{(\lambda)} P_{\mathbf{k},m}^{(\lambda)} e^{i(\mathbf{k}\cdot\mathbf{r})} - \bar{\mathbf{b}}_{\mathbf{k}}^{(\lambda)} P_{\mathbf{k},m}^{\dagger(\lambda)} e^{-i(\mathbf{k}\cdot\mathbf{r})}] \tag{20}$$

where μ_0 is the magnetic permeability of the vacuum ($\mu_0 = 1/\varepsilon_0 c^2$). To fully appreciate these expressions for the new auxiliary field operators, it is expedient to dwell briefly on their key features and elucidate the new symbols which appear in the preceding equations.

Compared with the mode expansions of their fundamental field counterparts, Eqs. (7) and (9), the most obvious difference apparent in Eqs. (19) and (20) relates to the introduction here of additional summations over m. This index labels the branches of polariton dispersion and runs from $m = 1, 2, \ldots M$, where $M = M_{\text{mol}} + 1$ and M_{mol} is the number of molecular frequencies. For example, in a two-level molecular system characterized by a single transition frequency, there are two branches to the dispersion curve. In general, the summations over $\mathbf{k}$ extend to $k \ll 2\pi/a$, where a is a characteristic intermolecular separation. Consequently the auxiliary operators are properly invoked only when dealing with the propagation and interactions in condensed media of infrared, optical, or ultraviolet light—where a description in terms of refractive index is entirely legitimate. Nonetheless, the theory properly accommodates not only transparent but also dispersive regions where the polariton wavevector and frequency are not linearly related, signifying resonant or near-resonant optical response. It also affords a means for the representation of photonic bandgap materials. Figure 1 illustrates the photonic and exciton-like regions for conventional two-, three- and multilevel systems. The index m, which identifies each of the dispersion branches in the general case, has to be incorporated in the definition of the polariton frequency, as given by

$$\omega_k^{(m)} = \frac{ck}{n(\omega_k^{(m)})} \tag{21}$$

where several normal frequencies are associated with each value of k, again as evident in Fig. 1. The mode expansions (19) and (20) also feature polariton annihilation and creation operators, $P_{\mathbf{k},m}^{(\lambda)}$ and $P_{\mathbf{k},m}^{\dagger(\lambda)}$, respectively, with similar properties to their vacuum counterparts of Eqs. (4) and (5). Finally, Eqs. (19) and (20) also feature the group velocity $v_g^{(m)}$, defined for each specific polariton mode as

$$v_g^{(m)} = c\left\{\frac{\partial\omega_k^{(m)} n(\omega_k^{(m)})}{\partial\omega_k^{(m)}}\right\}^{-1} = \frac{\partial\omega_k^{(m)}}{\partial k} \tag{22}$$

and again incorporating the frequency-dependent refractive index defined as

$$[n(\omega_k^{(m)})]^2 = 1 + \frac{\bar{\alpha}(\omega_k^{(m)})\rho/\varepsilon_0}{1 - \bar{\alpha}(\omega_k^{(m)})\rho/3\varepsilon_0} \tag{23}$$

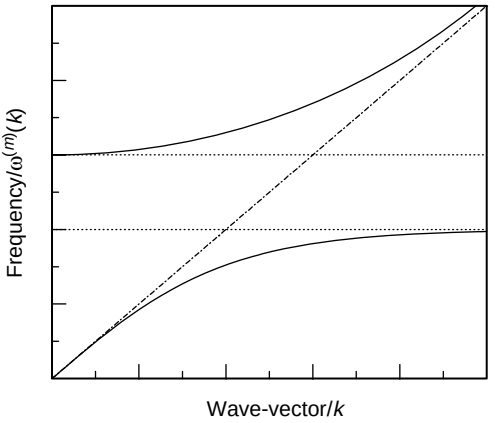

(a)

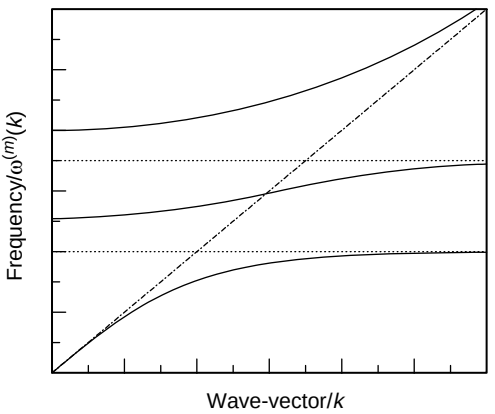

(b)

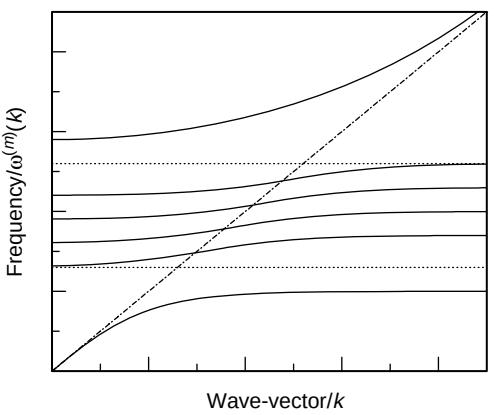

(c)

Figure 1. Schematic curves illustrate the dispersion relationship between the polariton frequency/$\omega^{(m)}(k)$ and the wave-vector/k. Figure 1(a) illustrates the dispersion if only a single molecular frequency is present (Hopfield model), and (b) the case of two molecular resonances; (c) depicts a situation in which a number of such dispersion branches are present.

representing a quantum extension of the Lorentz–Lorenz equation. Here $\bar{\alpha}$ is the average molecular polarizability of the homogeneous host, based on an electronically isotropic medium, and ρ is the number density of host molecules.

In the majority of applications to quantum and nonlinear optical phenomena, it is only the photon-like branches of the dispersion curves that are of interest, and the m index in the preceding expressions can generally be left implicit. Again, as we shall be concerned with photonic regions, it is legitimate to engage $a_{\mathbf{k}}^{(\lambda)}$ and $a_{\mathbf{k}}^{\dagger(\lambda)}$ in place of $P_{\mathbf{k}}^{(\lambda)}$ and $P_{\mathbf{k}}^{\dagger(\lambda)}$. In keeping with this policy, we shall from here on once again refer only to *photons*, although it is understood that the quanta involved are, strictly speaking, optical branch polaritons. The case of vacuum propagation can then be viewed as a special case of the more general formalism. For example, if the refractive index is set to unity in Eq. (19), the group velocity is simply c, the polariton operators become identical to those representing the annihilation and creation of pure photons, and the expression reduces directly to the fundamental electric field operator of Eq. (7), multiplied by ε_0.

At this juncture we have in place a formalism that fully accounts for the refractive and dissipative modifications of the fundamental fields due to the dispersive electronic properties of the optical medium. This has been achieved not by any phenomenological or other ad hoc approach, but from first principles, using the theoretical methods of molecular QED. As a result, the necessary local field corrections in condensed media naturally emerge from the detailed form of the auxiliary field operators, obviating the need to encompass them indirectly in terms of macroscopic bulk susceptibilities, as is necessary in the semiclassical theory.

IV. PERTURBATIVE DEVELOPMENT

With the full Hamiltonian given by Eq. (1), the time evolution of the system wavefunction ψ is determined by the time-dependent Schrödinger equation:

$$i\hbar \frac{\partial \psi(t)}{\partial t} = H\psi(t) \tag{24}$$

Solutions of high precision, fully incorporating electronic media effects, can be derived on the assumption that the coupling between matter and radiation is treated as a perturbation on the eigenstates of H_0, where

$$H_0 = H_{\text{bath}} + \sum_{\xi}{}' H_{\text{mol}}(\xi) \tag{25}$$

with

$$H_{\text{bath}} = H_{\text{rad}} + \sum_{\xi}{}'' (H_{\text{mol}}(\xi) + H_{\text{int}}(\xi)) \tag{26}$$

In Eq. (25) the prime on the summation denotes its limitation to those molecules whose transitions are engaged either directly or indirectly in the optical response. The double prime on the summation in Eq. (26) denotes the exclusion of those molecules. The eigenstates of H_0 thus contain products of the eigenstates of the optically prominent molecules and the dressed-photon eigenstates of H_{bath}. As usual, if the system is in an eigenstate of H_0 at time 0, the wavefunction at any later time t is expressible as

$$|\psi(t)\rangle = \exp\left(\frac{-iH_0 t}{\hbar}\right) U(t,0)|\psi(0)\rangle \tag{27}$$

defining a unitary time evolution operator $U(t,0)$ for the evolution of the system in the time interval $(0,t)$. Substitution of Eq. (27) into Eq. (24) leads to an exact result for $U(t,0)$ expressible as the following series expansion

$$U(t,0) = 1 + \sum_{m=1}^{\infty} (i\hbar)^{-m} \int_{t_0}^{t} \int_{t_0}^{t_1} \cdots \int_{t_0}^{t_{m-1}} \tilde{H}_{\text{int}}(t_1)\tilde{H}_{\text{int}}(t_2)\cdots\tilde{H}_{\text{int}}(t_m)\, dt_1\, dt_2 \cdots dt_m \tag{28}$$

where $\tilde{H}_{\text{int}}(t)$ is the interaction representation of the operator responsible for the coupling between light and matter, given by $\tilde{H}_{\text{int}}(t) = \exp(iH_0 t/\hbar) H_{\text{int}} \exp(-iH_0 t/\hbar)$. In the electric dipole approximation this results in the expression

$$\tilde{H}_{\text{int}}(t) = -\varepsilon_0^{-1} \boldsymbol{\mu} \cdot \tilde{\mathbf{d}}(\mathbf{r},t) \tag{29}$$

where the corresponding microscopic electric displacement operator, $\tilde{\mathbf{d}}(\mathbf{r},t)$ in the interaction representation, may be expressed as a sum of two parts:

$$\tilde{\mathbf{d}}(\mathbf{r},t) = \tilde{\mathbf{d}}^{(+)}(\mathbf{r},t) + \tilde{\mathbf{d}}^{(-)}(\mathbf{r},t) \tag{30}$$

$$\tilde{\mathbf{d}}^{(+)}(\mathbf{r},t) = i \sum_{\mathbf{k},\lambda,m} \left\{ \frac{\hbar v_g^{(m)} \omega_k^{(m)} \varepsilon_0}{2cVn_{\omega_k^{(m)}}} \right\}^{1/2} \left(\frac{n^2_{\omega_k^{(m)}} + 2}{3} \right) \mathbf{e}_{\mathbf{k}}^{(\lambda)} a_{\mathbf{k}}^{(\lambda)} \exp[i(\mathbf{k}\cdot\mathbf{r} - \omega_k^{(m)} t)] \tag{31}$$

$$\tilde{\mathbf{d}}^{(-)}(\mathbf{r},t) = -i \sum_{\mathbf{k},\lambda,m} \left\{ \frac{\hbar v_g^{(m)} \omega_k^{(m)} \varepsilon_0}{2cVn_{\omega_k^{(m)}}} \right\}^{1/2} \left(\frac{n^2_{\omega_k^{(m)}} + 2}{3} \right) \mathbf{e}_{\mathbf{k}}^{(\lambda)} a_{\mathbf{k}}^{\dagger(\lambda)} \exp[-i(\mathbf{k}\cdot\mathbf{r} - \omega_k^{(m)} t)] \tag{32}$$

In this form, the time-even and space-odd character of the electric displacement is again apparent. Also, development of the magnetization reveals its time-odd and space-even character.

In developing the quantum amplitude for an optical process, it is necessary to determine the matrix elements of the time evolution operator, and to this end it is frequently expedient to invoke an expansion in terms of operators rather than the embedded time integrals of Eq. (28). The method of resolvent operators, which affords a framework for both perturbative and nonperturbative analysis [28–30], proceeds through the introduction of a retarded Green function, $K_+(t) = U(t,0)\theta(t)$, together with its advanced counterpart, $K_-(t) = -U(t,0)\theta(-t)$, where $\theta(t)$ is the Heaviside function. These functions allow us to extend to infinity the temporal dependence of the evolution operator, enabling us to express the time evolution operator $U_I(t,t_0)$ as

$$U(t,0) = K_+(t) - K_-(t) = \frac{1}{2\pi i} e^{iE_f t/\hbar} \int_{-\infty}^{+\infty} e^{iE_f t/\hbar} [G_-(E) - G_+(E)]\, dE \tag{33}$$

where E_f denotes the (final) system energy and the retarded and advanced propagators, $G_+(E)$ and $G_-(E)$, respectively, are Fourier transforms of the retarded and advanced Green functions:

$$G_\pm(E) = \frac{1}{i\hbar} \int_{-\infty}^{+\infty} e^{iE\tau/\hbar} K_\pm(\tau)\, d\tau = \lim_{\eta \to 0+} (E - H \pm i\eta)^{-1} \tag{34}$$

At this stage it is convenient to define a set of subsystems, each containing one of the optically prominent molecules ξ and the bath. Introducing and expanding in perturbative fashion the corresponding resolvent operator [31]

$$\begin{aligned} T_{\mathrm{sub}(\xi)}(z) &= (z - H_0 - H_{\mathrm{int}}(\xi))^{-1} \\ &= (z - H_0)^{-1} + (z - H_0)^{-1} H_{\mathrm{int}}(\xi)(z - H_0)^{-1} \\ &\quad + (z - H_0)^{-1} H_{\mathrm{int}}(\xi)(z - H_0)^{-1} H_{\mathrm{int}}(\xi)(z - H_0)^{-1} \cdots \\ &= \sum_{p=0}^{\infty} [T_0(z) H_{\mathrm{int}}(\xi)]^p T_0(z) \end{aligned} \tag{35}$$

enables the requisite optical amplitude to be determined. Specifically, for a process associated with an initial system state $|i\rangle$ and a final system state $|f\rangle$, we have a quantum probability amplitude that can be evaluated from the equation

$$\begin{aligned} c_{fi} = \langle f|U(t,0)|i\rangle &= \frac{1}{2\pi i} e^{iE_f t/\hbar} \oint e^{-izt/\hbar} \langle f|T_{\mathrm{sub}(\xi)}(z)|i\rangle\, dz \\ &= \frac{1}{2\pi i} e^{iE_f t/\hbar} \sum_{p=0}^{\infty} \oint e^{-izt/\hbar} \langle f|[T_0(z) H_{\mathrm{int}}(\xi)]^p T_0(z)|i\rangle\, dz \end{aligned} \tag{36}$$

where the contour for integration encompasses the real axis. Using the method of residues to evaluate the contour integral, and discarding optical frequency oscillatory terms, we thus obtain

$$c_{fi} = \delta_{fi} - 2\pi i \delta\big(E_f - E_i\big) \sum_{\xi} M_{fi}(\xi) \tag{37}$$

The first term denotes the trivial nonprocess in which the initial and final states of the entire system are identical, and can be discarded for any real process. The subsequent term, in which the delta function serves to ensure overall energy conservation, leads to a rate equation expressed by the familiar Golden Rule [32–34]

$$\Gamma = \left(\frac{2\pi}{\hbar}\right) \left| \sum_{\xi} M_{fi}(\xi) \right|^2 \delta(E_f - E_i) \tag{38}$$

cast in terms of a transition matrix whose elements are

$$\begin{aligned} M_{fi}(\xi) &= \big\langle f_{\mathrm{sub}(\xi)} | H_{\mathrm{int}}(\xi) + H_{\mathrm{int}}(\xi) T_{\mathrm{sub}(\xi)} H_{\mathrm{int}}(\xi) | i_{\mathrm{sub}(\xi)} \big\rangle \\ &= \langle f_{\mathrm{sub}(\xi)} | H_{\mathrm{int}}(\xi) + \sum_{p=0}^{\infty} H_{\mathrm{int}}(\xi) [T_0 H_{\mathrm{int}}(\xi)]^p T_0 H_{\mathrm{int}}(\xi) | i_{\mathrm{sub}(\xi)} \rangle \end{aligned} \tag{39}$$

and where the resolvent operators T_0 and $T_{\mathrm{sub}(\xi)}$are evaluated for $z = E_0$.

V. TIME ORDERINGS AND STATE SEQUENCES

For each molecule ξ, every other molecule yields a vanishing contribution to the summands in Eq. (39). Hence, by invoking the completeness relation for the subsystem states, the matrix elements M_{fi} can succinctly be expressed as

$$\begin{aligned} M_{fi} = \langle f | H_{\mathrm{int}} | i \rangle &+ \sum_{r^{(1)}} \frac{\langle f | H_{\mathrm{int}} | r^{(1)} \rangle \langle r^{(1)} | H_{\mathrm{int}} | i \rangle}{(E_i - E_{r^{(1)}})} \\ &+ \sum_{r^{(2)}, r^{(1)}} \frac{\langle f | H_{\mathrm{int}} | r^{(2)} \rangle \langle r^{(2)} | H_{\mathrm{int}} | r^{(1)} \rangle \langle r^{(1)} | H_{\mathrm{int}} | i \rangle}{(E_i - E_{r^{(2)}})(E_i - E_{r^{(1)}})} \\ &+ \sum_{r^{(3)}, r^{(2)}, r^{(1)}} \frac{\langle f | H_{\mathrm{int}} | r^{(3)} \rangle \langle r^{(3)} | H_{\mathrm{int}} | r^{(2)} \rangle \langle r^{(2)} | H_{\mathrm{int}} | r^{(1)} \rangle \langle r^{(1)} | H_{\mathrm{int}} | i \rangle}{(E_i - E_{r^{(3)}})(E_i - E_{r^{(2)}})(E_i - E_{r^{(1)}})} + \cdots \end{aligned} \tag{40}$$

where all states and energies are eigenstates of H_0 and thus relate to the total system containing both the bath and the molecule, with the summations over the

virtual intermediate states $r^{(1)}, r^{(2)}, \ldots$ taken over all such states excluding i or f. In passing it is worth noting that this specifically does *not* exclude the *molecular* initial or final state from inclusion in the intermediate state summations, a point that has often been misunderstood but that is quite clear in the QED formulation. The representation of any m-photon interaction entails terms involving m-photon operators. In view of the linearity in the photon creation and annihilation operators of all the electric and magnetic multipole interactions, this representation generates its leading contribution from the term involving the mth power of H_{int}, and for most processes it is sufficient to consider only the leading nonvanishing term. Writing the system states explicitly as products of molecular and radiation states, we then have

$$\begin{aligned} M_{fi}^{(m)} = & \sum_{r_{\text{mol}}^{(1)}} \cdots \sum_{r_{\text{mol}}^{(m-1)}} \sum_{r_{\text{rad}}^{(1)}} \cdots \sum_{r_{\text{rad}}^{(m-1)}} \langle f_{\text{rad}}; f_{\text{mol}} | H_{\text{int}} | r_{\text{mol}}^{m-1}; r_{rad}^{(m-1)} \rangle \\ & \times \langle r_{\text{rad}}^{(m-1)}; r_{\text{mol}}^{(m-1)} | H_{\text{int}} | r_{\text{mol}}^{(m-2)}; r_{\text{rad}}^{(m-2)} \rangle \cdots \langle r_{\text{rad}}^{(1)}; r_{\text{mol}}^{(1)} | H_{\text{int}} | i_{\text{mol}}; i_{\text{rad}} \rangle \\ & \times [(E_{i_{\text{mol}}} - E_{r_{\text{mol}}^{(m-1)}}) + (E_{i_{\text{rad}}} - E_{r_{\text{rad}}^{(m-1)}})]^{-1} \cdots [(E_{i_{\text{mol}}} - E_{r_{\text{mol}}^{(1)}}) \\ & + (E_{i_{\text{rad}}} - E_{r_{\text{rad}}^{(1)}})]^{-1} \end{aligned} \tag{41}$$

In each of the $(m-1)$ summations over the intermediate radiation states $|r_{\text{rad}}^{(j)}\rangle$, there are only a limited number of possibilities that can make nonvanishing contributions, determined by the sequencing of the creation and annihilation events for the photons emitted and absorbed during the overall interaction. Each of these sequences is conventionally represented using Feynman time-ordered graphs. Calculations based on this method are commonly expedited by the construction of all topologically different diagrams connecting the same initial and final states; the summations over the intermediate states $|r_{\text{rad}}^{(1)}\rangle$ to $|r_{\text{rad}}^{(m-1)}\rangle$ in Eq. (41) are then equivalent to summations over the various time orderings. An alternative method based on state sequences [35] enables the complete set of interaction sequences for any process to be cast in the form of a single diagram. The latter method offers a more concise presentation and improved calculational expediency, particularly in the case of high-order interactions.

Optical frequency doubling affords a simple illustration of each of these diagrammatic methods. For clarity, it is expedient to write down the system states for the conversion process (although familiarity with either method enables this information to be read off directly from the diagrams). The initial and final states for the interaction are as follows:

$$|i_{\text{mol}}; i_{\text{rad}}\rangle = |E_0; q(\mathbf{k}, \lambda), q'(\mathbf{k}', \lambda')\rangle \tag{42}$$

$$|f_{\text{mol}}; f_{\text{rad}}\rangle = |E_0; (q-2)(\mathbf{k}, \lambda), (q'+1)(\mathbf{k}', \lambda')\rangle \tag{43}$$

Given that the molecule is initially in its ground state, there are initially q photons of the pump mode $(\mathbf{k}, \lambda)$ and q' photons of the harmonic mode $(\mathbf{k}', \lambda')$. There are three possible sequences of photon annihilation and creation (a, b, and c) that can provide a route from the initial to the final state, each involving different virtual intermediate states. To avoid confusion, the intermediate state labels $r^{(1)}$ and $r^{(2)}$ are redesignated here as r and s, respectively, and the latter appear below with superscripts to identify the route

$$\left.\begin{aligned} |r_{\mathrm{mol}}; r^a_{\mathrm{rad}}\rangle &= |E_r; (q-1)(\mathbf{k}, \lambda), q'(\mathbf{k}', \lambda')\rangle \\ |s_{\mathrm{mol}}; s^a_{\mathrm{rad}}\rangle &= |E_s; (q-2)(\mathbf{k}, \lambda), q'(\mathbf{k}', \lambda')\rangle \end{aligned}\right\} \tag{44}$$

$$\left.\begin{aligned} |r_{\mathrm{mol}}; r^b_{\mathrm{rad}}\rangle &= |E_r; (q-1)(\mathbf{k}, \lambda), q'(\mathbf{k}', \lambda')\rangle \\ |s_{\mathrm{mol}}; s^b_{\mathrm{rad}}\rangle &= |E_s; (q-1)(\mathbf{k}, \lambda), (q'+1)(\mathbf{k}', \lambda')\rangle \end{aligned}\right\} \tag{45}$$

$$\left.\begin{aligned} |r_{\mathrm{mol}}; r^c_{\mathrm{rad}}\rangle &= |E_r; q(\mathbf{k}, \lambda), (q'+1)(\mathbf{k}', \lambda')\rangle \\ |s_{\mathrm{mol}}; s^c_{\mathrm{rad}}\rangle &= |E_s; (q-1)(\mathbf{k}, \lambda), (q'+1)(\mathbf{k}', \lambda')\rangle \end{aligned}\right\} \tag{46}$$

as represented by the three time-ordered diagrams of Fig. 2. For example, in Fig. 2a, the sequence of interactions is as follows. First, a photon of the pump mode is annihilated by a molecule in its ground state $|0\rangle$, which thereby undergoes a transition to a state $|r\rangle$. A second pump photon is then annihilated, and the molecule proceeds to a state $|s\rangle$. Finally, a harmonic frequency photon is emitted, and the molecule returns to its ground state. Figures 2b and 2c represent the two other possible sequences in which emission of the harmonic photon precedes either one, or both of the pump photon interactions. It is important to emphasize that no *single* time-ordered diagram represents a physically distinguishable process; these diagrams are ultimately only calculational aids based on

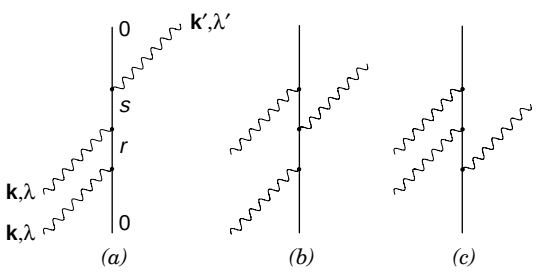

Figure 2. The three time-ordered diagrams representing second harmonic generation. Pump photons of wave vector $\mathbf{k}$ and polarization λ impinge on the molecule from the left and the subsequent harmonic $(\mathbf{k}', \lambda')$ leaves the molecular world line from the right. We assume the initial and final state of the molecule is the ground state 0; the intermediate states are labelled r and s.

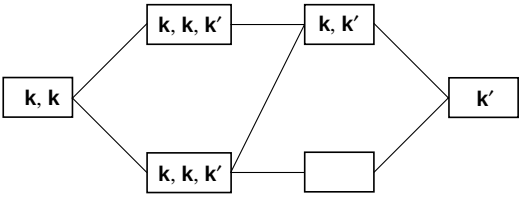

Figure 3. State sequence diagram for SHG. The intial state is represented by the solitary box in the column on the left and the final state by the corresponding the box on the right; columns with more then one box indicate virtual states r and s. An example is afforded by the uppermost route through the diagram, which corresponds identically to the time-ordering of Fig. 2(c).

the approximations of perturbation theory. Collectively, the photon creation and annihilation events that take place at each molecule appear *simultaneously*, as far as real experimental measurements with finite time resolution are concerned. However, the time–energy uncertainty relation does permit short-lived intermediate states that are not properly energy-conserving. This helps explain why it is necessary to include the diagrams corresponding to extremely counterintuitive time sequences such as that of Fig. 2c. Nonetheless, all possible interaction sequences must be included in calculating any matrix element.

The state sequence diagram of Fig. 3 accommodates *all three* routes between the initial and final states; those states are represented by boxes on the far left and far right of the diagram, respectively. The intervening columns represent intermediate system states r and s connected by links that represent valid operations by H_{int} on a preceding state. In these diagrams, lines thus represent interactions and vertices (where data boxes appear) represent states; in this sense they bear a reciprocal space relationship to the Feynman diagrams, where the converse applies.

VI. TENSOR REPRESENTATION

To proceed with the general development, it is useful to extract from the quantum amplitude those elements that involve properties belonging solely to the radiation and molecular tensors, respectively. Thus we formulate matrix elements through the appropriate tensor products for deployment in the Golden Rule.

Consider an m-photon process involving modes of radiation $(\mathbf{k}_m, \lambda_m), \ldots, (\mathbf{k}_1, \lambda_1)$, all potentially different, initially containing $q_m, \ldots, q_1$ photons, respectively. Equation (41) may be factorized as a tensor product of two terms, only one of which is dependent on any intrinsic molecular properties:

$$M_{fi}\{(\mathbf{k}_1, \lambda_1) \cdots (\mathbf{k}_m, \lambda_m)\} = (-1)^m \varepsilon_0^{-m} \alpha_{i_m \cdots i_2 i_1}(-\omega_m; \omega_1, \ldots, \omega_n) \times \rho_{i_m \cdots i_2 i_1}\{(\mathbf{k}_m, \lambda_m), \ldots, (\mathbf{k}_1, \lambda_1)\} \tag{47}$$

Specifically, this equation entails the m-fold tensor contraction of $\boldsymbol{\alpha}^{(m)}(\omega_m, \ldots, \omega_1)$, a rank-$m$ microscopic nonlinear polarisability tensor containing all the molecular variables (with a parametric dependence on the optical frequencies), with $\boldsymbol{\rho}^{(m)}\{(\mathbf{k}_m, \lambda_m), \ldots, (\mathbf{k}_1, \lambda_1)\}$, a tensor constructed solely from radiation parameters, including all the necessary local field corrections. Note the incorporation in Eq. (47) of a sign prefactor, serving to redefine each energy denominator so that the absorption of a photon is associated with a negative radiative frequency and emission with a positive frequency. This results in nonlinear polarisability expressions conforming to the usual conventions. An example might be n-harmonic generation where a tensor written as $\boldsymbol{\alpha}^{(m)}(-\omega_m; \omega_1, \ldots, \omega_1)$ indicates the absorption n photons of frequency ω_1 and emission of a single photon at a frequency $\omega_m \equiv n\omega_1$.

We postpone to a later section a detailed explanation of the explicit expressions for the molecular tensors $\boldsymbol{\alpha}^{(m)}$; we next identify the structure of the radiation tensor $\boldsymbol{\rho}^{(m)}$, which in the electric dipole approximation is given by the following:

$$\boldsymbol{\rho}^{(m)}\{(\mathbf{k}_m, \lambda_m), \ldots, (\mathbf{k}_1, \lambda_1)\} = \langle (m_m + 1)(\mathbf{k}, \lambda)|\mathbf{d}^{\perp}|(m_m)(\mathbf{k}, \lambda)\rangle, \ldots, \langle (m_1 - 1)(\mathbf{k}, \lambda)|\mathbf{d}^{\perp}|(m_1)(\mathbf{k}, \lambda)\rangle \tag{48}$$

In general, to incorporate the matrix elements of Eq. (47) into the rate equation (38), it is necessary to sum, over all molecules in the system, the tensor product entailed in the former—and to this end it proves useful to isolate the one part of the above radiation tensor that is molecule-specific. This simply reflects the fact that the tensor is a field quantity, sensitive to the position of the molecule at which it is evaluated, as follows from the phase factors in (19) and (20). The tensor representing the radiation field for the interaction at molecule ξ may, in fact, be written in the following general form, irrespective of the order or nature of the multipolar interactions involved:

$$\boldsymbol{\rho}(\xi) = \boldsymbol{\rho}' \exp(i\,\Delta\mathbf{k} \cdot \mathbf{R}_\xi) \tag{49}$$

Here ρ' is a position-independent radiation tensor, $\mathbf{R}_\xi$ is the position vector of the molecule relative to an arbitrary fixed origin, and $\Delta\mathbf{k}$ the wavevector mismatch for the process as defined by

$$\Delta\mathbf{k} = \sum_r^m g_r \mathbf{k}_r \tag{50}$$

where g_r assumes the value of $+1$ for each absorbed photon and -1 for each emitted photon. For instance, the radiation tensor for frequency doubling carries the phase factor $\exp[i(2\mathbf{k} - \mathbf{k}') \cdot \mathbf{R}_\xi]$, and hence $\Delta\mathbf{k} = (2\mathbf{k} - \mathbf{k}')$. Such features

are responsible for the all-important issue of coherence. Combining the above results, it thus transpires that any optical process rate may be written in a general Golden Rule form as

$$\Gamma = \frac{2\pi}{\hbar}\left|\sum_{\xi}^{N} \varepsilon_0^{-m}\alpha^{(\xi)}_{i_m\cdots i_2 i_1}\rho'_{i_m\cdots i_2 i_1}\exp\left(i\Delta\mathbf{k}\cdot\mathbf{R}_\xi\right)\right|^2 \delta\left(E_i - E_f\right) \tag{51}$$

This equation lies at the heart of the theoretical development; the precise structure of the molecular and radiation tensors it involves will depend on the detailed nature of the optical interaction to be modeled.

VII. CONSTRUCTION OF RADIATION TENSORS

Having stated that all optical interactions can be modeled through Eq. (51), we now outline the explicit details of both radiation and molecular tensors embedded in the matrix element. As we have shown, the radiative features that are of interest are cast in the tensor ρ introduced in Eq. (48). For any optical process the components of this tensor are explicitly given by a position-independent expression, which follows from Eq. (49):

$$\begin{aligned}\rho'\{(\mathbf{k}_m,\lambda_m),\ldots,(\mathbf{k}_1,\lambda_1)\} &= \rho'_{i_m\cdots i_1}\{(\mathbf{k}_m,\lambda_m),\ldots,(\mathbf{k}_1,\lambda_1)\}\\ \rho'_{i_m\cdots i_1}\{(\mathbf{k}_m,\lambda_m),\ldots,(\mathbf{k}_1,\lambda_1)\} &= \{-i^{(m)}\}s_{i_m\cdots i_1}\{(\mathbf{k}_m,\lambda_m),\ldots,(\mathbf{k}_1,\lambda_1)\}\\ &\quad\times\prod_{i=1}^{m}\left[\left(\frac{\hbar v_g^{(m)}\omega_k^{(m)}\varepsilon_0}{2cVn_{\omega_k}}\right)^{1/2}\left(\frac{n^2_{\omega_k}+2}{3}\right)\sqrt{q}\right]_{(|\mathbf{k}_i|)}\end{aligned} \tag{52}$$

Here, q_i is the number of photons in the ith mode within the quantization volume V. If no photons of a particular mode are initially present, as would be the case for spontaneous emission processes, q_i is equal to unity, as the photon creation operator then acts on the vacuum state. The symbol $\mathbf{s}\{(\mathbf{k}_m,\lambda_m),\ldots,(\mathbf{k}_1,\lambda_1)\}$ represents a polarization tensor defined by

$$S_{i_m\cdots i_1}\{(\mathbf{k}_m,\lambda_m),\ldots,(\mathbf{k}_1,\lambda_1)\} = e_{i_1}(\mathbf{k}_1,\lambda_1)\cdots e_{i_m}(\mathbf{k}_m,\lambda_m) \equiv e_{i_1}\cdots e_{i_m} \tag{53}$$

The arguments associated with each unit vector are now dropped for brevity. The polarization unit vectors $\mathbf{e}_i$ refer to each photon involved in the interaction process. The polarization vectors are represented as above for each photon that is annihilated, but created photons carry the overbar to represent complex

conjugation, thus allowing for the possibility that the light is circularly or elliptically polarised. It is also customary if two photons are from the same mode, as for example would be the case in single-color two-photon absorption or a harmonic process, to place parentheses around the appropriate indices to signify permutational symmetry.

In order to relate to the specific conditions produced by a given laser source, it is clearly necessary to express results in terms of physically meaningful radiation parameters in lieu of the artificial quantization volume V and photon number q that appear in Eq. (52). The procedure for this reformulation allows consideration of pump radiation states characterized by various forms of photon statistics, leading to results appropriate for several different kinds of intensity distribution. In an earlier review [1] it was shown how to develop theory in terms of quantum optical states more realistic than the zero-fluctuation number states $|q(\mathbf{k},\lambda)\rangle$ hitherto employed in the general formulation. Although these states are the most usual basis for QED calculations based on time-dependent perturbation theory, they are associated with infinite phase uncertainty and do not adequately represent any real laser input. One basis set of states that appears rather better suited to the modeling of laser radiation is the overcomplete set represented by the coherent states $|\beta(\mathbf{k},\lambda)\rangle$. These states, characterized for any given radiation mode by minimization of the uncertainty in phase and occupation number [36,37], are eigenstates of the corresponding annihilation operators, satisfying the result

$$a^{(\lambda)}(\mathbf{k})|\beta(\mathbf{k},\lambda)\rangle = \beta(\mathbf{k},\lambda)|\beta(\mathbf{k},\lambda)\rangle \tag{54}$$

where $\beta(\mathbf{k},\lambda)$ is a complex number whose modulus relates to the mean photon number q through $q = |\beta(\mathbf{k},\lambda)|^2$. It should nonetheless be mentioned that the employment of coherent or other states can, if caution is not exercised, produce spurious features resulting from the fact that they are not eigenstates of the radiation Hamiltonian, so that neither photon creation followed by annihilation nor annihilation followed by creation is an identity operation. This feature is commonly overlooked, but it provides one of the best reasons for working with number states if quantum optical aspects are not at issue.

Rate equations expressed in terms of mean photon number and quantization volume are still not directly applicable to experiment. Moreover, since the quantization volume is no more than a theoretical artifact, it must invariably cancel out in any final result. However, the ratio of these two quantities, which represents a mean photon density, is directly related to the mean irradiance, and the relationship may be derived as follows. Consider a quantization volume represented by a small cube of space of side length l and volume V through which the incident beam passes; by definition, this cube contains on average q photons of circular frequency ω_k, and its energy content is $q\hbar\omega_k$ (see Fig. 4). For

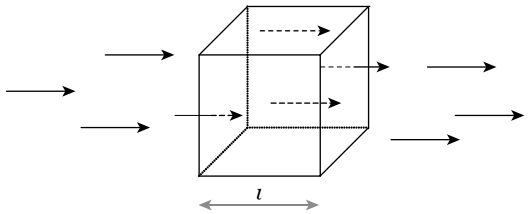

Figure 4. The schematic illustrates a photon flux through a quantization volume. Each side of the chosen cube is assigned a length l. The photons traverse the box in a time l/v_g where v_g is the group velocity in the medium.

a group of q photons with a mean group velocity v_g, it takes a time l/v_g for the energy $q\hbar\omega_k$ to traverse the cube; hence the mean irradiance $I(\omega_k)$ (power per unit beam cross-sectional area) is given by $\{q\hbar\omega_k/(l/v_g)\}/l^2$, so that

$$I(\omega_k) = \frac{q\hbar v_g \omega_k}{V} \tag{55}$$

In passing we may note that the mean interval τ between photon arrival times for any one molecule of physical cross section σ is directly related to $I(\omega_k)$ through

$$\tau = \frac{\hbar\omega_k}{I(\omega_k)\sigma} \tag{56}$$

The parameter τ is rarely featured in the literature but in the case of non-parametric excitation and decay processes in molecular media, its value relative to the decay lifetime affords a useful gauge of excitation efficiency.

For the generation of radiation through any *incoherent* optical process, the general freedom in propagation direction means that each photon is spontaneously created into any one of an infinite set of radiation states, subject to energy conservation. For a collection of free molecules, uncertainty in the molecular state energy, due to the presence of densely packed quasicontinuous vibrational and rotational energy levels, ensures that a density of states representation can legitimately replace the delta function of Eq. (51); see, for example, the work by Craig and Thirunamachandran [15].

Even in coherent processes whose nature serves to define the principal direction of the emergent radiation, and where the initial and final molecular states are necessarily identical, the general theory leads to quantum amplitudes in which the final state of the radiation field is not yet completely specified with regard to the wavevector and polarization of the emitted radiation. As such, the sums over all possible values of $\mathbf{k}'$ and λ' should remain in the general amplitudes of the radiation tensor $\boldsymbol{\rho}'$. However, the restrictions imposed on parametric

processes by virtue of energy conservation and wavevector matching conditions [1] ensures that radiation is emitted into a small pencil of solid angle centered around $\mathbf{k}' + d\mathbf{k}'$, where the prime indicates that the photon is emitted. In effecting the associated sums, we achieve a result of a form that correctly loses dependence on the quantization volume (i.e., except for processes occurring in geometrically confined microcavities where the quantization volume retains physical significance). In the limit of a large quantization volume, the sum over $\mathbf{k}'$ is conveniently replaced by an integral of the form

$$\frac{1}{V}\sum_{\mathbf{k}'} \underset{V\to\infty}{\Longrightarrow} \int \frac{d^3\mathbf{k}'}{(2\pi)^3} = \frac{1}{(2\pi)^3}\int_0^\infty \oint k'^2 dk' d\Omega \tag{57}$$

where it is understood that the solid angle $d\Omega$ extends over all angles. For coherent emission into a pencil of solid angle $d\Omega$ ($\ll 4\pi$ steradians) centered around $\mathbf{k}'$, it is legitimate to substitute for the sum over $\mathbf{k}'$ by

$$\sum_{\mathbf{k}'} \Longrightarrow \frac{d\Omega V}{(w\pi)^3}\int_0^\infty k'^2 dk' \tag{58}$$

Using Eq. (58), any remaining V factor can be successfully removed from the appropriate expressions.

To illustrate a case to be revisited in detail later, we explicitly derive the rate for coherent second-harmonic generation in a system containing M molecules. Using the general expression Eq. (52) for the radiation tensor together with the Golden Rule, and retaining a sum over the emitted harmonic in the matrix elements, we first obtain an expression of the form

$$\begin{aligned}\Gamma_{\text{coh}} = {} & \frac{2\pi}{\hbar\varepsilon_0^6}\left(\frac{\hbar v_g \omega_k \varepsilon_0}{2cVn_{\omega_k}}\right)^2 \left(\frac{n_{\omega_k}^2+2}{3}\right)^4 q(q-1) \\ & \times \sum_{\mathbf{k}',\lambda'} (\eta_M - M)\left(\frac{\hbar v_g' \omega_{k'}' \varepsilon_0}{2cVn_{\omega_{k'}'}}\right)\left(\frac{n_{\omega_{k'}'}^2+2}{3}\right)^2 |\beta_{i(jk)}(-2\omega;\omega,\omega)\bar{e}_i' e_j e_k|^2 \\ & \times \delta(\hbar\omega_k - 2\hbar\omega_k)\end{aligned} \tag{59}$$

Several points deserve mention. First, retention of the sum over the harmonic wavevector and polarization signifies an initial condition that assumes the absence of any harmonic radiation prior to interaction, so that no direction is favored on the basis of stimulated emission (i.e., although the emergent wavevectors are equal in magnitude, they may differ in direction). Secondly, although photon branch indices are suppressed for conciseness, they are to be

regarded as still implicit. Finally, the parentheses around the molecular tensor indices represent index symmetry. (This will be explained in more detail when we deal with the molecular tensors explicitly in the following sections.)

The delta function in Eq. (59) serves to ensure energy conservation, while the factor $(\eta_M - M)$ signifies the extent to which photon momentum is conserved, as determined by wavevector matching. As shown previously [1,38], we have $\eta_M = M^2$ in the limit of exact wavevector matching. Now, substituting Eqs. (55) and (58) into (59) allows the rate of coherent harmonic production, into an infinitesimal solid angle $d\Omega$, to be expressed as follows:

$$d\Gamma_{\text{coh}} = \frac{I^2(\omega_{\mathbf{k}})g^{(2)}_{\omega_k}d\Omega}{4\hbar(2\pi)^2c^2\varepsilon_0^3 n^2_{\omega_k}}\left(\frac{n^2_{\omega_k}+2}{3}\right)^4 \sum_{\lambda'}\int_0^\infty k'^2 dk' \frac{d\omega'_{k'}}{dk'}\left(\frac{\hbar\omega'_{}}{2cn_{\omega'_{k'}}}\right) \times \left(\frac{n^2_{\omega'_{k'}}+2}{3}\right)^2 |\beta_{i(jk)}(-2\omega;\omega,\omega)\bar{e}'_i e_j e_k|^2 \delta(\hbar\omega'_{k'} - 2\hbar\omega_k)\,(\eta_M - M) \tag{60}$$

Here the group velocity of the harmonic wave is written explicitly as $d\omega'_{k'}/dk'$, and we have introduced the second-order degree of coherence $g^{(2)}$ as appropriate for a generalization beyond number states

$$g^{(2)} = \frac{\langle q(q-1)\rangle}{\langle q\rangle^2} \tag{61}$$

where the angular brackets indicate expectation values based on the number state operators, $q \equiv a^\dagger a$. We proceed with the assumption that the output is polarized, thus obviating the need for the polarization sum λ'. Then, using the definition $k' = \omega'_{k'} n_{\omega'_{k'}}/c$ and exploiting delta function properties and after a little algebra, we finally arrive at the expression

$$d\Gamma_{\text{coh}} = \frac{I^2(\omega_k)g^{(2)}_{\omega_k}d\Omega\,\omega_k^3 n_{2\omega_k}}{4\hbar c^5\pi^2\varepsilon_0^3 n^2_{\omega_k}}\left(\frac{n^2_{\omega_k}+2}{3}\right)^4\left(\frac{n^2_{2\omega_k}+2}{3}\right)^2 \times |\beta_{i(jk)}(-2\omega;\omega,\omega)\bar{e}'_i e_j e_k|^2(\eta_M - M) \tag{62}$$

which is best recast in terms of a radiant intensity of harmonic emission by using

$$I(\mathbf{k}') = (\hbar\omega'_{k'})\frac{d\Gamma}{d\Omega} = (2\hbar\omega_k)\frac{d\Gamma}{d\Omega} \tag{63}$$

Significantly, the results of Eqs. (62) and (63) closely resemble those calculated using the more familiar vacuum electric field operators, modified by the

inclusion of refractive index-dependent correction factors (see, e.g., Refs. 1 and 15). This reflects the fact that the rates calculated for any interaction using those methods can, in some sense, incorporate the necessary media contributions if the matrix elements are phenomenologically modified by the factors $n_{\omega_k}^{-1/2}\{(n_{\omega_k}^2+2)/3\}$ or $n_{\omega'_{k'}}^{1/2}\{(n_{\omega'_{k'}}^2+2)/3\}$, for each absorbed or emitted photon, respectively, where n_{ω_k} is the frequency-dependent refractive index. This is a simple prescription that lacks the details of the underlying physics, including the implicit photonic branch indexing. The advantage of the complete method described in the course of this review is that it is directly amenable to systems of significantly greater optical complexity. In contrast to developments that directly dress the molecular response with the local field factors, casting the molecular optical response tensor as a microscopic representative of a bulk susceptibility, Eq. (62) explicitly retains all such factors whose value is determined by the properties of the input radiation, as modified within the bulk of the nonlinear medium.

VIII. PUMP PHOTONICS

Whilst the above is perfectly adequate for the description of processes observed with continuous-wave (cw) input, proper representation of the optical response to pulsed laser radiation requires one further modification to the theory. It is commonly thought difficult to represent pulses of light using quantum field theory; indeed, it is impossible if a number state basis is employed. However by expressing the radiation as a product of coherent states with a definite phase relationship, it is relatively simple to construct a wavepacket to model pulsed laser radiation [39]. The physical basis for this approach is that pulses necessarily have a finite linewidth and therefore in fact entail a large number of radiation modes, so that for the pump radiation, it is appropriate to construct a coherent superposition

$$|i_{\mathrm{rad}}\rangle = \prod_l |\alpha(\omega_l)\rangle \tag{64}$$

and where

$$|\alpha(\omega_l)| = q_l^{1/2} \tag{65}$$

represents the mean number of photons in the mode labeled by the (positive or negative) integer l. For simplicity, it may be assumed that each mode is associated with the same direction of propagation and polarization, so that the frequency label uniquely identifies each component. If the central frequency is ω_0 and the interval between adjacent modes is Ω, then we can write

$$\omega_l = \omega_0 + l\Omega \tag{66}$$

which, with $\Omega = \pi v_g(\omega_0)/L$ [$v_g(\omega_0)$ denoting the intracavity speed of light at frequency ω_0], serves to represent the frequency distribution of a laser with optical cavity length L. A phase relationship between the axial cavity modes, corresponding to perfect mode locking, can now be enforced by writing

$$\alpha(\omega_l) = q_l^{1/2} \exp[-i(\omega_l \tau)] + \varphi \tag{67}$$

with a suitable value for τ and arbitrary φ. When the initial state defined by (64) is made subject to this condition and employed in the calculation of matrix elements as in Eq. (41), this leads to the representation of a pulse train described by the following temporal envelope function $J(t)$ [39]:

$$J(t) = \sum_l (q_l \omega_l)^{1/2} \exp[-il\Omega(t+\tau)] \tag{68}$$

where the time t arises through evaluation of the matrix elements of $\tilde{\mathbf{d}}^{(+)}$ as given by Eq. (31). Choosing $\tau = -\pi/\Omega$ places time zero exactly in between two successive pulses, such that $J(0) \approx 0$ and the interaction is smoothly switched on. By extension of these principles to a continuous frequency distribution, single pulses of radiation can be entertained in the theory through the envelope function

$$J(t) = \int A(\omega) \exp[-i\omega(t+\tau)]\, dt \tag{69}$$

The net result of incorporating all these modifications in the theory of harmonic emission, or any other process entailing the annihilation of n photons from the pump radiation, is that we now have the following prescription:

$$\left[\frac{q!}{(q-n)!}\right] \to J^{2n}\omega^{-n} \tag{70}$$

For coherent state light, each and every coherence factor takes the value of unity, and it may be observed that the result of effecting Eq. (70) is that a time-dependent irradiance $I_\omega(t)$ now appears, properly defined through

$$I_\omega(t) = \left(\frac{\hbar c}{V}\right) J^2(t) \tag{71}$$

To complete the reformulation of results in terms of physically meaningful parameters, and to relax the unduly restrictive assumption of the last section, we now consider the possibility of stimulated emission for photons generated by the

optical process of interest, as, for example, in the case of strong harmonic pumping. This leads to a matrix element containing a factor $(q'+1)^{1/2}/V^{1/2}$, indicating that the rate becomes linearly dependent on $(q'+1)/V$. When q' is large, the rate is essentially proportional to the harmonic photon density. In the light of the preceding remarks on the pump radiation, it is nonetheless for many reasons inadvisable to work in terms of q'. Number states are hardly appropriate, nor is it sensible to suppose that all harmonic photons are delivered into a single radiation mode. Under conditions of strong emission pumping, it is better to gauge the mean number of n-harmonic photons by employment of the relation

$$q' = n^{-1}(q_0 - q) \tag{72}$$

where q_0 is the initial number of pump photons. Equation (72), which basically reflects energy conservation, may be regarded as an integrated form of the generalised Manley–Rowe relation

$$\frac{d\{I(\omega_{\mathbf{k}})/\omega_{\mathbf{k}}\}}{dz} = \frac{-qd\{I(\omega'_{\mathbf{k}'})/\omega'_{\mathbf{k}'}\}}{dz} \tag{73}$$

[40]. The q' that appears in the rate equations is best interpreted as a ratio of the stimulated to the spontaneous emission rate (see, e.g., Ref. 41).

IX. CONSTRUCTION OF MOLECULAR RESPONSE TENSORS

In this section we address the detailed form, and in particular the dispersion behavior, of the molecular response tensors. We note that the frequency dependence of nonlinear polarisabilities and their sum rules have been the subject of a series of incisive works by Bishop and others; see, for example, the paper by Bishop and DeKee [42]. In addressing dispersion behavior below, we follow the same general principles, but at the outset we invoke excited-state damping to allow for the incorporation of lineshape. This is a matter that, once its context is established below, we shall return to in the following section.

To begin, from Eqs. (41) and (47) the explicit result for the nonlinear polarizability $\boldsymbol{\alpha}^{(m)}$ that mediates an m-photon process may be written, in the electric dipole approximation, as follows:

$$\begin{aligned}\boldsymbol{\alpha}^{(m)} = &\sum_{r^{(1)}_{\mathrm{mol}}} \cdots \sum_{r^{(m-1)}_{\mathrm{mol}}} \sum_{r^{(1)}_{\mathrm{rad}}} \cdots \sum_{r^{(m-1)}_{\mathrm{rad}}} \langle f_{\mathrm{mol}}|\boldsymbol{\mu}|r^{(m-1)}_{\mathrm{mol}}\rangle\langle r^{(m-1)}_{\mathrm{mol}}|\boldsymbol{\mu}|r^{(m-2)}_{\mathrm{mol}}\rangle \cdots \langle r^{(1)}_{\mathrm{mol}}|\boldsymbol{\mu}|i_{\mathrm{mol}}\rangle \\ &[(\tilde{E}_{r^{(m-1)}_{\mathrm{mol}}} - \tilde{E}_{i_{\mathrm{mol}}}) + (E_{r^{(m-1)}_{\mathrm{rad}}} - E_{i_{\mathrm{rad}}})]^{-1} \cdots [(\tilde{E}_{r^{(1)}_{\mathrm{mol}}} - \tilde{E}_{i_{\mathrm{mol}}}) + (E_{r^{(1)}_{\mathrm{rad}}} - E_{i_{\mathrm{rad}}})]^{-1}\end{aligned} \tag{74}$$

The summations over all possible intermediate radiation states are accommodated by reference to the various contributing time orderings, or pathways through state-sequence diagrams, and generally result in a set of terms. Each term has a different frequency dependence, as determined by the structure of its energy denominator. The tildas appearing over the molecular energies in Eq. (74) represent a complex representation that includes the effects of damping, to be discussed in detail below. In general, all molecular states carry such damping; only in the special case of the lowest energy (ground) state is the damping redundant. When written with explicit reference to its frequency arguments, the ordering of tensor subscripts in $\boldsymbol{\alpha}^{(m)}$ is assumed to relate identically to the ordering of the frequencies. Thus, for example, in writing the component $\alpha^{(3)}_{ijk}(-\omega_3;\omega_2,\omega_1)$ of the nonlinear optical tensor that mediates sum-frequency conversion, the index i corresponds to the ω_3 photon interaction, j to the ω_2, and k to the ω_1 interaction. Since molecular response tensors are seldom completely index-symmetric [43], preserving an unambiguous correlation between indices and photon frequencies is a very necessary consideration. In the time-ordered diagrams, each interaction vertex carries the same index for the corresponding photon in each diagram, so that the subscript ordering on the molecular interaction vertices varies from diagram to diagram. On state-sequence diagrams, the same index set labels the interaction lines denoting state connections.

It is instructive to take as a first example the general expression for molecular polarizability, the response tensor that formally mediates elastic light scattering in the electric dipole approximation. The result is obtained by application of Eq. (74) with $m = 2$ (one photon is annihilated and another of the same frequency is created). Here there are only two time orderings, or state-sequence pathways, as illustrated in Figs. 5 and 6, respectively. Each generates a term whose numerator is a product of transition dipole moment components. For

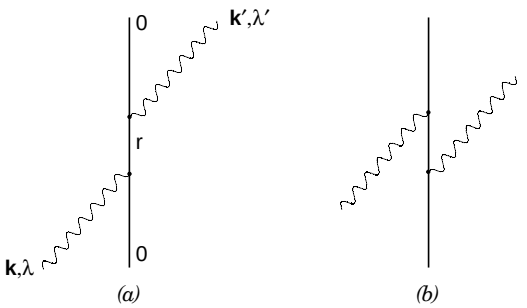

Figure 5. The two time-ordered diagrams required for light scattering. The incident light has wave-vector **k** and polarization λ and is scattered (re-emitted) with wave-vector and polarization **k**′ and λ′ respectively. The initial and final satate for the molecule is assumed to be the ground state 0; intermediate state carries the label r.

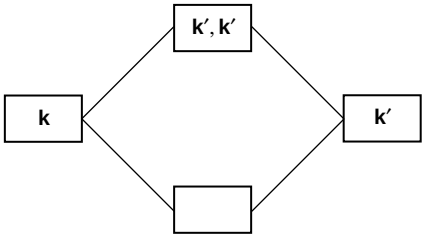

Figure 6. The state-sequence diagram for scattering.

example, from Fig. 5a, or the upper pathway in Fig. 6, we obtain the numerator $\langle f|\mu_i|r\rangle\langle r|\mu_j|i\rangle$. Calculation of each corresponding energy denominator using Eq. (74) requires us to identify the individual energy components. If we assume that the response is to be calculated for a molecule in its ground electronic state, then $E_{i_{\text{mol}}} = E_0$ and the radiation field consists of q photons of frequency ω, $E_{i_{\text{rad}}} = q\hbar\omega$. The intermediate state energies, $\left(\tilde{E}_{r_{\text{mol}}} + E_{r_{\text{rad}}}\right)$, are again calculated with the aid of the diagrams. In the intermediate state of the coupled system in Fig. 5a, a photon has been absorbed by the molecule, which is thereby promoted to an intermediate electronic state—corresponding to the state box in the center of the lower pathway in Fig. 6. Therefore the total intermediate state energy is the sum of the intermediate molecular energy $\tilde{E}_{r_{\text{mol}}}$ and the modified radiation field $E_{r_{\text{rad}}} = (q-1)\hbar\omega$. Following Eq. (74), and considering only the first state sequence, we have as one contribution to the molecular polarizability:

$$\alpha_{ij}^{(2;1a)}(-\omega;\omega) = \sum_r \frac{\langle 0|\mu_i|r\rangle\langle r|\mu_j|0\rangle}{\left(\tilde{E}_r - E_0 + (q-1)\hbar\omega - q\hbar\omega\right)} = \sum_r \frac{\langle 0|\mu_i|r\rangle\langle r|\mu_j|0\rangle}{\left(\tilde{E}_r - E_0 - \hbar\omega\right)} \tag{75}$$

Proceeding to evaluate in a similar manner the contribution associated with the alternative time ordering (Fig. 5b, and the upper pathway in Fig. 6), and then adding the result to (75), we arrive at the following final expression

$$\alpha_{ij}^{(2)}(-\omega;\omega) = \sum_r \left\{ \frac{\langle 0|\mu_i|r\rangle\langle r|\mu_j|0\rangle}{\left(\tilde{E}_{r0} - \hbar\omega\right)} + \frac{\langle 0|\mu_j|r\rangle\langle r|\mu_i|0\rangle}{\left(\tilde{E}_{r0} + \hbar\omega\right)} \right\} \tag{76}$$

using the standard energy difference notation $\tilde{E}_r - E_0 = \tilde{E}_{r0}$.

As an aside, it is useful to obtain from the Eq. (76) a result for the mean polarizability, whose value is required by Eq. (23). If the transition molecular dipoles are real (as is the case for nondegenerate transitions, or as may be enforced by a suitable choice of degenerate basis set), and the molecular

environment is randomly oriented, an isotropic average can be employed, and the mean polarizability is then expressed as

$$\bar{\alpha}(-\omega;\omega) = \frac{1}{3}\sum_r \left\{ \frac{|\langle r|\boldsymbol{\mu}|0\rangle|^2}{\left(\tilde{E}_{r0} - \hbar\omega\right)} + \frac{|\langle r|\boldsymbol{\mu}|0\rangle|^2}{\left(\tilde{E}_{r0} + \hbar\omega\right)} \right\}$$

$$= \frac{2}{3}\sum_r |\langle r|\boldsymbol{\mu}|0\rangle|^2 \left\{ \frac{\tilde{E}_{r0}}{\tilde{E}_{r0}^2 - \hbar^2\omega^2} \right\} \tag{77}$$

By explicitly including the wavevector and branch index dependence of the radiation frequency, and unfolding the detail of the molecular state damping, we conclude that the mean polarizability as used in Eq. (23) is

$$\bar{\alpha}\left(\omega_k^{(m)}\right) = \frac{2}{3\hbar}\sum_r \left\{ \frac{|\langle r|\boldsymbol{\mu}|0\rangle|^2 (\Omega_{r0} - \frac{i}{2}\gamma_r)}{\left(\Omega_{r0} - \frac{i}{2}\gamma_r\right)^2 - \omega_k^{(m)^2}} \right\} \tag{78}$$

where by factorizing $\hbar$ from the expression, Ω_{r0} represents each molecular frequency defined as $\Omega_{r0} = \Omega_r - \Omega_0$. The imaginary elements in Eq. (78) arise from the substitution $\tilde{E}_r = E_r - \frac{1}{2}i\hbar\gamma_r$, to properly accommodate finite excited-state lifetimes as discussed in the next section. It is represented explicitly here to illustrate that through Eqs. (78) and (23), the refractive index has both real and imaginary parts. The complex nature of (23), on passing through a particular molecular frequency, is illustrated in Fig. 7.

A second example, with $m = 3$, illustrates the nonlinear molecular polarizability responsible for second-harmonic generation. Here each tensor numerator contains a product of three transition dipole moments. Reading off from the appropriate diagram, for example, using Fig. 2a, we obtain the numerator $\mu_i^{0s}\mu_j^{sr}\mu_k^{r0}$. Here we again assume that the molecule starts and finishes in its ground electronic state, and we have introduced the shorthand notation $\mu_i^{0s}\mu_j^{sr}\mu_k^{r0} \equiv \langle 0|\mu_i|s\rangle\langle s|\mu_j|r\rangle\langle r|\mu_k|0\rangle$. Each denominator is a product of factors, one for each intermediate state, in each of which again the energy of the initial state is subtracted from the (complex) intermediate state energy. In the case of Fig. 2a, we find that for the intermediate state $|s\rangle$, the difference in molecular energies is $\tilde{E}_{s0}\left(= \tilde{E}_s - \tilde{E}_0\right)$, and the difference in photon energies $-2\hbar\omega$, thus giving a factor of $\left(\tilde{E}_{s0} - 2\hbar\omega\right)$. For the intermediate state $|r\rangle$, the difference in molecular energies is $\tilde{E}_{r0}$ and the difference in photon energies $-\hbar\omega$, giving a factor of $\left(\tilde{E}_{r0} - \hbar\omega\right)$. Proceeding in a similar way from Figs. 2b and 2c and summing, we thus obtain the following complete expression for the frequency-

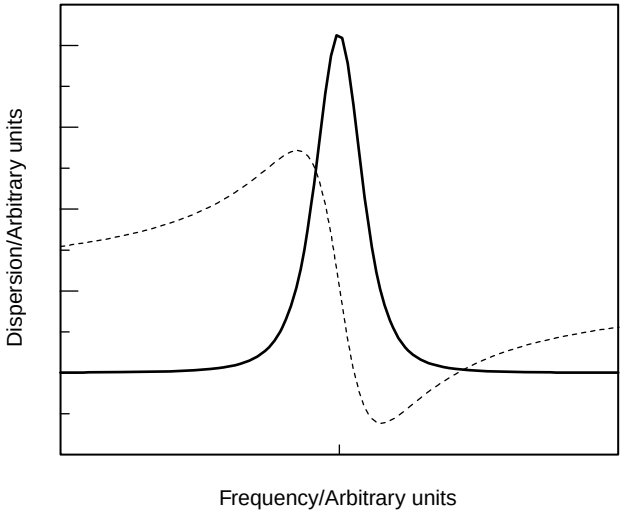

Figure 7. The dotted line (the real part of Eq. (23) utilizing Eq. (78) as the mean polarizability) illustrates the dispresion of the refractive index across an arbitrary molecular resonance. The solid line represents the imaginary part of the refractive index and only contributes close to the resonant frequency.

doubling molecular polarizability tensor (the molecular hyperpolarizability)

$$\beta_{ijk}(-2\omega;\omega,\omega) = \sum_s \sum_r \left[\frac{\mu_i^{0s}\mu_j^{sr}\mu_k^{r0}}{(\tilde{E}_{s0} - 2\hbar\omega)(\tilde{E}_{r0} - \hbar\omega)} + \frac{\mu_j^{0s}\mu_i^{sr}\mu_k^{r0}}{(\tilde{E}_{s0} + \hbar\omega)(\tilde{E}_{r0} - \hbar\omega)} + \frac{\mu_j^{0s}\mu_k^{sr}\mu_i^{r0}}{(\tilde{E}_{s0} + \hbar\omega)(\tilde{E}_{r0} + 2\hbar\omega)} \right] \tag{79}$$

where we have used the common nomenclature to represent the leading order of nonlinear molecular response, specifically, $\boldsymbol{\beta}(-2\omega;\omega,\omega) \equiv \boldsymbol{\alpha}^{(3)}(-2\omega;\omega,\omega)$.

A few further general remarks are in order at this stage. One is to note the fact that the sum over intermediate molecular states, as in Eqs. (76) and (79), in principle applies not only to electronic but also to vibrational levels. Although this issue initially received most attention in connection with molecular hyperpolarizabilities [44], it applies equally to other optical response tensors. The vibrational contributions, which were previously largely overlooked, have now been extensively studied and shown to be important in many applications [45,46]. Second, the polarizabilities associated with nonlinear parametric processes may in most circumstances be regarded as properties of the ground-state molecule, since it is the molecular ground state that usually constitutes the

initial and final molecular levels. Certainly it can be anticipated that under normal conditions the majority of conversion events will be mediated by ground (usually S_0) electronic state molecules, simply because of the overwhelming population of such molecules compared to those in excited states. However, other states may play the role of the initial/final state, and their corresponding polarizabilities can be evaluated in the same way. In fact, it transpires that the polarizabilities associated with electronic excited states can exceed those associated with the ground state by orders of magnitude, as has been shown both in theory and experiment [47–49]. Thus, if the appropriate excited state is optically pumped so as to provide a significant population of molecules, the observed polarizability characteristics of the medium can be significantly enhanced, or diminished. This is an important fact that we shall return to when discussing optically induced harmonic generation in more detail.

X. DAMPING

The issue of correctly signing the damping of energy denominators in optical response tensors has been the subject of much recent debate [see, e.g., Refs. 50–52]. This stems partly from a common confusion in the literature between two entirely different forms of damping; it also reflects attempts to impose conflicting conditions on the molecular response. The former obscurity is very easily dealt with, though; as will be shown below, it forms the ground in which seeds of the latter conflict have been sown.

First, the emergence of photon (more accurately, bath quantum, polariton) energies in the denominators of expressions such as Eqs. (76) and (79) originated in the development of the signal amplitude from Eq. (36). In the evaluation of the underlying contour integrals invoked at that stage, imaginary infinitesimals are commonly added to the photon energies to displace the poles from the real axis. Each photon energy thereby acquires an infinitesimal addendum, $\hbar\omega \to \hbar\omega + is$, with $s \to +0$. In the polarizability equation (76), for example, this modification introduces addenda of $-is$ and $+is$, respectively, to the two energy denominators—a prescription that also allows the tensor to retain the property of hermiticity. It has to be emphasized, nonetheless, that the result has no meaning other than in the specific case of the limit $s \to +0$.

The second type of resonance modification to energy denominators, alluded to earlier, is designed to reflect the finite lifetime of each molecular energy level, phenomenologically implemented by a modification of the corresponding energy

$$\tilde{E}_r = E_r \pm \frac{1}{2} i\hbar\gamma_r \tag{80}$$

where γ_r may be considered a sum of the inverse lifetimes associated with each line-broadening mechanism, and representing the *FWHM* (full width at

half-maximum) linewidth of the nonlinear response near resonance. Only the ground state is undamped, since its lifetime is taken as infinite. Using the positive sign in equation (80) results in the time dependence of each molecular state $|r\rangle$ acquiring within its phase factor $e^{-i\bar{E}_r t/\hbar}$ an exponential decay component. More significantly, the choice of the positive sign for the damping proves to be uniformly consistent with time-reversal symmetry, as will be discussed in more detail below. The result of implementing this correction in the polarizability equation (76), for example, is the addition of $+\frac{1}{2}i\hbar\gamma_r$ to each energy denominator, the sign the same in each term. In nonresonant processes, $\hbar\gamma_r$ is typically several orders of magnitude smaller than E_r, and its precise value is determined by the nature of the molecule and the local structure of the bulk phase. Near to resonance, the damping serves to give a realistic lineshape to the optical response. For example, in light scattering close to an optical absorption band where $\hbar\omega \approx E_{r0}$, the first term of Eq. (76) dominates and the corresponding rate acquires a Lorentzian lineshape. Resonance features play a particularly prominent role in the case of many large organic structures, whose ultrafast excited-state decay mechanisms produce damping factors on the terahertz scale. Detailed consideration of lineshape is also necessary in order to properly accommodate the dispersion behavior featured in the realization of wavevector matching for parametric processes.

Historically two conventions have been used extensively in the literature for setting the signs of the phenomenological damping factors. Although mutually incompatible, justifications for each convention have been made by appeal to causality—a different line generally being taken in the semiclassical and fully quantum-mechanical approaches to the interacting system of molecules and radiation. In earlier work [1] this issue was unresolved and the prevailing convention (variable signing, discussed in the following paragraphs) was adopted. Now it is clear that constant signing is correct; an example is instructive. The two conventions with respect to second-harmonic generation are as follows; in the semiclassical or variable-sign convention (vsc) the signs are chosen oppositely for interactions preceding and following in time the emission of the harmonic photon, as follows [53–55]:

$$\begin{aligned}\beta_{ijk}^{vsc}(-2\omega;\omega,\omega) = \sum_s \sum_r \Bigg[& \frac{\mu_i^{0s}\mu_j^{sr}\mu_k^{r0}}{(E_{s0} - 2\hbar\omega - \frac{1}{2}i\hbar\gamma_s)(E_{r0} - \hbar\omega - \frac{1}{2}i\hbar\gamma_r)} \\ & + \frac{\mu_j^{0s}\mu_i^{sr}\mu_k^{r0}}{(E_{s0} + \hbar\omega + \frac{1}{2}i\hbar\gamma_s)(E_{r0} - \hbar\omega - \frac{1}{2}i\hbar\gamma_r)} \\ & + \frac{\mu_j^{0s}\mu_k^{sr}\mu_i^{r0}}{(E_{s0} + \hbar\omega + \frac{1}{2}i\hbar\gamma_s)(E_{r0} + 2\hbar\omega + \frac{1}{2}i\hbar\gamma_r)} \Bigg]\end{aligned} \tag{81}$$

In the fully quantum-mechanical development [constant-sign convention, (csc)], as adopted in most of the literature on Raman scattering, all the signs of the damping are identical:

$$\beta_{ijk}^{\mathrm{csc}}(-2\omega;\omega,\omega) = \sum_s \sum_r \left[\frac{\mu_i^{0s}\mu_j^{sr}\mu_k^{r0}}{(E_{s0} - 2\hbar\omega - \frac{1}{2}i\hbar\gamma_s)(E_{r0} - \hbar\omega - \frac{1}{2}i\hbar\gamma_r)} + \frac{\mu_j^{0s}\mu_i^{sr}\mu_k^{r0}}{(E_{s0} + \hbar\omega - \frac{1}{2}i\hbar\gamma_s)(E_{r0} - \hbar\omega - \frac{1}{2}i\hbar\gamma_r)} + \frac{\mu_j^{0s}\mu_k^{sr}\mu_i^{r0}}{(E_{s0} + \hbar\omega - \frac{1}{2}i\hbar\gamma_s)(E_{r0} + 2\hbar\omega - \frac{1}{2}i\hbar\gamma_r)} \right] \tag{82}$$

The latter result (82) yields a quantum probability amplitude that, under Hermitian conjugation and time reversal, correctly equates to the corresponding amplitude for the time-inverse process of degenerate downconversion. To see this, we note that the matrix element for SHG invokes the tensor product $\beta_{ijk}(-2\omega;\omega,\omega)\rho_{i(jk)}$, where the brackets embracing two of the subscripts (jk) in the radiation tensor denote index symmetry, reflecting the equivalence of the two input photons. As shown previously [1], this allows the tensor product to be written without loss of generality as $\beta_{i(jk)}(-2\omega;\omega,\omega)\rho_{i(jk)}$, entailing an index-symmetrized form of the molecular response tensor,

$$\beta_{i(jk)}(-2\omega;\omega,\omega) = \frac{1}{2}\{\beta_{ijk}(-2\omega;\omega,\omega) + \beta_{ikj}(-2\omega;\omega,\omega)\} \tag{83}$$

Each of the six terms of the hyperpolarizability tensor so formed transforms into one of the six counterpart terms in $\beta_{i(jk)}(2\omega,-\omega,-\omega)$, the tensor for degenerate downconversion, on performing the combined operations of Hermitian conjugation and time reversal (the radiation tensor for downconversion is also obtained by performing the same procedure on $\rho_{i(jk)}$). For example, the last term of $\beta_{i(jk)}(-2\omega;\omega,\omega)$, in the order that logically follows from Eqs. (82) and (83), behaves as follows:

$$\frac{\mu_k^{0s}\mu_j^{sr}\mu_i^{r0}}{(E_{s0} + \hbar\omega - \frac{1}{2}i\hbar\gamma_s)(E_{r0} + 2\hbar\omega - \frac{1}{2}i\hbar\gamma_r)}$$

$$\xrightarrow{HT} \frac{\mu_i^{0r}\mu_j^{rs}\mu_k^{s0}}{(E_{s0} + \hbar\omega - \frac{1}{2}i\hbar\gamma_s)(E_{r0} + 2\hbar\omega - \frac{1}{2}i\hbar\gamma_r)}$$

and on interchanging the dummy state sum indices r and s, the result is exactly the first term of $\beta_{ijk}(2\omega;-\omega,-\omega)$ as follows from the form given by (82). The

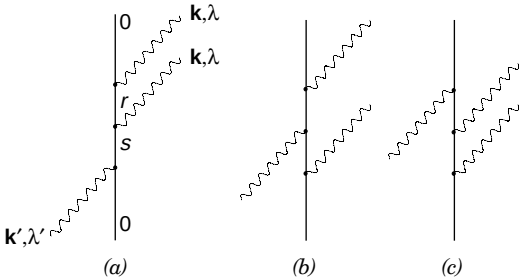

Figure 8. The three time-ordered diagrams for degenerate down-conversion, representing exact time reversal of the SHG orderings illustrated in Fig. 2. Consequently the emitted photons now carry the wave vector and polarization labels, **k** and λ, and the annihilated photon is characterized by $\mathbf{k}'$, λ'.

time reversal represented above is depicted in the time-ordered diagrams of Fig. 8. The two-step operation of *HT* is given above to clarify the action of the two operators, although it introduces assumptions that the indices relate to contractions with real polarization vectors and that the molecular states are all nondegenerate and time-even, consistent with spin-paired molecular orbitals. However, the combined operation is not subject to these conditions, so that the end result holds in general [11,24,50].

The variable-sign result Eq. (81) produces results that fail to satisfy such time-reversal symmetry, as shown by Andrews et al. [50]. The requirement for temporal symmetry remains unequivocal, despite the violation of time-reversal invariance by the system itself (its engagement of molecular interaction with the bath leading to state decay), specifically because of the inclusion of damping. The two conventions agree in ostensibly the most crucial signing, that which relates to potentially resonant denominator terms; they differ in "antiresonant" terms. Nonetheless, in certain processes they can lead to results with experimentally very significant differences.

The origin of confusion surrounding the correct form of damping is readily identified on comparison of Eqs. (81) and (82). In the latter, consistent signing is associated with the consistently positive signs of the energies E_{s0} and E_{r0}; in the former, the signing appears consistent with the variable signs of the photon energies $\hbar\omega$, $2\hbar\omega$. Thus, if the imaginary infinitesimals discussed earlier are directly substituted by physically meaningful and finite damping constants, spurious results conforming to the variable-sign rule emerge. Those results satisfy the Hermitian property of reciprocity, but that is not a principle of universal application [56]. Any prescription with variable assignment of signs can also introduce significant ambiguities in connection with processes entailing two or more outgoing waves, as, for example, in four-wave mixing.

The variable-sign convention would also logically lead to a secondary rule, that where static fields appear in electro- or magneto-optical processes, the interactions with which they are associated should carry no damping. However, from a quantum field theoretic viewpoint, static perturbations must induce damping [52]. All electromagnetic interactions are fundamentally mediated through the exchange of virtual photons (the gauge bosons). A static field involved in an electro-optical process in any given molecule is mediated in the same way. It owes its origin to the coupling between the charges within that molecule and those constituting the source of the static field. This coupling is expressed through the accommodation of interactions with virtual photons from modes of an infinite range, as with any electrodynamic interaction, and summation over the virtual photon wavevectors and polarizations thereby ensures a result that properly reflects the conservation of energy. Consequently, the case of a static field is no different in type from a time-varying field—except that, while causality is, of course, satisfied, explicit retardation features disappear. Hence the damping associated with any molecular excited state must be subject to damping, irrespective of the frequency of the electric field responsible for the perturbation. Damping factors are not frequency-dependent; each excited state has a damping of a characteristic magnitude, irrespective of the frequency of the perturbation with which it is associated. In this connection it has been shown that the correct constant-signing rule is necessary to uphold the principle that linear electro-optical response cannot occur in an isotropic liquid, whether chiral or not [57].

In general, detailed consideration of damping is especially important when operating near to resonance, which in general occurs when there exists a molecular state differing in energy from the initial state by an amount approaching the energy of one or more of the photons involved. For coherent parametric processes the need to operate in regions of dispersion, in order to satisfy wavevector matching conditions, is a well-known experimental technique. Operating in such frequency regions necessitates adoption of the polariton (rather than vacuum photon) formulation, as described in Section III. Inspection of the dispersion curves in Fig. 1, considering for simplicity case (a) with just one molecular frequency, clearly illustrates three areas of interest: (1) the diagonal curve segments represent photon-like radiation propagating through the media at transparent frequencies, (2) the horizontal regions exhibit exciton-like molecular resonances (photons impinging on the medium at such frequencies are readily absorbed into the molecular bulk), and (3) level-crossing areas signify a dispersive mixing of the molecular and radiation states. It is these latter regions in which it is commonly necessary to operate. Thus, depending on whether the radiation frequency is sufficiently above or below a particular molecular resonance will determine the branch index that is appropriate.

XI. INDEX SYMMETRY AND MOLECULAR STRUCTURE

A number of symmetry factors of quite distinct origins play a significant role in determining the nullity or nonnullity of the various components of any molecular optical response tensor (3^n components in the case of dipole coupling). Equally, symmetry considerations determine the number of linearly independent components. In second-harmonic generation, for example, the symmetrized tensor components must satisfy identities such as $\beta_{z(xy)} = \beta_{z(yx)}$, regardless of whether the molecule possesses the three- or higher-fold axis of symmetry necessary to confer degeneracy on the x and y axes. Consequently, of the $3^3 = 27$ tensor components, only 18 are independent. In general, for n-harmonic processes, the rigorously index-symmetric polarizability tensor has only $3(n+1)(n+2)/2$ independent components. The inherent structural symmetry of most molecules generally reduces this number still further.

It is most important to note that in many cases of harmonic emission, a more completely index-symmetric form of the polarizability tensor is implicated. Consider once again the prototypical example of optical nonlinearity afforded by harmonic generation. When any harmonic is generated from a plane-polarized beam, in an isotropic medium, it produces photons with the same polarization vector as the incident light. In such a case the radiation tensor ρ_{ijk} becomes fully index-symmetric, and arguments similar to those given above show that only the fully index-symmetric part of the hyperpolarizability tensor, $\beta_{ijk}(-2\omega;\omega,\omega)$, can be involved. This does not mean that the tensor itself is inherently fully index-symmetric, but it does mean that experiments of the kind described cannot determine the extent of any index antisymmetry.

This leads us to the issue of approximate index symmetry. Any nonlinear optical process involving only static (zero-frequency) fields is correctly described in terms of a classical response tensor, which is always fully index-symmetric. When optical frequencies are involved, the differences between the energy denominators of the various terms in the tensor remove this symmetry. The only exception, albeit an important one, is the linear polarizability. Since this entails the product of two transition moments connecting the same pair of states, permutational index symmetry is guaranteed. If, however, the photon frequencies all fall substantially below any electronic transition frequencies of the material, all energy denominators become approximately equal, ($\tilde{E}_{s0} \approx \tilde{E}_{r0}$ in the case of frequency doubling), and the tensor becomes in effect fully index-symmetric. Under such conditions the polarizability tensor for an n-harmonic process has only $(n+2)(n+3)/2$ independent components, for example, 10 in the case of frequency doubling. Index symmetry based on the assumption that such an approximation is valid, normally referred to as *Kleinman symmetry* [58] is nonetheless unjustified in a great many applications [43,59].

We now establish on the basis of physical symmetry the conditions for the existence of the m-photon optical response tensor $\boldsymbol{\alpha}^{(m)}$. For any parametric process, the initial and final molecular states are identical and normally carry the full ground-state symmetry of the molecule (or, in the case of a crystalline solid, that of the unit cell). Thus, since each term in the explicit expression (74) contains a product of m transition moments, the tensor can be nonvanishing only if the totally symmetric representation of the appropriate point group or space group is spanned by the product of $(n+1)$ translations (in the case of electric dipole, E1, coupling). The origin of this condition can be traced back to Eq. (41). Where the molecule or crystal possesses a center of symmetry, the symmetry condition can be met only in the generation of odd harmonics, where m is even and the product of translations is thus of *gerade* (even) symmetry. For the same reason free atoms cannot support the production of even harmonics, except under special conditions that effectively disrupt atomic symmetry.

Much more detailed symmetry information follows by considering the explicit group-theoretic basis. In general, the independent components of the response tensor form a basis for a reducible representation of the appropriate molecular or crystallographic group; the reduction of this representation into irreducible parts leads to results such as those given in Table I, in which $D^{(jp)}$ stands for the irreducible representation of weight j and parity p. In this table, based on the transformation properties associated the normal E1 coupling, the second-harmonic polarizability $\boldsymbol{\beta}(-2\omega;\omega,\omega)$ is represented as $\boldsymbol{\beta}^{\mathrm{SHG}}$ and the third-harmonic as $\boldsymbol{\gamma}^{\mathrm{THG}} \equiv \boldsymbol{\gamma}(-3\omega;\omega,\omega,\omega)$, although in each case it should be borne in mind that the same molecular tensors are involved in both coherent and incoherent harmonic processes. The first entry for each tensor gives the reduction based on consideration of only the index symmetry inherent in the interaction, as, for example, is denoted by the brackets around the subscripts in $\beta^{\mathrm{SHG}}_{i(jk)}$: the second entries give the results that apply under Kleinman assumption of full index symmetry, such as $\beta^{\mathrm{SHG}}_{(ijk)}$. In each case the entry in the final column gives r, the number of independent tensor components. This may be regarded as

TABLE I
Group-Theoretic Representations and Number of Components r of Second- and Third-Harmonic Polarizabilities

Coupling	Tensor	Representation	r
E1(E1^2)	$\beta^{\mathrm{SHG}}_{i(jk)}$	$2D^{(1-)} \oplus D^{(2-)} \oplus D^{(3-)}$	18
(E1^3)	$\beta^{\mathrm{SHG}}_{(ijk)}$	$D^{(1-)} \oplus D^{(3-)}$	10
E1(E1^3)	$\gamma^{\mathrm{THG}}_{i(jkl)}$	$D^{(0+)} \oplus D^{(1+)} \oplus 2D^{(2+)} \oplus D^{(3+)} \oplus D^{(4+)}$	30
(E1^4)	$\gamma^{\mathrm{THG}}_{(ijkl)}$	$D^{(0+)} \oplus D^{(2+)} \oplus D^{(4+)}$	15

a maximum, applicable to molecules totally lacking any intrinsic symmetry; any molecule with a twofold or higher axis of symmetry will inevitably manifest other relationships between its tensor components which will further reduce the number of independent parameters.

Any parametric nonlinear polarizability can be supported by a given molecule or crystal only as long as the totally symmetric representation of the corresponding point or space group is spanned by some components of the tensor. This remains true even for the parametric polarizabilities associated with molecular excited states; provided they are nondegenerate, the product of the initial and final state representations will generate the totally symmetric representation. In the very rare cases where the polarizability properties of molecules in degenerate excited states are required, the theory can be extended in an obvious way. Since components that transform under $D^{(0+)}$ invariably span the totally symmetric representation, it is immediately apparent from Table I that, on the basis of molecular symmetry, third-harmonic processes are universally allowed. Indeed, this is true for all odd harmonics; it is because the corresponding polarizabilities invariably carry components of $D^{(0+)}$ symmetry.

By contrast in the case of SHG, for example, only those species whose totally symmetric representation is spanned by $D^{(1-)}$, $D^{(2-)}$, or $D^{(3-)}$ components can support the hyperpolarizability tensor $\boldsymbol{\beta}^{SHG}$, and this excludes all centrosymmetric species. More interestingly, the condition is satisfied by all polar species, since these necessarily have $D^{(1-)}$ components transforming under the totally symmetric representation. In fact, among the common nonpolar molecular point groups, only the following permit a nonzero hyperpolarizability, by virtue of having $D^{(2-)}$ and/or $D^{(3-)}$ components transforming under their totally symmetric representation: S_4; C_{3h}; D_2; D_3; D_4; D_6; D_{3h}; D_{2d}; T; T_d [60]. If Kleinman symmetry is assumed, the hyperpolarizability tensor carries only $D^{(1-)}$ and $D^{(3-)}$ components: in this case the SHG potential of species with D_4 or D_6 symmetry, which have only $D^{(2-)}$ components, is not apparent.

Although index symmetry places constraints on the maximum number of independent elements for any given nonlinear susceptibility, that number is generally reduced to a significant degree by virtue of molecule, crystal, or site symmetry, where present. Two features are responsible for this; one is the fact that symmetry will generally dictate that certain tensor components are necessarily zero. For example, in any species with a mirror plane perpendicular to the z axis $\beta^{\mathrm{SHG}}_{z(zz)}$, must be zero since it has to equal its own negative. Second, structural symmetry will usually forge relationships between different components. For example, in species with a threefold axis of proper rotational symmetry, $\beta^{\mathrm{SHG}}_{x(xx)}$ has to equal minus $\beta^{\mathrm{SHG}}_{x(yy)}$. The explanation is that the product $x(x^2 + y^2)$ does not transform under the totally symmetric representation, and hence the linear combination $(\beta^{\mathrm{SHG}}_{x(xx)} + \beta^{\mathrm{SHG}}_{x(yy)})$ must be zero. For such reasons the

18 tensor components associated with SHG generally reduces to a far smaller number; in the extreme case of species with tetrahedral symmetry, there is in fact only one independent component (*xyz*).

Where local symmetry permits harmonic generation based exclusively on electric dipole coupling, the inclusion of higher-order multipolar contributions in the exact coupling equation (13) produces additional terms that are normally negligible. If electric dipole harmonic generation is forbidden, which, as we have seen, is the case for even harmonics in a centrosymmetric species, these higher-order terms can nonetheless become significant and may operate to effect weak harmonic emission. The exception is the case of an isotropic fluid, where global symmetry precludes the involvement of any higher multipoles in second-harmonic emission within the bulk [61–63]. Work by Cao and Zhu [64] has shown how the multipolar generation of a second harmonic signal in such systems necessitates the presence of a surface, from which the harmonic can emerge as a reflected beam. In other systems lacking full rotational symmetry, the higher multipoles can also be important. For example, if any one of the three *ungerade* electric dipole (E1) interactions involved in second-harmonic generation is replaced by a *gerade* electric quadrupole (E2) interaction, the operator product generates a $D^{(0+)}$ contribution as shown in Table II. Since this invariably spans the totally symmetric representation, the corresponding response tensor is nonzero even in centrosymmetric materials. In the first row of Table II the coupling E1(E1E2) refers to the polarizability associated with one electric dipole and one electric quadrupole annihilation of a pump photon, with electric dipole emission of the harmonic. The labeling E2(E1^2) in the second row relates to electric dipole annihilation of both pump photons and electric quadrupolar harmonic emission. In the third row the coupling (E1^{2}E2) can refer to either case, but the corresponding representation applies only under

TABLE II
Representations and Number of Components r of Leading Higher-Order Multipole Second-Harmonic Polarizabilities

Coupling	Tensor	Representation	r
E1(E1E2)	$\tilde{\beta}^{\mathrm{SHG}}_{i(jk)l}$	$D^{(0+)} \oplus 2D^{(1+)} \oplus 3D^{(2+)} \oplus 2D^{(3+)} \oplus D^{(4+)}$	45
E2(E1^2)	$\tilde{\beta}^{\mathrm{SHG}}_{(ij)(lk)}$	$D^{(0+)} \oplus D^{(1+)} \oplus 2D^{(2+)} \oplus D^{(3+)} \oplus D^{(4+)}$	30
(E1^{2}E2)	$\tilde{\beta}^{\mathrm{SHG}}_{(ijkl)}$	$D^{(0+)} \oplus D^{(2+)} \oplus D^{(4+)}$	15
E1(E1M1)	$\beta^{\mathrm{SHG}}_{ijk}$	$D^{(0+)} \oplus 3D^{(1+)} \oplus 2D^{(2+)} \oplus D^{(3+)}$	27
M1(E1^2)	$\beta^{\mathrm{SHG}}_{i(jk)}$	$2D^{(1+)} \oplus D^{(2+)} \oplus D^{(3+)}$	18
(E1^{2}M1)	$\beta^{\mathrm{SHG}}_{(ijk)}$	$D^{(1+)} \oplus D^{(3+)}$	10

the assumption of Kleinman index symmetry. Similar remarks apply if one of the electric dipole couplings is alternatively replaced by a gerade magnetic dipole (M1) interaction, though in this case the $D^{(0+)}$ representation arises only where the magnetic interaction is involved in the annihilation of a pump photon. Moreover, the $D^{(0+)}$ feature is not apparent if Kleinman symmetry is assumed.

XII. TWO-LEVEL SYSTEMS

From the results in the last section it is clear that for particular applied radiative frequencies or frequency multiples, close to resonance with particular molecular states, each molecular tensor will be dominated by certain terms in the summation of states as a result of their diminished denominators—a principle that also applies to all other multiphoton interactions. This invites the possibility of excluding, in the sum over molecular states, certain states that much less significantly contribute. Then it is expedient to replace the infinite sum over all molecular states by a sum over a finite set—this is the technique employed by computational molecular modelers, their results often producing excellent theoretical data. In the pursuit of analytical results for near-resonance behavior, it is often defensible to further limit the sum over states and consider just the ground and one electronically excited state. Indeed, the literature is replete with calculations based on two-level approximations to simplify the optical properties of complex molecular systems. On the other hand, the coherence features that arise through adoption of the celebrated Bloch equations are limited to exact two-level systems and are rarely applicable to the optical response of complex molecular media.

In the case of a single resonance, optical harmonic conversion is driven largely by transitions involving just the ground and resonant levels, so that the kinetics of the process approximates that of a two-level system. Indeed, in the realm of resonant multiphoton phenomena the two-level approximation is peculiarly appropriate for harmonic emission, whereas most nonparametric processes such as multiphoton absorption require three or more levels for their adequate representation. Consider once again, for example, the case of frequency doubling, where resonance amplification can occur at either the pump or the harmonic frequency. To begin, it is useful to separate the molecular tensor into a sum of two parts, in the first of which both the summations over intermediate states $|r\rangle$ and $|s\rangle$ are restricted to the ground level $|0\rangle$ and a resonant level $|u\rangle$; in the second, all other possibilities are accounted for. Hence we can write

$$\beta_{ijk}(-2\omega;\omega,\omega) = \beta_{ijk}^{\mathrm{TLA}}(-2\omega;\omega,\omega) + \beta_{ijk}^{\mathrm{others}}(-2\omega;\omega,\omega) \tag{84}$$

where the superscript "TLA" denotes the two-level approximation. It is to be noted at the outset that the $\boldsymbol{\beta}^{\text{others}}$ term does not completely exclude the states $|0\rangle$ and $|u\rangle$ from every intermediate state summation; for example, it accommodates contributions associated with $|r\rangle = |u\rangle$, $|s\rangle \neq \{|0\rangle, |u\rangle\}$.

Focusing first on the dominant two-level term [65], careful analysis of the tensor structure, with respect to the proper signs for the damping corrections and utilizing the freedom to add a j,k index-antisymmetric term (see later), yields the following result [59,66]:

$$\beta_{ijk}^{\text{TLA}}(-2\omega;\omega,\omega) = \left[\frac{\mu_i^{0u}\mu_j^{0u}\breve{d}_k}{(E_{u0}-2\hbar\omega-i\Gamma_u)(E_{u0}-\hbar\omega-i\Gamma_u)} + \frac{\mu_j^{0u}\breve{d}_j\mu_k^{0u}}{(E_{u0}+\hbar\omega-i\Gamma_u)(E_{u0}-\hbar\omega-i\Gamma_u)} + \frac{\breve{d}_j\mu_k^{0u}\mu_i^{0u}}{(E_{u0}+\hbar\omega-i\Gamma_u)(E_{u0}+2\hbar\omega-i\Gamma_u)}\right] \tag{85}$$

assuming only that the electric dipole transition moments are real, and for conciseness introducing the shorthand notation $\Gamma_u = \frac{1}{2}\hbar\gamma_u$. Where only diagonal components arise, as, for example, may apply for harmonic generation within a regular solid, the tensor product $\boldsymbol{\beta}^{TLA}\cdot\boldsymbol{\sigma}$ featured in the rate equation (51) reduces to a simpler structure first identified by Oudar and Chemla [67]. Both in its simpler form, and in the general expression Eq. (85), the most significant feature is the appearance in each term of the vector parameter $\breve{\mathbf{d}}$, defined by

$$\breve{\mathbf{d}} = \boldsymbol{\mu}^{uu} - \boldsymbol{\mu}^{00} \tag{86}$$

specifically, the difference between the static electric dipole moments of the resonant and ground states. Hence the two-level hyperpolarizability displays a linear dependence on the magnitude of $\breve{\mathbf{d}}$, which, for example, in extensively conjugated molecules can reasonably be assumed proportional to the length of the conjugation chain [67].

It is important to have included the ground state of the molecule in the sums over intermediate states for the dependence on $\breve{\mathbf{d}}$ to be recovered, and this proves significant for two reasons: (1) the result Eq. (85) shows that the two-level hyperpolarizability can be supported only by molecules with permanent ground- or excited-state dipoles, which means polar molecules; and (2) it is clear that there is considerable scope for the two-level response to be enhanced in polar molecules having a resonant excited state whose equilibrium geometry is appreciably different from that of the ground state, or in species exhibiting the characteristically strong absorption associated with a charge-transfer transition.

Similar features arise in the theory of multiphoton absorption [68–70] and also single-photon cooperative absorption [71,72]. In connection with second-harmonic generation, the result has added significance since most species that can support $\boldsymbol{\beta}(-2\omega;\omega,\omega)$, and thereby have the potential for frequency doubling, are, indeed, polar (see previous section).

Let us now consider more specifically the case of a medium possessing an excited state $|u\rangle$ close in energy to that of the emitted harmonic, $2\hbar\omega$. For practical application, this condition is generally more useful than resonance at the fundamental frequency, since the latter condition is likely to result in a substantial loss of pump power through conventional single-photon absorption. In view of its denominator structure, it is clearly the first term in Eq. (85) that will provide the major contribution to the nonlinear response tensor

$$\beta_{ijk}^{\mathrm{TLA}} \approx \frac{\mu_i^{0u}\mu_j^{0u}\breve{d}_k}{(\hbar\Delta\omega - i\Gamma_u)(\hbar\omega + \hbar\Delta\omega - i\Gamma_u)} \tag{87}$$

where $\Delta\omega$ represents the detuning from resonance: both the first and second terms of Eq. (85) dominate in the case of resonance at the fundamental frequency. If the molecule has no dipole and possesses a center of symmetry, it is well known that the all hyperpolarizability tensor components are null and no second-harmonic generation is possible. However, if only $\breve{\mathbf{d}}$ vanishes, as in the case of a tetrahedrally symmetric molecule, then only the two-level contribution to the tensor, $\boldsymbol{\beta}^{\mathrm{TLA}}(-2\omega;\omega,\omega)$, disappears. The remaining contribution $\boldsymbol{\beta}^{other}(-2\omega;\omega,\omega)$, as defined by Eq. (84), persists and is itself dominated by a term with essentially the same denominator structure as Eq. (87); specifically, the product of a near-resonant and an off-resonant term. For the general structure that then emerges, the reader is referred to Andrews [1].

It has been established in a series of works that a transformation of the electric dipole interaction is valid for deriving the optical characteristics of molecular systems with a response dominated by two electronic states [68–70; 73–77]. This procedure relates to the employment of a *fluctuation* dipole operator [78,79] as given by

$$H'_{\mathrm{int}} = -\varepsilon_0^{-1}[\boldsymbol{\mu} - \boldsymbol{\mu}^{00}] \cdot \mathbf{d}^{\perp} \tag{88}$$

in which the subtracted moment is the permanent dipole of the initial molecular state—usually the ground state. It has been proved how utilizing Eq. (88) for the form of the interaction operator leads to a new and expedient algorithm for the calculation of the requisite nonlinear optical polarizabilities [80], based on a novel interpretation of the appropriate time-ordered diagrams. In establishing the form for probability amplitudes of systems driven primarily by interactions

between the ground state $|0\rangle$, and one other higher electronic state $|u\rangle$, it proves legitimate and expedient simply to recast the permanent moments, where they arise as follows

$$\boldsymbol{\mu}^{uu} \to \boldsymbol{\mu}^{uu} - \boldsymbol{\mu}^{00} = \breve{\mathbf{d}}; \qquad \boldsymbol{\mu}^{00} \to 0 \tag{89}$$

while leaving any transition dipoles $(\boldsymbol{\mu}^{u0}, \boldsymbol{\mu}^{0u})$ unchanged. When the various time orderings for any optical processes of interest are drawn up, application of this rule enables expressions involving any connected route that entails the ground-state dipole $\boldsymbol{\mu}^{00}$ to be discarded, so long as those entailing the excited state dipole $\boldsymbol{\mu}^{uu}$ are re-interpreted to invoke $\breve{\mathbf{d}}$. This is the algorithm whose illustrative applications are described below. The method has been explicitly validated for all parametric and nonparametric processes, both degenerate and fully nondegenerate [80] and can be shown to correspond to a canonical transformation on the interaction Hamiltonian [14a,b; 81]. In every case its implementation leads in a matter of lines to results identical to those previously established by substantially more laborious means [66,69,70]. It may also be noted that the fluctuation dipole results are exact, when the correct constant-sign convention is used for damping; when variable signing is employed, the result is approximate only [66].

As an example, we again derive the two-level second harmonic tensor, this time using the algorithm outlined by Eq. (89). The three time-ordered diagrams as illustrated in Fig. 2a–c are once more employed. The route of molecular states between the initial (ground) state and the final (also ground) state runs through two virtual states, $|r\rangle$ and $|s\rangle$, and in the two-level approximation each of these is summed to represent one of two possibilities, either the ground state $|0\rangle$ or the excited state $|u\rangle$. The $(|0\rangle \leftarrow |s\rangle \leftarrow |r\rangle \leftarrow |0\rangle)$ sequences that arise are thus concisely expressible as 0000, 00u0, 0u00, 0uu0, corresponding to the dipole products $\boldsymbol{\mu}^{00}\boldsymbol{\mu}^{00}\boldsymbol{\mu}^{00}, \boldsymbol{\mu}^{00}\boldsymbol{\mu}^{0u}\boldsymbol{\mu}^{u0}, \boldsymbol{\mu}^{0u}\boldsymbol{\mu}^{u0}\boldsymbol{\mu}^{00}, \boldsymbol{\mu}^{0u}\boldsymbol{\mu}^{uu}\boldsymbol{\mu}^{u0}$, respectively. From the three time orderings we therefore have $3 \times 2^2 = 12$ contributions—each a product of three 'transition' dipoles (one or more of which may be permanent), divided by a product of two energy factors. Application of the algorithm determines that only the state sequence 0uu0 $(\boldsymbol{\mu}^{0u}\boldsymbol{\mu}^{uu}\boldsymbol{\mu}^{u0})$ need be considered in a suitable reinterpretation of the three time-ordered diagrams, since each of the other possibilities generates a $\boldsymbol{\mu}^{00}$ segment. Utilizing Fig. 2, we therefore obtain a two-level hyperpolarizability tensor exactly as expressed by Eq. (85). This is the simplest example of how the algorithm quickly generates results that would otherwise demand considerable algebraic manipulation. However, it is with higher-order amplitudes that the method is most obviously efficacious. Even in (85), the tensor structure obviates simple factorization in terms of $\breve{\mathbf{d}}$; higher orders have the additional complication that terms both linear and in powers of $\breve{\mathbf{d}}$ arise.

The process of third-harmonic generation (THG) serves both to illustrate the power of the new algorithm and to draw out some new physics. To derive the form of the susceptibility tensor, one needs to employ either the four time-ordered diagrams or the equivalent state-sequence diagram representing THG. Both diagrammatic representations are illustrated in Fig. 9. The state route connecting the initial and final (ground) states here runs through three virtual states, r, s, and t, and the two-level approximation requires each to be either the ground or the excited state. In this case, from the four time orderings we get a total of $4 \times 2^3 = 32$ contributions, each a product of four transition or permanent dipoles divided by three energy quotients. With the benefit of the algorithmic method delineated above, we can take the four time orderings and dispense with all except two of the following state sequences: 00000, 000u0, 00u00, 00uu0, 0u000, 0u0u0, 0uu00, 0uuu0. Specifically, discarding each sequence that includes the segment 00, we retain only 0u0u0 and 0uuu0. With proper reinterpretation of these remaining cases, we thus immediately obtain the following explicit result comprising only eight terms, of which each successive pair results from the successive time-ordered diagrams of Fig. 9a, also corresponding to all routes through the state-sequence

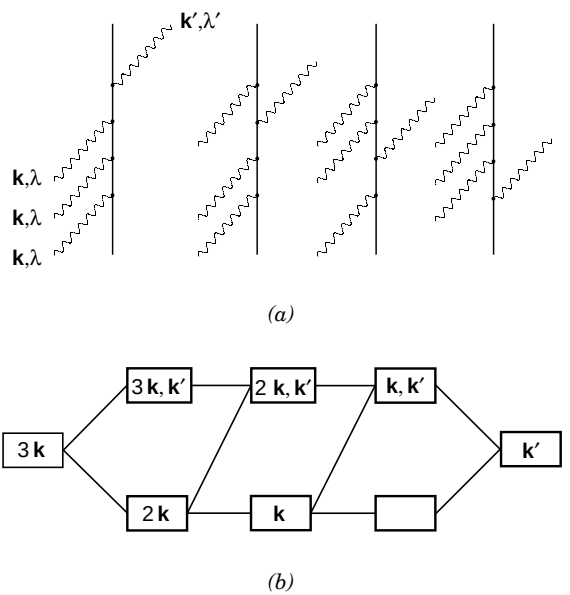

Figure 9. The four time-ordered diagrams characterizing third harmonic generation (a) and the state-sequence diagram representing the same process (b).

diagram of Fig. 9b. [80]

$$\begin{aligned}\gamma_{ijkl}(-3\omega;\omega,\omega,\omega) = {} & \frac{\mu_i^{u0}\mu_j^{u0}\mu_k^{u0}\mu_l^{u0}}{(E_{u0}-3\hbar\omega-i\Gamma_u)(-2\hbar\omega)(E_{u0}-\hbar\omega-i\Gamma_u)} \\ & + \frac{\mu_{i_1}^{u0}\breve{d}_j\breve{d}_k\mu_l^{u0}}{(E_{u0}-3\hbar\omega-i\Gamma_u)(E_{u0}-2\hbar\omega-i\Gamma_u)(E_{u0}-\hbar\omega-i\Gamma_u)} \\ & + \frac{\mu_j^{u0}\mu_i^{u0}\mu_k^{u0}\mu_l^{u0}}{(E_{u0}+\hbar\omega-i\Gamma_u)(-2\hbar\omega)(E_{u0}-\hbar\omega-i\Gamma_u)} \\ & + \frac{\mu_j^{u0}\breve{d}_i\breve{d}_k\mu_l^{u0}}{(E_{u0}+\hbar\omega-i\Gamma_u)(E_{u0}-2\hbar\omega-i\Gamma_u)(E_{u0}-\hbar\omega-i\Gamma_u)} \\ & + \frac{\mu_j^{u0}\mu_k^{u0}\mu_i^{u0}\mu_l^{u0}}{(E_{u0}+\hbar\omega-i\Gamma_u)(2\hbar\omega)(E_{u0}-\hbar\omega-i\Gamma_u)} \\ & + \frac{\mu_j^{u0}\breve{d}_k\breve{d}_i\mu_l^{u0}}{(E_{u0}+\hbar\omega-i\Gamma_u)(E_{u0}+2\hbar\omega-i\Gamma_u)(E_{u0}-\hbar\omega-i\Gamma_u)} \\ & + \frac{\mu_j^{u0}\mu_k^{u0}\mu_l^{u0}\mu_i^{u0}}{(E_{u0}+\hbar\omega-i\Gamma_u)(2\hbar\omega)(E_{u0}+3\hbar\omega-i\Gamma_u)} \\ & + \frac{\mu_j^{u0}\breve{d}_k\breve{d}_l\mu_i^{u0}}{(E_{u0}+\hbar\omega-i\Gamma_u)(E_{u0}+2\hbar\omega-i\Gamma_u)(E_{u0}+3\hbar\omega-i\Gamma_u)}\end{aligned} \tag{90}$$

where once again it is the index-symmetrized form, here entailing all permutations (jkl), that will feature in the observables. The transition moment $\boldsymbol{\mu}^{u0}$ is taken to be real and hence equal to $\boldsymbol{\mu}^{0u}$; also note that the tensor $\boldsymbol{\gamma}$ is minus that given as $\boldsymbol{\gamma}^{00}(-3\omega;\omega,\omega,\omega)$ elsewhere [80], because here each energy denominator expression carries an overall a minus sign, for consistency within the current work.

One aspect of Eq. (90) deserving comment is its amenability for the identification of resonances. Three-photon resonances are manifest in the first and second terms, through the appearance of the factor $(E_{u0}-3\hbar\omega-i\Gamma_u)$; two-photon resonances $(E_{u0}-2\hbar\omega-i\Gamma_u)$ are featured in the second and fourth, and single-photon resonances $(E_{u0}-\hbar\omega-i\Gamma_u)$ are seen in each of the first six. Since exploitation of the latter kind of resonance is in practice usually avoided because of the competing linear absorption with which it is associated, it is the two- and three- photon resonances that are of the most interest. Under suitable conditions, third-harmonic generation in either of those cases is driven largely by just two of the contributions to Eq. (90). Other contributions, signifying

minor corrections, are of much the same order of magnitude as those relating to the involvement of other molecular energy levels.

Further features are evident when the relative magnitudes of the dipole difference $|\mathbf{d}|$ and the transition dipole $|\boldsymbol{\mu}^{u0}|$ are considered. One immediately striking feature is the observation that the second, fourth, sixth, and eighth terms all disappear if $|\mathbf{d}| = 0$, leaving only terms associated with virtual excitation routes. [Note that no such routes were manifest in the second-harmonic result. If $|\mathbf{d}| = 0$ then the entire expression Eq. (85) becomes zero—any process involving an odd number of photons has to entail at least one 00 or *uu* segment in the interaction sequence.] In the third-harmonic case, in particular, both terms associated with two-photon resonances disappear—in other words, there can be no two-photon resonance enhancement of third-harmonic generation under such circumstances. If, however, $|\mathbf{d}| \gg |\boldsymbol{\mu}^{u0}|$, then the even terms of Eq. (90) dominate the optical response—and in the case of three-photon resonance, it is the second term that provides by far the leading contribution. Such considerations should play an important role in implementing strategies for the calculation of nonlinear optical response; for example in the case just cited, the dominant term is of a form that had not previously been identified as representing the major contribution.

XIII. OPTICAL COHERENCE IN DISPERSED PARTICLES

Despite the powerful symmetry rule that precludes the generation of even harmonics in optically isotropic media, except at surfaces, a number of experimental results have indicated exceptions to the rule, as detailed in the earlier review [1]. Most entail conditions resulting in a transient, local removal of isotropy, and are therefore well understood. Nonetheless, two quite different mechanisms have been found to mediate second-harmonic generation in macroscopically isotropic systems. In this section we consider a mechanism relating to optical coherence in small particles in suspension, or locally ordered domains within macroscopically structureless media. In the next section we shall focus on a six-wave form of interaction associated with very high pump laser intensities.

The coherent generation of second harmonics from particles in suspension was first found to operate in the generation of strongly directed SHG signals from photosynthetic bacterial membranes, randomly oriented in aqueous suspension [82,83]. The paradox was resolved when it was shown that the unusually strong signal detected from such isotropic suspensions is attributable to optical coherence within the separate particles of the suspension [84]. As such, the harmonic emission displays an amalgam of the characteristics associated with full coherence (second-harmonic generation) and incoherence (hyper-Rayleigh scattering). To understand this, it is necessary to return to the development of theory in Section VII. Consider a fluid or mesoscopically disordered material

(or any other optically isotropic system) within which there are small particles or local domains possessing a microscopically ordered structure. Examples of such systems include colloids, cell and membrane suspensions, and many plastics, glasses, and other modern materials. In systems of interest, each particle or domain includes a significant number of optical centers with strong optical dispersion at the frequency of the pump laser radiation or its harmonic. Let us suppose that such a system contains M randomly oriented particles (individually denoted below by the subscript m), each composed of n discrete molecules or other optical centres (denoted by the subscript ξ). Within each particle it is assumed that there is a structurally imposed orientational correlation, that is, a significant intrinsic rigidity, such that its net optical response can be cast in terms of an "effective hyperpolarizability" tensor given by

$$\beta^{00}_{(m)ijk} = \sum_{\xi}^{n} \beta^{00}_{(\xi)\lambda\mu\nu} l^{\xi}_{i\lambda} l^{\xi}_{j\mu} l^{\xi}_{k\nu} e^{i\,\Delta\mathbf{k}\cdot(\mathbf{R}_{\xi}-\mathbf{R}_{m})} \tag{91}$$

Here the hyperpolarizability of each individual optical center, $\beta^{00}_{(\xi)\lambda\mu\nu}$, is given a superscript label 00 to indicate that it relates to the electronic ground state (an assumption to be revisited later), and its position is given relative to the common Cartesian frame. The factor $l^{\xi}_{i\lambda}(l^{\xi}_{j\mu}, l^{\xi}_{k\nu})$ is the cosine of the angle between the space fixed axis $i(j,k)$ and the molecule fixed axis $\lambda(\mu,\nu)$. If the particles or ordered domains are small compared to the optical wavelengths involved, then so will be the internal distances $(\mathbf{R}_{\xi} - \mathbf{R}_{m})$, and thus in many circumstances—even in the complete lack of wavevector matching $(\Delta\mathbf{k} = 0)$—the phase factor in Eq. (91) can often be taken as effectively unity. However, we retain its explicit form for generality.

The rate of second-harmonic generation by the entire system of particles is expressible as a sum of two terms Γ_1 and Γ_2 as follows, where angular brackets denote the orientational average

$$\Gamma_1 = M\varsigma\langle|\beta^{00}_{(m)ijk}\bar{e}'_i e_j e_k|^2\rangle \tag{92}$$

$$\Gamma_2 = (\eta_M - M)\varsigma|\langle\beta^{00}_{(m)ijk}\bar{e}'_i e_j e_k\rangle|^2 \tag{93}$$

in which the latter, which represents a coherent addition of SHG amplitudes from *every* optical center in the system, corresponds exactly to the earlier Eq. (59) (which thereby serves to define the parameter ζ). When the particles are randomly oriented, Γ_2 vanishes as a result of the isotropic average, as is well known. However, since the corresponding average is conducted over the modulus square in the "incoherent" term, Γ_1, this contribution persists, representing an addition of the harmonic intensities produced by different particles. As determined by Eq. (91), these contributions in fact accommodate a coherent

addition of signals from the various optical centers that each particle contains. The analysis of angularly resolved measurements of the second harmonic [85] led to experimental verification of this interpretation, as shown in Fig. 10.

The coherent addition of second-harmonic signals, which can occur only in regions of local order, leads to intriguing possibilities for materials strongly pumped by an ultrafast source [86]. Here, the key feature is the relationship between the hyperpolarizabilities of optical centers in their ground and electronic excited states, under resonance conditions. To investigate this further, we return to the two-level model of the previous section, considering the role of other electronic levels subsequently. The hyperpolarizability for the upper state u is readily obtained using the transformed interaction Hamiltonian:

$$H''_{\text{int}} = -\varepsilon_0^{-1} \lfloor \boldsymbol{\mu} - \boldsymbol{\mu}^{uu} \rfloor \cdot \mathbf{e}^{\perp} \tag{94}$$

Here the algorithm given in (89) is modified by interchanging the labels 0 and u:

$$\boldsymbol{\mu}^{00} \to \boldsymbol{\mu}^{00} - \boldsymbol{\mu}^{uu} = -\mathbf{d}; \qquad \boldsymbol{\mu}^{uu} \to 0 \tag{95}$$

This has the effect of reversing the sign of $\mathbf{d}$ and also the energy difference E_{u0}, wherever each appears, although the Hermiticity of the dipole operator ensures that for nondegenerate states the transition dipole suffers no change:

$$\begin{aligned} \mathbf{d} &= \boldsymbol{\mu}^{uu} - \boldsymbol{\mu}^{00} \to -\mathbf{d} = -(\boldsymbol{\mu}^{uu} - \boldsymbol{\mu}^{00}) \\ E_{u0} &= E_u - E_0 \to -E_{u0} = E_{0u} \\ \boldsymbol{\mu}^{0u} &= \boldsymbol{\mu}^{u0} \end{aligned}$$

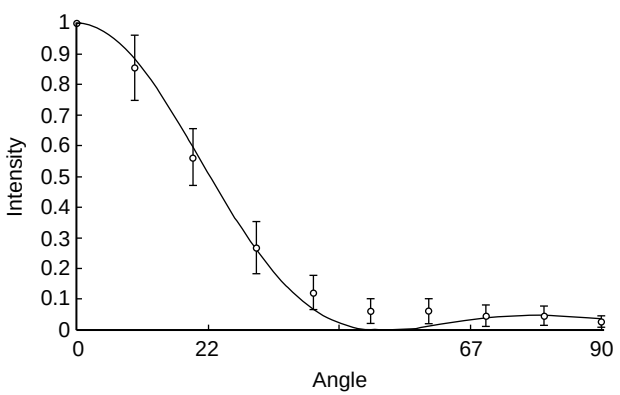

Figure 10. Intensity (arbitrary units) of optical SHG from a purple membrane suspension. Experimental data (Allcock et al. 1996) obtained with Nd:YAG laser pumping are shown by the open circles and the solid line represents the theoretical fit.

It then transpires that the upper-level hyperpolarizability tensor stands in the following simple relationship to its ground-state counterpart [86]:

$$\beta^{00}_{ijk}(-2\omega,\omega,\omega) = -\beta^{uu}_{ijk}(-2\omega,\omega,\omega) \tag{96}$$

Similar features arise when third-harmonic generation is considered. In passing we note that a variable-sign convention for the damping would lead to behavior of an analytical form substantially different from that discussed below.

Consider a system in which, prior to the input of the pump radiation responsible for the detected harmonic output, irradiation with a beam of the appropriate resonant frequency produces a significant population of the electronic level u among the optical centers in each particle or domain. With first-order decay kinetics, the probability that a certain center ξ is excited at time t is given by

$$P(\mathbf{R}_\xi, t) = P_0(\mathbf{R}_\xi)\exp(-k(t-t_0)) \tag{97}$$

where k is the decay constant and P_0 is the residual probability that the upper level is excited at time t_0, the time at which the pump radiation for SHG detection is applied. Particular interest expressed below focuses on the case of ultrafast excitation of sufficient intensity to elicit the onset of saturation, where $P_0 > 0.5$. While both excited- and ground-state species are present, the two processes described above contribute to an effective unit hyperpolarizability given by

$$\begin{aligned}\beta_{(m)ijk} &= \sum_{\xi}^{n}[(1-P(\mathbf{R}_\xi,t))\beta^{00}_{(\xi)\lambda\mu\nu} + P(\mathbf{R}_\xi,t)\beta^{uu}_{(\xi)\lambda\mu\nu}]l^{\xi}_{i\lambda}l^{\xi}_{j\mu}k\nu^{\xi}e^{i\Delta\mathbf{k}\cdot(\mathbf{R}_\xi-\mathbf{R}_m)}\\ &= \sum_{\xi}^{n}[(1-2P(\mathbf{R}_\xi,t))\beta^{00}_{(\xi)\lambda\mu\nu}]l^{\xi}_{i\lambda}l^{\xi}_{j\mu}l^{\xi}_{k\nu}e^{i\,\Delta\mathbf{k}\cdot(\mathbf{R}_\xi-\mathbf{R}_m)}\end{aligned} \tag{98}$$

leading to a harmonic intensity that features a characteristic decay and recovery in its temporal profile. Let us assume for simplicity that the probability of initial excitation is identical for all optical centers, removing the $\mathbf{R}_\xi$ dependence of $P(\mathbf{R}_\xi, t)$. Let us also denote by $\boldsymbol{\beta}$ the key factor

$$\boldsymbol{\beta} = \sum_{\xi}^{n}\beta^{00}_{(\xi)\lambda\mu\nu}l^{\xi}_{i\lambda}l^{\xi}_{j\mu}l^{\xi}_{k\nu}\bar{e}'_i e_j e_k e^{i\Delta\mathbf{k}\cdot(\mathbf{R}_\xi-\mathbf{R}_m)} \tag{99}$$

which will in general be a complex quantity by virtue of the damping involved in the hyperpolarizability tensor. For simplicity, assuming continuous-wave pump

radiation, the intensity of harmonic emission thus acquires a time dependence of the biexponential form

$$I \sim |\boldsymbol{\beta}|^2[1 - 4\exp(-kt') + 4\exp(-2kt')] \tag{100}$$

where $t' = t - t_0$ and $P_0(\mathbf{R}_\xi) \equiv 1$, giving a trace of the form $G(t) = 1 - 4\exp(-kt) + 4\exp(-2kt)$ as shown in Fig. 11.

To observe this exact time dependence in the second harmonic would require the satisfaction of certain criteria detailed below. Nonetheless, these conditions are largely a reflection of the simple two-level model employed, and in the following discussion we show that the major features of the result should be manifest in real systems of considerably greater electronic complexity. First, we note that with the two-level model a necessary condition for observation of a fall, and recovery of the harmonic output as illustrated in Fig. 11 is the creation of a transient population inversion by the preceding excitation laser pulse. The minimum output intensity (which will, in fact, be nonzero) would then be obtained at the time where the fractional population of the upper level u has fallen to exactly 0.5, matching the ground-state population in a two-level system. In practice, achieving initial population inversion is likely to require that the excitation pulse populate a higher level h that rapidly decays to u, where the latter plays the role of a population bottleneck as in conventional laser action. Although this emphasizes the fact that a two-level representation of the

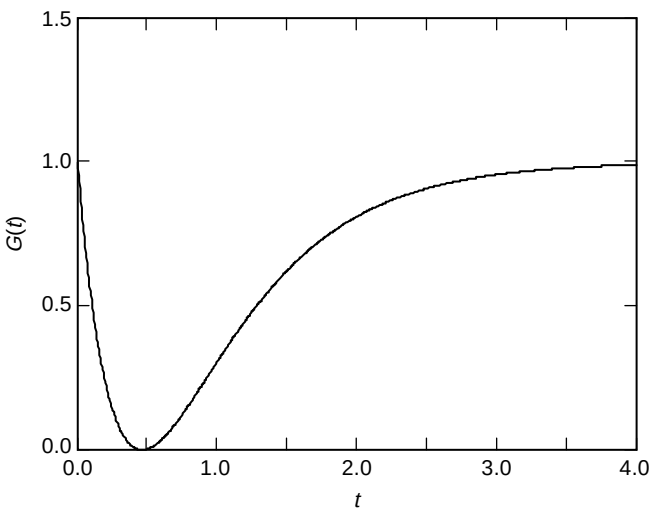

Figure 11. Schematic of the harmonic temporal profile *G(t)* from Eq. (100) in arbitrary units.

electronic energy levels is necessarily incomplete—as, indeed, it generally is—the inclusion of h and any other levels in the electronic structure of the optical centers will not significantly affect the results, provided those levels are no longer significantly populated once the pump for harmonic emission is applied. The harmonic signal will still be dominated by generation in centers in either the 0 or u state. Other electronic levels will certainly play the role of virtual states in the hyperpolarizabilities of each of those levels, adding a background contribution to each.

The effect of involving other levels in the calculations is assessed as follows, by considering what modifications to the preceding theory ensue. Both the tensors $\boldsymbol{\beta}^{00}$ and $\boldsymbol{\beta}^{uu}$ certainly acquire additional (and different) background contri butions, also complex, such that

$$\left.\begin{aligned} \sum_{\xi}^{n} \beta^{00}_{(\xi)\lambda\mu\nu}\, l^{\xi}_{i\lambda} l^{\xi}_{j\mu} l^{\xi}_{k\nu}\, \bar{e}'_i e_j e_k\, e^{i\,\Delta\mathbf{k}\cdot(\mathbf{R}_\xi - \mathbf{R}_m)} &\rightarrow \boldsymbol{\beta} + \tilde{\boldsymbol{\beta}} \\ \sum_{\xi}^{n} \beta^{uu}_{(\xi)\lambda\mu\nu}\, l^{\xi}_{i\lambda} l^{\xi}_{j\mu} l^{\xi}_{k\nu}\, \bar{e}'_i e_j e_k\, e^{i\,\Delta\mathbf{k}\cdot(\mathbf{R}_\xi - \mathbf{R}_m)} &\rightarrow -\boldsymbol{\beta} + \breve{\boldsymbol{\beta}} \end{aligned}\right\} \tag{101}$$

This results in a harmonic intensity with a more intricate time dependence of the form

$$I \sim |(\boldsymbol{\beta} + \tilde{\boldsymbol{\beta}}) - (2\boldsymbol{\beta} + \tilde{\boldsymbol{\beta}} - \breve{\boldsymbol{\beta}}) \exp(-kt')|^2 \tag{102}$$

which no longer factorises out the temporal profile $G(t')$. Separating the real and imaginary parts of each parameter $\boldsymbol{\beta} = \boldsymbol{\beta}' + i\boldsymbol{\beta}''$, $\tilde{\boldsymbol{\beta}} = \tilde{\boldsymbol{\beta}}' + i\tilde{\boldsymbol{\beta}}''$, $\breve{\boldsymbol{\beta}} = \breve{\boldsymbol{\beta}}' + i\breve{\boldsymbol{\beta}}''$, we thus have

$$\begin{aligned} I \sim\ & [(\boldsymbol{\beta}' + \tilde{\boldsymbol{\beta}}') - (2\boldsymbol{\beta}' + \tilde{\boldsymbol{\beta}}' - \breve{\boldsymbol{\beta}}') \exp(-kt')]^2 + [(\boldsymbol{\beta}'' + \tilde{\boldsymbol{\beta}}'') \\ & - (2\boldsymbol{\beta}'' + \tilde{\boldsymbol{\beta}}''\breve{\boldsymbol{\beta}}'') \exp(-kt')]^2 \end{aligned} \tag{103}$$

Of the two intensity contributions in Eq. (103) the first, associated with the real parts of the hyperpolarizabilities, will generally dominate, leading to a minimum in the harmonic emission at a time given by

$$t'_{\min} \sim k^{-1} \ln\left(\frac{2\boldsymbol{\beta}' + \tilde{\boldsymbol{\beta}}' - \breve{\boldsymbol{\beta}}'}{\boldsymbol{\beta}' + \tilde{\boldsymbol{\beta}}'}\right) \tag{104}$$

However, the effect of the second contribution in Eq. (103), corresponding to the imaginary parts of the hyperpolarizabilities and due to damping effects, will be to obviate complete cancellation of the harmonic signal at this time—only by a

spurious accident of hyperpolarizability values could the two harmonic intensity contributions of Eq. (103) be simultaneously zero. The characteristic fall and recovery of the harmonic remains.

In the light of the results presented above, it is useful to recall that the behavior we have identified, in the second-harmonic profile of a system of randomly oriented small particles or ordered domains in complex materials, owes its origin to the local quantum coherence between harmonic emission processes at different optical centers within each particle or domain. This behavior is dominated by features associated with a two-level optical response, but, provided the pump or harmonic frequencies are close to resonance, broadly similar effects are anticipated in systems of considerably greater electronic complexity. The effects of damping, which have to be included during operation close to resonance, and also the effects (as virtual states) of higher electronic levels, are to produce a background emission that prevents the harmonic from falling quite to zero during the probe pulse throughput. The characteristic signal recovery nonetheless remains a key feature, and its detailed form reflects the correct (constant sign) convention for effecting the optical damping. In this sense, observations might provide ground for experimental verification of the signing. Determination of the biexponential form of the harmonic profile will faithfully register the dynamics of excited-state decay.

The result has structural as well as kinetic implications. The local coherence, responsible for the partial cancellation of the harmonic signal after a characteristic delay time, is entirely dependent on a structural rigidity within each particle. This need not mean that all the optical centers are identically aligned, but that they do not rotate significantly with respect to each other (at least over the timescale for the harmonic measurements). The extent of recovery in the harmonic signal serves to register the extent of local coherence, and hence in many systems the localization of structural order. In any less than completely rigid system, it might be possible to assess the degree of local flexibility from the extent of harmonic recovery.

XIV. SIX-WAVE SECOND HARMONIC GENERATION

A spate of papers since the mid-1990s have reported theoretical and experimental studies of second-harmonic generation mediated by six-wave mixing (SWM), reflecting the new availability of laser sources with sufficient power and stability to make such observations possible [87–95]. Here we review the theory underlying the six-wave mechanisms for the evolution of a coherent second-harmonic signal in media where it is normally forbidden. As we shall see, the process $\omega + \omega + \omega + \omega \rightarrow 2\omega + 2\omega$ is invariably permitted, irrespective of local or bulk symmetry. We show how the initial results can be neatly adapted to model real molecular systems. We conclude by exhibiting the experimentally verified

form of a time-delayed harmonic that emerges if a pump probe system of beams is employed, which once again is a manifestation of quantum-optical interference.

To calculate the rate, we first construct a matrix element using the general equation (41) and substitute into the Golden Rule, Eq. (51). The detailed structure of the nonlinear polarizability $\boldsymbol{\alpha}^{(6)}_{\mathrm{SWM}}(-2\omega, -2\omega; \omega, \omega, \omega, \omega)$, which the process entails, is obtained using the state-sequence diagram of Fig. 12; in all there are $15\,(= 6!/4!2!)$ pathways linking the initial and final states to be taken into consideration, representing all topologically distinct orderings of the six electric dipole interactions involved. Again we might have used the time-ordered diagrams as an alternative—both, of course, lead to identical tensor expressions—but the concise representation of the state-sequencing is now clearly evident. For the explicit representation of the somewhat unwieldy resulting expressions, it is convenient to employ a more compact notation than we have used for lower-order polarisabilities. Here we follow Naguleswaran and Stedman [96], and neatly express $\boldsymbol{\alpha}^{(6)}_{\mathrm{SWM}}(-\omega', -\omega'; \omega, \omega, \omega, \omega)$ as

$$\begin{aligned}\boldsymbol{\alpha}^{(6)}_{\mathrm{SWM}}(-\omega', -\omega'; \omega, \omega, \omega, \omega) = \sum_{\pi} \sum_{r,s,t,u,v} \{(\mu^{0v}_{\pi(6)}\mu^{vu}_{\pi(5)}\mu^{ut}_{\pi(4)}\mu^{ts}_{\pi(3)}\mu^{sr}_{\pi(2)}\mu^{r0}_{\pi(1)}) \\ [\{\tilde{E}_{r0} + \hbar\eta_{\pi(1)}\omega_{\pi(1)}\}\{\tilde{E}_{s0} + \hbar(\eta_{\pi(1)}\omega_{\pi(1)} + \eta_{\pi(2)}\omega_{\pi(2)})\} \\ \times \{\tilde{E}_{t0} + \hbar(\eta_{\pi(1)}\omega_{\pi(1)} + \eta_{\pi(2)}\omega_{\pi(2)} + \eta_{\pi(3)}\omega_{\pi(3)})\} \\ \times \{\tilde{E}_{u0} + \hbar(\eta_{\pi(1)}\omega_{\pi(1)} + \eta_{\pi(2)}\omega_{\pi(2)} + \eta_{\pi(3)}\omega_{\pi(3)} \\ + \eta_{\pi(4)}\omega_{\pi(4)})\} \times \{\tilde{E}_{v0} + \hbar(\eta_{\pi(1)}\omega_{\pi(1)} \\ + \eta_{\pi(2)}\omega_{\pi(2)} + \eta_{\pi(3)}\omega_{\pi(3)} + \eta_{\pi(4)}\omega_{\pi(4)}\eta_{\pi(5)}\omega_{\pi(5)})\}]^{-1}\end{aligned} \tag{105}$$

where the sign of the photon label $\eta_{\pi(n)} = +1$ or -1 for emission or absorption, respectively. The sum over π leads to 30 unique permutations, allowing for

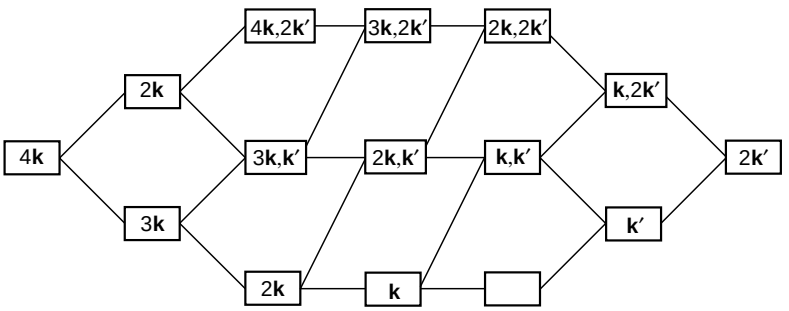

Figure 12. The state-sequence diagram representing SWM.

reversal of the time orderings of the signal photons, as is necessary for harmonics produced with differing wavevectors or polarizations. As an example of the energy denominator for a particular time ordering, consider the term for which $\pi(1) = n, \pi(2) = m, \pi(3) = l, \pi(4) = k, \pi(5) = j$, and $\pi(6) = i$. An energy denominator of the following form emerges

$$[(\tilde{E}_{r0} - \hbar\omega)(\tilde{E}_{s0} - 2\hbar\omega)(\tilde{E}_{t0} - 2\hbar\omega + \hbar\omega')(\tilde{E}_{u0} - 3\hbar\omega + \hbar\omega')r(\tilde{E}_{v0} - 4\hbar\omega + \hbar\omega')]$$

corresponding to the following temporal ordering: absorptions n and m (ω), emission l (ω'), absorptions k and j (ω) and finally emission i (ω').

It is worth drawing attention to the presence, and means of dealing with, the secular resonances that arise in high orders of optical nonlinearity. These features represent the fact that the quantum amplitudes for such processes can subsume the matrix elements for lower-order processes, apparently leading to spurious infinities. The various time orderings of the SWM interaction described here clearly include some that factor as a product of two sequential SHG time orderings, and it repays effort to examine in more detail their structure in the SWM polarizability tensor. Consider a situation where the molecular intermediate state $|t\rangle$ is represented by the molecular ground state $|0\rangle$ in the sum over t. When this occurs, certain energy denominators, such as E_{ti}, can suffer a complete cancellation of the radiation terms to uncover an expression of the form $E_{00} - i\Gamma_0 = -i\Gamma_0$; see, for example, Table III, which lists the energy denominators. As the ground-state lifetime, represented by Γ_0^{-1}, is considered infinite, a divergent signal is suggested. In order to circumvent these secular resonances, the molecular polarizability has to be reconstructed in such a way as to remove the possibility of infinite response [79]. We have reported the details for such a reconstruction explicitly for the SWM polarizability tensor [91]. The procedure is straightforward and entails properly taking the limit as the virtual state energy approaches that of the ground state.

Returning to the general form of the SWM interaction, it is next necessary to form the radiation tensor using the general expression of Eq. (52). Explicitly incorporating the degree of coherence of the input beam and assuming that there are initially no photons in the harmonic mode, the following equation, where $I\omega$ is the intensity of the pump radiation, is obtained for the rate of six-wave mixing:

$$\Gamma_{\mathrm{SWM}} = \left(\frac{4\pi\hbar}{\varepsilon_0^6}\right)\left(\frac{I_\omega}{2cn_\omega}\right)^4\left(\frac{n_\omega + 2}{3}\right)^8 \sum_{\mathbf{k}',\lambda'}\left(\frac{v_g'\omega'}{2cVn_{\omega'}}\right)^2\left(\frac{n_{\omega'} + 2}{3}\right)^4 g_\omega^{(4)}\eta_N$$
$$\times\, |\langle\alpha^{(6)}(-2\omega, -2\omega; \omega, \omega, \omega, \omega)\cdot\bar{\mathbf{e}}'\bar{\mathbf{e}}'\mathbf{eeee}\rangle|^2\delta(2\hbar\omega_{k'} - 4\hbar\omega_k) \qquad (106)$$

The result embodies the coherence factor η_N to account for the phase-matching characteristics of the process, leading to the familiar sinc^2 behavior, which

TABLE III
The Individual Intermediate State Energies Calculated for All 15 Pathways through the SWM State-Sequence Diagram of Fig. 12

Route	E_{ri}	E_{si}	E_{ti}	E_{ui}	E_{vi}
(i)	$(\tilde{E}_{r0} - 2\hbar\omega)$	$(\tilde{E}_{s0} - 2\hbar\omega)$	$(\tilde{E}_{t0} - 2\hbar\omega + \hbar\omega')$	$(\tilde{E}_{u0} - 3\hbar\omega + \hbar\omega')$	$(\tilde{E}_{v0} - 4\hbar\omega + \hbar\omega')$
(ii)	$(\tilde{E}_{r0} - \hbar\omega)$	$(\tilde{E}_{s0} - 2\hbar\omega)$	$(\tilde{E}_{t0} - 2\hbar\omega + \hbar\omega')$	$(\tilde{E}_{u0} - 3\hbar\omega + \hbar\omega')$	$(\tilde{E}_{v0} - 3\hbar\omega + 2\hbar\omega')$
(iii)	$(\tilde{E}_{r0} - \hbar\omega)$	$(\tilde{E}_{s0} - 2\hbar\omega)$	$(\tilde{E}_{t0} - 2\hbar\omega + \hbar\omega')$	$(\tilde{E}_{u0} - 2\hbar\omega + 2\hbar\omega')$	$(\tilde{E}_{v0} - 3\hbar\omega + 2\hbar\omega')$
(iv)	$(\tilde{E}_{r0} - \hbar\omega)$	$(\tilde{E}_{s0} - \hbar\omega + \hbar\omega')$	$(\tilde{E}_{t0} - 2\hbar\omega + \hbar\omega')$	$(\tilde{E}_{u0} - 2\hbar\omega + 2\hbar\omega')$	$(\tilde{E}_{v0} - 3\hbar\omega + 2\hbar\omega')$
(v)	$(\tilde{E}_{r0} + \hbar\omega')$	$(\tilde{E}_{s0} - \hbar\omega + \hbar\omega')$	$(\tilde{E}_{t0} - 2\hbar\omega + \hbar\omega')$	$(\tilde{E}_{u0} - 2\hbar\omega + 2\hbar\omega')$	$(\tilde{E}_{v0} - 3\hbar\omega + 2\hbar\omega')$
(vi)	$(\tilde{E}_{r0} + \hbar\omega')$	$(\tilde{E}_{s0} - \hbar\omega + \hbar\omega')$	$(\tilde{E}_{t0} - 2\hbar\omega + \hbar\omega')$	$(\tilde{E}_{u0} - 3\hbar\omega + \hbar\omega')$	$(\tilde{E}_{v0} - 3\hbar\omega + 2\hbar\omega')$
(vii)	$(\tilde{E}_{r0} + \hbar\omega')$	$(\tilde{E}_{s0} - \hbar\omega + \hbar\omega')$	$(\tilde{E}_{t0} - 2\hbar\omega + \hbar\omega')$	$(\tilde{E}_{u0} - 3\hbar\omega + \hbar\omega')$	$(\tilde{E}_{v0} - 4\hbar\omega + \hbar\omega')$
(viii)	$(\tilde{E}_{r0} - \hbar\omega)$	$(\tilde{E}_{s0} - \hbar\omega + \hbar\omega')$	$(\tilde{E}_{t0} - 2\hbar\omega + \hbar\omega')$	$(\tilde{E}_{u0} - 3\hbar\omega + \hbar\omega')$	$(\tilde{E}_{v0} - 4\hbar\omega + \hbar\omega')$
(ix)	$(\tilde{E}_{r0} - \hbar\omega)$	$(\tilde{E}_{s0} - \hbar\omega + \hbar\omega')$	$(\tilde{E}_{t0} - 2\hbar\omega + \hbar\omega')$	$(\tilde{E}_{u0} - 3\hbar\omega + \hbar\omega')$	$(\tilde{E}_{v0} - 3\hbar\omega + 2\hbar\omega')$
(x)	$(\tilde{E}_{r0} - \hbar\omega')$	$(\tilde{E}_{s0} - 2\hbar\omega)$	$(\tilde{E}_{t0} - 3\hbar\omega)$	$(\tilde{E}_{u0} - 3\hbar\omega + \hbar\omega')$	$(\tilde{E}_{v0} - 4\hbar\omega + \hbar\omega')$
(xi)	$(\tilde{E}_{r0} - \hbar\omega)$	$(\tilde{E}_{s0} - 2\hbar\omega)$	$(\tilde{E}_{t0} - 3\hbar\omega)$	$(\tilde{E}_{u0} - 3\hbar\omega + \hbar\omega')$	$(\tilde{E}_{v0} - 3\hbar\omega + 2\hbar\omega')$
(xii)	$(\tilde{E}_{r0} - \hbar\omega)$	$(\tilde{E}_{s0} - \hbar\omega + \hbar\omega')$	$(\tilde{E}_{t0} - \hbar\omega + 2\hbar\omega')$	$(\tilde{E}_{u0} - 2\hbar\omega + 2\hbar\omega')$	$(\tilde{E}_{v0} - 3\hbar\omega + 2\hbar\omega')$
(xiii)	$(\tilde{E}_{r0} - \hbar\omega)$	$(\tilde{E}_{s0} - 2\hbar\omega)$	$(\tilde{E}_{t0} - 3\hbar\omega)$	$(\tilde{E}_{u0} - 4\hbar\omega)$	$(\tilde{E}_{v0} - 4\hbar\omega + \hbar\omega')$
(xiv)	$(\tilde{E}_{r0} + \hbar\omega')$	$(\tilde{E}_{s0} + 2\hbar\omega')$	$(\tilde{E}_{t0} - \hbar\omega + 2\hbar\omega')$	$(\tilde{E}_{u0} - 2\hbar\omega + 2\hbar\omega')$	$(\tilde{E}_{v0} - 3\hbar\omega + 2\hbar\omega')$
(xv)	$(\tilde{E}_{r0} - \hbar\omega)$	$(\tilde{E}_{s0} - \hbar\omega + \hbar\omega')$	$(\tilde{E}_{t0} - \hbar\omega + 2\hbar\omega')$	$(\tilde{E}_{u0} - 2\hbar\omega + 2\hbar\omega')$	$(\tilde{E}_{v0} - 3\hbar\omega + 2\hbar\omega')$

demonstrates that the SWM process manifests coherence for emission in the forward z direction. This is nonetheless subject to optimal wavevector matching: $\Delta\mathbf{k} = 4\mathbf{k} - \mathbf{k}' \approx 0$.

The question of whether SWM can generate an observable signal in fluids requires further analysis, and calls for explicit evaluation of the ensemble average of the tensor product in Eq. (106) as

$$\langle \boldsymbol{\alpha}^{(6)} \cdot \bar{\mathbf{e}}'\bar{\mathbf{e}}'\mathbf{eeee}\rangle = \alpha^{(6)}_{(\lambda\mu)(\nu o\pi\rho)}\bar{e}'_i\bar{e}'_j e_k e_l e_m e_n \langle \ell_{i\lambda}\ell_{j\mu}\ell_{k\nu}\ell_{lo}\ell_{m\pi}\ell_{n\rho}\rangle \tag{107}$$

Applying a sixth-rank rotational average [97] immediately reveals that the rate equation entails an overall multiplier of the scalar product $(\mathbf{e}\cdot\mathbf{e})$, which vanishes for circular polarizations. The six-wave interaction is thus subject to the same embargo on conversion of a circularly polarized pump as the conventional SHG process [98]. In the case of a plane-polarized pump, ensemble averaging leads to the result;

$$\begin{aligned}\Gamma_{\mathrm{SWM}} = {} & \left(\frac{4\pi\hbar\omega_k^2}{\varepsilon_0^6}\right)\left(\frac{I_\omega}{2cn_\omega}\right)^4\left(\frac{n_{\omega_k}^2+2}{3}\right)^8 g^{(4)}_\omega \sum_{\mathbf{k}',\lambda'}\left(\frac{\nu'_g\omega'_{k'}}{2Vcn\omega'_{k'}}\right)^2\left(\frac{n^2_{\omega'_{k'}}+2}{3}\right)^4 \\ & \times |\{6(\mathbf{e}\cdot\mathbf{e}')^2-2\}\alpha^{(6)}_{(\lambda\mu)(\lambda\mu\nu\nu)} - \{2(\mathbf{e}\cdot\mathbf{e}')^2-3\}\alpha^{(6)}_{(\lambda\lambda)(\mu\mu\nu\nu)}|^2\eta_N \\ & \times \delta(2\hbar\omega'_{k'} - 4\hbar\omega_k)\end{aligned} \tag{108}$$

following simplication exploiting the inherent permutational symmetry in the first two and last four indices of the nonlinear response tensor. Equation (108) illustrates the fact that there need not be full retention of polarization in the emitted harmonic; indeed, the extent of depolarization ρ is given by

$$\rho = \frac{\Gamma_{\mathrm{SWM}}(\mathbf{e}'\perp\mathbf{e})}{\Gamma_{\mathrm{SWM}}(\mathbf{e}'\parallel\mathbf{e})} = \left|\frac{\{3\alpha_{\lambda\lambda(\mu\mu\nu\nu)} - 2\alpha_{\lambda\mu(\lambda\mu\nu\nu)}\}}{\{\alpha_{\lambda\lambda(\mu\mu\nu\nu)} + 4\alpha_{\lambda\mu(\lambda\mu\nu\nu)}\}}\right|^2 \tag{109}$$

whose value must lie in the range $0 \le \rho \le 9$. If full permutational (Kleinman) index symmetry applies to the components of the nonlinear susceptibility tensor, Eq. (109) reduces to the result $\rho = \frac{1}{25}$. Departure of the degree of depolarization from this value thus registers invalidity of the Kleinman assumption.

Before further developing the theory to a form more directly suited to a different kind of experimental application, we outline why SWM is a mechanism allowed for all possible molecular symmetries. By inspection of the index symmetry in the radiation tensor, it is clear that a harmonic signal can derive only from that part of the sixth-rank polarizability $\boldsymbol{\alpha}^{(6)}_{\mathrm{SWM}}$ that is symmetric with respect to permutation among the four indices related to the absorbed pump

photons, and also between the two indices relating to the two harmonic photons. Under the operations of the full rotation group SO(3), the group-theoretic representation of the tensor emerges as $2D^{(0+)} \oplus D^{(1+)} \oplus 4D^{(2+)} \oplus 2D^{(3+)} + 3D^{(4+)} \oplus D^{(5+)} \oplus D^{(6+)}$, accommodating a maximum of 90 independent components in the case of a molecule lacking any intrinsic symmetry. If full (Kleinman) index symmetry is assumed, the representation becomes $D^{(0+)} \oplus D^{(2+)} \oplus D^{(6+)}$, accounting for a total of just 28 independent components. In either case the crucial facet of the result is its incorporation of a $D^{(0+)}$ component, which invariably spans the totally symmetric representation of any point or space groups. Thus six-wave second-harmonic production entails a nonlinear polarizability that never vanishes for symmetry reasons; for example, it permits the process to be supported in centrosymmetric molecules or solids. Naturally, the six-wave process will be insignificant in media where the normal SHG process is allowed, since it derives from three orders higher perturbation theory.

Since the early 1990s, a number of studies on the generation of optically induced harmonics from isotropic suspensions of organic dyes have led to the characterization of SWM mechanisms (see, e.g., Refs. 88–90 and 92–95). However, it has generally been found experimentally expedient to induce the harmonic by seeding. This requires that samples be pumped not only with the four beams at the fundamental but also with a probe beam at the harmonic frequency, allowing for stimulated emission to enhance the interaction. The experimental setup is usually based on three distinct beams impinging on the sample. Of these, two are counterpropagating fundamental beams of frequency ω, with the third at a frequency of 2ω stimulating the second harmonic into a specific mode satisfying the wavevector matching conditions. A schematic experimental geometry is illustrated in Fig. 13. Under such conditions the number of time-ordered diagrams is increased from the original 15 to 180 ($=6!/2!2!$), indicating a reduction in the extent of permutational symmetry among both the product radiation and molecular polarizability indices.

Referring to the experimental geometry of Fig. 13, we can assign the radiation modes $r_1 = (\mathbf{k}_1, \lambda_1), r_2 = (\mathbf{k}_2 \lambda_2), r_3 = (\mathbf{k}_3, \lambda_3)$, and $r_4 = (\mathbf{k}_4, \lambda_4)$, recognizing that $\mathbf{k}_1 = -\mathbf{k}_2$ and $\mathbf{k}_3 = -\mathbf{k}_4$. Using the coherent representation for a SWM process, [Eq. (106)], and recognizing the appropriate index symmetry, we can write

$$\begin{aligned}\Gamma_{\mathrm{SWM}} = {} & \left(\frac{2\pi}{\varepsilon_0^6}\right)\left(\frac{I_1}{2cn_\omega}\right)^2\left(\frac{I_2}{2cn_\omega}\right)^2\left(\frac{n_\omega+2}{3}\right)^8 g_1^{(2)} g_2^{(2)}\left(\frac{I_3}{2cn_{2\omega}}\right)\left(\frac{n_{2\omega}+2}{3}\right)^2 \\ & \times \sum_{\mathbf{k}_4,\lambda_4}\left(\frac{\nu_g'\omega_{k_4}}{2cVn_{\omega_4}}\right)\left(\frac{n_{\omega_4}+2}{3}\right)^2 \eta_N \delta(\hbar\omega_{k_4} + 2\hbar\omega - 4\hbar\omega) \\ & \times |\alpha^{(6)}_{ij(kl)(mn)}(-\omega_{k_4}, -2\omega; \omega, \omega, \omega, \omega)\bar{e}_i^{(4)}\bar{e}_j^{(3)} e_k^{(2)} e_l^{(2)} e_m^{(1)} e_n^{(1)}|^2 \qquad (110)\end{aligned}$$

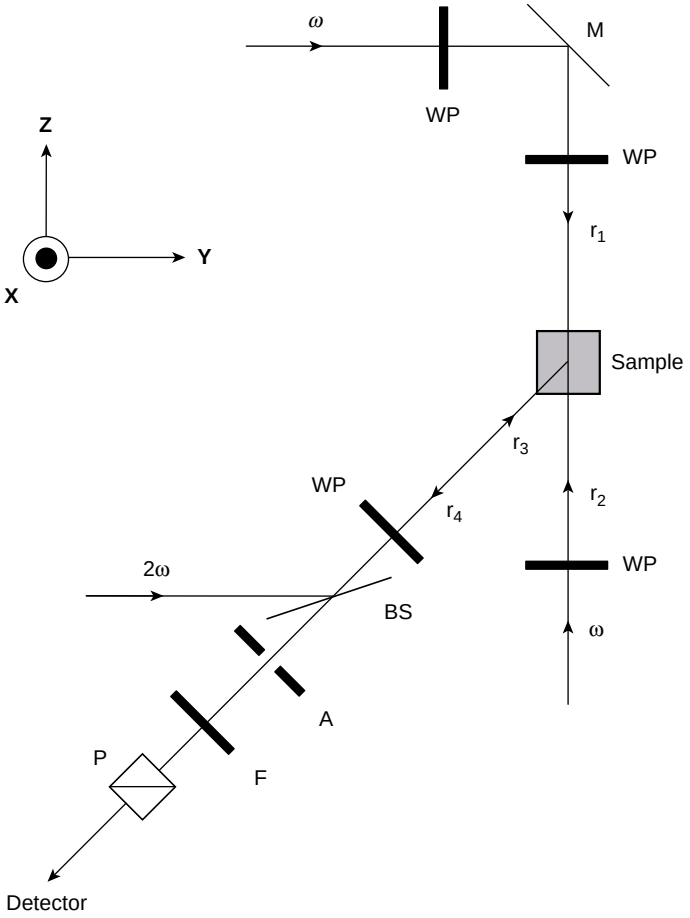

Figure 13. Schematic of a typical SWM experimental set-up. Counter-propagating fundamental beams of mode $r_1 = (\mathbf{k}_1, \lambda_1)$ and $r_2 = (\mathbf{k}_2, \lambda_2)$, each contribute two photons while the stimulating beam $r_3 = (\mathbf{k}_3, \lambda_3$ and signal beam $r_4 = (\mathbf{k}_4, \lambda_4)$ each gain one photon. The laboratory axes are illustrated and other symbols represent: A-Aperture, BS-beam splitter, C-chopper, F-bandpass filter, P-polarizer, M-mirror and WP-wave plate.

Note the dependence of the rate on the intensity of the stimulating harmonic or seeding beam at 2ω. On converting the sum over $\mathbf{k}_4$ to an integral, utilizing our knowledge of the delta function and converting to a harmonic intensity, we have

$$I_{\mathrm{SWM}} = \frac{1}{\varepsilon_0^6 (2\pi)^2} \left(\frac{I_1}{2cn_\omega}\right)^2 \left(\frac{I_2}{2cn_\omega}\right)^2 \left(\frac{n_\omega + 2}{3}\right)^8 g_1^{(2)} g_2^{(2)} \left(\frac{I_3}{2c}\right) \left(\frac{(2\omega)^4}{2c^3}\right) \left(\frac{n_{2\omega} + 2}{3}\right)^4 \eta_N$$
$$\times \sum_{\lambda_4} |\alpha^{(6)}_{ij(kl)(mn)}(-2\omega, -2\omega; \omega, \omega, \omega, \omega) \bar{e}_i^{(4)} \bar{e}_j^{(3)} e_k^{(2)} e_l^{(2)} e_m^{(1)} e_n^{(1)}|^2 \qquad (111)$$

where $g_i^{(2)}$ is the second-order degree of coherence of the ith mode. Notice how the artificial dependence on the quantization volume disappears. The interesting features of the optical response are embedded in the molecular polarizability/radiation tensor product. For an isotropic sample, we again have to perform a rotational average taken inside the modulus squared. Index symmetry exists only in the k, l and m, n index pairs, as indicated by parentheses. Therefore, on applying a sixth-rank average, we calculate the response as

$$\langle I_{\mathrm{SWM}} \rangle = \frac{\kappa}{105} \sum_{i=6}^{6} E_i A_i \tag{112}$$

Here κ represents all the molecule-independent and polarization-independent constants gathered into a single parameter; the E_i values represent the unique radiation polarization products

$$\begin{aligned} E_1 &= (\mathbf{e}^{(1)} \cdot \mathbf{e}^{(1)})(\mathbf{e}^{(2)} \cdot \mathbf{e}^{(2)})(\bar{\mathbf{e}}^{(3)} \cdot \bar{\mathbf{e}}^{(4)}) & E_3 &= (\mathbf{e}^{(1)} \cdot \mathbf{e}^{(2)})(\mathbf{e}^{(1)} \cdot \bar{\mathbf{e}}^{(3)})(\mathbf{e}^{(2)} \cdot \bar{\mathbf{e}}^{(4)}) \\ E_2 &= (\mathbf{e}^{(1)} \cdot \mathbf{e}^{(1)})(\mathbf{e}^{(2)} \cdot \bar{\mathbf{e}}^{(3)})(\mathbf{e}^{(2)} \cdot \bar{\mathbf{e}}^{(4)}) & E_4 &= (\mathbf{e}^{(1)} \cdot \mathbf{e}^{(2)})(\mathbf{e}^{(1)} \cdot \bar{\mathbf{e}}^{(4)})(\mathbf{e}^{(2)} \cdot \bar{\mathbf{e}}^{(3)}) \\ E_3 &= (\mathbf{e}^{(1)} \cdot \mathbf{e}^{(2)})(\mathbf{e}^{(1)} \cdot \mathbf{e}^{(2)})(\bar{\mathbf{e}}^{(3)} \cdot \bar{\mathbf{e}}^{(4)}) & E_5 &= (\mathbf{e}^{(1)} \cdot \bar{\mathbf{e}}^{(3)})(\mathbf{e}^{(1)} \cdot \bar{\mathbf{e}}^{(4)})(\mathbf{e}^{(2)} \cdot \mathbf{e}^{(2)}) \end{aligned} \tag{113}$$

and the A_i values represent the molecular response, in the following format:

$$\begin{bmatrix} A_1 \\ A_2 \\ A_3 \\ A_4 \\ A_5 \\ A_6 \end{bmatrix} = \begin{bmatrix} 8 & -5 & -5 & 4 & 4 & 5 \\ -5 & 11 & 4 & -6 & -6 & 4 \\ -5 & 4 & 11 & -6 & -6 & 4 \\ 4 & -6 & -6 & 16 & 2 & -6 \\ 4 & -6 & -6 & 1 & 16 & -6 \\ -5 & 4 & 4 & -6 & -6 & 11 \end{bmatrix} \begin{bmatrix} \boldsymbol{\alpha}_1 \\ \boldsymbol{\alpha}_2 \\ \boldsymbol{\alpha}_3 \\ \boldsymbol{\alpha}_4 \\ \boldsymbol{\alpha}_5 \\ \boldsymbol{\alpha}_6 \end{bmatrix} \tag{114}$$

Here each independent molecular polarizability invariant is explicitly defined as

$$\begin{aligned} \boldsymbol{\alpha}_1 &= \alpha^{(6)}_{ii(jj)(kk)} & \boldsymbol{\alpha}_4 &= \boldsymbol{\alpha}^{(6)}_{ij(ik)(jk)} \\ \boldsymbol{\alpha}_2 &= \alpha^{(6)}_{ij(ij)(kk)} & \boldsymbol{\alpha}_5 &= \boldsymbol{\alpha}^{(6)}_{ji(ik)(jk)} \\ \boldsymbol{\alpha}_3 &= a^{(6)}_{ii(jk)(jk)} & \boldsymbol{\alpha}_6 &= a^{(6)}_{jk(ii)(jk)} \end{aligned} \tag{115}$$

In this format we can easily derive expressions for the signal intensity of the harmonic for arbitrary electric field polarizations. By assuming a laboratory-frame coordinate axis as illustrated in the experimental setup shown in Fig. 13,

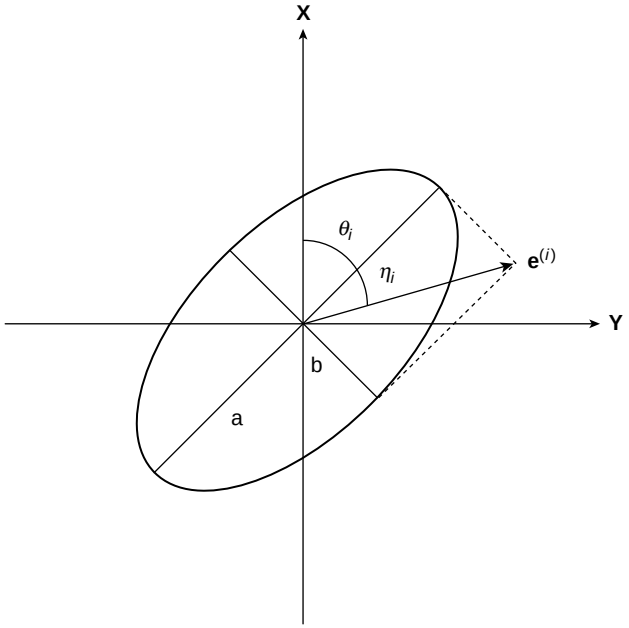

Figure 14. General representation for an arbitrarily polarized light beam, with polarization vector $\mathbf{e}^{(i)}$ as represented by Eq. (116). The definition of the azimuth θ_i and ellipticity $\eta_i = \tan^{-1}(b/a)$ is as illustrated with respect to the **X**- and **Y**-axis with the **Z**-axis pointing into the plane of the paper.

the polarization vectors for the four fields, characterized by their azimuth and ellipticity as defined in Fig. 14, are concisely expressed as

$$\begin{aligned}
\mathbf{e}^{(1)} &= (\cos\theta_1\cos\eta_1 - i\sin\theta_1\sin\eta_1)\hat{\mathbf{x}} + (\sin\theta_1\cos\eta_1 + i\cos\theta_1\sin\eta_1)\hat{\mathbf{y}} \\
\mathbf{e}^{(2)} &= (\cos\theta_2\cos\eta_2 - i\sin\theta_2\sin\eta_2)\hat{\mathbf{x}} - (\sin\theta_2\cos\eta_2 + i\cos\theta_2\sin\eta_2)\hat{\mathbf{y}} \\
\mathbf{e}^{(3)} &= (\cos\theta_3\cos\eta_3 - i\sin\theta_3\sin\eta_3)\hat{\mathbf{x}} - (\sin\theta_3\cos\eta_3 + i\cos\theta_3\sin\eta_3)\hat{\mathbf{y}} \\
&\quad \times (\cos\delta\hat{\mathbf{y}} - \sin\delta\hat{\mathbf{z}}) \\
\mathbf{e}^{(4)} &= (\cos\theta_4\cos\eta_4 - i\sin\theta_4\sin\eta_4)\hat{\mathbf{x}} + (\sin\theta_4\cos\eta_4 + i\cos\theta_4\eta_4)\hat{\mathbf{y}} \\
&\quad \times (\cos\delta\hat{\mathbf{y}} - \sin\delta\hat{\mathbf{z}})
\end{aligned} \tag{116}$$

By placing a plane polarizer in the signal collection geometry ($\eta_4 = 0$) and collecting the signal separately along $\hat{\mathbf{x}}(\theta_4 = 0)$ and $\hat{\mathbf{y}}(\theta_4 = \pi/2)$ directions, we are free to select any particular set of polarizations for the applied fields. As an example of the many controlled polarization plots possible, consider the applied

fields all linearly polarized along the $\hat{\mathbf{x}}$ axis except for beam $\mathbf{e}^{(1)}$, which makes an angle θ_1 to the others. The signal intensity then reduces from Eq. (112) to

$$\langle I_{\mathrm{SWM}}^{(\hat{\mathbf{x}})-\mathrm{pol}} \rangle = \frac{\mathrm{K}}{105} |(A_1 + A_2) + (A_3 + A_4 + A_5 + A_6)\cos^2\theta_1|^2 \tag{117}$$

$$\langle I_{\mathrm{SWM}}^{(\hat{\mathbf{y}})-\mathrm{pol}} \rangle = \frac{\mathrm{K}}{105} \left| \frac{1}{2}(A_5 + A_6)\sin 2\theta_1 \cos\delta \right|^2 \tag{118}$$

where δ is the angle at which the seeding and signal fields propagate with respect to the laboratory $(\hat{\mathbf{x}}, \hat{\mathbf{y}})$ plane. The calculated signal for collection along the $\hat{\mathbf{x}}$ and $\hat{\mathbf{y}}$ axis can be plotted as a function of angle θ_1. This is illustrated in Fig. 15. By performing a number of similarly designed experiments, detailed information on the six-wave mixing polarizability tensor can be extracted.

The seeding of molecular harmonics is in some sense a throwback to experiments where second harmonics were first observed in condensed-matter isotropic systems. For example, in glass fibers it was observed that a harmonic was produced after long exposures to fundamental frequency laser light [99,100]. It was later found that, by introduction of a low intensity seeding beam at the harmonic frequency, the onset of the harmonic in the glass was essentially instantaneous [101]. It was at this time that the proposal of a SWM mechanism

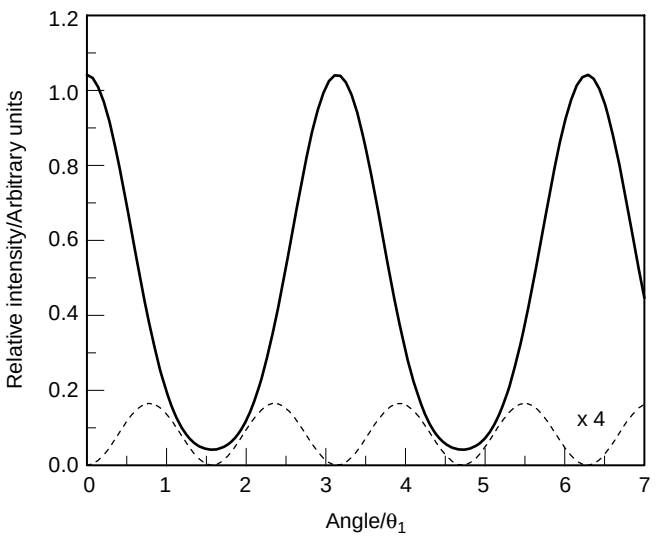

Figure 15. The solid and dotted lines represent theoretically calculated traces for SWM signals collected under the polarization conditions pertaining to Eqs. (117) and (118), respectively. The solid trace is normalized and the dotted line scaled by a factor of 4. The results are calculated assuming all molecular parameters $A_1 - A_6$ yield equal contributions.

was first made [102,103]. However, it is necessary to accommodate additional features that are observed in the generation of harmonics from suspensions of organic dyes that absorb at the harmonic frequency. In such media the temporal behavior of the harmonic evolution is generally considered consistent with some degree of molecular alignment as a result of the optical perturbations to the environment [104]. Such perturbations would necessarily be physically distinct from the process of harmonic production, although engendered by the same optical input beams. This represents a move away from the instantaneous SWM mechanism, allowed for all molecular symmetries, focusing instead on time-dependent molecular orientational symmetry breaking. Here we illustrate how, with a resonant seeding harmonic, the concept of a molecular population diffraction grating can be employed as an alternative and more readily comprehensible means of eliciting the physics of harmonic evolution. This is a quantum optical effect that does not require the invocation of light-induced orientation. Its foundation is based on a selective absorption process that is a direct result of a molecular ensemble initially having an isotropic array of molecules.

The first task then is to show that, in the presence of the two writing beams r_2 and r_3, the created population grating is of just the correct periodicity to efficiently generate phase-matched second-harmonic photons from the probe beam r_1. As a result, the r_4 signal photons emerge at the second-harmonic frequency and propagate in the direction exactly opposite that of seeding beam r_3, according to the dictates of wavevector matching. We shall suppose that the seeding pulses from modes r_2 and r_3 are coincident with the sample at time $t = 0$, and then at $t = \tau$ the pulse from the probe beam r_1 arrives. The sample is absorbing at the harmonic frequency, and so transition to the excited state is expected. Nonetheless, there are two ways to accomplish this in the presence of the two differing input frequencies: (1) two-photon absorption of photons solely from the fundamental beam and (2) single-photon absorption of photons from the harmonic beam. (This principle was first considered in connection with ionization processes by Baranova and Zel'dovich, [105].) We thus need to consider two time orderings as shown in Fig. 16. The matrix element (quantum probability amplitude) for the transition in a particular molecule ξ is thus written as

$$M_{fi}^{(\xi)} = M_{fi}^{(\xi,a)} + M_{fi}^{(\xi,b)} \tag{119}$$

where $M_{fi}^{(\xi,a)}$ is the matrix element for graph (a) of Fig. 16 and $M_{fi}^{(\xi,b)}$ is that for graph (b). By rigorously following the procedures for forming the matrix elements as outlined in earlier sections, these quantities can be written as

$$M_{fi}^{(\xi,a)} = \left(\frac{\hbar \nu_g \omega_k}{2c\varepsilon_0 V n_{\omega_k}}\right)\left(\frac{n_{\omega_k}^2 + 2}{3}\right)^2 \sqrt{\langle q_2\rangle\langle(q_2-1)\rangle}\,\alpha_{(ij)}^{10}(\omega,\omega)e_i^{(2)}e_j^{(2)}e^{i\,2\mathbf{k}_2\cdot\mathbf{R}_\xi} \tag{120}$$

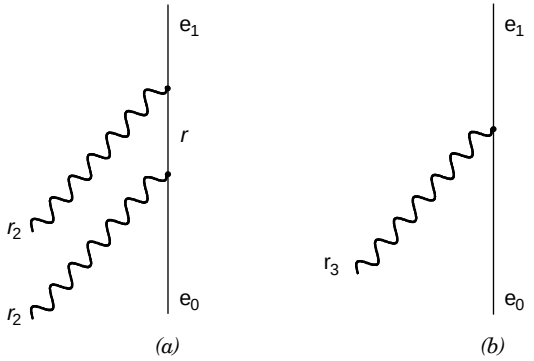

Figure 16. The time-ordered diagrams associated with the formation of an appropriate molecular grating for SHG. The two writing beams r_2 and r_3 populate the upper electronic state via two- and single-photon absorption respectively.

and

$$M_{fi}^{(\xi,b)} = i\left(\frac{\hbar\nu'_g\omega'_{k'}k'}{2cV\varepsilon_0 n_{\omega_{k'}}}\right)^{1/2}\left(\frac{n^2_{\omega'_{k'}}+2}{3}\right)\sqrt{\langle q_3\rangle}\mu_i^{10}e_i^{(3)}\,e^{i\mathbf{k}_3\cdot\mathbf{R}_\xi} \tag{121}$$

In these equations the position of the molecule is described by the vector $\mathbf{R}_\xi$; the wavevectors of the two beams of modes r_2 and r_3 are $\mathbf{k}_2$ and $\mathbf{k}_3$ respectively, with $\langle q_2\rangle$ and $\langle q_3\rangle$ the corresponding mean photon numbers (mode occupancies); and $\mathbf{e}^{(n)}$ is a unit vector describing the polarization state of mode r_n. In deriving Eqs. (120) and (121), the state vectors describing the radiation fields have been assumed to be coherent laser states, and so, for example, $\langle q_2\rangle = \langle\alpha^{(2)}|\hat{n}|\alpha^{(2)}\rangle$, where $|\alpha^{(2)}\rangle$ is the coherent state representing mode 2 and $\hat{n}$ is the number operator; a similar expression may be written for $\langle q_3\rangle$. Also, the molecular parameters apparent in Eqs. (120) and (121) are the components of the transition dipole, μ_i^{10}, and the index-symmetric second-order molecular transition tensor, $\alpha_{(ij)}^{10}(\omega,\omega)$.

The rate at which the excited state is populated is once again given by recourse to the Golden Rule [Eq. (51)] and clearly three contributions are apparent:

$$\Gamma = \frac{2\pi}{\hbar}|M_{fi}^{(\xi)}|^2\rho_F^{(1)} = \Gamma_1 + \Gamma_2 + \Gamma_3 \tag{122}$$

where

$$\Gamma_1 = \frac{2\pi\rho_F^{(1)}}{\hbar}\left(\frac{\hbar v_g \omega_k}{2c\varepsilon_0 V n_{\omega_k}}\right)^2 \left(\frac{n_{\omega_k}^2+2}{3}\right)^4 \langle q_2\rangle\langle(q_2-1)\rangle|\alpha_{(ij)}^{(10)} e_i^{(2)} e_j^{(2)}|^2 \tag{123}$$

$$\Gamma_2 = \frac{2\pi\rho_F^{(1)}}{\hbar}\left\{ -i\left(\frac{\hbar v_g \omega_k}{2c\varepsilon_0 V n_{\omega_k}}\right)\left(\frac{n_{\omega_k}^2+2}{3}\right)^2 \left(\frac{\hbar v'_g \omega'_{k'}}{2c\varepsilon_0 V n_{\omega'_{k'}}}\right)^{1/2}\left(\frac{n_{\omega'_{k'}}^2+2}{3}\right) \right. \tag{124}$$

$$\left. \sqrt{\langle q_3\rangle\langle q_2\rangle\langle(q_2-1)\rangle}\,\alpha_{(ij)}^{10}\bar{\mu}_k^{10} e_i^{(2)} e_j^{(2)} \bar{e}_k^{(3)}\, e^{i(2\mathbf{k}_2-\mathbf{k}_3)\cdot\mathbf{R}_\xi} + \text{c.c}\right\}$$

and

$$\Gamma_3 = \frac{2\pi\rho_F^{(1)}}{\hbar}\left(\frac{\hbar v'_g \omega'_{k'}}{2c\varepsilon_0 V n_{\omega'_{k'}}}\right)\left(\frac{n_{\omega_k}^2+2}{3}\right)^2 \langle q_3\rangle|\mu_i^{10} e_i^{(3)}|^2 \tag{125}$$

As the transition is to a particular molecular electronic manifold, we have utilized the convenient density of states representation in the expressions. We see that the rate at which the exited state is populated depends on the position of the molecule, through Γ_2—and also on the molecular orientation, through the matrix elements. It is this Γ_2 term that produces the grating within the sample. We note here that the periodicity of the grating, determined by $e^{i(2\mathbf{k}_2-\mathbf{k}_3)\cdot\mathbf{R}_\xi} \equiv e^{-i(2\mathbf{k}_1+\mathbf{k}_3)\cdot\mathbf{R}_\xi}$, is exactly that required for phase-matched second-harmonic generation from the probe beam, where the signal is created in precisely the opposite direction to the harmonic pump beam.

Thus far we have a position-dependent rate $\Gamma(\mathbf{R}_\xi)$ at which the upper state is populated during application of the two writing beams. If we take the effective time for which the beams are applied as Δt, the probability that molecule ξ is excited immediately after the pulses have passed is $P(\mathbf{R}_\xi) = \Gamma(\mathbf{R}_\xi)\Delta t$. The probe pulse arrives after a delay of $\tau(>\Delta t)$ seconds, during which time the molecule, if excited, may relax. We suppose that it relaxes to the ground state via a simple exponential decay. At time τ the probability that the molecule is excited is hence

$$P(\mathbf{R}_\xi, \tau) = \Gamma(\mathbf{R}_\xi)\Delta t\, e^{-k_{10}(\tau-\Delta t)} \tag{126}$$

where k_{10} is the decay constant. It is useful to assume that the molecules remain clamped in between light pulses, so that we can ignore any movement (rotational or translational) that may occur during these finite periods. This physically reasonable assumption is primarily made for calculational expediency; it may be

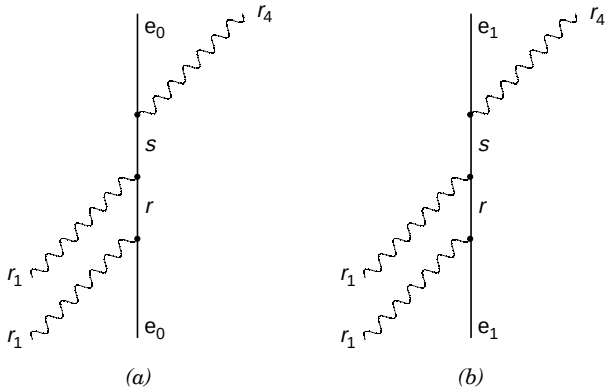

Figure 17. Representative time-ordered diagrams illustrating the harmonic formation from molecules in (a) the ground electronic state e_0 and (b) the excited state e_1.

dispensed with, but only at the cost of substantially increased complexity [93]. This means that the probe pulse encounters the associated population distribution in the sample and the harmonic is then produced from it. Again two possibilities arise, as illustrated in Fig. 17 (in which only the dominant of three contributory time orderings is shown). Writing as $M_{fi}'^{(\xi,a)}$ and $M_{fi}'^{(\xi,b)}$ the quantum-optical matrix elements for these component processes, the effective matrix element for harmonic production will be

$$M_{fi}'^{(\xi)} = \big(1 - P(\mathbf{R}_\xi, \tau)\big) M_{fi}'^{(\xi,a)} + P(\mathbf{R}_\xi, \tau) M_{fi}'^{(\xi,b)} \tag{127}$$

reflecting a statistical weighting of the appropriate quantum amplitudes. For a two-level system, Eq. (127) is exact, and follows from use of the completeness relation for the molecular states. The two components involved in the harmonic generation process are, in fact, identical in terms of the photonics, differing only in their molecular mediation, and so we have

$$\begin{aligned} M_{fi}'^{(\xi,a)} = {} & -i\left(\frac{\hbar \nu_g \omega_k}{2c\varepsilon_0 V n_{\omega_k}}\right)\left(\frac{n_{\omega_k}^2 + 2}{3}\right)^2 \left(\frac{\hbar \nu_g' \omega_{k'}'}{2c\varepsilon_0 V n_{\omega_{k'}'}}\right)^{1/2} \left(\frac{n_{\omega_{k'}'}^2 + 2}{3}\right) \\ & \times \sqrt{\langle q_1 \rangle (\langle q_1 \rangle - 1)}\, \beta_{i(jk)}^{00} \bar{e}_i^{(4)} e_j^{(1)} e_k^{(1)}\, e^{i(-2\mathbf{k}_2 + \mathbf{k}_3)\cdot \mathbf{R}_\xi} \end{aligned} \tag{128}$$

and

$$\begin{aligned} M_{fi}'^{(\xi,b)} = {} & -i\left(\frac{\hbar \nu_g \omega_k}{2c\varepsilon_0 V n_{\omega_k}}\right)\left(\frac{n_{\omega_k}^2 + 2}{3}\right)^2 \left(\frac{\hbar \nu_g' \omega_{k'}'}{2c\varepsilon_0 V n_{\omega_{k'}'}}\right)^{1/2} \left(\frac{n_{\omega_{k'}'}^2 + 2}{3}\right) \\ & \times \sqrt{\langle q_1 \rangle (\langle q_1 \rangle - 1)}\, \beta_{i(jk)}^{11} \bar{e}_i^{(4)} e_j^{(1)} e_k^{(1)}\, e^{i(-2\mathbf{k}_2 + \mathbf{k}_3)\cdot \mathbf{R}_\xi} \end{aligned} \tag{129}$$

where $\langle q_1 \rangle$ is the mean number of photons in mode r_1. The index-symmetric hyperpolarizbilities are exactly as those given in previous sections (where the upper level was designated u). They are distinguished by the fact that the harmonic stems from the labeled states 0 and 1, respectively; as before, the repeated superscripts indicate that the molecules return to their initial state following the interaction. As shown in the last section, a two-level model would require that the hyperpolarizability of the upper level be precisely minus that of the ground state, as in Eq. (96). In the SWM systems of experimental interest, the two-level model is too restrictive; however, it can certainly be anticipated that the upper- and lower-level hyperpolarizabilities will substantially differ, a feature that proves crucial for the following analysis.

To continue, we now compile the total matrix element for SHG from the ensemble through

$$M'_{fi} = -i\left(\frac{\hbar \nu_g \omega_k}{2c\varepsilon_0 V n_{\omega_k}}\right)\left(\frac{n^2_{\omega_k}+2}{3}\right)^2\left(\frac{\hbar \nu'_g \omega'_{k'}}{2c\varepsilon_0 V n_{\omega'_{k'}}}\right)^{1/2}\left(\frac{n^2_{\omega'_{k'}}+2}{3}\right)$$
$$\times \sqrt{\langle q_1\rangle(\langle q_1\rangle - 1)}\bar{e}^{(4)}_i e^{(1)}_j e^{(1)}_k \sum_{\xi}\{\beta^{00}_{i(jk)} + P(\mathbf{R}_\xi, \tau)\Delta\beta_{i(jk)}\}\, e^{i(-2\mathbf{k}_2+\mathbf{k}_3)\cdot\mathbf{R}_\xi} \tag{130}$$

where the difference in the hyperpolarizabilities between the upper and lower states has been written

$$\Delta\beta_{i(jk)} = \beta^{11}_{i(jk)} - \beta^{00}_{i(jk)} \tag{131}$$

The rate of production of SHG from the ensemble given by the Golden Rule is

$$R = \frac{2\pi\rho^{(2)}_F}{\hbar}\left|\sum_{\xi} M'^{(\xi)}_{fi}\right|^2$$

where $\rho^{(2)}_F$ is the density of states for the second (reading) process. Taking an orientational average and effecting the usual split into incoherent (single site) and coherent (multi-site interference) terms, we have

$$\langle R\rangle = \frac{2\pi\rho^{(2)}_F}{\hbar}\left\langle \sum_{\xi}|M'^{(\xi)}_{fi}|^2 + \sum_{\xi\neq\xi'} M'^{(\xi)}_{fi}\bar{M}'^{(\xi')}_{fi}\right\rangle$$

The dominant contribution to SHG is hence the coherent term

$$R_{\text{coh}} = \frac{2\pi\rho^{(2)}_F}{\hbar}\sum_{\xi\neq\xi'}\langle M'^{(\xi)}_{fi}\rangle\langle \bar{M}'^{(\xi')}_{fi}\rangle \tag{132}$$

where we have assumed that differing molecules in the solution are orientationally uncorrelated, as is the case for the majority of pairs in the

system. For any one particular molecule, one can simply employ Eq. (130), excluding the sum over ξ. Referring back to that equation and effecting the orientational average for individual molecules leads to disappearance of the first term within the parenthesis, as is usual for SHG in isotropic media. The second term, however, contains "hidden" orientational factors through $P(\mathbf{R}_\xi, \tau)$, as a result of which the average is nonzero. Using Eq. (126) we thus have

$$\langle \Gamma(\mathbf{R}_\xi)\Delta t\, e^{-k_{10}(\tau-\Delta t)}\Delta\beta_{i(jk)}\rangle = \langle(\Gamma_1+\Gamma_2+\Gamma_3)\Delta\beta_{i(jk)}\rangle\Delta t\, e^{-k_{10}(\tau-\Delta t)} \tag{133}$$

Of the three contributory terms, it is Γ_2 that is responsible for the observed signal, as it is the only term to exhibit the necessary phase matching when inserted into Eq. (130). We thus ignore the other two terms in (133). The assumption is justified by experiments where no SHG signal is observed if either of the writing beams r_2 or r_3 is blocked [106]. Using the Γ_2 term in Eq. (133), we now find

$$\begin{aligned}\langle \Gamma(\mathbf{R}_\xi)\Delta t\, e^{-k_{10}(\tau-\Delta t)}\Delta\beta_{i(jk)}\rangle = {} & i\frac{2\pi\rho_F^{(1)}}{\hbar}\left(\frac{\hbar\nu_g\omega_k}{2c\varepsilon_0 V n_{\omega_k}}\right)\left(\frac{n_{\omega_k}^2+2}{3}\right)^2\left(\frac{\hbar\nu'_g\omega'_{k'}}{2c\varepsilon_0 V n_{\omega'_{k'}}}\right)^{1/2}\\ & \times\left(\frac{n_{\omega'_{k'}}^2+2}{3}\right)[\langle q_3\rangle\langle q_2\rangle(\langle q_2\rangle-1)]^{1/2}\\ & \times\langle\{\alpha_{(lm)}^{10}\bar{\mu}_n^{10}e_l^{(2)}e_m^{(2)}\bar{e}_n^{(3)}\, e^{i(2\mathbf{k}_2-\mathbf{k}_3)\cdot\mathbf{R}_\xi}+\text{c.c.}\}\\ & \times\Delta\beta_{i(jk)}\rangle\Delta t\, e^{-k_{10}(\tau-\Delta t)}\end{aligned}$$

with the exponential explicitly exhibiting the phase-matching (and the complex conjugate term accounting for the fact that SHG can be produced from a fundamental beam propagating in the opposite direction, as also observed experimentally). The phase-matched, orientationally averaged matrix element is hence

$$\begin{aligned}\langle M_{fi}'^{(\xi)}\rangle = {} & \frac{\pi\rho_F^{(1)}}{\hbar}\left(\frac{\hbar\nu_g\omega_k}{2c\varepsilon_0 V n_{\omega_k}}\right)^2\left(\frac{n_{\omega_k}^2+2}{3}\right)^4\left(\frac{\hbar\nu'_g\omega'_{k'}}{2c\varepsilon_0 V n_{\omega'_{k'}}}\right)\left(\frac{n_{\omega'_{k'}}^2+2}{3}\right)^2\\ & \times\sqrt{\langle q_3\rangle\langle q_2\rangle(\langle q_2\rangle-1)\langle q_1\rangle(\langle q_1\rangle-1)}\\ & \times\langle\alpha_{(lm)}^{10}\bar{\mu}_n^{10}\Delta\beta_{i(jk)}\rangle e_l^{(2)}e_m^{(2)}\bar{e}_n^{(3)}\bar{e}_i^{(4)}e_j^{(1)}e_k^{(1)}\Delta t\, e^{-k_{10}(\tau-\Delta t)}\end{aligned} \tag{134}$$

which is necessarily position-independent, so that the phase-matching double sum in Eq. (132) can be evaluated for the ensemble of N molecules as $N(N-1)\approx N^2$ for large N. The resulting rate of SHG production is

$$\begin{aligned}R_{\text{coh}} = {} & \frac{2\pi^3(\rho_F^{(1)})^2\rho_F^{(2)}}{\hbar^3}(N\,\Delta t)^2\left(\frac{\hbar\nu_g\omega_k}{2c\varepsilon_0 V n_{\omega_k}}\right)^4\left(\frac{n_{\omega_k}^2+2}{3}\right)^8\left(\frac{\hbar\nu'_g\omega'_{k'}}{2c\varepsilon_0 V n_{\omega'_{k'}}}\right)^2\left(\frac{n_{\omega'_{k'}}^2+2}{3}\right)^4\\ & \times\langle q_3\rangle\langle q_2\rangle(\langle q_2\rangle-1)\langle q_1\rangle(\langle q_1\rangle-1)\\ & \times|\langle\alpha_{(lm)}^{10}\bar{\mu}_n^{10}\Delta\beta_{i(jk)}\rangle e_l^{(2)}e_m^{(2)}\bar{e}_n^{(3)}\bar{e}_i^{(4)}e_j^{(1)}e_k^{(1)}|^2\, e^{-2k_{10}(\tau-\Delta t)}\end{aligned} \tag{135}$$

Casting the result in terms of the mean intensities of the beams, with $\omega'_{k'} \equiv 2\omega_k$, the final expression for coherent SHG from the grating may be written as

$$I_{\text{sig}}^{(2\omega)} = \frac{(\rho_F^{(1)})^2 (k') g_1^{(2)} g_2^{(2)} (N\,\Delta t)^2}{256\hbar^2 c^5 \varepsilon_0^6} (I_1^{(\omega)} I_2^{(\omega)})^2 I_3^{(2\omega)} \times |\langle \alpha_{(lm)}^{10} \bar{\mu}_n^{10} \Delta\beta_{i(jk)} \rangle e_l^{(2)} e_m^{(2)} \bar{e}_n^{(3)} \bar{e}_i^{(4)} e_j^{(1)} e_k^{(1)}|^2 e^{-2k_{10}(\tau-\Delta t)} \tag{136}$$

where $I_n^{(\omega)}$ is the mean intensity of the nth beam of frequency ω and $g_n^{(2)}$ is its degree of second-order coherence. Equation (136) thus exhibits the correct dependence on the intensities of the three input beams (quadratic with respect to the two fundamental beams and linear in the harmonic writing beam) and also the sample density ($I_{\text{sig}}^{(2\omega)} \propto N^2$). Dynamically this equation yields a simple exponential decay due to relaxation of the molecules from the excited to ground state; the timescale for the decay is therefore governed by the intrinsic fluorescence lifetime.

The polarization dependence of Eq. (136) is exactly that found previously for the case of coincident pulses, represented herein as Eq. (111). It is therefore interesting to compare the two results and their respective dependences on the molecular tensor components. Evaluating the sixth-rank average for Eq. (136), we find

$$\langle I_{\text{sig}}^{(2\omega)} \rangle = \frac{(\rho_F^{(1)})^2 (k')^3 g_1^{(2)} g_2^{(2)} (N\Delta t)^2}{256\hbar^2 c^5 \varepsilon_0^6} (I_1^{(\omega)} I_2^{(\omega)})^2 I_3^{(2\omega)} \left| \frac{1}{105} \sum_{i=1}^{6} E_i A'_1 \right|^2 e^{-2k_{10}(\tau-\Delta t)} \tag{137}$$

where the modified linear matrix $\mathbf{A}'$ now contains a molecular response through

$$\begin{bmatrix} A'_1 \\ A'_2 \\ A'_3 \\ A'_4 \\ A'_5 \\ A'_6 \end{bmatrix} = \begin{bmatrix} 8 & -5 & -5 & 4 & 4 & 5 \\ -5 & 11 & 4 & -6 & -6 & 4 \\ -5 & 4 & 11 & -6 & -6 & 4 \\ 4 & -6 & -6 & 16 & 2 & -6 \\ 4 & -6 & -6 & 2 & 16 & -6 \\ -5 & 4 & 4 & -6 & -6 & 11 \end{bmatrix} \begin{bmatrix} \bar{\mu}_\gamma^{10} \alpha_{(\beta\beta)}^{10} \Delta\beta_{\gamma(\alpha\alpha)} \\ \bar{\mu}_\beta^{10} \alpha_{(\beta\gamma)}^{10} \Delta\beta_{\gamma(\alpha\alpha)} \\ \bar{\mu}_\gamma^{10} \alpha_{(\alpha\beta)}^{10} \Delta\beta_{\gamma(\alpha\beta)} \\ \bar{\mu}_\beta^{10} \alpha_{(\alpha\gamma)}^{10} \Delta\beta_{\gamma(\alpha\beta)} \\ \bar{\mu}_\gamma^{10} \alpha_{(\alpha\gamma)}^{10} \Delta\beta_{\beta(\alpha\beta)} \\ \bar{\mu}_\alpha^{10} \alpha_{(\gamma\gamma)}^{10} \Delta\beta_{\beta(\alpha\beta)} \end{bmatrix} \tag{138}$$

The linear matrix $\mathbf{E}$ is exactly that as previously defined, in Eq. (113). The polarization characteristics are similar *in form* to those of the coincident-pulse case. Hence, although one would not expect them to be exactly the same because

of their different dependence on molecular properties, polarization analysis is unlikely to unambiguously differentiate the contributory mechanisms. The latest analysis shows experimental results exactly in agreement with this theory [93].

XV. CONCLUSION

In this review we have described some of the advances in the quantum electrodynamical formulation of theory for molecular photonics. We have shown how the framework described in an earlier review has now been extended to new areas of application, and reformulated for application to real dispersive media—as reflected in the new treatment of refractive, dissipative, and resonance properties. With all its conceptual splendor, conventional quantum optics has not generally been pursued at this level of detail on its dielectric host, and it is our hope that this work will help match its precepts with quantitative accuracy. Applications of the new theory have revealed new quantum optical features in two quite different aspects of the familiar process of second harmonic generation, one operating through local coherence within small particles and the other, a coherence between the quantum amplitudes for fundamental and harmonic excitation. Where the salient experiments have been performed, they exactly match the theoretical predictions. The theoretical foundation we have discussed therefore shows promise for the delivery of accurate insights into other optical processes yet to be characterized, and it should be well placed to facilitate the determination of meaningful data from the associated experiments.

Acknowledgments

We are pleased to acknowledge helpful comments and insights from friends and colleagues at various stages of preparing this review, and especially from Robert Jenkins, Gediminas Juzeliunas, Geoff Stedman, and T. Thirunamachandran.

References

1. D. L. Andrews, *Modern Nonlinear Optics*, in M. Evans and S. Kielich (Eds.), *Adv. Chem. Phys.* **85** (Part 2), 545–606.
2. T. Kinoshita, *Quantum Electrodynamics*, World Scientific, River Edge, NJ 1990.
3. E. A. Power, *Introductory Quantum Electrodynamics*, Longmans, London, 1964.
4. S. Haroche, in J. Dalibard, J.-M. Raimond and J. Zinn-Justin (Eds.), *Fundamental Systems in Quantum Optics*, Elsevier, Amsterdam, 1992.
5. P. W. Milonni, *The Quantum Vacuum*, Academic, San Diego, 1994.
6. G. Compagno, R. Passante, and F. Persico, *Atom-Field Interactions and Dressed Atoms*, Cambridge Univ. Press, 1995.
7. S. M. Barnett, A. Aspect, and P. W. Milonni, *J. Phys. B*, *Atom. Mol. Opt. Phys.* **33**, L143–L149 (2000).
8. V. Chernyak and S. Mukamel, *J. Chem. Phys.* **100**, 2953–2974 (1994).
9. D. L. Andrews and P. Allcock, *Chem. Soc. Rev.* **24**, 259–265 (1995).

10. G. Juzeliunas and D. L. Andrews, *Adv. Chem. Phys*. **112**, 357–410 (2000).
11. G. E. Stedman, private communication, 2000.
12. P. W. Milonni, in S. Diner, D. Fargue, G. Lochak, and F. Selleri (Eds.), *The Wave-Particle Dualism*, Reidel, Dordrecht, 1984.
13. R. G. Woolley, *Int. J. Quantum Chem*. **74**, 531–545 (1999).
14. R. G. Woolley, (a) *Proc. Roy. Soc. Lond*. **A456**, 1803–1819; 2000; (b) R. G. Woolley, private communication, 2000.
15. D. P. Craig and T. Thirunamachandran, *Molecular Quantum Electrodynamics* Academic, London, 1984.
16. B. J. Dalton, E. S. Guerra, and P. L. Knight, *Phys. Rev. A* **54**, 2292–2313 (1996).
17. M. Göppert-Mayer, *Ann. Physik* **9**, 273–294 (1931).
18. E. A. Power and S. Zienau, *Phil. Trans. Roy. Soc. Lond. Ser. A* **251**, 427–454 (1959).
19. R. G. Woolley, *Proc. Roy. Soc. Lond*. **A321**, 557–572 (1971).
20. M. Babiker, E. A. Power, and T. Thirunamachandran, *Proc. Roy. Soc. Lond*. **A338**, 235–249 (1974).
21. E. A. Power and T. Thirunamachandran, *Am. J. Phys*. **46**, 370–378 (1980).
22. E. A. Power and T. Thirunamachandran, *Phys. Rev. A* **60**, 4936–4942 (1990).
23. B. J. McKenzie and G. E. Stedman, *J. Phys. C*, *Solid State Phys*. **12**, 5062–5075 (1970).
24. S. Naguleswaran, Ph.D. thesis, Univ. Canterbury, NZ, 1998.
25. G. Juzeliunas and D. L. Andrews, *Phys. Rev. B* **49**, 8751–8763 (1994).
26. P. W. Milonni, *J. Mod. Opt*. **42**, 1991–2004 (1995).
27. G. Juzeliunas, *Phys. Rev. A* **53**, 3543–3558 (1996).
28. C. Cohen-Tannoudji, J. Dupont-Roc, and G. Grynberg, *Atom-Photon Interactions*, Wiley, London, 1992.
29. S. Mukamel, *Principles of Nonlinear Optical Spectroscopy*, Oxford Univ. Press, Oxford, 1995.
30. L. C. Davila-Romero, Ph.D. thesis, Univ. East Anglia, 1999.
31. P. O. Löwdin, in C. H. Wilcox (Ed.), *Perturbation Theory and Its Applications in Quantum Mechanics*, Wiley, New York, 1965.
32. E. Fermi, *Nuclear Physics*, Univ. Chicago Press, Chicago, 1950.
33. P. A. M. Dirac, *The Principles of Quantum Mechanics*, Clarendon Press, Oxford, 1958.
34. L. I. Schiff, *Quantum Mechanics*, 3rd ed., McGraw-Hill, New York, 1968.
35. R. D. Jenkins and D. L. Andrews, *J. Phys. Chem. A* **102**, 10834–10842 (1998).
36. W. H. Louisell, *Quantum Statistical Properties of Radiation*, Wiley, New York, 1973, pp. 104–109.
37. R. Loudon, *The Quantum Theory of Light*, 2nd ed., Clarendon, Oxford, 1983.
38. D. Marcuse, *Principles of Quantum Electronics*, Academic, New York, 1980.
39. D. L. Andrews, *J. Phys. B*, *Atom. Mol. Phys*. **11**, 2655–2664 (1978).
40. J. M. Manley and H. E. Rowe, *Proc. Inst. Radio Eng*. **47**, 2115–2116 (1959).
41. H. Haken, *Laser Theory*, Springer, Berlin, 1984, p. 91.
42. D. M. Bishop and D. W. DeKee, *J. Chem. Phys*. **104**, 9876–9887 (1996).
43. G. Wagnière, *Appl. Phys. B* **41**, 169–172 (1986).
44. D. S. Elliott and J. F. Ward, *Mol. Phys*. **51**, 45–63 (1984).
45. D. M. Bishop, *Rev. Mod. Phys*. **62**, 343–374 (1990).

46. D. M. Bishop and B. Kirtman, *J. Chem. Phys*. **95**, 2646–2658 (1991).
47. Q. L. Zhou, J. R. Heflin, K. Y. Wong, O. Zamani-Khamiri, and A. F. Garito, *Phys. Rev. A* **43**, 1673–1676 (1991).
48. J. R. Heflin, D. C. Rodenberger, R. F. Shi, M. Wu, N. W. Wang, Y. M. Cai, and A. F. Garito, *Phy. Rev. A.* **45**, R4233–R4236 (1992).
49. D. C. Rodenberger, J. R. Heflin, and A. F. Garito, *Nature* **359**, 309–311 (1992).
50. D. L. Andrews, S. Naguleswaran, and G. E. Stedman, *Phys. Rev. A* **57**, 4925–4929 (1998).
51. A. D. Buckingham and P. Fischer, *Phys. Rev. A* **61**, 035801 (2000).
52. G. E. Stedman, S. Naguleswaran, D. L. Andrews, and L. C. Dávila-Romero, *Phys. Rev. A* **63**, 047801 (2001).
53. N. Bloembergen, Nonlinear Optics, Benjamin, New York, 1965.
54. D. C. Hanna, M. A. Yuratich, and D. Cotter, *Nonlinear Optics of Free Atoms and Molecules*, Springer, Berlin, 1979.
55. Y. R. Shen, *The Principles of Nonlinear Optics*, Wiley-Interscience, New York, 1984.
56. J. Berger, *Eur. J. Phys*. **11**, 155–159 (1990).
57. L. C. Dávila-Romero, S. Naguleswaran, G. E. Stedman, and D. L. Andrews, *Nonlin. Opt*. **23**, 191–201 (2000).
58. D. A. Kleinman, *Phys. Rev*. **126**, 1977–1979 (1962).
59. R. Wortmann, P. Krämer, C. Glania, S. Lebus, and N. Detzer, *Chem. Phys*. **173**, 99–108 (1993).
60. D. L. Andrews, *Spectrochim. Acta* **46A**, 871–885 (1990).
61. D. L. Andrews, *J. Phys. B, Atom. Mol. Phys*. **13**, 4091–4099 (1980).
62. D. L. Andrews and N. P. Blake, *Phys. Rev. A* **38**, 3113–3115 (1988).
63. G. E. Stedman, *Modern Nonlinear Optics*, in M. Evans and S. Kielich (Eds.), *Adv. Chem. Phys*. **85** (Part 2), 489–543.
64. G. X. Cao and D. Zhu, *Phys. Rev. B* **51**, 2418–2426 (1995).
65. N. Bloembergen, and Y. R. Shen, *Phys. Rev*. **133**, A37–A49 (1964).
66. D. L. Andrews and W. J. Meath, *J. Phys. B, Atom. Mol. Phys*. **28**, 4633–4641 (1993).
67. J. L. Oudar and D. S. Chemla, *J. Chem. Phys*. **66**, 2664–2668 (1977).
68. B. Dick and G. Hohlneicker, *J. Chem. Phys*. **76**, 5755–5760 (1982).
69. W. J. Meath and E. A. Power, *Mol. Phys*. **51**, 585–600 (1984a).
70. W. J. Meath and E. A. Power, *J. Phys. B, Atom. Mol. Phys*. **17**, 763–781 (1984b).
71. D. L. Andrews and P. Allcock, *Chem. Phys. Lett*. **231**, 206–210 (1994).
72. A. J. Sadlej and P. W. Fowler, *Chem. Phys. Lett*. **245**, 59–65 (1995).
73. S. Leasure and R. E. Wyatt, *Chem. Phys. Lett*. **61**, 625–629 (1979).
74. M. A. Kmetic and W. J. Meath, *Phys. Lett. A* **108**, 340–343 (1985).
75. A. E. Kondo, W. J. Meath, S. H. Nilar, and A. J. Thakkar, *Chem. Phys*. **186**, 375–394 (1994).
76. P. Tran, W. J. Meath, B. D. Wagner, and R. P. Steer, *J. Chem. Phys*. **100**, 4165–4170 (1994).
77. B. N. Jagatap and W. J. Meath, *Chem. Phys. Lett*. **258**, 293–300 (1996).
78. K. A. Brueckner, *Phys. Rev*. **100**, 36–55 (1955).
79. D. M. Bishop, *J. Chem. Phys*. **100**, 6535–6542 (1994).
80. D. L. Andrews, L. C. Dávila Romero, and W. J. Meath, *J. Phys. B, Atom. Mol. Opt. Phys*. **32**, 1–17 (1999).

81. G. Juzeliunas, L. C. Dávila Romero, and D. L. Andrews, work in progress.
82. Q. Song, C. Wan, and C. K. Johnson, *J. Phys Chem*. **98**, 1999–2001 (1994).
83. P. K. Schmidt and G. W. Rayfield, *Appl. Opt*. **33**, 4286–4292 (1994).
84. D. L. Andrews, P. Allcock, and A. A. Demidov, *Chem. Phys*. **190**, 1–9 (1995).
85. P. Allcock, D. L. Andrews, S. R. Meech, and A. J. Wigman, *Phys. Rev. A* **53**, 2788–2791 (1996).
86. D. L. Andrews and L.C. Dávila Romero, *Proc. SPIE* **4098**, 284–293 (2000).
87. D. L. Andrews, *Nonlin. Opt.* **8**, 25–32 (1994).
88. J. M. Nunzi, F. Charra, C. Fiorini, and J. Zyss, *Chem. Phys. Lett*. **219**, 349–354 (1994).
89. C. Fiorini, F. Charra, and J.-M. Nunzi, *J. Opt. Soc. Am. B* **11**, 2347–2358 (1994).
90. C. Fiorini, J.-M. Nunzi, F. Charra, I. D. W. Samuel, and J. Zyss, *Int. J. Nonlin. Opt. Phys*. **5**, 653–670 (1996).
91. P. Allcock and D. L. Andrews, *J. Phys. B, Atom. Mol. Opt. Phys*. **30**, 3731–3742 (1997).
92. I. D. Hands, S. J. Lin, S. R. Meech, and D. L. Andrews, *J. Chem. Phys*. **109**, 10580–10586 (1998).
93. I. D. Hands, S. J. Lin, S. R. Meech, and D. L. Andrews, *Phys. Rev. A* **62**, 023807 (2000).
94. S. Lin, I. D. Hands, D. L. Andrews, and S. R. Meech, *J. Phys. Chem. A* **103**, 3830–3836 (1999).
95. S. Lin, I. D. Hands, D. L. Andrews, and S. R. Meech, *Opt. Commun*. **174**, 285–290 (2000).
96. S. Naguleswaran and G. E. Stedman, *J. Phys. B, Atom. Mol. Opt. Phys*. **29**, 4027–4040 (1996).
97. D. L. Andrews and T. Thirunamachandran, *J. Chem. Phys*. **67**, 5026–5033 (1977).
98. C. L. Tang and H. Rabin, *Phys. Rev. B* **3**, 4025–4034 (1971).
99. Y. Sasaki and Y. Ohmori, *Appl. Phys. Lett*. **39**, 466–468 (1981).
100. U. Österberg and W. Margulis, *Opt. Lett*. **11**, 516–518 (1986).
101. R. H. Stolen and H. W. K. Tom, *Opt. Lett*. **12**, 585–587 (1987).
102. N. B. Baranova and B. Ya. Zel'dovich, *JETP Lett*. **45**, 717–720 (1987).
103. B. Ya. Zel'dovich and Yu. E. Kapitskii, *JETP Lett*. **51**, 441–444 (1990).
104. T. J. Driscoll and N. M. Lawandy, *J. Opt. Soc. Am. B* **11**, 355–371 (1994).
105. N. B. Baranova and B. Ya. Zel'dovich, *J. Opt. Soc. Am. B*, *Opt. Phys*. **8**, 27–32 (1991).
106. S. R. Meech, private communication, 2000.
D. L. Andrews and P. Allcock, *J. Phys. B*, *Atom. Mol. Opt. Phys*. **30**, 3731–3742 (1997).

SYMMETRY IN ELECTRODYNAMICS: FROM SPECIAL TO GENERAL RELATIVITY, MACRO TO QUANTUM DOMAINS

MENDEL SACHS

Department of Physics, State University of New York at Buffalo, Buffalo, New York

CONTENTS

This chapter is based on the part of my research program in general relativity on electromagnetism. Most of it has been published, since the late 1950s, and is referred to in the bibliography. The analysis of the theory of electromagnetism based on its underlying symmetry in relativity theory is reassembled here with added discussion.

1. INTRODUCTION

An important lesson from Einstein's theory of relativity is that the underlying symmetry of any scientific theory reveals many far-reaching physical implications that are not obvious at first glance. In regard to the subject of electrodynamics and its unification with optics, the initially discovered relations in the nineteenth century, between electrical charges and their motions and the resulting electric and magnetic fields of force, led to a set of partial differential equations for the laws of electrodynamics. The formalism was not completed until Maxwell saw the need, *based on symmetry*, for an extra term in the equation that relates current density to a resulting magnetic field. His addition of the extra term, called "displacement current," then yielded the full expression of "Maxwell's equations." The latter were recognized as the laws of electrodynamics, which were then seen to incorporate the laws of optics.

Indeed, it was Maxwell's generalization of the laws of electrodynamics that revealed that the radiation solutions of these equations, which would not have appeared in the earlier version (without the displacement current term) predicted all the known optical phenomena. After Maxwell's investigation of these optical implications of electrodynamics, other portions of the spectrum of radiation solutions were predicted and discovered empirically: radiowaves, X- rays, infrared radiation, and gamma rays. Thus, it was Maxwell's intuitive feeling for the need of symmetry in his laws of electrodynamics that led to the full unification of electrodynamics and optics in the expression of Maxwell's equations.

James Clerk Maxwell died in 1879, the same year that Albert Einstein was born. Sixteen years later Einstein recognized that Maxwell's equations are *covariant* with respect to the Lorentz transformations between relatively moving inertial frames of reference, that is, reference frames that are in constant relative motion in a straight line. Thus, Einstein recognized in 1895 that the laws of electrodynamics, expressed with Maxwell's field equations, must be in one-to-one correspondence in all possible inertial frames of reference, *from the view of any one of them* [1].

The set of transformations of the spacetime coordinates that project the laws of electrodynamics from any observer's reference frame to any other (continuously connected) inertial frame such that the laws remain unchanged is the *symmetry group* of the theory of special relativity. It was discovered that this is

the Poincaré group [2]. Einstein then asserted, 10 years later in 1905, that not only the laws of electrodynamics and optics, but *all* the laws of nature must be covariant under the transformations of the symmetry group of relativity theory. This is the assertion of "the theory of special relativity." It is a statement of the objectivity of the laws of nature regarding all possible inertial frames of reference [3].

In the next stage, Einstein generalized this symmetry rule to assert that all of the laws of nature must remain objective (covariant) with respect to transformations between frames of reference that are in arbitrary types of relative motion. This is the "theory of general relativity." As a first step, the theory of general relativity led to a new explanation for the phenomenon of gravitation, agreeing with the successful predictions of Newton's theory of universal gravitation, but predicting more effects not predicted by the classical theory. General relativity thereby superceded Newton's law of universal gravitation [4].

A significant feature of general relativity is the role of geometry in the mathematical representation of *all* of the laws of nature. For Einstein found that the Euclidean (flat) spacetime was not an adequate logic to represent the laws of interacting matter and radiation. Instead, he had to generalize to Riemannian (curved) spacetime geometry. The implication was that all the laws of nature, including the laws of electrodynamics and optics, must be field laws that are mapped in such a curved spacetime. Later on, in his quest for a unified field theory, Einstein did insist that one should exploit not only the geometric logic of the spacetime language but also its algebra. Here he referred to the underlying group of general relativity—which I have called "the Einstein group". In a 1945 article [5], Einstein said: "Every attempt to establish a unified field theory must start, in my opinion, from the group of transformations which is no less general than that of the continuous transformations of the four coordinates."

At the outset, then, it is important to recognize in our study of a generalization of the laws of electrodynamics based on the full symmetry of relativity theory that its covariance is in terms of a *continuous group* [6] (whether we refer to special relativity or to general relativity). Such a group does not admit the discrete reflections in space or time. Further, because of the requirement of incorporating laws of conservation of energy, momentum and angular momentum, in the flat spacetime limit of the theory, *Noether's theorem* prescribes that the transformations that define the covariance in relativity theory must be analytic [7]. In other words, the relativistically covariant solutions of the laws of nature must be regular (i.e., nonsingular) *everywhere* [8]. Such groups of continuous, analytic transformations (the Poincaré group for special relativity [2] and the Einstein group for general relativity) are *Lie groups* [9]. They prescribe the algebraic logic of the theory of relativity.

Section II includes an outline of the generalization of the vector potential of electromagnetic theory so as to include a gauge-invariant *pseudovector* part.

This is allowed because of the lack of reflection symmetry in the relativity groups. In Section III the full form of the equations of electrodynamics in terms of the irreducible representations of the Lie groups of relativity theory will be shown. It is a two-component spinor formalism that follows from a factorization of the standard vector representation of the Maxwell formalism. In Section IV the theory will be extended to its full form in general relativity. It will be shown that the 16-component quaternion metrical field equation emerges as a factorization of Einstein's (10-component) symmetric tensor field equations in general relativity, once the reflection symmetry elements are removed from the underlying covariance group. It is then demonstrated that these 16 independent field equations may be rewritten as a sum of 10 second-rank symmetric tensor equations, corresponding exactly with the Einstein field equations, plus 6 second-rank antisymmteric tensor equations. It is shown that the latter may be put into a form that corresponds exactly with the formal structure of Maxwell's equations. Thus, it is because of removing the reflection symmetry elements from the underlying group of general relativity, that one arrives at the factorized field equations that fully unify the gravitational features of matter, in terms of Einstein's field equations, with the electromagnetic features of matter in terms of the Maxwell field equations. The *route* toward achieving a unified field theory from general relativity is then to follow the rules of the underlying Lie group by removing the reflection symmetry elements from the symmetry group of Einstein's tensor field equations, thereby yielding a natural structure of the formalism in terms of spinor and quaternion variables. It will be seen in this analysis that, in accordance with a *generalized Mach principle* [10], the electromagnetic field of a charged body vanishes in a vacuum.

In Section V it will be shown that the quaternion structure of the fields that correspond to the electromagnetic field tensor and its current density source, implies a very important consequence for electromagnetism. It is that the local limit of the time component of the four-current density yields a *derived* normalization. The latter is the condition that was *imposed* (originally by Max Born) to interpret quantum mechanics as a probability calculus. Here, it is a derived result that is an asymptotic feature (in the flat spacetime limit) of a field theory *that may not generally be interpreted in terms of probabilities*. Thus, the derivation of the electromagnetic field equations in general relativity reveals, as a bonus, a natural normalization condition that is conventionally imposed in quantum mechanics.

II. A GENERALIZATION OF THE ELECTROMAGNETIC POTENTIAL

After the momentous discovery by C. S. Wu and her collaborators in 1957 that the weak interaction violates parity (spatial reflection) [11], I addressed the

question of whether there may be any empirical evidence for the violation of parity in the electromagnetic interaction [12]. It was thought that only the weak interaction violates space-reflection symmetry. But if, in the final analysis, there is a unified field theory in which the weak and the electromagnetic forces, as well as all of the other forces of nature, are manifestations of a single force field, then there is an implication in the experimental result of Wu et al. that the electromagnetic and the nuclear forces also violate space-reflection symmetry, as well as time reversal symmetry. Indeed, the *continuous group* that underlies relativity theory implies that *all* discrete symmetries must be excluded from the laws of nature.

At that time, in the 1950s, there was a problem whereby the calculations from quantum electrodynamics for the Lamb shift, $2S_{1/2} - 2P_{1/2}$ in the states of hydrogen, were not in exact agreement with the measurements. Thus it occurred to me that a small violation of parity symmetry in the electromagnetic interaction might be responsible for this discrepancy.

My investigation proceeded along the following lines [12]. The conventional coupling of an external electromagnetic potential field A_μ to an electrical four-current density of matter j^μ is in terms of the *scalar* interaction Lagrangian

$$L_{\text{int}}^{(s)} = j^\mu A_\mu = e\psi^{(e)+}\gamma^0\gamma^\mu\psi^{(e)}A_\mu \tag{1}$$

$\psi^{(e)}$ is the (four-component) bispinor electron field that solves the Dirac equation

$$[\gamma^\mu(\partial_\mu + ieA_\mu) + m]\psi^{(e)} = 0 \tag{2}$$

It is assumed here that the electromagnetic vector potential A_μ is a (polar) four-vector field. Thus the Lagrangian $L_{\text{int}}^{(s)}$ is a scalar function in space and time.

If parity should be violated, A_μ may be generalized by adding an (axial) pseudovector part, B_μ to A_μ. The Lagrangian then generalizes to a sum of a scalar part and a pseudoscalar part, $L_{\text{int}} = L_{\text{int}}^{(s)} + L_{\text{int}}^{(ps)}$, where the latter part, $e\psi^+\gamma^0\gamma^\mu\psi B_\mu$, is clearly a pseudoscalar function.

Then what is the source of B_μ in electromagnetic theory? Are there restrictions on A_μ that should also apply to B_μ? The answer is "yes"—it is the restriction of gauge invariance in order to yield a unique representation for the electric and magnetic field variables. Additionally, gauge invariance is the necessary and sufficient condition for the existence of conservation laws in the formalism—in this case the requirement of the conservation of electrical charge [13]. The latter follows from the continuity equation,

$$\partial^\mu j_\mu = 0 \tag{3}$$

The gauge covariance is in two parts: (l) gauge invariance of the first kind, that is, invariance of the formalism under the phase change $\psi \to \psi \exp(i\eta)$, where, at this stage, $\eta(x)$ is an arbitrary scalar field; and (2) gauge invariance of the second kind—applied to the vector potential, this is the change: $A_\mu \to A_\mu + ie\partial_\mu \eta$. The latter is the addition of a four-gradient of the scalar field η to the original potential A_μ. Applying these two types of gauge transformations to the Dirac equation (2) then leaves it covariant, thus, its form is left unchanged.

A. The Unique Form of B_μ

The form of the pseudovector potential B_μ that is gauge-invariant would be a field that effectively interchanges the roles of the electric and magnetic field variables in the interaction Hamiltonian that couples a charge q to external electric and magnetic fields. For such a form leaves the electromagnetic interaction with charged matter still dependent only on the electric and magnetic field variables, directly.

The idea is as follows. The electromagnetic field intensity solution of Maxwell's equations, expressed in terms of the four-dimensional curl of the vector potential, is

$$F_{\mu\nu} = \partial_\mu A_\nu - \partial_\nu A_\mu \tag{4}$$

where the antisymmetric second-rank tensor $F_{\mu\nu}$ is the combination of the electric and magnetic field variables, **E** and **H**, as follows: $F_{0k} = -F_{k0} = E_k$, $F_{jk} = -F_{kj} = H_n$ and $F_{\mu\mu} = 0$, where $j \neq k \neq n = 1, 2, 3$ and the "0" subscript is the time component. $F_{\mu\nu}$ are the solutions of Maxwell's equations:

$$\partial^\nu F_{\mu\nu} = 4\pi j_\mu, \quad \partial_{[\rho}, F_{\mu\nu]} = 0 \tag{5}$$

The bracket in the second equation in (5) denotes a cyclic sum, and we use units (henceforth in this article) with $c = 1$. Combining the definition of $F_{\mu\nu}$ as the four-dimensional curl of a 4 vector, as in Eq. (4), Maxwell's equations in terms of the vector potential are:

$$\Box A_\mu = 4\pi j_\mu \tag{6}$$

where $\Box$ is the D'Alembertian operator $\partial^2/\partial t^2 - \nabla^2$, and the vector potential is subject to the *Lorentz gauge*, $\partial^\mu A_\mu = 0$, which, in turn, corresponds to selecting the phase $\eta(x)$ to be a solution of the wave equation, $\Box\eta = 0$.

Since j_μ is a 4-vector field and $\Box$ is a scalar operator, it follows that A_μ is a (polar)vector field. Let us now choose the (axial) pseudovector field B_μ that accompanies A_μ so that 1) it satisfies the same Lorentz gauge as A_μ, that is, $\partial^\mu B_\mu = 0$, and it solves the field equation (that accompanies (6) for A_μ:

$$\Box B_\nu = -i\xi\left(\frac{4\pi}{2}\right)\varepsilon_{\mu\nu\lambda\rho}\int \partial_\rho j_\lambda \, dx_\mu \tag{7}$$

where $\varepsilon_{\mu\nu\lambda\rho}$ is the totally antisymmetric Levi–Civita symbol, with $\varepsilon_{0123} = +1$. ξ is an undertermined parameter at this stage of the analysis; it is, physically, a measure of the ratio of reflection nonsymmetric terms to the reflection-symmetric terms in the generalized four-potential expression of electrodynamics, as discussed above.

A solution of Eq. (7) that is compatible with the continuity equation, $\partial^\mu j_\mu = 0$, which in turn leads to the conservation of charge, is

$$B_\nu = -\left(\frac{i\xi}{2}\right)\int \varepsilon_{\mu\nu\lambda\rho}\partial_\rho A_\lambda \, dx_\mu \tag{8}$$

The integration above is defined to be an *indefinite line integral*. (It is, by definition, a function of the spacetime coordinates x, not dependent on limits in the line integral. For example, the line integral $\int x\, dx$ is *defined* here to be $x^2/2$). The integrand in Eq. (8) is the dual of the electromagnetic field tensor, $F_{\mu\nu} = \varepsilon_{\mu\nu\lambda\rho}F_{\lambda\rho}$; that is, it replaces the electric and magnetic field variables, $\mathbf{E} \leftrightarrow \mathbf{H}$. In terms of these variables, the pseudovector potential may be expressed as follows: $B_\nu = \{\mathbf{B}, B_0\}$, where

$$\mathbf{B} = \left(\frac{\xi}{2}\right)\int(\mathbf{H}\,dt + \mathbf{E}\times d\mathbf{r}), B_0 = \left(\frac{i\xi}{2}\right)\int \mathbf{H}\cdot d\mathbf{r} \tag{9}$$

B. The Case of Constant Fields

If $\mathbf{E}$ and $\mathbf{H}$ are constant fields (i.e., independent of the space and time coordinates), then they would come out of the integral signs in Eq. (9). With the reflection nonsymmetric Lagrangian density $L_{\text{int}} = j^\mu(A_\mu + B_\mu)$, Lagrange's equation of motion then reduces to the following equation of motion of a test body with charge q:

$$\frac{d\mathbf{p}}{dt} = \mathbf{F}_v + \mathbf{F}_{pv}$$

where $\mathbf{p}$ is the particle's momentum,

$$\mathbf{F}_v = q[\mathbf{E} + \mathbf{v}\times\mathbf{H}] \tag{10}$$

is the usual vector (polar) Lorentz force in electrodynamics and

$$\mathbf{F}_{pv} = -q\xi[\mathbf{H} - \mathbf{v}\times\mathbf{E}] \tag{11}$$

is a pseudovector (axial) contribution, which I have called the "anti-Lorentz force." The latter predicts that a charge q would move along the lines of the

magnetic field **H**. Even if the value of the parameter ξ should be extremely small, a very large magnitude of the magnetic field intensity **H**, say, in the interior or near a rotating galaxy, may make this prediction observable in astrophysical measurements. The second term in $\boldsymbol{F}_{pv}$ predicts a motion of a charge q in an external electric field **E** such that it would rotate perpendicularly to the plane of its velocity vector **v** and the imposed constant electric field **E**.

C. The Generalized Dirac Hamiltonian

The behavior of an electron in an electromagnetic field, in the context of the quantum theory, is determined from the solutions of the Dirac equation. Here the free-particle momentum operator is replaced with the generalized 4-momentum operator, $p_\nu + e(A_\nu + B_\nu)$. The Dirac equation then takes the form

$$\{\gamma^\nu(p_\nu + e(A_\nu + B_\nu) - im\}\psi = 0 \tag{12}$$

where $p_\nu = -i\partial_\nu$ (units are used with $h/2\pi = 1$) and the "Dirac matrices" are:

$$\gamma^\nu = \{\boldsymbol{\gamma}, \beta\}, \gamma = -i\beta\boldsymbol{\alpha},\ \gamma^4 = \beta$$

and $\boldsymbol{\alpha}, \beta$ are the 4×4 matrices defined in terms of the Pauli matrices: $\boldsymbol{\alpha}_{12} = \boldsymbol{\alpha}_{21} = \boldsymbol{\sigma}, \boldsymbol{\alpha}_{11} = \boldsymbol{\alpha}_{22} = 0,\ \beta_{11} = -\beta_{22} = I, \beta_{12} = \beta_{21} = 0, I$ is the unit 2-matrix, and $\gamma_\mu\gamma_\nu + \gamma_\nu\gamma_\mu = 2\delta_{\mu\nu}$ (where $\mu, \nu = 1, 2, 3, 4$).

The generalized Dirac equation was applied to the case of the hydrogen atom [14]. It was to investigate whether the added potential B_μ in the Dirac Hamiltonian in Eq. (12) would predict a contribution to the Lamb shift, exclusive of quantum electrodynamics. The exact solutions of (12) were determined for the hydrogen atom. The very interesting (and unexpected!) result was found that the added potential did not lift the accidental degeneracy in the states of hydrogen. In other words, there was no prediction of any contribution to the Lamb shift from B_μ that might have accounted for the small difference between the experimental observations and the predictions of quantum electrodynamics (in the late 1950s).

The pseudovector four-potential B_μ may still contribute to other effects in the microscopic domain. For example, it would predict that a particle, such as a neutron, would have an electric dipole moment, whose value is proportional to the term in the Dirac Hamiltonian $\xi\sigma \cdot \mathbf{E}$ [12]. However, after much experimental investigation into the possibility of the neutron electric dipole moment, it has not been found [15]—that is, in the context of this theory, the parameter ξ, if it were nonzero, must be too small (the order of 10^{-13}) for this effect to be observed.

A later analysis was based on a spinor formulation of the electromagnetic field theory, to be discussed in the next section. It was found that this general-

ization, based on full conformance to the reflection nonsymmetric field theory, which is in accordance with the symmetry group of relativity theory, the Lamb shift is, indeed, fully predicted, exclusive of quantum electrodynamics. The predictions were in agreement with the empirical facts, within the experimental error, for the hydrogen states with principal quantum numbers $n=2,3,4$ [16].

III. FACTORIZATION OF MAXWELL'S EQUATIONS TO A SPINOR FORM

In the context of Einstein's theory of relativity, we must ask whether Maxwell's expression of the electromagnetic theory is the most general representation consistent with the symmetry requirements of relativity. The answer is negative because the symmetry of Maxwell's equations based on *reducible* representations of the group of relativity theory. Then there must be additional physical predictions that remain hidden that would not be revealed until the most general (*irreducible*) expression of the electromagnetic field theory is used.

Two equivalent forms of Maxwell's field equations in terms of the standard vector formalism are Eq. (5), or (6) with the Lorentz gauge $\partial^{\mu}A_{\mu} = 0$. The former is in terms of the antisymmetric second-rank tensor solution $F_{\mu v}$, which is a combination of the electric and magnetic field variables. The latter is in terms of the vector potential, A_{μ}, shown in Eq. (6) [as well as Eq. (7) in terms of the pseudovector potential B_{μ}, assuming that the parameter ξ is nonzero]. (Experimental results to this point in time indicate that indeed this parameter is zero to within experimental accuracy [15]—even though the symmetry of relativity theory has no reason to exclude it. Henceforth, we will assume that this parameter is zero.)

The symmetry requirements of the theory of relativity have geometric and algebraic modes of expression. From the geometric view in special relativity, the continuous spacetime transformations that leave the laws of nature covariant (i.e., unchanged in form) in all possible inertial frames of reference, *from the view of any one of them*, are the same set of transformations that leave invariant the squared differential metric:

$$ds^2 = (dx^0)^2 - dr^2 \tag{13}$$

In general relativity, where the relative motion between frames is not inertial, the geometric invariant of the resulting "curved" spacetime is

$$ds^2 = g^{\mu\nu}(x)dx_{\mu}dx_{\nu} \tag{14}$$

where μ and ν are summed from 0 to 3 and $g^{\mu\nu} = g^{\nu\mu}$ is the 10-component metric tensor with the flat spacetime limit that takes Eq. (14) into (13), that is, in

the local limit of a flat spacetime: $g^{\mu\nu}(x) \to [g^{00} = 1, g^{kk} = -1, (k = 1, 2, 3)$ and $g^{\mu \neq \nu} = 0]$.

The idea of covariance is then that the same set of spacetime transformations that leave the differential metric (13) in special relativity, or (14) in general relativity, unchanged (invariant) also leave all the laws of nature covariant (unchanged in form) under these transformations between reference frames. The metric (13) in special relativity, or (14) in general relativity, then guides one to the forms of the covariant laws of nature, in accordance with the theory of (special or general) relativity. This is the role of the differential metrics—*they are not to be considered as "observables" on their own*!

A significant point here is that it is not the *squared invariant* ds^2 that is to underlie the covariance of the laws of nature. It is rather the *linear invariant* ds that plays this role. How, then, do we proceed from the squared metric to the linear metric? That is to say, how does one take the "square root" of ds^2? The answer can be seen in Dirac's procedure, when he factorized the Klein–Gordon equation to yield the spinor form of the electron equation in wave mechanics:- the Dirac equation. Indeed, Dirac's result indicated that by properly taking the square root of ds^2 in relativity theory, extra spin degrees of freedom are revealed that were previously *masked*.

The symmetry group of relativity theory tells the story. For the *irreducible representations* of the Poincaré group (of special relativity) or the Einstein group (of general relativity) obey the algebra of quaternions. The basis functions of the quaternions, in turn, are two-component spinor variables [17].

We start out then with a factorized metric in special relativity, which has the quaternion form:

$$ds = \sigma^{\mu} dx_{\mu} \equiv \sigma^0 dx_0 - \boldsymbol{\sigma} \cdot d\mathbf{r} \tag{15}$$

where σ^0 is the unit two-dimensional matrix and $\sigma^k (k = 1, 2, 3)$ are the three Pauli matrices. The set $\{\sigma^{\mu}\}$ form the four basis elements of a quaternion (analogous to the two basis elements $\{1, i\}$ of a complex number).

In the global extension to general relativity, the geometric generalization from the flat spacetime description to a curved spacetime, the basis elements $\sigma^{\mu} \to q^{\mu}(x)$, so that the factorized invariant differential element becomes

$$ds = q^{\mu}(x)\, dx_{\mu} \tag{16}$$

This quaternion differential is a generalization of the Riemannian metric. The 4-vector *quaternion fields* $q^{\mu}(x)$ then replace the second-rank, symmetric tensor fields $g^{\mu\nu}(x)$ as the fundamental metric of the spacetime. The metric field $q^{\mu}(x)$ is a 4-vector, whose four components are each quaternion-valued. This is then a 16-component field, rather than the 10-component metric tensor field $g^{\mu\nu}$ of the standard Riemannian form.

The 16-component quaternion metric field is then a generalization of the 10-component metric tensor field to represent gravitation. The increase in the number of components satisfies the group requirement of general relativity theory—that the Einstein group is a 16-parameter Lie group, indicating that there must be 16 essential parameters to characterize the irreducible representations of the group. This implies that there must be 16 independent field equations to underlie the spacetime metric. These are the 16 essential parameters of the Einstein group. They are the derivatives of four coordinates $x^{\mu'}(x)$ of one reference frame with respect to those of another: $\partial x^{\mu'}/\partial x^{\nu}(\mu, \nu = 0, 1, 2, 3)$ The basic reason for the increase in the number of components of the metric field q^{μ}, compared with $g^{\mu\nu}$, is that the reflection symmetry elements of the spacetime have been removed from the underlying symmetry group of the latter. [It is the same reason why the removal of the reflection symmetry elements from the covariance of the Klein–Gordon operator yields the extra (spinor) degrees of freedom in the factorized Dirac operator in quantum mechanics.] Thus, the factorized metric (16) has no reflection symmetry while the "squared" metric in special relativity (14) does have reflection symmetry in space and time.

The key to the generalization achieved is then the removal of the reflection symmetry elements in the space and time coordinates in the laws of nature. This then leads to the Poincaré group (of special relativity) or the Einstein group (of general relativity), since these are Lie groups—groups of only continuous, analytical transformations of the spacetime coordinate systems that leave the laws of nature covariant.

Let us now focus on the irreducible expressions of the electromagnetic field equations in special relativity, using the quaternion calculus. We will then come to their form in general relativity.

Following from the quaternion differential metric (15), we have the first-order quaternion differential operator:

$$\sigma^{\mu}\partial_{\mu} = \sigma^{0}\partial_{0} - \sigma \cdot \nabla$$

The basis functions of this operator are the two-component spinor variables. Guided by the two-dimensional Hermitian structure of the representations of the Poincaré group, we may make the following identification between the spinor basis functions $\phi_{\alpha}(\alpha = 1, 2)$ of this operator and the components $(E_k, H_k)(k = 1, 2, 3)$ of the electric and magnetic fields, in any particular Lorentz frame:

$$\begin{aligned}
&(\phi_1)_1 = G_3, (\phi_1)_2 = G_1 + iG_2, (\phi_2)_1 = G_1 - iG_2, (\phi_2)_2 = -G_3 \\
&(\Upsilon_1)_1 = -4\pi i(\rho + j_3)\ (\Upsilon_1)_2 = -4\pi i(j_1 + ij_2)\ (\Upsilon_2)_1 = -4\pi i(j_1 - ij_2) \\
&(\Upsilon_2)_2 = -4\pi i(\rho - j_3) \qquad (17)
\end{aligned}$$

where $G_k = H_k + iE_k$. It is then readily verified that the two uncoupled, two-component spinor equations:

$$\sigma^\mu \partial_\mu \phi_\alpha = \Upsilon_\alpha (\alpha = 1, 2) \tag{17'}$$

precisely duplicate the standard form (5) of Maxwell's equations [18].

It is important to note at this stage of the analysis that the generalization achieved in going from the vector representation (5) to the spinor representation (17′) of the electromagnetic field equations is not merely a rewriting of the Maxwell equations. This is because the spinor formalism has more degrees of freedom than does the vector formalism; thus it makes more predictions, in addition to duplicating the predictions of the (less general) vector form of the theory. This will be demonstrated in the following paragraphs.

Under the Poincaré group of transformations of special relativity, when $x^\mu \to x^{\mu,} = \alpha^\mu_\nu x^\nu$, where $\{\alpha^\mu_\nu\}$ are the vector transformations, covariance of the spinor field equations (17′) is preserved *if and only if* [17]

$$\phi_\alpha(x) \to \phi'_\alpha(x') = S\phi_\alpha(x), \;\; \Upsilon_\alpha(x) \to \Upsilon'_\alpha(x') = S^{+-1}\Upsilon_\alpha(x) \tag{18}$$

where the spinor transformations S relate to the vector transformations α^μ_ν according to the equation

$$S^+ \sigma^\mu S = \alpha^\mu_\nu \sigma^\nu \tag{19}$$

Equation (19) then yields the double-valued spinor transformation:

$$S(\theta_{\mu\nu}) = \exp\left(\frac{\sigma^\mu \sigma^\nu \theta_{\mu\nu}}{2}\right) \qquad (\mu, \nu = 0, 1, 2, 3) \tag{20}$$

Note that this equation is not summed over $(\mu, \nu).\theta_{\mu\nu}$ are the constant (i.e., x-independent) parameters that define the 10 transformations in the x_μ–x_ν plane of the 10-parameter Poincaré group: three Eulerian angles of rotation in space, three components of the relative speed between inertial frames, and the four translations in space and time.

The solutions $F_{\mu\nu}$ of the standard (reducible) vector form of electromagnetic field theory transform as a second-rank (covariant) tensor

$$x \to x' \Rightarrow F_{\mu\nu}(x) \to F'_{\mu\nu}(x') = \alpha^\lambda_\mu \alpha^\rho_\nu F_{\lambda\rho}(x) \tag{21}$$

Thus the *identification* (17) $\phi_\alpha(F_{\mu\nu})$ is not to be understood as form-invariant regarding the dependence (17) of the spinor variables ϕ_α on the tensor variables $F_{\mu\nu}$ in any other Lorentz frame. In other words, the Lorentz transformation of

$\phi_\alpha(F_{\mu\nu})$ does not transform form-invariantly into $\phi'_\alpha(F'_{\mu\nu})$ under the Lorentz transformations of the Poincaré group, $x \to x'$. Of course, this is because ϕ_α transforms as a spin-$\frac{1}{2}$ basis function of the irreducible representations of the group of relativity while $F_{\mu\nu}$ transforms as the basis functions of the spin-1 (reducible) representations of the group.

The terms of the respective (reducible) tensor and the (irreducible) spinor expressions of the electromagnetic laws that must correspond in all Lorentz frames are those that identify with physical observations. These are the conservation laws of electromagnetism. They derive, in turn, from the invariants of the theory.

In accordance with the transformation properties (18), it follows that the Hermitian products

$$I_{\alpha\beta} = \phi_\alpha^+ \Upsilon_\beta \qquad (\alpha, \beta = 1 \text{ or } 2) \tag{22}$$

are four complex number invariants, thus corresponding to eight real-number invariants. Particular linear combinations of these invariants may then be set up to correspond to the standard invariants of the vector form of electromagnetic theory. Since there are more independent invariants here than in the standard theory, there must be more invariants and physical predictions that have no counterpart in the standard form of the theory.

According to the spinor calculus [19], further invariants, in addition to (22), that correspond with the standard invariants of electromagnetic field theory, are

$$I_1 = \phi_1^{\text{tr}} \varepsilon \phi_2 \Leftrightarrow (E^2 - H^2) + 2\mathbf{i}\mathbf{E} \cdot \mathbf{H} \tag{23a}$$

$$I_2 = \Upsilon_1^{\text{tr}} \varepsilon \Upsilon_2 \Leftrightarrow \rho^2 - j^2 \tag{23b}$$

where the superscript "tr" stands for the transpose of the spinor variable and ε is the two-dimensional Levi–Civita symbol, with $\varepsilon_{01} = -\varepsilon_{10} = 1$, and $\varepsilon_{00} = \varepsilon_{11} = 0$.

We see here that the real and imaginary parts of the complex invariant I_1 correspond to the two invariants of the standard form of electromagnetic theory, namely, the scalar and the pseudoscalar terms. They appear together here in a single complex function because of the reflection-nonsymmetric feature of this theory. The invariant I_2 corresponds to the real-valued modulus of the four-current density of the standard theory.

A. The Conservation Equations

It follows from the spinor field equation (17′) that these equations may be rewritten in the form of four complex conservation equations:

$$\partial_\mu(\phi_\alpha^+ \sigma^\mu \varphi_\beta) = \phi_\alpha^+ \Upsilon_\beta + \Upsilon_\alpha^+ \phi_\beta \tag{24}$$

If we set $\alpha = \beta = 1$ in (24) and add this to the equation with $\alpha = \beta = 2$, it follows from the identification (17) that their sum corresponds to the standard form of the conservation equation:

$$\frac{1}{2}\partial^0(E^2 + H^2) + \operatorname{div}(\mathbf{E} \times \mathbf{H}) = -4\pi \mathbf{E} \cdot \mathbf{j} \tag{25a}$$

$$\partial^0(\mathbf{E} \times \mathbf{H}) = \rho \mathbf{E} + \mathbf{j} \times \mathbf{H} \tag{25b}$$

Thus we see that four of the conservation equations in (24) correspond to all four conservation equations of the standard theory; one is the conservation of energy (25a) (Poynting's equation), and the other three are the conservation of the three components of momentum (25b) of the standard form of electromagnetic field theory. But since (24) are eight real-number valued equations rather than four, the spinor formalism predicts more facts than the standard vector Maxwell formalism—it is a true generalization.

B. Faraday's Interpretation

With Faraday's interpretation of the electromagnetic field as a "potentiality" of force exerted by charged matter, then to be actualized by a test body at the spacetime point x where it is located, there must be a separate field of force for each charged source. Thus, Maxwell's equations (5) must be labeled for each source field

$$\partial^\nu F^{(n)}_{\mu\nu} = 4\pi j^{(n)}_\mu, \qquad \partial_{[\rho} F^{(n)}_{\mu\nu]} = 0 \tag{26}$$

for the nth source field. Similarly, the spinor expression of the electromagnetic equations are

$$\sigma^\mu \partial_\mu \phi^{(n)}_\alpha = \Upsilon^{(n)}_\alpha \tag{27}$$

It is important to note that while there are fields for each source of the system, they are all mapped in the same spacetime x, rather than separate spacetimes for each source. This is the *nonlocal* feature of this field theory since there are no individual trajectories for charged discrete particles. This interpretation eliminates the problem of the self-energy of the electron, as a singular, charged particle of matter [20].

The conserved energy in the vector representation with Faraday's interpretation is then

$$\sum_n \sum_{m \neq n} \left(\frac{1}{16\pi}\right)(\mathbf{E}^{(m)} \cdot \mathbf{E}^{(n)} + \mathbf{H}^{(m)} \cdot \mathbf{H}^{(n)}) \tag{28}$$

rather than the standard form:

$$\left(\frac{1}{8\pi}\right)(E^2 + H^2) \tag{29}$$

The form (29) is derived from integrating the conservation law (25a) over all of space and using Gauss' law. It includes the self-energy terms ($m = n$) as well as the free-field (radiation) terms that are independent of any sources. The latter terms are automatically absent from the expression (28), which is finite from the outset and entails no "free radiation."

In the spinor formalism (27), the four *complex* conservation equations, with Faraday's interpretation are

$$\partial_\mu \sum_n \sum_{m\neq n} \phi_\alpha^{(n)+} \sigma^\mu \phi_\beta^{(m)} = \sum_n \sum_{m\neq n} (\phi_\alpha^{(n)+} \Upsilon_\beta^{(m)} + \Upsilon_\alpha^{(n)+} \phi_\beta^{(m)}) \tag{30}$$

The right-hand side of this scalar equation, which consists of four complex relations, then entails eight real-number scalar equations. As in the vector formalism, there are no self-energy terms present.

It is to be noted that some of the eight equations may be expressed in one-to-one correspondence with all four conservation equations of the standard Maxwell formalism. But there are other conservation equations here that have no counterpart in the standard formalism of electromagnetism. It further implies that indeed this is a true generalization of the Maxwell form of electromagnetism.

It is interesting to note here a difference between the standard theory and the Faraday interpretation that relies on the Mach principle. Consider the complex conservation equation (30) with $\alpha = \beta = 1$. The imaginary part of this complex equation is

$$\partial_\mu \sum_n \sum_{m\neq n} (\phi_1^{(m)+} \sigma^\mu \phi_1^{(n)} - \phi_1^{(n)+} \sigma^\mu \phi_1^{(m)}) = \sum_n \sum_{m\neq n} (\phi_1^{(m)+} \Upsilon_1^{(n)} - \Upsilon_1^{(n)+} \varphi_1^{(m)}) + (\Upsilon_1^{(m)+} \phi_1^{(n)} - \phi_1^{(n)+} \Upsilon_1^{(m)})$$

If $m = n$, as included in the standard Maxwell theory, the extra four conservation equations above reduce to $0=0$, which is an ambiguity. However, with the restriction from Faraday's interpretation that requires that $m \neq n$, the ambiguity is removed and the extra conservation equations remain.

Let us now sum up the generalization of electromagnetic field theory thus far. The starting point is that the symmetry group that underlies Einstein's theory of relativity is a Lie group—a group of continuous, analytic transformations that preserve the covariance of all the laws of nature. This is the rule that all laws of nature remain in one-to-one correspondence in all continuously connected

reference frames, *from the view of any one of them*. This group does not entail any discrete transformations in space or time.

In Section I of this chapter it was shown that the only gauge-invariant way to express this extension in the context of the vector potential expression of the electromagnetic field theory is to add to the standard (polar) vector potential A_μ an (axial) pseudovector contribution B_μ. This has the effect of interchanging the roles of the electric and the magnetic field variables in the coupling of a charged body to this field. Although this addition is theoretically permitted, it was found to not imply any significant empirical contributions, for the magnitudes of fields studied thus far in the experimental domain. Future experimental studies of very high magnetic fields, such as the interiors of galaxies, may reveal possible observable consequences in astrophysical studies.

In Section II, the group requirement that removes the reflection transformations was met head-on, without the need to add any new potential terms. It was seen that the most general expression of electromagnetic field theory, which excludes reflections in spacetime in the underlying symmetry group, follows from a factorization of the vector representation of the Maxwell theory to a first-rank spinor form. This is a natural generalization, following from the *irreducible representations* of the covariance group of relativity theory that leads to extra physical predictions, because of the extra degrees of freedom in the spinor variables.

In the next section, the final generalization of full symmetrization will be carried out, whereby the spinor–quaternion expression of the laws of electromagnetism will be extended from special relativity to general relativity. This extension automatically fuses the laws of electromagnetism with those of gravity. It will be shown that the generalized formalism for electromagnetism is obtained from a factorization of Einstein's field equations. The new formalism is presented in terms of a replacement of Einstein's tensor metric field with a vector field whose four components are each quaternion-valued. Thus, the new metric variable $q^\mu(x)$ has 16 independent components, rather than the 10 (of the symmetric tensor $g^{\mu\nu}$ of the Einstein formalism) or the 6 (of the antisymmetric tensor $F^{\mu\nu}$ of the Maxwell formalism). From the factorized metrical field equations in q^μ, it will be seen how the Einstein formalism and the Maxwell formalism are recovered, although now identifying each with the single quaternion field and its related spinor calculus in a curved spacetime.

IV. EXTENSION OF ELECTROMAGNETIC FIELD THEORY TO GENERAL RELATIVITY

A. The Group

In accordance with the principle of general covariance—which is the underlying axiom of the theory of general relativity—the expressions of all laws of nature in all possible continuously connected frames of reference, from the view of any

one of them, must be in *one-to-one correspondence*. The different reference frames, in turn, relate to each other in terms of continuous, differentiable transformations, which we call "motion." (The differentiability of these transformations to all orders, requiring that they be analytic, is dictated by the requirement of the inclusion of the laws of conservation of energy, momentum, and angular momentum in the special relativity limit of the theory; this is in accordance with Noether's theorem [7].) When the relative motion is inertial, characterized by 3 constant parameters of relative velocity, 3 (Eulerian) angles of rotation, and 4 translations, the underlying set of transformations forms the 10-parameter Lie group of special relativity. It is the Poincaré group **P** [2]. This is a special limit of the coordinate-dependent (noninertial) transformations group of general relativity—the Einstein group **E**. It is a 16-parameter Lie group whose representations are a global extension of the representations of the Lie group **P** [21].

It is important to recognize that, in physics, **P** is an *asymptotic limit* of **E**, but **P** is *not* a subgroup of **E**. This is for the physical reason that **P** is exact only in the case of a vacuum—wherein the entire universe would be empty! For in the field theory of general relativity, if there should be matter, *anywhere in the universe*, the continuous, analytic fields associated with this matter must be nonzero *everywhere*. In this case, the parameters that relate a reference frame to any other must be spacetime-dependent. Thus, special relativity can be viewed only as an asymptotic limit of general relativity. Its representations may be approached asymptotically from those of general relativity, as closely as we please, *but not reached in an exact sense!* The Einstein group **E** is a form of a topological group **T**.

B. A Mathematical Diversion on the Nature of E—Pontjagin's Theorem

1. Three general conditions are noteworthy here: Because **E** prescribes the invariance associated with continuous changes from any point of the function space of field solutions, to any other that is arbitrarily close, **E** must be *locally compact*.
2. Because of the rejection of the discontinuous reflections in the spacetime, the topological space of this group must be *connected*; that is, it cannot be decomposed into two or more disjoint sets.
3. Since the elements of this topological space are a countable number of fields $\{\psi^{(1)}(x), \ldots, \psi^{(n)}(x)\}$—corresponding to the countable modes of the closed system—and since the continuous changes of these field variables in their own neighborhoods $\{\delta\psi^{(1)}, \ldots, \delta\psi^{(n)}\}$ are induced by the transformations of the group, it follows that the complete set of neighborhoods of the topological space is *countable*. The topological group T is then said to satisfy the *second axiom of countability.*

Pontjagin's theorem is as follows [22]. Let **T** be a locally compact, connected topological field satisfying the second axiom of countability. Then **T** is isomorphic with one of the three topological fields: (1) the field of real numbers, (2) the field of complex numbers, and (3) the field of quaternions.

Since the Einstein group **E** corresponds to the topological group **T**, the most general mathematical system to express the laws of physics in general relativity is then the set of quaternions [23]. Reducing the quaternion-valued field from four dimensions to two leads to the complex-number-valued field and further reduction to one dimension leads to the real-number-valued field. (The word "field" here refers to an "algebraic field" [22].) The latter two sets may be seen as subsets of the first, reductions where one loses not only dimensionality but also the important feature of noncommutability of the quaternion number system. The quaternion field then expresses the laws of nature to be compatible with the covariance requirement of the group of general relativity **E**.

C. The Electromagnetic Field Equations in General Relativity

The vector representation (5) of Maxwell's equations extends to general relativity by globalizing the ordinary derivatives to covariant derivatives that entail the affine connection $\Gamma^{\lambda}_{\mu\nu}$ of the curved spacetime [24]. Thus, (5) takes the following form in the curved spacetime

$$F^{;\nu}_{\mu\nu} = 4\pi j_{\mu} \tag{31a}$$

$$F^{[\mu\nu}_{;\lambda]} = 0 \tag{31b}$$

where the square brackets denote the cyclic sum and

$$F^{\alpha\beta}_{;\gamma} \equiv \partial_{\gamma} F^{\alpha\beta} + \Gamma^{\alpha}_{\rho\gamma} F^{\rho\beta} + \Gamma^{\beta}_{\rho\gamma} F^{\alpha\rho} \tag{32}$$

The affine connection coefficients in terms of the metric tensor are [24]

$$\Gamma^{\rho}_{\mu\alpha} = \frac{1}{2} g^{\rho\lambda}(\partial_{\mu} g_{\lambda\alpha} + \partial_{\alpha} g_{\mu\lambda} - \partial_{\lambda} g_{\alpha\mu})$$

The two-component spinor form of electromagnetic field theory (17′) is generalized in the curved spacetime by (1) globally extending the Pauli matrices to the quaternion elements, $\sigma^{\mu} \to q^{\mu}(x)$, and (b) generalizing the ordinary derivatives to covariant derivatives of the spinor variables. This entails the "spin–affine connection fields" Ω_{μ} as follows:

$$q^{\mu}(x)\phi_{\alpha;\mu} \equiv q^{\mu}(x)(\partial_{\mu} + \Omega_{\mu})\phi_{\alpha} = \Upsilon_{\alpha} \tag{33}$$

where

$$\Omega_\mu = \frac{1}{4}(\partial_\mu q^\rho + \Gamma^\rho_{\tau\mu} q^\tau) q^*_\rho \tag{34}$$

and q^*_ρ is the quaternion conjugate to q_ρ, corresponding to time reversal (or space reflection) of q_ρ. (From here on, the asterisk over the quaternion variables denotes the *quaternion conjugate*, not the *complex conjugate*. The former is obtained by reversing the sign of the time component of the quaternion variable.)

D. The Global Spinor Lagrangian for Electromagnetism

The Lagrangian density that gives, on variation, the topologically covariant field equations (33) is an explicit function of the spinor variables, $\phi_1, \phi_1^+, \phi_2, \phi_2^+$ and their respective covariant derivatives. (The dagger superscript denotes the Hermitian conjugate of the function.) It has the form:

$$L_M = \{ i g_M \sum_\alpha (-1)^\alpha [\phi^+_\alpha (q^\mu \phi_{\alpha;\mu} - 2\Upsilon_\alpha) + \text{H.c.}\} (-g)^{1/2} \tag{35}$$

where "H.c." stands for the Hermitian conjugate of the term preceding it and

$$(-g)^{1/2} = i\varepsilon_{\mu\nu\lambda\rho} q^\mu q^{\nu *} q^\lambda q^{\rho *}$$

is the *metric density*. The multiplicative constant g_M in (35) has the dimension of a *length*—it is the one extra fundamental constant in this theory. Its appearance results from the generalization that is effected when the Lagrangian is expressed in terms of the spinor variables rather than the usual vector variables. Since the spinor variables ϕ_α have the dimension of an electric field intensity, the terms summed have a dimension of energy density per length; thus g_M has the dimension of a length so that the Lagrangian has the proper dimension of energy density.

The magnitude of g_M was determined from the prediction that this spinor formalism yields the Lamb shift in hydrogenic atoms. It follows from the new terms in the spinor formulation of electromagnetism that appear in the Dirac Hamiltonian, which are not present in the standard Dirac equation for hydrogen [16]. These extra terms then predict a lifting of the accidental degeneracy in the states of hydrogen, thus the Lamb shift. The new fundamental constant g_M was found to have a magnitude that is the order of 2×10^{-14} cm. This gives results that are in agreement with the experimental facts on the Lamb shifts $nS_{1/2} - nP_{1/2}$ for the principal quantum numbers for hydrogen, $n = 2, 3, 4$.

E. Derivation of the Maxwell Field Formalism from General Relativity

The covariance groups underlying the tensor forms of the respective Einstein and the Maxwell field equations are reducible. This is because they entail reflection symmetry, not required by relativity theory, as well as the required continuous symmetry of the Einstein group **E**. When the Einstein field equations are factorized, they yield the irreducible form, which are then in terms of the quaternion and spinor variables, rather than the tensor variables. Such a generalization must then extend the physical predictions of the usual tensor forms of general relativity of gravitation and the standard vector representation of the Maxwell theory (both in terms of second-rank tensor fields, one symmetric and the other antisymmetric) because the new factorized variables have more degrees of freedom than did the earlier version variables.

The starting point then to achieve the factorization of the Einstein equations is the factorized differential line element in the quaternion form, $ds = q^{\mu}(x)dx_{\mu}$, where q^{μ} are a set of four quaternion-valued components of a 4-vector. Thus ds is, geometrically, a scalar invariant, but it is algebraically a quaternion. As such, it behaves like a second-rank spinor of the type $\psi \otimes \psi^*$, where ψ is a two-component spinor variable [17].

We then see that the basic variable that represents the generalized spacetime that is appropriate to general relativity is a 16-component variable. One may then speculate at the outset that these 16 independent components of the metrical field relate to the 10 components of the gravitational field plus 6 components of the Maxwell field, in terms of a single unified field that incorporates both gravitation and electromagnetism. We will now see that this is, indeed, the case.

Since there is no reflection symmetry in the quaternion formulation, the "reflected" quaternion $q^{\mu}*$ must be distinguishable from q^{μ}. The conjugate differential line element to ds is $ds* = q^{\mu*}dx_{\mu}$. The product of the quaternion and conjugate quaternion line elements is then the real-number-valued element that corresponds to the squared differential element of the Riemannian geometry:

$$ds\ ds^* = -\left(\frac{1}{2}\right)(q^{\mu}q^{\nu*} + q^{\nu}q^{\mu*})dx_{\mu}\ dx_{\nu} \Leftrightarrow \sigma_0\, g^{\mu\nu}dx_{\mu}\ dx_{\nu}$$

Thus the symmetric second-rank metric tensor $g^{\mu\nu}$ of Einstein's formulation of general relativity corresponds to the symmetric sum from the quaternion theory, $(-\frac{1}{2})(q^{\mu}q^{\nu*} + q^{\nu}q^{\mu*})$. [The factor $(-\frac{1}{2})$ is chosen in anticipation of the normalization of the quaternion variables.] Thus we see that ds is a factorization of the standard Riemannian squared differential metric $ds^2 = g^{\mu\nu}dx_{\mu}\ dx_{\nu}$.

The following is an outline that leads to a derivation of the factorization of the Einstein formalism that gives back the gravitational and the electromagnetic equations from a unified quaternion–spinor formalism.

F. The Variables of a Riemannian Spacetime in Quaternion Form

Let us now exploit the feature of the quaternion metrical field that it has configuration degrees of freedom, as a 4-vector, as well as spinor degrees of freedom, as a second-rank spinor of the type: $\psi \otimes \psi^*$ [25].

Since the quaternion q^μ is a 4-vector, the product $q^\mu q^*_\mu$ must be invariant under the continuous spacetime transformations *and* the reflections in spacetime. It then follows that the covariant derivatives and the second covariant derivatives of the quaternion fields must vanish. Since $q^\mu \sim (\psi \otimes \psi^*)^\mu$, it follows that (with $\alpha, \beta = 1, 2$)

$$0 = (q_{\mu;\rho;\lambda} - q_{\mu;\lambda;\rho})_{\alpha\beta} = [(\psi_{\alpha;\rho;\lambda} - \psi_{\alpha;\lambda;\rho})\psi^*_\beta + \psi_\alpha(\psi_{\beta;\rho;\lambda} - \psi_{\beta;\lambda;\rho})] + ([q_{\mu;\rho;\lambda}] - [q_{\mu;\lambda;\rho}]) \tag{36}$$

The squared bracket in Eq. (36) denotes the behavior of the quaternion field with respect to its vector degrees of freedom alone. The covariant derivatives of the two-component spinor variables are as follows: $\psi_{;\rho} = (\partial_\rho + \Omega_\rho)\psi$ and the "spin–affine connection" has two alternative (equivalent) forms [17]:

$$\Omega_\rho = \left(\frac{1}{4}\right)(\partial_\rho q^\mu + \Gamma^\mu_{\tau\rho} q^\tau) q^*_\mu = -\left(\frac{1}{4}\right) q_\mu (\partial_\rho q^{\mu^*} + \Gamma^\mu_{\tau\rho} q^{\tau^*}) \tag{37}$$

Ω_ρ is the term that must be added to the ordinary derivative of a spinor field in a curved spacetime in order to define its derivative covariantly; that is, so that the spinor variable is integrable in the curved spacetime.

The first two terms on the right-hand side of Eq. (36) denote the changes with respect to the spinor indices; the third term denotes the changes in configuration space. Their explicit forms are

$$\psi_{;\rho;\lambda} - \psi_{;\lambda;\rho} = (\partial_\lambda \Omega_\rho + \Omega_\lambda \Omega_\rho - \partial_\rho \Omega_\lambda - \Omega_\rho \Omega_\lambda)\psi \equiv K_{\lambda\rho}\psi \tag{38}$$

where $K_{\rho\lambda} = -K_{\lambda\rho}$ is the *spin curvature tensor.* It is clearly a second-rank, antisymmetric tensor in configuration space. Since the left-hand side of this equation is a first-rank spinor in spinor space, the spin curvature tensor on the right, $K_{\rho\lambda}$, must be a second-rank spinor that contracts with the first-rank spinor ψ on the right to yield a first-rank spinor function. The spin–affine connection field Ω_ρ, on the other hand, is a 4-vector in configuration space, but it is not covariant in spinor space. This is clear since it is the term that must be added to

the ordinary (noncovariant) derivative of the spinor variable in order to make its derivative in a curved spacetime covariant.

In the third term in Eq. (36), where the square bracket represents the changes in q_μ as a four vector, we have

$$[q_{\mu;\rho;\lambda}] - [q_{\mu;\lambda;\rho}] = R_{\kappa\mu\rho\lambda} q^k \tag{39}$$

This defines the *Riemann curvature tensor*, $R_{\kappa\mu\rho\lambda}$, wherein q_μ could be any covariant 4-vector.

Substituting (38) and (39) into (36), the relation between the spin curvature tensor and the Riemann curvature tensor follows:

$$K_{\rho\lambda} q_\mu + q_\mu K^\dagger_{\rho\lambda} = -R_{\kappa\mu\rho\lambda} q^\kappa \tag{40}$$

where the dagger denotes the Hermitian adjoint of the function.

In a similar fashion, application of the preceding analysis to the conjugated quaternion fields yields the accompanying equation to (40):

$$K^\dagger_{\rho\lambda} q^*_\mu + q^*_\mu K_{\rho\lambda} = R_{\kappa\mu\rho\lambda} q^{\kappa^*} \tag{41}$$

Multiplying (40) on the right with the conjugated quaternion q^*_γ and (41) on the left with the quaternion q_γ, then adding the resulting equations and using the identity

$$q_\gamma q^{\kappa^*} + q^\kappa q^*_\gamma = 2\sigma_0 \delta^\kappa_\gamma$$

where σ_0 is the unit two-dimensional matrix, the following correspondence is derived between the Riemann curvature tensor and the spin curvature tensor:

$$\sigma_0 R_{\kappa\mu\rho\lambda} = \frac{1}{2}(K_{\rho\lambda} q_\mu q^*_\kappa - q_\kappa q^*_\mu K_{\rho\lambda} + q_\mu K^\dagger_{\rho\lambda} q^*_\kappa - q_\kappa K^\dagger_{\rho\lambda} q^*_\mu) \tag{42}$$

Next, contracting $R_{\kappa\mu\rho\lambda}$ with the contravariant metric tensor $g^{\mu\lambda}$ yields the correspondence with the Ricci tensor $R_{\kappa\rho}$:

$$\sigma_0 g^{\mu\lambda} R_{\mu\kappa\rho\lambda} \equiv \sigma_0 R_{\kappa\rho} = \frac{1}{2}(K_{\rho\lambda} q^\lambda q^*_\kappa - q_\kappa q^{\lambda *} K_{\rho\lambda} + q^\lambda K^\dagger_{\rho\lambda} q^*_\kappa - q_\kappa K^+_{\rho\lambda} q^{\lambda^*}) \tag{43}$$

Finally, the scalar curvature field R follows from the further contraction of the Ricci tensor (43) with the metric tensor, giving

$$\sigma_0 R = \frac{1}{2}(K_{\rho\lambda} q^\lambda q^{\rho *} - q^\rho q^{\lambda *} K_{\rho\lambda} + q^\lambda K^\dagger_{\rho\lambda} q^{\rho *} - q^\rho K^\dagger_{\rho\lambda} q^{\lambda *}) \tag{44}$$

G. The Quaternion Field Equations

The Lagrangian density whose vanishing variation leads to the field equations in q^{λ} is chosen to be the trace of the scalar curvature:

$$L_E = (\mathrm{Tr}\ R)(-g)^{1/2} = \frac{1}{2}\mathrm{Tr}(q^{\rho *}K_{\rho\lambda}q^{\lambda} + \mathrm{H.c})(-g)^{1/2} \tag{45}$$

If we signify by L_M the part of the Lagrangian density that yields the matter variables on variation with respect to the quaternion variables, then the total Lagrangian density is $L = L_E + L_M$. Its variation with respect to the conjugated quaternion variables then yields the field equations [25]:

$$\frac{1}{4}(K_{\rho\lambda}q^{\lambda} + q^{\lambda}K^{\dagger}_{\rho\lambda}) + \frac{1}{8}Rq_{\rho} = kT_{\rho} \tag{46a}$$

Variation with respect to the quaternion variables yields the conjugated quaternion field equation:

$$-\left(\frac{1}{4}\right)(K^{\dagger}_{\rho\lambda}q^{\lambda *} + q^{\lambda *}K_{\rho\lambda}) + \frac{1}{8}Rq^{*}_{\rho} = kT^{*}_{\rho} \tag{46b}$$

(Note that the source term T_{ρ} is a quaternion and T^{*}_{ρ} is a conjugated quaternion.)

The quaternion field equations (46a,b) are then the factorization of Einstein's tensor field equations:

$$R_{\mu\nu} - \left(\frac{1}{2}\right)g_{\mu\nu}R = kT_{\mu\nu} \tag{47}$$

The solutions of the latter equations are the 10 components of the symmetric second-rank metric tensor $g_{\mu\nu}$. The solutions of the factorized equations (46a) [or (46b) are the 16 components of the quaternion metrical field q_{ρ} (or q^{*}_{ρ}). We will now see that this 16-component metrical quaternion field, indeed, incorporates the gravitational and the electromagnetic fields in terms of their earlier tensor representations. Gravitation entails 10 of the components in the symmetric second-rank tensor $g_{\mu\nu}$. Electromagnetism entails 6 of the components (the 3 components of the electric field and the three components of the magnetic field), as incorporated in the second-rank antisymmetric tensor $F_{\mu\nu}$.

To demonstrate the natural unification of the gravitational and electromagnetic aspects of the quaternion field equation (46a) and its conjugate equation (46b), we follow this procedure. Multiply (46a) on the right with the conjugated quaternion solution q^{*}_{γ}, and the conjugated equation (46b) on the left with q_{γ}.

Then adding (with the constant k on the right) and subtracting (with the constant k' on the right) we obtain the following positive/negative pair of equations:

$$\frac{1}{2}(K_{\rho\lambda}q^{\lambda}q^{*}_{\gamma} - (\pm)q_{\gamma}q^{\lambda *}K_{\rho\lambda} + q^{\lambda}K^{\dagger}_{\rho\lambda}q^{*}_{\gamma} - (\pm)q_{\gamma}K^{\dagger}_{\rho\lambda}q^{\lambda *}) + \frac{1}{4}(q_{\rho}q^{*}_{\gamma} \pm q_{\gamma}q_{\rho^{*}})R = 2\begin{pmatrix} k \\ k' \end{pmatrix}(T_{\rho}q^{*}_{\gamma} \pm q_{\gamma}T^{*}_{\rho}) \tag{48}$$

Examination of eqs. (42)–(44) shows that Eq. (48) (positive) is in one-to-one correspondence with Einstein's second-rank symmetric tensor equation (47).

H. The Electromagnetic Field Equations

The antisymmetric second-rank tensor equations (48) (negative), corresponding to six independent relations, may be reexpressed in terms of the Maxwell field theory (5) by taking the covariant divergence of (48) (negative), with

$$F_{\rho\gamma} = Q\left[\frac{1}{4}(K_{\rho\lambda}q^{\lambda}q^{*}_{\gamma} + q_{\gamma}q^{\lambda *}K_{\rho\lambda} + q^{\lambda}K^{\dagger}_{\rho\lambda}q^{*}_{\gamma} + q_{\gamma}K^{\dagger}_{\rho\lambda}q^{\lambda *}) + \frac{1}{8}(q_{\rho}q^{*}_{\gamma} - q_{\gamma}q^{*}_{\rho})R\right] \tag{49}$$

In this expression for the electromagnetic field intensity tensor, Q is a constant of proportionality with the dimension of charge, inserted on both sides of Eq. (48) (negative). The four-current density is

$$j_{\gamma} = \left(\frac{Qk'}{4\pi}\right)(T^{;\rho}_{\rho}q^{*}_{\gamma} - q_{\gamma}T^{;\rho *}_{\rho}) \tag{50}$$

The role of the *Mach principle* is revealed at this stage of the analysis. Since $F_{\rho\lambda}$ depends on the spin curvature tensor $K_{\rho\lambda}$, which automatically vanishes in a vacuum (i.e., a flat spacetime), the electromagnetic field, and therefore the previously considered electric charge of any quantity of matter in a vacuum, must vanish. Thus, not only the inertial mass but also the electric charge of a "particle" of matter does not exist when there is no coupling to other matter. I have generalized this idea in the field theory based on *general relativity*, to the case where *all* previously considered *intrinsic properties* of discrete matter, in addition to inertial mass and electric charge, vanish identically in a vacuum. This view exorcises all of the remaining features of the discrete, separable "elementary particle" of matter. It is replaced with a view of matter in terms of a closed, continuous field theory, according to the theory of general relativity. I have called this view of matter, whereby all of its previously considered intrinsic properties are explained in terms of coupling within the closed system, *the generalized Mach principle* [10].

I. The Conservation of Charge

Since $F_{\rho\gamma}$ is an antisymmetric tensor in spacetime and since the components of the ordinary affine connection $\Gamma^{\gamma}_{\alpha\beta}$ are symmetric in the indices $(\alpha\beta)$, it follows that the 4-divergence of the current density j_γ automatically vanishes. In other words, as in the standard formulation, the equation of continuity follows from taking the covariant divergence of Maxwell's equation (31a):

$$j^{;\gamma}_{\gamma} = \frac{1}{4\pi} F^{;\rho;\gamma}_{\rho\gamma} = 0 \tag{51}$$

It then follows from the integral form of (51) (in the local domain) that the integral of the time component j_0 over all of 3-space is time-conserved. This assumes that there is no current flow in or out of the surface containing the charge $Q = \int j_0 \, d^3x$, which gives rise to the electromagnetic field of force $F_{\rho\gamma}$.

J. The Absence of Magnetic Monopoles

The form (48) (negative) for the electromagnetic field intensity was seen to yield four out of the eight of Maxwell's equations associated with the current source, as shown in Eq (31a). It also follows that the four of Maxwell's equations without source terms

$$F^{[\mu\nu}_{;\lambda]} \equiv F^{\mu\nu}_{;\lambda} + F^{\lambda\mu}_{;\nu} + F^{\nu\lambda}_{;\mu} = 0 \tag{52}$$

are predicted by the quaternion structure of $F_{\rho\gamma}$ as given in (49). This implies the absence of magnetic monopoles [26] since, if they did exist, the right-hand side of (52) would be nonzero.

This result is a consequence of the dependence of the definition of $F_{\rho\lambda}$ of the spin curvature tensor, $K_{\rho\lambda}$, according to Eq. (49) (as well as $q_{\rho;\lambda} = 0$). This is because the spin curvature tensor $K_{\rho\lambda}$ is the four-dimensional curl of a 4-vector in configuration space:

$$K_{\rho\lambda} = \partial_\lambda \Omega_\rho - \partial_\rho \Omega_\lambda + \Omega_\lambda \Omega_\rho - \Omega_\rho \Omega_\lambda = \Omega_{\rho;\lambda} - \Omega_{\lambda;\rho} = -K_{\lambda\rho} \tag{53}$$

which, in turn, follows from the transformation of the spin–affine connection Ω_ρ *in configuration space* as a four-vector. It then follows that the cyclic sum $K_{[\rho\lambda;\gamma]} = 0$.

This result, according to Eq. (49), in turn, implies that Eq. (52), $F_{[\rho\lambda;\gamma]} = 0$, must be true, indicating that there are no magnetic monopoles in this formulation of the electromagnetic field equations—for if there were, there would be a nonzero source term in Eq. (52).

Thus we have seen that the factorized quaternion field equations (46a) (or their conjugated equations (46b)) -the irreducible form of electromagnetism

according to the underlying group of general relativity—indicates a lack of magnetic monopoles, in agreement with the standard formulation of the Maxwell field theory. The factorized field formulation of general relativity, in terms of the 16-component quaternion metrical field, q^{μ}, then automatically fuses the laws according to the Einstein formulation, and the laws of electromagnetism, according to the Maxwell formulation, in a *unified field theory* of the gravitational and electromagnetic manifestations of matter.

It is important to recognize at this stage of the analysis that the unified field equations (46) entail more physical predictions than do the respective earlier versions of gravitation—Einstein's field equations—and electromagnetism—Maxwell's field equations. We have already seen extra predictions from the spinor form of the electromagnetic field equations. Though this theoretical analysis does not focus on the expression of electromagnetism in terms of potential fields, extra predictions may indeed also follow in the quaternion-spinor formulation from the structuring of the electromagnetic $B^{(3)}$ potential field, as derived in the theory of M. Evans and his collaborators [27].

V. ELECTROMAGNETISM AND WAVE MECHANICS

A. Derivation of Born's Probability Calculus

The conventional conceptual content of quantum mechanics was initiated by the Copenhagen School when it was recognized that one could express the linear Schrödinger wave mechanics [28] in terms of a probability calculus, whose solutions are represented with a Hilbert function space. Max Born then interpreted the wave nature of matter in terms of a spatially distributed *probability amplitude*—a wave represented by a complex function—to accompany the material particle as it moves from one place to another. The Copenhagen view was then to *define* the basic nature of matter in terms of the measurement process, with an underlying probability calculus, wherein the probability densities (for locating the particles of matter/volume) are the real-number-valued moduli of the matter wave amplitudes.

But this was not Schrödinger's intention in his formulation of wave mechanics [29]! Rather, it was to complete the Maxwell field formulation of electromagnetic theory by incorporating the empirically verified wave nature of matter in the source terms on the right-hand sides of Maxwell's equations.

The "matter field" was originally postulated by Louis de Broglie, and discovered in the electron diffraction studies of Davisson and Germer [30] and of G. P. Thomson [31]. From Schrödinger's understanding of the matter field of, say, an electron, it must be represented in the source terms (charge and current density) of Maxwell's equations, as the moduli of these waves.

Integration of the *local limit* of Eq. (50) for the four-current density source of Maxwell's equations, together with the boundary condition that the

three-current part of this density, j_k, vanishes on the bounding surface of a volume that contains the total charge Q, then gives the law of conservation of electric charge:

$$\sigma^0 Q = \int j_0 \, d^3x = \text{constant in time} \tag{54}$$

[The insertion of the unit matrix σ^0 on the left takes account of the matrix structure (27) of the current density in the quaternion formulation.]

The local limit of j_0 in Eq. (50) is

$$j_0 = -\left(\frac{Qk'}{4\pi}\right)\partial^\rho (T_\rho^{(1)} + T_\rho^{(1)*}) \tag{55}$$

where $T_\rho^{(1)}$ is the local limit of the matter source of the quaternion metric field equation. In terms of the Lagrangian density for the matter variables, its form is $-\delta L_M/\delta q^{\rho *}$.

Taking determinants of both sides of Eq. (55) then yields the value of the constant k' as

$$k' = \frac{-(4\pi)}{|\int \partial^\rho (T_\rho^{(1)} + T_\rho^{(1)*}) d^3x|}$$

where the vertical bars denote the determinant.

Thus, the four-current density j_γ of this expression of the Maxwell theory has the following general form in a curved spacetime:

$$j_\gamma = Q(T_\rho^{;\rho} q_\gamma - q_\gamma T_\rho^{;\rho *})/\left|\int \partial^\rho (T_\rho^{(1)} + T_\rho^{(1)*}) d^3x\right| \tag{56}$$

The matter density, interpreted in conventional quantum mechanics as a probability density, is then

$$\sigma^0 \rho = \frac{j_0}{Q} = (q_0 T_\rho^{;\rho *} - T_\rho^{;\rho *} q_0^*)/\left|\int \partial^\rho (T_\rho^{(1)} + T_\rho^{(1)*}) d^3x\right| \tag{57}$$

In the local limit, $q_0 \to \sigma_0, q_0^* \to \sigma_0^* = -\sigma_0 \, T_\rho^{;\rho} \to \partial^\rho T_\rho^{(1)}$

Thus, we have

$$\text{loc lim}\left|\int \rho \; d^3x\right| = 1 \tag{58}$$

Equation (58) is the normalization condition that was *postulated* by Max Born, in his interpretation of Schrödinger's nonrelativistic wave mechanics as a probability calculus. As we see here, the *derived* normalization is not a general relation in the full, generally covariant expression of the field theory.

We also see from the general form (56) that the three-current density part of j_γ is

$$\frac{j_k}{Q} = \frac{q_k T_\rho^{;\rho^*} - T_\rho^{;\rho} q_k^*}{|\int \partial^\rho (T_\rho^{(1)} + T_\rho^{(1)*}) d^3x|}$$

This expression predicts a coupling of the gravitational field (in terms of q_k) with the matter field components T_ρ to define a gravitational current contribution. The latter is not foreseen in the conventional theories that neglect the gravitational coupling to matter fields.

B. Summary

We have seen in this section that the factorization of Einstein's symmetric, second-rank tensor field equations (10 relations) to a quaternion form (16 relations) not only yields the gravitational and electromagnetic manifestations of matter in a unified field theory but also reveals a feature of quantum mechanics. In particular, it was found that in the flat-space approximation to the curved-space representation in general relativity, the time component of the electromagnetic four-current density corresponds in a one-to-one way with the probability density of quantum mechanics. Its integration over all of space in this limit is found to be unity.

This is a result that was postulated (not derived from first principles) when Born attempted to identify quantum mechanics with a probability calculus. The result of this analysis, in which the normalization follows as a derivation from general relativity, together with a rigorous derivation of the quantum-mechanical equations from general relativity [32] then enforces the view of a paradigm change in physics. It is from that of quantum theory, which has dominated the last two-thirds of the twentieth century, to that of general relativity, as a theory of electromagnetism, gravity, and matter, in all domains. This is a shift to a paradigm for the laws of matter based fully on the views of continuity, determinism, and holism, in terms of the nonsingular field concept.

> It seems clear that the present quantum mechanics is not in its final form. Some further changes will be needed, just about as drastic as the changes made in passing from Bohr's orbit theory to quantum mechanics. Some day, a new quantum mechanics, a relativistic one, will be discovered, in which we will not have these infinities occurring at all. It might very well be that the new quantum mechanics will have determinism in the way that Einstein wanted. This

determinism will be introduced only at the expense of abandoning some other preconceptions that physicists now hold. So, under these conditions I think it is very likely, or at any rate quite possible, that in the long run Einstein will turn out to be correct, even though for the time being physicists have to accept the Bohr probability interpretation [33].

References

1. A. Einstein, *The Meaning of Relativity*, 5th ed., Princeton Univ., 1955. English translations of some of the initial papers on relativity theory are available in A. Einstein, H. A. Lorentz, H. Weyl, and H. Minkowski, *The Principle of Relativity*, Dover, 1923.
2. Y. S. Kim and M. E. Noz, *Theory and Applications of the Poincare Group* Reidel, 1986. One of the pioneering books on group theory that clearly explicates the spinor role in relativistic covariance is E. P. Wigner, *Group Theory and Its Application to the Quantum Mechanics of Atomic Spectra*, Academic, New York, 1959.
3. M. Sachs, *Relativity in Our Time*, Taylor & Francis, 1993.
4. The mathematical details of the approach of Einstein's general relativity in approaching Newton's theory of universal gravitation are outlined in R. J. Adler, M.J. Bazin, and M. Schiffer, *Introduction to General Relativity*, 2nd ed., McGraw-Hill, New York, 1975, Chap. 10. Further details are discussed in Ref. 3, Chap. 19.
5. A. Einstein, *Ann. Math.* **46**, 578 (1945).
6. L .P. Eisenhart, *Continuous Groups of Transformations* Dover, 1961.
7. Noether's theorem is derived in E. Noether, *Goett. Nachr.* 235 (1918). It is explained further in C. Lanczos, *The Variational Principles of Mechanics*, Toronto, 1966, Appendix II and in R. Courant and D. Hilbert, *Mathematical Methods of Physics*, Interscience, 1953, Vo. I, p. 262. Application to fields is clearly demonstrated in N. N. Bogolubov and D. V. Shirkov, *Introduction to the Theory of Quantized Fields*, 3rd ed., Interscience, 1980, Sec. 1.2.
8. In J. J. Thomson (Ed.), *James Clerk Maxwell: A Commemorative Volume: 1831–1931*, Cambridge Univ., 1931, Einstein said: "I incline to the belief that the physicists will ... be brought back to the programme which may suitably be called Maxwell's: the description of Physical Reality by fields which satisfy without singularity a set of Partial differential equations." In a letter that Einstein wrote to David Bohm in 1953, he said: "If it is not correct that reality is described as a continuous field, then all my efforts are futile," *Einstein Archives*, Jewish National and University Library, The Hebrew University of Jerusalem, Call No. 1576:8–053.
9. A complete discussion of Lie groups is contained in H. Weyl, *The Theory of Groups in Quantum Mechanics*, Dover, 1931, Sec. 15 (translated by H. Robertson).
10. I have discussed the generalized Mach principle in: M. Sachs, *General Relativity and Matter*, Reidel, 1982, Sec. 1.7.
11. C. S. Wu, E. Ambler, R. W. Hayward, D. D. Hoppes, and R. P. Hudson, *Phys. Rev.* **105**, 1413 (1957).
12. M. Sachs, *Ann. Phys.* **6**, 244 (1959).
13. M. Sachs, *General Relativity and Matter*, Reidel, 1982, Sec. 4.7.
14. M. Sachs and S.L. Schwebel, *Ann. Phys.* **8**, 475 (1959).
15. N. F. Ramsey, *Phys. Rep.* **43**, 409 (1978).
16. M. Sachs, *Quantum Mechanics from General Relativity*, Reidel, 1986, Sec. 8.2.
17. Ref. 13, Chap. 3.

18. Ref. 13, Chap. 5.
19. Ref. 13 (3.31).
20. M. Sachs, in T. W. Barrett and D. M. Grimes (Eds.), *Advanced Electromagnetism*, World Scientific, Singapore, 1995, p. 551.
21. M. Sachs, *Lett. Nuovo Cimento* **21**, 123 (1978).
22. L. Pontrjagin, *Topological Groups*, Princeton Univ., 1939, p. 173.
23. In a letter to P. G. Tait in 1871, J. C. Maxwell said the following about the use of quaternions in the laws of physics: ''the virtue of the 4nions lies not so much as yet in solving hard questions as in enabling us to see the meaning of the question and its solutions,'' *Archives*, Cavendish Laboratory, Cambridge Univ.
24. For a derivation of the affine connection in the tensor formalism, see Ref. 4.
25. Ref. 13, Chap. 6.
26. M. Sachs, *Nuovo Cimento* **114B**, 123 (1999).
27. M. W. Evans and J.-P. Vigier, in M. W. Evans, J.-P. Vigier, S. Roy, and S. Jeffers (Eds.), *The Enigmatic Photon, Vol. 1. The Field* $B^{(3)}$ Kluwer, 1994; ibid., Vol. 3, Kluwer, 1996.
28. M. Sachs, *Annales de la Fondation Louis de Broglie* **17**, 163 (1992).
29. M. Sachs, *Einstein Versus Bohr* (Open Court, 1988), Chap. 5.
30. C. J. Davisson and L.H. Germer, *Phys. Rev.* **30**, 705 (1927).
31. G. P. Thomson, *Proc. Roy. Soc.* (London) **A117**, 600 (1928).
32. M. Sachs, *General Relativity and Matter*, Reidel, 1982, Chap. 4.
33. P. A. M. Dirac, ''The Early Years of Relativity'', in G. Holton and Y. Elkana (Eds.), *Albert Einstein: Historical and Cultural Perspectives*, Princeton Univ. Press, 1982, p. 79.

AUTHOR INDEX

Numbers in parentheses are reference numbers and indicate that the author's work is referred to although his name is not mentioned in the text. Numbers in *italic* show the pages on which the complete references are listed.

SUBJECT INDEX